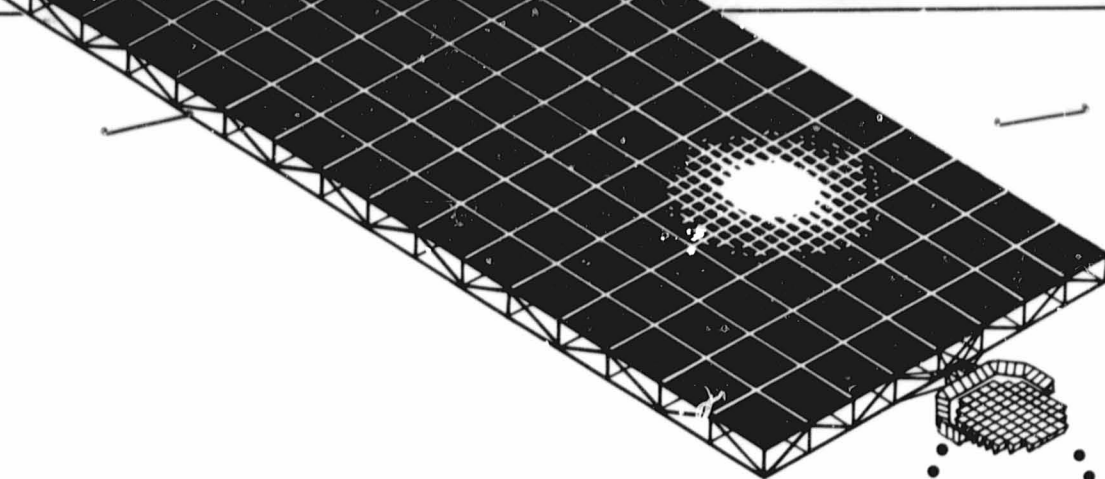


General Disclaimer

One or more of the Following Statements may affect this Document

- This document has been reproduced from the best copy furnished by the organizational source. It is being released in the interest of making available as much information as possible.
- This document may contain data, which exceeds the sheet parameters. It was furnished in this condition by the organizational source and is the best copy available.
- This document may contain tone-on-tone or color graphs, charts and/or pictures, which have been reproduced in black and white.
- This document is paginated as submitted by the original source.
- Portions of this document are not fully legible due to the historical nature of some of the material. However, it is the best reproduction available from the original submission.

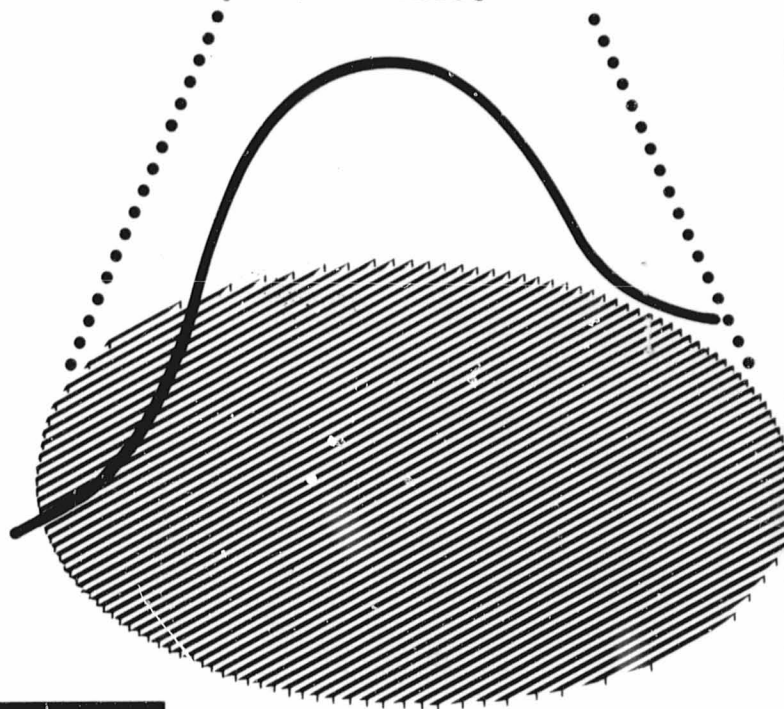


1439

(NASA-TM-84064) WORKSHOP ON MICROWAVE POWER
TRANSMISSION AND RECEPTION. WORKSHOP PAPER
SUMMARIES (NASA) 1366 p HC A99/MF A01
CSCL 10A

N82-12538
THRU
N82-12568
Unclass
02688

G3/44



NASA Solar Power
Satellite

Workshop on
Microwave Power
Transmission
and Reception

Workshop
Paper
Summaries

Jan
15-18
1980

National Aeronautics and
Space Administration

Lyndon B. Johnson Space Center
Houston, Texas 77058

FOREWORD

This volume contains the summary papers of the SPS Workshop on Microwave Power Transmission and Reception held at the Johnson Space Center, Houston, Texas, January 15-18, 1980. These papers are summaries of the material presented during six technical sessions: Microwave System Performance, Phase Control, Power Amplifiers, Radiating Elements, Rectenna and Solid State Configurations. As part of the DOE/NASA Concept Evaluation Program, a set of conclusions were reached based on numerous analytical and experimental investigations. These papers provide a comprehensive record of the material developed to support those conclusions at the Workshop.

It is hoped that this volume will be a useful contribution to the continuing evaluation process of the SPS Microwave Power Transmission and Reception System.

R. H. Dietz
SPS Microwave Systems
Johnson Space Center

SYSTEM PERFORMANCE SESSION

)

SYSTEM PERFORMANCE CONCLUSIONS

G. D. Arndt

NASA - Johnson Space Center

1. System Sizing

- o Reduced Power Levels
- o Antenna Diameters Smaller than 1 Km

The initial sizing for the satellite power station was a 1-kilometer transmit array with 5 gigawatts of DC power out of the rectenna. There are, however, some advantages in having a smaller system size. Commercial utility companies can probably handle 1-gigawatt increments easier than 5 gigawatts; the implementation cost of 1-gigawatt system is lower; and the sidelobe radiation levels near the rectenna are lower. Disadvantages of smaller systems include lower end-to-end microwave transmission efficiency and an increase in the overall cost of electricity (mills per kilowatt-hour).

The downlink operating frequency is another trade-off consideration. The SPS reference system operates at 2.45 gigahertz, which is the center of a 100-megahertz band reserved for government and nongovernment industrial, medical, and scientific (IMS) use. This band has the advantage that all communication services operating within the 2450 ± 50 megahertz limits must accept any interference from other users. There is another IMS band at 5.8 gigahertz which should be considered. One way to reduce the terrestrial land usage requirements for the SPS rectenna is to increase the operating frequency while maintaining the same antenna size. This reduction in rectenna size must, however, be traded off against the large temporary degradation in transmission efficiency under extremely adverse weather conditions at the higher frequency.

The end-to-end microwave transmission efficiency for smaller SPS systems operating at different frequencies will not be determined. The nominal microwave transmission efficiency, from the rotary joint in the satellite to the DC/DC power interface at the output of the rectenna; is shown in figure 1. This end-to-end efficiency, for a frequency of 2450 megahertz, may be written

$$\text{Microwave Eff} = 0.805 \text{ Eff}_{\text{coll}} \times \text{Eff}_{\text{conv}} \quad (1)$$

For the reference system, $\text{Eff}_{\text{coll}} = 0.88$ and $\text{Eff}_{\text{conv}} = 0.89$, and the microwave link efficiency is 63 percent. This efficiency will be used as a reference for comparing smaller SPS systems. In equation 1, the rectenna collection efficiency Eff_{coll} is a function of incident power density and incremental rectenna area while the conversion efficiency Eff_{conv} varies only with power density. The RF-DC conversion efficiency

Figure 1

Nominal efficiencies for the
microwave system (2450 MHz)

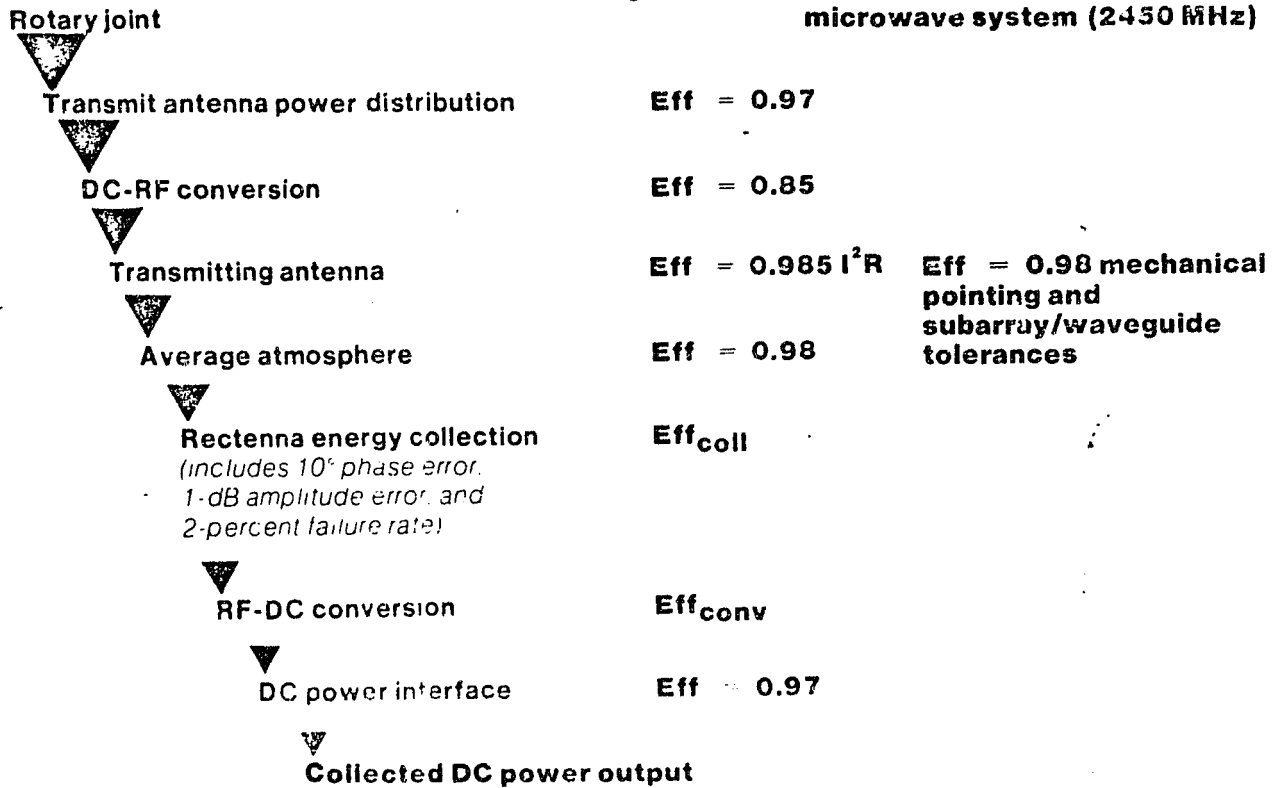
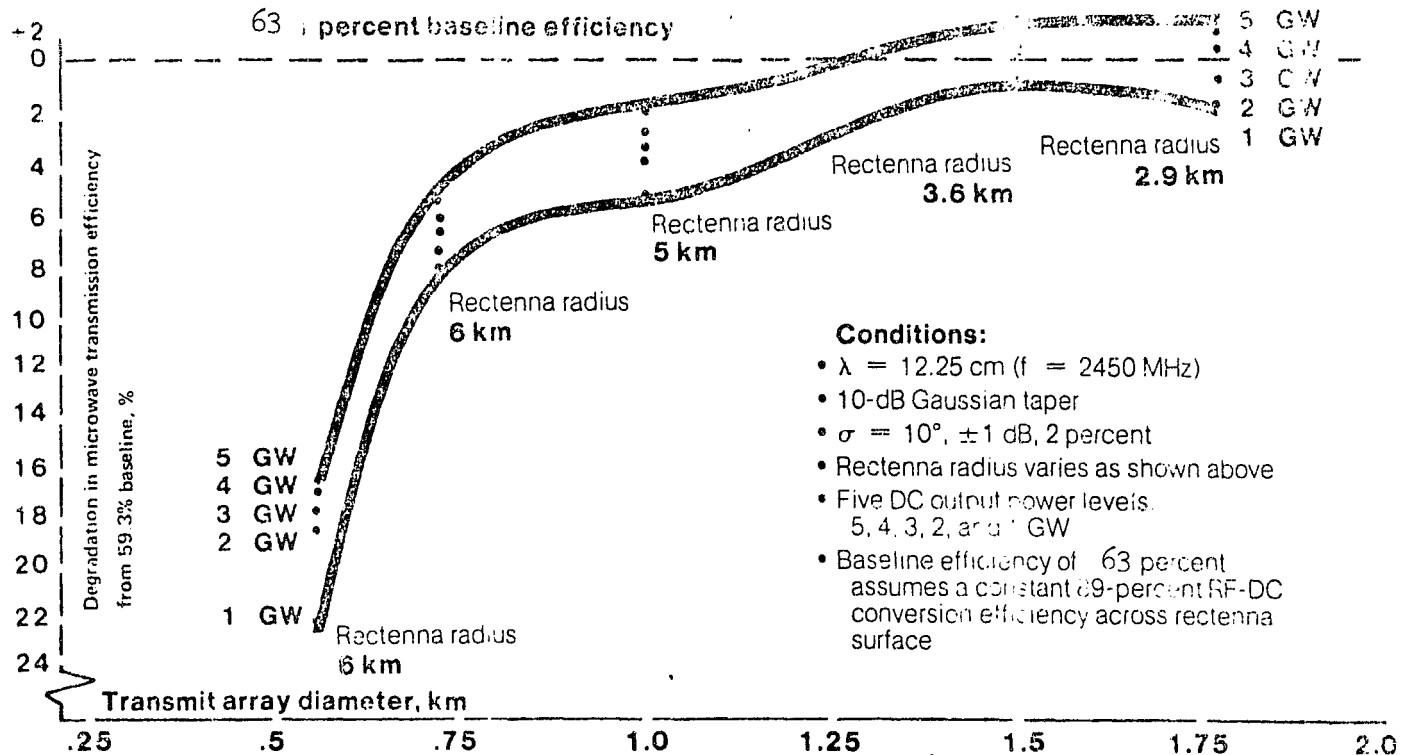


Figure 2

SPS performance at 2450 MHz as a function of antenna size and power



depends on the input power level to the rectifying diodes connected to the half-wave dipole elements in the rectenna. During the past several years, excellent progress has been made in developing higher efficiency diodes, particularly at lower levels. This RF-DC conversion efficiency, which is the collection efficiency of the individual dipole elements times the diode rectifying efficiency, varies from 70 percent at 0.04 milliwatt per square centimeter to 90 percent at 10 milliwatts per square centimeter as a function of incident power density. These data assume a 3 percentage point improvement in the next decade over the present achievable conversion efficiency.

The degradations in end-to-end microwave efficiency for smaller SPS sizes are summarized in figures 2 and 3 for operating frequencies of 2450 and 5800 megahertz respectively. The 63 percent reference efficiency is that performance expected for a 1-kilometer, 5-gigawatt SPS system operating with a constant 89 percent RF-DC conversion efficiency in the rectenna. The difference in performance between the 5-gigawatt and the 1-gigawatt systems as shown in figure 2 is due to a reduction in rectenna conversion efficiency at the reduced power density levels associated with the 1-gigawatt system. Also, for transmit arrays with a diameter less than 1 kilometer, the power beam is dispersed over a wider area at the ground due to reductions in antenna gain. This dispersion reduces the amount of energy intercepted by the rectenna and further reduces the RF-DC conversion efficiency. The data indicate that smaller SPS powers are feasible, provided the antenna size is not reduced; that is, a 1-kilometer, 1-gigawatt SPS system will have only a 4 to 5 percent (percentage points) reduction in microwave transmission efficiency as compared to a 5-gigawatt system.

The transmission efficiency for systems operating at 5800 megahertz as given in figure 3 is interesting in that there is very little degradation in performance at the reduced power levels. The reason is that the power density levels at the rectenna are considerably higher for the 5800-megahertz systems, and hence little degradation in RF-DC conversion efficiency occurs as the power is reduced. There is also a constant degradation relative to the 59.3 percent reference efficiency due to lower efficiencies in several of the microwave subsystems operating at the higher 5800-megahertz through a heavy rain, rectennas for these systems could have intermittent power reductions unless located in dry, southwest regions.

There is a significant reduction in rectenna size at the higher frequency as shown in figure 3. If rectenna costs and land usage requirements become major factors, operating at 5800 megahertz should be seriously considered.

2. Startup/Shutdown Operations

- o Three sequences for startup/shutdown provide satisfactory performance

An SPS in synchronous orbit experiences solar eclipses by the earth, moon, and other SPS. The most important of these eclipses are by the earth, both in occurrence and duration. The satellite will be eclipsed daily by the earth for approximately six weeks during the spring and fall equinoxes, March 21 and September 21, respectively. Specifically there will be 43 eclipses centered around the spring equinox and 44 in the fall, for a total of 87 times per year. These eclipse periods will vary each day, with the time building up to a maximum of 75 minutes at the equinox. Except for the first and last days of each series, the satellite is totally eclipsed.

Because of switching conditions and transients in the DC power distribution system, the microwave system will be brought up (or shutdown) in controlled increments, rather than having on-off switching of 7 GW of power. The resultant microwave radiation patterns can vary greatly, depending upon the sequences used for energizing the antenna. The beam patterns have been evaluated in order to reduce the environmental effects of the microwave radiation from the antenna under transient operating conditions.

Let us now examine what happens to the solar array during an eclipse. Both the solar cells and the structures will cool off quickly. The structure will drop to 70°K (-335°F) during the longest (72 minutes) occult period (Ref. 5). The solar cell temperature drops from its normal operating value of 310°K to 110°K at the end of 70 minutes. After emerging from the earth's shadow, cell temperatures rise quickly, particularly if the cells are open-circuited. A solar cell's output is a function of temperature and the cells will produce a higher output power for a few minutes until the temperature stabilizes. Since the voltage regulation to the klystron tubes is +5%, the tubes cannot be energized until near steady-state operating temperatures are reached in the solar array.

The operational procedure would be to open-circuit the solar cells prior to emergence from occultation, close to the DC power circuits in the solar array after the solar cell temperatures have stabilized near 310°K (a few minutes depending the length of the eclipse period), and then sequentially energize the klystron tubes in an optimum manner to minimize radiation effects.

The pattern characteristics for the main beam, sidelobes, and grating lobes were examined for eight types of energizing configurations which include:

1. Random - the antenna is starting at the center and progressing outward
2. Concentric rings - starting at the center and progressing outward
3. Concentric rings - beginning at the outer and progressing to the center
4. Line strips - center to the outside edge
5. Line strips - outside edge to the center

Figure 3 SPS performance at 5800 MHz as a function of antenna size and power

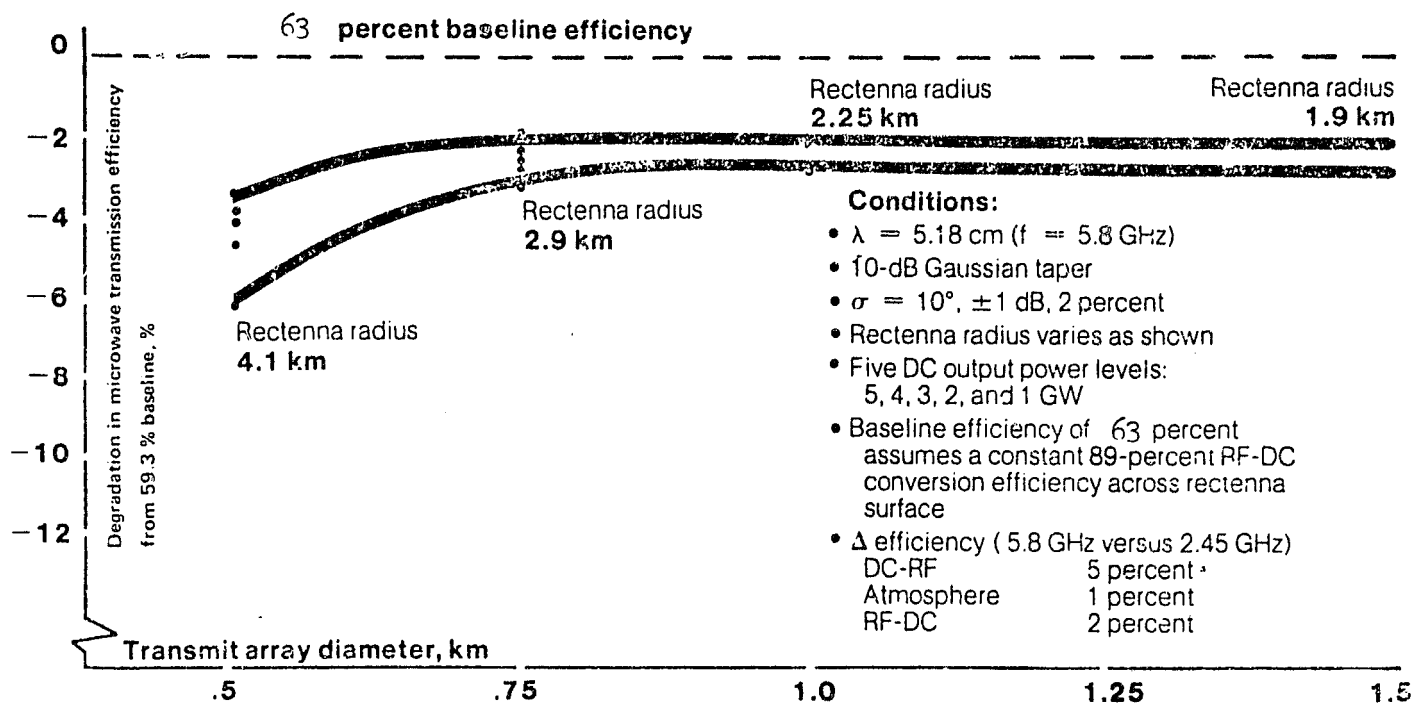
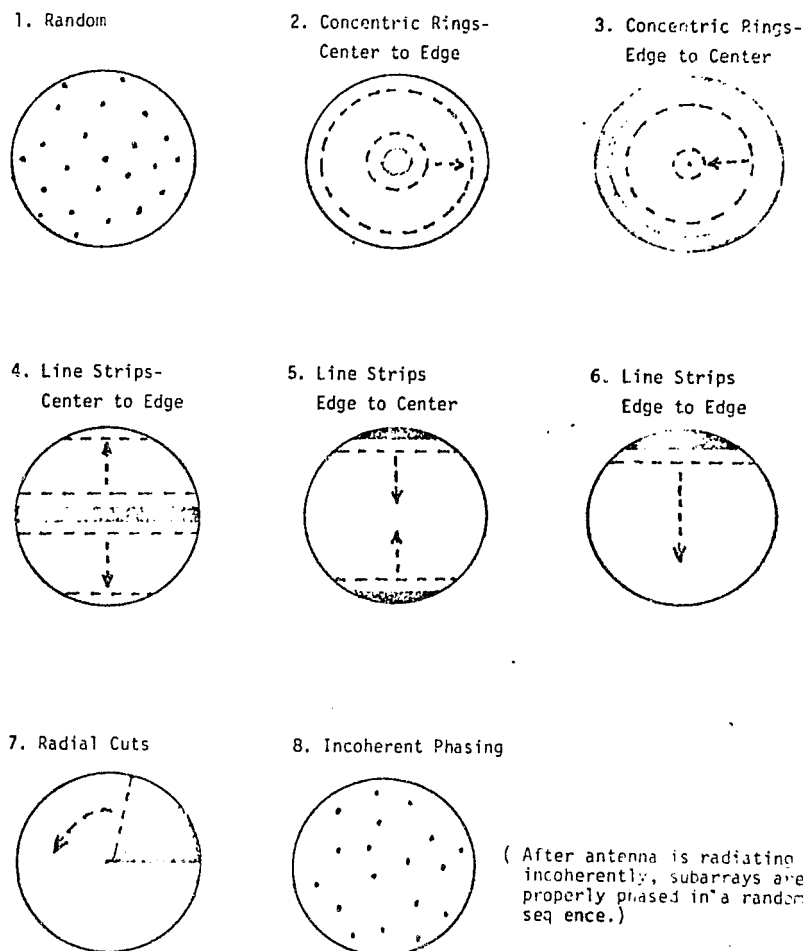


Figure 4. Antenna Startup/Shutdown Configurations



Note: Increments of 10 power are used for all sequences. Antenna illumination is a 10 dB Gaussian taper.

Figure 5. Sidelobe Patterns for the Pardon Sequence

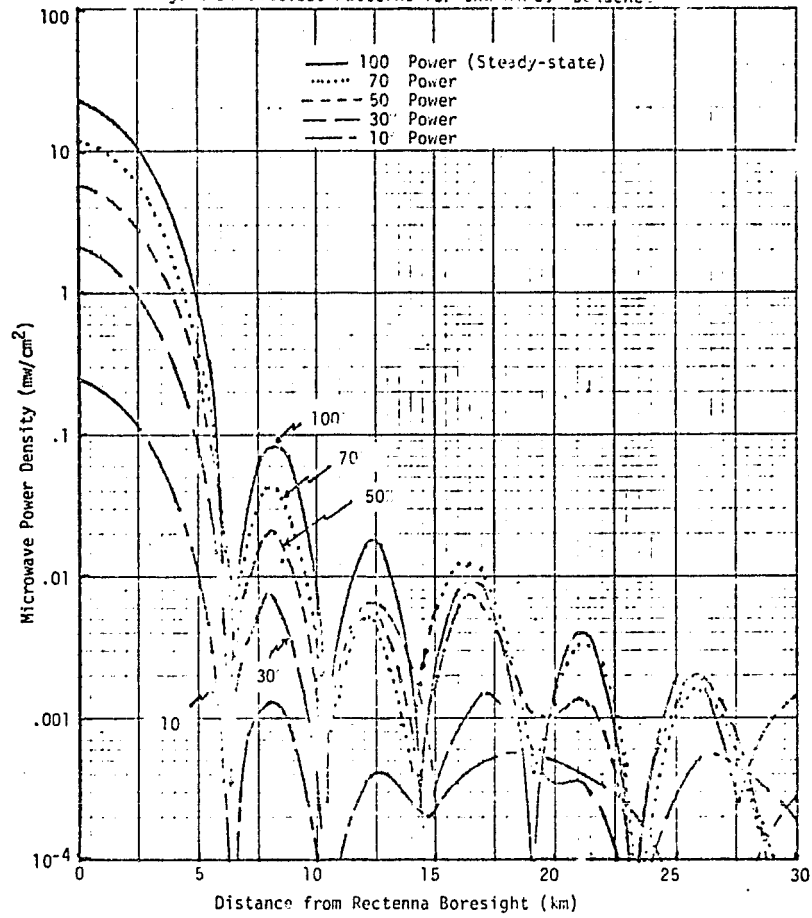
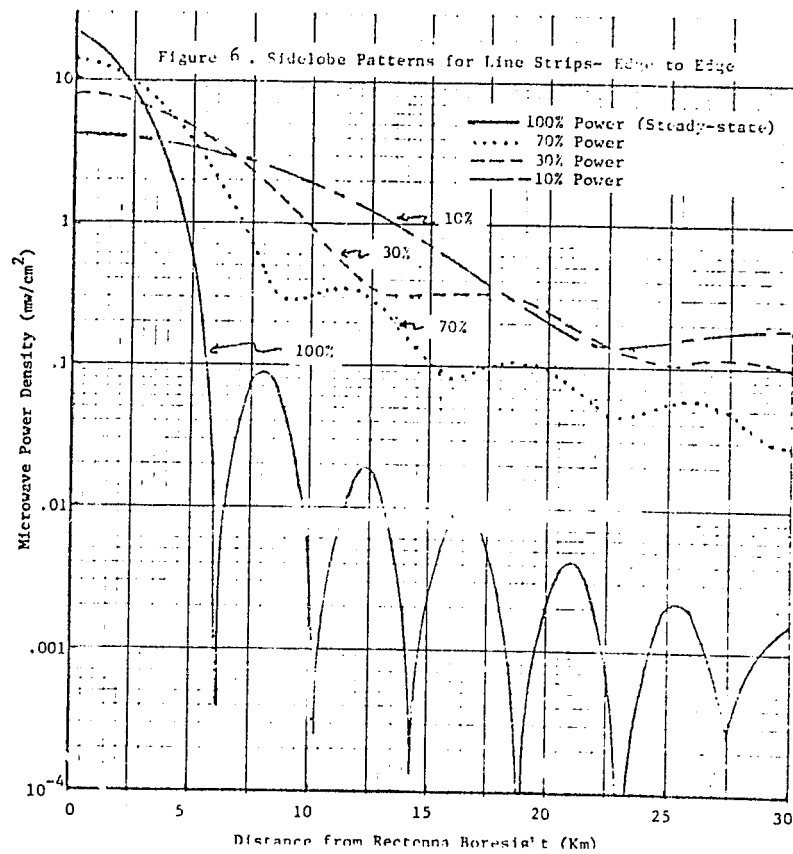


Figure 6. Sidelobe Patterns for Line Strips- Edge to Edge



6. Line strips - edge-to-edge
7. Radial cuts
8. Incoherent phasing

In each of these sequences shown in figure 4, the amount of antenna power is increased in ten discrete steps. For each of the configurations the reference error tolerances for random amplitude and phase errors throughout the antenna are included. The results are obtained through computer programs which simulate the 7220 subarrays as individual radiators properly phased together.

To briefly summarize the results, three sequences provided satisfactory performance in that the resultant sidelobe levels during startup/shutdown were lower than the steady-state levels present during normal operations. These three sequences were:

- o random
- o incoherent phasing
- o concentric rings - center to edge

As an example of the performance of the random sequence, the random startup is well-behaved in that the partial power patterns closely resemble the full power characteristics, only reduced in amplitude as shown in figure 5. As the radiated power is decreased the effective antenna area decreases, and the far sidelobe levels increase. The peaks and nulls of the sidelobes remain spatially stationary as the antenna radiating area changes.

An example of a poor startup/shutdown sequence is shown in figure 6, i.e., line strips - edge to edge. By taking successive vertical strips at one edge of the antenna and progressing to the other edge, the peaks and nulls of the sidelobes moves inward towards the rectenna with additional power. These patterns have sidelobe levels several orders of magnitude greater than for steady-state. In conclusion a proper choice of sequences should not cause environmental problems due to increased microwave radiation levels during the short time periods of energizing/de-energizing the antenna.

3. Antenna/Subarray Mechanical Alignments

- o Alignment requirements determined by grating lobe peaks and scattered power levels
- o Antenna alignment requirement is 1 min or 3 min depending upon phase control configuration.

There are two types of mechanical misalignments: (1) a systematic tilt of the entire antenna structure produced by attitude control system errors, and (2) a random tilt of the individual subarrays produced by antenna bending or subarray alignment errors. The rectenna collection efficiency (which is an indication of the amount of scattered power) as a function of systematic (structure) and random (subarray) tilts is shown in figure 7. It is interesting to note that the two tilts have the same degradation in collection efficiency per arc

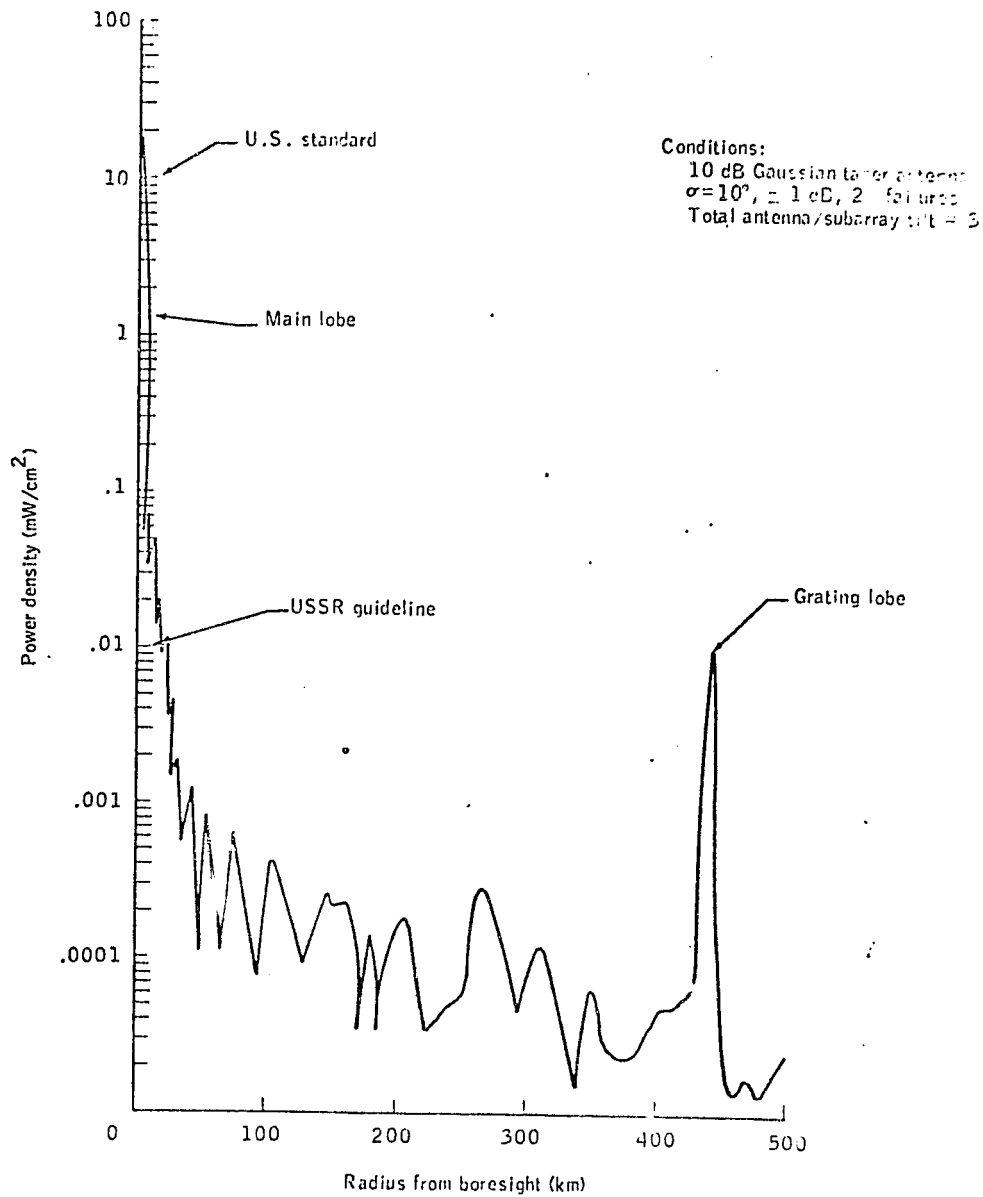
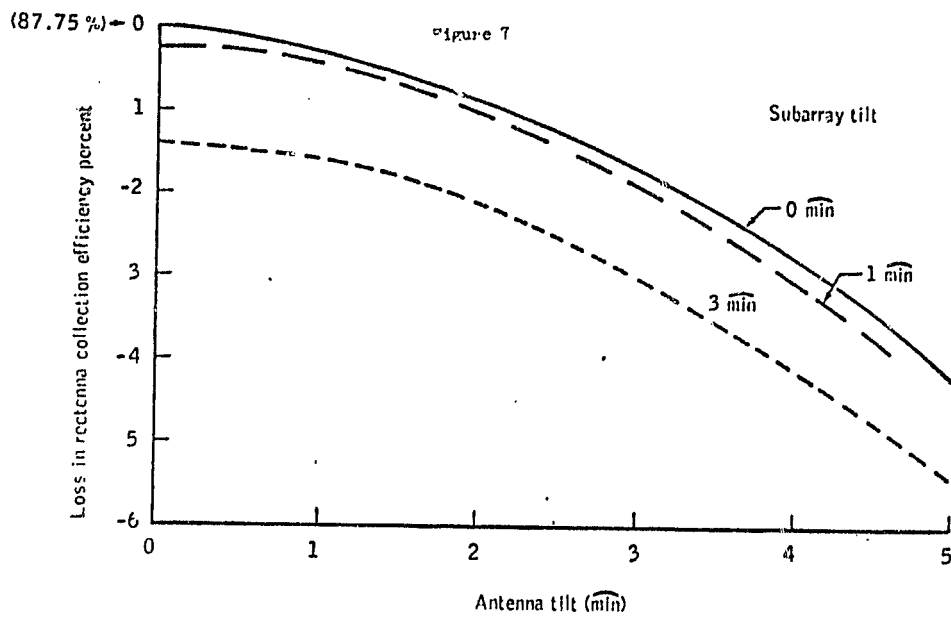


Figure 7 - Peak power density for sidelobes and grating lobe as a function of range from rectenna.

minute of misalignment. It will be shown later that the systematic tilt has an order of magnitude greater effect on grating lobe levels than the random tilts.

The antenna and subarray/power module misalignments produce well-defined grating lobes. The grating lobes occur at spatial distances corresponding to angular directions off-axis of the antenna array where the signals from each of the subarrays add in-phase. When the mechanical boresights of the subarrays are not aligned with the pilot beam transmitter at the rectenna, the phase control system will still point the composite beam at the rectenna; however, some of the energy will be transferred from the main beam into the grating lobes. The grating lobes do not spatially move with misalignment changes but their amplitudes are dependent upon the amount of mechanical misalignment. The distance between maxima for the grating lobes is inversely proportional to the spacings between phase control centers on the transmit antenna. If the phase control is provided to the 10.4 meter X 10.4 meter subarray level, grating lobe peaks occur every 440 Km. If the phase control system is extended down to the power module level, the grating lobes will be spatially smeared and the peaks greatly reduced in amplitude. This improvement in grating lobe pattern would be due to differences in spacings between the power tubes within the antenna. An example of the first grating lobe peak for a total antenna/subarray tilt of 3.0 arc-minutes is shown in figure 8.

Based upon environmental considerations, the grating lobes are constrained to be less than $.01 \text{ mw/cm}^2$. The total mechanical alignment requirements for both the subarrays and the total antenna can be determined from this constraint. The amplitudes of the grating lobes for phase control to the power module level and an antenna tilt of 1 min is shown in figure 9. The locations and spacings of these grating lobes across the continental United States with the rectenna centrally located are shown in figure 10.

Conclusions from the antenna simulation studies are:

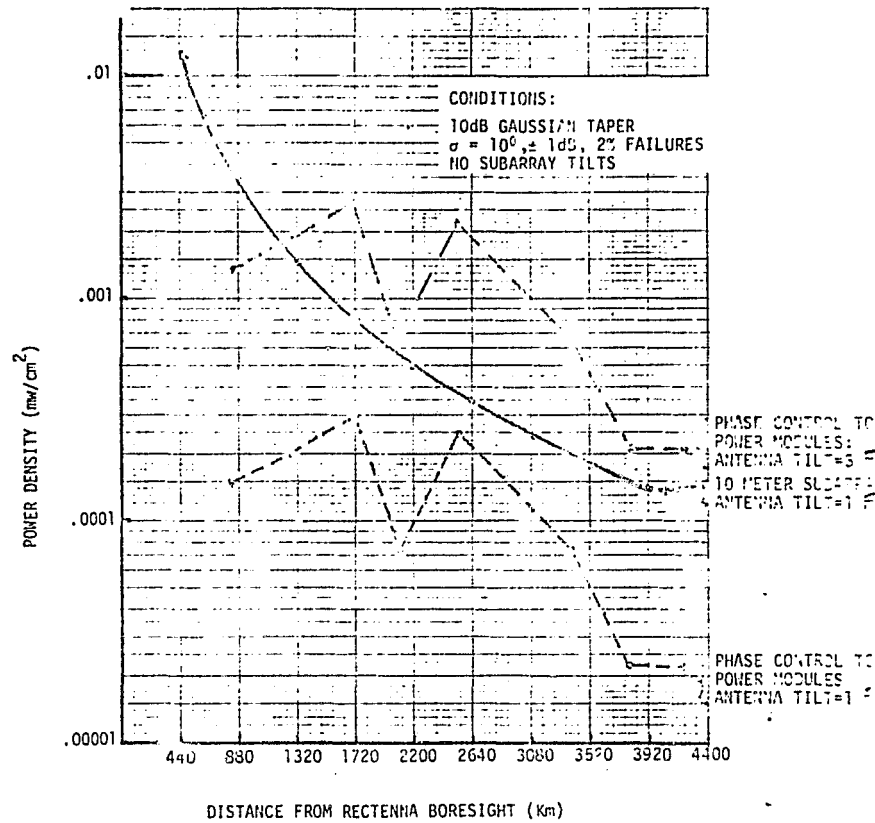
- (1) Systematic (antenna) tilt has an order of magnitude greater effect on grating lobe peaks than random (subarray) tilt.
- (2) The systematic tilt must be less than 1 min for phase control to the 10 meter square subarray level and 3 min for phase control to the power module level in order for the grating lobe peaks to meet the guideline of $.01 \text{ mw/cm}^2$.
- (3) Random (subarray) tilt is limited to 3 min in order to maintain a 2% or less drop in rectenna collection efficiency. The random tilt has a profound impact on the amount of scattered microwave power but only a very small contribution to the grating lobe peaks.

4. Scattered Microwave Power

- o System error parameters have been defined to minimize scattered power

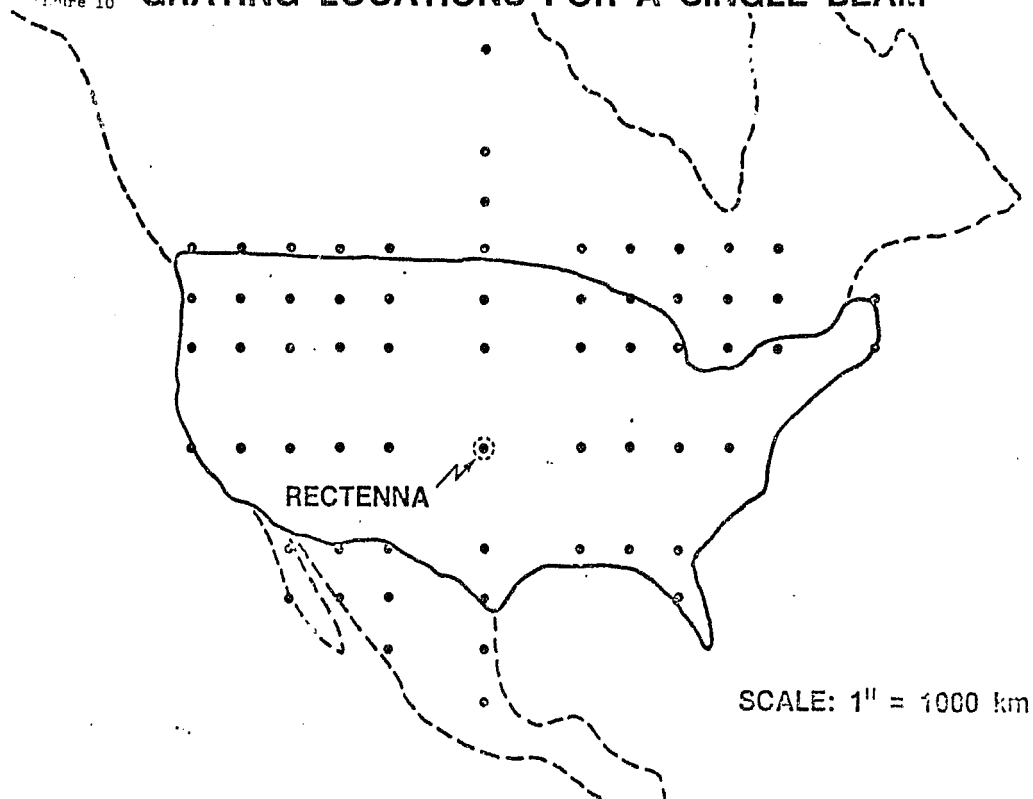
ORIGINAL PAGE IS OF POOR QUALITY

FIGURE 9
GRATING LOCATIONS FOR 10 METER SUBARRAYS AND PHASE
CONTROL TO POWER MODULES (TUBES)



NASA-S-79-11121

Figure 10 GRATING LOCATIONS FOR A SINGLE BEAM



The relative importance of the electrical and mechanical tolerances on the rectenna collection efficiency is summarized in figure 11. The baseline error parameters are $\sigma = 10^\circ$ rms phase error, ± 1 dB amplitude error, 2% failures, .25 inch mechanical gap between the 10. meter X 10. meter subarrays, antenna tilt < 1 min (attitude control) and subarray tilt < 3 min. The scattered microwave power is the extra power lost (not incident upon the rectenna) due to the error tolerances. The rectenna would intercept 95.3% of the total power transmitted by a perfect system; the error tolerances reduce this amount of received power to 86.0% of the transmit power.

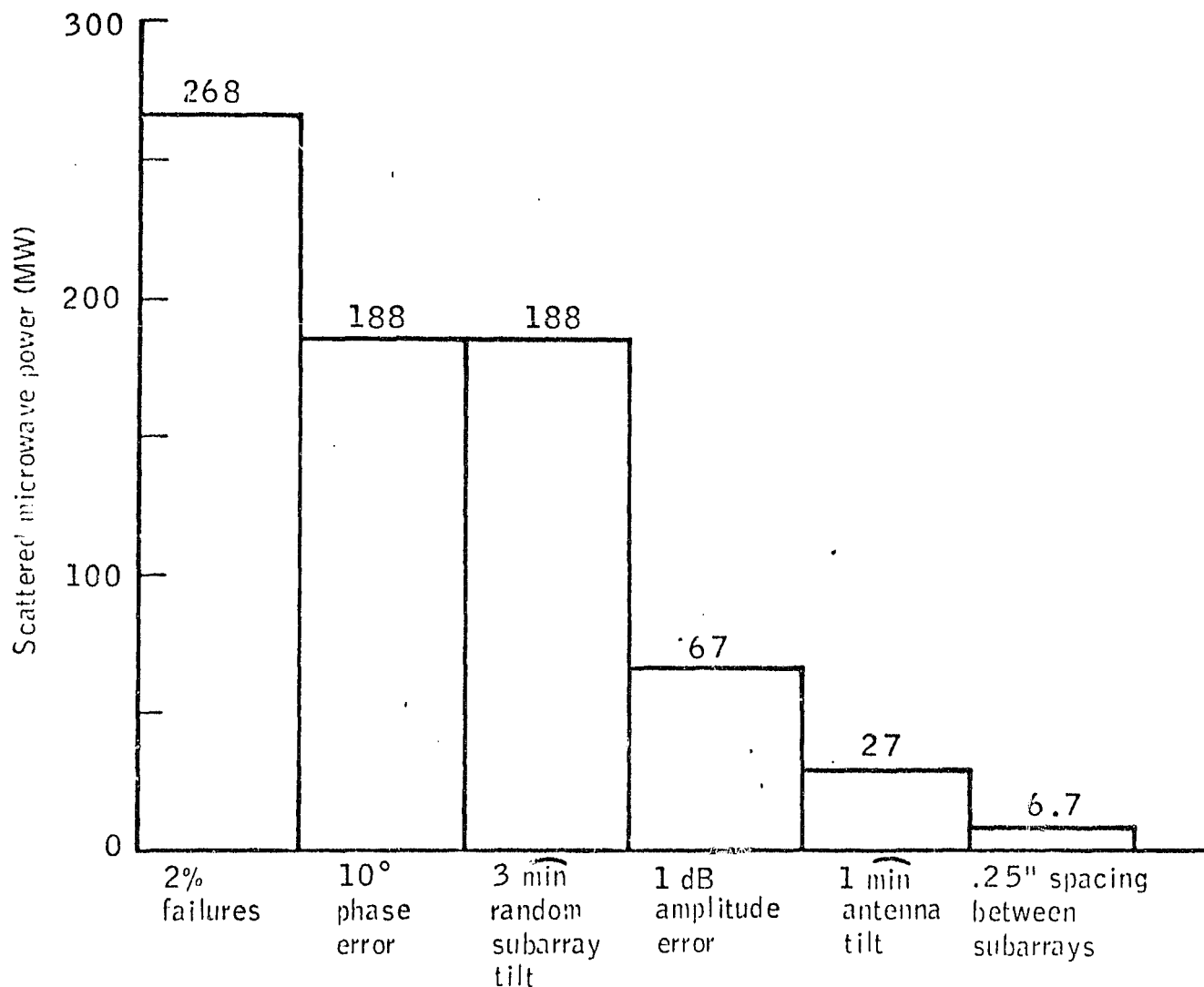


Figure 11 - Scattered microwave power due to electrical and mechanical errors. (10 meter subarray).

Reference System Description
Gordon Woodcock/Boeing

Initial MPTS Study Results
O. Maynard/Raytheon

unavailable at time of printing

SPS LARGE ARRAY SIMULATION

S. Rathjen B. R. Sperber, E. J. Nalos, Boeing Aerospace Company

1.0 INTRODUCTION

The computer simulation has been developed with the objective of producing a flexible design and verification tool for the SPS reference design. The computer programming efforts have been directed primarily to beam pattern analysis. The following reasons have been specified as the purpose of the computer programs: verification of the reference design, definition of feasible departures such as quantized distributions, the study of far-out sidelobe roll-off characteristics, the analysis of errors and failures, illumination function analysis to develop beam patterns for efficient collection, and beam shaping synthesis to meet environmental constraints.

2.0 ARRAY SIMULATION PROGRAMS

Three types of computer simulations have been developed to study the SPS microwave power transmission system (MPTS). The radially symmetric array simulation is low cost and is utilized to investigate general overall characteristics of the spacetenna at the array level only. "Tiltmain," a subarray level simulation program, is used to study the effects of system errors which modify the far-field pattern. The most recently designed program, "Modmain," takes the detail of simulation down to the RF module level and so to date is the closest numerical model of the reference design.

Early in the computer program development stage, radially symmetric array simulations were written to model various power taper distributions and to compare their beam efficiencies.

The radially symmetric simulations have been used to study a variety of spacetenna distribution functions enabling comparisons of the on-axis power densities, the far field patterns, and their associated beam efficiencies.

The "Tiltmain" array simulation is much more complex than the circularly symmetric simulation due to the fact that "Tiltmain" models the spacetenna as comprised of 7220 subarrays. In "Tiltmain," the ground-grid is specified as a planar circular area where the electric fields are determined. The field at any particular point on the grid is computed using scalar wave equations with approximations that make them accurate in the Fresnel Zone. The equations are not valid for the very near field, but give very good results in the Fresnel Zone, $D^2/\lambda > R > 2D^2/\lambda$, and the far field $R > 2D^2/\lambda$ where D is the diameter of a circular spacetenna or the diagonal of a rectangular spacetenna, λ is the wavelength of the transmission signal, and R is the range from the spacetenna to the ground-grid. The electric field at any particular point is determined by calculating the field from each subarray in the spacetenna to the given grid point and then summing all the fields to give the total field at that grid point.

The total power collected by the ground-grid is calculated by multiplying the power density at a point by the incremental area associated with that point to give the power over that area, and then summing up the power from each sample. Efficiencies with respect to the total power collected on the ground-grid and with respect to the total input power of the orbiting spacetenna are calculated at incremental grid distances out of the specified diameter.

"Modmain" is the most complex simulation of the MPTS to date in that the spacetenna is modelled not only as 7220 subarrays (as in "Tiltmain") but each subarray is modeled as a composition of RF transmitter modules. "Modmain" models over 100,000

modules and simulates phase errors, amplitude errors, failures, and systematic as well as random tilt.

The "Tiltmain" simulation was unable to model below the subarray level because its program structure caused data storage limitations problems; "Modmain" is structured in such a way as to overcome this disadvantage. Previously, the amplitude and phase of each subarray was stored in an array and recalled for each ground point. With "Modmain" the amplitude and phase of every module is not stored but the contribution of a module at each ground point is calculated and stored before moving on to the next module where the contribution is added to the previous ground point contributions.

3.0 REFERENCE DESIGN VERIFICATION

The computer programs have been used to investigate different antenna aperture illumination functions. An optimized aperture distribution will maximize the RF power intercepted by the ground rectenna and minimize the sidelobes and grating lobes. The types of illumination functions investigated include: Gaussian, cosine on a pedestal, uniform, reverse phase, inflected Bessel, and quadratic on a pedestal. Each of these was evaluated in terms of maximum power density at the transmit array and the rectenna, sidelobe levels, beam shape, and beam efficiency. Several Taylor series tapers were also explored with general results indicating that sidelobe levels decrease as the amount of taper increases.

Figure 1 shows five spacetenna distribution functions and the required spacetenna size and power densities to produce the same peak power density on the ground and the same size main beam. Figure 2 depicts the five far-field patterns showing the relative levels of the sidelobes. It was found that a 10 dB Gaussian taper has the best performance and that when quantized into at least eight levels produced nearly the same results as a theoretical continuously variable function. From antenna layout considerations, a 10-step, 10 dB Gaussian taper was then chosen for the aperture illumination (See Figure 3). The farther out sidelobes were compared for the continuous and ten-step quantized Gaussian tapers. The results show very little difference between the two cases.

In order to verify the energy distribution at distances far away from antenna boresight, it was necessary to determine the roll-off characteristics of the entire antenna. This was done by a numerical integration technique applied to the radiation pattern of the 10 dB Gaussian taper distribution. It was established that the sidelobes rolled off at 30 dB/decade of angle. This coincidentally is the roll-off rate of a uniform circular aperture. Next, the error plateaus were computed from the assumed error magnitudes and the number of subarrays associated with three different subarray sizes. The aperture efficiency was also obtained by numerical integration. Next the subarray roll-off characteristics were obtained by numerically integrating the square aperture distribution for each of 19 different cuts over a 45° sector of \emptyset . These cuts were then averaged at each θ . The resultant subarray sidelobes also roll off at 30 dB/decade of angle. There is an additional error plateau associated with the randomly scattered power by each slot in the subarray. This second plateau will in theory roll off in accordance with the radiation pattern of the slot.

The lowest integral element in the MPTS is the klystron module, composed of a klystron, its feed and radiating waveguides, thermal control, solid state driver and RF control, power distribution, power return, and the support structure. The factors in selecting the klystron module sizes include: RF power density and thus the thermal environment, ease of quantizing the spacetenna aperture distribution, and awareness of klystron module interfaces. The high power density at the center of the beam is generated by 36 klystrons, each rated 70 KW, radiating RF from an area slightly larger than 108 m^2 (area of subarray). The 36 klystrons are organized into a 6 by 6 matrix. At the edge of the 10 dB tapered antenna a

subarray should have 3.60 klystrons. Since 3.60 is not an integer number, each edge subarray has 4.0 klystrons formed into a 2 by 2 matrix. Matrix configurations were similarly established for each power density step in the taper. Due to the klystron module system interfaces and the thermal limitations, the smallest possible size module is 1.5 by 1.5 meters.

The reference system calls for phase control at the klystron module level. Current thinking defines this level rather than phase control at the subarray level because of the belief that the modules cannot be assembled together accurately enough to retain a uniform phase front. The uniform phase front for the subarray could not be achieved due to the tilt of the modules and the distributed phase errors which occur within the subarray. Figure 4 shows the comparison between subarray and klystron module phase control level as a function of random tilt. The peak power density on the Earth is closely correlated to the beam efficiency and so Figure 4 shows that the klystron module phase control level is significantly better than subarray level control.

Simulations made to compare phase control level as a function of random phase error is shown in Figure 5. The results indicate a range of values for both systems, meaning that for 10° of random phase error both phase control systems have a random range of values statistically which are equal as would be expected.

Grating lobes are peaks in radiation occurring at angular directions off axis of the spacetenna where the signals from each of the subarrays add in-phase. The lobe amplitudes are a function of the mechanical alignment of the modules and the spacetenna pointing whereas the spatial position of the lobes is dependent upon the modules sizes. When there is no mechanical misalignment (no tilt of modules or spacetenna), the grating lobes appear to be split because the peaks of the "array factor" fall directly in the nulls of the subarray pattern. As tilt occurs, the peaks move out of the nulls, quickly increasing their amplitude because of the steep slope of the subarray pattern nulls. Figure 6 shows a comparison between grating lobe amplitudes for module and subarray phase control levels when two arc minutes of spacetenna tilt is simulated. Once again phase control at the module level shows a significant advantage over control at the subarray level.

4.0 SHAPED BEAM SYNTHESIS

In order to improve the overall collection efficiency by increased beam flatness out to the rectenna edge as well as provide an additional means of sidelobe control, beam synthesis with resultant phase reversals at some portions of the spacetenna was considered. These phase reversals are obtained by a fixed phase shifter at the klystron input and represent a first step towards a continuously variable phase distribution across the spacetenna, should this be more desirable. The results indicate that it is possible to synthesize a pattern that is considerably more flat-topped than the 10 dB Gaussian or other patterns that we have investigated. The price paid for this improvement is increased spacetenna size or a larger rectenna.

It is possible to increase the flatness of the beam without limit with arbitrarily large apertures and large numbers of beam components. Figure 7 compares the 10 dB Gaussian taper with the reverse phase taper and the continuous phase synthesis. The comparison shows the differences in the amplitude and phase illumination tapers across the spacetenna as well as the far-field patterns. Results show that reshaped beam pattern with "squared" main beams are possible but at the expense of larger transmit antennas or larger rectennas.

The idea of adding a suppressor ring to the spacetenna was investigated in the hope of significantly reducing the first sidelobe level. Figure 8 presents the results of this

study. The upper left diagram shows the layout of the spacetenna with its uniform distribution out to 0.72 times the normalized radius and the suppressor ring of width W . The diagram on the upper right shows the linear relationship between beam efficiency and the first sidelobe level as the ring width changes. $.98 R_0$ means that the width of the suppressor ring is bound by the edges $.98 R_0$ and R_0 . Looking at the lower right diagram shows the effect of changing the phase of the suppressor ring as well as the ring width. From this diagram it may be concluded that an in-phase ring is better than one which is out of phase. The lower left diagram shows the far-field pattern produced for the suppressor ring case where the inside edge of the suppressor ring is at $.94 R_0$. Although the first sidelobe is lower by about 5 dB than the case without a suppressor ring a significant loss in beam efficiency accompanies this achievement.

A dual suppressor ring case was looked into with a 10 dB taper rather than the uniform illumination and a larger spacetenna radius of 2 km. Figure 9 presents the illumination across the large array with the ring closest in out-of-phase by 180° and the second ring in-phase with the array. The far-field pattern for this case is shown in Figure 10 with a sidelobe level about the same as the referenced design but a main beam radius which is about 2.35 Km less.

A study was made to look at using defocusing and phase taper for beam shaping. Cases where the beam was focused at infinity showed much lower peak power density and much broader beams. These results indicate that reshaped beams with reduced peak levels are possible at the expense of larger spacetennas or rectennas.

Quadratic phase taper was utilized to look at shaped beam synthesis. In Figure 11, the far-field patterns for 4 cases with uniform amplitudes and different quadratic phase tapers are compared. As ϕ_{max} increases the on-axis power density decreases (see Figure 11) and the beam efficiency decreases significantly (see Figure 12). Figures 13 and 14 show the far-field patterns and efficiencies for quadratic phase taper with the Gaussian rather than the uniform amplitude taper. These results show that the reference Gaussian taper without quadratic phase error is the most efficient pattern. Figure 15 presents a table which shows how the quadratic phase taper may be utilized to design alternate SPS systems.

5.0 SPS SYSTEM SIMULATION

In this final section three types of SPS system simulations are described: a) Incoherent phasing, b) startup/shutdown operations, and c) multiple beams. Incoherent phasing was simulated to investigate the effect of complete phase control failure. The results show that the far-field pattern takes on a constant value in the rectenna and sidelobe region. The constant value is about $.003 \text{ mw/cm}^2$ over 5 dB below the Russian exposure level.

Computer simulations were utilized by JSC to investigate the performance of the MPTS during startup/shutdown operations. (See paper by G. D. Arndt and L. A. Berlin entitled "Microwave System Performance For A Solar Power Satellite During Startup/Shutdown Operations" on p. 1500 in Vol. II of the Proceedings of the 14th Intersociety Energy Conversion Engineering Conference.) Three sequences are recommended—random, incoherent phasing, and concentric rings-center to edge. The use of incoherent phasing is attractive in that it allows the antenna to be energized in any sequence. In conclusion the question of energizing the antenna has several practical solutions and should not present environmental problems.

The possibility of transmitting several power beams from an SPS has intrigued various researchers for some time. Recently, some computer runs were made to verify the capability of transmitting multiple beams using a modified version of the large array program TILMAIN. The scheme used to generate the beams was the simplest possible

one imaginable; namely, splitting the main beam along an axis by spatially modulating the illumination function by a factor $\cos(k r \sin \theta)$ when: $k = 2\pi/\lambda$, r = subarray displacement from center, θ = beam split angle. Results of a simply split 6.5 G.W. reference Gaussian are shown on Figure 16, and are as predicted except for the central lobe which did not diminish as the split angle was increased to 6×10^{-4} radians. The central peak may be due to an in-phase residual component in the spatial modulation or a grating lobe effect. Understanding and eliminating the central peak will be among our future efforts along with investigating various other multiple beam effects.

6.0 CONCLUSION

The computer simulations described have proven to be powerful versatile tools in the prediction of RF performance of the space solar power satellite. They are continually being refined and their use is being extended into the planning of initial experimental verification of the array performance.

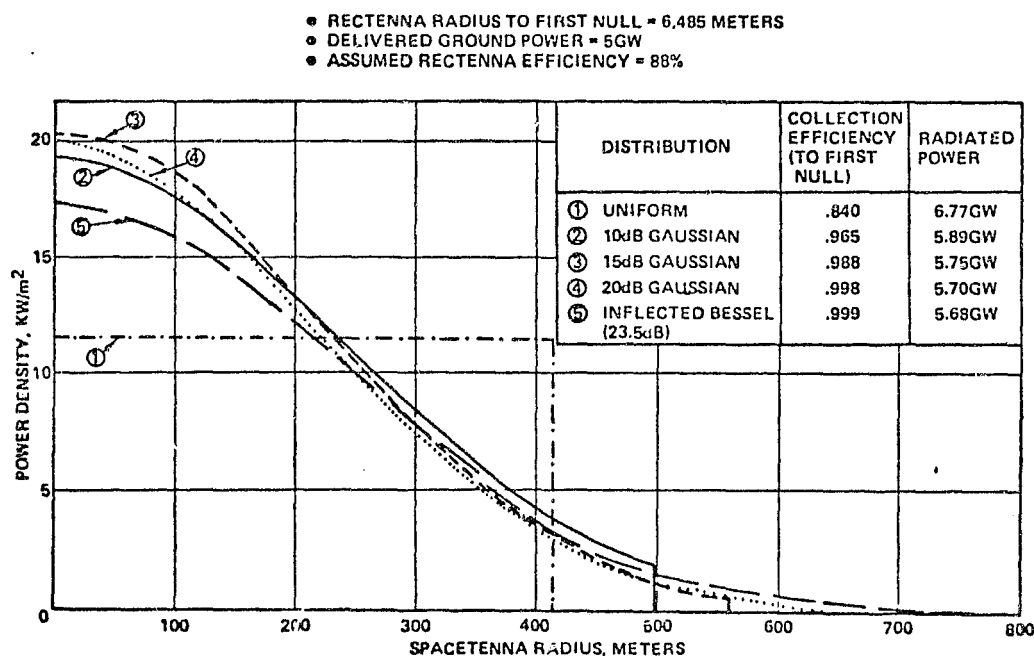


FIGURE 1

FIGURE 2

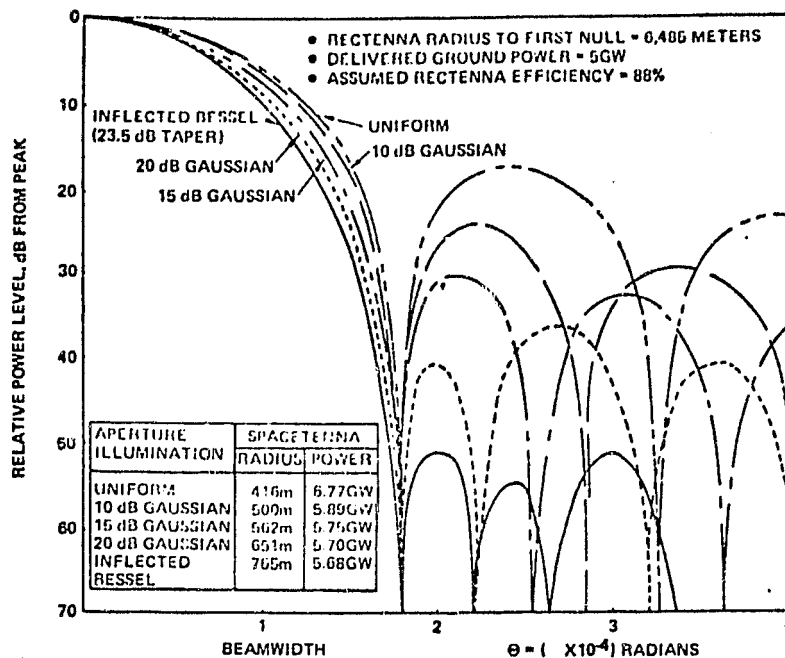


FIGURE 3

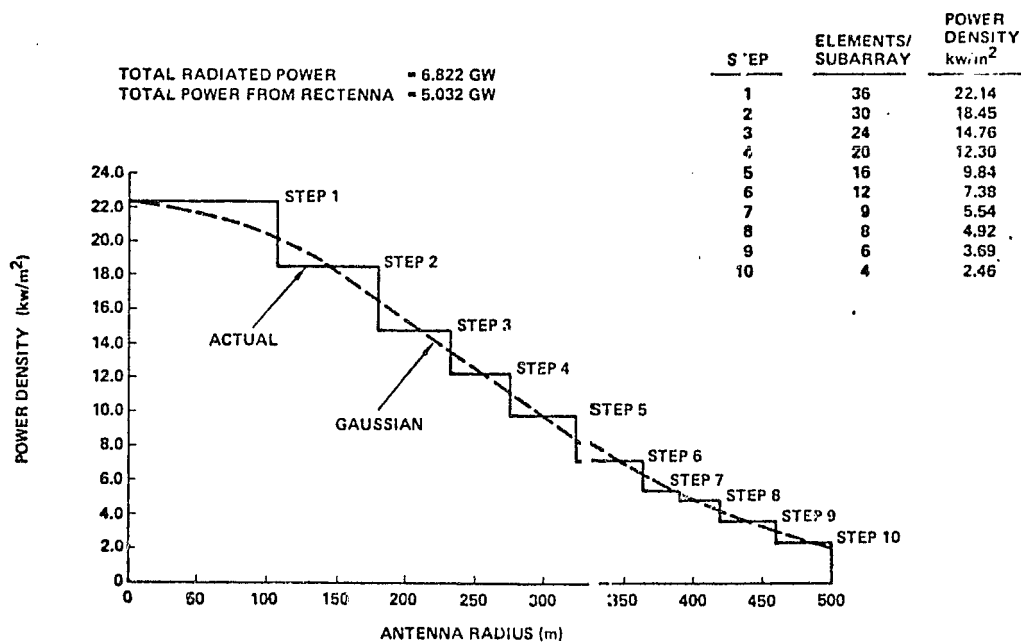
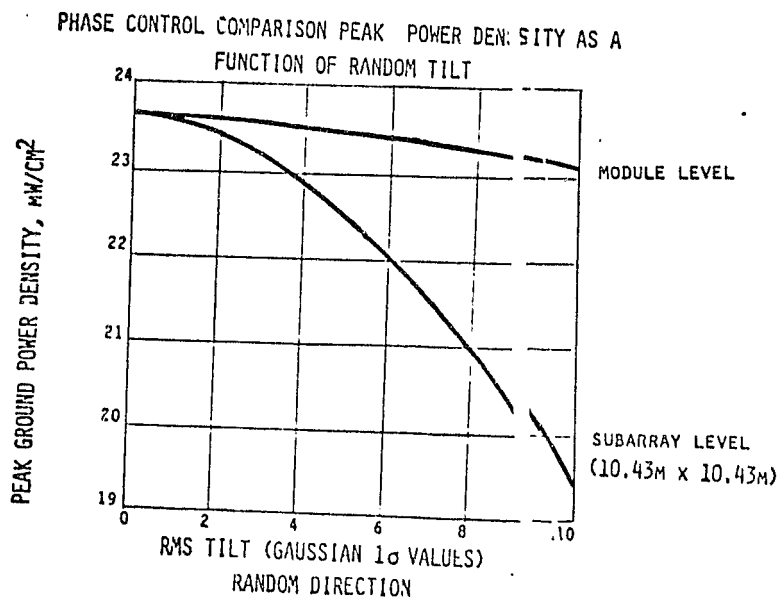


FIGURE 4



PHASE CONTROL LEVEL COMPUTER SIMULATION

FIGURE 5

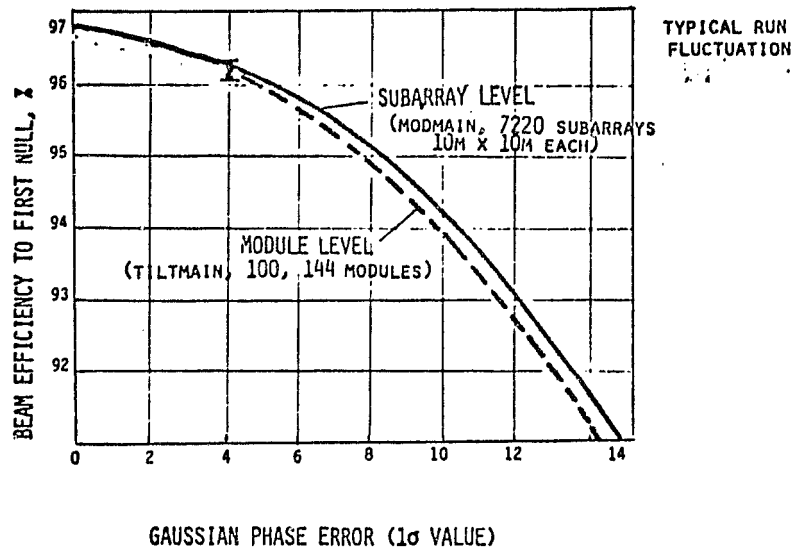


FIGURE 6

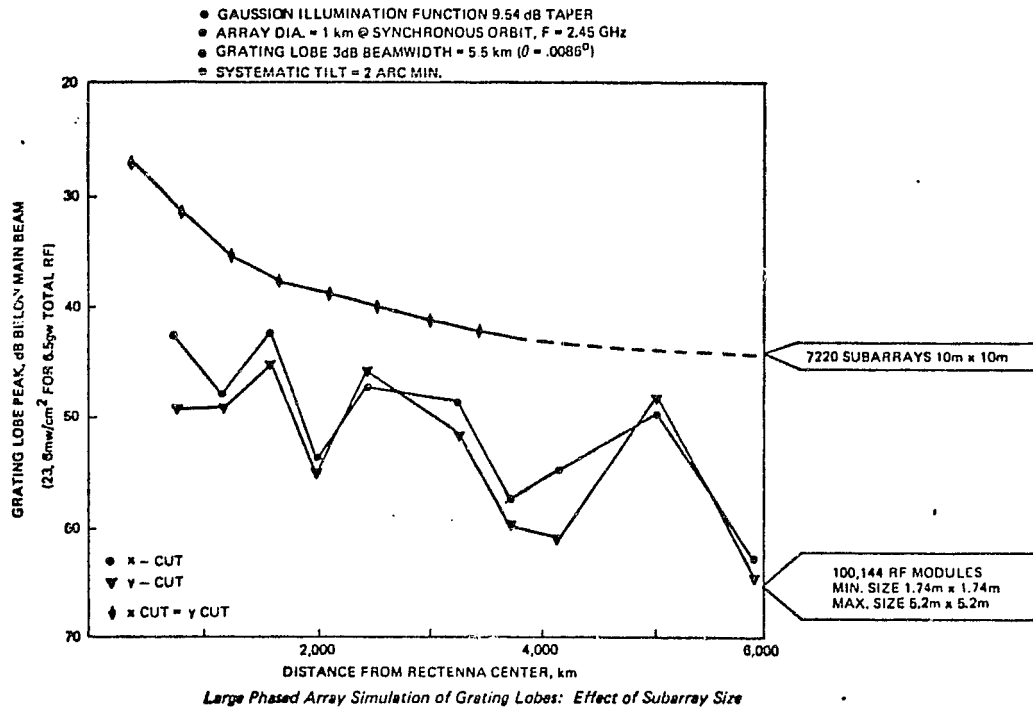
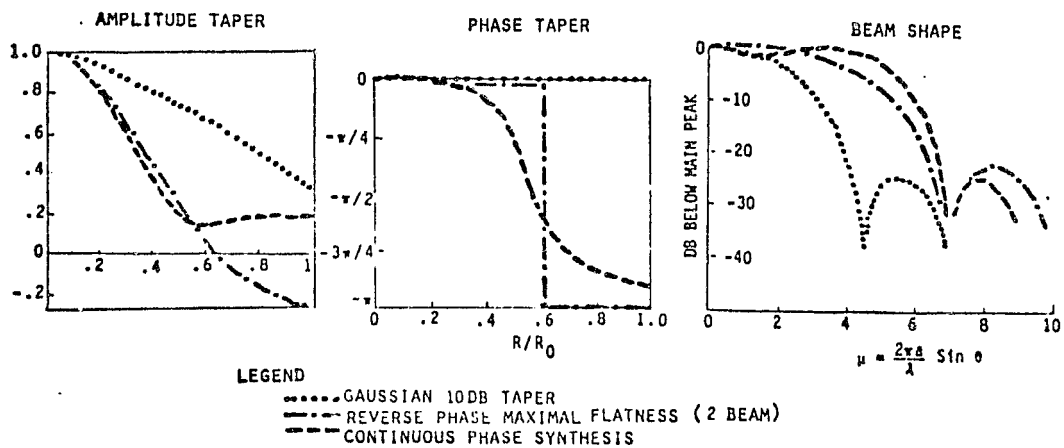
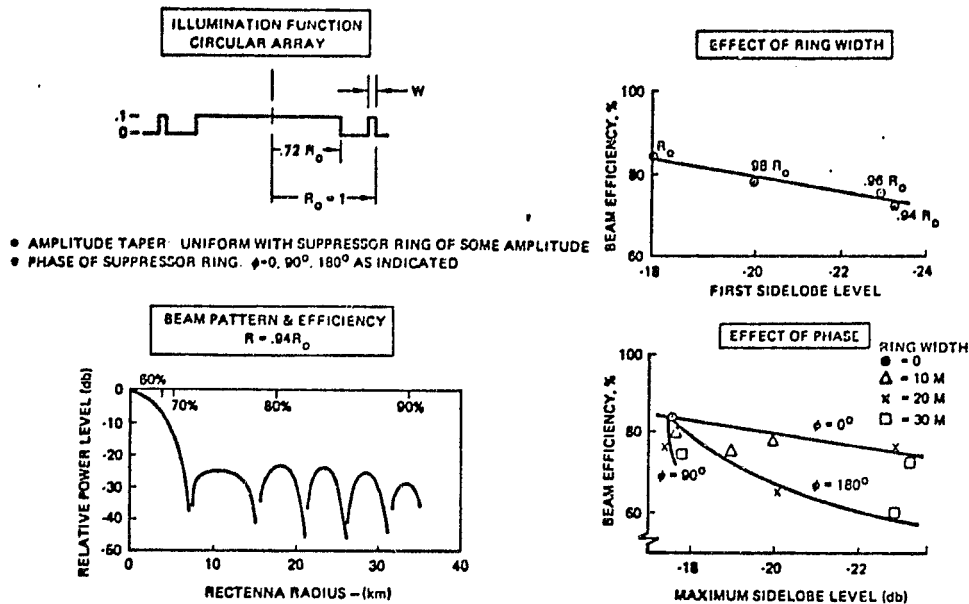


FIGURE 7



SPS Shaped Beam Synthesis

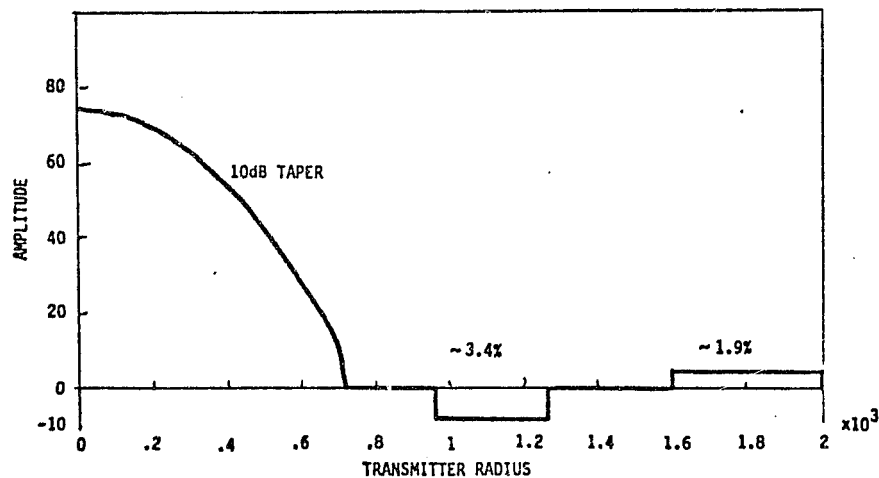
FIGURE 8



DUAL RING

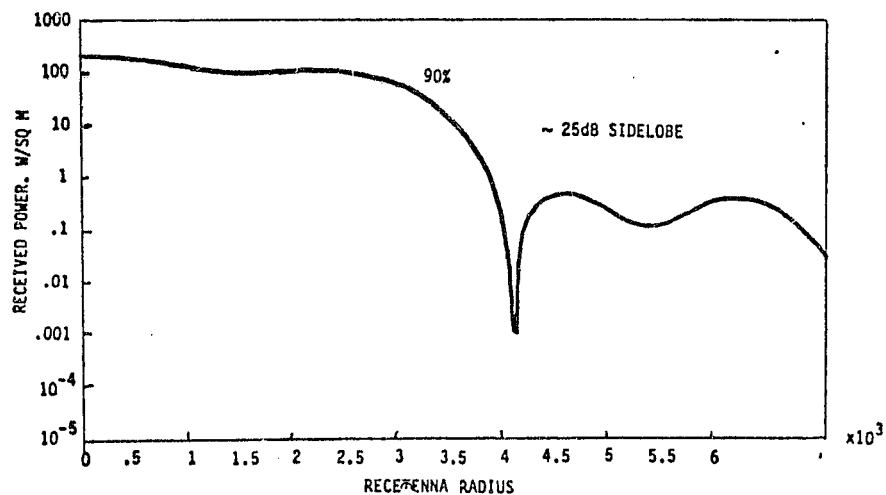
SPACETENNA ILLUMINATION FUNCTION

FIGURE 9



DUAL RING FAR-FIELD PATTERN

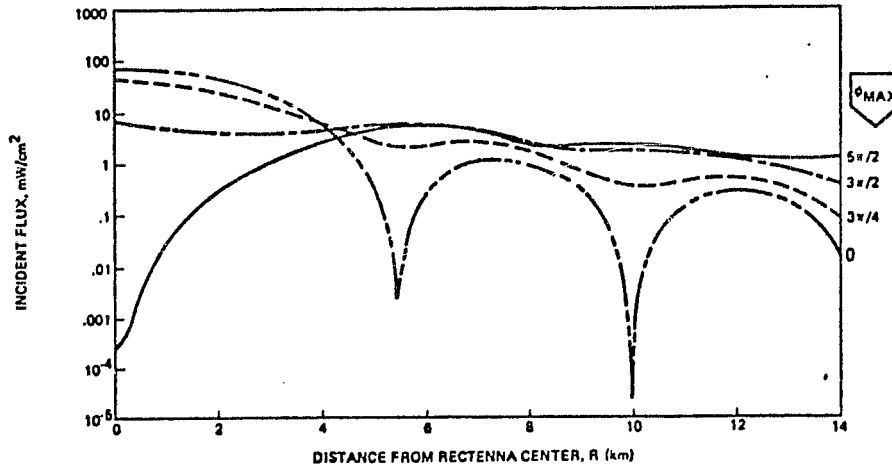
FIGURE 10



SPS Shaped Beam Synthesis

AMPLITUDE TAPER - UNIFORM
 PHASE TAPER - QUADRATIC $\phi = \phi_{MAX} (R/R_0)^2$
 SPACE ANTENNA 1 KM DIA., 2.45 GHz 22kW/m² 5GW

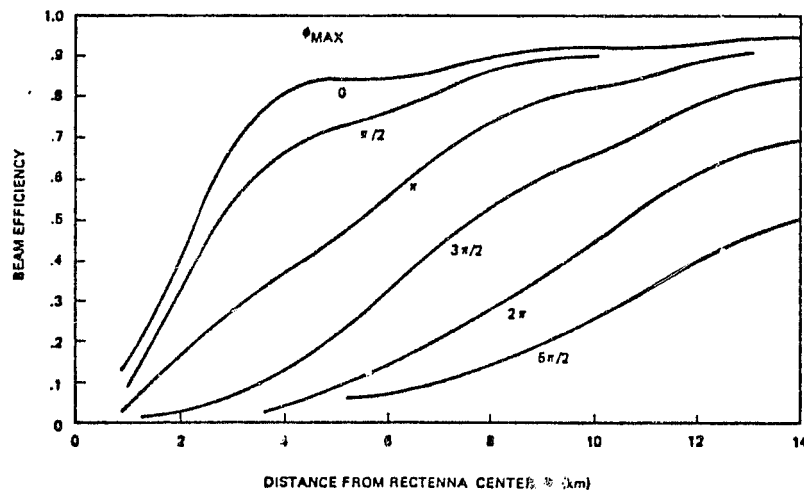
FIGURE 11



SPS Shaped Beam Synthesis

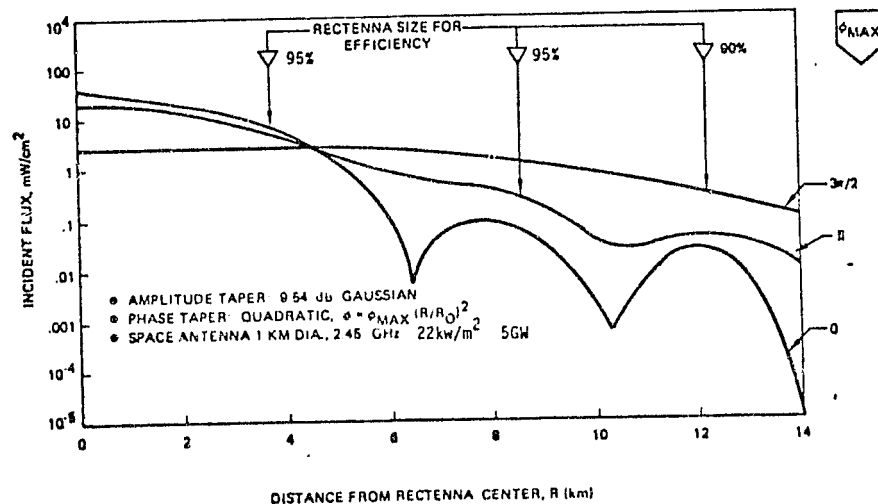
• AMPLITUDE TAPER: UNIFORM
 • PHASE TAPER: QUADRATIC, $\phi = \phi_{MAX} (R/R_0)^2$
 • SPACE ANTENNA 1 KM DIA., 2.45 GHz

FIGURE 12



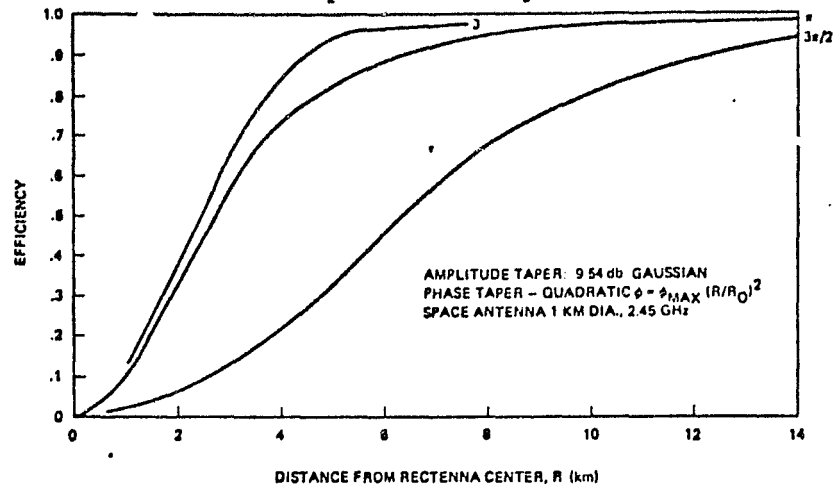
SPS Shaped Beam Synthesis

FIGURE 13



SPS Shaped Beam Synthesis

FIGURE 14

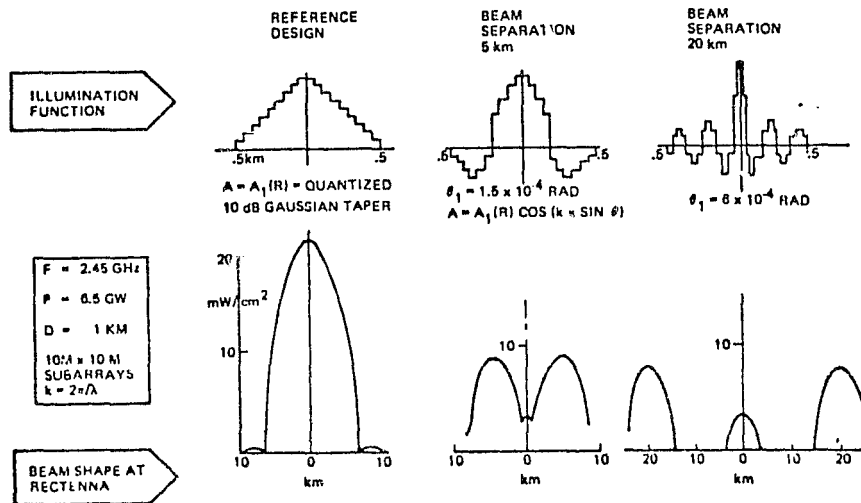


ALTERNATE SPS DESIGNS USING BEAM DEFOCUSING QUADRATIC PHASE TAPER $\phi = \phi_{MAX} (R/R_0)^2$

FIGURE 15

5GW 1KM 22KW/M ²					KLYSTRON BASELINE 5GW
ϕ_{MAX}	PEAK ON AXIS POWER mW/CM ²	RECTENNA DIAM, KM	POWER FLUCTUATION CR. TO EDGE	EFFICIENCY %	
0	23	10KM	23:1	97	
1.2π	5.8	22	35:1	95	
3π/2	2.1	28	48:1	92	
10GW 1.4KM 22KW/M ²					POTENTIAL 10GW KLYSTRON DESIGN
1.2π	23	15.7KM	35:1	95	
2GW 1.5KM 5KW/M ²					SOLID STATE SPS (BOEING)-2GW
1.2π	20 5.8	6.7 14.7	23:1 35:1	97 95	
4GW 2.1KM 5KW/M ²					POTENTIAL SPS 4GW DESIGN
1.2π	20	10.5	35:1	95	

FIGURE 16



Antenna Construction Techniques
R. Ried/JSC

unavailable at time of printing

AN ACTIVE ALIGNMENT SCHEME FOR THE MPTS ARRAY

By

Richard Iwasaki
Axiomatix
Los Angeles, California

In order to maximize the efficiency of the microwave power transmission system (MPTS), the surface of the array antenna must be extremely flat, which is difficult to achieve using passive techniques over the 1 km dimensions of the array. In order to achieve and maintain this required flatness, a rotating laser beam used for leveling applications on earth has been utilized as a reference system. A photoconductive sensor with a reflective collecting surface is used to determine the displacement and polarity of any misalignment and automatically engage a stepping motor to drive a variable-length mechanism to make the necessary corrections. Once aligned, little power is dissipated since a nulling bridge circuit that centers on the beam is used, an important alignment feature since even laser beams broaden considerably at 1 km distances. A three-point subarray alignment arrangement is described which independently adjusts, in the three orthogonal directions, the height and tilt of subarrays within the MPTS array and readily adapts to any physical distortions of the secondary structure (such as that resulting from severe temperature extremes caused by an eclipse of the sun). Finally, it is shown that only one rotating laser system is required since optical blockage is minimal on the array surface and that it is possible to incorporate a number of redundant laser systems for reliability without affecting the overall performance.

PRECEDING PAGE BLANK NOT FILMED

1.0 ROTATING LASER BEAM REFERENCE SYSTEM

A commercially available rotating laser system, the Laser Level, appears to satisfy many of the requirements for achieving flatness over a very large area. A key element for achieving flatness is the use of a pentaprism for attaining exact perpendicularity about the rotating axis. A unique feature of the pentaprism is the automatic compensation of any tilting resulting from errors such as misaligned bearing surfaces.

The Helium-Neon laser source must use a collimator to minimize the inherent beam broadening, a limiting factor for defining alignments at long distances. It is estimated that the beam diameter expands from 1 mm at the laser to 3 inches at 500 m, and the sensor system must be able to accommodate this wide range of beam diameters.

2.0 OPTICAL SENSORS

A photoconductive sensor configuration has been devised to attain alignment with the center of a laser beam, for any laser beam diameter. The basis for this design is the use of a nulling-bridge detector circuit that utilizes symmetry about the separation (about 0.1 mm) of two colinear photoconductive strips which total five inches in length. The conductivity of the photoconductor increases with laser beam illumination so that equal illumination results in identical resistance and therefore a null in the resistive bridge. This null condition, when properly biased, dissipates very little power.

If the two colinear strips are asymmetrically illuminated as a result of the beam center being offset, however, the nulling condition is lost and a voltage imbalance occurs. The magnitude and polarity of this voltage imbalance can be used to drive an electric motor to realign the sensors as part of a negative feedback loop until null is again realized.

The 0.1 mm separation permits operation close to the rotating laser system, whereas the 5 inch overall length easily accommodates the 3 inch diameter laser beam at extremities of the array. Tapering of the tips of the photoconductive strips near the gap will compensate for relative signal strength changes by providing a variable resistance along the strip. Further improvements in the laser light collection

efficiency can be obtained by using optical matching by protective thin film coatings and by shaping the glass supporting structure into a paraboloidal or semi-circular shape and metallizing it to form a reflective surface.

Redundancy can be readily implemented by having multiple adjacent photoconductive strips, each driving separate variable length motors. Using a pin-and-socket arrangement, these multiple photoconductive sensors can be as easily replaced as vacuum tubes.

The locations of the three photoconductive sensors required to align each subarray are just above the attachment points, which are referred to as the three point support.

3.0 THREE POINT SUBARRAY MOUNT

In order to reduce the number of adjustments required to align the subarrays, a three point mount with a single support has been studied. The entire subarray is attached to any secondary structure configuration by only a single sturdy support. This single support can readily adapt to any tilting arising from physical distortions of the secondary structure by simply adjusting the height of the subarray.

The initial alignment procedure, during fabrication, can use the rotating laser beam reference plane to adjust the position of the single support mount. Installation consists of sliding this mount into a keyed slot built into the secondary structure and centering the beam on the photoconductive sensor located at the center of the subarray where the single support is attached. The two orthogonal tilting directions are controlled by two variable length struts which form a triangular truss with the support and subarray. Each tilting direction is independent of the other so that iterative adjustment procedures are avoided. During fabrication, an astronaut would visibly align the photoconductive sensors above the struts within the laser beam reference plane, and subsequent adjustments would be implemented by the active alignment instrumentation.

4.0 OPTICAL SENSOR POSITIONING

The use of a rotating laser beam reference system requires that a clear field of view to all sensors is desirable such that only one laser system is necessary to align all the subarrays. Since there are supporting structures located beneath the subarrays, obviously the flat radiating surface of the array is a better choice.

If the rotating laser system is in the center of the array and the optical sensors are 0.125 inches wide, then the closest sensors 7.1 m away would subtend an angle of 0.05° . Sensors located at farther distances would subtend even smaller angles. For example, the second set 11.2 m away subtends 0.03° . Using the square symmetry of the array, it is possible to illuminate all of the sensors by offsetting the laser at least 0.125 inches from the exact center. Larger width photoconductive sensors can be used and would correspondingly subtend larger angles, but the offset concept is still valid. Adjustable position sockets for the photoconductive sensors can provide some flexibility in the event of inadvertent blockage.

If redundant rotating laser systems are used, a common baseplate is recommended to ensure that both reference planes are coincident. Multiple laser systems (with pentaprisms assumed to be 2 cm wide) placed 1 m apart in line with the service corridors discussed in section 6.0 will not obscure the required field of view of each other.

Electromagnetic interference arising from the microwave power radiated from the array is reduced by the normal orientation of the photoconductive sensor to the array and its 5 inch length, which, on the basis of a dipole on a ground plane, has minimal coupling effects. Also, the metallizing of the sensor, with the possible addition of wire grids on the exposed optical face, should not permit interference. The effective cavity formed by the metallized sensor is also non-resonant to the radiated microwave frequency. Therefore the placement of the sensors on the array face is not unreasonable.

5.0 VARIABLE LENGTH MECHANISMS

In developing the concepts for an active alignment system, two of the dominating criteria were to use simple designs and attempt to

incorporate redundancy provisions suitable for operation in space, especially in view of the reluctance of using electric motors for long duration missions.

The variable length mechanism, which is basically a worm gear drive driven by a stepping motor, is the only electromechanical device used for this active alignment scheme. The redundant variable length mechanisms are short segments serially located along the strut, each independently driven by a separate photoconductive sensor nulling bridge circuit. If for some reason one motor or the bearings of one variable length mechanism fails, then the other redundant systems intrinsically maintain the variable length capability. And if multiple failures occur, replacement of the entire strut consists of removing and installing only two pins in a U-clamp arrangement.

The center support attachment is unique in that it uses a universal ball joint about which the subarray can readily pivot in any direction. The side orthogonal support struts, designated arbitrarily as azimuth (Az) and elevation (El), pivot about the axis formed by the central universal ball joint and the opposite side strut attachment point. Since three points in space define a plane and if these three photoconductive sensors align themselves to the laser beam reference plane, then the subarray is considered aligned. And on a macroscopic scale, if all subarrays are aligned, the array itself is aligned.

Since worm gear drives move by the rotation and translation along a pitched thread, the actual physical movement can be made quite small by means of gearing ratios and stepping motors. Further, by geometrical considerations of the triangular struts, the actual amount of tilting for a given amount of variable length change is quite small. Therefore an extremely high degree of resolution is achievable in adjusting the orientation of the subarray and therefore the array itself. Once this premise is accepted, then it is easy to imagine that the design engineers can extend the concept so that the desired practical resolution is feasible, by the proper choice of pitched threads and the specifications for the stepping motor.

6.0 MAINTENANCE SERVICE CORRIDORS

One aspect of the three-point support is the existence of a square matrix of service corridors or passageways directly under the subarrays for rapid accessibility for necessary repairs. A service vehicle traversing these corridors will be at most only half a subarray dimension away from any position in the array. In addition, since there are only three supports per subarray, the supporting under-structure is not cluttered.

The matrix of corridors also presents the possibility of incorporating a shadow-masking alignment monitoring scheme using 170 laser beams on two adjacent sides passing through strategically placed apertures under the subarrays and incident on detecting sensors on the opposite side. Misalignment is indicated by the loss of signals in both intersecting laser beams, thereby immediately locating the source of the problem.

7.0 MONOPULSE POINTING SYSTEM

A related topic of discussion to the alignment scheme is the accurate pointing of the MPTS array towards the effective location of a pilot beam, which may vary due to refractive variations of the ionosphere. One method which might be considered is a monopulse tracking system that senses the phase differentials of an encoded pilot beam and points the array in the proper direction. Although this scheme will not permit rapid compensation, if the ionospheric fluctuations are slow, the pointing accuracy will be adequate such that instantaneous fine pointing adjustment by an auxiliary retrodirective pilot beam phase reference system is possible.

Four receiving antennas, mounted within a microwave baffle to reduce coupling effects to the radiated microwave power, located at the extremities of the array, will allow active tracking of the pilot beam source located at the rectenna.

IONOSPHERIC POWER BEAM STUDIES

LEWIS M. DUNCAN
LOS ALAMOS SCIENTIFIC LABORATORY

WILLIAM E. GORDON
RICE UNIVERSITY

23 MW/cm²

A POWER DENSITY LEVEL OF 23 MW/cm² HAS ACHIEVED THE STATUS OF A FIRM DESIGN SPECIFICATION BASED ON THEORETICAL CALCULATIONS OF A THRESHOLD FOR MICROWAVE-IONOSPHERE NONLINEAR INTERACTION (THERMAL RUNAWAY).

THERMAL RUNAWAY IS NO LONGER A VALID THEORETICAL CONCEPT ALTHOUGH FOR COMPARABLE POWER DENSITIES ENHANCED ELECTRON HEATING IS OBSERVED TO CHANGE THE ELECTRON TEMPERATURE BY A FACTOR OF TWO OR THREE, BUT NOT BY AN ORDER OF MAGNITUDE.

THERE IS, SO FAR, NO EXPERIMENTAL EVIDENCE TO SUPPORT 23 MW/cm² AS AN UPPER LIMIT.

THE QUESTION TO BE POSED AND ANSWERED IS AT WHAT POWER DENSITIES IS THE IONOSPHERE MODIFIED IN A WAY THAT PRODUCES UNACCEPTABLE COMMUNICATION EFFECTS AND/OR ENVIRONMENTAL IMPACTS?

ARECIBO TEST RESULTS

CASE 1 HEATING WAVE PENETRATED THE IONOSPHERE

FREQUENCY	OHMIC HEATING AS A FRACTION OF 5 GW SPS HEATING	DIAMETER OF HEATED VOLUME RELATIVE TO SPS HEATED VOLUME	CROSS SECTION FOR FIELD-ALIGNED SCATTER IS LESS THAN
6-10 MHz	1%	3.00	$4 \times 10^{-3} \text{ M}^2$
430 MHz	40%	0.10	$4 \times 10^{-3} \text{ M}^2$
2380 MHz	5%	0.01	10^{-3} M^2

ARECIBO TEST RESULTS

CASE 2 HEATING WAVE REFLECTED BY THE IONOSPHERE (NOT THE SPS CONDITION)

PLASMA INSTABILITIES ARE EXCITED BY THE HF HEATER WAVE LEADING TO FIELD-ALIGNED STRIATIONS THAT SCATTER RADIO WAVES.

FIELD-ALIGNED RADIO-SCATTERING CROSS-SECTIONS UP TO 10^3 m^2 .

SINCE THE EXCITATION OF THESE INSTABILITIES REQUIRES A MATCHING OF THE HEATER FREQUENCY TO THE IONOSPHERIC PLASMA FREQUENCY, A CONDITION THAT IS NOT MET BY THE SPS, THEY WILL NOT BE EXCITED. NO OTHER INSTABILITIES ARE PRESENTLY KNOWN THAT THE SPS FREQUENCY WILL EXCITE.

THE SIMULTANEOUS ILLUMINATION OF THE IONOSPHERE BY THE SPS FREQUENCY AND A SECOND FREQUENCY SEPARATED BY ABOUT 15 MHz OR LESS COULD PRODUCE THE INSTABILITIES DESCRIBED ABOVE.

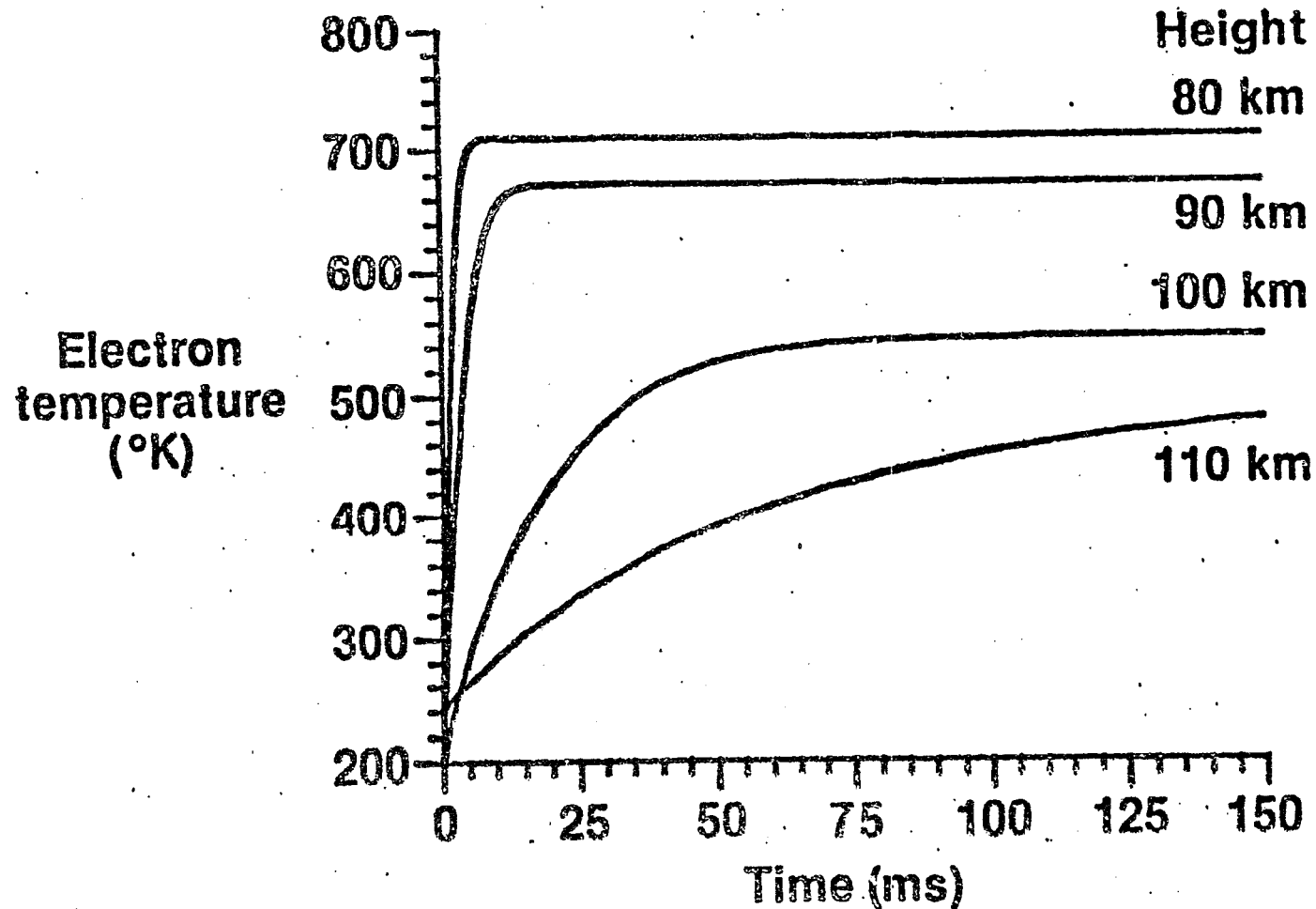
26

4

ENHANCED ELECTRON HEATING BY THE SPS BEAM

- (1) WILL INCREASE ELECTRON TEMPERATURES BY UP TO A FACTOR OF THREE OR MORE, MOSTLY IN THE LOWER IONOSPHERE.

Power flux = 23 mW/cm²
Frequency = 2450 MHz
Standard midlatitude atmosphere



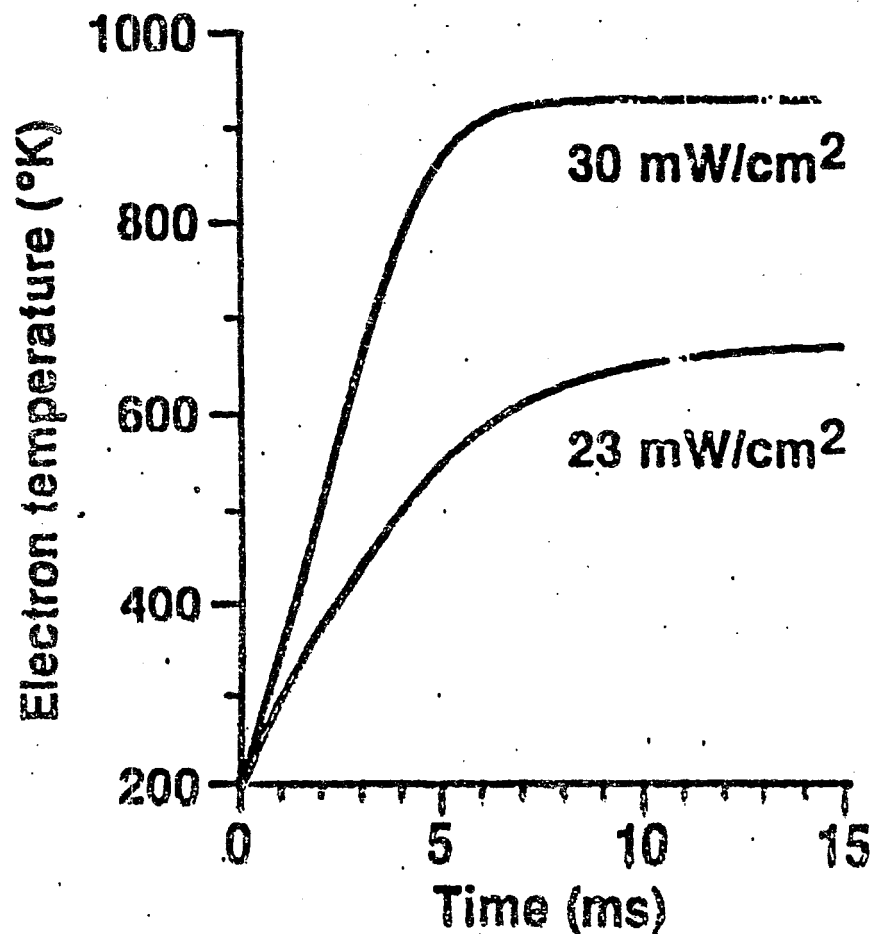
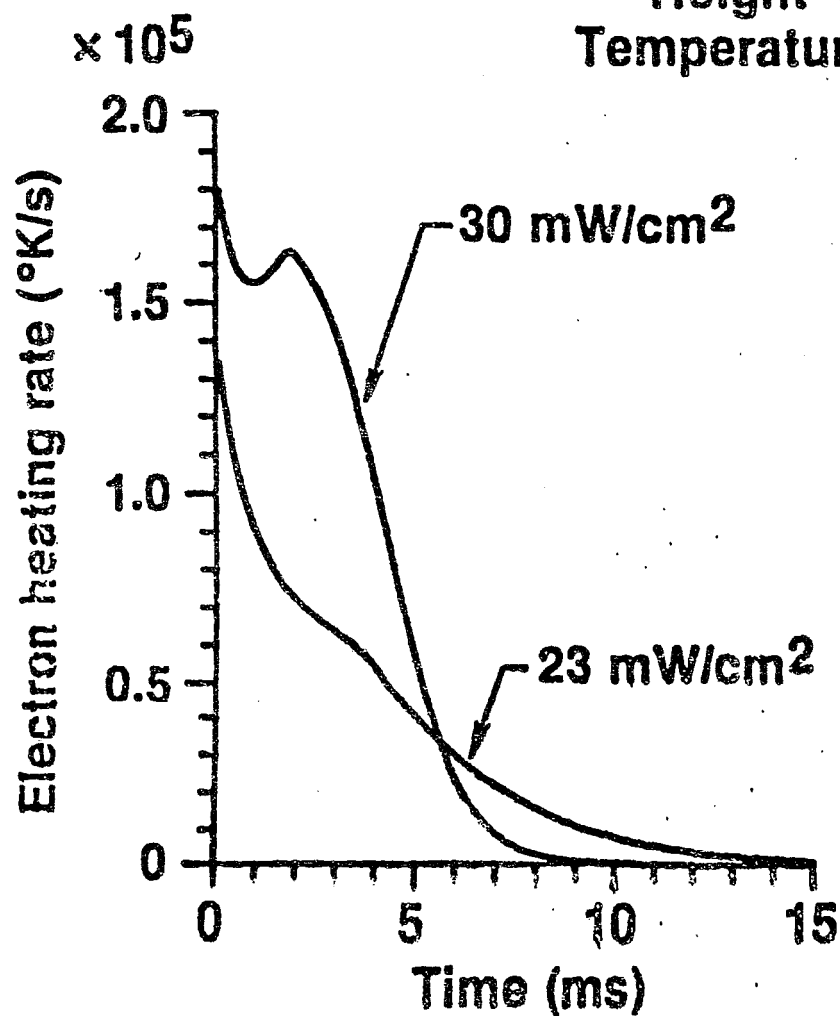
ENHANCED ELECTRON HEATING BY THE SPS BEAM

(2) IS PREDICTED TO BE DEPENDENT ON THE INCIDENT POWER DENSITY.

Frequency = 2450 MHz

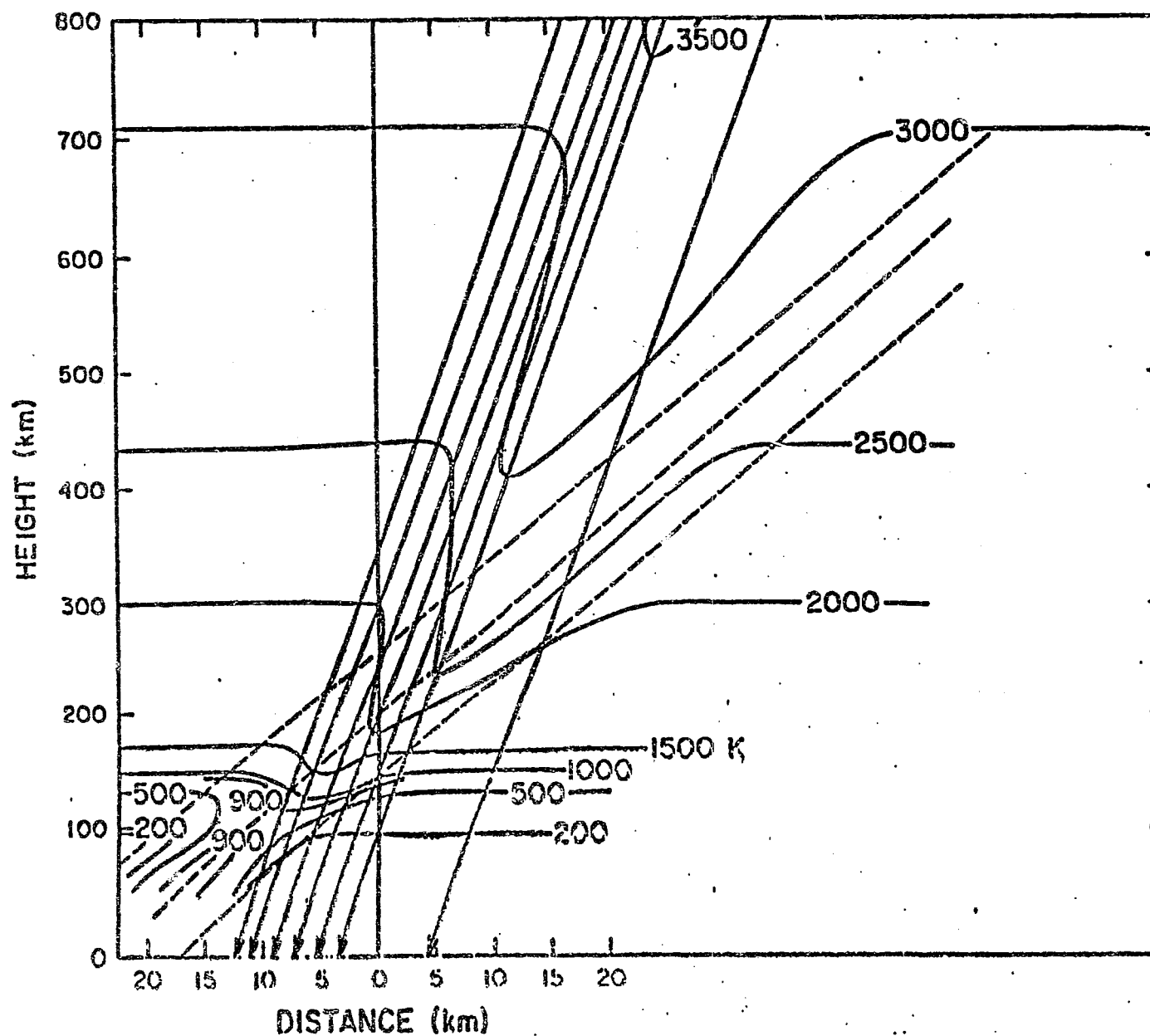
Height = 90 km

Temperature = 187°K.



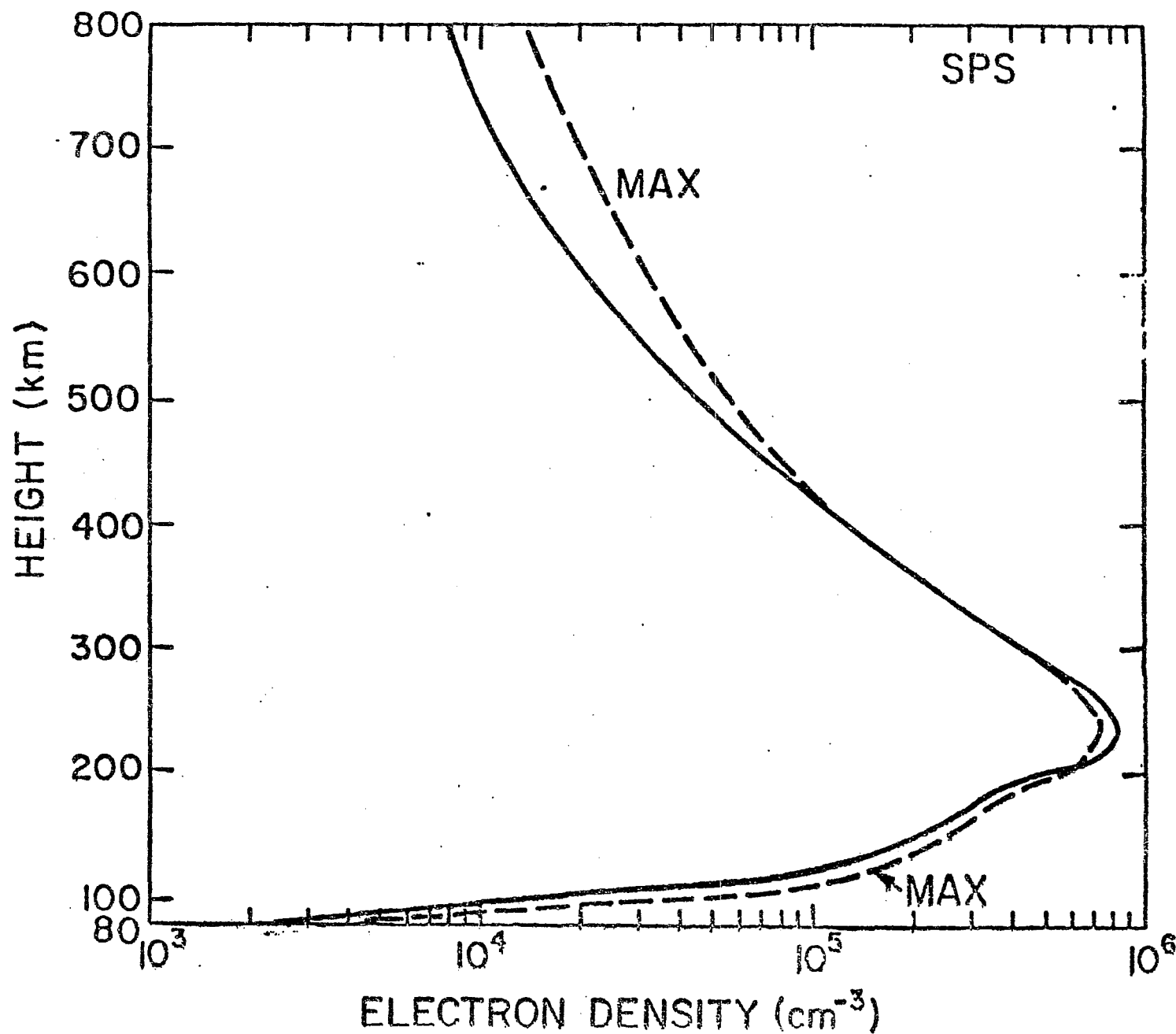
ENHANCED ELECTRON HEATING BY THE SPS BEAM

- (3) WILL INCREASE ELECTRON TEMPERATURES IN AND NEAR THE BEAM BY SMALL FACTORS.



ENHANCED ELECTRON HEATING BY THE SPS BEAM

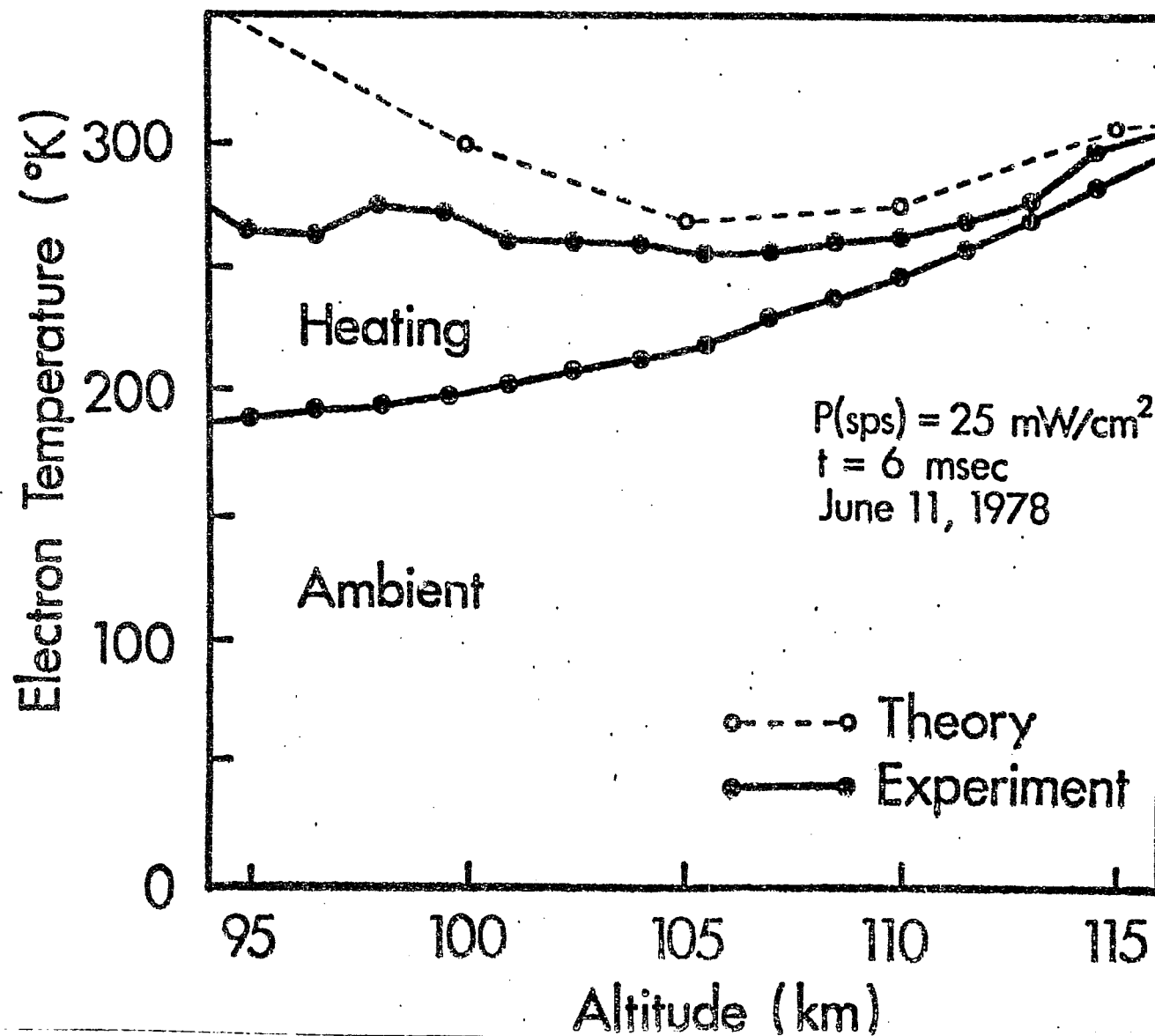
(4) WILL CHANGE THE ELECTRON DENSITY IN THE BEAM BY SMALL AMOUNTS.



04

8

OBSERVATIONS OF ENHANCED ELECTRON HEATING AT ARECIBO ARE CLOSE TO, BUT BELOW,
THE PREDICTED INCREMENTS.

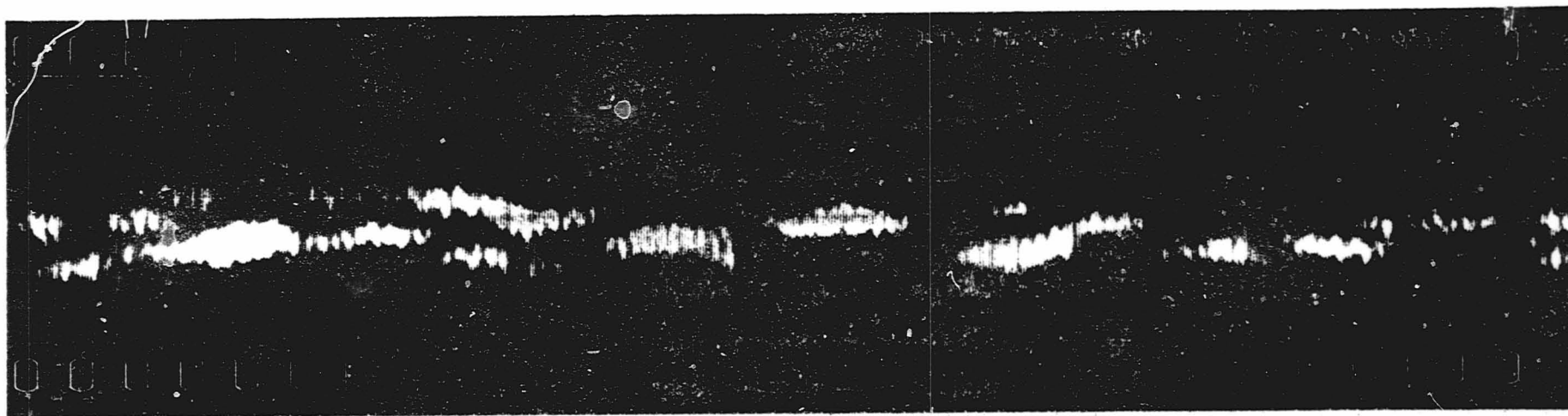


COMPARISON OF 5800 MHz AND 2450 MHz

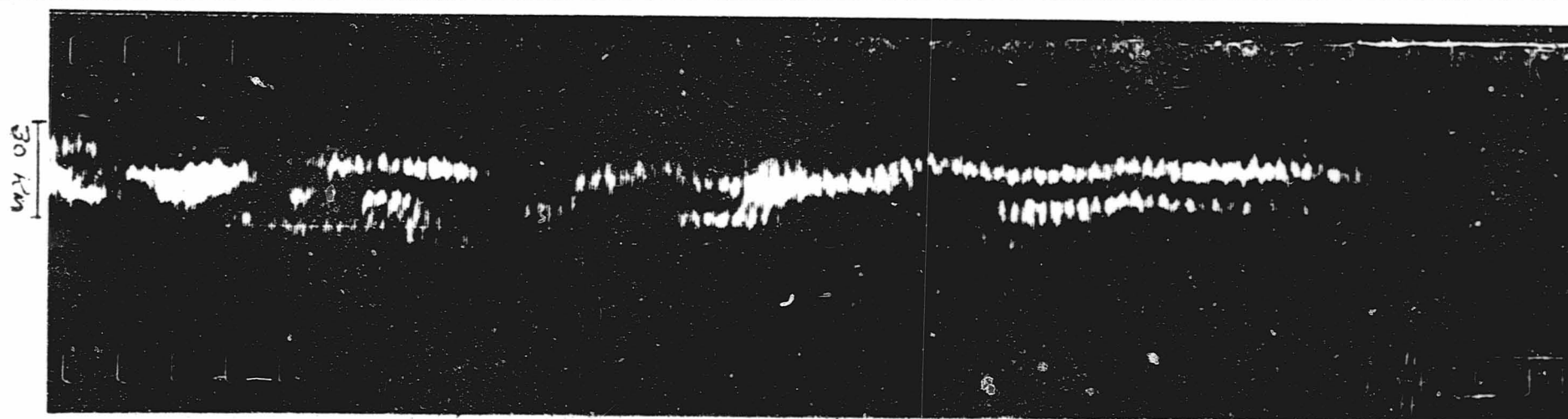
<u>MEDIUM</u>		<u>2450 MHz</u>	<u>5800 MHz</u>
IONOSPHERE		1 KW	0.25 KW
NEUTRAL ATMOSPHERE AT 60° ELEVATION ANGLE		90 MW	100 MW
RAIN (25MM/HR OVER 20 KM PATH IN BEAM)		45 MW	1.450 GW
HAIL (1.93 cm DIAMETER HAILSTONES, 10 KM PATH THROUGH THE BEAM)	DRY	0.2 GW	1.7 GW
	WET	2.7 GW	4.99 GW

RADAR ECHOES FROM FIELD-ALIGNED STRIATIONS

ORIGINAL PAGE IS
OF POOR QUALITY



RADAR ECHOES FROM FIELD-ALIGNED STRIATIONS

OF 1000 000000
1000000 000000
1000000 000000

PROPOSED EXPERIMENTAL STUDIES FOR ASSESSING IONOSPHERIC PERTURBATIONS ON SPS UPLINK PILOT BEAM SIGNAL

Santimay Basu and Sunanda Basu
Emmanuel College
Boston, MA 02115

Introduction

The microwave beam of the proposed Solar Power Satellite (SPS) at geosynchronous altitude is to be formed and directed by phase information derived from a pilot signal at 2.45 GHz transmitted from ground and received in a number of module locations on the SPS antenna. The frequency of the pilot signal has been chosen to be sufficiently low as to avoid the effects of strong scattering by turbulence in the neutral atmosphere and yet high enough to avoid any possible refractive effects caused by the ionized upper atmosphere. However, the ionosphere is known to contain irregular variation of concentration due to natural processes and the downlink microwave beam has also been predicted to interact with the ionosphere to cause artificial irregularities (Perkins and Valeo, 1974; Perkins and Roble, 1978; Duncan and Behnke, 1978). Thus the uplink pilot signal has to propagate through the ionosphere containing natural and possibly some artificial irregularities. In view of the fact that microwave signals from communication satellites suffer considerable perturbations both in intensity and phase in the equatorial and auroral zones there has been some concern that the uplink pilot signal may suffer perturbations with possible consequences to the formation of the downlink high power microwave beam. While there may exist some satisfaction regarding the SPS site location at midlatitudes avoiding the intense belt of equatorial and auroral irregularities, there is evidence for the occurrence of ionospheric irregularities at midlatitudes causing considerable perturbations of signal intensity at VHF and even at GHz. Though these effects due to natural irregularities are usually smaller at midlatitudes as compared to the equatorial zone, the effective perturbations at midlatitudes may become magnified if a geostationary satellite acquires finite orbital inclination. The generation of artificial irregularities by ionospheric heating in the underdense mode and the effects thereof on transionospheric microwave propagation remain totally

unexplored from the experimental standpoint. In the following sections we shall provide some evidence of the occurrence of natural irregularities at midlatitudes based on scintillation measurements by the use of VHF and GHz transmissions from geostationary satellites and satellite in-situ measurements. We shall then provide an outline of our proposed measurements related to the detection, lifetime and drift of artificial irregularities generated by ionospheric heating in the underdense mode.

Formulation of the Problem

Figure 1 illustrates that in the presence of fluctuations of ionospheric electron concentration confined within a layer of thickness L_e , an incident plane wave undergoes phase fluctuations as it emerges from the layer. For small phase fluctuations, the emerging wavefront contains only phase perturbations without any fluctuations in intensity. As the wavefront propagates towards the observer's plane, phase mixing occurs and thereby spatial intensity fluctuations also develop. In the presence of a relative motion between the propagation path and the irregularities, the spatial variations of intensity and phase sweep past the observer's receiving system giving rise to temporal variations in phase and intensity called phase and intensity scintillations. In the practical situation, such as for the SPS case, or radio wave scintillation measurements, the ionospheric irregularities between the transmitter and the receiver are located in the far zone of the transmitter so that the radiation can be well approximated by a spherical wave. On the other hand, the beam nature of the wave has to be considered when the irregularities are located in the near zone of the transmitter as frequently encountered in optical propagation (Ishimaru, 1978). In the case of spherical wave propagation between a transmitter and receiver separated by a distance L and the scatterers at a variable distance η from the transmitter the correlation functions of intensity (I) and phase (ϕ) over the receiving plane in the weak-scatter regime are given by:

$$\begin{aligned}
 B_I(L, \rho) &= \langle I(L, \rho_1) I(L, \rho_2) \rangle \\
 &= (2\pi)^2 \int_0^L d\eta \int_0^\infty \kappa d\kappa J_0(\kappa\eta\rho/L) |H_r|^2 \phi_n(\kappa)
 \end{aligned} \tag{1}$$

$$\begin{aligned}
B\phi(L, \rho) &= \langle \phi(L, \rho_1) \phi(L, \rho_2) \rangle \\
&= (2\pi)^2 \int_0^L d\eta \int_0^\infty \kappa d\kappa J_0(\kappa \eta \rho / L) |H_i|^2 \Phi_n(\kappa)
\end{aligned} \quad (2)$$

where

ρ - dimension transverse to propagation path
 κ - irregularity wave number
 $\Phi_n(\kappa)$ - irregularity wave number spectrum
 k^n - wave number of the propagating wave

$$|H_r|^2 = k^2 \sin^2 |\eta(L-\eta)\kappa^2/2kL|$$

$$|H_i|^2 = k^2 \cos^2 |\eta(L-\eta)\kappa^2/2kL|$$

The variance of intensity and phase may be obtained by putting $\rho = 0$ in equations (1) and (2). These equations may be used to obtain the respective variances from a knowledge of the irregularity spectrum. In solving the equations for the ionospheric case, it must be considered that the irregularities in the inertial subrange cause the diffraction effects as distinct from the case of geometrical optics. Measurement of variances and temporal spectra allow a determination of the strength of turbulence which may then be used to derive the structure functions of phase and intensity. In principle, direct measurements of phase and intensity correlations are possible using the spaced receiver technique with variable baselines.

Strong Ionospheric Irregularities at Midlatitudes

At Ramey Air Force base near Arecibo, Puerto Rico, nighttime scintillation events accompanied by long period (30 mins to 1 hour) variations of total electron content have been routinely observed (Kersley et al., 1979; Basu et al., 1979). The top panel in Figure 2 shows the temporal (local time = UT-4.5 hours) variations of total electron content measured with a radio polarimeter by the use of 137 MHz transmissions from geostationary satellite, SMS-1. The bottom panel shows that the fluctuations in total electron content were accompanied by intensity scintillations in excess of 15 dB.

Satellite in-situ observations have also revealed existence of such large and small scale structure near Arecibo. The

solid line in Figure 3 shows the spatial variation of ion concentration, N (or electron concentration for charge neutrality at F region heights) recorded by the ion drift meter on board the Atmosphere Explorer E satellite. The AE-E data has been kindly made available to us by W.B. Hanson. The ion concentration is sampled 16 times per sec. The irregularity amplitude $\Delta N/N$ computed from 3-sec intervals of N data are indicated by the circles. The satellite altitude, longitude, magnetic local time and latitude are indicated in the diagram. Long period spatial variations of electron concentration, as well as, steep horizontal gradients at a latitude close to that of Arecibo may be noted. Such steep gradients are accompanied by small scale irregularities with amplitudes exceeding 10%. Such levels of irregularity amplitude ($\Delta N/N$) and ambient density (N) provides ΔN values which can explain observed scintillation events near Arecibo shown in Figure 2 if we assume a layer thickness of about 100 km (Basu and Basu, 1976).

In Figure 4 we show a case of similar perturbations of total electron content accompanied by 1 dB fluctuation of intensity at 1.7 GHz (Fujita et al., 1978). Such levels of GHz scintillation activity with a maximum of 2.3 dB are often observed near the June solstice at Kashima, Japan with ETS-II satellite, for which the propagation path is nearly aligned with the earth's magnetic field. It may be of interest to note that the magnetic dip location of Kashima is nearly identical to that of Arecibo although the geographic latitude is higher than Arecibo. An equivalent enhancement of scintillation activity may be encountered at U.S. sites such as, Boulder or Arecibo, if the geostationary satellite acquires finite orbital inclination. Such large amplitude natural irregularities may cause phase perturbations at the SPS frequency. Their effects on both the pilot and power beams should be carefully assessed.

Proposed Measurement of Phase and Intensity Scintillation Effects During Ionospheric Heating

We have made plans to perform several experiments in conjunction with RF ionospheric heating both in the overdense and underdense modes at Arecibo and at Platteville. In December, 1979, we had planned to make use of the Arecibo heating facility and perform ground and airborne measurements of the effects of ionospheric heating. Figure 5 shows the observing geometry, the shaded region indicating the heated volume at 5 MHz. From Roosevelt Roads, Puerto Rico, we planned to receive the 249 MHz transmissions from LFS-9 and obtain the variance and temporal spectra

of phase and intensity scintillations at that frequency. In view of the finite orbital inclination of LES-9 satellite, the locus of the intersection of the propagation path with 300 km ionospheric height lies within the heated volume between 06-10 UT. In addition, the AFGL Airborne Ionospheric Observatory agreed to provide supporting measurements of phase and intensity scintillations using LES-9 and Fleetsatcom satellites (Figure 5) 6300 Å airglow and ionosonde measurements. The Fleetsatcom satellite was chosen to probe the ionosphere outside the heated volume and detect the presence of naturally occurring irregularities. The aircraft was also expected to scan the heated region to define the extent of the perturbed volume. Simultaneous diagnostic incoherent scatter measurements from Arecibo Observatory were requested for determining the electron concentration and temperature.

Unfortunately, the Arecibo Heating Facility could not be made operational in December, 1979 so that the above experiments had to be postponed. However, we have drawn up a back-up plan for similar experiments using the LES-8 satellite in conjunction with the heating facility at Platteville during Feb-March, 1980 (Rush et al., 1979). In addition to some of the experiments outlined above, we have planned to include spaced receiver scintillation measurements to obtain ionospheric drift. We also propose to set up an observing station such that a field aligned propagation path can be viewed through the heated volume. These measurements will provide an estimate of the phase and intensity structure functions. Experimental support for the above program will be provided by Dr. J. Aarons of AFGL. At a later date, we shall utilise the phase coherent spread spectrum signals from NAVSTAR-GPS satellites at 1575 MHz and 1227 MHz to make accurate phase scintillation measurements in the GHz range. These results are expected to provide a direct input to the design of the SPS system. However, it is essential that the heating facilities at Arecibo and Platteville be upgraded as proposed by Gordon and Duncan (1978) and Rush et al., (1979) to meet the SPS power density levels at F-region altitudes before accurate experimental results can be provided for predicting SPS ionospheric and telecommunication systems impact.

This work was partially supported by National Science Foundation Grant No. ATM 78-25264 and Air Force Geophysics Laboratory Contract F19628-78-C-0005.

References

- Basu, S. and S. Basu, Geophys. Res. Lett., 3, 681, 1976.
- Basu, S., S. Basu, S. Ganguly and J.A. Klobuchar, Simultaneous Incoherent Scatter and Scintillation/Total Electron Content Observations in the Mid-latitude Ionosphere, presented at National Radio Science Meeting, URSI, Boulder, Colorado, November, 1979.
- Duncan, L.M. and R.A. Behnke, Phys. Rev. Lett., 41, 998, 1978.
- Fujita, M., T. Ogawa and K. Koike, J. Atmos. Terr. Phys., 40, 963, 1978.
- Gordon, W.E. and L.M. Duncan, NASA Report No. NAS9-15212, July, 1978.
- Ishimaru, A., Wave Propagation and Scattering in Random Media, Academic Press, New York, 1978.
- Kersley, L., J. Aarons and J.A. Klobuchar, J. Geophys. Res., 1979 (in press).
- Perkins, F.W. and E.J. Valeo, Phys. Rev. Lett., 32, 1234, 1974.
- Perkins, F.W. and R.G. Roble, J. Geophys. Res., 83, 1611, 1978.
- Rush, C.M., J.C. Carroll and E.J. Violette, Report No. NTIA-TM-79-27, U.S. Dept. of Commerce, October, 1979.

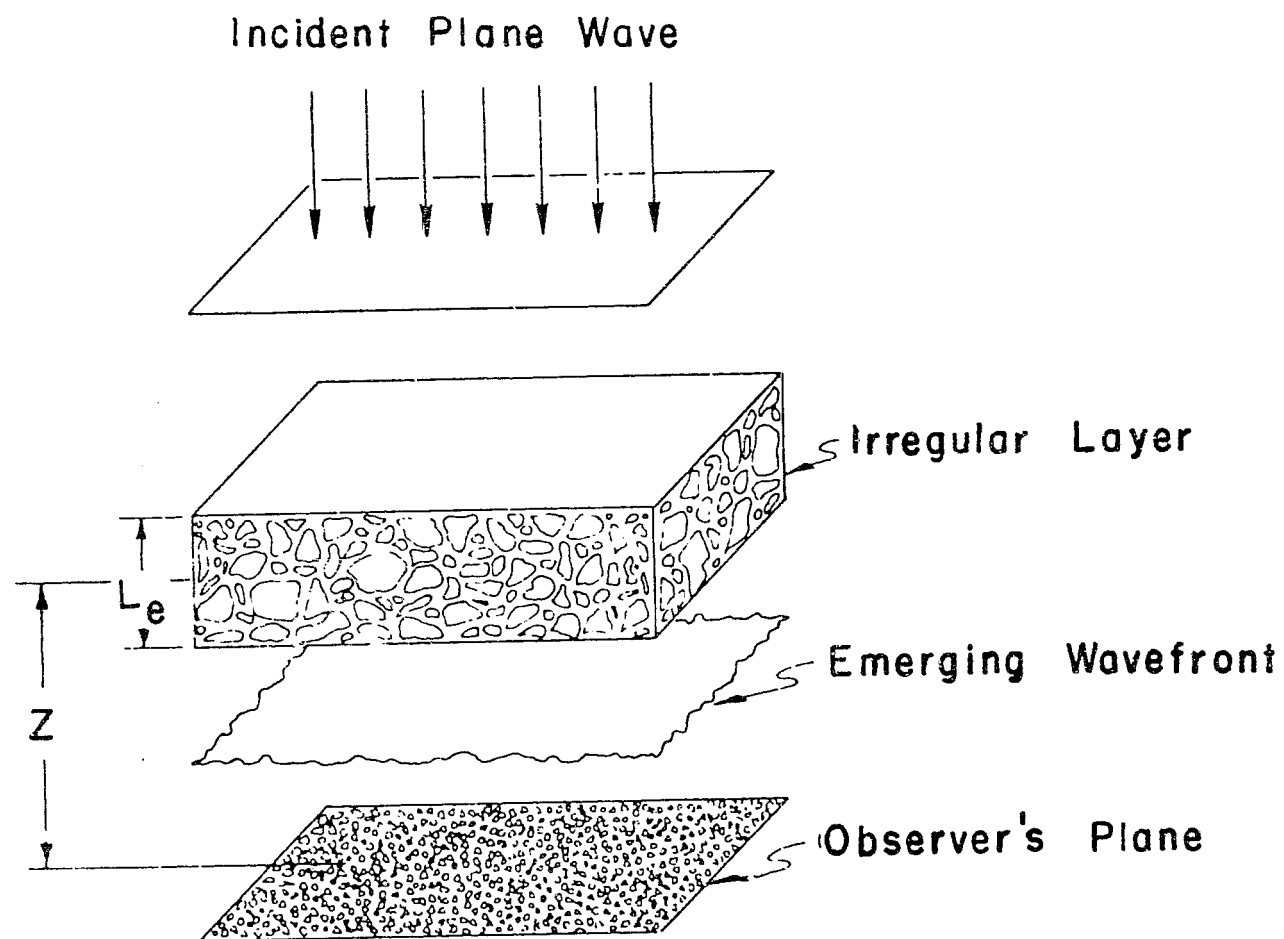


Figure 1. Geometry of the scintillation problem

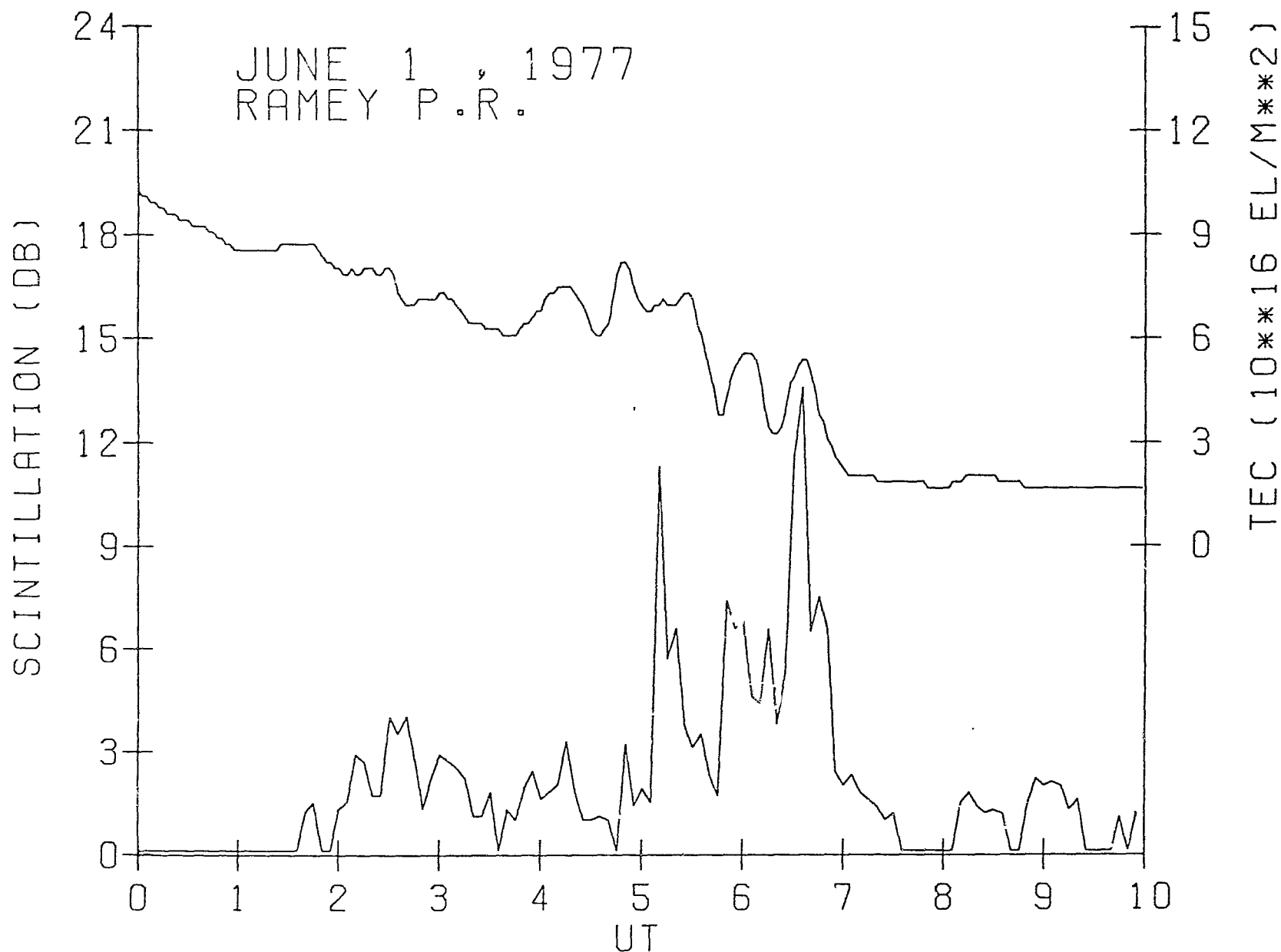


Fig. 2. Total electron content (top panel) and scintillation (lower panel) measurements obtained at Ramey Air Force Base, P.R., using SMS-1 at 137 MHz on June 1, 1977 showing large amplitude scintillations correlated with content fluctuations. This diagram was made available by J.A. Klobuchar of AFGL.

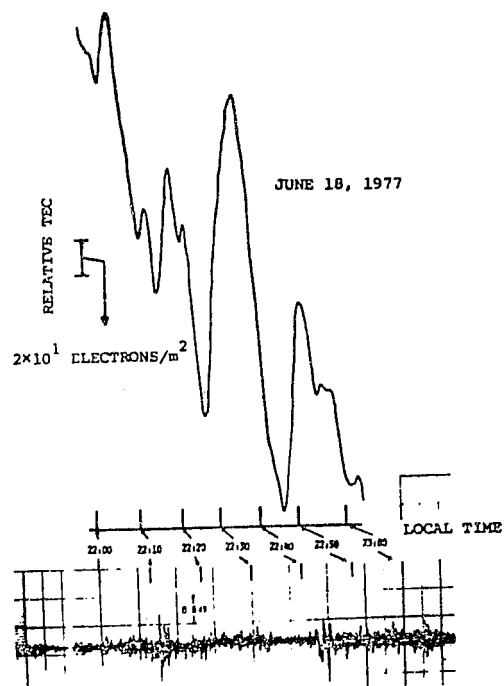


Figure 4. Example of nighttime scintillation (lower) and irregular variation of TEC (upper) observed at Kashima on June 18, 1977.

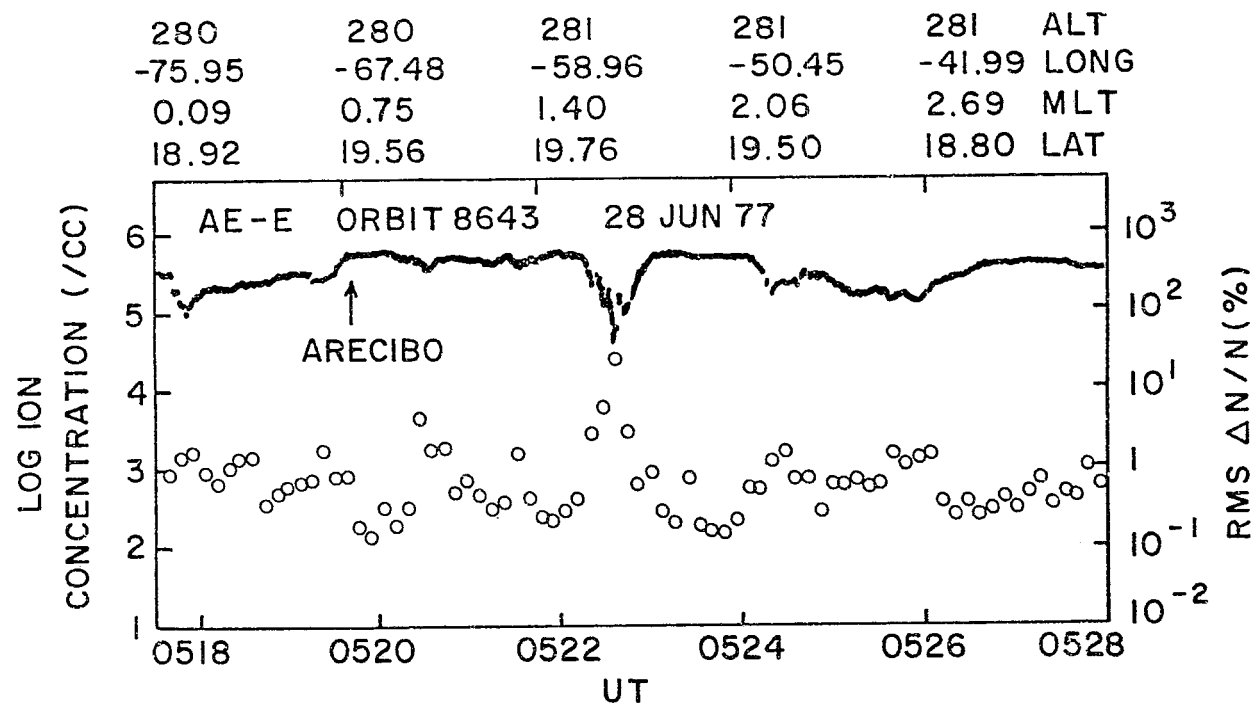


Figure 3. Atmospheric Explorer E orbit near Arecibo showing large amplitude irregularities.

SATELLITE POSITIONS FOR DEC. 20, 1979
300km INTERSECTIONS FROM ROOSEVELT ROADS, P. R.

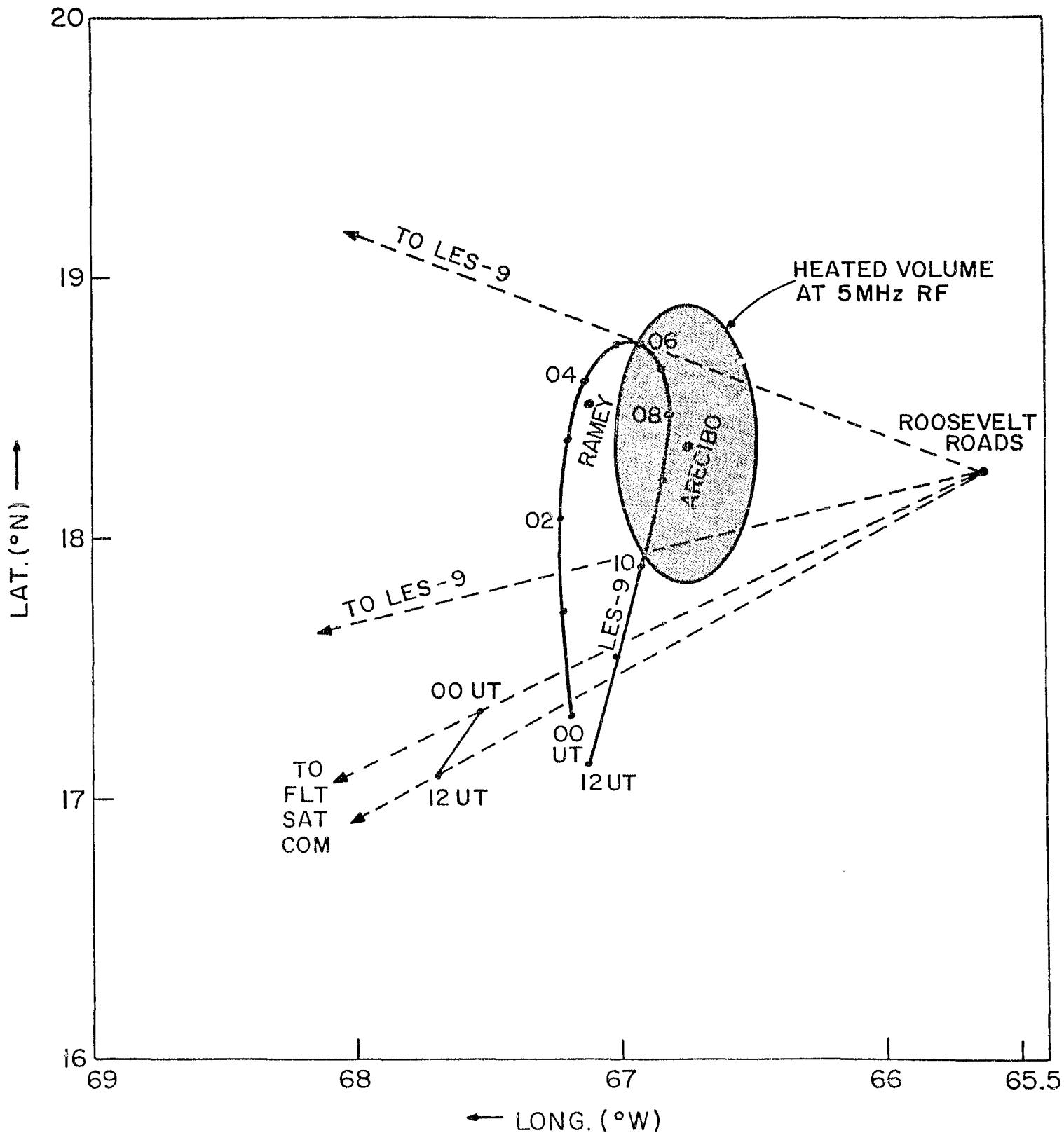


Figure 5. Observing geometry of LES-9 and Fleetsatcom satellites during proposed ionospheric heating from Arecibo.

*Ionospheric Perturbations on Uplink Pilot Beam Signal
(Theoretical) and Plattville Heating Test Results
E. Morrison/ITS*

unavailable at time of printing

PHASE CONTROL SESSION

Active Retrodirective Arrays
Ralph Chernoff/JPL

unavailable at time of printing

PRECEDING PAGE BLANK NOT FILMED

PERFORMANCE ANALYSIS AND SIMULATION OF
THE SPS REFERENCE PHASE CONTROL SYSTEM*

W. C. Lindsey and C. M. Chie
LinCom Corporation
P.O. Box 2793D
Pasadena, CA 91105

ABSTRACT

This short paper provides a summary overview of the SPS reference phase control system as defined in a three phase study effort (see Refs. 1-5). It serves to summarize key results pertinent to the SPS reference phase control system design. These results are a consequence of extensive system engineering tradeoffs provided via mathematical modeling, optimization, analysis and the development/utilization of a computer simulation tool called SOLARSIM.

1.0 INTRODUCTION

The SPS reference phase control system investigated under contract to the Johnson Space Center is reviewed in Section 2. The next section is devoted to the analysis and selection of the pilot signal and power transponder. The SOLARSIM program development and the simulated SPS phase control performance are treated in Section 4.

2.0 THE SPS CONCEPT AND THE REFERENCE PHASE CONTROL SYSTEM

Figure 2.1 illustrates the major elements required in the operation of an SPS system which employs retrodirectivity as a means of automatically pointing the beam to the appropriate spot on the Earth. From Figure 2.1 we see that these include: (1) the transmitting antenna, hereafter called the spacetenna, (2) the receiving antenna, hereafter called the rectenna, and (3) the pilot signal transmitter. The rectenna and pilot signal transmitter are located on the Earth. The purpose of the spacetenna is to direct the high-power beam so that it comes into focus at the rectenna. The pilot signal, transmitted from the center of the rectenna to the spacetenna, provides the signal needed at the SPS to focus and steer the power beam.

As seen from Fig. 2.1 the SPS phase control system is faced with several key problems. They include: (1) path delay variations due to imperfect SPS circular orbits, (2) ionospheric effects, (3) initial beam forming, (4) beam pointing, (5) beam safing, (6) high power amplifier phase noise effects, (7) interference (unintentional and intentional), etc.

2.1 SPS-Transmitting System Concept

From the system engineering viewpoint, the SPS transmitting system which incorporates retrodirectivity is depicted in Fig. 2.2. As seen

*This work was performed at LinCom Corporation for NASA Johnson Space Center Houston, TX, under contract NAS 9-15782.

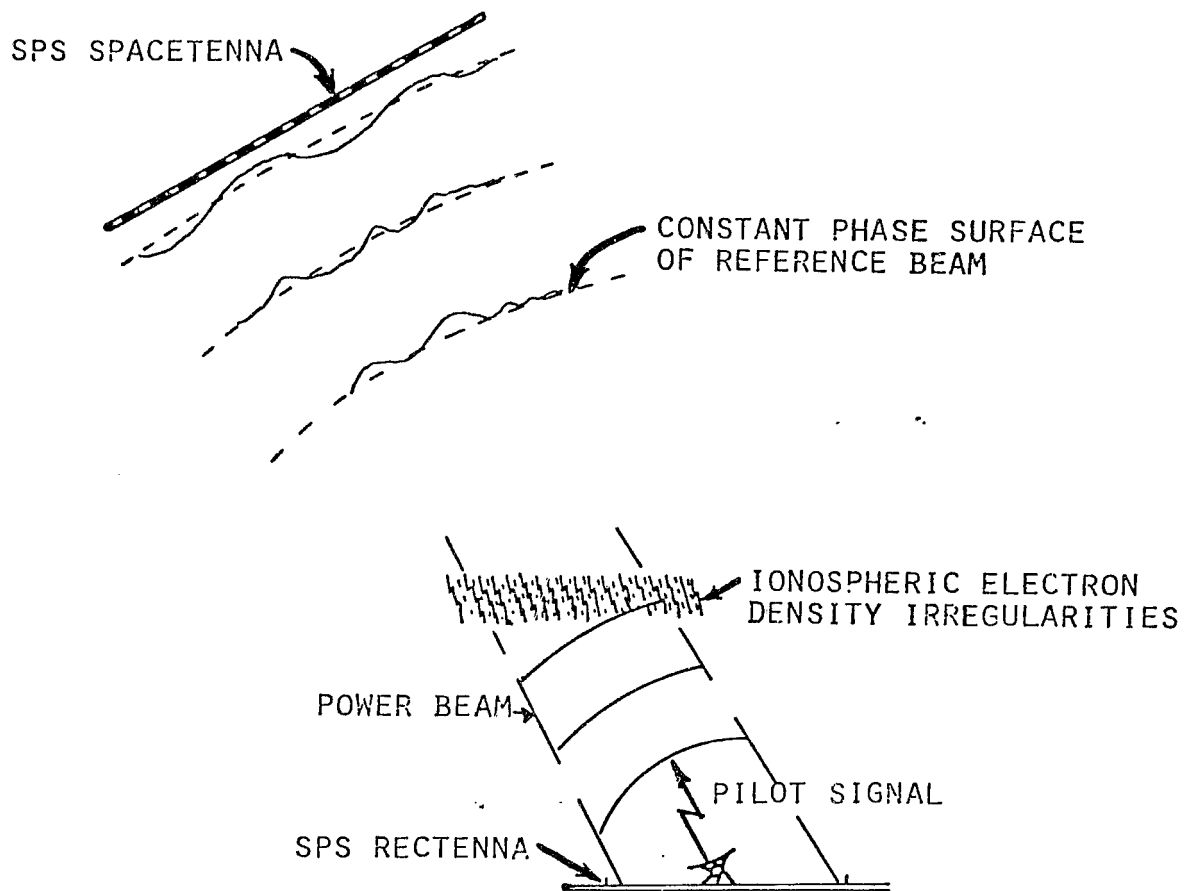


Figure 2.1. Space Based Solar Power Satellite and Earth Based Energy Collection System Concept.

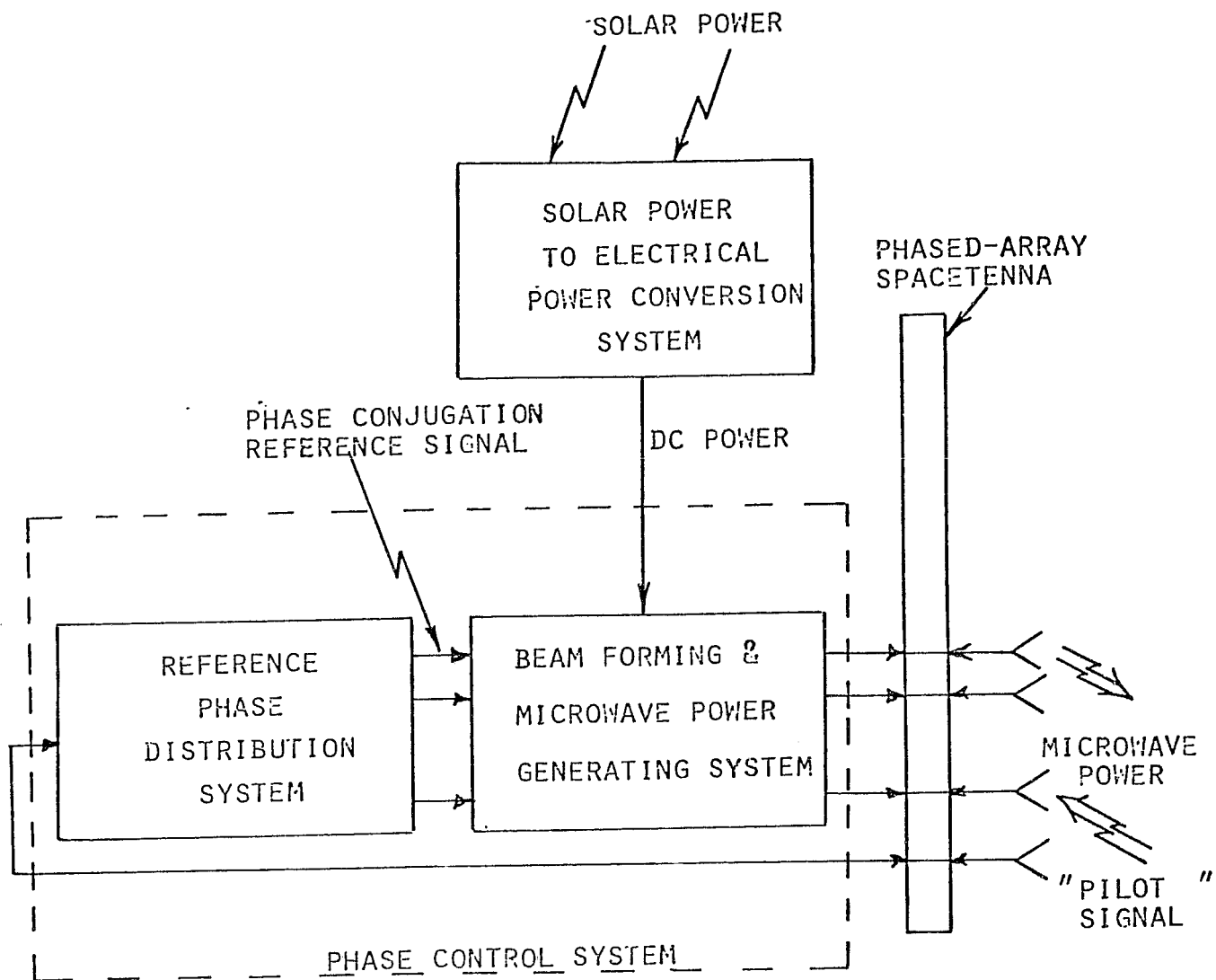
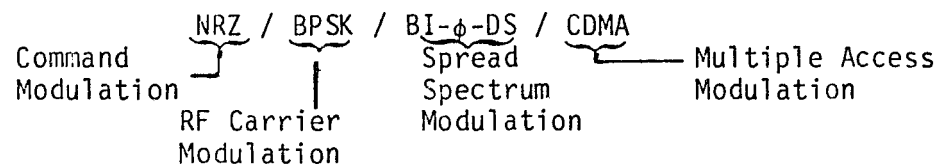


Figure 2.2. Solar Power Satellite (SPS) Transmission System (Phase Conjugation).

from Fig. 2.2 the SPS Transmission System consists of three major systems: (1) The Reference Phase Distribution System, (2) The Beamforming and Microwave Power Generating System, and (3) The Solar Power to Electrical Power Conversion System.

2.2 Reference System SPS Pilot Waveform

The reference system SPS pilot waveform utilizes: (1) NRZ command modulation, (2) split phase, direct sequence pseudo-noise or spread spectrum modulation, BI- ϕ -DS. This combined data-code modulation is used to bi-phase modulate (BPSK) the RF carrier. Multiple access in the SPS network is to be achieved via code division multiple access techniques (CDMA). Thus the baseline SPS pilot waveform is characterized via four modulation components summarized by the symbols:



A functional diagram indicating the mechanization of the pilot transmitter is shown in Fig. 2.3. As illustrated the data clock and code clock are coherent so that the uplink operates in a data privacy format. The purpose of the spread spectrum (SS) code generator is several fold. First it provides link security, second it provides a multiple access capability for the operation of a network of SPSs, and third, the anti-jamming protection is provided for both intentional radio frequency interference (RFI) and unintentional RFI such as those arising from a neighboring SPS on the adjacent orbit. Proper choice of this code modulation will also provide the needed isolation between the uplink and the downlink, since a notch filter can be placed around the carrier frequency at the SPS receiver input to blank out the interferences without destroying the uplink signal (see pilot signal spectrum in Fig. 2.3). The selection of the PN code parameters to achieve the code isolation and processing gain required will be addressed in Section 3.

2.3 Reference Phase Control System

The reference phase control system concept was presented in detail in Ref. 3; its major features are summarized in this section. Based upon earlier study efforts (Refs. 3,4), a phase control system concept has been proposed which partitions the system into three major levels. Figure 2.4 demonstrates the partitioning and represents an expanded version of Fig. 2.2. The first level in Fig. 2.4 consists of a reference phase distribution system implemented in the form of phase distribution tree structure. The major purpose of the tree structure is to electronically compensate for the phase shift due to the transition path lengths from the center of the spacetenna to each phase control center (PCC) located in each subarray. In the reference system, this is accomplished using the Master Slave Returnable Timing System (MSRTS) technique. The detailed mathematical modeling and analysis of the MSRTS technique is provided in Ref. 4. Based upon extensive tradeoffs

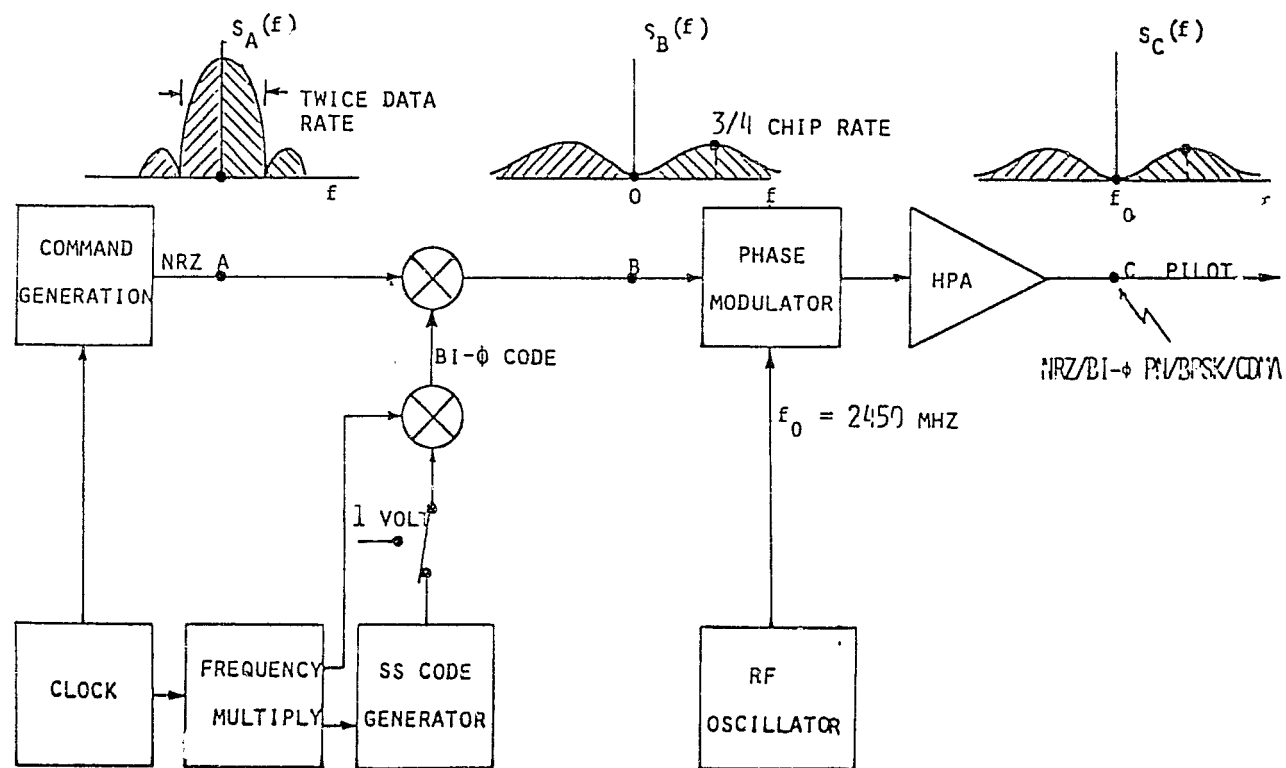


Figure 2.3. Reference System Pilot Signal Transmitter Functional Diagram.

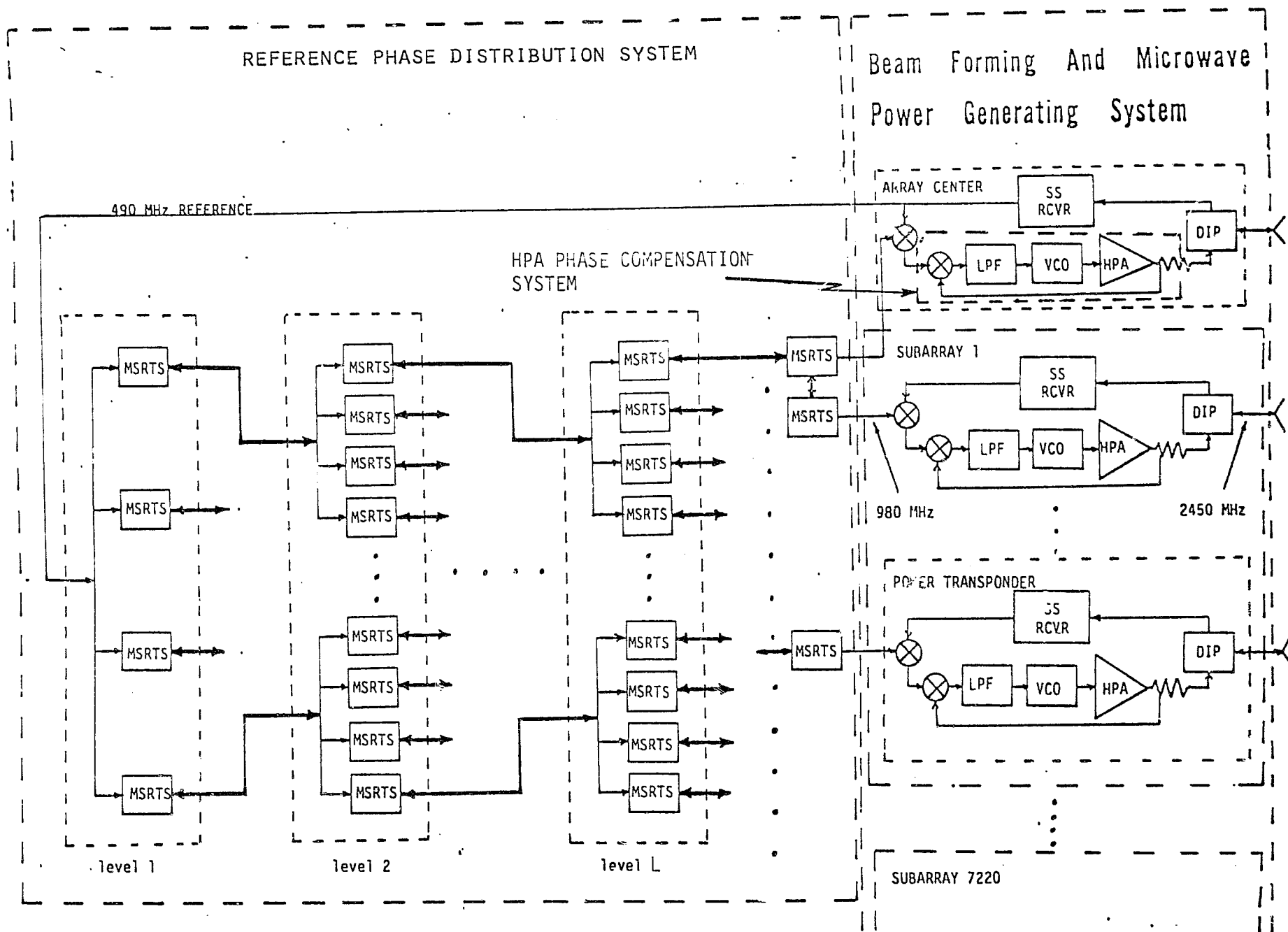


Figure 2.4. Reference Solar Power Satellite Transmission System.

using SOLARSI and appropriate analysis during the Phase II study, a four level tree is selected to be the reference phase distribution system configuration.

The second level is the Beam Steering and Microwave Power Generation System which houses the SPS Power Transponders. This transponder consists of a set of phase conjugation multipliers driven by the reference phase distribution system output and the output of a pilot spread spectrum receiver (SS RCVR) which accepts the received pilot via a diplexer connected to a separate receive horn or the subarray itself. The output of the phase conjugation circuits serve as inputs to the third level of the phase control system. The third level of phase control is associated with maintaining an equal and constant phase shift through the microwave power amplifier devices while minimizing the associated phase noise effects (SPS RFI potential) on the generated power beam. This is accomplished by providing a phase-locked loop around each high power amplifier.

2.4 Reference System-SPS-Power Transponder

In addition to distributing the constant phase reference signal over the spacenna, a method for recovering the phase of the received pilot signal is required. Figure 2.5 represents the functional diagram of the SPS power transponder. This includes the pilot signal receiver, phase conjugation electronics and the high power amplifier phase control system.

In the mechanization of the SPS power transponders, two receiver "types" will be required; however, most of the hardware will be common between two receivers. One receiver, the Pilot Spread-Spectrum Receiver, is located at the center of the spacenna or the reference subarray. It serves two major functions: (1) acquires the SS code, the carrier and demodulates the command signal, (2) provides the main input signal to the Reference Phase Distribution System.

The second receiver "type" will be located in the Beam Forming and Microwave Power Generating System. Its main purpose is to phase conjugate the received pilot signal and transpond power via the j-th spacenna element, $j = 1, 2, \dots, 101, 552$.

In the case that data transmitting capability is not implemented for the pilot signal, the Costas loop can be replaced by a CW loop. This avoids the need for provisions to resolve the associated Costas loop induced phase ambiguity.

3.0 PILOT SIGNAL DESIGN AND POWER TRANSPONDER ANALYSIS

The key technical problem areas concerning the reference phase control system design and specifications are the SPS pilot signal design and power transponder analysis. Figure 3.1 illustrates the radio frequency interference (RFI) scenario.

The interferences are generated by different mechanisms: (1) self jamming due to the power beam leakage from the diplexer/circulator; (2) mutual coupling from adjacent transponders, (3) thermal noise and (4)

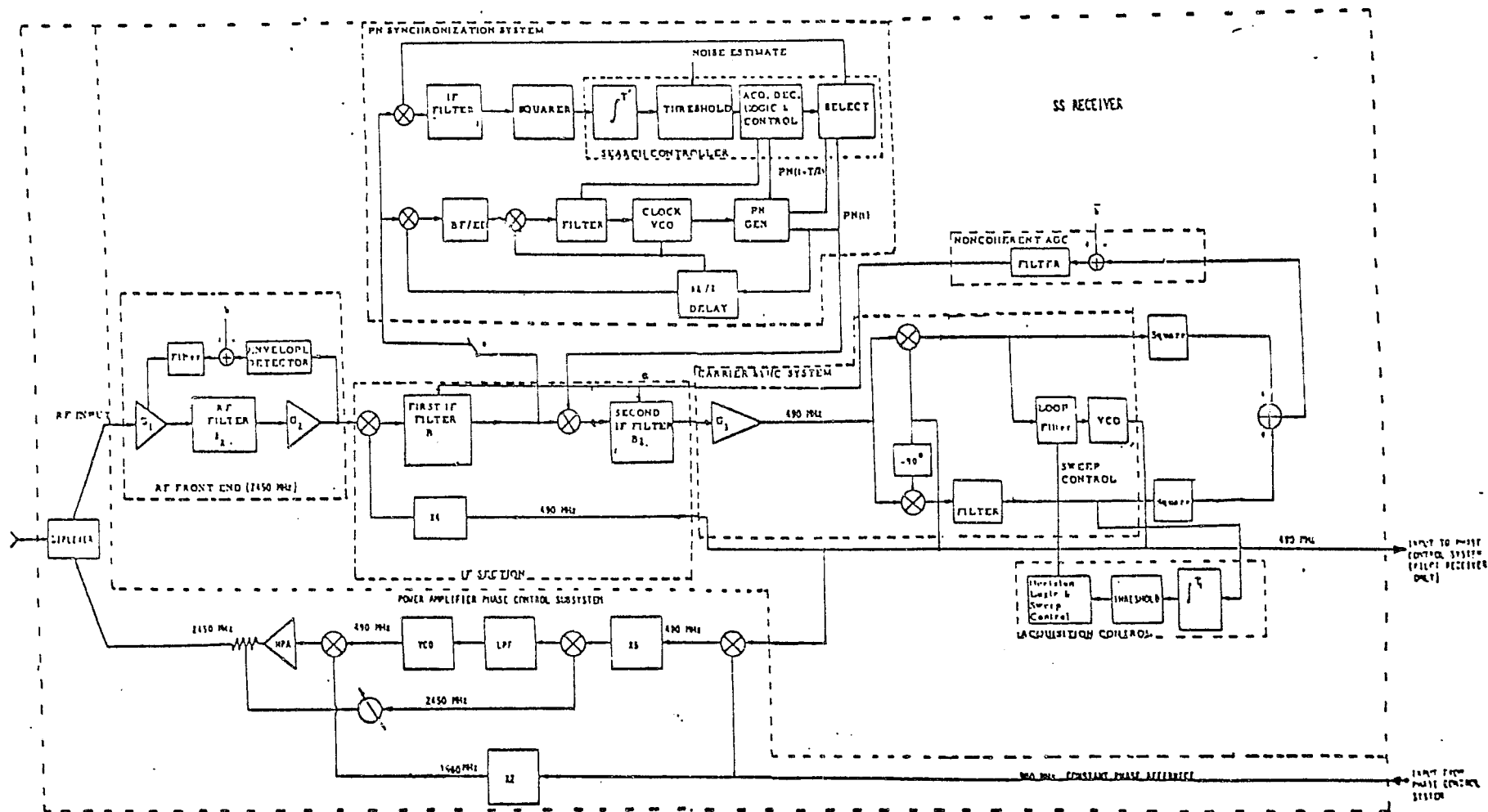
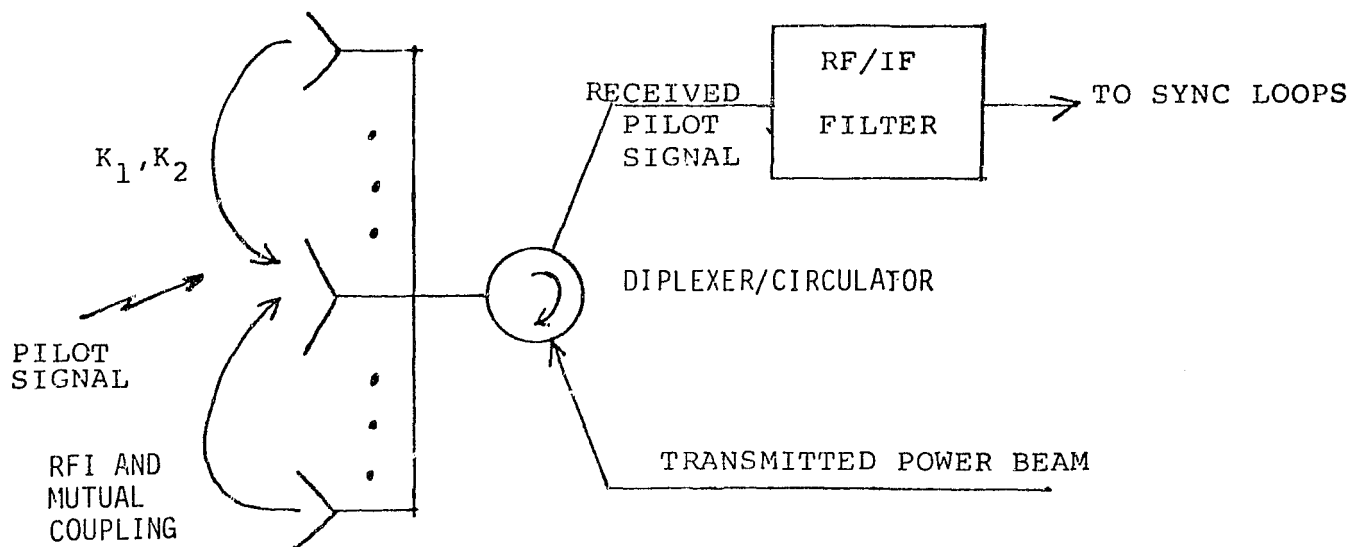
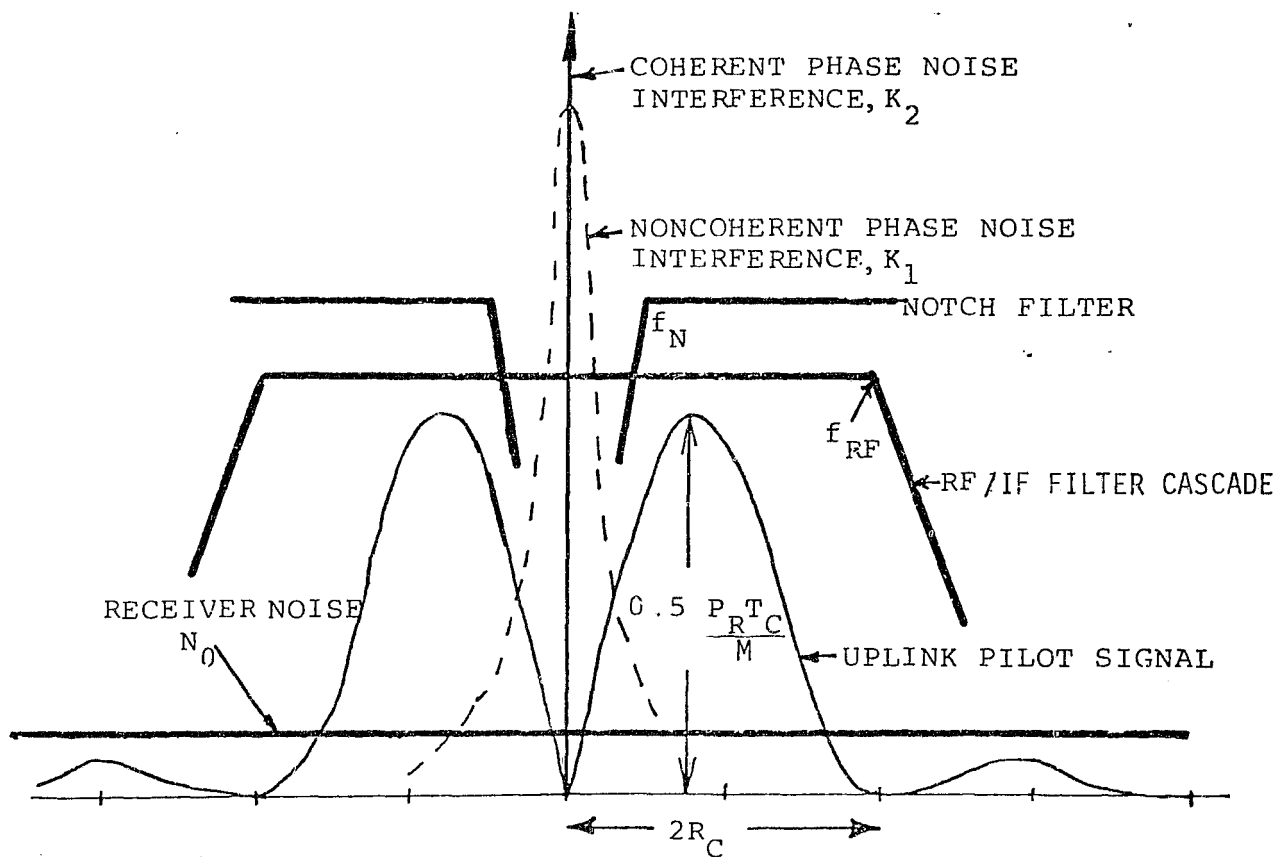


Figure 2.5. Central SPS Power Transponder Located at Spacetenna Center.



(a) SPS Power Transponder Front End (Conceptual)



(b) Signal and Noise Spectrum

Figure 3.1. Signal and Noise Spectrum into SPS Transponder.

interference from adjacent SPSs. The signal and interference spectrum at the input to the SPS transponder is depicted in Fig. 3.1. In general, the combined phase noise interference from the power beams consists of a coherent and a noncoherent term. Depending on the mechanization of the antenna structure and diplexer/circulator characteristics, these terms are associated with gains K_1 and K_2 . Note that the phase noise interferences are concentrated around the carrier frequency (2450 MHz). The uplink pilot signal on the other hand has no power around this frequency. Its power spectrum peaks at $f = 0.75 R_c$, with a value proportional to the produce of the received power (P_r) and the PN chip rate (R_c), and inversely proportional to the PN code length (M). The parameters R_c and M are related to the processing gain of the PN spread signal and determines its interference suppression capability. The RF filter characteristic is mainly determined by the waveguide antennas, which have bandwidths ranging from 15 to 45 MHz depending on the array area. Our goal is to optimally select (1) the pilot signal so that it passes the RF filter with negligible distortions, and (2) a practical notch filter that rejects most of the phase noise interferences. When this is done, one can be assured that the reconstructed pilot signal phase after the sync loops is within a tolerable error for the retrodirective scheme.

3.1 Pilot Signal Parameter Selection

SOLARSIM is developed to enable performance tradeoffs of pertinent design parameters such as pilot signal transmitter EIRP, PN code requirement, chip rate and RF front end characteristics (notch filter). The computer model is based upon a mathematical framework which includes the analytical models for power spectral density of the pilot signal, various sources of interference, the RF front end, the PN tracking loop and the pilot tracking loop. The resulting design values are provided in a later section.

3.2 Power Transponder Analysis

Analytical models are developed for the SPS transponder tracking loop system that include: (1) the PN despreader loop, (2) the pilot phase tracking (Costas) loop and (3) the PA phase control loop. The phase reference receiver that feeds the phase distribution system is also modeled. Various sources of potential phase noise interferences are identified and their effects on the performance of the individual loops are modeled. In particular, a model of the phase noise profile of the klystron amplifier based on a specific tube measurement is introduced. Important implications on the PA control loop design are also addressed.

An analytical model for evaluating the overall performance of the SPS transponder is given. The phase fluctuation at the output of the transponder is shown to be directed related to the various noise processes through the closed-loop transfer functions of the tracking loops. These noise processes are either generated externally to the transponder circuitry such as ionospheric disturbances, transmit frequency instability, or externally such as receiver thermal noise, power beam interferences, data distortions, VCO/mixer phase noise and the phase variations introduced by the reference distribution tree.

3.3 Summary of Results

The important findings and preliminary specifications the transponder design parameters and results based upon SOLARSIM and the analytical models discussed in Sections 3.1 and 3.2 can be summarized as follows:

- EIRP = 93.3 dBW
- PN Chip Rate ~ 10 Mcps
- RF filter 3 dB cutoff frequency ~ 20 MHz
- Notch filter 3 dB cutoff frequency ~ 1 MHz
- Notch filter dc attenuation ~ 60 dB
- PN Code period ~ 1 msec
- Costas loop phase jitter ≤ 0.1 deg for 10 Hz loop bandwidth
- Channel Doppler is negligible
- Klystron phase control loop bandwidth ≥ 10 kHz

In arriving at these design values, we have used extensively the capabilities of SOLARSIM to perform the necessary tradeoffs. Figure 3.2 represents a typical design curve generated via SOLARSIM and used to pick the RF filter 3 dB cutoff frequency. The details and other tradeoffs performed are documented in Ref. 5, Vol. II.

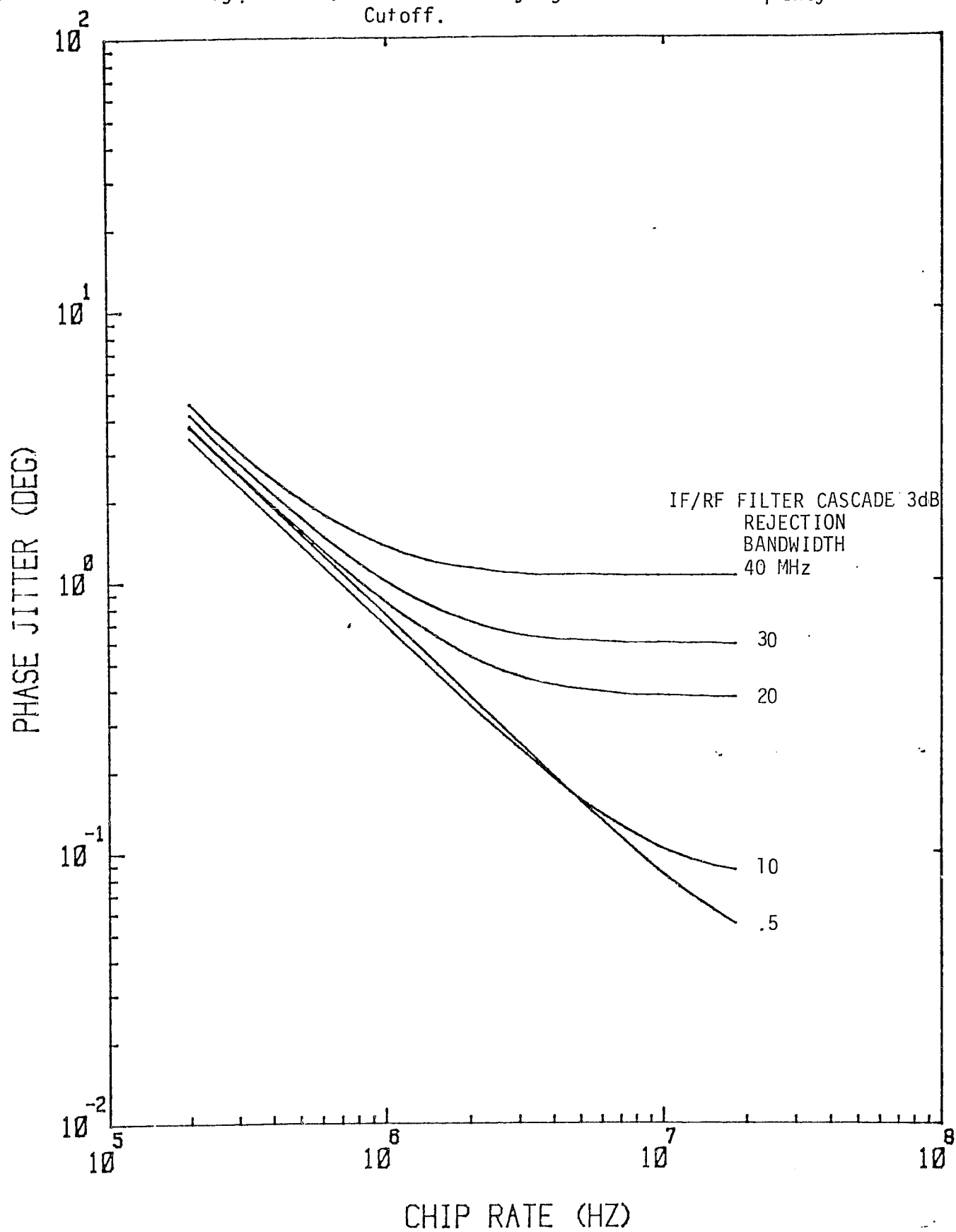
The preliminary results are generated using a tentative model of RFI with coupling coefficients $K_1 = K_2 = 20$ dB. Explicitly, we assumed that the transponder input sees a CW interference with power equal to 0.65 KW and a phase noise (1/f type) interference at about 20 W. Of course, when these values are changed significantly, our predictions have to be modified. For this reason, the development and verification of an acceptable model for the effects of mutual coupling on the phase array antenna based upon the "near field" theory is extremely important and essential in the near future.

A maximum-length linear-feedback shift register sequence, i.e., m-sequences generated by a 12 stage shift register with a period equal to 4095 is recommended as the spread spectrum code. In the code division multiple access situation, the theoretical optimal solution is to use the set of 64 bent function sequences of period 4095, enabling as much as 4095 simultaneous satellite operation of the SPS network. The bent sequences are guaranteed to be balanced, have long linear span and are easy to initialize. However, the set of maximum length sequence of period 4095, though suboptimal, may suffice. This depends of course on the code partial correlation requirement and the number of satellites in the network. The design detail is discussed in Ref. 5, Vol. II.

At this point our results indicate that it is feasible to hold the antenna array phase error to less than one degree per module for the type of disturbances modeled in this report. However, there are irreducible error sources that are not considered herein and their effects remain to be seen. They include: (a) reference phase distribution errors, (b) differential delays in the RF path.

4.0 SPS PERFORMANCE EVALUATION VIA SOLARSIM

Figure 3.2 . Effect of Varying Notch Filter Frequency Cutoff.



Because of the complicated nature of the problem of evaluating performance of the SPS phase control system and because of the multiplicity and interaction of the problems as they relate to subsystem interfaces, the methods of analysis and computer simulation (analytical simulation) have been combined to yield performance of the SPS system. The result is the development of SOLARSIM--a computer program package that allows a parametric evaluation of critical performance issues. The SOLARSIM program and its various subroutines have been exercised in great detail to provide system engineering tradeoffs and design data for the reference system. In what follows, we shall focus on the key results obtained from one of the SOLARSIM subroutines, viz., POWER TRANSFER EFFICIENCY.

4.1 System Jitters and Imperfections Modeled in POWER TRANSFER EFFICIENCY

The system jitters and imperfections can be grouped into two main classes: (1) jitters arising due to spacetenna electrical components which include such effects as the amplitude jitter and the phase jitters of the feed currents and (2) jitters arising due to the mechanical imperfections of the spacetenna which include the subarray tilts (mechanical pointing error), tilt jitters and the location jitters. The location jitters include the transmitting and receiving elements and arise from the misplacement of the radiating elements.

4.2 Definition of Power Transfer Efficiency

The power transfer efficiency adopted is defined by:

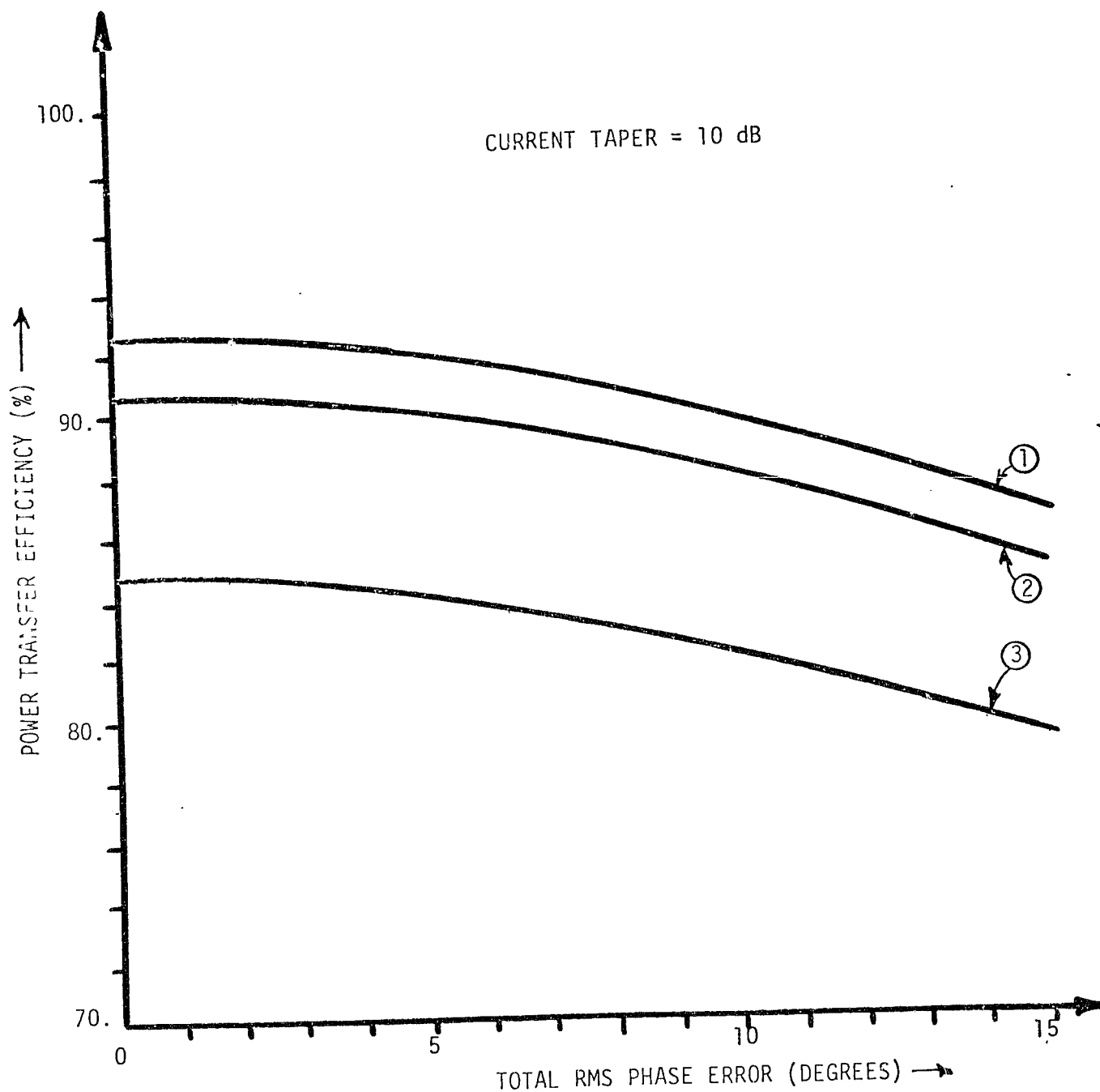
$$\text{POWER TRANSFER EFFICIENCY} = \frac{\text{Power Received by the 10 km Diameter Rectenna}}{\text{Total Power Radiated by the Spacetenna}}$$

This definition is convenient because the multiplying constants due to the propagation through the medium cancel out from the numerator and denominator.

4.3 Effects of System Imperfections on SPS Efficiency

Figures 4.2 - 4.3 summarize the effects of the various system imperfections on the SPS power transfer efficiency obtained through SOLARSIM. In Figure 4.1, the power transfer efficiency is plotted against the total phase error produced by the SPS phase control system. For a mechanically perfect system with no location jitters and mechanical pointing errors or jitters (curve ①), the total rms phase error is restricted to less than 10° at RF to yield a 90% efficiency. Curve ② depicts the influence of the mechanical pointing error (assumed to be $10'$ with a jitter of $2'$) when the location jitters are absent. As can be seen from the figure, for a total phase error of 10° the power transfer efficiency of the spacetenna drops down to 87.3%. When the location jitters of 2% of λ is added for the transmitting and receiving elements, this number drops down to 82.0% (see Curve ③). It is expected that the SPS system will operate in the region between Curve ① and ③. In this case, the power transfer efficiency will be less than 90% for a typical rms phase error of 10 degrees.

Figure 4.1. SPS Power Transfer Efficiency vs RMS Phase Error.



LEGEND

- ① MECHANICAL POINTING ERROR (MPE) = 0, LOCATION JITTER (LJ) = 0, JITTER ON MECHANICAL POINTING = 0
- ② MPE = 10', LJ = 0, JITTER ON MPE = 2'
- ③ MPE = 10', LJ = 2% of λ , JITTER ON MPE = 2'

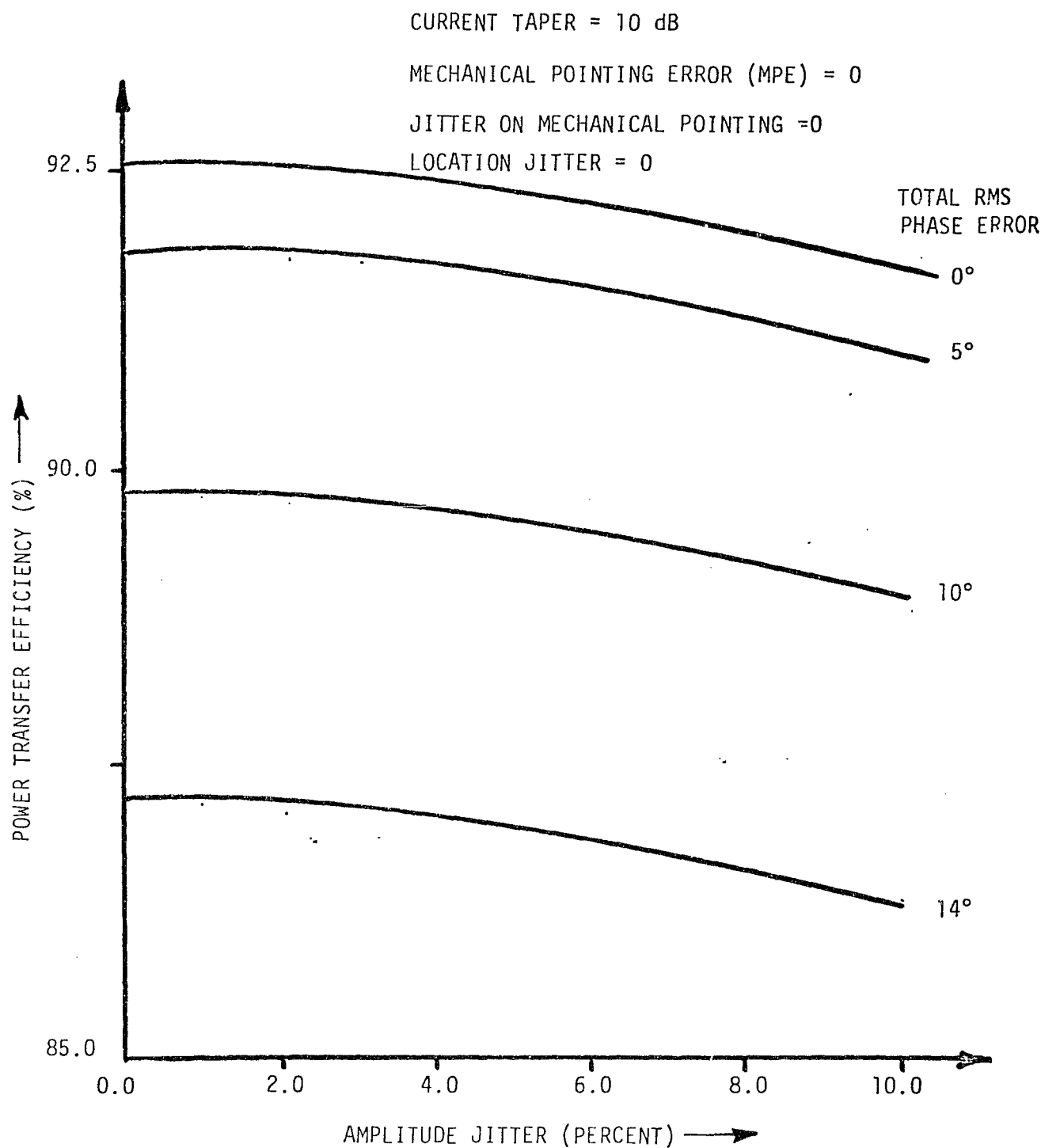


Figure 4.2. Effect of Amplitude Jitter on SPS Power Transfer Efficiency.

CURRENT TAPER = 10 dB

MECHANICAL POINTING ERROR = 0

JITTER ON MECHANICAL POINTING = 0

PHASE JITTER = 0

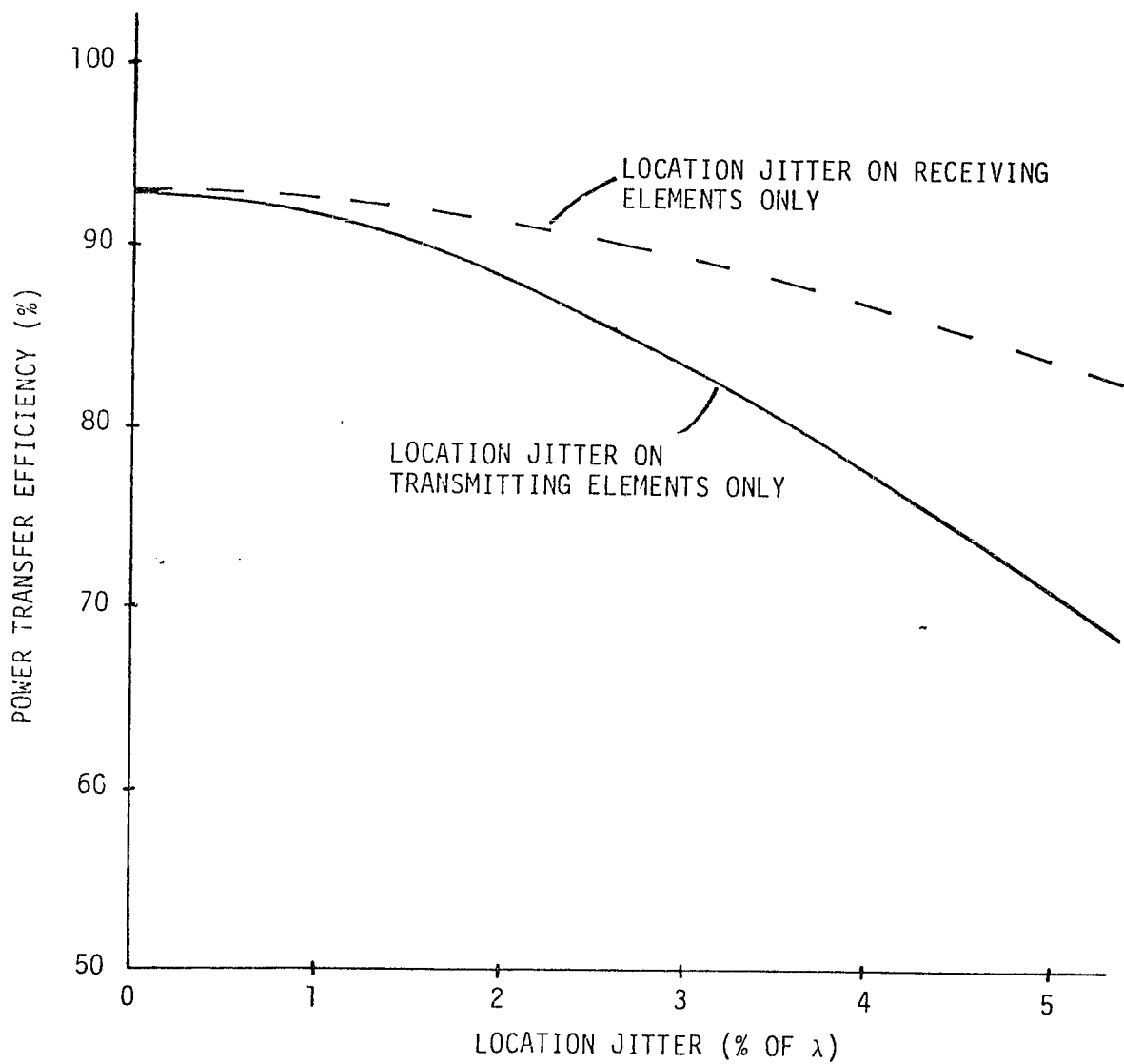


Figure 4.3 Effect of Location Jitters on the Otherwise Perfect SPS.

4.3.1 Current Amplitude Jitter

The effect of the current amplitude jitter is shown in Fig. 4.2 for a mechanically perfect system. As can be seen from the figure, for an amplitude jitter of 5%, the power transfer efficiency of the mechanically perfect spacetenna with the current phase jitter of 0° is 92.3%. This value drops to 91.63% for the total phase error of 5° and to 89.57% for a total phase error of 10° . One can conclude that the power transfer efficiency is relatively insensitive to the amplitude jitters.

4.3.2 Location Jitters

Figure 4.3 investigates the effects of location jitters on the power transfer efficiency of an otherwise perfect SPS. As can be seen from the figure, the degradation of efficiency is severe: for a location jitter on each radiating element of $2\% \lambda$ the power transfer efficiency drops to 88.3%. As a comparison, Fig. 4.1 shows that for a rms phase error of 7° ($2\% \lambda = 7.2^\circ$) the efficiency is down to 91.2%. It is noticeable that the effect produced by location jitters on the receiving (conjugating) elements is comparable to the effect produced by the phase error. This is true because both these effects enter into the transmission system at the same physical point, i.e., the center subarray. On the other hand, power transfer efficiency is rather sensitive to the location jitter on the radiating elements.

REFERENCES

1. Lindsey, W. C., and Kantak, A. V., "Automatic Phase Control in Solar Power Satellite Systems," Prepared for NASA/JSC, TR-7809-0977, September 1977, LinCom Corporation, P.O. BOX 2793D, Pasadena, CA.
2. Lindsey, W. C., "A Solar Power Satellite Transmission System Incorporating Automatic Beam Forming, Steering and Phase Control," prepared for NASA/JSC, TR-7806-0977, June 1978, LinCom Corporation, P.O. BOX 2793D, Pasadena, CA.
3. Lindsey, W. C., and Kantak, A. V., "Automatic Phase Control in Solar Power Satellite Systems," Prepared for NASA/JSC, TR-7802-0977, February 1978, LinCom Corporation, P.O. BOX 2793D, Pasadena, CA.
4. Lindsey, W. C., Kantak, A. V., Chie, C. M., and Booth, R. W. D., "SPS Phase Control System Performance Via Analytical Simulation, Phase II," Prepared for NASA/JSC, TR-7903-0977, March 1979, LinCom Corporation, P.O. BOX 2793D, Pasadena, CA.
5. Lindsey, W. C., Kantak, A. V., and Chie, C. M., "SPS Phase Control Performance Via Analytical Simulation Phase III," Vols. I-IV, Prepared for NASA/JSC, TR-0180-0779, January 1980, LinCom Corporation, P. O. BOX 2793D, Pasadena, CA.

DESIGN AND BREADBOARD EVALUATION OF THE SPS
REFERENCE PHASE CONTROL SYSTEM CONCEPT

P. M. Hopkins and V. R. Rao

Lockheed Engineering and Management Services Company, Inc.

1. INTRODUCTION

Efficient operation of a very large phased array such as the proposed solar power satellite [1], requires precision focusing and pointing of the power beam; i.e., the power beam must have a planar wavefront directed precisely at the center of the target antenna (rectenna). To maintain such a power beam requires real-time phase compensation at each subaperture in order to adjust for structural deformations and other transitory factors. In the current solar power satellite (SPS) baseline, the spaceborne antenna (Spacenna) is an active retrodirective array [2], [3]. A pilot signal transmitted from the center of the rectenna is phase-conjugated at each subaperture (power module) of the spacenna, thereby assuring that the radiated composite wave is focused on the target. This scheme requires a large amount of precision electronic circuitry on the spacenna. Specifically, pilot receivers must be located at each power module and an adaptive distribution network is required in order to provide a properly phased reference signal at each conjugator [4], [5].

In order to verify theoretical and simulation results, a project was initiated by the Tracking and Communication Systems Department of Lockheed Electronics Company to design, develop, and test a breadboard system comprising a pilot receiver and transmitter, phase distribution system, and power transponder. This breadboard system is to be used in the Electronic Systems Test Laboratory (ESTL) at the Johnson Space Center. The total breadboard system will include one pilot transmitter, one pilot receiver, nine phase distribution units, and

two power transponders. It will be shown in the following sections of this paper that with this complement of equipment, segments of a typical phase distribution system can be assembled to facilitate the evaluation of significant system parameters.

The major objectives of the project are to determine the achievable accuracy of a large phase distribution system, the sensitivity of the system to parameter variations, and the limitations of commercially available components in such applications.

2. ACCOMPLISHMENTS

The design and development of a breadboard Master-Slave Returnable Timing System (MSRTS) was the first objective of the project. Nine units were planned; three were completed and used for prototype evaluation tests. Six remaining units are in final assembly.

2.1 MSRTS BREADBOARD

The MSRTS breadboard system is of a modular design with three major elements. These are the Phase Tracking Unit (PTU), the Interface/Return Unit (IRU) and the Main Frame. Modular construction permits the equipment to be configured in various ways as required to model portions of the proposed SPS phase distribution tree network. A simplified functional diagram of a single MSRTS stage is shown in Figure 1. Figure 2 shows the tree distribution structure for which the breadboard MSRTS is designed.

The major components of the PTU are Voltage Controlled Oscillator (VCO), loop filter, circulator, mixers and a phase detector. The phase lock loop circuitry is used to advance the phase of VCO to compensate for the effect of the delay introduced by the path between nodes of a tree structure.

At the IRU, two functions are performed. First, a portion of the received reference signal is returned to the preceding PTU via the single interconnecting cable. This return signal arrives at the PTU with a phase delay proportional to the line length. The delay is measured in the phase detector

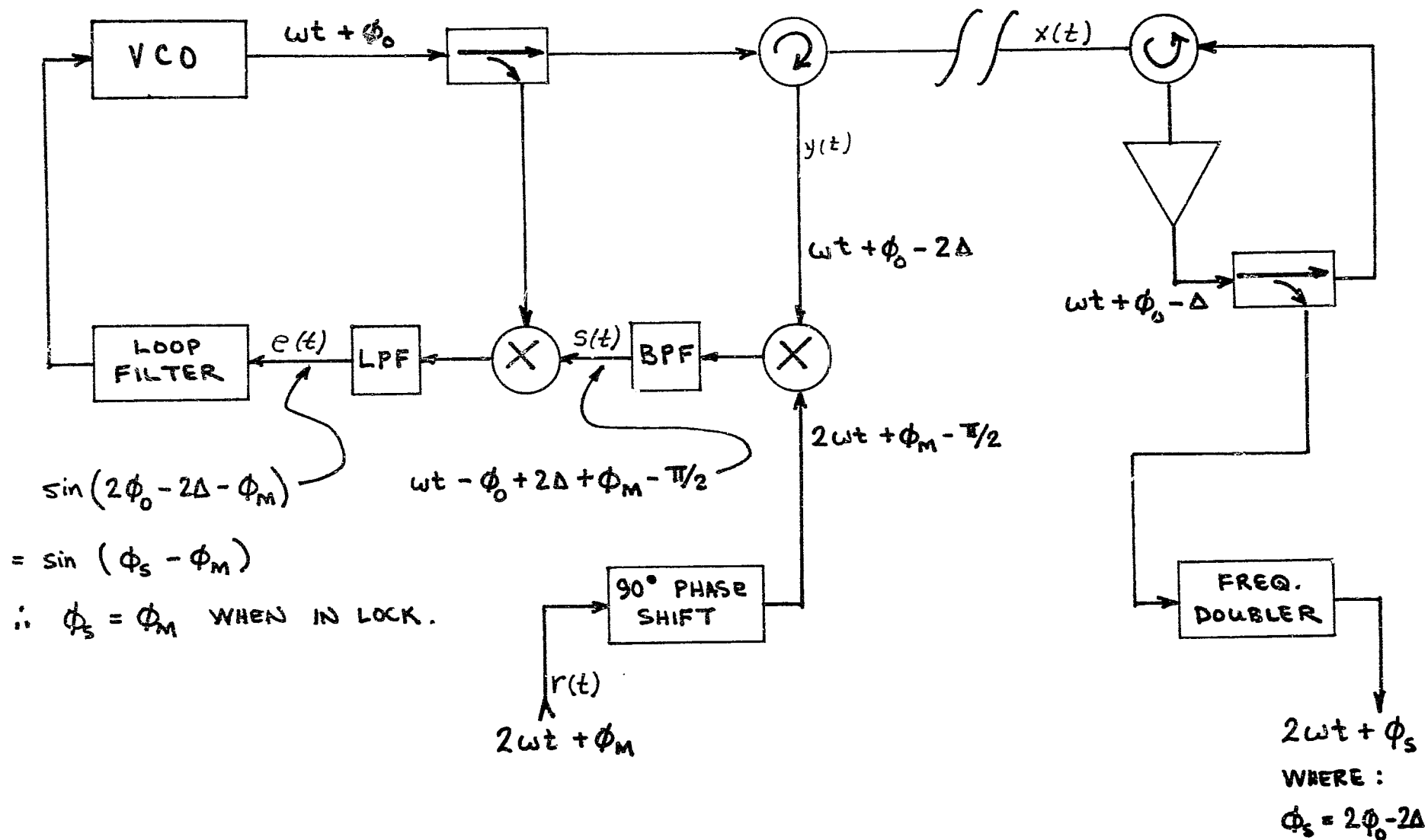


Figure 1: Simplified functional diagram of MSRTS.

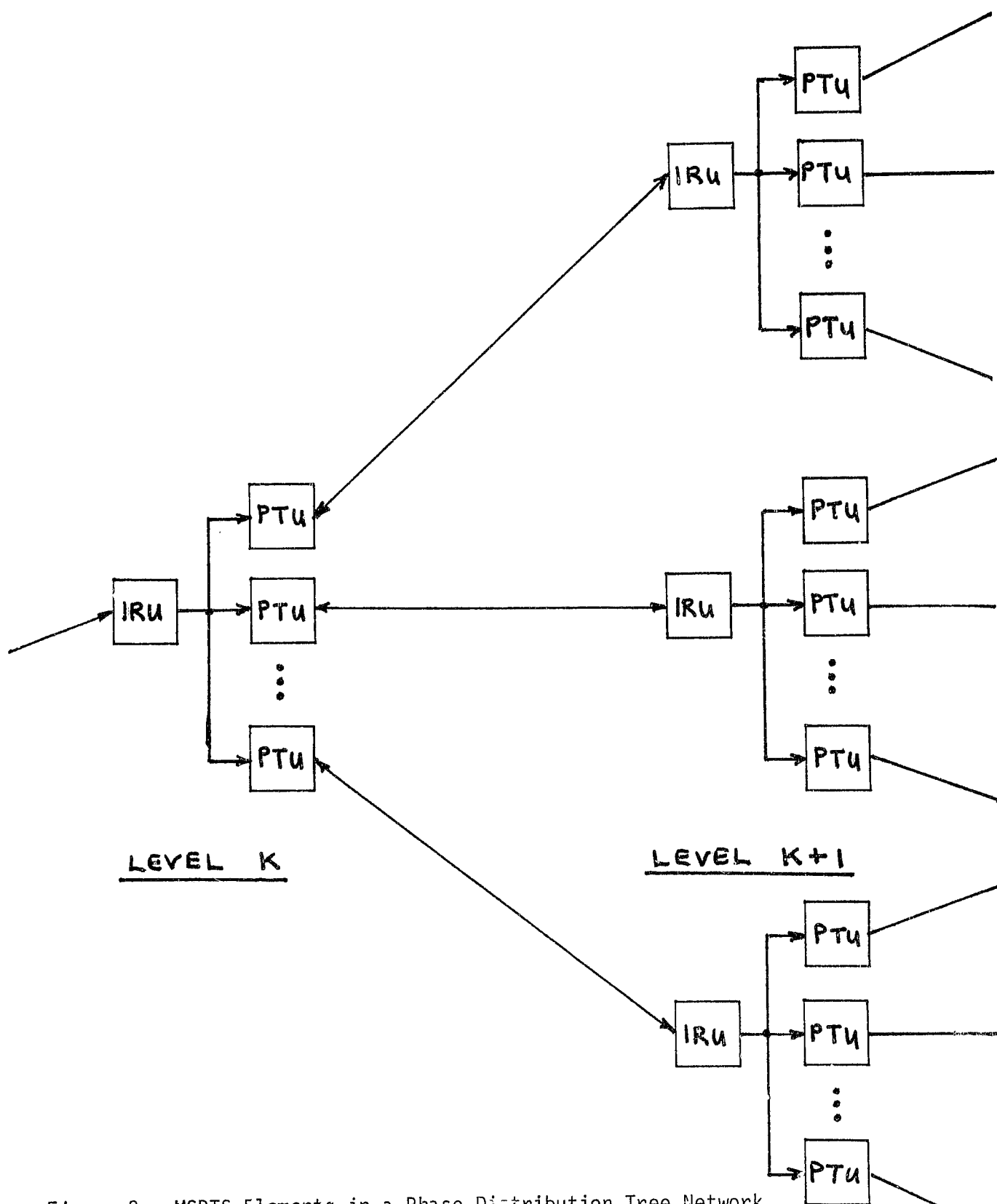


Figure 2. MSRTS Elements in a Phase Distribution Tree Network

of the PTU, and the VCO phase is appropriately adjusted so that the reference phase is correct at the IRU input. Second, the reference signal at the IRU is doubled in frequency to match the reference input to the PTU. When the PTU is phase locked, the phase of the IRU output signal is the same as the phase of the preceding PTU input signal, within the accuracy limitations of the hardware. Each IRU can provide up to four outputs.

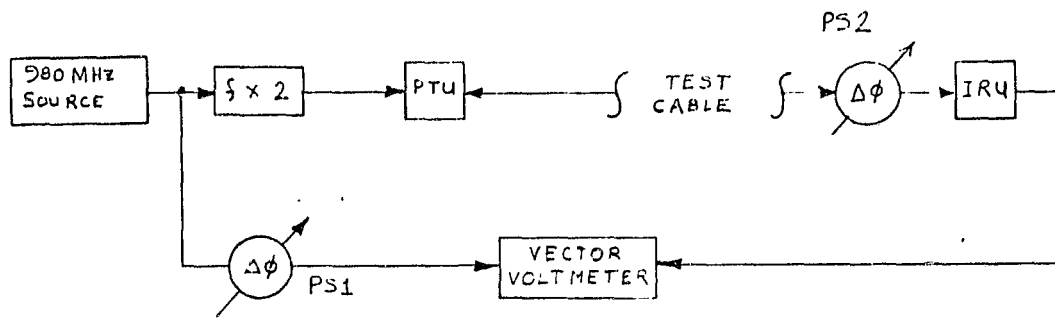
The Main Frame contains supplies and a patch panel that facilitates the interconnection between PTU's and IRU's mounted in separate mainframes. Each mainframe is capable of supporting a total of three PTU's and/or IRU's.

2.2 MSRTS BREADBOARD TEST RESULTS

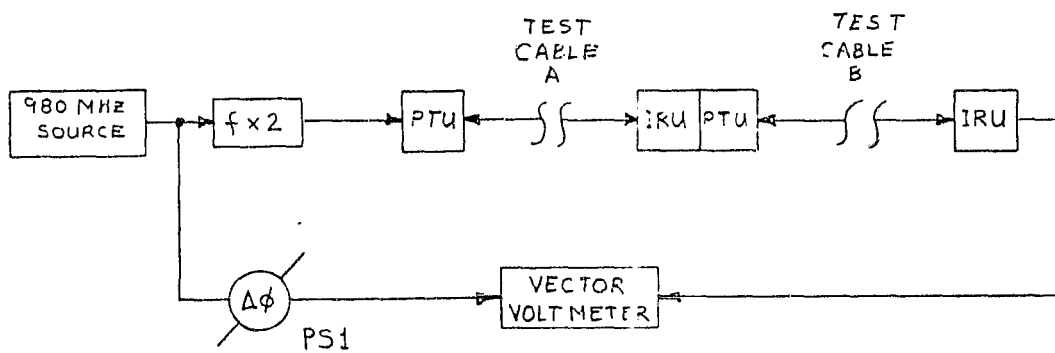
Three prototype MSRTS breadboard units were used in a variety of test configurations to evaluate the accuracy of phase control and the effects of component imperfections. These test configurations included those shown in Figure 3.

For example, the three-node series network of Figure 3c was tested with 30 different cable combinations, using RG-14 coaxial cable in lengths between 200 and 250 feet (60 - 80 meters); that is, after initial adjustment of the test configuration with zero phase error on the vector voltmeter, 30 different combinations of cables were substituted for Test Cables A and B. For each combination, the resulting phase error was measured and recorded. The results are presented in the histogram of Figure 4, which indicates a standard deviation of error of 4.2° . This experiment is intended to demonstrate the accuracy of the breadboard MSRTS with arbitrary cable lengths. It is important to note that the cables were not cut to precise measurements.

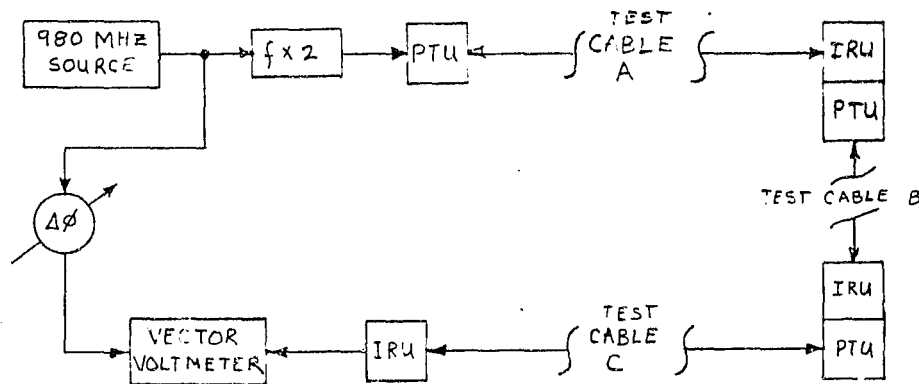
Another type of phase error measurement was made with the configuration of Figure 3a. Minor variations in electrical line length were introduced by means of a phase shifter (PS2). The phase error at the vector voltmeter was initially nulled with PS2 set to zero. Then PS2 was varied from 0 to 180° , equivalent to a half-wave variation in cable length. The resulting phase error is shown in Figure 5.



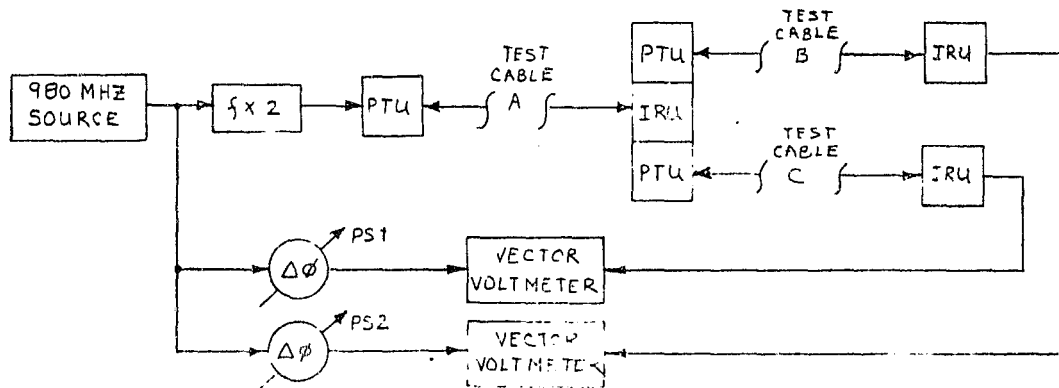
a) TWO-NODE



b) THREE-NODE SERIES



c) FOUR-NODE SERIES



d) FOUR-NODE NMF

Figure 3. MSRTS Breadboard Test Configuration

STANDARD DEVIATION OF 30 TRIAL SAMPLE = 4.2 DEGREES

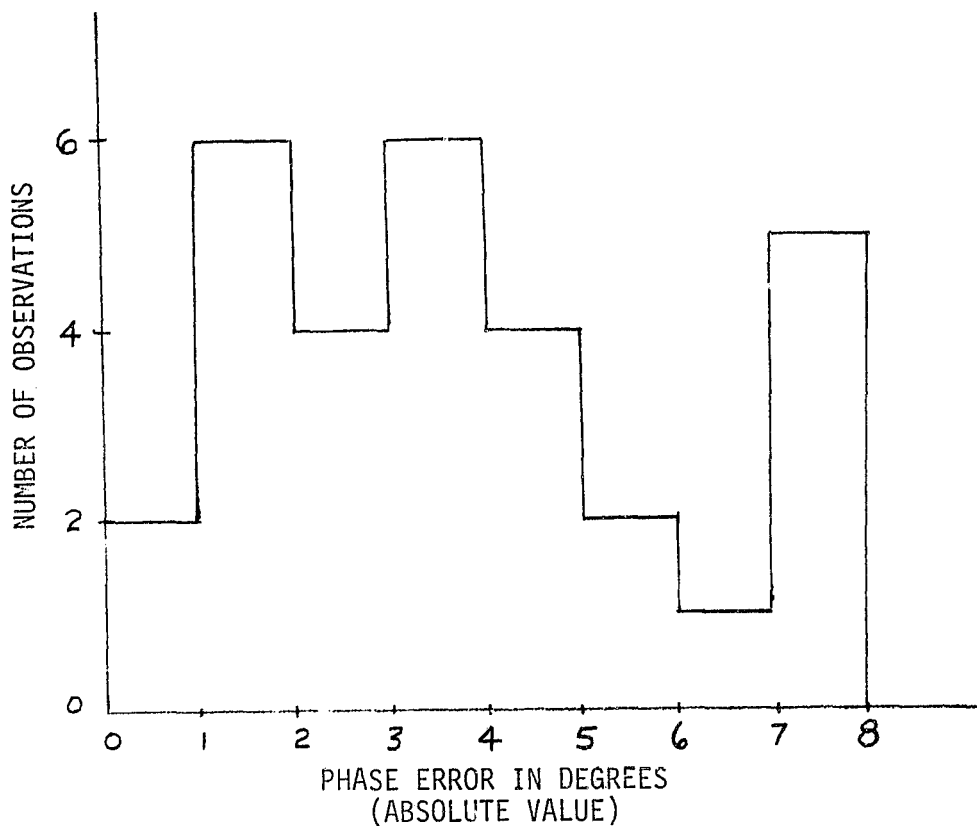


Figure 4. Histogram of Three-Node Test Results

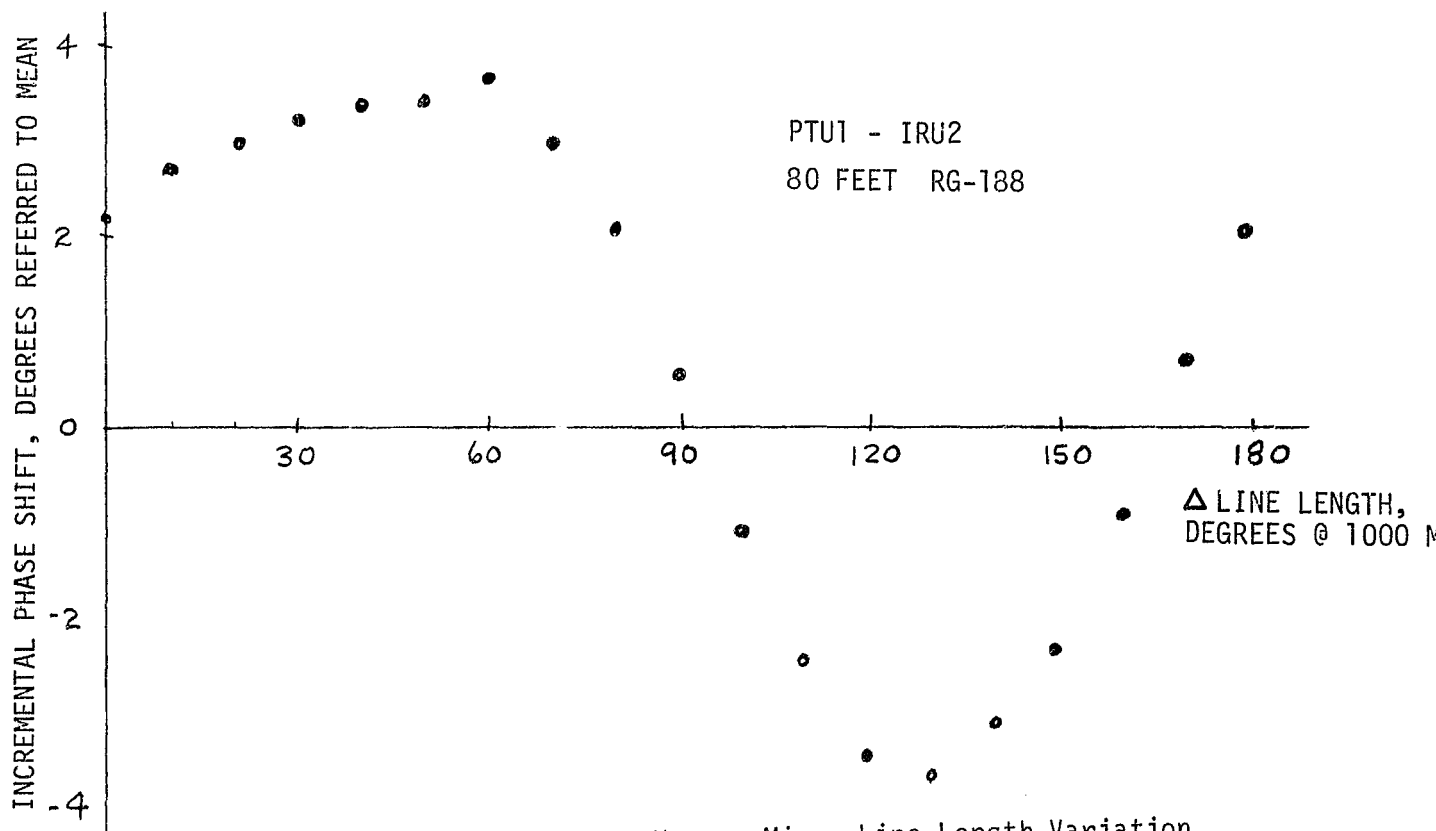


Figure 5. Phase Error Versus Minor Line Length Variation.

2.3 INTERPRETATION OF TEST RESULTS

A detailed report of the MSRTS breadboard test results has been prepared [6]. The conclusions from that report are summarized in the following:

- Satisfactory performance can be obtained using readily available components under closely controlled conditions.
- Commercially available components exhibit non-ideal behavior which is critical to MSRTS performance, e.g. port-to-port isolation of mixers and circulators was not sufficient to prevent extraneous signals which can cause phase errors. These effects can be minimized with compensating networks.

3. CONTINUING DEVELOPMENT

The breadboard MSRTS will be used as part of a larger breadboard system which models the total SPS phase control concept. A pilot transmitter will generate a pseudonoise (PM) code-modulated spread spectrum pilot carrier at 2450 MHz. A central pilot receiver will phaselock to the pilot carrier and provide a reference for the MSRTS. At the final level of the MSRTS tree, each IRU will provide a reference phase signal for a power transponder. Each power transponder will receive the pilot carrier, phase-conjugate, and retransmit. The ESTL breadboard system, shown functionally in a typical test configuration in Figure 6, will consist of the following units.

- One Pilot Transmitter
- One Central Pilot Receiver
- Nine MSRTS Elements
- Two Power Transponders
- One Klystron Power Amplifier

These units can be interconnected in various test configurations. Tests will be performed to evaluate the feasibility of the MSRTS phase control concept and to determine the sensitivity of the phase control system to variations in system parameters. In addition, techniques for suppressing the phase noise of the klystron power amplifier will be investigated.

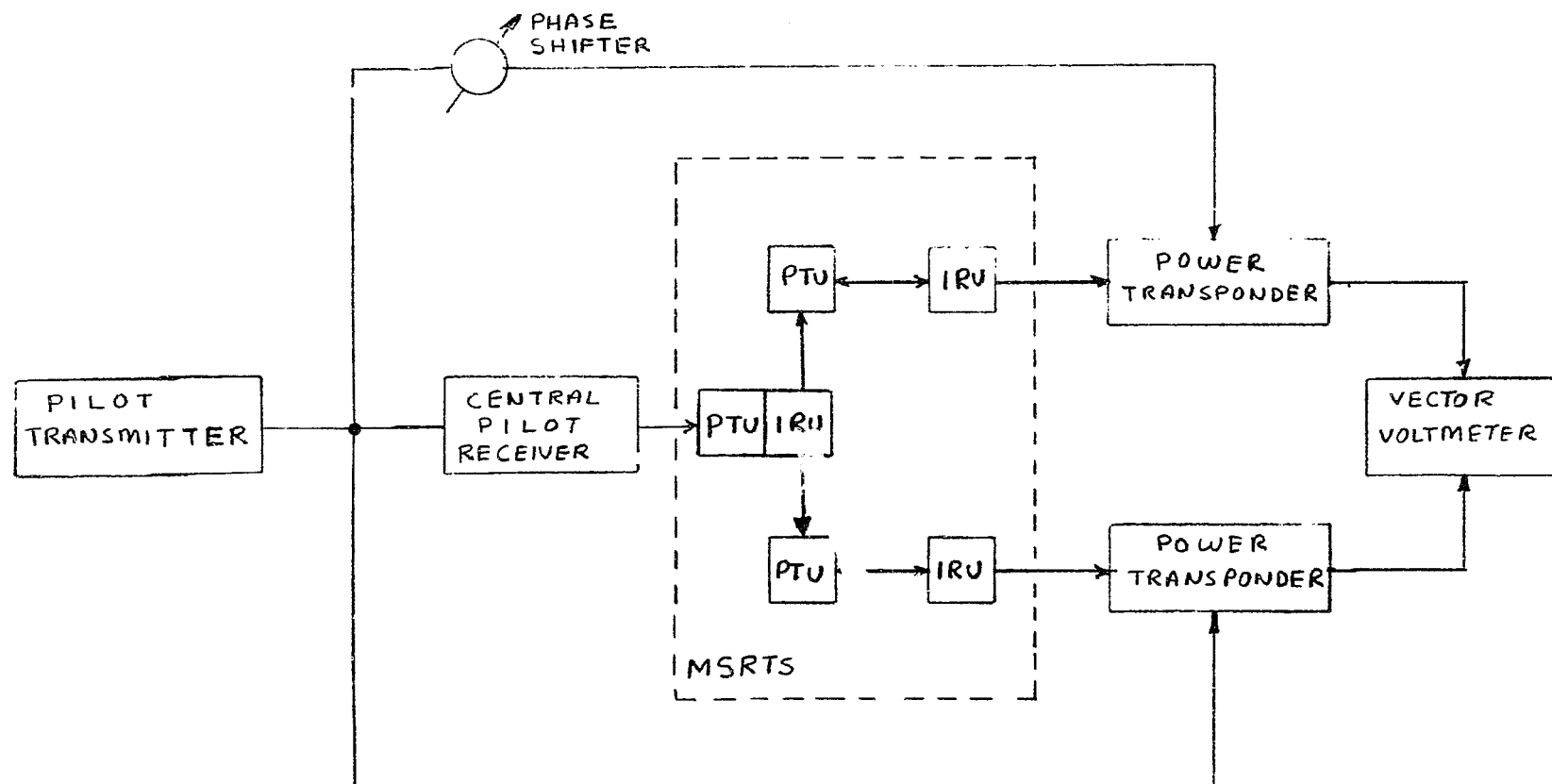


Figure 6. Breadboard SPS Phase Control System in Typical Test Configuration

Design and development of the ESTL breadboard system will be completed by March 1980. The test and evaluation program will be completed by July 1980.

4. ACKNOWLEDGEMENTS

The work described in this paper was performed under NASA Contract Number NAS 9-15800. The design, development, and initial testing of the breadboard MSRTS was done by Dr. James C. Vanelli of Lockheed Electronics Company, Inc.

5. REFERENCES

1. "Initial Technical, Environmental and Economic Evaluation of Space Solar Power Concept." NASA Lyndon B. Johnson Space Center, Houston, Texas, JSC-11568, August 31, 1971.
2. Skolnick, M. I. and King, D. D.: "Self-Phasing Array Antennas." IEEE Transactions on Antennas and Propagation, Volume AP-12, pp. 142-149, March 1964.
3. Ghose, R. N.: "Electronically Adaptive Antenna Systems." IEEE Transactions on Antennas and Propagation, Volume AP-12, pp. 161-169, March 1964.
4. Lindsey, W. C. and Kantak, A. V.: "Automatic Phase Control in Solar Power Satellite Systems." Lincom Technical Report TR-7802-0977, February 15, 1978.
5. Lindsey, W. C.: "A Solar Power Satellite Transmission System Incorporating Automatic Beamforming, Steering and Phase Control." Lincom Technical Report TR-7806-0977, 1978.
6. Vanelli, J. C.: "Design and Testing of a Master-Slave Returnable Timing System for the Solar Power Satellite." Lockheed Electronics Company, Houston, Texas, LEC-10474/EE7-79-714, December 1979.

COHERENT MULTIPLE TONE TECHNIQUE FOR
GROUND BASED SPS PHASE CONTROL*

C. M. Chie
LinCom Corporation
Pasadena, CA 91105

1.0 Introduction

The ground based phase control concept has been under study at LinCom as an alternative approach to the reference SPS phase control system (See Refs. 1,2,3). The details of the ground based phase control system study are documented in Ref. 4. In this short paper we summarize the coherent multiple tone technique used for the ground based phase measurement waveform design and phase control system.

2.0 Ground-Based Phase Control Concept

The ground based phase control system achieves beam forming by adjusting the phases of the individual transmitters on board SPS. The phase adjustments are controlled by ground commands. To specify the correct amount of adjustments, the phases of the power beams from each individual transmitter arriving at the rectenna center must be measured, the appropriate corrections determined (to ensure that all power beams arrive at the same phase) and relayed to the SPS. The proposed scheme to be considered is sequential in nature, i.e., the phase measurement is performed one at a time for each individual transmitter at approximately one-second intervals (measurement time allocated is 10 μ sec). The phase corrections are updated once every second. A 10-bit phase quantization for the corrections giving 0.35° resolution is envisioned. The uplink command data rate is on the order of 10 Mbps. The functional operation of the ground-based phase control concept is summarized in Fig. 1. As evident from the figure, the key issues that need to be addressed are:

*This work was performed at LinCom Corporation for the NASA Johnson Space Center, Houston, TX, under Contract No. NAS9-15782.

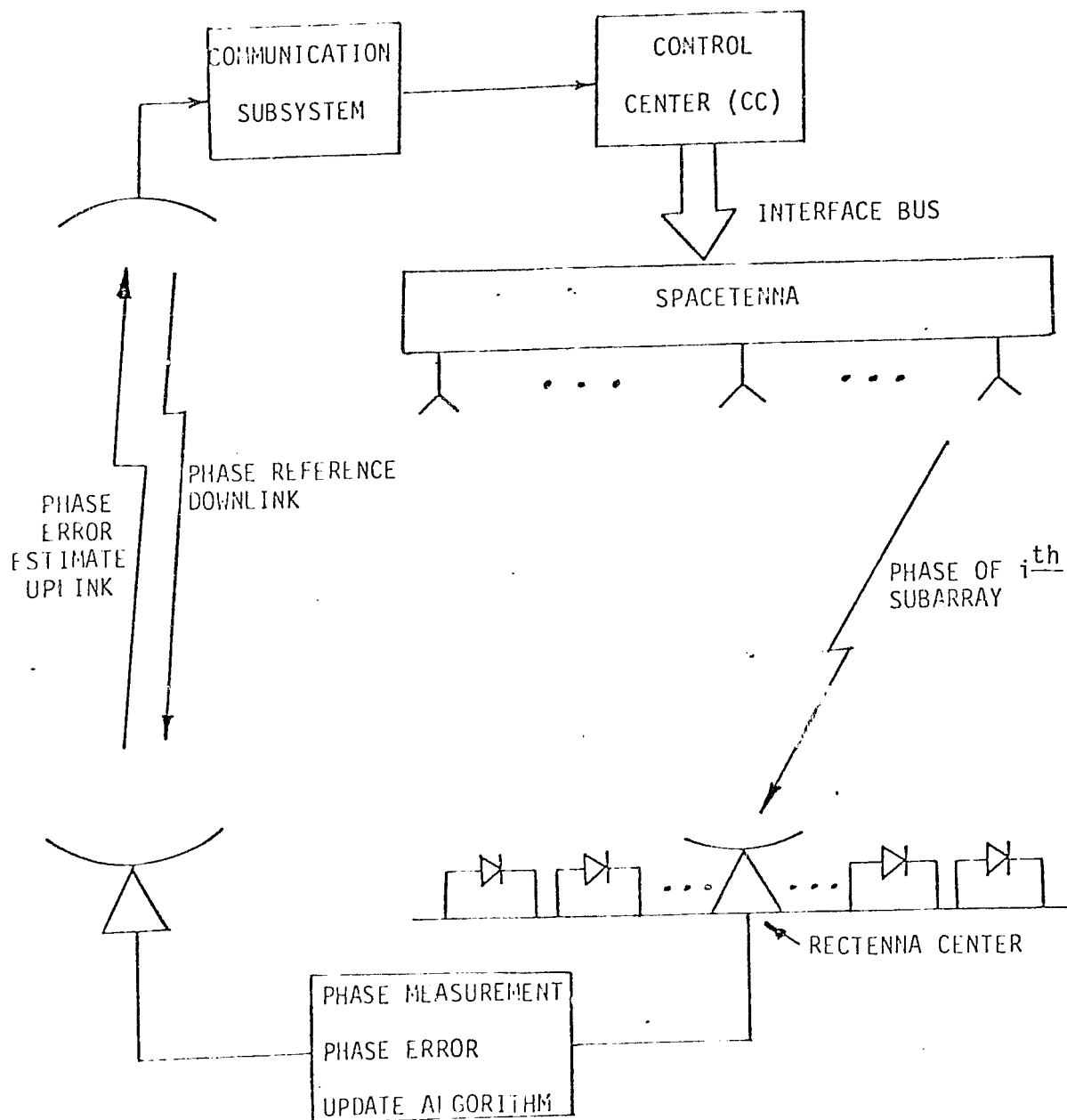


Figure 1. Ground Based Phase Control System Concept with Major Functional Blocks.

- (1) measurement waveform design and selection,
- (2) phase measurement pilot reference design and selection,
- (3) uplink phase corrections command link format and design, and
- (4) system synchronization techniques.

3.0 Two-Tone Phase Measurement Scheme with Coherent Subcarrier

In the basic two-tone measurement scheme, two side tones at $f_0 \pm \Delta f$ are transmitted from the satellite to the ground receiver. A phantom carrier can be reconstructed from the sidetones by passing the signal through a squaring circuit. The output will then have a CW component with frequency $2f_0$ and a phase component equal to $(\phi_1 + \phi_2)$, where ϕ_1 and ϕ_2 are the channel induced phase shifts at $f_0 + \Delta f$ and $f_0 - \Delta f$, respectively. This phase shift is very close to double the one that would have occurred if the downlink signal were a single sinusoid at frequency f_0 . If we divide the $2f_0$ component by two, we obtain the average phase $\frac{\phi_1 + \phi_2}{2}$. Unfortunately, the divide by two circuit results in a $0^\circ - 180^\circ$ ambiguity.

4.0 Four-Tone Phase Measurement Scheme

The four-tone measurement scheme given in Fig. 2 is a simple modification of the two-tone scheme. Basically, we first use frequencies at $f_0 \pm 2\Delta f$ for phase error measurement with introduces π ambiguity. Then we use frequencies at $f_0 \pm \Delta f$ for ambiguity resolution. The scheme works as follows. The transmitted signal at the input to the transmitting antenna is (neglecting multiplicative constants)

$$s_1(t) = \cos\left[\omega_0\left(1 + \frac{\ell}{N}\right)t + \left(1 + \frac{\ell}{N}\right)\theta_i + \frac{2\pi k \ell}{N}\right] \\ + \cos\left[\omega_0\left(1 - \frac{\ell}{N}\right)t + \left(1 - \frac{\ell}{N}\right)\theta_i - \frac{2\pi k \ell}{N}\right] \quad \ell = 0, 1, 2$$

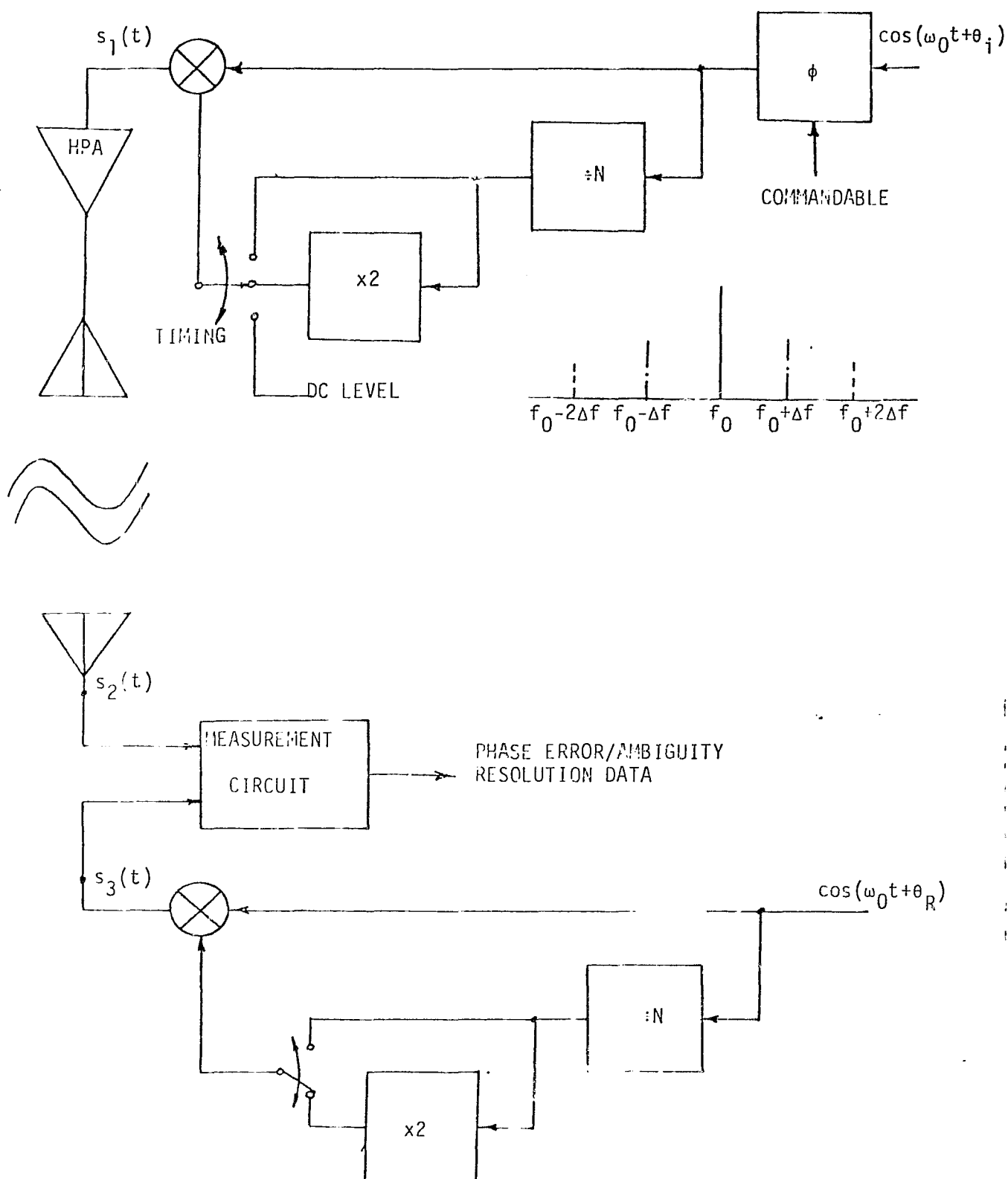


Figure 2. Four-Tone Phase Measurement Scheme.

where θ_i includes the commandable phase shift, $\frac{2k\pi}{N}$ is the ambiguity introduced by the divide by N circuit, $f = \frac{f_0}{N}$, and $\ell = 0, 1, 2$ depending on whether the PM is in the power mode (1), ambiguity resolution mode (2), or phase error measurement mode (3). At the receiver on the ground,

$$s_2(t) = \cos[\omega_0(1 + \frac{\ell}{N})t + (1 + \frac{\ell}{N})\theta_i + \frac{2\pi k\ell}{N} + \varphi_+(\ell)] \\ + \cos[\omega_0(1 - \frac{\ell}{N})t + (1 - \frac{\ell}{N})\theta_i - \frac{2\pi k\ell}{N} + \varphi_-(\ell)]$$

where $\varphi_+(\ell)$ and $\varphi_-(\ell)$ are the phase shifts introduced by the channel.

The reference signal $s_3(t)$ is given by

$$s_3(t) = \cos[\omega_0(1 + \frac{\ell}{N})t + (1 + \frac{\ell}{N})\theta_R + \frac{2\pi \ell m}{N}] \\ + \cos[\omega_0(1 - \frac{\ell}{N})t + (1 - \frac{\ell}{N})\theta_R - \frac{2\pi \ell m}{N}]$$

where θ_R is the phase of the ground reference, and $\frac{2\pi m}{N}$ is the ambiguity introduced by the ground divide by N circuit. If the operations are synchronized, we can then measure up to modulo 2π at the output of the measurement circuit, the phases

$$\varphi_+(\ell) + (1 + \frac{\ell}{N})(\theta_i - \theta_R) + \frac{2\pi \ell}{N}(k - m) = \phi_+(\ell) + 2\pi M_+(\ell) \quad (1)$$

$$\varphi_-(\ell) + (1 - \frac{\ell}{N})(\theta_i - \theta_R) - \frac{2\pi \ell}{N}(k - m) = \phi_-(\ell) + 2\pi M_-(\ell) \quad (2)$$

Actually, in (1) and (2), $\phi_+(\ell)$ and $\phi_-(\ell)$ are the measured phases and $M_+(\ell)$ and $M_-(\ell)$ are integers so that the absolute values of $\phi_+(\ell)$ and $\phi_-(\ell)$ can be restricted to π . Note that we are interested in determining $[\varphi_+(\ell) + \varphi_-(\ell)]/2$ modulo 2π . For $\ell=2$, we know from (1) and (2) that

$$\frac{\varphi_+(2) + \varphi_-(2)}{2} = \frac{\phi_+(2) + \phi_-(2)}{2} + [M_+(2) + M_-(2)]\pi - (\theta_i - \theta_R) \quad (3)$$

Now if we can resolve whether $[M_+(2) + M_-(2)]$ is even or odd, we can determine $[\varphi_+(2) + \varphi_-(2)]/2 + (\theta_i - \theta_R)$ modulo 2π . This information is

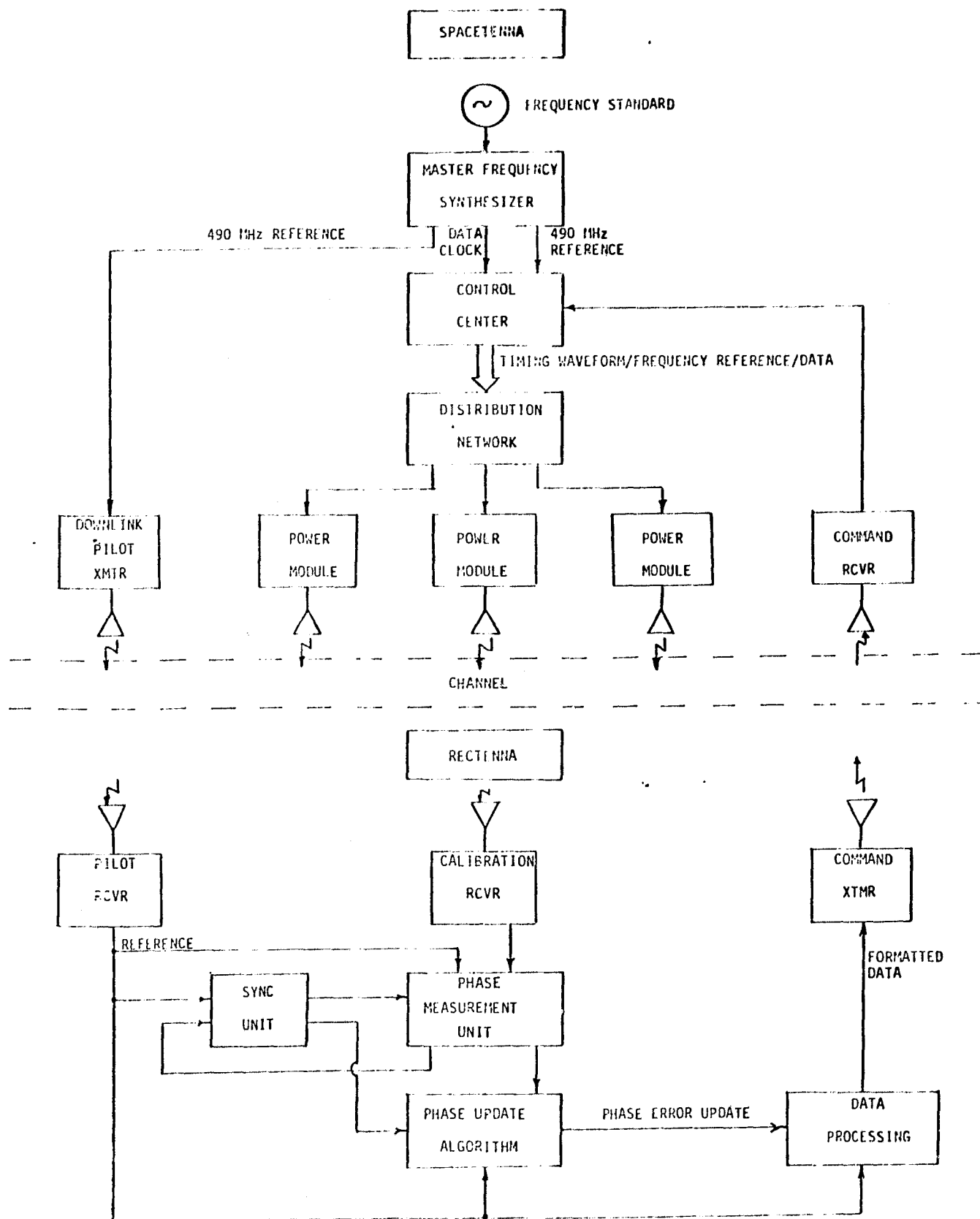


Figure 3. SPS Ground Based Phase Control Functional Block Diagram Showing System Timing Hierarchy.

provided by comparing

$$\varphi_+(1) - \varphi_-(1) = -\frac{2}{N}(\theta_i - \theta_R) - \frac{4\pi}{N}(k-n) + \phi_+(1) - \phi_-(1) + [M_+(1) - M_-(1)]2\pi \quad (4)$$

$$\frac{\varphi_+(2) - \varphi_-(2)}{2} = -\frac{2}{N}(\theta_i - \theta_R) - \frac{4\pi}{N}(k-n) + \frac{\phi_+(2) - \phi_-(2)}{2} + [M_+(2) - M_-(2)]\pi \quad (5)$$

If Δf is designed properly ($\Delta f < 50$ MHz) the left hand side of (4) and (5) are nearly equal. See Ref. 4 for a discussion on ionospheric effects. Equating (4) and (5) we have

$$\frac{\phi_+(2) - \phi_-(2)}{2} + [M_+(2) - M_-(2)]\pi \equiv \phi_+(1) - \phi_-(1) \pmod{2\pi} \quad (6)$$

Since we can measure $\phi_+(2)$, we can determine from (6) whether $[M_+(2) - M_-(2)]$ is odd or even. This then determines whether $[M_+(2) + M_-(2)]$ is odd or even, since $[M_+(2) - M_-(2)] + [M_+(2) + M_-(2)] = M_+(2)$ must be even. With this information, we can solve for $[\varphi_+(2) + \varphi_-(2)]/2 + (\theta_i - \theta_R)$ modulo 2π in (3).

5.0 Baseline System for Ground-Based Phase Control

The implementation of the ground-based phase control concept is determined by the phase control waveform designs employed. Based on our waveform selections, functional subsystems to implement the ground-based phase control concept are identified and functionally represented. The resultant ground-based phase control functional block diagram is depicted in Fig. 3 and includes:

- Satellite Signal Processing
 - Time-Frequency Control
 - Processing Control Center
 - Signal Distribution Network
 - Processing Power Module
 - Downlink Pilot Transmitter

- Uplink Command Receiver
- Ground Based Signal Processing
 - Pilot Beacon Receiver
 - Calibration Receiver
 - Phase Measurement Unit
 - Synchronization Unit
 - Phase Update Algorithm
 - Data Processing Unit
- Uplink Command Transmitter

The ground-based system envisioned employs satellite based frequency/timing reference with an IF frequency of 490 MHz. A 4-tone measurement scheme using frequencies at $2,450 \pm 9.57$ MHz and $2,450 \pm 19.14$ MHz is selected. Each power module devotes 10 μ sec per second for phase correction measurement, representing a minimal loss in total power transmitted. Two frequencies are chosen for the downlink and one frequency for uplink; the downlink pilot signal center frequency is set at 4.9 GHz.

Our preliminary investigation indicates that the effects of power beam interference and thermal noise on the phase measurement error can be controlled to a tolerable level. The ground based system can also function if the ionosphere is nonturbulent in nature and the satellite's tilt rate is limited to 0.5 min/sec .

6.0 Limiting Factors of the Feasibility of Ground-Based Phase Control System

The feasibility of the ground-based phase control concept becomes unclear if the conditions on the ionosphere and the satellite motion are not met. The ground-based phase control system can only correct for random phase fluctuations which have a correlation time that is large

compared with 1.25 sec. The noise components which are faster than 1.25 sec is uncompensated for and result in a degradation on transmission efficiency. Unfortunately, measured ionosphere data which is suitable for the SPS system is not readily available. (Most data are concerned with spatial correlations rather than temporal correlations. Also, most data are measured from low orbit satellites rather than geostationary satellites.) The other limiting factor is the statistical behavior of the random pointing error exhibited by the spacetenna. Again, the fast component of this error is not corrected for and it contributes to efficiency degradation. At this point, we feel that the development and specification of models for ionospheric phase disturbance and satellite motion is essential. It is hoped that our findings can serve as a guideline for any parallel efforts in studying these two factors.

REFERENCES

1. Lindsey, W. C., and Kantak, A. V., "Automatic Phase Control in Solar Power Satellite Systems," Prepared for NASA/JSC, TR-7809-0977, September 1977, LinCom Corporation, Pasadena, CA.
2. Lindsey, W. C., "A Solar Power Satellite Transmission System Incorporating Automatic Beam Forming, Steering and Phase Control," Prepared for NASA/JSC, June, 1978, LinCom Corporation, Pasadena, CA.
3. Lindsey, W. C., and Kantak, A. V., "SPS Phase Control System Performance via Analytical Simulation," Prepared for NASA/JSC, February, 1979, LinCom Corporation, Pasadena, CA.
4. Chie, C. M., "A Ground Based Phase Control System for the Solar Power Satellite," Prepared for NASA/JSC, January, 1979.

AN INTERFEROMETER-BASED PHASE CONTROL SYSTEM

James H. Ott

James S. Rice

Novar Electronics Corporation, Barberton, Ohio

ABSTRACT

An interferometer-based phase control system for focusing and pointing the SPS power beam is discussed. The system is ground based and closed loop. One receiving antenna is required on earth. A conventional uplink data channel transmits an 8-bit phase error correction back to the SPS for sequential calibration of each power module. Beam pointing resolution is better than 140 meters at the Rectenna.

INTRODUCTION

Key to focusing and pointing the SPS power beam is the maintenance of precise phase relationships among the transmitted signals of each Spacetenna subarray. Specifically, the signals transmitted by each power module must arrive at the center of the Rectenna in phase. This results in a power beam having a planar wavefront pointed at the center of the Rectenna. However, structural deformations in the Spacetenna can, if not compensated for, alter the phases of the power module signals at the Rectenna by altering the path lengths of the signals between the power modules and the Rectenna. In addition, variations within the Spacetenna circuitry can also alter the phases of the signals.

Novar Electronics Corporation has developed an interferometer-based phase control system.¹ This approach, which we call Interferometric Phase Control (IPC), has three significant characteristics which differentiate it from the Reference System retrodirective approach.

1. Interferometric Phase Control is a ground based closed loop system.
Unlike in the retrodirective approach, the phase correction information is obtained on earth by measuring the resultant power transmission of the Spacetenna power modules and comparing them against a reference.
2. The Spacetenna's power modules are calibrated sequentially.
A signal from a reference transmitter near the center of the Spacetenna is sequentially phase compared with a calibration transmission of each of the power modules.
3. During normal power transmission, the frequency of each power module is shifted slightly during phase calibration.
Maintenance of a properly focused and pointed power beam can be accomplished concurrently with the normal transmission of power from the SPS by using frequencies for calibration which are different from the power beam frequency.

SYSTEM DESCRIPTION

On or near the Rectenna site, an antenna called the Phase Measurement Antenna (PMA) receives the transmission from the Spacetenna Reference Transmitter (SRT) and the particular power module being phase tuned (calibrated). Analysis of these signals provides sufficient information to generate a phase error correction term which is sent up to the on-board phase control circuitry, shown in Figure 1, of the power module undergoing calibration.

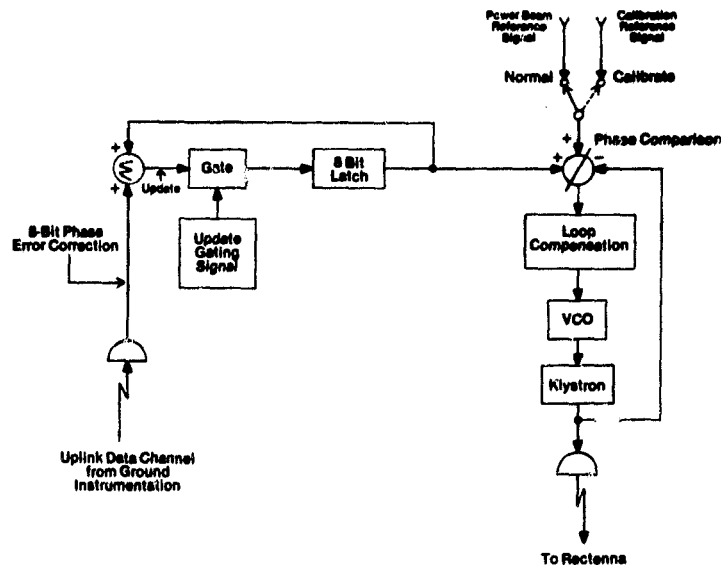


FIGURE 1
POWER MODULE PHASE CONTROL CIRCUITRY

Phase Tuning During Normal Power Transmission

Simultaneous with the transmission of the power beam, coherent signals at three different frequencies are transmitted from the Spacetenna. Two of these signals are transmitted from the SRT, which is located near the center of the Spacetenna, and one is transmitted from the power module being phase tuned, as shown in Figure 2. The two signals transmitted from the SRT are respectively called s_1 and s_{r1} , and the signal transmitted by the power module being phase tuned is called s_2 . The frequency of s_1 is midway between that of s_{r1} and s_2 so that the beat frequency of s_1 and s_2 is the same as that of s_1 and s_{r1} .

At the PMA, simple mixing and filtering circuitry detects two difference frequency signals. One signal is due to s_1 and s_2 . The other, which is called a phase reference signal, is that due to s_1 and s_{r1} . These two beat frequency signals are then phase compared.

The phase comparison gives the phase difference between the two beat frequency signals which is a function of π -axis deformations* in the power module being phase tuned plus biases in the phase feed network of the SPS. Certain components of the phase difference change with a change in frequency, others do not. Since the power module being phase tuned is transmitting at a frequency different from the power beam frequency, it is necessary to distinguish between these frequency dependent and frequency independent components in order to determine the phase

*deformations in a direction toward or away from the Rectenna.

correction that will be correct at the power beam frequency. This is done by shifting s_{r1} and s_2 to a different set of frequencies, according to a phase ambiguity error avoidance criterion, and making a second phase difference measurement. These two phase difference measurements are numerically adjusted by -2π , 0, or $+2\pi$ according to a second phase ambiguity error avoidance criterion. These two numerically adjusted phase differences provide sufficient information to calculate the phase error correction² transmitted back to the SPS power module being phase tuned. This phase error correction can be made with an 8-bit binary word sent to the SPS via a data channel. An 8-bit accuracy produces a phase resolution of $360^\circ / 2^8 \approx 1.4^\circ$. This is sufficient to give a power beam pointing resolution better than 140 meters at the Rectenna.

A tradeoff exists between satellite bandwidth requirements and the power module updating rate which is limited by filter settling times. It is anticipated that the frequency separation between s_1 , s_2 , s_{r1} and the power beam will be on the order of 1 MHz. At these frequency separations, the update interval for an entire Spacetenna could be on the order of a few seconds. It is possible that this will be fast enough to correct for any changes that will occur at the Spacetenna due to deformations, thermal effects, etc.

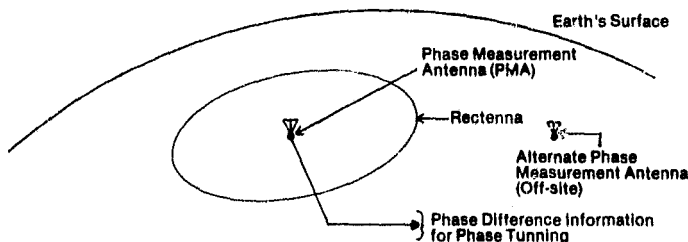
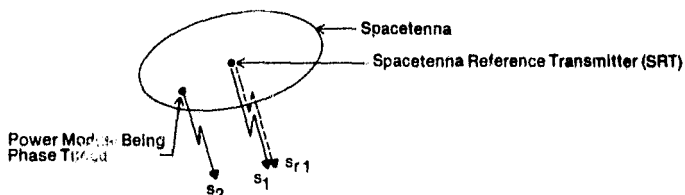


FIGURE 2
INTERFEROMETRIC PHASE CONTROL
Pictorial representation of relationship between space-
tenna signals and ground instrumentation.

Phase Tuning During Startup

It is also possible to use this interferometer technique to phase tune the power modules at the power beam frequency during initial startup or maintenance. This would be necessary to calibrate the phase tuning system used during normal power transmission for any phase vs. frequency nonlinearities. In this case, the measured phase difference is the phase error correction.

IONOSPHERIC EFFECTS

With the ground based closed loop interferometer phase control approach, ionospheric effects are limited to phase errors introduced into the space-to-earth transmission path only.

Although, the PMA is shown to be at the center of the Rectenna, it is not necessary that it be located there or even within the Rectenna site. Off-site measurement has the advantage that the signals being phase tuned do not have to pass through an ionosphere that may be subjected to undetermined heating effects by the power beam.

An important advantage of Interferometric Phase Control is its inherent ability to make use of statistical error reduction techniques to minimize any ionospheric effects. This includes time averaging and/or spatial averaging using several on and off-site phase measurement antennas.

PREDICTION OF DEFORMATION DYNAMICS/MAPPING

It should be pointed out that once the Spacetenna has been initially phase tuned, learning curves or adaptive modeling techniques could be used to predict the dynamics of Spacetenna structural deformations. With such predictions, it is felt that the capability would then exist to phase tune the entire Spacetenna based on frequency measurements of only a "few" key power modules and occasional measurements of the rest. By adding two additional receiving antennas on the earth so that there are three earth antennas spaced a few kilometers apart and not in a straight line, additional phase measurements can be made. These measurements provide information to "map" the face of the Spacetenna, that is, to determine the relative distance, direction and motion of each power module with respect to the SRT. This provides the capability for performing a transverse modal analysis, from the earth, of select samples of power modules on the face of the Spacetenna. In addition, the interferometer phase control technique provides the ability to automatically identify defective power modules.

CONCLUSIONS

Interferometric Phase Control (IPC) was originally developed as a closed loop, ground control approach for focusing and steering the power beam because of Novar's concern over effects that the ionosphere might have on the pilot beam of the retrodirective system. IPC could provide a useful adjunct to the retrodirective system to mitigate phase biasing problems with the retrodirective system and to provide a backup system if there are times when the atmosphere/ionosphere precludes use of a retrodirective system. Until definitive studies have been completed on the atmospheric/ionospheric effects on the retrodirective system, Novar recommends the simultaneous development of power beam control techniques using both the retrodirective approach and IPC.

REFERENCES

1. J. H. Ott and J. S. Rice: "Digital SPS Phase Control Using Traveling Wave Interferometry" Novar Electronics Corporation Technical Report, October, 1978.
2. Ibid., p. 32.

A SONIC SATELLITE POWER SYSTEM MICROWAVE POWER TRANSMISSION SIMULATOR

James H. Ott
James S. Rice
Novar Electronics Corporation, Barberton, Ohio

ABSTRACT

A simulator is described which generates and transmits a beam of audible sound energy mathematically similar to the SPS power beam. The simulator provides a laboratory means for analysis of ground based closed loop SPS phase control and of ionospheric effects on the SPS microwave power beam.

INTRODUCTION

Novar Electronics Corporation is in the final stages of constructing and testing a Satellite Power System Microwave Transmission Simulator. In a ground based laboratory environment, the simulator generates and transmits a beam of audible sound energy which is mathematically similar to the microwave beam which would transmit energy to earth from a Solar Power Satellite.

SIMULATOR DESCRIPTION

Figure 1 shows the major functional parts of the simulator. The Sonic Spacetenna (Figure 2) is 1.3 meters in diameter and contains 3200 independent transmitting elements. These elements are connected in a 64 row by 64 column matrix. Each column is driven by a driver which multiplexes each of the 64 rows 32,000 times per second. This enables the simulator's computer to control the amplitude, phase, and frequency of each of the 3200 transducers. The simulator is designed to transmit a coherent sonic power beam at 12 kHz. Any illumination taper, e.g., Gaussian, can be programmed and the resultant ground pattern studied. A computer, RAM Memory, 300 MB disc drive, and line printer are incorporated to provide a very high degree of experimental flexibility.

SIMULATOR CAPABILITIES

A unique feature of Novar's Sonic Simulator is its ability to provide actual photographs of the transmitted power beam. Figure 3 shows a scanning system which provides an intensity modulated raster of the sonic beam. By adding a phase signal to the intensity modulator, the phase coherence can also be photographed. This technique, developed at Bell Labs in the early 1950's will provide photographic records similar to Figure 4.

As soon as the Sonic Simulator is operational (mid-February, 1980), its initial use will be to generate a collimated coherent sonic beam to verify that the beam divergence and sidelobe characteristics are in satisfactory agreement with the aperture illumination equations which have been used to define the SPS microwave beam.

The concept of "ground based" phase control implies a closed loop phase control system which makes corrections in deviations in SPS beam pointing and focusing from ground based measurements of the received power beam. In other words, ground based phase control is a servo control system which like any servo system has a measurable transfer function, frequency response, step response, noise factor, resolution, loop stability, etc. Novar is using its

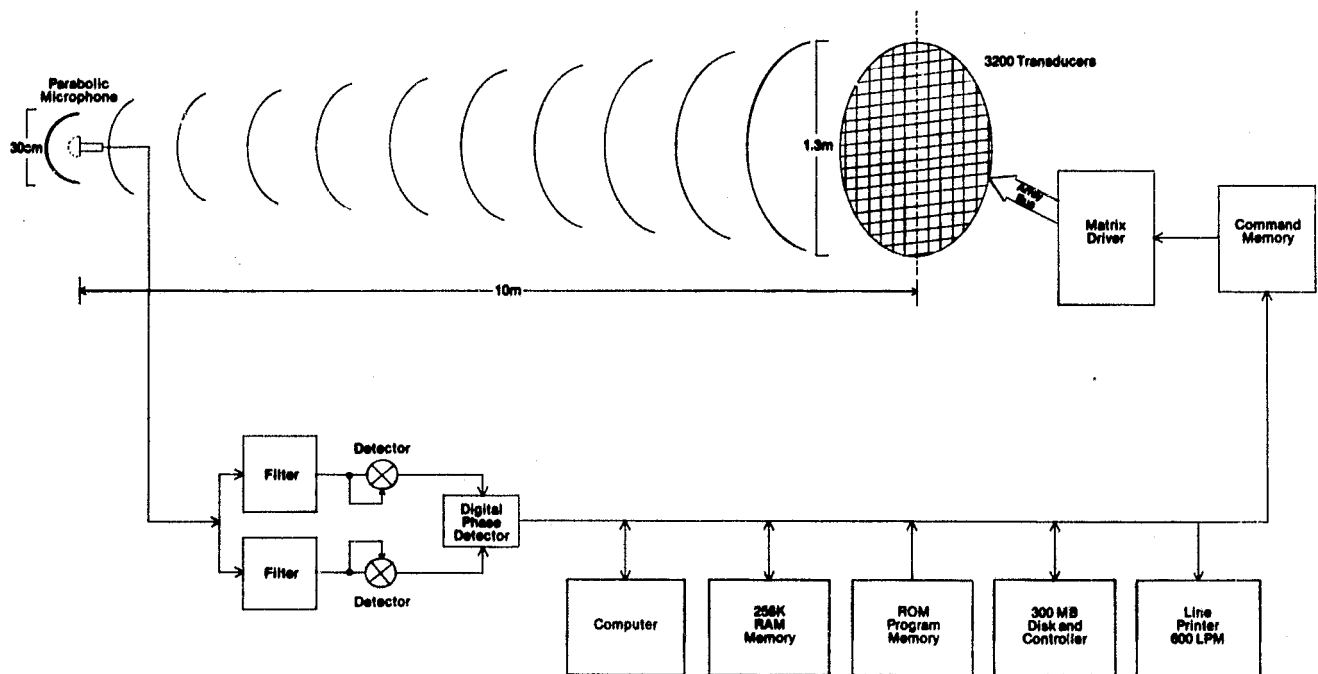


FIGURE 1
SONIC SPS PHASE CONTROL SIMULATOR
MAJOR FUNCTIONAL BLOCKS

interferometer phase control technique to focus and point the sound beam. The open and closed loop characteristics of the Sonic Simulator will be measured. A descriptive servo loop diagram and transfer function will be developed and all measured characteristics will be tested for agreement with control system theory. The next step will then be to analyze and mitigate the effects of unwanted interfering inputs such as air currents in the laboratory and the reflection of the sonic beam off walls.

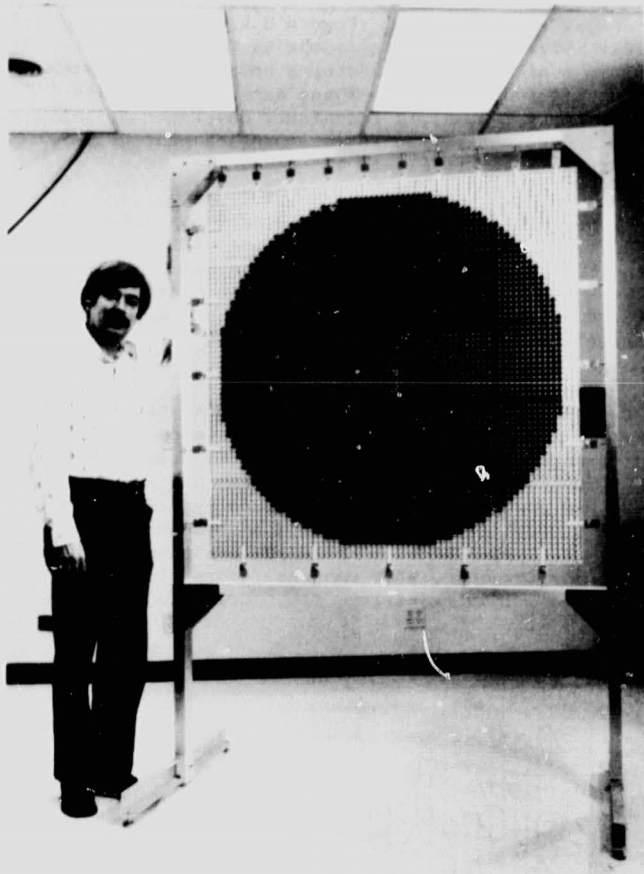


FIGURE 2
SONIC SPACETENNA

The Sonic Simulator can be readily forced to deal with the same noise characteristics as the ionosphere would introduce into the real world SPS phase control system. This would be accomplished by altering the propagation of the simulator's sonic beam through the use of sculptured reflecting surfaces and controlled air turbulence.

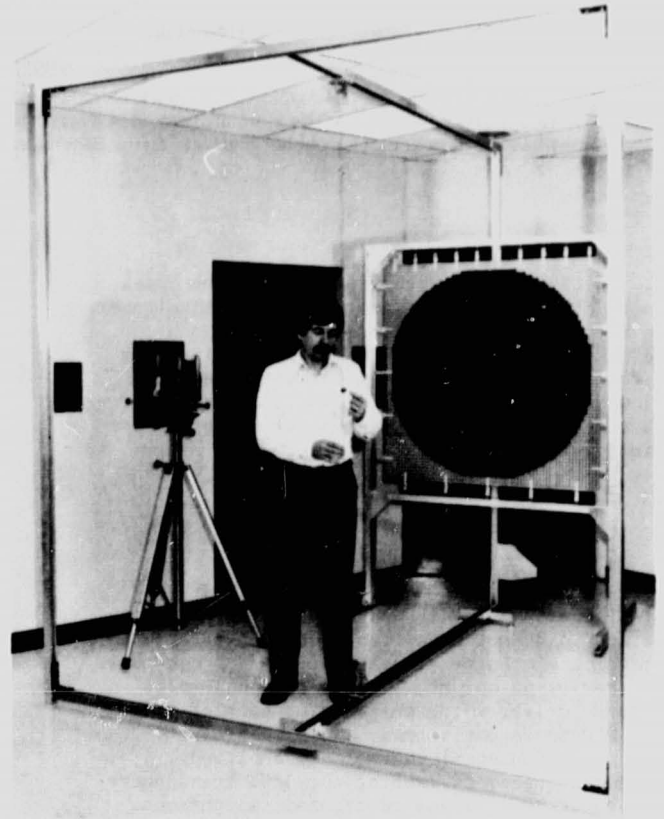


FIGURE 3
PHOTOGRAPHIC SCANNING SYSTEM
A precision mechanical scanning system provides an actual photograph of the sonic beam. The camera lens remains open in a darkened room while the sound-to-light modulator (device being pointed at) provides a light output proportional to the intensity of the sonic beam. The modulator is scanned up and down and forward and backward to provide a photograph of a cross section of the beam.

Ionospheric effects will impact an SPS Phase Control System similar to the way that noise and offset error impact any closed loop servo system. Therefore, conventional control system synthesis techniques should be able to reduce SPS phase control errors due to ionospheric effects.

Analytical techniques will be developed to permit the validation of these sonic propagation models against measured ionospheric parameters. This would, for example, lead to the quantitative correlation of ionospheric electron density patterns with the sound reflecting surface's roughness and placement.

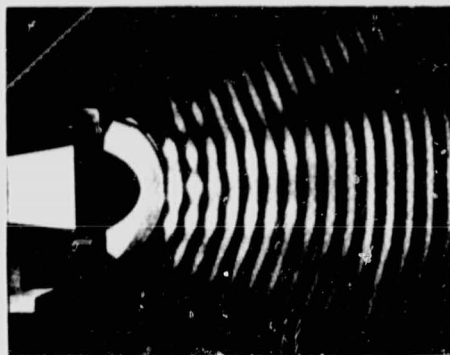
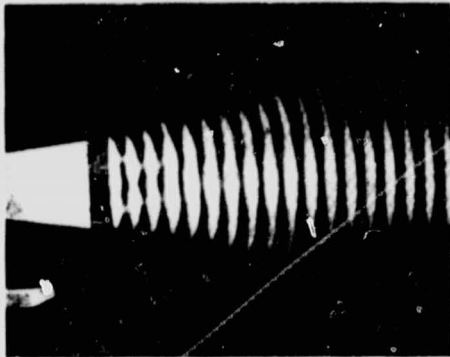


FIGURE 4
REPRESENTATIVE PHOTOGRAPH OF A MECHANICALLY
SCANNED SONIC BEAM (Bell System Technical Journal,
1951)

CONCLUSIONS

It is expected that a number of conclusions can be provided regarding the applicability of the sonic simulation technique to the future development of the SPS power transmission system. If conclusions are favorable, we would expect that the sonic simulator will provide a low cost alternative to many of the time consuming orbiting satellite experiments that would otherwise be necessary.

REFERENCE

1. W. E. Kock and F. K. Harvey, "A Photographic Method for Displaying Sound Waves and Microwave Space Patterns," Bell System Technical Journal, Vol. 30, July 1951, pp. 564-587.

SPS PHASE CONTROL STUDIES

W. W. Lund, B. R. Sperber, G. R. Woodcock
Boeing Aerospace Company

1.0 INTRODUCTION

To properly point and form the SPS microwave power beam, the outputs of the power amplifiers in the transmitting array must be phased in a specific and coherent fashion. The purpose of the SPS phase control system is to bring this about reliably.

A number of different phase control schemes can be, and have been, envisioned. The one selected for the SPS baseline system is a retrodirective CW phase conjugating system using a spread spectrum uplink signal and a reference phase signal that is distributed via fiber optics. The basis of this selection is relative technical simplicity and requisite assurance of success.

The operational principle of the retrodirective phase control system is that if a signal E_{Received} , described by

$$E_{\text{Received}} = \cos (wt + \phi_{\text{ref}} + \phi_{\text{rec}}) \quad (1)$$

is received, a phase conjugated signal

$$E_{\text{Transmitted}} = \cos (wt + \phi_{\text{ref}} - \phi_{\text{rec}}) \quad (2)$$

is transmitted. If this is done all over the transmitting aperture, the resulting beam will leave in the inverse direction of the incoming pilot beam.

Problematic technical aspects in implementing the scheme above are that the received and transmitted frequency spectra are dissimilar and that the reference phase ϕ_{ref} against which the received phase ϕ_{rec} is measured must be the same all over the transmitting array. (Regarding tolerable systematic phase shift, it may be noted that a phase shift of 3×10^{-2} radians will scan the beam approximately 40 meters.)

Transmitter noise, receiver noise and pilot beam power determine how close the pilot beam frequencies of the spread-spectrum uplink can be to the downlink. Studies at Boeing and elsewhere have yielded values for this offset in the range of 5 to 50 MHz. In the case of the most recent Boeing pilot link study, the network of considerations used was as shown on Figure 1, yielding the characteristics of the final system as a function of transmitting frequency notch filter cutoff frequency f_c , pilot beam receiving aperture and desired signal to noise of the received pilot signal shown on Figure 2.

For accurate pointing it is important that the received pilot signal be scaled to generate the transmitted downlink signal instead of merely translated. I.e., if the downlink frequency is f_0 , the pilot frequency is $f_0 + \Delta f = \omega/2\pi$ and the received field is given by Equation (1), the downlink should be:

$$E_{\text{transmitted}} = \cos \left[f_0 (f_0 + \Delta f)^{-1} (wt + \phi_{\text{ref}} - \phi_{\text{rec}}) \right] \quad (3)$$

instead of

$$E_{\text{transmitted}} = \cos \left[(\omega - 2\pi\Delta f)t + \phi_{\text{ref}} - \phi_{\text{rec}} \right] \quad (4)$$

The reason for this is that if frequencies are not scaled but translated by some amount Δf , the transmitted beam is incorrectly steered off the pilot beam axis by an amount W . W depends on the transmitting aperture tilt θ , the range of R and the transmitting frequency f according to the "squint" formula:

$$W = R \theta \Delta f f_0^{-1} . \quad (5)$$

For the baselined spread spectrum pilot signal Δf is effectively 0.

Selection of the specific spread spectrum uplink signal scheme and the decoding of the uplink at the receiver is pending further study of ways to mitigate ionospheric and tropospheric distortions of the uplink wavefront. The basic problem is that the index of refraction in the beam propagation path depends on the atmospheric pressure, composition, temperature and the degree of ionization; and in the troposphere the index of refraction increases with increasing density while in the ionosphere the opposite is true. A secondary problem is geometry: if there is only a single pilot beam just a small central portion of the propagation path through the troposphere and ionosphere is sampled. Finally, the effects of the power beam on the temperature and density of the ionosphere must not interfere with phase control or beam pointing.

The effect of phase errors on the transmitted beam is to distort the wavefront. The effect of average phase errors can be treated as a function of position in classical optical fashion to get beam offset, defocusing, astigmatism, distortion and similar quantities. The effect of random RMS phase errors $\bar{\delta}^2$, assumed not a function of position, is to reduce the main beam efficiency by the factor

$$\eta_{\text{random}} = e^{-\bar{\delta}^2} . \quad (6)$$

Because in general there is a residual on-axis $\bar{\delta}^2$ over a single phase controlled area proportional to that area, the above equation qualitatively illustrates the reason for the recent change in the baselined level of phase control from the sub-array level to the klystron power module level. The approximately factor of 10 average decrease in phase controlled area contributed to a smaller effective $\bar{\delta}^2$. The revenues from the extra received power of the now more efficient power beam over a satellite lifetime were found to adequately compensate for the increased phase control system cost. Other benefits associated with phase control to the module level include increased pointing accuracy and decreased waveguide tuning mismatches.

2.0 BASELINE PHASE CONTROL SYSTEM DESCRIPTION

The baselined phase control system, illustrated on Figure 3, consists of 101,552 klystron module level power amplifier phase control subsystems, as shown on Figure 4, and an 816-2/3 MHz reference phase distribution network of fiber optical cables and master slave returnable timing system repeater units as shown in Figure 5.

The reference phase distribution tree (to be described in more detail in the next section) has four levels culminating at the klystron module with no more than a 1:36 output branching, and constitutes most of the physical and operational (but not functional) complexity of the system. Its purpose is to provide identical phase reference phase signals to all klystron modules for use in conjugating the pilot to get the power downlink.

The klystron power amplifier phase control subsystems contain the phase control system's functional complexity insofar as they each receive and decode the

Reference phase control system element costs, estimated by standard aerospace avionics cost estimating methodology from the computerized Boeing Program Cost Model data base. After estimation of the first unit cost on the basis of platform, function and service factors the costing methodology used was to discount the per unit cost on a 70% learning curve through the 1000th unit. After this was assumed to saturate and per learning unit costs were constant. Table I summarizes characteristics of the phase control system units on board subarrays, while Table II summarizes the segments of the reference phase distribution system at levels above the subarray level.

The primary results of the cost estimations are that the phase control system costs total well under \$100 million and are dominated by the costs of the phase control pilot beam receivers. With more detailed reference satellite phase control system specifications there can be a requisite reduction in cost uncertainties. However, it should be noted that substantial (factor of two or more) reductions in phase control system cost are unlikely because current aerospace and electronic industry technology routinely deals with production runs such as those required for the SPS phase control system on equipment of comparable complexity.

spread spectrum pilot link signal, make any necessary corrections, conjugate it using the 816-2/3 MHz reference phase signal from the phase distribution tree and actively compensate for phase shifts suffered in the power amplifier and waveguide feed networks.

Fiber optic cabling was chosen over conventional coax for the reference phase distribution because of its lower mass, lower signal attenuation, and the fact that it has no short circuit failure mode. It also has lower phase delay and costs less. However, the phase delay variations are not low enough to eliminate the need of feedback (i.e., returnable timing systems) on all but the subarray (Level 4) reference phase control tree level. At the lowest level the length is so short that temperature induced variations in phase shift are judged to be tolerable.

NASA-funded technology development work at Boeing is currently developing 980 MHz fiber optic transmitters and receivers for SPS use. The expected successful completion of these and their demonstration with a 1 km cable should substantially verify that fiber optic technology can distribute the reference phase.

3.0 BASELINE SYSTEM RELIABILITY AND REDUNDANCY

It is clear that any reference phase control system that refers phases to central points has critical links when system reliability is considered. Because of this, the most central units in the reference system have been made redundant and autonomous.

The baseline transmitting array has three autonomous master reference phase receivers, which each transmit a reference phase signal via separate and redundant fiber optic cable links to each of twenty active Level 1 sector phase distribution units. (See Figure 7) These units select valid phase control signals and distribute them via redundant fiber optic cables to twenty Level 2 (group) distribution units. The group distribution units in turn tree the signal out further to 19 subarrays each. At the subarray, a last distribution unit sends the signal to each klystron module, where it is used as a reference for conjugation of the phase control pilot signal receiver output. The klystron is held in proper relation to the conjugated pilot beam signal by a control loop of its own that compensates for its internal phase shifts with temperature, time, and voltage.

An analysis of the basic reliability of the baseline configuration was performed by G.E. under subcontract to Boeing. The element reliabilities and basic configuration assumed are shown in Figures 7 and 8. For purposes of analysis the phase control system was considered as four segments. The first segment starts at the master reference receivers and continues through the sector reference distribution unit's selection switch SW_1 . The second segment is from the output of SW_1 to the output of the subarray group signal splitter B_{19} . A third segment runs from this splitter through to the output of the subarray splitter B_{mn} . Finally, the last segment was analyzed from the B_{mn} output to the klystron input.

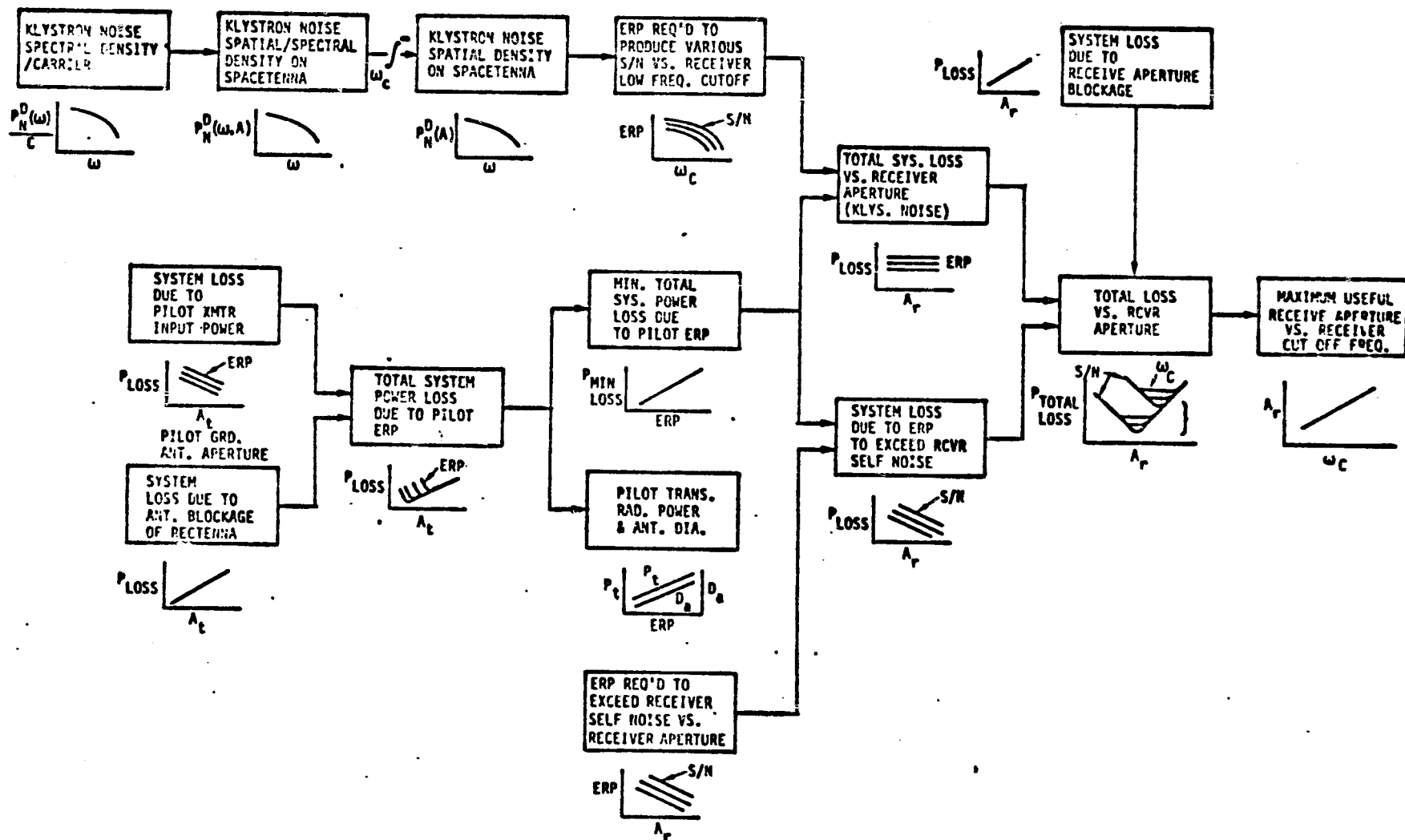


FIGURE 1. PILOT LINK ANALYSIS FLOW CHART

Table I. Intracubarray Phase Control System
Production Cost Characteristics

Subarray Type	Number of Klystrons	Subarrays of This Type	PCR Mass (kg)	PCR Cost (\$)	RPDS Mass (kg)	RPDS Cost (\$)	Length Cable (m)	Cable Mass (kg)	Cable Cost (\$)
1	4	1028	4.4	2240	1.0	595	33	3.7	73
2	6	1052	6.6	3360	1.0	595	49	5.4	108
3	8	612	8.8	4480	1.0	595	61	6.9	138
4	9	664	9.9	5040	1.0	595	72	8.0	160
5	12	900	13.2	6720	1.0	595	95	10.6	212
6	16	784	17.6	8960	1.0	595	132	14.5	290
7	20	628	22.0	11200	1.0	595	167	18.2	365
8	24	644	26.4	13440	1.0	595	197	21.6	433
9	30	632	33.0	16800	1.0	595	232	26.0	521
10	36	276	39.6	20160	1.0	595	296	32.5	649
TOTAL		7220	112 T	\$57M	7 T	\$4M		91 T	\$1M

Table II. Intersubarray Phase Control System
Production Cost Characteristics

Item	No. Req'd.	Avg. Unit	Per SPS (M)
Master Reference Receiver and Reference Phase Transmitter	3	424K	1.272
Cables	60	4.6K	0.276
Slave Repeaters	400	25.1K	10
Level 2 Cables	380	2.5K	0.95
			\$12.5M

Level 3 cables are common with
area-subarray data harness (see WBS 1.1.3)

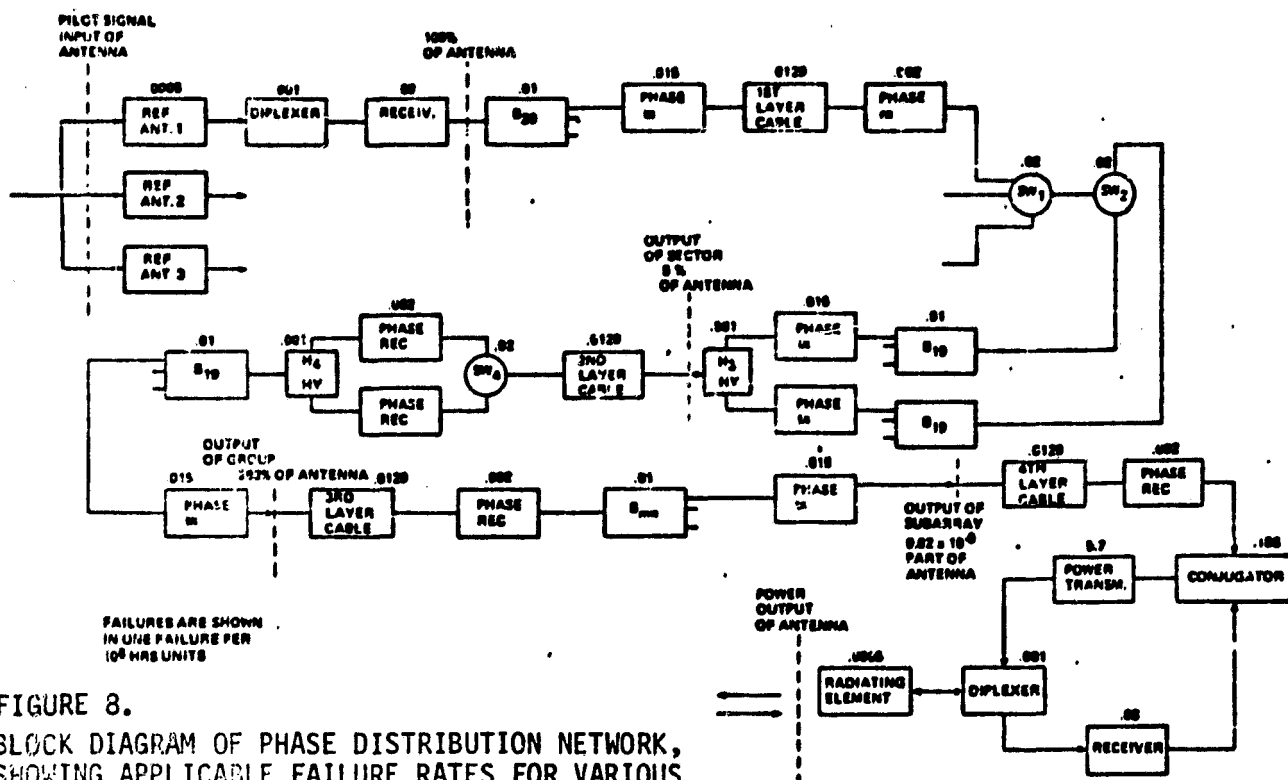


FIGURE 8.
BLOCK DIAGRAM OF PHASE DISTRIBUTION NETWORK,
SHOWING APPLICABLE FAILURE RATES FOR VARIOUS
COMPONENTS.

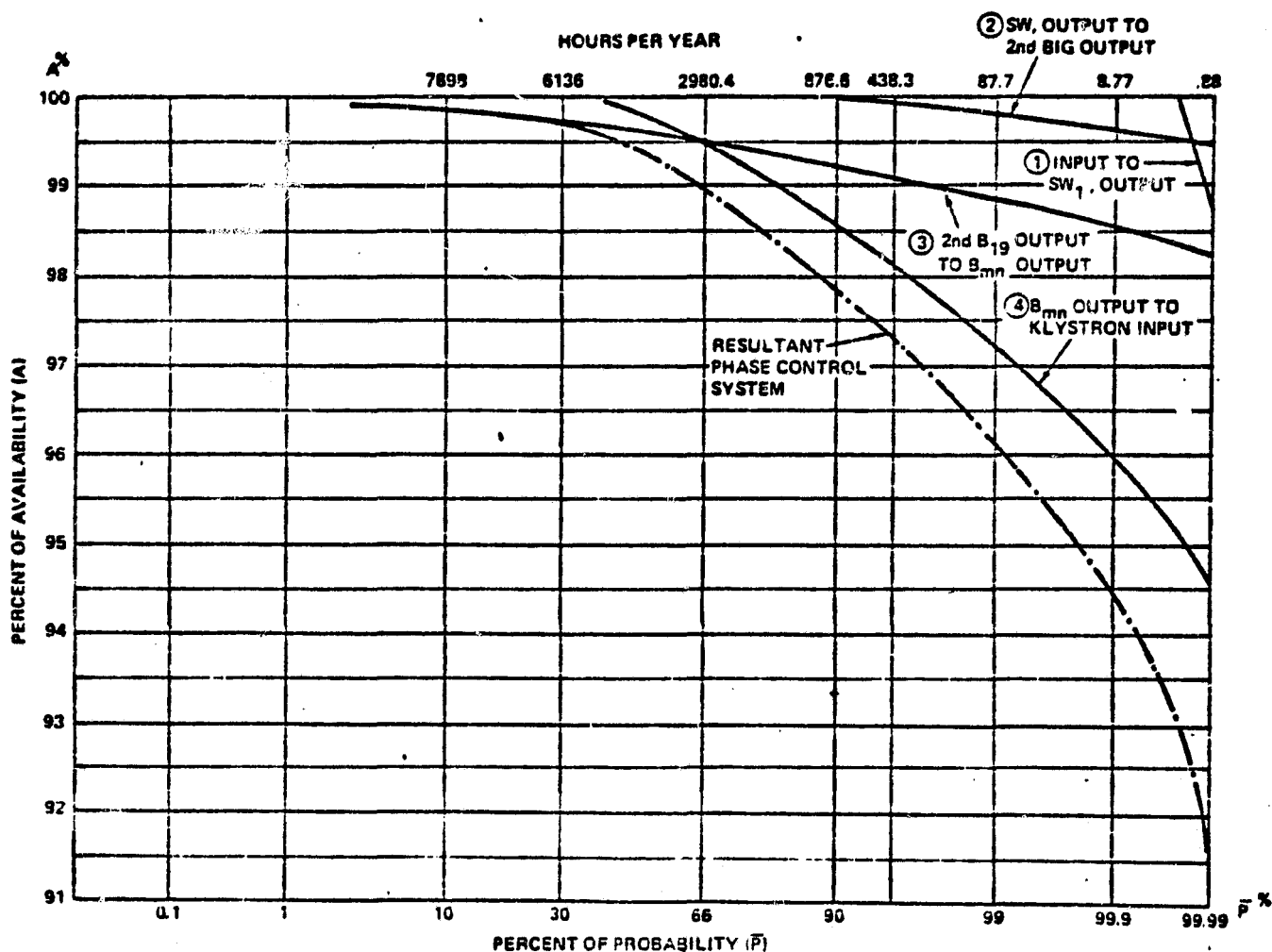


FIGURE 9. AVAILABILITY VS PROBABILITY FOR SPACE ANTENNA PHASE CONTROL SYSTEM
FROM INPUT OF PILOT RECEIVE ANTENNA TO KLYSTRON DRIVE INPUT.

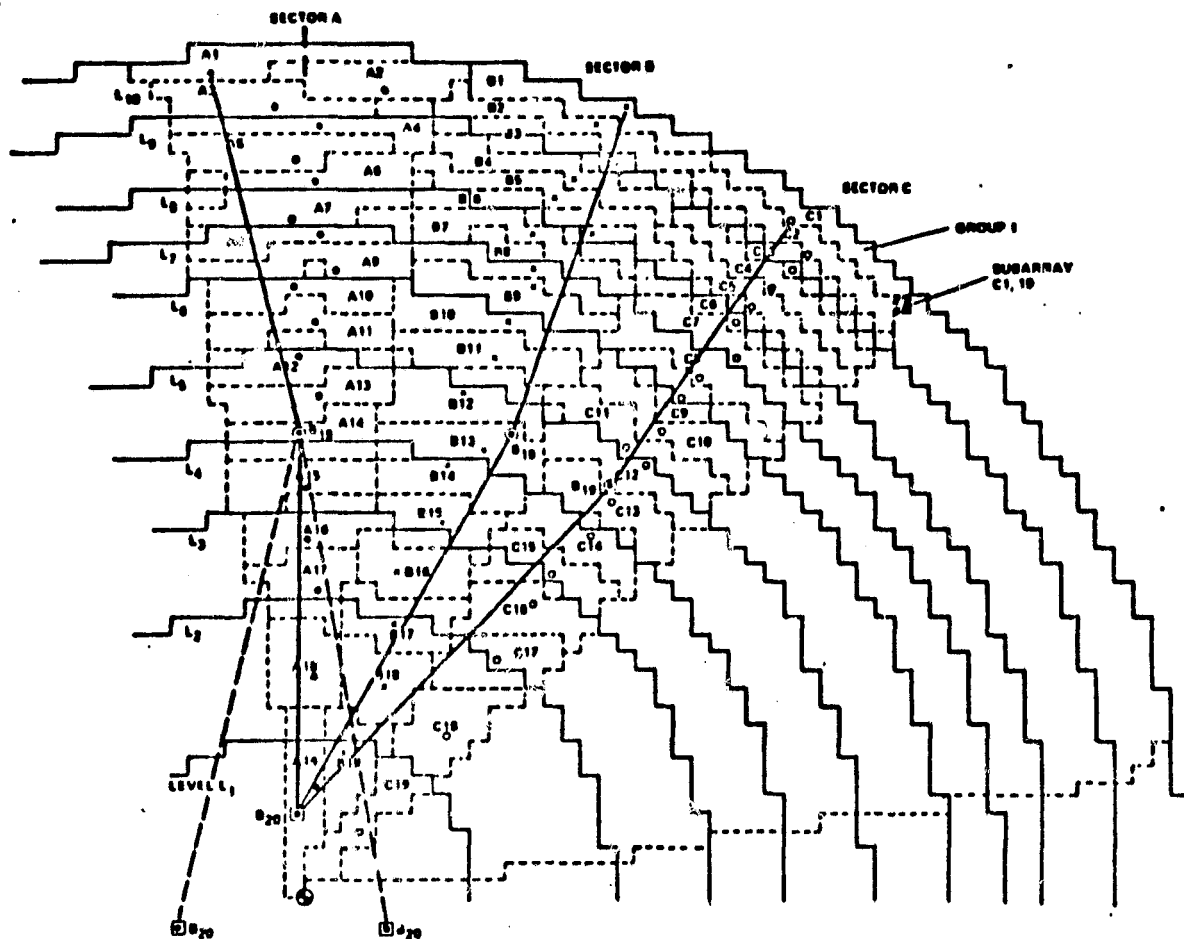


FIGURE 6. LOCATION OF REFERENCED PHASE REPEATER STATIONS OF SECTORS AND GROUPS

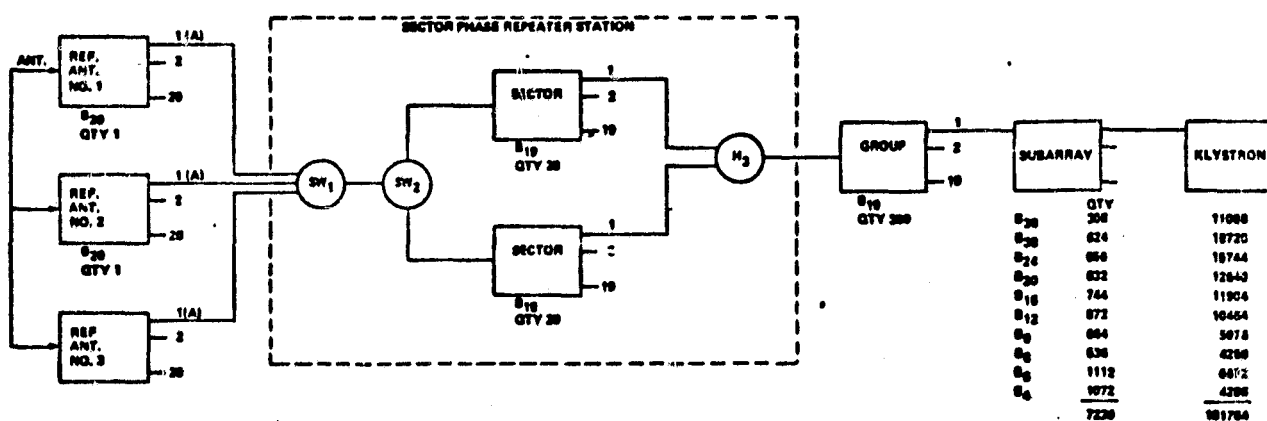


FIGURE 7. REDUNDANCY CONCEPT OF PHASE DISTRIBUTION NETWORK

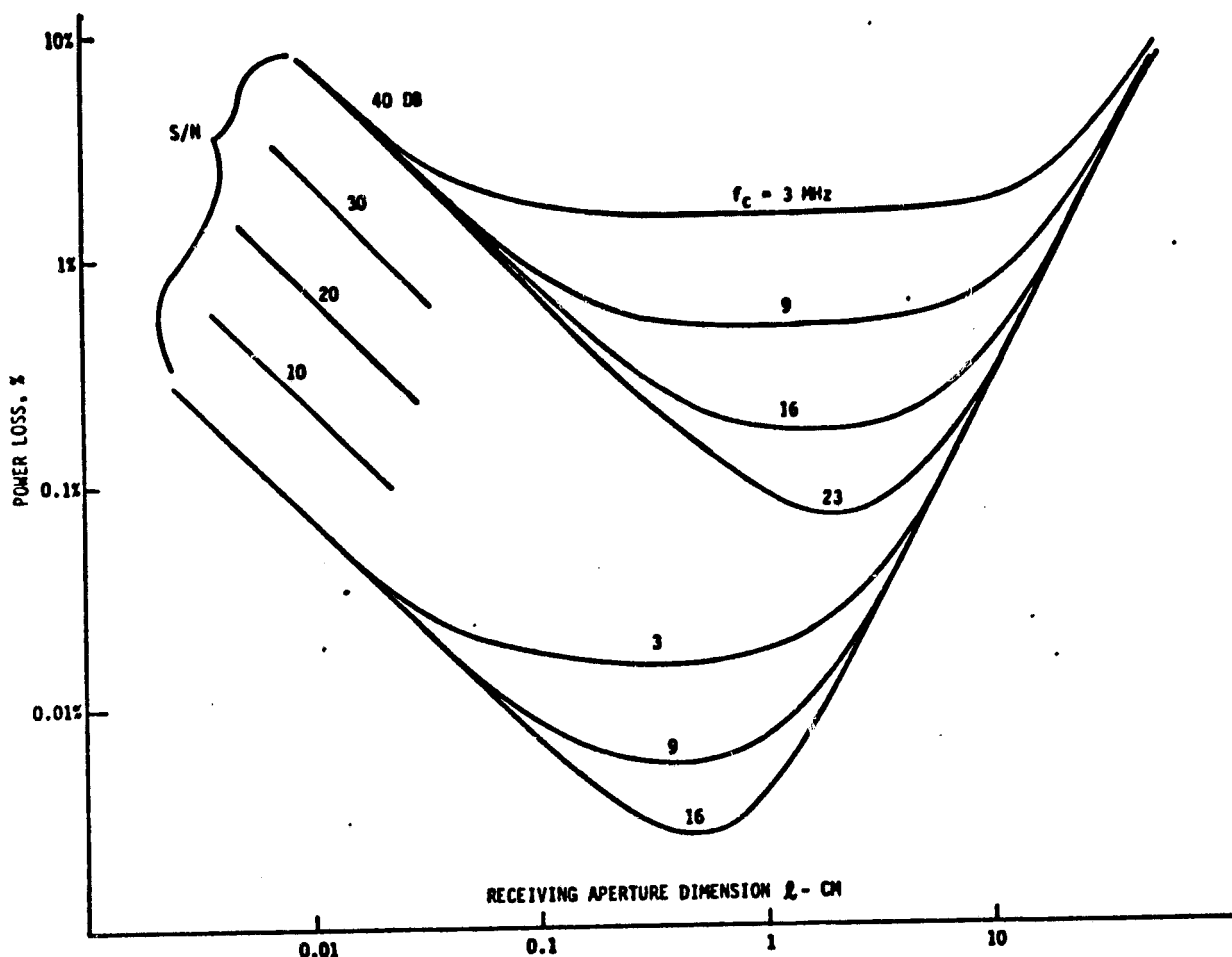


FIGURE 2. TOTAL SYSTEM LOSS VS. RECEIVE APERTURE

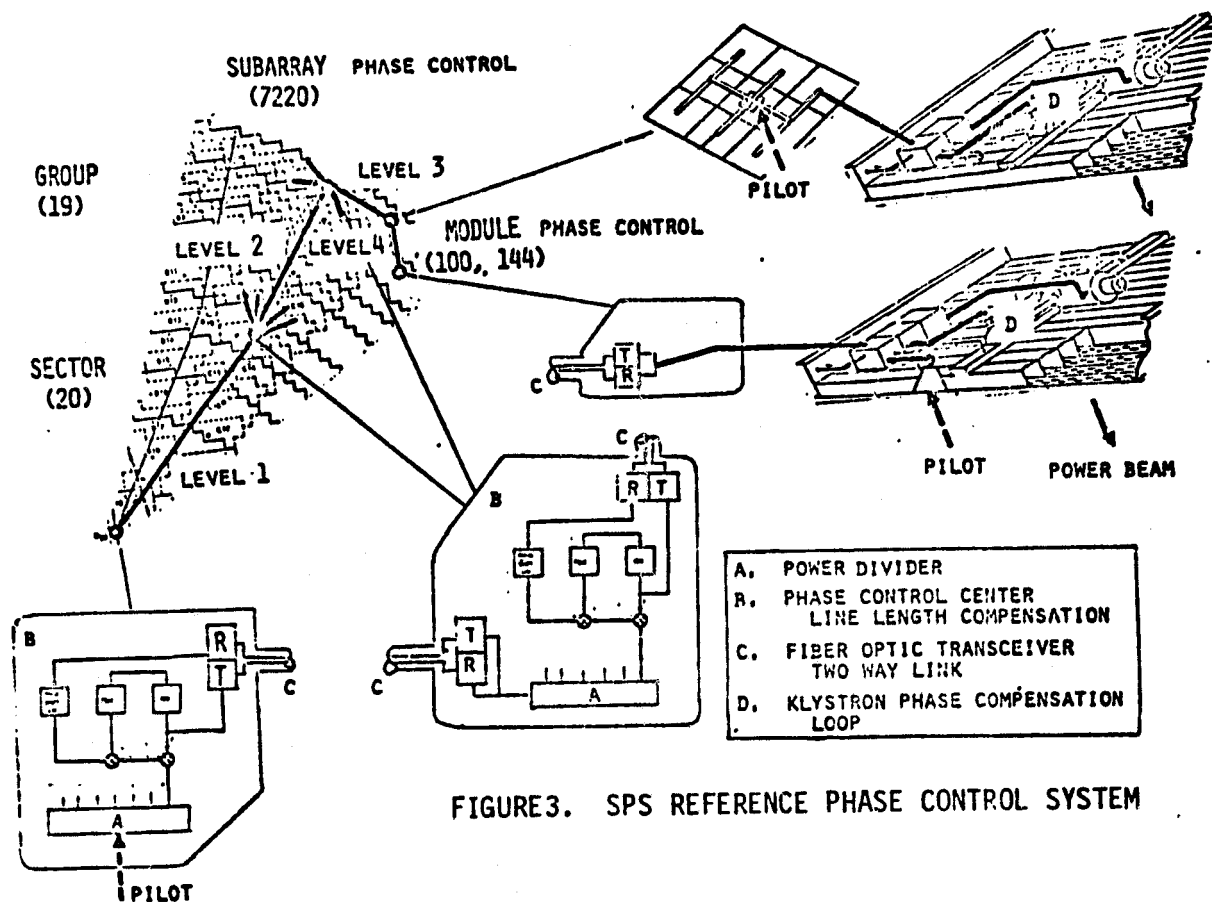


FIGURE 3. SPS REFERENCE PHASE CONTROL SYSTEM

SPS FIBER OPTIC LINK ASSESSMENT

T. O. Lindsay, E. J. Nalos
Boeing Aerospace Company

1. INTRODUCTION

Fiber optic technology has been tentatively selected in the SPS baseline design to transmit a stable phase reference throughout the microwave array. Over a hundred thousand microwave modules will be electronically steered by the phase reference signal to form the power beam at the ground receiving station. The initially selected IF distribution frequency of the phase reference signal has been set at 980 MHz or a submultiple of it.

Fiber optics offers some significant advantages in view of the SPS application. Optical transmission is highly immune to EMI/RFI, which is expected to be severe when considering the low distribution power (<1mW). In addition, there will be savings in both mass, physical size, and potentially in cost.

2. FIBER OPTIC LINK VERIFICATION PROGRAM

2.1 TASK DESCRIPTION

The purpose of the present program is to demonstrate feasibility of a fiber optic link at 980 MHz for SPS application. The specific tasks are: 1) Analyze existing optical fibers for use in the phase distribution fiber/optic link with emphasis on phase change effects and ability to transmit high frequency IF signals; i.e., low attenuation and adequate bandwidth; 2) Analyze suitable optical emitters and detectors to determine feasibility of operation and usage at 980 MHz; 3) Select and purchase optical emitters, detectors, and fibers for link development; 4) Design and construct impedance matching systems for matching the optical emitter and detector to laboratory equipment; and 5) Assemble and test a two-way link at 980 MHz consisting of matched detectors, emitters, and a two-fiber cable of minimum length of 200 meters.

In the present phase control system for SPS, a two-way link is required in the phase distribution system at each level to achieve phase compensation for phase changes induced by temperature changes and other property changes in the electronic circuit.

2.2 FIBER OPTIC LINK DESIGN

The results of the component selection for the fiber optic link are summarized in Table 1 below.

TABLE 1: COMPONENT SELECTION FOR FIBER OPTIC TEST LINK

Component	Type	Features
Emitter	GaAlAs Multi-Mode Injection Laser Diode	1. Moderate cost 2. High power 3. High modulation bandwidth
	GaAlAs Single-Mode Injection Laser Diode*	1. High power 2. High coupling eff. 3. High bandwidth 4. Low distortion
	Light Emitting Diode (LED)	5. Low threshold 6. High reliability 7. Narrow spectral width 1. No threshold current 2. Low distortion 3. Low cost 4. Stable operating point

TABLE 1: COMPONENT SELECTION FOR FIBER OPTIC TEST LINK (Continued)

Component	Type	Features
Detector	Silicon Avalanche Photodiode*	<ol style="list-style-type: none"> 1. Gain - BW product \approx 80 GHz 2. High RCVR S/N 3. Moderate cost
	Silicon PIN Photodiode	<ol style="list-style-type: none"> 1. Low bias voltage 2. Stable operating point 3. Low cost
Fiber	Step-index glass Multi-mode	<ol style="list-style-type: none"> 1. Low cost 2. Low attenuation
	Graded-index glass Multi-mode*	<ol style="list-style-type: none"> 1. Moderate cost 2. High bandwidth 3. Low attenuation
	Step-index glass Single-mode	<ol style="list-style-type: none"> 1. Extremely high bandwidth 2. Low attenuation 3. Poor coupling efficiency

*Selected for link development

As a result of the investigations, multi-mode graded index fiber was chosen due to its high bandwidth, low attenuation, availability, and high coupling efficiency with injection laser diodes; single-mode injection laser diode was selected for its high bandwidth, high output, and excellent linearity; and an avalanche photodiode was selected because of its high bandwidth and superior sensitivity.

The link will operate at a wavelength of 820 nm where present laser diodes and avalanche photodiodes are readily available and offer good reliability. Fiber attenuation although not minimum, reaches an acceptable value at 820 nm also.

The injection laser diodes were purchased from Nippon-Electric in Japan; the two-fiber cable was obtained from Siecor (fibers manufactured by Corning Glass Works); and the avalanche photodiodes from RCA.

One of the problems to be solved for the 980 MHz feasibility link was to develop simple, but effective, signal coupling techniques for the emitter and detector. The approach chosen is illustrated schematically in Figure 2. The use of the 47Ω resistor in series with the injection laser diode causes approximately 50Ω to be seen by the driver amplifier and it also aids in converting the driver output to a current source which is needed by the diode for linearity. The output signal current from the avalanche photodiode flows directly into the 50Ω input impedance of the laboratory amplifier. In both cases, the dc biasing networks are isolated from the signal paths by shorted quarter-wave microstrip techniques.

2.3 EXPERIMENTAL RESULTS

The results of an initial test to couple 980 MHz through a sample link are shown by Figure 2. The fiber length was 300 meters and the type is similar to that to be used in the two-way link development. Results are listed for two values of detector biasing. The output voltage waveforms were monitored using a sampling oscilloscope and, in both cases, the trace was stable and noise-free.

The test setup was similar to that shown in Figure 3. The emitter and detector modules are towards the right foreground shown with a length of coiled fiber optic cable. Laboratory equipment includes a 980 MHz frequency synthesizer, a vector voltmeter, oscilloscope, preamplifier, and biasing and monitoring equipment.

The emitter and detector modules used in the initial test are shown in Figure 4a and 4b. The thermal environment aboard the SPS is expected to be widely variable with values anticipated between -50°C and $+150^{\circ}\text{C}$. Therefore, a major subject of interest involves the variation in propagation time through a fiber as temperature is changed. Propagation time is directly related to the transmitted phase and is known to be affected by thermal expansion and refractive index variation. Data was also taken to determine the magnitude of the phase variation versus temperature as illustrated in Figure 6. The phase sensitivity is not low enough to obviate the need for phase compensation except possibly for the shortest (last) level of phase distribution.

For a one-way link length of 200 meters, the transmitted phase would vary approximately 2.5 degrees for every $^{\circ}\text{C}$ of temperature change at 980 MHz. This rate is acceptable with the present phase control system because of the two-way link length compensation. The two lengths of fiber will be adjacent for the total link, providing accurate tracking and matching.

At the outer levels of the phase reference distribution network, the link lengths average 10 meters and comprise over 90% of all of the elements. It may be possible to eliminate the return link in such cases as the phase shift will be greatly reduced for the short runs, averaging 0.125 degrees of shift per $^{\circ}\text{C}$.

As fiber optic technology progresses, longer wavelengths should be investigated where bandwidth and attenuation characteristics are superior for fused silica fibers. It is anticipated that phase shift sensitivity may be reduced at longer wavelengths because of dispersive changes in the refractive index. Fiber optics represent a promising approach for the phase distribution system for the SPS and merit further development to realize their full potential.

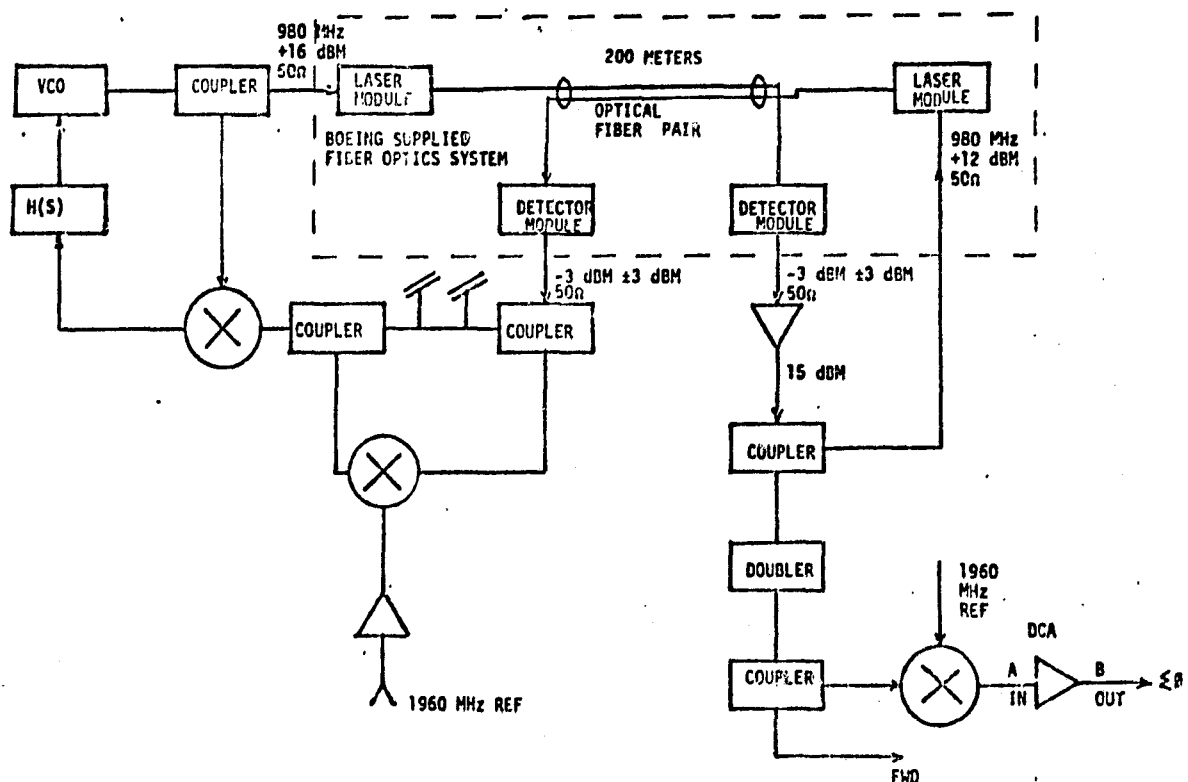
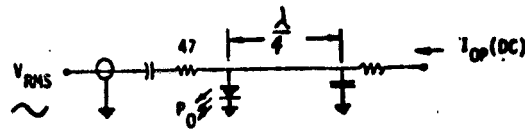


FIGURE 1 TEST CONFIGURATION FOR 2 WAY FIBER OPTIC LINK.

ORIGINAL PAGE IS
OF POOR QUALITY

EMITTER MODULE:

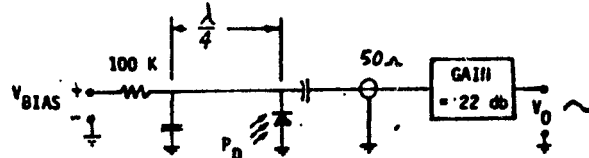
I_{THRESH} = 60 ma
 I_{OP} = 67 ma DC
 V_{MOD} = 0.7 V RMS
 P_O = 262 μ Watts I_{IN}



DETECTOR MODULE:

V_{BIAS}	185 Volts	315 Volts
V_O	71 MV RMS	283 MV RMS
P_O	19.1 μ Watt	19.1 μ Watt

Out



FIBER: CORNING IVPO

Length = 303 Meters
 Atten = 3.9 db/km @ 900 nm
 BW = 870 MHz-km
 N.A = 0.218

FIGURE 2 FIBER OPTIC LINK DESIGN SPECIFICATIONS

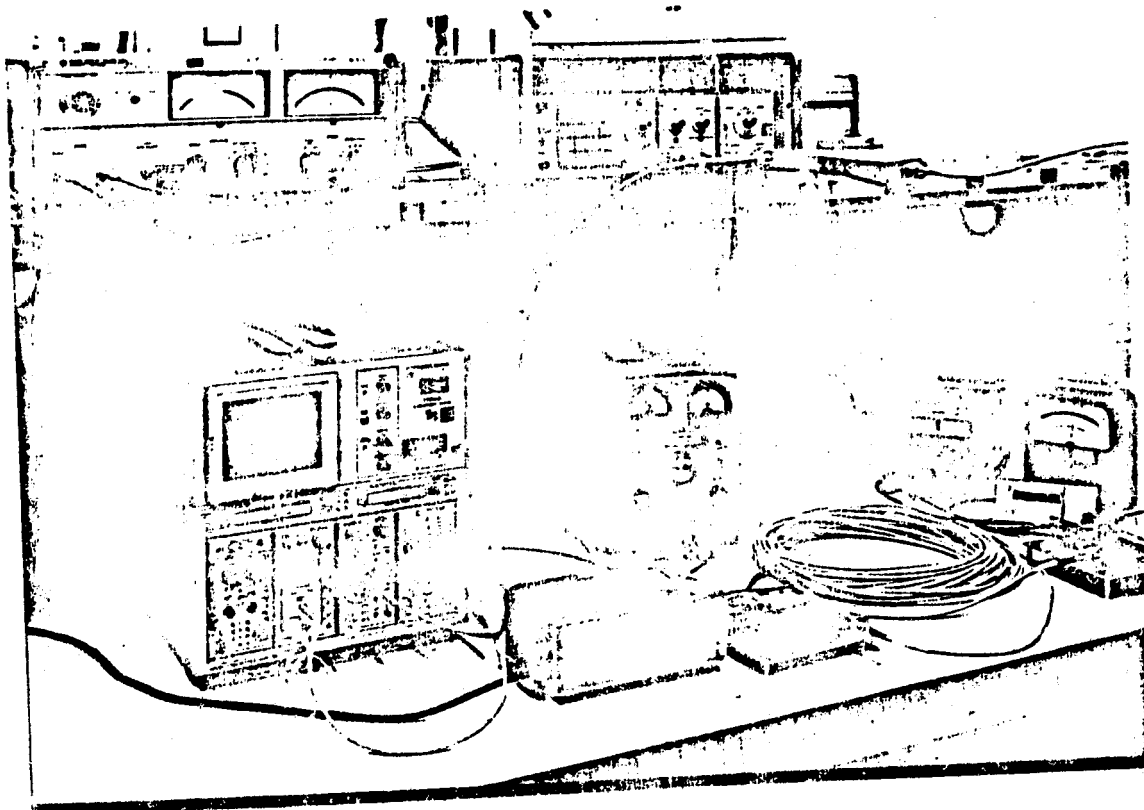


FIGURE 3 INITIAL 980 MHz LINK TEST SETUP

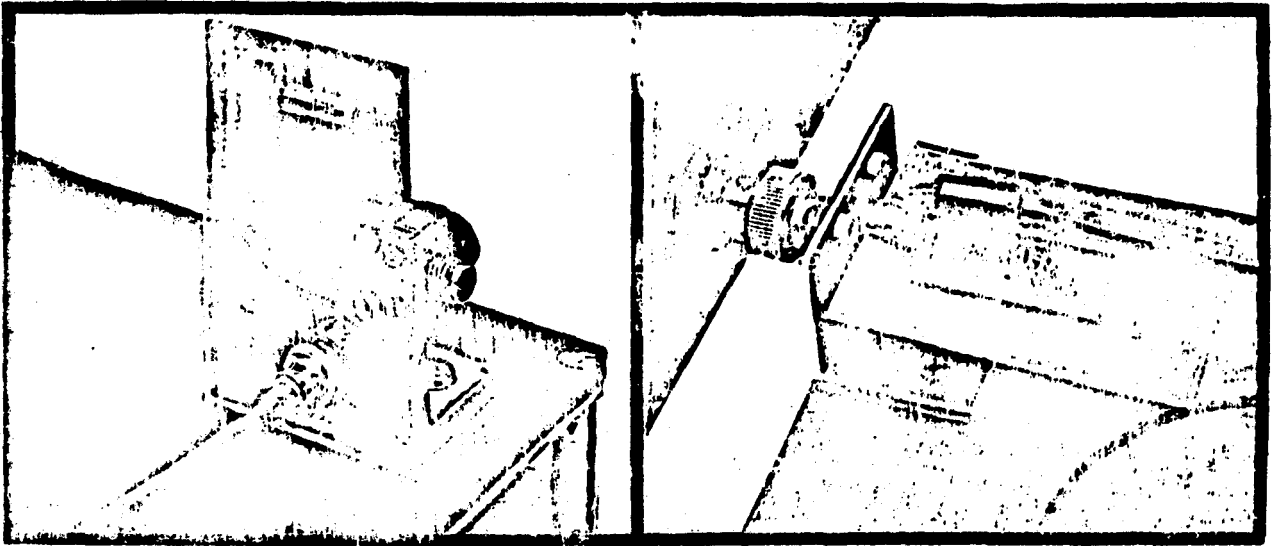


FIGURE 4A EMITTER MODULE BOARD. FIGURE 4B DETECTOR MODULE BOARD

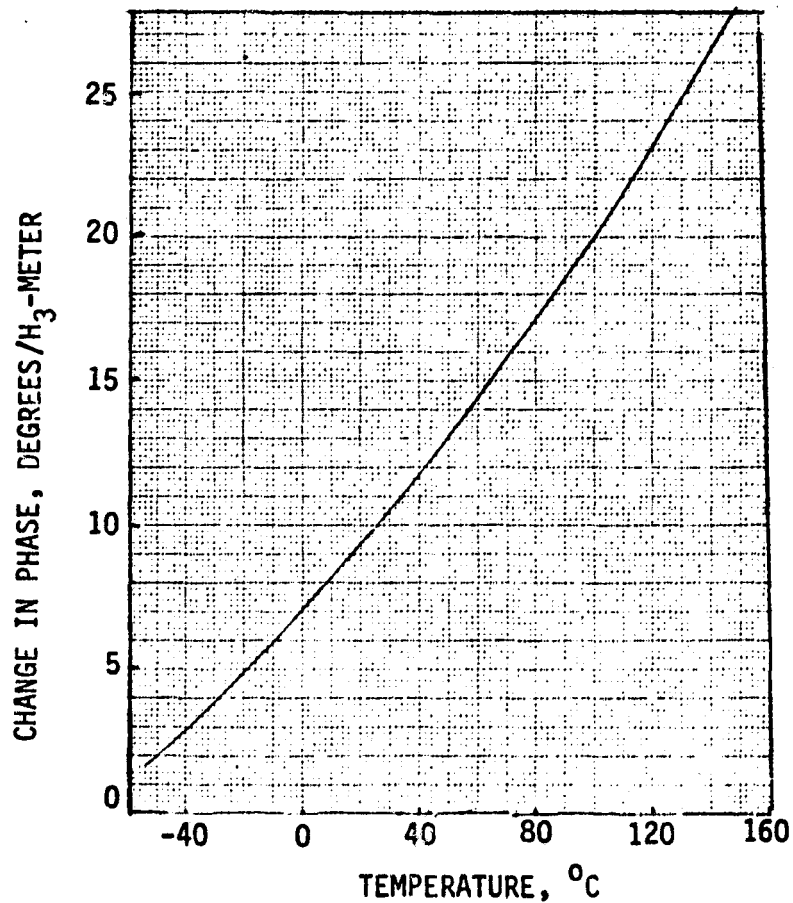


FIGURE 5 PHASE CHANGE OF GRADED INDEX FIBER vs. TEMPERATURE

- CORNING FIBER 303 METERS LONG
- FREQUENCY 980 MHZ

IONOSPHERIC EFFECTS IN ACTIVE RETRODIRECTIVE ARRAY AND MITIGATING SYSTEM DESIGN

A. K. Nandi and C. Y. Tomita
Rockwell International

Abstract

The operation of an active retrodirective array (ARA) in an ionospheric environment (that is either stationary or slowly-varying) is examined. The restrictions imposed on the pilot-signal structure as a result of such operation are analyzed. A 3-tone pilot beam system is defined which first estimates the total electron content along paths of interest and then utilizes this information to aid the phase conjugator so that correct beam pointing can be achieved.

I. INTRODUCTION

In order to make the solar power satellite system perform correctly, it is necessary to point the high power downlink beam towards a specific point on ground. The downlink beam is narrow and pointing accuracy requirements are stringent. One way of achieving this objective is to use the retrodirective array such that the down-going power beam points in the same direction from which a ground-originated pilot signal came. In this approach, the downlink wavefront is obtained by conjugating the phases of various segments of the uplink (pilot) wavefront. For operational reasons, the uplink and downlink frequencies cannot be identical. Both the uplink and downlink wavefronts are required to travel through the ionosphere. The object of this note is to examine system operation constraints imposed by the ionosphere and find possible remedies. The discussion that follows is based on the assumption that the ionosphere is stationary or slowly-varying. Also, heating effects on the medium due to the downlink power beam are not taken into account.

II. IONOSPHERIC EFFECTS ON SINGLE-TONE PILOT BEAM

It is well-known that an important feature of the retrodirective array is that the down-coming beam is phase coherent when it arrives at the source.¹ This statement is rigorously correct only if the propagation medium is non-dispersive spatially homogeneous and temporally stable. In case of the ionosphere, one or more of the above conditions are violated. Under certain conditions, beam pointing error can occur and phase coherence at the source can be lost.

Consider the situation shown in Figure 1. Assume the uplink and downlink frequencies are given by f_u and f_D , respectively ($f_u \neq f_D$). The (path-dependent) phase shift at f_u on one particular radio link can be written as²

$$\phi(f_u) = \frac{2\pi f_u L}{C} - \frac{b}{2\pi f_u C} \int_0^L N \, d\ell \quad (1)$$

where

$$b = \frac{e^2}{2\epsilon_0 m}; \quad e = \text{electron charge, } m = \text{electron mass,} \\ \epsilon_0 = \text{free-space permittivity} \\ = 1.6 \times 10^3 \text{ mks}$$

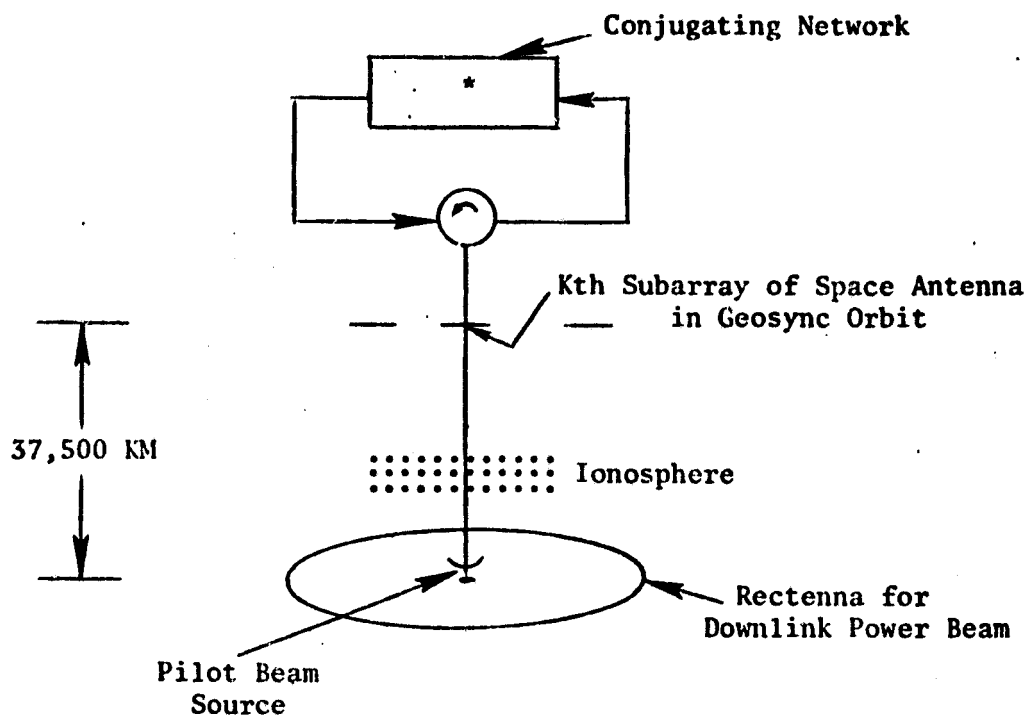


FIGURE 1.

L is the physical path length involved and $\int_0^L N d\ell$ is the integrated electron density along the path under consideration ($\approx 10^{17} - 10^{19}$). Note the second quantity on the right hand side of Equation (1) accounts for ionospheric effects on a CW tone. On using appropriate constants, one can write

$$\begin{aligned} \phi(f_u) &= \frac{2\pi f_u L}{C} - 40.5 \times \frac{2\pi}{f_u C} \int_0^L N d\ell \\ &= \frac{2\pi f_u L}{C} - \frac{K_u}{f_u} \end{aligned} \quad (2)$$

Since one is interested in knowing the phase shift at f_D , a reasonable estimate of the phase can be obtained by multiplying $\phi(f_u)$ by f_D/f_u (this estimate becomes increasingly accurate as $f_u \rightarrow f_D$). Thus,

$$\begin{aligned} \bar{\phi}(f_D) &= f_D/f_u \times \phi(f_u) \\ &= \frac{2\pi f_D L}{C} - \frac{K_u}{f_u^2} \cdot f_D \end{aligned} \quad (3)$$

On conjugating this phase, one obtains

$$\bar{\phi}^*(f_D) = - \frac{2\pi f_D L}{C} + K_u \frac{f_D}{f_u^2} \quad (4)$$

The downlink signal at the transmitting end can be written as

$$S_{\text{down}}^T(t) = \cos \left[\omega_D t + 2\pi f_D \frac{L}{C} - K_u \frac{f_D}{f_u^2} \right] \quad (5)$$

The downlink signal at the receiving end is given by

$$S_{\text{down}}^R(t) = \cos \left[\omega_D t - \left(K_u \frac{f_D}{f_u^2} - \frac{K_D}{f_D} \right) \right] \quad (6)$$

For a temporally stable ionosphere and ignoring second-order effects, one can set $K_u = K_D$ in Equation (6) and obtain

$$S_{\text{down}}^R(t) = \cos \left[\omega_D t - K_u \left(\frac{f_D}{f_u^2} - \frac{1}{f_D} \right) \right] \quad (7)$$

If, in addition, the propagation medium is assumed non-dispersive, then the second term on the right hand side of Equation (7) involving K_u could be equated to zero. In the present situation, this kind of assumption is highly unrealistic. Note in Equation (7), K_u applies to a particular radio path and will, in general, be different on different paths because of ionospheric inhomogeneity. A consequence of this fact is that the phase coherence (at source) property of the downlink signal mentioned earlier does no longer hold good. Furthermore, if a coherent phase perturbation occurs due to some ionospheric large-scale features (such as a wedge), then even a beam pointing error is possible. The magnitude of these effects need to be evaluated for worst-case ionospheric conditions. The two tone pilot beam system which aims at alleviating some of the ionospheric problems mentioned above is discussed next.

III. TWO-TONE PILOT BEAM SYSTEM

If two tones (symmetrically situated around the downlink frequency) are used on the uplink transmission, then under appropriate conditions an average of the phases of the uplink tones can be taken to be a good estimate of the phase at the downlink frequency. The idea here is that the phase errors caused by a stationary ionosphere can be largely eliminated by this approach. Let f_1 and f_2 be the two tones constituting the pilot beam and symmetrically located around the downlink frequency f_D . The choice of the offset Δf is based on conflicting requirements and is not discussed here.

Using the notation as before, for a given link one can write

$$\phi(f_1) = 2\pi f_1 \frac{L}{C} - \frac{40.5}{f_1} \times \frac{2\pi}{C} \int_0^L N \, d\ell = \phi_1 \quad (8)$$

and

$$\phi(f_2) = 2\pi f_2 \frac{L}{C} - \frac{40.5}{f_2} \times \frac{2\pi}{C} \int_0^L N \, d\ell = \phi_2 \quad (9)$$

Then

$$\begin{aligned} \bar{\phi} &= \frac{\phi(f_1) + \phi(f_2)}{2} \\ &= 2\pi f_D \frac{L}{C} - \frac{40.5}{f_D} \times \frac{2\pi}{C} \int_0^L N \, d\ell; \quad \left| \frac{\Delta f}{f_D} \right| \ll 1 \\ &= \phi(f_D) \end{aligned} \quad (10)$$

Note $\bar{\phi}$ is a desirable quantity as far as correct retrodirective array operation is concerned. Normally, all one needs to do is to conjugate this quantity and use it as the phase of the downlink signal leaving the space antenna. However, the arithmetic averaging indicated in Equation (10) can give wrong answers for $\bar{\phi}$ (often called Π ambiguities). This can happen if

$$(i) \quad \phi(f_2) - \phi(f_1) = K(2\pi) + \Delta; \quad |\Delta| < 2\pi \text{ and } K \text{ is odd integer}$$

and/or

(ii) asynchronous dividers are used.

It is clear that in spite of its inherent attractiveness, the 2-tone pilot beam system cannot be used because of the Π ambiguities that can occur during phase averaging.

IV. THREE-TONE PILOT BEAM SYSTEM

Before proceeding with the main task of solving the phase conjugation problem in an ionospheric environment, it is worthwhile to find out whether ϕ_1 and ϕ_2 could indeed differ by integral multiples of 2π when typical SPS parameters are used. For the present problem, it is sufficient to show that ionospheric effects alone can give rise to phase differences which are multiples of 2π . A measure of this effect is obtained by multiplying ϕ_1 (Equation (8)) by f_2/f_1 and subtracting ϕ_2 (Equation 9)). Thus

$$\begin{aligned} \Delta\phi &= \frac{f_2}{f_1} \phi_1 - \phi_2 \\ &= 2\pi \times \left\{ \frac{40.5}{C} \times \int_0^L N \, d\ell \times \left[\frac{1}{f_2} - \frac{f_2}{f_1^2} \right] \right\} \end{aligned} \quad (11)$$

Let

$$f_D = 2.45 \times 10^9 \quad (12a)$$

$$\text{and } \begin{cases} f_1 = f_D - \Delta f \end{cases} \quad (12b)$$

$$f_2 = f_D + \Delta f \quad (12c)$$

then, the number of 2π phase changes obtained for different values of $\int N \, d\ell$ and Δf is shown in Table 1.

Table 1. Number of Ambiguities (η) Vs. Δf

Δf MHz	f_1 GHz	f_2 GHz	$10^{19} \frac{\text{el/m}^2}{\eta}$	$10^{18} \frac{\text{el/m}^2}{\eta}$
100	2.350	2.550	92	9.2
50	2.400	2.500	45	4.5
10	2.440	2.460	8.9	0.89
5	2.445	2.455	4.4	0.44
1	2.449	2.451	0.9	0.09

$\int N \, d\ell$

It is clear from Table 1 that in order to avoid ionospheric ambiguity for the strongest concentration under consideration, Δf should not exceed 1 MHz. Other operational constraints render such a choice unacceptable.

In what follows, a 3-tone approach due to Burns and Fremouw is used to resolve the ambiguity problem.³ It is based on a direct measurement of $\int N \, d\ell$ along the paths of interest and then using this information to estimate the path related phase shift at the downlink frequency f_D .

Consider a frequency-amplitude pattern as shown in Figure 2 where the three uplink tones f_1 , f_2 and f_3 are coherent at ground. Indeed, the three tones can be generated by a low-deviation phase-modulated transmitter. Thus, using equations similar to Equation (8) for three frequencies f_1 , f_2 and f_3 , one can write

$$\begin{aligned} \delta\phi_A &= \phi_2 - \phi_1 \\ &= \frac{2\pi}{C} \left\{ (f_2 - f_1) L - 40.5 \times \int N \, d\ell \times \left(\frac{1}{f_2} - \frac{1}{f_1} \right) \right\} \end{aligned} \quad (13)$$

and

$$\begin{aligned} \delta\phi_B &= \phi_1 - \phi_3 \\ &= \frac{2\pi}{C} \left\{ (f_1 - f_3) L - 40.5 \times \int N \, d\ell \times \left(\frac{1}{f_1} - \frac{1}{f_3} \right) \right\} \end{aligned} \quad (14)$$

The second difference of phase shift is given by

$$\begin{aligned} \delta_2\phi &= \delta\phi_A - \delta\phi_B \\ &= \frac{2\pi}{C} \times 40.5 \times \int N \, d\ell \times \left[\frac{2}{f_1} - \frac{1}{f_3} - \frac{1}{f_2} \right] \end{aligned} \quad (15)$$

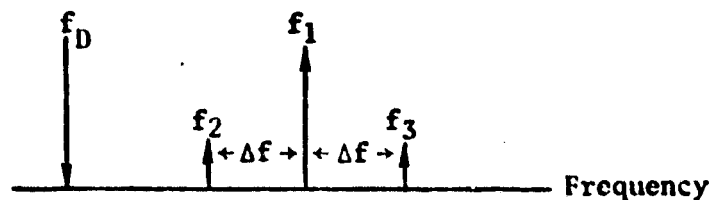


Figure 2.

For suitably chosen Δf , one obtains

$$\delta_2\phi \approx -\frac{2\pi}{C} \times 40.5 \times \int N \, d\ell \times \frac{2 \Delta f^2}{f_1^3} \quad (16)$$

Suppose one needs to avoid a 360° ambiguity in $\delta_2\phi$ for values of $\int N \, d\ell$ less than 10^{19} . From Equation (16), one easily finds

$$\Delta f^2 \approx -\delta_2\phi \times f_1^3 / \left(\frac{2\pi}{C} \times 40.5 \times 2 \times \int N \, d\ell \right) \quad (17)$$

Let

$$\begin{aligned} f_1 &= 2.45 + 0.153125 \text{ (this choice will be justified later)} \\ &= 2.603125 \text{ GHz} \end{aligned} \quad (18)$$

Then

$$\begin{aligned} \Delta f^2 &\approx (2\pi) \times (2.6 \times 10^9)^3 \times C / (2\pi \times 81 \times 10^{19}) \\ &= 0.651 \times 10^{16} \end{aligned}$$

or

$$\Delta f \approx 80.6 \text{ MHz} \quad (19)$$

Thus, with $\Delta f \leq 80.6 \text{ MHz}$ and assuming that $\delta_2\phi$ can be measured, then $\int N \, d\ell$ can be calculated rather easily from Equation (16). An implementation that measures $\delta_2\phi$ with relative ease is shown in Figure 3.

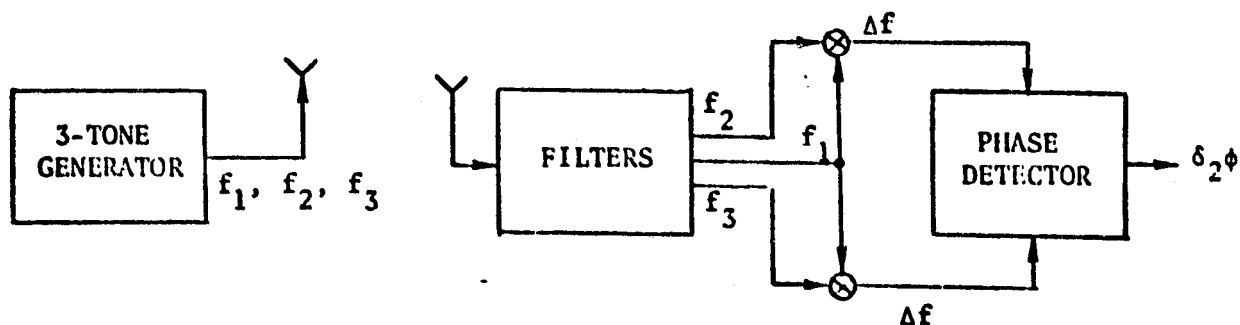


Figure 3. Measurement of $\delta_2\phi$

Reordering Equation (16), one easily obtains

$$\begin{aligned}\hat{N} &= \text{computed value of } \int N \, d\ell \\ &= \frac{f_1^3}{2 \Delta f^2} \times \frac{C}{2\pi} \times \frac{1}{40.5} \times (-\delta_2 \phi)_{\text{measured}} \\ &= \alpha \cdot (-\delta_2 \phi)_{\text{measured}}\end{aligned}\quad (20)$$

For $f_1 = 2.603 \text{ GHz}$ and $\Delta f = 80.0 \text{ MHz}$, one can compute

$$\alpha = 1.6 \times 10^{18} \quad (21)$$

Based on S/N ratio considerations, the accuracy of the \hat{N} computation in Equation (20) is determined by the accuracy of $\delta_2 \phi$ measurement and is given by

$$\alpha_{\hat{N}} = \alpha \cdot \sigma_{\delta_2 \phi} \quad (22)$$

Once an estimate of $\int N \, d\ell$ for a given link is found, one needs to perform several steps of signal processing starting with the phase at f_1 and finishing with the conjugated phase at f_D . These steps are shown in Figure 4.

It is fair to point out that the conjugator used is a modified version of the one in Reference 1. With the additional boxes, the new conjugator clearly takes into account steady-state ionospheric effects.

For the present configuration, the uplink and downlink frequencies are related by the equation*

$$\frac{n}{n+2} \cdot f_1 = f_D$$

or

$$f_1 = \frac{n+2}{n} f_D \quad (23)$$

For $f_D = 2.45 \text{ GHz}$ and $n = 32$, one obtains

$$f_1 = 2.603125 \text{ GHz (see Equation (18)).}$$

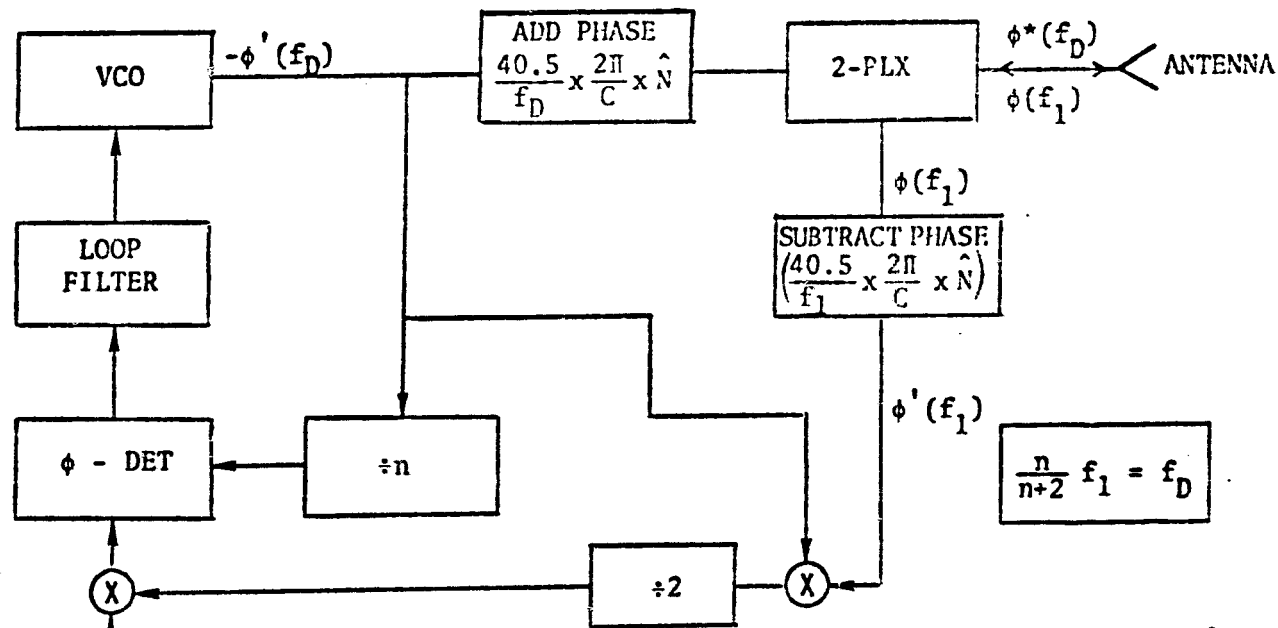
It is interesting to examine the output $\phi^*(f_D)$ of the conjugator in Figure 4. On taking differentials, one obtains

$$\Delta \phi^*(f_D) \approx \frac{40.5}{f_D} \times \frac{2\pi}{C} (1 - f_D^2/f_1^2) \Delta \hat{N} \quad (24)$$

One using $f_D = 2.45 \text{ GHz}$ and $f_1 = 2.603 \text{ GHz}$, the above equation simplifies to

$$\Delta \phi^*(f_D) \approx 3.95 \times 10^{-17} \Delta \hat{N} \quad (25)$$

*Note the mode of operation indicated here is different from that in Ref. 1.



$$\begin{aligned}\phi_o(f_1) &= \text{Ref. Phase} \\ &= \omega_1 \frac{L_0}{C} - \frac{40.5}{f_1} \times \frac{2\pi}{C} \times \int_0^{L_0} N \, d\ell \\ &= \text{Constant at all subarrays}\end{aligned}$$

$$\phi(f_1) = \omega_1 \frac{L}{C} - \frac{40.5}{f_1} \times \frac{2\pi}{C} \times \int_0^L N \, d\ell$$

$$\phi^*(f_D) = -\phi'(f_D) + \frac{40.5}{f_D} \times \frac{2\pi}{C} \times \hat{N}$$

$$= \frac{n}{n+2} [2\phi_o(f_1) - \phi'(f_1)] + \frac{40.5}{f_D} \times \frac{2\pi}{C} \times \hat{N}$$

$$= \text{const.} - \omega_D \frac{L}{C} + \frac{40.5}{f_D} \times \frac{2\pi}{C} [\hat{N}(1 - \frac{f_D^2}{f_1^2}) + \frac{f_D^2}{f_1^2} \int_0^L N \, d\ell]$$

Figure 4. Modified Chernoff Conjugator

so that

$$\Delta \hat{N} = 2.53 \times 10^{16} \times \Delta \phi^*(f_D) \quad (26)$$

Suppose one requires an rms accuracy of 10° ($= .174$ rad) on $\phi^*(f_D)$. Then the required accuracy on N is given by

$$\begin{aligned} \sigma_{\hat{N}} &= 2.53 \times 10^{16} \times .174 \\ &= 4.41 \times 10^{15} \end{aligned} \quad (27)$$

On going back to Equation (22), one finds

$$\begin{aligned} \sigma_{\delta_2} &= \sigma_{\hat{N}}/\alpha, \quad \alpha = 1.6 \times 10^{18} \\ &= 2.76 \times 10^{-3} \end{aligned} \quad (28)$$

Squaring the quantity on the right hand side of Equation (28) and on using some results in Reference 3, one obtains a value for (P_R/σ^2) .** Thus,

$$\begin{aligned} P_R/\sigma^2 &= (S/N) \text{ ratio at the receiver sketched in Figure 3} \\ &= \frac{8}{\text{Var } (\delta_2 \phi)_{\text{opt}}} \\ &= \frac{8}{7.62} \times 10^{-6} \\ &= 1.05 \times 10^6; \text{ i.e., } 60 \text{ dB} \end{aligned}$$

As far as Figure 4 is concerned, several comments are in order. Firstly, the use of the same \hat{N} for both uplink and downlink phase compensations need justification. Secondly, the conjugator suffers from divider ambiguity problems. This makes it necessary to phase conjugate at IF and then suitably multiply the conjugator output frequency to 2.45 GHz. Preliminary design of a 3-tone conjugator operating at IF has been completed and will be reported elsewhere.

V. CONCLUSION

An attempt has been made above to incorporate the role of the ionosphere in ARA system design. A conjugator has been sketched that compensates for steady-state ionospheric effects. Work is currently in progress to evaluate the magnitudes of ionospheric wedge effects. Based on (limited) available data² and because of geometry considerations (the proximity of the ionosphere to the rectenna), it appears unlikely that any compensation towards ionospheric effects would be necessary. However, in order to make a definite conclusion, more data on wedge structure are desirable. In addition, this problem needs examination in the light of ionospheric heating effects due to the downlink power beam.

** P_R is the total 3-tone signal power received and σ^2 is the noise power out of any one of the tone filters that have identical bandwidths.

REFERENCES

1. Chernoff, R. C., "Large Active Retrodirective Array for Space Application," IEEE Trans. on Antennas and Propagation, pp 489-496, July 1979.
2. Lawrence, R. S., Little, C. G., and Chivers, H. J., "A Survey of Ionospheric Effects Upon Earth-Space Radio Propagation," Proc. IEEE, pp 4-27, January 1964.
3. Burns, A. A. and Fremouw, E. J., "A Real-Time Correction Technique for Transionospheric Ranging Error," IEEE Trans. on Antennas and Propagation, pp 785-790, November 1970.

POWER AMPLIFIER SESSION

HIGH EFFICIENCY SPS KLYSTRON DESIGN

E. J. Nalos, Boeing Aerospace Company

1. Introduction

Considerable data has now been accumulated on the feasibility of an 80-85% high power klystron design from previous studies. The most likely compact configuration to realize both high efficiency and high gain (~ 40 dB) is a 5-6 cavity design focused by an electromagnet. A refocussing section will probably be required for efficient depressed collector operation. An outline of a potential klystron configuration is given in Figure 1. The selected power output of 70 kW CW resulted from a maximum assumed operating voltage of 40 kV. The basic klystron efficiency cannot be expected to exceed 70-75% without collector depression. Although impressive gains have been achieved in raising the basic efficiency from 50% to 70% or so with a multi-stage collector, the estimated efficiency improvement due to 5-stage collector at the 75% level is only about 8%, resulting in an overall efficiency of about 83%. These estimates need to be verified by experiment, since the velocity distribution of the spent klystron beam entering the collector is not precisely known. It appears that the net benefit of a 5-stage collector over a 2-stage collector is between 1.5 - 3.5 kW per tube. This has the double benefit of less electrical power to be supplied as well as less thermal power in the collector to be dissipated. Table 1 indicates an estimated energy balance in the klystron which leads to the above estimates. A modulating anode is incorporated in the design to enable rapid shutoff of the beam current in case the r.f. drive should be removed. In this case, the collector would become overheated since it would receive the full beam power.

2. Depressed Collector Design

One of the greater uncertainties in the design is the velocity distribution of electrons in the output gap, particularly for a high basic efficiency tube. Experimental verification will be required for the selection of proper depressed voltages at each collecting electrode. Varian has reported that about 10% of the electrons develop twice the d.c. beam voltage in a 50% efficient tube. We estimate that this will be reduced to perhaps 2% for an 80-85% efficient tube. To obtain initial specifications for the collector supply, an estimate was made of the possible voltage ratios required, as indicated in Figure 2.

3. Voltage Regulation

The requirements on the modulating anode and body voltage are dictated primarily by phase fluctuations. At 40 kV, $\phi \approx 3000^\circ$ and at 41 kV, this calculation yields 29720° . Thus, $d\phi/dt = -370^\circ$ per kv. If a 10° phase error were allowable in the klystron, this would translate into a regulation requirement of $\pm 0.67\%$ at 40 kV, provided that klystron-to-klystron phase errors are not correlated. Although it is likely that voltage fluctuations on all klystrons on a given d.c. - d.c. converter will go up and down together, the time delays in distribution, of the order of fractions of microseconds, will make them appear as though they were uncorrelated at a given instant at all klystron terminals. With this in mind, the initial regulation requirement on the modulating anode and body supply was set at 0.5%. Since it is contemplated to include the klystron in a phase compensation loop, it may be possible to relax this requirement when the loop performance is verified.

PRECEDING PAGE BLANK NOT FILLED

4. Electron Beam Focusing Design

The focusing options for the klystron include: (1) solenoid ElectroMagnetic (EM) focusing, (2) Multiple-pole electromagnetic focusing with periodic field reversals, introducing the possibility of Permanent Magnet (PM) implementation, (3) Periodic Permanent Magnet (PPM) focusing used successfully on low and medium power tubes (mostly TWT's); and 4) Combined PM/PPM focusing wherein the PM section at the output is used to retain good efficiency and good collimation in the high power r.f. region. The low risk approach of (1) was recommended in order to achieve the highest efficiency, but R&D efforts in a combined PM/PPM approach should be investigated for possible later incorporation.

In order to achieve a conservative design, we have initially selected a capability of achieving 1,000 Gauss in the solenoid when operating at 300°C. Selecting a minimum ID dimension compatible with directly winding the solenoid on the tube involves a trade study of the required solenoid power and weight as a function of solenoid OD. Figure 3 shows the trade of solenoid power and weight with coil OD.

It is anticipated that the solenoid will consist of copper sheet with glass-like insulation between layers, wound directly on the tube body. With factory adjusted cavity tuning, there will be no protruding tuners. It is possible that the solenoid may be used for baking out the tube in space.

As a matter of interest, the performance parameters of a 50 KW PM focused klystron were estimated in Table 2. With the design assumptions postulated, it does not appear to offer any advantages over an efficiently focused solenoid design.

5. Design Approach to Long Life

The objective of SPS is the achievement of 30 year life and since the main component of the MPTS system is the r.f. transmitter, its consideration is of paramount importance. The major transmitter elements which contribute to life are summarized in Table 3. The achievement of uniform tube-to-tube performance will require stringent materials control, well defined construction techniques, and special design features such as temperature compensated cavity frequency control.

An initial risk assessment of the unknowns on the space environment have led us to favor a closed envelope approach as a reference design. Some of the concerns with open envelope operation near the Shuttle vehicle deal with outgassing from non-metallic skin of heavy molecules and absorbed volatile species: cabin leaks (oxygen); fuel cell flash evaporators (water vapor); Vernier control rocket engine exhaust; and main rocket engine outgassing (water vapor). The degree to which such contaminants can be localized, and the pumping speed of space, etc., have yet to be determined.

The NASA objective of 30 year life, in the light of current experience and understanding thus has to be based on the following phased approach:

- . Conservative Design:

- Emission; R.F., Thermal and Stress: Derating

- . Determination of Appropriate Manufacturing Procedures

- . Adequate Protective Features

- Modulating Anode

- System Monitoring Requirements

- . Adequate Test Program on Ground
 - Failure Mode Identification
 - Infant Mortality Elimination - Burn-in
- . Understanding of Space Environment
 - Processing in Space
 - Open Envelope Operation
- . Definition of Maintenance Philosophy
 - Allowable Down Time
 - In-place Repair Feasibility
- . Development of Improved MTBF Analytical Model
- . Space Test Verification

There are promising developments in transmitter life which lend some credibility to the 30 year life objective. For instance, the best ten high power klystrons running on the BMEWS system have seen 9 years of life and are still running. With proper burn-in procedures, current space based TWT's are being qualified for 7 years life. Over 100 such tubes currently in space have been running for well over 2 years. It is our expectation that within the SPS development time-frame, tube MTBF's approaching 30 years with the suggested design approach will be feasible. It is important to recognize that significant life test programs on the ground will be required not only for cathodes, but the entire r.f. envelope.

5.1 Cathode Design

The mechanisms limiting thermionic cathode life are primarily evaporation rate of the cathode material, cathode matrix properties, and impurities. The cathode-tube interaction is paramount in realizing long life, regardless of how good the cathode may be in a diode test. The approach to realize 30 year life must be based on minimizing tube-cathode interactions through conservative design, good beam focusing and proper selection of materials to minimize poisoning gases produced by electron bombardment. The most likely candidates, based on present knowledge, are either a tungsten matrix cathode operating at a temperature of slightly above 1000°C or a nickel matrix cathode operating at about 800°C. The lower temperature would be preferable from the life point of view but factors such as migration and reactivation feasibility tend to favor the higher temperature cathode. Our current assessment, based on discussions with the tube industry suggests that it would probably be unwise to utilize some of the newer cathodes until sufficient life test data has been accumulated. Encouragement with respect to long life in thermionic cathodes can be derived from the work at Bell Telephone Laboratories on the so-called Coated Powder Cathode (CPS), which is in use on long life repeaters, capable of 50,000 hours life at current densities approaching 1 amp/cm², much higher than those proposed for the SPS Klystron (<.2 amps/cm²).

5.2 Tube MTBF Considerations

Ideally, a failure model of the transmitter would be desired, in which no failures occurred until wearout mechanisms set in; i.e., avoidance of early mortality. To some degree this can be achieved by a burn-in procedure to identify and remove infant mortality victims. It is anticipated that with the reference design tube, partial or full bakeout in space will be feasible, avoiding the need to perform costly burn-in on the ground. Also, with mass production, automated manufacture, good quality control, and maintenance, infant mortality can be minimized.

With roughly $N = 100,000$ tubes, if a maximum of 2% of all klystrons are allowed to fail at scheduled SPS shutdown, (every 6 months), the required tube MTBF would be approximately

$$\frac{(.02N)}{N} (\text{Tube MTBF}) = 6 \text{ months} - .5 \text{ years; i.e., MTBF} = (50)(.5) = 25 \text{ years.}$$

This is compatible with the reference klystron design; however, a more refined reliability model needs to be developed, of which the exponential failure model is but one case corresponding to a constant failure rate. With proper burn-in procedures, and as better understanding of failure modes is developed, the SPS klystron may require a much lower MTBF to meet the above criteria. With a proper burn-in period, infant mortality failures can be avoided and failures shifted toward cathode wearout limitations. The required burn-in period for current space qualified TWT's is of the order of 1,500 hours. Further understanding of the required tube MTBF under these conditions will evolve with the ground based development program implementation.

6. Klystron Tube Protection

The tube interacts with the subarray through the waveguide feed system. The primary requirement is maintenance of a good r.f. match under all conditions. During initial processing or if mismatched, either external or internal arcing may occur. Commercial waveguide components are available to visually detect arcs and use a trigger signal to disconnect the tube rapidly, in this case by connecting the modulating anode to cathode. This can occur in much less than 1 μ sec, adequate to prevent damage.

With loss of r.f. drive, the entire electron beam power appears at the collector. The conventional klystron is designed to handle this power. In our case, the collector is designed to handle only the spent electron beam after normal r.f. interaction. If the loss of r.f. drive is sensed at the klystron input, the modulation-anode power supply will be used to shut off the electron beam.

The most likely region of dc arcing is between cathode structure and modulation-anode and between the modulating anode and the r.f. circuit. In the event of an arc, the energy stored in the modulation-anode power supply RC circuit is discharged. Ordinarily the arc extinguishes after a brief interval and normal tube performance is restored automatically. Should some unknown fault cause persistent non-clearing arcing, arc logic could be designed to sense repeated loss of r.f. output and to shut down the modulation-anode power supply.

Persistent repeated nonclearing rf arcing in the klystron rf load or output system may result in tube damage. The rf arc logic protection circuit is designed to sense reflected rf power caused by the arcing and to shut down the modulation-anode power supply pending correction of the problem.

7. Operation Under Reduced Voltage

One advantage of the klystron is the fact that efficiency does not deteriorate significantly with voltage. The effect of solar cell voltage degradation on klystron power output is indicated in Figure 4 for the condition that the klystron characteristics remain on the V-I portion of the solar cells corresponding to maximum d.c. output. This condition can only be achieved if the perveance of the tube is slightly changed. If the modulating anode is mounted on a diaphragm, such an adjustment could be made. This feature would also be useful for adjustment of tube-to-tube uniformity. It is seen that if the solar cells are not refurbished, the efficiency remains high, but the power output drops significantly. On this basis, it was decided to refurbish solar cells and not require the transmitter to adjust perveance for solar cell optimal matching.

8. Klystron Power Output Trade Study

The reference klystron represents an initial point design within the given NASA guidelines. It is intended primarily as a vehicle to demonstrate its potential in the SPS application. If the operating voltage at GEO can be increased to a value above 40 kv other klystron power levels become of interest.

One of the advantages of the linear beam amplifier such as a klystron is the fact that the different interaction regions, i.e., beam formation, r.f. interaction, and beam collection are physically separate and hence distribute the thermal stresses over a large area. The most critical portion of the klystron from the thermal point is the output gap. The output gap interception for two typical values of beam transmission (95% and 98%) is indicated in Figure 5. The capability of the output gap to handle this interception is given for two values of heat rejection capability: 0.25 and 0.5 kw/cm² of area. This could be either heat pipe cooling or pumped fluid cooling.

It is seen that for a 4% beam interception and $W = 0.25 \text{ kw/cm}^2$, the maximum beam voltage is about 67 kv, corresponding to a power level in excess of 200 kw. If the perveance were increased from $S = 0.3$ to 0.5×10^{-6} , still within the regime of potentially high efficiency, this power level would correspond to 580 kw. This has encouraged us to investigate two additional point designs, at 250 kw and at 500 kw, respectively, the parameters for which are summarized in Table 4.

The efficiency including solenoid power is somewhat higher than that for the reference design. It is worth noting that even with a longer tube, the efficiency increases by about 2% points due to lower incremental solenoid requirements at higher power. The specific mass decreases from about 0.8 kg/kw at 70 kw to less than 0.4 kg/kw at 500 kw CW. Thus, it appears advantageous to consider a higher power klystron design should the voltage constraints permit it.

The cost of a single klystron tube is estimated from the cost trends in Figure 6. For a 70 kw CW tube, the mass production cost is estimated at \$2800. The acquisition cost of r.f. tubes and 10-year replacement cost of spares, based on a projected transportation cost to space of \$60 per kg, for a system output of 6 GW RF in space, are summarized in Table 5. The transportation costs comprise about 47 to 62% of the total cost. Again, with the assumptions made, it appears advantageous to go to as high power per tube as possible. As the ground-based development program proceeds, the results of these trade studies will be used in updating the present baseline design, not only for the klystron transmitter candidate, but for other transmitters as well.

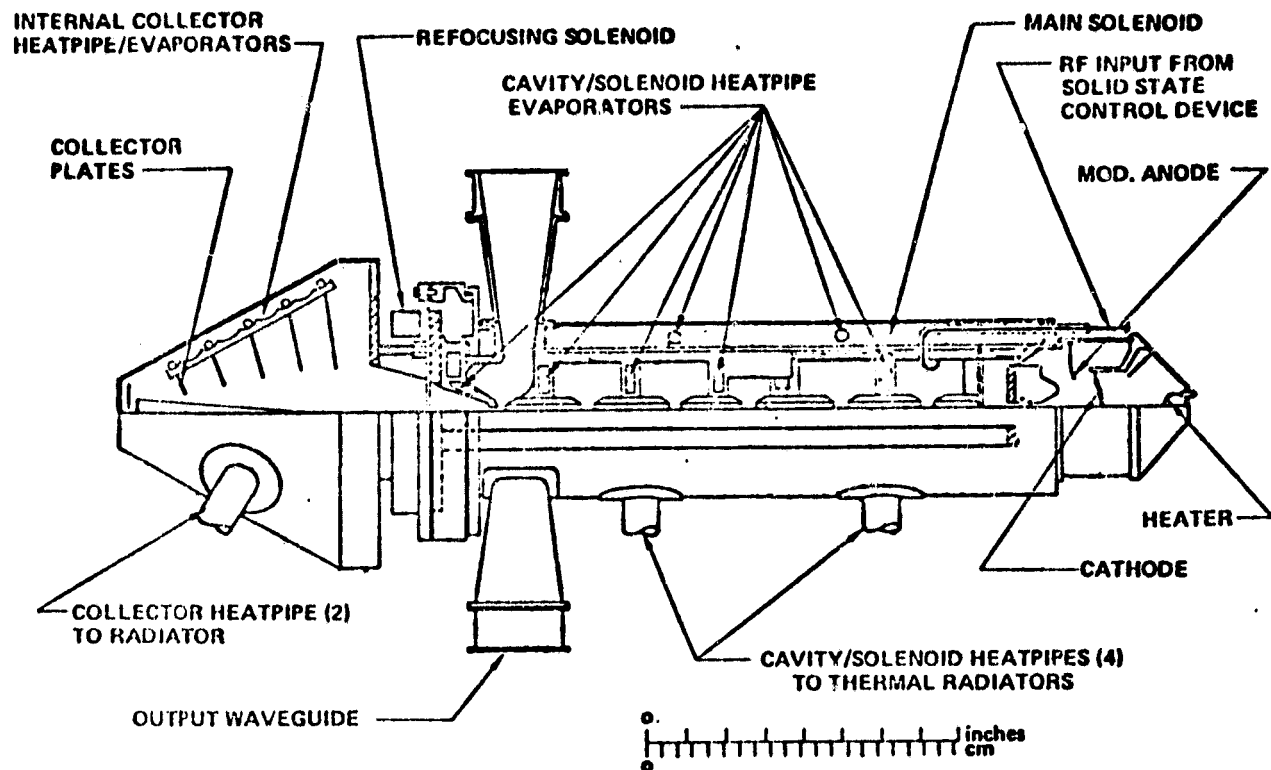
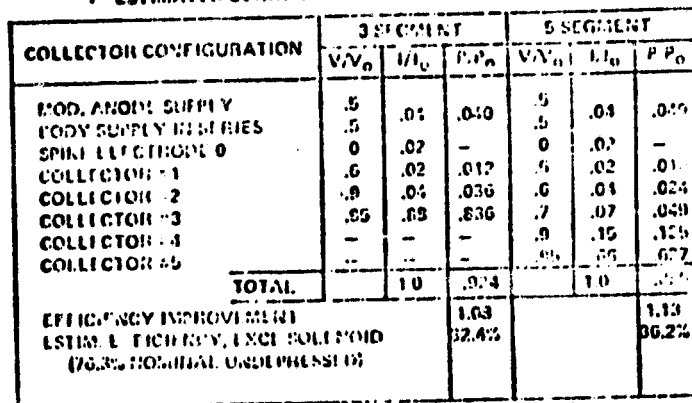


Figure 1 Reference Klystron Configuration

Table 1 Energy Balance in Reference Klystron Design

	2-SEGMENT COLLECTOR	5-SEGMENT COLLECTOR
BEAM POWER	92.62 Kw	92.62 Kw
RF LOSS IN DRIVER CAVITIES	.40 Kw	.40 Kw
RF POWER PUTPUT ¹	70.66 Kw	70.66 Kw
OUTPUT CAVITY RF LOSS	2.19 Kw	2.19 Kw
OUTPUT INTERCEPTION LOSS ²	1.62 Kw	1.62 Kw
POWER ENTERING COLLECTOR	17.75 Kw	17.75 Kw
COLLECTOR RECOVERY	7.10 @ 40%	10.65 @ 60%
THERMAL LOSS IN COLLECTOR	10.65 Kw	7.1 Kw
NET BEAM POWER	85.52 Kw	81.97 Kw
EFFICIENCY EXC. SOLENOID	82.6%	86.2%
NET EFFICIENCY ³	81.2%	84.6%

1. ELECTRONIC EFFIC. (.79) x OUTPUT CIRCUIT EFFICIENCY (.97) x REMAINING POWER (92.22 Kw)
2. BASED ON 4% INTERCEPTION @ $V_{o/3}$ (33%) and $2 V_{o/3}$ (67%) i.e., .0178 $V_{o/3}$
3. INCLUDING 1.5 Kw FOR SOLENOID AND HEATER POWER.



COPPER SOLENOID 3" ID, 1000 GAUSS, 16.5" LONG

- ② AS ABOVE, WITH 3.86 kg/kw FOR 300°C HEAT REJECTION.

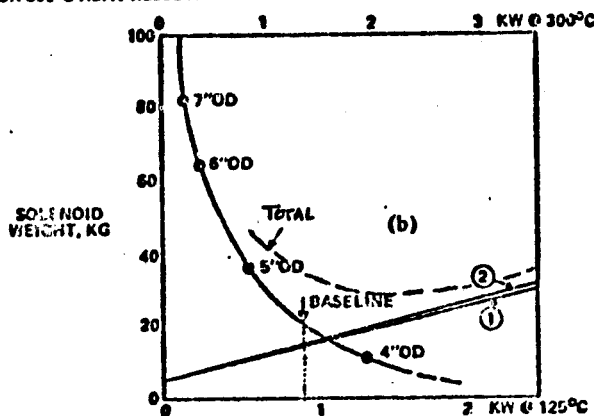


Figure 3 Solenoid Design for High Power Klystron

Table 2 50 KW Permanent Magnet Klystron Design

VOLTAGE/CURRENT	38KV, 1.81 AMPS
PERVANCE/BEAMPOWER	S=.244, P ₀ = 69KW
ELECTRONIC EFFICIENCY	0.75
CIRCUIT EFFICIENCY	0.97
RF POWER OUTPUT	50KW
HEATER POWER	.1KW
DRIVER RF LOSSES	.005V ₀ I ₀ = .3KW
OUTPUT INTERCEPTION LOSS	.025V ₀ I ₀ = 1.72KW
RF OUTPUT CAVITY LOSS	.03(50) = 1.50KW
POWER INTO COLLECTOR	15.42KW
COLLECTOR THERMAL INPUT	8.51KW REMOVED @ 500°C

PASSIVE COOLING -

ACTIVE COOLING -
RADIATOR & HEAT PIPES LIQUID METAL CYCLE @ 2.2/1.5KG/KW FOR 275°C
@ .94/.43KG/KW FOR 500°C

WEIGHT ESTIMATE

TUBE & POLEPIECES	12.0KG
COLLECTOR - 5 SEGMENT	6.0
MAGNETS	7.5
RADIATOR DISTANCE	0
COOLING @ 275°C	5.4
COOLING @ 500°C	4.2

o SPECIFIC WEIGHT = .78 TO .83
KG/KG

6 EFFICIENCY = 80.7%

TOTAL WEIGHT 35.1 - 41.5KG

Table 3. Features Affecting Transmitter Life**BEAM FORMATION**

CATHODE MANUFACTURING MATERIAL PROCESSING
 EMISSION SUPPRESSION FROM SURFACES
 CATHODE BASE MATERIAL PURITY-POISONING MECHANISM
 EVAPORATION RATES FROM IMPREGNATED CATHODES
 HEATER WARMUP
 BURN-IN PERIOD-NO INFANT MORTALITY

BEAM FOCUSING

SOLENOID DESIGN/MATERIALS-SPACE BAKEOUT FEASIBILITY AND CONTROL
 MAGNETIC CIRCUIT MATERIAL SELECTION SmCo_5 , ALNICO, FLUX CONDUCTORS

RF CIRCUIT

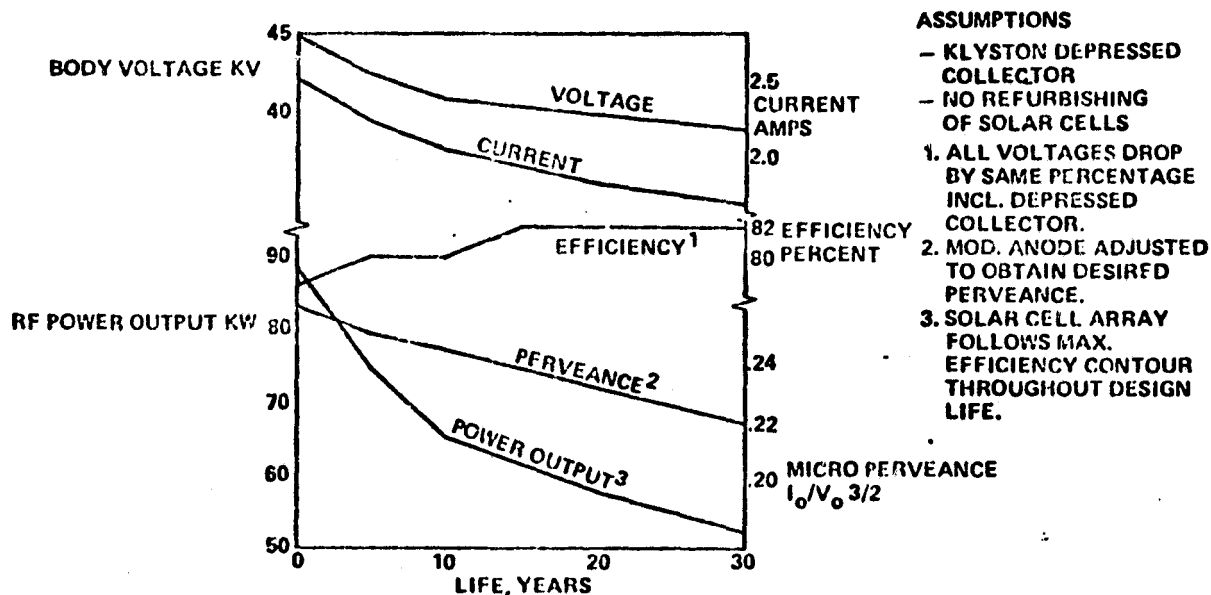
COPPER ALTERNATIVES FOR CAVITIES
 PROPERTIES OF LOSSY INTERNAL CERAMICS
 OUTPUT WINDOW POWER LIMITS BeO , Al_2O_3

BODY AND COLLECTOR

LEAKAGE OF INSULATORS
 SUPPRESSION OF SECONDARY EMISSION

EXTERNAL

LEAD AND CONNECTOR COMPATIBILITY

**Figure 4** Klystron Performance When Optimally Matched to Solar Cell Output

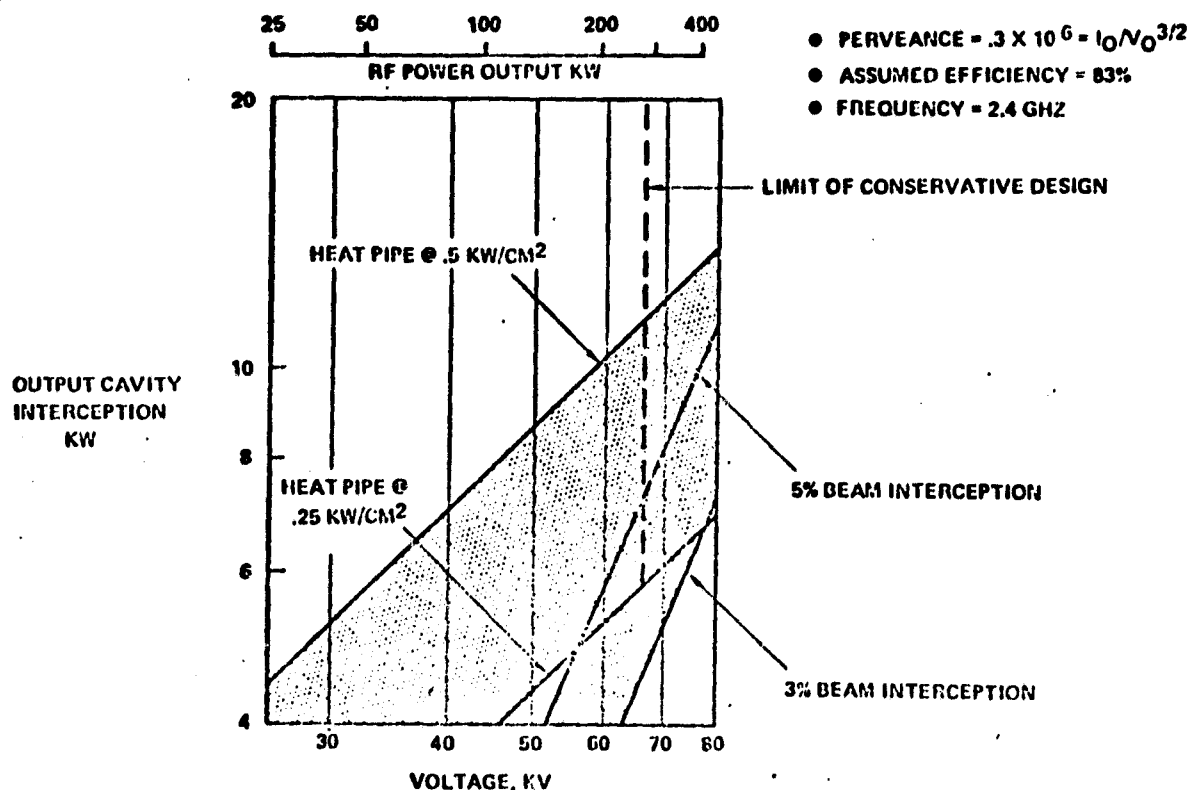


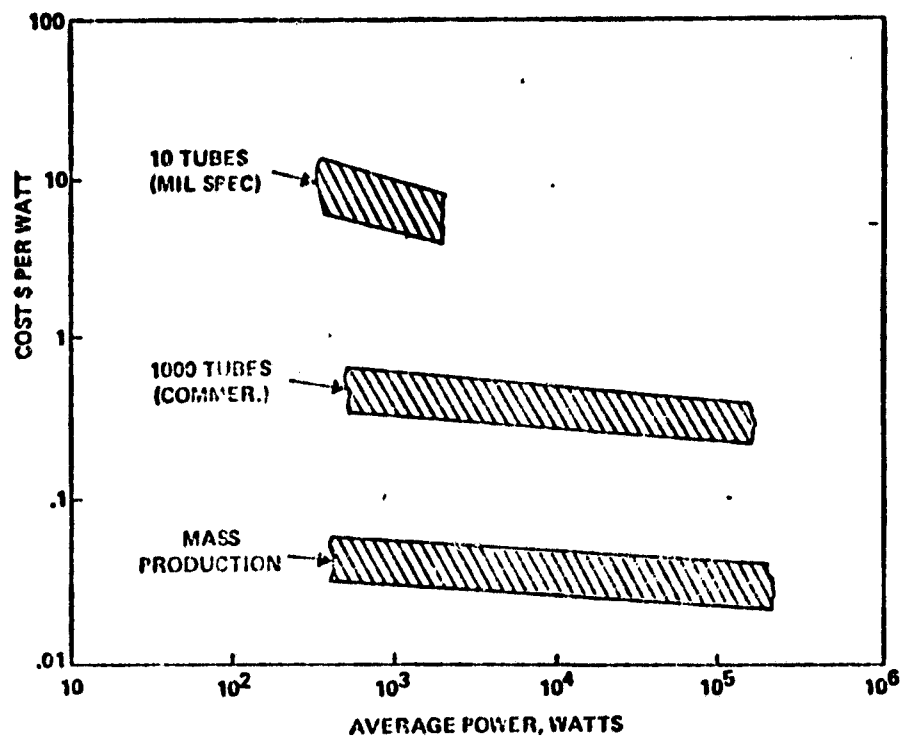
Figure 5. High Power CW Limitations of High Efficiency Klystron

Table 4 Alternate High Power Klystron Designs

POWER VOLTAGE/CURRENT PERVEANCE $K \times 10^{-6}$ RF SECTION LENGTH $\sim \sqrt{V_0}$	70.6kw 42kv/2.2amps 25 16.5in		250kw 65kv/5amps .30 20.5in		500kw 80kv/8.2amps .36 22.8in	
	WEIGHT, kg	POWER, kw	WEIGHT	POWER	WEIGHT	POWER
TUBE WEIGHT CAVITY, SEALS, BODY ETC. $\sim 1.2 \sqrt{V_0}$	10kg		15kg		16.6kg	
COLLECTOR WEIGHT (EST.) $\sim V_0 I_0$	7.0kg		13.2kg		18.7kg	
SOLENOID (EST.) @ 300°C, 1 KGAUSS, $P \sim B^2 \times L \sim \sqrt{V_0} K$	20kg	2kw	24.8kg	2.93kw	27.9kg	3.98kw
HEATER AND REFocusing COIL		1.0kw		1.50kw		2.0kw
RF LOSSES		4.2kw		14.7kw		29.8kw
RADIATOR AND HEAT PIPES	0	1m	0	1m	0	1m
WEIGHT AND POWER DISSIP'N REQ'D @ 300°C	9.5	14.5	25.3	33.6	47.3	72.0
WEIGHT AND POWER DISSIP'N REQ'D @ 500°C	4.9	9.3	16.7	32.1	33.8	64.9
TOTAL WEIGHT KG	51.4	60.8	95.0	123.7	144	199.8
SPECIFIC WEIGHT KG PER KW	.727	.860	.380	.495	.288	.400
EFFICIENCY INC. SOLENOID	80.51%		82.43%		82.67%	

LEGEND:

- SOLENOID FOCUSING, FIVE STAGE COLLECTOR, 45% RECOVERY.
- RF LOSSES AT INPUT, OUTPUT, PLUS 4% INTERCEPTION LOSS TOTAL 4.45% OF $V_0 I_0$
- USEFUL RF OUTPUT = $.7529 V_0 I_0$
- COLLECTOR THERMAL DISSIPATION = $.105 V_0 I_0$
- COLLECTOR POWER RECOVERED = $.0860 V_0 I_0$
- EFFICIENCY = 83.4% EXCLUDING SOLENOID
- HEAT PIPES (1/0 METER) + RADIATOR WEIGHT ESTIMATED @ 2.01/1.32kg/kw @ 300°C (BODY AND SOLENOID)
- @ .94/1.45kg/kw @ 500°C (COLLECTOR)
- S BAND DESIGN WITH SOLENOID @ 300°C, ID = 3" OD = 4"



(B) COST VARIATION WITH POWER LEVEL AND QUANTITY

Figure 6 Cost Trends in High Power CW Transmitters

Table 5. RF Transmitter Acquisition & 10 Year Replacement Cost

SPS-1546

CANDIDATE	POWER PER UNIT, Kw	NUMBER PER SYSTEM	ACQUISITION COST						REPLACEMENTS/MONTH	REPLACEMENT COST	SPECIFIC COST \$/KW	SPECIFIC WEIGHT	MASS		TRANS. PORT COST	SYSTEM COST
			PER UNIT \$K	PER. SYSTEM \$M				INITIAL ACQ'N					10 YR REPLACEMENT			
				MTBF, YEARS	REPLACEMENTS/MONTH	REPLACEMENT COST	SPECIFIC COST \$/KW						INITIAL ACQ'N	10 YR REPL.		
						SM			Kn/Kw	10 ³ kn		SM	SM			
1	50	120x10 ³	2.7	324	28	357	116	70	.8	4.8	1.7	283	102	830		
2	70	85,000	2.8	238	26	272	91	40	.75	4.76	1.8	266	108	723		
3	250	24,000	7.0	168	24	84	70	28	.4	2.4	1.0	144	60	442		
4	500	12,000	10	120	20	50	60	20	.3	1.8	.9	108	54	342		

LEGEND

CANDIDATE

1. IM FOCUSED KLYSTRON 38kv
2. EM FOCUSED KLYSTRON 42kv
3. EM FOCUSED KLYSTRON 65kv
4. EM FOCUSED KLYSTRON 80kv

TRANSPORT COST AT \$ 60/k₃ TO ORBIT
 EXPONENTIAL FAILURE RATE
 PASSIVE COOLING
 NO BURN-IN COSTS INCLUDED

***Klystron
LaRue/Varian***

unavailable at time of printing

ANALYTIC INVESTIGATION OF EFFICIENCY AND PERFORMANCE
LIMITS IN KLYSTRON AMPLIFIERS USING MULTIDIMENSIONAL
COMPUTER PROGRAMS; MULTI-STAGE DEPRESSED COLLECTORS; AND
THERMIONIC CATHODE LIFE STUDIES.

by

H. G. Kosmahl
NASA Lewis Research Center
Cleveland, Ohio

Introduction

In 1972 this author together with L.U. Albers performed an extensive parametric investigation of the extraction of energy in output gaps of klystron amplifiers, using our own 3-D computer programs. Due to complexity of the program which used a hydrodynamic, axially and radially deformable disk-ring model and the resulting long computing time we limited our investigation, Ref. 1, to the output gap, by far the most important and difficult part of the klystron interaction. As inputs best results from independent studies at G.E. by T. Mihran, Ref. 2 and at Varian, Ref. 3, by E. Lien were used to initiate the starting conditions for the electrons and the RF voltage using our program. Although this method of computation is less exact than processing the entire klystron interaction in 3-Dimensions we verified that, for a confined flow focused beam throughout the penultimate cavity, radial velocities remain very small and the beam is highly laminar. It was, therefore, concluded that possible errors resulting from treating only the output cavity in 3-D would remain small.

Discussion of Results

We proceed now with the discussion of the computer results. Figure 1 shows the cross-section of the ring model used in computations and the degree of complexity and care applied to compute accurately the radial and axial deformation of the rings and the space charge forces. The price paid for this effort - the computing time - was felt to be justified for the one time verification. Figure 2 shows typical axial and radial space charge functions. In agreement with basic theory the radial functions obey Gauss' law inside the beam and the axial space charge force is zero at the tunnel wall $r=a$.

Efficiency

Let us now turn to the discussion of computed efficiencies. Figure 3 shows a plot of efficiency versus $\beta_e a$ for two bunching levels, $i_1 = 1.81 I_0$ and $i_1 = 1.64 I_0$, $B = 2.5 X B_{BR}$, and 0.5μ perveance. The voltage swings α are 1.10, 1.05, and 1.0, respectively. The $1.81 I_0$ bunching is characterized by a very compact bunch with a small velocity spread and absence of a typical antibunch disk since the maximum velocity past the output gap is only $1.14 u_0$. As can be seen from the plots, the efficiency seems to decrease linearly with increasing $\beta_e a$ with a slope of approximately 2.5 percent points efficiency loss for each 0.1 radian increase in $\beta_e a$. Note that b/a , β_e , and 2.1 were held constant and only a was permitted to increase. Thus at large $\beta_e a$ values the aspect ratio a/b is

* A paper presented at the SPS Microwave Systems Workshop, at JSC, Houston, TX
16 Jan 1980

small; the RF fields penetrate deeper into the tunnels than in cases of narrow tunnels. We observed that many disks were caught in the long fringes and experienced a post-acceleration when the RF field reverses its phase. This phase reversal is also responsible for the increase in current interception that is marked in percentage points, since the radial RF fields action changes from converging into diverging. Computations at $\beta_0 a \gg 1$ were not continued due to a rapid increase in interception to impractical levels.

The above finding of increasing η with decreasing $\beta_0 a$ is confirmed by a number of new experimental results in high-efficiency klystrons and TWT designs, mainly at Varian (3), but it seems to disagree with the estimates of Mihran (4), and the very early finding by Cutler (5). It should be remembered that Mihran's conclusions were based on the behavior of rigid disks and did not treat the energy extraction, while Cutler's experiments with helical structures cannot be considered representative of a solid wall tunnel and a discrete gap with regard to RF and space-charge fields. The author knows that the constant bunching level assumed for computing the straight lines of Figure 3 cannot be strictly realized in practical designs. The value $\beta_0 a = 0.5$ is probably as small as can be realized at high frequencies and further decrease in $\beta_0 a$ would only increase the demands upon the focusing fields to excessive levels.

A physical explanation for the behavior presented in Figure 3 was recently found by researchers at Varian, notably E. Lien, who showed that a favorable conversion of second harmonic bunching into fundamental bunching takes place at small values $\beta_0 a$.

Another important selection criteria for high efficiency designs is the choice of perveance which, in turn, is a measure of space charge forces in the beam. Large space charge increases the degree of the velocity spread in beams of all tube types and also decreases the efficiency of depressed collectors. If we again assume constant bunching, then Figure 4 demonstrates clearly the destructive effects of increasing perveance on the electronic efficiency of the output gap. Note also the increase of interceptions. On the other hand, to achieve high overall efficiency, the circuit efficiency, η_K must be as high as possible which requires larger values of perveances. Thus, a compromise is required. This author suggested a value around 0.25 μ perv. as most reasonable selection.

Still another selection must be made concerning the length of the output gap. The results are plotted in Figure 5 with θ_0 , the output gap length in radius, as parameter and the output voltage α_{out} as abscissa. Fortunately, within a range of $\theta_0 = 20^\circ$ to 40° , η remains insensitive to gap length.

Parametric Optimization of the Output Gap Performance

If one assumes, as we did throughout this paper, that the quality and magnitude of the bunching used in this study was very close to a practical optimum, then it should be possible to perform a parametric computer optimization of the electronic klystron efficiency. Note that the value of $\zeta_1/I_0 = 1.81$ obtained by E. Lien is close to the theoretical limit $\zeta_1/I_0 = 2$ and that this design resulted in a very compact bunch and absence of a typical antibunch disk since

the maximum velocity past the output gap was only $1.14 u_0$. With this justification we proceed to discuss Figure 6 which is the most important result of this study.

Figure 6 is a summary of some of our computations executed for disk distribution and klystron design parameters as supplied by Mihran from General Electric and Lien from Varian. Our results are plotted with solid and dotted lines as η versus phase. Available for comparison were results published by Mihran et al. (2) and by Varian (3), both with one-dimensional programs. The top circle indicates an 83 percent value as computed by Lien (3), (and private communication) who measured 75 percent with 2 percent RF interception and the triangle, an 82 percent value as computed by Mihran et al. (2). Note that both investigators used almost identical bunching levels with, however, different $\beta_e a$ values of 0.485 and 0.75, respectively. Disregarding at first interception (which cannot be computed with one-dimensional models) it is seen from Figure 6 that Lien's number is about 3 percent and Mihran's about 10 percent points higher than our result (which indicates 6 percent current interception at $\eta = 0.806$). The strong dependence of η on $\beta_e a$ is evident. A more sensible evaluation is possible if not only measured and computed efficiencies but also interceptions are compared. Turning now to Table I which summarizes measured (by Lien) and computed (author's program) results, excellent agreement in efficiencies is evident. At $a = 1.08$ the agreement in interception is also very good and becomes less good with decreasing a where measurements indicate some residual interception while our program indicates none.

It is believed that this difference is more due to the "nonideal" features of tubes than to program errors. Also, the level of interception in Lien's klystron was very small to begin with.

A comparison between Mihran's measurements of $\eta = 0.62$ with our computations was not possible because Mihran's measurements were carried out at a perveance of 0.72×10^{-6} instead of 0.5×10^{-6} and disk distribution for the higher perveance was not available.

In computing the above cases the correct field distribution between the tunnel tips, as discussed in Ref. 6, was used. The detail is illustrated in Figure 7, case (C) where the ratio of the E_z field at the tunnel tips to that in a middle of the gap at $r=a$ was approximately 2.5. Using the correct, actual field and not the uniform one is important for the trajectories of slow electrons moving close to $r=a$.

Conclusions

A very accurate mathematical model and computer program for the computation of electronic interaction, electron trajectories, interceptions, and efficiency was developed for the output cavity of a klystron amplifier. It is concluded that one-dimensional programs yield efficiencies that are approximately 10 percent points too high at η levels > 0.7 . It has been confirmed that $\eta \approx 0.75$, with a few percent interception, is possible and that $\eta \approx 0.8$ could be obtained with 6 percent "ideal" interception. With the augmentation by a novel depressed collector, overall efficiencies of 80-85 percent seem possible. A very important conclusion is the result that η increases linearly with decreasing $\beta_e a$, at least in the range $0.4 < \beta_e a < 1.0$. Another important conclusion is that efficiency increases initially with interceptions. At $\eta > 0.7$ transverse velocities of many rings are comparable to axial components and exit angles up to 30° were observed.

Multi-Stage Depressed Collectors

The combination of LeRC developed Multi-Stage Depressed Collectors (MDC) and Spent Beam Refocusing Schemes has led to demonstration of highest collector and overall efficiency when applied to TWT's with moderate electronic efficiencies ($\eta_e < 25\%$), Ref. 7. MDC efficiencies in excess of 97% were measured on dc beams of medium perveance ($0.5 \mu \text{ perv}$) and more than 85% MDC efficiency on spent beams with 20% electronic efficiency. This author developed simple relations for predicting the MDC and the overall efficiency, η_{ov} , for TWT's in Ref. (8):

$$\eta_{cd} = \eta_{dc} \left[1 - \frac{1}{N-1} \frac{f(\mu \text{ perv}) \sqrt[3]{\eta_e \cdot \mu \text{ perv}}}{2 - f(\mu \text{ perv}) \cdot \sqrt[3]{\eta_e \cdot \mu \text{ perv}}} \right]. \quad (1)$$

$$\eta_{ov} = \frac{\eta_{ck} \cdot \eta_e}{1 - \eta_{cd} + \eta_{cd} \left(\eta_e + \frac{P_{INT}}{P_o} \right) + \frac{P_{sol}}{P_o}} \quad (2)$$

(P_{int} , P_{sol} designate, respectively, the intercepted and solenoid power).

These relations may be derived, Ref. (8), from a more basic relation derived by this author, also in Ref. (8), for the smallest (normalized) energy of an electron in the spent beam of a helical TWT:

$$\frac{V_{min}}{V_o} = 1 - f(\mu \text{ perv}) \cdot \sqrt[3]{\eta_e \cdot \mu \text{ perv}} \quad (3)$$

The factor $f(\mu \text{ perv})$ is a simple function of the perveance ranging from $f(0) = 1.26$ to $f(2) = 0.8$ for helical TWT's. It assumes different (from those quoted above) but as yet unknown values for coupled cavity TWT's and klystrons. Relation (3) holds also below saturation and does not contain any small signal quantities. Were $f(\mu \text{ perv})$ known for klystrons it could be then applied to eqs. (1) and (2).

During the earlier days of our collector work at LeRC we did some collector work in conjunction with klystrons of microperv .75 at C-Band and 0.5 at Ku band and $\eta_e \approx 40\%$. Highest then achieved collector efficiencies were approximately 65% resulting in overall efficiencies of about only 50% due to interception and poor circuit efficiencies (less than 90%). A klystron with 80% electronic efficiency has a very unfavorable velocity spread that will make the design of a MDC even more difficult because of the presence of majority of rings at the output whose velocities are $< 0.2 u_o$. This author doubts that a MDC efficiency of more than 50% could be practically realized. This

fact plus the presence of interception, circuit losses ($\eta_{ck} \approx 0.95$), the solenoid power and a complex power supply are likely to limit the effective RF output efficiency to below 85%.

Cathodes

Cathode performance and cathode life are the main limiting factors to the reliability and long life of microwave amplifiers. The Microwave Amplifier Group at LeRC was and is, for this reason, engaged and committed to testing and analyzing high performance impregnated tungsten matrix cathodes since 1971. Figure A shows the results of long life tests, carried out in real tubes at a density of $2A/cm^2$ on a large number of samples. At $2A/cm^2$ the standard Philips B-cathode has a useful life of about 40,000 hours. The M cathode, the most promising and interesting of the matrix type cathodes, is expected to perform for 8-10 years at $2A/cm^2$ judging from the recorded performance to date. Since the SPS klystron would require a cathode loading density of only 1 or less A/cm^2 , commensurate with a true cathode temperature of about $980^\circ C$, an educated guess would lead us to an estimated life of perhaps 20 years. Actual test results of this duration are, of course, not available at all and great caution must be exercised in making predictions for system life exceeding 15 years.

References

1. H.G. Kosmahl and L.U. Albers: " Three-Dimensional Evaluation of Energy Extraction in Output Cavities of Klystron Amplifiers. IEEE - TRANS on E.D., Vol. ED-20, No. 10, October 1973, pp. 883-890.
2. T.G. Mihran, G.M. Branch, and G.J. Griffin, "Design and Demonstration of a klystron with 62 percent efficiency," IEEE TRANS on E.D., Vol. ED-18, pp. 124-133, Feb. 1971.
3. E. Lien, " High Efficiency Klystron Amplifier," presented at the 8th Int. Conf. Microwave and Optical Generation and Amplification, Amsterdam, The Netherlands, Sept. 1970.
4. T.G. Mihran, "The Effect of Drift Length, Beam Radius and Perveance on Klystron Power Conversion Efficiency." IEEE Trans. on E.D., Vol. ED-14, pp. 201-206, April 1967.
5. C. C. Cutler, "The Nature of Power Saturation in Traveling Wave Tubes," Bell System Tech. Journal, Vol. 35, pp. 841-876, July 1956.
6. H. G. Kosmahl and G.M. Branch. "Generalized Representation of Electric Fields in Interaction Gaps in Klystrons and Traveling Wave Amplifiers." IEEE Trans. E.D., Vol. ED-20, pp. 621-629, July 1973.
7. IEEE - Transactions on E.D., Vol. ED-26, October 1979, pp. 1589-1598 and 1662 - 1664
8. H.G. Kosmahl, "How to Quickly Predict the Overall TWT and the Multistage Depressed Collector Efficiency." IEEE Trans. on E.D. Vol. ED-27, March 1979

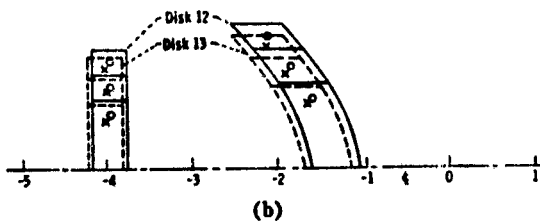


Fig. 1. (a) Effect of source ring on reference ring. (b) Typical overlapping and deformation of disks 12 and 13. Crosses and circles indicate centers of rings. Position -4 is prior and position -2 past the output gap.

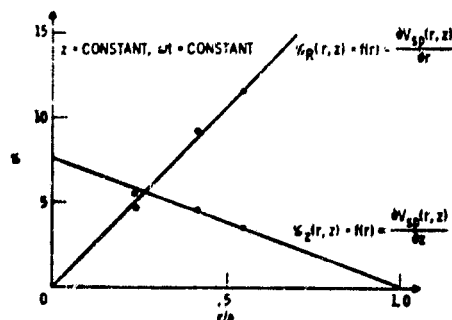


Fig. 2. Typical axial and radial space-charge functions of the beam in the output gap.

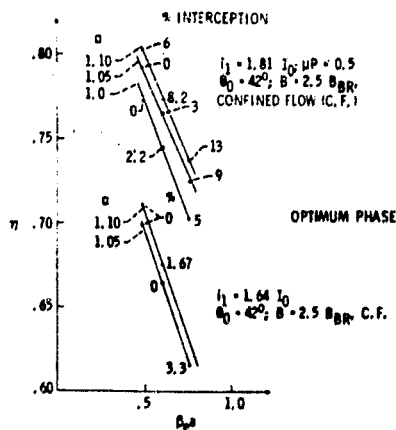


Fig. 3. Efficiency versus $\beta_a a$ with voltage swing α_0 as parameter. Current interception is listed in percent points.

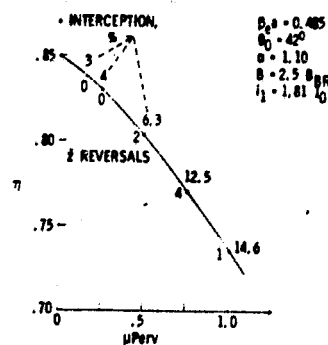


Fig. 4. Efficiency versus perveance assuming constant bunching level. Interceptions and velocity reversals are listed at computed points.

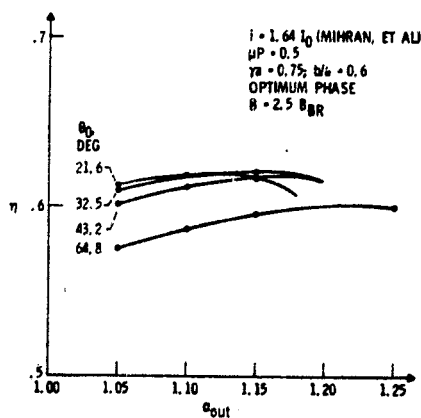


Fig. 5. Efficiency versus output voltage $\alpha = \phi/t_0$ with output gap angle θ_0 as parameter; phase adjusted for highest efficiency.

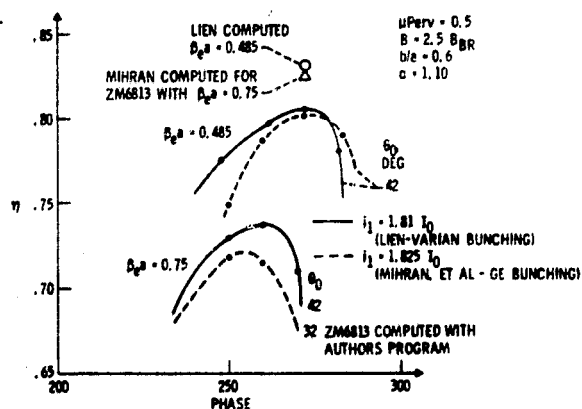


Fig. 6. Internal conversion efficiency computed with authors program for General Electric and Varian high-efficiency designs.

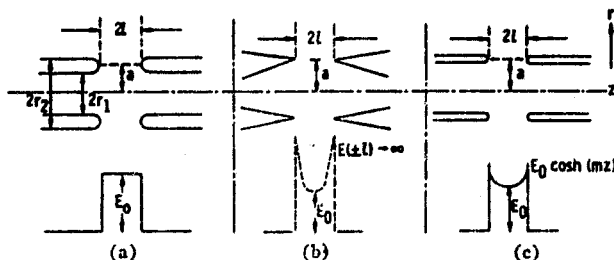


Fig. 7. Electric fields for three differently shaped tunnel tips. (a) Constant field ($E_0 = \text{constant at } r = a$); blunt tips and relatively.

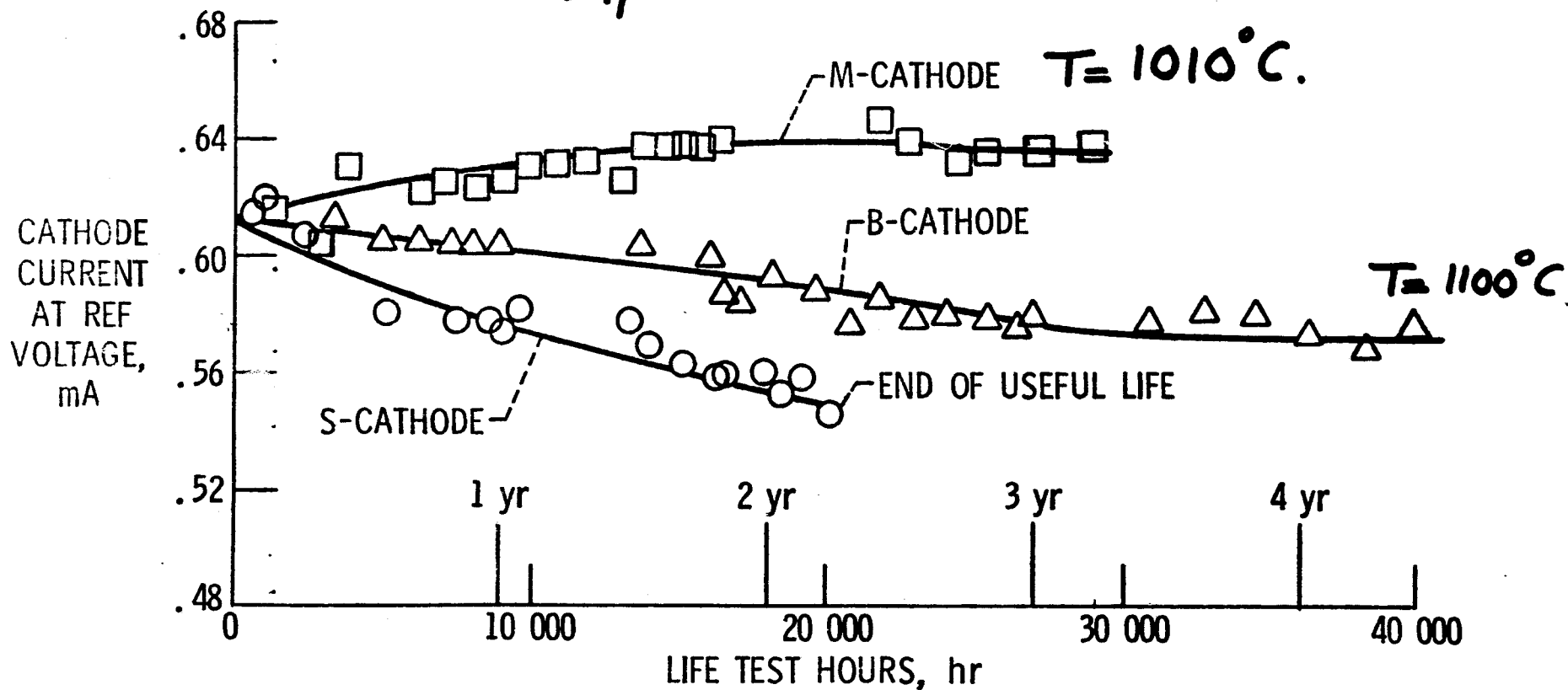
TABLE I
COMPARISON BETWEEN MEASURED EFFICIENCIES
AND INTERCEPTIONS FOR A VARIAN DESIGN
 $I_1 = 1.81 I_0$; $\beta_a a = 0.485$; $\mu p_{\text{rev}} = 0.5$

α	Measured (Lien) η	percent	Authors' Computed η	percent
1.08	0.751	1.9	0.775	1.5
0.953	0.705	1.6	0.709	0.5
0.903	0.681	1.4	0.679	0

Fig 8.

LIFE TEST STUDY OF STATE-OF-ART CATHODES

2 A/cm²



**PROGRESS REPORT ON THE ADAPTING OF THE CROSSED-FIELD
DIRECTIONAL AMPLIFIER TO THE REQUIREMENTS OF THE SPS**

William C. Brown
Raytheon Company
New Products Center
Waltham, Massachusetts 02154

Presented at the MICROWAVE POWER AMPLIFIER SESSION OF THE SPS MICROWAVE SYSTEMS WORKSHOP
January 15-18, 1980, Lyndon B. Johnson Space Center, Houston, Texas

ABSTRACT

Progress in adapting the crossed-field directional amplifier to the SPS is reviewed with special emphasis upon (1) recent developments in controlling the phase and amplitude of the microwave power output, (2) a perceived architecture for its placement in the subarray, and (3) recent developments in the critical pivotal areas of noise, potential cathode life, and efficiency.

Introduction and Background

The first proposed use of the crossed-field directional amplifier in the solar power satellite dates back to 1969 and 1970.¹ Since then there have been a number of successive discoveries and developments resulting in an ever-increasing better fit between the device and the severe requirements that are imposed upon the generator by the SPS.

First proposed by the author in the form of a 200 to 400 kW liquid cooled amplatron¹, the crossed-field device approach was soon changed to a passively cooled amplatron in the power range of five to ten kW because of the high desirability of passive cooling in the SPS satellite as pointed out by O.E. Maynard.² Such a tube was designed and the first phase of its development completed.

In 1975 R.M. Dickinson of JPL proposed that because of its high efficiency, simplicity, relatively low mass, and already established high production volume and low cost, the microwave oven magnetron be incorporated into a directional amplifier package and considered for the SPS. While subsequently investigating this approach the author made two important discoveries: the first, that the microwave oven magnetron, when operated with a ripple-free DC power source and with no externally applied filament power, has an extremely high signal to noise ratio⁴; the second, that under these conditions the carburized thoriated tungsten cathode can be operated at such low temperatures that a potential life of more than 50 years is indicated under the high-vacuum and highly controlled operating conditions in space.^{5,6}

The potential role of the magnetron directional amplifier in the SPS is now being further evaluated under a NASA-MSFC contract.⁷ This investigation first involves an extension of the laboratory data base on the magnetron directional amplifier utilizing the microwave oven magnetron. This data, when combined with information obtained from other sources, will then make it possible to accurately define the projected characteristics of a higher powered version of the magnetron directional amplifier for SPS use, and to define a program of technology development that would result in the development of such an amplifier.

Because of the basic similarities of the magnetron and amplatron in their construction configurations and performance characteristics it is found that much of the experience gained in adapting the amplatron to SPS use is directly applicable to a similar adaptation

of the magnetron directional amplifier.

The current study involves a penetrating look at all of the interfaces associated with the magnetron directional amplifier. At least one level of higher integration must be examined, and in some instances, more. The study has progressed far enough to yield a specific architecture that is shaped by these interfaces and that appears to have many attractive features.

One of the most important developments of the current activity is the precise control of both the amplitude and phase of the microwave power output from the amplifier by feedback control systems utilizing phase and amplitude references. The method by which amplitude is controlled is of overall SPS system interest in that it can be adapted to match the entire microwave generating system to the solar photovoltaic area at the point of maximum operating efficiency.

The material which follows is intended to provide the reader with: (1) a brief summation of those features of the crossed-field device that are of a desirable nature for the SPS; (2) a comparison of the amplatron and the magnetron directional amplifier for orientation purposes; (3) knowledge of the recently established architecture of the subsection of the subarray into which the amplifier is placed; (4) an introduction to the recently developed method for accurately controlling the phase and the amplitude of the microwave power output; (5) discussions of several very important pivotal areas relating to noise, tube life, and efficiency and (6) a summation of areas of concern needing additional attention.

Features of the Crossed-Field Microwave
Generator that are Desirable for the SPS

- **High Efficiency:** Overall efficiencies in excess of 85% have been demonstrated in an off-the-shelf magnetron used for industrial microwave heating and in certain laboratory models of the amplatron. An efficiency in excess of 80% at power levels (3 kW) low enough to utilize passive cooling has also been obtained.
- **High Signal to Noise Ratio:** Random noise level in a 1 MHz band down 100 dB or more at frequencies above and below carrier frequency by more than 10 MHz. The noise level may be lower because instrumentation is the limitation.
- **Potential Life of 50 Years or More:** Such life is possible by operating at low emission current densities that allow the low operating temperatures that have a proven association with extremely long life of carburized thoriated tungsten cathodes.

- **Low Ratio of Mass to Microwave Power Output:** The current estimate by the author is 0.4 kilograms per kilowatt of microwave power at the tube output. This includes the weight of the passive radiator but not the buck-boost coils which are considered a power conditioning function.
- **Accurate Control of the Phase and Amplitude of the Microwave Power Output:** By use of a set of phase and amplitude references and a set of phase and amplitude sensors the phase can be controlled to within ± 1 degrees and amplitude to within $\pm 3\%$.
- **Potential to Perform the Bulk of the System Power Conditioning Requirements:** The buck-boost coils necessary for output amplitude control of the magnetron can take on the added function of adjusting the input of the microwave system to operate at the optimum output voltage for the solar array.
- **Minimal X-Ray Radiation:** The crossed-field tube energy conversion mechanism generates negligible radiation, permitting maintenance functions during operation of the SPS.
- **Only One Voltage and Two Terminals Required for Normal Microwave Tube Operation:** Auxiliary power is required for a few seconds to heat up the cathode and initiate emission.
- **Simplicity of Construction:** The crossed-field device, particularly in its magnetron form, is very simple in construction.
- **High Degree of Maturation in Production and Cost:** Currently, more than two million magnetrons that closely resemble a similar tube for the SPS are manufactured annually for the microwave oven.

Definition of Crossed-Field Directional Amplifiers - Comparison of Amplitron and Magnetron Directional Amplifier

A directional amplifier is defined as a device which passes energy in both directions but which amplifies in only one direction. There are at least three ways, as shown in Figure 1, in which a crossed-field device may be used as a directional amplifier. The first is in a self-contained device called the amplitron.^{8,9} The amplitron is unique among the devices in that it needs no assist from auxiliary devices to obtain its directional amplification. It is a relative broadband device and has a very small phase change from input to output as a function of a change in frequency, magnetic field, or DC current level as compared with other crossed-field directional amplifiers and linear beam tubes, as well. This feature is advantageous in many applications where a high degree of phase stability is needed. The device does have limited gain of about 10 dB. The device is widely used in radar systems.

The second way is the combination of a magnetron oscillator and ferrite circulator which converts the magnetron oscillator into an amplifier with a bandwidth over which gain can be obtained.¹⁰ The bandwidth is dependent upon the level of the drive relative to the level of the power output of the device. Typically, a bandwidth of 15 MHz can be obtained at 2.45 GHz with a gain of 20 dB while 5 MHz is possible with a gain of 30 dB. At these gains and within these bandwidths, the efficiency will remain high and nearly constant. The very high signal-to-noise ratio is independent of bandwidth and gain.

The total range of phase shift within the device as the drive frequency is shifted over this bandwidth is approximately 180°. The center of the frequency range over which amplification occurs is at a frequency dependent upon the operating current level of the tube, the temperature of the tube envelope, and other secondary factors.

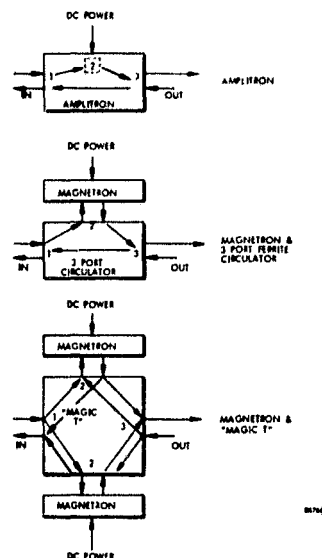


Figure 1. Directional Amplifier Approaches Utilizing Crossed-Field Devices.

As shown in Figure 1, the principle can also be carried out by means of a "magic T" or, synonymously, a 3 dB hybrid, an alternative method originally suggested for the SPS by R.M. Dickinson. A matching of the characteristics of the two tubes is required in the hybrid, but a ferrite circulator is not required.

It should be noted that the operating theory of the directional amplifier is well established.¹⁰ They are often called "reflection amplifiers" or "locked oscillators". The principle is probably more often employed for solid state amplifier devices than for vacuum tubes.

It is important to realize that the magnetron device and the amplitron are very closely related so that development work that is done on one may be directly applicable to the other, as indeed is the case in the SPS. A set of scaling laws and design equations apply equally well to both devices in establishing their power level, voltage and current inputs, efficiency, cathode size, and other basic parameters. Both devices even use the same slow wave circuit, with which the electrons interact. However, the manner in which connections are made to this internal circuit is the basis of distinguishing these devices. As shown in Figure 2, the circuit is made reentrant in the magnetron and one output connection is made to the device, while the internal circuit in the amplitron is cut and the ends of it matched to external transmission lines.

Overall Architecture of the Subarray Employing the Magnetron Directional Amplifier

Physically placing the microwave generator in the subarray and making the proper allowances for its many electrical and mechanical interfaces with other components

and with space itself introduces the perennial systems design problem of making all the parts fit. This problem is currently being worked on as a necessary part of the MSFC study to project the characteristics of the magnetron directional amplifier and to define the technology development program to fully develop the magnetron directional amplifier.⁷

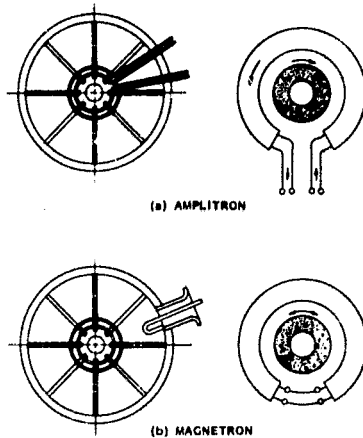


Figure 2. Diagram Illustrating the Basic Differences of Construction and Operation Between the Amplitron and the Magnetron.

It is believed that the development of the subsection shown in Figure 3 represents a substantial advancement toward the ultimate solution of this problem. The design recognizes and solves the following problems:

1. The microwave generators must dispose of their heat directly to space by operating at temperatures in the 200° to 300°C range. On the other hand, solid state devices which may be needed for many purposes cannot reliably operate at temperatures higher than 150°C and lower temperatures are preferable.

The design takes care of this problem by having the generators radiate heat in only one direction. Heat normally radiated toward the face of the array is largely reflected by a thin insulation blanket. There is also a substantial temperature drop across the thin walled waveguide construction. The solid state devices are located either on the face of the slotted waveguide array or in the slots immediately back of the face which are a property of the proposed method for fabrication of the thin-walled slotted waveguide radiators. Such components may be easily attached to heat radiating sinks on the front surface, if need be.

2. Phase and amplitude sensors, phase and amplitude references, and electronics associated with the control loops for phase and amplitude control must be incorporated. The architecture of Figure 3 provides the means of putting both the references and sensors for both amplitude and phase at the point where they are needed most-right at the radiating surface of the antenna. All solid state devices that are associated with the control electronics are located in the same area where they can be operated in a relatively cool environment.

In the architecture the phase and amplitude references are fed from the backbone of the subarray through flat ducts welded to the surface of the slotted waveguide arrays. These ducts serve an additional function in that they are very effective stiffeners of the thin aluminum faces of the waveguide array. However, the fact that these ducts run all the way to

the edge of the subarray governs the number of tubes and area of slotted waveguide array that are in the subsection. Thus, the whole subsection may be considered as a plug-in unit and this concept replaces the earlier held concept that each tube and its slotted waveguide array section represented a plug-in unit.

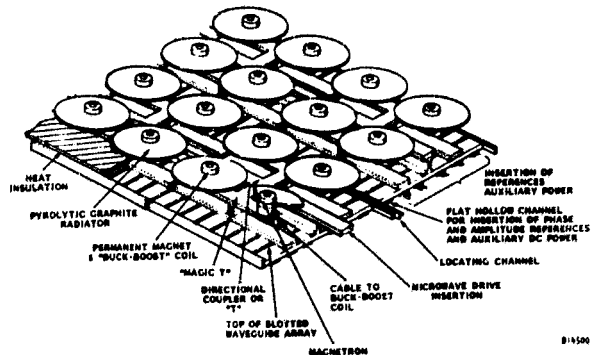


Figure 3. Assembly Architecture for the Magnetron Directional Amplifier in the Antenna Subarray. Two Subsections are Shown. Microwave Drive and All References and Auxiliary Power are Inserted from the "Backbone" of the Subarray. The Array has Two Distinct Temperature Zones. The Top is Used to Radiate the Heat. The Bottom is Used for Mounting of Solid State Components.

3. Interface with the microwave drive source. In Figure 3 the microwave drive source is not shown but it is derived from another magnetron directional amplifier identical to the ones directly attached to the waveguide radiators. At a gain level of 20 dB, one magnetron directional amplifier can drive between 50 and 100 other magnetron directional amplifiers. The microwave drive for any one subsection, as shown, is delivered to the intended tube through a waveguide which runs the length of the subsection and serves all the tubes. The energy may be siphoned off by a number of different techniques including directional couplers and the standing wave techniques used in the design of the slotted waveguide radiators.

After the power is taken off the central waveguide feed it enters one port of a "magic T", or alternatively, one of the ports of a ferrite circulator (not shown). Two magnetrons with matched performance are placed at either end of the Magic T, unequally separated in distance from the center by a quarter wavelength. The combined power of these generators then comes out of the fourth port of the device directly into the slotted waveguide array.

4. One of the interesting features of this architecture is that the cathode and magnetic circuits are operated at ground potential. This permits the power for initial heating of the filament and for energizing the buck-boost coils on the magnetron to be operated at ground potential. The anode and its radiator are isolated from ground potential by means of alumina ceramics which also support the anode and the magnetic circuit. The output of the magnetron is a coaxial probe which excites the waveguide without physical contact and therefore can remain at anode potential.

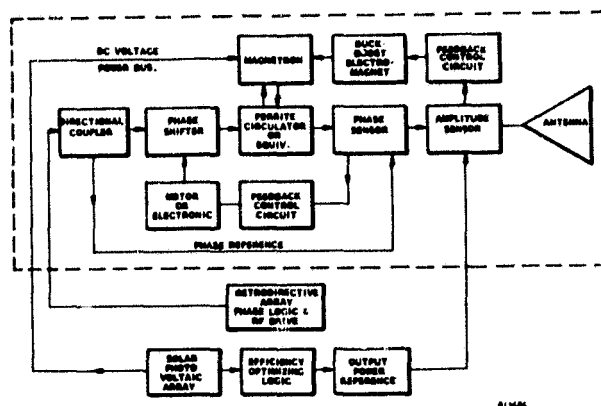
5. Sources of auxiliary power. Not shown in Figure 3 but located along the spine feeding the subsection array are sources of the auxiliary DC power needed

Incorporation of Phase and Amplitude Tracking in the Magnetron Directional Amplifier

The control of the output amplitude in the face of many factors that tend to change that amplitude is also essential for generating an efficient microwave beam. In the case of a crossed-field device the output amplitude can be controlled to a predetermined value by another control loop which makes use of small electromagnets that can be used to boost or buck the residual field provided by permanent magnets.

It is of importance to note that the magnetron directional amplifier will be operating in an efficiency-saturated mode so that modest changes in operating voltage will have only a minor impact upon operating efficiency. Thus the optimized efficiency of the solar cell array will predominate in the combined operating efficiency of solar array and microwave generators.

absorption by the solar cell array. A central computer establishes the most efficient operating point (maximum power output) of the solar cell array and then adjusts the reference power output of the banks of magnetron directional amplifiers, making certain of course not to err on the side of asking for more power than is available from the array.



The phase and amplitude tracking system requires a set of references and a set of sensors. These references and sensors are located at the front face of the slotted waveguide array where the most accurate sensing of the phase and amplitude can be made and where the solid-state sensing and control devices can find a temperature environment that they can tolerate.

The phase control system makes use of a phased-controlled signal from a central source, a sample of the output power, and a balanced detector which compares their phases. The error signal can be used to operate a number of different types of phase shifters positioned in the input side of the magnetron directional amplifier.

Noise Emission Properties of the Amplitron, Magnetron, and Magnetron Directional Amplifier

The lack of historic data on the noise performance of CW crossed-field devices and the consequent inability to predict their behavior in the SPS application where the noise level of the transmitter is

a highly critical issue understandably became a major factor in the preliminary selection of a generator approach in the reference design. In the recent time frame people within the SPS microwave system community have become aware of the very low noise data that has been obtained from the microwave oven magnetron^{4,5} which is now serving as a scaled-down version of an SPS magnetron and to a lesser degree they are aware of the low noise data that was obtained from the amplatron development.

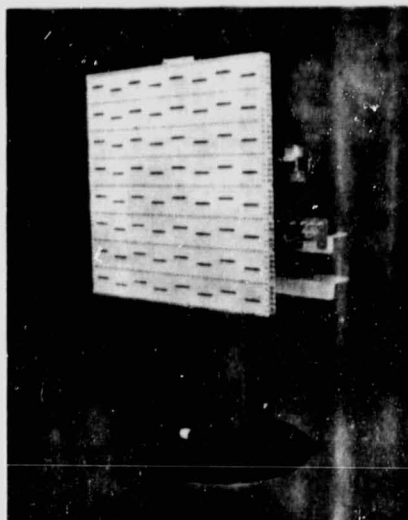


Figure 5. Test Bed for the Phase and Amplitude Tracking Investigation, Shown with Slotted Waveguide Load as an Option.

The early lack of data in this area is understandable when it is considered that the production of random noise outside of an area immediately around the signal (where it is important in communication or doppler radar applications) has been of little concern or interest in the past. However, just the converse is true in the SPS application where the high power level of the transmitter makes it mandatory to have very high ratios of carrier signal to random noise everywhere but immediately close to the carrier. Even after the importance of this noise was realized it was necessary to make special noise measuring setups to obtain more sensitive measurements of noise. In these setups the carrier signal was greatly attenuated in order to allow the noise to be visible as exhibited on a sensitive spectrum analyzer.

Many measurements of signal to noise ratio over frequency ranges of as much as ± 1000 MHz either side of the carrier have been made on magnetron directional amplifiers with this equipment. A typical set of measurements is shown in Figure 6.⁴ The data was taken both with normal external power applied to the filament and with no external power applied. The reader's attention is to be focused on the very high signal to noise ratio that is obtained over a frequency sweep of 200 MHz with no external power applied. The signal to noise ratio is 100 dB for a 1 MHz band of noise. This corresponds to a signal to noise ratio of 130 dB per 1 KHz of noise which is greater than the 125 dB quoted for the klystron in the reference design. Sweeps of ± 1000 MHz around the carrier also exhibit equally large signal to noise ratios. The reader is reminded that with these signal to noise levels even a 10 gigawatt transmitter would be radiating only one watt of noise for each megahertz of the

frequency spectrum.

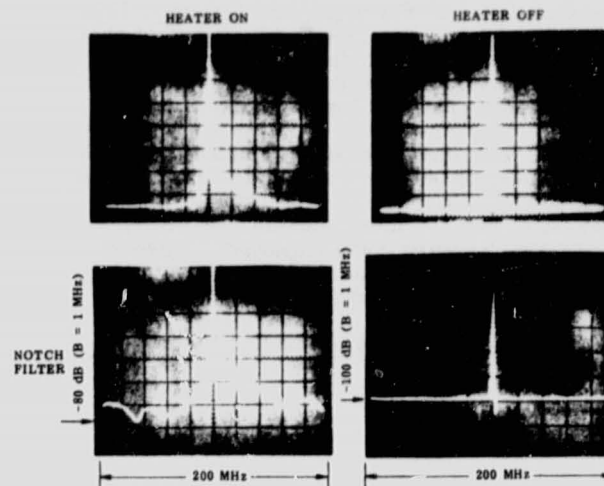


Figure 6. Spectrum of Locked Magnetron.

The signal to noise level may be substantially better than 100 dB/MHz because the measurements are still limited by equipment sensitivity. The sensitivity is currently being increased by 20 dB so that signal to noise ratios of as great as 120 dB/MHz can be measured.

It should be noted that while these noise measurements were made with a device gain of approximately 20 dB, the noise behavior remains independent of gain at high gain levels. At high gain levels the drive source appears as a small reflection factor (0.1 for a gain of 20 dB) and this has a negligible impact upon the behavior of the tube.

It should also be noted that these low noise measurements have been observed on magnetrons made by different manufacturers and in different time periods, but not on all magnetrons that have been randomly selected. However, no studies of a statistical nature have been made nor probably should be made until more sensitive measuring equipment is available. And it may be more effective to devote any limited future effort to better understanding the sources of noise in the magnetron.

There is currently no government support of any investigation into the sources of noise in the crossed-field device. However, Raytheon Company did carry on a modest effort in this area in 1979 in which special external probing equipment was built to examine the fine structure of magnetron operation with the hope of determining some of the factors that greatly impact the noise performance. Some of these results are very interesting but a discussion of their logic and implications would be so lengthy and involved that it would be outside the scope of this summary article.

Measurements of close-in phase modulation noise added by the magnetron directional amplifier¹¹ were also made when it was operating with a gain of approximately 20 dB. These measurements indicated a carrier-to-noise level that was typically 115 dB for a 1 KHz band of noise in the range of 10 KHz to 100 KHz removed from the carrier frequency. This represents excellent performance.

The discussion is now turned to harmonic generation. In this area there was no particular issue between the crossed-field and klystron device

approach since it is known that both of these devices along with all other classes of microwave generators produce harmonics. It was apparent, however, that there was little data on the quantitative level of these harmonics in any device, partly for the reason that it is difficult to make such measurements in waveguide where the harmonics usually become accessible.

However, a method of making measurements in a small coaxial line and water load attached immediately to the output of the magnetron and matched into it with a normal loaded Q, thus avoiding the problem of multiple mode propagation, was employed. Measurements made on two representative tubes, designated as #11 and #12, are given below.¹²

Frequency	HARMONIC LEVELS	
	#11 *dbc	#12 *dbc
f_o	0	0
$2 f_o$	-71	-69
$3 f_o$	< -51	-85
$4 f_o$	-86	-93
$5 f_o$	-62	-64

*dbc - decibels below carrier level

These findings are somewhat better than had been anticipated. The unexpected anomaly of the significant energy at the 5th harmonic is an indication of the difficulty of the a priori assessment of the more complicated characteristics of any microwave generator that may be designed for the SPS.

Investigation into the Designing of Magnetrons with Cathode Life of 50 Years

It is well known from the theory and experience associated with properly carburized thoriated tungsten cathodes that such cathodes can have extremely long life if they are operated at low temperatures in a good vacuum.^{13,14} An investigation of the application of this knowledge to the design of long life cathodes for SPS magnetrons was precipitated by a question raised by a NASA representative about the life of tubes with carburized thoriated tungsten cathodes that had exhibited very high signal to noise ratio when power from the external heater source was set to zero.⁶ The resulting investigation not only indicated that very long life can be achieved but also led to the discovery of an apparently overlooked feedback mechanism in the magnetron that maintains the emitting surface of the cathode at a temperature just sufficient to supply the needed current that flows from the cathode to the anode.¹⁵ This mechanism assures that the tube will determine its own long life, independent of external circumstances with the exception of compromised high vacuum and demand for increased anode current beyond the design value.

The investigation that was made began with the use of an optical pyrometer to observe the brightness temperature of the magnetron cathodes through optically transparent windows in specially constructed tubes. The arrangement is shown in Figure 7. The tube is fitted inside of a magnetic solenoid so that the magnetic field and therefore the operating voltage of the tube can be varied. Most measurements were made without the application of any external heater power to the filament.

It was observed that the only parameter that had a significant impact upon the cathode temperature was anode current. It had previously been assumed, for

example, that cathode bombardment power would increase with greater magnetic field and greater power input. By contrast, it was observed that when the anode current was held constant and the magnetic field varied over a range of two to one to give an increase of power input by approximately the same amount, the cathode temperature remained the same to within $\pm 10^\circ\text{C}$, or not much greater than the resolution of the optical pyrometer.

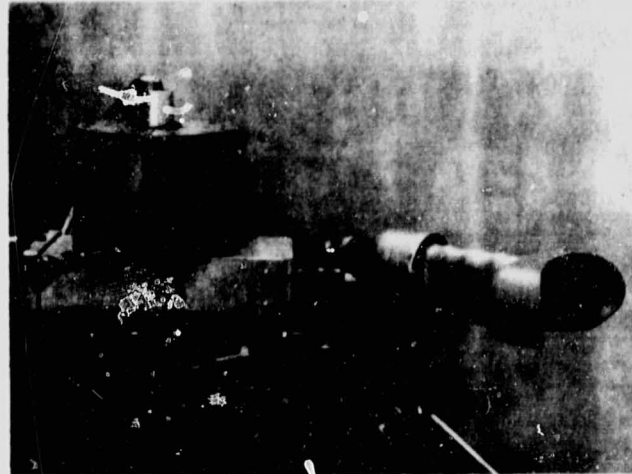


Figure 7. Test Arrangement for Viewing the Temperature of the Filament-Type Cathode in the Microwave Oven Magnetron as a Function of Anode Current, Applied Magnetic Field, and Microwave Load. Optical Pyrometer is in the Right Foreground. Transparent Window is Visible Outside of Solenoid-Type Electromagnet.

The variation of cathode temperature with anode current is shown in Figure 8. The slope of this curve is nearly the same as that obtained from the Richardson-Dushman equation which predicts temperature limited emission density as a function of true temperature. If the Richardson equation is matched to the true temperature of 1896° Kelvin that corresponds to a brightness temperature of 1500°C, then a reasonable value for the constant A of the equation is obtained. The emission as a function of temperature may then be obtained and as the three points on Figure 8 indicate follows closely the experimental data.

It has been established from life test evaluations that the life of a carburized tungsten cathode is a very steep function of the operating temperature. The difference between life at 2000°K and 1900°K is a factor of ten.

From the great body of design data that is based upon many laboratory investigations as well as life test data, an operating temperature of 1900° Kelvin is associated with a potential life of 500,000 hours or more than 50 years, as derived from the curves and the notes on Figure 9, if the cathode is made from 0.040 inch diameter wire that is 50% carburized.^{13,14} This is a reasonable design and a reasonable operating temperature for a cathode that could be used in a magnetron designed for SPS use.

Of course, life test data for 50 years is not available. But the design data of Figure 7 would have predicted a life of 130,000 hours for each of a lot of 12 tubes manufactured by Machlett for use in the WWV transmitter. The filament wire was 0.035 inch in diameter and 20% carburized, and the tubes were run at 1950° Kelvin. The 12 tubes had a total running

time of 850,000 hours and there had been no failures when the equipment was retired from service. Some of the tubes had been operated at 86,000 hours or 2/3 of the predicted life. Considering that there were no failures among the 12 tubes this test would indicate that the use of Figure 7 is conservative practice.

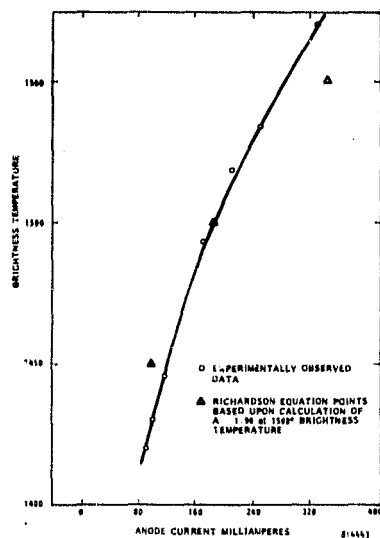


Figure 8. Cathode Brightness Temperature and Associated Points of Temperature Limited Emission as Function of Anode Current in the Microwave Oven Magnetron.

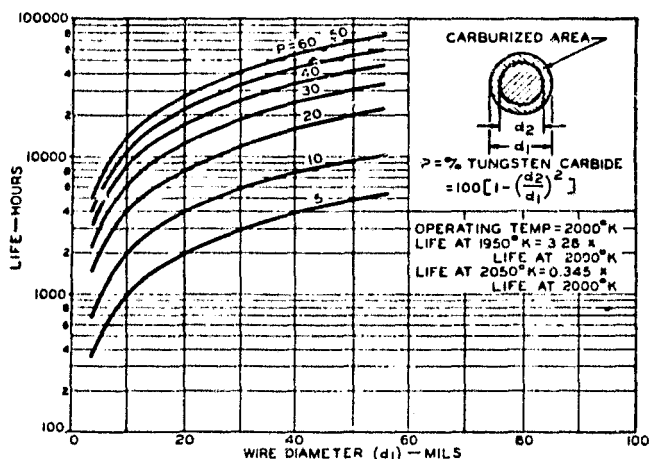


Figure 9. Thoriated-Tungsten Filament Life Curves as Function of Wire Diameter and % Carburization. Note Increase or Decrease in Life as Function of Temperature as Noted.

These tubes were also high power and high voltage tubes, similar to the projected SPS magnetron and subject to the same cathode failure mechanisms if the vacuum inside of the tube were not sufficiently good.

The conclusion is that a very good argument can be made for extremely long cathode life in the proposed SPS magnetron. The argument is based upon observations of low operating cathode temperatures in operating magnetrons, an internal mechanism that will automatically keep the cathode temperature as low as possible over closely controlled operating conditions in the SPS, an enormous body of experience and information on the carburized thoriated tungsten cathode that is well documented in published papers and books and the correlation of the long life of the Machlett tubes with predicted life.

Crossed-Field Device Efficiency

Crossed-field electron tubes of the magnetron and amplatron type are properly recognized as the most efficient of microwave generator devices. But the highest electronic efficiency, defined as the efficiency with which DC power is converted into microwave power, is associated with a high ratio of the magnetic field B to a design parameter B_0 which is proportional to frequency as shown in Figure 10. But the theoretical electronic efficiency is always degraded to some degree by the circuit efficiency, and can be degraded by improper design of the interaction area and other design parameters as well. When the B/B_0 ratio is high and the tube otherwise properly designed the measured electronic efficiency has exceeded 90% as exhibited by the commercially available 8684 magnetron. For reasons largely related to the physical size and cost of the permanent magnet, crossed-field devices are almost always designed in the range of B/B_0 of four to six. This is true of the microwave oven magnetron whose operating characteristics have recently been intensively evaluated.

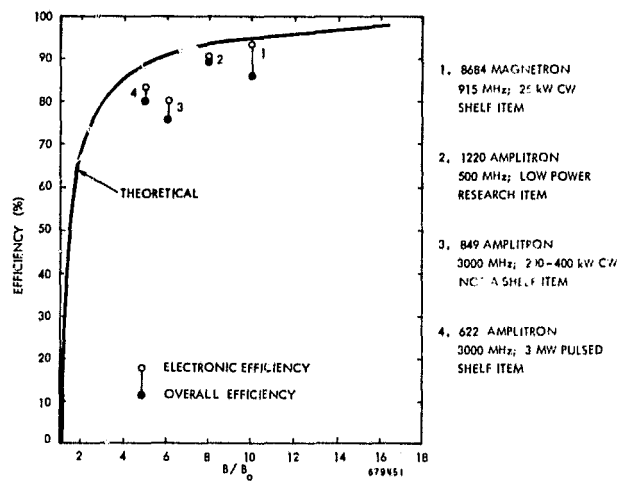


Figure 10. Magnetron Efficiency as a Function of B/B_0 Ratio.

However, the microwave oven magnetron can have its permanent magnet removed and be operated in an electromagnet. When this has been done the measured overall efficiency can be considerably increased as shown in Figure 11. The measurement of $82 \pm 1\%$ efficiency was carefully measured after extensive preparation and precaution and then a balance was made between the DC power input and the sum of the microwave power output and the power dissipated in the anode as an additional precaution.¹⁶ After taking a carefully measured circuit efficiency of 95% into account, the electronic efficiency was computed to be

86%. To this may be added at least one and perhaps two percentage points to take into account the amount of backbombardment power that was needed to heat the cathode to a temperature sufficient to provide the emission (No external filament power was used).

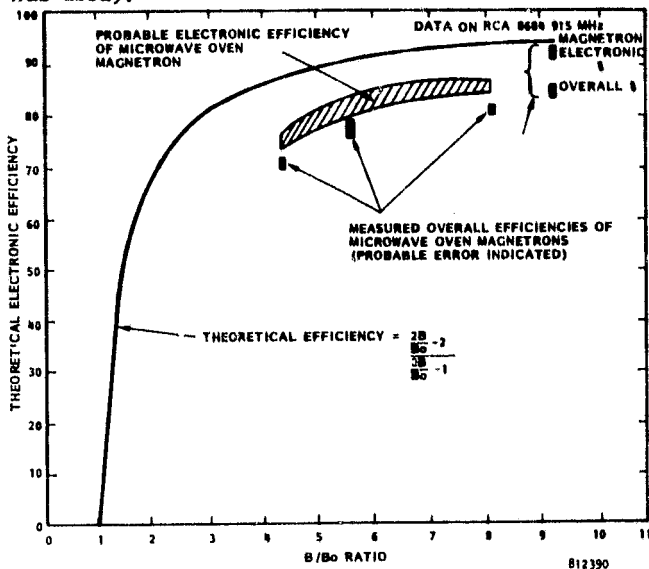


Figure 11. Theoretical and Experimentally Observed Electronic Efficiencies of Conventional Microwave Oven Magnetron and 915 MHz Magnetron. Electronic Efficiency is Efficiency of Conversion of DC Power into Microwave Power. Overall Efficiency Includes Circuit Inefficiencies which can be Ascertained from Cold Test Data.

Although this efficiency may seem high, actually it is from six to eight percent lower than it should be, and considerably below that of the 8684 previously referred to and also shown in Figure 11. The reason for the degraded efficiencies that seem to occur for all B/B_0 ratios is not fully understood. A contaminated field pattern does exist in the tube in the cathode-anode interaction area and there may be some leakage current, although small, around the end shields. But there are probably other factors as well.

To the author's knowledge there has never been a dedicated effort to maximize the efficiency of the crossed-field device, with but one exception. The one exception was an effort made on an amplatron device and resulted in an overall efficiency of $90\% \pm 3\%$ (Figure 10). It therefore seems probable that if there were a dedicated effort to optimize the design for efficiency an efficiency of 90% could be achieved from an SPS tube. The procedure would be to use high B/B_0 ratios, make certain that the end shield and pole piece design were proper, make certain the cathode potential always remained at a neutral potential with respect to the vanes, contour the vane tips, and design for high circuit efficiency.

Areas of Concern Needing Additional Attention

Although the magnetron directional amplifier has been operated at very high carrier-to-noise levels, confidence in such performance and the potential to improve on that performance must be based upon an improved understanding of what causes the noise. Recent experiments would seem to indicate that the random noise that is observed is not an inherent property of the basic energy conversion mechanism in the crossed-field device but is rather associated with one or more extraneous mechanisms that are complex

and difficult to comprehend. It is expected that various hypotheses may be generated to explain them but that there will be little confidence in these hypotheses until special tubes are constructed to test them.

Similarly, in the area of efficiency, there is the concern for the microwave six to eight percentage points in efficiency in the microwave oven magnetron and more than that in the experimental amplatron. Presumably, most of this efficiency loss can be accounted for by the contaminated field patterns in the interaction area; therefore tubes with good field patterns should be constructed to check this hypothesis.

Of particular concern are complications arising from the desire to operate the SPS tube at relatively high magnetic field to obtain high efficiency and at high ratios of voltage to current to assure long cathode life, but measurements of signal to noise from the microwave oven magnetron run with these conditions indicates a lower signal to noise ratio. It should be noted that under these conditions the rather primitive end-geometry arrangement to contain the space charge may allow current leakage from the interaction area that can lead to noise. The condition may be further exacerbated by a change in the shape of the magnetic field caused by magnetic saturation of the pole tip.

To better understand these areas of concern it seems clear that some special experiments requiring a special experimental tube will be needed.

BIBLIOGRAPHY

1. W.C. Brown, "High Power Generators of the Crossed-Field Type" in Journal of Microwave Power, Special Issue on Satellite Solar Power Station, Volume 5, No. 4, Dec. 1970. pp. 245-259.
2. "Microwave Power Transmission System Studies" Raytheon Contractor Report ER75-4368 NASA CR-134886, December 1975.
3. W.C. Brown, "Design, Fabrication and Testing of a Crossed-Field Amplifier for Use in the Solar Power Satellite" NASA CR-159410 Contract NAS3-20374 LeRC.
4. Raytheon Briefing Document on "Crossed-Field Directional Amplifier for Use in the Solar Power Satellite" - to JSC and MSFC in September 1978.
5. "Microwave Beamed Power Technology Improvement", JPL Contract # 955104 with Raytheon Company. Monthly Progress Report #9 for March, 1979.
6. Technical Letter of September 12, 1978 to Robert O. Piland from W.C. Brown.
7. "Satellite Power System (SPS) Magnetron Tube Assessment Study" MSFC Contract NAS8-33157 with Raytheon Company.
8. W.C. Brown, "Description and Operating Characteristics of the Platinotron - a New Microwave Tube Device", Proceedings of the IRE, Vol. 45, No. 9, pp. 1209-1222, Sept., 1957.

9. W.C. Brown, "The Platinotron: Amplitron and Stabilotron", in E.C. Okress, *Crossed-Field Microwave Devices*, Vol. 2, Academic Press, 1961, pp. 165-209.
10. E.E. David, "Phasing by RF Signals" in E.C. Okress, *Crossed Field Microwave Devices*, Vol. 2, Academic Press, 1961, pp. 375-399.
11. Microwave Beamed Power Technology Improvement, JPL Contract #955104, with Raytheon, Monthly Progress Report #10 for April 1979.
12. Microwave Beamed Power Technology Improvement, JPL Contract #955104, with Raytheon, Monthly Progress Report #14 for August 1979.
13. W.H. Kohl, "Handbook of Materials and Techniques for Vacuum Devices" Reinhold Publishing Corp, 1967, pp. 487-491.
14. Ayer, R.B., "High-power Industrial Vacuum Tubes Having Thoriated Tungsten Filaments," AIEE Trans., 72, Pt. 1, 121-125, (May 1953).
15. "Microwave Beamed Power Technology Improvement," JPL Contract #955104 with Raytheon Monthly Progress Report #5 for Nov. 1978.
16. "Microwave Beamed Power Technology Improvement," JPL Contract #955104 with Raytheon Monthly Progress Report #10 for April 1979.

RADIATING ELEMENTS SESSION

. RECEDING PAGE BLANK NOT FILMED

C. D. Lunden, W. W. Lund
E. J. Nalos, Boeing Aerospace Company

1.0 SPS ANTENNA ELEMENT EVALUATION

The SPS transmitting array requires an architecture which will provide a low weight, high efficiency and high structural rigidity. Several candidate antenna configurations include the parabolic dish, the parabolic cylinder, the lens and the waveguide slot array. As discussed below, the waveguide slot array is preferred over the other options.

Parabolic dishes are widely used on earth. For SPS application, they could be readily laid up in six-foot diameters with lightweight graphite-epoxy materials. On the other hand, the area efficiency of such an array is relatively low. Moreover, a zero spillover feed configuration is not presently apparent.

An array of parabolic cylinders with line-source feeds could give better area efficiency than an array of dishes, but would suffer from feed blockage.

A lens, using lightweight waveguide structures, with zero blockage behind-the-lens feedhorns can have high efficiency and little spillover, but the SPS center-to-edge illumination tapers would give a spatial "lumpiness" which would produce undesirable grating lobes in the far-field pattern.

As noted above, waveguide slot arrays constitute the most desirable option. Consequently, such an array has been chosen for the SPS. Waveguide slot arrays offer high efficiency, uniform illumination, and are fairly lightweight. Bandwidths of such arrays are narrow, typically 1/2-2%. Although this does not directly impact the SPS, which transmits power at a single frequency of 2.45 GHz, the narrow bandwidth does constrain the thermal and mechanical tolerances of the antenna.

2.0 SLOTTED WAVEGUIDE MODULE DESIGN VERIFICATION

2.1 EXPERIMENTAL PROGRAM

The purpose of this program is to better define the electronic aspects of an SPS specific waveguide slot array. The specific aims of the program are as follows:

- o To build a full-scale half-module, 10 stick, array, the design parameters for which are to be determined by analytical considerations tempered by experimental data on a single slotted radiating stick.
- o To experimentally evaluate the completed array with respect to antenna pattern, impedance and return loss.
- o To measure swept transmission amplitude and phase to provide a data base for design of a receiving antenna.

2.2 ARRAY CONFIGURATION

The first step in module design is to fix the gross dimensions, including the module length and width, and the dimensions of the radiating sticks and the feed waveguide. Because the feedguide is a standing wave device in which the coupling slots must be spaced by $\lambda_g/2$, where λ_g is the guide wavelength, and because λ_g is a function of waveguide width, the radiating stick and feedguide dimensions are not independent.

The SPS baseline design calls for a half-module of ten 1.6 m long sticks of 6 cm x 9 cm cross-section. For these dimensions, at the SPS frequency, the feedguide dimensions are also 6 cm x 9 cm. To assess the desirability of the baseline configuration, the ohmic losses of several alternative configurations of equal area were calculated. The I^2R losses for these are plotted in Figure 1 as functions of radiating stick

in the loss curve is quite shallow. Also, the values of the minima do not appear to be very configurationally sensitive. On the other hand, it was determined in the course of this study that end-feeding of the feedguide may afford somewhat lower loss than expected of the baseline configuration which utilizes center-feeding.

Based on the above considerations, it was decided to configure the experimental module according to the baseline design. The commercially manufactured waveguide which most nearly approximates the baseline guide, is WR-340, with dimensions of 4.32 x 8.64 cm. Because this was not available in sufficient quantity, WR-284 waveguide was used instead for the developmental module. Because this waveguide is narrower than the baseline, and because it would be used for both the radiating sticks and the feedguide, the design frequency of the developmental module was increased from 2.45 GHz to 2.86 GHz. With 6061 Aluminum feedguide, the ohmic losses in the module are expected to be less than 1%.

2.3 WAVEGUIDE STICK DESIGN

The design of the waveguide stick entails the assignment of values to both the slot offset from the waveguide centerline and the slot length. The slot length, l , is chosen so that the slot is resonant at the design frequency. The slot offset is chosen to give the desired slot conductance. This is determined by impedance matching considerations. Thus, for a waveguide stick containing N identical shunt slots, the desired value of normalized slot conductance, g , is just $g = 1/N$.

For a single isolated stick, the choice of slot length and slot offset is relatively straightforward. The slot length is given to good approximation by $l = \lambda_0/2$, where λ_0 is the free-space wavelength. The conductance and slot offset are related to sufficient accuracy by a well known equation.

Tentative radiator stick dimensions in WR-284 waveguide are:

Slot Spacing	3.0 inch	Slot Offset	.187 inch
Slot Length	1.98 inch	Slot Normalized	.055
Slot Width	.125 inch	Conductance	
		Number of Slots	18 or 20

Where several sticks are placed in close proximity, however, as they are in the SPS module, the design problem is exacerbated by mutual coupling between the sticks. That is, the slots in any particular stick are now loaded by the slots in the neighboring stick and will necessarily exhibit resonant frequencies and conductances which differ significantly from those predicted by single stick equations.

The changes in stick behavior due to mutual coupling effects are shown in Figure 2. Here, both the resonant frequency and the reflection coefficient of a single stick at resonance change noticeably in the presence of a second stick. A theoretical analysis of this problem, based on an adaptation of a mutual coupling analysis for an array of dipoles (L. Stark, Radio Science 1, 361, 1966) is shown in Figure 3. As might be expected, the effects converge rather rapidly, suggesting that a particular slot does not interact to any significant extent with other slots that are more distant than third or fourth neighbors. Figure 3 also shows that mutual coupling effects are also present between neighboring slots of a single stick.

Because of the mutual coupling problem, the choice of slot length and offset has been pursued in an iterative manner beginning from the single stick analytical values. Data for several iterations with two waveguide sticks, are shown in Table 1. Because the slot offsets, once machined, are fixed, stick impedance in these data was varied by changing the number of slots by the means of a sliding short in the waveguide. Adjacent

sticks were fed in-phase using home built four-hole directional couplers machined in one end of each stick, permitting swept return-loss/coupling measurements without interference by guide flanges.

2.4 FEED GUIDE DESIGN

The radiating waveguide sticks are fed in-phase by a feed waveguide whose axis is perpendicular to those of the radiating sticks. Like the radiating sticks, the feedguide supports a standing wave. The power is coupled from the feedguide to each radiating stick through a resonant (length = $\lambda_0/2$) coupling slot which is inclined to the feedguide axis. The transformed radiating stick impedance seen by the feedguide is proportional to $\sin^2 2\theta$, where θ is the inclination angle. The phase of the power coupled to the stick is inverted as the coupling slot is reflected in the feedguide axis. For maximum power transfer to the 10 radiating sticks, each stick must present an impedance to the feedguide of one-tenth the feedguide characteristic impedance. This dictates a rather small coupling slot inclination of about 7° . To maintain proper phasing of the radiating sticks, the coupling slots are alternately reflected in the feedguide axis.

Tentative feed stick dimensions in WR-284 6061 aluminum waveguides for the 1/2-module are:

Slot Spacing	3.0 inch	Slot Normalized Resistance	.10
Slot Length	2.0 inch	Slot Number	10.
Slot Width	.125 inch		
Slot Offset Angle	7.		

3.0 RECEIVING TECHNIQUES EVALUATION

The receiving antenna receives a pilot signal from earth with phase information to keep all modules in-phase. Symmetry considerations argue for the pilot signal to originate from the center of the SPS earth receiving array. Ionospheric phase shift and Faraday rotation call for the pilot signal to be centered on the SPS power frequency with the phase information in symmetrically disposed sidebands. The purposes of the receiving techniques evaluation were to:

- o Conduct a shared antenna versus separate receiving antenna analysis to determine feasible pilot beam budget and receiving antenna constraints due to power module.
- o Design and select a pilot-beam receiving antenna technique compatible with a power beam array which must allow simultaneous transmission of an S-Band carrier and reception of the anticipated pilot-beam spread-spectrum signal.

The pilot beam link analysis established that very small low gain pilot receiving antenna elements imbedded in the transmitting array are significantly superior to any scheme of diplexing, because: (1) The total system power losses are two orders of magnitude lower with a separate antenna than with any state-of-the-art diplexing device; (2) The small antenna, due to its inherent broad bandwidth, is fully compatible with a spread spectrum signal; whereas the transmit array is not, (3) The small, low gain antenna represents a much lower development risk than a diplexing device.

Also from the pilot beam link analysis, formalisms have evolved from which to determine values of pilot transmitter power and antenna aperture, as well as pilot receiving antenna aperture. The transmitter power and aperture depend foremost upon the requisite pilot link effective radiated power, ERP. The ERP, in turn, depends upon the signal-to-noise requirement of the pilot link receiver; and hence, the noise environment in which the receiving system must operate. Consequently, the ERP requirements were found to be extremely sensitive to the cut-off frequency of a required receiver I.F. notch filter.

The relationship between transmitting antenna diameter and system power loss (efficiency) is shown in Figure 4. This relationship is not monotonic due to the fact that increasing the antenna diameter produces two opposing effects. It reduces the amount of pilot transmitter power required to produce the requisite ERP, while simultaneously increasing the degree of rectenna blockage. At low diameters, the transmitter power effect dominates, and the loss decreases with increasing diameter; whereas, at larger diameters, rectenna blockage becomes most important, and the system loss increases with increasing diameter. Thus, for a particular ERP, there is a rather limited set of pilot transmitter power/aperture combinations which gives minimum system loss.

The relationship between system losses and pilot-link receiving aperture is shown in Figure 5. For small apertures, an increase in aperture reduces system losses due to a decrease in the required ERP. At large apertures, the system losses increase with increasing aperture, due to receiving antenna blockage of the spacetenna. The specific nature of this relationship depends on the required signal-to-noise ratio, S/N, in the pilot receiver and also on the bandwidth, f_c , of the intermediate frequency notch-filter. As S/N is increased, the pilot ERP must increase, and so also must the system losses. As f_c is decreased, more of the power transmitter noise spectrum is passed by the receiver I.F. This increase in noise must be overcome by an increase in pilot link transmitter power.

As shown in Figure 5, the optimum receiving aperture, under any foreseeable conditions, is quite small. Consequently, the pilot-link receiving antenna requirement can be satisfied by a simple dipole or slot antenna. Adaptations of these to the SPS array are shown in Figure 6. The slot antenna is inserted in a notch cut in the outer portion of adjacent waveguide narrow walls. The dipole is positioned at a distance $\lambda_0/4$ above the array by a small rigid coax feed, which like the slot, is slipped through a hole in the waveguide walls. These antennas may be dimensioned either to be resonant or non-resonant. The aperture of the resonant structure is larger, but so also is the effect on the impedance of the neighboring transmitting-antenna radiating slots. To the extent that the lower aperture can be tolerated, the non-resonant structure is preferred.

An important consideration in the pilot link design is the isolation of the pilot receiver from noise inherent to the high-power down-link signal. With the dipole, isolation can be improved by rotating the antenna so that it is cross-polarized to the power transmitting antenna. An alternate noise-cancelling scheme utilizes two dipoles per receiving antenna, as shown in Figure 6. These are separated by $\lambda_0/4$ and can therefore be connected to pass, as would a directional coupler, radiation coming from the earth, while rejecting that which is earthbound.

One of the candidate receiving antennas in Figure 6, the slot, or "credit-card" receiving antenna, has been built and sweep-tested. It consists of a 1.75" x .062" teflon-glass microcircuit board shorted around three edges to form a low-impedance waveguide cavity.

4.0 ANTENNA EFFICIENCY MEASUREMENTS

The antenna pattern will be measured on one of the six antenna ranges at Boeing. Besides observing the far-field rule $R > 2D^2/\lambda \geq 180$ ft., high paths and sharp-beam range illuminators will be employed to minimize multipath errors. For the ranges at the Boeing Developmental Center, multipath errors at beam-center are estimated to be well under $\pm .1$ db. Gain is measured using a Scientific Atlanta SA-1740 Precision Amplifier-Receiver, and SA-12-1/70 Standard gain horn. Measurement accuracies are estimated as follows:

Standard-gain Horn (Δ gain)	$\pm .2$ db
Match	$\pm .2$ db
Switch mismatch differences between two positions	$\pm .2$ db
Receiver/mixer linearity	$\pm .2$ db
Total RSS Value	$\pm .4$ db or $\pm 9\%$ in power

By hardwiring the SPS array to the standard gain horn, with their beams pointed near 90° apart to avoid crosstalk, the rf switch and its inherent uncertainty can be eliminated.

The antenna efficiency is obtained from the experimental measurement of gain, with respect to a reference horn, and directivity, D . Since the directivity is the gain of a lossless antenna, the ratio of these values represents the efficiency of the antenna. The gain is obtained from the measured value of incremental gain above a calibrated standard horn. The directivity is expressed as the ratio of the maximum radiation intensity, U_{\max} to the average radiation intensity \bar{U} , which is given by $\bar{U} = 1/4\pi \int U(\theta, \phi) d\Omega$.

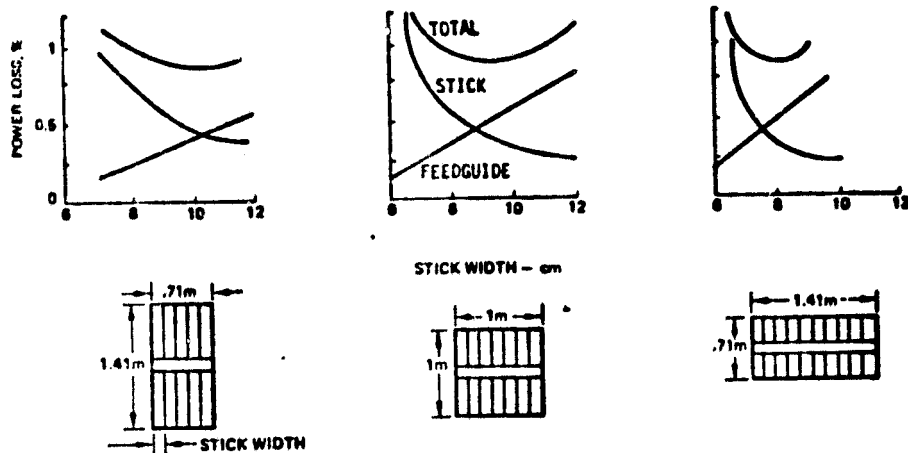
The directivity measurement is carried out separately by rotating the antenna continuously through selected azimuth and elevation angles and integrating the far field contributions over a solid sphere, thus obtaining the directivity with reference to an isotropic radiator as $D = U_{\max}/\bar{U}$.

The efficiency is obtained from the ratio of two separately measured experimental values, $\eta = G/D$. With currently available antenna range accuracy, this measurement is typically determined to $\pm .4$ db accuracy. The resulting efficiency value will give an indication of ohmic losses in the waveguide feed system and in the radiating sticks. In the SPS baseline design, this loss is estimated to be less than 0.1 db, and the antenna range measurement will thus provide a crude verification only.

TABLE: I ITERATIVE DESIGN PROCEDURE FOR RADIATING STICK PARAMETERS

STICK NUMBER	NO. OF SLOTS ¹ FOR BEST MATCH		SLOT ³ OFFSET	SLOT LENGTH	COMMENT
	SINGLE STICK	WITH ² NEIGHBOR			
1	22	20	.18"	2.04"	RESONANCE @ 2800 MHz SLOT TOO LONG
2	16	14	.20"	1.94"	RESONANCE @ 2880 MHz SLOT TOO SHORT TOO MUCH CONDUCTANCE PER SLOT
3	18	16	.187"	1.98"	RESONANCE AT 2875MHz
4	18	18	.180"	2.00"	EXPECT 2860 MHz ⁴

1. SLIDING SHORT MEASUREMENT: VSWR AT RESONANCE < 1.1
2. NON-DUPLICATE STICKS ARE USED TO APPROXIMATE MUTUAL COUPLING EFFECT
3. AFFECTS PRIMARILY SLOT CONDUCTANCE
4. DESIRED FREQUENCY FOR FEED GUIDE TO BE IDENTICAL TO RADIATING STICK GUIDE (WR240)



- NOT SENSITIVE TO MODULE ASPECT RATIO
- NOT VERY SENSITIVE TO WAVEGUIDE SIZE
- STICK STANDING WAVES SUGGEST END FEEDING PREFERABLE

Figure 1 : RF Module $P^2 R$ Optimization

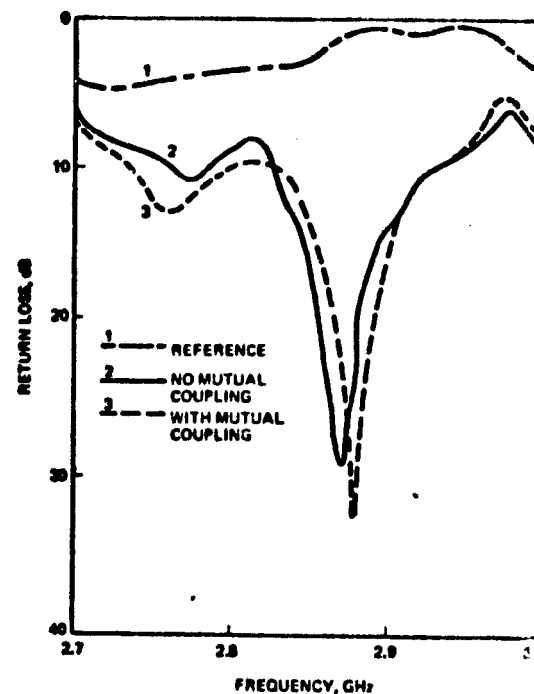


Figure 2: Effect of Mutual Coupling - Two Stick Measurement

ANALYTICAL EXPRESSION¹

$$\frac{V}{V_0} = \frac{4 \cdot S_y S_H (1 - \cos^2 \theta)}{b^2 \lambda^2 [1 + \cos^2 \theta] + \left(\frac{\lambda}{2b}\right)^2} \approx \left(\frac{2}{\lambda} \sqrt{1 + \frac{\lambda^2}{4b^2}}\right)^2 \approx \left(\frac{2b}{\lambda}\right)^2$$

WHERE

$$m = n = k$$

$$m = 1, n = 4$$

$$m \neq n \neq 0$$

$$\left[\frac{\sin\left(\frac{\pi y}{L_y}\right)}{\frac{\pi y}{L_y}} \right]^2 \left[\frac{\sin\left(\frac{\pi x}{L_x}\right)}{\frac{\pi x}{L_x}} \right]^2 \left[\frac{\left(\frac{\pi}{L_y}\right)^2 + 1}{\sqrt{\left(\frac{\pi}{L_y}\right)^2 + \left(\frac{\pi}{L_x}\right)^2}} \right]$$

1 = % THE NUMBER OF NEIGHBORING SLOTS CONSIDERED IN THE 'Y' PLANE

4 = % THE NUMBER OF NEIGHBORING SLOTS CONSIDERED IN THE 'X' PLANE

• = GUIDE I.D. WIDTH

• = GUIDE I.D. WIDTH

• = GUIDE I.D. HEIGHT

S_y = SLOT 'Y' PLANE SPACING

S_H = SLOT 'H' PLANE SPACING

• = SLOT OFFSET

• = SLOT OFFSET

• = SLOT WIDTH

V = SLOT SHUNT ADMITTANCE

V_0 = GUIDE CHARACTERISTIC

1. MODIFICATION OF STARK'S DIPOLE EXPRESSION TO SLOTS

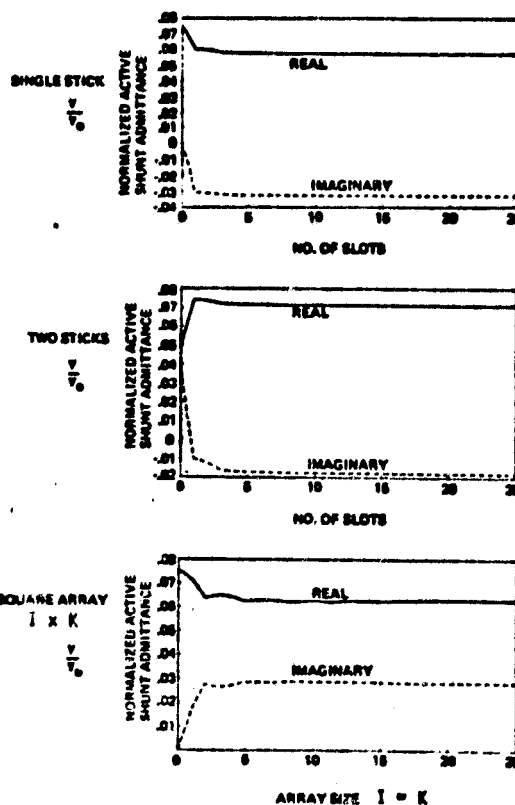


Figure 3: Estimate of Mutual Coupling in SPS Slotted Waveguide Array

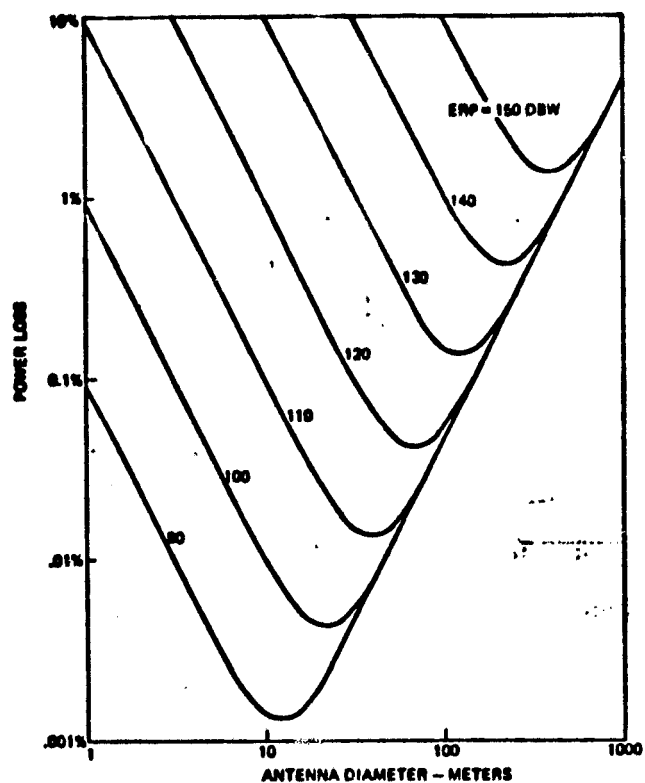


Figure 4 : System Power Loss Vs. Pilot Transmit Antenna Diameter and ERP Required

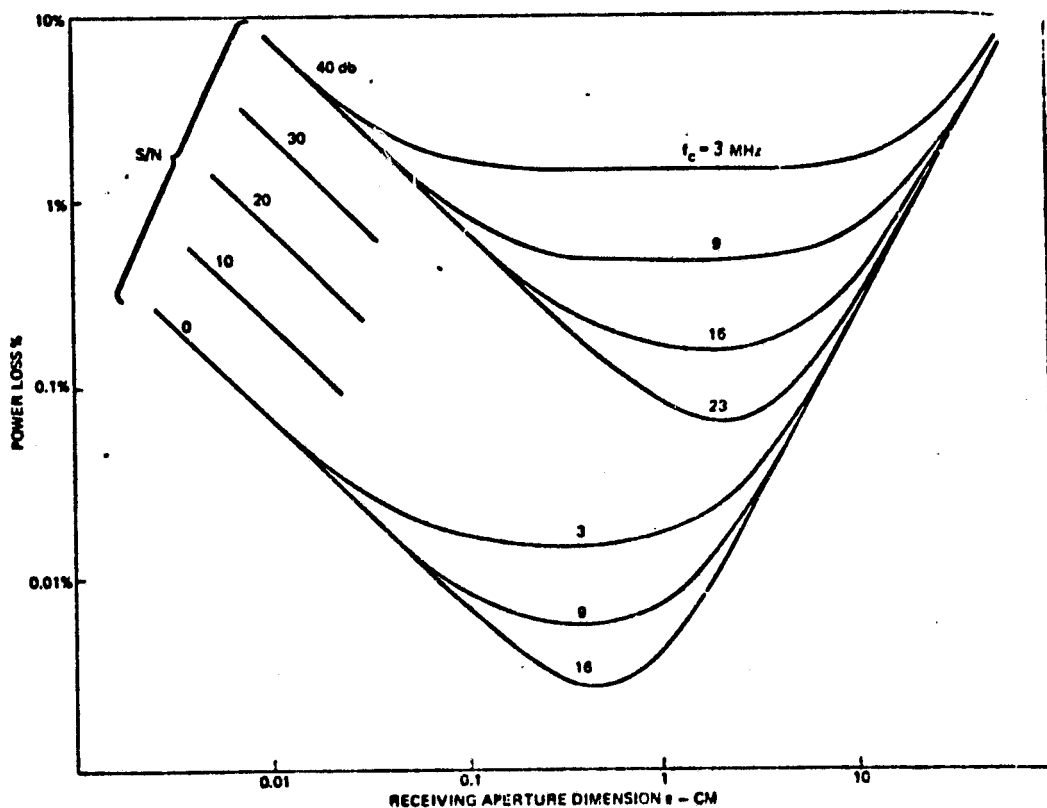


Figure 5 : Total System Loss Vs. Receive Aperture

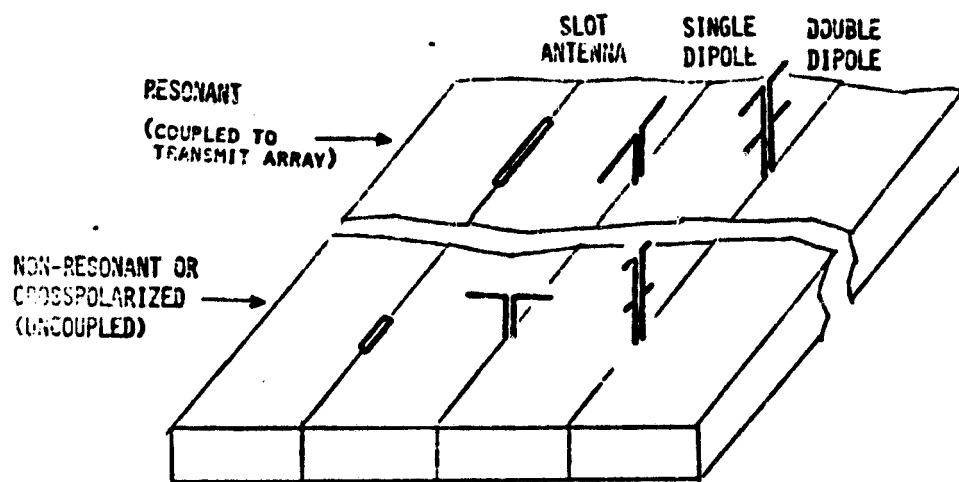


FIGURE 6: POTENTIAL SPS PILOT-LINK RECEIVING ANTENNA CONFIGURATIONS.
THE DOUBLE DIPOLE CONFIGURATIONS AFFORD PARTIAL NOISE
CANCELLATION.

THE RESONANT CAVITY RADIATOR (RCR)

K. G. Schroeder
R. L. Carlise
C. Y. Tomita

ROCKWELL INTERNATIONAL

D/8

N82-12556

1. INTRODUCTION

The fundamental theory of MW antenna operation and basic array technology development status was used in the design of the 1-km diameter 5-Gw SPS microwave antenna. However, the aperture size and the high efficiency requirements make the MW antenna extremely complex. Studies have shown that the slotted waveguide array is one of the most efficient radiators for the antenna. Subsequent analyses have shown that the temperature interface between waveguides and dc-RF conversion tubes can cause severe thermal design problems on the array. An alternate design, the Resonant Cavity Radiator, is described here.

2. RADIATING ELEMENT DESIGN

2.1 Basic RCR Principle

Conventional waveguide designs such as the TE_{10} mode waveguide slotted array make tube installation fairly complex. To solve the resultant temperature interface problem and possibly increase the RF efficiency of the radiator, Rockwell developed the resonant cavity radiator (RCR). The RCR is a resonant cavity box excited with the TE_{10} mode. Physically, the RCR is a conventional standing waveguide radiator with the common walls removed. The RCR has three significant potentials. They are:

1. Improvement in efficiency.
2. Lighter weight.
3. Simpler structure which allows the RCR to be integrated with the RF tube to alleviate the thermal interface problem.

2.2 RCR Theoretical Attenuation Estimates

The loss mechanisms of the RCR can be best explained by comparison to conventional arrays. The typical flat plate antenna array is formed by placing side-by-side several sections of rectangular waveguide as shown in Figure 1.

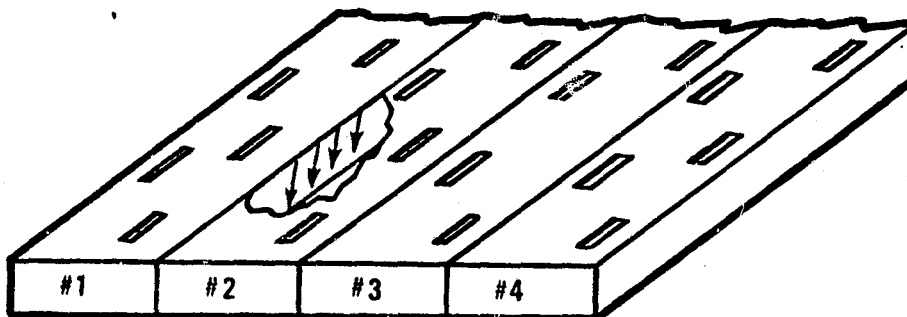


Figure 1. Typical TE_{10} SWR Array

PRECEDING PAGE BLANK NOT FILMED

The mode that propagates down each waveguide is the dominant TE₁₀. The mode designation simply describes a particular electric-magnetic field configuration that satisfies Maxwell's equations. A portion of the top wall in waveguide No. 2 in Figure 1 is cut away to show the current flowing in the side wall. Not shown is the adjacent currents flowing in waveguide No. 1. These currents (waveguide No. 1) are flowing in the opposite direction and because the system is symmetrical, they are of equal magnitude. If the side walls are removed as in the RCR, these two equal and opposite currents cancel. Since conduction losses are simply I²R losses, any reduction in surface currents will make the antenna array more efficient.

The closed-form analytical expression for conduction losses for a silver-plated RCR supporting the TE_{m,0} modes is given as:

$$\alpha_c = \frac{2.8738 \times 10^{-4}}{b \sqrt{1 - \left(\frac{m\lambda}{2a}\right)^2}} \left[1 + \frac{2b}{a} \frac{m\lambda^2}{2a} \right] \frac{\text{dB}}{\text{meter}} \quad (1)$$

For an "a" dimension of 4.460 inches and a "b" dimension of 2.130 inches (11.319 cm by 5.40 cm) the loss calculated from the above equation is tabulated in Table 1. This shows that for a typical array length of 2.5 meters, a TE₇₀ RCR has the potential of saving 4.3×10^6 watts of power. Weight savings in the MW antenna is achieved by two design features: (1) the RCR is designed with no side walls with the exception of the cavity walls, and (2) it can be designed to be structurally integrated with a magnetron or klystron heat dissipator because of the simplicity of the structure.

2.3 Typical Integration Between RCR and Tube

Figure 2 shows a typical anode heat radiator integrated with the RCR bottom. The area required for heat dissipation computed by Rockwell indicates that the RCR has more than sufficient area to dissipate the excess heat. In the aperture high-density area, only 0.76 percent of the total RCR area is required to replace a 48-cm magnetron anode. The RCR bottom wall can be constructed of pyrolytic graphic composite, or equivalent, and plated for high RF conduction. The plating technique of pyrolytic graphite to operate at extremely high temperatures should be investigated in future studies. The potential weight savings of the RCR is then the removal of the side walls and the weight reduction achieved by incorporating heat dissipation in the waveguide bottom wall. The integrated assembly also provides techniques for solving the high-temperature interface problem. It should be noted that the RCR may offer other advantages for ease of maintenance and assembly.

Table 1: Theoretical Power Saving of RCR Over Conventional Standing Wave TE₁₀ Slotted Arrays .

Mode	(α) dB/Meter	Loss Differential for 2.5m (dB)	Power Savings 5-GW/Base
TE _{1,0}	8.068×10^{-3}	-	
TE _{2,0}	7.193×10^{-3}	.00218	2.51×10^6
TE _{3,0}	6.901×10^{-3}	.00291	3.35×10^6
TE _{4,0}	6.755×10^{-3}	.00328	3.77×10^6
TE _{5,0}	6.668×10^{-3}	.00350	4.02×10^6
TE _{6,0}	6.609×10^{-3}	.00364	4.19×10^6
TE _{7,0}	6.567×10^{-3}	.00375	4.3×10^6
TE _{8,0}	6.530×10^{-3}	.003845	4.42×10^6
TE _{10,0}	6.490×10^{-3}	.00394	4.53×10^6

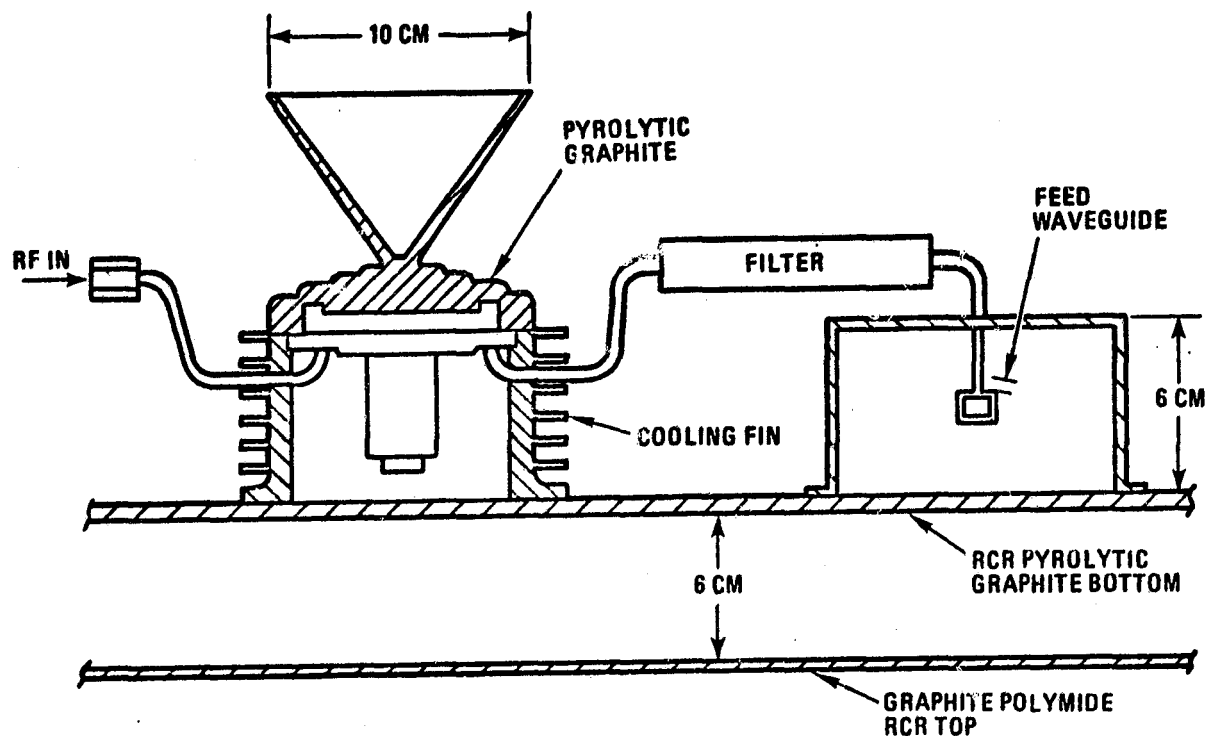


Figure 2. Magnetron Modified Heat Sink (Input-Output Connections May be Different)

2.4 Measurement Results

One of the primary uncertainties with the RCR is the suppression of higher order modes. One of the easiest ways of detecting higher order mode existence is by observing radiation patterns. Higher order modes will collimate in off-boresight locations, causing null filling and higher sidelobes. Rockwell developed special feed techniques which led to the reduction of higher order modes. To prove the technique does suppress higher order modes, scaled tests were conducted. A TE₇₀ RCR shown in Figure 3 was fabricated and tested with results shown in Figures 4 and 5. The RCR was uniformly excited for -13 dB peak sidelobe level. Measured sidelobe levels in the E and H planes were -13 dB for good correlation. Off-axis patterns also were taken at predicted higher order mode locations. No existence of higher order mode propagation was found. These tests were performed on a limited scale; however, it definitely proves that the RCR has a potential for a major breakthrough in array technology. Efficiency verification tests will be performed by Rockwell to verify theoretical predictions.

3. SUBARRAY DESIGN

Rockwell's design of the MPTS transmit array consists of 6993 subarrays, each 10 meters square. The optimum size of the subarray is a function of the electronic scanning range of the antenna. A small subarray allows more electronic scanning range; however, the total number of electronic scanning circuits increases with the increased number of subarrays. With a subarray larger than 10 meters square, the pointing requirements of the subarray is extremely tight, therefore undesirable. The baseline subarray size of 10m by 10m requires the subarray to be pointed to within + 1 arc minutes for less than 0.5-percent loss. Typical power plots in dB and percent of the subarray is shown in Figures 6 and 7. A typical subarray may consist of 20 to 50 RCR's, depending on the power density of the subarray.

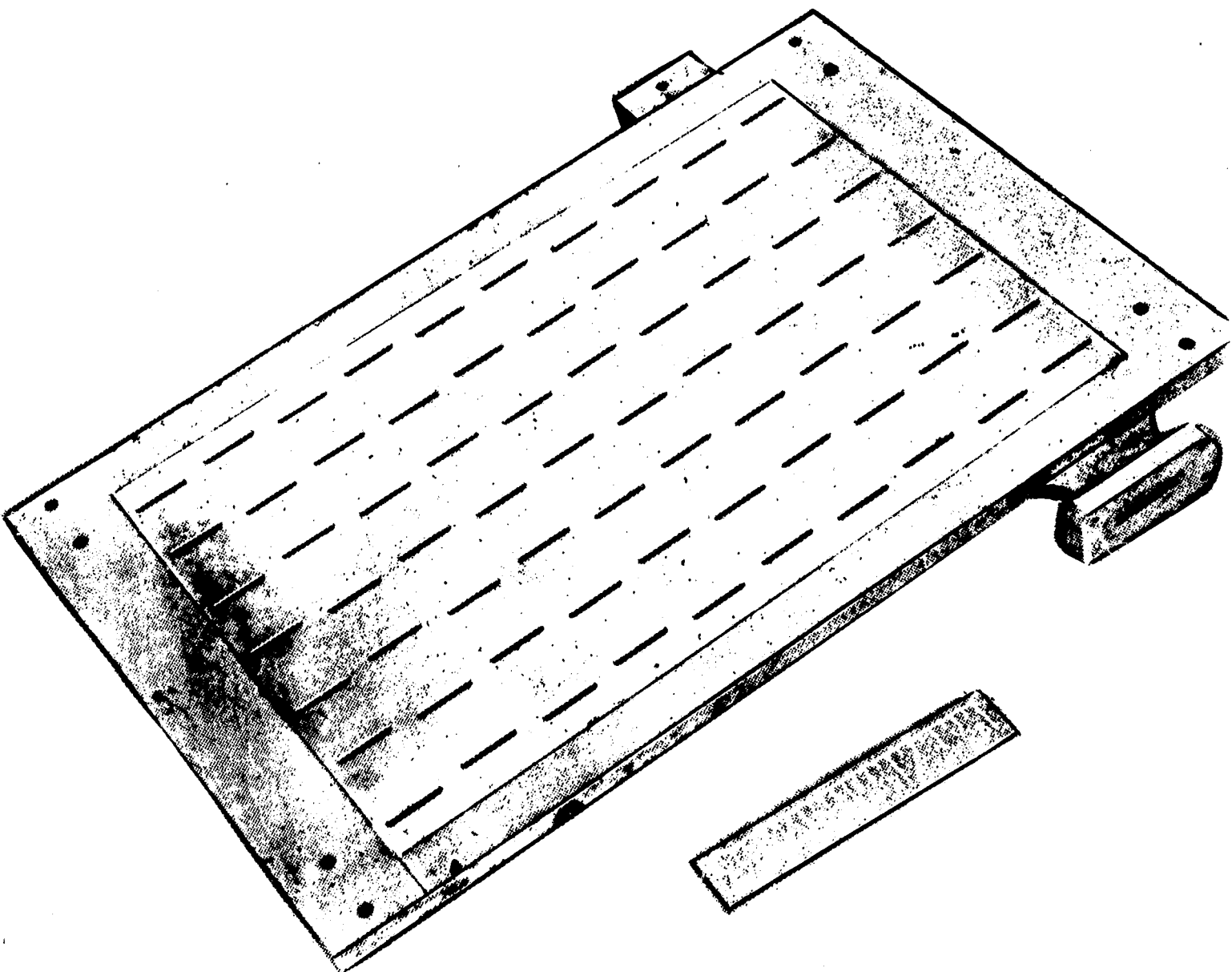


Figure 3. Experimental RCR

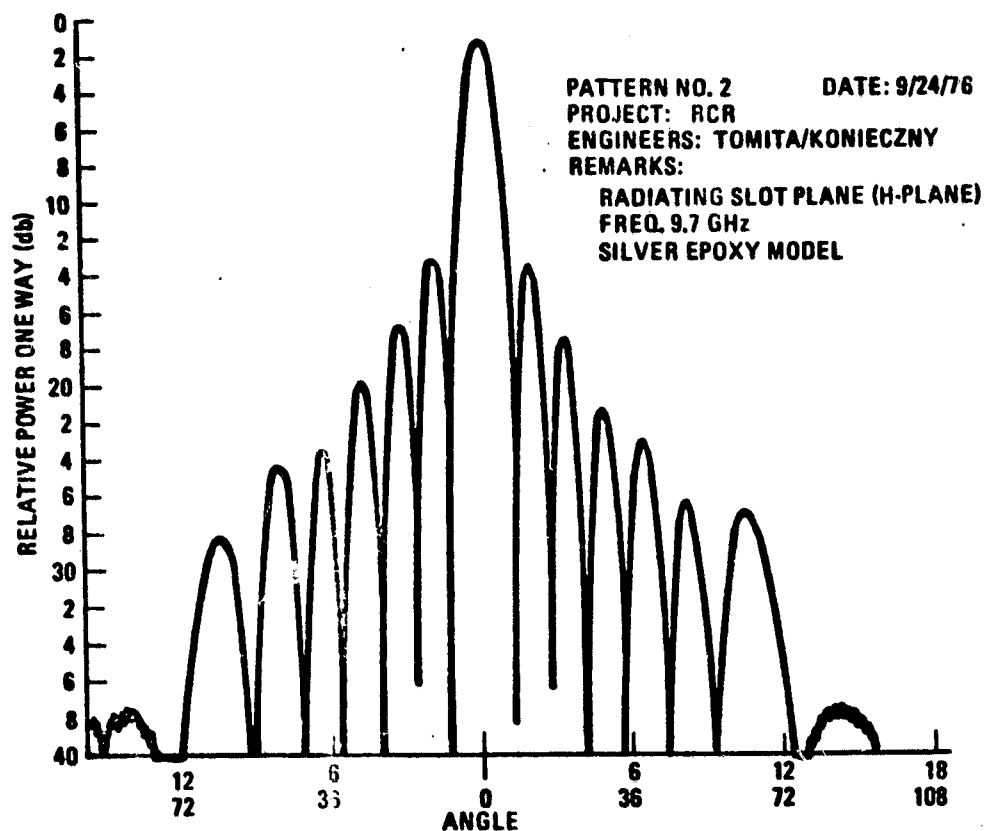


Figure 4. RCR H-Plane Pattern

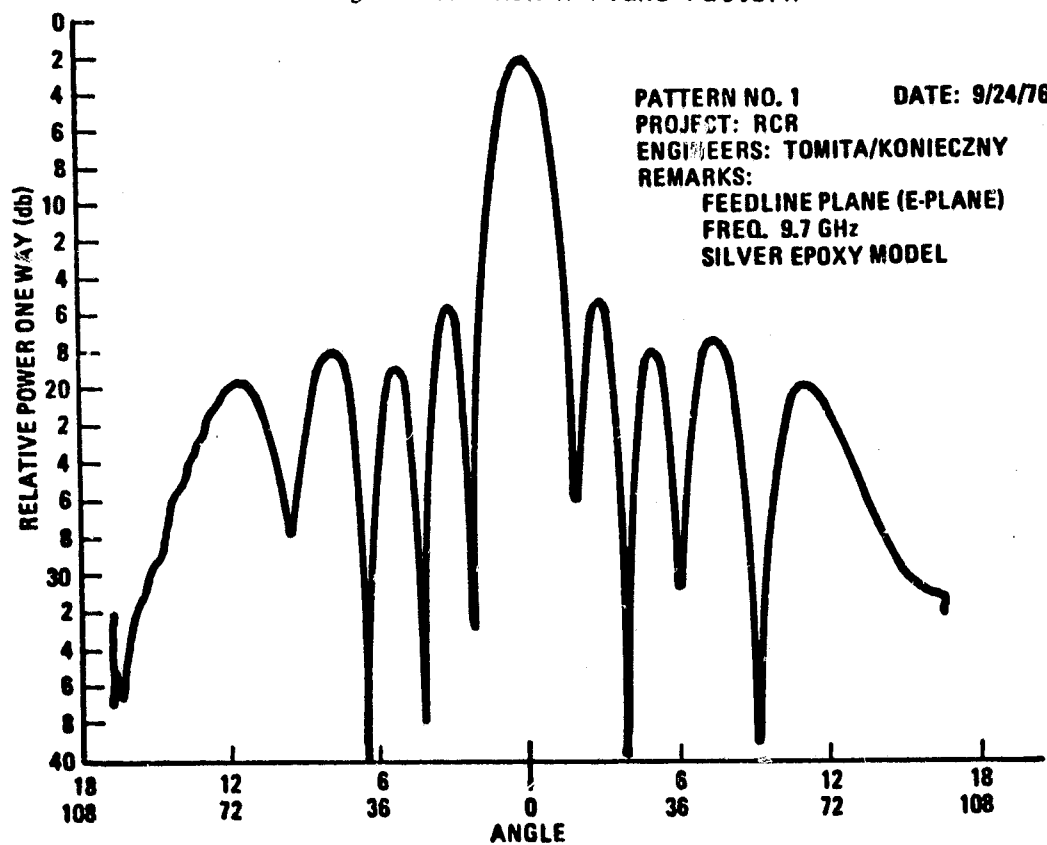


Figure 5. RCR E-Plane Pattern

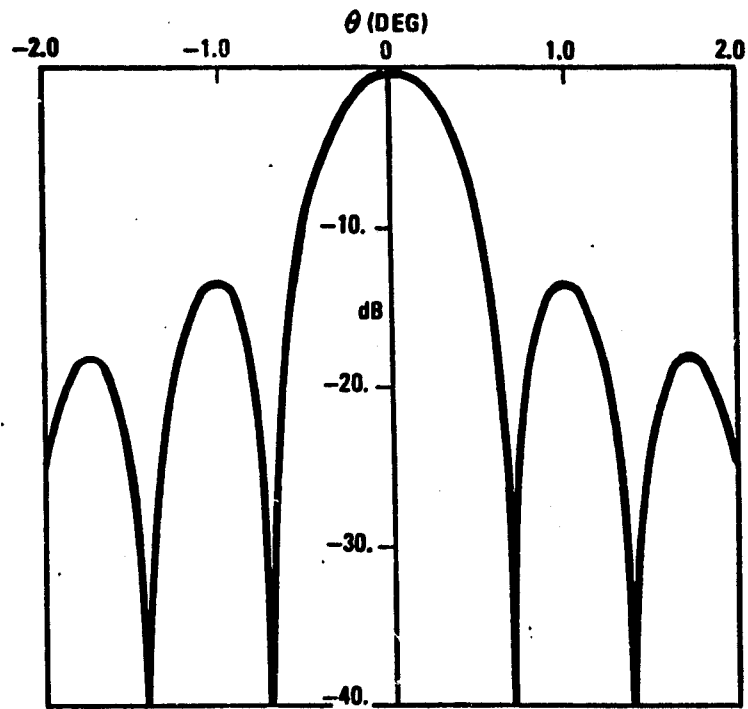


Figure 6. Far-Field Radiation Pattern
(10-Meter Square Subarray)

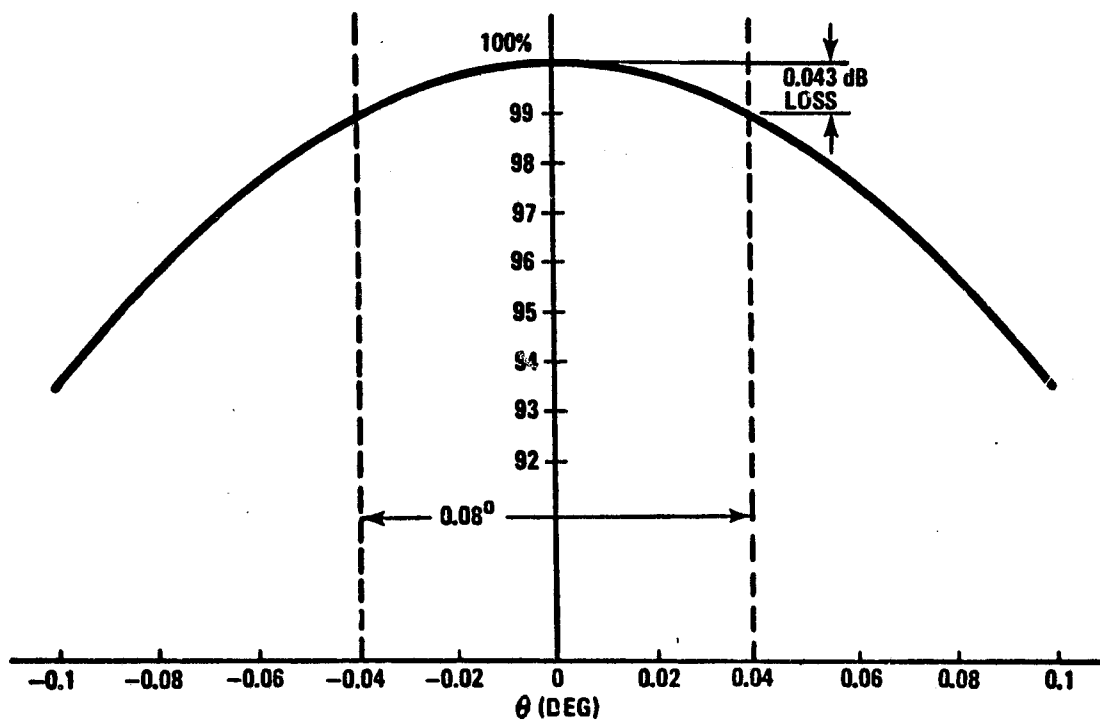


Figure 7. 10-Meter Square Element Factor

4. TUBE SUBARRAY INSTALLATIONS

One of the prime advantages of the RCR is its adaptability to numerous magnetron or klystron tube installations. Rockwell has studied various tube/RCR integrated and non-integrated concepts to determine potential solutions to the weight and high-temperature interface problem. Figures 8 through 11 illustrate various magnetron and klystron mounting techniques to the RCR. Figure 8 which shows magnetron mounting, illustrates the configuration where the back face of the RCR is integral to the magnetron. It should be recognized that these techniques are advanced and unproven; however, it offers the MPTS antenna designer alternative installation concepts. The simplicity of the RCR for maintenance also is shown in Figure 8. The RCR modes for various installation concepts will vary as a function of the power density or structural integrity. In the low density areas such as shown in Figure 9, a TE₇₀ RCR may be used. In the higher density areas of the array a TE₃₀ RCR can be used. The interconnecting feed lines of the RCR as shown in Figures 9 through 11 represent implementation of the old version of Rockwell's phased array retrodirective network. Separate pilot and reference pick-up antennas are used in the new phase control system, similar to the one described in connection with the solid-state concepts.

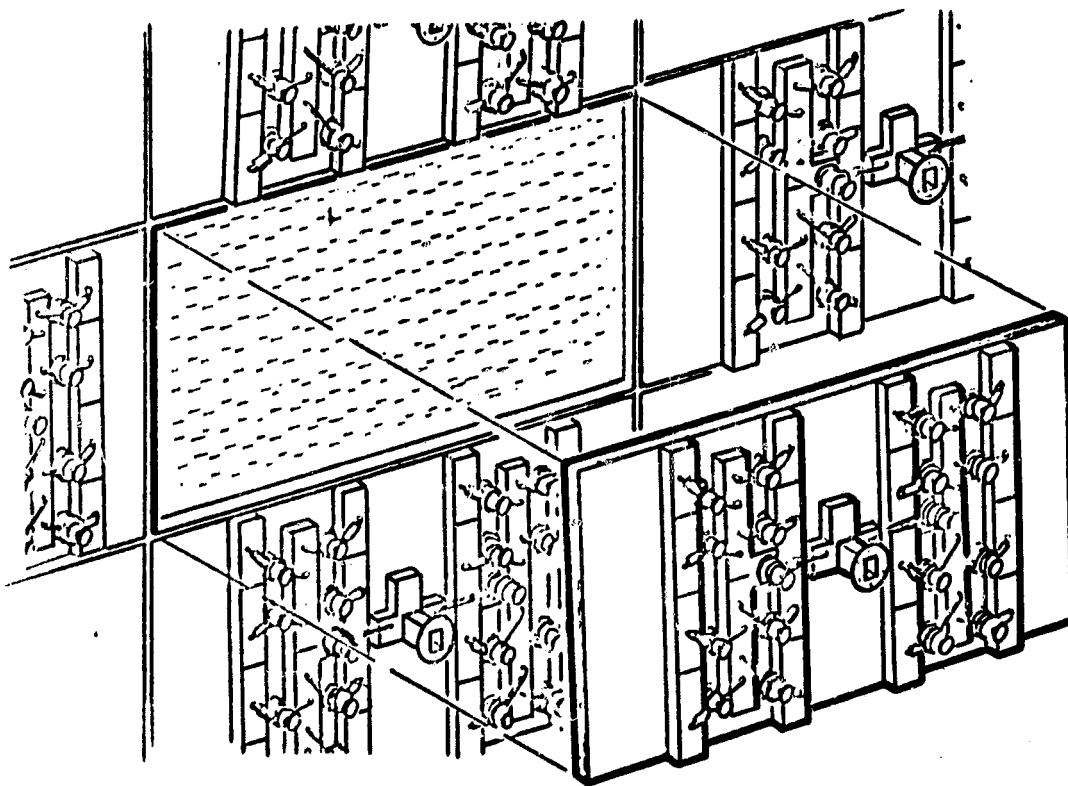


Figure 8. RCR Element Maintenance

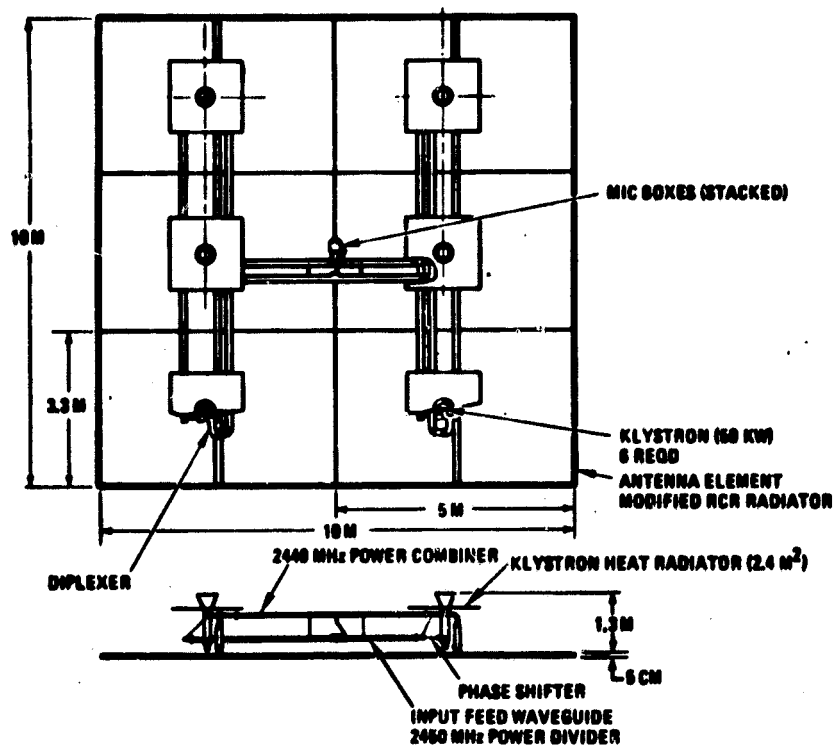


Figure 9. Low-Density 10-Meter-Square Subarray

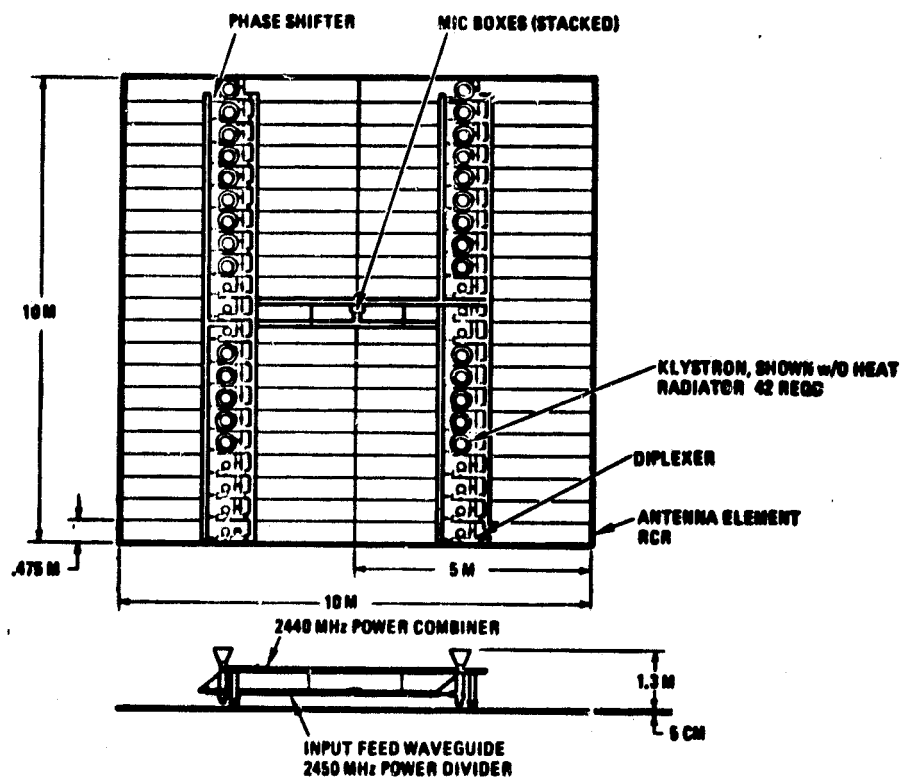


Figure 10. High-Density 10-Meter-Square Subarray

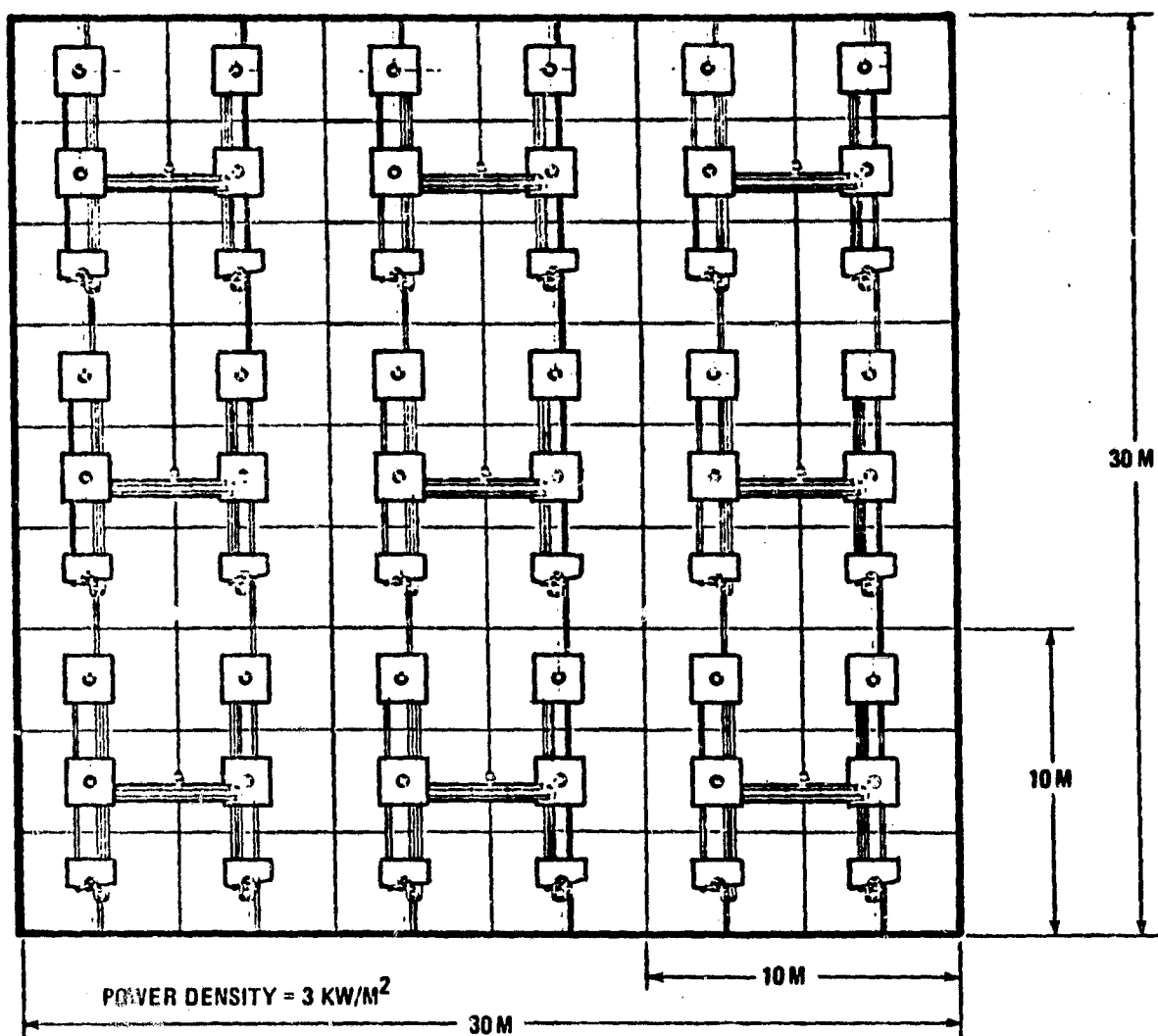


Figure 11. Low-Density 30-Meter-Square Layout Array

**EVALUATION OF "THICK WALL"
WAVE GUIDE ELEMENT**

**ERVIN J. NALOS
BOEING AEROSPACE**

1-48

The SPS transmitting array requires an architecture which will provide a low weight, high efficiency and high structural rigidity. Several candidate antenna configurations include the parabolic dish, the parabolic cylinder, the lens and the waveguide slot array. As discussed below, the waveguide slot array is preferred over the other options.

Parabolic dishes are widely used on earth. For SPS application, they could be readily laid up in six-foot diameters with lightweight graphite-epoxy materials. On the other hand, the area efficiency of such an array is relatively low. Moreover, a zero spillover feed configuration is not presently apparent.

An array of parabolic cylinders with line-source feeds could give better area efficiency than an array of dishes, but would suffer from feed blockage.

A lens, using lightweight waveguide structures, with zero blockage behind-the-lens feedhorns can have high efficiency and little spillover, but the SPS center-to-edge illumination tapers would give a spatial "lumpiness" which would produce undesirable grating lobes in the far-field pattern.

As noted above, waveguide slot arrays constitute the most desirable option. Consequently, such an array has been chosen for the SPS. Waveguide slot arrays offer high efficiency, uniform illumination, and are fairly lightweight. Bandwidths of such arrays are narrow, typically 1/2-2%. Although this does not directly impact the SPS, which transmits power at a single frequency of 2.45 GHz, the narrow bandwidth does constrain the thermal and mechanical tolerances of the antenna.

2.0 SLOTTED WAVEGUIDE MODULE DESIGN VERIFICATION

ORIGINAL PAGE 19
OF POOR QUALITY

2.1 EXPERIMENTAL PROGRAM

The purpose of this program is to better define the electronic aspects of an SPS specific waveguide slot array. The specific aims of the program are as follows:

- o To build a full-scale half-module, 10 stick, array, the design parameters for which are to be determined by analytical considerations tempered by experimental data on a single slotted radiating stick.
- o To experimentally evaluate the completed array with respect to antenna pattern, impedance and return loss.
- o To measure swept transmission amplitude and phase to provide a data base for design of a receiving antenna.

2.2 ARRAY CONFIGURATION

The first step in module design is to fix the gross dimensions, including the module length and width, and the dimensions of the radiating sticks and the feed waveguide. Because the feedguide is a standing wave device in which the coupling slots must be spaced by $\lambda_g/2$, where λ_g is the guide wavelength, and because λ_g is a function of waveguide width, the radiating stick and feedguide dimensions are not independent.

The SPS baseline design calls for a half-module of ten 1.6 m long sticks of 6 cm x 9 cm cross-section. For these dimensions, at the SPS frequency, the feedguide dimensions are also 6 cm x 9 cm. To assess the desirability of the baseline configuration, the ohmic losses of several alternative configurations of equal area were calculated. The I^2R losses for these are plotted in Figure 1 as functions of radiating stick

sticks were fed in-phase using home built four-hole directional couplers machined in one end of each stick, permitting swept return-loss/coupling measurements without interference by guide flanges.

2.4 FEED GUIDE DESIGN

The radiating waveguide sticks are fed in-phase by a feed waveguide whose axis is perpendicular to those of the radiating sticks. Like the radiating sticks, the feedguide supports a standing wave. The power is coupled from the feedguide to each radiating stick through a resonant (length = $\lambda_0/2$) coupling slot which is inclined to the feedguide axis. The transformed radiating stick impedance seen by the feedguide is proportional to $\sin^2 2\theta$, where θ is the inclination angle. The phase of the power coupled to the stick is inverted as the coupling slot is reflected in the feedguide axis. For maximum power transfer to the 10 radiating sticks, each stick must present an impedance to the feedguide of one-tenth the feedguide characteristic impedance. This dictates a rather small coupling slot inclination of about 7° . To maintain proper phasing of the radiating sticks, the coupling slots are alternately reflected in the feedguide axis.

Tentative feed stick dimensions in WR-284 6061 aluminum waveguides for the 1/2-module are:

Slot Spacing	3.0 inch	Slot Normalized Resistance	.10
Slot Length	2.0 inch	Slot Number	10.
Slot Width	.125 inch		
Slot Offset Angle	7.		

3.0 RECEIVING TECHNIQUES EVALUATION

The receiving antenna receives a pilot signal from earth with phase information to keep all modules in-phase. Symmetry considerations argue for the pilot signal to originate from the center of the SPS earth receiving array. Ionospheric phase shift and Faraday rotation call for the pilot signal to be centered on the SPS power frequency with the phase information in symmetrically disposed sidebands. The purposes of the receiving techniques evaluation were to:

- o Conduct a shared antenna versus separate receiving antenna analysis to determine feasible pilot beam budget and receiving antenna constraints due to power module.
- o Design and select a pilot-beam receiving antenna techniques compatible with a power beam array which must allow simultaneous transmission of an S-Band carrier and reception of the anticipated pilot-beam spread-spectrum signal.

The pilot beam link analysis established that very small low gain pilot receiving antenna elements imbedded in the transmitting array are significantly superior to any scheme of diplexing, because: (1) The total system power losses are two orders of magnitude lower with a separate antenna than with any state-of-the-art diplexing device; (2) The small antenna, due to its inherent broad bandwidth, is fully compatible with a spread spectrum signal; whereas the transmit array is not, (3) The small, low gain antenna represents a much lower development risk than a diplexing device.

Also from the pilot beam link analysis, formalisms have evolved from which to determine values of pilot transmitter power and antenna aperture, as well as pilot receiving antenna aperture. The transmitter power and aperture depend foremost upon the requisite pilot link effective radiated power, ERP. The ERP, in turn, depends upon the signal-to-noise requirement of the pilot link receiver; and hence, the noise environment in which the receiving system must operate. Consequently, the ERP requirements were found to be extremely sensitive to the cut-off frequency of a required receiver I.F. notch filter.

The relationship between transmitting antenna diameter and system power loss (efficiency) is shown in Figure 4. This relationship is not monotonic due to the fact that increasing the antenna diameter produces two opposing effects. It reduces the amount of pilot transmitter power required to produce the requisite ERP, while simultaneously increasing the degree of rectenna blockage. At low diameters, the transmitter power effect dominates, and the loss decreases with increasing diameter; whereas, at larger diameters, rectenna blockage becomes most important, and the system loss increases with increasing diameter. Thus, for a particular ERP, there is a rather limited set of pilot transmitter power/aperture combinations which gives minimum system loss.

The relationship between system losses and pilot-link receiving aperture is shown in Figure 5. For small apertures, an increase in aperture reduces system losses due to a decrease in the required ERP. At large apertures, the system losses increase with increasing aperture, due to receiving antenna blockage of the spacetenna. The specific nature of this relationship depends on the required signal-to-noise ratio, S/N , in the pilot receiver and also on the bandwidth, f_c , of the intermediate frequency notch-filter. As S/N is increased, the pilot ERP must increase, and so also must the system losses. As f_c is decreased, more of the power transmitter noise spectrum is passed by the receiver I.F. This increase in noise must be overcome by an increase in pilot link transmitter power.

As shown in Figure 5, the optimum receiving aperture, under any foreseeable conditions, is quite small. Consequently, the pilot-link receiving antenna requirement can be satisfied by a simple dipole or slot antenna. Adaptations of these to the SPS array are shown in Figure 6. The slot antenna is inserted in a notch cut in the outer portion of adjacent waveguide narrow walls. The dipole is positioned at a distance $\lambda_0/4$ above the array by a small rigid coax feed, which like the slot, is slipped through a hole in the waveguide walls. These antennas may be dimensioned either to be resonant or non-resonant. The aperture of the resonant structure is larger, but so also is the effect on the impedance of the neighboring transmitting-antenna radiating slots. To the extent that the lower aperture can be tolerated, the non-resonant structure is preferred.

An important consideration in the pilot link design is the isolation of the pilot receiver from noise inherent to the high-power down-link signal. With the dipole, isolation can be improved by rotating the antenna so that it is cross-polarized to the power transmitting antenna. An alternate noise-cancelling scheme utilizes two dipoles per receiving antenna, as shown in Figure 6. These are separated by $\lambda_0/4$ and can therefore be connected to pass, as would a directional coupler, radiation coming from the earth, while rejecting that which is earthbound.

One of the candidate receiving antennas in Figure 6, the slot, or "credit-card" receiving antenna, has been built and sweep-tested. It consists of a 1.75" x .062" teflon-glass microcircuit board shorted around three edges to form a low-impedance waveguide cavity.

4.0 ANTENNA EFFICIENCY MEASUREMENTS

The antenna pattern will be measured on one of the six antenna ranges at Boeing. Besides observing the far-field rule $R > 2D^2/\lambda \geq 180$ ft., high paths and sharp-beam range illuminators will be employed to minimize multipath errors. For the ranges at the Boeing Developmental Center, multipath errors at beam-center are estimated to be well under $\pm .1$ db. Gain is measured using a Scientific Atlanta SA-1740 Precision Amplifier-Receiver, and SA-12-1/70 Standard gain horn. Measurement accuracies are estimated as follows:

Standard-gain Horn (Δ gain)	+ .2 db
Match	+ .2 db
Switch mismatch differences between two positions	+ .2 db
Receiver/mixer linearity	+ .2 db
Total RSS Value	+ .4 db or + 9% in power

By hardwiring the SPS array to the standard gain horn, with their beams pointed near 90° apart to avoid crosstalk, the rf switch and its inherent uncertainty can be eliminated.

The antenna efficiency is obtained from the experimental measurement of gain, G , with respect to a reference horn, and directivity, D . Since the directivity is the gain of a lossless antenna, the ratio of these values represents the efficiency of the antenna. The gain is obtained from the measured value of incremental gain above a calibrated standard horn. The directivity is expressed as the ratio of the maximum radiation intensity, U_{\max} to the average radiation intensity \bar{U} , which is given by $\bar{U} = 1/4\pi \int U(\theta, \phi) d\Omega$.

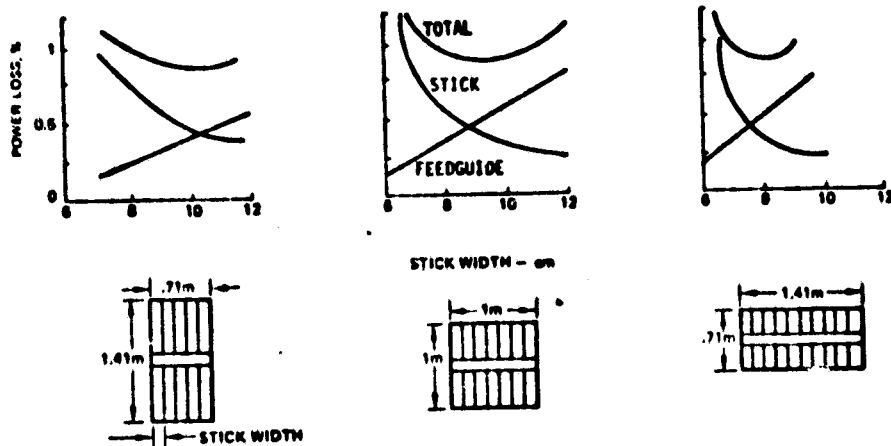
The directivity measurement is carried out separately by rotating the antenna continuously through selected azimuth and elevation angles and integrating the far field contributions over a solid sphere, thus obtaining the directivity with reference to an isotropic radiator as $D = U_{\max}/\bar{U}$.

The efficiency is obtained from the ratio of two separately measured experimental values, $\eta = G/D$. With currently available antenna range accuracy, this measurement is typically determined to $\pm .4$ db accuracy. The resulting efficiency value will give an indication of ohmic losses in the waveguide feed system and in the radiating sticks. In the SPS baseline design, this loss is estimated to be less than 0.1 db, and the antenna range measurement will thus provide a crude verification only.

TABLE: I ITERATIVE DESIGN PROCEDURE FOR RADIATING STICK PARAMETERS

STICK NUMBER	NO. OF SLOTS ¹ FOR BEST MATCH		SLOT ³ OFFSET	SLOT LENGTH	COMMENT
	SINGLE STICK	WITH ² NEIGHBOR			
1	22	20	.18"	2.04"	RESONANCE @ 2800 MHz SLOT TOO LONG
2	16	14	.20"	1.94"	RESONANCE @ 2880 MHz SLOT TOO SHORT TOO MUCH CONDUCTANCE PER SLOT
3	18	16	.197"	1.98"	RESONANCE AT 2875MHz
4	18	18	.180"	2.00"	EXPECT 2860 MHz ⁴

1. SLIDING SHORT MEASUREMENT: VSWR AT RESONANCE < 1.1
2. NON-DUPLICATE STICKS ARE USED TO APPROXIMATE MUTUAL COUPLING EFFECT
3. AFFECTS PRIMARILY SLOT CONDUCTANCE
4. DESIRED FREQUENCY FOR FEED GUIDE TO BE IDENTICAL TO RADIATING STICK GUIDE (WR240)



- NOT SENSITIVE TO MODULE ASPECT RATIO
- NOT VERY SENSITIVE TO WAVEGUIDE SIZE
- STICK STANDING WAVES SUGGEST END FEEDING PREFERABLE

Figure 1 : RF Module $P^2 R$ Optimization

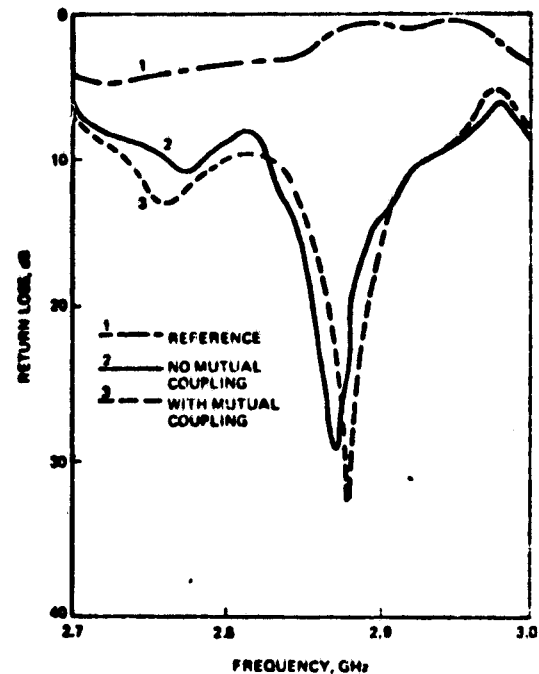


Figure 2: Effect of Mutual Coupling - Two Stick Measurement

ANALYTICAL EXPRESSION¹

$$\frac{V}{V_0} = \frac{a_0 b_0 S_M (1 - j\alpha)}{b^2 [1 - \alpha^2] + (\frac{1}{2})^2} = \left(\frac{1}{2} \sqrt{1 - \frac{1}{2}} \right) = \left(\frac{m}{n} \right)$$

WHERE

$$m = 4n + 1$$

$$n = \sum_{k=1}^m \left[\frac{1 - \left(\frac{m}{k} \right)^2}{\left(\frac{m}{k} \right)^2} \right] \left[\frac{1 - \left(\frac{m}{k} \right)^2}{\left(\frac{m}{k} \right)^2} \right] \left[\left(\frac{m}{k} \right)^2 + 1 \right]$$

$$m = 1, 2, 3, \dots$$

$$n = 1, 2, 3, \dots$$

$$m = 1, 2, 3, \dots$$

$$n = 1, 2, 3, \dots$$

1 = % THE NUMBER OF NEIGHBORING SLOTS CONSIDERED IN THE 'V' PLANE

2 = % THE NUMBER OF NEIGHBORING SLOTS CONSIDERED IN THE 'W' PLANE

a = GUIDE I.D. WIDTH

b = GUIDE I.D. WIDTH

b = GUIDE I.D. HEIGHT

b₀ = SLOT 'V' PLANE SPACING

b_M = SLOT 'W' PLANE SPACING

x = SLOT OFFSET

x = SLOT OFFSET

s = SLOT WIDTH

v = SLOT SHUNT ADMITTANCE

v₀ = GUIDE CHARACTERISTIC

1. MODIFICATION OF STARK'S DIPOLE EXPRESSION TO SLOTS

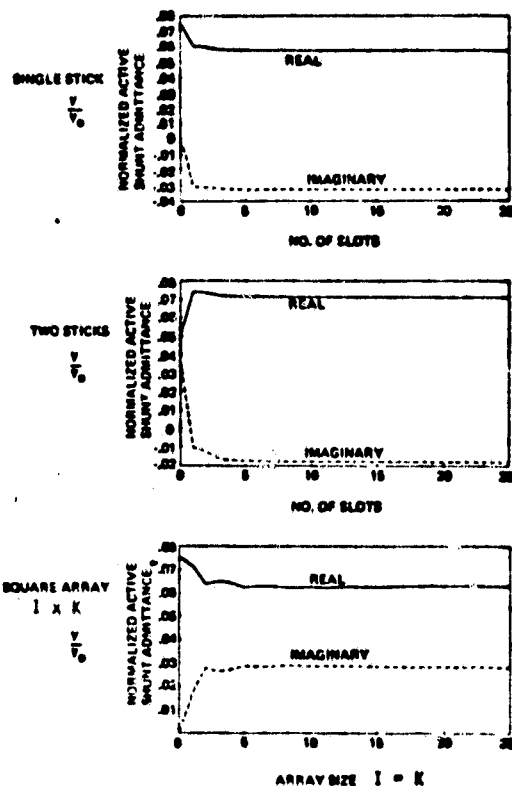


Figure 3: Estimate of Mutual Coupling in SPS Slotted Waveguide Array

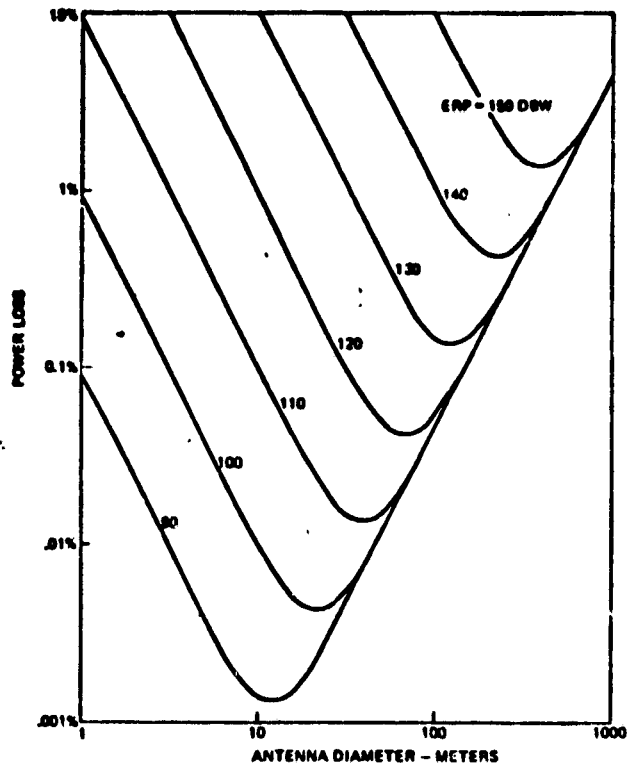


Figure 4 System Power Loss Vs. Pilot Transmit Antenna Diameter and ERP Required

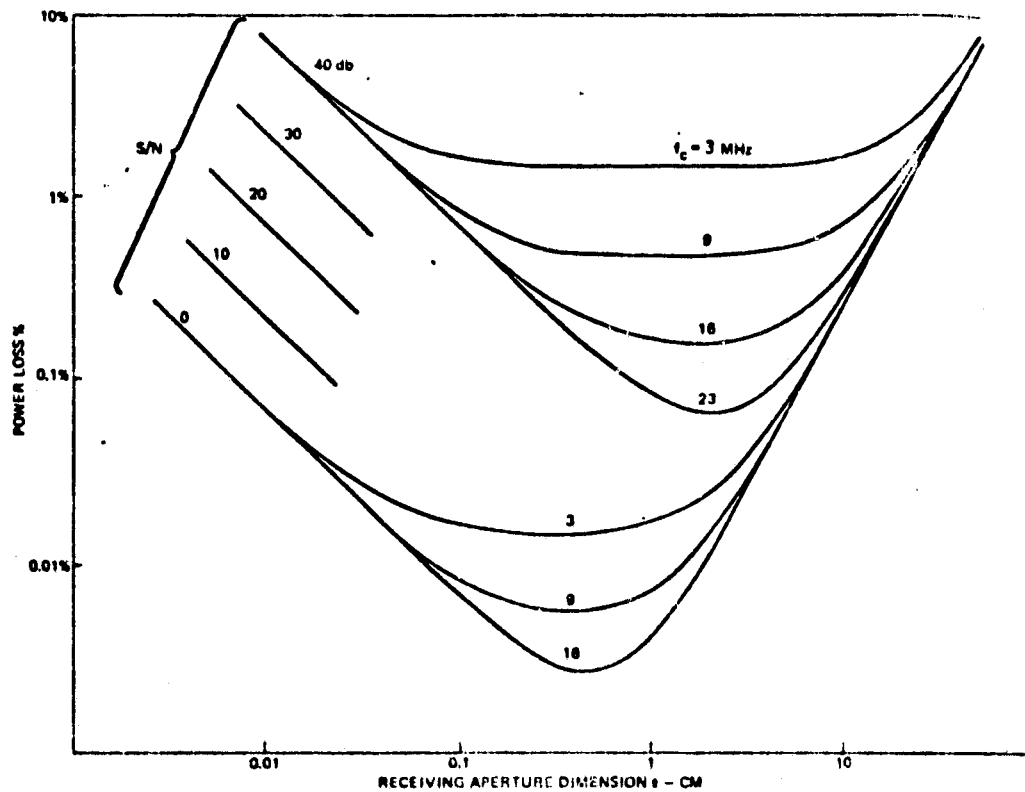


Figure 5 : Total System Loss Vs. Receive Aperture

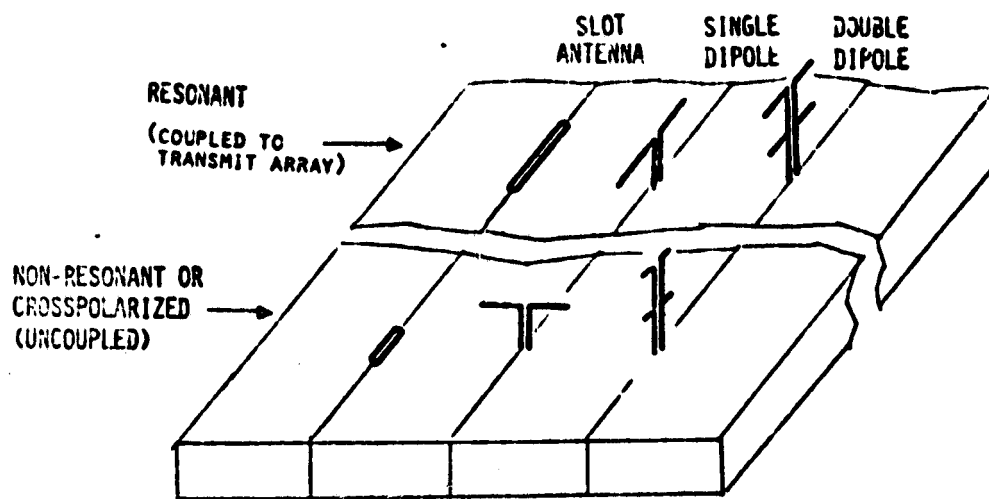


FIGURE 6: POTENTIAL SPS PILOT-LINK RECEIVING ANTENNA CONFIGURATIONS.
THE DOUBLE DIPOLE CONFIGURATIONS AFFORD PARTIAL NOISE CANCELLATION.

METHOD FOR PRECISION FORMING OF LOW-COST, THIN-WALLED SLOTTED WAVEGUIDE ARRAYS FOR THE SPS

William C. Brown
Raytheon Company
New Products Center
Waltham, Massachusetts 02154

Presented at the RADIATING ELEMENTS SESSION OF THE SPS MICROWAVE SYSTEMS WORKSHOP
January 15-18, 1980, Lyndon B. Johnson Space Center, Houston, Texas

ABSTRACT

A method for the precision-forming of thin-walled, slotted-waveguide arrays has been devised. Models have been constructed with temporary tools and evaluated. The application of the method to the SPS requirements is discussed.

Introduction

The method for forming thin-walled slotted waveguide arrays that will be described grew out of a necessity to narrow down the broad range of estimated cost for slotted waveguide arrays in ground based arrays. In most items that are designed for automated production the cost of the material is the dominant element of cost. Therefore the use of thin material is attractive because of the large reduction in material cost. Then, if a rapid, inexpensive method of fabrication can be devised, the cost of the slotted waveguide arrays will be low and can be accurately estimated.

Such a fabrication method had been devised in principle by the author. An opportunity then arose to build working models of the design as part of a contract with JPL for the improvement of microwave beamed power technology, using a slight modification of their electrical design for such an array.

The working models that were made from 0.020 inch material were mechanically so strong and the fabrication technique so well adapted to even

thinner material that the potential for a slotted waveguide array made from 0.005 inch or even thinner material for the SPS applications is very good.

Early estimates of the mass of a slotted waveguide array for the 1 kilometer diameter transmitting antenna for the SPS were based on the use of 0.020 inch thick aluminum material and these estimates may still persist and show up in current estimates of mass for the SPS. An array based on the use of 0.005 inch material in place of the 0.020 inch would save nearly 2.5×10^6 kilograms of material. Savings in transportation costs alone would be 250 million dollars if transportation costs were only \$100 per kilogram.

The fabrication of thin-walled guides can also be accomplished with great precision. Tolerances of $\pm 2-3$ mils should be possible.

Finally it appears, as shown in Figure 1, that the arrays can be relatively easily fabricated in space from rolls of aluminum foil which represents an ideal packing factor for transportation purposes.

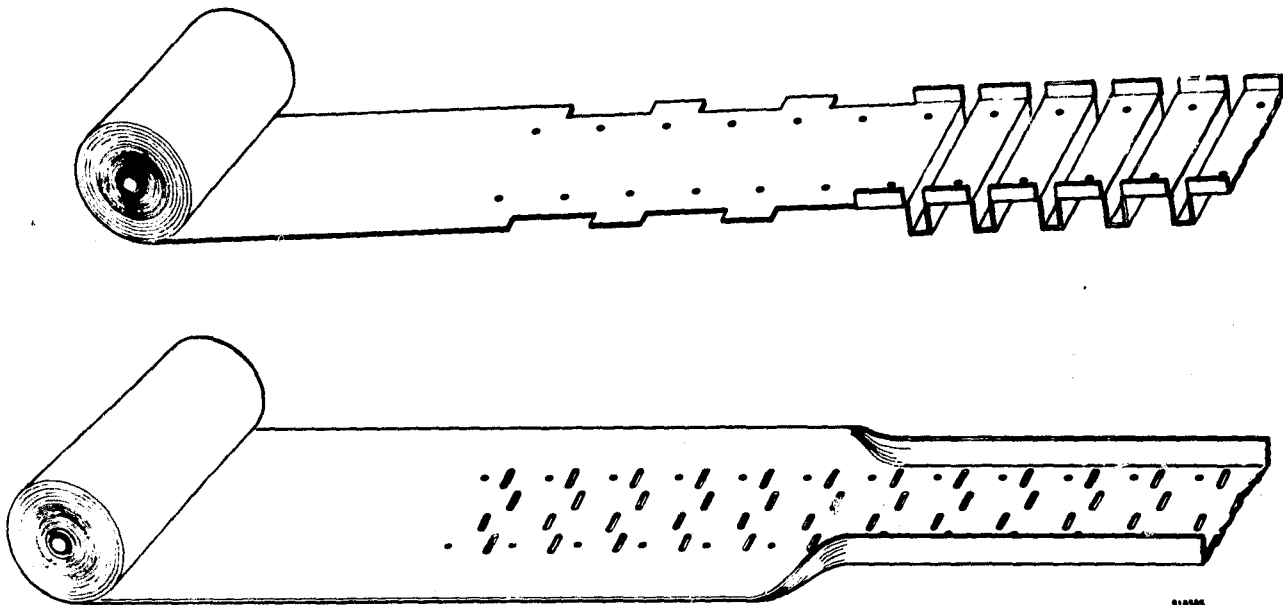


Figure 1. Proposed Method for Precision Forming and Assembly of Low-Cost, Thin-Walled, Slotted Waveguide Arrays for the SPS.

Description of Fabrication Method

The slotted waveguide array as shown in Figure 1 consists basically of a folded top plate whose corrugations contribute the three sides of the waveguide and a bottom plate into which the radiating slots are punched. The two sections then flow together and are joined to each other either by resistance spot welding or by laser beam welding to form the finished assembly shown in Figure 2.

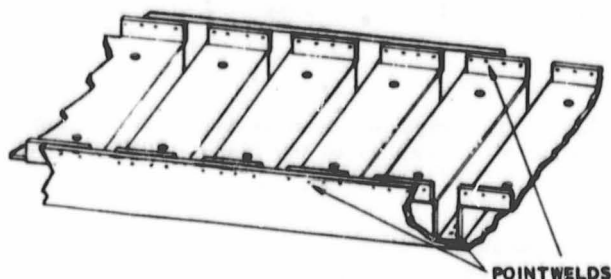


Figure 2. Finished Assembly.

The holes which are punched into the material are spaced accurately from each other and serve to accurately locate the material in the bending fixture which is also accurately machined and ground. The holes also serve to jig the top and bottom halves to each other for accurate assembly.

The method as originally proposed by the author utilized a third piece in the assembly that joined the top and bottom at their ends. An improvement to simply eliminate the end plate by the upward fold of the end of the top and bottom pieces as shown in Figure 1 is the suggestion of R.M. Dickinson.

It is possible that the broad faces of the waveguide members, both top and bottom, may need some stiffening to avoid bending and "oil canning". The thin flat channels that are proposed to house the phase and amplitude references and auxiliary power lines perform this function on the slotted surface. The unslotted surfaces could be embossed to stiffen them.

The individual slotted waveguides in the array are fed from a feed waveguide shown in Figure 3 as the transverse waveguide. Transfer of energy is made through diagonal slots between the feed waveguide and radiating waveguides. The feed waveguide is attached to the array by means of pop rivets.

Construction and Evaluation

Two 8 x 8 (8 slots in 8 waveguides) arrays were constructed from 0.020 inch aluminum with the use of temporary tooling of a simple nature. The $\frac{1}{4}$ inch separation between waveguides that is necessary in the forming process and which have become attractive as a region in which to mount solid state devices and through which to run cables made it necessary to adjust the dimensional specifications of the JPL design which was designed for a different fabrication method.

The slotted face plate, folded waveguide section, and the end channels were assembled to each other by spot welding. Back and front view of the finished assembly are shown in Figures 3 and 4.

In the absence of any antenna testing range a method was evolved to test the array by electrically probing each slot for amplitude and phase, as shown in Figure 5. This arrangement gave the phase and

amplitude information tabulated in Table I. When readings around the outside are disregarded because of edge effects, the rms phase and amplitude percentage deviation of the remaining sections are 6.22° and 10% respectively. With the outer elements included the phase deviation is 8.89°.

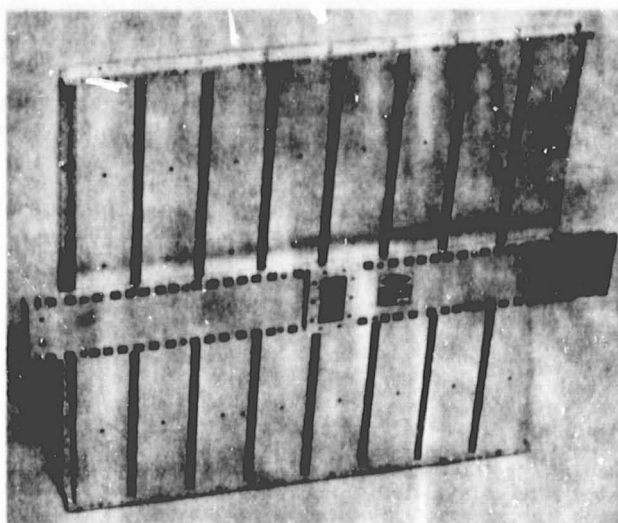


Figure 3. Back View of the 8 x 8 Slotted Waveguide Array as Constructed from 0.020 Inch Aluminum Sheet Throughout and Assembled by Means of Spot Welding.

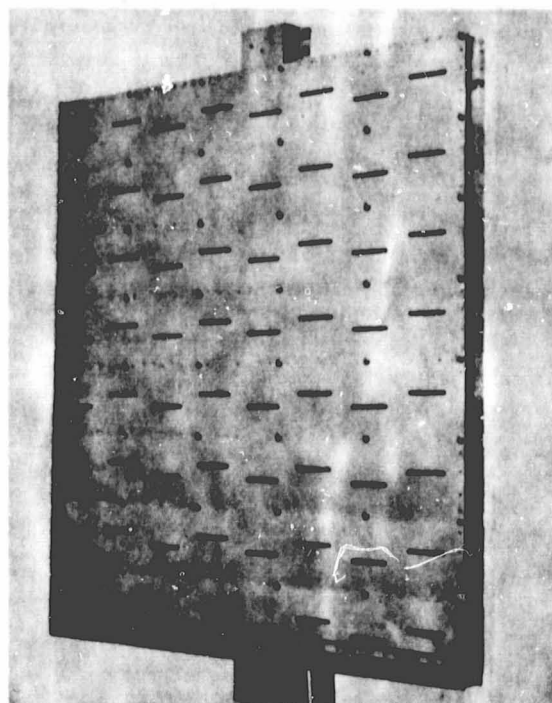


Figure 4. Front View of the 8 x 8 Slotted Waveguide Array as Constructed from 0.020 Inch Aluminum Sheet Throughout and Assembled by Means of Spot Welding.

Finally, the antenna range data taken by JPL on the array that was made for them as a portion of the contractual work effort for them is presented in Figures 6 and 7.

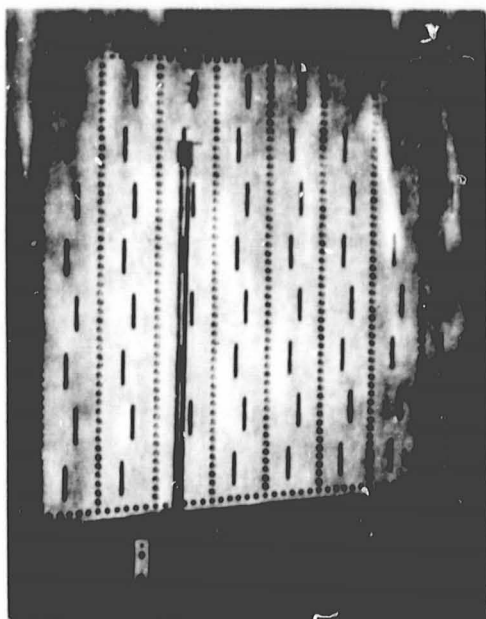


Figure 5. Probe Arrangement for Measuring Phase and Amplitude of Microwave Power Radiated at Individual Slots. The Phase and Amplitude Sensed by the Probe were Compared by Means of a Hewlett-Packard Network Analyzer with the Amplitude and Phase of the Power Input to the Single Waveguide Feed to the Slotted Waveguide Array.

TABLE I
Matrix Array of Amplitude and Phase Information on Thin Metal Slotted Array #1

Col.		1	2	3	4	5	6	7	8
Row									
1	Phase	105	100	109	110	103	96	93	105
	Amp	.53	.57	.67	.70	.64	.61	.62	.62
2	Phase	104	84	80	82	91	94	79	90
	Amp	.61	.51	.59	.67	.71	.72	.59	.40
3	Phase	94	80	88	89	85	85	94	106
	Amp	.45	.58	.63	.71	.64	.58	.56	.56
4	Phase	105	79	80	73	80	89	72	94
	Amp	.61	.56	.60	.73	.73	.69	.65	.40
5	Phase	120	81	86	76	70	85	84	120
	Amp	.50	.60	.59	.72	.68	.52	.58	.50
6	Phase	96	80	74	83	92	90	79	91
	Amp	.68	.53	.57	.68	.72	.69	.60	.39
7	Phase	89	73	83	82	80	86	91	104
	Amp	.49	.60	.67	.69	.61	.60	.54	.55
8	Phase	100	86	90	93		96	88	160
	Amp	.59	.60	.53	.63		.70	.57	.45

Overall array is an 8 x 8 matrix

"Internal" array is a 6 x 6 matrix

Test data obtained by dipole probe placed in front of each radiating slot.

RMS of phase deviation of internal array is 6.22°.

RMS of phase deviation of overall array is 8.89°.

RMS of amplitude variation of internal array is 0.0628 from a mean value of 0.627.

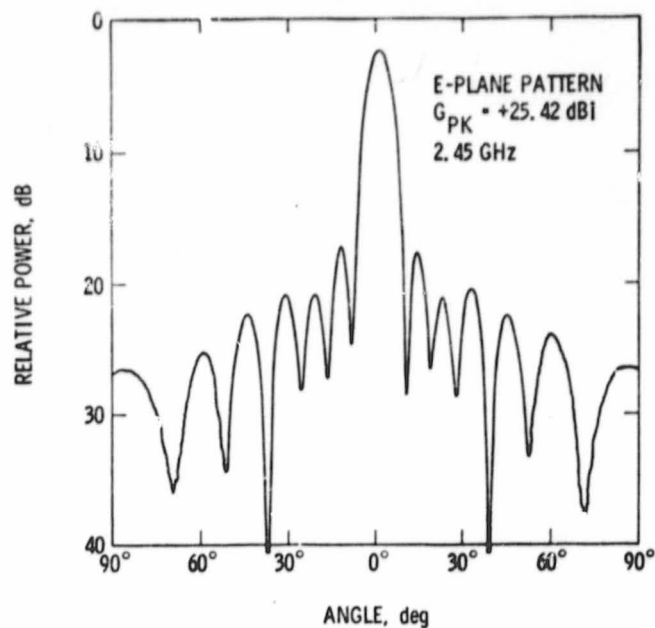


Figure 6. Antenna Pattern for 8-Slot x 8-Stick Slotted Waveguide Antenna.

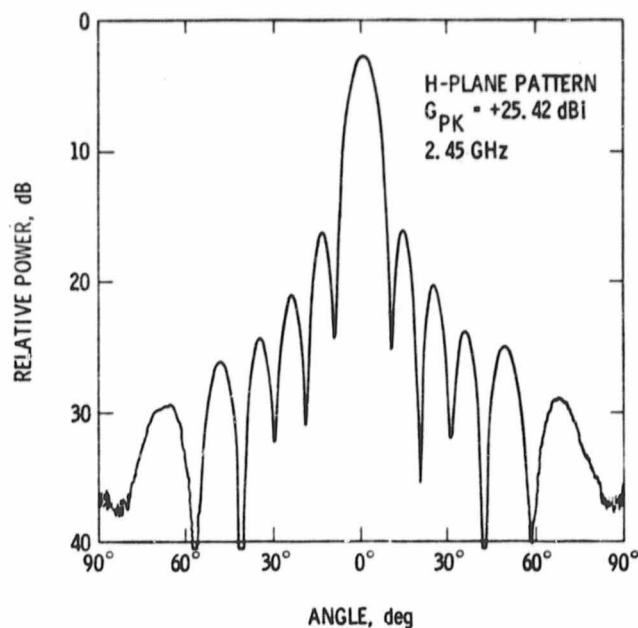


Figure 7. Antenna Pattern for 8-Slot x 8-Stick Slotted Waveguide Antenna.

CONSIDERATIONS FOR
HIGH ACCURACY RADIATION EFFICIENCY
MEASUREMENTS FOR THE
SOLAR POWER SATELLITE (SPS) SUBARRAYS

D. J. Kozakoff, J. M. Schuchardt and C. E. Ryan

Georgia Institute of Technology
Engineering Experiment Station
Atlanta, Georgia 30332

INTRODUCTION

The relatively large apertures to be used in SPS [1], small half-power beamwidths, and the desire to accurately quantify antenna performance dictate the requirement for specialized measurements techniques. The subject matter presented herein is under investigation as part of a program at Georgia Tech to address the key issues*.

The objectives of the program include the following:

- 1) For 10-meter square subarray panels, quantify considerations for measuring power in the transmit beam and radiation efficiency to $\pm 1\%$ (± 0.04 dB) accuracy.
- 2) Evaluate measurement performance potential of far-field elevated and ground reflection ranges and near-field techniques.
- 3) Identify the state-of-the-art of critical components and/or unique facilities required.
- 4) Perform relative cost, complexity and performance tradeoffs for techniques capable of achieving accuracy objectives.

The precision required by the techniques discussed below are not obtained by current methods which are capable of $\pm 10\%$ (± 0.4 dB) performance. In virtually every area associated with these planned measurements, advances in state-of-the-art are required.

ERROR SOURCES

In general, the RF and physical environment and the electronic instrumentation all contribute to the overall measurement error. Ideally, the RF source is stable in amplitude and frequency, the transmitted wave arrives at the receiver as a true plane wave free of objectionable reflections, and the atmospheric effects are negligible. The receiver must be ideal and error free, and the gain antenna reference is accurately known. In the real world, one must deal with the errors which occur as the instrumentation departs from the ideal performance listed above.

For SPS subarray antenna pattern measurements, the critical error sources have been quantified into four categories shown in Table 1. The objective of this investigation is controlling these error sources to yield an overall gain uncertainty of ± 0.04 dB. Because of the large size of an SPS subarray (81.67-wavelengths at 2.45 GHz), antenna range effects are given

* Contract NAS8-33605

the largest allowance in the error budget. The errors allocated to transmitter/receiver sources require advances in state-of-the-art of associated microwave electronics. However, even with currently available equipment, because of single frequency operation, and the fact that receiver and transmitter are phase-locked and thermally stabilized, errors can be accurately controlled. Use of a microcomputer will permit error compensation of such factors as the nonlinearity of receiver and detector.

Controlling the antenna structure for measurement will require developing a cradle assembly that will hold the antenna rigid. Preliminary weight estimates indicate approximately 2.5 tons for a prototype subarray assembly. Ambient temperature, solar energy and wind effects can be controlled somewhat by selecting the measurement time period. However, since several thousand 10-meter apertures may need to be measured during the course of the SPS program, unique test facilities are anticipated. For instance, shielding from the adverse external parameters listed above can be achieved through use of a large dome radome.

Antenna measurements can be made with the test antenna either receiving or transmitting because of the reciprocity theorem. However, in the case where the SPS array is transmitting and the goal is to determine power in the transmit beam via beam integration, unique problems arise. Figure 1 illustrates one measurement concept being considered.

FAR-FIELD MEASUREMENT CONCEPTS

The predominant error contributors for far-field measurements are 1) field nonuniformity due to ground reflection, 2) gain loss due to quadratic phase error (near-field effects), and extraneous reflections. The National Bureau of Standards has investigated error budgets associated with far-field measurements [2]. For SPS, an adopted far-field error subbudget is shown in Table 2. The large size of an SPS subarray dictates a far-field criteria of greater than $6 D^2/\lambda$ to maintain quadratic phase error loss below 0.01 dB.

Field nonuniformity can be controlled via an elevated range concept where the receive antenna null is placed at the midpoint reflection point as depicted in Figure 2. Tradeoff calculations indicate the required tower heights for elevated range distances greater than $6 D^2/\lambda$ are not practical, however, consideration for a mountain top to mountain top range with an elevation of 600 feet and a measurement range of 7 miles appears very attractive.

Consideration was given to use of a ground reflection range facility. Here, transmit and receive tower heights are selected so that the reflection from the ground adds in phase to the direct ray path. A negative feature is that a relatively large range is required to obtain a sufficiently flat amplitude wavefront over the vicinity of the test antenna. Figure 3 relates the transmit and receive tower heights as a function of range. Under the constraint of a minimum and maximum tower height of 20 and 100 feet, respectively, and minimum range of 3 miles based on near-field criteria; the shaded area indicates regions where satisfactory operation may be obtained. The criteria for a sufficiently flat amplitude wavefront over the test zone is currently under investigation. Initial calculations indicate the performance of a 4-mile ground reflection range with receive and transmit tower heights of 30 and 70 feet, respectively, provided a wavefront within 0.1 dB over a 10-meter zone, but only with use of high efficiency absorber barricades at the midrange point.

POSITIONER CONSIDERATIONS

The large weight handling requirement (2.5 tons minimum)*, and small angular accuracy requirements, indicate that the positioner is a potential problem area based on units currently available. It has been determined that the positioner must be able to resolve a sample within 0.0016 degrees corresponding to a 19 bit encoder to resolve the beam power within a ± 0.04 dB accuracy.

A survey was made of available antenna positioners, and is summarized in Table 3. The positional accuracy of off-the-shelf positioners is on the order of 0.005 degrees. Available positioner data indicate positioning of anything larger than the 10-meter subarray will not be possible based on the weight projections.

The fractional power in the beam based on a uniformly illuminated 10-meter square aperture is plotted in Figure 4. Here, it is seen that the main beam (± 0.312 degrees) encompasses approximately 79 percent of the transmitted energy.

Based on these results, a concept was devised providing desired scan performance as illustrated in Figure 5. Here, a small angle positioner (SMAP) provides very accurate scan capability over a ± 1.5 degree sector for the purpose of beam integration. The larger gimbal arrangement provides coarse positioning over the complete ± 20 degree sector. Positioner hardware providing greater angular scan does not currently exist. From the plot of fractional beam power (Figure 4) approximately 89% of the total radiated power is accounted for within $\pm 1.5^\circ$ scan; over 99% of the power is radiated in the ± 20 degree sector.

NEAR-FIELD MEASUREMENTS

Near-field techniques utilize a calibrated probe antenna to measure the amplitude and phase of the field close to the antenna aperture. Two orthogonally-polarized probes, or a single linear-polarized probe oriented in the vertical and horizontal directions are used, together with a probe compensation technique [8, 9] to obtain the complete radiation characteristics of the antenna under test (AUT). This measurement procedure requires an automated facility capable of reading the measured data in digital form for the required computer processing. The planar near-field measurement technique is particularly attractive for SPS since the SPS subarray does not have to be moved during the measurement, i.e. only the probe antenna is moved.

Recent work at Georgia Tech has demonstrated that accurate antenna patterns can be obtained via near-field techniques [4, 5]. The National Bureau of Standards has shown that for planar near-field scanning, the near-field derived patterns are more accurate than far-field measured patterns when considering all error sources involved [6].

Martin Marietta [3] has implemented an indoor planar near-field measurements facility capable of measurement of antennas up to 50-foot diameter. The benefits of this facility include all weather operation, a thermally controlled environment (maintained within 2°F), and an RF anechoic environment. RCA has also implemented an indoor planar near-field facility for acceptance testing of the AN/SPY-1 phased array antenna for the AEGIS system [10].

* This weight estimate is based on using either conventional aluminum waveguide (without klystrons) or ultra-thin aluminum waveguide with klystrons included.

Near-field measurements can also be implemented by employing cylindrical or spherical probe scanning. However, in the spherical technique it is necessary to move the AUT while holding the probe fixed. In the case of SPS, spherical near-field scanning cannot be used because of the difficulty of gimbaling the heavy subarray in order to scan over a full sphere. However, planar and cylindrical scanning concepts are applicable. A planar scan concept is shown in Figure 6 and a cylindrical concept in Figure 7. Either system has potential to be implemented outdoors, however, the effects of thermal changes on scanning mechanism and instrumentation and the fact that an outdoor facility is subject to environmental conditions, makes an indoor near-field facility far more attractive and practical.

Tradeoff studies at Georgia Tech have suggested that the planar near-field concept has potential for array measurements of an SPS mechanical module (30 square meters). Problem areas to be resolved include computer requirements and the complexity of scanning over a much larger surface with acceptable precision. A previous study performed by Georgia Tech for NASA indicated that the cylindrical near-field technique is attractive for the measurement of electrically and physically large ground station antennas [11].

Previous studies at Georgia Tech have considered the cost tradeoffs of far-field measurements versus a near-field measurement [8, 11]. The results of these investigations for both large phased array and large reflector antennas demonstrate that costs are less for the near-field facility, and that the projected measurement accuracy is superior to that which could be obtained on a high quality far-field antenna measurement range.

However, the capital investment and operating costs of the near-field facility are functions of the required measurement accuracy. For example if the on-axis antenna gain is to be determined to within 0.01 dB, the measurement probe axial position accuracy must be within 0.1 wavelength, i.e. 0.048 inches for the SPS. Also, the scan width-to-diameter ratio must be at least 1.5. Thus, this requirement has a direct effect on the mechanical design of the near-field measurement system.

In order to obtain a complete representation of the antenna pattern from a planar or cylindrical near-field scan, the field is normally sampled at $1/2$ wavelength intervals along the linear scan dimension. If the AUT is electrically large, the required Fourier transform processing can become burdensome. However, it has been shown that the sample spacing can be increased by almost an order of magnitude if only the main-beam and first sidelobes are to be defined [4, 11].

In order to obtain accurate polarization information on the antenna pattern, the polarization characteristics of the measurement probe must be carefully characterized over the maximum possible dynamic range. Work at RCA [7] has also indicated that careful probe polarization design is necessary too if a very accurate gain determination is required. For instance, assuming an SPS antenna polarization ratio of 30 dB, a probe polarization ratio of 20 dB will result in a gain measurements error of approximately 0.25 dB. Thus, a very stringent requirement is placed on probe polarization ratio; a requirement of 30 dB, or better, is anticipated.

CONCLUSIONS

Because of the large electrical size of the SPS subarray panels and the requirement for high accuracy measurements, specialized measurement facilities are required. Most critical measurement error sources have been identified for both conventional far-field and near-field techniques. Although the adopted error budget requires advances in state-of-the-art of microwave instrumentation, the requirements appear feasible based on extrapolation from today's technology.

Additional performance and cost tradeoffs need to be completed before the choice of the preferred measurement technique is finalized.

REFERENCES

1. "Solar Power Satellite Concept Development and Evaluation Program," U.S. Department of Energy and NASA Report, October 1978.
2. "Accuracy Considerations in the Measurement of the Power Gain of a Large Microwave Antenna," M. Kanda, 1974 IEEE/AP-S Symposium, Georgia Tech, Atlanta, June 1974.
3. "Near-Field Pattern Measurement Facility," C. E. Kirchoff, 1979 Antenna Applications Symposium, U. of Illinois, September 1979.
4. "Probe Compensated Near-Field Measurements Basic Theory, Numerical Techniques, Accuracy," W. M. Leach, Jr., E. B. Joy and D. T. Paris, IEEE/AP-S Symposium, Georgia Tech, June 1974.
5. "Antenna Compensated Near-Field Measurements to Obtain Far-Field Patterns of Aperture Antennas and Phased Arrays," H. A. Ecker, et al, IEEE/AP-S Symposium, Georgia Tech, June 1974.
6. "Upper Bound Errors in Far-Field Antenna Parameters Determined From Planar Near-Field Measurements: Part 1-Analysis," A. D. Kaghjian, National Bureau of Standards Technical Note 667, October 1975.
7. "Automated Near-Field Test Set for Phased Array Production," D. Staiman, 1979 Antenna Applications Symposium, U. of Illinois, September 1979.
8. "Correction of Near-Field Antenna Measurements Made with an Arbitrary But Known Measuring Antenna," D. M. Kerns, Electronics Letters, Vol. 6, May 1970.
9. "Plane Wave Scattering Matrix Theory of Antenna and Antenna-Antenna Interaction: Formulation and Application," D. M. Kerns, Journal of Research of the Nation Bureau of Standards, Vol. 80B, No. 1, January 1976.
10. "Implimenting a Near-Field Antenna Test Facility," W. A. Harmening, Microwave Journal, Vol. 22, No. 9, September 1979
11. "A Study of the Application of Near-Field Measurements for NASA Requirements," B. J. Cown, C. E. Ryan, Jr., A. L. Bridges and J. D. Adams, Final Engineering Report, Contract NAS5-2234, Georgia Institute of Technology, March 1976.

TABLE 1

TOTAL RSS = .04 dB



Figure 1. Equipment Configuration for Antenna Measurements.

TABLE 2
ANTENNA RANGE MEASUREMENTS
ERROR SUB-BUDGET

<u>ERROR COMPONENT</u>	<u>ALLOWABLE VALUE</u>	<u>COMMENTS</u>
Field Uniformity	0.015 dB	Maximum amplitude taper at edge of SPS subarray approx. 0.04 dB
Quadratic Phase Error	0.010 dB	Requires range greater than $6 D^2/\lambda$
Standard Gain Antenna Uncertainty	0.020 dB	Gain standard needs to be developed
Atmospheric Effects	0.005 dB	Atmospheric effects cancelled by reference
VSWR	0.005 dB	VSWR loss calibrated out
Extraneous Reflections	0.025 dB	Extraneous reflections -57 dB down
RSS Subtotal		0.037 dB

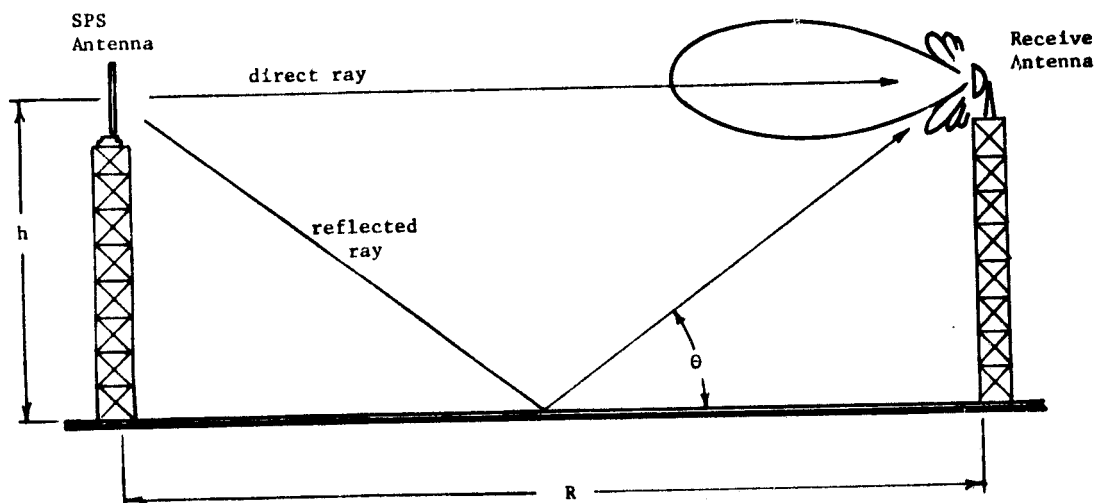
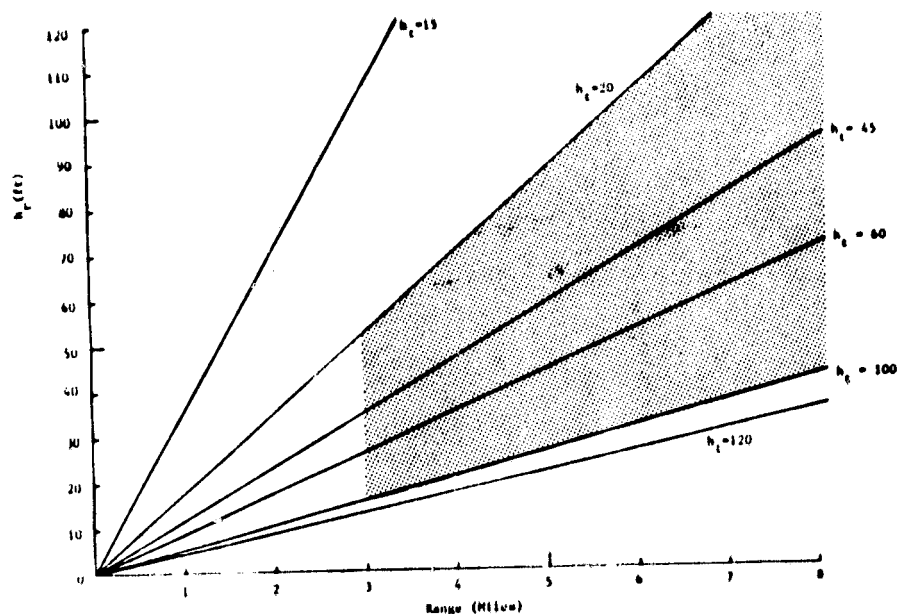


Figure 2. Elevated Antenna Range.



Note: Darkened area is allowable operating region.

Figure 3. Relation Between Receive Antenna Height (h_r), and Transmit Antenna Height (h_t) for a Ground Reflection Antenna Range.

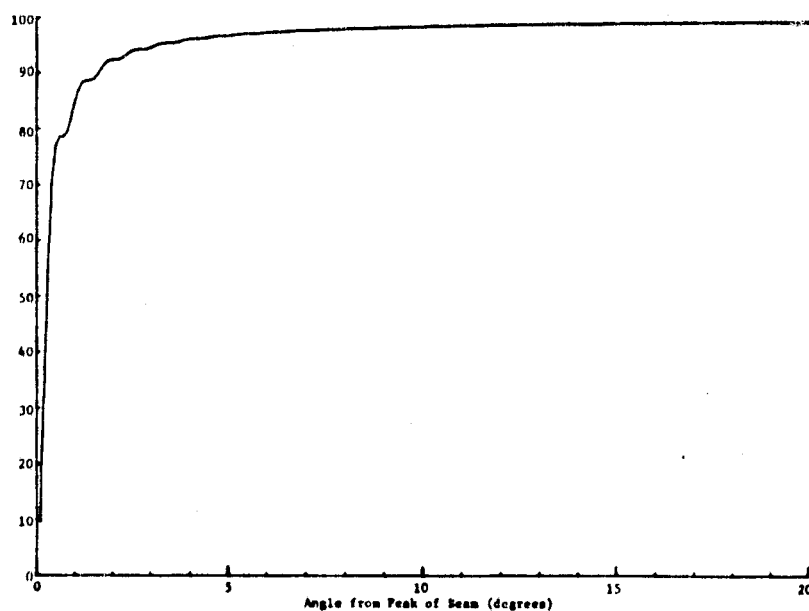
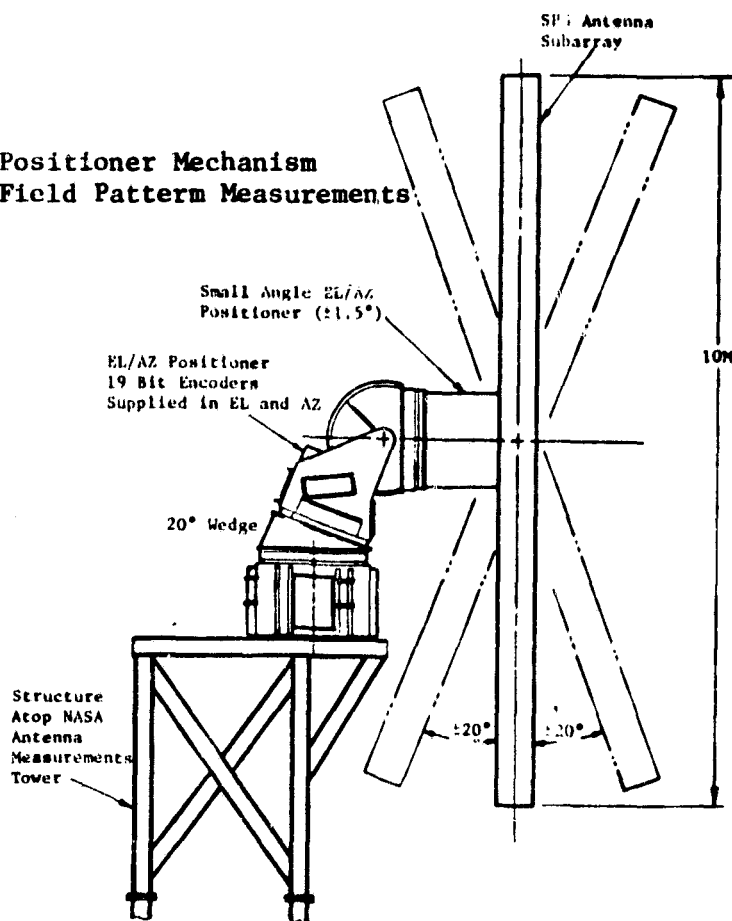


Figure 4. Fractional Beam Power for SPS Subarray Pattern.

**Figure 5. Antenna Positioner Mechanism
For Far-Field Pattern Measurements.**



**TABLE 3
SUMMARY OF POSITIONER PERFORMANCE**

Scientific Atlanta Series**	Maximum Moment (Kft-lb)	Estimated Moment Arm* (ft)	Maximum Subarray Wt.		Cost***		
			Klbs	Tons	Elev./Az.	SMAP	Total
85	150	9.5	15.8	7.9	\$440K	\$400K	\$840K
45	75	7.5	10	5	\$111K	\$100K	\$211K

* Elevation over azimuth plus SMAP configuration.

** NOTE: the series 85 has a maximum vertical load limit of 25 tons.

*** November 1979 estimates.

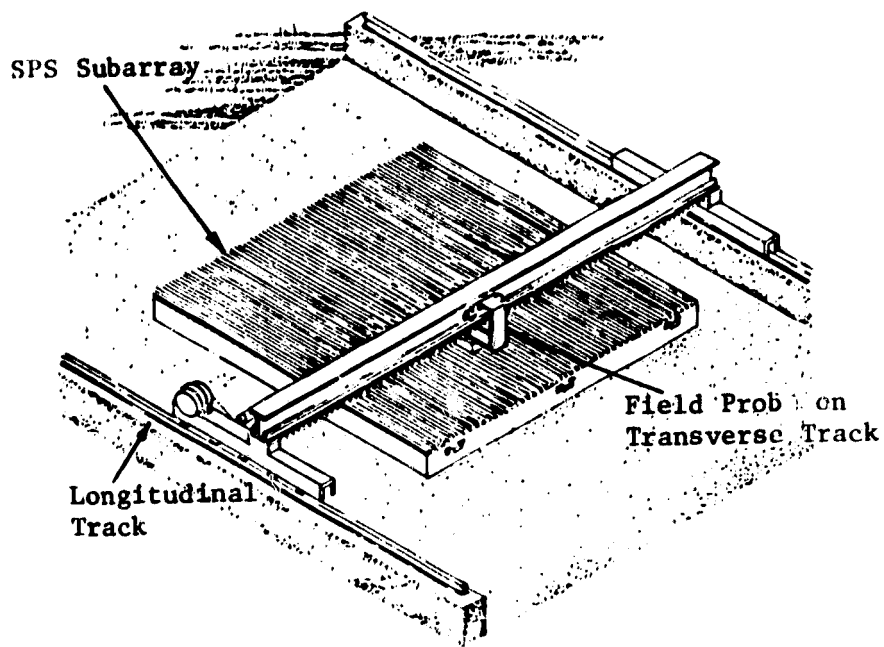


Figure 6. Planar Scanner Concept for Near-Field Measurements.

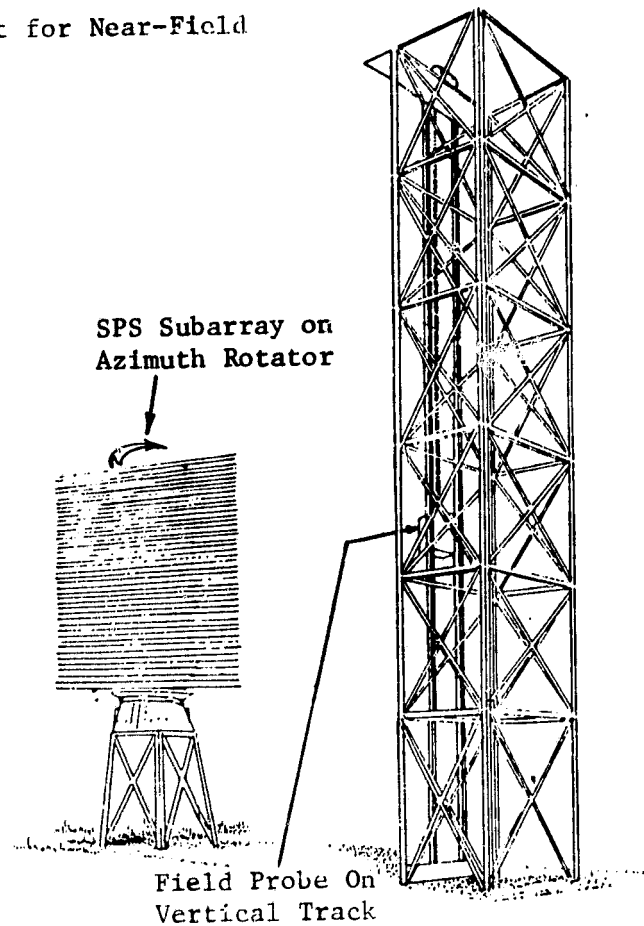


Figure 7. Cylindrical Scanner Concept for Near-Field Measurements.

RECTENNA SESSION

THE HISTORY OF THE DEVELOPMENT OF THE RECTENNA

William C. Brown
Raytheon Company
New Products Center
Waltham, Massachusetts 02154

Presented at the RECTENNA SESSION OF THE SPS MICROWAVE SYSTEMS WORKSHOP
January 15-18, 1980, Lyndon B. Johnson Space Center, Houston, Texas

ABSTRACT

The history of the development of the rectenna is first reviewed through its early conceptual and developmental phases in which the Air Force and Raytheon Company were primarily involved. The intermediate period of development which involved NASA, Jet Propulsion Laboratory, and Raytheon is then reviewed. Some selective aspects of the current SPS rectenna development are examined.

Introduction

The chairman of this session believes that the perspective given by a history of the development of the rectenna would be of value to those now becoming involved with the application and further development of the rectenna for the SPS. He has asked me to present this history because he is aware that I have been closely and continuously involved with the development of the rectenna since its inception in 1963.

The concept and development of the rectenna arose in response to the need for a device that could be attached to a high altitude atmospheric platform and absorb and rectify microwave power from a microwave beam pointed at the vehicle. After the initial development of the rectenna under Raytheon and Air Force sponsorship for this purpose the rectenna development was carried on further and in a different direction by the author himself. In 1968, NASA became interested in the rectenna and its development in the context of transferring power from one space vehicle to another. This was followed by NASA's interest in the device for the receiving end of a system that would transfer electrical power from geosynchronous orbit to the earth.

Throughout this time period of 17 years, the development of the rectenna has been heavily disciplined by the various applications for which it has been considered. The result has been the accumulation of a large amount of experience which covers many facets of interest, including electrical design and performance, various physical formats, methods for accurate efficiency measurement and validation, life test data, and other items. Its development has also been characterized by contributions from many individuals whose involvement has been in two different areas. The first area is related to technical contributions. The second area is related to sponsorship. The development of the rectenna could not have proceeded very far without the encouragement and support of individuals within and outside the government who have understood the significance of free space power transmission by microwaves and the relevance of the rectenna development to this concept.

In presenting this history the author is treating the early conceptual and developmental phase as an interaction between many technological forces and developments, and people, which is the true nature of history. The history of the intermediate period is identified with the work supported by MSFC, JPL, LeRC and that was largely carried out by Raytheon. It is presented in a more summarized fashion with the

presentation focused on technological improvements and refinements. A final section is devoted to what might be considered as technological forecasting which is a projection of the past history combined with the subjective view of the author as to the impact of current and future technological and sociological events.

Early History of the Rectenna

The early development of the rectenna must be examined in the context that its conception and development grew out of the needs for a satisfactory receiving terminal for a microwave power transmission system. In this context we must take into account the factors which gave rise to an interest in the concept of microwave power transmission itself.

The first serious thought about power transmission by microwaves grew out of the development of microwaves for radar in which power was concentrated in relatively narrow beams as contrasted to the "broadcast" mode associated with low frequency radio. However, the element that really gave substance to the concept and distinguished it from the situation that existed when Hertz first demonstrated wireless power transmission with narrow beams using parabolic reflectors and spark gap generators, were newly developed electron tubes that could generate relatively large amounts of power at high efficiencies.

Still, there was no active postwar activity on microwave power transmission until it became recognized that with new approaches microwave generators could be developed to produce levels of CW microwave power about 100 times greater than from generators then available.^{1,2,3} Concurrent with this recognition was the inference that one of the potential useful applications of microwave power transmission would be microwave powered high altitude atmospheric platforms for communication and surveillance purposes.

This recognition stimulated Raytheon, under the guidance of Ivan Getting, Vice President for Engineering, to perform an in-depth study of such a platform in a helicopter format and to make a proposal to the Department of Defense in 1959 to develop such a vehicle.⁴ The reason why this is important in the development of the rectenna is that for the first time it became widely recognized that there was no efficient means of converting the microwave back into DC or low frequency electrical power at the receiving end of the system. This stimulated the Air Force to award several contracts to study this problem. One of these investigations that was to become a key element in the development of the rectenna was awarded to Purdue University and involved the use of

semiconductor diodes as power rectifiers.⁵

While this development at Purdue was proceeding, the development of super power microwave tubes had been started at Raytheon under the sponsorship of the Department of Defense and had achieved CW power outputs of over 400 kW at an efficiency exceeding 70% at a frequency of 3.0 GHz. Recognizing the potential application to free space power transmission the author had persuaded Raytheon Company to support the development of a close-spaced thermionic diode as a rectifier and the demonstration of a complete microwave power transmission system.⁶ Such a demonstration using the close-spaced thermionic diode and the physical arrangement of Figure 1 was successfully made in May 1963 with a power output of 100 watts which was used to drive a DC motor.⁷ Among those witnessing the demonstration was John Burgess, Chief Scientist at the Rome Air Development Center, who saw the potential of a microwave powered atmospheric platform for line of sight communication over long distances.

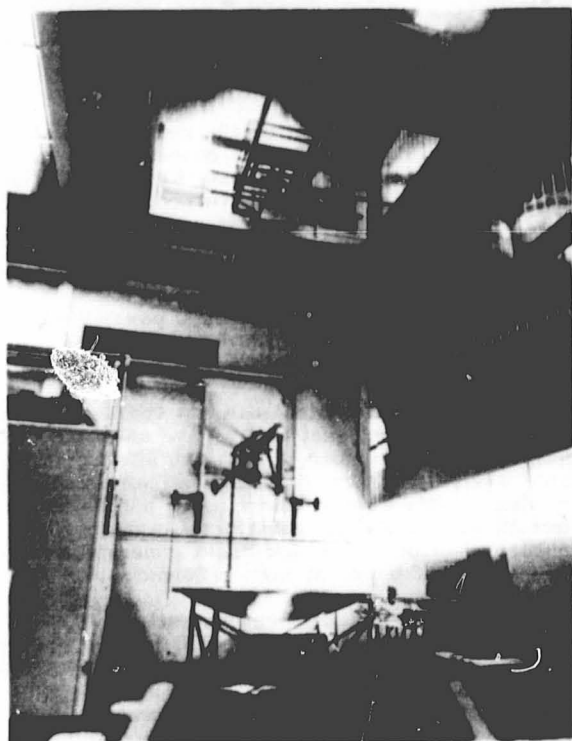


Figure 1. First experiment in the efficient transfer of power by means of microwaves at the Spencer Laboratory of Raytheon Company in May 1963. In this experiment microwave power generated from a magnetron was transferred 5.48 meters and then converted with DC power with an overall efficiency of 16%. A conventional pyramidal horn was used to collect the energy at the receiving end and a close-spaced thermionic diode was used to convert the microwaves into DC power of 100 watts. The collection and rectification arrangement was directive and not very efficient.

To encourage the chief scientist's interest the author privately constructed a small helicopter whose rotor was driven by a conventional electric drill motor supplied with power by a cable and demonstrated that it could carry aloft one of the closely spaced thermionic diodes. This demonstration was a major factor in motivating the chief scientist to set aside

discretionary funds for the development and demonstration of a small microwave powered platform. These funds became available in July of 1964, a year later.

Meanwhile it had become evident that the receiving arrangement used in Figure 1 had serious flaws for use in a microwave powered platform. The horn as a collecting element was much too directive for the expected roll and pitch of a vehicle and its collection efficiency was also poor. The close-spaced thermionic diode rectifier also proved to be a very short lived device. It was at this point that the author met by chance a college friend, Thomas Jones, in the Boston airport. Jones had become the head of the Electrical Engineering Department at Purdue University and told the author about the work going on there on the use of semiconductor diodes as microwave power rectifiers. The author immediately made a trip to Purdue and met Roscoe George, who had been carrying out most of the research activity. Professor George has been using dense arrays of closely spaced diodes within an expanded waveguide and had achieved as much as 40 watts of DC power output from microwaves in the 2 to 3 GHz range of frequency with respectable efficiencies.⁸ Although he had not made any measurements with free space radiation, he had shown how the microwave semiconductor diode, previously ignored as a power rectifier because of its very low individual power handling capability, could be combined in large numbers to produce reasonable amounts of DC power. In the absence of any other successfully developed microwave power rectifier the author was obviously drawn to the semiconductor diode approach. However, the use of George's dense arrays within a waveguide attached to a receiving horn would not solve the low collection efficiency and directivity of the receiving horn itself.

It was from this dilemma that the concept of the rectenna arose. The proposed solution was to take the individual full wave rectifiers out of the waveguide, attach them to half wave dipoles, and put a reflecting plane behind them. Once conceived⁹ the development of the rectenna, driven by its need for the proposed microwave powered helicopter, proceeded rapidly. Professor George was employed as a consultant to proceed with this approach and to make measurements on the characteristics of such a device.

With the arrangement of 28 rectenna elements shown in part in Figure 2 a power of 4 watts of DC power at an estimated collection and rectification efficiency of 50% and a power of 7 watts at an estimated efficiency of 40% were achieved.¹⁰ Of primary importance was the highly non-directive nature of the aperture (Figure 3) that had been anticipated because of the termination of each dipole antenna in a rectifier which effectively isolated the elements from each other in a microwave impedance sense except for the secondary effect of the mutual coupling of the dipoles. This feature of the rectenna that distinguishes it from the phased array antenna is of the greatest practical importance.

Although this achievement may be considered as the first major milestone in rectenna development the very small power handling capacity of the diodes limited the power output per unit area to values unsuitable for a helicopter experiment. For the helicopter experiment George suggested vertical strings of diodes separated by approximately a half wavelength, but the power density was still much too low. Placed close to each other in a plane to obtain the necessary power density, the impedance of the diode plane was very low and most of the power was reflected. The author solved this problem by placing a matching

network in front of it consisting of a plane array of rods spaced at an appropriate distance from the plane of the diode array. The final helicopter rectenna is shown in Figure 4. It was comprised of 4480 IN82G diodes, and had a maximum power output of 270 watts which was more than enough to power the helicopter rotor. The weight of the array was about three pounds or about 11 pounds per kilowatt of DC output.^{11,12}

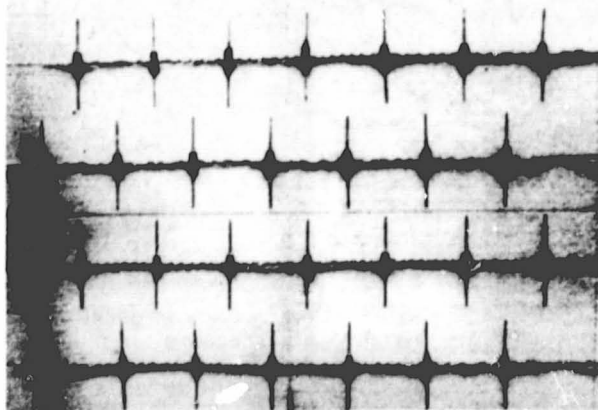


Figure 2. The first rectenna. Conceived at Raytheon Company in 1963, it was built and tested by R. George of Purdue University. Composed of 28 half-wave dipoles spaced one-half wave-length apart, each dipole terminated in a bridge-type rectifier made from four IN82G point-contact semi-conductor diodes. A reflecting surface consisting of a sheet of aluminum was placed one-quarter wavelength behind the array.

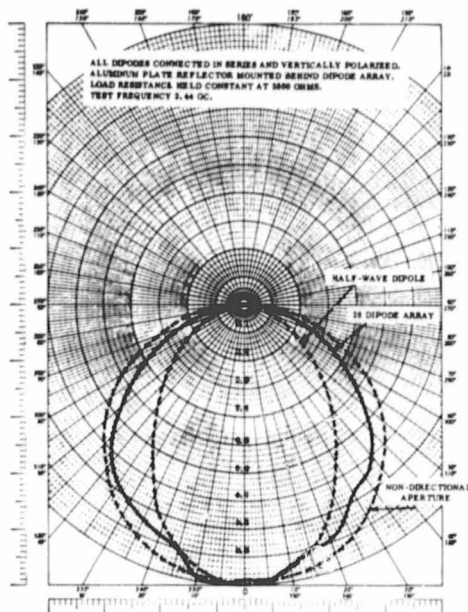


Figure 3. Directivity of the Half-Wave Dipole Array Shown in Figure 2. Directivity was essentially the same about both axes of rotation. Array has slightly less directivity than single half-wave dipole.

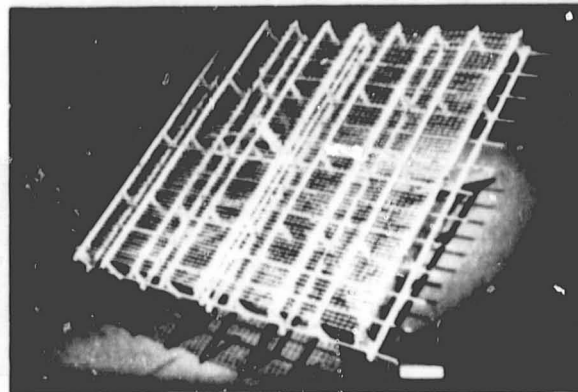


Figure 4. The special rectenna made for the first microwave-powered helicopter. The array is 0.6 meters square and contains 4480 IN82G point-contact rectifier diodes. Maximum DC power output was 270 watts.

A microwave power helicopter flight with this string type rectenna was made on July 1, 1964 prior to the start of work effort on an Air Force contract, to demonstrate continuous flight for ten hours. The Air Force contract was the basis for needed refinements and several notable demonstrations, including the 11,12 specified ten hour continuous flight of the vehicle. Figure 5 shows the helicopter in flight. It was necessary, of course, to use laterally constraining tethers to keep the helicopter on the microwave beam but this limitation was later removed by a study and experimental confirmation that the microwave beam could be used successfully as a position reference in a control system in an automated helicopter which would keep itself positioned over the center of the beam.¹²

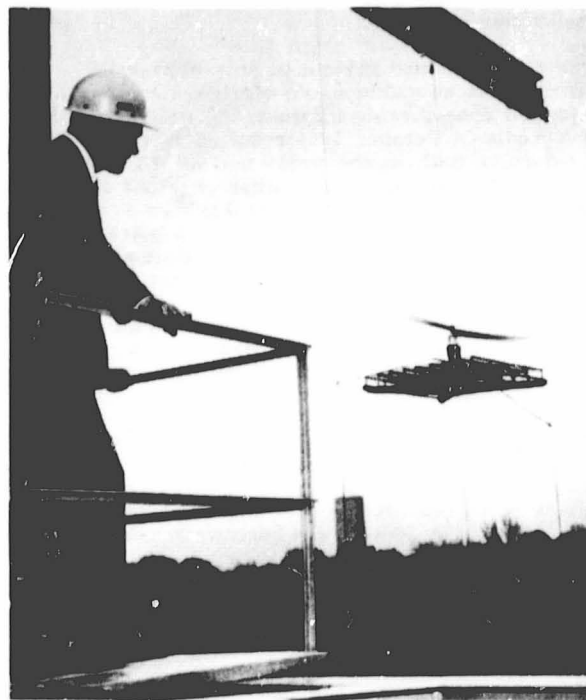


Figure 5. Microwave powered helicopter in flight 18.28 meters above a transmitting antenna. The receiving array for collecting the microwave power and converting it to DC power was made up of several thousand point contact silicon diodes. DC power level was approximately 200 watts. The date of the demonstration was October 1964.

The development of the string type rectenna (Figure 6) is of more than historical significance because it represents an approach in which large numbers of rectifying diodes can be spread over a surface to accommodate a high power density influx of microwave radiation or to operate in the vacuum of space where it may be desired to decrease to a minimum the mass required to transport heat from the diode sources to the heat sinks, in all probability passive radiators. The current status of microwave diodes (1979 technology) is such as to minimize the need for the "string-type" or equivalent arrays. Most applications currently envisaged do not call for incident microwave radiation of a density level beyond what the half wave dipole array with the greatly improved diodes can handle.

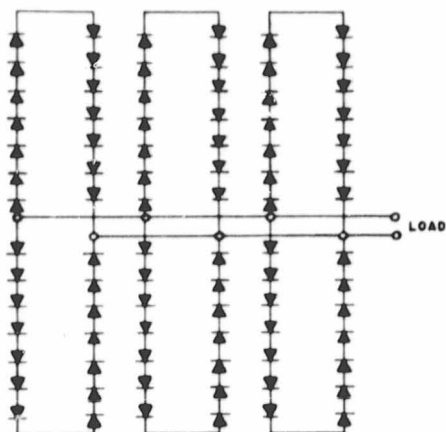


Figure 6. Schematic Drawing Showing Arrangement of Dipoles and Interconnections within a Diode Module used in Helicopter rectenna.

As the first airborne vehicle to stay aloft from power derived from any kind of an electromagnetic beam, it excited considerable interest. A demonstration to the mass media in October 1964 resulted in considerable exposure both in the press and on TV. Probably as a result of this, the author received a letter from a representative of Hewlett Packard Associates enclosing some newly developed Schottky barrier diodes which were indicated to be a substantial improvement over the point contact diodes that had been used. Tests made on the individual diodes (Type 2900) indicated that indeed they were much more efficient and would have more power handling capability. This combined with their smaller size made them of a great deal of potential interest.

Unfortunately, the Air Force elected not to further develop the microwave powered platform. It did, however, support the successful development and demonstration of a helicopter which would automatically position itself over the center of a microwave beam.¹²

In the time period from 1965 until 1970 there was no direct support of rectenna development from either government or industry. However, a substantial amount of development work on the rectenna was carried out by the author using personal funds and time during the 1967 to 1968 time period. This work was primarily aimed at incorporating the improved Schottky-barrier diodes into a very light weight rectenna structure that reverted back to the format of half wave dipoles terminated in a full-bridge rectifier. The resulting array is shown in Figure 7. The array, with a mass of only 20 grams, produced 20 watts of power output for an improvement in the power to mass

ratio of a rectenna by a factor of five. However, the rectenna of Figure 7 was also important in that it was used to make a demonstration of microwave power transmission that may have been an important factor in the decision by MSFC to continue with the development of microwave power transmission and the rectenna.

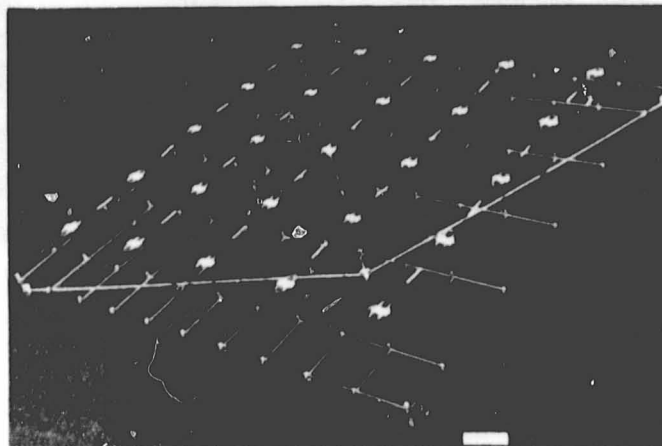


Figure 7. Greatly improved rectenna made in 1968 from improved diodes (HP2900) which became commercially available in 1965. The 0.3 meter square structure weighed 20 grams and delivered 20 watts of DC output power.

Development Under MSFC Sponsorship

The interest in the rectenna at MSFC is believed to have grown out of an interest of Associate Director Ernest Stuhlinger in some kind of free space power transmission within a space based community that would contain a collection of physically separated satellites. A country wide survey of technical approaches to this problem made by William Robinson of MSFC identified the work that had been done on microwave power transmission at Raytheon. At his and Dr. Stuhlinger's suggestion a demonstration was given to Dr. Werner von Braun and his entire staff. In the kind of demonstration that would probably not be permissible today the author set up a three foot parabolic reflector at one end of the long table as the source of a microwave beam of about 100 watts. At the other end of the table the author held the rectenna of Figure 7 now attached to a small motor with a small propeller on it. The microwave beam was used to supply power to the motor and the author would interpose his body between the source and the rectenna to demonstrate that the power was coming from the microwave beam.

Interest within MSFC resulted in setting up a small in-house facility for laboratory effort under W.J. Robinson and a contract with Raytheon for a system study in 1969. Initially the system study did not involve any supportive technology development. It soon became evident, however, that a barrier to any further interest at MSFC in microwave power transmission lay in demonstrating a minimal overall system efficiency. The contract was hastily amended to permit Raytheon to construct the hardware for an overall efficiency measurement to be made at MSFC.

The system, shown in Figure 8, was hastily put together and demonstrated at MSFC in September 1970. The specified minimal overall efficiency of 19% was achieved with a measured efficiency of 26%.¹³ This demonstration focused interest upon further increasing the efficiency of the rectenna and of the

overall system. Over the next four years there was a succession of improvements in overall system efficiency, primarily because of improvements in both the collection and rectification efficiency of the rectenna.¹⁵ The focus in this time period was upon the development of the technology rather than upon an application. However, it is believed that the emergence of the solar power satellite concept in the 1968 to 1974 time frame and its need for high efficiency exerted considerable influence upon the drive for better efficiency from all parts of the microwave power transmission system.



Figure 8. Test set-up of microwave power transmission system at Marshall Space Flight Center in September 1970. The magnetron which converts DC power at 2450 MHz is mounted on the waveguide input to the pyramidal horn transmitting antenna. The rectenna in the background intercepts most of the transmitted power and converts it to DC power. Ratio of DC power out of rectenna to the rf power into the horn was 40.8%. Overall DC-to-DC efficiency was 26.5%.

The MSFC demonstration of September 1970 indicated a number of deficiencies in the system including a rectenna collection efficiency of only 74% versus the theoretical maximum of 100%. This low collection efficiency was associated with improper spacing of the rectenna elements from each other in the rectenna array. The elements were therefore spaced more closely to each other in a hexagonal format, (Figure 9) and, in addition, the DC output of each rectenna element was terminated in a separate resistor to obtain a much greater range of data on the behavior of the rectenna. With the changed geometry the collection efficiency was increased to about 93%.

The decision to terminate each rectenna element in a separate resistor involved a change in the manner in which the DC power was collected and instrumented. The output of each rectenna element was brought back through the reflector plane where it could be directly monitored with DC meters. This arrangement provided such an enhanced capability to study and understand the performance of the rectenna that it was retained in the further development of it (See Figure 10 for an adaptation to a later MSFC rectenna.) The construction however is not economical and is not recommended for most applications.

It was during this period that an arrangement to separate the measurement of the collection efficiency from the rectification efficiency of the rectenna was developed. The individual rectenna element was placed

at the end of a section of waveguide that was expanded into a small horn with an aperture of about 100 square centimeters. A metallic reflecting plane was placed behind the rectenna element and this plane also was used to seal the end of the waveguide so that no microwave power could leave the closed system. This made it possible to accurately measure the DC output power and the microwave power absorbed by the element and thus to accurately measure an efficiency, defined here as the rectification efficiency. Such an efficiency, of course, includes any circuit losses in the rectenna element itself. The test fixture environment in which the rectenna element was placed simulated to a first approximation the environment of the surrounding rectenna into which the rectenna element would eventually be placed. This test arrangement was a key factor in reducing costs for the development of the rectenna.

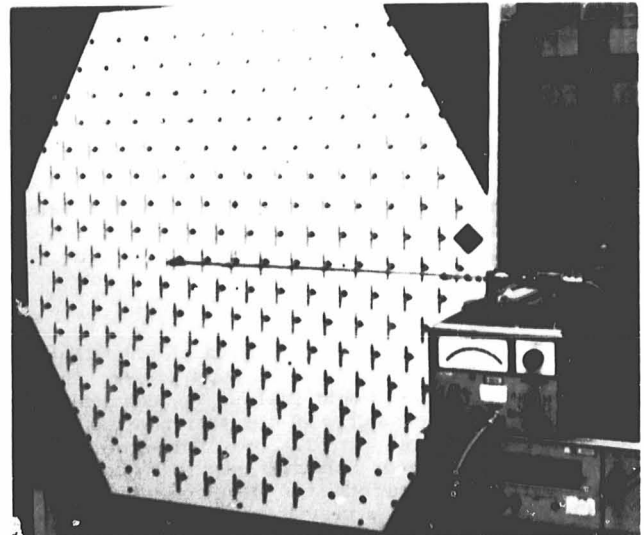


Figure 9. Close up view of rectenna used in measurements of overall system (DC to DC) efficiency. There were 199 elements in a four foot diameter hexagonal array. Rectenna was illuminated with a near gaussian shaped beam with a power density at the center about forty times that at the edges. The probe in front is used to measure the standing wave pattern in space. Probe measurements indicated that after suitable adjustment of DC load resistance and spacing of elements from the reflecting plane a reflection of less than 1% could be obtained, indicating an absorption efficiency approaching 100%. Although overall rectenna efficiency is generally difficult to measure because of edge effects and difficulty of measuring power density in the beam the unique aspects of the test facility made it possible to estimate overall capture and rectification efficiency of 82% for the rectenna within a $\pm 2\%$ error.

The collection efficiency of the rectenna has always been difficult to measure. The termination of a large aperture horn with a large number of rectenna elements, an arrangement which would seem to logically follow the test arrangement for a single element, loses its validity for collection efficiency because many modes are set up within the horn if there is any dissymmetry at all in the rectenna arrangement. Most of the power in these modes gets absorbed in the elements themselves and very little flows back into the throat of the horn and into the waveguide where any measurement of reflected power could be made. The best way to measure collection efficiency is to measure the standing wave pattern directly in front of the center of freely

exposed rectenna of sufficient area to minimize diffraction effects from the edge. The measurement is made more valid if the impinging beam has a gaussian distribution, the reflection factor is small and the reflected wave also assumed to be gaussian. These conditions prevail in the arrangement of Figure 11.

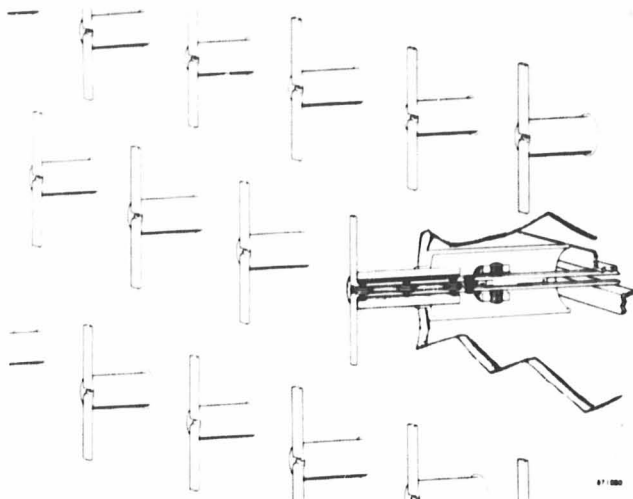


Figure 10. Sketch of the Marshall Space Flight Center rectenna which was constructed in spring of 1974. Cutaway section of rectenna element shows the two section input low pass filter, the diode, and a combination tuning element and by-pass capacitor.

Because the diode rectifier is such an important element in the collection and rectification process, a search for diodes which would improve the efficiency and power handling capability of the rectenna has been a continuing procedure. In 1971, Wes Mathei suggested that the Gallium Arsenide Schottky-barrier diode that had reached an advanced state of development for Impatt devices might be a very good power rectifier and provided a number of diodes for testing.¹⁶ These devices were indeed much better. Their revolutionary behavior in terms of higher efficiency and much greater power handling capability rapidly became the basis for the planning of improved rectenna performance.

The knowledge of the superior performance of this device was coincident with the advancement of the concept of the Satellite Solar Power Station by Dr. Glaser of the A.D. Little Co.¹⁷ The earliest investigation of a rectenna design for this concept indicated that the economics of its construction would be crucial and that mechanical and electrical simplicity of the collection and rectification circuitry would be of paramount importance. This factor, combined with the fact that no harmonic filters had existed in previous rectenna element designs but would be necessary in any acceptable microwave power transmission system, motivated a completely new direction of rectenna element development. This new direction was the development of a rectenna element employing a single diode in a half-wave rectifier configuration with wave filters to attenuate the radiation of harmonics and to store energy for the rectification process.

The construction of such a rectenna element and its insertion into a DC bus collection system is shown in Figure 10. This rectenna element was used in the first phase of the MSFC sponsored work at Raytheon to construct a rectenna 1.21 meters in diameter which was illuminated by a gaussian beam horn (Figure 9). The combined collection and rectification efficiency of this rectenna was measured at $82 \pm 2\%$. The overall DC to DC efficiency was measured at 48%.

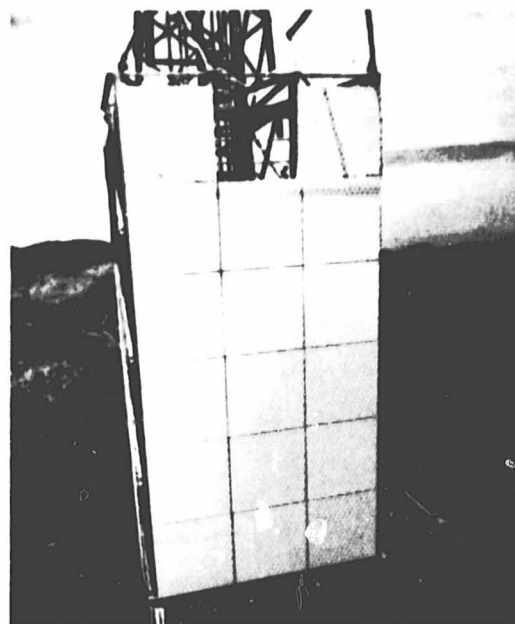


Figure 11. Photo of 24.5 Square Meter Rectenna erected in 1975 at the Venus Site of the Goldstone Facility of the Jet Propulsion Laboratory. Power was transferred by microwave beam over a distance of 1.6 km and converted into over 30 kW of cw power which was dissipated in lamp and resistive load. Of the microwave power impinging upon the rectenna, over 82% was converted into DC power. The rectenna consisted of 17 subarrays, each of which was instrumented separately for efficiency and power output measurements. Each rectenna housed 270 rectenna elements, each consisting of a half-wave dipole, an input filter section, and a Schottky-barrier diode rectifier and rectification circuit. The DC outputs of the rectenna elements were combined in a series-parallel arrangement that produced up to 200 volts across the output load. Each subarray was protected by means of a self-resetting crowbar in the event of excessive incident power or load malfunction. Each diode was self-fused to clear it from short-circuiting the array in the event of a diode failure.

Development Under JPL Sponsorship

By 1973 the solar power satellite concept (then the SSPS) had become an important enough consideration to interest the Office of Applications within NASA to support the development of the microwave power transmission portion of the system. Although it would have been logical to continue the effort at MSFC because of their initial involvement, MSFC indicated that the subject matter was outside of their main interests and that they did not wish to pursue its development further. As a result both JPL and LeRC became involved in efforts that involved the demonstration and further development of the rectenna, and the rectenna became increasingly identified with the SPS.

The JPL activity was involved with the demonstration of the transfer of power over a distance of one mile and at a DC power level of 30 kilowatts, nearly two orders of magnitude greater than had been accomplished in the laboratory. (Figure 11)^{18,19} This work effort was carried out in the 1974 to 1975 time period and has undoubtedly been the most important contribution to the establishment of confidence within the NASA and aerospace community in the feasibility of microwave power transmission. Although the emphasis

was upon demonstration rather than technology development it did provide some opportunity for additional development, those aspects involving the interface with the useful load on the output side of the array, life test data and improvement and certification of overall efficiency. An unfortunate aspect of the demonstration was that for risk minimizing purposes the uneconomic three level construction of dipoles, reflecting plane, DC power and bussing was retained. However, later work with LeRC featured the development and testing of the economic two level construction.

From the rectenna development point of view the JPL activity included the following accomplishments:

- Demonstrated the parallel-series connection of the DC output power from parallel rows of rectenna elements.
- Developed plated-heat-sink GaAs Schottky-barrier diodes with carefully controlled thickness of epitaxial layer to maximize efficiency.
- Demonstrated "fail-safe" nature of the diodes. If a diode should short out the adjacent parallel connected diodes force enough current through the package of the shorted diode to burn out a one mil diameter wire which acts as a fuse in the package.
- Demonstrated the value of crowbars in protecting diodes from load faults and from excessive incident microwave power but also the desirability of complementing them with capacitors placed across the output terminals of the diode array to absorb short duration spikes of output power from any cause.
- A mechanical design of the rectenna element itself that was much improved over the element developed under MSFC sponsorship.
- The initiating of life test on 199 rectenna elements and diodes arranged in groups that were exposed to different values of incident microwave power.
- Improved the setup in Raytheon's laboratory to demonstrate high overall (DC to DC) system efficiency and then provided certification of the data upon which the calculation of an overall efficiency of 54% was based.²⁰ The rectenna that was used in this experiment is shown in Figure 9. The overall collection and rectification efficiency of the rectenna was found to be $82 \pm 2\%$ in this experiment.

Development Under LeRC Sponsorship

Lewis Research Center carried out two activities for the Office of Applications having to do with the rectenna. One, carried out in 1974 and 1975 was a broad study of the entire microwave power transmission system for the SPS. Various approaches to the collection and rectification problem were investigated. Investigation included an examination of all rectifier approaches and all receiving antenna approaches. The rectenna approach was found to be unique in the solution of this problem.²¹

The other LeRC activity dealt exclusively with the improvement of the rectenna²² and made important contributions as follows:

Improvements in Efficiency

Improvements in rectenna element efficiencies to values slightly in excess of 90% were achieved. These

efficiencies were with DC outputs in excess of 4 watts, which is above that currently planned for the SPS. However, notable improvements were made in efficiency at low power densities with improved diodes and higher impedance rectenna elements. The results are shown in Figure 12. Further, directions in which to obtain higher efficiency, particularly at the lower power levels, were discovered.

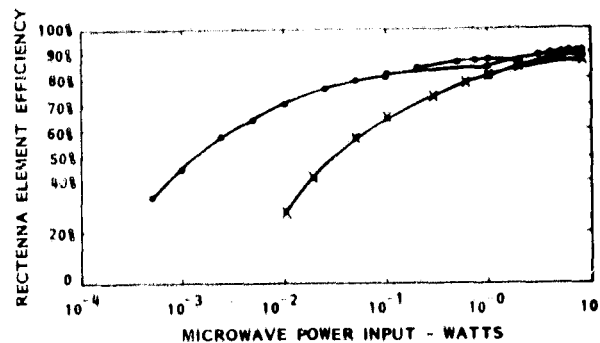


Figure 12. A summary of the efficiencies achieved with new diode in various new rectenna configurations as a function of power level, compared with performance of a standard element used in the JPL Goldstone rectenna and shown as the lower curve.

Improvement in Confidence in Collection and Rectification Efficiency Measurements

A considerable improvement in the confidence of efficiency measurements on the rectenna element was established by equating the microwave power absorbed by the rectenna element to the sum of the DC power output, the losses measured in the diode, and the circuit losses as measured experimentally and by computer simulation. The losses in the diode were measured by a unique substitution method developed at Raytheon and explained in reference 22. The balancing of microwave power input and total power output, as shown in Figure 13, is a good check on the measurement of microwave power input which is traceable to a 100 milliwatt microwave standard at the Bureau of Standards through a secondary standard sent there for calibration, and a calibrated 20 dB directional coupler with which the secondary standard is applied to the test set for the rectenna element.

Mathematical Modeling and Computer Simulation

The mathematical modeling of the rectenna element and simulating its performance on a computer was successfully carried out. Although other computer modeling had been successfully carried out,²² this was the first time that the computer program modeling was for the same rectenna element on which accurate experimental measurements of circuit and diode losses had been made.

The computer simulation generally gave results that confirmed the experimental results, as may be seen from an examination of Figure 13, but upon occasion indicated differences which have led to investigations to resolve the differences. For example, the diode losses were first computed on the basis of the theoretical design of the diode and found to be less than those measured. It was found that the forward voltage drop as measured by DC voltage measurements was greater than that predicted from theory leading to the conclusion that the ohmic contact

is not purely ohmic but retains some Schottky barrier characteristics which contribute to the voltage drop.

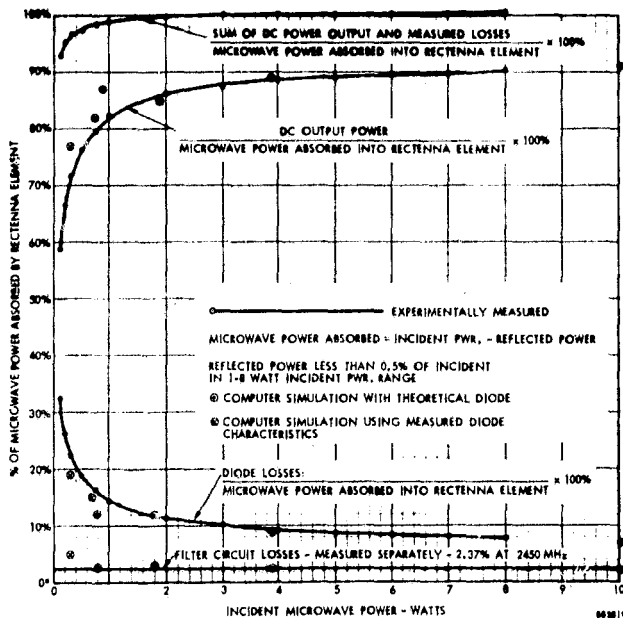


Figure 13. The DC power output, losses in the microwave diode, and losses in the input filter circuit are shown as a percentage of the microwave power absorbed by the rectenna element as a function of incident microwave power level. The sum of all of these is then compared with the absorbed microwave power. Comparison with computer simulation computations is also shown.

A typical set of diode losses as obtained from the computer simulation may be of interest. Total losses were 13.03% of the input power of which 2.08% was skin loss, 2.52% loss in the diode series resistance in the forward conduction period, 1.23% loss in the non-conducting portion of the cycle, and 7.22% loss in the Schottky junction itself. The total losses observed experimentally were 12.8%, an agreement that is probably better than can be justified.

Development of Improved Diodes

The power loss represented by the voltage drop in the Schottky barrier is an important loss in the diode, and it is the major one when the operating power level is low, even when the impedance level of the circuit is raised to minimize these losses. GaAs Schottky barrier diodes commonly use platinum as a barrier metal because it behaves better than other materials for use of the diode as an Impatt device. Tungsten has a lower work function than platinum and would be preferable in a rectenna element. Such diodes were developed and indeed found to have lower loss and to be more suitable for rectenna element application.

Suppression of Harmonic Energy

A means of reducing harmonic energy radiated from the dipole antenna was investigated. A shorted line $\frac{1}{4}$ wavelength long placed across the terminals of the dipole appears as an open circuit to the fundamental but as a short circuit to the second harmonic. The power in the second harmonic is therefore reflected back into the rectenna element. It was found that this technique will reduce the second harmonic level by as much as 25 dB but the impact of the

harmonic reflection upon the overall efficiency needs more evaluation. The technique can be incorporated with no additional cost into the rectenna element in the two-plane format. The third harmonic may be treated in a similar fashion but it is necessary to complicate the physical format of the rectenna element to incorporate it.²²

Development of a Rectenna Design that is Both Environmentally Sound and is Suited to Low Cost High Speed Production

The development of basic technology for the rectenna for the full scale SP3 is well advanced, but the adaptation of this basic technology to a rectenna that is environmentally sound and that can be made at low cost in large volume production was recognized as an area of special study. Effort on this part of the program resulted in the outline of a mechanical design based upon the two-plane rectenna system in which all of the important elements of the rectenna, including the bussing of DC power, are carried out in the foreplane. This foreplane is shown schematically in Figure 14. In effect this design reverts back to some of the earliest rectennas but with greatly improved components and better understanding. A mechanical design of the entire rectenna coupled with the fabrication and electrical testing of a portion of the foreplane was carried out. The overall mechanical design is shown in Figure 15 while the electrically operative foreplane portion is shown in Figure 16.

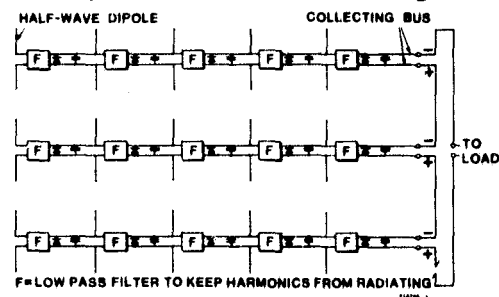


Figure 14. Interconnection arrangement of half-wave dipoles, wave filters, rectifier circuits, and collecting buses in the foreplane of a two-plane rectenna system.

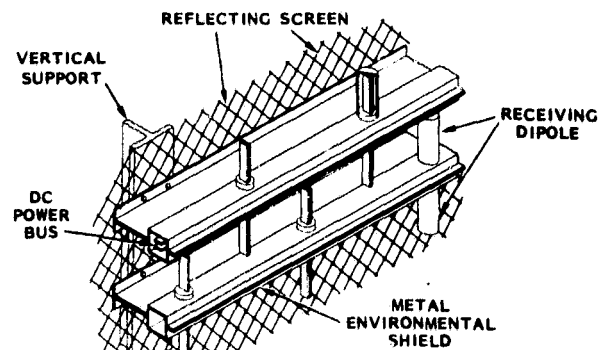


Figure 15. Proposed design of Rectenna motivated by environmental protection and cost considerations. In this design the environmental shield becomes an important load-bearing member of the structural design.

The foreplane shown in Figure 16 was thoroughly evaluated for performance. A special arrangement made it possible to test each of the five foreplane elements in the single rectenna element test fixture while all five remained within the foreplane assembly. The average efficiency of the elements was 88%. To determine its compatibility within a large array of elements

the foreplane of Figure 16 was inserted into the 199 element array shown in Figure 17. A careful check was made on any effect it might have had on the performance of the rectenna as a whole, by means of reflection measurements of the kind shown in Figure 9 and by comparison of the power obtained from the five element array with the sum of the power from the five standard rectenna elements it replaced. From the almost imperceptible impact that was noted, it was concluded that the rectenna design depicted in Figures 15 and 16 is electrically satisfactory.

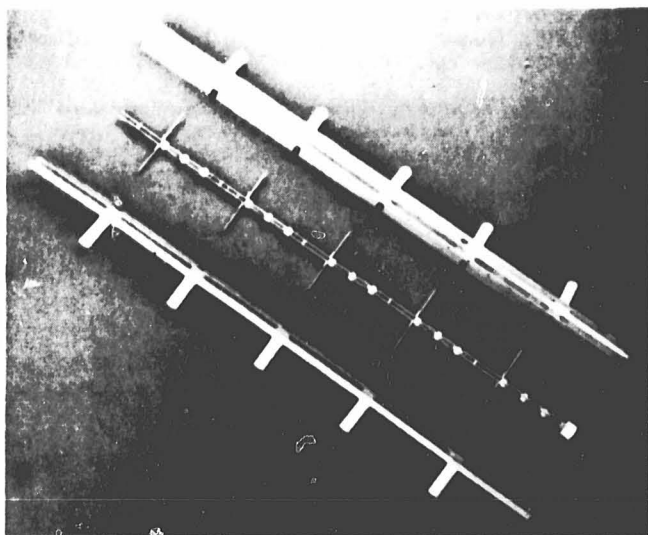


Figure 16. Basic core structure design of the foreplane illustrating the joining of individual rectenna elements to each other to form a linear, easily-fabricated structure performing the functions of DC power bussing and microwave collection and rectification.

Assessment of Life of Rectenna Element

Figure 18 provides a summation of the life test data taken up to a total of slightly over 800,000 diode hours. It is noted that there were no failure of diodes in rectenna elements operated at DC power levels below 6 watts. Even those failing at higher power levels may have been associated with infant or operator-induced failures. There was only one unequivocal self-induced life failure of a diode and that occurred in the group operating at 6 to 8 watts of DC power output.

All of the diodes that were used were the plated-heat-sink GaAs Schottky barrier diodes that were made as part of the effort under the JPL supervised program at Raytheon. The life test was made possible because of the availability of the complete microwave power transmission system and the 199 element rectenna shown in Figure 9. With this arrangement there is a distribution of power density over the rectenna by a factor of about 40.

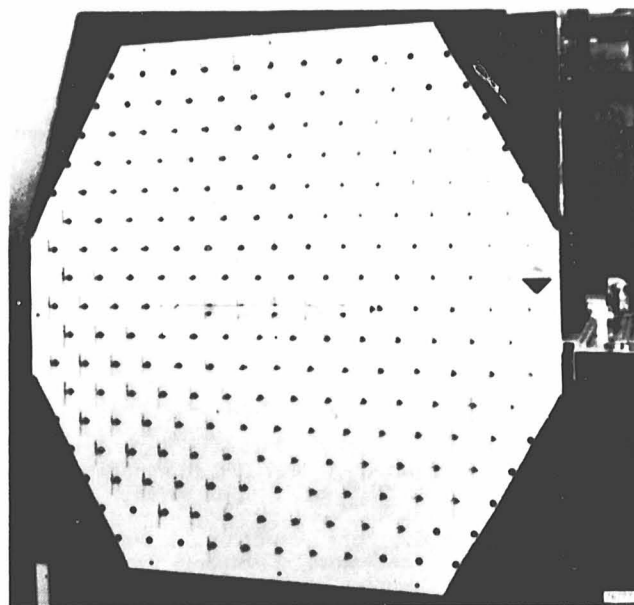


Figure 17. The test set-up for checking the foreplane type of rectenna array. The five element foreplane structure is placed at the center of the larger rectenna array as shown. The DC output is dissipated in a resistive load. The collected power from the foreplane can then be compared with the power that would have been collected from the five elements that it replaced. Reflected power measurements were also made with the probe arrangement shown in Figure 9.

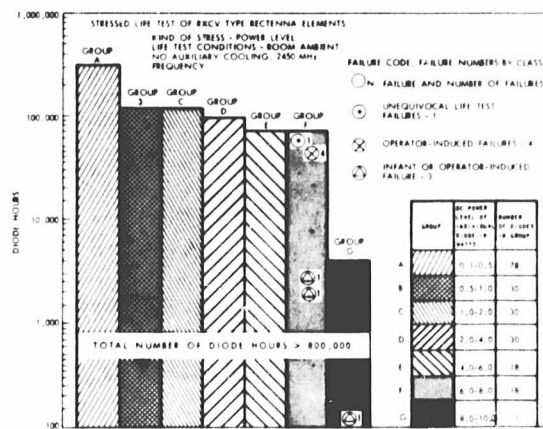


Figure 18. Diode Life Test Results Using Rectenna shown in Figure 9. Rectenna contains 199 rectenna elements which are subjected to a wide range of incident power.

Recent Developments and Future Trends

The SPS rectenna design approach of Figure 15 was structurally analyzed in considerable detail by the author.²³ Material requirements and costs were estimated. To save on material, which is the chief element of cost, airframe design practices should be used, and extensive scaled wind tests should be performed in the early design stages to forestall excessive design safety factors for wind loading.

A set of studies leading to additional understanding of the rectenna have been sponsored by Johnson Space Center, with R.J. Gutmann of RPI being the principal investigator for a number of these.²⁴

The most recent trend in rectenna development is the thin-film printed-circuit rectenna for high altitude atmospheric platform and space use. It is not believed to be suitable for the SPS rectenna because of its fragility and higher cost per unit area than the rigid construction of Figure 15. Its application to the high altitude platform, however, may lead to a better general understanding and acceptance of microwave power transmission in the SPS.

Bibliography

1. Brown, W.C., and G. Perloff, "High Power CW X-Band Amplitron," 1960 IRE International Conv. Record, vol. VIII, pt. 3, pp. 52-55.
2. Brown, W.C., "The Amplitron, A Super Power Microwave Generator," Electronic Progress, Raytheon Company, Burlington, Mass., July-August 1960.
3. Brown, W.C., "A Survey of the Elements of Power Transmission by a Microwave Beam," 1961 IRE International Conv. Record, vol. IX, pt. 2, pp. 93-106.
4. "Raytheon Airborne Microwave Platform (RAMP) System" Technical Proposal prepared for U.S. Air Force, May 21, 1959.
5. Sabbagh, E.M., et al., "Microwave Energy Conversion," WADD Tech. Rept. No. 61-48, pt. II, op. cit., Nov. 1961.
6. Brown, W.C. "Thermionic Diode Rectifier" in Okress, Microwave Power Engineering, Academic Press, Vol. II, pp. 295-298.
7. Brown, W.C., "Experiments in the Transportation of Energy by Microwave Beam," 1964 IEEE International Conv. Record, vol. XII, pt. 2, pp. 8-17.
8. George, R.H., "Solid-State Rectifiers" in Okress, Microwave Power Engineering, Academic Press Vol. II, pp. 275-293.
9. U.S. Patent No. 3,434,678, March 25, 1969, W.C. Brown, et al.
10. Brown, W.C., and George, R.H., "Rectification of Microwave Power" in "Microwave Power Engineering," IEEE Spectrum. October 1964, pp. 88-92.
11. W.C. Brown, "Experimental Airborne Microwave-Supported Platform," Tech. Rept. RADC-TR-65-188, 1965.
12. W.C. Brown, "Experiments Involving a Microwave Beam to Power and Position a Helicopter," IEEE Trans. Aerospace Electron, System, vol. AES 5, pp. 692-702, Sept. 1969.
13. W.J. Robinson, "Wireless Power Transmission in a Space Environment" J. Microwave Power, vol. 5, December 1970.
14. W.C. Brown, "Progress in the Efficiency of Free-Space Microwave Power Transmission", Journal of Microwave Power, Vol. 7, No. 3, pp. 223-230.
15. W.C. Brown, "Free-Space Microwave Power Transmission Study, Combined Phase III and Final Report", Raytheon Report No. PT-4601, Sept. 1975. NASA Contract No. NAS-8-25374.
16. W.C. Brown, "The Technology and Application of Free-Space Power Transmission by Microwave Beam", Proceedings of the IEEE, vol. 62, No. 1 Jan. 1974, pp. 11-25.
17. P.E. Glaser, "Power from the Sun: Its Future", Science, Vol. 162, pp. 857-861, Nov. 22, 1968.
18. R.M. Dickinson, "Evaluation of a Microwave High-Power Reception-Conversion Array for Wireless Power Transmission", Tech. Memo 33-741, Jet Propulsion Lab, Cal. Inst. Tech. Sept. 1, 1975.
19. "Reception - Conversion Subsystem (RXCv) for Microwave Power Transmission System", Raytheon Report No. ER75-4386, JPL Contract No. 953968, Sept. 1975.
20. R.M. Dickinson, W.C. Brown, "Radiated Microwave Power Transmission System Efficiency Measurements", Tech. memo 33-727 Jet Prop. Lab. Cal. Inst. Tech, March 15, 1975.
21. "Microwave Power Transmission System Studies" Raytheon Contractor Report ER75-4368 NASA CR-134886, December 1975.
22. W.C. Brown, "Electronic and Mechanical Improvement of the Receiving Terminal of a Free-Space Microwave Power Transmission System", Raytheon Contractor Report PT-4964 NASA CR-135194, Aug. 1977.
22. J. Nahas, "Final Report, Simulation and Experimental Studies of Microwave-to-DC Energy Conversion Systems", Prepared for NASA, Lewis Research Center, under Grant No. NSG-3070.
23. SPS System Evaluation Phase III Study Document - Executed by Boeing, Raytheon, General Electric Boeing D180-24635-1.
24. R.J. Gutmann, J.M. Borrego "Solar Power Satellite Rectenna Design Study" Contract NAS 9-15453, December, 1978.

RECTENNA SYSTEM DESIGN

G. R. Woodcock, Boeing Aerospace Company
R. W. Andryczyk, General Electric

1.0 INTRODUCTION

The function of the rectenna in the solar power satellite system is to convert the downcoming microwave power beam to electrical grid power. Due to its large physical size (a typical rectenna site is a 10 KM x 14 KM ellipse) and element composition (many repetitive components), the projected cost savings of automatic mass production are of prime importance. Control of the satellite power beam and its distribution also takes place at facilities on the rectenna site. These critical functions have minor cost impacts and are not treated in this document.

The fundamental processes at the rectenna consist of rectifying the incident r.f. field into d.c. current using Schottky barrier diodes, filtering the rectified output, combining it and processing it to higher voltages for distribution. Hierarchical combination and processing of currents is done several times to integrate the relatively low power per diode to electrical grid power magnitudes. Provisions for power control for equipment protection and load management exist at each step in the hierarchy.

2.0 RECEIVING ANTENNA OPTIONS

Figure 1 illustrates the basic design choices based on the desired microwave field concentration prior to rectification and on the ground clearance requirement for the rectenna structure. For an optimized system, these parameters depend on positions within the site, local terrain and incident r.f. field. For purposes of the present study, a non-concentrating inclined planar panel with a 2 meter minimum clearance configuration was selected as representative of the typical rectenna.

3.0 RECEIVING ELEMENT OPTIONS

Figure 2 illustrates some of the options that have been considered for receiving antenna elements. Dipoles in various implementations represent the most straightforward way of receiving a linearly polarized incident field compatible with the slotted waveguide transmitting array, and are relatively easy to analyze. However, other options, including elements that receive circularly polarized fields, have been considered.

Figure 3 shows capture area as a function of element width and length for a number of different types of elements. A trade study of diode power for maximum rectification efficiency (5-10 watts per diode) as opposed to long life with passive cooling (<5 watts per diode) suggests a power level per diode of somewhere between 1 and 5 watts. (See Table 1).

TABLE 1: SINGLE DIODE RECTENNA (DIPOLE) ELEMENT

Element Power Level (Watts)	Equivalent Power* Density mW/CM ²	Achieved Element Efficiency %	Projected Element Efficiency %
8	160	91	91
1	20	88	90
0.5	10	86	88
0.2	4	84	86
0.1	2	82	85

*Proposed Power Density at SPS Rectenna Center - 23 mW/CM²

Proposed Power Density at SPS Rectenna Edge - 1 mW/CM²

The baselined modified half-wave dipole, with a capture area of 70 CM^2 (typical) will provide between 1-2 watts of power per diode at the center of the rectenna (23 mW/CM^2) indicating good efficiency. More directional elements or dipole arrays must be used as we go out to the rectenna edge ($\approx 1 \text{ mW/CM}^2$); for instance, a 4×4 dipole array would again provide 1 watt per diode. Care must be exercised not to select too large an array which would pose problems of directional reception and increased losses in the r.f. collection lines. The design chosen integrates the dipoles and their associated power and microwave circuitry inside an aluminum environmental shield and support structure which readily lend themselves to mass production methods.

4.0 BASELINE RECTENNA DESCRIPTION

A representative rectenna design at a 35° latitude is described, characterized by a 5 GW Gaussian tapered beam with a peak incident microwave power of 23 mW/CM^2 . Power is collected out to the point where the interception efficiency is 95%. The basic receiving element of the baseline rectenna is a dipole above a ground plane. The dipole assembly also contains a filtering and matching circuit to match the dipoles to the incoming wave with a reflection coefficient of better than -20 db. It is assumed that all dipoles are identical throughout the rectenna. The number of dipoles in the rectenna is approximately 1.3×10^{10} in a $7.9 \text{ CM} = .64 \lambda$ triangular array format.

Component designs for the rectenna are varied to most effectively match the incident power flux in ten rings. Basically, all microwave system components of a given type are similar within a ring. However, power bussing and control segmentation at the 5-10 mW power level and above extends across ring boundaries. Local d.c. voltages on the panels are designed not to exceed $\pm 3.25 \text{ KV}$.

Due to the power density variation over the rectenna aperture, a single type of radiating element or a single type of rectifier cannot provide optimum conversion efficiency. Either a number of radiating element types or a number of diode types must be provided. Presently, one single type of diode is assumed which is operated with four different types of antenna elements. It is assumed that besides the dipole element already described these antenna elements are formed by using the basic dipoles in arrays containing 2, 4, or 8 dipoles. The corresponding assemblies are called Type 1, 2, 3, and 4 receiving arrays. There are approximately 7.654×10^9 arrays (diode assemblies) in the overall antenna.

The array assemblies are combined into panels which are the smallest assembly units from the fabrication point of view. 10 m^2 was selected for the panel area, with a N-S plane dimension of 3 m and E-W plane dimension of 3.33 m. Figure 4 shows a typical panel assembly in the center of the rectenna. It is assumed that all panel sizes are identical. This requires 7,060,224 panels in the rectenna. There are four different types of panels, corresponding to the four different types of receiving arrays. Although the dipoles and diodes are identical for all panels, the combining-matching-filtering circuits and the diode wiring represent four types. Table 2 summarizes the characteristics of the panels.

Ring	$\frac{\text{mW}}{\text{cm}^2}$	$\frac{\text{W}}{\text{Panel}}$	$\frac{\text{V}}{\text{Panel}}$	Dipoles	Diodes	$\frac{\text{V}}{\text{Diode}}$	$\frac{\text{W}}{\text{Diode}}$	$\frac{\text{V}}{\text{Panel}}$	$\frac{\text{A}}{\text{Panel}}$	$\frac{\text{ohm}}{\text{Panel}}$
1	23.33	2333	1738.8	$43 \times 43 = 1849$	1849	17.96	.9398	772.3	2.25	1100
2	18.76	1876	1375.2	1849	1849	16.11	.7437	692.7	1.98	1100
3	14.38	1438	1043.3	1849	1849	14.11	.5642	606.7	1.72	1100
4	11.42	1142	828.1	$2 \times 30 \times 31 = 1860$	930	17.73	.8904	549.6	1.50	1136
5	8.67	867	625.6	1860	930	15.44	.6727	478.6	1.31	1136
6	6.72	672	468.1	1860	930	13.59	.5033	421.3	1.11	1136
7	5.34	534	365.4	1860	930	12.12	.3929	375.7	.973	1136
8	4.24	424	292.1	$4 \times 21 \times 22 = 1848$	462	15.32	.6322	337.0	.866	1152
9	3.49	349	236.5	1848	462	13.90	.5119	305.8	.773	1152
10	3.14	314	214.0	$8 \times 15 \times 15 = 1800$	225	18.90	.9311	283.5	.755	1100

TABLE 2:

RECTENNA
PANEL
CHARACTERI-
ZATION

Units are combined from panels in such a manner that nominally 1,000 panels are in one unit and the N-S dimension of a unit is always $32 \times 3.662 = 117.18$ m, which means that the number of panel rows in the N-S plane is always 32. This allows a standardization of the unit layouts to a minimum of seven types. Figure 5 shows the overall layout of the rectenna with the ring boundaries and the number of units within each ring. Note that the N-S dimension of the units are standardized to 117.18 m everywhere within the rectenna and only the E-W dimension of the units varies from ring to ring.

The last assembly which is formed at DC is called "group". This brings the power output into the 5-10 MW range. In order to keep the voltage levels relatively low, groups are formed from the units by parallel connections only. The power from the unit output is brought to group centers, or blocks, where the DC to AC inverters are located, by relatively long transmission lines that are parallel-connected at the group centers only. Blocks handle approximately 70 MW of power each.

Selection of the layout for the rectenna AC system between the individual DC/AC converters and the bulk power transmission system depends on the location and the power levels of the DC/AC converters as well as on the needs of the bulk power transmission system. A one-line diagram for the rectenna AC system in which the DC output from the dipoles is collected into 40 MW DC/AC converter stations is shown in Figure 6. The 40 MW converter station output is transmitted by underground cable to 200 MW transformer station where the voltage is stepped up to 230 kV, then collected in 1,000 MW groups and transformed to 500 kV for interphase with the bulk transmission system. The switchyards are shown arranged as reliable "breaker and a half" schemes where single contingency outages may be sustained without loss of power output capability. The selection of the voltage level for the ultimate bulk power transmission interface with the utility grid, as well as the possibility of interconnecting two or more of the 1,000 MW switching stations together should be optimized based on detailed information about the connecting utility system. The solution, shown in Figure 6, integrated in a utility system with a control structure, as indicated in Figure 7, is one of several possible choices.

Availability calculations for the baseline rectenna design (Figure 8) were performed, the results of which are that 80% of the rated satellite power is available 96.8% of the time, and that scheduled no-power periods total only 208 hours per year.

To define the requirements for a given specific situation, load flow and system stability studies are required. It is likely, however, that the SPS power system would be far more stable than a conventional power plant of the same rating. This would mean that the transmission distances could be increased for a given line loading without need for as much series compensation as in conventional power plants.

When substantial amounts of power are to be transported for distances of 400 miles or more, the consideration of a high-voltage DC (HVDC) as the transmission load is often indicated. The HVDC system is ideally suited for long distance bulk power transport since it does not suffer from stability effects and can even be used to improve the stability of the AC system to which it is connected. The DC system is asynchronous and can easily transmit power between independent power systems such as those of the Eastern and the Western United States. HVDC technology is advanced and the systems have been well received. A 6,300 MW system in Brazil is currently in the proposal stages with full scale operation scheduled for 1985. It appears that a DC system or a combination of DC and AC systems could be applied to the Solar Power Satellite system with few difficulties.

5.0 SCATTERING AND RADIO FREQUENCY INTERFERENCE

The microwave transmission link must meet a stringent standard of electromagnetic cleanliness which states that out-of-band power must be more than 150 db down from the link power. Even though stray power reflected from and/or radiated by the

rectenna generally travels in an upward direction, there are enough scattering mechanisms for harmonics from the diode rectifier and associated noise to warrant the serious question of meeting this requirement. Some of the approaches and their implications are summarized in Raytheon data of Table 3 below.

TABLE 3: APPROACHES TO DECREASE HARMONIC RECTENNA RADIATION

<u>Approach</u>	<u>Expected Improvement in 2nd, 3rd and 4th Harmonics</u>	<u>Implications</u>
o More filter sections of current design	Approx. 14 db per section	o No physical room, 1% loss for each section.
o Stub lines to short higher harmonics at dipole terminals	~30 db	o Mechanical tolerance problem.
		o 2nd harmonic reduction easily added.
		o 3rd and higher harmonics require added width to core section.
		o Less than 1% decrease in circuit efficiency.
		o Could degrade the electronic efficiency.
o Incorporate stub lines as part of filter sections	~60 - 80 db	o Mechanical tolerance problem.
		o Requires additional width of core section.
		o Some circuit efficiency degradation.
		o Could degrade the electronic efficiency.
o Full wave rectification	~15 db	o Doubles or quadruples number of diodes.
		o Greatly complicates electrical circuit and mechanical construction.

In the baseline design, two low pass filter sections which attenuate the second and higher order harmonics by over 25 db separate the rectifier from the outside world. More filter sections add approximately 17 db more suppression, each at a cost of approximately 1% efficiency loss. Other alternatives, also with an efficiency penalty, are to use stub line filters or full wave rectification. All of these approaches have mechanical configuration problems that, while solvable, will increase rectenna diode array assembly costs. Given these difficulties, it may become necessary to seek SPS-assigned bands at the first few harmonic frequencies.

Another type of scattering which affects system design is Fresnel edge diffraction from the rectenna panel edges. A slight overlapping of panels can reduce these losses but does increase total panel area and cost. The expected capture loss and resultant efficiency loss is estimated at between 1 to 2%.

6.0 RECTENNA SYSTEM OPTIMIZATION

Optimization of a rectenna system design to minimize costs is carried out at several levels. It is always desirable from the cost per unit power standpoint to transmit as much power through the transmission link as the ionospheric medium and beam pattern constraints will allow. The rectenna should be increased in size until the incremental rate of return from sales of the intercepted power are marginal. Such a procedure is illustrated in Figure 8 where the incremental revenue per square meter is balanced by the incremental cost per unit rectenna area at the optimum.

Much of the cost of the rectenna is in the structural support material required to support it against wind drag and snow loads. Different types of rectenna panels were considered. The baseline design chosen is an intermediate between the inexpensive but draggy flat panels and the more expensive, low drag panels which have circuit topology problems. The present rectenna panel support structure evolved from stiff edge-supported panels to a hierarchical more centrally supported frame which uses much less material.

7.0 RECTENNA CONSTRUCTION

Construction of the rectenna is, by necessity, highly automated. Starting with prefabricated dipole assembly components, a dipole machine (Figure 9), manufactures completed dipole/diode assemblies at a high rate. These are then combined with other prefabricated parts to manufacture receiving element sticks. The sticks, metal frame and ground plane are then tack-welded together to form panels (Figure 10).

The completed panels are then taken to the rectenna site where specialized equipment, shown on Figure 11, prepares the site through the emplacement of panel support arches. The panels are then lowered on the support arches, fastened and connected electrically.

There must, of necessity, be some rather conventional construction at the rectenna for the grid power system and the pilot beam transmitter(s), but these constitute only a small fraction of the construction cost.

8.0 RECTENNA COST

The rectenna investment and maintenance cost breakdown for the baseline design is indicated in Table 4.

TABLE 4: SPS RECTENNA COST BREAKDOWN PER MAJOR TASK

<u>Task</u>	<u>Labor</u>	<u>Eqmt.</u>	<u>Material</u>	<u>Freight</u>	<u>Total</u>
Initiate Site Preparation	503	301	4,479	255	3,40
Complete Site Preparation	1,400	1,047	18,780	884	15,4
Foundation and Supporting Structure	24,550	64,093	182,842	32,181	303,6
Manufacture and Install Panels	24,296	145,134	928,664	3,455	1,101,5
TOTAL (\$'s in Thousands)	50,752	210,575	1,088,247	36,775	1,386,2

Land costs are excluded, but are typically less than 5% of the anticipated cost for typical sites considered. If desired, the land underneath the rectenna may be used for factories or intensive agriculture.

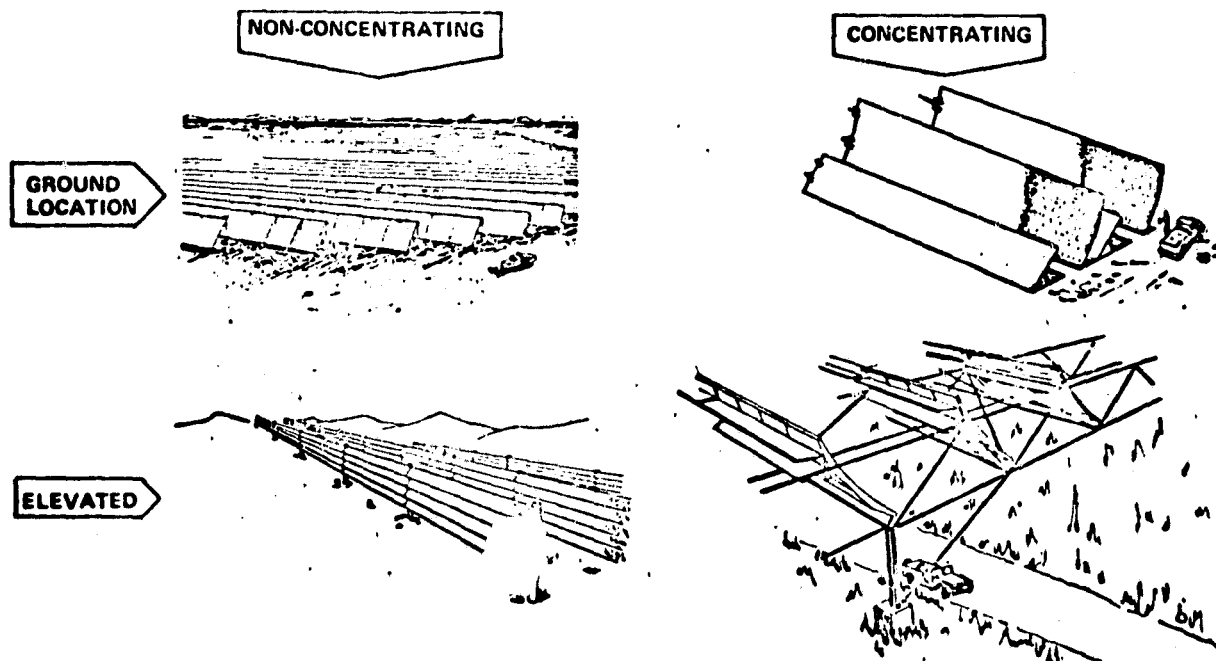


Figure 1: Potential Rectenna Configurations

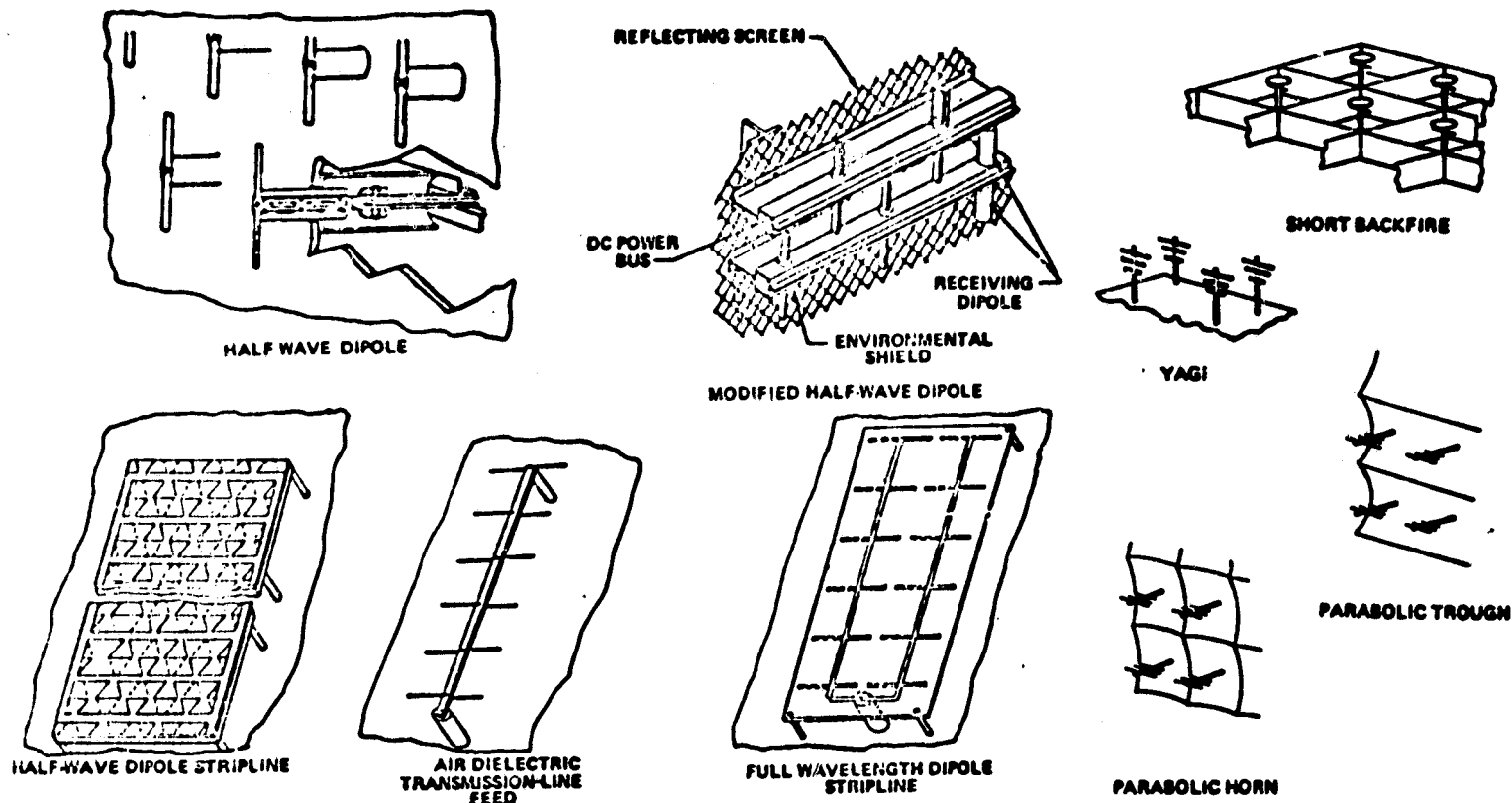


Figure 2: Rectenna Receiving Element Options

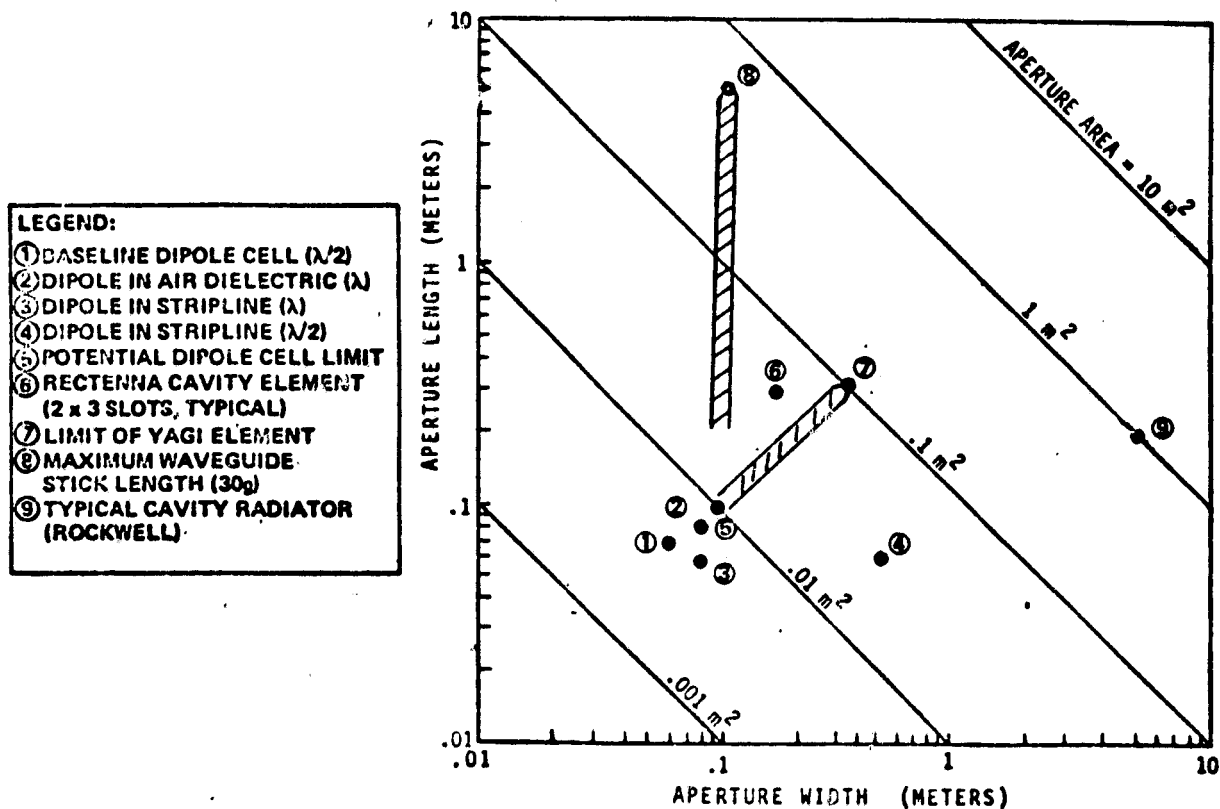


Figure 3: Rectenna Element Capture Areas

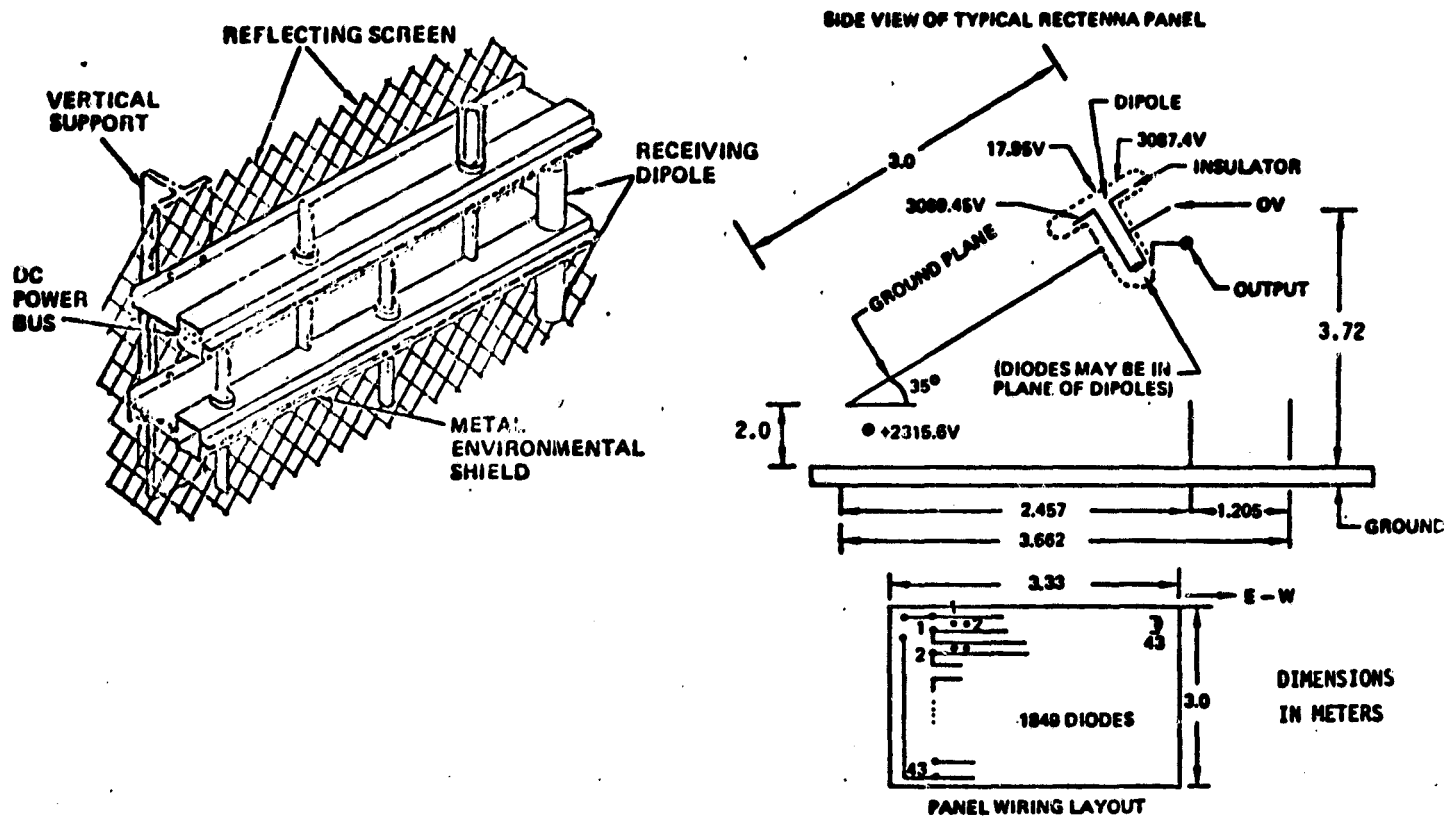


Figure 4: Typical Panel Configuration at Rectenna Center

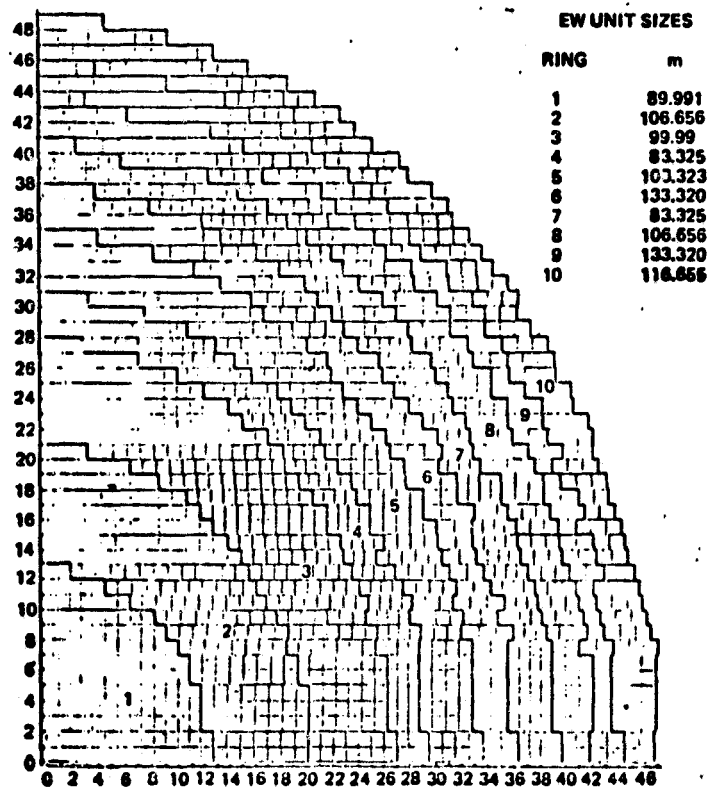


Figure 5: Rectenna Ring and Unit Boundary Map

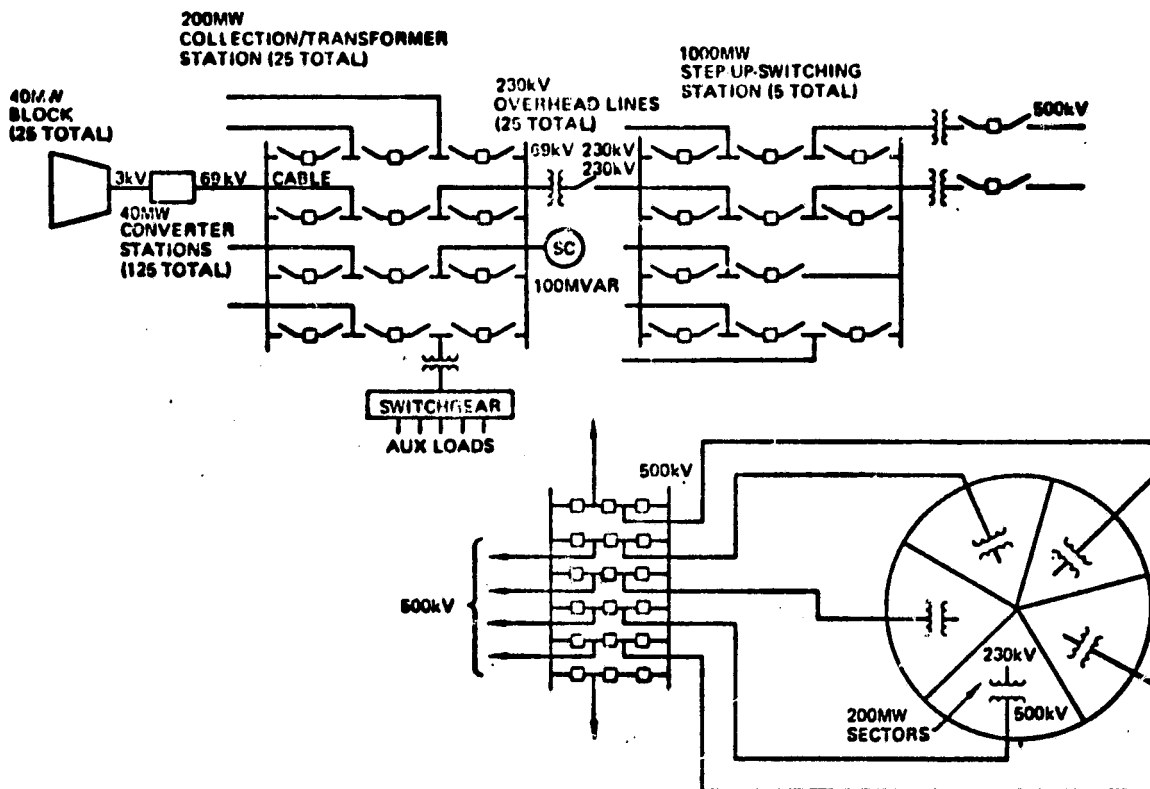


Figure 6:
Grid
Connection
Approach

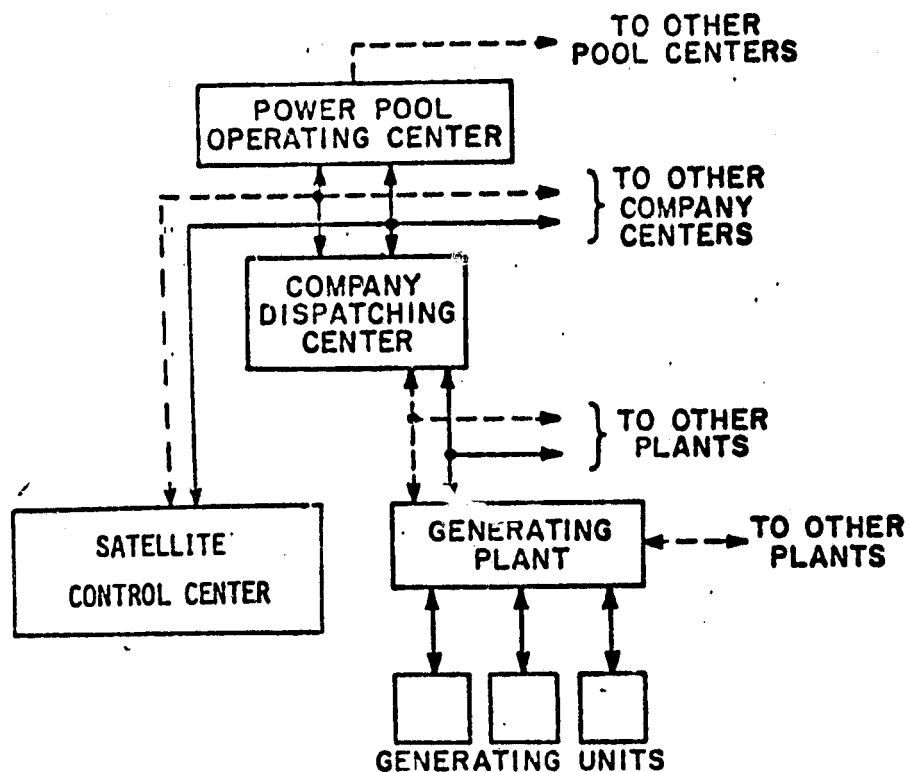


Figure 7:
Utility System
Control Structure

—————> CONTROL SIGNALS
- - - - -> DATA LINKS (VOICE OR TELETYPE)

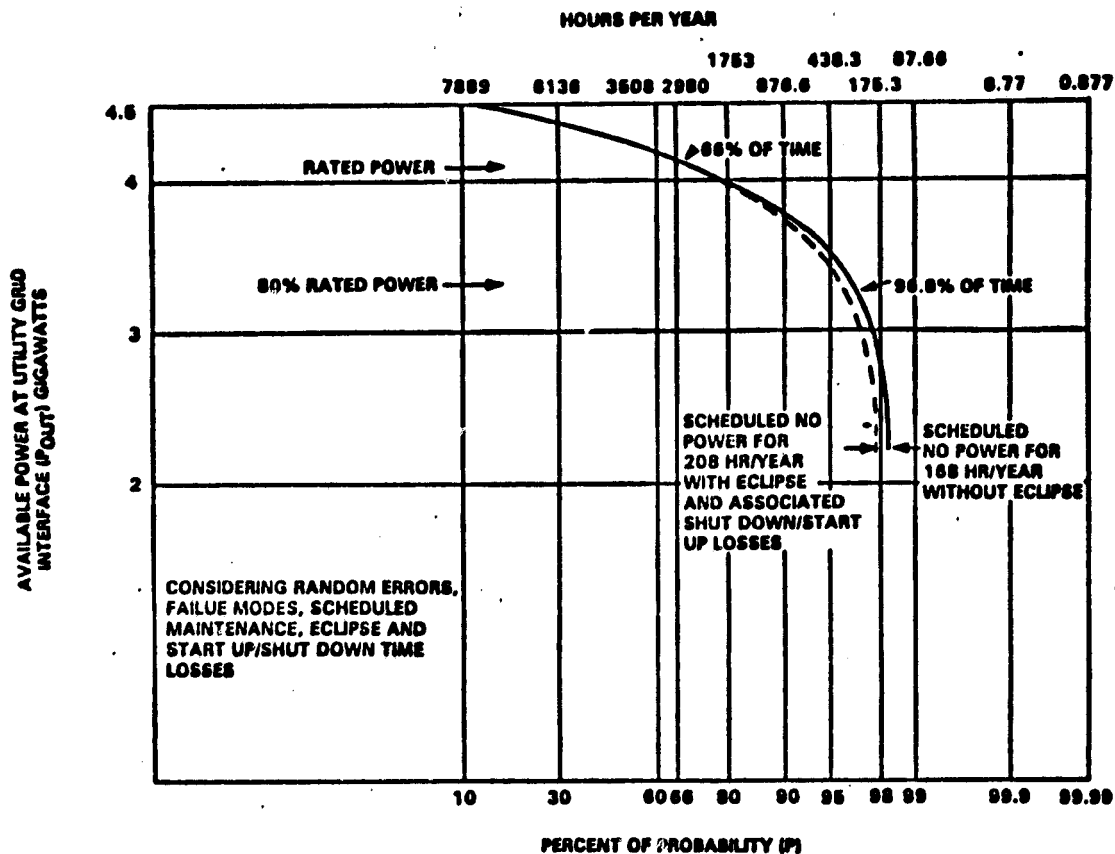
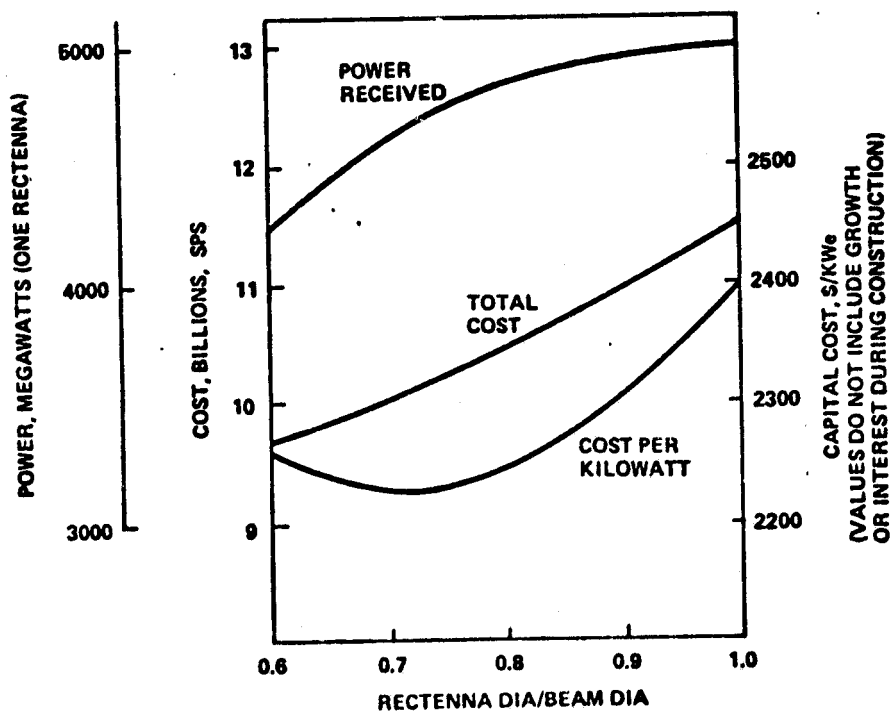


Figure 8: SPS Power Availability

SPS-1388



(Note: Beam diameter is the entire main lobe to the first null.)

Figure 9: Rectenna Size Optimization

ORIGINAL PAGE IS
OF POOR QUALITY

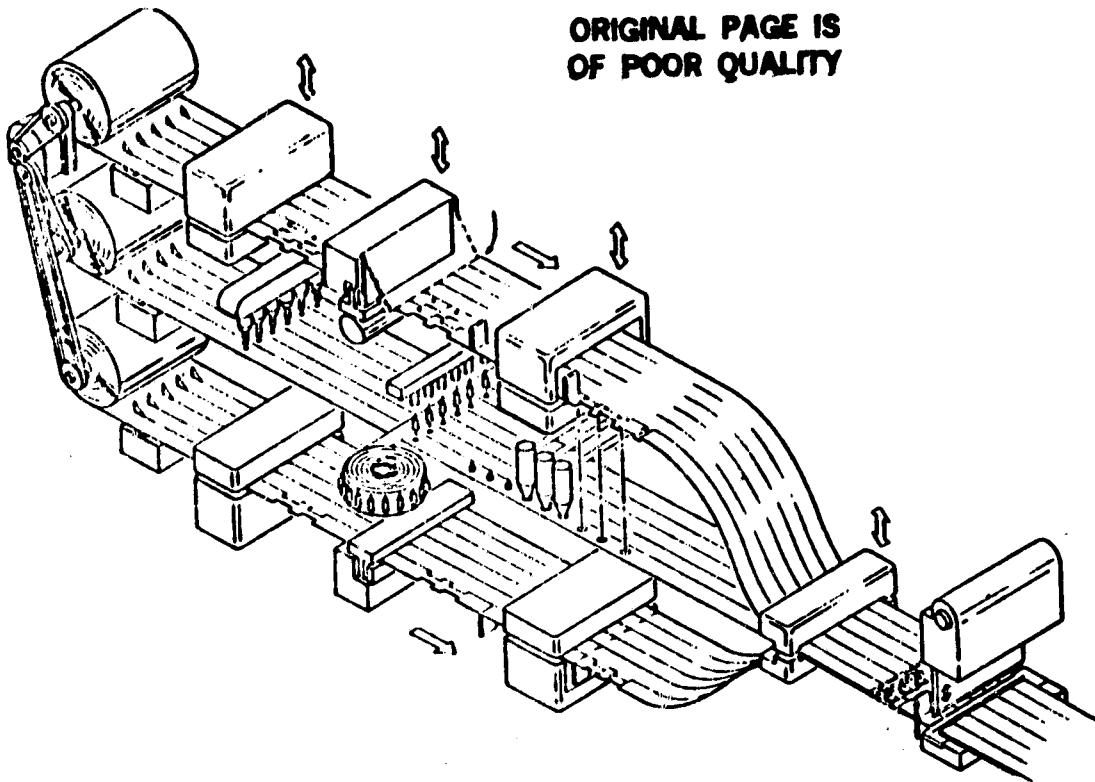


Figure 10: Dipole Machine

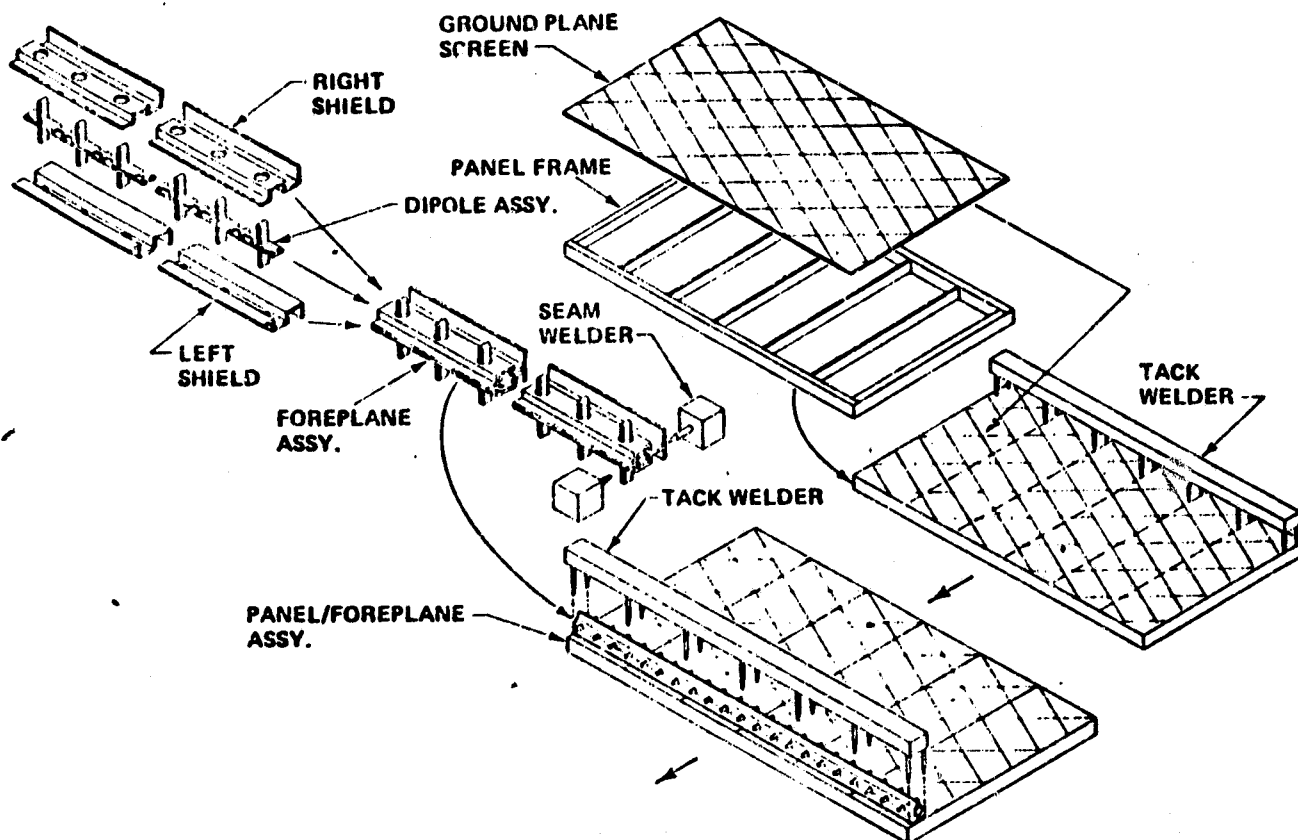


Figure 11: Rectenna Panel Fabrication Sequence

Rectenna Session: Micro Aspects
Dr. Ronald J. Gutmann
Rensselaer Polytechnic Institute

There are two micro aspects of the rectenna design which will be addressed in this presentation: evaluation of the degradation in net rectenna RF to DC conversion efficiency due to power density variations across the rectenna (power combining analysis) and design of Yagi-Uda receiving elements to reduce rectenna cost by decreasing the number of conversion circuits (directional receiving elements). The first of these micro aspects involves resolving a fundamental question of efficiency potential with a rectenna, while the second involves a design modification with a large potential cost saving. These tasks were investigated under contract with JSC during 1978.

Power Combining Analysis

In the rectenna, numerous rectifier circuits share a common DC load to achieve useful power levels. The rectifier outputs can be combined in series and/or parallel to enhance the voltage and/or current level respectively, with previous rectennas designed with first stage parallel combining followed by series combining.

A fundamental question in this receiving, rectification and power combining process is caused by the power taper of the incident microwave beam. The incident power density can vary by 10 dB over the rectenna area since a high percentage of the transmitted microwave power needs to be collected and the power beam sidelobe level must be kept reasonably low. Since the output (DC terminal) characteristics of the rectifier are power dependent, rectifiers at different power levels that share a common DC load cannot be operated at optimum conditions. With individual rectifiers near 90% maximum efficiency, the resultant efficiency degradation could be significant. In this work the efficiency degradation that results when an array of microwave power rectifiers shares a common DC load was evaluated for the first time.

In analyzing the degradation, we assume that the output load line or volt-ampere (V-I) characteristics of each of the rectifying circuits to be combined are known. This V-I characteristic can be determined by either

a circuit analysis of the rectenna element, by a computer simulation or by direct measurement of the output voltage and current for several load resistances. It is assumed that the V-I characteristics are a function of some parameter θ of the rectenna element (in our case incident RF power). Given the V-I characteristics, it is possible to determine the operating point for maximum power output.

In Fig. 1 we show the V-I characteristics of two dissimilar rectenna elements as well as the points at which each of them deliver maximum power if operating independently. The same figure shows that if the elements are operated in parallel (common output voltage) or in series (common output current), they will not operate at their optimum power output and their combined power output will be less than if operated independently. We have developed expressions for the power combining inefficiency (reduction in output power compared to collected power assuming each rectifier operated in its own optimum DC load) for both series and parallel combining. (1,2)

In order to evaluate the power combining inefficiency an accurate output equivalent circuit model of the conversion circuitry is needed. This was obtained using two independent approaches. First, an approximate closed form circuit model of the rectifier was developed assuming an ideal diode and lossless circuit elements. The output load line was then obtained analytically. Second, a more precise computer simulation model was used, and the output equivalent circuit was obtained by varying the DC load resistance and plotting the resultant output load line.

We have shown that assuming an ideal diode, the circuit indicated in Figure 2A has yielded 100% conversion efficiency if $L_3 - C_3$, $L_5 - C_5$ etc. form odd harmonic parallel resonant circuits, C_1 series resonates the resultant inductive impedance at the fundamental frequency and $R_L = (\pi^2/8) R_s$. (1,2) Figure 2B indicates the more exact computer simulation model, a reasonable representation of the actual circuitry used in experimental rectennas. The models and the resulting load lines will be discussed further in the presentation.

When using these models and various assumed power density variations, we find that parallel combining is marginally better than series combining and that the closed form analytical model slightly underestimates the power

combining inefficiency compared to the computer simulation results. Assuming a uniform power density distribution, the power combining inefficiency is 1.0% when the ratio of maximum to minimum power density is 2.0 to 1.0, reducing to 0.3% if the ratio is 1.4 to 1.0. This has an important effect on the design of the rectenna DC power combining network, favoring ring combining rather than row combining particularly near the rectenna edge.

Directional Receiving Elements

A principal advantage of the rectenna concept for the receiver in free-space microwave power transmission systems is that the effective receiver pattern is sufficiently non-directional (i.e. beamwidth sufficiently large) that receiver steering is not required. However in evaluating the requirements for a solar power satellite (SPS) with a small orbit eccentricity in a near zero inclination geostationary orbit, it became apparent that the half wave dipole separated by $\approx 0.2 \lambda$ from a conducting ground plane has a more non-directional pattern than needed. That is the beamwidth of the receiver pattern at which 1% of the incident power is not received (0.04 dB beamwidth)* is much larger than the off normal incidence due to orbit considerations. Since the rectenna cost is projected to be $\sim 25\%$ of the total system cost, consideration of more directional receiving elements is clearly desirable.

In most applications fewer RF to DC conversion circuits (favoring directional elements) and power beam pointing requirements (favoring non-directional elements) are expected to dominate the directionality issue. An additional factor with the present GaAs Schottky diode rectifiers and present SPS design values is that higher RF to DC conversion efficiency is possible at higher power levels (power density limited by nonlinear interactions in ionosphere and possibly biological factors), thus favoring somewhat more directional elements. An additional disadvantage to directional receiving elements are more stringent requirements for a stable rectenna structure and precise element tolerances.

In considering alternate receiving elements at the modest gain enhancement considered desirable, we focused on the Yagi-Uda element because of

* Since efficient power transmission is paramount in the SPS application, a 1% beamwidth is more applicable than either the 3 dB or 1 dB beamwidth used in many microwave applications.

its simplicity. Including proximity effects in an actual array configuration was beyond the scope of our program. Instead we utilized antenna performance of isolated Yagi-Uda arrays in arriving at the expected electrical performance depicted in Table 1.^(1,3)

Based upon this electrical performance we designed three and six element Yagi-Uda arrays, with and without ground plane reflector, in both conventional baseline construction and in printed circuit form. Design of three element Yagi-Uda elements without ground planes are depicted in Fig. 3. These designs will be discussed further in the presentation.

The resultant costs obtained are in our investigation presented in Table 2, the trend toward lower cost with increased rectenna element gain being apparent. As expected, the cost reduction per unit rectenna area varies between the ratio of element densities (dependent upon effective area of each receiving element) and the square root of this ratio (dependent upon linear density of element rows). The net result is clear: THERE IS A LARGE RECTENNA COST SAVING POSSIBLE BY UTILIZATION OF MORE DIRECTIONAL RECEIVING ELEMENTS LIKE YAGI-UDA ELEMENTS. In a typical SPS rectenna there would be $\sim 75 \text{ km}^2$ area, so that a cost reduction of $\$/\text{m}^2$ is equivalent to a 75 million dollar reduction in capital costs. Thus savings of 300 to 450 million dollars per rectenna may be possible with the more directional Yagi-Uda element (capital costs in 1978 dollars).

The comparison between conventional construction and printed circuit implementation is less apparent. The printed circuit estimates are based upon less detailed design, but these results do not indicate a substantial reduction with printed circuit implementation. Only if socket and DC buss bar cost can be reduced will a large cost advantage result. These may be possible with careful structural designs requiring less material usage and low cost manufacturing, 5 mm diameter aluminum buss bars being assumed in our work. However, the conversion efficiency of printed circuit implementations will be somewhat lower, so baseline construction definitely seems preferred.

We have shown that more directional receiving elements are expected to lower rectenna costs in free-space microwave power transmission systems such as the SPS where the microwave power beam is relatively stationary with respect to the rectenna. Yagi-Uda receiving elements are considered

most desirable when moderate gains of perhaps 8 to 14 dB (with respect to an isotropic radiator) are optimum. Yagi-Uda antennas become undesirably awkward at higher gain, and alternatives such as short back-fire antennas should be considered. However it is believed that higher gain may result in unrealistically stringent power beam-rectenna alignment requirements in the SPS.

References

1. R. J. Gutmann and J. M. Borrego, "Solar Power Satellites Rectenna Design Study: Directional Receiving Elements and Parallel-Series Combining Analysis", Rensselaer Polytechnic Institute Report under Contract NAS9-15453 with NASA Johnson Space Center, December 1978.
2. R. J. Gutmann and J. M. Borrego, "Power Combining in an Array of Microwave Power Rectifiers", IEEE Trans. Microwave Theory and Techniques, MTT-27, December 1979.
3. R. J. Gutmann and R. Gworek, "Yagi-Uda Receiving Elements in Microwave Power Transmission System Rectennas", Journal of Microwave Power, 14, September 1979.

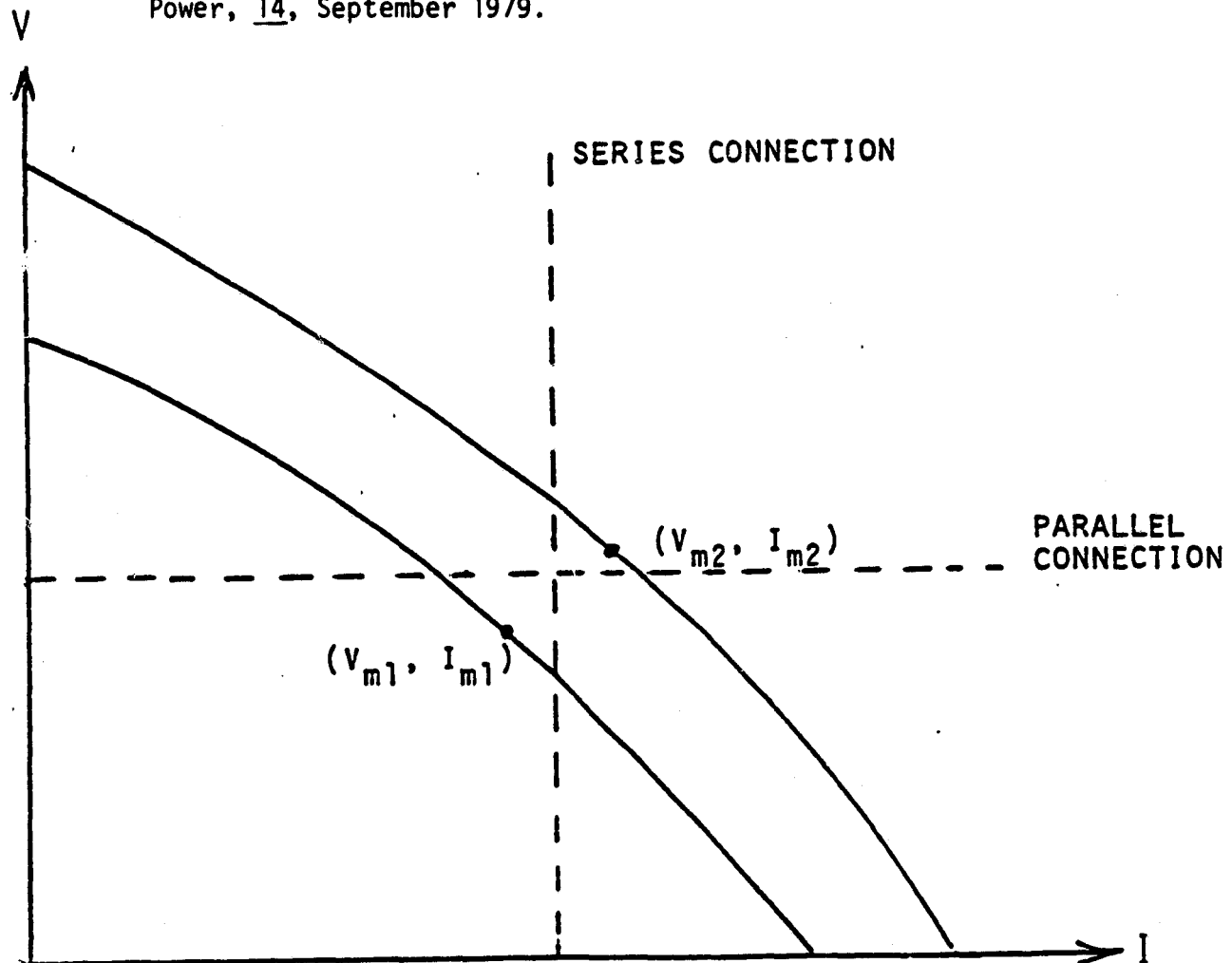


Figure 1 Output Load Line for Two Different Rectifiers

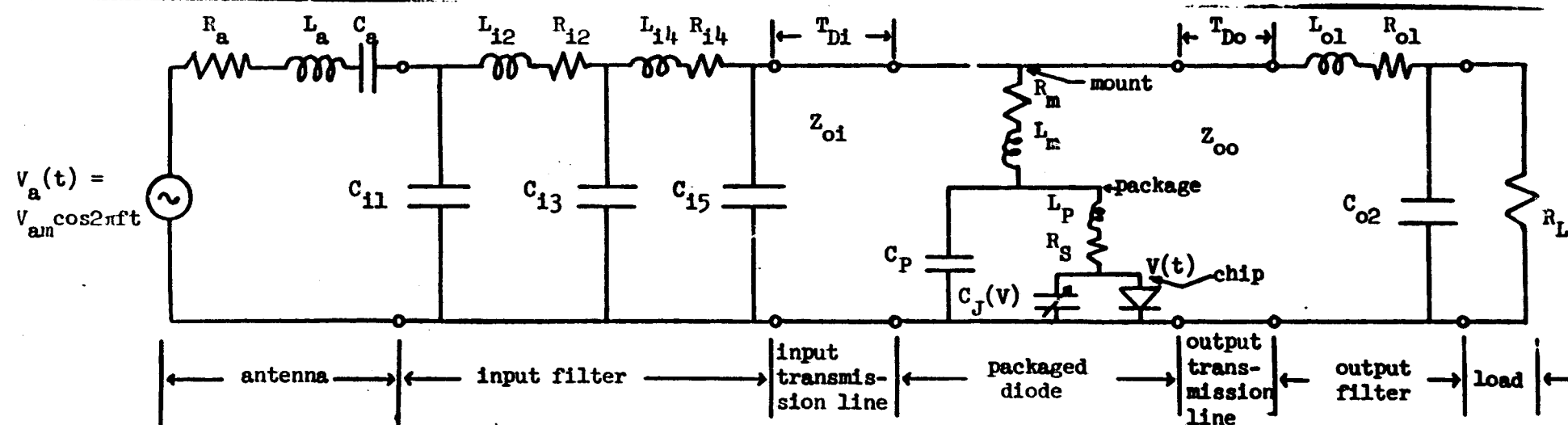
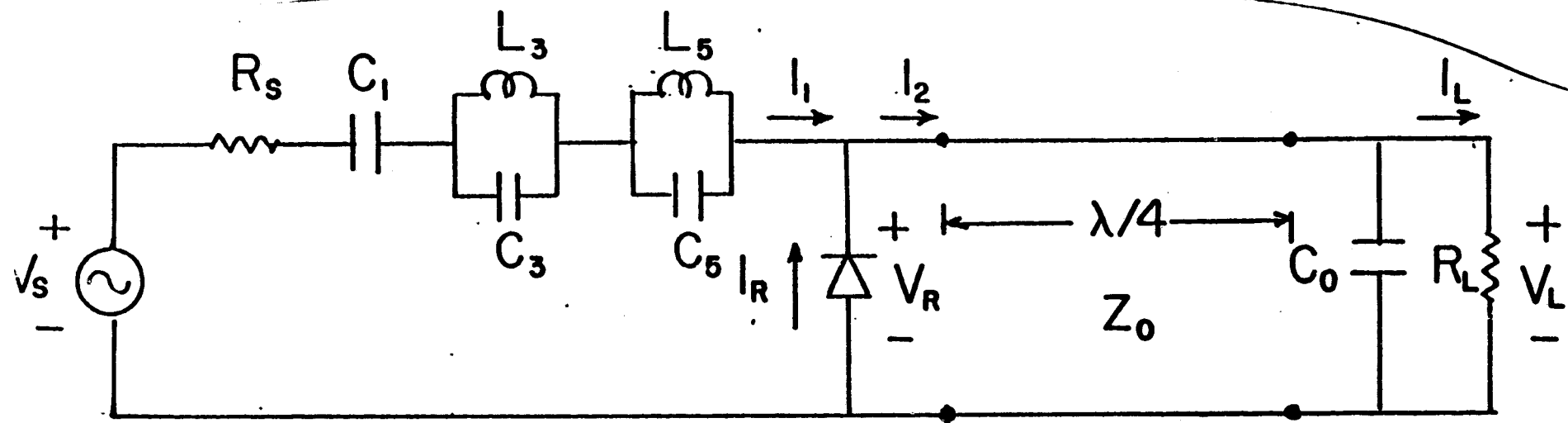


Figure 2 Equivalent Circuit Models for Microwave Rectifier
 (A) Ideal Circuit Model
 (B) Realistic Circuit Model of Baseline Rectifier

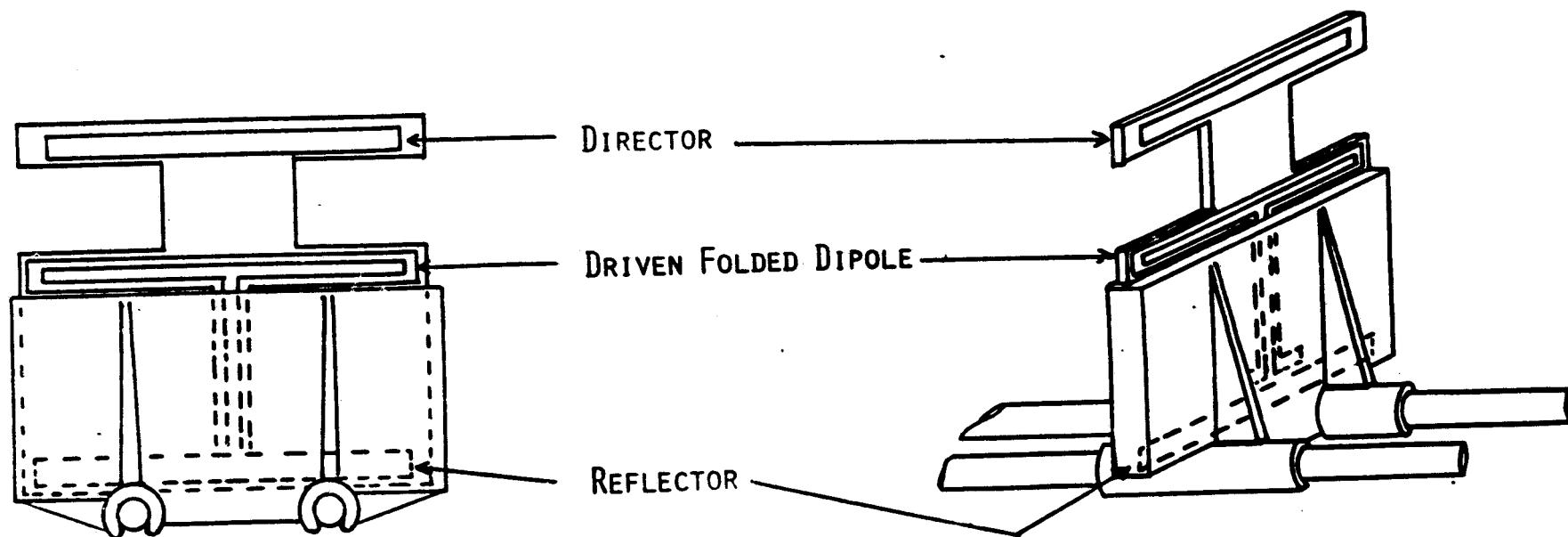
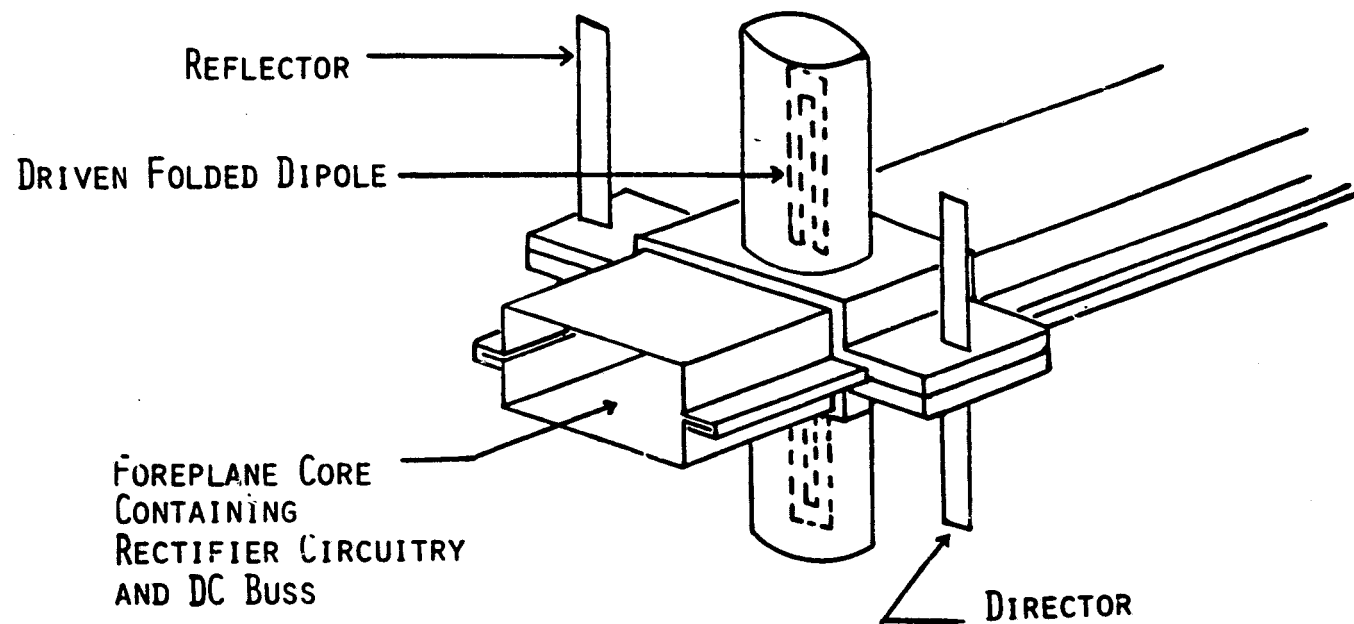


Figure 3 Three Element Yagi-Uda Receiving Array
 (A) Baseline Construction
 (B) Printed Circuit Construction

Table I

Expected Optimal Performance of Yagi-Uda Receiving Elements

	<u>Gain (wrt Isotropic) dB</u>	<u>F/B Ratio dB</u>	<u>Receiving Element Reduction Factor*</u>
3 Element-Low F/B ratio	11	5	2.82
3 Element-Moderate F/B ratio	10	15	2.24
3 Element-High F/B ratio	8.5	25	1.58
6 Element-Low F/B ratio	14	5	5.62
6 Element-Moderate F/B ratio	13	15	4.47
6 Element-High F/B ratio	11.5	25	2.82

* Relative to 6.5 dB Half-Wave Dipole Separated by $.20\lambda$ from a Conducting Ground Plane

ORIGINAL PAGE IS
OF POOR QUALITY

A. Printed Circuit Board Implementation

(costs are given in $\$/m^2$)

	<u>Half-wave Dipole with ground plane</u>	<u>3 element Yagi with ground plane</u>	<u>without ground plane</u>	<u>6 element Yagi without ground plane (average size)</u>
Element Density ($\frac{\text{elem.}}{m^2}$)	192	81	123	57
Socket	\$.92	\$.39	\$1.12	\$.52
DC buss bar	2.78	1.81	2.23	1.55
Printed Circuit Board	.24	.24	.42	.44
Ground Plane	<u>1.91</u>	<u>1.91</u>	<u>.00</u>	<u>.00</u>
Cost/ m^2	\$5.85	\$4.35	\$3.77	\$2.51
Diodes at \$.01 each	<u>1.92</u>	<u>.81</u>	<u>1.23</u>	<u>.57</u>
Total Cost/ m^2	\$7.77	\$5.16	\$5.00	\$3.08

B. Conventional Type Construction

(costs are given in $\$/m^2$)

	<u>Half-wave Dipole with ground plane</u>	<u>3 element Yagi with ground plane</u>	<u>without ground plane</u>	<u>6 element Yagi without ground pla</u>
Element Density ($\frac{\text{elem.}}{m^2}$)	192	81	123	57
Foreplane Core	\$3.13	\$1.47	\$2.09	\$1.09
Aluminum Shield/ Structural Member	2.14	1.40	.92	.64
Yagi-Uda Additions	.00	.30	.71	.76
Ground Plane	<u>1.91</u>	<u>1.91</u>	<u>.00</u>	<u>.00</u>
Cost/ m^2	\$7.18	\$5.08	\$3.72	\$2.49
Diodes at \$.01 each	<u>1.92</u>	<u>.81</u>	<u>1.23</u>	<u>.57</u>
Total Cost/ m^2	\$9.10	\$5.89	\$4.95	\$3.06

Table 2 Rectenna Cost Estimates (excluding rectenna frame)

Macro Aspects
A. Few/Rice University

unavailable at time of printing

A THEORETICAL STUDY OF MICROWAVE BEAM ABSORPTION BY A RECTENNA

James H. Ott
James S. Rice
Donald C. Thorn

Novar Electronics Corporation, Barberton, Ohio

ABSTRACT

The results of a theoretical study of microwave beam absorption by a Rectenna is given. Total absorption of the power beam is shown to be theoretically possible. Several improvements in the Rectenna design are indicated as a result of analytic modeling. The nature of Rectenna scattering and atmospheric effects are discussed.

INTRODUCTION

A workable Solar Power Satellite system will depend upon the efficient free-space transmission of energy to earth via an environmentally benign microwave beam. The "Rectenna", a large array of dipole-diode devices which captures and rectifies microwave power from satellites, embodies an emerging technology pioneered by William C. Brown¹ of Raytheon. Brown² and Richard Dickinson³ of JPL have reported tests on experimental Rectenna arrays which have achieved microwave to dc conversion efficiencies exceeding 80%. However, classical antenna theory tells us that an isolated dipole must re-radiate as much energy as it delivers to a properly matched load. Because of a frequently expressed concern over whether or not this antenna theory was in contradiction with experimental Rectenna results, Novar Electronics Corporation undertook the task of developing a theoretical model which describes the absorption of a microwave beam by a very large Rectenna. In view of the size and scope of the SPS program, it is important to theoretically determine whether a rectenna array or the reference system design can totally absorb the power beam--that is, produce no scattering. In addition, it is desirable to study the microwave absorption process in order to provide a theoretical model for the simulation of design improvements and, because of concerns about possible electromagnetic interference from the rectenna, to obtain additional insights into the rectenna's scattering properties.

Novar's work demonstrates not only that the theoretical absorption limit is in fact 100% but that the number of elements required for total absorption per unit area can be greatly reduced, significantly reducing the cost of the Rectenna. Results further indicate that Rectenna panels can be made to totally absorb at any angle of incidence by adjusting reflector and element spacing and load impedance. This suggests a flat or terrain conforming Rectenna eliminating the need for the "billboard" or "Venetian blind" design and essentially conforming to the terrain. Also, the screen reflector should be able to be replaced by parasitic reflector dipole elements.

Deviations from conditions required for total absorption give rise to scattering, and the resulting losses due to variations from design center values for several parameters are shown. The directionality of fundamental and harmonic scattering from a Rectenna is described. Among the factors causing scattering that were studied are microwave beam depolarization and amplitude fluctuations caused by disturbances in the atmosphere. Included in this category is "diffracted signal enhancement", the diffractive effects of large objects flying over the Rectenna, which can be expected to cause transient signal increases as large as 9 dB which must be taken into account in the rectenna design.

Because of the difficulty in trying to analyze a large array of interacting dipoles using mutual impedance analysis, it was necessary to develop another type of mathematical model descriptive of the microwave

power absorption process. Two such models were derived from Maxwell's equations. These models quantify conditions for total absorption of the power beam by a Rectenna and provide values for scattering losses due to deviations in each condition.

CURRENT SHEET RECTENNA MODEL

The first model is based on the current sheet equivalency of a large planar array above a reflector as shown in Figure 1. The current sheet has the properties of resistive absorbers described by Jasik⁴ and Kraus⁵. The model is mathematically characterized by an expression for the fraction of an incident plane wave's power that is reflected from the sheet.

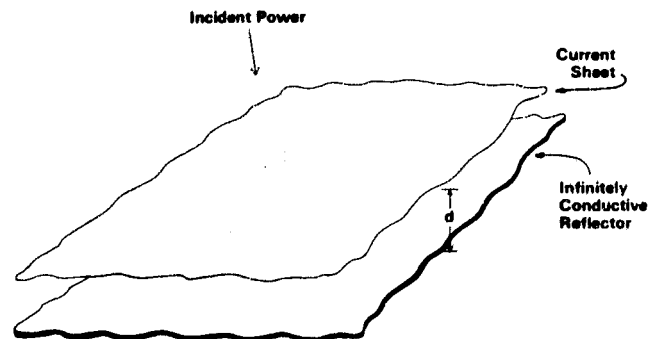


FIGURE 1
CURRENT SHEET RECTENNA MODEL

This expression, which agrees with Jasik, and for which no derivation could be found in the literature, is determined as follows. First, Maxwell's equations are solved to obtain general expressions for the electric and magnetic fields in the region above the current sheet and in the region between the current sheet and the reflector surface.

Next, the boundary conditions are satisfied at the infinitely conductive reflector surface and then at the current sheet as the thickness of the current sheet is allowed to become very thin. This yields expressions for the waves at the surface of the current sheet. The expressions are then solved simultaneously for the power reflection coefficient, the fraction of power reflected by the current sheet. It is expressed by either Equation 1a or 1b, following, depending upon the polarization of the incident wave.*

*Polarization is defined by the relationship of the incident wave's electric field vector, \underline{E} , to the plane of incidence, the plane determined by rays in the directions of propagation of the incident and reflected waves. When \underline{E} is parallel to the plane of incidence, the wave is said to be parallel polarized. When \underline{E} is perpendicular to the plane, the wave is said to be perpendicularly polarized. (Any other polarization can be decomposed into a combination of parallel and perpendicular polarization.)

Parallel Polarization

$$|\rho_{\parallel}|^2 = \frac{\left(\frac{\sqrt{\mu/\epsilon}}{R_0} \cos\theta - 1\right)^2 + \cot^2\left(\frac{2\pi d}{\lambda} \cos\theta\right)}{\left(\frac{\sqrt{\mu/\epsilon}}{R_0} \cos\theta + 1\right)^2 + \cot^2\left(\frac{2\pi d}{\lambda} \cos\theta\right)} \quad (1a)$$

Perpendicular Polarization

$$|\rho_{\perp}|^2 = \frac{\left(\frac{\sqrt{\mu/\epsilon}}{R_0} \sec\theta - 1\right)^2 + \cot^2\left(\frac{2\pi d}{\lambda} \cos\theta\right)}{\left(\frac{\sqrt{\mu/\epsilon}}{R_0} \sec\theta + 1\right)^2 + \cot^2\left(\frac{2\pi d}{\lambda} \cos\theta\right)} \quad (1b)$$

where:

- R_0 is the resistance of the current sheet in ohms per square*,
- θ is the angle of incidence of the received wave as measured from the normal,
- d is the separation between the current sheet and reflector,
- λ is the wavelength,
- ϵ and μ are the permittivity and permeability, respectively.

The expressions above demonstrate that total absorption is theoretically possible for normal incidence ($\theta = 0$) when $d = \lambda/4$ and $R_0 = \sqrt{\mu/\epsilon} = 377$ ohms for free space. The power reflection coefficient and reflected power as functions of deviations in R_0 , d , or θ from those values required for total absorption at normal incidence are shown in Figure 2.

The model further predicts that a Rectenna can be designed for total absorption for beam angles off normal incidence.† This leads to the possibility of a Rectenna that can be built to lie flat on the ground and be essentially "terrain conforming". This type of Rectenna array has several advantages over the "billboard" or "venetian blind" construction of the reference system: 1) much less excavation is required, 2) there is the potential to suspend the elements and reflector screen above farms, buildings, etc., and 3) less scattering is anticipated because there are no "billboard" edges to cause diffraction of the power beam.

This current sheet Rectenna model provides a "macroscopic view" of the microwave absorption process. Novar has developed a second model which provides an insight into the role played by the individual Rectenna elements. Moreover it provides an independent theoretical confirmation of the ability of the Rectenna to totally absorb the power beam.

WAVEGUIDE RECTENNA MODEL

The second model quantifies the electromagnetic modes (field configurations) in the immediate vicinity of a Rectenna element in the Rectenna array and gives limits for the element spacing which permit total power beam absorption by preventing unwanted modes from propagating (scattering). This model is based on the properties of a special waveguide described by Wheeler⁶ in his analysis of certain aspects of a large planar array. Specifically, the waveguide has

special "imaging" characteristics and has the ability to allow only plane wave propagation. The waveguide is rectangular in shape with a probe (monopole) inserted through the middle of one of the walls. However unlike "conventional" waveguides, the two walls parallel to the monopole are nonconductive and "magnetic" ($\mu = \infty$, $\sigma = 0$), with the other two walls being perfectly conductive ($\sigma = \infty$). When we solve the equations describing the nature of wave reflections at

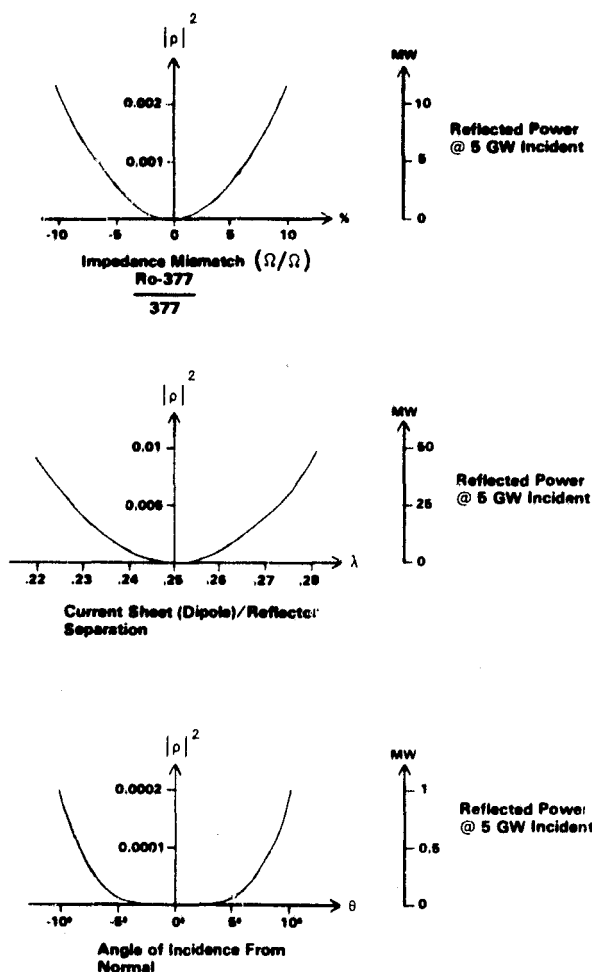


FIGURE 2
POWER REFLECTION COEFFICIENT AND REFLECTED POWER LEVEL OF THE CURRENT SHEET RECTENNA MODEL AS A FUNCTION OF VARIOUS PARAMETERS

*Resistance per square is the resistance between opposite edges of a square slab of resistive material and therefore is independent of the size of the square.

†With λ fixed, and given any θ , there is an R_0 and d such that $|\rho|^2 = 0$.

the walls, it is found that a monopole in this type of waveguide, which we will call a "mixed-wall" waveguide, produces an infinite array of image dipoles with currents of identical magnitude and phase as depicted in Figure 3.* Conversely, an infinite array of identical dipoles with currents of identical magnitude and phase can be replaced by a single monopole in a mixed-wall waveguide to analyze the behavior of a dipole as illustrated by Figure 4. Since the power beam is nearly uniform in power density over quite a large area, dipoles within a fairly large arbitrarily selected area of the Rectenna will have currents nearly uniform in magnitude and phase which can be closely approximated for that area by an infinite array. Thus the behavior of a dipole which defines the center of this area can be accurately modeled by the behavior of a monopole in a mixed-wall waveguide.

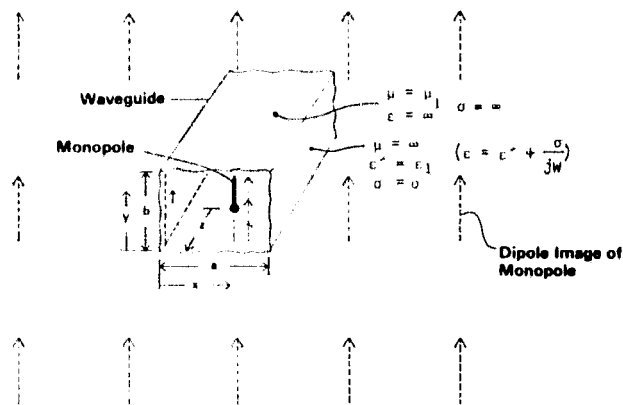


FIGURE 3
IMAGING PROPERTIES OF MIXED-WALL
WAVEGUIDE WITH MONOPOLE

The first step in analysis of this monopole's behavior is to determine what modes can propagate in the mixed-wall waveguide† and under what conditions. We want the TEM mode to be the only mode that can propagate. This TEM mode is the same field configuration as that of the power beam, i.e., a plane wave. If other modes propagate, scattering is taking place. Since the side walls of a mixed-wall waveguide as shown in Figure 3 are non-conductive and "magnetic", the mixed-wall waveguide is similar to a strip-line for the TEM modes. Thus this waveguide will support the TEM mode at the power beam frequency independent of the waveguide dimensions.

Next, the properties of the mixed-wall waveguide for the higher order modes are derived in order not only to determine the conditions required for their evanescence but also to allow us to describe the near fields around the monopole. To do this, Maxwell's equations are solved to obtain wave equations which are then modified by mathematical decomposition to put them into an efficient form for solution. The wave equations are then solved to obtain general equations for the magnetic and electric fields in the mixed-wall waveguide. These equations are functions of pairs of integers, one integer of which is associated with the "a" dimension in Figures 3 and 4, and the other with "b". Specific values for the inte-

gers in a pair defines a mode. The higher order modes have either transverse magnetic or transverse electric fields.‡ These are respectively designated the TM_{fg} and the TE_{mn} modes, where f and n are 0,1,2,3,...; g and m are 1,2,3,....

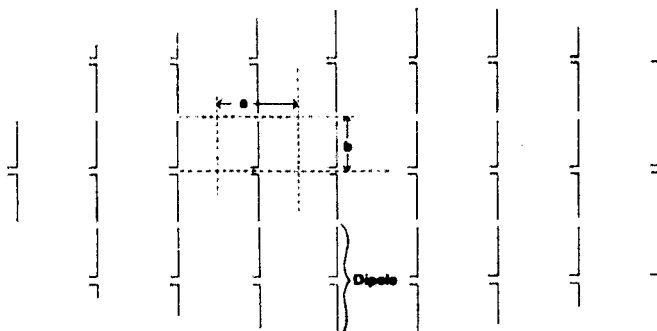


FIGURE 4
SECTION OF INFINITE ARRAY OF DIPOLES MODELED BY
A MONOPOLE IN A "MIXED-WALL" WAVEGUIDE

Inspection of the mode equations shows that the lowest cutoff frequency for higher order TM modes is associated with TM_{01} and that for the TE modes is the TE_{10} . This means that at a given frequency the smallest critical dimensions for propagation are associated with those two modes. The next larger critical dimension is associated with the TE_{20} .

The TE_{10} mode is actually non-existent in our mixed-wall waveguide/monopole configuration because it is not generated when the monopole is located in the center of this special type of waveguide.** This results in the critical dimensions for higher mode

*Analogous to the study of optical reflections from mirrors, the "method of images" shows that the fields within the mixed-wall waveguide boundaries are the same as though there was no waveguide but only the monopole and an infinite number of identical magnitude and phase images.

†Modes, which are the various field configurations that can exist within a waveguide, have the property that for a given frequency they are evanescent (non-propagating) for waveguide dimensions less than certain critical values, which are called "cutoff" dimensions, and can propagate for any dimensions greater than those values. Each mode has its own set of cutoff dimensions. Conversely, for a given set of waveguide dimensions, there is a critical frequency for each mode (called the cutoff frequency) below which the mode is evanescent and above which it can propagate.

‡Transverse means no component in the $\pm z$ direction in Figure 3.

**Note that "mode-hopping", the generation of modes due to waveguide imperfections, is not a problem here because the waveguide is assumed to be ideal.

propagation being determined by the TM_{01} and the TE_{20} . Specifically, for evanescence of all higher modes, those critical dimensions restrict the waveguide dimensions to be less than one wavelength in the "a" direction and less than one half wavelength in the "b" direction. (This is equivalent to a Rectenna element spacing of just under one wavelength.)

The total electric field, \underline{E} , and the total magnetic field, \underline{H} , in the mixed-wall waveguide are each sums of the various field configurations or modes that exist in the waveguide. Now \underline{E} and \underline{H} are vector sums of respective field components in the x, y, and z directions of Figure 3. Thus for "+ z directed" field components, \underline{E} and \underline{H} can be represented by the equations given in Table I, where A_{mn} and B_{fg} are respectively the maximum amplitudes of H_z and E_z , K_{00} is the maximum amplitude of the H field of the TEM wave. The α 's and β 's at the bottom of the table are respectively the real and imaginary parts of the expressions shown for the γ 's. The terms involving double summations represent the "sums of the higher order modes". The leading terms in the equations for E_y and H_x are the equations for the TEM mode. If the higher order modes are evanescent, then the double summation terms are components of the fields associated with reactive power.

If a reflector or shorting plate is inserted in the waveguide behind the monopole, as shown in Figure 5, the situation is equivalent to the infinite array of dipoles in Figure 4 being backed by a reflector. A set of equations analogous to those in Table I can then be generated for the "-z directed" field components of the waves reflected from the shorting plate. Summing the +z and -z directed field components in the neighborhood of the monopole gives rise to a set of equations of the same form as those in a conventional waveguide backed by a shorting plate. These equations establish matching requirements on the monopole and load impedances and spacing of the monopole from the shorting plate so that the non-evanescent wave does not propagate back up the waveguide toward the source. Since it is well known that a probe in a conventional waveguide backed by a shorting plate can totally absorb all power flowing down the waveguide⁷, it is therefore expected that a probe (monopole) in a mixed-wall waveguide can also totally absorb all power flowing down that type of waveguide. Therefore total absorption of the plane wave power beam by a dipole in a Rectenna is expected when the separation between dipoles is within limits dictated by the mixed-wall waveguide model's dimensions which restrict propagation in that waveguide to the TEM mode.

Since the waveguide dimensions which restrict propagation to the TEM mode is less than λ in the "a" direction and less than $\lambda/2$ in the "b" direction of Figures 3 and 4, and since the separation between the centers of the dipoles is "a" by "2b" as can be seen from Figure 4, then the maximum allowable separation of the centers of dipoles for total absorption of a plane wave, for the rectangular grid configuration of Figure 4, is just under one wavelength.

$$H_z = 0 + \sum_{m=1}^{\infty} \sum_{n=0}^{\infty} A_{mn} \sin \frac{m\pi x}{a} \cos \frac{n\pi y}{b} e^{-\alpha_{mn} z}$$

$$E_z = 0 + \sum_{f=0}^{\infty} \sum_{g=1}^{\infty} B_{fg} \cos \frac{f\pi x}{a} \sin \frac{g\pi y}{b} e^{-\alpha_{fg} z}$$

$$E_x = 0 + \sum_{m=1}^{\infty} \sum_{n=0}^{\infty} \frac{j\omega\mu n\pi}{k_{cmn}^2} A_{mn} \sin \frac{m\pi x}{a} \sin \frac{n\pi y}{b} e^{-\alpha_{mn} z}$$

$$+ \sum_{f=0}^{\infty} \sum_{g=1}^{\infty} \frac{-\alpha_{fg} f}{k_{cfg}^2} B_{fg} \sin \frac{f\pi x}{a} \sin \frac{g\pi y}{b} e^{-\alpha_{fg} z}$$

$$E_y = \frac{\mu}{\epsilon} K_{00} e^{-j\beta_{00} z} + \sum_{m=1}^{\infty} \sum_{n=0}^{\infty} \frac{j\omega\mu m\pi}{k_{cmn}^2} A_{mn} \cos \frac{m\pi x}{a} \cos \frac{n\pi y}{b} e^{-\alpha_{mn} z}$$

$$+ \sum_{f=0}^{\infty} \sum_{g=1}^{\infty} \frac{\alpha_{fg} g\pi}{k_{cfg}^2} B_{fg} \cos \frac{f\pi x}{a} \cos \frac{g\pi y}{b} e^{-\alpha_{fg} z}$$

$$H_x = K_{00} e^{-j\beta_{00} z} + \sum_{m=1}^{\infty} \sum_{n=0}^{\infty} \frac{\alpha_{mn} m\pi}{k_{cmn}^2} A_{mn} \cos \frac{m\pi x}{a} \cos \frac{n\pi y}{b} e^{-\alpha_{mn} z}$$

$$+ \sum_{f=0}^{\infty} \sum_{g=1}^{\infty} \frac{j\omega\epsilon g\pi}{k_{cfg}^2} B_{fg} \cos \frac{f\pi x}{a} \cos \frac{g\pi y}{b} e^{-\alpha_{mn} z}$$

$$H_y = 0 + \sum_{m=1}^{\infty} \sum_{n=0}^{\infty} \frac{-\alpha_{mn} n\pi}{k_{cmn}^2} A_{mn} \sin \frac{m\pi x}{a} \sin \frac{n\pi y}{b} e^{-\alpha_{mn} z}$$

$$+ \sum_{f=0}^{\infty} \sum_{g=1}^{\infty} \frac{j\omega\epsilon g\pi}{k_{cfg}^2} B_{fg} \sin \frac{f\pi x}{a} \sin \frac{g\pi y}{b} e^{-\alpha_{fg} z}$$

$$\gamma_{mn} = \alpha_{mn} + j\beta_{mn} = \sqrt{k^2 - \left(\frac{m\pi}{a}\right)^2 - \left(\frac{n\pi}{b}\right)^2} = \sqrt{k^2 - k_{cmn}^2}$$

$$\gamma_{fg} = \alpha_{fg} + j\beta_{fg} = \sqrt{k^2 - \left(\frac{f\pi}{a}\right)^2 - \left(\frac{g\pi}{b}\right)^2} = \sqrt{k^2 - k_{cfg}^2}$$

$$\beta_{00} = k = \frac{2\pi}{\lambda}$$

TABLE I

ELECTROMAGNETIC FIELD EQUATIONS FOR A MIXED-WALL WAVEGUIDE

Equations shown are for total "+ z directed" portion of the field components in a mixed-wall waveguide. With appropriate sign changes, equations express the "- z directed" components.

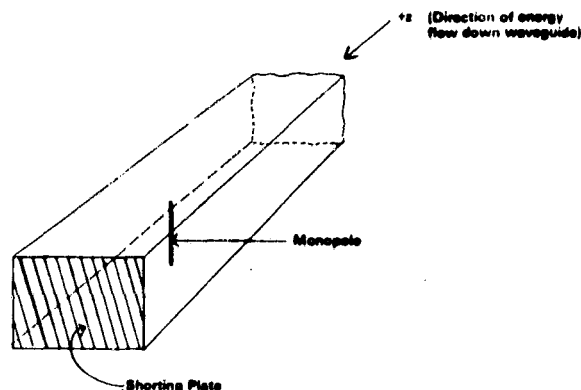


FIGURE 5
MONOPOLE IN MIXED-WALL WAVEGUIDE
BACKED BY SHORTING PLATE

ELEMENT DENSITY

The existence of non-evanescent higher order modes corresponds to the existence of grating lobes. Analysis of the generation of grating lobes indicates that the maximum separation between dipole centers for avoidance of grating lobes with the triangular grid configuration used in the Reference System is just under 1.15λ . It is understood that the present separation between dipole centers in the Reference System is just under 0.6λ . The number of Rectenna dipole-diode elements needed for total power beam absorption can be significantly reduced over the number needed for the Reference Systems as shown below.

	NUMBER OF DIPOLE-DIODE ELEMENTS REQUIRED (NORMAL INCIDENCE)
Reference System Design	18 billion
Triangular Grid Configuration With Maximum Allowable Dipole Spacing	4.5 billion
Rectangular Grid Configuration With Maximum Allowable Dipole Spacing	5.2 billion

In addition, greater diode efficiency is indicated when the number of Rectenna dipole elements is reduced since the power density per diode is higher.

PARASITIC REFLECTING DIPOLES

Total absorption of energy by the monopole in a conventional waveguide requires that the shorting plate in the waveguide be approximately a quarter wavelength behind the monopole. This distance is also expected to be proper for the mixed-wall waveguide. Since the shorting plate corresponds to the Rectenna reflector, and since it is expected that the shorting plate can be replaced by a parasitic reflecting mono-

pole as can be done easily in a conventional waveguide and still totally absorb the energy traveling down the waveguide, then the Rectenna reflector should be replaceable by parasitic dipole elements, as depicted in Figure 6.

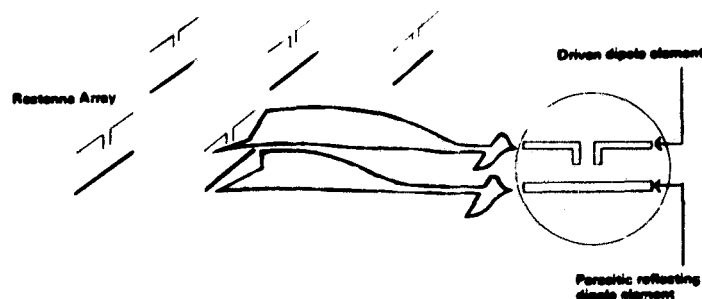


FIGURE 6
RECTENNA WITH PARASITIC REFLECTING
DIPOLE ELEMENTS

HARMONIC FILTER

None of the preceeding analysis permits the dipole terminals to see a non-linear load for total absorption. What is required in a Rectenna element for total absorption is a harmonic filter, as depicted in Figure 7, that presents a linear load to the dipole terminals at the fundamental frequency such that the load voltage and current seen by the dipole are pure sinusoids not in phase quadrature, i.e. that the linear load has a real component.

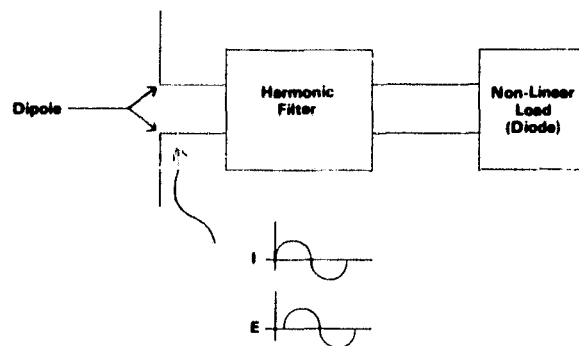


FIGURE 7
RECTENNA ELEMENT HARMONIC FILTER

FUNDAMENTAL SCATTERING

Specular scattering of the power beam, depicted in Figure 8, is expected to result from most deviations in the Rectenna's parameters. The smaller the deviation anomaly, the broader will be the specular lobe. Single, isolated element failures (short or open diodes) will appear to radiate as isotropic sources above a reflector.

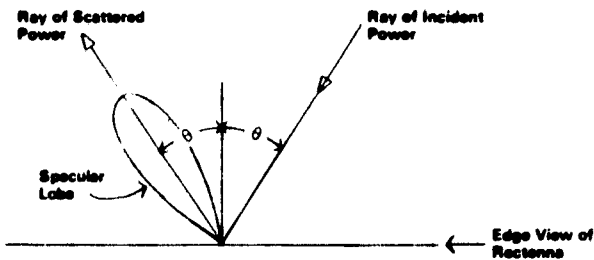


FIGURE 8
DEPICTION OF SPECULAR SCATTERING
FROM FACE OF RECTENNA
Frequency is the power beam fundamental

HARMONIC SCATTERING

The Rectenna dipole-filter-diode assembly and power bus are expected to be most significant sources of harmonic scattering. The harmonic energy will be concentrated in grating lobes, as shown in Figure 9. Random Rectenna imperfections will broaden the lobes.

ATMOSPHERIC EFFECTS

Atmospheric phenomena cause polarization shifts and amplitude fluctuations in an electromagnetic wave at microwave frequencies 8,9,10,11,12,13. However, only infrequent depolarizing events up to 20 dB (1% scattered power) have been observed in microwave down-link transmissions with greater than 10 meter apertures. Based on these observations, depolarization is not expected to be a significant source of scatter.

Amplitude fluctuations cause scattering by disrupting the uniform illumination of the Rectenna. In addition, this disruption of the RF power level from design values for the diodes causes impedance mismatches resulting in further scattering. Existing earth-space propagation measurements to date ¹³

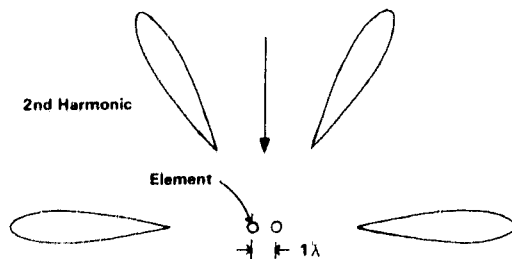


FIGURE 9a
EXAMPLE OF ELEVATION OF HARMONIC RADIATION

Figure depicts 2nd harmonic scattering for normal incidence of power beam when the element spacing is equal to λ at the fundamental frequency.

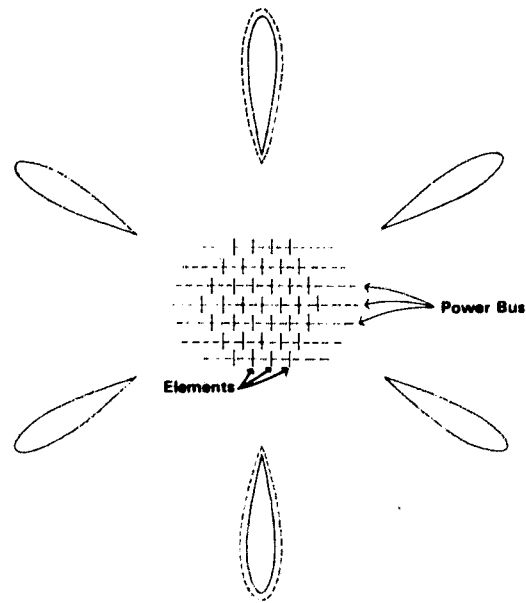


FIGURE 9b
AZIMUTHS OF HARMONIC RADIATION

"Dotted" lobe due to power bus.

FIGURE 9
GRATING LOBE NATURE OF HARMONIC
SCATTERING FROM A RECTENNA

indicate a maximum of 0.1 dB amplitude fluctuations for 2-3 GHz at elevation angles above 20° (which would cause insignificant scattering).

There are factors which impair the application of previous earth station measurements to the SPS. In all studies found, there is significant aperture averaging. The minimum aperture area for those studies is about $5000\lambda^2$ as compared to about $1\lambda^2$ or so of each "independent" receiving element in the Rectenna. This indicates that the amplitude fluctuations may be appreciably greater than 0.1 dB for the Rectenna. Another factor is that the measurement data, taken at C and S bands, were obtained from modulated signals. Most deep fades are frequency sensitive. Therefore for modulated signals, which have their power spread over a spectrum of frequencies, the observed amplitude fluctuations would be expected to be less than those of the monochromatic SPS power beam.

As of this writing, Novar Electronics Corporation intends to receive, at its earth station located in Summit County, Ohio, special monochromatic calibration signals from RCA's new F3 Satcom* in order to observe aperture averaging effects and monochromatic signal fading characteristics. Aperture areas of approximately $1200\lambda^2$ and on the order of $1\lambda^2$ will be used to comparatively receive the signals (which are transmitted for satellite installation test purposes to determine EIRP contours).

*Scheduled to be stationed in orbit at the end of December, 1979

DIFFRACTED SIGNAL ENHANCEMENT

A large object flying through the power beam over the Rectenna causes diffraction patterns to be generated at the Rectenna as depicted in Figure 10. Preliminary experimental evidence has been obtained. Depending on the size and shape of the object, increases in signal levels as large as 9 dB are possible. Therefore, Rectenna diodes should have tolerance to the resulting spot-transient signal enhancement to protect against overvoltage transients from fast aircraft and also against diode overheating from slower objects.

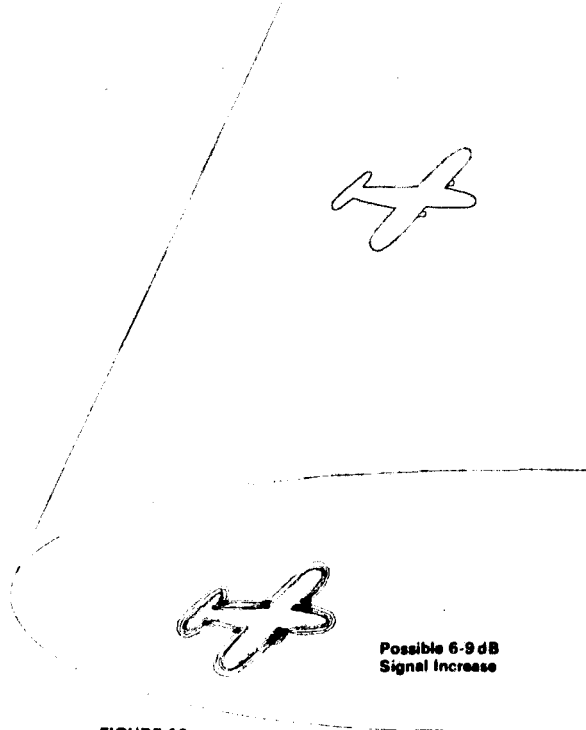


FIGURE 10
DIFFRACTION ENHANCEMENT AT RECTENNA
CAUSED BY OBJECT FLYING THROUGH THE
POWER BEAM

CONCLUSIONS

Analytic modeling shows that it is theoretically possible for a Rectenna to totally absorb microwave energy, i.e., produce no scattering. The number of elements required is significantly less than indicated in the Reference System. The Rectenna can be designed for total absorption at off-normal angles of incidence and it is expected that the Rectenna's reflecting screen can be replaced with parasitic reflecting dipoles.

Further space-earth transmission studies are required. The application of existing data to the SPS is impaired because these were from measurements of modulated signals received by large aperture antennas.

REFERENCES

1. W. C. Brown, "The Technology and Application of Free-Space Power Transmission by Microwave Beam," Proceedings of the IEEE, Vol. 62, No. 1, January 1974, pp. 11-25.
2. W. C. Brown: "Optimization of the Efficiency and Other Properties of the Rectenna Element," 1976 IEEE MTT-S International Microwave Symposium Digest of Technical Papers, pp. 142-144.

3. R. M. Dickinson: "Performance of a High-Power 2.388-GHz Receiving Array in Wireless Power Transmission Over 1.54 km", 1976 IEEE MTT-S International Microwave Symposium Digest of Technical Papers, pp. 139-141.
4. H. Jasik (Ed): Antenna Engineering Handbook, McGraw-Hill Book Company, 1961. (The Salisbury screen is described in Sec. 32, page 36.)
5. J. D. Kraus: Electromagnetics, McGraw-Hill Book Company, Inc., 1953. (The "Space cloth" is discussed, starting on page 407.)
6. H. A. Wheeler: "The Radiation Resistance of an Antenna in an Infinite Array or Waveguide" Proc. I.R.E. Vol. 36, No. 4, April 1948, pp. 478-487. (Introduces concept of waveguide to image interchange) (Gives radiation resistance of each element of an infinite rectangular array on the basis of a special waveguide.) (States ability of individual antenna in guide with reflector to have 100% absorption.)
7. J. C. Slater: Microwave Transmission. McGraw Hill Book Company, Inc., 1942 (Good basic treatment including a careful discussion of the limitation of "impedance" in waveguides. Discusses dipole-waveguide connection on page 296.)
8. R. R. Taur: "Ionospheric Scintillation at Frequencies Above 1 GHz" Cosmat Technical Review, Vol. 4, No. 2. Fall, 1974.
9. J. P. Basart, G. K. Miley, and B. G. Clark: "Phase Measurements with an Interferometer Baseline of 11.3 km" IEEE Trans. on Antennas and Propagation. Vol. AP18, No. 3, May 1970, pp. 375-379. (Provides a good insight into phase variations due to the atmosphere.)
10. D. J. Fang: "Attenuation and Phase Shift of Microwaves due to Canted Raindrops" Cosmat Technical Review Vol. 5, No. 1. Spring, 1975.
11. D. J. Fang and J. Jih: "A Model of Microwave Propagation Along an Earth Satellite Path" Cosmat Technical Review Vol. 6, No. 2. February 1976.
12. M. C. Thompson, Jr. and H. B. James: "Antenna Aperture Size Effect on Tropospheric Phase Noise" IEEE Transactions on Antennas and Propagation Vol. AP. November, 1966. pp. 800-802.
13. R. K. Crane and D. W. Blood: "Handbook for the Estimation of Microwave Propagation Effects--Link Calculations for Earth-Space Paths (Path Loss and Noise Estimation)" Environmental Research & Technology, Inc. Technical Report No. 1, p. 7376 - TRI, June 1979.

In addition to the publications listed above, the authors gratefully acknowledge the assistance provided in personal communications from R. K. Crane, D. J. Fang, P. W. Hannan, R. K. Moore, R. R. Taur, and H. A. Wheeler.

RECTENNA ARRAY MEASUREMENT RESULTS

Richard M. Dickinson
Telecommunications Science and
Engineering Division Staff
Jet Propulsion Laboratory
Pasadena, CA 91103

ABSTRACT

The measured performance characteristics of a rectenna array are reviewed and compared to the performance of a single element. It is shown that the performance may be extrapolated from the individual element to that of the collection of elements.

Techniques for current and voltage combining have been demonstrated. The array performance as a function of various operating parameters is characterized and techniques for overvoltage protection and automatic fault clearing in the array have been demonstrated. A method for detecting failed elements also exists.

Instrumentation for deriving performance effectiveness is described. Measured harmonic radiation patterns and fundamental frequency scattered patterns for a low level illumination rectenna array are presented.

INTRODUCTION

Prior to a definite commitment for a significant application of Beamed RF Power, performance characteristic data must be obtained for use by design engineers and systems analysts. The operating performance of a rectenna array under various conditions of load, RF power input level, temperature, polarization, angle of incidence, state of maintenance, and frequency is required. Fundamental performance factors are the transfer efficiency, relating dc power output to available RF power input, and the level and distribution of scattered fundamental and emitted harmonic radiation from the array. Secondary performance factors are the output voltage and converter temperature. The existing measured performance data on rectenna arrays will be reviewed and recent results will be discussed.

MEASURED RECTENNA ARRAY PERFORMANCE

High efficiency (greater than 50%) rectenna array characteristics were documented in Ref. 1, for the condition of highest collection-conversion efficiency performance associated with a demonstration of overall system end to end dc transfer efficiency. The array consisted of 199 half wave gallium arsenide Schottky barrier diodes connected to half wave dipoles through a two section low pass filter projecting through a flat solid ground plane. The elements were arranged in a triangular lattice whose outline configuration was a hexagon. The collecting area per element was about 52 cm². The incident flux density ranged from 203 mW/cm² to 2.5 mW/cm² in a gaussian distribution over the aperture of the array. (A 19 dB taper.) The dc load collection consisted of 21 separate concentric rings of adjustable resistances tailored to the ring radius. A one tenth wavelength dipole probe in front of the array measured about 1.11 to 1 VSWR on axis under matched conditions.

PRECEDING PAGE BLANK NOT FILMED

The peak collection-conversion efficiency of an individual element was measured as $87 \pm 1.5\%$, whereas the average efficiency of the entire array at approximately 0.5 KW output dc power was 82.7% of the available RF power incident upon the array (not counting the estimated 4% spillover energy). The array transfer efficiency decreased less than 2% for a 16.7% decrease in RF input power level.

The next large rectenna array was tested at Goldstone, CA (Ref. 2) and consisted of 4590 elements arranged in 17 subarrays of 270 elements each arranged in a triangular grid pattern. The subarrays were grouped in a three column arrangement with the top center subarray absent, as shown in Fig. 1. Fig. 2 and 3 are of the array performance characteristics and capabilities for use of the instrumented output data. The measured performance can in general be accurately predicted from general transmission line reflection coefficient theory as concerns the load variations, and the polarization and angle of incidence performance follows array theory. Computer models (Ref. 3, 4) for the diode and associated RF circuitry are able to predict the element performance as a function of the input RF amplitude, however, the array performance is poorer than predicted in most cases, by a few percent. This may be due to the effects of mutual coupling in the array, which are not modeled in a single element analysis. Nevertheless, over a 10 dB range of input power density, the rectenna array performance may be adequately predicted within a few percent, based upon measured diode characteristics.

Figure 4 compares the transfer efficiency performance of a single element, the average element in a subarray of 270 elements, and the average element in an array of 4590 elements over a 6 dB range of RF power density input. The performance of a large array may be extrapolated with confidence from the single element.

CURRENT AND VOLTAGE COMBINING AND PROTECTION

Figure 5 shows the wiring diagram of one of the 270 element subarrays. By insulating the dc buss from the subarray frame the paralleled rows of rectenna element outputs may be seriesed in order to raise the output voltage, while still presenting an adequate output impedance level to the individual element.

The subarray rows are self-clearing of short circuited diode faults by the fusing open of the one mil diameter gold bond wires in the packaged diodes under the combined short circuit current developed by 45 rectennas in parallel. The failed elements may be detected while operating by the increased reflected power at a VSWR probe over the element, or alternatively while the array is inoperative, by briefly individually illuminating each element while monitoring the dc output (termed "sniffing").

Overvoltage protection from loss of load, excessive RF input level or interruption of input, was accomplished in the Goldstone tests by the self actuated crowbar in Fig. 5. A voltage limiter would be less traumatic for the load than a crowbar however.

INSTRUMENTATION

Fig. 5 also shows the isolated load central element for a subarray, that is used to provide a measure of the input RF power flux density. An RF shielded thermistor is employed to measure the temperature of the central buss bar in the subarray. Calibrated shunts and precision voltage dividers

were employed to sample the output current and voltage levels. A fixed track, movable probe positioned in front of the subarray to measure the reflected power would be an expensive, but useful instrument to monitor the subarray performance under various operating conditions. It could be integrated into a sniffing and maintenance positioning assembly perhaps, that travels over the array surface.

SCATTERED FUNDAMENTAL AND RADIATED HARMONIC CHARACTERISTICS

Figure 6 shows a 42 element rectenna array undergoing pattern recording of its emitted harmonics as a function of various operating parameters. Figures 7 and 8 show the measured harmonics and the scattered fundamental patterns for certain conditions. These patterns are typical for a wide range of parameters. The significant facts are that the scattered fundamental is distributed over a broad range of angles, and that the fourth harmonic is of higher magnitude than the third harmonic. The array was underexcited due to equipment limitations, with the peak RF to dc conversion efficiency being only 35%, however the results are expected to be applicable to a normally functioning array. Future designs will probably require more filtering of harmonics in order to control them and permit the array to meet applicable radio regulations (Ref. 5). The scattered fundamental frequency radiation may be controlled to a degree by varying the dc load value, the incident flux density level, or the dipole to ground plane spacing, each of which affects the impedance match of the array, and thus provides a potential parameter for control of the reflected fundamental magnitude. Figure 9 shows the variation in efficiency and dc power output for a particular subarray as the spacing is varied.

The RF frequency could also be varied to effect an impedance match. Figure 10 shows the bandwidth measurements for the 42 element array for two different illumination conditions. Such a design characteristic would have to be integrated with the harmonic filter design also.

CONCLUSIONS AND RECOMMENDATIONS

Adequate theory and design information exists that has been compared with full scale measurements, to provide engineers and systems analysts with the characterization of rectennas performance to within the order of a couple of percent. Particularly for high power level of incident flux density applications. The data for scattered fundamental and emitted harmonics could use some theoretical modeling to gauge the preliminary measurements. Also, bandwidth analysis and modeling for degraded modes such as partially obscured apertures and inadequate maintenance or repair need to be undertaken to round out the rectenna complete characterization.

Refinements such as automatic feedback control of rescattered fundamental by changing the ground plane spacing or load, frequency, or incident power density should be studied to evaluate their effectiveness and life cycle cost in meeting applicable radio regulations.

It should be stated that the above conclusions are based principally on measured results of half wave dipole arrays, and some of the conclusions are applicable to other elements such as yagis, only if the same array characteristics can in practice be achieved. The stipulation applies to any high gain element array.

Better harmonic filtering and active dc load management within a tapered density array along with an efficient and effective overvoltage limiter need to be developed, along with rapid repair techniques also. Long life environmental protection is still a continuing requirement for certain applications, along with light weight and waste heat dissipation for space and high altitudes.

REFERENCES

1. Dickinson, R., and Brown, W., Radiated Microwave Power Transmission System Efficiency Measurements, Technical Memorandum 33-727, Jet Propulsion Laboratory, Pasadena, California, May 15, 1975.
2. Dickinson, R., Evaluation of a Microwave High-Power Reception-Conversion Array for Wireless Power Transmission, Technical Memorandum 33-741, Jet Propulsion Laboratory, Pasadena, California, September 1, 1975.
3. Nahas, J., "Modeling and Computer Simulation of a Microwave-to-dc Energy Conversion Element," IEEE Trans. Microwave Theory Tech., Vol. MTT-23, No. 12, December 1975, pp. 1030-1035.
4. Brown, W., "Optimization of the Efficiency and Other Properties of the Rectenna Element," 1976 IEEE MTT-S International Microwave Symposium Digest of Technical Papers, pp. 142-144.
5. Edition of 1976 Radio Regulations Published by the General Secretariat of the International Telecommunications Union, Geneva, 1976.

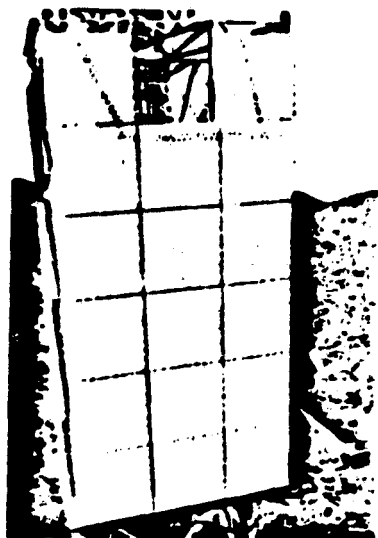


Fig. 1. The RXCV Array

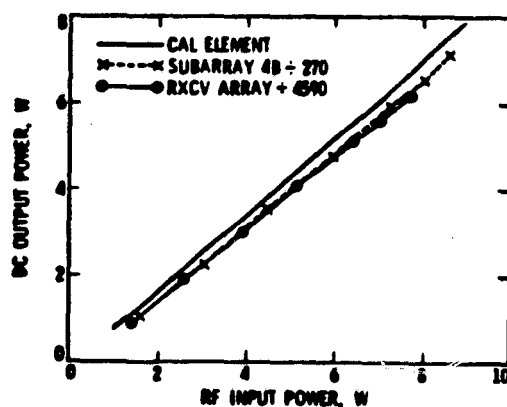


Fig. 4. Transfer Efficiency Performance Comparison

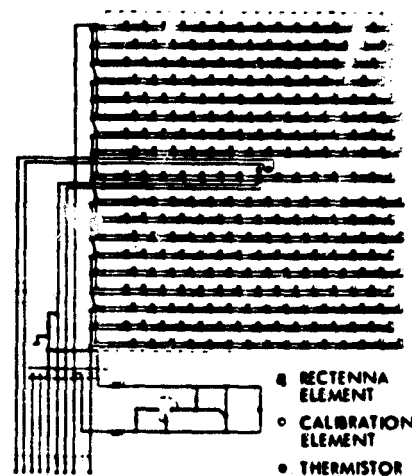
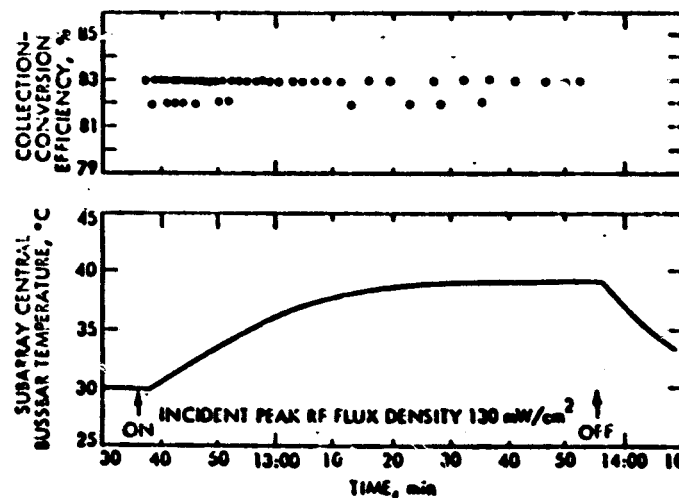
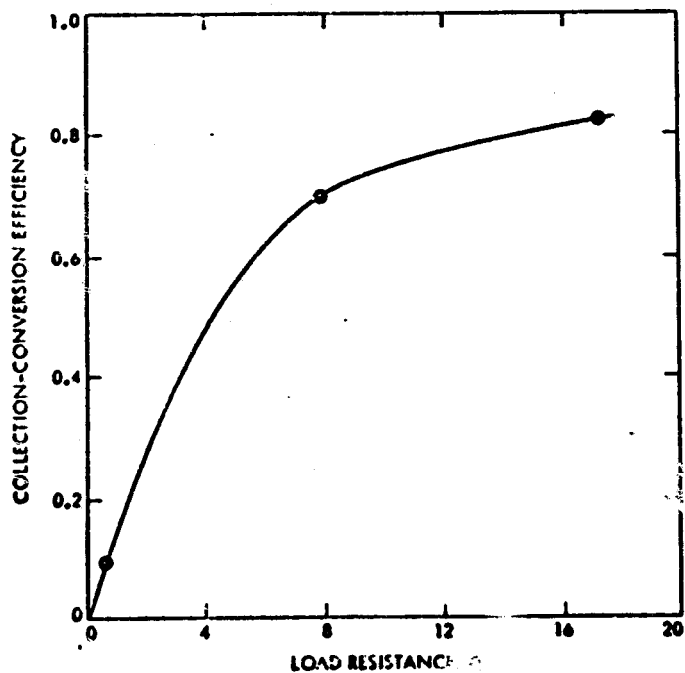
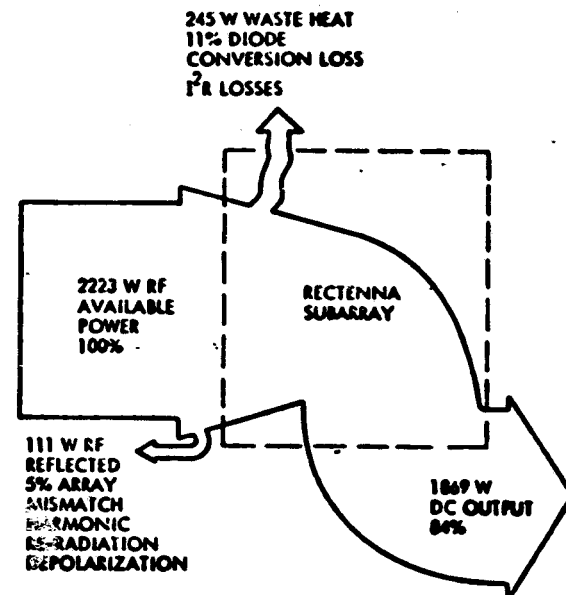
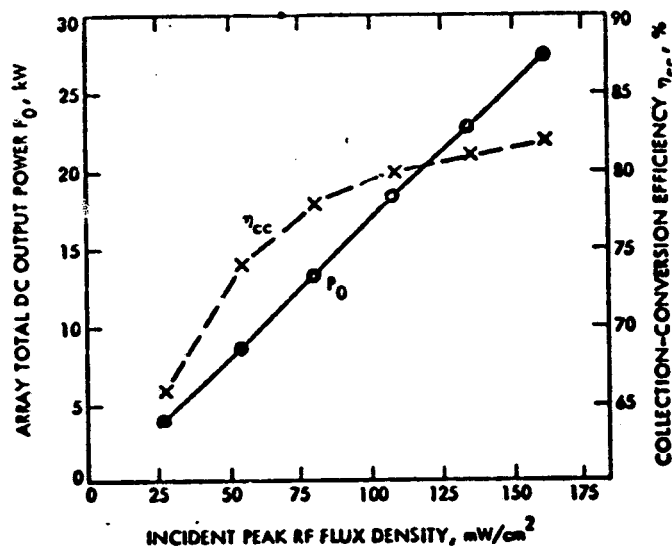
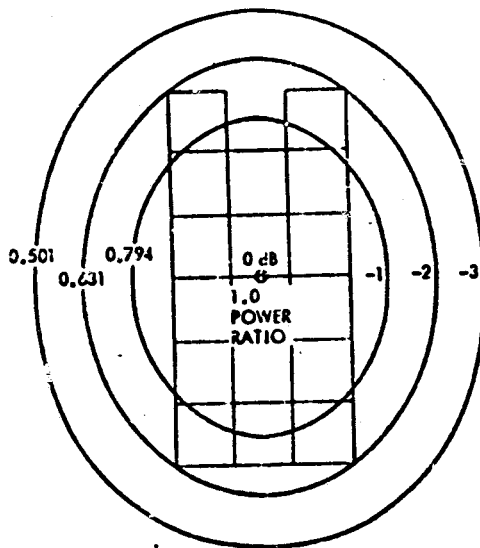


Fig. 5. Subarray Wiring Diagram

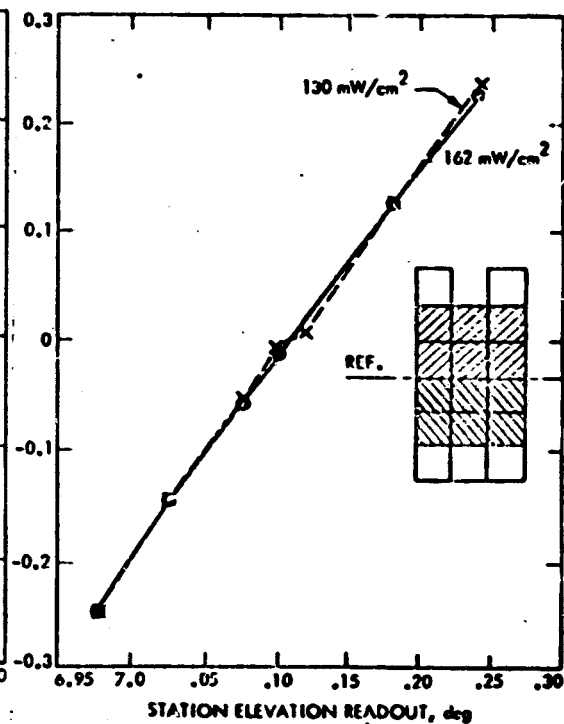
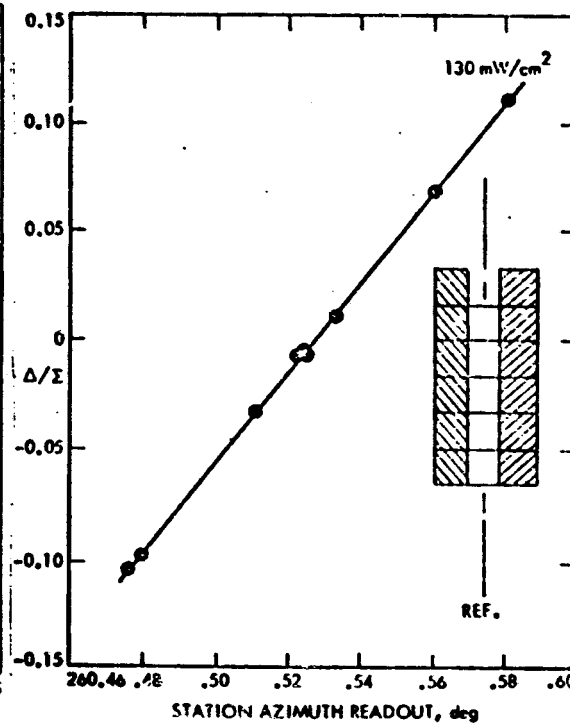
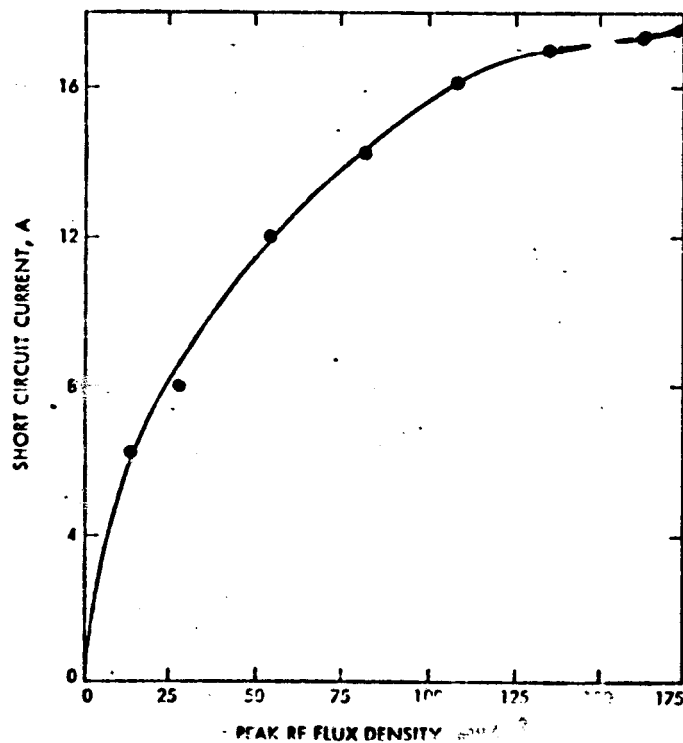
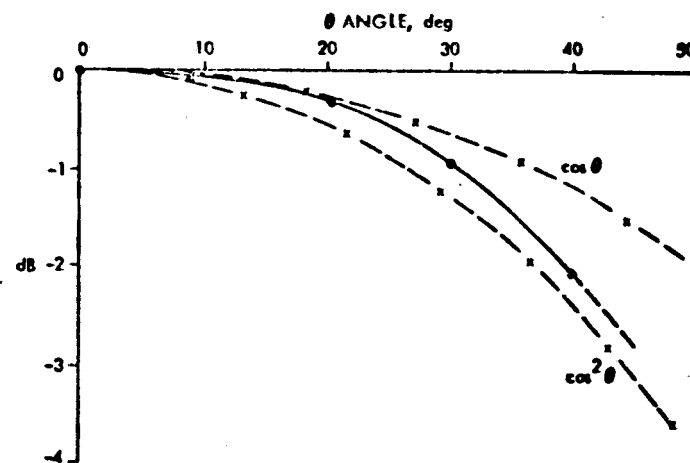
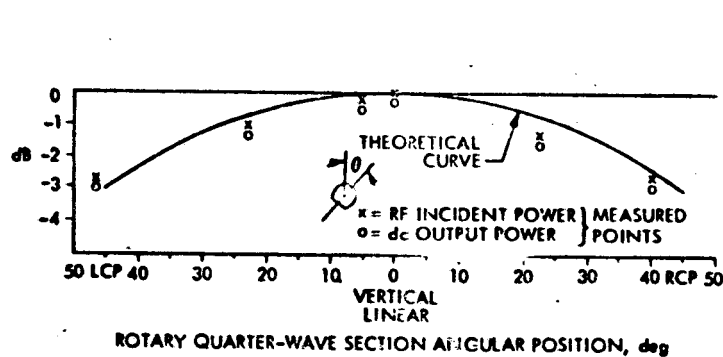


MICROWAVE RECEPTION-CONVERSION ARRAY PERFORMANCE I



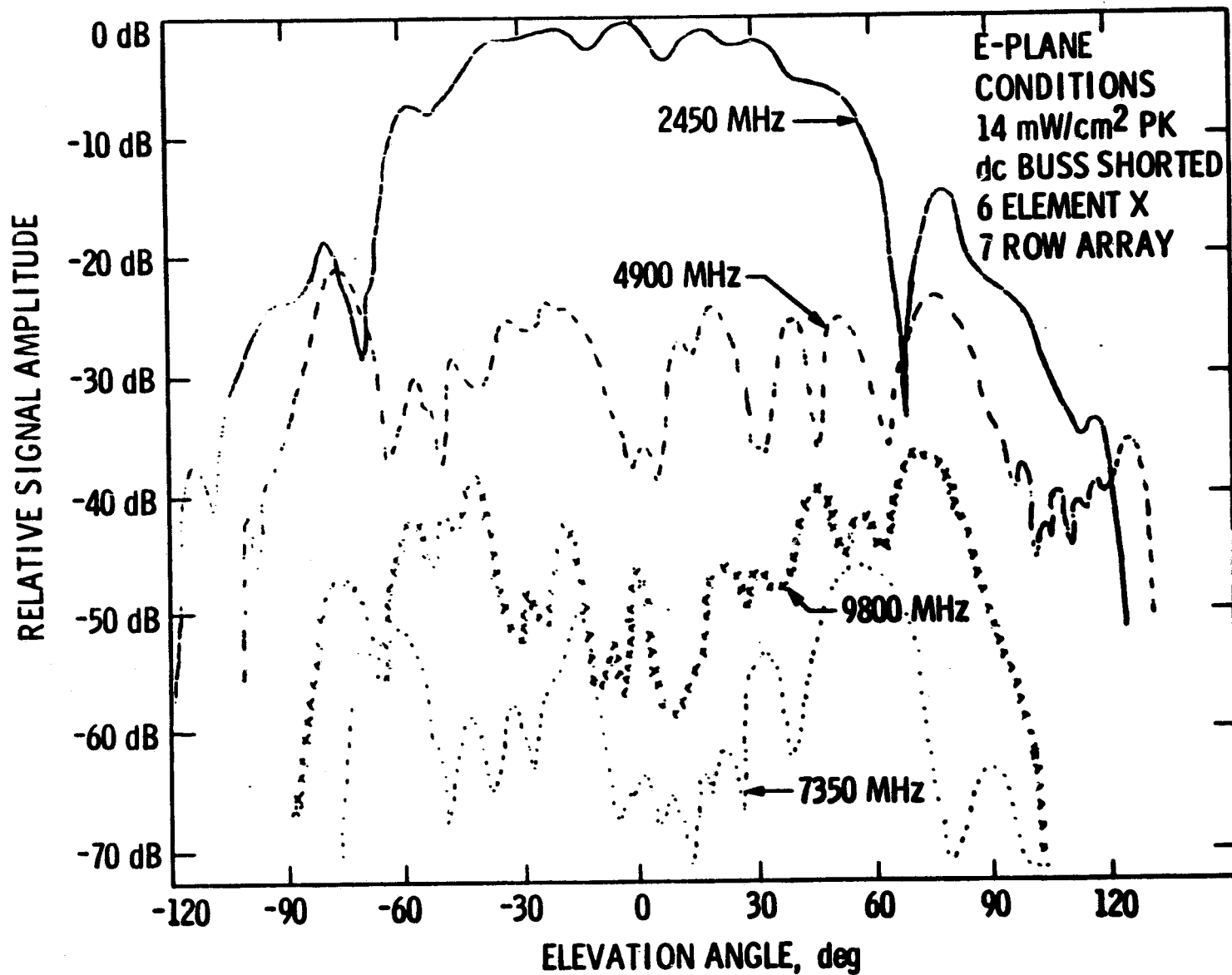


MICROWAVE RECEPTION-CONVERSION ARRAY PERFORMANCE II





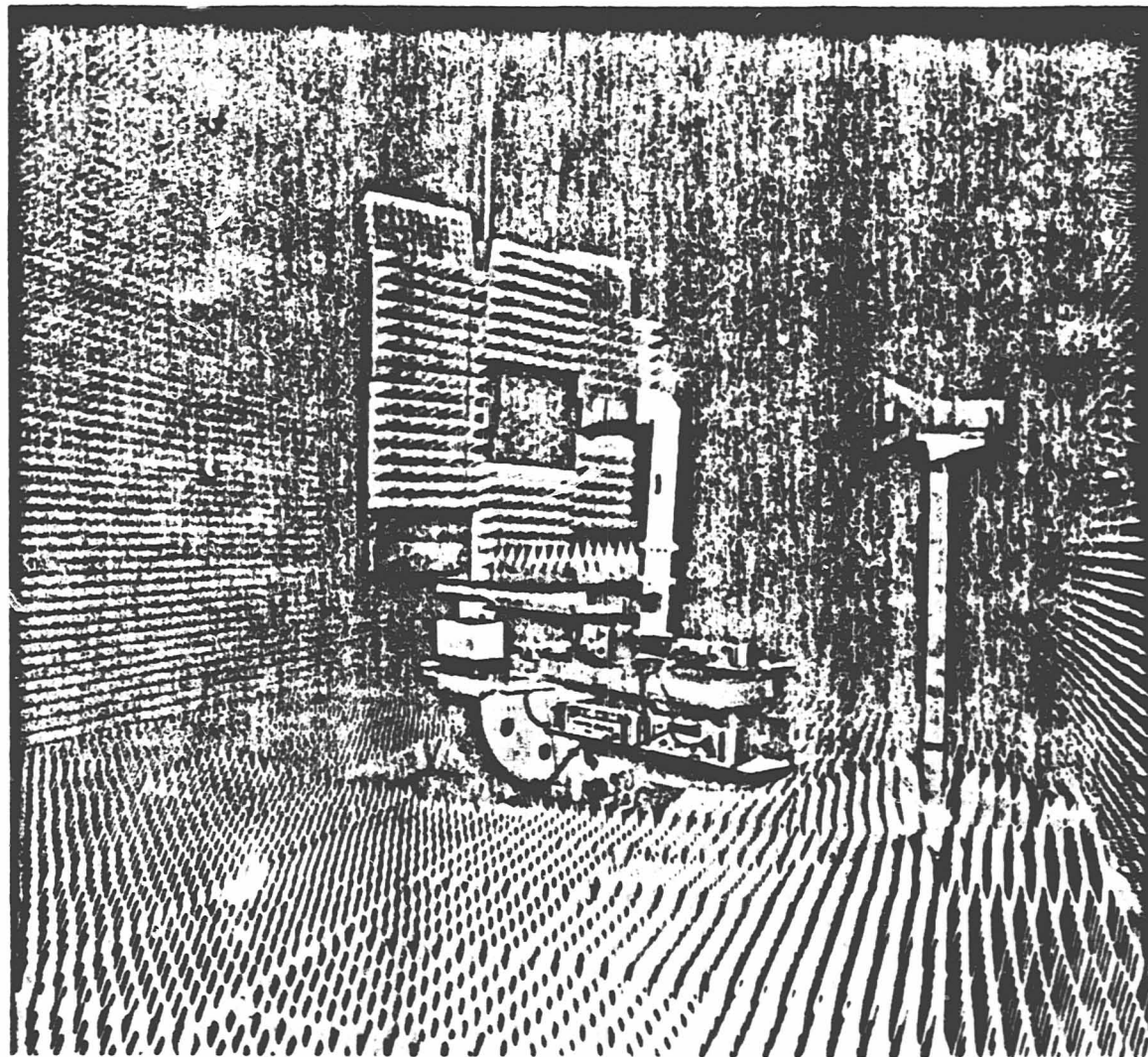
BEAMED RF POWER TECHNOLOGY RECTENNA RESCATTER AND EMISSIONS





BEAMED RF POWER TECHNOLOGY

RECTENNA SUBARRAY FUNDAMENTAL SCATTER & HARMONIC EMISSION RADIATION PATTERNS



ORIGINAL PAGE IS
OF POOR QUALITY

R. M. DICKENSON

SPS ASSESSMENT REVIEW

JUNE 1979



BEAMED RF POWER TECHNOLOGY

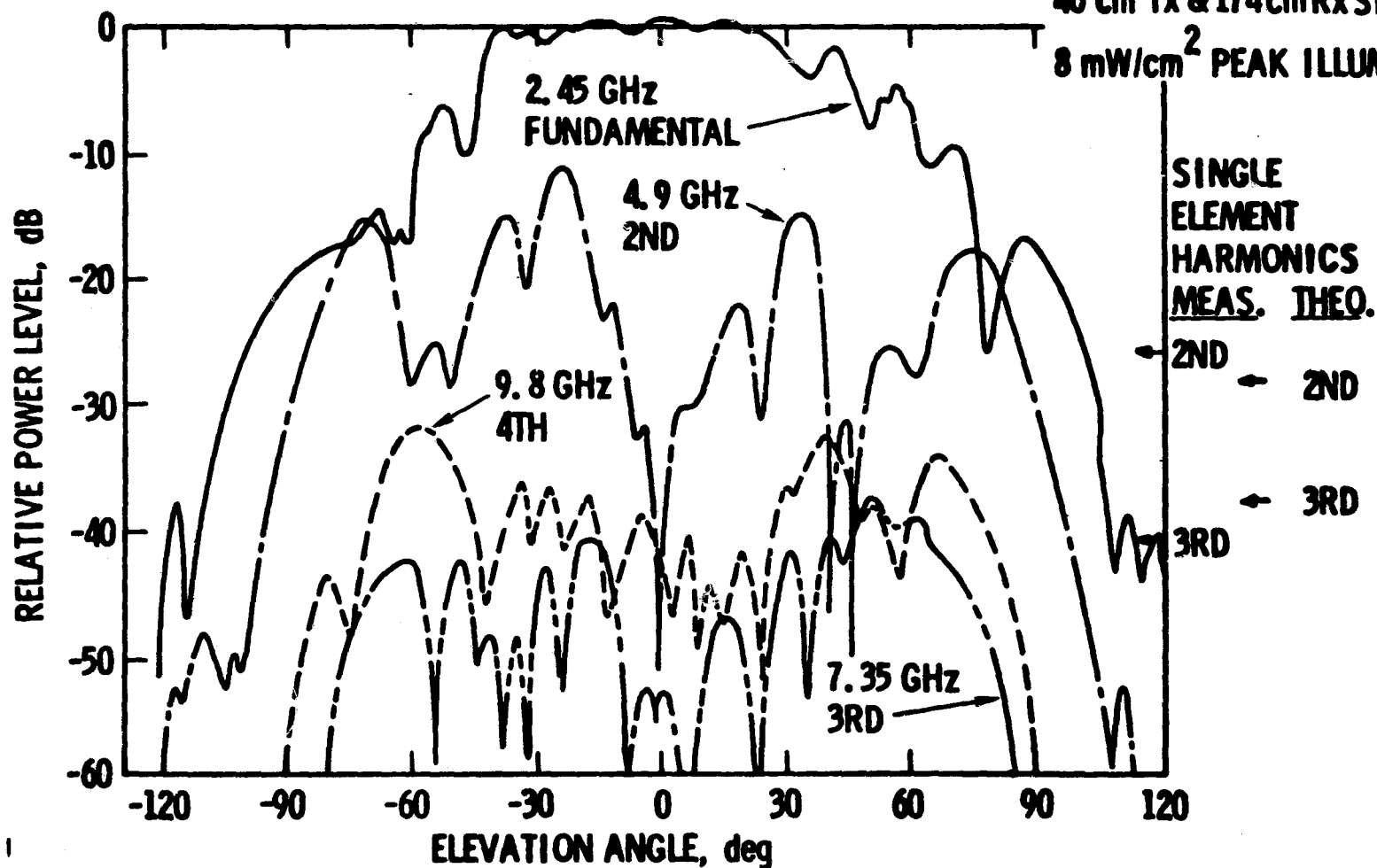
RECTENNA RESCATTER AND EMISSIONS

E-PLANE CONDITIONS

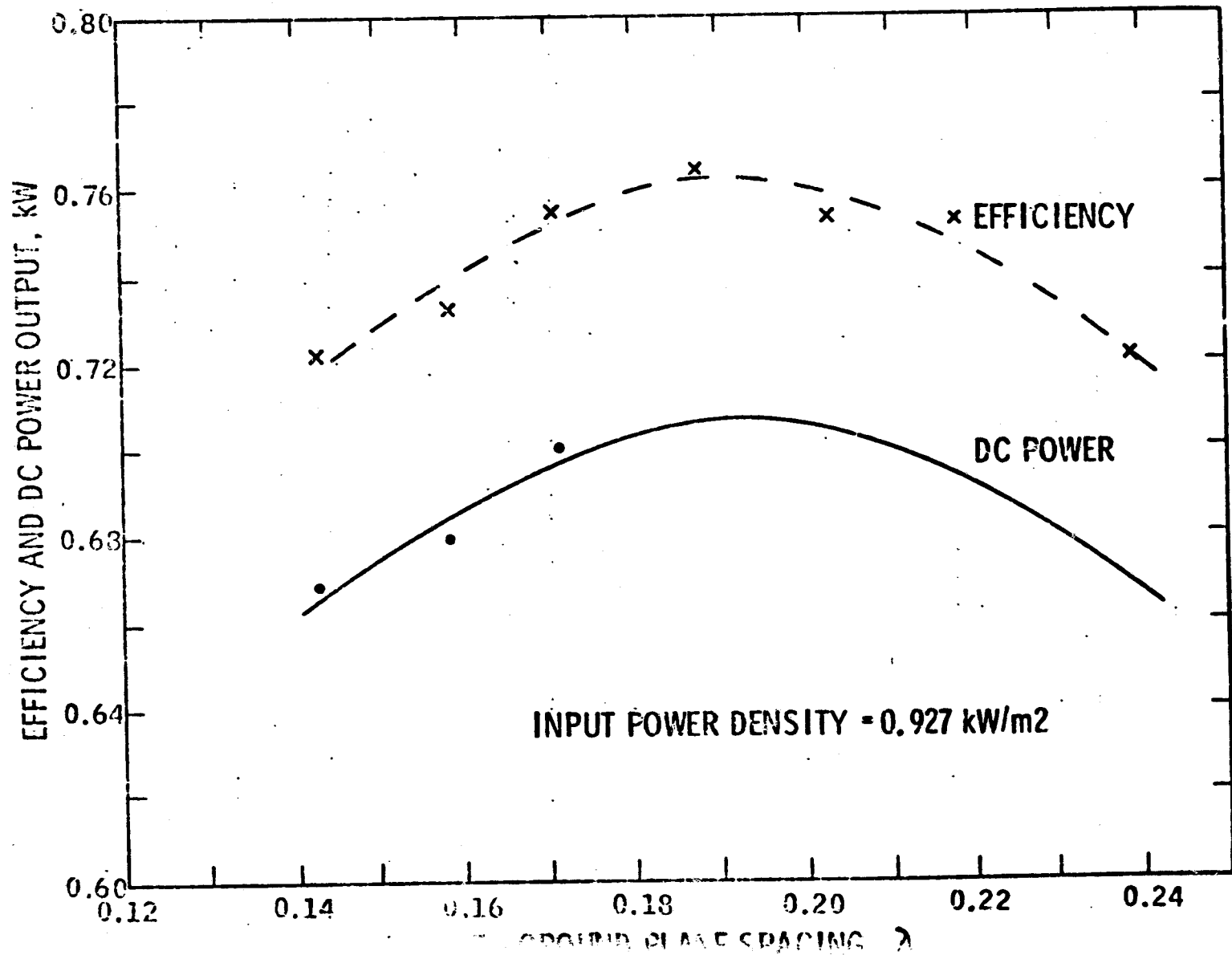
$R_L = 15 \Omega / \text{ROW } 6 \times 7 \text{ SUBARRAY}$

40 cm Tx & 174 cm Rx SPACING

8 mW/cm^2 PEAK ILLUMINATION



POWER OUTPUT AND EFFICIENCY VS GROUND PLANE SPACING



SOLID STATE CONFIGURATIONS SESSION

MICROWAVE POWER
TRANSMISSION SYSTEM
WORKSHOP

SESSION ON SOLID STATE

INTRODUCTION

"Why should we study a solid state SPS" is a valid question and one that we do not have a complete system answer for at this time. The first chart is an attempt to list some of the reasons a solid state SPS should be investigated. Solid state is no magical solution to SPS designs but it does attack three very important aspects of SPS - the potential for low cost through mass manufacturing techniques that are well established, reliability, and essentially maintenance free operation. Solid state was not considered in the original Raytheon study for LRC in 1975 on the microwave system. Low efficiency and power levels of a kilowatt or larger made them unattractive for SPS. NASA decided to investigate the possibility of a solid state design that incorporated a much lower device power requirement. A design was developed requiring 120W devices or amplifiers which appeared more reasonable but still very difficult for S-band.

The next step was to determine if solid state devices could potentially be highly efficient. An analytical approach was selected to investigate this potential. Dr. Roulston of Waterloo University performed the analysis and indicated there were no fundamental limitations on the efficiency of solid state devices. Further study by the systems contractors and NASA has produced two concepts that will be given a more detailed systems analysis. These concepts produced amplifier power requirements of 5 to 30 watts. One concept simply substituted a solid state

antenna for the reference Klystron antenna. The other concept produced an entirely new SPS conceptual design and was called a solar cell solid state sandwich design. Both of these designs will be discussed by other summaries in this section. However, it should be noted that all solid state designs have thus far been characterized by larger antennas, smaller rectennas, and less delivered power than the SPS reference concept. There is no solid state reference concept at present because of the systems analysis on solid state concepts is not complete. Much data has been generated by numerous sources on the solid state concepts. The following summaries in this section are just representative of the study effort. Thus far Rockwell, Boeing, Raytheon and RCA have been directly involved in the solid state studies. The last two charts list the preliminary conclusions and issues related to this solid state study effort. Solid state continues to be a viable alternative to the reference Klystron concept and is included in the six year planning document (Ground Based Exploratory Development - GBED) now being finalized.

255

MSFC SOLID STATE ACTIVITY

WHY SOLID STATE

- o HIGHER RELIABILITY THAN TUBES
(- 10^6 HOURS VS. 10^4 HOURS)**
- o TECHNOLOGY BASE**
- o POTENTIAL FOR LOW COST**
- o SYSTEM COSTS OPTIMIZES AT LOWER POWER OUTPUT
AT UTILITIES (1.0-1.5 GW)**
- o POTENTIAL FOR REDUCING FRONT END COST**
- o MORE EASILY ADAPTABLE TO FLIGHT/GROUND TEST**
- o START-UP - SHUT-DOWN**

SOLID STATE CONCLUSIONS

1. Solid state SPS concepts have not had the same depth of systems definition as the reference concept; however, preliminary results indicate the following.
 - a. The system sizing parameters optimize such that lower power is delivered to the utility grid.
 - b. The transmit antenna is larger primarily because of the thermal limitations.
 - c. The rectenna land requirement is smaller.
 - d. Weight per delivered kilowatt is projected to be more.
 - e. Maintenance projections are better because of the higher reliability.
2. Type of Power Amplifier - Based on studies to date, the GaAs FET is the preferred solid state power amplifier.
3. Antenna Unit Costs - Solid state antennas will have high parts count similar to the solar array, and therefore unit costs are a critical item.
4. Mitigating Designs - Conceptual designs have to some degree mitigated the issues of thermal and low voltage power distribution.
5. Items of Concern - Techniques of phase distribution, (possibly to more points on the array), and power distribution (on the end mounted configuration more DC-to-DC converters are required) are major items of concern in the solid state concept.
6. Technology - Associated technology development is more likely for solid state due to the advancing technology base.
7. Continued Investigation - Based on current findings, continued investigation of solid state concepts and issues is warranted.

SOLID STATE ISSUES

- o Efficiency
- o Operating Temperature
- o Low Voltage Distribution
- o Harmonic Noise Suppression
- o Power Combining
- o Subarray Size
- o Monolithic Technology
- o Life Time
- o Mutual Coupling
- o Amplifier gain
- o Input to Output Isolation
- o Charge Particle and UV Radiation Effects

MODIFIED REFERENCE SPS WITH SOLID STATE TRANSMITTING ANTENNA

G. R. Woodcock, B. R. Sperber, Boeing Aerospace Co.

1.0 INTRODUCTION

The motivations for considering solid state microwave power amplifiers for the solar power satellite transmitting antenna have been the possibilities of greatly increased system reliability due to elimination of electron tube cathodes, a lower mass per unit power and transmitting array area due to the high power densities obtainable in semiconductors (the active region of a power GaAs FET has a power density exceeding 10^{15} W m^{-3} !), and, probably, cost savings due to development of small hardware items that can be handled by individuals instead of organizations.

In order to provide a fair assessment of where we stand today with regard to solid state SPS technology, the design described here is close to that of the NASA/DOE reference and is implemented using today's solid state technology with only a small "push." The small push is raising the efficiency of DC-RF conversion from the .68 obtained by RCA in 1975 to somewhat over .8 of the solid state SPS. This is generally considered feasible by semiconductor industry representatives.

Other solid state SPS configurations can yield somewhat better performance. However, these generally do not provide as fair a vehicle for comparison with the reference and usually also incorporate somewhat more advanced technologies.

2.0 SOLID STATE MICROWAVE POWER AMPLIFIER TECHNOLOGY

Currently a wide variety of solid state devices suitable for use as microwave amplifiers exist. These include bipolar and field effect transistors, many types of two-terminal devices (tunnel, Gunn, IMPATT, BARITT and TRAPATT diodes) and electron bombarded semiconductors (EBS). (EBS have been included as being solid state since the electron beam only supplies a small control current, with the bulk of the supply current staying in the semiconductor.) For those active devices with over two terminals, there are several classes of circuit configurations that the active devices may be used in. Finally, there is a growing number of commonly used solid state materials out of which components may be fabricated, using several types of process at each step of the fabrication.

State of the art power-added efficiency, gain and single device power as a function of frequency for various types of CW microwave output solid state devices are shown on Figures 1 through 3. As technology evolves the curves will move towards the upper right-hand corners of the graphs.

Given the results of Figure 1, it would appear that there is no hope of achieving efficient solid state DC-microwave conversion in the near future. All the two terminal devices have efficiencies less than .36, which is so low as to make their use for SPS impractical. Most of the three terminal devices are not much better. However, in the case of three-terminal devices, the classes of amplifiers presently used (Classes A and B for GaAs FETs and Class C for bipolar transistor amplifiers) inherently limit their efficiency. Other classes of amplifiers, summarized on Figure 4, can have efficiencies approaching unity.

In fact, to achieve the desired efficiencies of .8 or greater requires that the devices be used in "switched mode" types of amplifiers, which attain high efficiency by minimizing the I-V product time integral over the operating cycle. This generally requires device switching times about a factor of ten less than the RF period. Experimental amplifiers with efficiencies of over 90% have been built at frequencies above 100 MHz. NASA-sponsored microwave amplifier studies have recently been initiated to determine the feasibility of high efficiency at microwave frequencies.

Because of the many high frequency components in the waveforms characteristics of fast switches, efficient switching amplification devices must have large bandwidths. This leads to different device noise properties than those at the narrowband SPS reference system klystron tubes. While the switching amplifiers do have frequency selective output circuits that transform the switched waveform into a sine wave, these will not be nearly as selective as a 5-cavity klystron. However, the solid state design will benefit due to its small module size giving a larger ground footprint than that of the larger klystron module.

Achieved device gains vs frequency are shown on Figure 2. There is a striking difference between small-signal and power gain for FETs. At the SPS frequency of 2.5 GHz bipolars have about 8 db gain while GaAs FETs yield around 10 db. In general, GaAs FETs have several db more gain than bipolars throughout the spectrum. As for the other devices, IMPATTs can have gains of over 20 db and electron beam semiconductors are projected to yield about 20 db. The low gain of Static Induction Transistors (SITs) at 1 GHz eliminates them from consideration at present, although they appear to have great potential for further development due to their high power bandwidth product.

The power per device is an important SPS parameter since the number of devices which can be efficiently combined in a module is limited by circuit losses and the power per module determines the RF power density per unit transmitting array area. The single device power chart (Figure 3) shows that silicon bipolar transistors, GaAs FETs and multi-mesa IMPATTs can all handle powers above 10 watts, which is an adequate power level for SPS application. Of the devices considered here, only E-beam semiconductor devices are capable of generating a power level of 100 watts per device which would be adequate for one device per radiating element. For the other devices, power combining will be necessary.

The fundamental failure modes in semiconductor devices are wearout failure modes that tend to be concentrated at surfaces, both internal and exposed, and are generally electrochemical in origin. In the case of the internal surfaces, transport of species to and away from interfaces eventually degrades contacts. In the case of external surfaces, impurities can come in from outside to form compounds and high electric fields can cause breakdown.

EBS cathodes presently have an expected lifetime of 2×10^5 hours, over an order of magnitude less than that required for a 30-year satellite, so they appear unsuitable. The two remaining solid state amplifier candidates are GaAs FETs and Si bipolar transistors. Si bipolar lifetimes are limited by electromigration of emitter finger metallizations due to localized high current densities. This gives relatively sudden and complete hard (open or short circuit) failures, whereas GaAs FETs seem to suffer from contact degradation which decreases performance gradually.

Of the three terminal devices, GaAs Field Effect Transistors (FET's) and Si-bipolar transistors provide approximately equal power capability at 2.45 GHz and appear potentially feasible for SPS use. GaAs FET's were selected as the preferred DC-RF conversion devices because they have higher gain than silicon bipolars, higher power added efficiencies, roughly equal power capabilities at 2.5 GHz and lower device metallization current densities leading to better expected reliabilities. GaAs FET's for SPS application could be fabricated separately and mounted in hybrid fashion or combined with other components on larger GaAs chips in integrated circuits. The latter alternative is preferred because of its significantly lower costs in mass production, although it does entail somewhat more development. For conservatism and in consideration of the fact that efficient "switched mode" amplifiers require gain at frequencies higher than the fundamental, the maximum single device powers in the solid state baseline design satellite were chosen to be 7.5 watts. For devices like this, a reasonable operating voltage is 15 volts.

A current small signal GaAs FET lifetime versus temperature curve is shown on Figure 5. There is currently no lifetime data on power GaAs FET's in the literature. When it appears, it is likely to be somewhat worse than Figure 5, but Figure 5 probably represents lifetimes achievable with development of the relatively new GaAs FET technology. It should be noted that solid state devices fail with log-normal statistics. Since the SPS failure criterion is loss of 2% the transmitting array with no maintenance, the mean time to failure required for the device is about a factor of ten more than the SPS life. Thus the average junction temperature for SPS GaAs FET's should be no higher than 140°C.

Figure 6 shows current and projected GaAs FET costs with an estimated 70% production rate improvement curve (i.e., units produced at the rate of $2n$ per year cost 70% as much as units produced at the rate of n per year). For the anticipated projected rates, the cost per unit power for GaAs FET's are nearly the same as the projected cost per unit power for klystrons. In practice, integrated circuits with several stages of driver amplifiers and other circuitry will be incorporated with the power amplifier. Since production costs are roughly equivalent to chip size and the output FET is anticipated to use approximately 70% of the total semiconductor area, the above cost estimates are adequate to first order.

3.0 SOLID STATE ANTENNA MODULE INTEGRATION

Cost effective integration of the low power, low voltage solid-state devices into mass producible antenna array elements represents the prime challenge in solid-state microwave power transmitter design. The "natural" array element size of about a wavelength squared and radiative cooling considerations for the peak microwave density areas at the transmitting array center yield 11 devices per λ^2 at an anticipated 5.5 kW m^{-2} radiated microwave power per unit area. For central array modules of the modified reference solid-state SPS both a small module size and combining of several devices were used to get the 4-FET $.6\lambda \times .6\lambda$ microstrip cavity combining module shown in Figure 7.

To avoid the power combining losses associated with circuit hybrids, the power from 4 solid-state amplifiers is combined by direct coupling of each amplifier's output to the radiating antenna structure. The resulting savings in transmitter efficiency range from 4% to 10%, depending upon the configurations being compared. The selected power-combining antenna consists of a printed (metallized) microstrip circuit on a ceramic type dielectric substrate which is backed by a shallow lightweight aluminum cavity which sums the power of four microwave sources. The antenna behaves like two half wavelength slot-line antennas coupled together via a common cavity structure. Feedback is taken from sampling probes in the module

cavity and used to correct for amplifier phase errors. This insures that the insertion phase of each module is identical even though the power amplifiers are fabricated to relatively loose (low cost) insertion phase requirements.

The modules are fabricated by starting with metallized (microstrip) 25 mil thick alumina dielectric cards which are attached to a 7.5 mil thick aluminum sheet metal carrier. A 7.5 mil thick stamped aluminum back plate is then attached, covering the substrate and all circuit components. This back cover defines the antenna cavity as well as shielding the otherwise exposed electronic components on the substrate. The high thermal conductivity of the aluminum components and of the alumina substrate allows the module's waste heat to spread to all surfaces as evenly as possible.

For the lower power density areas of the array an alternate dipole radiator module configuration is proposed. (See Figure 8.) This module design is approximately a third the mass per unit area of the 4-FET cavity radiator module because it has nearly no ceramic and significantly less metallization.

4.0 ANTENNA INTEGRATION

Variations of the basic cavity radiator and dipole radiator modules have been used to define a 1.42 km diameter transmitting antenna with a 9.54 db 10-step Gaussian taper similar to that of the reference SPS. Since its peak transmitted power per unit area is $\frac{1}{4}$ that of the reference satellite, its grid output power is half that of the reference, or 2.5 Gw.

Antenna quantization scheme specifications are summarized on Figure 9. There are seven basic module types of varying mass. As the 4-FET cavity radiator and 2-FET dipole module powers are reduced the module masses may also be reduced by removing superfluous metal not required for lateral thermal conduction. The 2-FET cavity radiator can also take advantage of reduced dielectric mass. No claim is made that these designs are optimized; they represent hopefully conservative estimates for likely module configurations.

To reduce I^2R power bussing losses the 15 volt modules must be connected in a series-parallel arrangement. The connection hierarchy selected for the $(.6\lambda \text{ by } .6\lambda)$ cavity radiator modules has four modules in parallel to form units called rows. Twelve rows are connected in series to form strings. Three strings in parallel make up a panel, which is the least replaceable unit. One hundred forty-four panels in a 12×12 series-parallel matrix form subarrays of the same size $(10m \times 10m)$ as in the current baseline, with a subarray voltage drop of 2.16 kv. Two subarrays are connected in series to give a 4.32 kv distribution voltage.

In the case of subarrays using the slightly larger $(.6\lambda \times .8\lambda)$ dipole module the hierarchy is the same except that the rows only have three modules in parallel.

A reliability assessment of the described cavity radiator module subarray hierarchy as a function of probability of amplifier failure, Q , is summarized in Figure 10. In case only one amplifier failure per row is permitted, string failures will cause 2% rf power reduction (with 50% probability) in 22 years for an amplifier MTBF of 3.5×10^6 hours. The random failures at this time cause an additional 0.8% of amplifiers to have failed so that the total rf power reduction at this time is 2.8%. If two amplifier failures per row are allowed, the power loss due to string failures of 2% and random amplifier failures of 3.2% together

result in a subarray power loss of 5.2% after 63 years. These results indicate that, for the SPS requirement of less than 2% rf converter failures in a 30 year period, the objectives of maintenance-free operation are achievable. This provides encouragement for further effort to address the issues of series-parallelizing such large strings.

An additional reliability feature beyond those considered in the assessment of all the module designs for string protection is the use of an external high temperature resistor which is shunted in to dissipate the nominal module power when the power amplifier in a module becomes open-circuited. By making the resistors small filaments a visual indication of failure is provided.

Although the failure reliability aspects of the above series-parallel configuration appear workable, other valid questions remain. The modules each have separate inputs that must be kept from coupling to neighboring outputs over the power supply lines. This is believed feasible but has not yet been experimentally demonstrated. Also, in a real system startup and shutdown transients are experienced. There must be kept from "rattling around" in the series-parallel matrix and selectively blowing out modules. Protection against these transients is believed assured if all the modules present similar impedances to the power line and have some over-voltage protection.

5.0 SATELLITE CONFIGURATION

A trade study done to decide on the preferred power distribution system to the 4.32 kv subarray pairs from the solar array compared directly bussed DC, high voltage AC and high voltage DC with DC-DC convertors. The results are shown on Figure 11 in the form of conductor and power loss make-up array mass as a function of conductor temperature. Direct DC won out despite a low power bussing efficiency of .73. However, it should be noted that should power convertor technology improvements result in 25% power convertor mass reductions, high voltage DC with DC-DC convertors would be the preferred option.

Satellite efficiency and sizing, done in a fashion similar to the NASA/DOE reference SPS design, clearly shows the impact of the buss losses on Figure 12.

The completed 2.5 GW modified reference SPS configuration is shown on Figure 13. The technology of the non-microwave subsystems is the same as the reference except for elimination of the antenna yoke by using linear actuators between the antenna edge and the rotary platform and the use of a pentahedral main satellite bay structure. Both changes reduce satellite mass somewhat.

Figure 14 gives a mass and cost summary. Total mass per unit transmitted power is up 30% from the reference because of DC bussing and DC-microwave conversion inefficiencies, with costs tracking. A second pass through the design, concentrating on increasing power bussing efficiency to achieve mass reductions, might reduce this difference but it is unlikely to erase it.

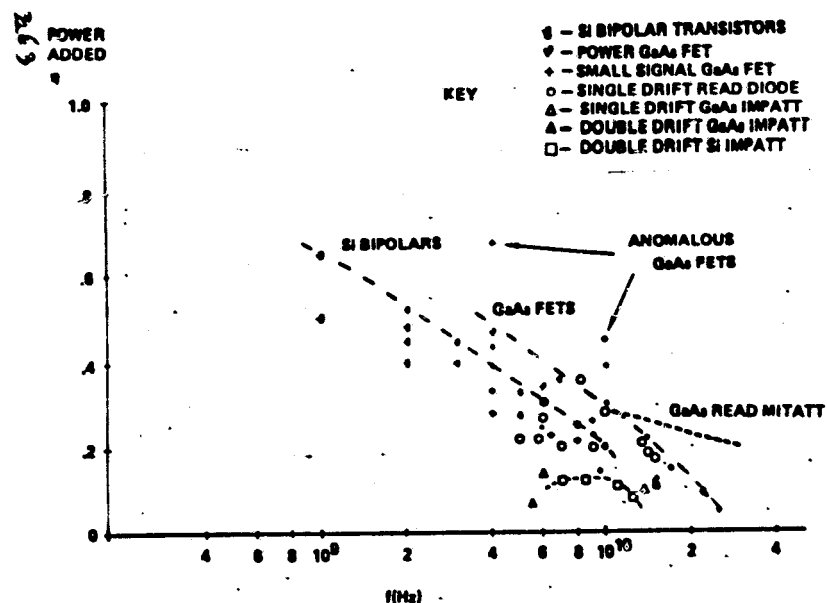


Figure 1. CW Solid State Device Efficiency vs Frequency—1978

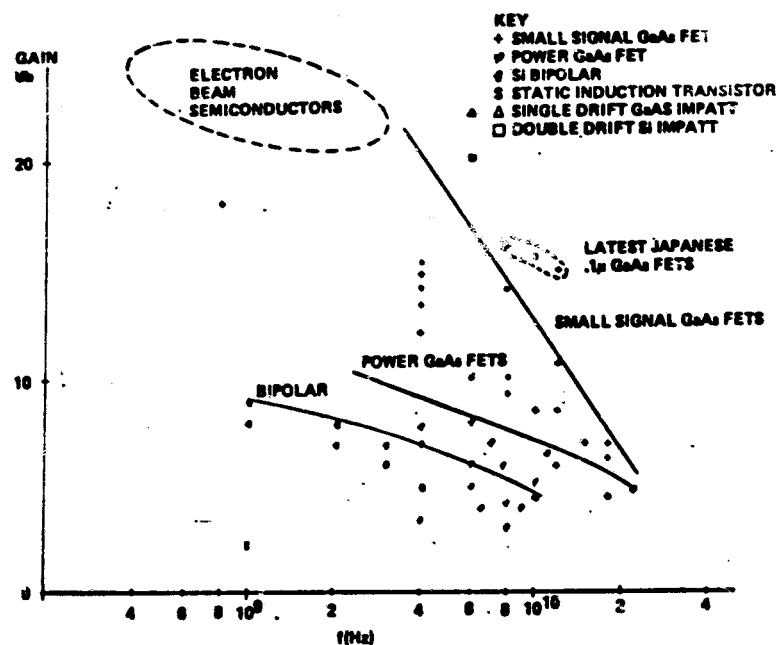


Figure 2. Solid State Device Gain vs Frequency—1978

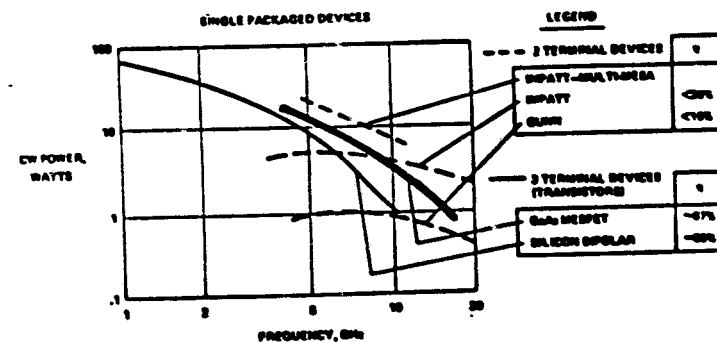


Figure 3. Solid State CW Power vs Frequency—1978

Figure 4. Characteristics of Various Amplifier Classes

Amplifier Class		Maximum Power-added Efficiency for Sine Wave Output	Typical Efficiency Values Achieved	@ Frequency	Duty Cycle at Maximum Efficiency	Active Device Saturated ?	Active Device Cut Off ?
Switched Mode Amplifiers	A	.5	.3	@ 1 GHz	1.0	No	No
	B	.785	.5	@ 1 GHz	.5	No	Yes
	C (Unsatuated)	.89%	.6	@ 2.5 GHz	.5	No	Yes
	D	1.0	.9	@ 10 MHz	.5	Yes	Yes
	E	1.0	.9	@ 100 MHz	.5	Yes	Yes
	F	1.0	.9	@ 10 MHz	.5	Yes	Yes
	S	1.0	.8	@ 100 KHz	Variable > 1	Yes	Yes
	Multivoltage	1.0	.8	@ 10 MHz	Variable	Yes	Yes
G	.818	.7	@ 100 KHz	Variable	Yes	Yes	

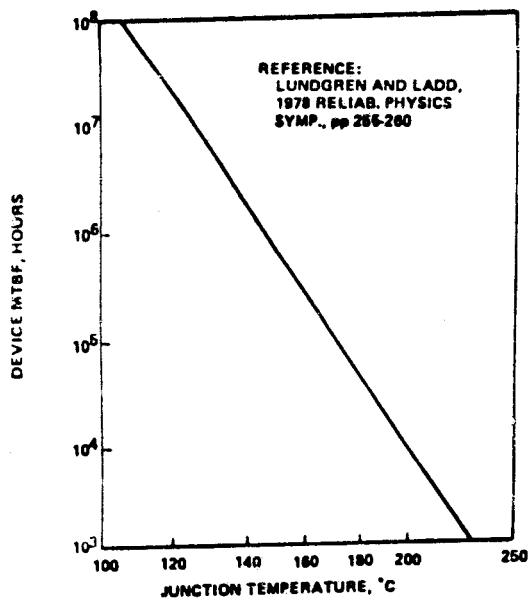


Figure 5. Small Signal GaAs FET Lifetime vs Junction Temperature

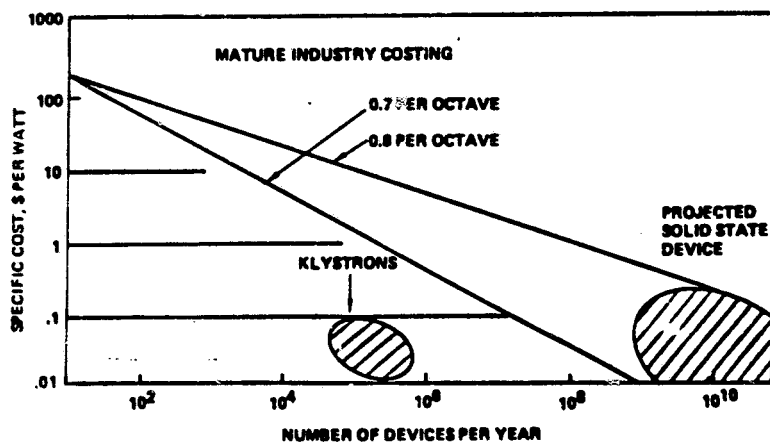


Figure 6. Projected GaAs FET Costs

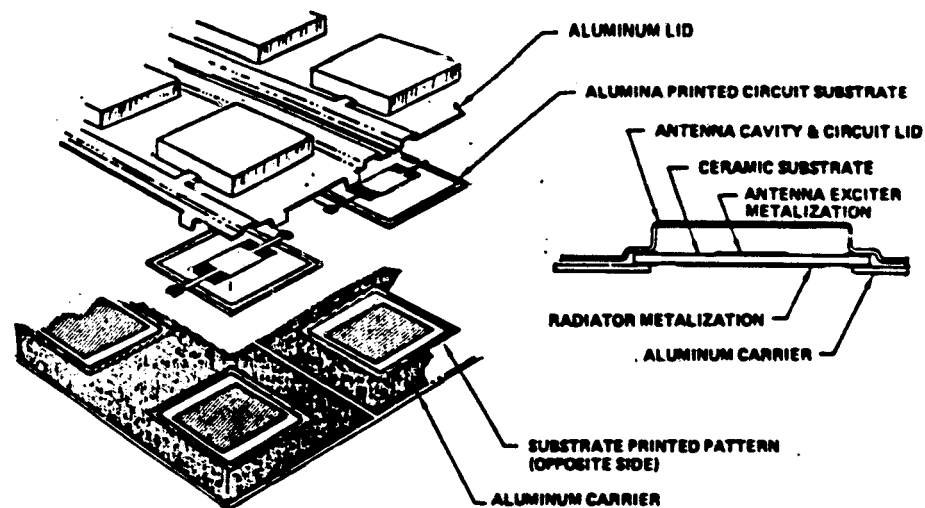


Figure 7. Solid State Combiner-Radiator Module

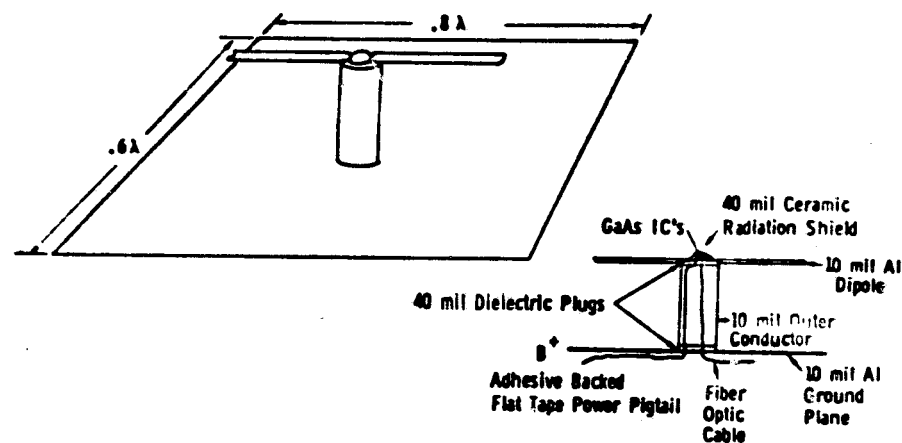


Figure 8. Solid State Dipole Radiator Module

STEP	OUTSIDE RADIUS (m)	STEP AREA (m ²)	NUMBER OF SUBARRAYS	MODULE TYPE	MODULE POWER (W)	(P/A) _{RF} (Kw/m ²)	(M/P) _{RF} (kg km ⁻¹)	STEP MODULE MASS (T)	NO. FETS (M)
1	124.8	48,970	456	High Power 4-FET, Cavity Radiator (4.06 kgm ⁻²)	28.7	5.50	.742	200	37.82
2	249.6	146,830	1,360	"	24.0	4.45	.917	600	112.80
3	322.4	130,820	1,208	Reduced Power 4-FET Cavity Radiator (3.58 kgm ⁻²)	19.2	3.56	1.006	468	100.20
4	384.8	138,640	1,280	"	16.0	2.97	1.207	496	108.17
5	457.6	192,680	1,784	2-FET Cavity Radiator (3.06 kgm ⁻²)	12.8	2.37	1.289	590	73.99
6	520.0	191,680	1,776	2 FET Dipole (1.47 kgm ⁻²)	12.8	1.78	.826	582	55.24
7	561.6	141,390	1,312	"	9.6	1.33	1.101	208	40.81
8	582.4	74,795	696	"	8.5	1.18	1.244	110	21.65
9	644.8	238,950	2,208	1 FET Dipole (1.47 kg m ⁻²)	6.4	.89	1.652	351	34.34
10	707.2	264,880	2,448	"	4.3	.59	2.476	389	38.07
TOTALS			14,528					3,694	621.09

Figure 9. Solid State Transmitting Antenna Quantization

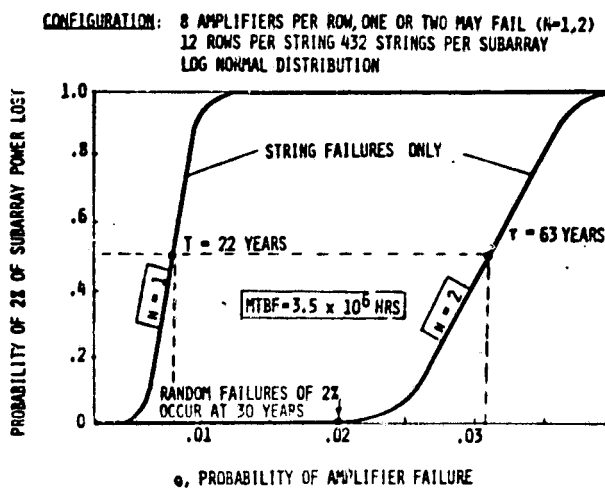


Figure 10. Solid State SPS Array Center Subarray Reliability

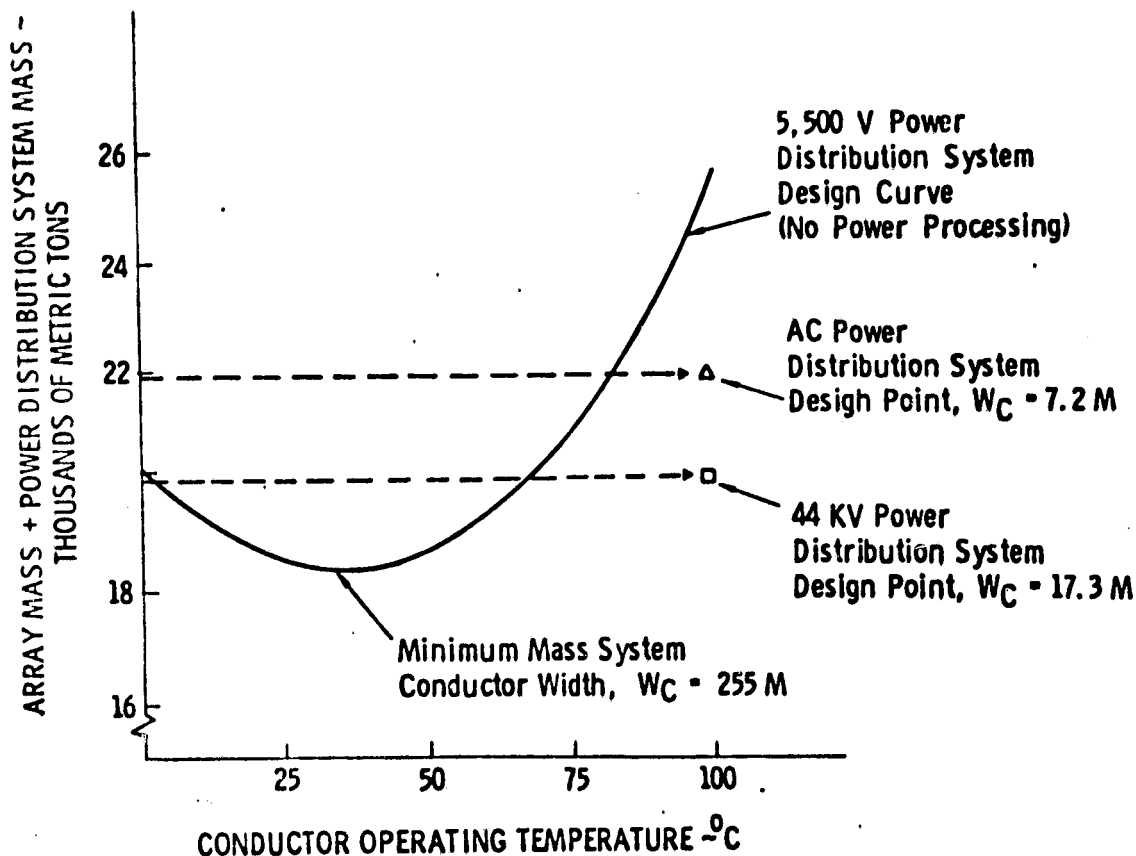


Figure 11. Power Distribution System Analysis

<u>ITEM</u>	<u>EFFICIENCY</u>	<u>MEGAWATTS</u>	
Array Mismatch			
Array Mismatch	.965	6050	Ideal Array Output
Main Bus I ² R	.729	5838	
Antenna Distr	.97	4256	Total Antenna Input
DC-RF Conversion	.8	4128	
Waveguide I ² R	N/A	3303	Total RF Radiated Power
Ideal Beam	.965	3303	
Inter-Subarray Losses	.976	3187	
Intra-Subarray Losses	N/A	3110	
Atmosphere Loss	.98	3110	
Intercept	.95	3048	
Rectenna RF-DC	.89	2896	Incident on Rectenna
Grid Interface	.97	2577	
	.413	2500	Net to Grid

TOTAL ARRAY OUTPUT 6050 MW
TOTAL SOLAR ARRAY AREA = 33.8 km²

Figure 12. Solid State SPS Efficiency and Sizing

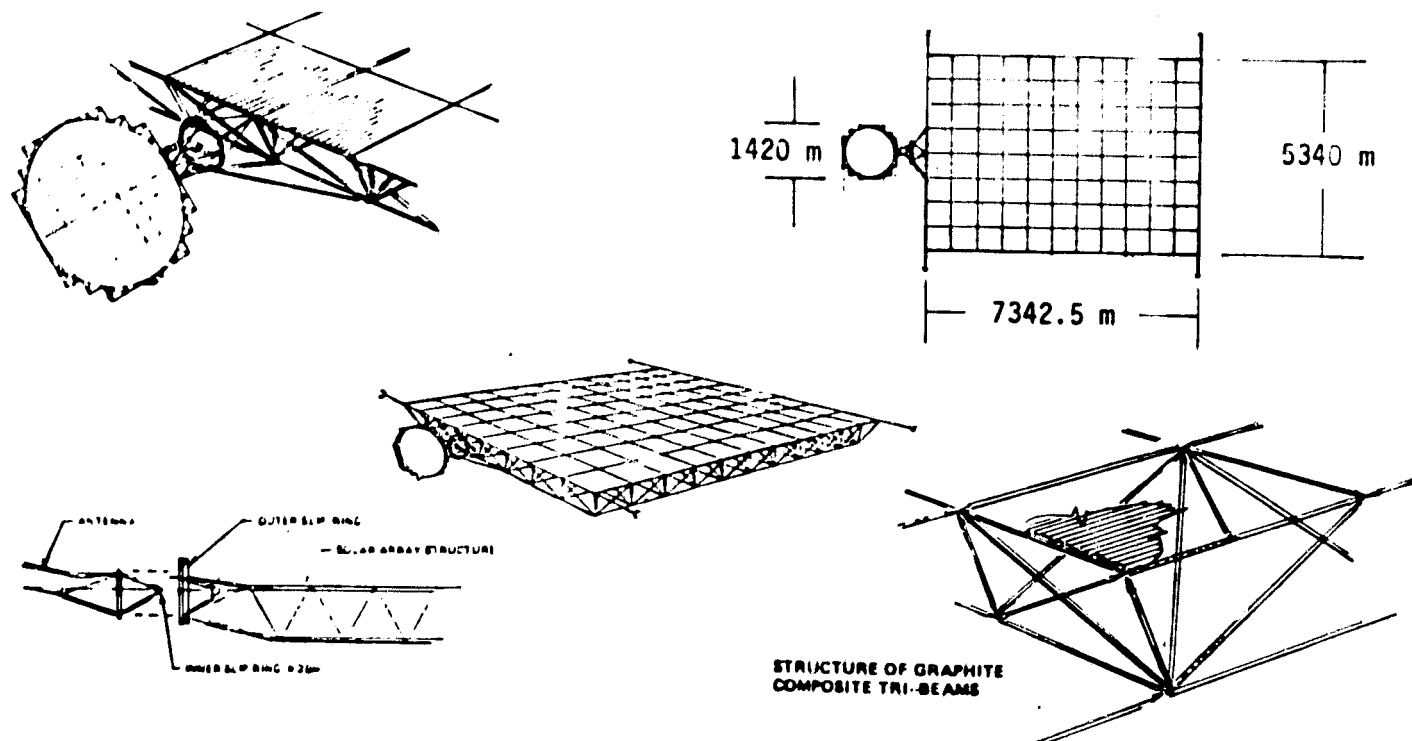


Figure 13. 2.5 Gw Solid State SPS Configuration

	MASS (MT)	ESTIMATING BASIS	(COST (\$M))
1.1 SPS	<u>35,204</u>		<u>4,541</u>
1.1.1 ENERGY CONVERSION	<u>22,087</u>		<u>2,350</u>
1.1.1.1 STRUCTURE	<u>2,851</u>	Detailed Estimate	<u>275</u>
1.1.1.2 CONCENTRATORS	(0)	Not Required	(0)
1.1.1.3 SOLAR BLANKETS	14,409	Scaled from Reference	1,355
1.1.1.4 POWER DISTRIB.	4,400	Detailed Estimate	530
1.1.1.5 THERMAL CONTROL	(0)	Allocated to Subsystems	(0)
1.1.1.6 MAINTENANCE	427	Scaled from Reference	190
1.1.2 POWER TRANSMISSION	<u>6,365</u>		<u>1,134.5</u>
1.1.2.1 STRUCTURE	<u>460</u>	Scaled from Reference	<u>38</u>
1.1.2.2 TRANSMITTER	4,480	Detailed Estimate	888.5
1.1.2.3 POWER DISTR. & COND.	1,262	Scaled from 1.1.1.4	124
1.1.2.4 PHASE DISTR.	25	Scaled from Reference	51
1.1.2.5 MAINTENANCE	20	Docking Ports Only	20
1.1.2.6 ANTENNA MECH. POINTING	118	Scaled by Mass x Area	13
1.1.3 INFO MGMT & CONTROL	145	Scaled from Ref.	73
1.1.4 ATT. CONT. & STA.KP.	<u>146</u>	Scaled From Ref	<u>110</u>
1.1.5 COMMUNICATIONS	<u>0.2</u>	Same as Ref.	<u>8</u>
1.1.6 INTERFACE	<u>113</u>	Est. Based on Simplification	<u>46.3</u>
1.1.7 GROWTH & CONTINGY.	<u>6,348</u>	Same % as Reference	<u>819</u>

Figure 14. Solid State SPS Mass and Cost Summary

SPS SOLID STATE ANTENNA POWER COMBINER

G. W. Fitzsimmons, Boeing Aerospace Company

1. INTRODUCTION

Solid state dc-rf converters offer potential improvements in reliability, mass and low voltage operation, provided that anticipated efficiencies in excess of 80% can be realized. Field effect transistors offer the greatest potential in the SPS frequency band at 2.45 GHz. To implement this approach it is essential that means be found to sum the power of many relatively low power solid state sources in a low-loss manner, and that means be provided to properly control the phase of the outputs of the large number of solid state sources required.

To avoid the power combining losses associated with circuit hybrids it was proposed that the power from multiple solid state amplifiers be combined by direct coupling of each amplifier's output to the radiating antenna structure. The resulting savings in transmitter efficiency ranges from 4% to 10% depending upon the configurations being compared. The selected power-combining antenna consists of a unique printed (metalized) microstrip circuit on a ceramic type dielectric substrate which is backed by a shallow lightweight aluminum cavity which sums the power of four microwave sources. The antenna behaves like two one-half wavelength slot-line antennas coupled together via their common cavity structure. A significant feature of the antenna configuration selected is that the radiated energy is summed to yield a single radiated output phase which represents the average insertion phase of the four power amplifiers. This energy may be sampled and, by comparison with the input signal, one can phase error correct to maintain the insertion phase of all solid state power combining modules at exactly the same value. This insures that the insertion phase of each SPS power combining antenna module is identical even though the power amplifiers are fabricated to relatively loose (low cost) insertion phase requirements.

The concept, illustrated in Figure 1, shows two solid state power amplifier modules with two outputs each at 5 watts delivering power to the antenna. The power amplifiers derive their input from an integrated circuit which performs the function of phase error correction so that each module has the same insertion phase. The phase error correction circuit employs two probes to sample the phase of the of the radiated power. This phase is then compared with that at the module input. A ceramic substrate is proposed to dissipate the heat of the power amplifiers via radiation. The high thermal conductivity of the ceramic substrate and of the aluminum cavity and ground plane will spread the heat so that all surfaces will participate in the cooling process.

The material that follows describes an initial program to verify the suitability of this concept for SPS. An appropriate microstrip antenna is being developed which will be evaluated when driven from four solid state power amplifiers.

2. EXPERIMENTAL VERIFICATION PROGRAM

The objective of the program is to demonstrate the suitability of a 2.45 GHz power combining microstrip slot-line antenna, when fed by four solid state

amplifiers, to the needs of a solar power satellite. The program entails the design and fabrication of a four feed microstrip antenna and a stripline antenna phasing network which will be integrated with four transistor amplifiers to demonstrate that the total solid state module (amplifiers plus antenna) will operate as an efficient power combining-radiating system. The antenna developed will be evaluated for gain, pattern and efficiency on the antenna range with and without the amplifiers. The amplifiers will be connected directly to the antenna without benefit of isolators so that their interaction via the antenna will be unimpeded. The combined output power of the amplifiers will be approximately 1/2 watt.

Figure 2 contains a sketch of the power combining microstrip antenna to be evaluated. The dielectric substrate is metalized on both sides. The underside, within the cavity, contains the four microstrip feed lines which are coupled to the two radiating slots on the top side via two narrow slotlines. In order to feed the antenna, two of the rf inputs are required to be 180° out of phase with the remaining two. An antenna feed network is thus required which will provide the four 0°-180° equal amplitude outputs.

The antenna feed network, the power amplifiers and the microstrip antenna will be connected as indicated in Figure 3a. The four cables connecting the amplifiers and the antenna are required to have equal electrical lengths as are the cables connecting the antenna feed network and the amplifiers. This is necessary to retain proper phasing of the antenna.

3. EXPERIMENTAL PROGRAM STATUS

3.1 FEED NETWORK

Three solid state antenna module feed networks have been assembled and measurements on all have been made. Two of the feed networks are needed to accomplish the antenna range tests. The stripline feed network, (Figure 4a), consists of two 0°-180° rat race ring hybrids fed by a single in-phase two-way power divider. The circuit metalization pattern was etched into the top circuit cover plate as a label for the finished feed. Figure 4b contains a photograph of the automatic network analyzer being used to measure the feed network performance.

The insertion loss and insertion phase measurements over a 500 MHz bandwidth indicate (Figure 5) that at the design frequency, the insertion loss of all ports is nearly equal. The insertion phase error window at 2.45 GHz is 1.5° wide, or $\pm .75^\circ$. The measured results for all feed networks at 2.45 GHz are as follows:

Serial No.	Phase Balance	Loss Balance	Insertion Loss	Isolation & Return Loss
001	$\pm .73^\circ$	$\pm .03$ dB	.154 dB	25 dB
002	$\pm .39^\circ$	$\pm .03$ dB	.189 dB	25 dB
003	$\pm .81^\circ$	$\pm .015$ dB	.172 dB	25 dB
GOAL	$\pm 1^\circ$	$\pm .05$ dB	.2 dB	20 dB

The measured insertion phase to all ports of each network deviate from a mean value by less than one degree, which was the design goal. The measured loss was less than 0.2 dB for each of the units over and above the 6.02 dB that results from the four way power division. This value will be used again when the antenna efficiency is calculated. A more important parameter is loss balance, which is so small that it is hardly measurable ($\pm .03$ dB). Thus, the power delivered to all ports is within 0.7% of the mean value.

The isolation between the feed network output ports is greater than 25 dB for all units. This minimizes the interaction between amplifiers in the final configuration, by preventing reflected power from the input of each amplifier from reaching the input of one or more of the other amplifiers. Thus, the amplifiers are operated as if they were each driven from an isolated source. This is a particularly good operating procedure where one is primarily interested in how well the power combining antenna performs, and in how well the solid state amplifiers interact with each other within the antenna circuitry.

The impedance match realized at each port results in a VSWR < 1.12 , with a return loss greater than 25 dB. In actual operation, a low output VSWR and good isolation is only available if the input power to the feed network is derived from a well-matched source.

3.2 POWER AMPLIFIERS

The four 2.45 GHz power amplifiers have been supplied by Tron-Tech, Inc. of Eatontown, N. J. and, to date, have only been evaluated under small signal conditions. (Table 1) As can be seen, the amplifiers meet many of the specifications and are out on others. More tests are scheduled to determine how the amplifiers perform under the required drive condition needed to yield 1/8 watt of output power. Until these additional tests are completed, it is premature to speculate on the degree of suitability of the four amplifiers.

Table 1. AMPLIFIER SPECIFICATIONS & SMALL SIGNAL MEASURED VALUES

Parameter	Specification	Measured by Boeing (small signal)
Frequency	2.45GHz	2.45GHz
Power out @ 1 dB gain compression	+21 dBm	Not measured
Gain	6 dB min.	7.76 dB - 8.18 dB
Gain match	$\pm .5$ dB max.	$\pm .21$ dB
VSWR in:	2.5:1 max.	3.65:1 (one unit)
out:	1.5:1 max.	1.66:1 (two units)
Phase match	$\pm 5^\circ$ max.	$\pm 2.4^\circ$
Phase control	$\pm 10^\circ$ min.	$\pm 2^\circ$ by varying B^+ according to Tron-Tech.
Gain Control	by varying B^+	Installed separate loss cont. which yields ± 1.5 dB according to Tron-Tech.
Infinite VSWR save at full power		verified by Tron-Tech.

The amplifiers were specified to be fail-safe under conditions of infinite VSWR at all phases. This was required to insure that the amplifiers wouldn't fail during test. Such a failure would preclude the collection of antenna data with the amplifiers attached. Since the amplifiers are designed to operate Class A, the small signal data exhibited in Table 1 may not change very much under large signal tests.

3.3 RADIATING ELEMENT

A four feed microstrip antenna has been developed which appears suitable for the task at hand. It evolved through a series of steps which began with a microstrip to slot-line coupler and graduated from a single feed slot line antenna to a dual fed slot-line antenna and finally, the four feed design illustrated in Figure 3b. Figure 3b shows the metalization pattern (actual scale) on each side of the microstrip dielectric substrate. The four microstrip lines (shown shaded) cross under and couple their energy to the four narrow slotlines which transport the signal to the wide radiating slots (shown in black). The antenna substrate is 2.6 inches square and is backed by a 2.5" x 2.5" x 0.30" cavity, which couples the radiating slots together.

The antenna, when fed by the feed network described earlier, exhibits a bandwidth at the 15 dB return loss points of approximately 100 MHz. A preliminary pattern taken with the antenna on the range is shown in Figure 6. The peak gain as measured is approximately 8 dB; however, not accounting for 0.43 dB of feed network and cabling losses. The pattern is well behaved with the first sidelobes approximately 23 dB down. A second "cleaned-up" model will now be fabricated to initiate full range testing with and without the power amplifiers.

4. TEST PLAN

The primary purpose of the antenna range testing is to determine the efficiency of the four feed antenna with and without the amplifiers. The efficiency is derived by dividing the antenna gain G by the antenna directivity D . The antenna gain will be determined by a 3-antenna method in which antenna spacing is measured to better than 1/2%. This method is expected to yield gain accuracies of ± 0.3 dB.

The antenna directivity D is defined as the ratio of the peak radiated power to the average isotropic radiated power (average power radiated over the unit sphere). To arrive at the average isotropic radiated power, one must measure and total up the radiated power over the spherical surface with the unknown antenna at its center, and average that value by dividing by the number of measurements. Typically, a $2^\circ \times 2^\circ$ cell is employed which requires 16,200 measurements. The error associated with the directivity measurement is approximately $\pm .25$ dB.

The antenna feed system insertion loss will be measured on the automatic network analyzer (HP 8542B), which is periodically certified by Hewlett-Packard using standards traceable to NBS to an accuracy of ± 0.15 dB ($\pm 3.51\%$) for devices of low insertion loss. Thus, when the feed system insertion loss is

subtracted from the measured gain, the feed system measurement uncertainty will be added to the previously stated uncertainties. The RSS value of the combined efficiency is thus, $\pm \sqrt{(.30)^2 + (.25)^2 + (.15)^2} = \pm .42\text{db} = \pm 10\%$ Cross-polarized radiation for the SPS application is considered wasted power, and therefore, it will also be measured and included when determining the antenna efficiency.

With the basic antenna characterized for gain, pattern and efficiency, antenna range measurements will then be made with the solid state power amplifiers inserted and operating with a combined output power of approximately one-half watt. The measurement of interest is the difference between the range received power with and without the inclusion of the solid state power amplifiers. The difference should be equal to the gain of the amplifiers. This difference will verify the degree in which the antenna sums the available power of the four amplifiers. Pattern measurements will also be taken to compare with those taken without the power amplifiers. As a final test to verify the entire procedure, the integrated amplifier-antenna system will be tested for directivity and gain, and the overall efficiency will be calculated.

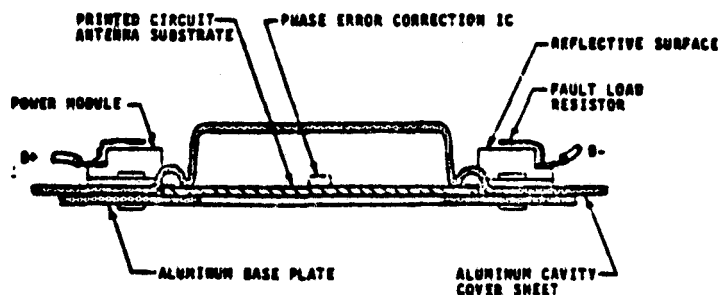
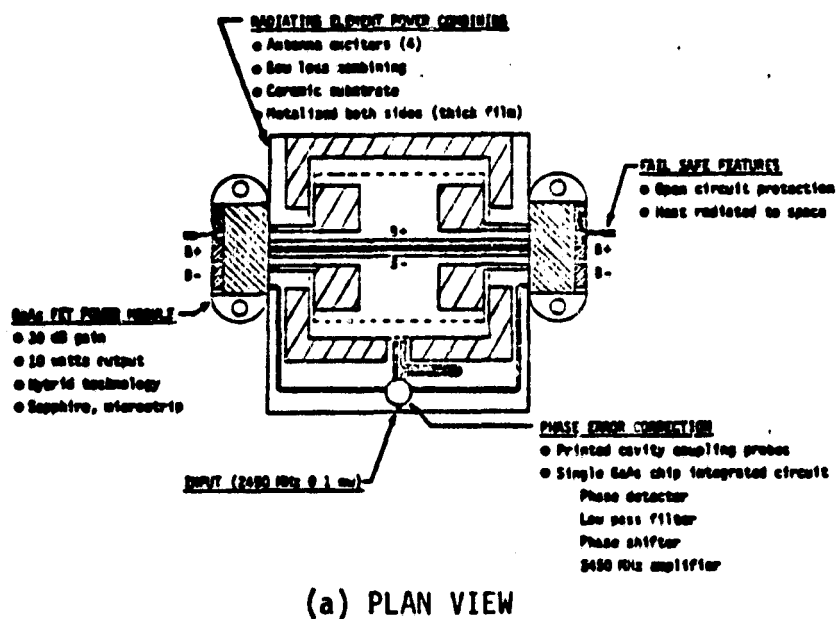


FIGURE 1 SOLID STATE POWER COMBINING MODULE CONCEPT (20 WATTS)

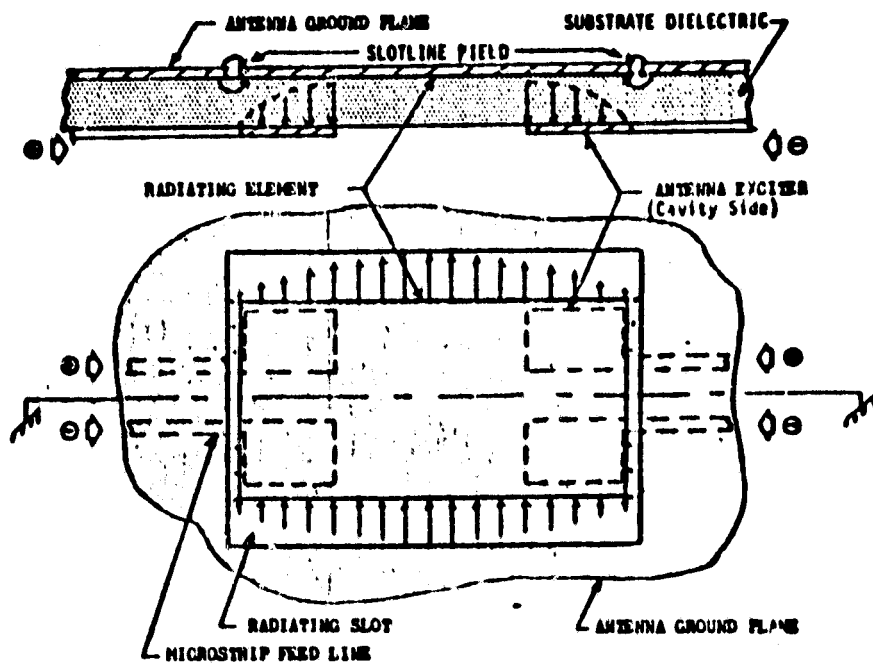
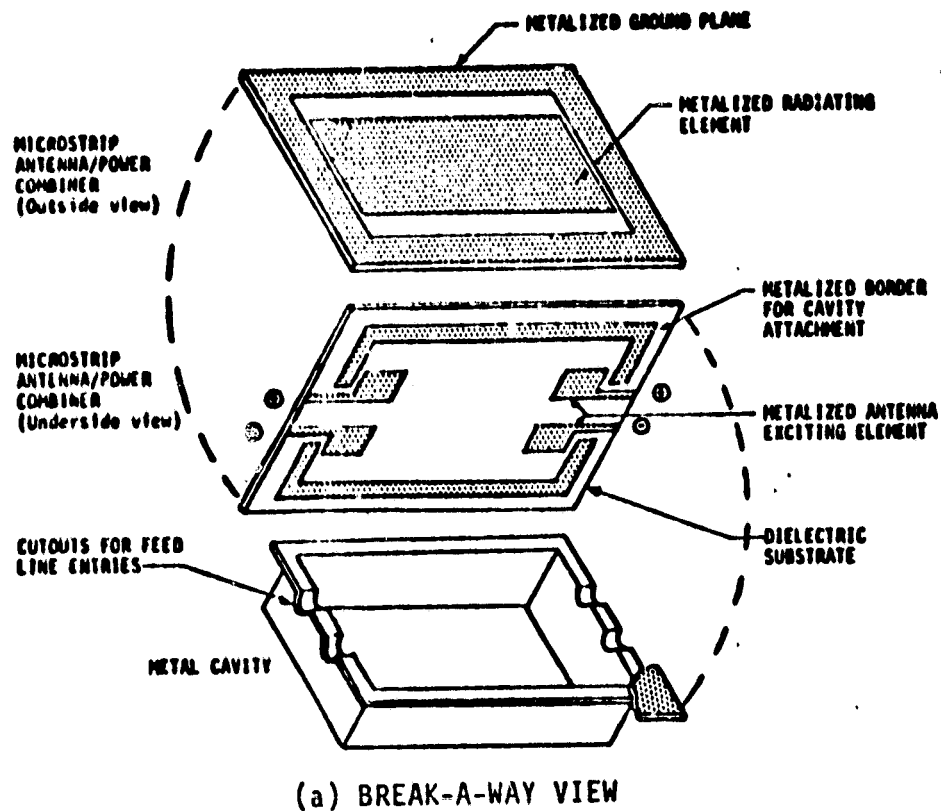


FIGURE 2 POWER COMBINING MICROSTRIP SLOTLINE ANTENNA

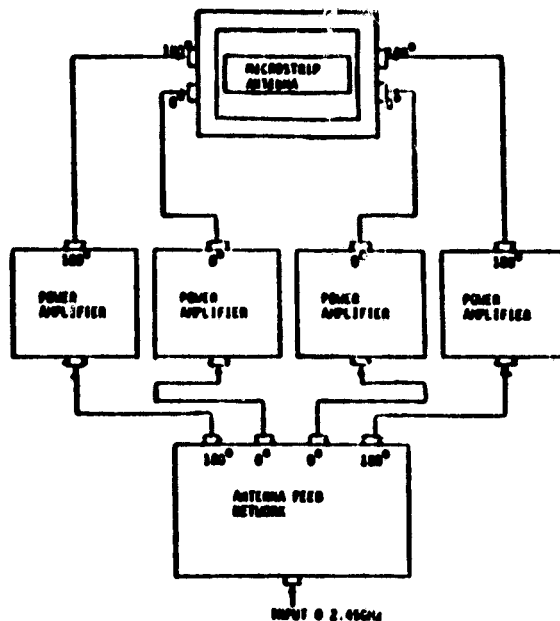


FIGURE 3a POWER COMBINING ANTENNA, FEED NETWORK & POWER AMPLIFIER
BLOCK DIAGRAM

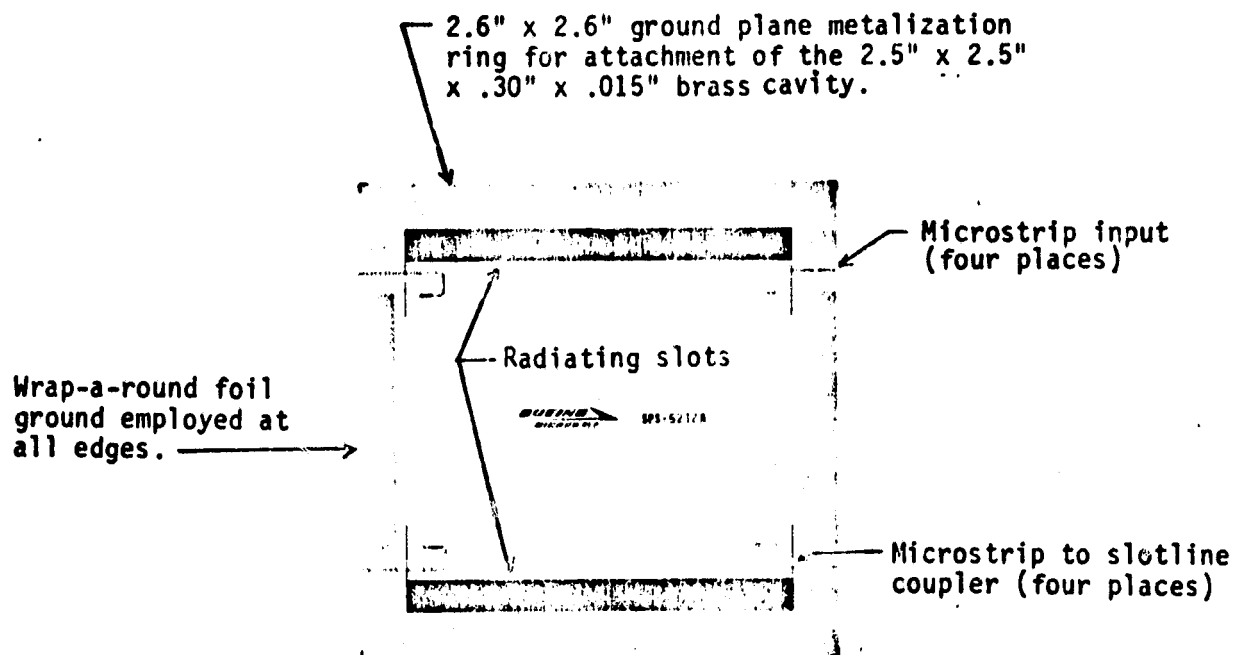


FIGURE 3b COPPER METALIZATION PATTERN FOR FOUR FEED MICROSTRIP ANTENNA

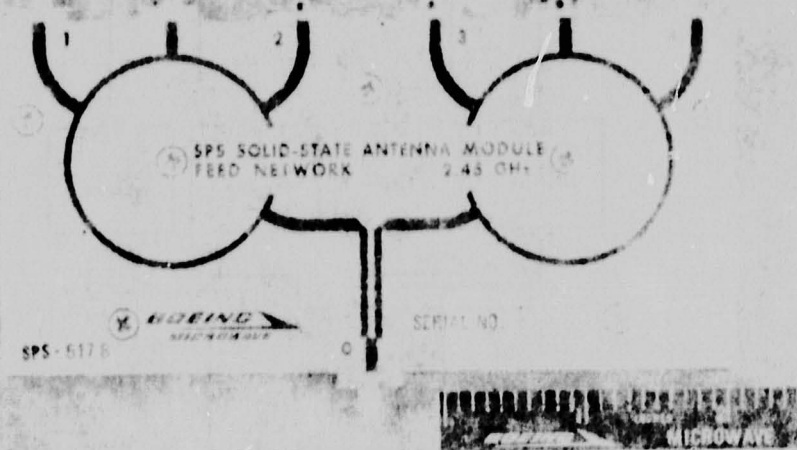


FIGURE 4a STRIPLINE FEED NETWORK

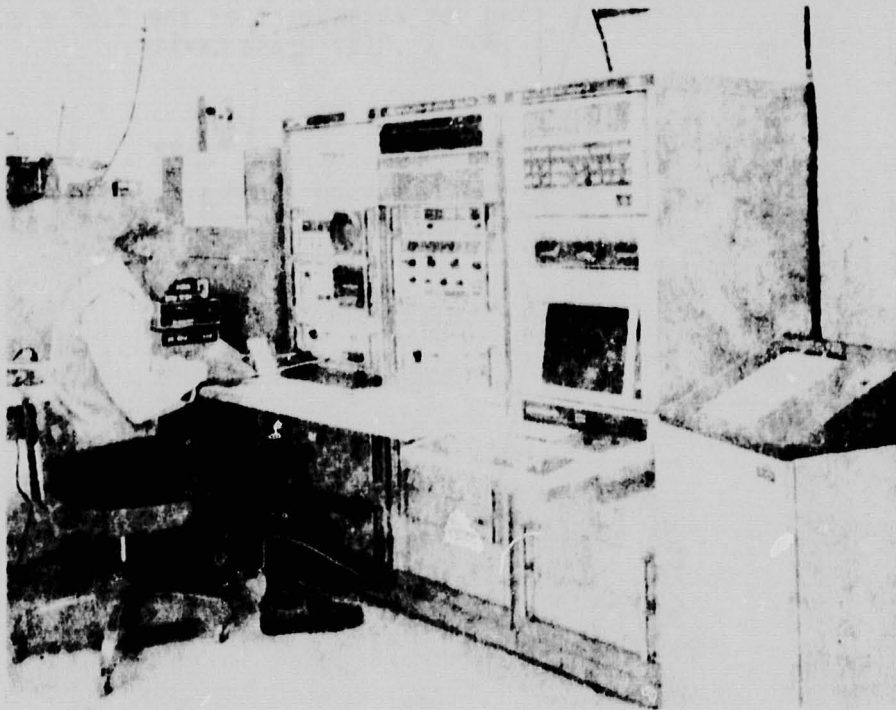
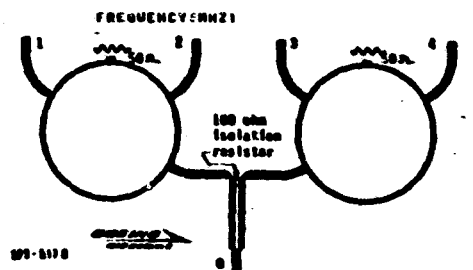
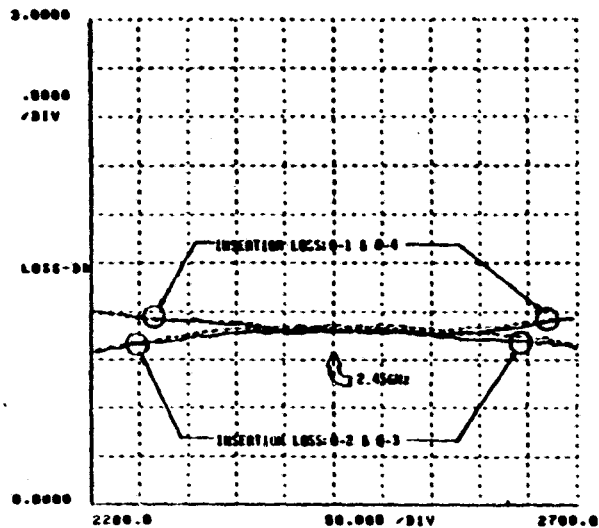


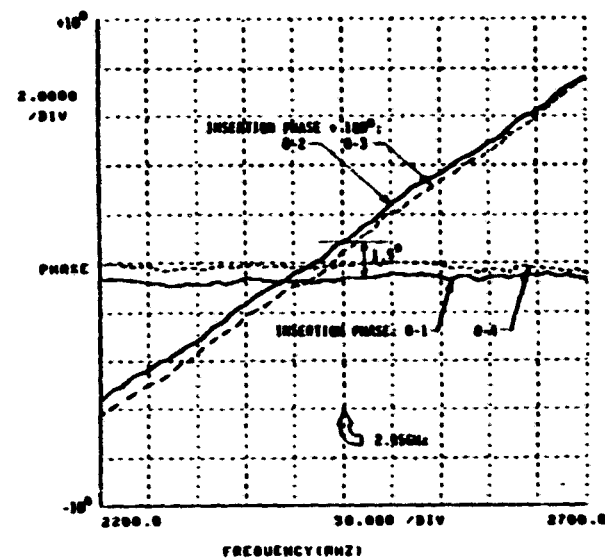
FIGURE 4b AUTOMATIC NETWORK ANALYZER

THE BOEING CO. GWF
SPS SOLID-STATE ANTENNA MODULE FEED
NETWORK
2.45 GHz
SPS-5170, SER. #01
SEPTEMBER 10, 1970



INSERTION LOSS

THE BOEING CO. GWF
SPS SOLID-STATE ANTENNA MODULE FEED
NETWORK
2.45 GHz
SPS-5170, SER. #01
SEPTEMBER 10, 1970



INSERTION PHASE

FIGURE 5 INSERTION LOSS AND INSERTION PHASE VERSUS FREQUENCY FOR THE STRIPLINE FEED NETWORK.

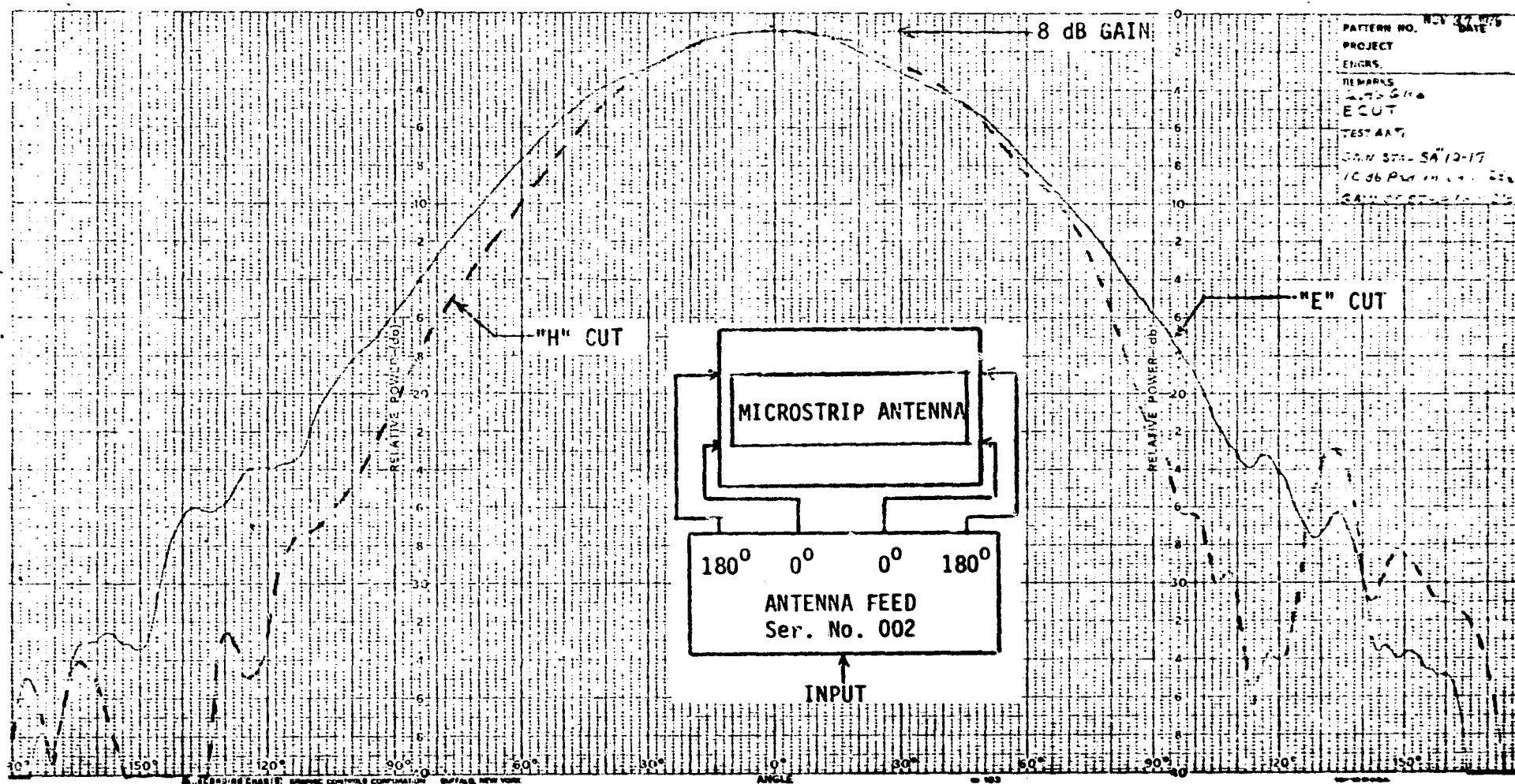


FIGURE 6 ANTENNA RANGE GAIN PATTERN FOR THE FIRST POWER COMBINING MICROSTRIP ANTENNA (FEED NETWORK NO. 2)

SOLID-STATE SYSTEMS CONCEPTS

K. G. Schroeder

I. K. Petroff

ROCKWELL INTERNATIONAL

SOLID-STATE RETRODIRECTIVE PHASED ARRAY CONCEPTS FOR MICROWAVE

POWER TRANSMISSION FROM A SOLAR POWER SATELLITE

1.0 INTRODUCTION

This paper describes two prototype solid-state phased array systems concepts for potential use in the Solar Power Satellite (SPS). In both concepts, the beam is centered on the rectenna by means of phase conjugation of a pilot signal emanating from the ground. Also discussed is on-going solid-state amplifier development.

The basic systems concepts are now described in more detail.

2.0 OVERVIEW OF SOLID-STATE ARRAY CONCEPTS

Two different solid-state array concepts are being developed at this time: The End-Mounted Space System (Figure 1) and the Sandwich (Figure 2). Both concepts use the same element and spacing, but in the end-mounted system 36-watt amplifiers are mounted on the ground-plane, whereas in the sandwich the amplifiers are elevated to the dipoles, and their waste heat is dissipated by beryllium oxide discs. The feed lines are underneath the ground-plane, and a coaxial transmission line is carried all the way to the amplifier input. (See section on RF Signal Distribution). Figure 4 in Section 4 shows the sandwich dipole layout in close-up view.

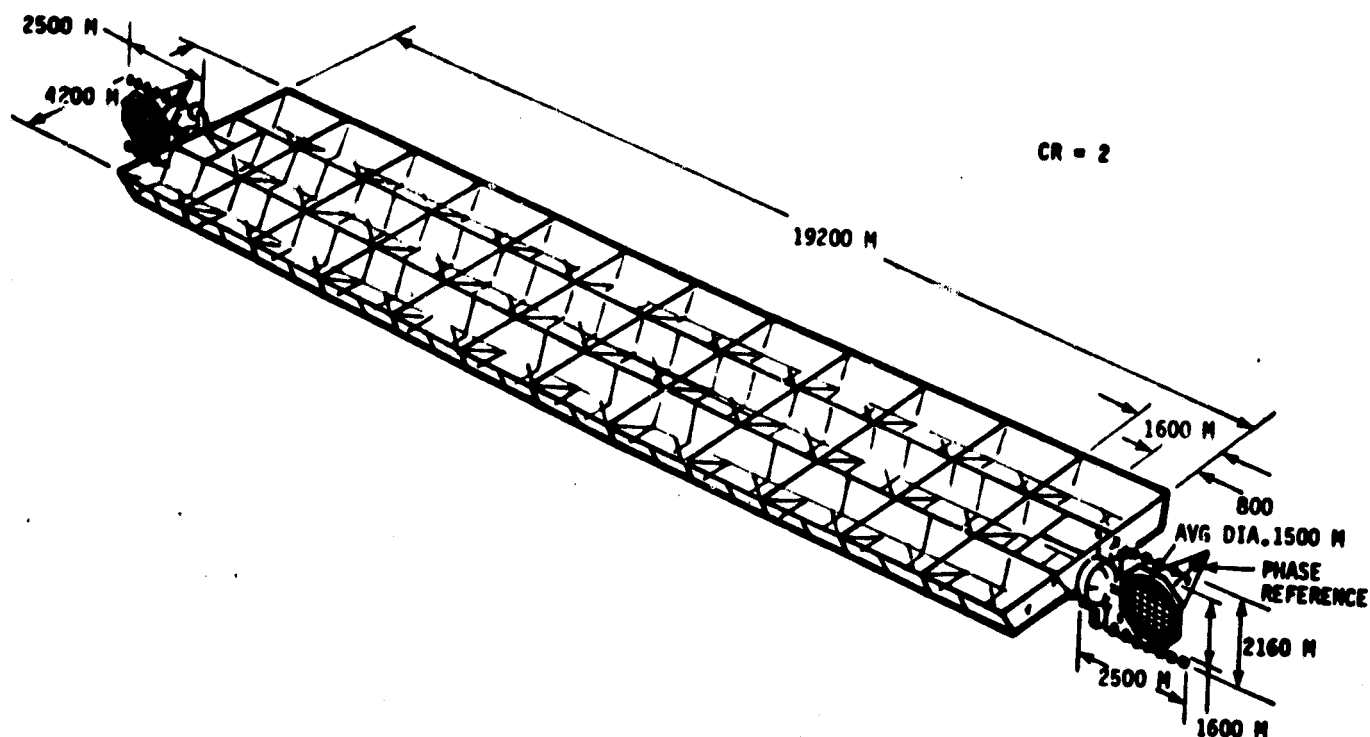
3.0 SOLID-STATE PHASE CONTROL3.1 REFERENCE PHASE DISTRIBUTION

Phase conjugation at the 10 meter by 10 meter subarray is used to steer the beam. The reference phase signal is distributed over the spacetenna aperture via a radio link. Figure 3 illustrates this method giving a perspective view of the top of the aperture. Two important features are: (a) the phase reference signal originates from a single transmit location at the rear of the aperture; and (b) phase reference and pilot antennas are orthogonally polarized with respect to the power dipoles to avoid feedback loops. Instead of an endfire (e.g., "Cigar") array, broadside arrays can be used for reference and pilot pick-up. Both configurations shall be considered in more detail in future studies.

The phase reference signal is distributed as follows:

From the shaped-beam illuminator antenna an RF signal is distributed over a cone with maximally 90 degrees beamwidth. All reference pick-up antennas see approximately the same signal strength. The local oscillator and driver amplifier is redundant. Large variations in aperture flatness can be compensated modulo 2π since bandwidth is of no concern for the reference phase signal. The phase at each subarray pick-up point is normalized with respect to a perfectly flat

FIGURE 1. END-MOUNTED SOLID STATE CONCEPT (REF. 1)

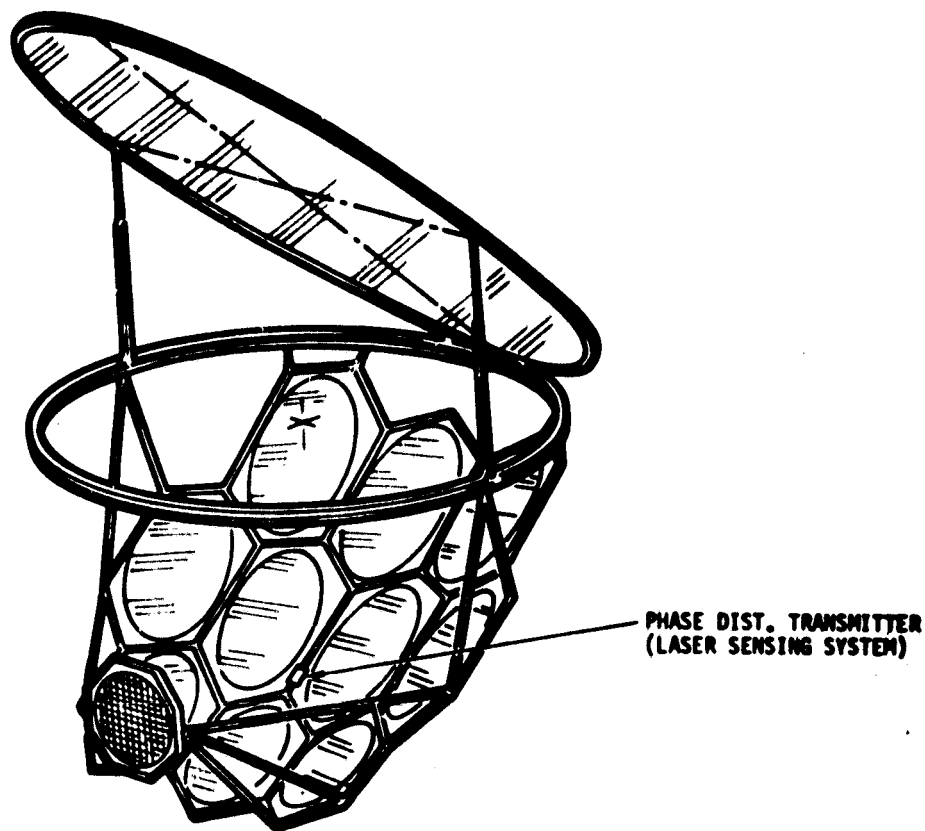


END-MOUNTED SOLID-STATE CONCEPT CHARACTERISTICS

- o GaAs SOLAR ARRAY
- o GEOMETRIC CR = 2.0
- o DUAL END-MOUNTED MICROWAVE ANTENNAS
- o AMPLIFIER BASE TEMPERATURE = 125°C
- o AMPLIFIER EFFICIENCY = 0.8
- o ANTENNA POWER TAPER ~ 10dB
- o ANTENNA DIAMETER = 1.35 km
- o POWER AT UTILITY INTERFACE = 2.61 GW PER ANTENNA
(5.22 GW TOTAL)
- o RECTENNA BORESIGHT DIAMETER = 7.51 km PER RECTENNA

Ref. 1) After: G. M. Hanley, SPS Concept Definition Study (Exhibit D),
First Performance Review - 10 October 1979.

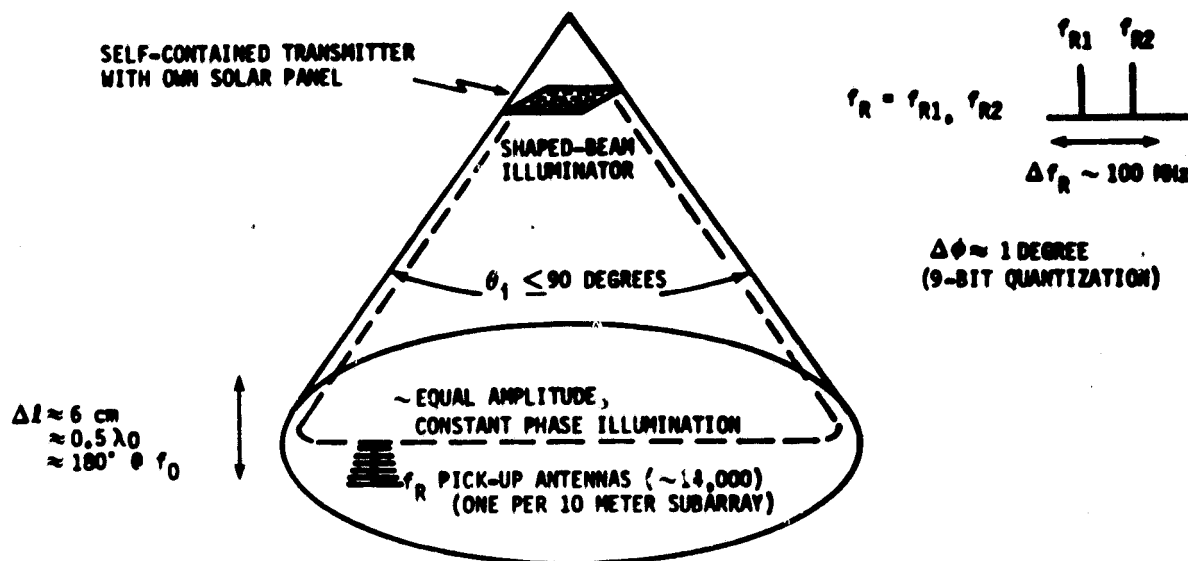
FIGURE 2. SOLID STATE SANDWICH CONCEPT RECOMMENDED FOR POINT DESIGN
(REF. 1)



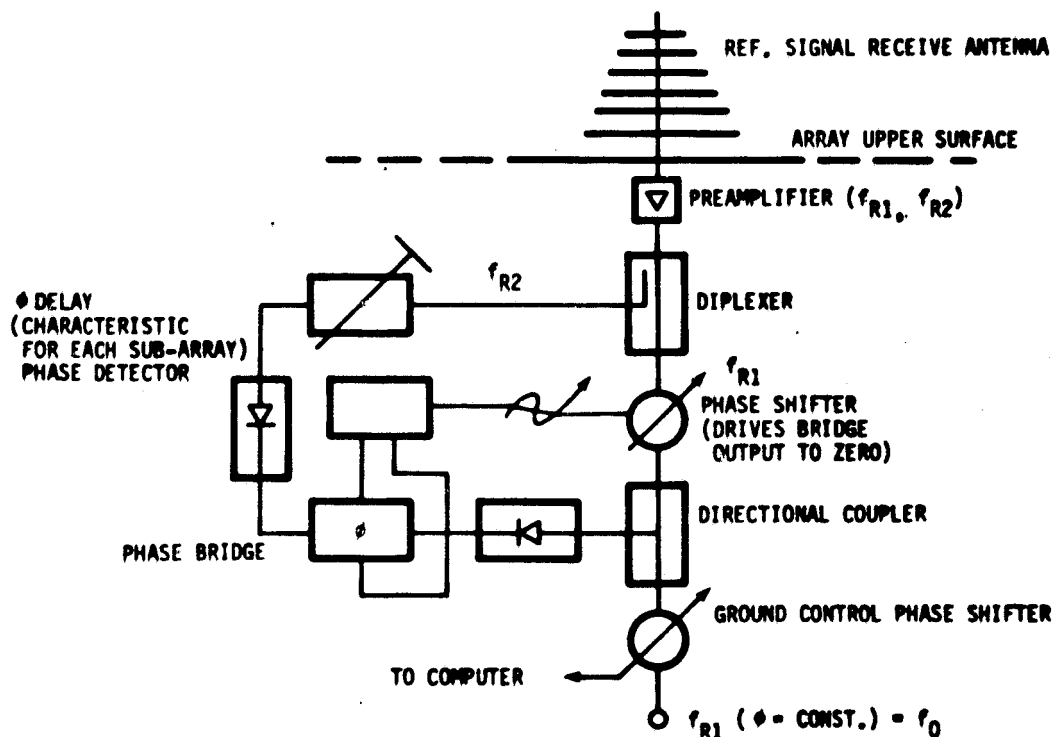
RECOMMENDED SOLID-STATE SANDWICH CONCEPT CHARACTERISTICS

<u>CHARACTERISTIC</u>	<u>PRIMARY</u>	<u>SECONDARY</u>
SOLAR ARRAY TYPE	GaAs	MULTI-BANDGAP
EFFECTIVE CR	6	5 TO 6
SOLAR ARRAY TEMP. ($^{\circ}\text{C}$)	200	200
AMPLIFIER BASE TEMP. ($^{\circ}\text{C}$)	125	125
AMPLIFIER EFFICIENCY	0.8	0.8
ANTENNA TAPER RATIO (dB)	0	0
ANTENNA DIAMETER (Km)	1.77	1.64 TO 1.58
POWER AT UTILITY INTERFACE (GW)	1.26	1.47 TO 1.54
RECTENNA BORESIGHT DIA. (Km)	5.10	5.39 TO 5.68

FIGURE 3. PHASE REFERENCE SIGNAL DISTRIBUTION SYSTEM AND
REFERENCE SIGNAL CONTROL LOOP



NOTE: PICK-UP ANTENNA ORTHOGONALLY POLARIZED WITH RESPECT TO POWER BEAM
TOTAL ISOLATION $I_T \geq 40 + 60 \text{ dB} \geq 100 \text{ dB}$
CROSS POL FRONT-TO-BACK RATIO (CAN BE MADE $> 100 \text{ dB}$)



uniform aperture by means of a servo loop shown in the bottom part of Figure 3. For each subarray center location, a phase delay differential ("reference standard") is computed which occurs for the two generating frequencies f_{R1} and f_{R2} if the receiving antenna is located on a perfect plane. These delays can be calculated, and tuned in the lab to fractions of a degree. The output of the phase bridge then drives a phase shifter until the path delay differential equals that of the reference standard.

Since this circuit is used at every subarray, the subarray center points are electrically normalized to show $\phi = \phi_0$ constant across the entire array. This provides the conjugation circuit with the required reference phase.

3.2 RETRODIRECTIVE BEAM CONTROL

A retrodirective control circuit which compensates for pilot-generated beam shifts (without ionospheric effects) is the Chernoff circuit, with additional isolation added by (a) separating the pilot and power frequency paths, (b) using orthogonally polarized radiating elements; and (c) providing the remaining isolation in separate bandpass filters. The total required filter isolation is 70 dB, according to preliminary pilot system calculations.

This pilot system is predicated on ~ 100 dBw pilot power. The proposed implementation of this pilot system consists of a circular array of low to medium-gain elements placed at the periphery of the rectenna, on top of utility poles if necessary to avoid interference from the power collection and transmission system.

The system provides vastly improved reliability over a single-dish, concentrated amplifier pilot system, and also provides such a wide power tube when the near-field beam enters the ionosphere that certain ionospheric effects will be mitigated. If ionospheric tests show that delay compensation through the ionosphere is required, a three-tone pilot system will be used as described in the Phase Control Session.

3.3 RF SIGNAL DISTRIBUTION SYSTEM

The current baseline distribution system for the conjugated RF signal is the same for both solid-state concepts.

Seven levels of corporate divisions provide equiphase feeding to the 16,384 elements in each 10m x 10m subarray.

The salient features of this distribution network are: weight of 0.67 million killograms for the total array using UT-47M; 250°C temperature capability; approximately 10dB ohmic loss (in addition to 42dB splitting loss). All layers of coax are pressed together behind the ground-plane, and very little thermal resistance is presented to the heat being radiated rearward from the ground-plane in the end-mounted concept, and toward the ground-plane (from the solar cells) in the sandwich concept. The composite heat transfer will be established by the spacing between the ground plane and the solar cells in the case of the sandwich.

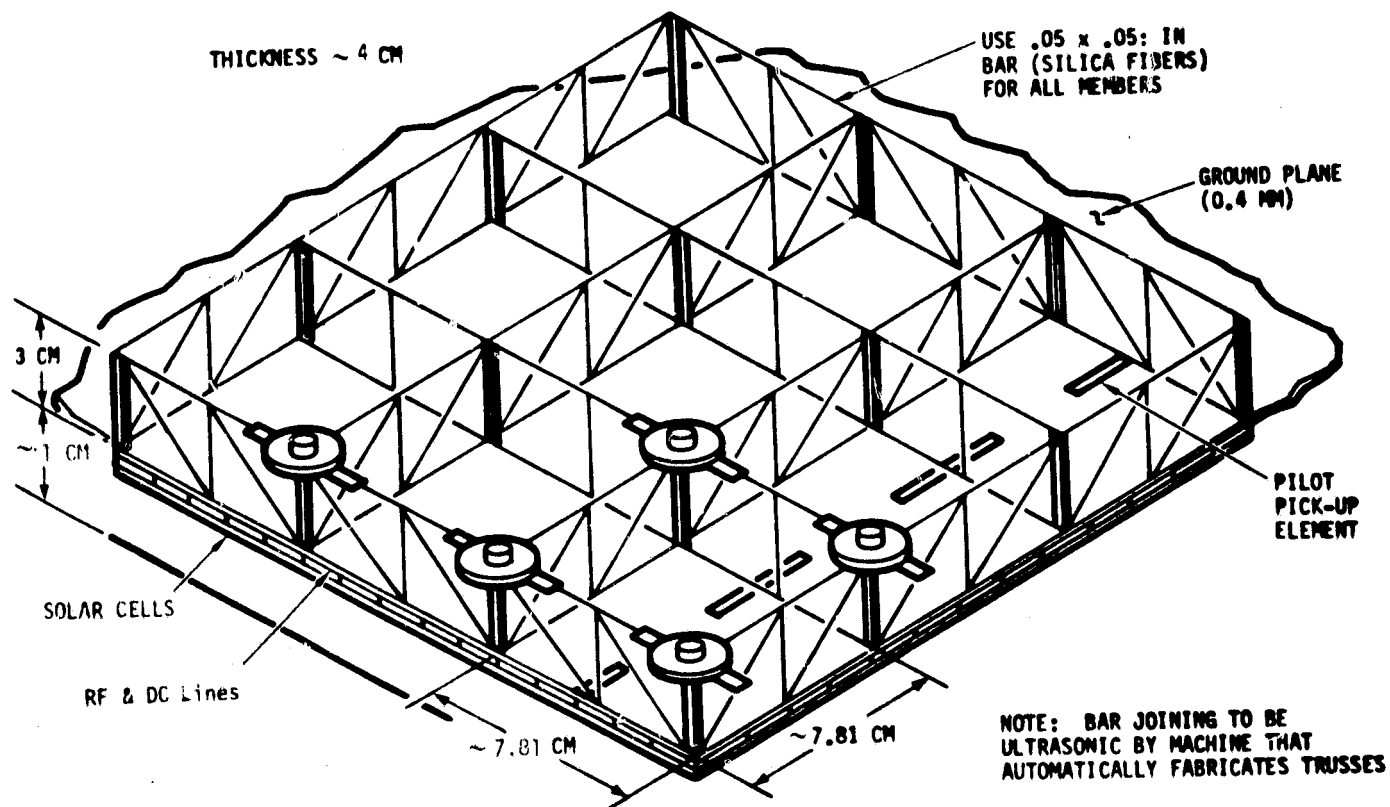
SOLID-STATE RADIATORS

A number of elements have been considered for the reference phase pick-up and pilot-tone pick-up elements: Helices; disc-on-rod antennas; yagis; dipole arrays; slot arrays; patch-type microstrip arrays; and arrays of various other strip-type radiators.

For the power radiators, all of the above array elements (except for high-gain end-fire arrays) have been considered but thin dipoles were selected because a) they lead to a minimum power requirement for the amplifier module; b) provide the necessary heat removal characteristics, and c) yield maximum reliability.

Figure 4 shows the dipole layout selected for the sandwich concept. The pilot pick-up slots are interspersed, but the power dipoles can be removed from this section if additional isolation is required, and/or space is required for the conjugation circuit.

FIGURE 4. SANDWICH ANTENNA WITH DIPOLES OVER GROUND PLANE



5.0 SOLID-STATE POWER AMPLIFIERS

The assessment of solid-state devices for r-f conversion in the SPS microwave power transmission system has included to date both an analytical effort and an amplifier development program.

5.1 Analytical Studies

The analytical study was carried out for Rockwell International at the University of Waterloo, Canada. The first phase of the study consisted of a computer simulation of bipolar transistors, in Class C and Class E type circuits. Both silicon and GaAs bipolar transistors were modelled. In the second part of the study, GaAs MESFETs were modelled in Class B and Class C circuits. Work is currently in progress to obtain Class E results.

The study was undertaken as an evaluation of transistors for the microwave space power system. The goal was the determination of transistor fabrication parameters suitable for power conversion efficiencies of at least 80% with power gains of at least 10 dB.

5.2 Bipolar Transistor Simulation

The simulation is carried out by using two basic programs. The first program generates a circuit model of the transistor, from inputs consisting of the impurity profile and lifetimes, plus geometry data. The second program is a circuit analysis program where the device model is incorporated into the desired external circuit. The results of the bipolar transistor analysis indicated that GaAs devices perform better at high temperatures with respect to efficiency than Si devices of similar geometrical parameters as shown in Figures 5 and 6. A comparison of Class C with Class E operation for the silicon transistor at 27°C, shows that at high power levels (20 watts) the saturated Class-C mode gives the best results (Figure 7), while at lower power levels (10 watts) Class C gives better results at gains below 13 dB and Class E performs better at higher gains, (Figure 8).

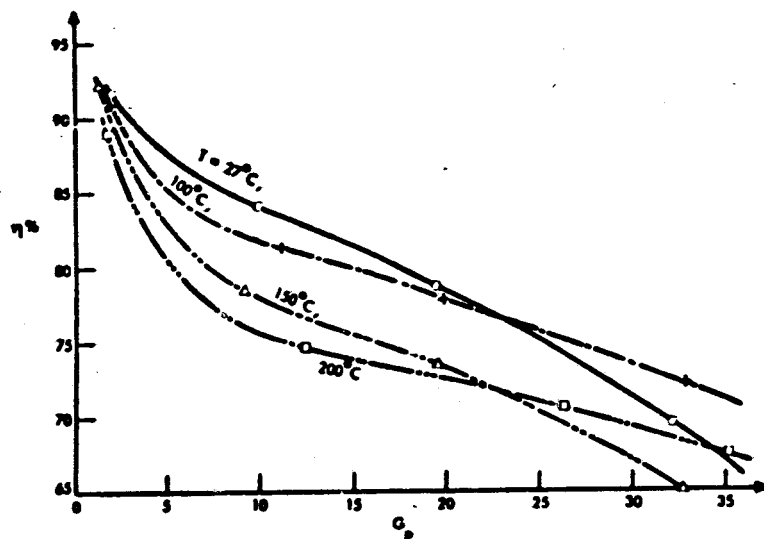


FIGURE 5. Results of High Temperature Study for the Silicon Transistor at 2.45 GHz

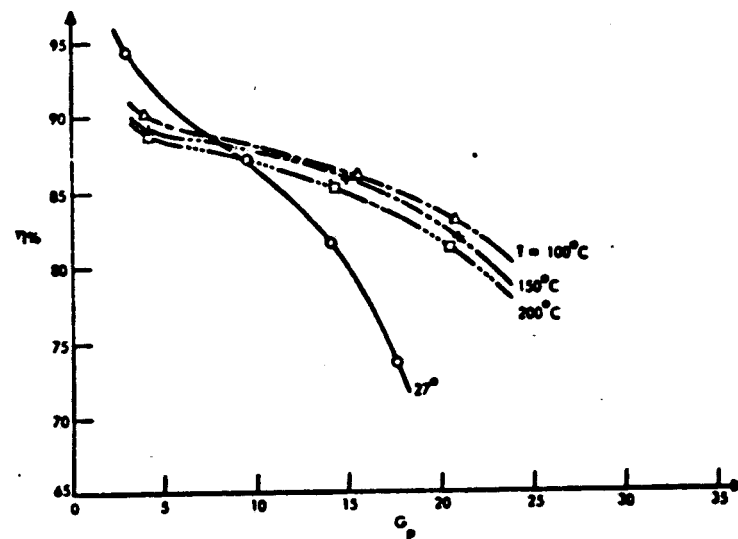


FIGURE 6. Results of High Temperature Study for the GaAs Transistor at 2.45 GHz

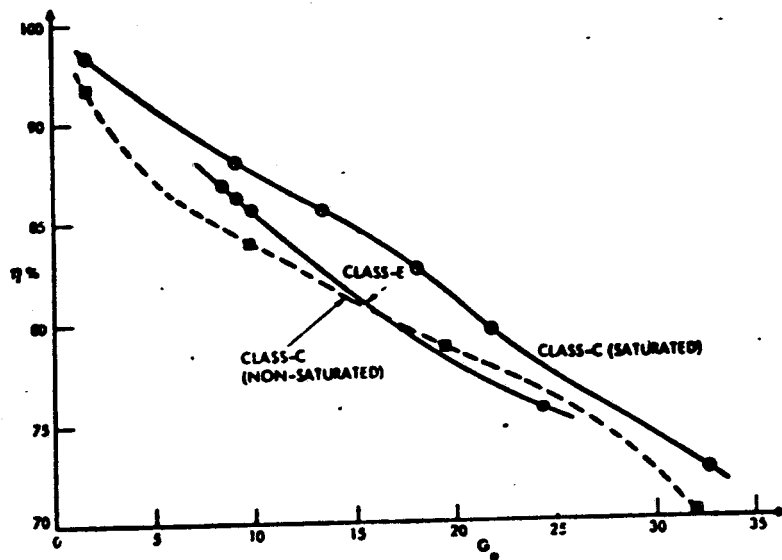


FIGURE 7. Efficiency vs Power Gain at 2.45 GHz and High Power Level for Silicon

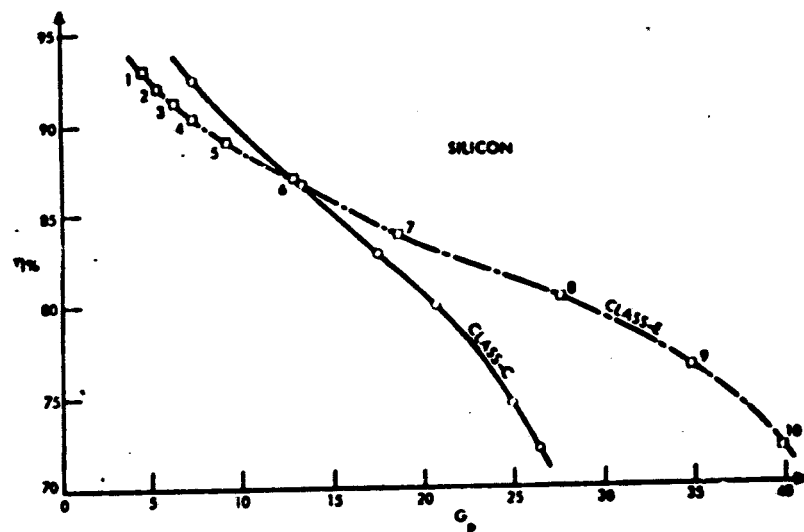


FIGURE 8. Efficiency vs Power Gain at 2.45 GHz and Low Power Level for Silicon

5.3 GaAs MESFETs Simulation

This study, currently in progress, follows the procedure used for the bipolar transistor simulation. A circuit model is generated by an appropriate program and is fed into the circuit analysis program. The devices modelled, so far, were basic one-cell structures, with low overall power output capability. The power output, power gain and efficiency obtained for the five structures modelled so far are shown in Figure 9. This figure shows plots of power added efficiency versus P_{out}/P_{max} for each device, where the three values shown correspond to conduction angles of 80° , 120° and 180° . The dashed lines indicate a mode of operation which cannot be attained physically, because the gate source voltage exceeds the breakdown voltage for that transistor.

6.0 POWER AMPLIFIER DEVELOPMENT

The goal of the power amplifier development program is to demonstrate that efficient operation at a 5 to 10 watt power level can be achieved with off the shelf GaAs power FETs and to show that the performance can be improved with optimized devices of similar type. The high efficiency power amplifiers are being developed for Rockwell International by RCA and will be discussed in a subsequent presentation.

GaAs devices were selected because of data showing that GaAs performs better than silicon at the temperatures likely to be encountered in the SPS environment. Several transistor structures should be investigated to establish possible trade-offs with respect to power level, comparative efficiencies and reliability. Schottky barrier FETs are the first choice for testing at the experimental level in view of the high degree of activity in their development due to their use as power devices at microwave frequencies.

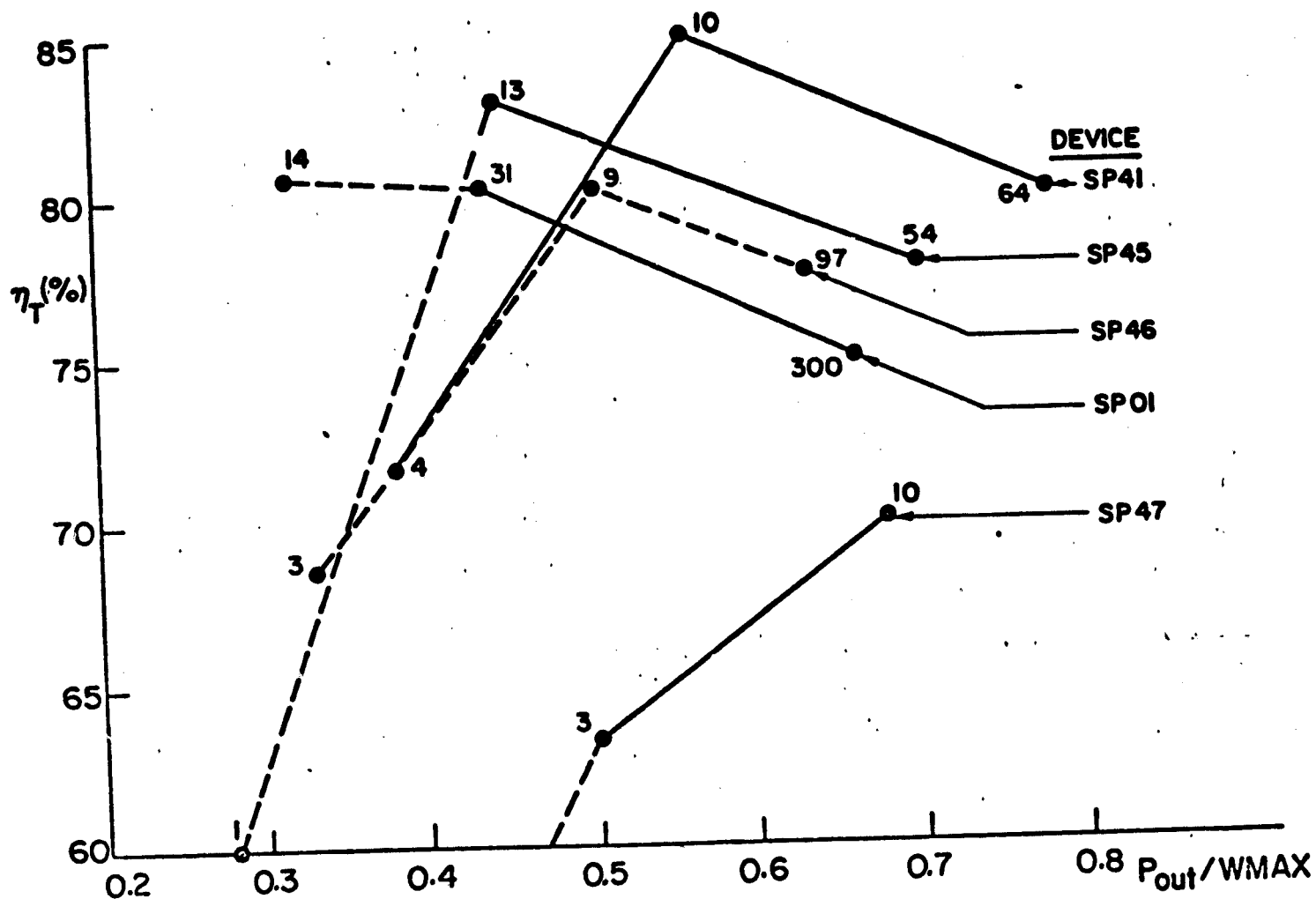


FIGURE 9. Total Efficiency vs (Output power/Wmax) for Sinusoidal Drive at 2.45 GHz for Five Different FETs. NOTE: The numbers indicate power gains.

SOLID-STATE DEVICE TECHNOLOGY FOR SOLAR POWER SATELLITE*

NASA, Johnson Space Center sponsored a program, "Analysis of S-Band Solid-State Transmitters for the Solar Power Satellite," based on the assumption that a high-efficiency solid-state SPS transmitter may be feasible.

The objectives of the study were to:

- o expand the understanding of the SPS transmitter concept and relate it to the possible utilization of solid-state (rather than thermionic) elements in the antenna array;
- o explore the need for technology development in the areas of devices, circuits, and interface configurations for a solid-state antenna array;
- o recommend specific technology advancement programs that could impact future SPS designs.

An additional task, added toward the end of the program in agreement with the Technical Monitor, was to construct a sample solid-state amplifier, based on existing gallium arsenide FET devices, so that power, gain, and efficiency relationships could be experimentally explored.

The study was designed to explore independently aspects of the devices, the circuits, and the overall antenna system. Only toward the end of the investigations were these three elements brought together to provide an overall view of the solid-state antenna concept and to recommend follow-on technology investigation programs.

DEVICE INVESTIGATIONS

For any system configuration, devices providing the maximum possible power at the highest possible efficiency would obviously be desirable. In practice, however, power must be traded off against efficiency, with efficiency the paramount parameter. When these factors are considered, gallium arsenide rather than silicon appears to be the favored material for the SPS application; the device used would be some kind of field-effect transistor of the type that combines high efficiency and relative ease of fabrication.

Thermal and electrical designs for both Schottky-barrier and junction-type FETs were presented at the conclusion of the study. Their purpose, rather than serve as device designs to be actually developed, was to highlight the considerations likely to influence the choice of future programs. No clearcut preference of one over the other was discerned at that point in the study. Devices providing 4 watts at greater than 80% power-added efficiencies were considered feasible.

*RCA presentation at NASA, Johnson Space Center, Houston, TX, 17 January 1980.

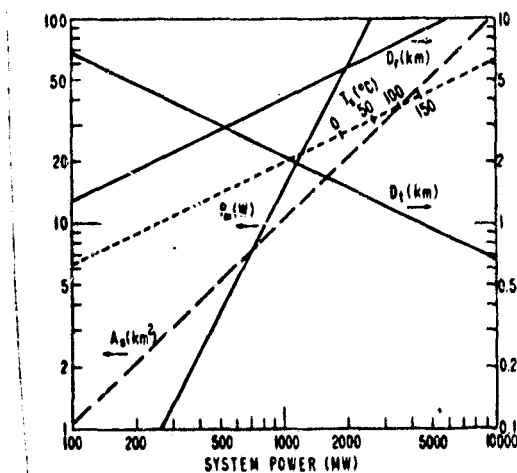
An actual amplifier stage was constructed with commercially available devices. It provided 3 watts of output power at an efficiency of 58% -- results considered very good indeed. The unit was delivered to JSC at the conclusion of the study.

One of the important recommendations of this part of the study was the undertaking of a follow-on experimental and theoretical program to ascertain the factors contributing to high-efficiency operation of microwave FETs. Previous experience with specialized large-signal computerized equipment pointed to the benefits of using this apparatus for the recommended follow-on study program.

ANTENNA SYSTEM INVESTIGATIONS

The Reference System (DOE/NASA Report, October 1978) served as a basis for the first phase of the antenna system investigations.

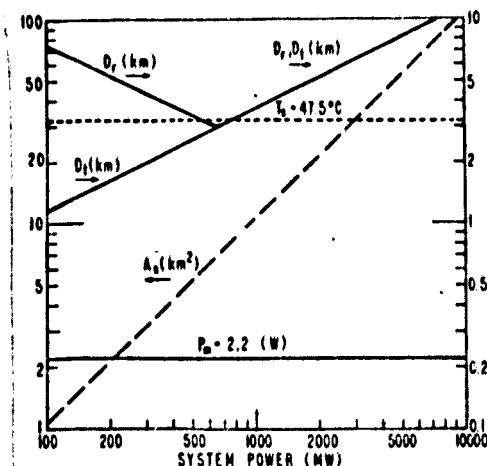
If it is attempted simply to replace the thermionic devices contemplated in the Reference System by clusters of solid-state devices whose power is combined to form equivalent transmitting elements, penalties in voltage-distribution losses, power combining losses, and thermal problems must be seriously considered. From detailed analyses performed during our study, it soon became apparent that a solid-state replacement program of this nature, while it may contribute toward the overall reliability of the system, would fall short in terms of the operational parameters -- particularly in terms of a Factor of Merit measured in watts per kilogram.



SPS design nomograph - 10-db taper.

At that point in the study, again with the concurrence of the Technical Monitor, emphasis was placed on a concept that considered direct conversion of sunlight into microwave power-generating modules, thereby obviating the need for voltage distribution altogether and essentially solving the thermal problems. Some specific problem areas peculiar to this approach were addressed in

the study -- e.g., the relative orientations of the solar array and the microwave antenna, the spacing of the antenna elements and, most importantly, the near-field properties of such an antenna.



SPS design nomograph - uniform distribution.

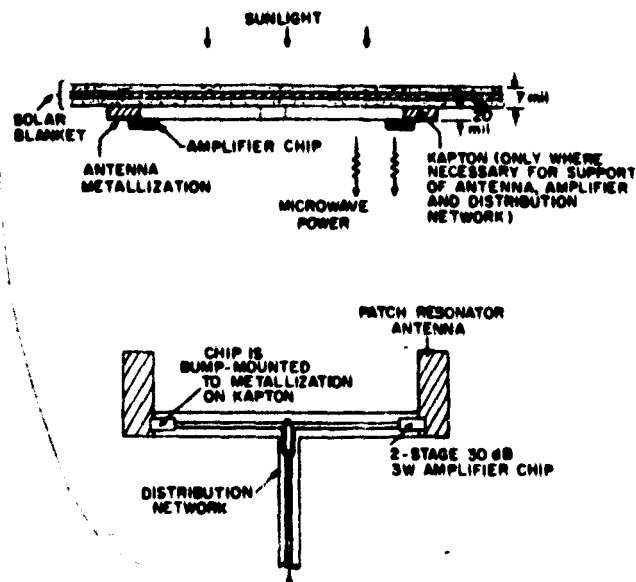
It was concluded that this type of system has Factor of Merit (W/kg) advantages over the Reference System, and that a tubular beam can indeed be created; a judicious choice of phase tapers made it possible to smooth power variations over the rectenna. Computer simulations of this type of antenna beam were performed at the conclusion of the study. Recommendations for adapting this approach, after further study, were made.

We recommended that studies aiming at a fuller understanding of the factors affecting high-efficiency operation of microwave FETs and the circuitry associated with them be vigorously pursued. Large-signal waveform analysis of FET operation was identified as a necessary factor of these studies.

MODULE INVESTIGATIONS

The module study quickly yielded the (not unexpected) notion that the efficiency of the power module is the most important design parameter, since it impacts very strongly the overall SPS cost in terms of dollars per watt of output power. Here again power combining losses and primary power distribution problems pointed toward the concept of the solar-powered module; an analysis of the practical power limits placed the module somewhere between 0.5 and 30 watts, with the power-vs-efficiency tradeoff pointing toward an optimum value of 1.5-3 watts.

Two design concepts were shown in which modules were placed on a $1.3\lambda \times 1.3\lambda$ grid, with 16-module clusters controlled by a single receiver module and providing 50 watts of transmitter power per cluster. As was the case with the device designs, both module designs (a "high Q" version and a "patch resonator" approach) were meant to represent the approach rather than be specific.



Patch - resonator design.

The most important recommendation resulting from the module study was a strong indication that any future efficiency optimization attempt should consider the device-module interface as part of the problem. Thus the large-signal waveform analysis recommended for the device studies should be combined with similar analyses for the module circuitry.

CONCLUSIONS AND RECOMMENDATIONS

The JSC study program yielded the following conclusions:

- o It does not appear prudent to simply replace the thermionic microwave power converters in the Reference System by equivalent clusters of solid-state devices.
- o On the other hand, real benefits can be obtained if the system architecture takes full advantage of the operating parameters of solid-state microwave devices. This leads to a concept of direct utilization of the solar-panel-generated power by low-power microwave amplifiers (the so-called SMART concept).
- o The postulated 80% power-added efficiency of the microwave amplifiers appears ultimately achievable. Gallium arsenide FETs are the logical device candidates for this service.

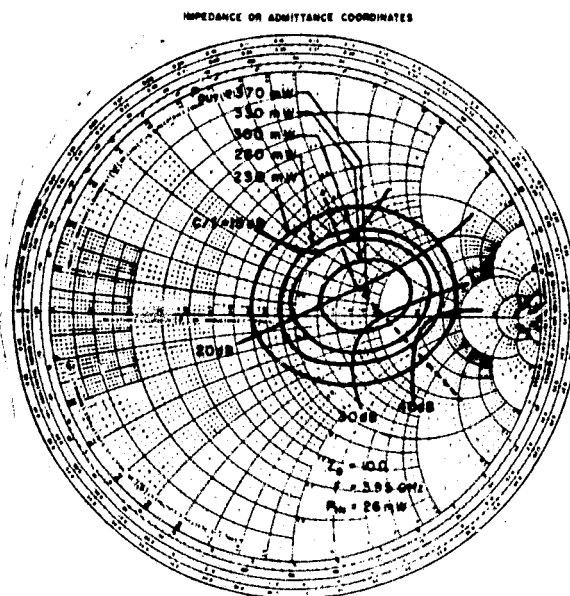
SPS SOLID-STATE AMPLIFIER

NASA, Marshall Space Center through Rockwell International, is presently sponsoring the "SPS Solid State Amplifier Development Program."

This program represents an extension of the effort performed as part of the JSC study: its main purpose is to gain a better understanding of the factors contributing to the high-efficiency performance of GaAs FETs. Large-signal waveform analysis techniques are a major investigative tool in the program.

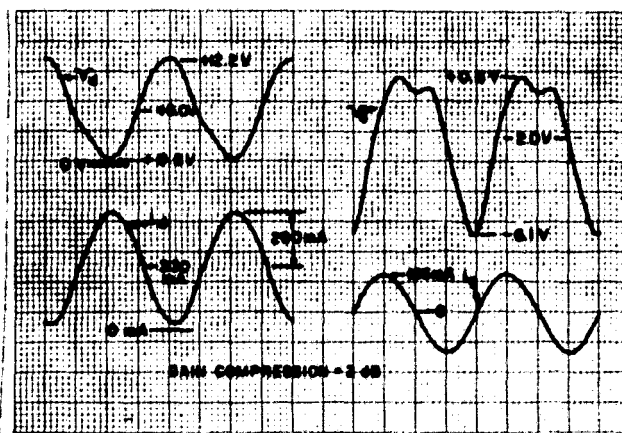
The program is divided into two consecutive tasks, with present effort still under Task A. This calls for the demonstration of an amplifier having an output power of 5 watts, a gain of 8 dB, and a power-added efficiency of 50%. In Task B the power output, gain, and efficiency to be demonstrated are increased to 10 watts, 10 dB, and 65%, respectively. To date a survey of available devices from a total of six domestic and foreign manufacturers of GaAs FETs was made, and circuits using various devices are being built and analyzed as the transistors are received. While "Class E" operation was and continues to be of interest for the SPS application because of its potential for very high efficiency, it is by no means certain that such mode of operation can be obtained at microwave frequencies, and the work under the program is not restricted to multipole operation of the FETs.

As previously mentioned, computer-aided analysis techniques are used extensively in the program, not only in the normal small-signal device characterization mode, but also to define the available tradeoffs under large-signal operating conditions. Examples of such techniques are the automatic plotting of circles of constant efficiency, constant gain, constant power output, and constant intermodulation distortion on special instrumentation which exists at RCA Laboratories.



Microwave CAD large-signal analysis.

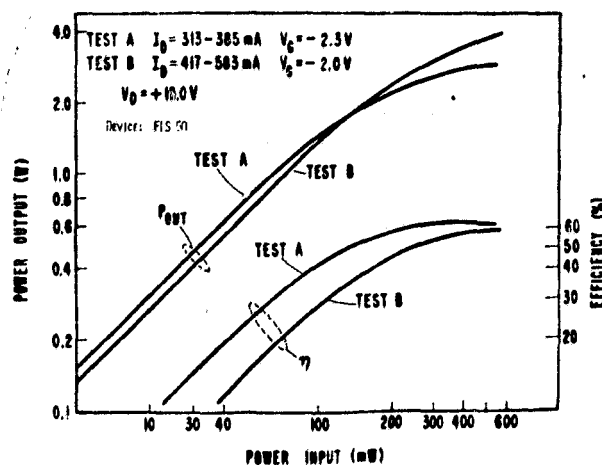
In addition, we have demonstrated a technique for synthesizing current and voltage waveforms under FET amplifier full operating power. This approach is also a powerful analytic tool in our investigation.



Full-power-measured voltage and current waveforms.

While the effort is still in progress and any attempts at projections of final results (even in Task A) are still considered premature, some very significant findings have already been made. When optimized for maximum efficiency at the SPS frequency, a power amplifier stage using a transistor designed for 12 GHz operation yielded 71% power-added efficiency, a very impressive figure that exceeds the requirements of Task B.

This result was obtained at a power output close to 1 watt and a gain in excess of 11 dB. The mode of operation may be described as an inverted Class AB, since the drain current is highest at low rf drive and lowest at full rf drive -- the rf voltage turns off the device during a substantial fraction of the rf cycle, hence the high efficiency. However, when the same type of operation was attempted with a transistor of the same manufacturer (but rated at somewhat lower power output at 12 GHz), low efficiency was observed at 2.45 GHz, but at a power output much closer to the rated value. These results are presently



Test results - max. power and max. efficiency tuning.

under intensive investigation. The current and voltage waveform analyses are expected to shed some light on the hitherto unexplained aspects of this type of FET performance.

Both Task A and Task B will make use of power-combining circuits in the final amplifier configuration. A study of such circuits is included in the program.

SOLID-STATE SPS TECHNOLOGY FORECAST

Solid-State Technology is in a period of rapid growth in both the microwave and the signal-processing areas. Specific applications of this technology in a variety of spaceborne systems occur with increasing frequency and effectiveness. The roots of this great interest in solid-state devices, components, and integrated circuits have been, on the one hand, the commercial computer industry and its integrated-circuit logic components and, on the other, the military-systems interest in microwave solid-state devices. This trend is quite independent of the SPS concept. Thus the SPS will reap tremendous benefits from the very large investments made in this technology, investments that are certain to continue in the future.

The directions of technology research pertinent to the SPS concept span the entire gamut of fields familiar to the solid-state industry--materials, devices, circuits, processing methods, and automated test procedures. In the semiconductor materials area, gallium arsenide is presently the most important compound for microwave applications, while ternary and quaternary materials are being investigated for use, particularly at the higher microwave frequencies. The silicon-on-sapphire technology is likely to provide the SPS solid-state antenna with an excellent technology base for substrate materials.

New device concepts, in addition to the FET which presently appears to be the best candidate for amplifiers at the SPS frequency, are the vertical FET, the power MOS transistor, the SIT, and matrix transistors, all of which are in advanced stages of exploration at the present time.

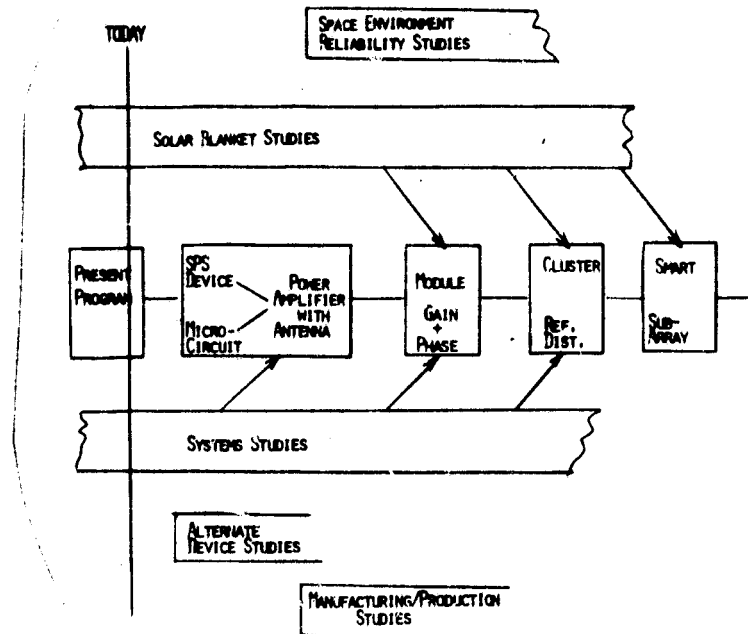
The most important area in circuit development is the return, after a hiatus of some years, to the concept of microwave lumped-circuit design. Lumped circuits designed for microwave frequencies extend FET operation to very high microwave frequencies. At 2.45 GHz, they permit extreme miniaturization of the amplifiers, making large distributed antenna arrays feasible.

Finally, modern processing methods -- e.g., ion-beam milling and plasma etching -- are likely to extend the techniques of the integrated-circuit chips to microwave circuits, while the selective implantation of impurities by means of ion implantation and laser annealing techniques point toward the fabrication of monolithic components directly on semi-insulating gallium arsenide.

These comments are not intended to imply that the SPS components -- both for signal-processing and for conversion to microwaves -- will not require specific and vigorous development. The attached diagram is a rough indication of the various microwave components which require study, development, and refinement in manufacturing techniques. We feel that the two most important areas requiring immediate attention are the following:

- o THE CONFIRMATION THAT A SMART-TYPE SOLID-STATE ANTENNA IS INDEED WORTHY OF SERIOUS CONSIDERATION AND SHOULD THEREFORE FORM PART OF THE MAIN-STREAM OF SPS STUDIES.

o THE INITIATION OF A SOLID-STATE POWER AMPLIFIER DEVELOPMENT PROGRAM AIMED SPECIFICALLY AT HIGH-EFFICIENCY SPS APPLICATION. THIS EFFORT SHOULD INCLUDE THE ACTIVE DEVICE AND THE MICROCIRCUIT MATCHING, INCLUDING ANTENNA, IN A SINGLE PACKAGE.



***Solid State Sandwich Concept
O. Maynard/Raytheon***

unavailable at time of printing

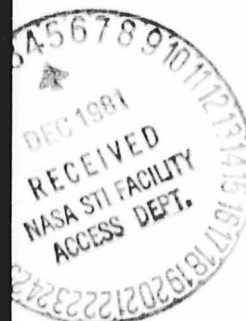


National Aeronautics and
Space Administration

Lyndon B. Johnson Space Center
Houston, Texas 77058

1

**General
Session**



NASA	Solar Power Satellite	Workshop on Microwave Power Transmission and Reception
------	--------------------------	---

**Session
Presentations**

**Jan
15-18
1980**



The presentation material herein was used in the General Session of the Solar Power Satellite Workshop on Microwave Power Transmission and Reception held at the Lyndon B. Johnson Space Center, January 15-28, 1980. The workshop was conducted as part of the technical assessment process of the DOE/NASA Solar Power Satellite Concept Evaluation Program. All aspects of Solar Power Satellite microwave transmission and reception were addressed including studies, analyses, and laboratory investigations. Conclusions from these activities were presented as well as recommended follow-on work. The workshop was organized into eight sessions as follows:

- *General*
- *Microwave System Performance*
- *Phase Control*
- *Power Amplifiers*
- *Radiating Elements*
- *Rectenna*
- *Solid State Configurations*
- *Planned Program Activities*

The material contained herein supplements the workshop papers which were published and distributed at the time of the workshop. Together they are a comprehensive documentation of the numerous analytical and experimental activities in the field of microwave power transmission and reception.

- *Additional information regarding the workshop may be obtained by*

contacting: R.H. Dietz
EE4/SPS Microwave Systems
National Aeronautics &
Space Administration
Lyndon B. Johnson Space Center
Houston, Texas 77058
713 483-4507

1

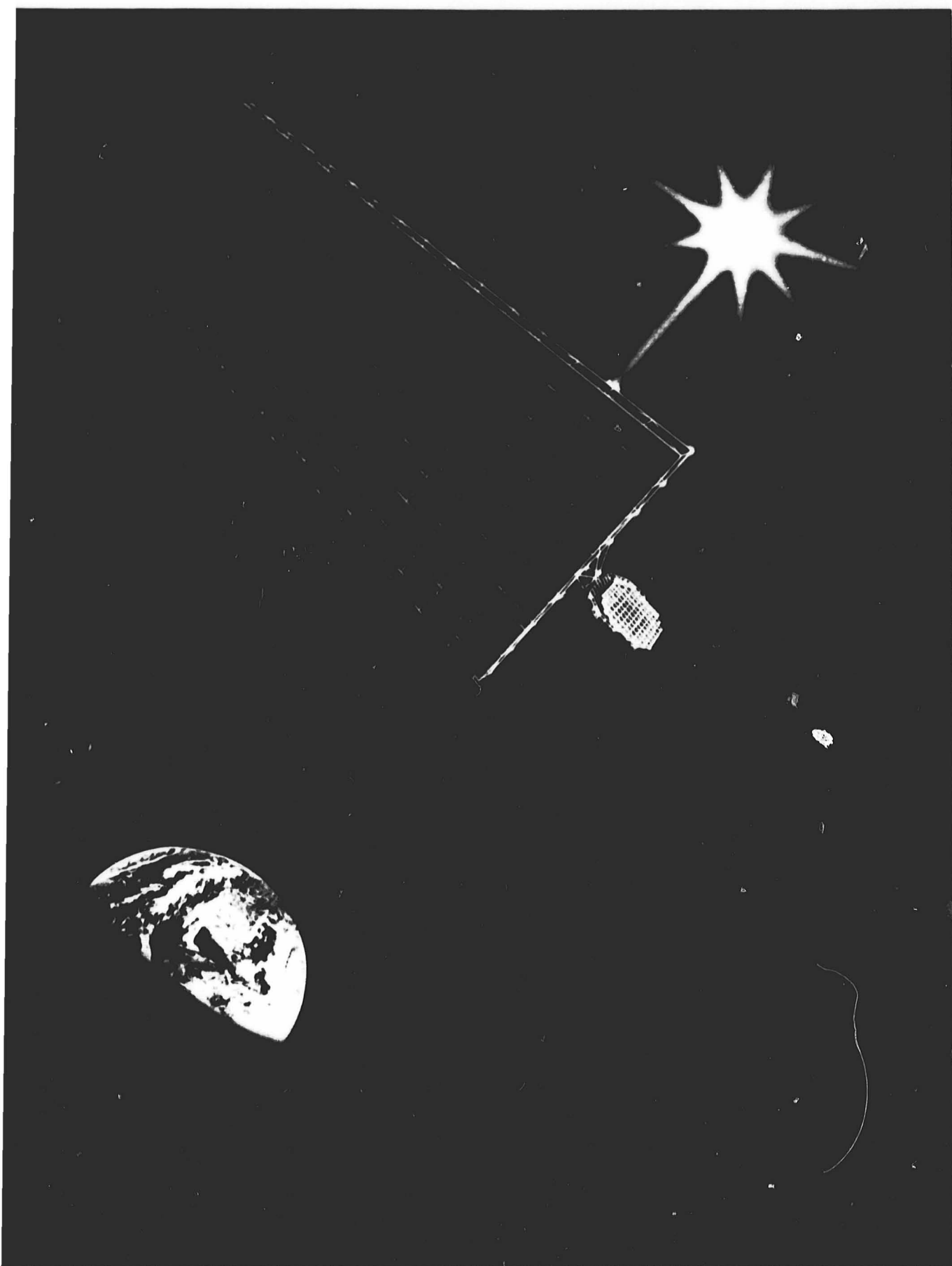
General Session *contents*

- | | |
|-----------|--|
| 1 | DOE / NASA Concept Evaluation Program
Robert O. Piland, Lyndon B. Johnson Space Center |
| 7 | Solar Power Satellite Technical Overview
L. E. Livingston, Lyndon B. Johnson Space Center |
| 33 | Early Solar Power Satellite Concepts
Gordon Woodcock, Boeing |
| 45 | Microwave Systems Summary/Conclusions
Introduction to Planned Program Activities
R. H. Dietz, Lyndon B. Johnson Space Center |

DOE / NASA Concept Evaluation Program

***Robert O. Piland
Lyndon B. Johnson Space Center***

NASA
S78-10349



NASA

Solar Power
Satellite

Chronology

Activity 68 69 70 71 72 73 74 75 76 77 78 79 80

Concept presented ▲

Initial system study ■

NASA assessment ■

Congressional study ■

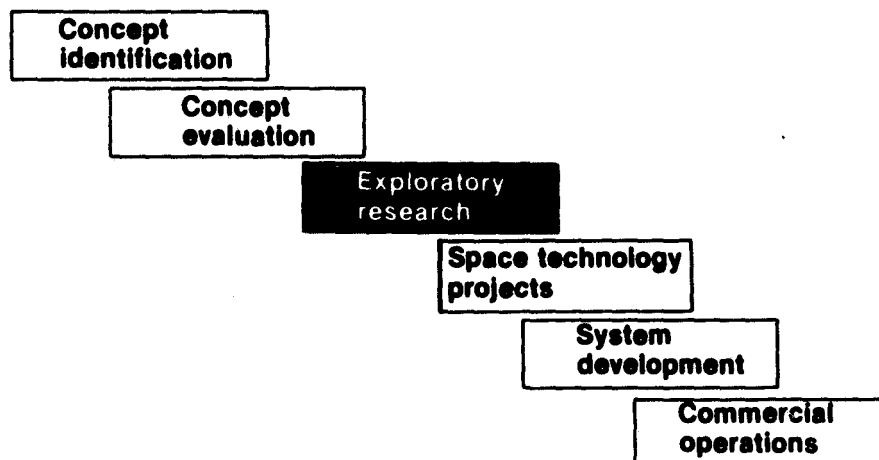
NASA in-house studies ■

DOE assessment ■

DOE /NASA evaluation program //

NASA

Evolutionary program phasing



PRECEDING PAGE BLANK NOT FILMED

Objective		To develop by the end of 1980, an initial understanding of the economic practicality and the social and environmental acceptability of the Solar Power Satellite concept.				
Funding	Program components		77	78	79	80 Total
	NASA	Systems definition	2500	1700	1300	800 6300
	DOE	Environment, health, safety	220	1940	2050	1740 5950
		Societal assessment	164	537	537	322 1560
		Comparative assessment	95	376	754	585 1790
			2979	4553	4641	3427 15600
Program Milestones			77	78	79	80
	Program initiation		●			
	Baseline concept selection					
		Preliminary		●		
		Final			○	
	Program recommendation					
		Preliminary				○
		Updated				○
		Final				○

TECHNICAL WORKSHOP

OBJECTIVES

ASSESS AND CRITIQUE:

- THE ASSUMPTIONS, METHODOLOGIES AND CONCLUSIONS OF THE STUDIES
- THE IDENTIFIED CRITICAL ISSUES AND THE FOLLOW-ON WORK BEING RECOMMENDED.

SPS CONCEPT EVALUATION PROGRAM

SCOPE

- COLLECTION AND CONVERSION OF SOLAR ENERGY IN SPACE
- 'POSITIVE' TRANSMISSION OF ENERGY TO EARTH FOR COLLECTION AND CONVERSION.
- SPACE CONSTRUCTION MATERIALS FROM EARTH - USE OF NON-TERRESTRIAL MATERIALS STUDIED OUTSIDE OF PRESENT PROGRAM
- SPACE-BASED SOLAR REFLECTOR CONCEPTS NOT INCLUDED - 'SOLARES' CONCEPT STUDIED OUTSIDE OF PRESENT PROGRAM.

***Solar Power Satellite
Technical Overview***

***L. E. Livingston
Lyndon B. Johnson Space Center***

SPS OVERVIEW

SPACECRAFT DESIGN DIVISION

L. E. LIVINGSTON

- SUMMARY OF MAJOR CONCLUSIONS REACHED TO DATE
- PRESENT DISCUSSION LIMITED TO BASIC SPS CONCEPT:
 - SOLAR ENERGY COLLECTED AND CONVERTED TO ELECTRICITY IN GEOSYNCHRONOUS ORBIT (GEO)
 - MICROWAVE TRANSMISSION OF ENERGY TO EARTH
- ALTERNATE CONCEPTS NOT CONSIDERED:
 - LASER TRANSMISSION
 - LOW ALTITUDE SOLAR COLLECTORS
 - ORBITING MIRRORS
 - ETC.

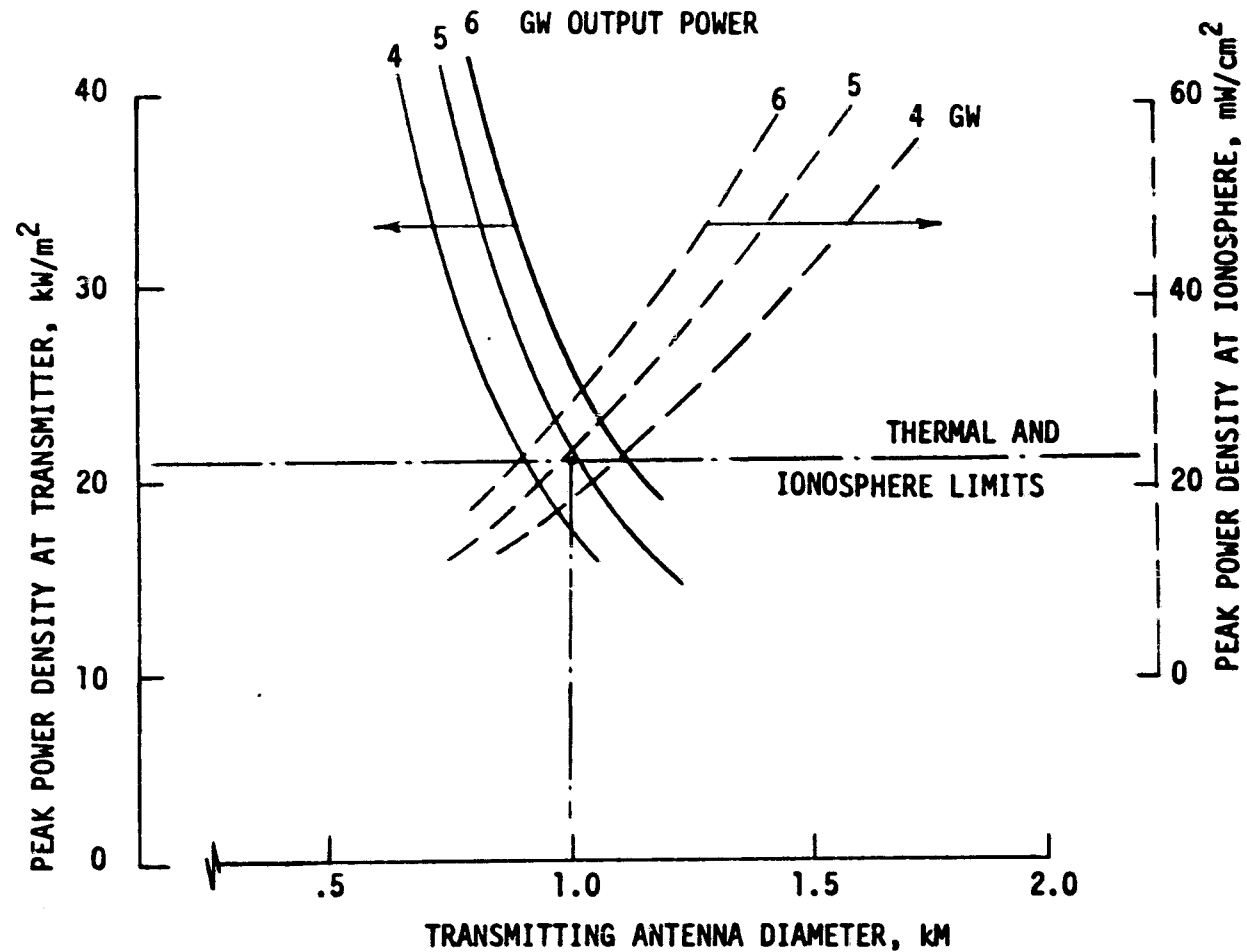
CS

SPS SYSTEM	SPACECRAFT DESIGN DIVISION	
	L. E. LIVINGSTON	

- SPS CAN BE BASELOAD SOURCE OF ELECTRICAL POWER
 - CONTINUOUS SOLAR ILLUMINATION EXCEPT FOR OCCULTATIONS UP TO 75 MINUTES DAILY FOR 6 WEEKS AT EQUINOXES (99%)
 - MINIMUM LOSSES DUE TO WEATHER EFFECTS
 - MOST FAILURE MODES RESULT IN GRADUAL OR PARTIAL POWER LOSS RATHER THAN ABRUPT, TOTAL OUTAGE

- MAXIMUM POWER PER MICROWAVE LINK ~5 GW
 - CAN BE AS LOW AS 3 GW WITH MODEST COST PENALTY

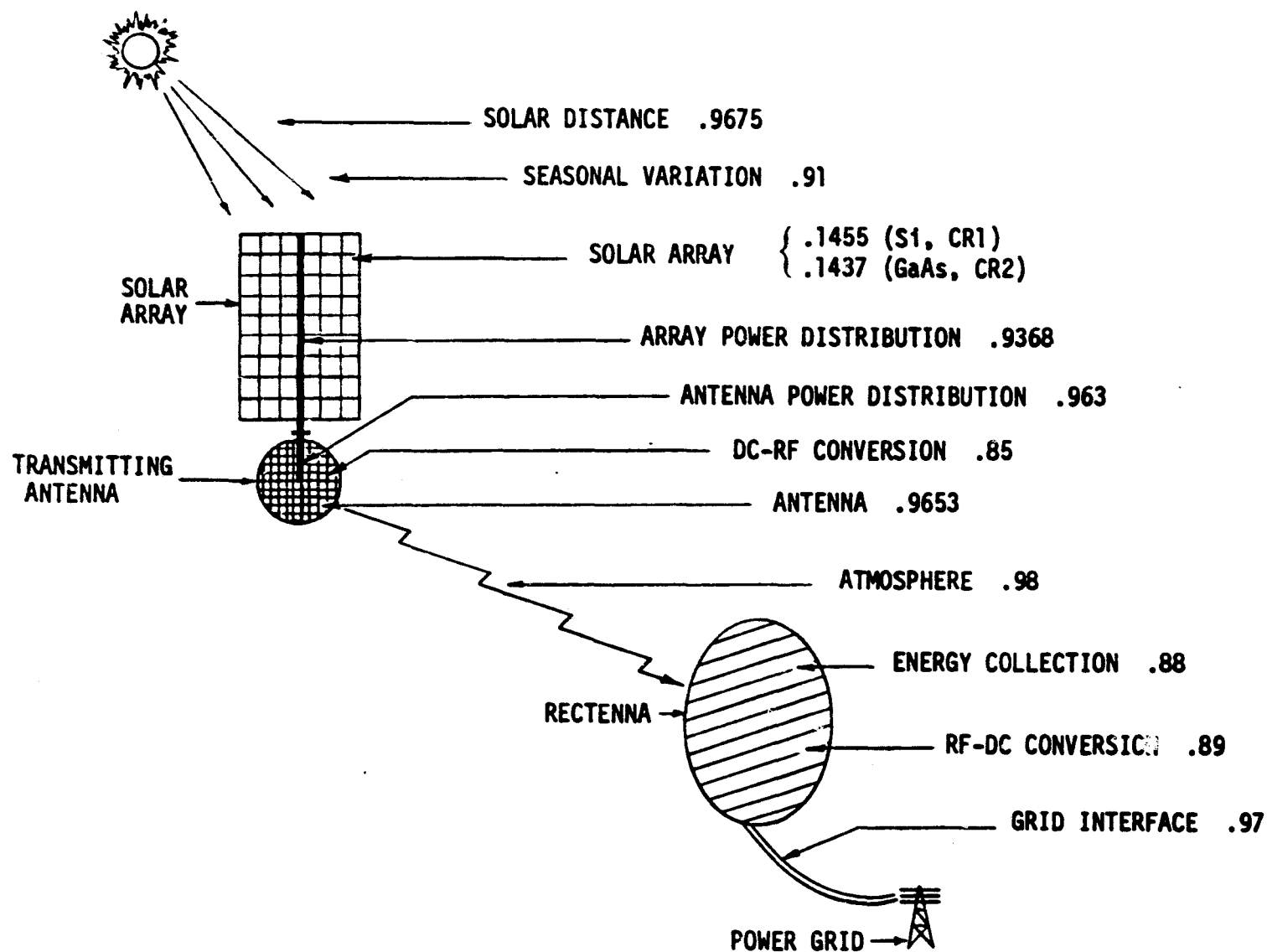
- 10 dB TAPER
- 2.45 GHz
- NOMINAL EFFICIENCY CHAIN



NOMINAL EFFICIENCY CHAIN

SPACECRAFT DESIGN DIVISION

L. E. LIVINGSTON

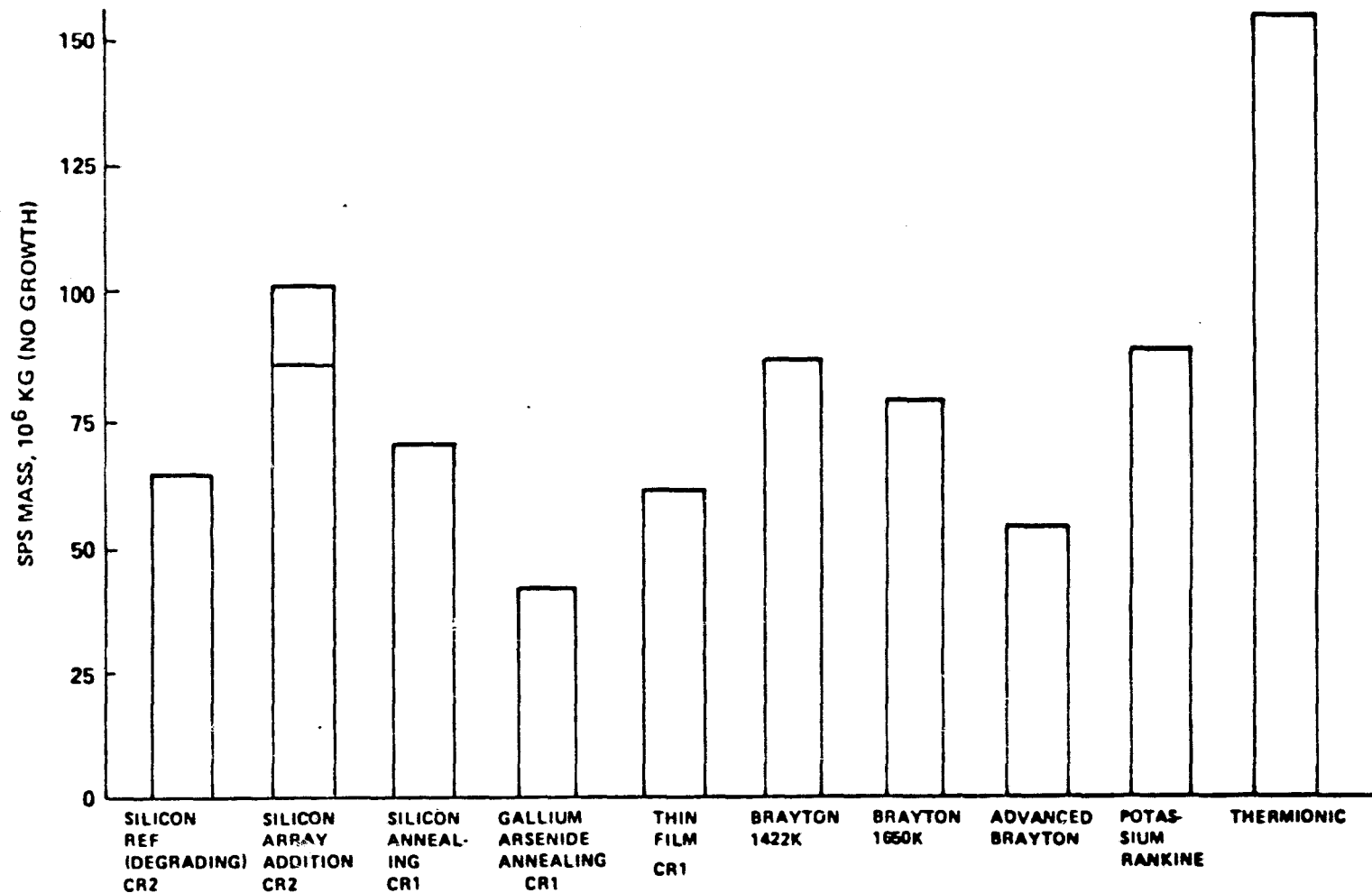


ENERGY CONVERSION - SPS MASS

SPACECRAFT DESIGN DIVISION

L. E. LIVINGSTON

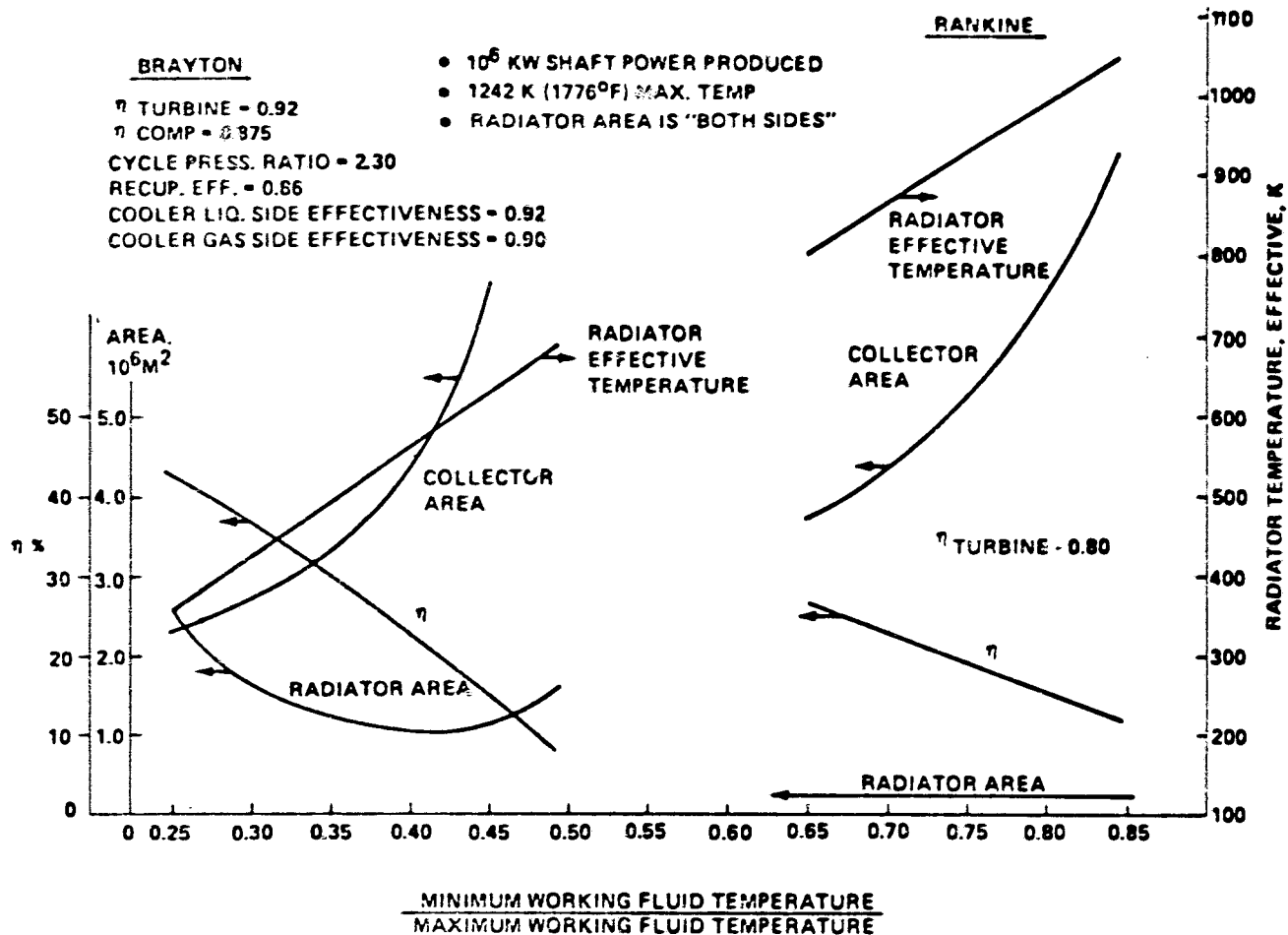
MASS COMPARISON INDICATES ELIMINATION OF THERMIONICS



ENERGY CONVERSION - CYCLE TEMPERATURE RATIO

SPACECRAFT DESIGN DIVISION

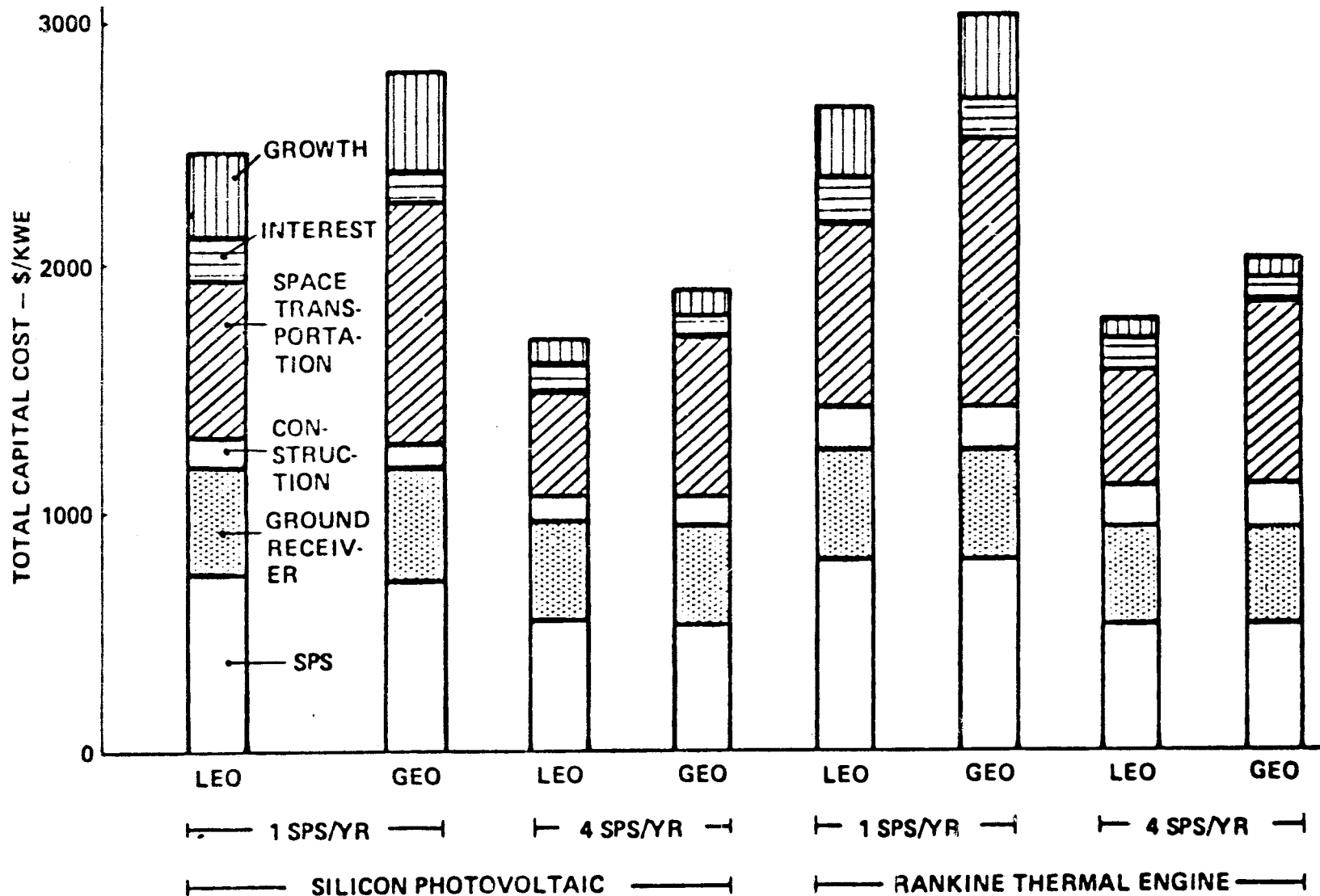
L. E. LIVINGSTON



ENERGY CONVERSION - CAPITAL COST

SPACECRAFT DESIGN DIVISION

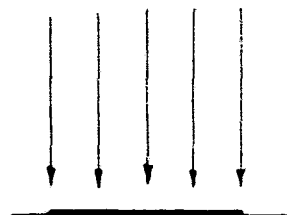
L. E. LIVINGSTON



CELL MATERIAL AND CONCENTRATION RATIO

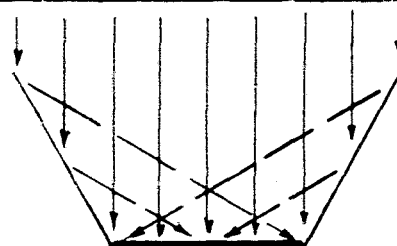
SPACECRAFT DESIGN DIVISION

L. E. LIVINGSTON



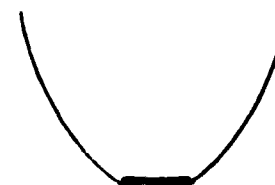
CR1

SIMPLE CONSTRUCTION
HIGHER CELL EFFICIENCY



CR2

LOWER MASS
FEWER CELLS



CR>2

COMPLEX CONSTRUCTION
LOW EFFICIENCY



SILICON - CR1:

EFFICIENCY LOSS FROM INCREASED TEMPERATURE NEGATES
ADVANTAGES OF CONCENTRATION

GALLIUM ARSENIDE - CR2:

SMALL EFFICIENCY LOSS MORE THAN COMPENSATED BY MASS
AND MATERIAL SAVING

POWER DISTRIBUTION

SPACECRAFT DESIGN DIVISION

L. E. LIVINGSTON

- HIGH-VOLTAGE DC SYSTEM HAS MINIMUM MASS FOR PHOTOVOLTAIC SPS WITH SEPARATE ANTENNA
 - OPTIMUM VOLTAGE DEPENDS ON DC-RF CONVERSION SYSTEM
 - PLASMA INTERACTIONS MAY LIMIT VOLTAGE
 - ORDERS-OF-MAGNITUDE IMPROVEMENT IN SWITCHING SPEED OF STATE-OF-THE-ART DC SWITCHGEAR REQUIRED
- AC SYSTEM MAY BE PREFERABLE FOR THERMAL ENGINE CONVERSION SYSTEM
 - AC GENERATORS
 - ROTARY TRANSFORMER INSTEAD OF SLIPRING
 - COMPONENT STATE-OF-THE-ART CLOSER TO REQUIREMENTS
- LARGE DISTRIBUTION SYSTEM MASS PENALTY FOR SOLID-STATE DC-RF CONVERSION IN SEPARATE ANTENNA
- ROTARY JOINT WITH SLIPRINGS IS FEASIBLE

MICROWAVE POWER TRANSMISSION

SPACECRAFT DESIGN DIVISION

L. E. LIVINGSTON

- MICROWAVE POWER TRANSMISSION AT MULTI-GW LEVEL IS FEASIBLE
- 2.45 GHz FREQUENCY DESIRABLE
 - PROPAGATION THROUGH ATMOSPHERE
 - ISM BAND UTILIZATION
 - ANTENNA, RECTENNA SIZES
 - HARDWARE TECHNOLOGY PROJECTIONS
- PLANAR, SLOTTED-WAVEGUIDE PHASED ARRAY IS MOST EFFICIENT TRANSMITTING ANTENNA
- 10 dB, 10-STEP GAUSSIAN TAPER OPTIMUM FOR RECTENNA COLLECTION EFFICIENCY
- SUBARRAY SIZE 10m x 10m
 - COMPROMISE BETWEEN MECHANICAL, ELECTRICAL REQUIREMENTS
 - 1 ARC MIN ANTENNA FLATNESS, 3 ARC MIN SUBARRAY ALIGNMENT

MICROWAVE POWER TRANSMISSION (CONTINUED)

SPACECRAFT DESIGN DIVISION

L. E. LIVINGSTON

- POWER AMPLIFIERS:

- KLYSTRON FEASIBLE: HIGH GAIN, HIGH POWER, LOW NOISE; HEAT PIPE COOLING
- AMPLITRON LESS SUITABLE: PASSIVE COOLING; LOW GAIN, LOW POWER, HIGH NOISE
- MAGNETRON WARRANTS FURTHER INVESTIGATION: LOW NOISE, HIGH EFFICIENCY, SIMPLE DESIGN

- PHASE CONTROL:

- ELECTRONIC FOCUSING AND STEERING REQUIRED
- CODED SIGNAL CAN PROVIDE SECURITY
- RETRODIRECTIVE SYSTEM: FAST RESPONSE; POSSIBLE CALIBRATION PROBLEM
- GROUND-BASED SYSTEM: SELF-CALIBRATING; SLOW RESPONSE
- HYBRID SYSTEM POSSIBLE

- INDIVIDUAL RECTENNA ELEMENTS FEEDING RECTIFYING CIRCUITS IS MOST EFFECTIVE APPROACH BASED ON ANALYSIS AND RESEARCH

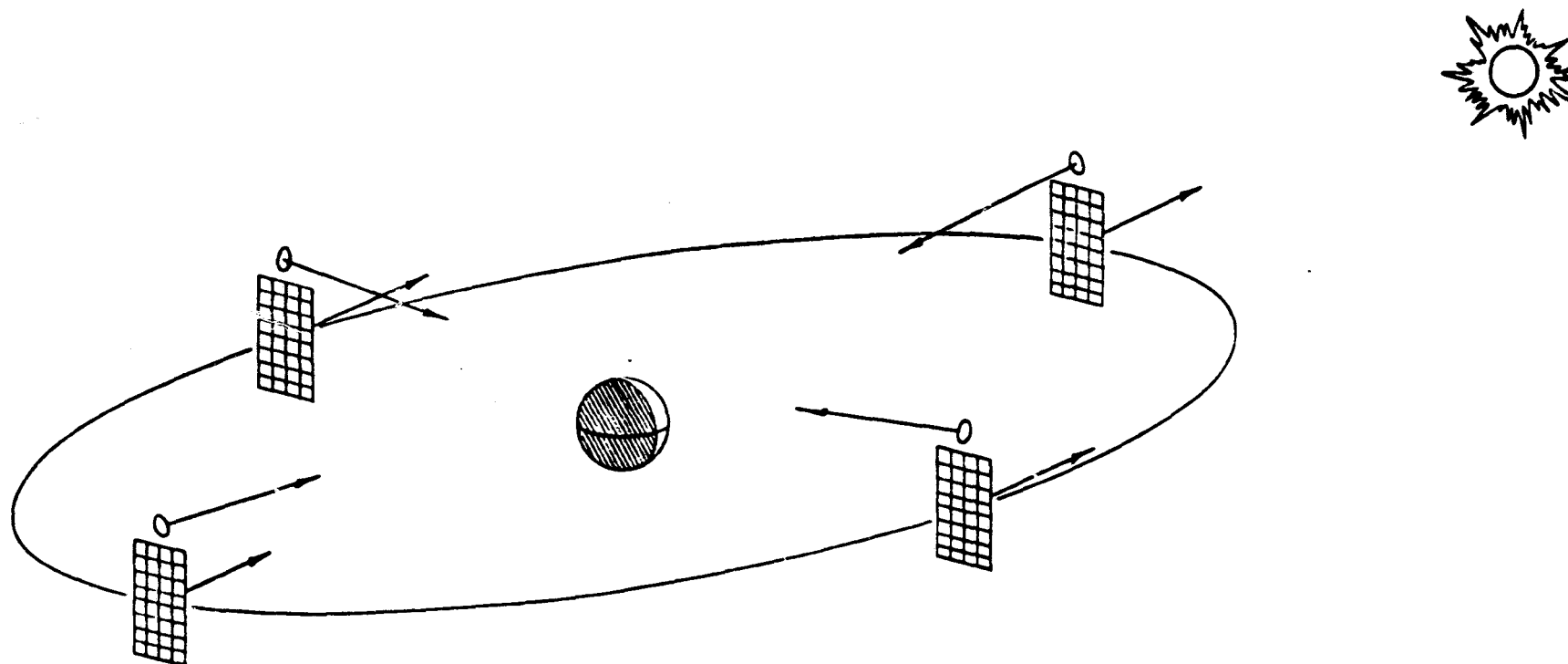
- SOLID STATE SYSTEMS:

- MAXIMUM POWER ABOUT 2.5 GW
- LARGER TRANSMITTING ANTENNA, SMALLER RECTENNA
- LESS MAINTENANCE
- ADVANCING TECHNOLOGY BASE
- FURTHER INVESTIGATION WARRANTED

SPS ORIENTATION

SPACECRAFT DESIGN DIVISION

L. E. LIVINGSTON



STATIONKEEPING AND ATTITUDE CONTROL

SPACECRAFT DESIGN DIVISION

L. E. LIVINGSTON

- SOLAR RADIATION PRESSURE IS PREDOMINANT ORBIT PERTURBATION
 - CONTINUAL CORRECTION NECESSARY TO AVOID EAST-WEST MOTION THROUGH ADJACENT ORBIT POSITIONS
 - ANNUAL PROPELLANT ~60 TONNES
- GRAVITY GRADIENT TORQUE IS PREDOMINANT ATTITUDE DISTURBANCE
 - SOLAR RADIATION PRESSURE ALSO SIGNIFICANT FOR ASYMMETRICAL CONFIRMATIONS
 - BOTH DISTURBANCES CONTROLLABLE WITH DIFFERENTIAL THRUSTING DURING CONTINUOUS ORBIT CORRECTIONS; VERY LITTLE ADDITIONAL PROPELLANT REQUIRED
- ANTENNA POINTING CONTROLLABLE BY MOMENTUM EXCHANGE DEVICES

STRUCTURE/CONTROL/MATERIALS	SPACECRAFT DESIGN DIVISION	
	L. E. LIVINGSTON	

- BECAUSE LOADS ARE LOW, STRUCTURE REPRESENTS A SMALL PART OF THE SPS MASS
- STRUCTURAL DESIGN IS GOVERNED BY STIFFNESS REQUIREMENTS FOR DYNAMIC STABILITY
- TRANSIENT THERMAL ENVIRONMENT IS MAJOR CONSIDERATION
 - DAILY OCCULTATIONS AT EQUINOXES
 - MPTS DAILY SOLAR CYCLE DISTORTS ANTENNA
- GRAPHITE COMPOSITE MATERIAL WITH LOW CTE ATTRACTIVE FOR STRUCTURE
 - THERMAL OSCILLATIONS MINIMIZED WITHOUT ACTIVE CONTROL
 - HIGH ELASTIC COEFFICIENT ENHANCES STIFFNESS
 - SIMPLIFIED DESIGN
 - 30-YEAR LIFE NOT YET ESTABLISHED
- ALUMINUM USABLE
 - MUCH LARGER THERMAL DEFLECTIONS
 - HIGHER THERMAL STRESSES
 - INCREASED STRUCTURAL MASS
 - MORE COMPLEX DESIGN
- PERFORMANCE VERIFICATION IS ONLY POSSIBLE BY ANALYSIS

SPACE CONSTRUCTION

SPACECRAFT DESIGN DIVISION

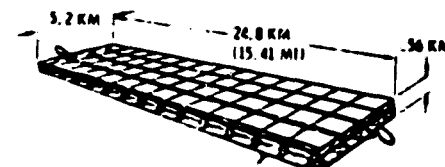
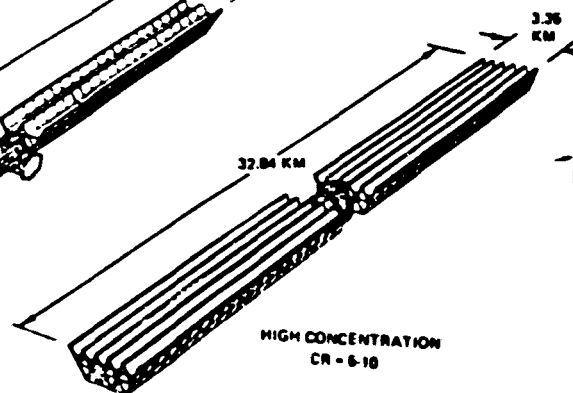
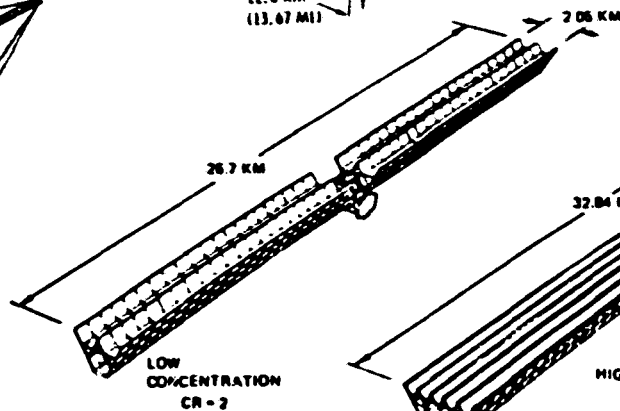
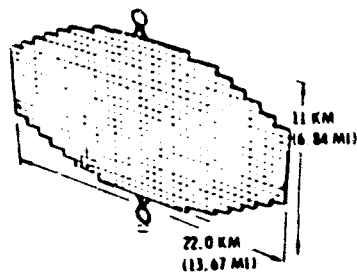
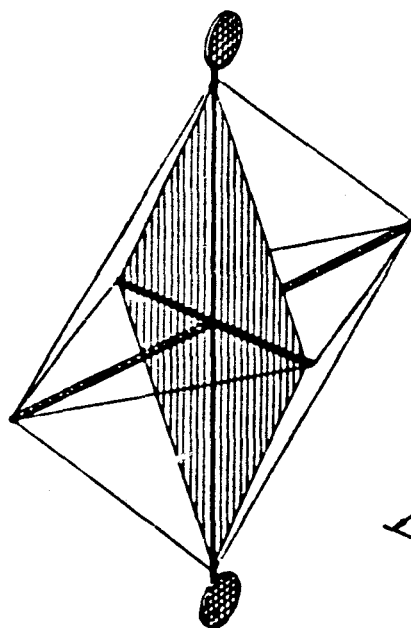
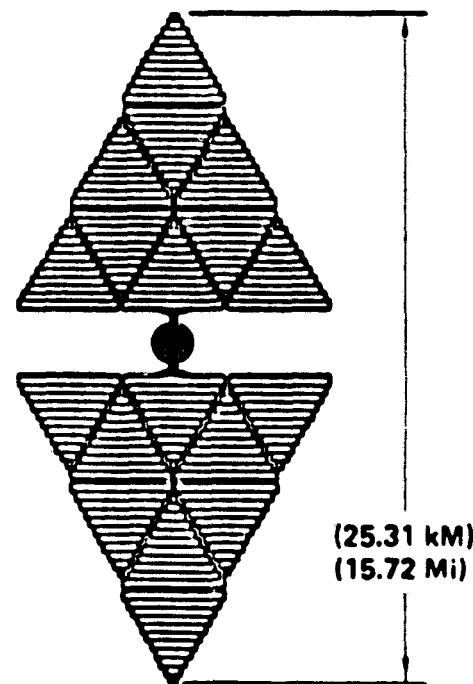
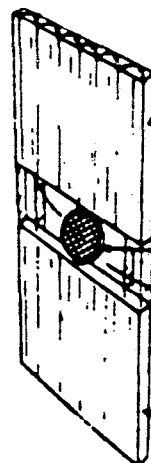
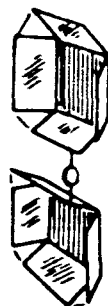
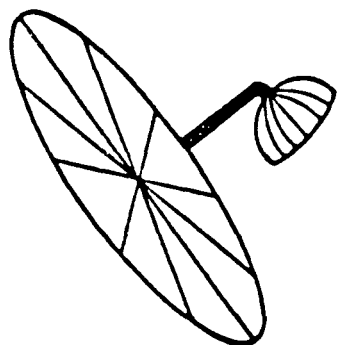
L. E. LIVINGSTON

- SPS MUST BE CONSTRUCTED IN ORBIT
- SIX-MONTH CONSTRUCTION TIME FOR 5 GW SATELLITE IS TECHNICALLY FEASIBLE
- EASE OF CONSTRUCTION IS A MAJOR DRIVER IN CONFIGURATION SELECTION
 - FEW DISTINCT OPERATIONS REPEATED MANY TIMES EASIER TO AUTOMATE
 - SIMPLE GEOMETRY

PHOTOVOLTAIC CONFIGURATION CONCEPTS

SPACECRAFT DESIGN DIVISION

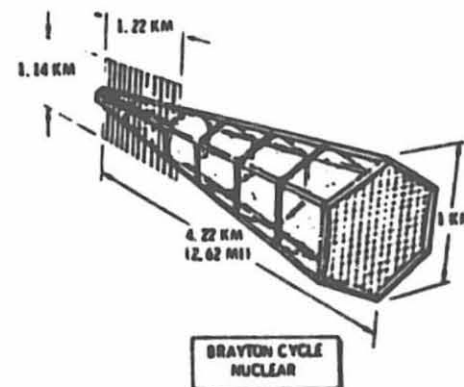
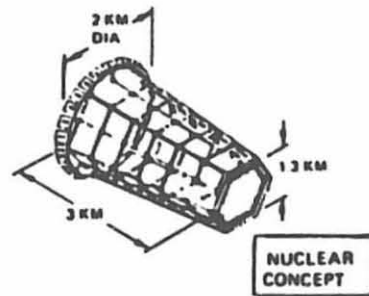
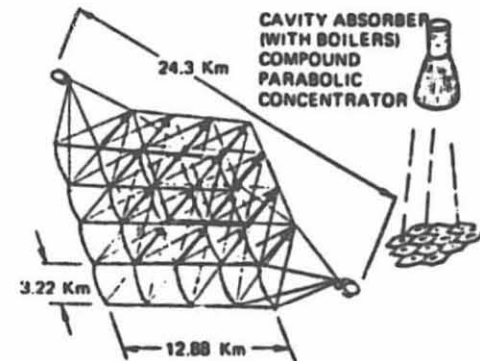
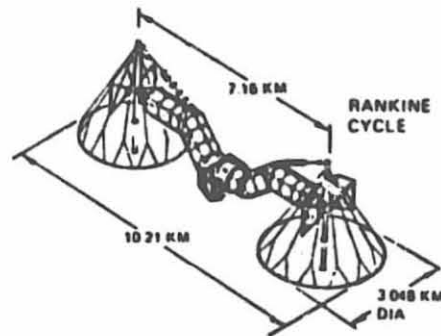
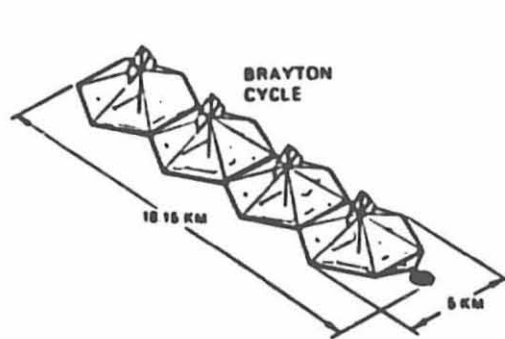
L. E. LIVINGSTON

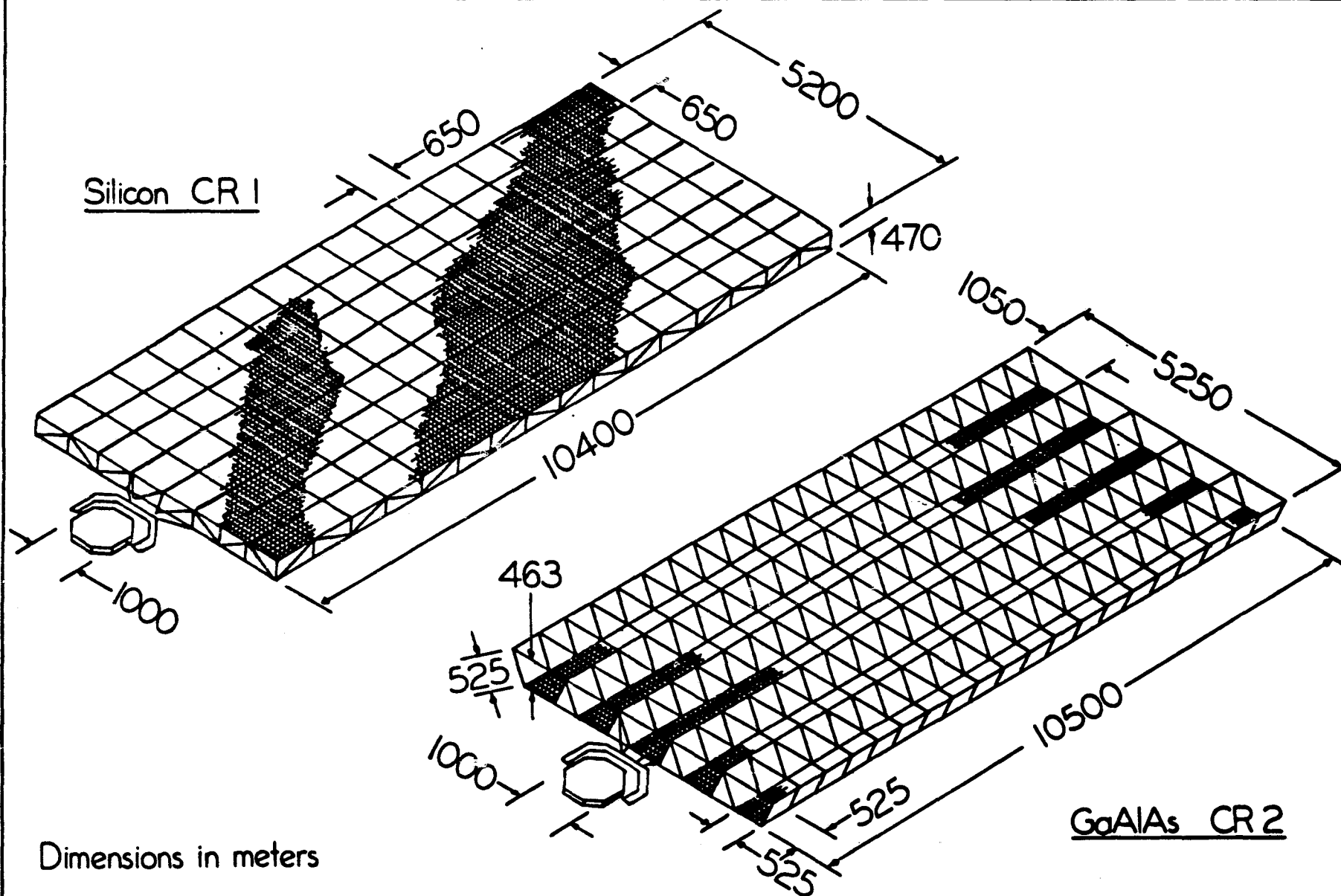


SOLAR/THERMAL AND NUCLEAR CONFIGURATION CONCEPTS

SPACECRAFT DESIGN DIVISION

L. E. LIVINGSTON





Dimensions in meters

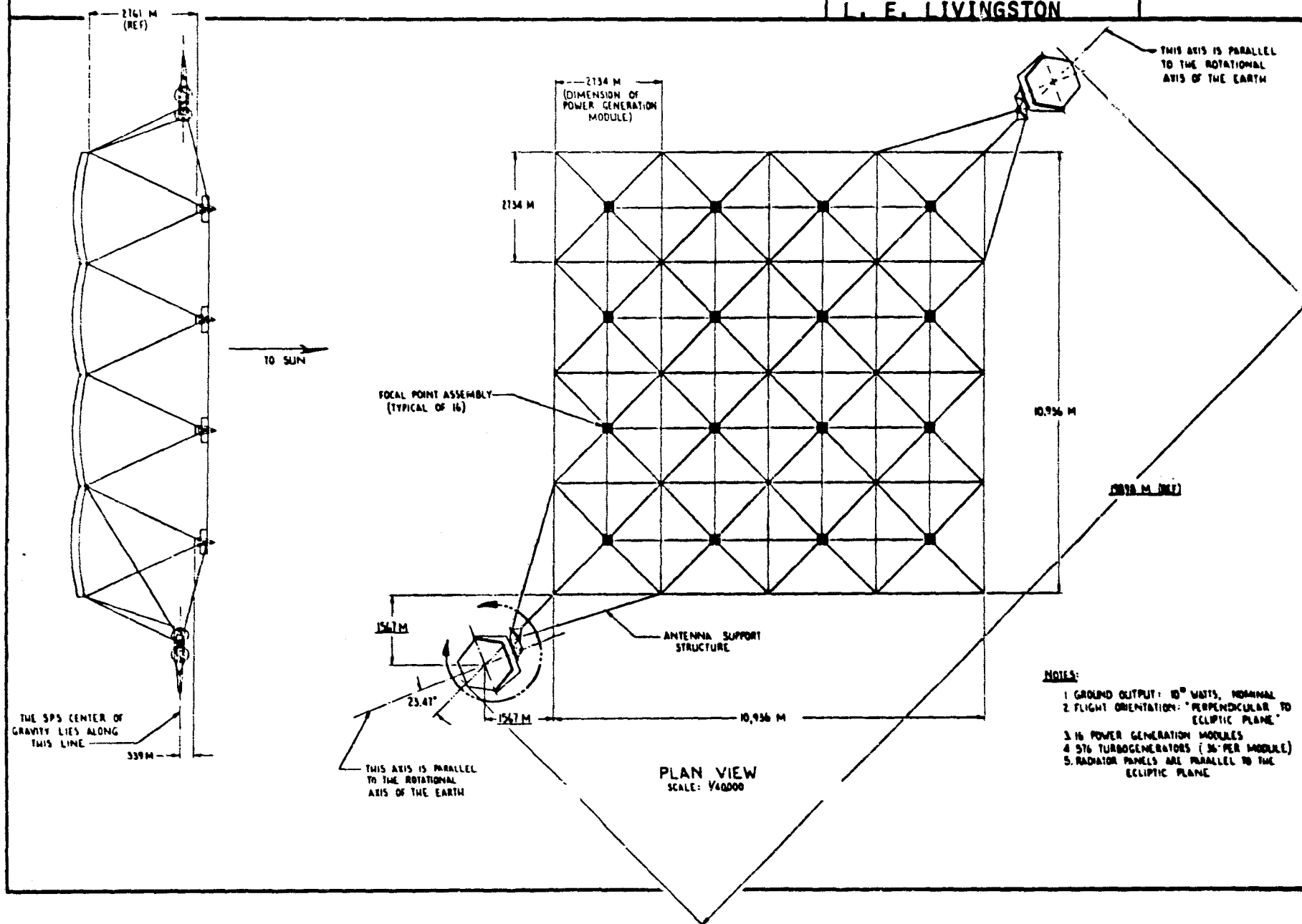
LEO/GEO CONSTRUCTION	SPACECRAFT DESIGN DIVISION	
	L. E. LIVINGSTON	

- CONSTRUCTION IS POSSIBLE IN EITHER LEO OR GEO
- LEO CONSTRUCTION:
 - AERODYNAMIC AND GRAVITY GRADIENT LOADS MAKE CONSTRUCTION OF COMPLETE SPS IMPRACTICAL
 - MODULAR SECTIONS OF SPS CAN BE CONSTRUCTED IN LEO AND TRANSPORTED INDIVIDUALLY TO GEO FOR FINAL ASSEMBLY
 - MOST PERSONNEL AT LEO
 - POSSIBLE SELF-POWERED TRANSFER TO GEO
- GEO CONSTRUCTION
 - MONOLITHIC STRUCTURE
 - FEWER PASSAGES THROUGH EARTH'S SHADOW
 - REDUCED COLLISION HAZARD FROM DEBRIS

RANKINE CYCLE SPS

SPACECRAFT DESIGN DIVISION

L. E. LIVINGSTON



MAINTENANCE	SPACECRAFT DESIGN DIVISION	
	L. E. LIVINGSTON	

- MAINTENANCE OF OPERATIONAL SATELLITES WILL BE NECESSARY TO KEEP TRANSMITTED POWER AT REQUIRED LEVELS
- MAINTENANCE FACILITIES CAN BE INCORPORATED IN CONSTRUCTION BASE
- 60-SATELLITE FLEET WILL REQUIRE ROUGHLY 1000 MAINTENANCE PERSONNEL ON ORBIT

SPACE TRANSPORTATION EARTH - LEO	SPACECRAFT DESIGN DIVISION	
	L. E. LIVINGSTON	

- TRANSPORTATION, PRIMARILY EARTH-TO-LEO CARGO, REPRESENTS ABOUT 1/4 OF SPS CAPITAL COST
- BALLISTIC HLLV
 - SMALLER, LIGHTER
 - LOWER DEVELOPMENT COST
- WINGED HLLV
 - EASIER RECOVERY AND REUSE
 - LOWER OPERATING COST
 - USABLE FOR PERSONNEL TRANSFER
- CHOICE INFLUENCED BY LAUNCH RATE REQUIRED
- DEPRESSED TRAJECTORY CAN PREVENT DIRECT INJECTION OF HLLV EXHAUST INTO IONOSPHERE

SPACE TRANSPORTATION LAUNCH SITES	SPACECRAFT DESIGN DIVISION	
	L. E. LIVINGSTON	

- KSC:
 - COULD SUPPORT CONSTRUCTION RATES UP TO 10 GW PER YEAR
 - SONIC OVERPRESSURE AND NOISE CAN BE KEPT WITHIN ACCEPTABLE LIMITS

- EQUATORIAL:
 - MORE FREQUENT LAUNCH WINDOWS
 - LESS PLANE CHANGE BY OTV
 - OFFSHORE SITES PRACTICAL IN WATER DEPTHS OF AT LEAST 600 FEET
 - TERRESTRIAL TRANSPORTATION COST AND TRANSIT TIME (LOST REVENUE) ARE SIGNIFICANT CONSIDERATIONS

- SOLAR-POWERED ARGON ION ENGINE SYSTEM (EOTV):
 - LOWER OPERATING COST
 - LONG TRIP TIMES SUITABLE ONLY FOR CARGO
 - DEGRADATION FROM RADIATION IN VAN ALLEN BELTS

- CHEMICAL SYSTEM:
 - COST ABOUT \$1B MORE PER 5 GW SATELLITE
 - USABLE FOR BOTH CARGO AND PERSONNEL

***Early
Solar Power Satellite
Concepts***

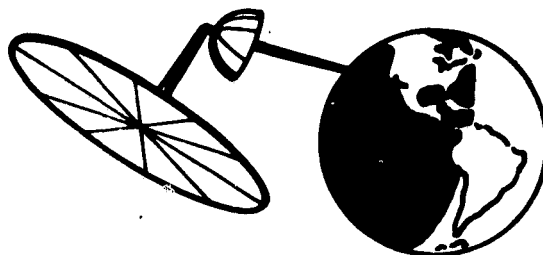
***Gordon Woodcock
Boeing***

NASA

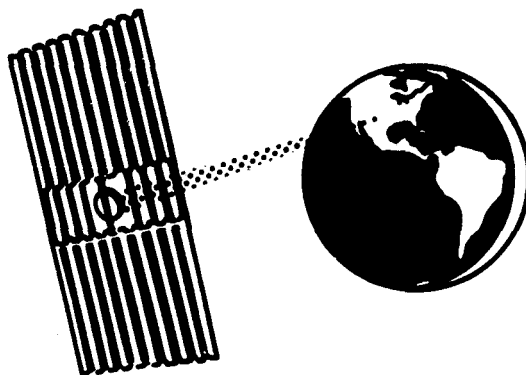
Solar Power Satellite

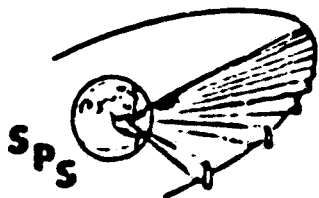
Early Concepts

1968 Glaser



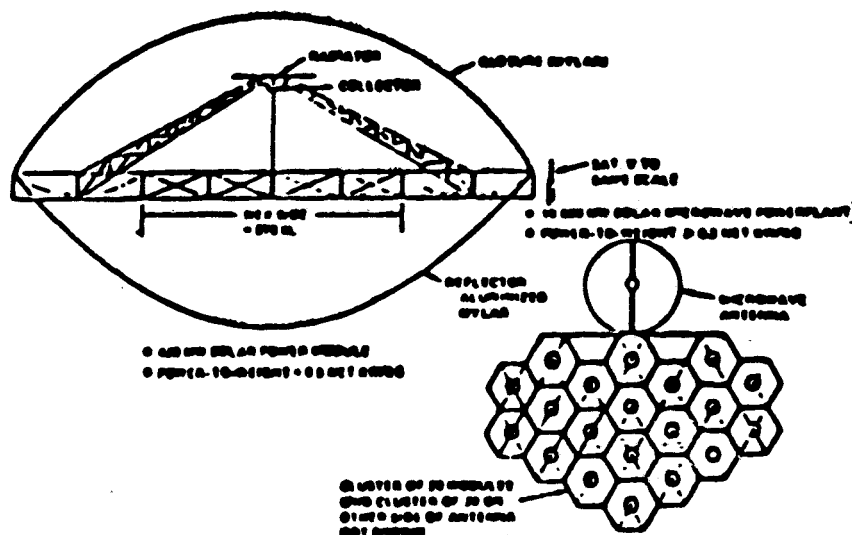
1973 ADL/Grumman/Raytheon/
Spectrolab Study for
NASA LeRC



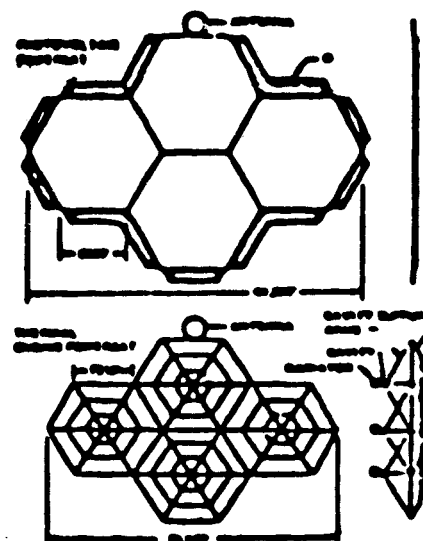


Configuration Concepts Circa 1972-4

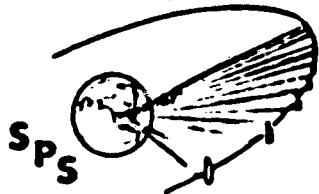
COXING



SOLAR-BRAYTON POWER SYSTEM CONCEPT



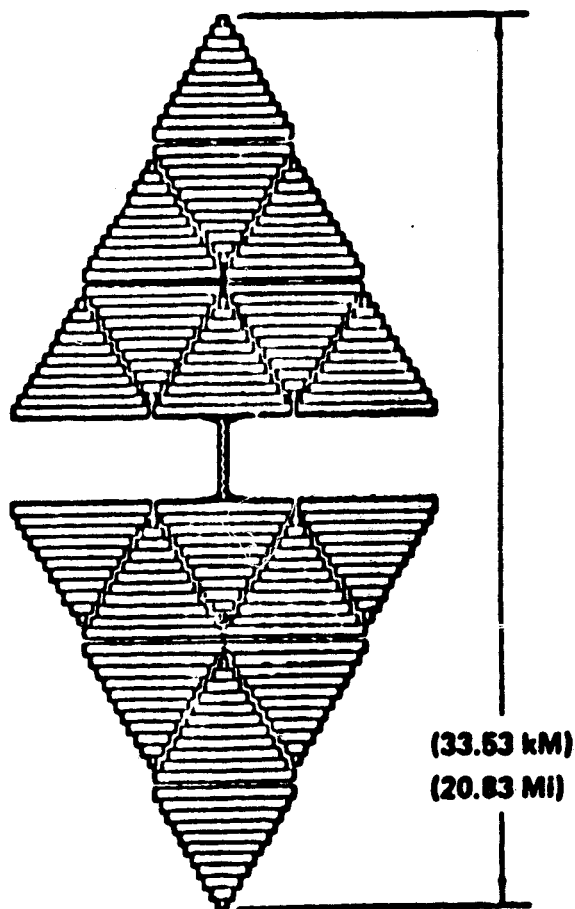
"THEREFORE, WHILE RECOGNIZING THAT SOLAR CELLS MAY ULTIMATELY PROVE TO BE THE BEST SOLUTION, WE EXAMINED THE ALTERNATIVE OF A SOLAR CONCENTRATOR AND HEAT ENGINE."



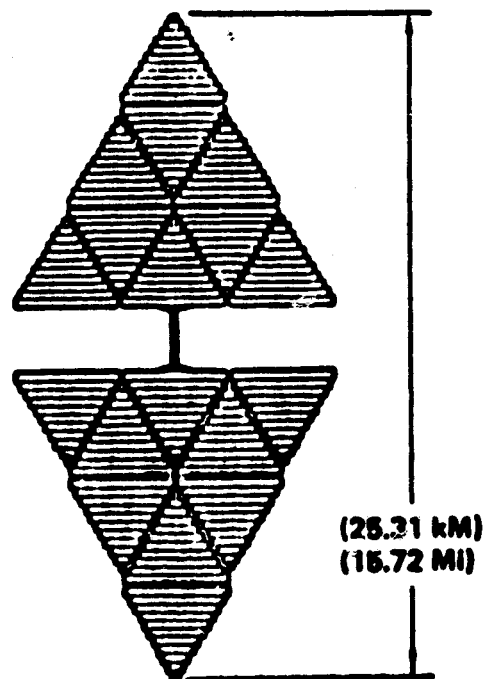
Comparison of Power Satellite Option Sizes

BOEING

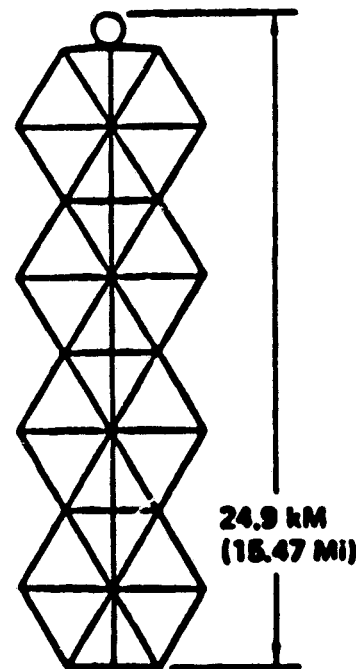
SILICON PHOTOVOLTAIC



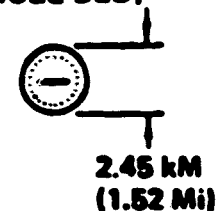
GaAs PHOTOVOLTAIC



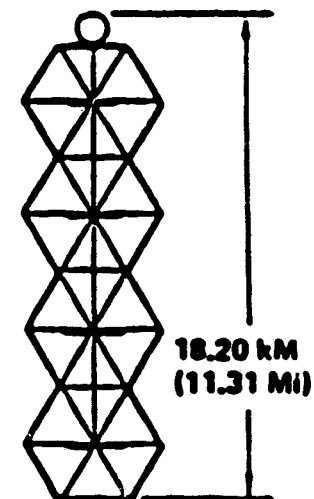
THERMIONIC



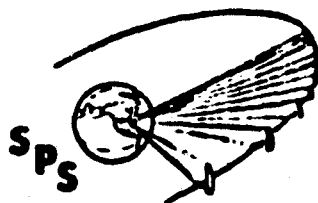
NUCLEAR (ROTATING PARTICLE BED)



BRAYTON

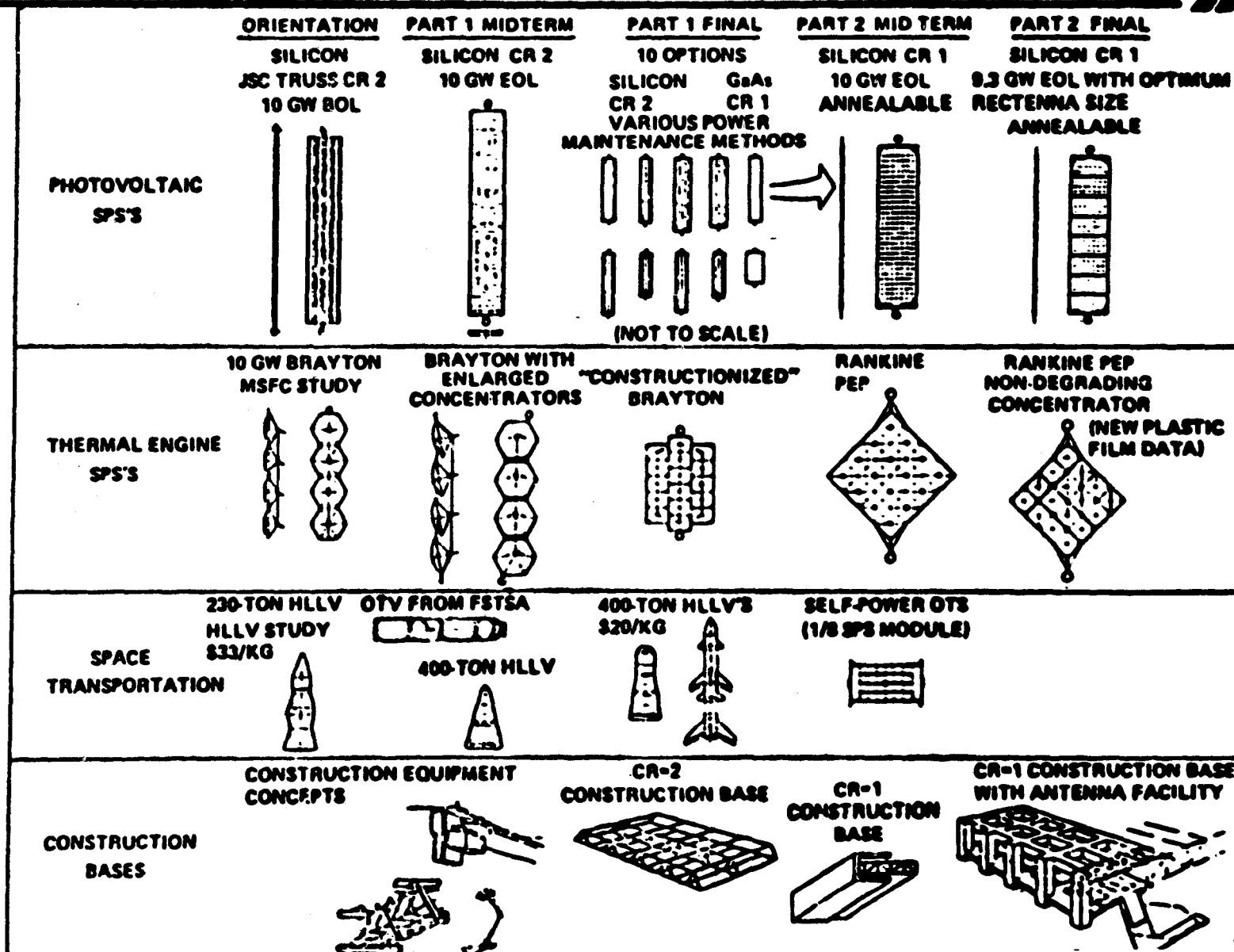


ALL ARE TO SAME SCALE, END-OF-LIFE CONFIGURATION)








SPS System Definition Study Design Evolutions

BRING





PROPELLANT PRODUCTION REQUIREMENTS SPS CONSTRUCTION AT 10,000 MEGAWATTS/YR

		METRIC TONS/YR				TOTAL 	PLANT CAPITAL COST \$M79	
	HLLV	POTV	EOTV	PLV	TONS/DAY			
LO ₂	2,671,000	3,722	1,060	57,700	9,000 	650	}	From Coal & Air
LCH ₄	642,600	-0-	-0-	18,700	2,200 	615		
LH ₂	123,704	745	353	3,036	420 	500		
ARGON	-0-	-0-	14,400	-0-	47 	-0-		

 Capacity required at start of program; includes 20% margin

 1979 U.S. capacity is about 30,000 tons/day

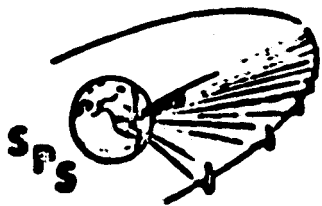
 About 0.2% of U.S. Natural Gas Consumption in 1977

 Today's capacity is 100 T/Day

 Byproduct of LO₂ Plant

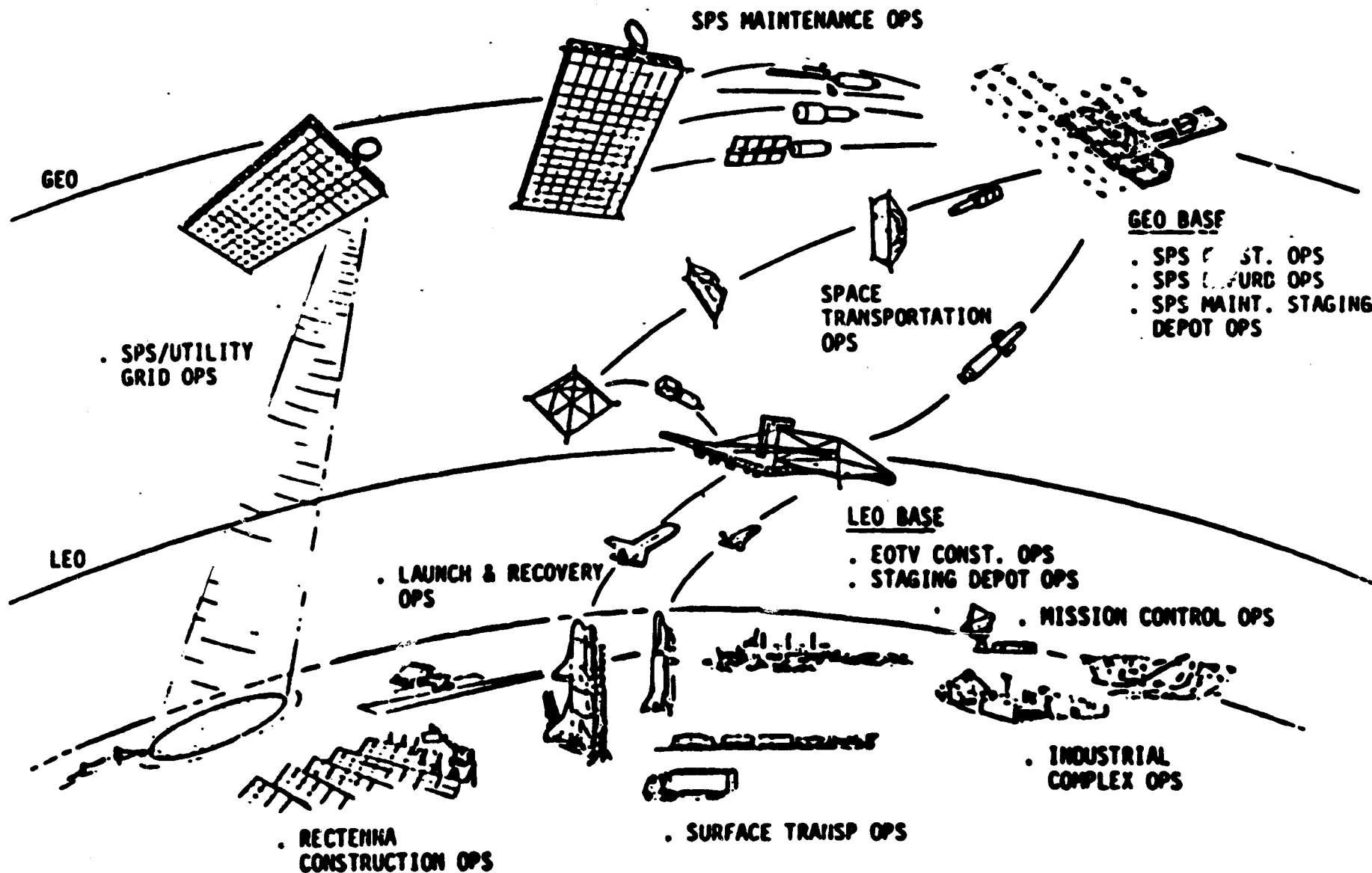
 12,250 T/D coal + 1000 megawatts electric power. Coal use is 0.7% of U.S. '77

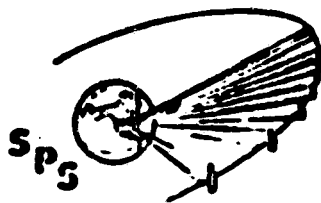
ORIGINAL PAGE IS
OF POOR QUALITY



INTEGRATED SPS PROGRAM OPERATIONS

BEING





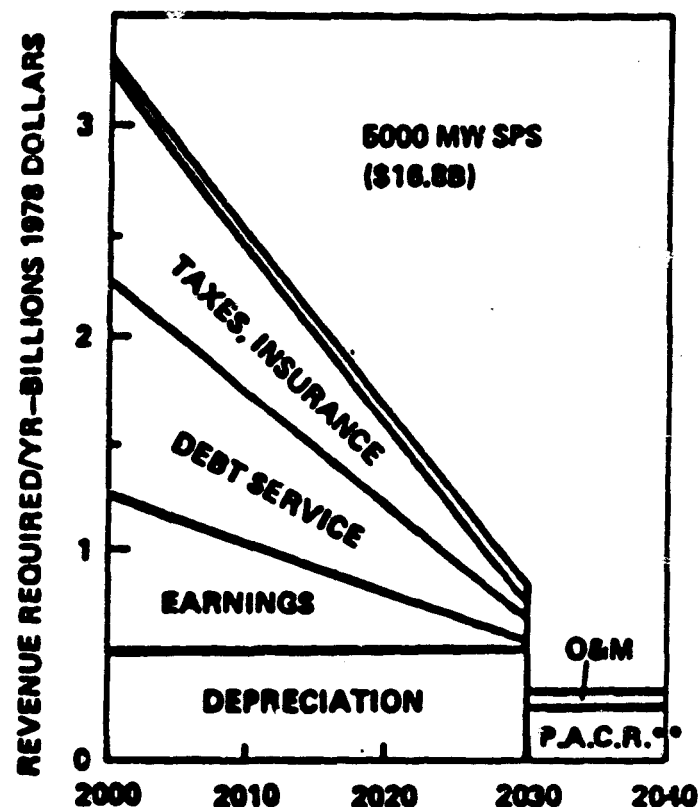
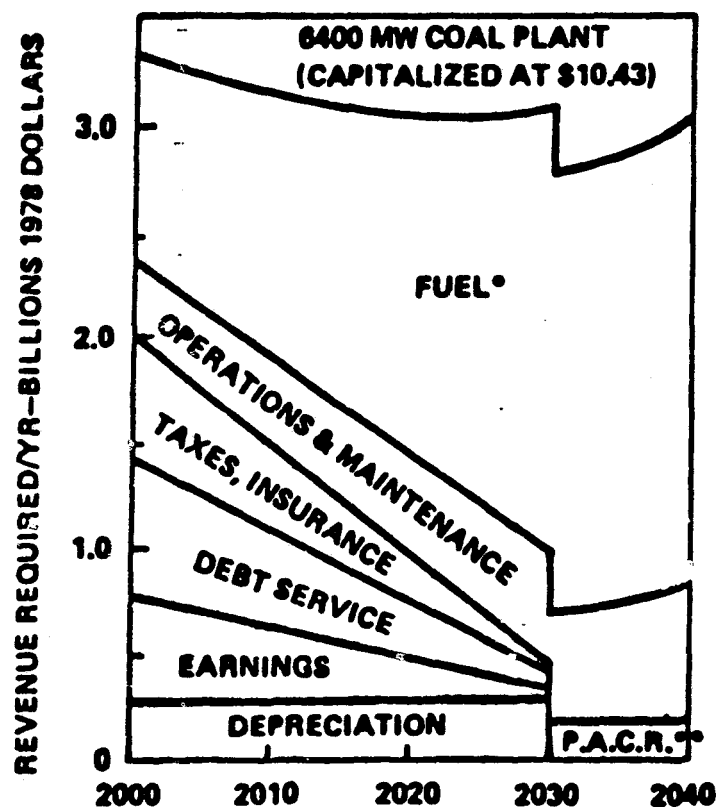
SPS RECURRING COST SUMMARY

(1979 Dollars)

NRIND

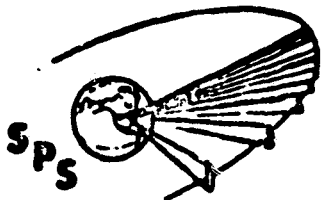
SPS HARDWARE AS COSTED	4946	
LESS IMPLICIT AMORTIZATION OF INVESTMENT	<u>473</u> 4473	(Half of 10.61% per annum on 8924 M for factories and production equipment)
SPACE TRANSPORTATION	3120	Based on SPS mass with growth'
CONSTRUCTION OPERATIONS	961	Includes 10 support people on the ground per space worker as well as construction base spares
GROUND TRANSPORTATION	35	
RECTENNA	2578	
MISSION CONTROL	10	
PROGRAM MANAGEMENT & INTEGRATION	495	Equivalent to 14,000 direct people
COST ALLOWANCE FOR MASS GROWTH	<u>766</u>	17% of net SPS hardware cost
TOTAL DIRECT OUTLAY	12,432	

Annual Revenue Requirements in 1978 Dollars

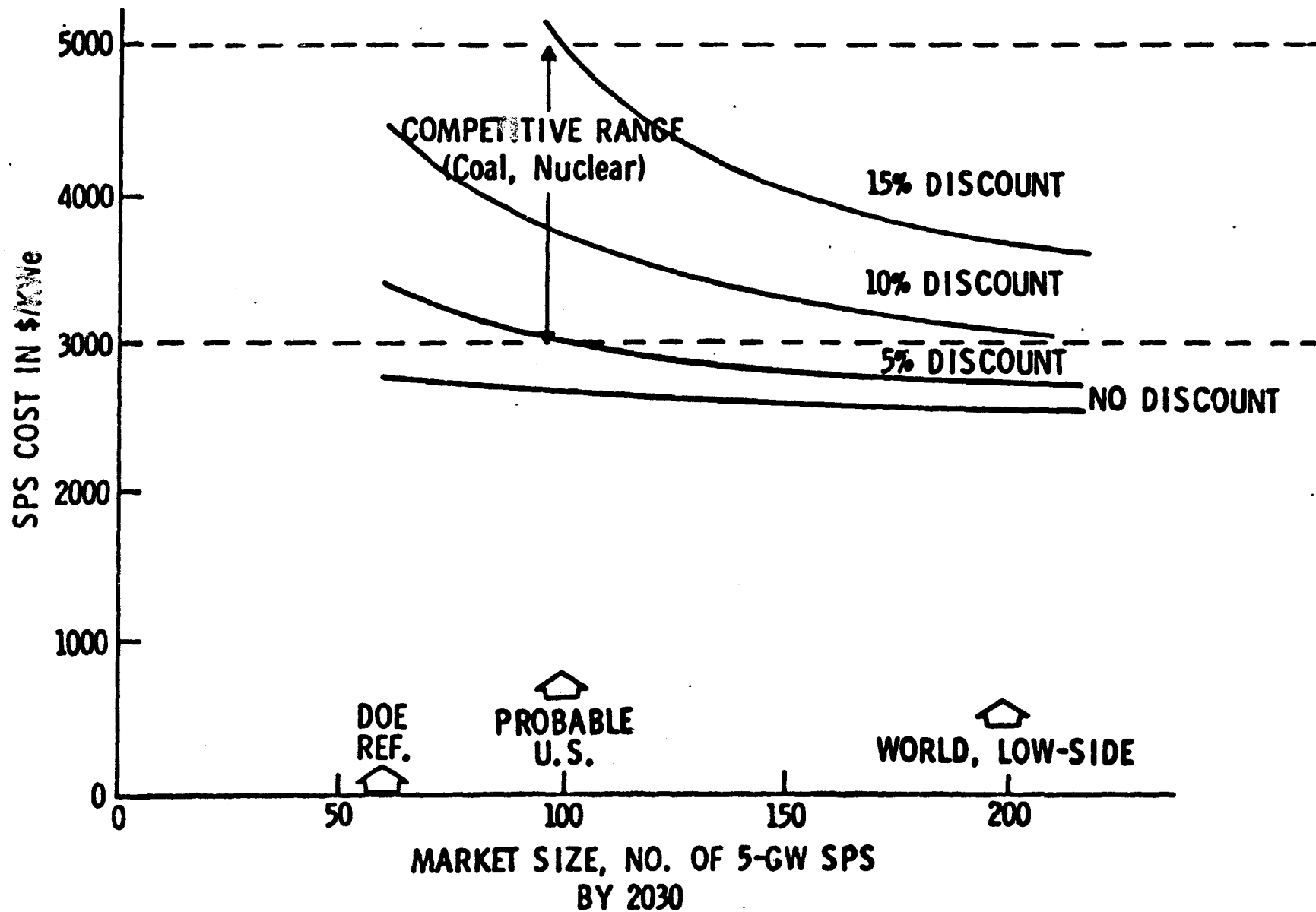


* FUEL PRICE ESCALATING AT 6%/YEAR IN 1978, DROPS LINEARLY TO 2%/YEAR BY 2020, STAYS AT 2%/YEAR THROUGH 2040

** POST AMORTIZATION CAPITAL RELATED
(EARNING, DEBT SERVICE, TAXES AND INSURANCE ON 10% OF CAPITAL INVESTMENT)



AMORTIZATION OF NONRECURRING COST



***Microwave Systems
Summary/Conclusions***

***Introduction to
Planned Program Activities***

***R. H. Dietz
Lyndon B. Johnson Space Center***

~~44~~
~~WIRE~~ INTENTIONALLY DELETED

NASA

**Solar Power
Satellite**

Outline

- Concept Evaluation Program
- Historical Background
- Reference System Overview
- Solid State Configurations
- Conclusions

NASA

**Solar Power
Satellite**

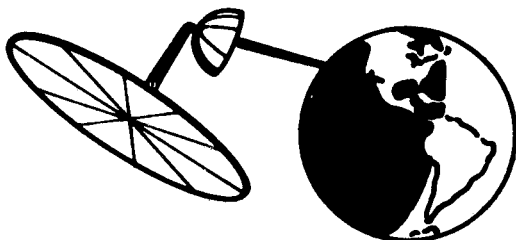
**Concept Evaluation
Program**

Objective To develop by the end of 1980, an initial understanding of the economic practicality and the social and environmental acceptability of the Solar Power Satellite concept.

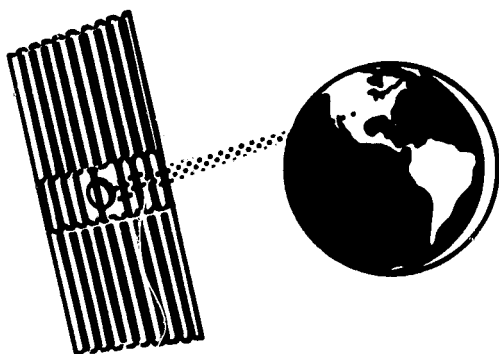
Funding	Program components	77	78	79	80	Total
NASA	Systems definition	2500	1700	1300	800	6300
DOE	Environment, health, safety	220	1940	2050	1740	5950
	Societal assessment	164	537	537	322	1560
	Comparative assessment	95	376	754	565	1790
		2979	4553	4841	3427	15600

Program Milestones	77	78	79	80
Program initiation	●			
Baseline concept selection				
<i>Preliminary</i>		●		
<i>Final</i>			○	
Program recommendation				
<i>Preliminary</i>				○
<i>Updated</i>				○
<i>Final</i>				○

1968 Glaser



**1973 ADL/Grumman/Raytheon/
Spectrolab Study for
NASA LeRC**

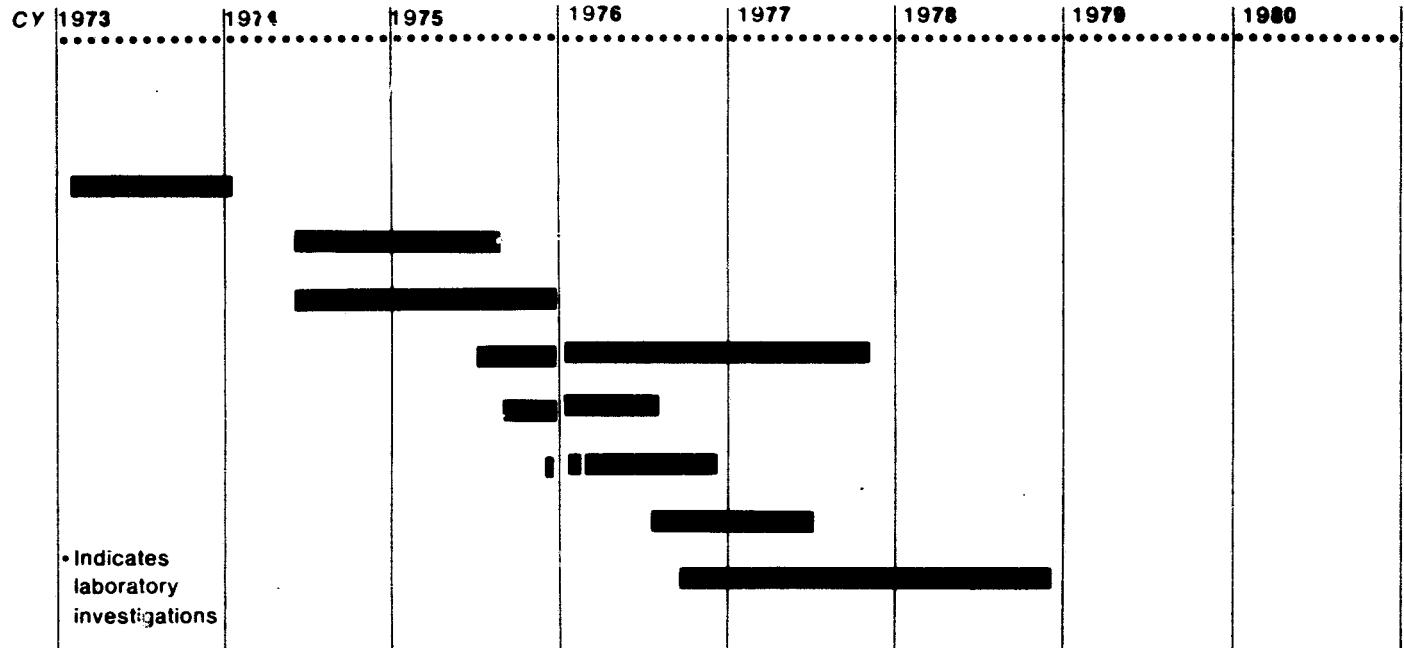




Solar Power Satellite

Studies/Experiments Microwave Power Transmission and Reception

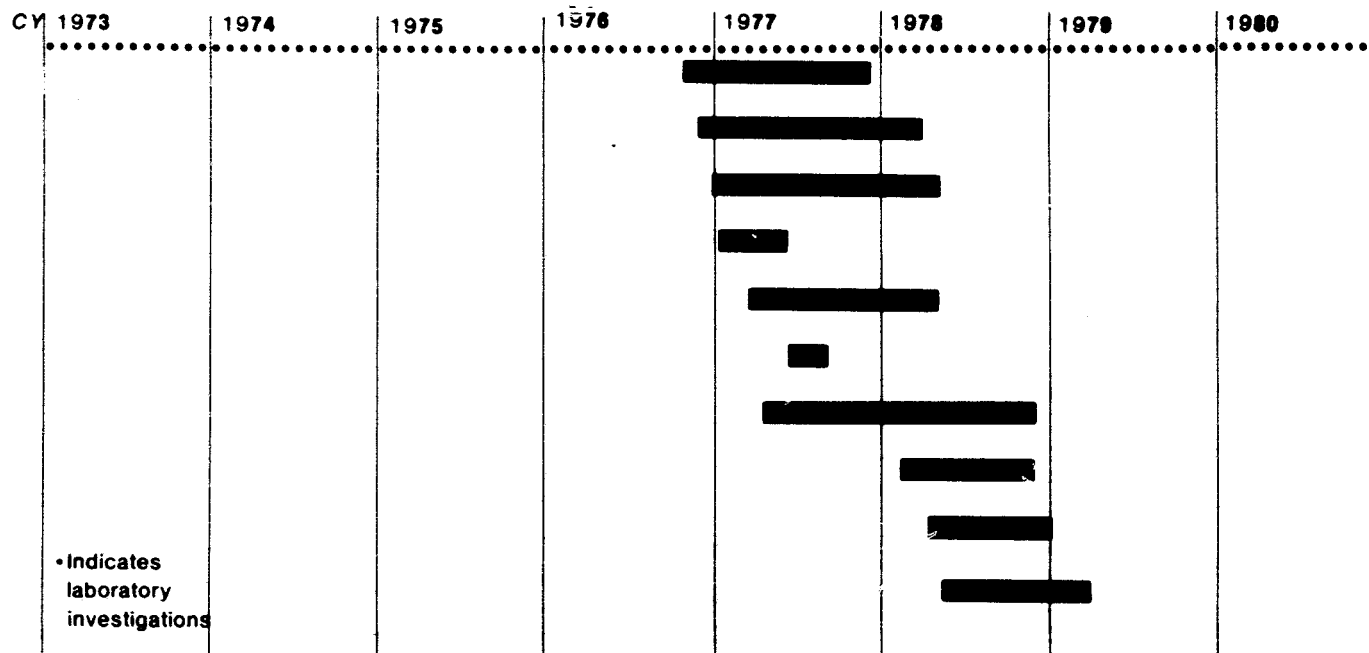
- 1 1964-MW Transmission Experiments -
Brown
- 2 1969-1974/Orbit to Orbit Feasibility -
MSFC/Raytheon - \$130K
- 3 MPTS feasibility - ADL/LeRC -
\$250/25K
- 4 Lab DC-DC η /Goldstone rectenna -
JPL/Raytheon - \$785K
- 5 Complete MPTS Study -
LeRC/Raytheon - \$408K
- 6 Rectenna improvements -
LeRC/Raytheon - 98K
- 7 Initial Technical/Env/Econ SPS Eval -
JSC
- 8 SPS Engineering/Economic Analysis -
MSFC
- 9 SPS Concept Evaluation -
MW System Trades - JSC
- 10 Phase 1 Technology development
of CFA-LeRC/Raytheon - \$235K



NASA

Solar Power
Satellite

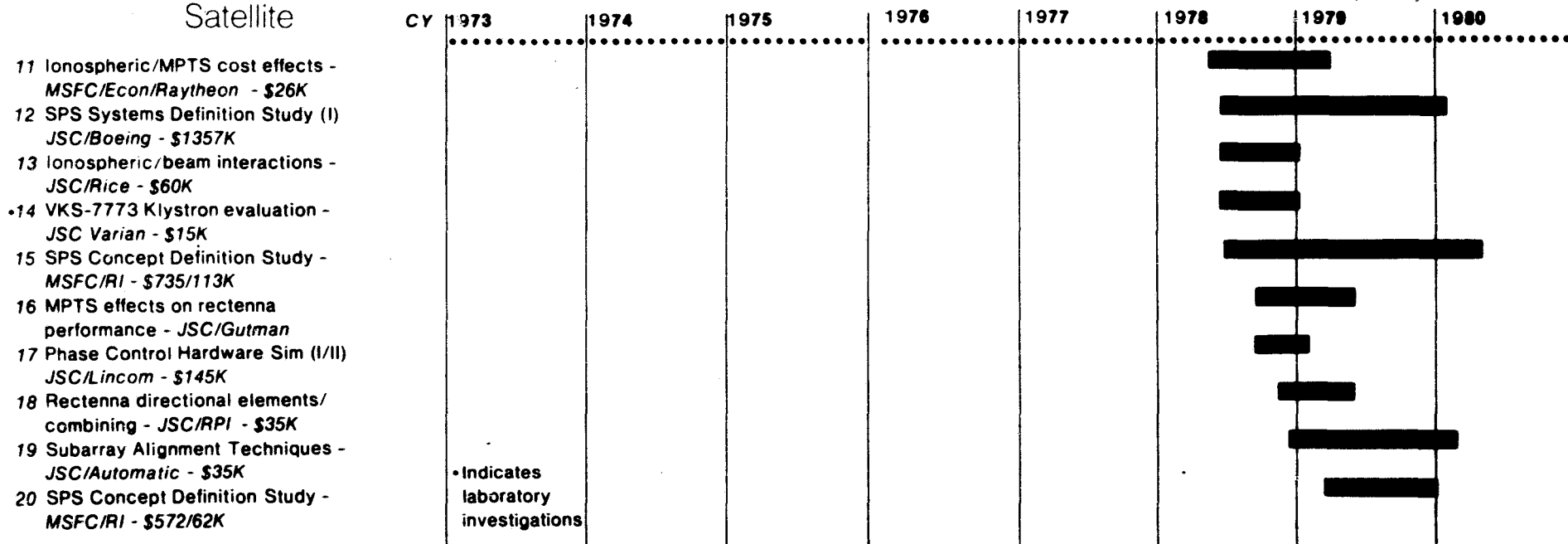
Studies/Experiments Microwave Power Transmission and Reception





Solar Power Satellite

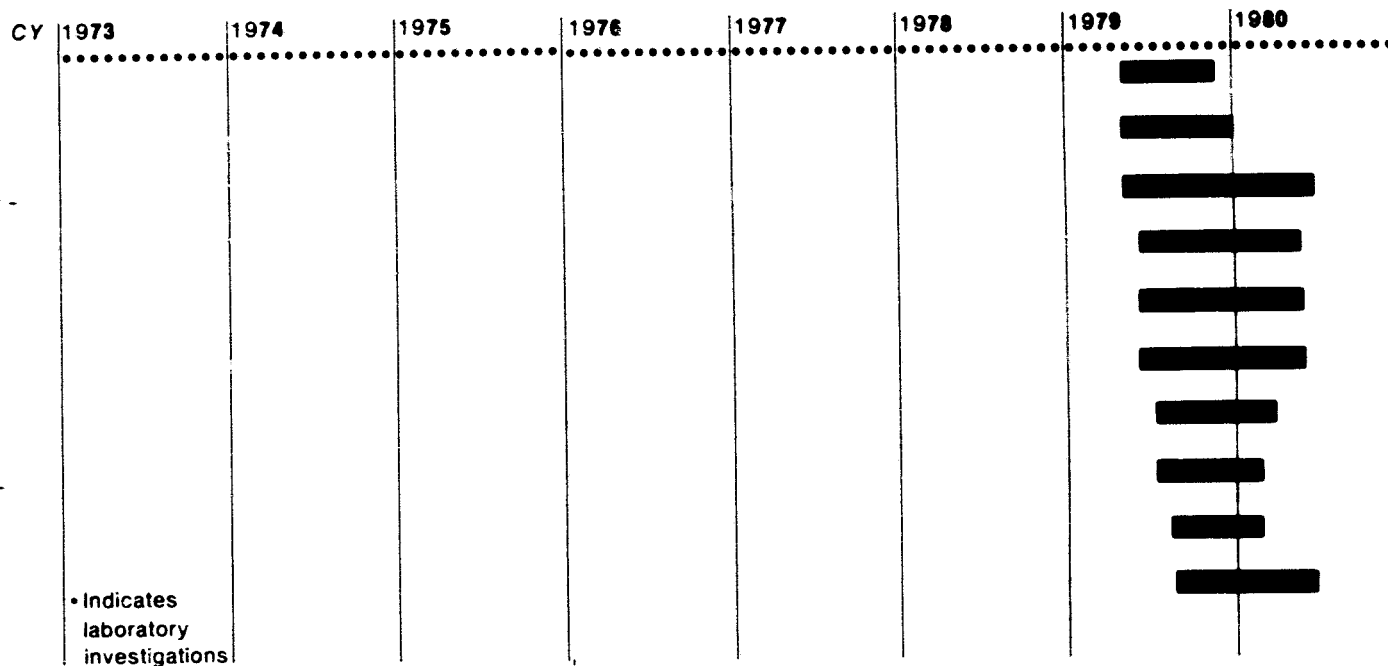
Studies/Experiments Microwave Power Transmission and Reception



NASA

Solar Power
Satellite

Studies/Experiments Microwave Power Transmission and Reception

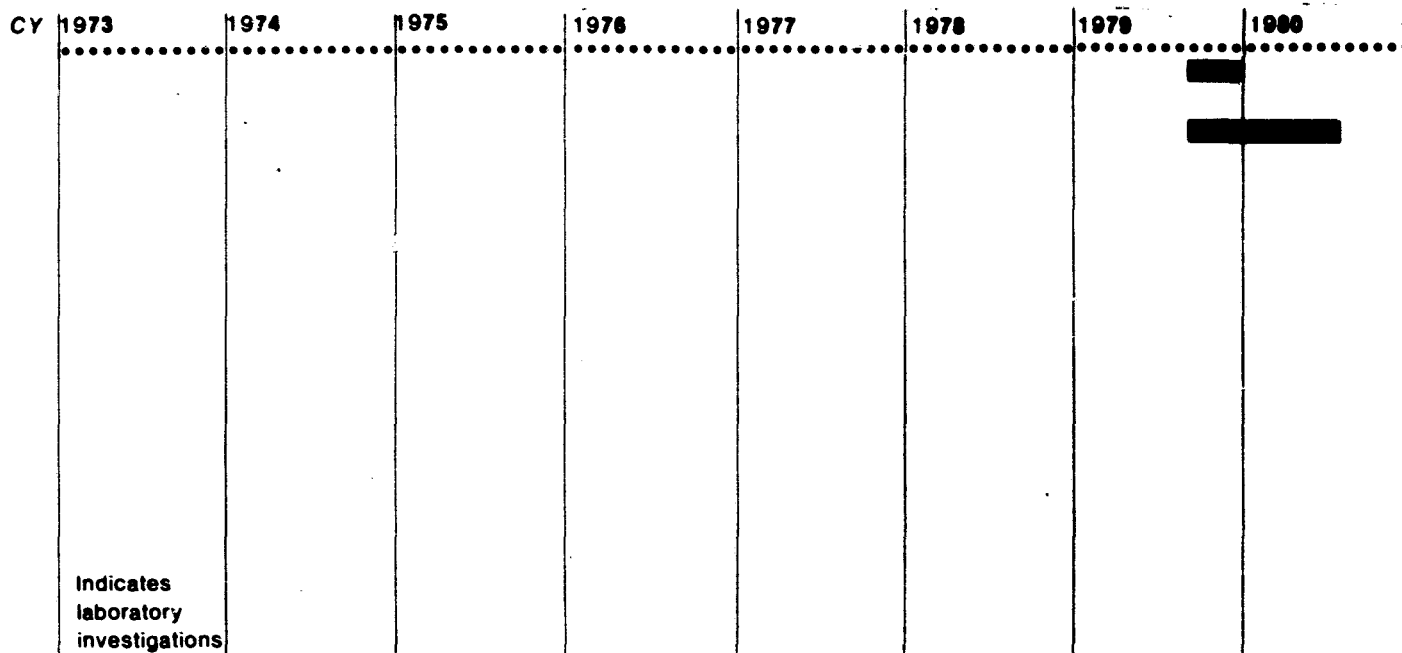


NASA

Solar Power
Satellite

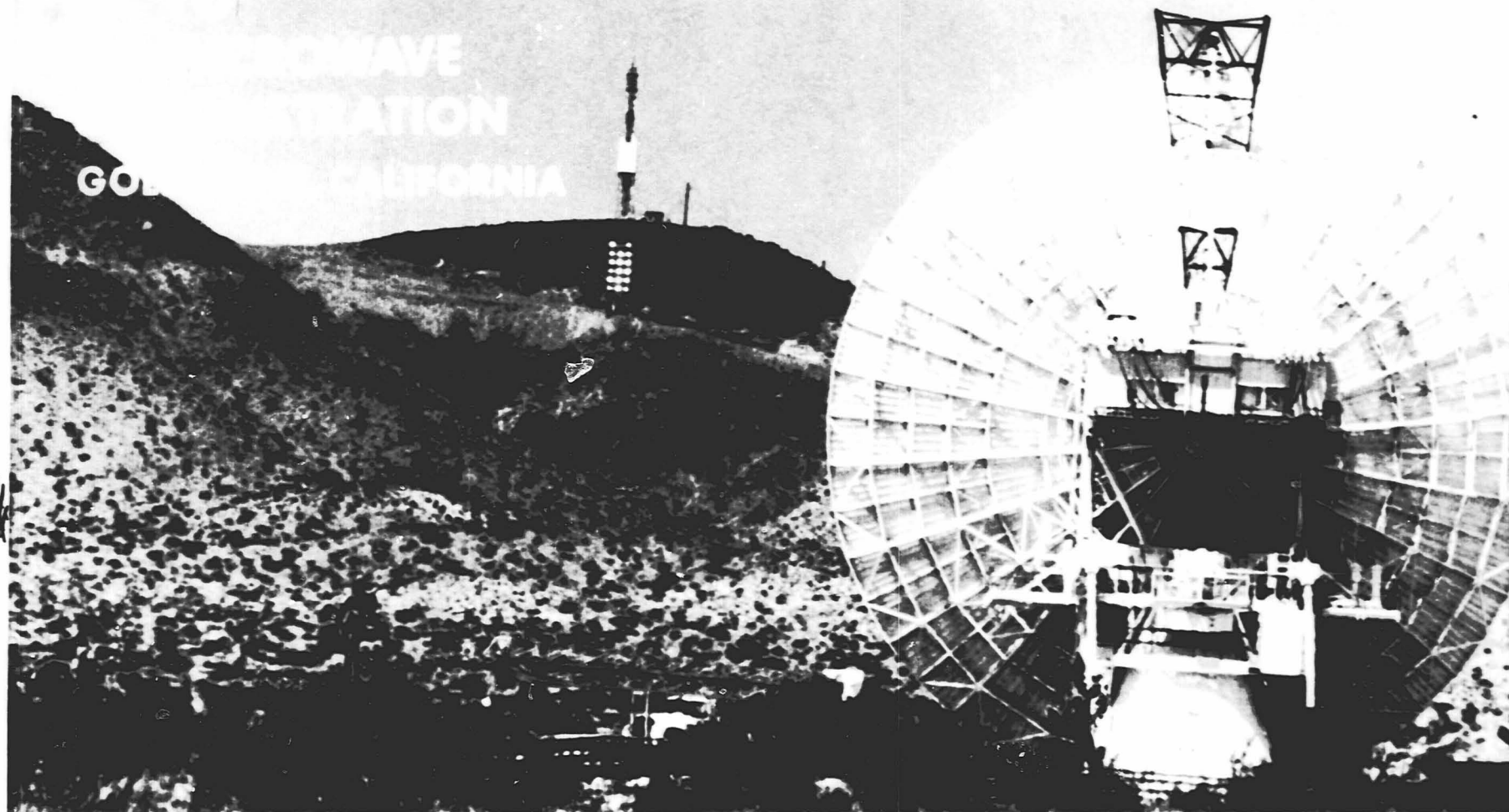
Studies/Experiments Microwave Power Transmission and Reception

- 41 High Accuracy rf Measurement
Techniques - MSFC/GIT - \$20K
- 42 Magnetron Tube Assessment -
MSFC/Raytheon - \$150K



NASA-S-75-12505

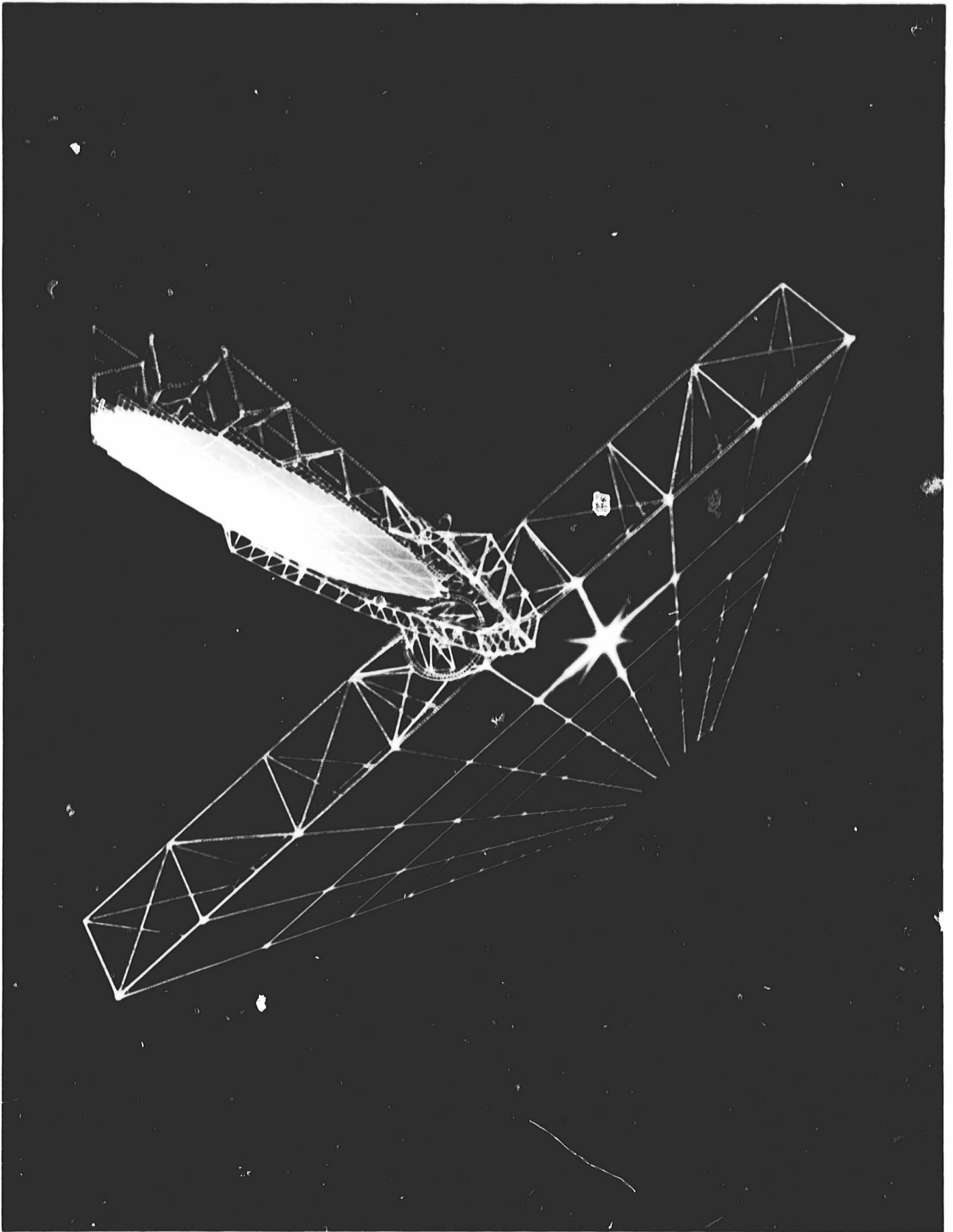
POWER TRANSMISSION SYSTEM



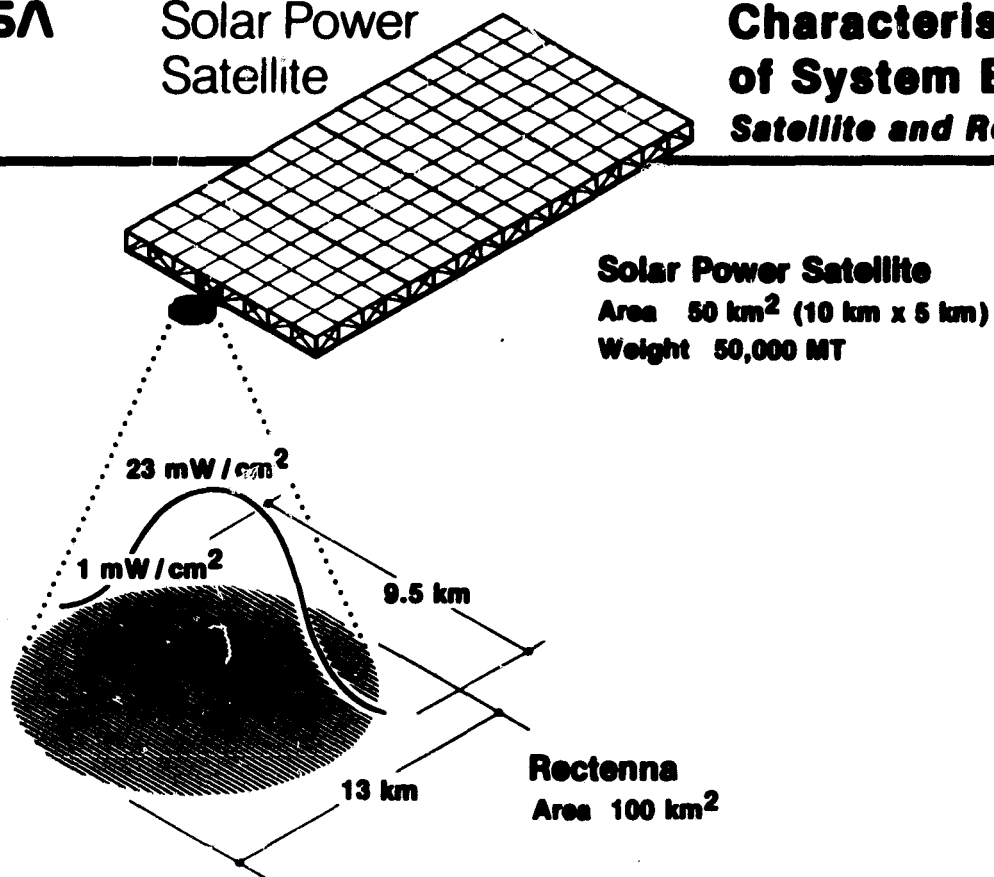
- TRANSMITTER DIAMETER - 26 m
- MICROWAVE FREQUENCY - 2388 MHz

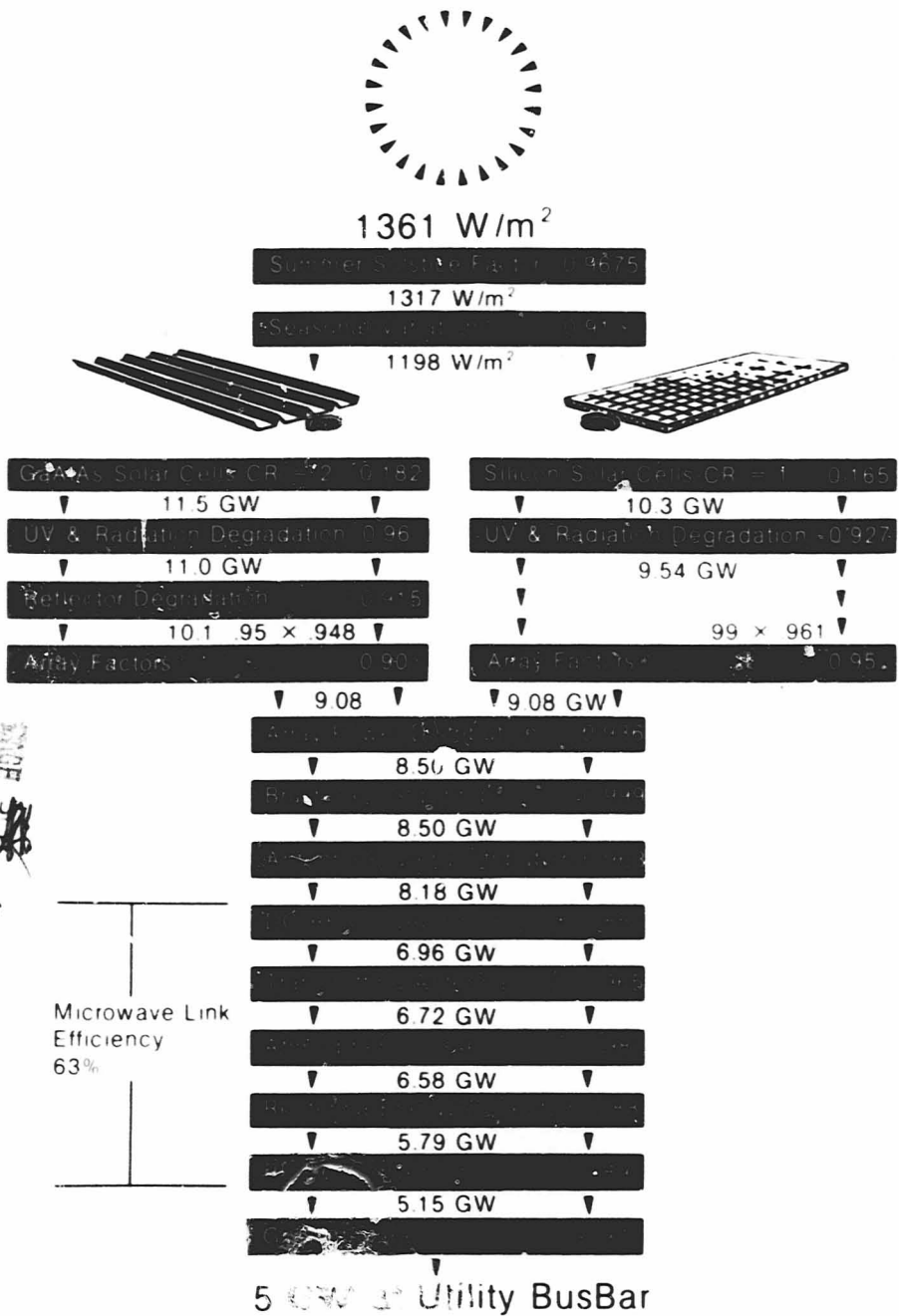
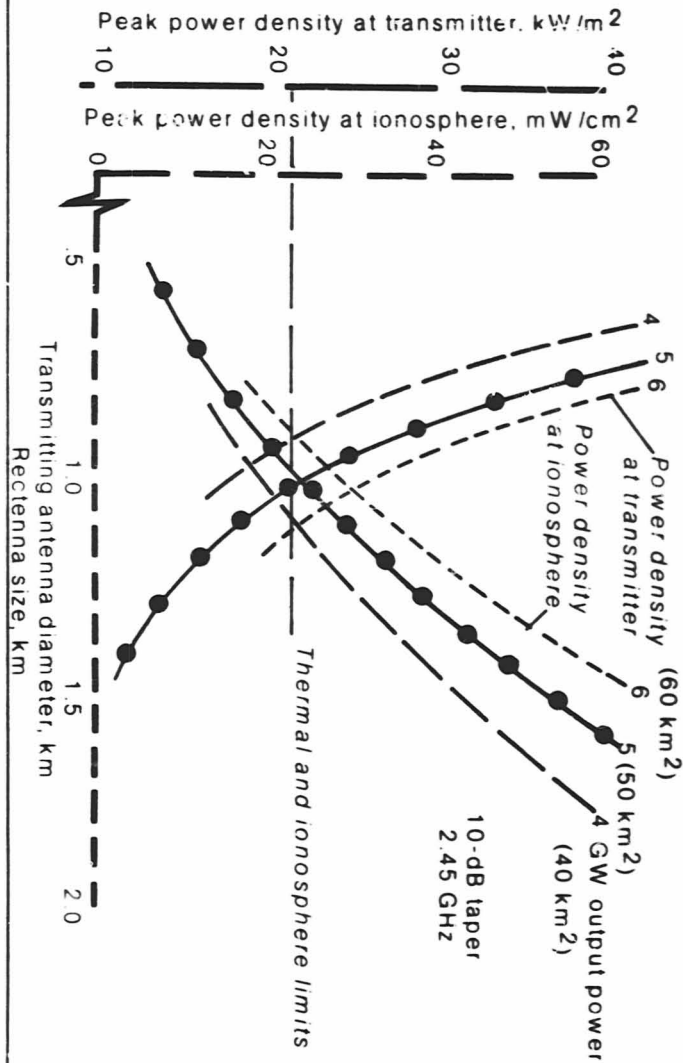
- RANGE (TRANSMITTER TO RECEIVER) - 1.5 km
- SYSTEM EFFICIENCY - 82.5%

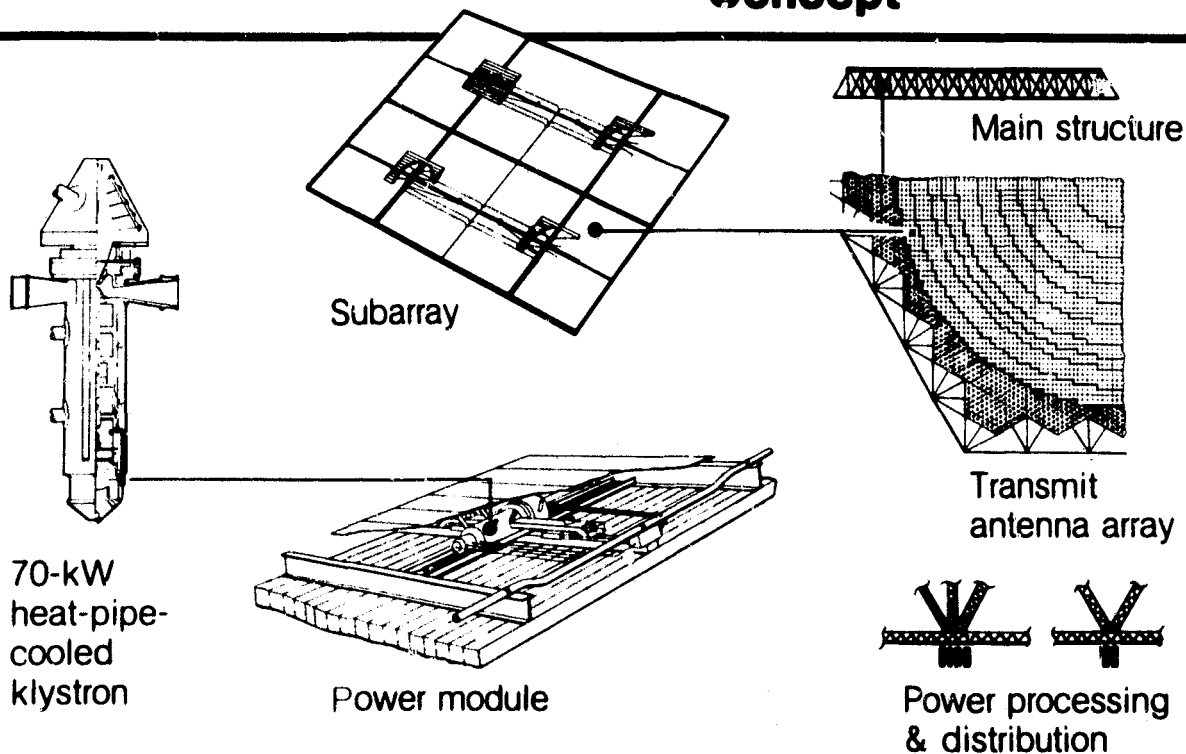
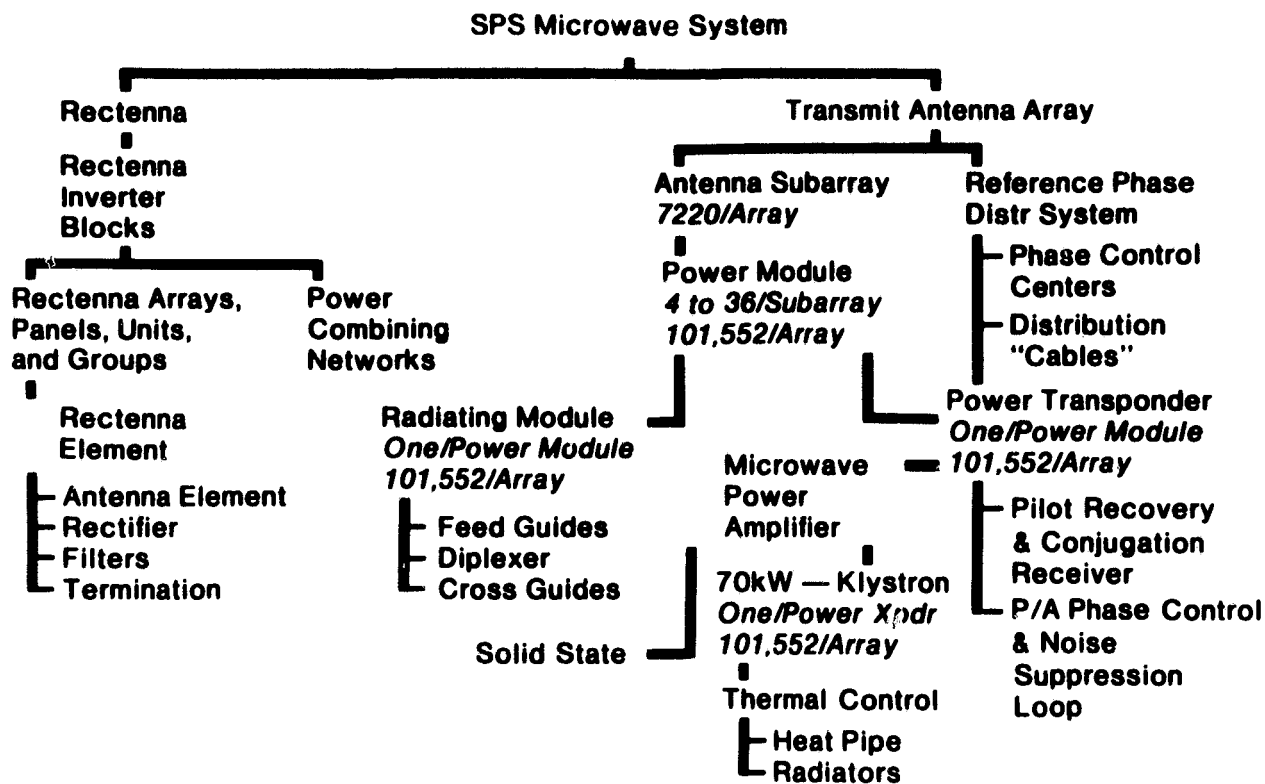
-
- Data drawn from NASA & contractor studies
 - 5,000 megawatt SPS, one transmitter
Silicon and gallium arsenide solar cell options
 - Klystron transmitter
Magnetron & solid state recognized as potential options
 - GEO construction with independent electric OTV
 - TWO-stage vertical take-off, horizontal landing
rocket HLLV
-





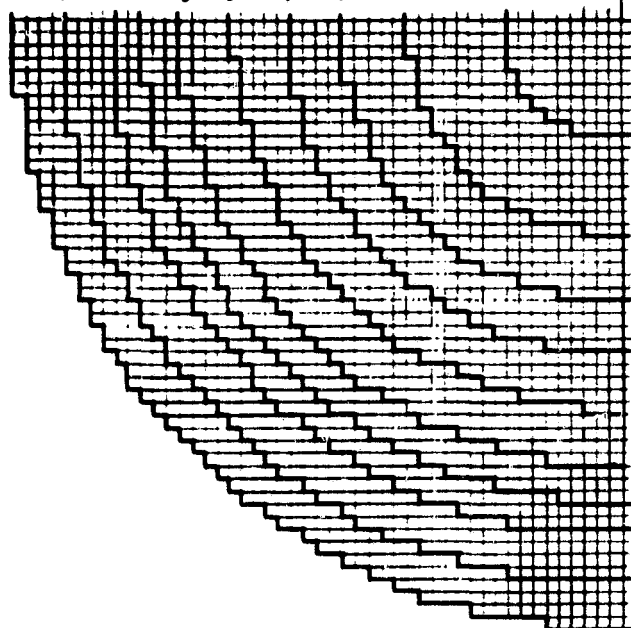






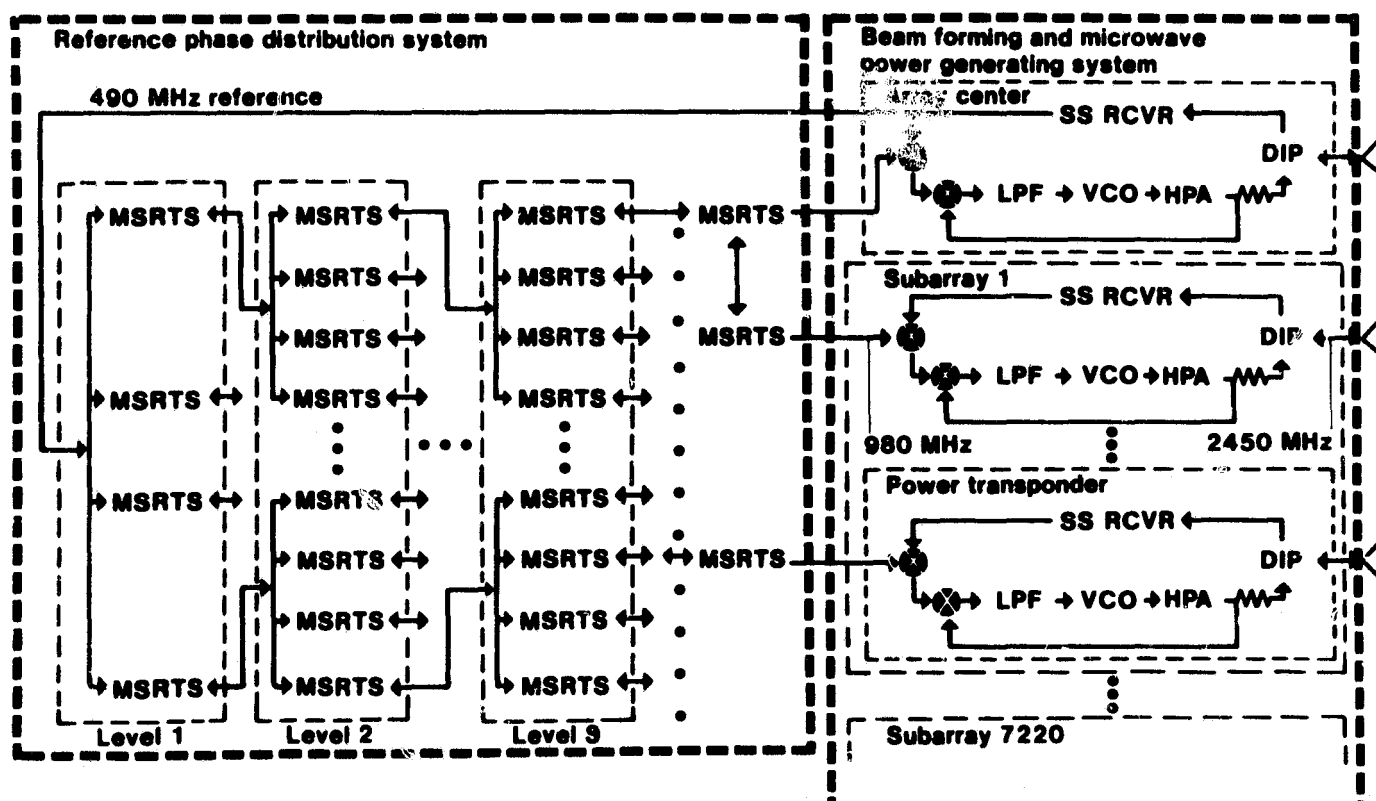
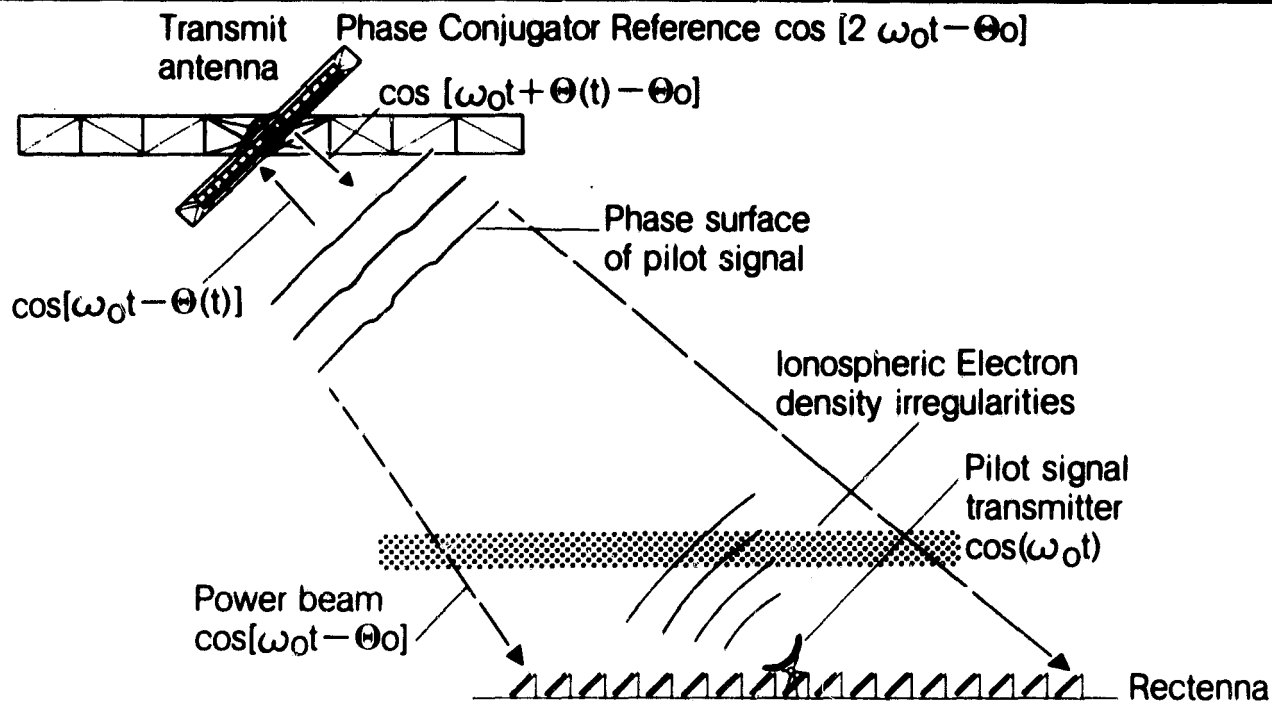
NASA**Solar Power
Satellite****Transmitting
Antenna***Power Taper Integration*

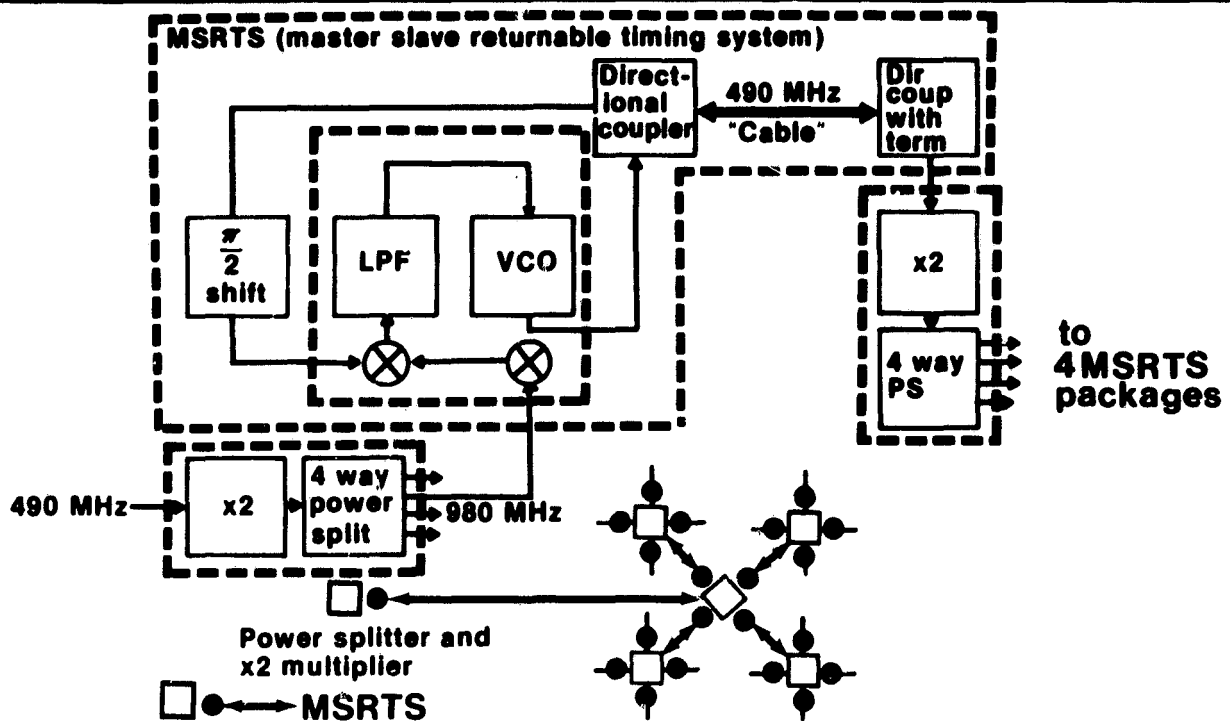
500.6m
458.9m
417.2m
396.3m
365.1m
323.3m
271.2m
229.5m
177.3m
93.9m



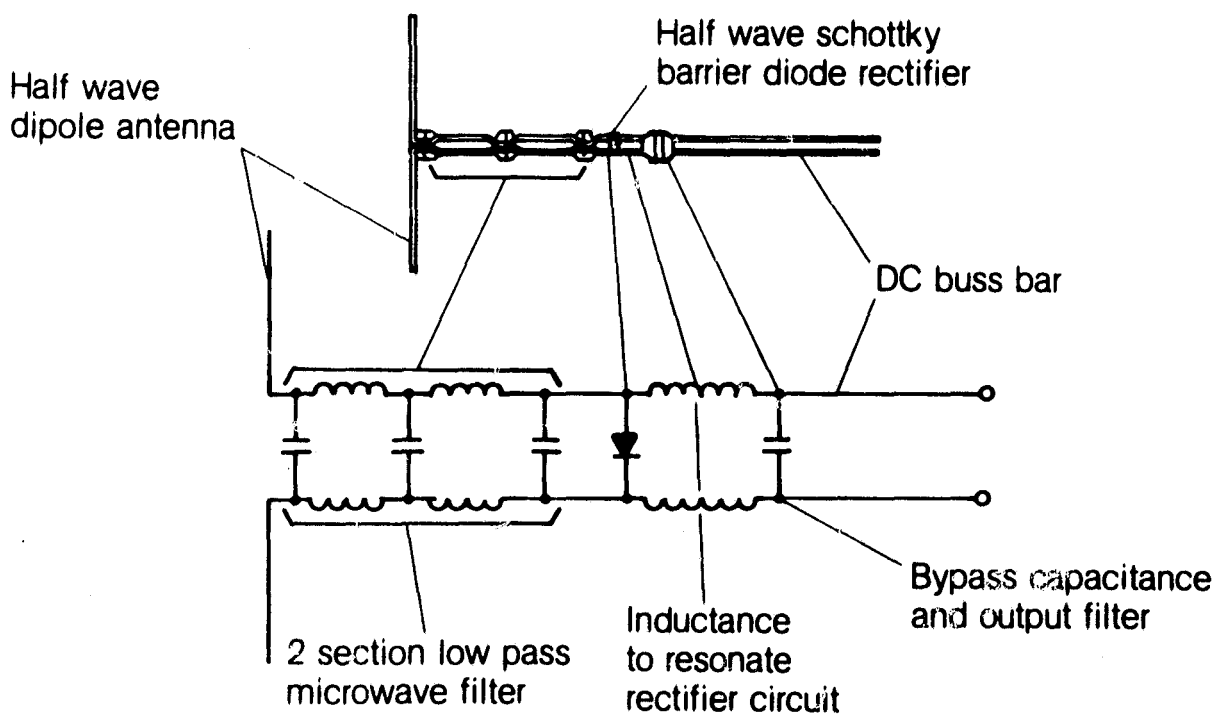
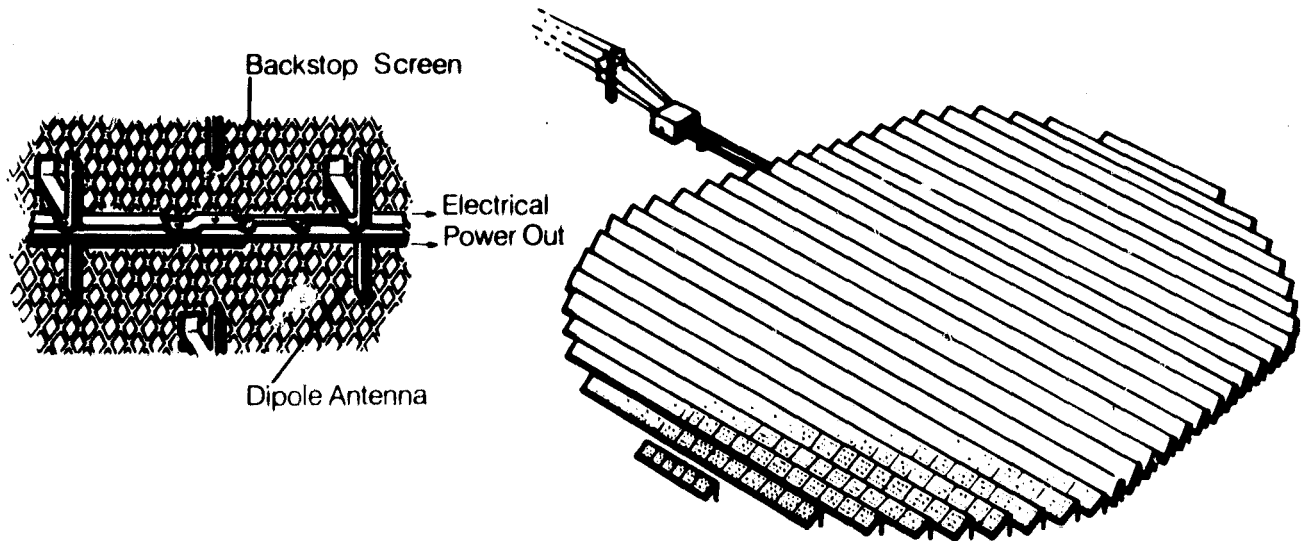
Step	Number Subarrays	Number Klystrons/ Subarrays	Number Klystrons
1	276	36	9,936
2	632	30	18,960
3	644	24	15,458
4	628	20	12,560
5	784	18	12,544
6	900	12	10,800
7	664	9	5,976
8	612	8	4,896
9	1,052	6	6,312
10	1,028	4	4,112
Totals	7,220		101,552

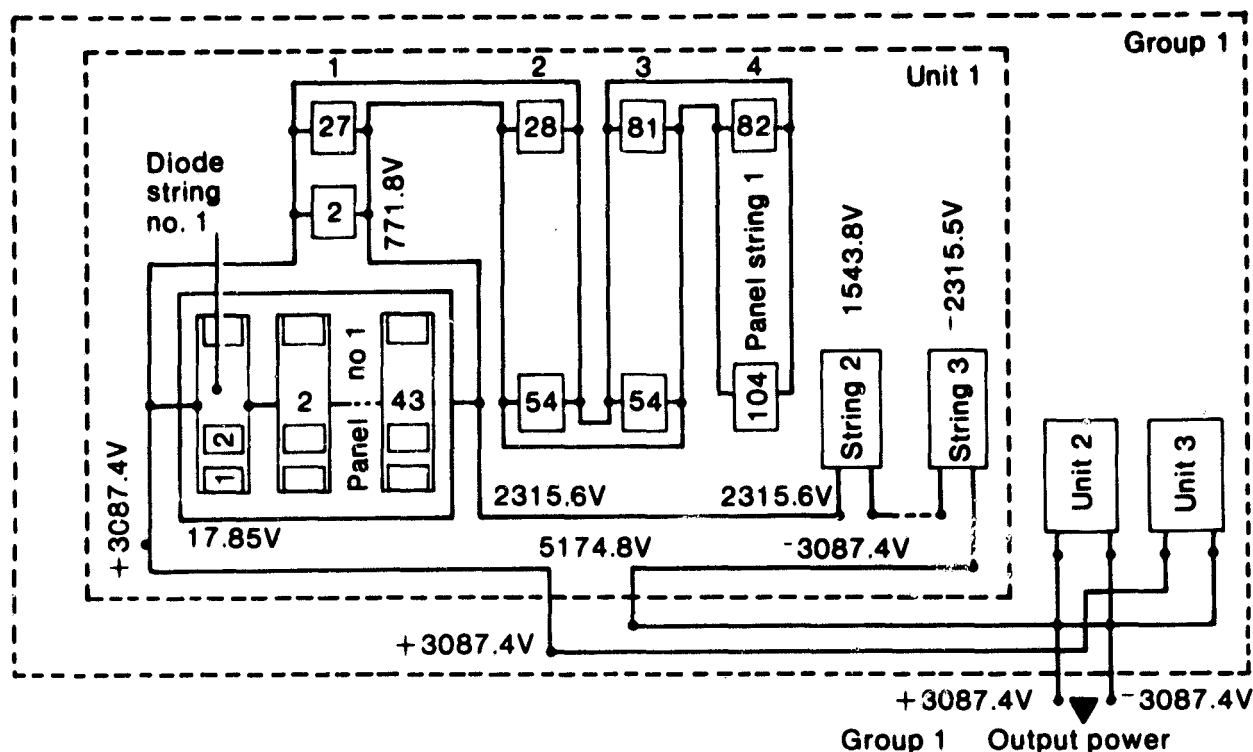
NASA**Solar Power
Satellite****Array Pattern
Roll-Off
Characteristics**





Item	Amplatron	Klystron	Solid State
Power	5 kW with 10 ⁵ tubes	50 - 250 kW with 10 ⁵ tubes	1 - 3 W (5-10 W)
Efficiency	85 - 90%	80 - 85%	80%
Cathode	Cold pure metal (avall life data 10,000 hrs.)	Thermionic oxide/matrix (avall life data 50,000 hrs.)	
Gain	7 dB	40 dB	20 dB
Voltage	20 kV	40 - 65 kV	12 to 20 V
Spurious signal AM (Typ.)	-100 dB/kHz 10 MHz from carrier	-125 dB/kHz 5 kHz away from carrier	unknown
M T B F	Comparable to klystron	Comparable to amplatron	approx. 100 years
Thermal dissipation	Concentrated interaction region	Distributed, collector can run 500-700°C, require heat pipes	100-125° C passive
Specific cost	\$20/kW	\$20 to \$40 /kW	unknown
Specific weight	0.4 kg/kW	0.4 to 0.8 kg/kW	0.01 to 0.03 kg/kW
Array interface	Series operation no feed waveguides	Power adjusts to voltage changes, corporate feed	Device to antenna element





Frequency 2.45 GWz

Output power to power grid 5 GW per antenna

Transmit array size 1 km in diameter

Subarray size 10.4 m × 10.4 m (7220 per antenna)

Power radiated from transmit array 6.85 GW

System efficiency 63%

Array aperture illumination a 10-step, truncated Gaussian amplitude distribution with 10 dB edge taper

Error budget Total rms phase error for each subarray = 10°

Maximum mean phase error at edge of transmit array = 2°

Amplitude tolerance across subarray = ± 1 decibel

Failure rate of DC-RF power converter tubes = 2% (a maximum of 2% have failed at any one time)

NASA**Solar Power
Satellite****Microwave System**
typical parameters

Antenna/ subarray mechanical alignment ± 3 arc minutes, with the grating lobes constrained to $\leq .01$ mW/cm² for a 108 m² subarray

Power density levels *center of rectenna* 23 mW/cm²

edge of rectenna 1 mW/cm²

first side lobe .08 mW/cm² (approximately 9 Km from center of rectenna)

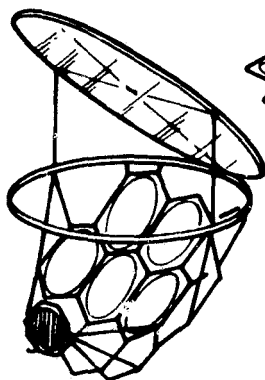
Out-of-band noise < CCIR requirement of -180 dBW/m²Hz for arrival angles greater than 25°

Beam formation and steering retrodirective phased array

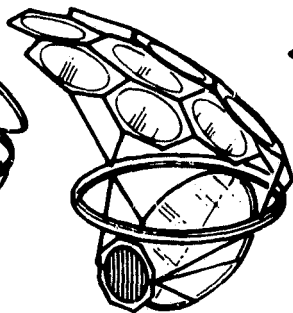
DC-RF power amplifier Klystron

RF radiators aluminum slotted waveguide

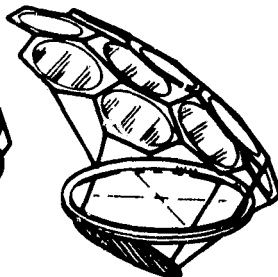
NASA**Solar Power
Satellite****Solid State
Sandwich Concepts**

**1**

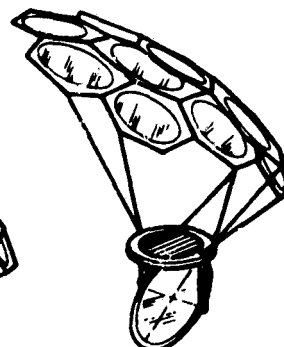
**Flat primary/
faceted
secondary**

**2**

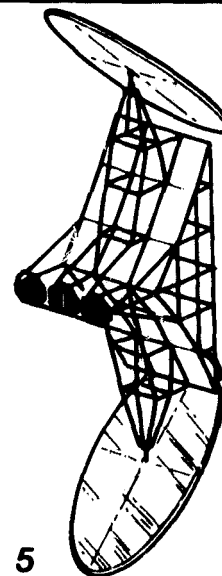
**Flat secondary/
faceted
primary**

**3**

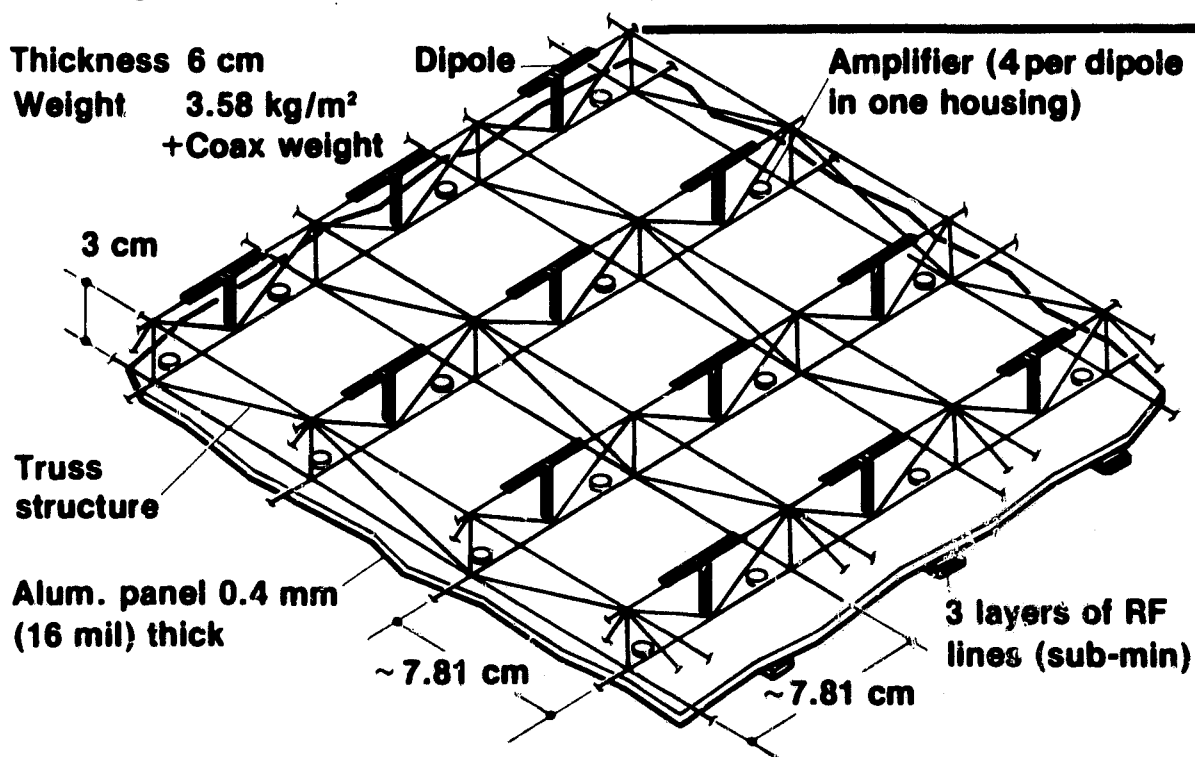
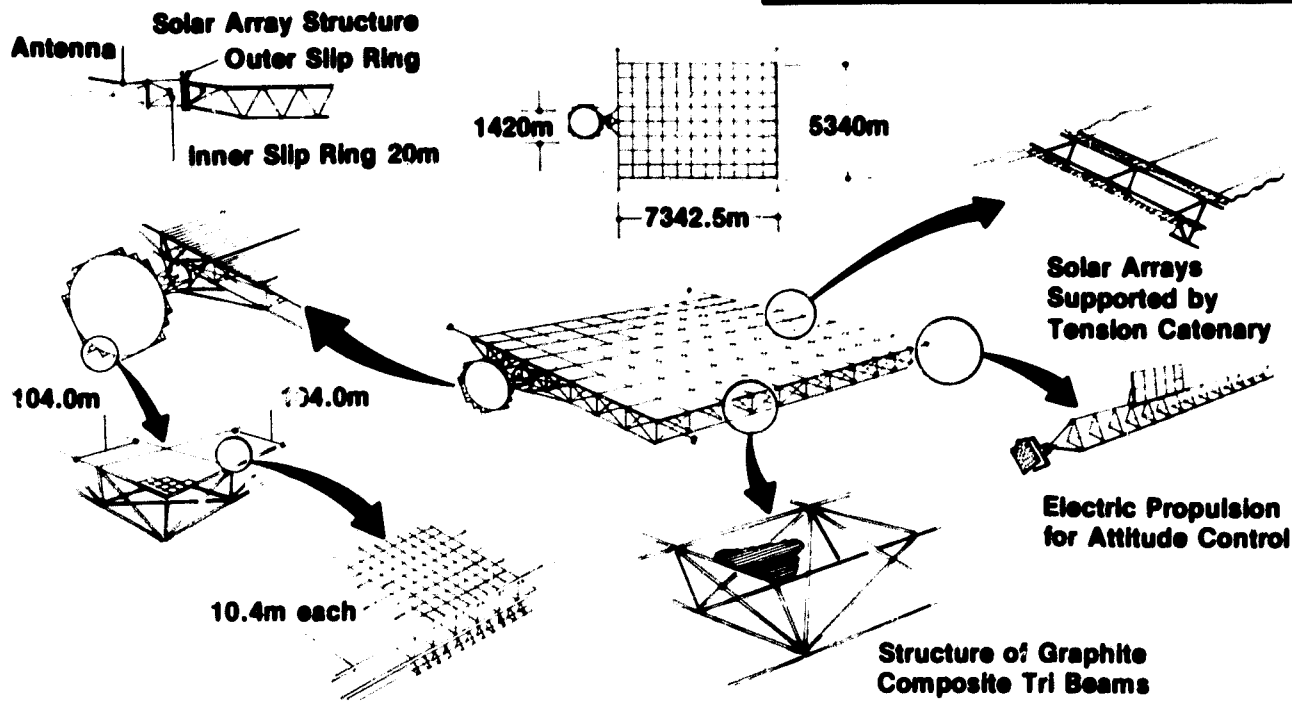
**Inclined
antenna/single
faceted reflector**

**4**

**RF reflector/
single multi-
faceted reflector**

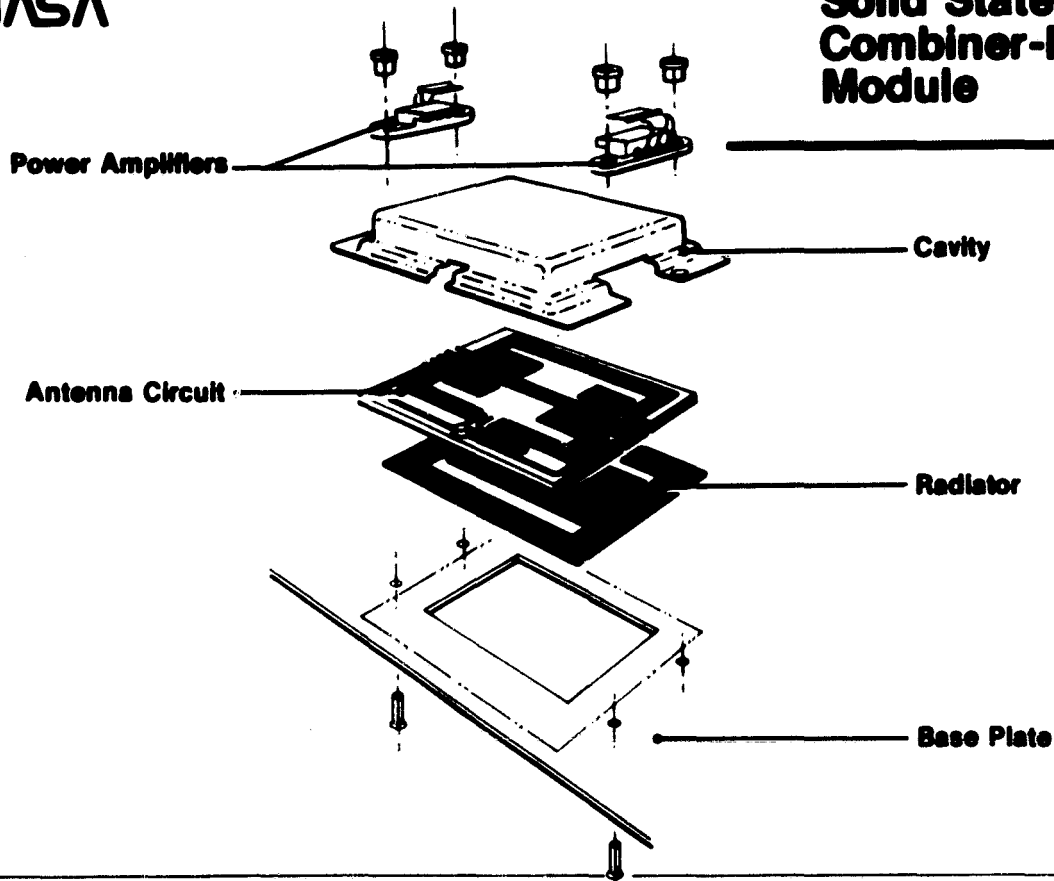
**5**

**Multi-antenna
concept**



NASA

Solid State Combiner-Radiator Module



NASA

Solar Power Satellite

Microwave System Options

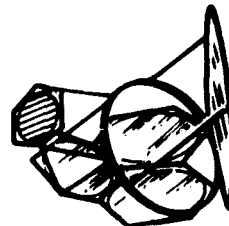
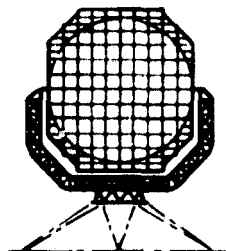
RF Converter

Antenna mounted

Solar cell mounted (concentration ratio = 3)

Optical reflector

RF reflector



**SPS
Design**

**Klystron
or CFA**

Solid state

Solid state

Solid state

**Power output
to grid**

5 GW

2.5 GW

0.7 GW

0.2 GW per km² solar cells

**Space antenna
diameter**

1 km

1.4 km

2.7 km

High power waveguide

**Rectenna diameter
at 23mW/cm²**

10 km

7.1 km

3.3 km

Not determined

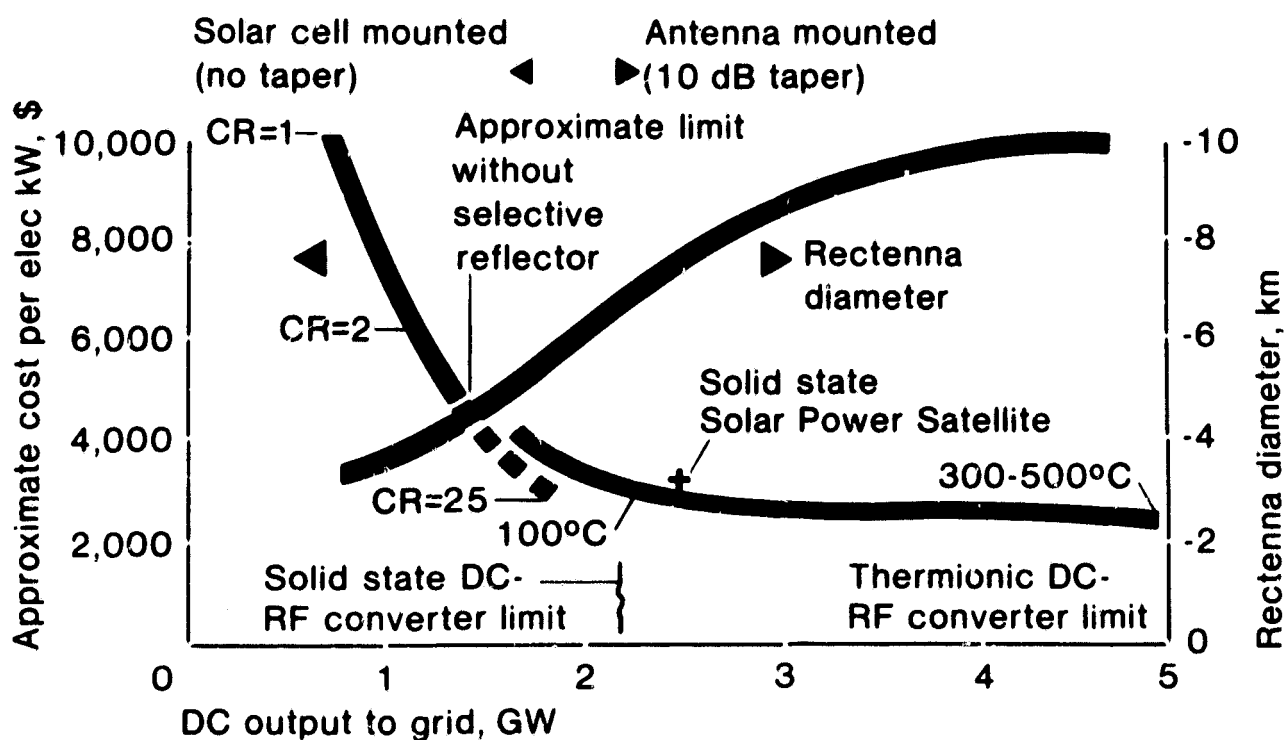
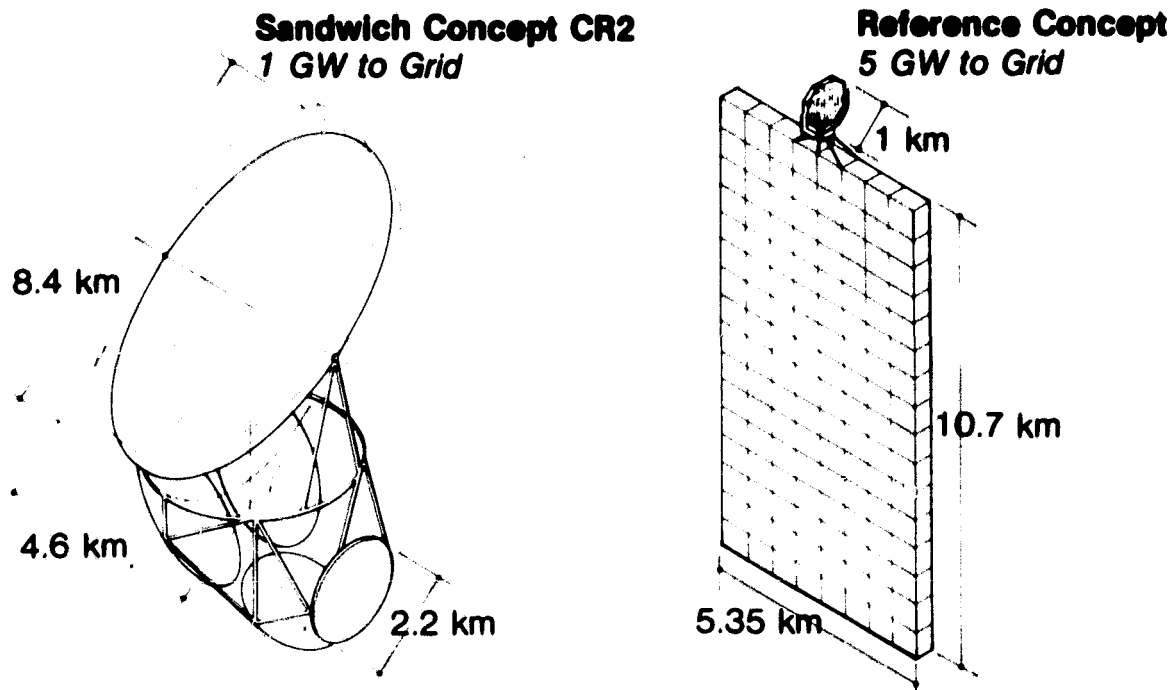
Antenna

10 dB taper

10 dB taper

Uniform

Advanced horn feed paraboloid



- 1 **Microwave Power Transmission** Transferring gigawatt power levels between two points using microwaves is feasible.
- 2 **One Antenna vs Multiple Antennas** Each SPS microwave power transmission system should use one transmit antenna with contiguous radiating subarrays rather than multiple separate antennas.
- 3 **Frequency** The power transmission frequency of 2.45 GHz has been determined to have advantages for power transmission and reception based on system tradeoffs including (1) transmit antenna and rectenna sizing, (2) propagation effects through the atmosphere, (3) hardware technology projections, and (4) ISM band utilization.
- 4 **Microwave System Sizing** Transmit antenna size (1 km), rectenna size (10 km minor axis) and power delivered to the utility grid (5 GW) have been determined based on the minimum cost of electricity per kilowatt hour. The tradeoffs assumed a maximum thermal limit on the transmit antenna of 21 kW/m², (tube configuration), maximum power density through the ionosphere of 23 mW/cm², and the current projections of microwave system efficiencies. A microwave system using solid state power amplifiers will have a different thermal limit and different system efficiencies, resulting in different system sizes.

- 5 **Type of Transmitting Antenna** The transmitting antenna should be a planar phased array in order to meet the requirement of maximum power transfer efficiency.
- 6 **Type of Receiving Antenna** An SPS rectenna concept theoretically capable of recovering all RF energy impinging on its surface with direct RF-to-DC conversion provides the required maximum conversion efficiency.
- 7 **Antenna Construction and Subarray Alignment** Construction of a 1 km diameter antenna array with a ± 1 minute alignment tolerance appears to be within the state of the art if low CTE (coefficient of thermal expansion) materials are used. Antenna subarray alignments, both initially and realtime, can be maintained to ± 3 minutes by the use of Azimuth-Elevation mounts and laser measurement techniques.
- 8 **Power Beam Stability** Based on analytical simulations and experimental evaluations it appears feasible to automatically point and focus the power beam with minimum beam wander ($\pm 0.001^\circ$) and automatic fail safe operation (rapid beam defocusing).

NASA**Concept Development
and
Evaluation Program****Assessment
Information
Organization**

**Basic information reports from analyses, experiments
workshops**

- DOE/NASA
- National Laboratories
- Universities
- Governmental Agencies
- Industry
- Consultants

▼
**Reference
System
Definition
Report**

▼
**Environmental
Assessment
Report**

▼
**Social
Assessment
Report**

▼
**Comparative
Assessment
Report**



▼
Ground Based Exploratory Development Program

NASA**Solar Power
Satellite****DOE/NASA GBED
Program**

**Overall
Goal**

- To provide information required to make a rational decision on whether to proceed to a technology verification phase of the SPS program

Approach

- Information generated through experiment, demonstration, and analysis, and would include:
 - Further development of system concept
 - Test/Demonstration of components necessary to construct and operate the system
 - Analysis of environmental effects and their mitigation
 - Assessment of economic factors including financing options
 - Programs to understand and solve problems in the international, institutional, and public concern areas

PRECEDING PAGE BLANK NOT FILMED

NASA**Solar Power
Satellite****DOE/NASA GBED
Program**

**Program
Results**

- Data base that specifies/reduces uncertainty in all critical areas so that a decision can be made for or against a commitment to a technology verification program
 - Selection of preferred system(s)
 - Definition of a technology verification program, including required space projects

**Areas
to be
addressed**

- Systems analysis and technology
- Environmental research and assessment
- International affairs, institutional relations, and public concerns

NASA**Solar Power
Satellite****GBED - Systems Analysis
and Technology
Objectives**

- Resolve technology issues that affect decision to proceed to technology verification phase
 - Conduct carefully planned, critical experiments/ demonstrations in ground laboratories and in space as necessary
 - Reduce uncertainty with respect to
 - *Performance*
 - *Reliability*
 - *Feasibility of production, construction, operation, and maintenance*
 - *Costs, while conforming to environmental/ societal constraints*
-

NASA**Solar Power
Satellite****GBED - Systems Analysis
and Technology
*Objectives***

- Support environmental, societal, and comparative assessments by providing analytical and experimental data as required
- Define preferred overall system concepts, including alternate compatible subsystems
- Define plans and projects that would be required in a post-GBED technology verification phase

NASA**Solar Power
Satellite****GBED - Systems Analysis
and Technology
*Technical Areas***

- System definition studies
 - Solar energy conversion
 - Electrical power processing and distribution
 - *Power transmission and reception*
 - Space structures, controls, and materials
 - Space operations
 - Space transportation
-

NASA**Solar Power
Satellite**

GBED Plan Format

Issue Trees**1.0 System
Definition****Milestone/Flow Chart****1.0 System
Definition
Studies**

Project Summary Sheets

- 1.0 System definition studies
- 1.1 Reference system
- 1.2 Alternate concepts
- 1.3 Technology impacts
- 1.4 Environmental/societal and comparative assessment impacts
- 1.5 System analysis and planning

NASA**Solar Power
Satellite**

GBED Plan Format

Issue Trees**4.0 Power
Transmission
and
Reception****4.1 Microwave
Systems****Milestone/Flow Chart****4.0 Power
Transmission
and
Reception****4.1 Microwave
Systems**

Project Summary Sheets

- 4.0 Power transmission and reception
- 4.1 Microwave systems
 - 4.1.1 Power amplifier performance (tube/solid-state)
 - 4.1.2 Microwave system performance (tube/solid state)
 - 4.1.3 Phase control system performance (tube/solid-state)
 - 4.1.4 Transmit antenna performance (tube/solid-state)
 - 4.1.5 Rectenna element performance

- **Can the required performance be attained for SPS viability?**
 - *System efficiency*
 - *Focusing and pointing control*
 - *RFI*
- **Can required long life and/or maintainability characteristics be achieved?**
- **Can manufacturing techniques be devised to provide systems and components of required performance, production rates, and costs?**

- **Provides quantitative data for microwave system**
 - **feasibility and performance verification**
- **Uses existing specialized facilities including anechoic chamber, EMC laboratory, antenna range, electronic systems test laboratory and environmental chamber**
- **Includes microwave system integration and testing at full scale antenna subarray level**
- **Integration and testing will provide data which can be extrapolated to the full scale SPS system**

- Includes decision point for solid-state versus power tube
 - *Continue with solid-state, drop power tube project*
 - *Continue with power tube, drop solid-state*
 - *Continue with both solid-state and power tube development*
- Microwave subsystem development continues throughout program after supporting system integration and test phases

**General
objectives**

- **Investigate critical technology areas**
 - Phase control
 - Power amplifiers
 - *Power tubes*
 - *Solid-state*
 - Radiating module
 - Rectenna
 - System integration and performance
 - **Develop microwave system and subsystem hardware**
 - **Verify system performance through subsystem and system ground testing**
 - **Obtain required data for predicting performance of the full scale SPS microwave system**
 - **Establish SPS microwave system criteria and guidelines for continued development**
 - **Investigate potential microwave system/environmental impact areas**
-

NASA**Solar Power
Satellite**

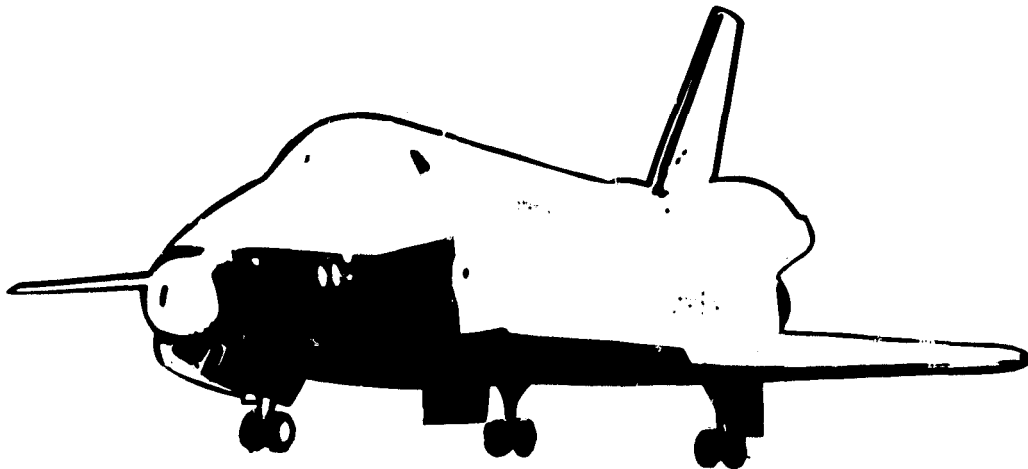
**Microwave GBED
Summary**

- Approach**
- **Early test/facilities requirements definition phase**
 - Microwave system integration and test
 - Subsystem projects
 - **Establish system integration and testing project**
 - Coordinate all microwave activities
 - Progressive system integration tests
 - *Power amplifier/phase control*
 - *Power module using low power klystron*
 - *Power module environmental (high power klystron with heat-pipe radiator)*
 - *Transmit subarray (10.4 M x 10.4 m) using up to 36 power modules*
 - *Rectenna panel/subarray integrated microwave system*

NASA**Solar Power
Satellite**

**Microwave GBED
Summary**

- Approach**
- **Establish subsystem projects**
 - Klystron
 - Klystron thermal control
 - Solid-state power amplifier/SPS system
 - Phase control system
 - Radiating module
 - Rectenna
 - **Utilize existing specialized facilities**
 - **Obtain quantitative performance data at system/subsystem levels**
 - **Extrapolate performance to full scale SPS**
 - **System feasibility assessment and performance verification**
-



The Shuttle provides transportation for space experiments and projects



National Aeronautics and
Space Administration

Lyndon B. Johnson Space Center
Houston, Texas 77058



2

**Microwave
System
Performance**



**NASA Solar Power
Satellite**

**Workshop on
Microwave Power
Transmission
and Reception**

**Session
Presentations**

**Jan
15-18
1980**



The presentation material herein was used in the Microwave System Performance Session of the Solar Power Satellite Workshop on Microwave Power Transmission and Reception held at the Lyndon B. Johnson Space Center, January 15-28, 1980. The workshop was conducted as part of the technical assessment process of the DOE/NASA Solar Power Satellite Concept Evaluation Program. All aspects of Solar Power Satellite microwave transmission and reception were addressed including studies, analyses, and laboratory investigations. Conclusions from these activities were presented as well as recommended follow-on work. The workshop was organized into eight sessions as follows:

- *General*
- *Microwave System Performance*
- *Phase Control*
- *Power Amplifiers*
- *Radiating Elements*
- *Rectenna*
- *Solid State Configurations*
- *Planned Program Activities*

The material contained herein supplements the workshop papers which were published and distributed at the time of the workshop. Together they are a comprehensive documentation of the numerous analytical and experimental activities in the field of microwave power transmission and reception.

- *Additional information regarding the workshop may be obtained by contacting: R.H. Dietz*

EE4/SPS Microwave Systems
National Aeronautics &
Space Administration
Lyndon B. Johnson Space Center
Houston, Texas 77058
713 483-4507

2

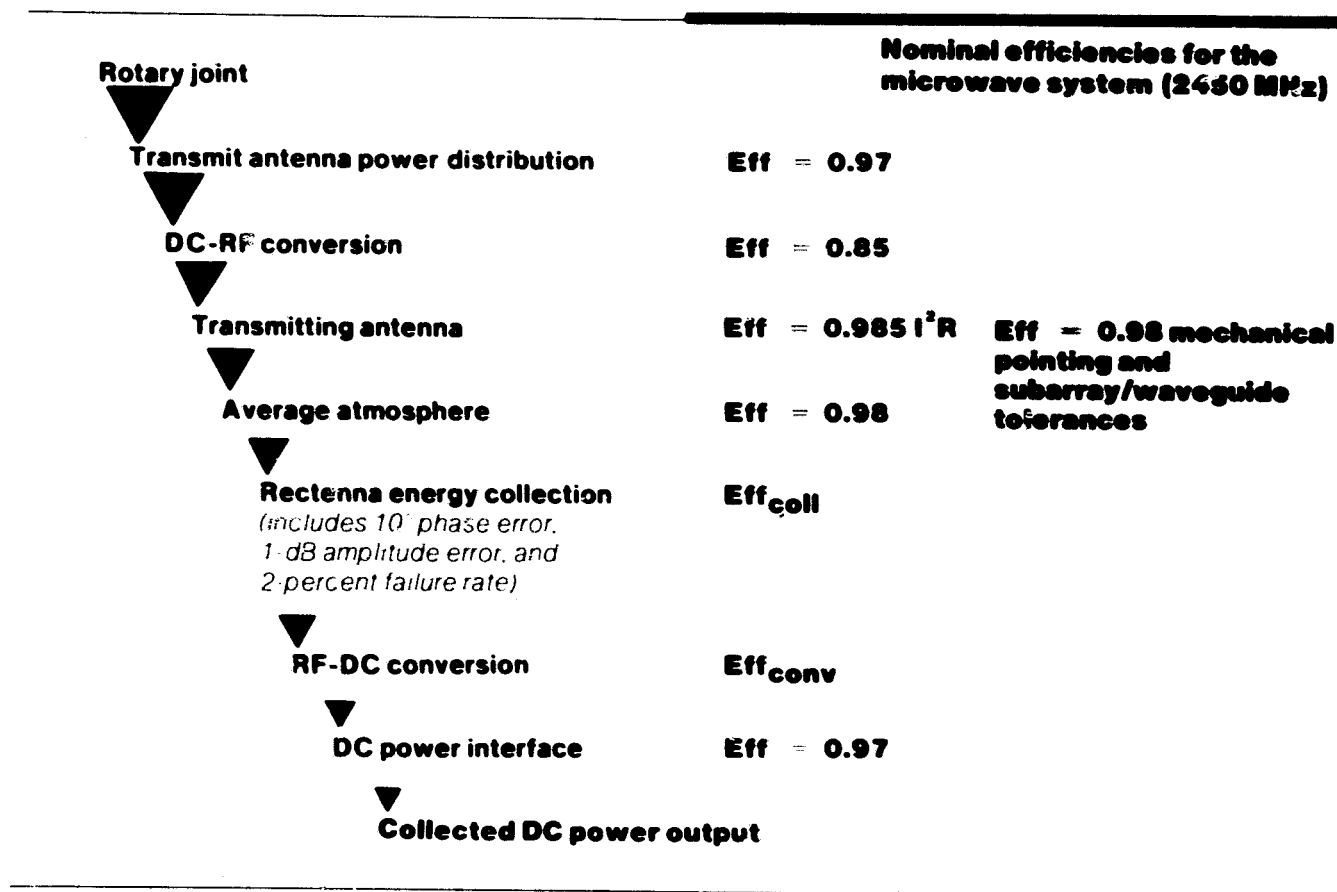
Microwave Performance Session *contents*

1	Reference System Conclusions D. Arndt, Lyndon B. Johnson Space Center
13	Reference System Description Gordon Woodcock, Boeing
27	Initial MPTS Study Results O. Maynard, Raytheon
115	Antenna Illumination and Beam Shaping Studies Dr. Erv Nalos, Boeing
135	Antenna Construction Techniques R. Ried, Lyndon B. Johnson Space Center
155	Subarray Alignment Techniques R. Iwasaki, Axiomatix (x)
193	Ionospheric Power Beam Studies W. Gordon, Rice University
205	Ionospheric Perturbations on Uplink Pilot Beam Signal (Experimental) Basu and Basu, Emanuel University
217	Ionospheric Perturbations on Uplink Pilot Beam Signal (Theoretical) and Plattville Heating Test Results K. Davis, Battelle Northwest Labs and D. Arndt, Lyndon B. Johnson Space Center

Reference System Conclusions

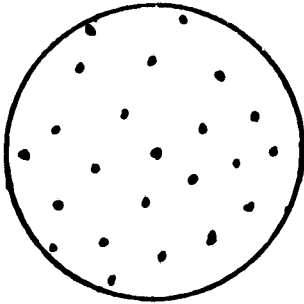
*D. Arndt
Lyndon B. Johnson Space Center*

PRECEDING PAGE BLANK NOT FILLED

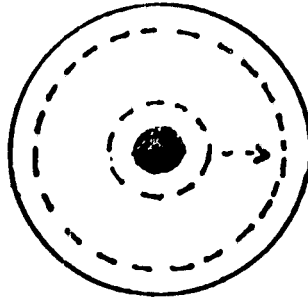


Antenna Startup/Shutdown Configurations

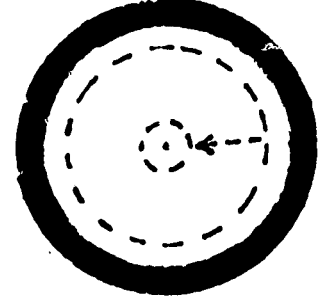
1. Random



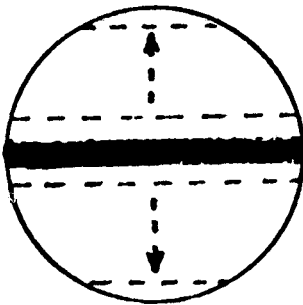
2. Concentric Rings-
Center to Edge



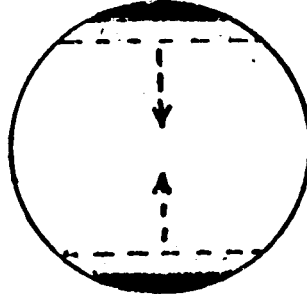
3. Concentric Rings-
Edge to Center



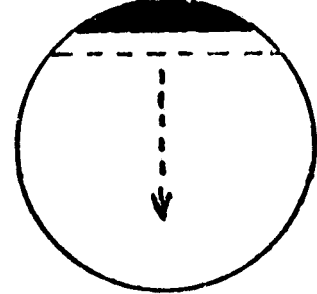
4. Line Strips-
Center to Edge



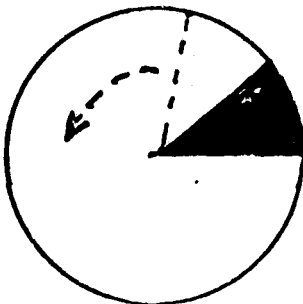
5. Line Strips
Edge to Center



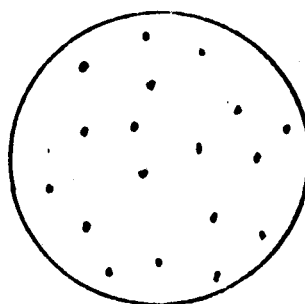
6. Line Strips
Edge to Edge



7. Radial Cuts



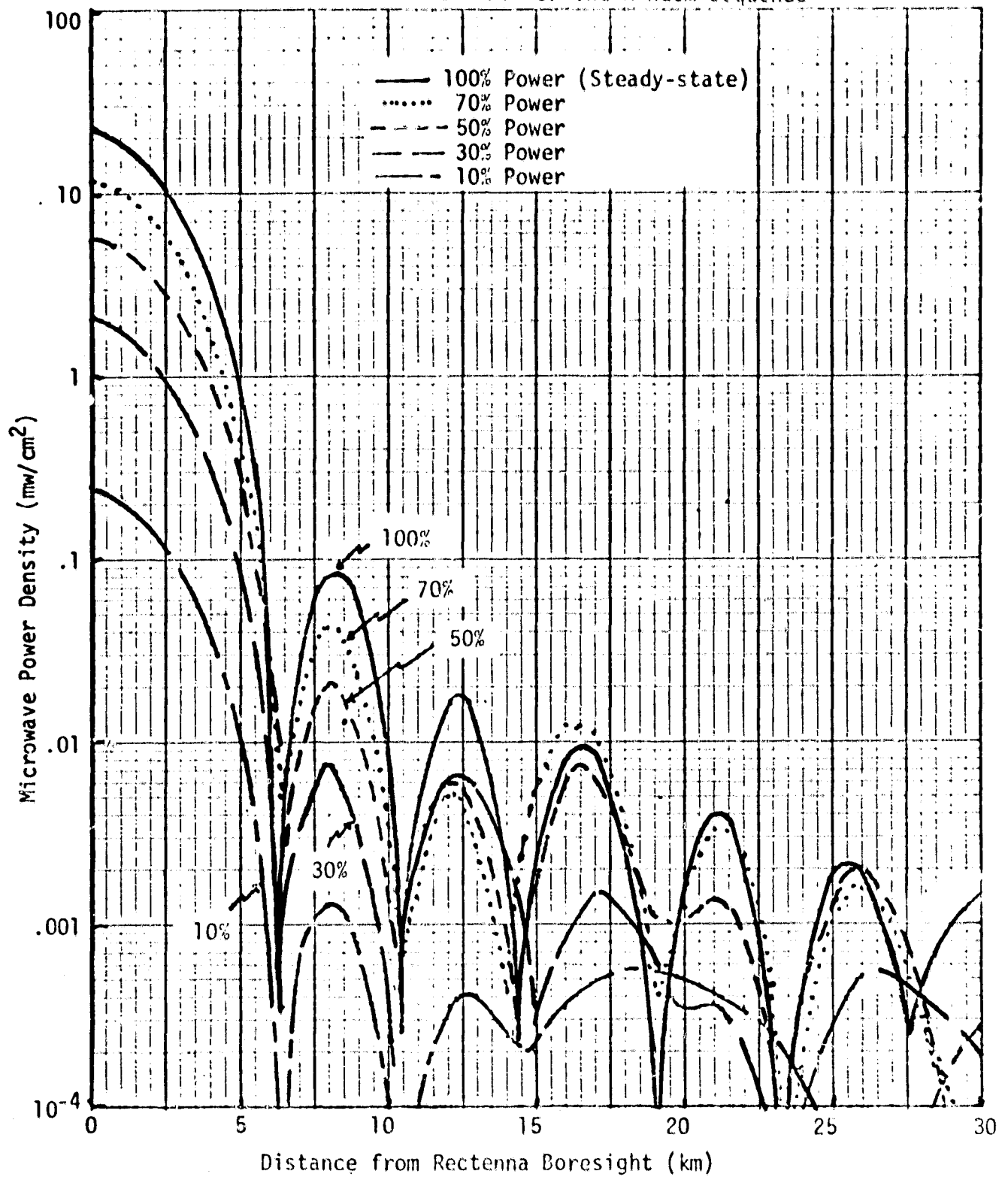
8. Incoherent Phasing

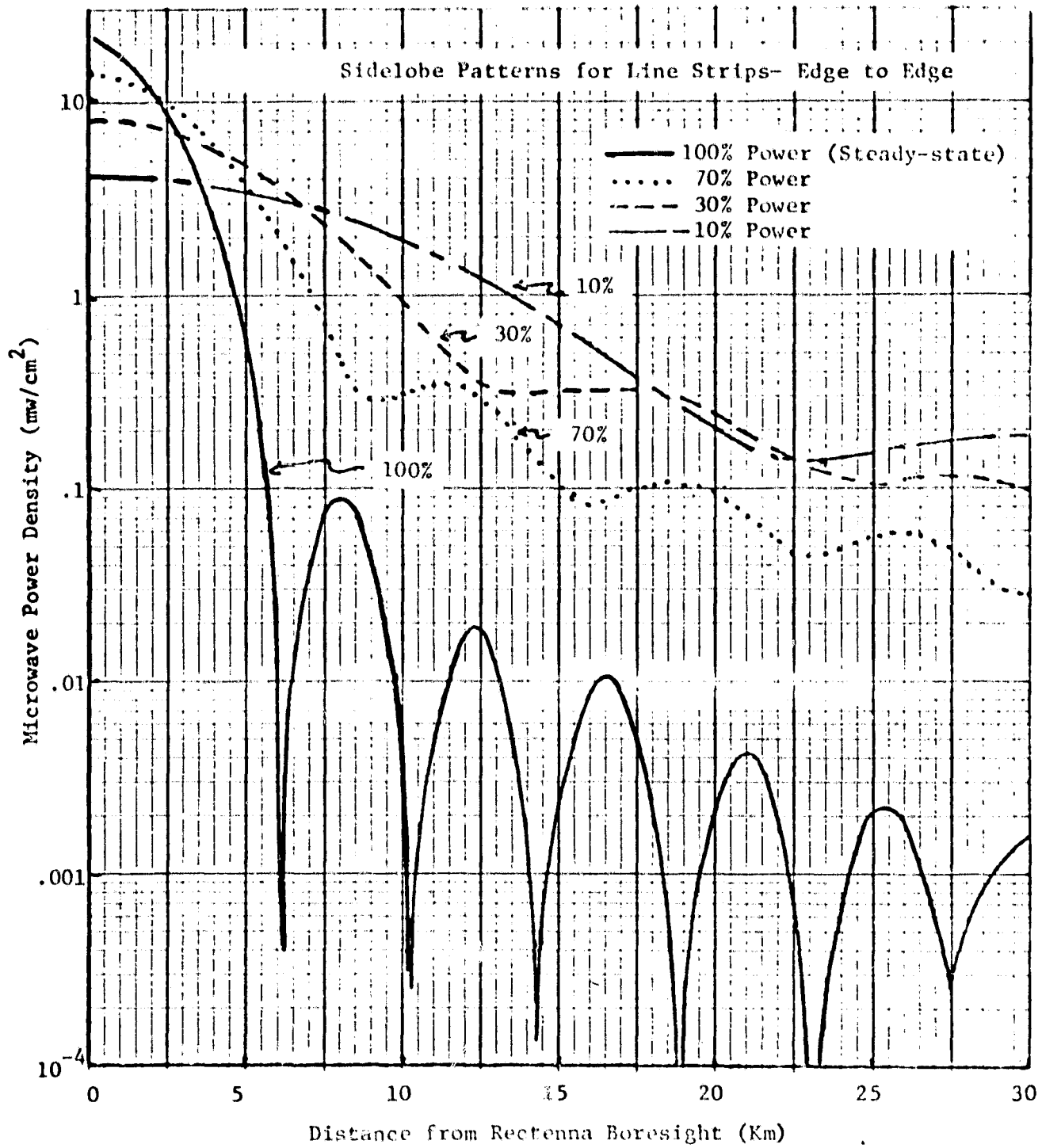


(After antenna is radiating incoherently, subarrays are properly phased in a random sequence.)

Note: Increments of 10% power are used for all sequences. Antenna illumination is a 10 dB gaussian taper.

Sidelobe Patterns for the Random Sequence





(87.75 %) ← 0

Loss in rectenna collection efficiency percent

1
-2
3
-4
5
-6

0

1

2

3

4

5

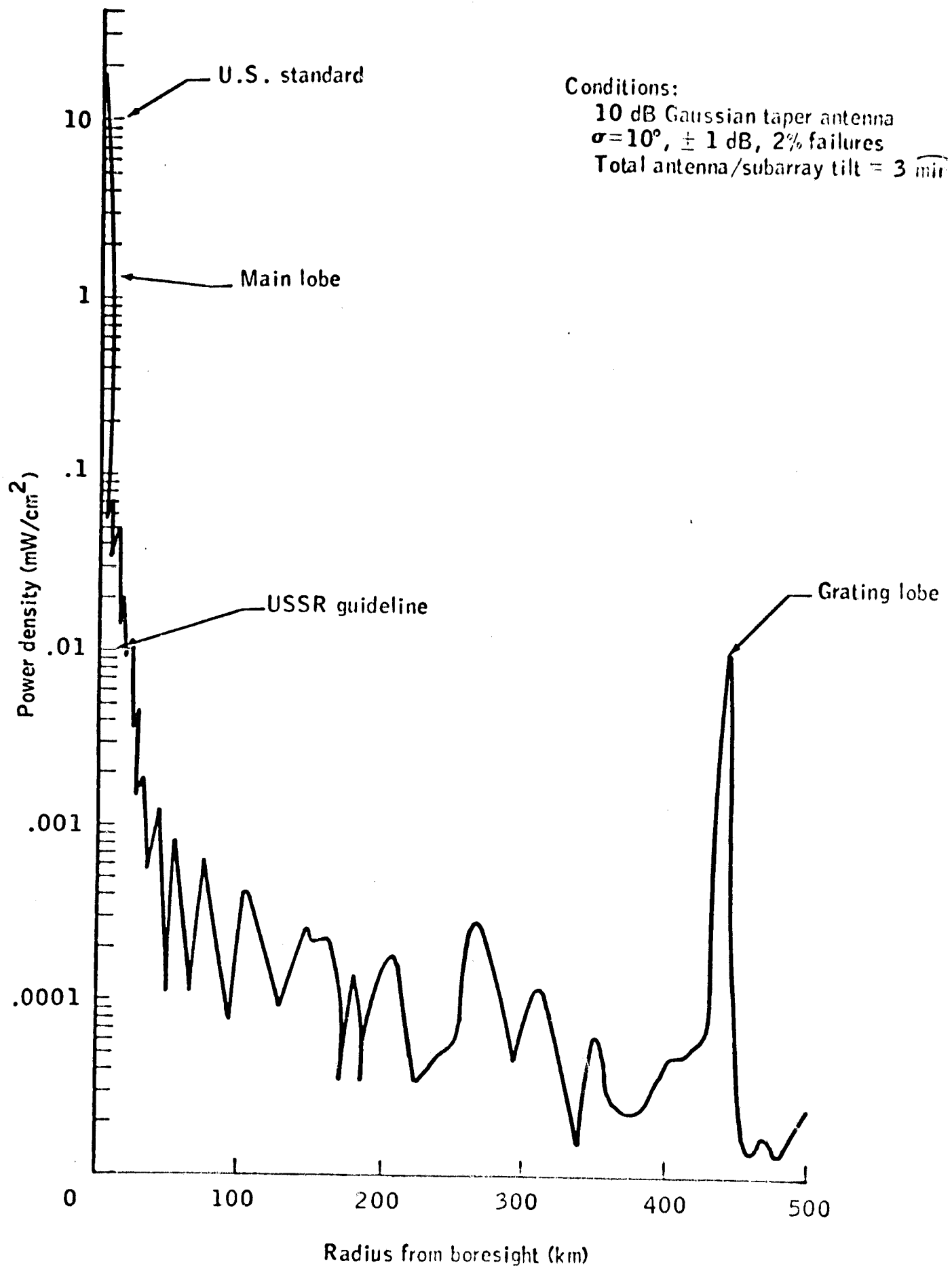
Antenna tilt ($^{\circ}$)

Subarray tilt

0 $^{\circ}$

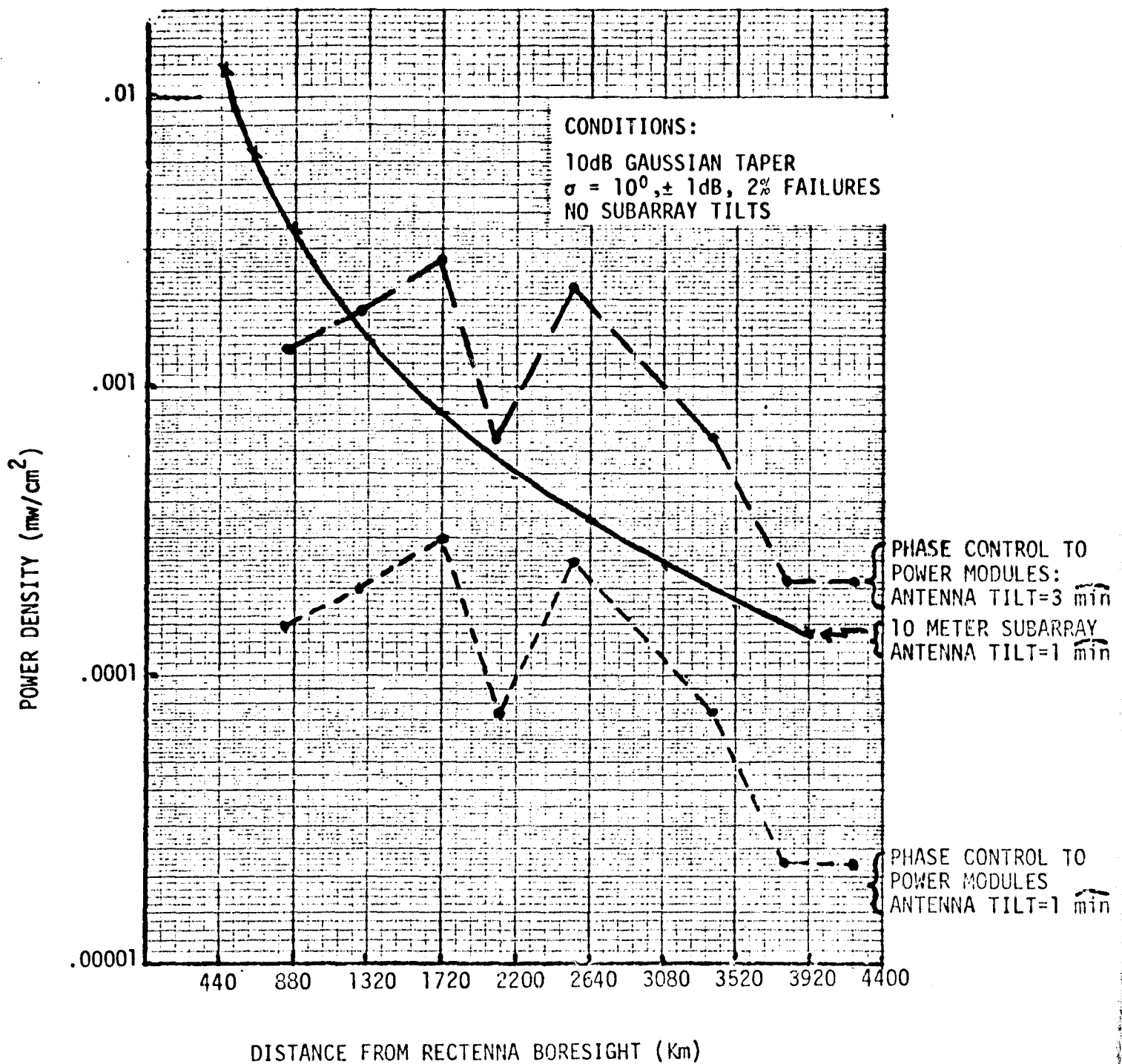
1 $^{\circ}$

3 $^{\circ}$



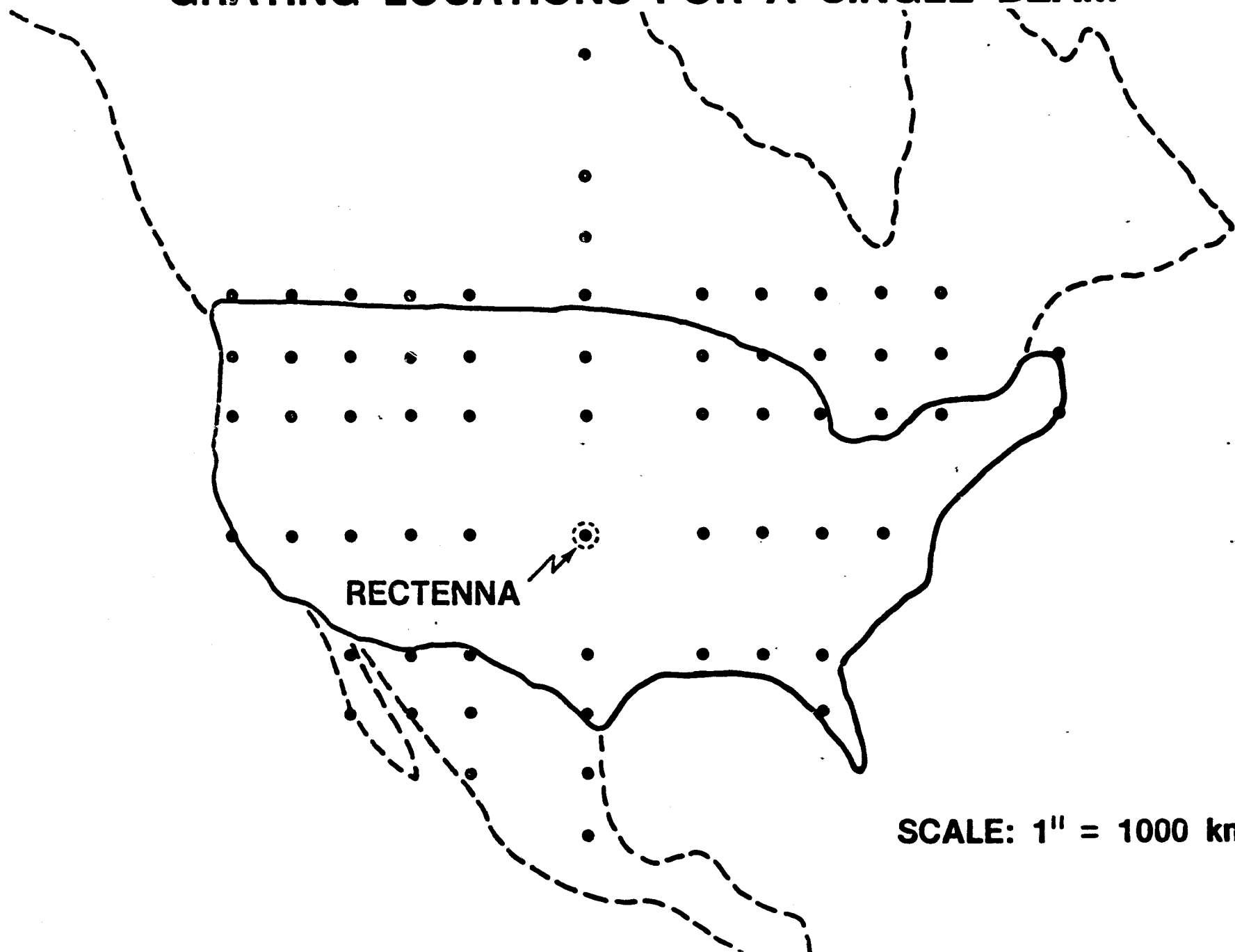
Peak power density for sidelobes and grating lobe as a function of range from rectenna.

GRATING LOBE PEAKS FOR 10 METER SUBARRAYS AND PHASE CONTROL TO POWER MODULES (TUBES)

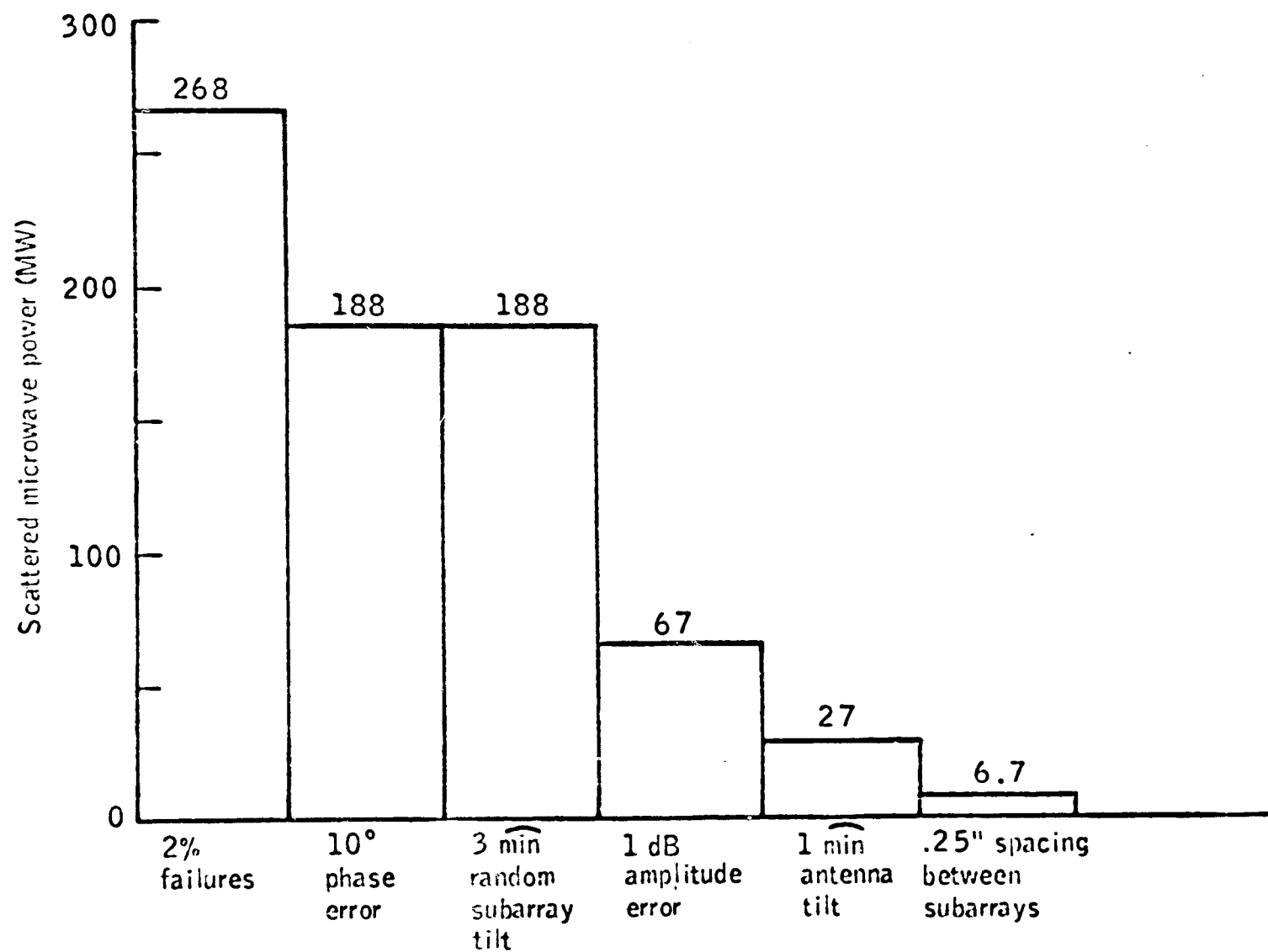


GRATING LOCATIONS FOR A SINGLE BEAM

10



SCALE: 1'' = 1000 km



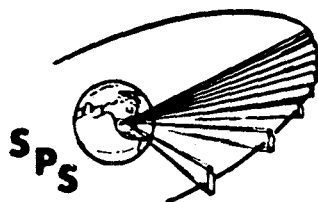
Scattered microwave power due to electrical and mechanical errors.
(10 meter subarray).

12

Reference System Description

Gordon Woodcock
Boeing

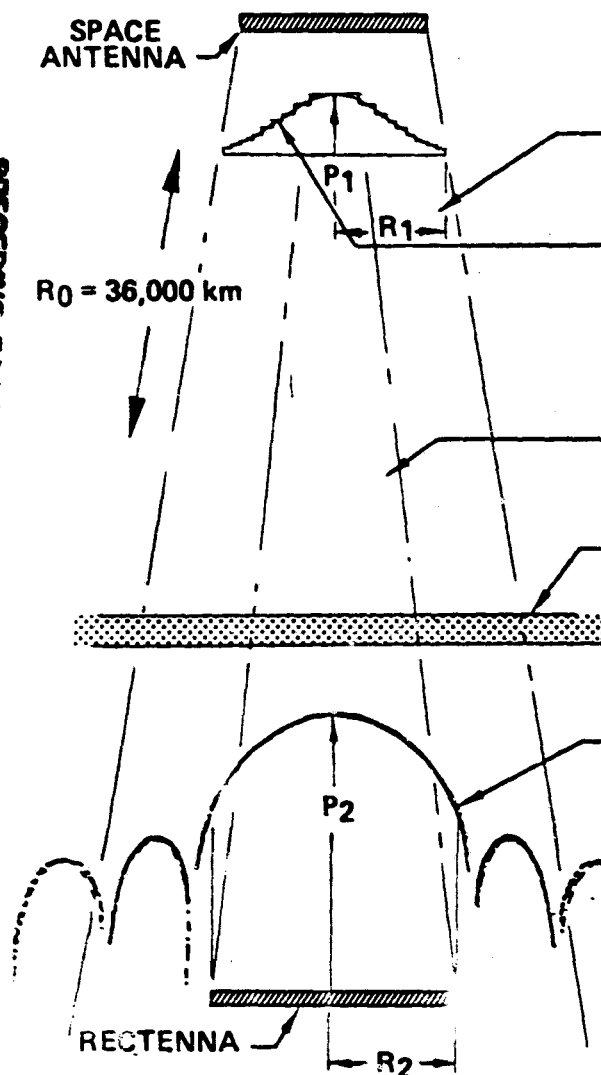
PRECEDING PAGE BLANK NOT FILMED



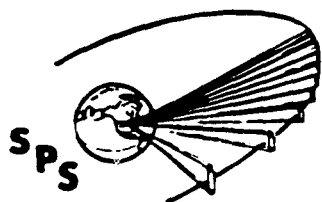
Design Constraints In Microwave Beam Link

BOEING

PRECEDING PAGE BLANK NOT FILMED



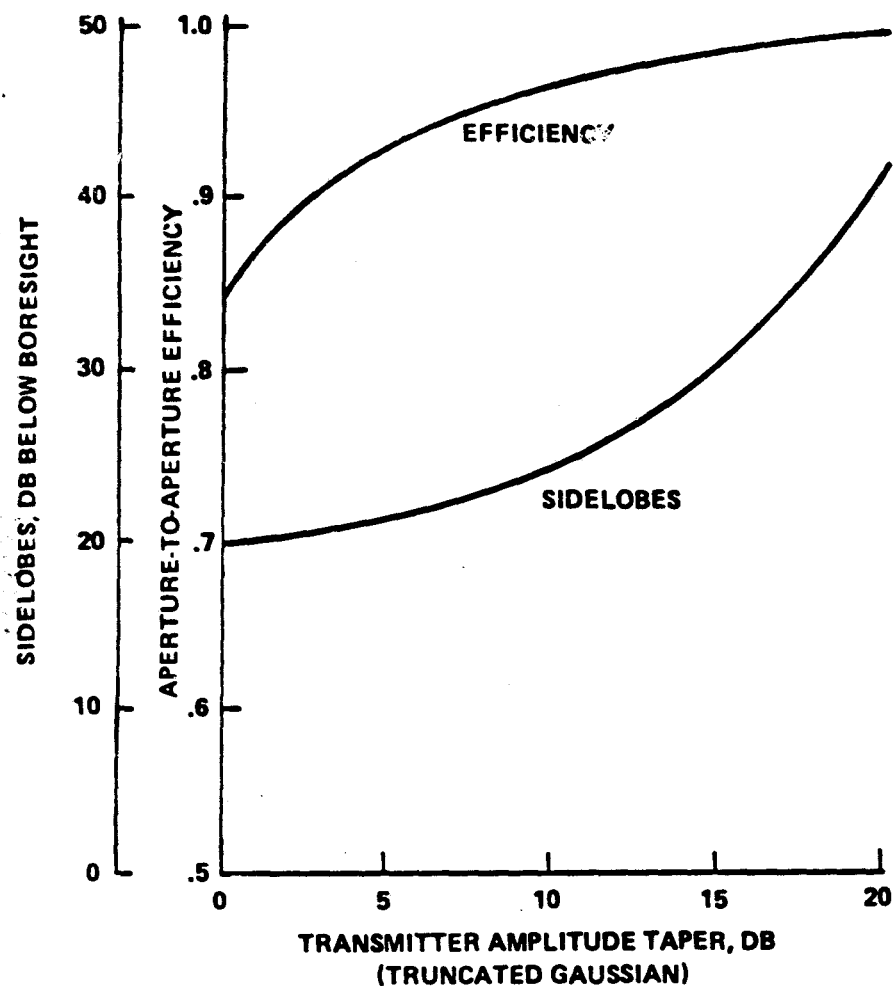
- ① PROPAGATION EFFECTS: SELECT $\lambda < 3\text{GHz}$;
INDUSTRIAL BAND @ 2.45GHz
 $\lambda = .12\text{ METERS}$
- ② HIGH EFFICIENCY $>95\%$ } SELECT TAPERED ILLUMINATION
LOW SIDELobe LEVEL $>20\text{db}$ } FUNCTION WITH $>10\text{db}$ POWER TAPER
- ③ THERMAL LIMIT PASSIVE RADIATIVE COOLING 4.5kw/m^2
I.E. PEAK RF POWER DENSITY = $P_1 = 3/(1-\eta)$
WHERE η = DC-RF CONVERSION EFFICIENCY
- ④ IONOSPHERIC HEATING LIMIT $P_2 = 23\text{ mw/cm}^2$
- ⑤ EDGE RECTENNA CONVERSION EFFICIENCY $>85\%$
- ⑥ SIDELobe & GRATING LEVEL OUTSIDE RECTENNA
BELOW ESTABLISHED STANDARDS



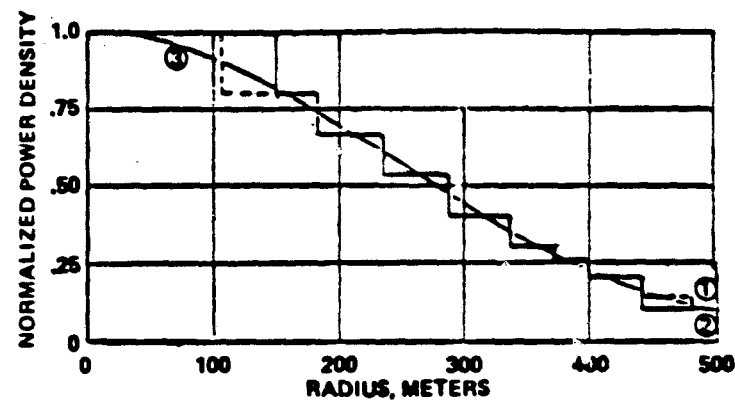
EFFECT OF TAPER AND BASELINE CHOICE

BOEING

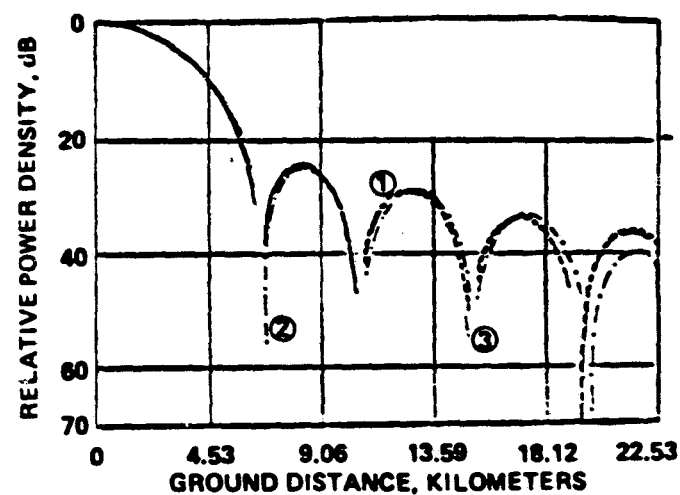
EFFECT OF AMPLITUDE TAPER



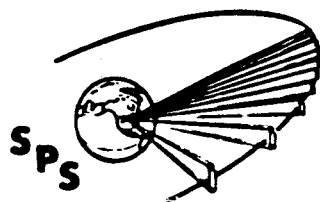
REFERENCE TAPER



(A) TRANSMITTER DISTRIBUTION FUNCTIONS

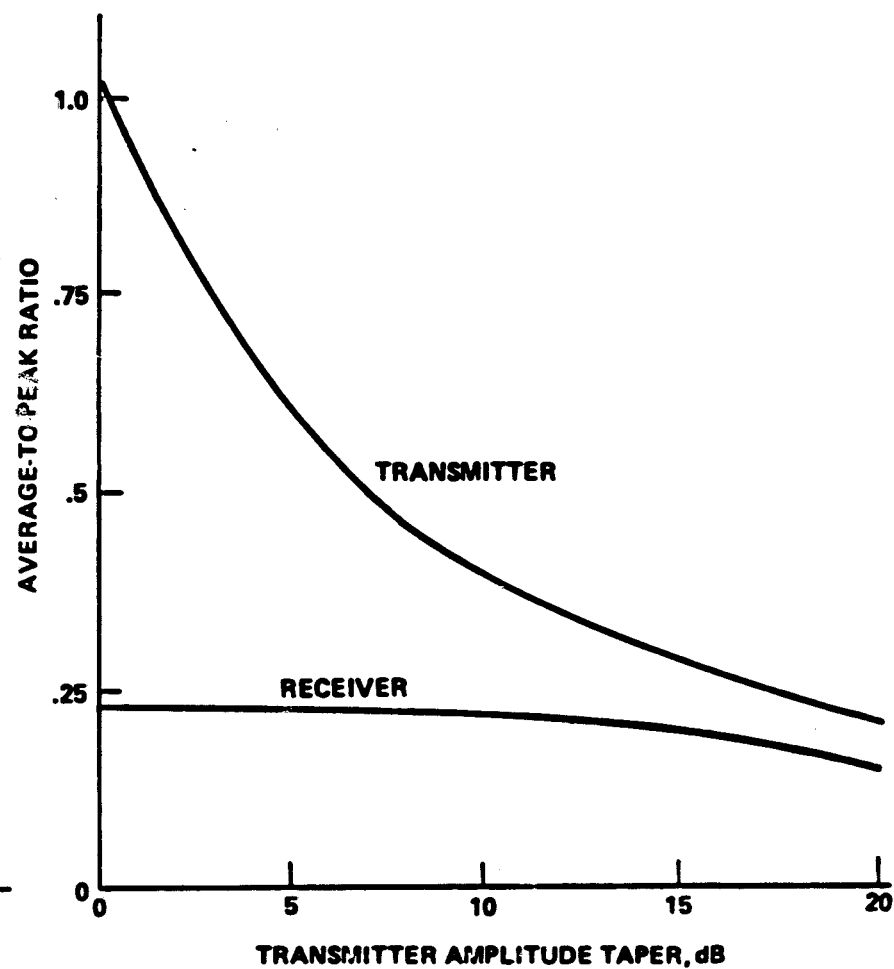
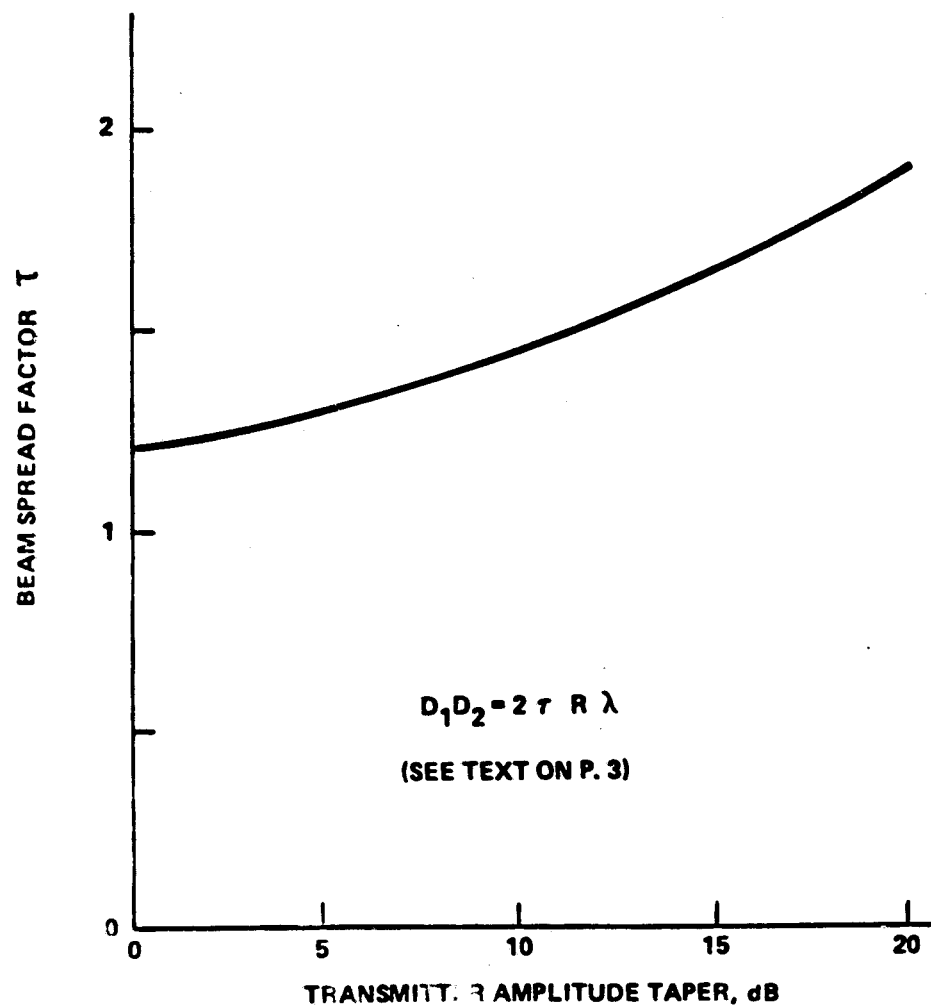


(B) FAR FIELD GROUND DISTRIBUTION

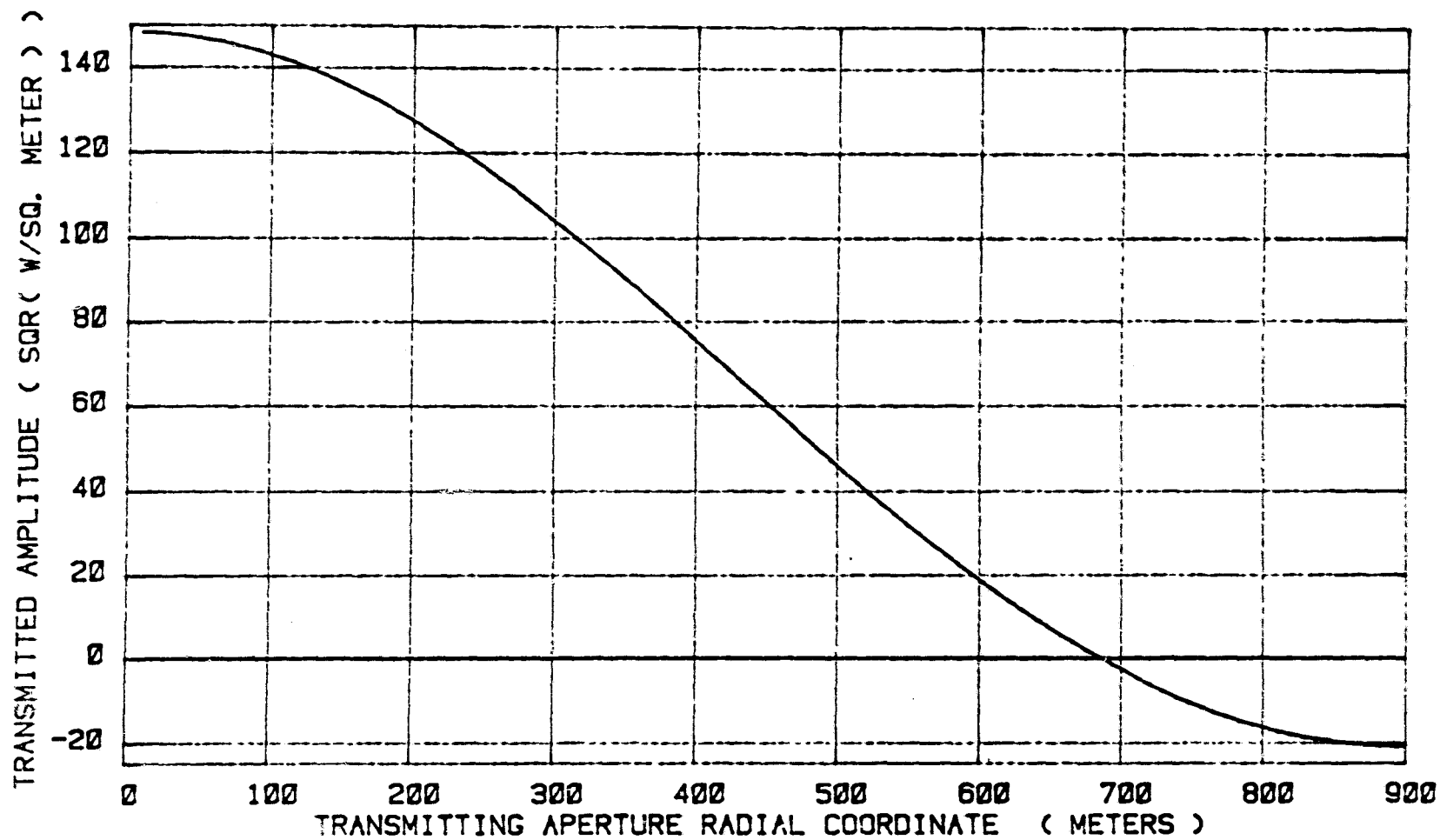


TAPER INFLUENCE ON BEAM SPREADING

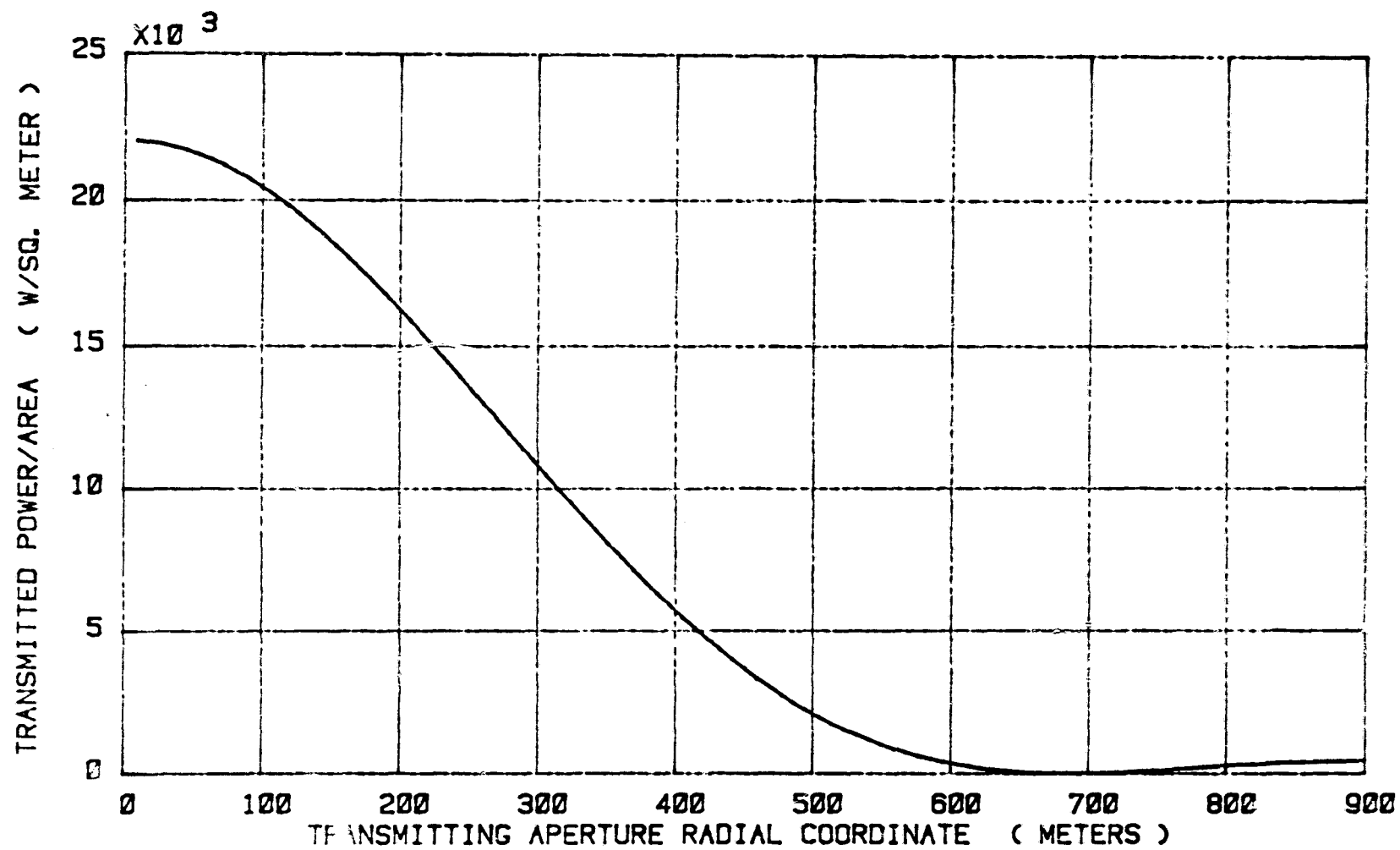
BOEING



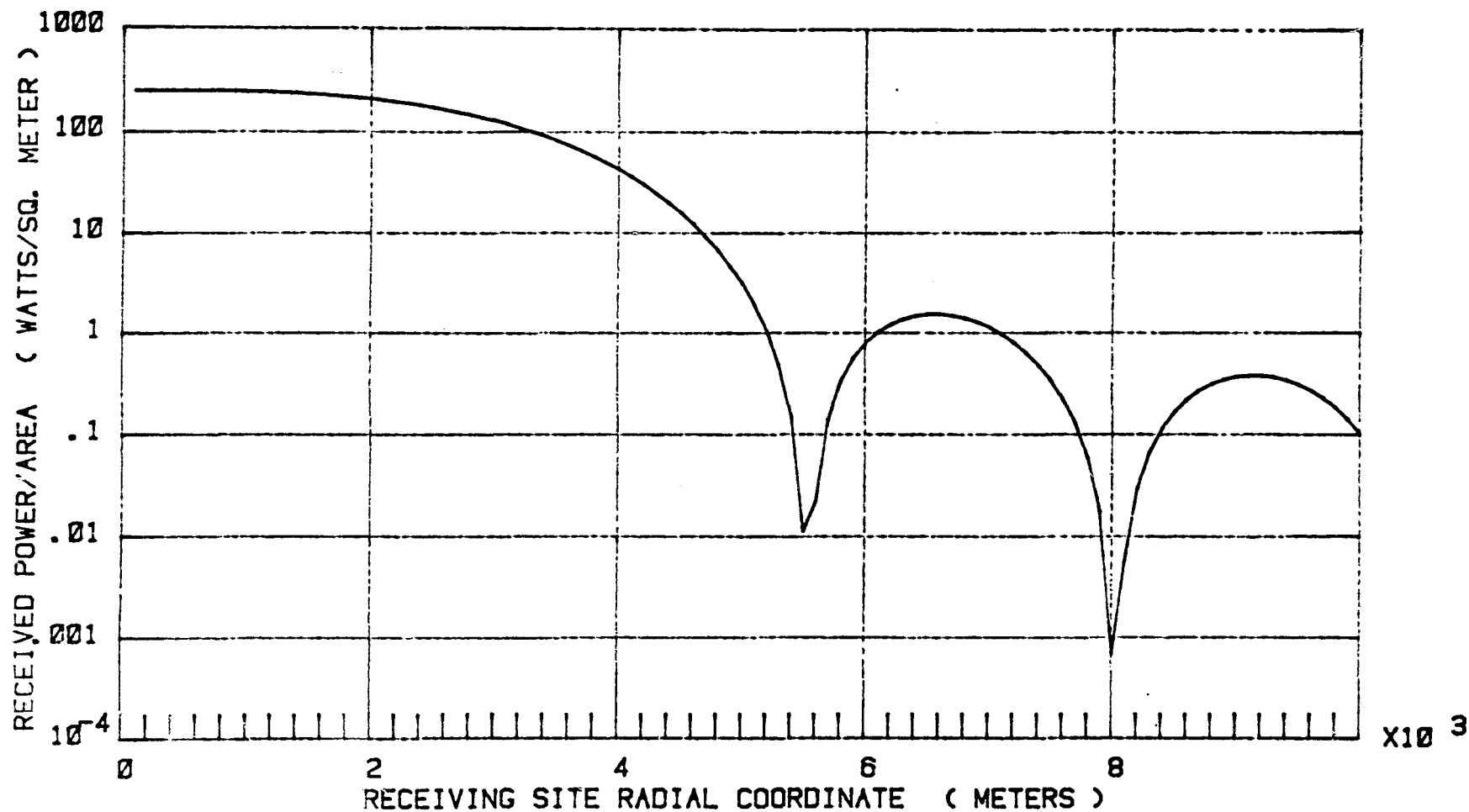
INFLECTED BESSEL $K=4.35$



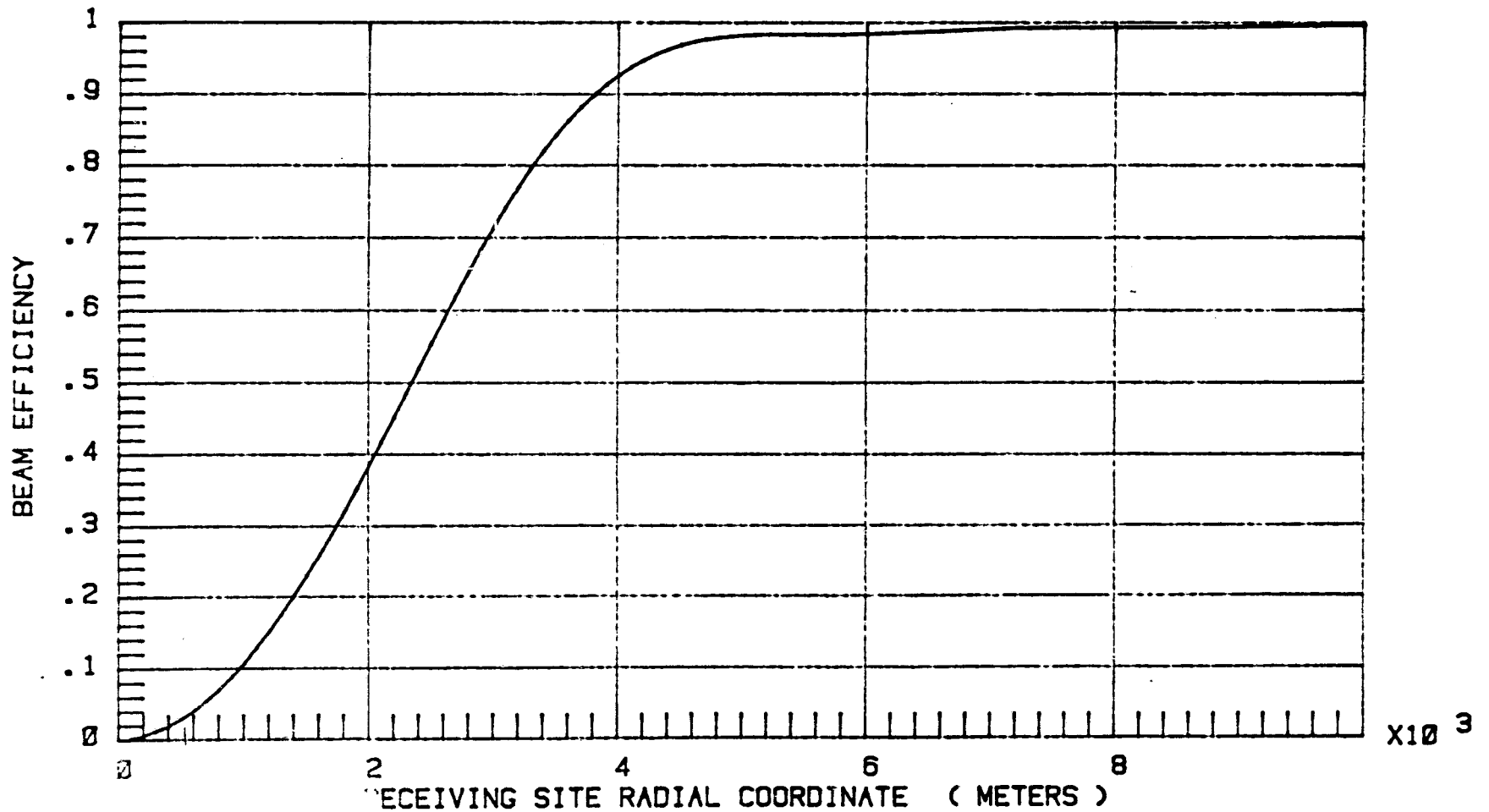
INFLECTED BESSEL K=4.35

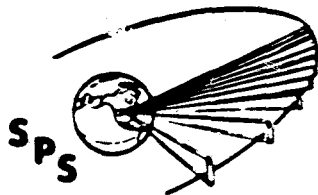


INFLECTED BESSEL $K=4.35$



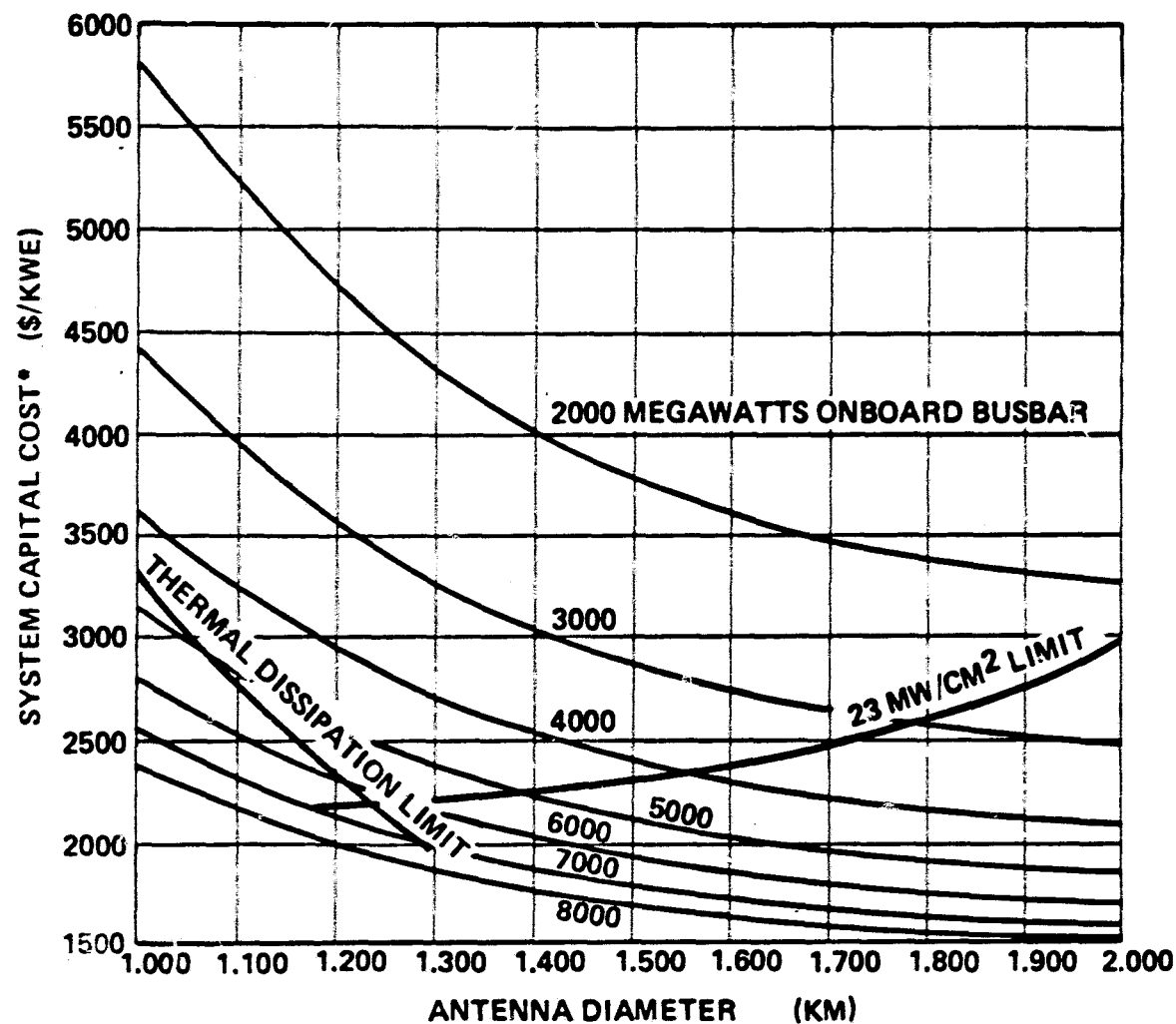
INFLECTED BESSEL $K=4.35$





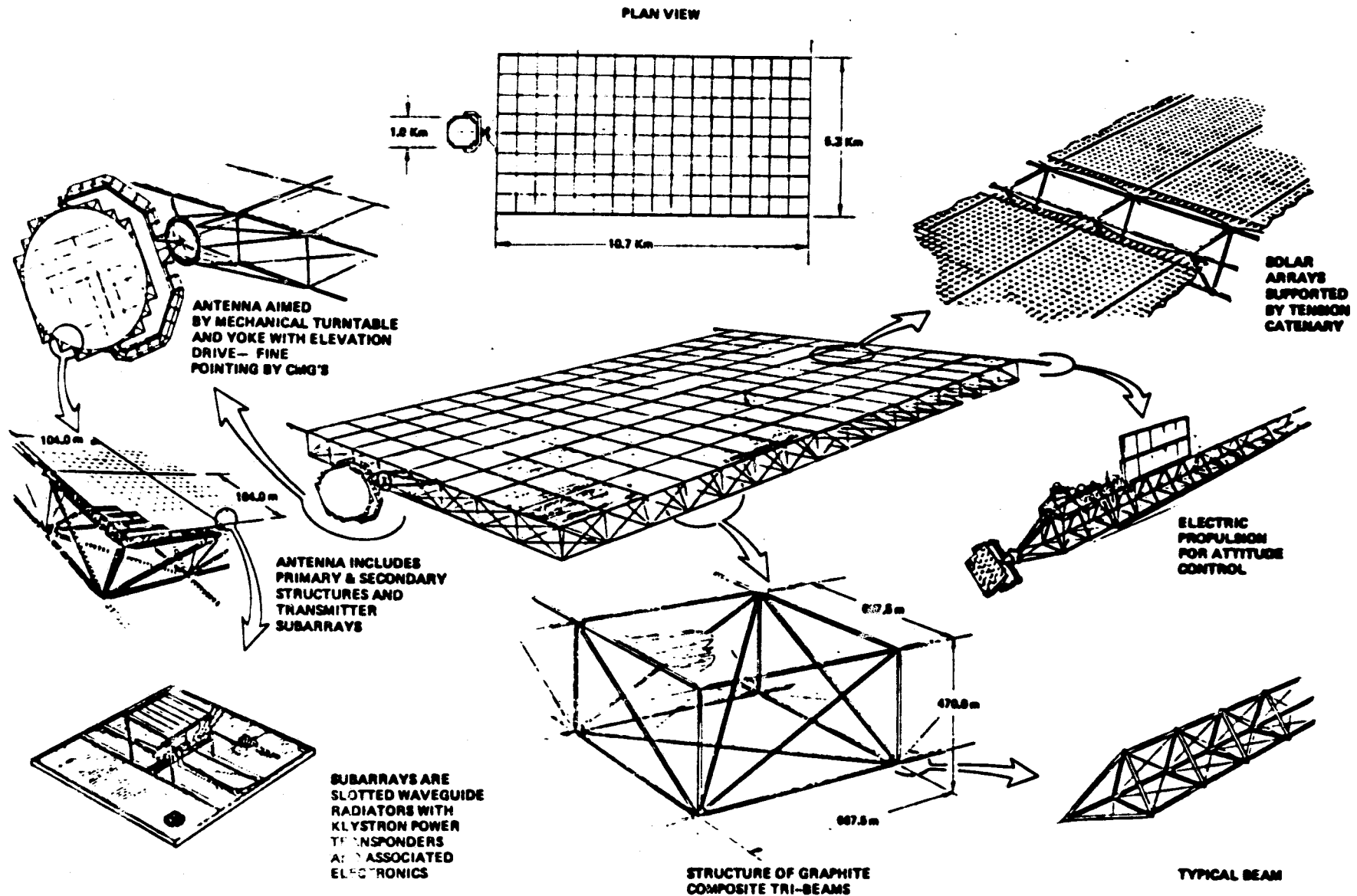
Transmitter Constraints Determine Minimum Cost Design Point

BOEING -

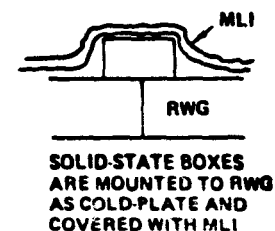
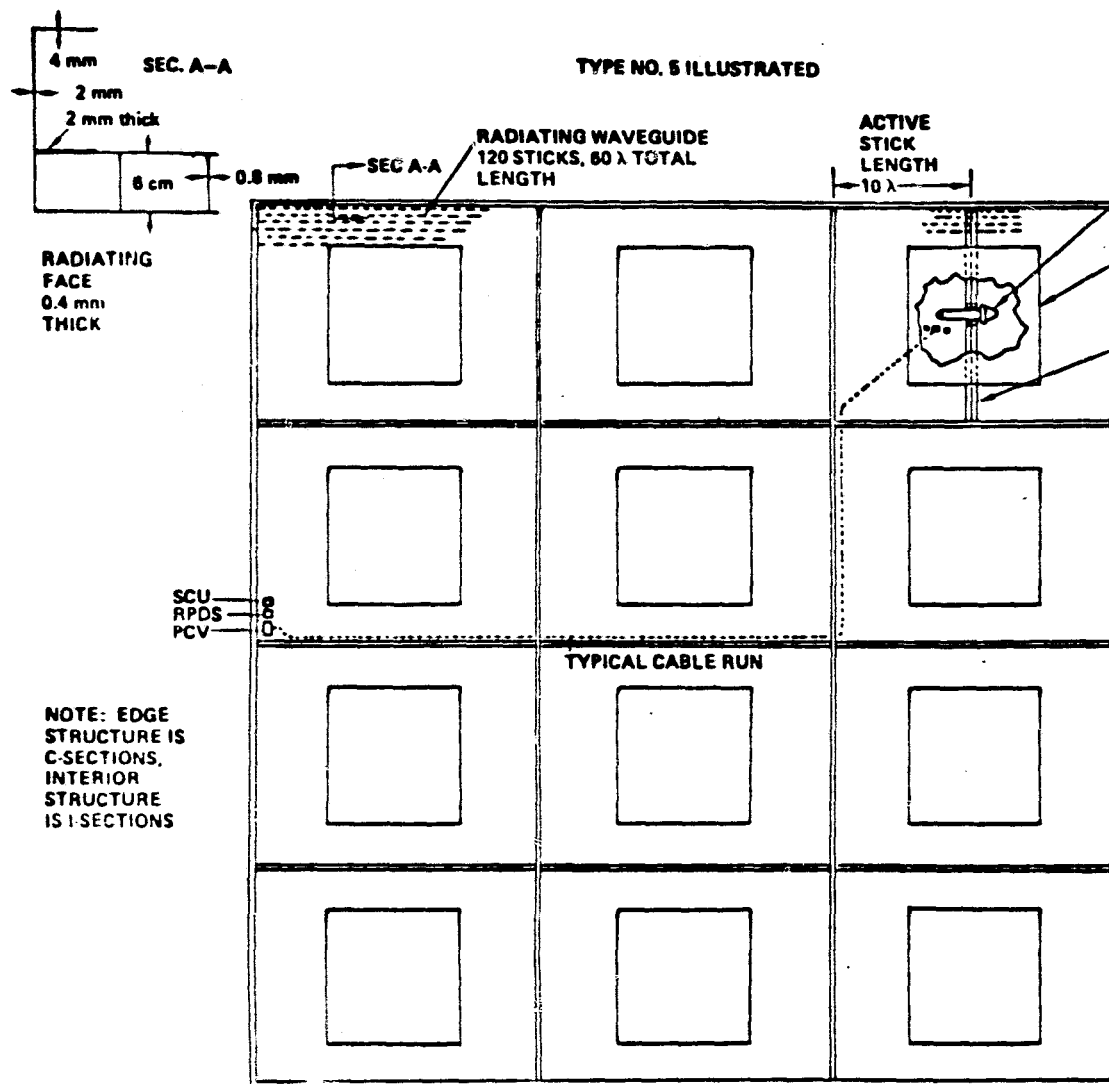


*ASSUMES BEAM-DIAMETER RECTENNA

SPS Silicon Solar Array Reference Design Concept



ORIGINAL PAGE IS
OF POOR QUALITY

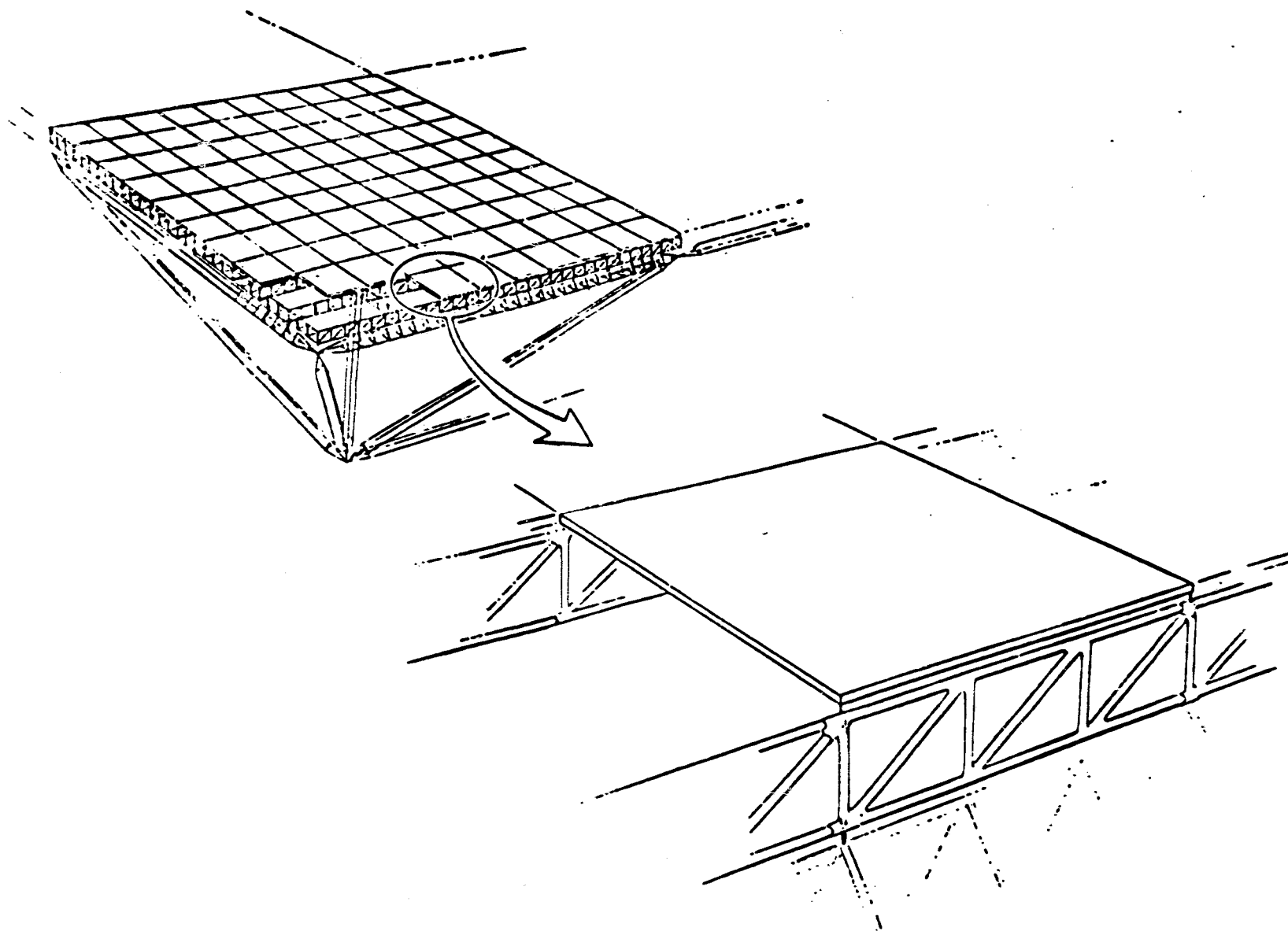


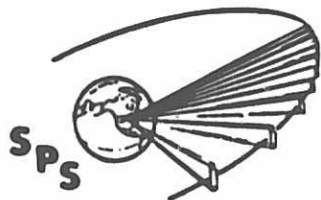
SOLID-STATE BOXES
ARE MOUNTED TO RWG
AS COLD-PLATE AND
COVERED WITH MLI

SUBARRAY ARRANGEMENTS

ARRANGEMENT TYPE	NO. KLAYSTRONS	RWG STICK LENGTH
1	4	15 λ
2	6	10 λ
3	8	15 λ
4	9	10 λ
5	12	10 λ
6	16	15 λ
7	20	8 λ
8	24	5 λ
9	30	5 λ
10	36	5 λ

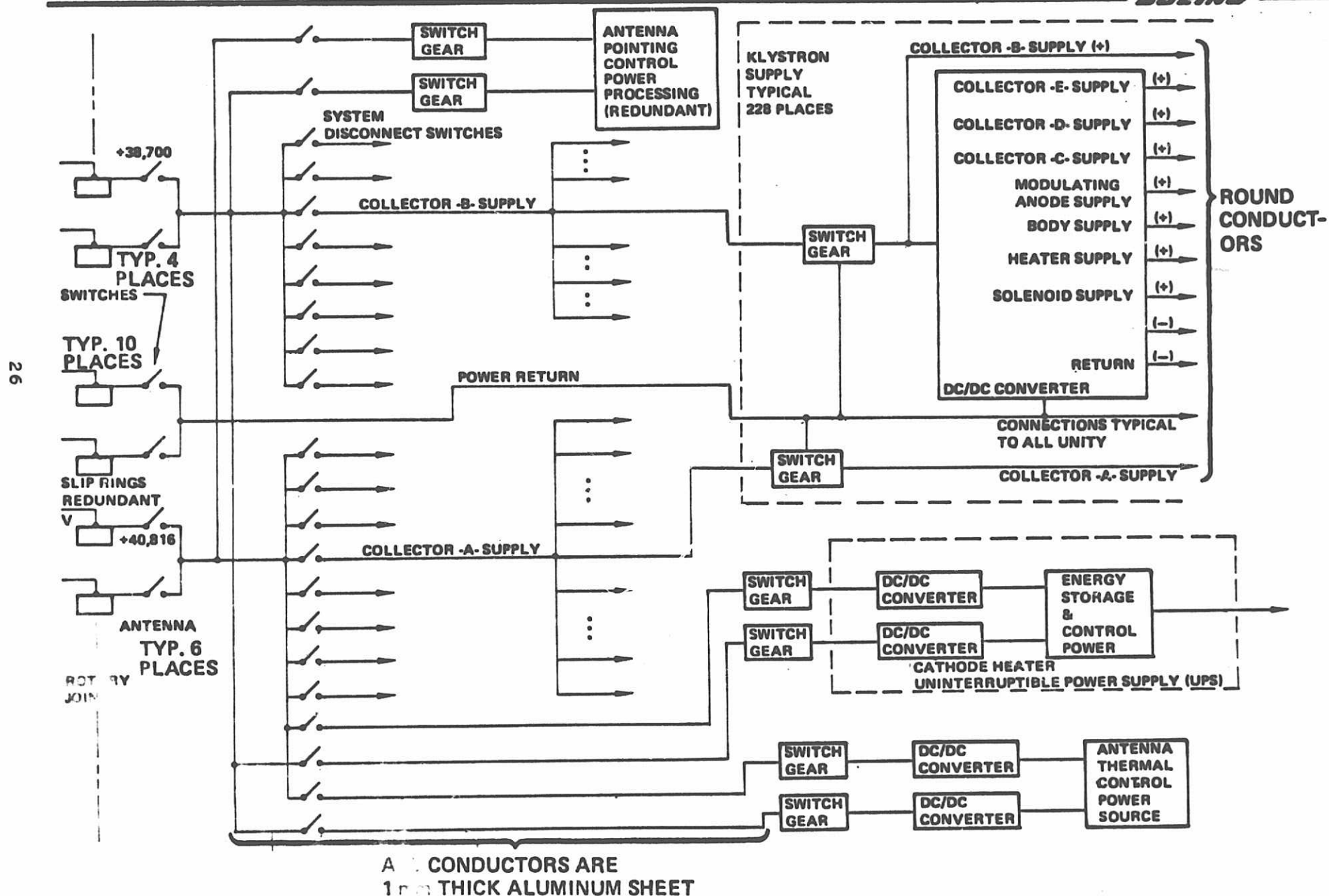
NOTE: TYPE NO. 6 USES SINGLE-FEED OUTPUT





MPTS Power Distribution System Block Diagram

BOEING



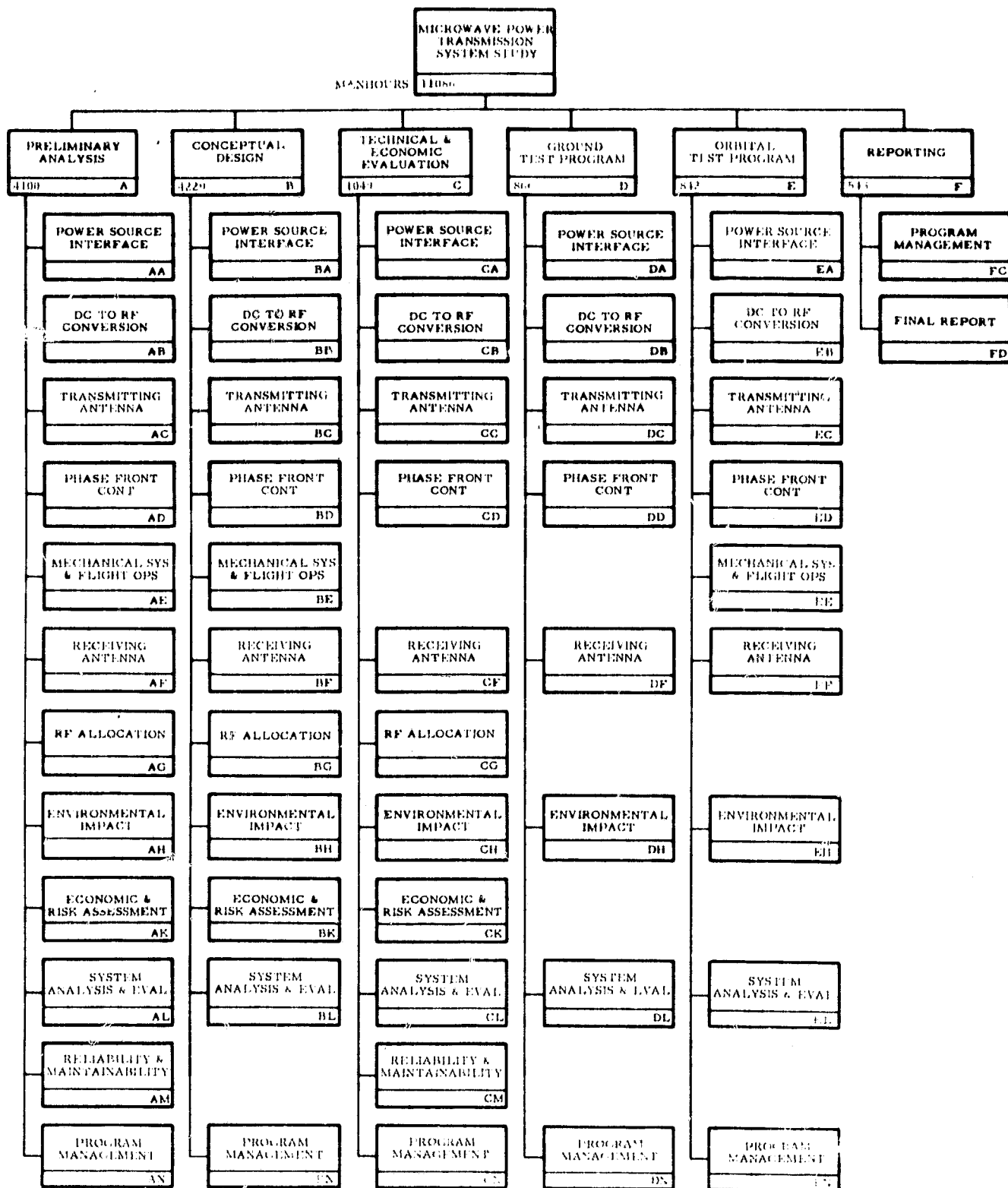
Initial MPTS Study Results

***O. Maynard
Raytheon***

RAYTHEON'S PARTICIPATION IN SOLAR POWER SATELLITE PROGRAM RELATED WORK - SYSTEM STUDIES AND TECHNOLOGIES

DESCRIPTIVE TITLE	PRIOR TO 1970	PERIOD OF PERFORMANCE												CUSTOMER	PRIME	SUB	RELATED REPORT NUMBER
		70	71	72	73	74	75	76	77	78	79	80	81				
Microwave Powered Helicopter	1964													USAF	Raytheon		RADC-TR-65-188
Orbit-to-Orbit Power Transmission	1969													NASA-MSFC	Raytheon		PT-4601
MPTS in Satellite Solar Power Station														In-House			ER77-4038
Feasibility Study of SPS														NASA-LeRC	Arthur D. Little	Raytheon Grumman Spectrolab	NASA CR-2357
Microwave Power Transmission System Studies														NASA-LeRC	Raytheon	Shared Applic's & Grumman	NASA CR-134886
Reception-Conversion Subsystem (RXCV) for Microwave Power Transmission System														NASA	JPL	Raytheon	ER75-4386
RF to DC Collector/Converter Technology Development														NASA-LeRC	Raytheon		NASA CR-135194
Design and Fabrication of Crossed Field Amplifier														NASA-LeRC	Raytheon		NASA CR-159410
Areas of Investigation Relationships to Development Approaches														In-House			
Space Station System Analysis Study														NASA-MSFC NASA-JSC	GAC H&AC	Raytheon Raytheon	
Space Based Solar Power Conversion and Delivery System Study														NASA-MSFC	ECON	Raytheon	ECON 77-145-1 S/C ECON-0003
Satellite Power System Development Plan Summary														In-House			
DOD Applications & DARPA Advanced Technology Development (Relevant Space Based Investigations)														SAMSO RADC	TRH/GAC Raytheon	Raytheon	
SPS System Evaluation Phase III - Rectenna Technology Study														NASA-JSC	Boeing	G.E. Raytheon	D18G-24635-1 PT-5155
SPS & Alternate Technology Comparisons														ANL	UE&C Inc.	Consultant	UE&C-ANL-79031
Crossed Field Directional Amplifiers For Use in the Solar Power Satellite														In-House			
SPS Pilot Beam & Communication Link Study														NASA-MSFC	Raytheon		NAS9-33157
SPS Pilot Beam Ionospheric Effects Discussion of Critical Issues														In-House			Draft 6/79
Solid State SPS Microwave Generation and Transmission Study														NASA-MSFC	Raytheon		
Magnetron Tube Assessment														NASA-MSFC	Raytheon		

PRECEDING PAGE BLANK NOT FILMED



Work Breakdown Structure

MICROWAVE POWER TRANSMISSION SYSTEM STUDIES

- INTRODUCTION -

TASKS

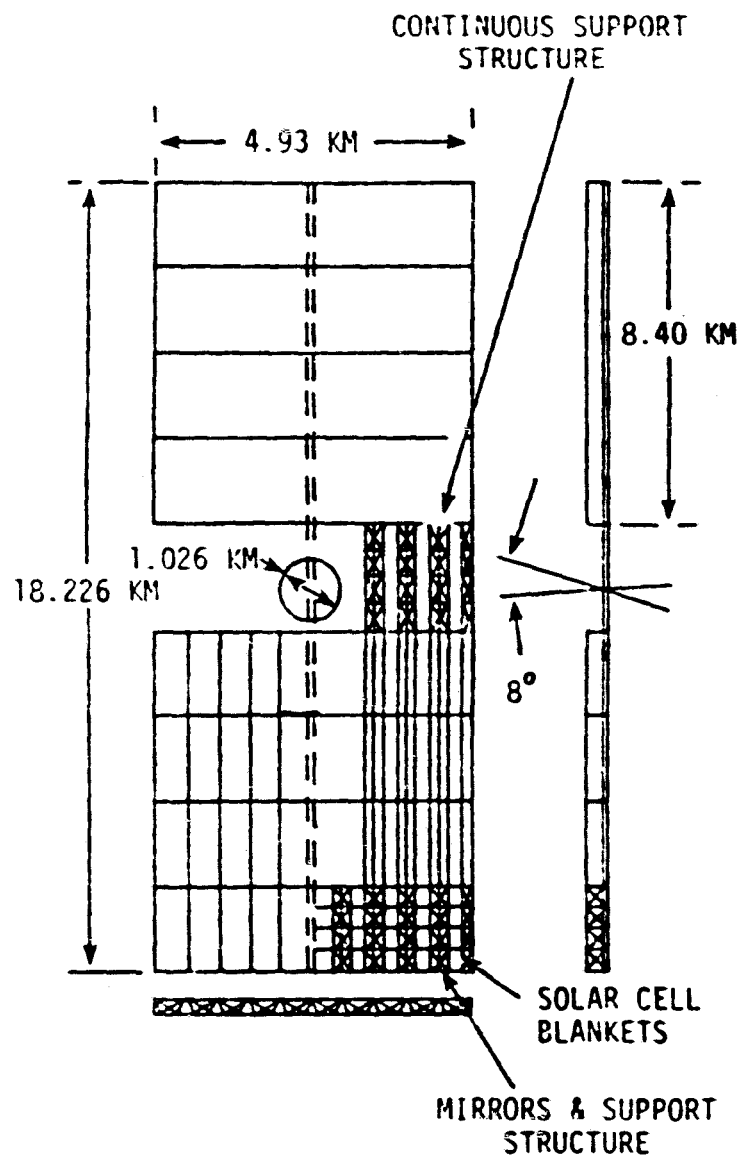
- PRELIMINARY ANALYSIS
- CONCEPTUAL DESIGN
- TECHNICAL AND ECONOMIC EVALUATION OF SYSTEMS
- DEVELOPMENT OF GROUND TEST PROGRAM
- DEVELOPMENT OF ORBITAL TEST PROGRAM
- REPORTING

MAJOR VARIABLES

- GROUND POWER OUTPUT
- OPERATING FREQUENCY
- DC-RF CONVERTER POWER LEVEL
- DC-RF CONVERTER TYPE
 - AMPLITRON
 - KLYSTRON
- TRANSMITTING ANTENNA SUBARRAY SIZE
- TRANSMITTING ANTENNA POWER LEVELS
- TECHNIQUES FOR COOLING TRANSMITTER TUBES
- BEAM CONTROL TECHNIQUES
- TRANSMITTING ANTENNA ILLUMINATION PATTERN
- PEAK RECEIVING ANTENNA POWER DENSITY

CONSIDERATIONS

- SOCIO-ECONOMIC CONSIDERATIONS
- POWER SOURCE
- OPERATIONS AND MAINTENANCE
- FLIGHT OPERATIONS
 - TRANSPORTATION SYSTEM
 - RE-SUPPLY
 - SPS FLIGHT MECHANICS
 - ORBITAL ASSEMBLY SYSTEM
- ASSURANCE TECHNOLOGIES
 - RELIABILITY
 - SAFETY
 - ENVIRONMENTAL IMPACT



NOMINAL CHARACTERISTICS

BOL POWER OUTPUT: 5375 MW

MASS: 27,200,00 kg

ORBIT: GEOSYNCHRONOUS

LIFE: 30 YEARS

OPERATING FREQ.: 2.45 GHz

DC-TO-DC EFFICIENCY: 58%

SOLAR ARRAY EFF.: 9.2% BEGINNING
OF LIFE

CONC. RATIO: 2

ANTENNA TAPER: 10db

SOLAR CELL MATERIAL: Si

The Satellite Solar Power System
Configuration Used in this Study

CONCLUSIONS AND RECOMMENDATIONS

- PLANAR PHASED ARRAY ~ 1 KM DIAMETER OF AL OR COMPOSITES WEIGHING $\sim 6 \times 10^6$ KG.
- 18M X 18M SLOTTED WAVEGUIDE SUBARRAYS ELECTRONICALLY CONTROLLED TO DIRECT POWER BEAM AT GROUND WITH RMS ERROR OF ~ 10 M.
- 5 KW CROSSED FIELD DIRECTIONAL AMPLIFIERS IN SERIES OR 50 KW KLYSTRONS IN PARALLEL.
- RECTENNA (~ 10 KM DIA) OF DIPOLES EACH INTEGRATED WITH A SOLID STATE DIODE AND FILTERS WHICH CONVERT MICROWAVE BACK TO DC POWER.
- RECOMMENDED OPERATING FREQUENCY: 2.45 GHZ.
- RECOMMENDED GROUND POWER OUTPUT = 5.0 GW WITH 20 MILLIWATTS/CM² POWER DENSITY PEAK.
- MPTS EFFICIENCY IS $\sim 60\%$.
- MPTS COST INCLUDING ORBITAL ASSEMBLY AND TRANSPORTATION IS ~ 500 \$/KW. TRANSPORTATION COST ASSUMED TO BE 200\$/KG.
- CRITICAL TECHNOLOGY ITEMS OF MPTS NEEDING EARLY DEVELOPMENT ARE:
 - DC TO MICROWAVE CONVERTERS
 - MATERIAL
 - ELECTRONIC PHASE CONTROL SUBSYSTEMS
 - TRANSMITTING ANTENNA WAVEGUIDE INCLUDING INTERFACE WITH MICROWAVE CONVERTERS
 - STRUCTURE
- SIX-YEAR, THREE-PHASE CRITICAL TECHNOLOGY DEVELOPMENT PROGRAM RECOMMENDED AT ROM \$27M.
- ORBITAL TEST PROGRAM OBJECTIVES DEFINED WHICH RELY ON SHUTTLE TRANSPORTATION SYSTEM TO DEVELOP AND DEMONSTRATE ORBITAL ASSEMBLY TECHNIQUES AND TO ESTABLISH LEARNING FOR COST AND SCHEDULE PROJECTIONS AT R 4 \$3,500M.

SUMMARY AND CONCLUSIONS
INITIAL MPTS STUDY RESULTS - SUBSYSTEMS AND TECHNOLOGY

ISSUES/CONSIDERATIONS

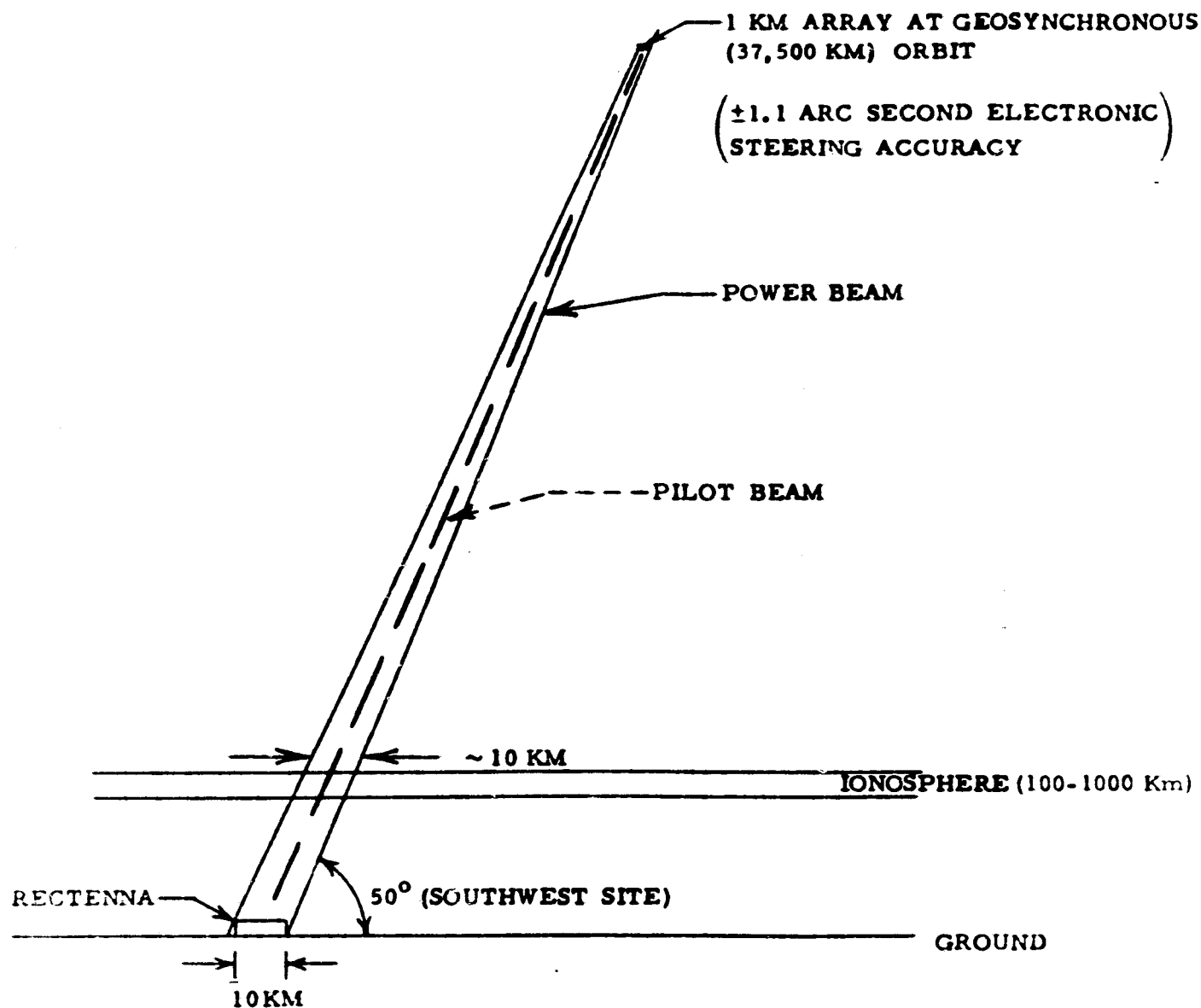
ENVIRONMENTAL EFFECTS - PROPAGATION

RESOLUTION/STATUS

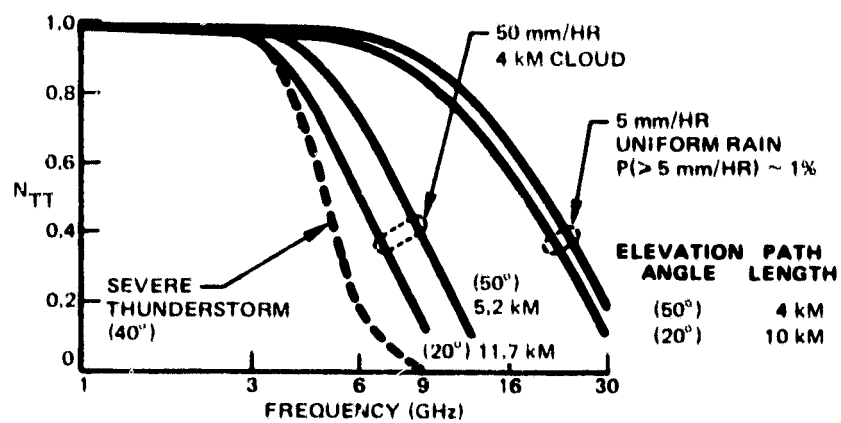
- RECENT DATA INDICATE THAT IONOSPHERIC EFFECTS ON PILOT BEAM STABILITY AND PHASE MEASUREMENT ACCURACY WILL NOT BE INCONSEQUENTIAL. SEVERAL THREE-FREQUENCY APPROACHES ARE POTENTIALLY SUITED TO THE SOLUTION OF THE VARIOUS PROBLEMS.
- FARADAY ROTATION HAS SMALL EFFECT. DURING AMBIENT CONDITIONS, $\sim 0.5\%$ LOSS; DURING DISTURBED CONDITIONS, $\sim 3\%$ LOSS. ORIENTATION OF RECEIVE ANTENNA TO AMBIENT ROTATION REDUCES LOSS FOR DISTURBED CONDITIONS TO 1% TYPICALLY 3 TIMES A YEAR. ANALYSIS OF TEC AS A FUNCTION OF TIME FOR EACH LOCATION IS NEEDED.

ENVIRONMENTAL EFFECTS - PROPAGATION
- FOR FREQUENCIES IN 1 TO 3 GHz RANGE -

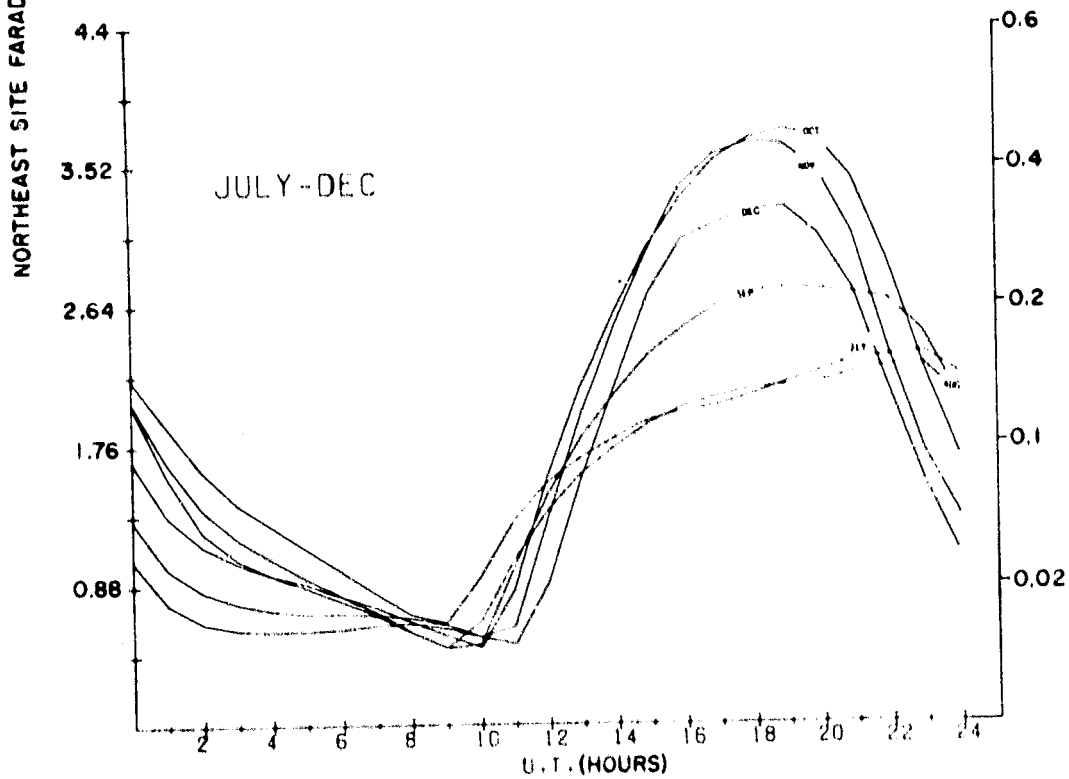
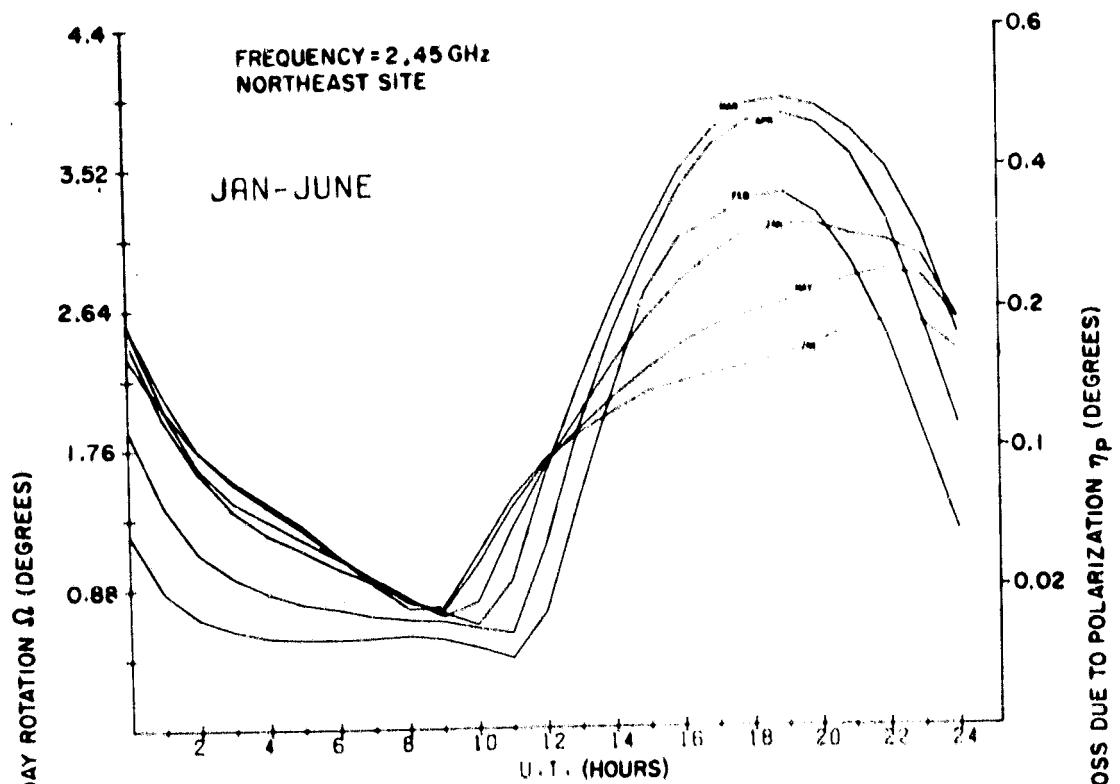
- ABSORPTION AND SCATTERING EFFECTS ARE SMALL EXCEPT FOR WET HAIL.
- REFRACTION CHANGES AND GRADIENTS:
 - CAUSE NEGLIGIBLE DISPLACEMENT OR DISPERSION OF THE HIGH POWER BEAM
 - DO NOT DEGRADE SIGNIFICANTLY A GROUND BASED PILOT BEAM PHASE FRONT AS SEEN AT TRANSMITTING ANTENNA
- RECENT DATA INDICATE THAT IONOSPHERIC EFFECTS ON PILOT BEAM STABILITY AND PHASE MEASUREMENT ACCURACY WILL NOT BE INCONSEQUENTIAL.
 - SEVERAL THREE-FREQUENCY APPROACHES ARE POTENTIALLY SUITED TO SOLUTION OF THE VARIOUS PROBLEMS AND COULD BE ADOPTED TO MAKE THE PILOT BEAM CAPABLE OF OPERATING WITHIN RATIONAL PERFORMANCE SPECIFICATIONS IN EXPECTED CONDITIONS OF IONOSPHERIC BIAS AND STOCHASTIC FLUCTUATIONS.
- FARADAY ROTATION HAS ONLY SMALL EFFECT FOR A LINEARLY POLARIZED RECEIVING ANTENNA.
- CHANGES IN ELECTRON DENSITY CAUSED BY POWER DENSITIES OF 20 mW/cm^2 AND ABOVE AT 2.45 GHz NEED TO BE INVESTIGATED FOR POSSIBLE EFFECTS ON OTHER IONOSPHERIC USERS.
- POSSIBILITY OF HARMONIC RADIATION FROM THE IONOSPHERE (RFI EFFECTS) SHOULD BE INVESTIGATED.



Schematic Representation of Power Beam and Pilot Beam



Transmission Efficiency - Molecular Absorption and Rain



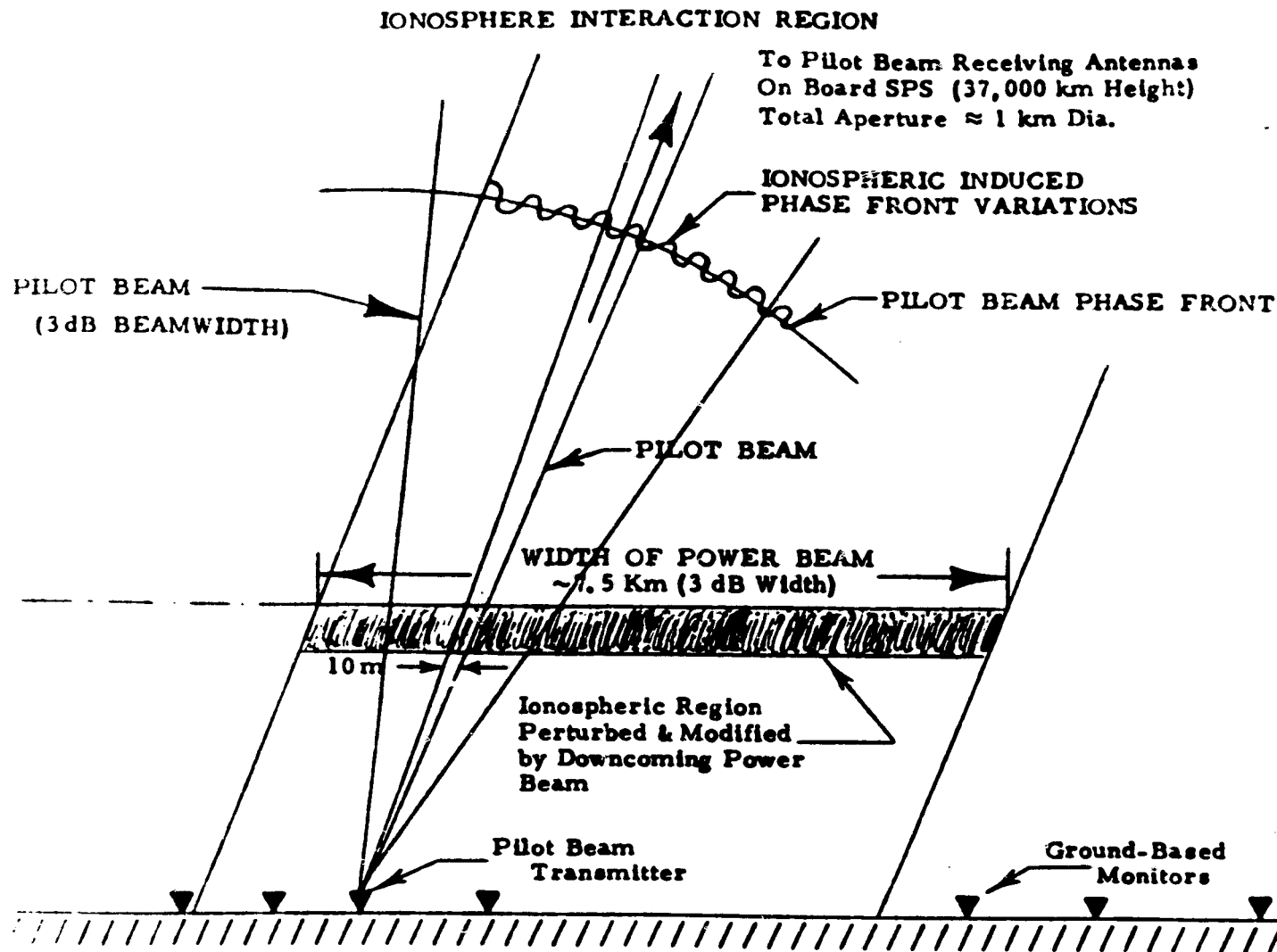
Diurnal and Seasonal Variation in Faraday Rotation Ω
and Polarization Mismatch "Loss" η_p

FARADAY ROTATION FOR NORTHEAST SITE

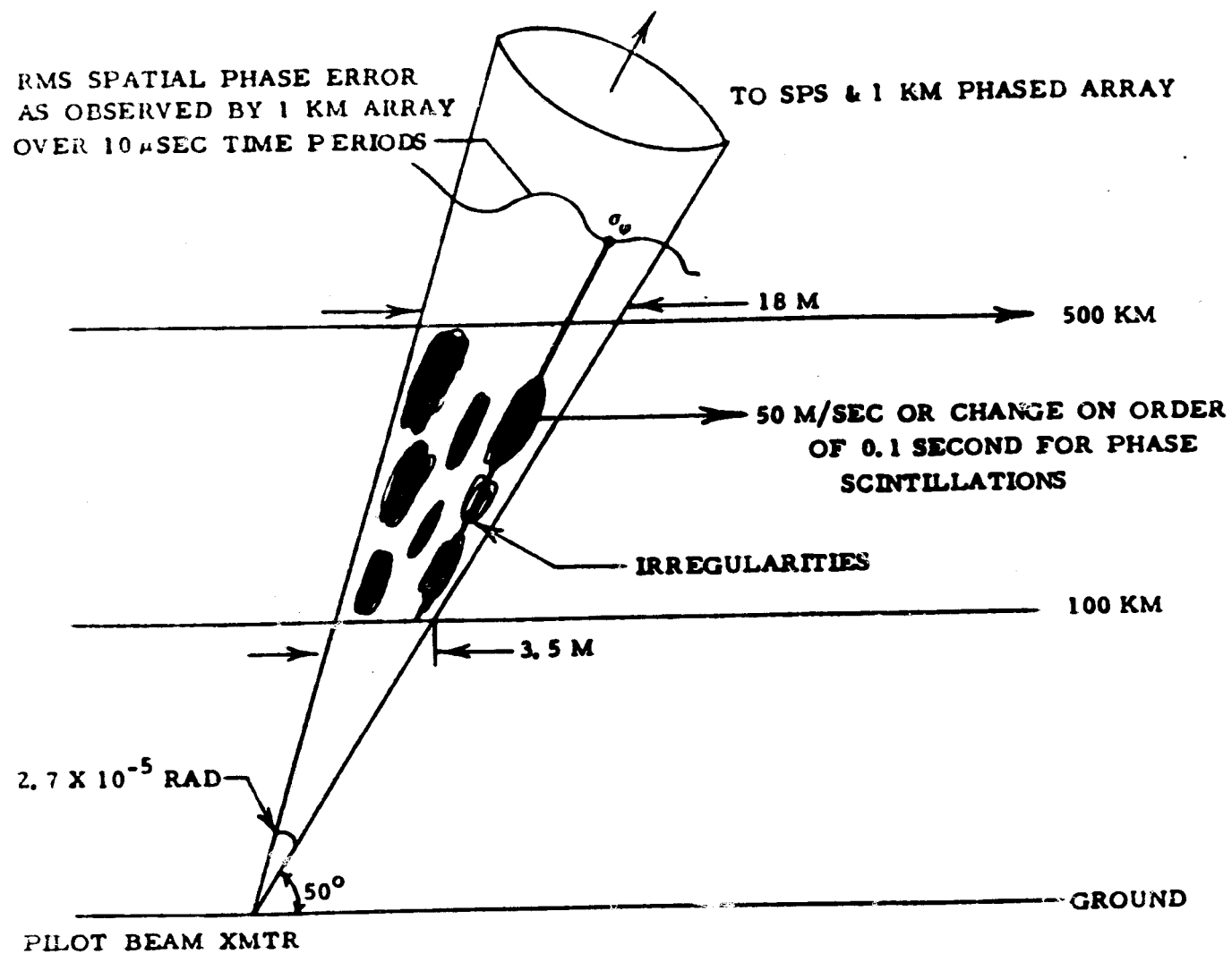
- $\alpha \propto \frac{K}{f^2}$ (TEC)
- DATA BASE TEC DATA FROM HAMILTON, MASS. (42.6°N, 70.8°W) (1967-1973 TIME FRAME)
- FOR AMBIENT CONDITIONS FARADAY ROTATION PRODUCES $\approx 0.5\%$ LOSS @ 2.45 GHz
- DURING DISTURBED CONDITIONS TEC INCREASES AND FARADAY ROTATION (FOR TEC OF 8.47×10^{17} ELECTRONS/M²) PRODUCES $\approx 3.0\%$ LOSS.
- COMPENSATE FOR DISTURBED CONDITIONS - (ORIENT RECEIVE ANTENNA TO AMBIENT ROTATION) REDUCES LOSS FOR DISTURBED CONDITIONS TO 1% TYPICALLY 3 TIMES A YEAR.
- WHERE LOSS IS IMPORTANT A STATISTICAL ANALYSIS OF TEC AS FUNCTION (TIME, LOCATION) WOULD BE REQUIRED.

SUMMARY OF PHASE I PILOT BEAM STUDY

AREA	RESULTS OF STUDY	RECOMMENDATIONS
Ionospheric Interactions	<p>Baseline concept not valid in presence of unstable transmission path.</p> <p>Alternate approaches recommended.</p> <p>Mitigating strategy to reduce phase fluctuations presented.</p>	<p>Investigate alternate approaches vis-a-vis ionospheric interactions.</p> <p>Investigate mitigating strategies to reduce RMS phase error.</p> <p>Investigate impact of time fluctuations of power on interface to power grid.</p> <p>Develop experimental program for GBER (power beam heating).</p>
Pilot Beam System	<p>Pilot System sized.</p> <p>Levels of RFI from pilot beam provided.</p> <p>(Depends on freq. separation from carrier and size of subarray).</p>	<p>Utilize approach which maximizes M. This might conflict with ionospheric effects and should be studied.</p> <p>Study implementation of alternate approaches described above.</p> <p>RF vs IF phase conjugation still requires study.</p>
Communication System	<p>Requirement established.</p> <p>Off-the-shelf standard comm. gear.</p> <p>Low Power - 25 mW data links, 1 W TV links</p>	<p>Study decentralized vs centralized concepts (not a high priority item).</p>



Expanded view of ionospheric interaction region for both pilot beam and power beam



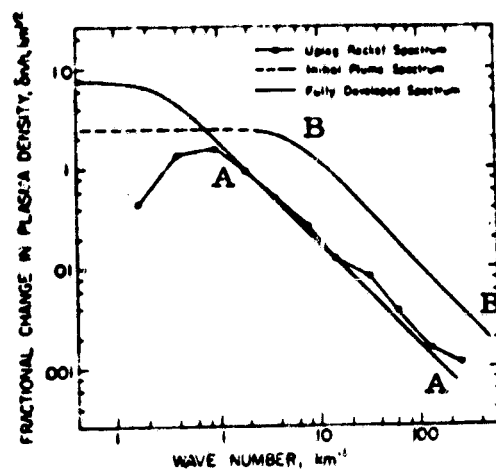
Expanded view of ionospheric interaction region for pilot beam

MITIGATING STRATEGIES TO REDUCE IONOSPHERIC INDUCED
PHASE FLUCTUATION

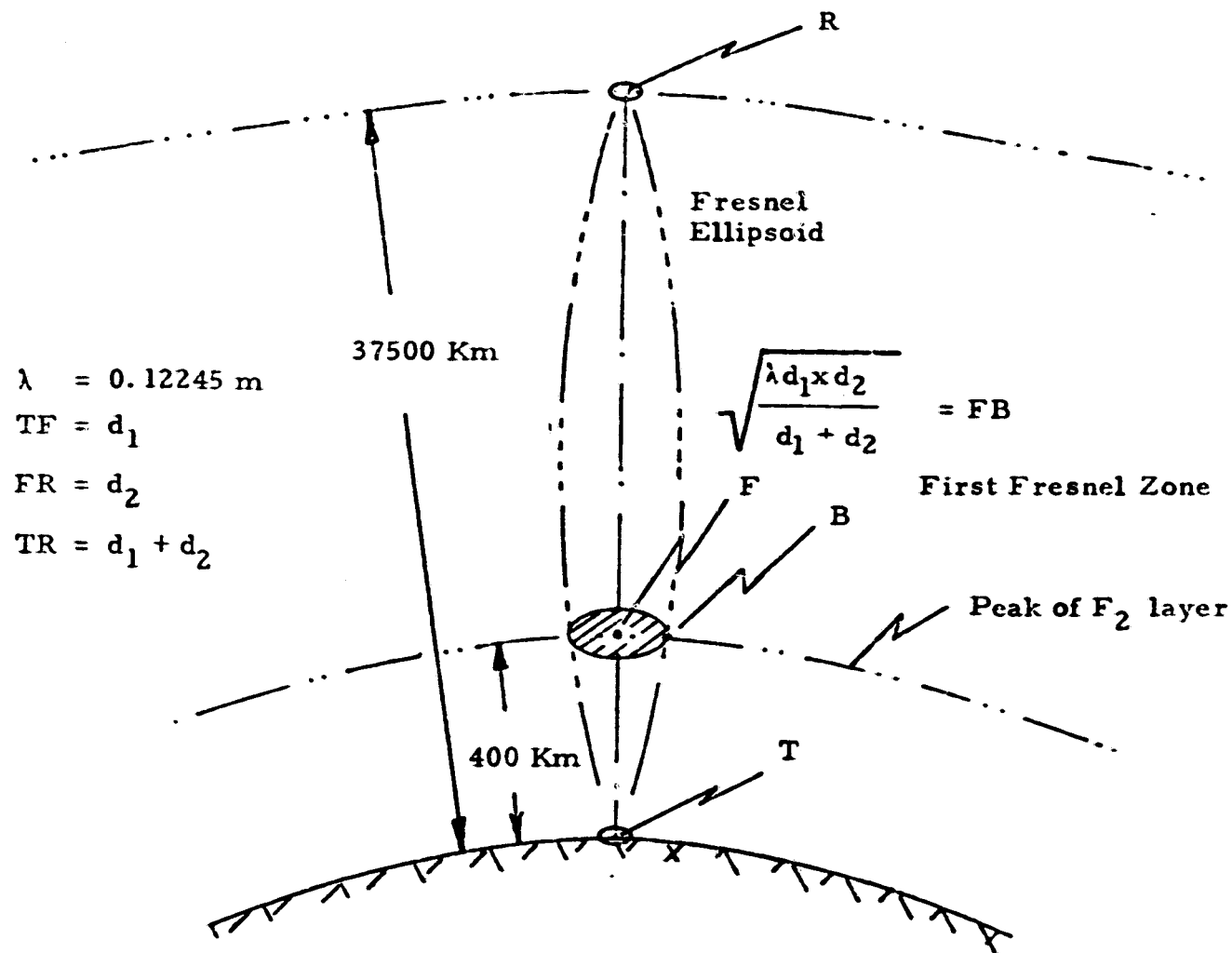
<u>METHOD</u>	<u>IMPLEMENTATION</u>	<u>IMPROVEMENT</u>
SPATIAL DIVERSITY	TWO OR MORE XMITERS ON GROUND SO PILOT BEAM TRAVERSES DIFFERENT IONOSPHERES	$(\text{NO. OF TRANSMITTERS})^{-1/2}$
TEMPORAL DIVERSITY	AVERAGE PHASE FLUCTUATIONS IN TIME PERIOD LONG COMPARED TO STABILITY OF PROPAGATION PATHS	$\left(\frac{\text{INTEGRATION TIME}}{\text{IONOSPHERE TIME CONSTANT}} \right)^{-1/2}$
FREQUENCY DIVERSITY		
INCOHERENT	NOT APPLICABLE	PHASE FLUCTUATIONS TRACK INCOHERENT AVERAGE DOES NOT SIGNIFICANTLY IMPROVE PERFORMANCE
COHERENT	TRACK PHASE FLUCTUATIONS ON TWO FREQUENCIES OR THREE FREQUENCIES	

IONOSPHERIC COLUMNAR ELECTRON DENSITY

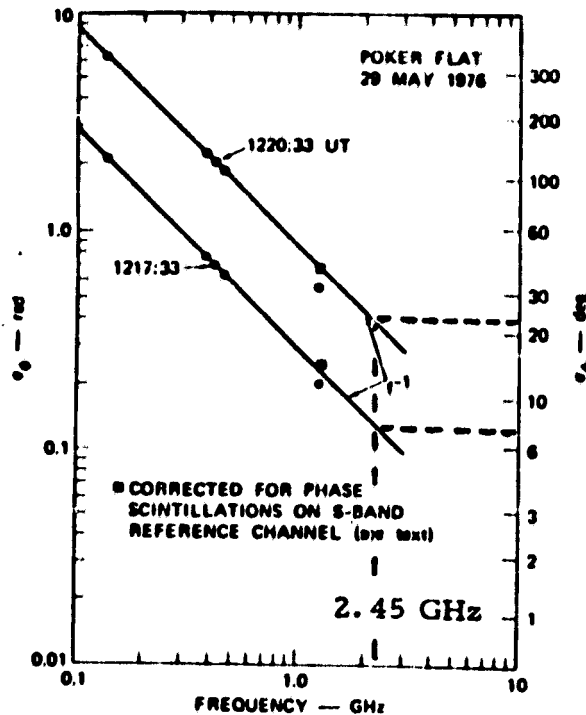
- o This function is a random process in the time domain. It has a non-zero mean.
- o This mean value is called the ionospheric "bias."
- o The "bias" is slowly changing with time (1 sample every 15 minutes is an appropriate sampling rate).
- o Superimposed to the "bias" there are random fluctuations (ionospheric scintillation phenomenon). Typical scintillation rates are between 0.1/minute to 10/minute, requiring sampling rates of approximately one every 3 minutes to one every 2 seconds respectively.



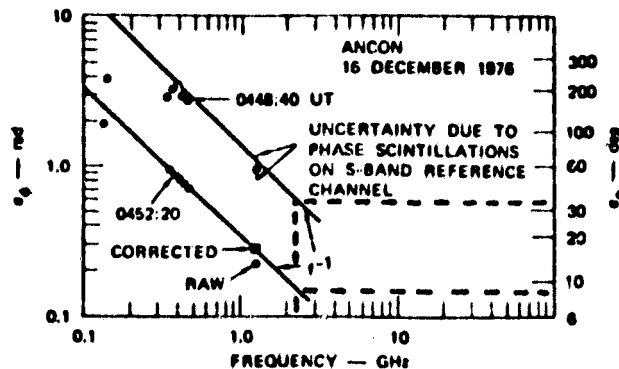
The dashed line is a model spectrum used by Costa and Kelley (1976) to characterize the breakup of density gradients in upwelling structures. The solid line is a spectrum used by Basu and Basu (1976) to typify extended topside irregularities. (From Basu and Kelley, 1977)



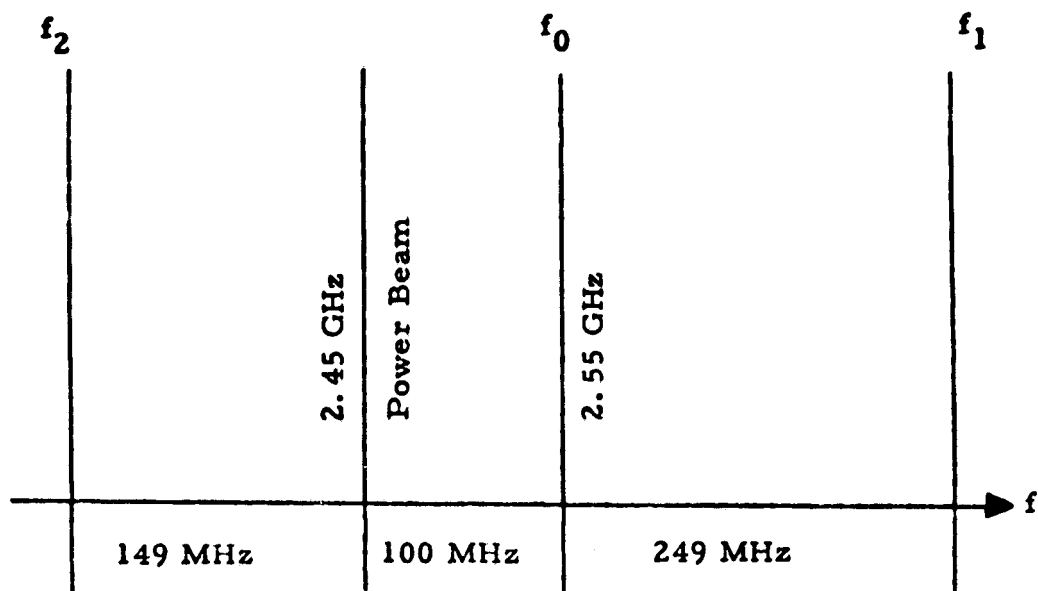
Fresnel Ellipsoid of the Pilot Beam Ray



Frequency dependence of phase-scintillation index, during two 20 sec periods of the pass above Poker Flat, 29 May 1976 compared with an f^{-1} dependence.
(from Fremouw et al, 1978)

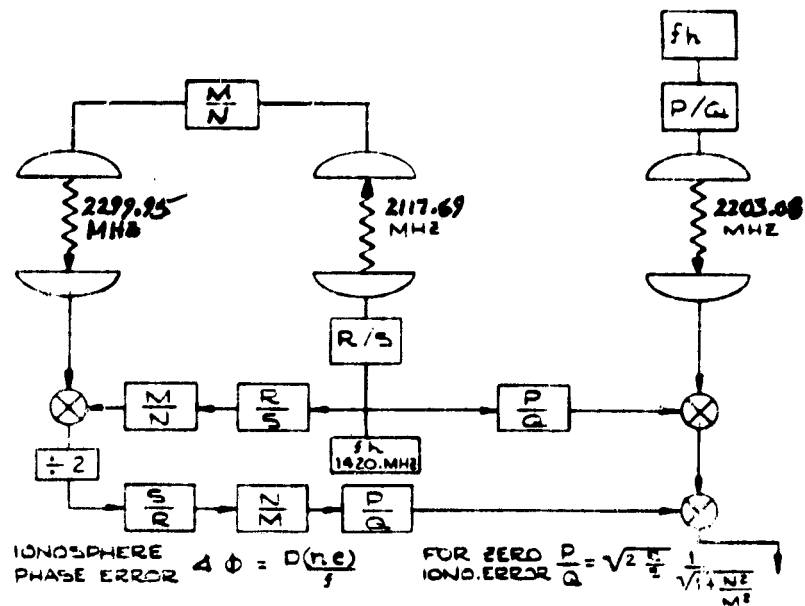


Frequency dependence of phase scintillation index during two 20 sec periods of pass recorded at Ancon on 16 Dec. 1976, compared with an f^{-1} dependence arbitrarily passed through the 413 MHz data point.
(from Fremouw et al, 1978)

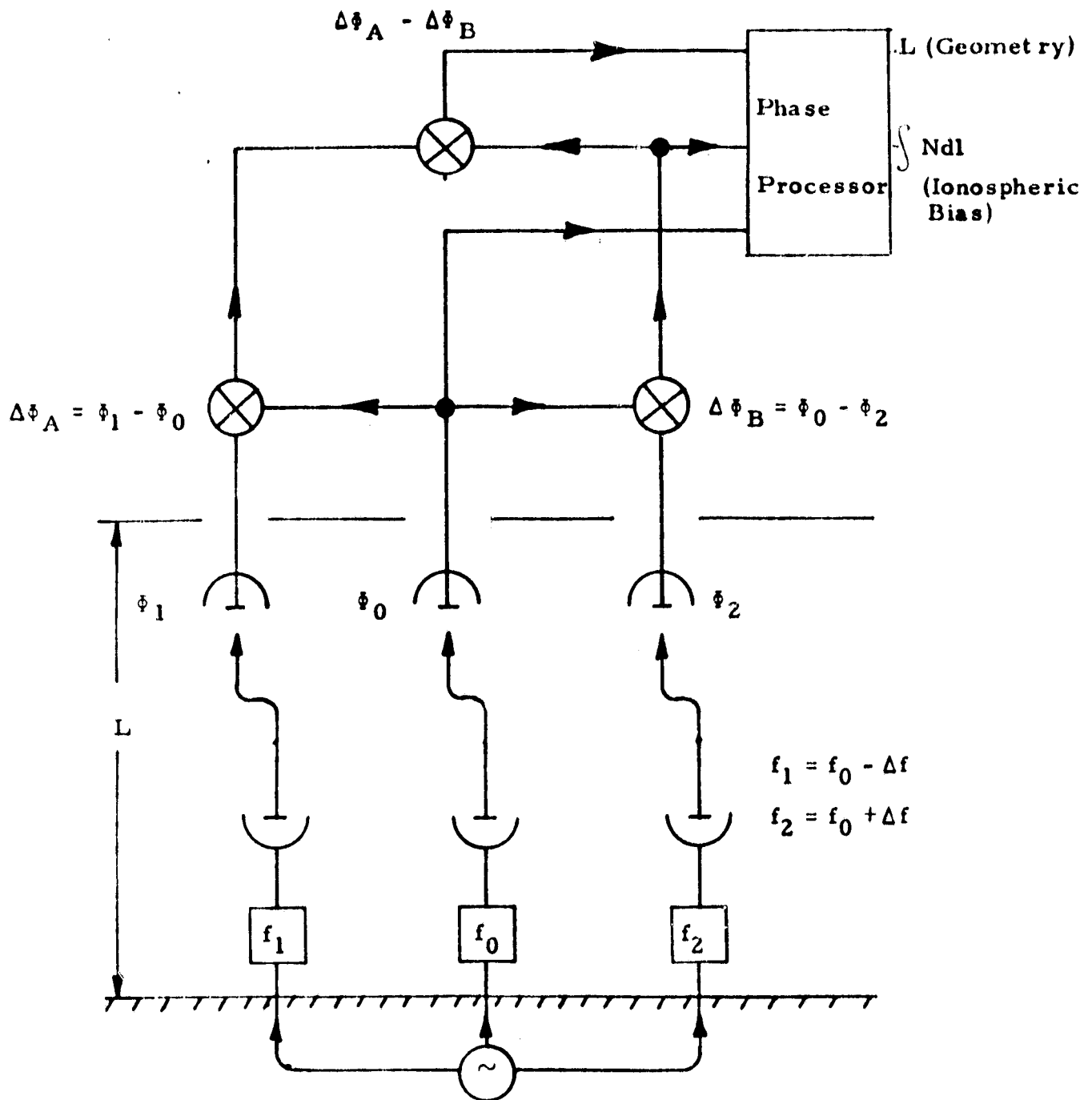


Possible Frequency Allocation

REDSHIFT DOPPLER AND IONOSPHERIC ERROR CANCELLING SYSTEM



Schematic Concept of the Doppler-Cancelling System.
(Vessot and Levine, 1977)



Common Master Oscillator

Three Frequency Approach - Simplified Block Diagram of Proposed Mechanization

SUMMARY AND CONCLUSIONS
INITIAL MPTS STUDY RESULTS - SUBSYSTEMS AND TECHNOLOGY

ISSUES/CONSIDERATIONS

DC-RF CONVERSION

POWER INTERFACE AND DISTRIBUTION CONTROL

RESOLUTION/STATUS

- OPERATING FREQUENCY RANGE OF INTEREST IS:
KLYSTRON: 1.0 GHZ TO 30 GHZ & 2.45 GHZ IS GOOD
CFDA: 1.5 GHZ TO 3.06 GHZ & 2.45 GHZ IS PREFERRED
- POWER ADDED PER TUBE IS:
KLYSTRON: 4.8 KW
CFDA: 5 TO 10 KW
- EFFICIENCY FOR TUBE IS:
KLYSTRON: 80% GOAL
CFDA: 85% WITH 90% AS REALISTIC GOAL
- CONFIGURATION
KLYSTRON: PARALLEL RF FOR DRIVE & 5 STAGES
CFDA: AMPLITRON - CASCADE RF FOR DRIVE
MAGNETRON - PARALLEL RF FOR DRIVE
- VOLTAGE
KLYSTRON: 40 KV
CFDA: 20 KV

DC-RF CONVERSION

GENERAL

- COLD PURE METAL CATHODES FOR LONG LIFE. RECENT INVESTIGATIONS INDICATE HEATERS FOR START-UP OF CFA DEVICES CAN BE DESIGNED FOR LONG LIFE.
- PYROGRAPHITE RADIATORS FOR EFFICIENT WASTE HEAT DISSIPATION. HEAT PIPES NEEDED FOR KLYSTRON TRANSFER OF HEAT TO RADIATORS.
- SAMARIUM COBALT PERMANENT MAGNET FOR LIGHT WEIGHT AND LOW COST. RECENT STUDIES INDICATE ELECTROMAGNETS MAY ALSO BE DEVELOPED FOR NOMINAL WEIGHT AND COST PENALTIES.
- OPERATING FREQUENCY 1.5 GHZ TO 3.0 GHZ FOR CFA WITH 2.45 GHZ PREFERRED. FOR KLYSTRON FREQUENCY IS 1.0 GHZ TO 3.0 GHZ WITH 2.45 GHZ CONSIDERED AS "GOOD".
- OPEN TUBE CONSTRUCTION, POSSIBLY WITH CONTAMINANT BAFFLE, FOR HIGH RELIABILITY, SIMPLE THERMAL CONTROL AND LOW WEIGHT.
- FOR AMPLITRON, CASCADE CONFIGURATION REQUIRED BECAUSE OF LOW GAIN CHARACTERISTICS. FOR MAGNETRON AND KLYSTRON, PARALLEL CONFIGURATION RECOMMENDED.

FOR CFA

- POWER ADDED 5 KW TO 10 KW PER TUBE WITH 5 KW PREFERRED.
- EFFICIENCY WITH RF NOISE AND HARMONIC FILTERS IS CONSERVATIVE 85%; IMPROVEMENT TO 90% IS REALISTIC GOAL.
- REGULATION OF CONSTANT CURRENT OR CONSTANT PHASE BY MOVABLE POLE PIECE OR IMPULSE MAGNET TECHNIQUE FOR HIGH EFFICIENCY.

FOR KLYSTRON

- SOLENOID FOCUSING AND POWER OUTPUTS OF 48 KW OR GREATER, WITH OUTPUT POWER DIVIDERS TO THE WAVEGUIDE.
- COLLECTOR DEPRESSION NEEDED FOR HIGHEST EFFICIENCY: REQUIRES FURTHER STUDY TO DETERMINE PRACTICALITY OF REACHING 80% EFFICIENCY.
- FIVE-STAGE DESIGN INCLUDING A SECOND HARMONIC BUNCHING CAVITY TO REDUCE NOISE BANDWIDTH.

POWER INTERFACE AND DISTRIBUTION (ORBITAL)

GENERAL

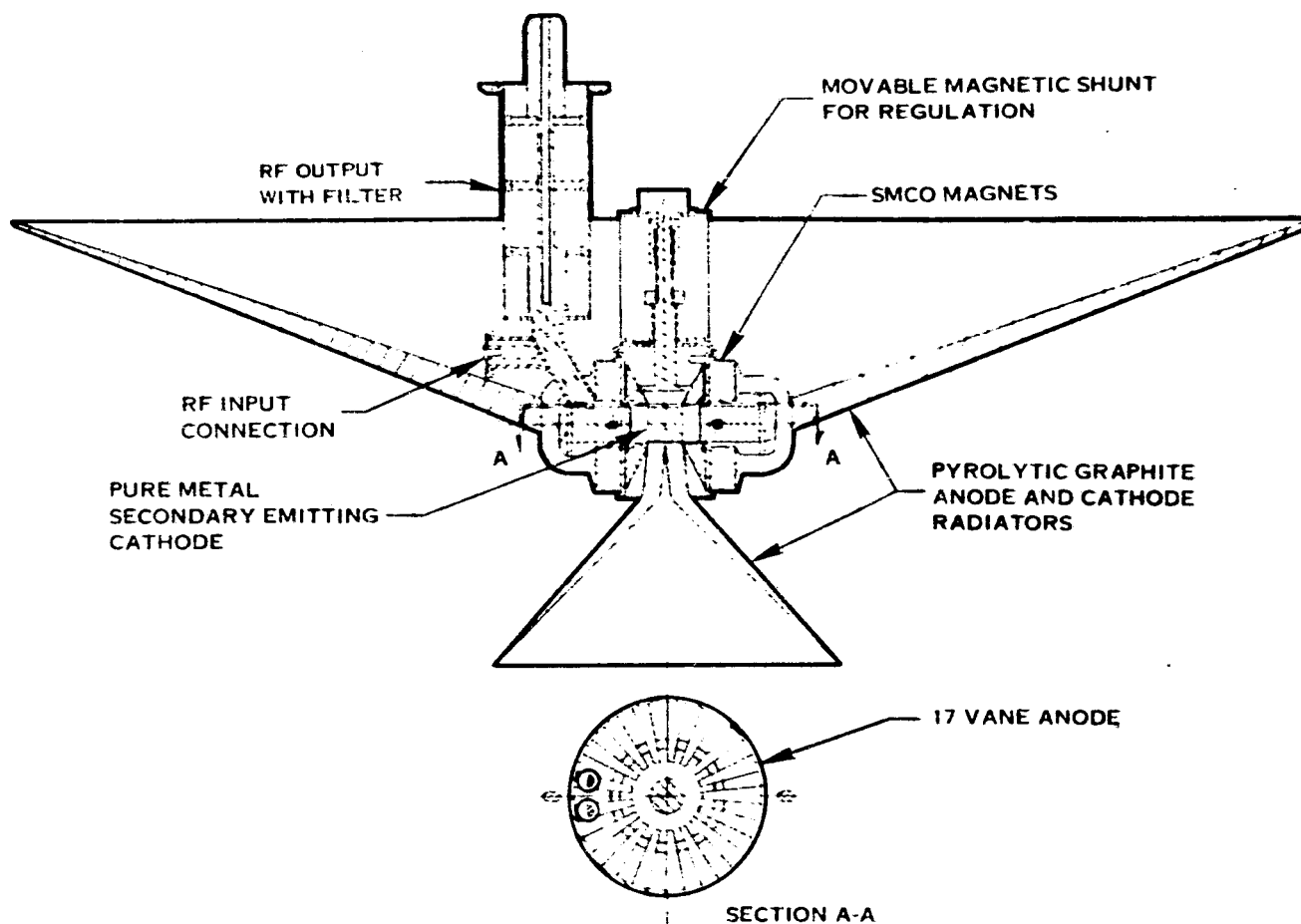
- RECYCLING SWITCHGEAR (CROWBAR) NEEDED FOR PROTECTION AGAINST TUBE ARCING.

FOR CFA

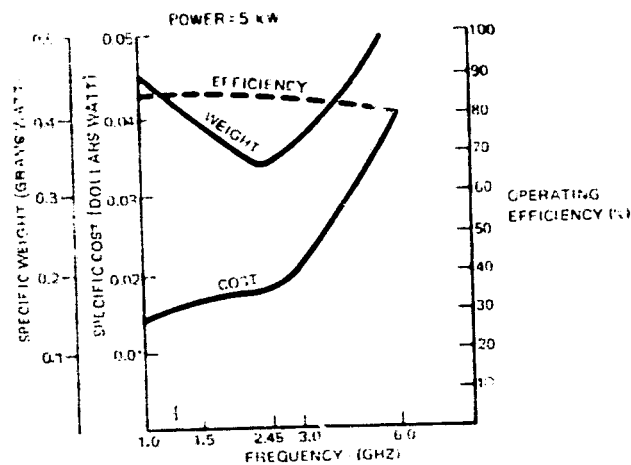
- CONSTANT CURRENT REGULATION AT THE CONVERTER TO MAXIMIZE POWER OUTPUT AND MINIMIZE PHASE SHIFT VARIATIONS WITH VOLTAGE CHANGES.
- POWER SOURCE VOLTAGE SHOULD BE 20 KV DC

FOR KLYSTRON

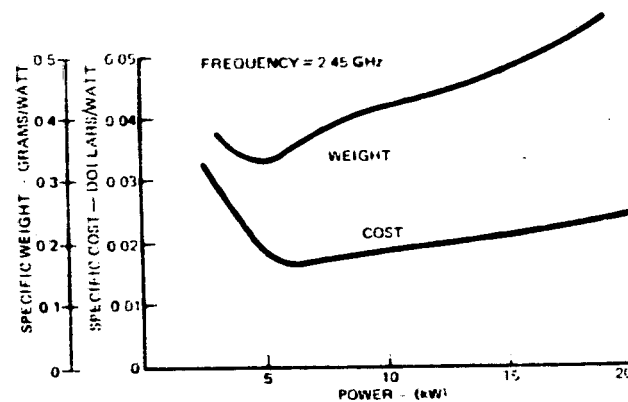
- UNREGULATED OPERATION TO MAXIMIZE POWER OUTPUT.
- POWER SOURCE VOLTAGE SHOULD BE 40 KV FOR PRIMARY POWER.



Amplitron Assembly



Amplitron Weight/
Cost/Efficiency Vs.
Frequency



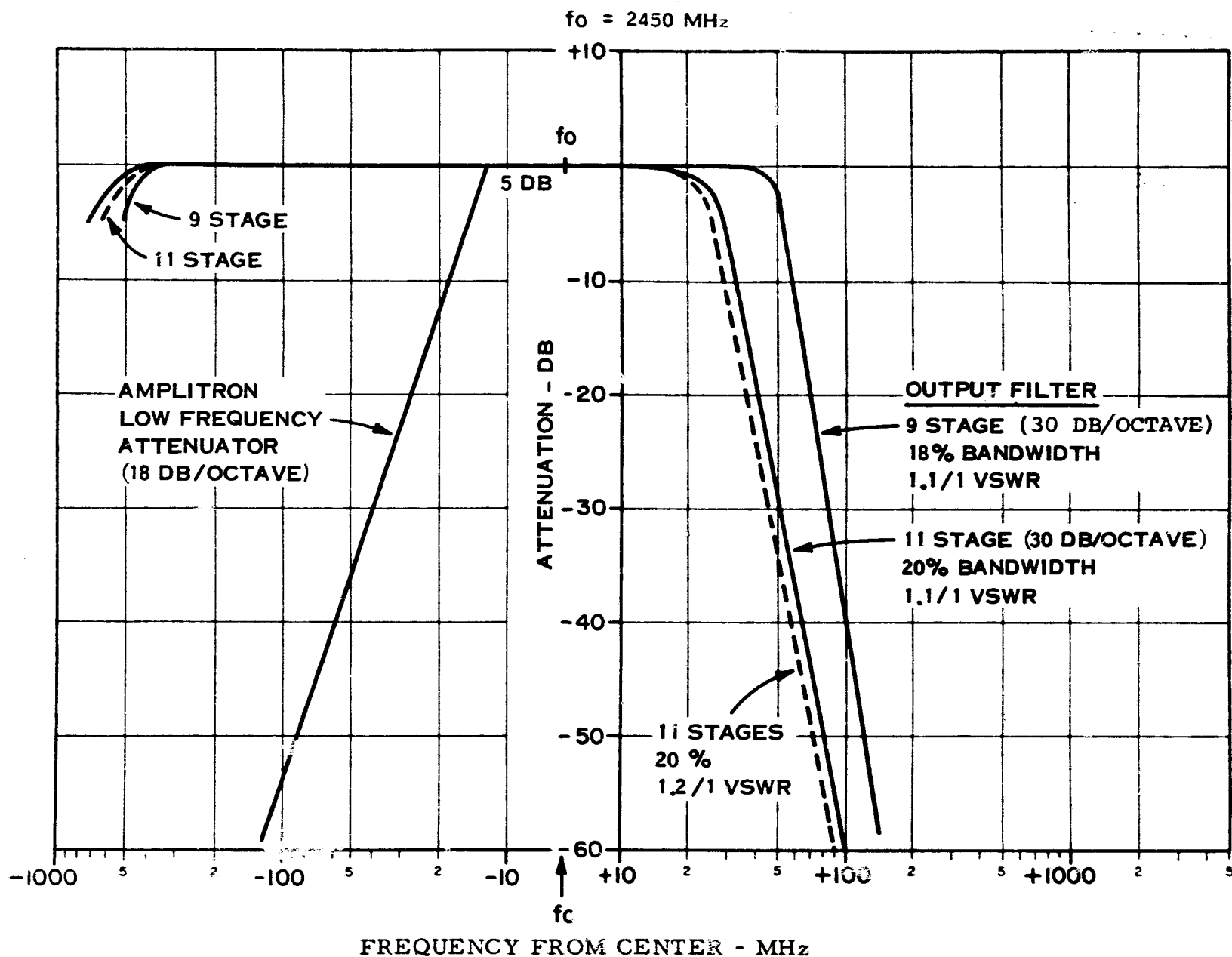
Amplitron Weight and
Cost Vs. Power

ANODE	108 GRAMS
ANODE RADIATOR	1000
CATHODE	9
CATHODE RADIATOR	71
MAGNET	260
POLES	100
INPUT AND OUTPUT	40
MOTOR AND DRIVE	30
	1618 GRAMS — 3.56 LB
SPECIFIC WEIGHT	0.33 g/w
SPECIFIC COST	0.018 \$/w

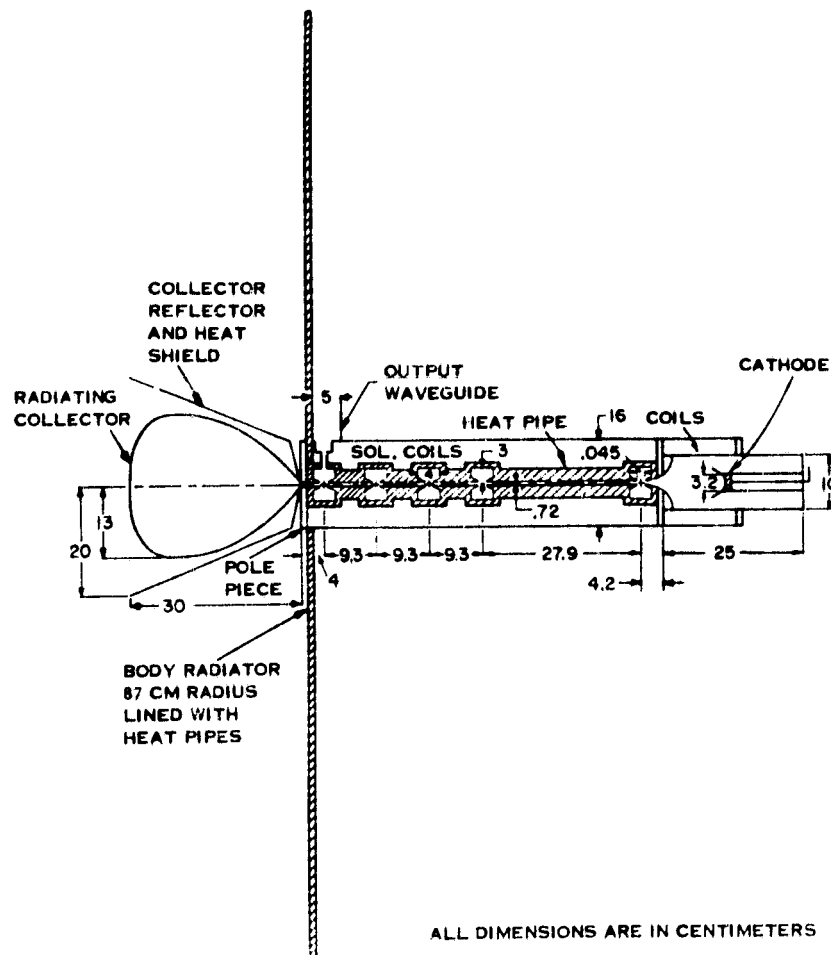
MPTS 5 kW
Amplitron Parameters

RF POWER ADDED	5000 WATTS
ANODE ELECTRON BOMBARDMENT	371
ANODE CIRCUIT LOSSES	177
CATHODE DISSIPATION	199
DC INPUT POWER	5747 WATTS
GROSS EFFICIENCY	87%
OUTPUT FILTER DISSIPATION	125 WATTS
NET EFFICIENCY	85%

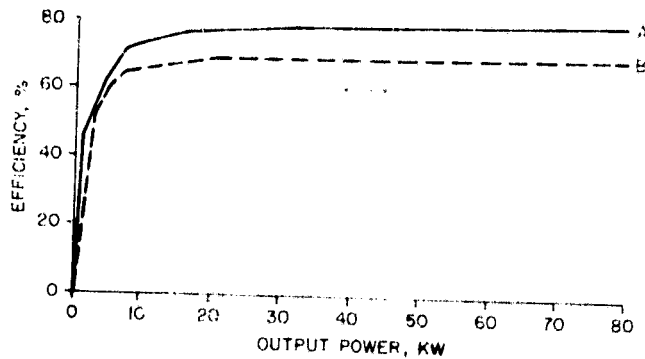
MPTS 5 kW Amplitron
Power Budget



Amplitron Equivalent Filter Characteristics ($f_o = 2450 \text{ MHz}$)



Outline of 48 kW Klystron with Solenoid Focusing



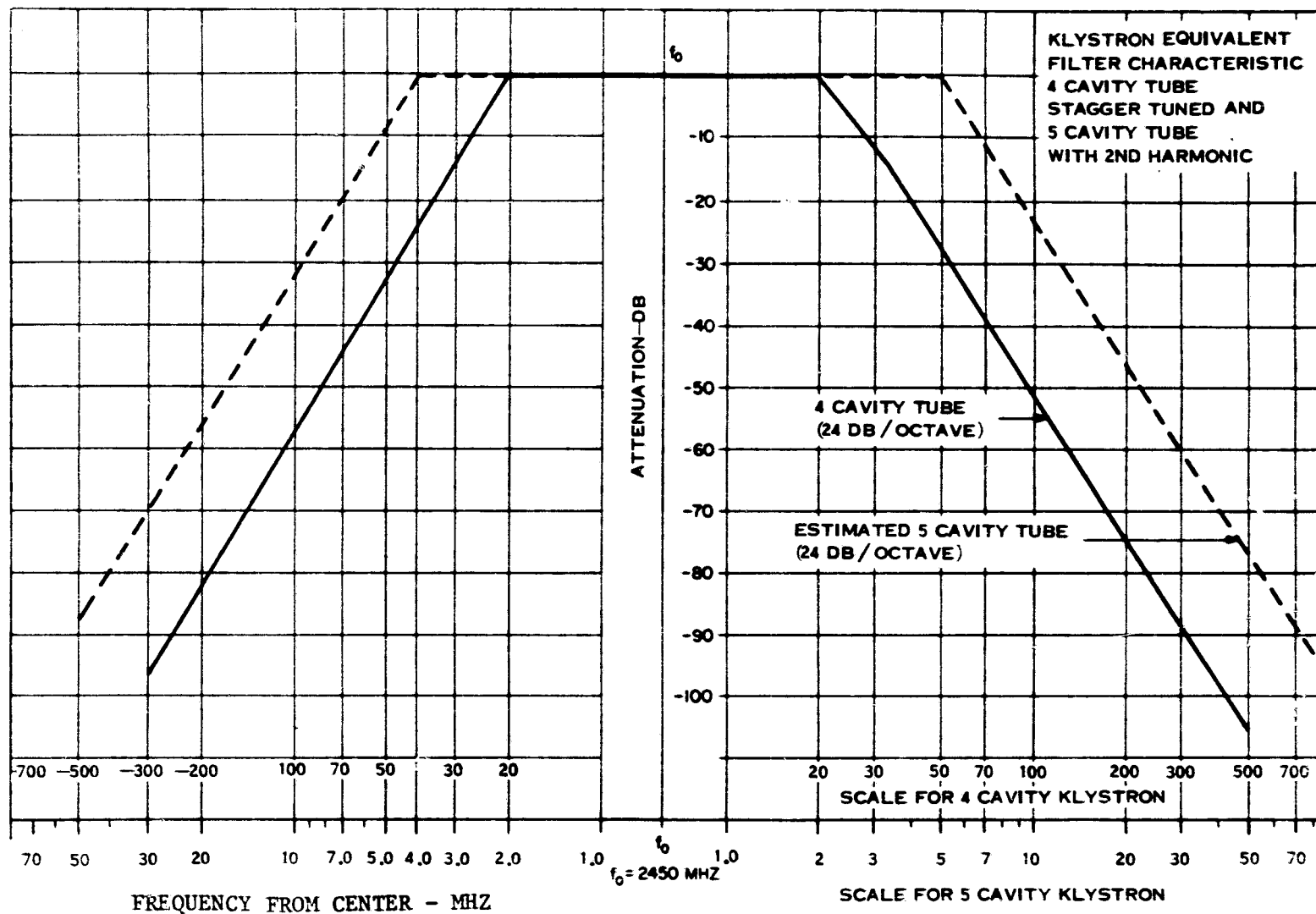
A - ASSUME 84 PERCENT ELECTRONIC EFFICIENCY } 1 KW CONSUMED
 B - ASSUME 75 PERCENT ELECTRONIC EFFICIENCY } BY SOLENOID
 AND HEATER

Efficiency Vs Output Power for Solenoid-Focused Klystron

ELECTRICAL			
VOLTAGE	38.9 KV	OUTPUT POWER	48362 WATTS
CIRCUIT	1.54 A	OUTPUT CAVITY LOSSES	
GAIN	31 dB	SKIN LOSSES	2038
MICROPERVEANCE	0.2	INTERCEPTION	384
		OTHER INTERCEPTION	461
		HEATER POWER	60
		SOLENOID	1000
		COLLECTOR DISSIPATION	8755
		TOTAL BEAM POWER	60000 WATTS
		OTHER POWER	1060
		TOTAL INPUT	61060 WATTS
		NET EFFICIENCY	79.2%
WEIGHTS			
MAGNET PLUS POLE PIECES	16300 GRAMS		
TUBE	32374		
TOTAL	48674 GRAMS		
SPECIFIC WEIGHT	1.01 g/w		
COST			
SPECIFIC COST	0.039 \$/w		

MPTS 48 kW Klystron
Parameters

MPTS 48 kW
Klystron Power
Budget



Klystron Equivalent Filter Characteristic

	No Regulation	Constant Current	Constant Output Power
Beam Power	Varies as $V_0^{5/2}$ Part of available power unused	Varies as V_0 All available power used	Constant, but power is wasted at voltages above design minimum
Focusing and Efficiency	Experimental tests required	Experimental tests required	Beam Transmission falls with solenoid power. Efficiency is greatest at minimum voltage; least at maximum voltage.
Construction	Simplest: no modifications needed to constant-power tube	Requires a gridded gun	Requires a complex and heavy collector
Phase Change at Output	About 22° for each percent voltage change	About 22° for each percent voltage change	None
Stability	Most stable	Focusing may be unstable at low voltage	Collector may be unstable at low voltage

Klystron Voltage Control

SUMMARY AND CONCLUSIONS
INITIAL MPTS STUDY RESULTS - SUBSYSTEMS AND TECHNOLOGY

ISSUES/CONSIDERATIONS

TRANSMITTING ANTENNA

RESOLUTION/STATUS

- PLANAR ACTIVE PHASED ARRAY APPROXIMATELY 1 KM DIA.
- TRUNCATED GAUSSIAN WITH TAPER OF 5 TO 10 DB
QUANTIZED INTO ABOUT 5 REGIONS OF UNIFORM POWER.
- SECTORED INTO SLOTTED WAVEGUIDE SUBARRAYS
18M X 18M OR SMALLER DEPENDING ON SIZE, WEIGHT
AND COST OF PHASE CONTROL, COMMAND CONTROL AND
DRIVER ELECTRONICS FOR EACH SUBARRAY.
- ALUMINUM, GRAPHITE EPOXY AND GRAPHITE POLYIMIDE
ARE CANDIDATE WAVEGUIDE MATERIALS.
- INITIAL AND PERIODIC ALIGNMENT OF LARGE
SUBARRAYS MAY BE REQUIRED.

TRANSMITTING ANTENNA

- CIRCULAR, PLANAR, ACTIVE PHASED ARRAY ON THE ORDER OF 1 KM IN DIAMETER.
- ANTENNA ILLUMINATION WILL BE TRUNCATED GAUSSIAN WITH TAPER OF 5 DB TO 10 DB QUANTIZED INTO ABOUT 5 REGIONS OF UNIFORM POWER.
- ANTENNA SECTORED INTO SUBARRAYS OF NOMINAL DIMENSION 18M X 18M. THIS LARGE SIZE PRIMARILY DRIVEN BY HIGH ESTIMATES FOR PHASE CONTROL, COMMAND CONTROL AND DRIVER ELECTRONICS FOR EACH SUBARRAY INDEPENDENT OF SUBARRAY SIZE. REFINEMENT OF THESE ESTIMATES IS REQUIRED.
- SUBARRAYS ARE SLOTTED WAVEGUIDE RADIATORS FOR HIGH OVERALL BEAM FORMATION AND INTERCEPTION EFFICIENCY OF AT LEAST 95% FOR A CONTIGUOUS RECTENNA WITHIN THE MAIN LOBE.
- WAVEGUIDE WALL THICKNESS NOMINALLY 0.5 MM BUT ADDITIONAL INVESTIGATION MAY SHOW THIS CAN BE REDUCED: WIDTH IS 12 CM AND DEPTH IS 6 CM.
- ALUMINUM, GRAPHITE EPOXY, AND GRAPHITE PLOYIMIDE ARE CANDIDATE MATERIALS FOR SLOTTED WAVEGUIDE.
 - ALUMINUM REQUIRES STRUCTURAL SEGMENTING AND VARIATION OF OPERATING FREQUENCY TO COMPENSATE FOR LONGITUDINAL THERMAL DISTORTIONS.
 - GRAPHITE POLYIMIDE OFFERS HIGHEST TEMPERATURE MARGIN WITH MINIMAL DISTORTION, BUT ALL COMPOSITES MUST BE EVALUATED FOR STABILITY AND OUTGASSING PROPERTIES.
 - WAVEGUIDE MANUFACTURE AND SUBARRAY ASSEMBLY ON ORBIT IS RECOMMENDED TO ACHIEVE FAVORABLE LAUNCH VEHICLE PACKAGING DENSITY. SMALLER SUBARRAYS MAY REDUCE OR ELIMINATE THIS NEED.
 - MICROWAVE INTERFEROMETERS ARE RECOMMENDED FOR MPTS AND SPS ATTITUDE CONTROL AND FOR INITIAL AND PERIODIC ALIGNMENT OF SUBARRAYS USING SCREWJACK ACTUATORS ON EACH SUBARRAY. SMALLER SUBARRAYS MAY REDUCE OR ELIMINATE THIS NEED.

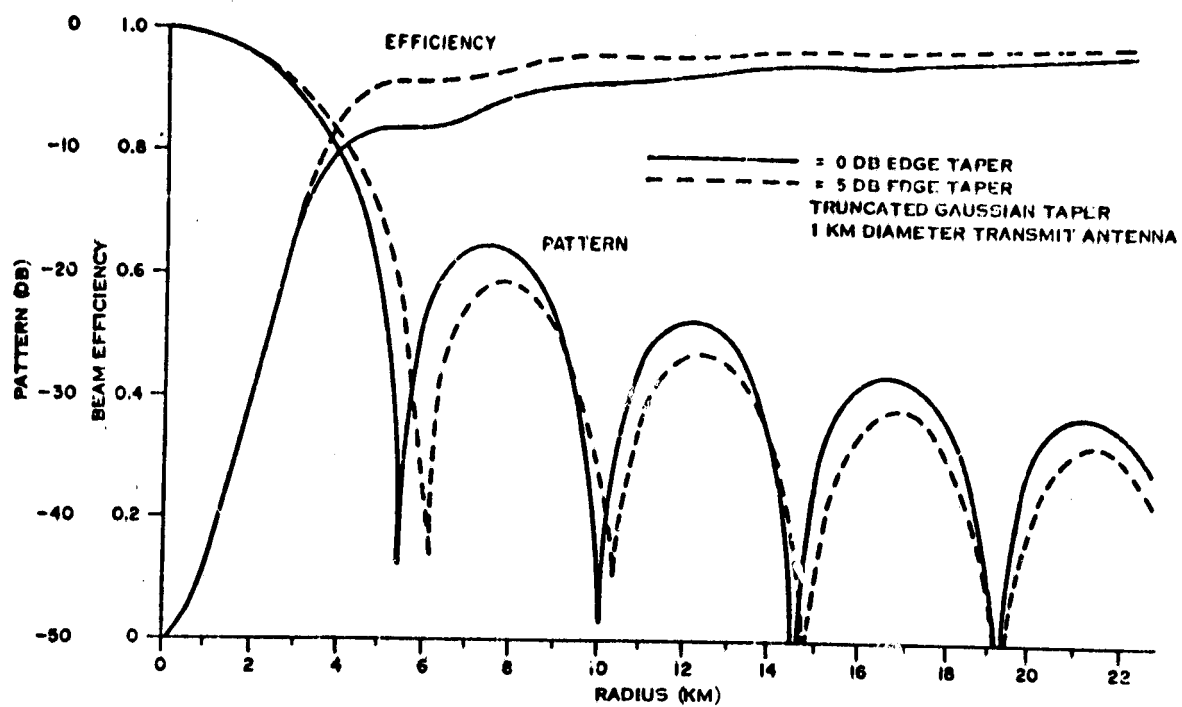
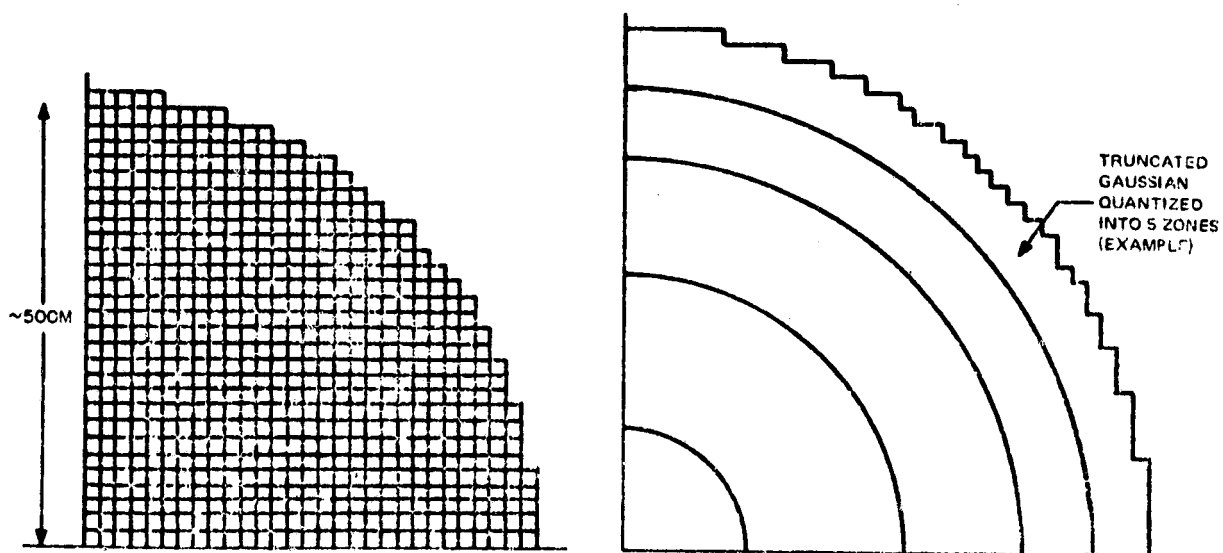


Figure 16 Taper Effect on Pattern and Efficiency



Array-Subarray Organization

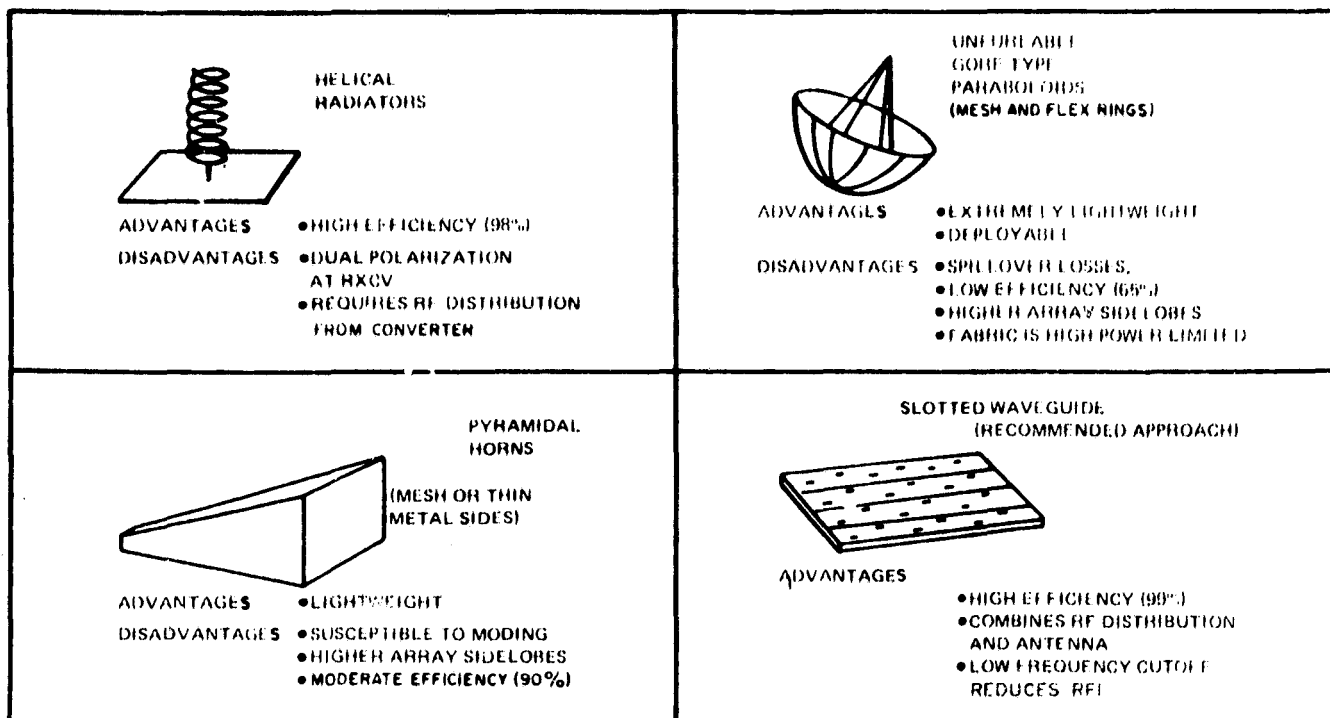
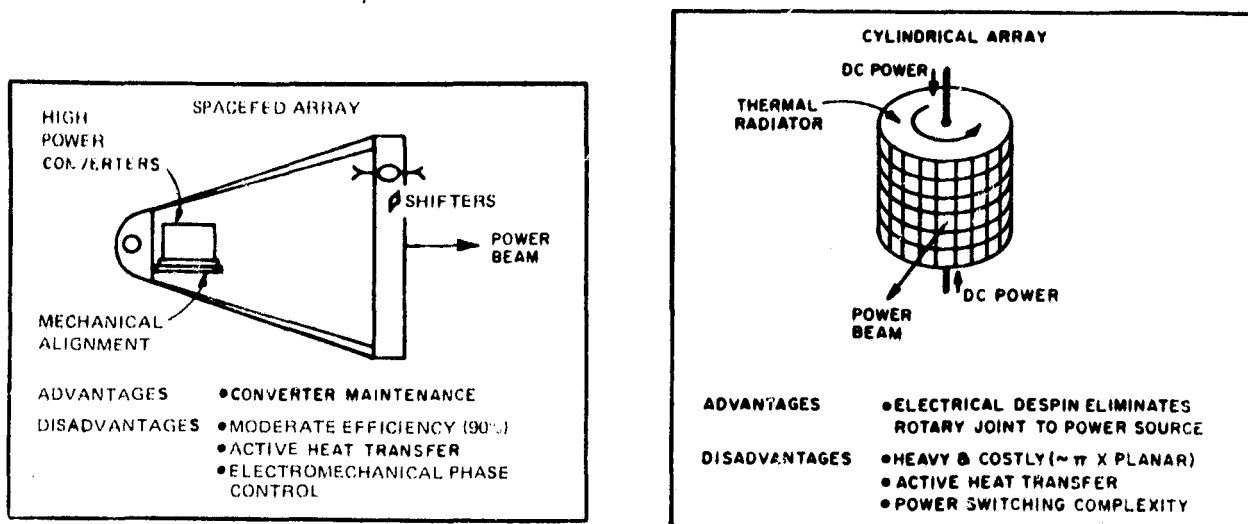
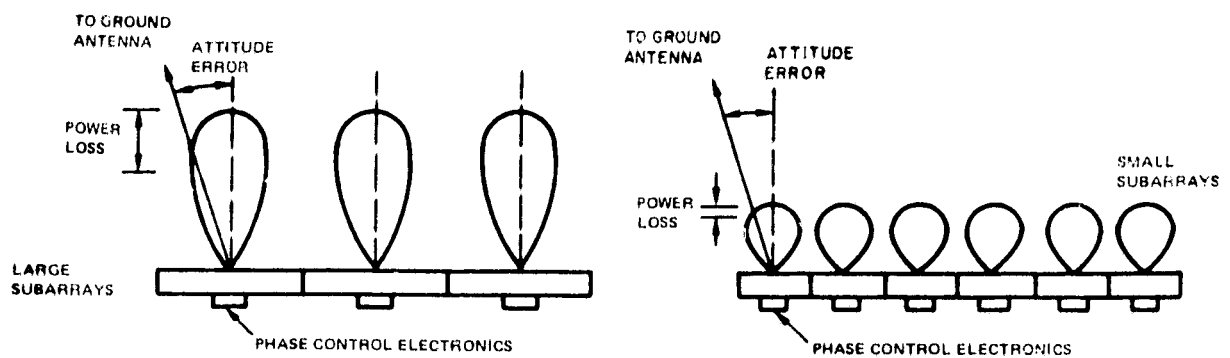


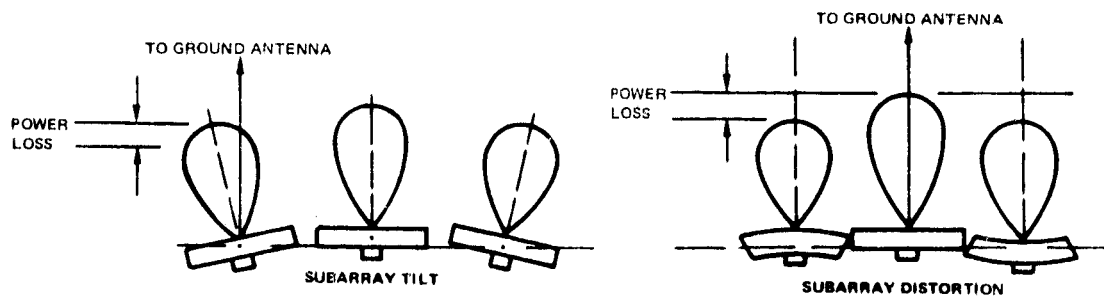
Figure 20 Subarray Types



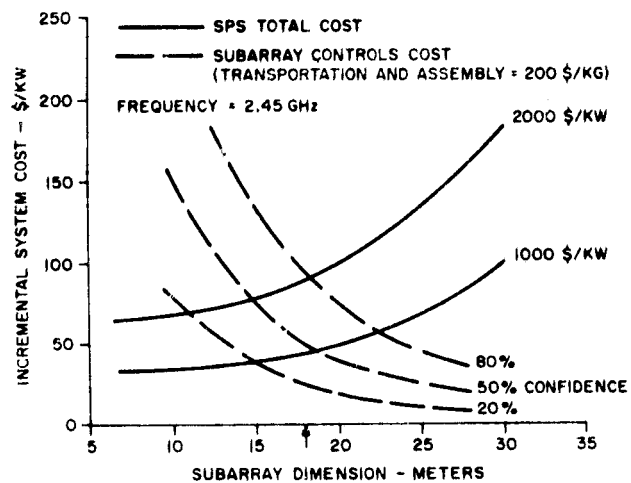
Alternative Array Types



OVERALL ARRAY ATTITUDE CONTROL

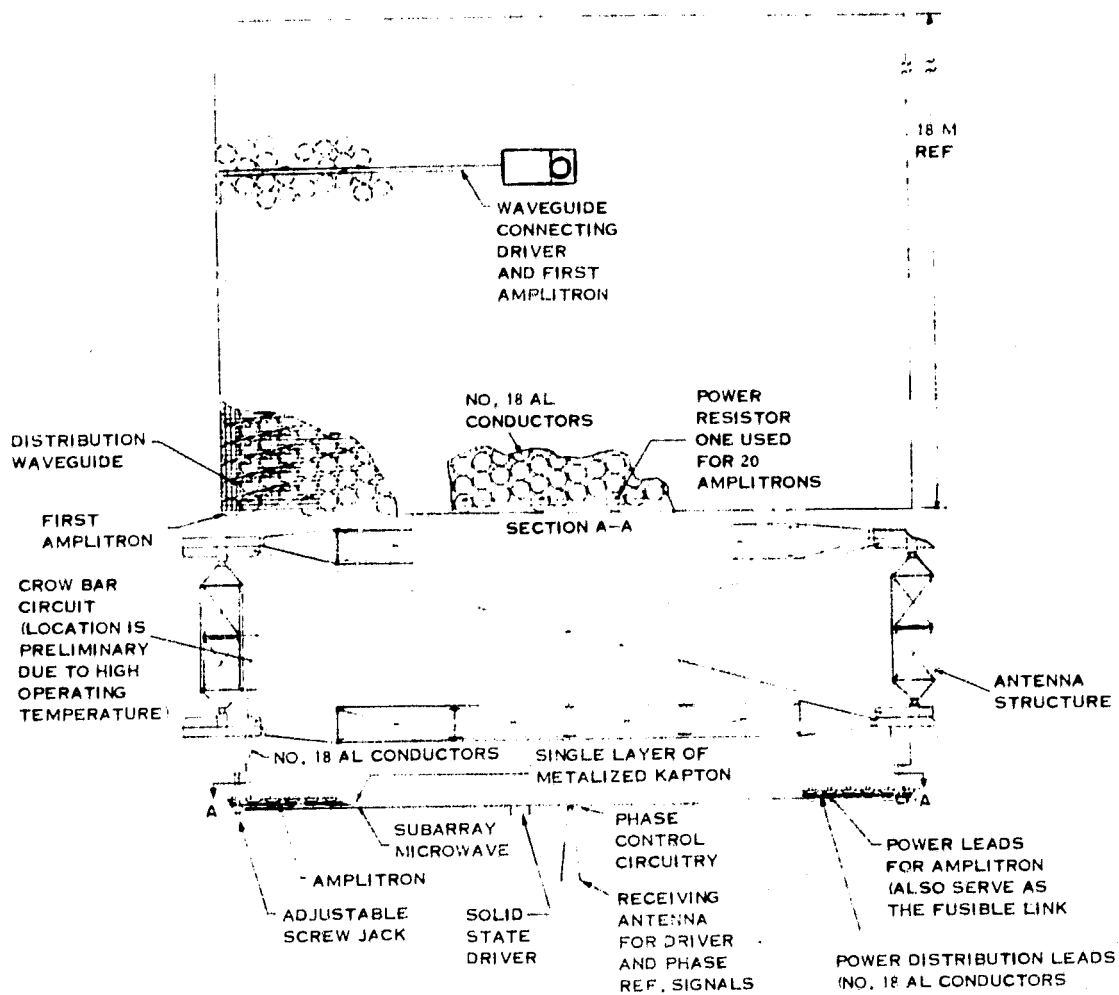


Subarray Size Considerations

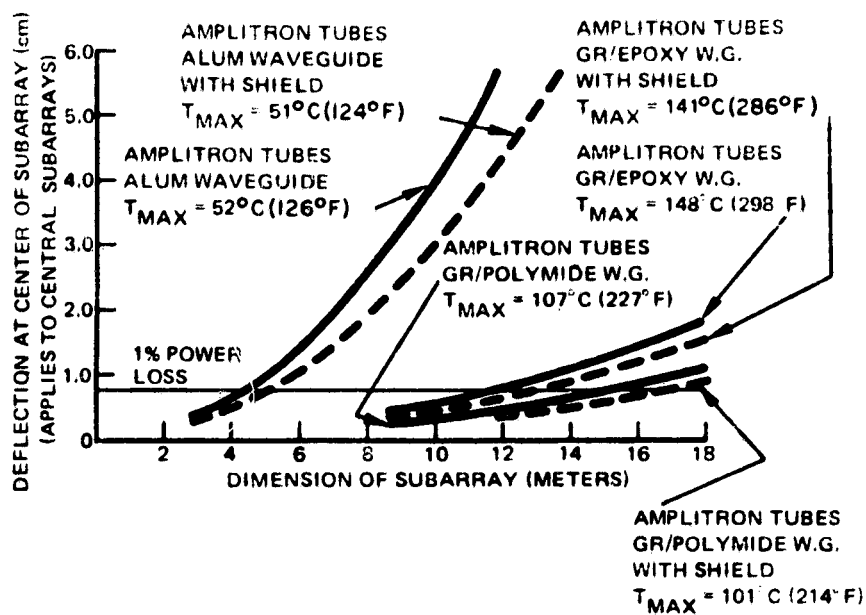


SPS Incremental Cost vs Subarray Size

ORIGINAL PAGE IS
OF POOR QUALITY



Subarray Layout



Subarray Deflection vs Size

SUMMARY AND CONCLUSIONS
INITIAL MPTS STUDY RESULTS - SUBSYSTEMS AND TECHNOLOGY

ISSUES/CONSIDERATIONS

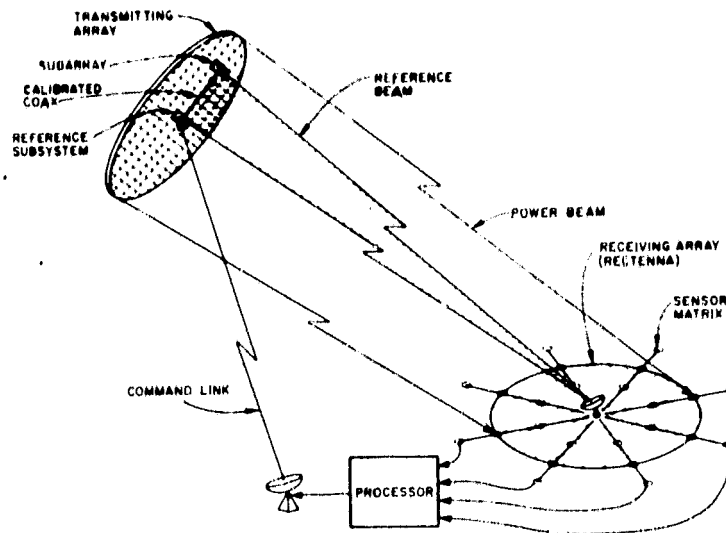
PHASE FRONT CONTROL

RESOLUTION/STATUS

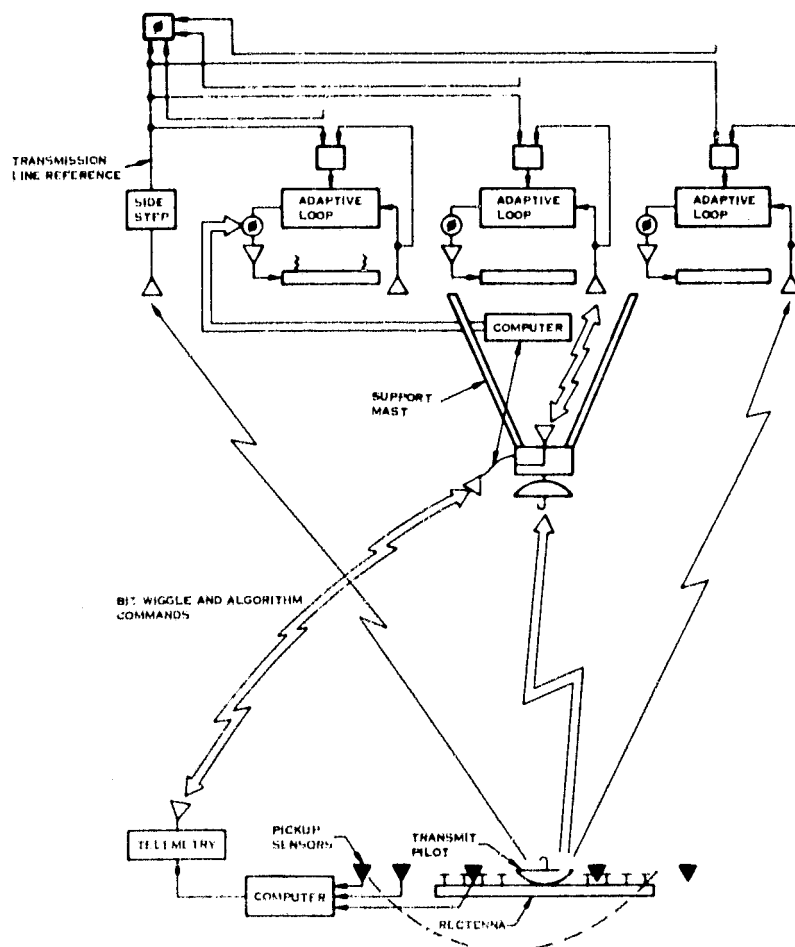
- ADAPTIVE (RETRODIRECTIVE) APPROACH NEEDED FOR MAXIMUM EFFICIENCY.
- COMMAND APPROACH NEEDED FOR SAFETY AND BACK-UP.
- ADAPTIVE PHASE CONTROL MECHANIZATION
 - CALIBRATED TRANSMISSION LINE AND/OR SUBARRAY-TO-SUBARRAY TRANSFER OF REFERENCE PHASE DATA
 - ANTICIPATE ADVERSE IONOSPHERIC MODEL
 - ORTHOGONAL POLARIZATION OF POWER/PILOT SIGNAL DESIRED

PHASE FRONT CONTROL

- ADAPTIVE (RETRODIRECTIVE) APPROACH NEEDED FOR MAXIMUM EFFICIENCY.
- COMMAND APPROACH NEEDED FOR SAFETY AND BACK-UP.
- CALIBRATED TRANSMISSION LINE AND/OR SUBARRAY-TO-SUBARRAY TRANSFER OF REFERENCE PHASE DATA FOR ADAPTIVE PHASE CONTROL MECHANIZATION.
- PHASE ESTIMATION FOR COMMAND MECHANIZATION.
- INVESTIGATE BIT WIGGLE TECHNIQUE AS DIAGNOSTIC TOOL.
- DETAILED INVESTIGATIONS SHOULD BE CONDUCTED TO MINIMIZE PHASE CONTROL ELECTRONICS COSTS, WEIGHT AND BLOCKAGE FOR EACH SUBARRAY.



Command and Adaptive Phase Front Control Concepts



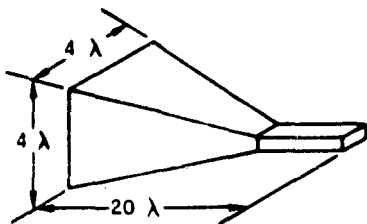
MPTS Phase Front Control Approaches

GROUND PILOT CHARACTERISTICS

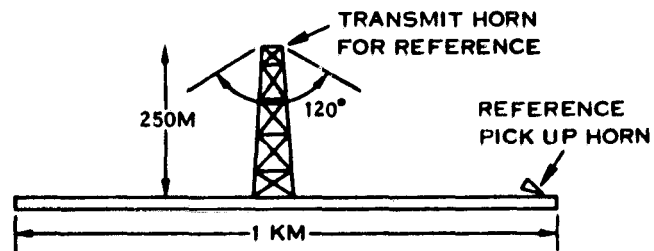
PILOT ANTENNA = 30 FEET DIAMETER PARABOLOID ($60\% \eta$, $F/D = 0.4$, GAIN = 63.4 DB)
 RECEIVE HORN GAIN ≈ 20 DB
 RECEIVED PILOT SIGNAL = -57 DBM
 TRANSMIT PILOT LEVEL = 132 WATTS CW

SPACE FED APPROACH (FRONT SIDE)

ON-ORBIT REFERENCE



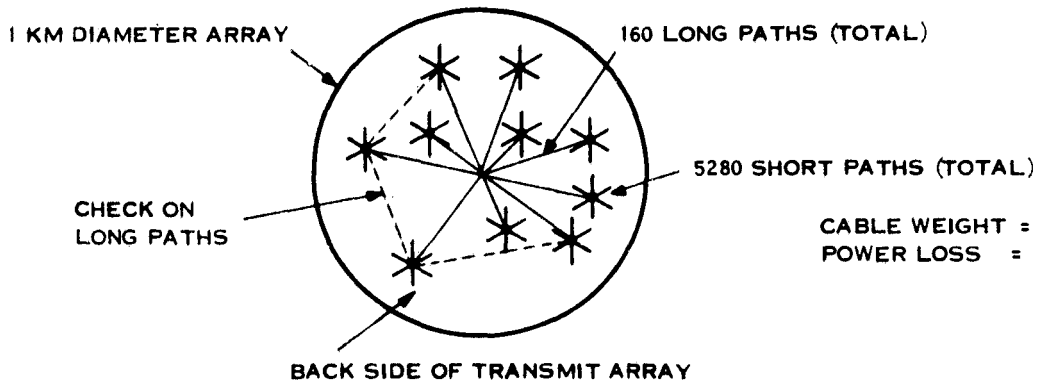
REFERENCE RECEIVE HORN
 PYRAMIDAL OR CONICAL
 (CORRUGATED OR DUAL MODE)



120 DEGREES 10 DB BEAMWIDTH FOR TRANSMIT
 HORN $\Rightarrow 1\lambda \times 1\lambda$ APERTURE AND ≈ 10 DB GAIN

RECEIVE HORN GAIN ≈ 20 DB
 TRANSMIT HORN GAIN AT ARRAY EDGE ≈ 0 DB
 TRANSMIT HORN TO ARRAY EDGE DISTANCE = 559 M
 REQUIRED REFERENCE POWER = 3.3 KW

TRANSMISSION LINE APPROACH



CABLE WEIGHT = 3700 KG
 POWER LOSS = 424 W

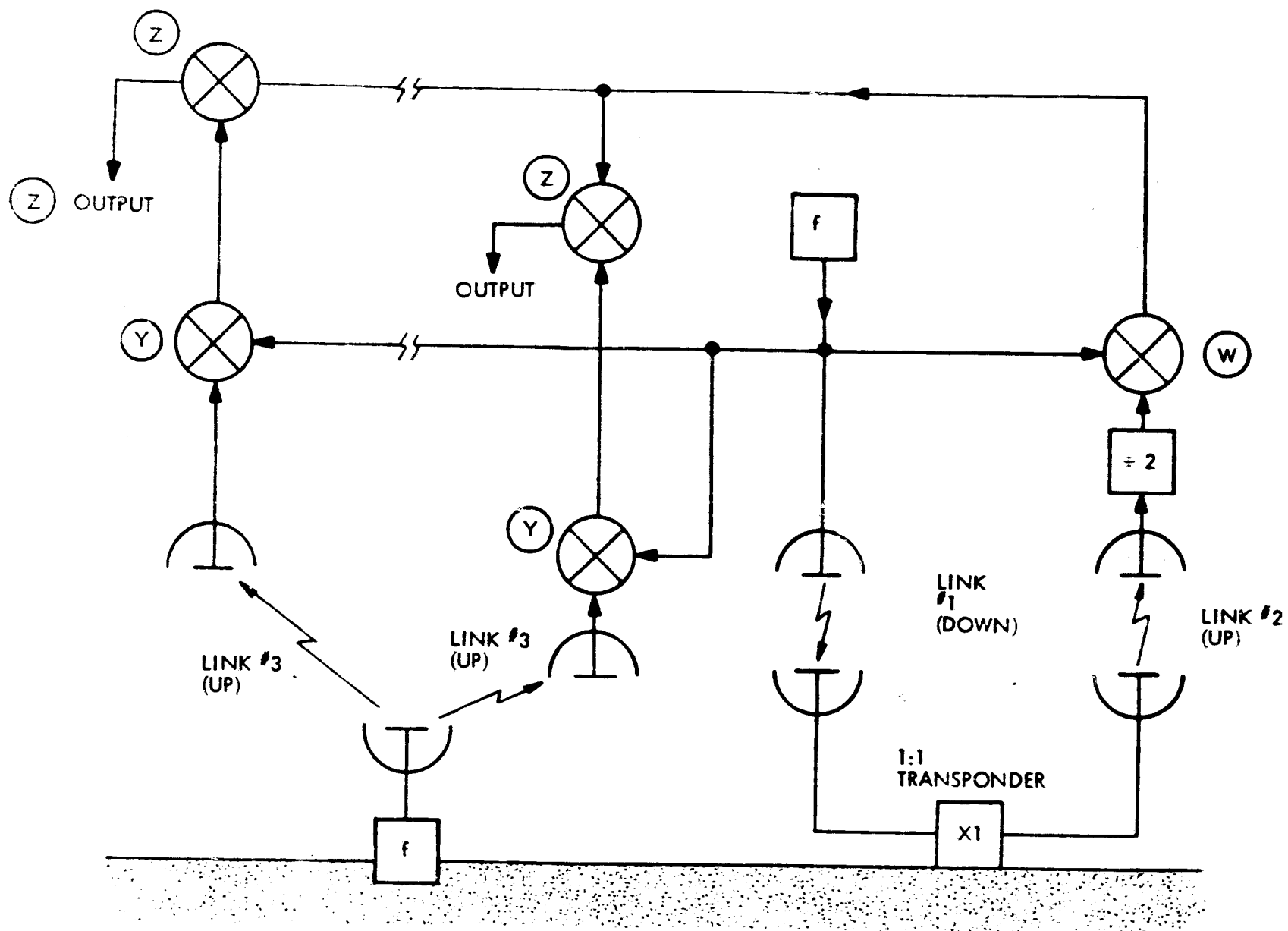
Ground Pilot and Phase Distribution

SUMMARY OF PHASE I PILOT BEAM STUDY

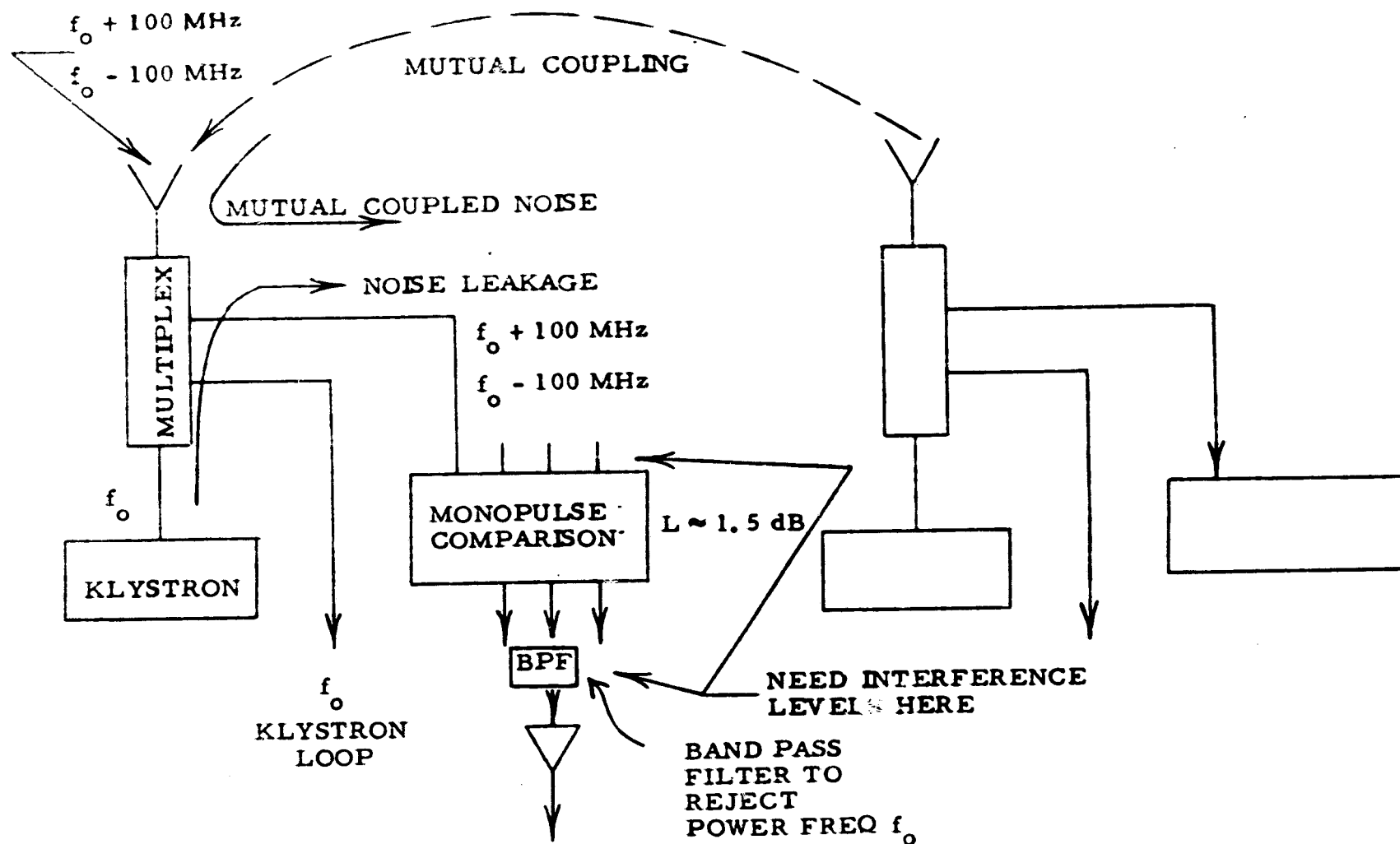
AREA	RESULTS OF STUDY	RECOMMENDATIONS
Ionospheric Interactions	<p>Baseline concept not valid in presence of unstable transmission path.</p> <p>Alternate approaches recommended.</p> <p>Mitigating strategy to reduce phase fluctuations presented.</p>	<p>Investigate alternate approaches vis-a-vis ionospheric interactions.</p> <p>Investigate mitigating strategies to reduce RMS phase error.</p> <p>Investigate impact of time fluctuations of power on interface to power grid.</p> <p>Develop experimental program for GBER (power beam heating).</p>
Pilot Beam System	<p>Pilot System sized.</p> <p>Levels of RFI from pilot beam provided.</p> <p>(Depends on freq. separation from carrier and size of subarray).</p>	<p>Utilize approach which maximizes Δf. This might conflict with ionospheric effects and should be studied.</p> <p>Study implementation of alternate approaches described above.</p> <p>RF vs IF phase conjugation still requires study.</p>
Communication System	<p>Requirement established.</p> <p>Off-the-shelf standard comm. gear.</p> <p>Low Power - 25 mW data links, 1 W TV links</p>	<p>Study decentralized vs centralized concepts (not a high priority item).</p>

MITIGATING STRATEGIES TO REDUCE IONOSPHERIC INDUCED
PHASE FLUCTUATION

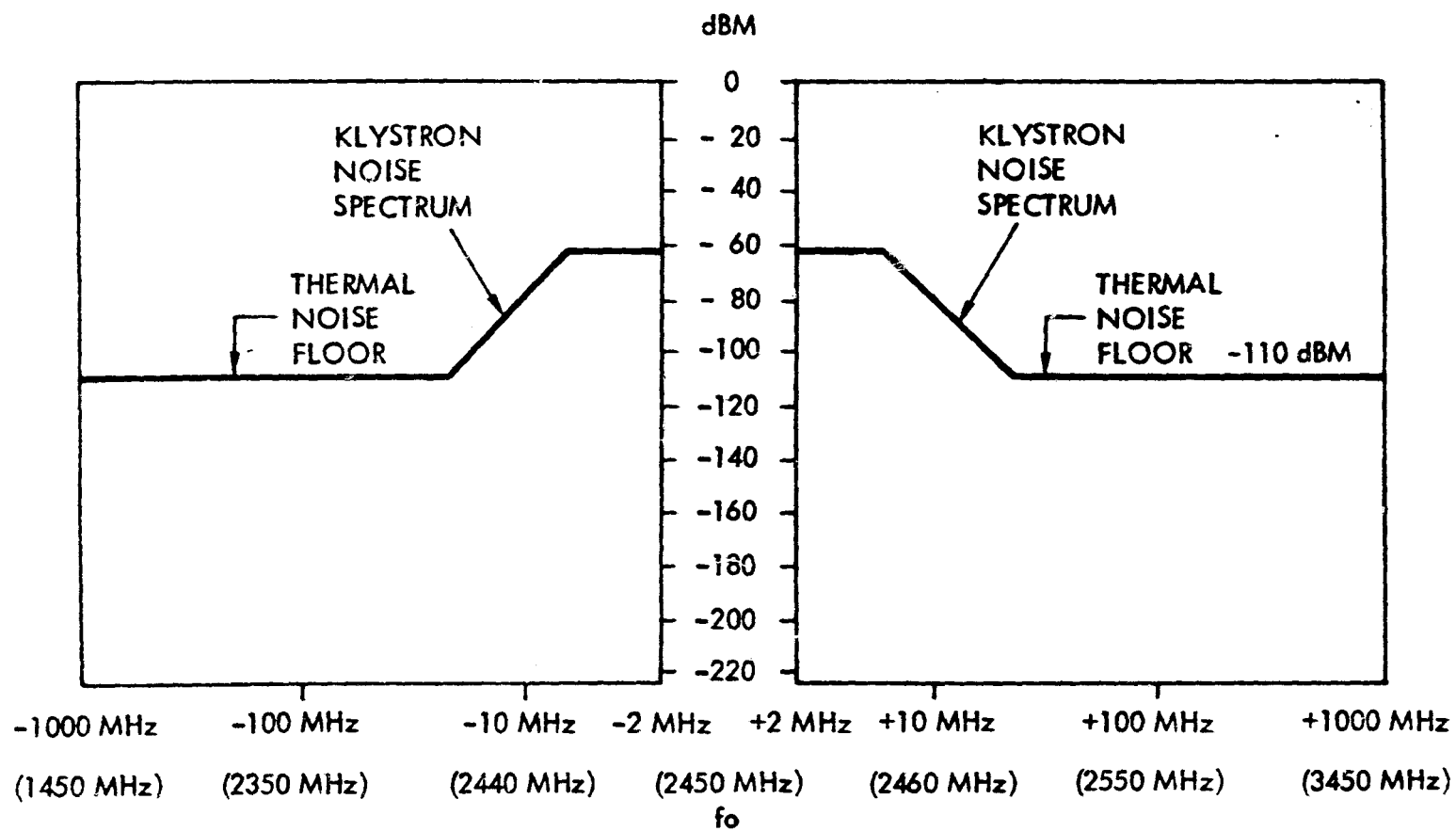
<u>METHOD</u>	<u>IMPLEMENTATION</u>	<u>IMPROVEMENT</u>
SPATIAL DIVERSITY	TWO OR MORE XMTRS ON GROUND SO PILOT BEAM TRAVERSES DIFFERENT IONOSPHERES	$(\text{NO. OF TRANSMITTERS})^{-1/2}$
TEMPORAL DIVERSITY	AVERAGE PHASE FLUCTUATIONS IN TIME PERIOD LONG COMPARED TO STABILITY OF PROPAGATION PATHS	$\left(\frac{\text{INTEGRATION TIME}}{\text{IONOSPHERE TIME CONSTANT}} \right)^{-1/2}$
FREQUENCY DIVERSITY		
INCOHERENT	NOT APPLICABLE	PHASE FLUCTUATIONS TRACK INCOHERENT AVERAGE DOES NOT SIGNIFICANTLY IMPROVE PERFORMANCE
COHERENT	TRACK PHASE FLUCTUATIONS ON TWO FREQUENCIES OR THREE FREQUENCIES	



Simplified Block Diagram of Approach No. 1



Interference Sources at SPS Subarray



Total Interference vs Pilot Beam Frequency

PILOT TRANSMITTER SIZING INTERFERENCE LEVELS

- RECEIVER THERMAL NOISE = $k t_o B NF L$

$$\begin{aligned}
 k &= 1.38 \times 10^{-23} \text{ w-s/}^{\circ}\text{k} &= -228.6 \text{ dBw} \\
 t_o &= 290^{\circ}\text{K} &= 24.6 \text{ dB} \\
 B &= 1.0 \text{ MHz} &= 60.0 \text{ dB} \\
 NF & &= 2.5 \text{ dB} \\
 L & &= \frac{1.5 \text{ dB}}{-140.0 \text{ dBw}} = -110.0 \text{ dBm}
 \end{aligned}$$

- DIPLEXER LEAKAGE OF KLYSTRON NOISE AT PILOT FREQ

$$\begin{aligned}
 \text{KLYSTRON CARRIER POWER, 50 KW} &= 77.0 \text{ dBm} \\
 \text{NOISE IN 1 MHz (PASSBAND)} &= -100.0 \text{ dBc/MHz} \\
 \text{KLYSTRON ROLLOFF @ 100 MHz } \Delta F &= -80.0 \text{ dB} \\
 \text{DIPLEXER ISOLATION} &= \frac{-30.0 \text{ dB}}{-133.0 \text{ dBm}}
 \end{aligned}$$

- MUTUAL COUPLING NOISE FROM OTHER KLYSTRONS

$$\begin{aligned}
 \text{KLYSTRON CARRIER, 50 KW} &= 77.0 \text{ dBm} \\
 \text{NOISE IN 1 MHz} &= -100.0 \text{ dB} \\
 \text{KLYSTRON ROLLOFF @ } \Delta F = 100 \text{ MHz} &= -80.0 \text{ dB} \\
 \text{MUTUAL COUPLING} &= \frac{-40.0 \text{ dB}}{-143.0 \text{ dBm}}
 \end{aligned}$$

Based on JSC
SPS production
cost of \$32.9B/
10 GW = \$230/KW

<u>S/I</u>	<u>σ</u>	<u>LOSS IN POWER</u>	<u>POWER LOST (XMIT 7.36 GW)</u>	<u>COST TO SYSTEM TO REPLACE</u>
30 dB	1.8°	0.1%	8.07 MW	\$1.9M
40 dB	0.6°	0.01%	807 KW	\$186K

$$S/I = 30 \text{ dB} \Rightarrow S = -80 \text{ dBm} = -110 \text{ dBw} = 10^{-11} \text{ WATTS}$$

$$\frac{P_T G_T A}{4\pi R^2} = 10^{-11} \text{ WHERE } R = 3.8 \times 10^7 \text{ m} \text{ \& } A = 0.5 (10.2\text{m}) (11.64\text{m}) = 59.4\text{m}^2$$

USE FULL SUBARRAY

$$P_T G_T = 3.054 \times 10^3$$

$$G_T = \eta \left(\frac{\pi D}{\lambda} \right)^2 = 45.4 \text{ dB FOR } D = 10\text{m}, \lambda = 0.12\text{m}, \eta = 50\%$$

$$P_T = 0.089 \text{ WATTS @ } \Delta F = 100 \text{ MHz}$$

P_T & G_T vs. ΔF (10.2m x 11.64m SUBARRAY)

<u>ΔF (MHz)</u>	<u>Antenna Dia. m</u>	<u>G_T (dB)</u>	<u>P_T^*</u>
1	10	45.4	44.6 KW
1	30	54.9	5.0 KW
5	10	45.4	44.6 KW
5	30	54.9	5.0 KW
10	10	45.4	141 W
30	10	45.4	0.1 W
100	10	45.4	0.1 W

* $P_T \approx 25$ times greater if
1/50 subarray used (central
Klystron module) and
aperture $\eta \sim 100\%$.

Thermal
Noise Limited

Pilot Transmitter Sizing

SUMMARY AND CONCLUSIONS
INITIAL MPTS STUDY RESULTS - SUBSYSTEMS AND TECHNOLOGY

ISSUES/CONSIDERATIONS

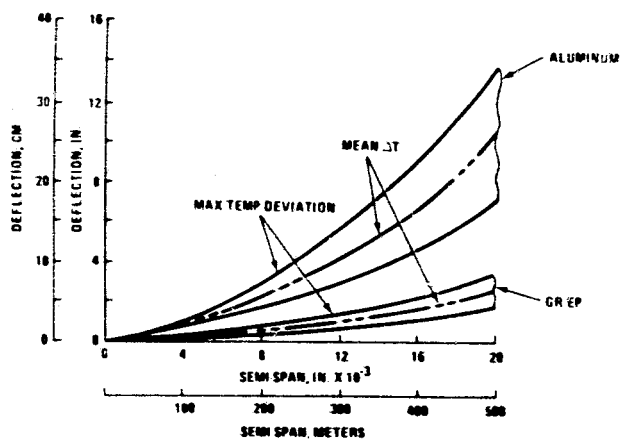
MECHANICAL SYSTEMS AND FLIGHT OPERATIONS

RESOLUTION/STATUS

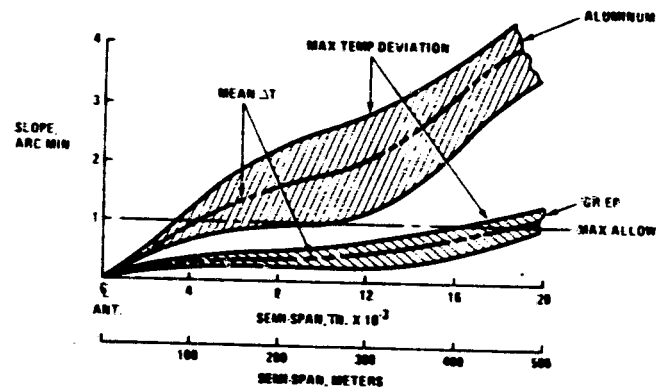
- ALUMINUM, GRAPHITE EPOXY, AND GRAPHITE-POLYIMIDE
TYPES OF MATERIALS RECOMMENDED FOR FURTHER
INVESTIGATION
 - LOW THERMAL DISTORTION REQUIRED AND HIGH
TEMPERATURE OPERATION WITH HIGH POWER DENSITIES
- OUTGASSING OF MATERIALS AND VEHICLES TO BE
INVESTIGATED TO ASSURE NO ADVERSE CONTAMINATION
OF OPEN ELECTRONICS.

MECHANICAL SYSTEMS AND FLIGHT OPERATIONS

- MATERIALS - ALUMINUM, GRAPHITE EPOXY, AND GRAPHITE POLYIMIDE - ARE RECOMMENDED AS CANDIDATES.
- COMPOSITES ARE ATTRACTIVE FOR LOW THERMAL DISTORTION AND HIGH TEMPERATURE OPERATION (POLYIMIDE), BUT ULTRA-VIOLET COMPATIBILITY AND OUTGASSING LEADING TO RF GENERATOR CONTAMINATION NEED INVESTIGATING.
- SEVERAL MORE PURELY STRUCTURAL ORIENTED CONCLUSIONS AND RECOMMENDATIONS ARE INCLUDED IN SECTION 1 OF NASA CR-134886.



Typical Antenna
Deflections Due to
Thermal Gradients



Typical Slopes of
Structure Due to
Thermal Gradients

SUMMARY AND CONCLUSIONS
INITIAL MPTS STUDY RESULTS - SUBSYSTEMS AND TECHNOLOGY

ISSUES/CONSIDERATIONS

RECEIVING ANTENNA

RESOLUTION/STATUS

- ARRAY OF INDEPENDENT ELEMENTS TO COLLECT AND RECTIFY INCIDENT MICROWAVE POWER FOR LOW COST AND HIGH EFFICIENCY.
- LINEARLY POLARIZED DIPOLE WITH GaAs SCHOTTKY BARRIER DIODE RECOMMENDED.
- RECTENNA EFFICIENCY IS 84% WITH 90% GOAL.
- SUPPORT STRUCTURE REQUIRES IN-DEPTH DEVELOPMENT OF CRITERIA AND CONCEPTS FOR LOW COST.
- POWER INTERFACE TO USER NETWORK NEEDS DEVELOPMENT TO REACH 92% AND GREATER EFFICIENCY.

RECEIVING ANTENNA

- AN ARRAY OF SMALL INDEPENDENT ELEMENTS ABLE TO COLLECT AND RECTIFY INCIDENT MICROWAVE POWER IS REQUIRED FOR LOW COST AND HIGH EFFICIENCY.
- A LINEARLY POLARIZED DIPOLE WITH GaAs SCHOTTKY BARRIER DIODE IS RECOMMENDED.
- RECTENNA COLLECTION AND CONVERSION EFFICIENCY IS 84% AND A REALISTIC DEVELOPMENT GOAL IS 90%.
- SUPPORT STRUCTURE IS MAJOR COST ITEM REQUIRING FURTHER IN-DEPTH STUDY OF TERRAIN, SOILS MECHANICS, AND ENVIRONMENTS TO BE ESTABLISHED.
- POWER INTERFACE TO THE USER NETWORK NEEDS DEVELOPMENT TO REACH 92% AND GREATER EFFICIENCIES.

REQUIREMENT FOR RECEPTION & RECTIFICATION OF SPACE-TO-EARTH POWER TRANSMISSION	ANTENNA APPROACH			
	ARRAY OF CONTIGUOUS HORNS	ARRAY OF CONTIG- UOUS REFLECTORS & FEED HORNS	PHASED ARRAY OF SMALL-APERTURE ELEMENTS WITH COMMON MICRO- WAVE LOAD	ARRAY OF SMALL- APERTURE ELEMENTS WITH INDEPENDENT MICROWAVE LOAD (RECTENNA)
NON-DIRECTIVE APERTURE	NO	NO	NO	YES
HIGH ABSORPTION EFFICIENCY	<70%	<70%	~100%	~100%
HIGH RECTIFICATION EFFICIENCY	YES	YES	YES	YES
VERY LARGE POWER HANDLING CAPABILITY	YES	YES	YES	YES
PASSIVE RADIATION OF WASTE HEAT	NO	NO	NO	YES
HIGH RELIABILITY	YES	YES	YES	YES
LONG LIFE	YES	YES	YES	YES
LOW RADIO FREQUENCY INTERFERENCE (RFI)	YES	YES	YES	YES
CAPABLE OF BEING CONSTRUCTED IN LARGE APERTURE SIZE	YES	YES	YES	YES
EASY MECHANICAL TOLERANCE REQUIREMENTS	NO	NO	NO	YES
LOW COST	NO	NO	NO	YES

Comparison of Antenna Approaches in Meeting Requirements for Reception and Rectification in Space-to-Earth Power Transmission

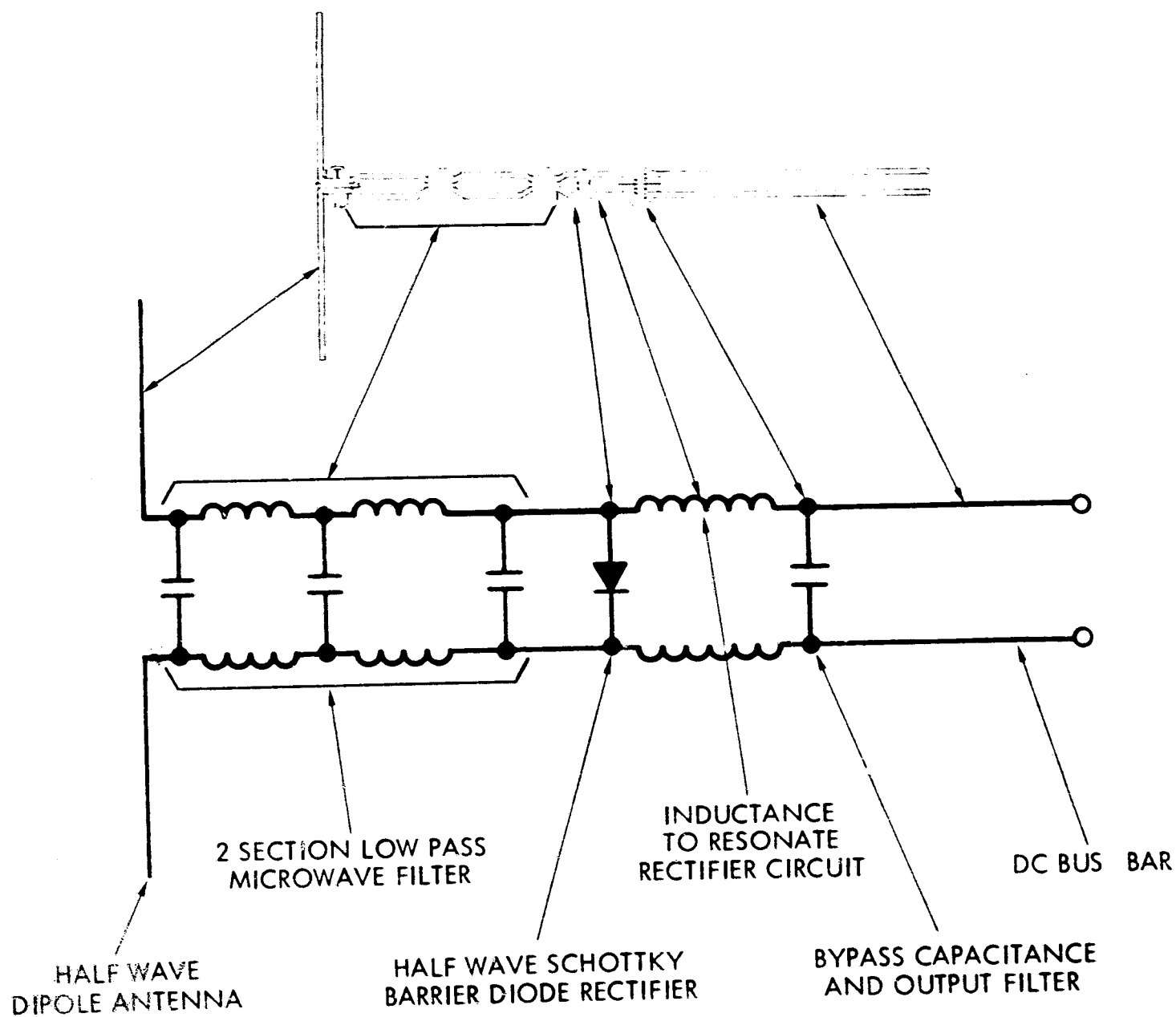
CLASS	SUBCLASS	STATUS* REACHED	MAXIMUM EXPERIMENTAL EFFICIENCY (%)	MAXIMUM EXPERIMENTAL POWER (WATTS)	FREQUENCY BAND	DEVICE IMPEDANCE
COLLINEAR BEAM	TWT	CONCEPTUAL	-----	-----	---	HIGH
COLLINEAR BEAM	KLYSTRON	CONCEPTUAL	-----	-----	---	HIGH
CROSSED-FIELD	INJECTED BEAM	EARLY DEVEL.	42	162 (CW)	S	HIGH
CROSSED-FIELD	MAGNETRON	EARLY DEVEL.	22	25,000 (PEAK)	L	MEDIUM
CROSSED-FIELD	CYCLOTRON	EARLY DEVEL.	12	12,000 (PEAK)	L	MEDIUM
DIODE	MULTIPACTOR	CONCEPTUAL	-----	-----	---	MEDIUM
DIODE	THERMIONIC	EARLY DEVEL.	55	900 (CW)	LS	LOW
DIODE	SEMI-CONDUCTOR	ADVANCED	90	10 (CW)	S	LOW

* FROM 1966 TO PRESENT-TIME THERE HAS BEEN NO SIGNIFICANT SUPPORT OF MICROWAVE RECTIFIER DEVICE TECHNOLOGY. IMPROVEMENTS IN SEMICONDUCTOR DEVICES HAVE RESULTED AS SPIN-OFFS FROM OTHER APPLICATIONS.

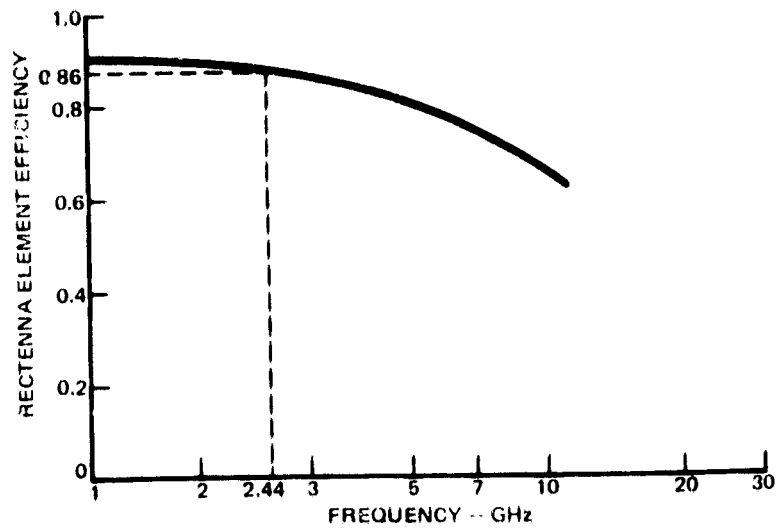
** ALL OF THESE DEVICES ARE DESCRIBED IN OKRESS, MICROWAVE POWER ENGINEERING.

Microwave Rectifier Device Technology **

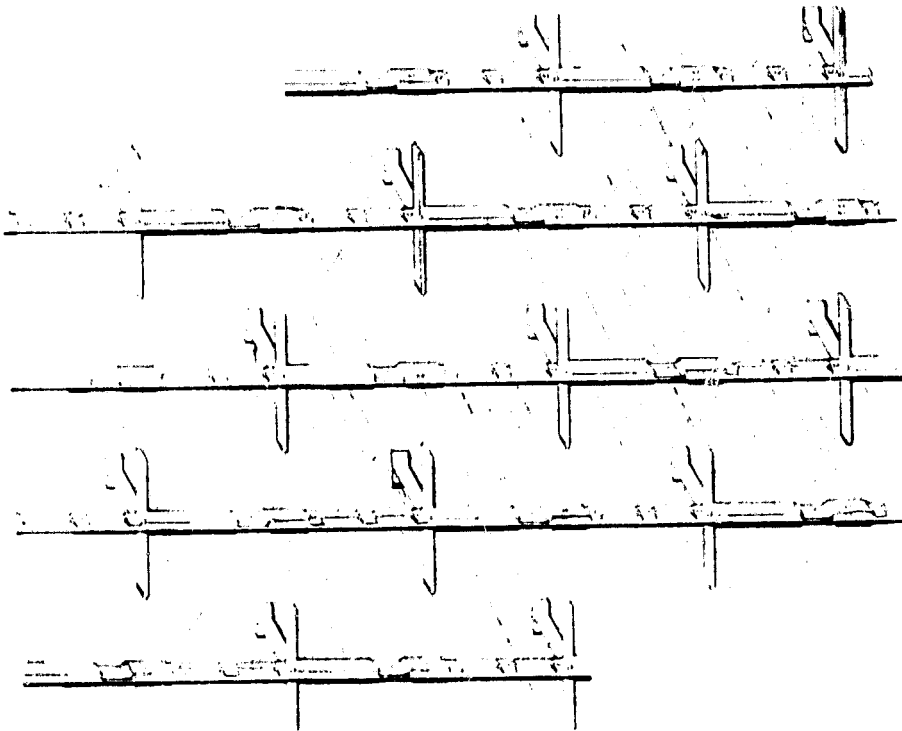
ORIGINAL PAGE IS
OF POOR QUALITY



Simplified Electrical Schematic for the Rectenna Element



Rectenna Element Efficiency vs Frequency



Rectenna Elements

SUMMARY AND CONCLUSIONS
INITIAL MPTS STUDY RESULTS - SUBSYSTEMS AND TECHNOLOGY

ISSUES/CONSIDERATIONS

RADIO FREQUENCY INTERFERENCE AND ALLOCATION

RESOLUTION/STATUS

- 2.45 GHz RECOMMENDED.
- HARMONIC FILTERS ARE NEEDED.
- SENSITIVE RECEIVING SYSTEMS NEED NOTCH FILTERS TO PROTECT AGAINST MPTS HARMONICS.
- MULTIPLE SPS INSTALLATIONS REQUIRE IN-DEPTH INVESTIGATION.

RADIO FREQUENCY INTERFERENCE AND ALLOCATION

GENERAL

- 2.45 GHZ IS RECOMMENDED AS OPERATING FREQUENCY.
- HARMONIC FILTERS AT THE RF GENERATORS ARE NEEDED TO MEET COMMERCIAL SERVICE REGULATIONS.
- RADIO ASTRONOMY AND SIMILAR SENSITIVE RECEIVING SYSTEMS WILL NEED NOTCH FILTERS TO PROTECT AGAINST MPTS HARMONICS.
- MULTIPLE SPS INSTALLATIONS REQUIRE FURTHER IN-DEPTH INVESTIGATION.

FOR CFA

- BANDPASS FILTER NEEDED TO IMPROVE PERFORMANCE RELATIVE TO RADIO ASTRONOMY NOISE REGULATIONS.
- NOISE LEVEL WITH FILTER ADDED IS ESTIMATED TO EXCEED RADIO ASTRONOMY ISOTROPIC REGULATIONS BETWEEN 2.3 GHZ AND 2.7 GHZ, AND TO EXCEED RADIO ASTRONOMY 60 DB ANTENNA REGULATIONS ABOVE 1.9 GHZ. EARLY DEVELOPMENT OF CFA AND FILTERS REQUIRED TO ESTABLISH NOISE CHARACTERISTICS.

FOR KLYSTRON

- NOISE LEVEL EXCEEDS RADIO ASTRONOMY ISOTROPIC REGULATIONS ONLY IN USA INDUSTRIAL BAND OF 2.4 TO 2.5 GHZ.
- NOISE LEVEL EXCEEDS RADIO ASTRONOMY 60 DB ANTENNA REGULATIONS BETWEEN 2.1 GHZ AND 2.85 GHZ.

$$P_D = \frac{N P_T G_{SA} C}{4 \pi R^2}$$

$$N = 1$$

$$P_T = 7.362 \text{ GW}$$

$$4 \pi$$

$$R^2 (3.8 \times 10^7 \text{ m})$$

$$G_{SA}$$

$$C (-160 \text{ dBc/Hz})$$

dB

0.0 dB

98.7 dBW

-11.0 dB

-151.6 dB

36.9 dBi

-160.0 dBc/Hz

-187.0 dBW/m² Hz

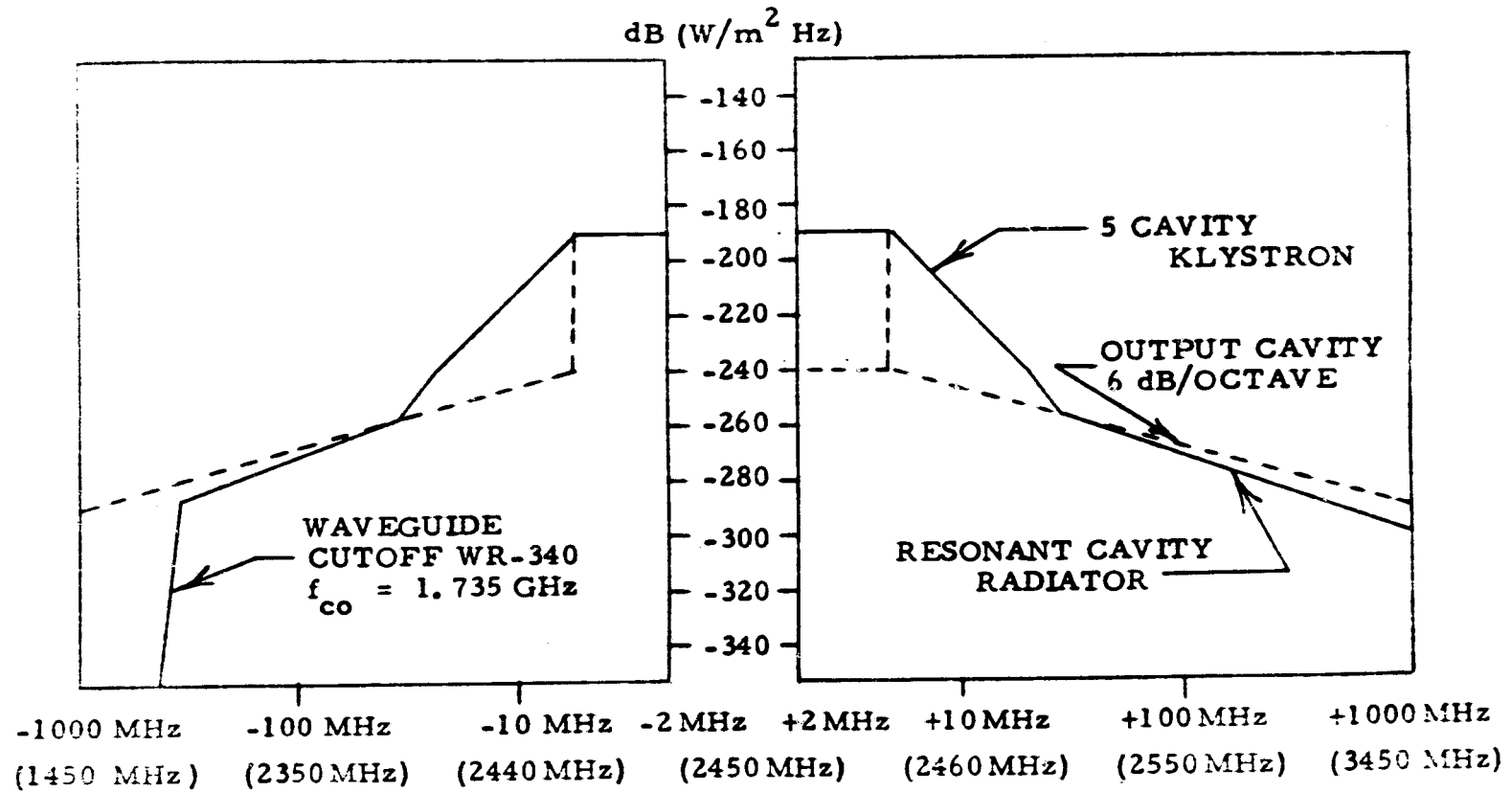
CLOSE-IN NOISE LEVEL

Noise on Earth From SPS Array

NO. SPS SYSTEMS

NOISE LEVEL INCREASE (dB)

1	0
30	14.8
60	17.8
120	20.8



SPS Noise Level at Earth (Single SPS)

SUMMARY AND CONCLUSIONS
INITIAL MPTS STUDY RESULTS - SUBSYSTEMS AND TECHNOLOGY

ISSUES/CONSIDERATIONS

RISK ASSESSMENT

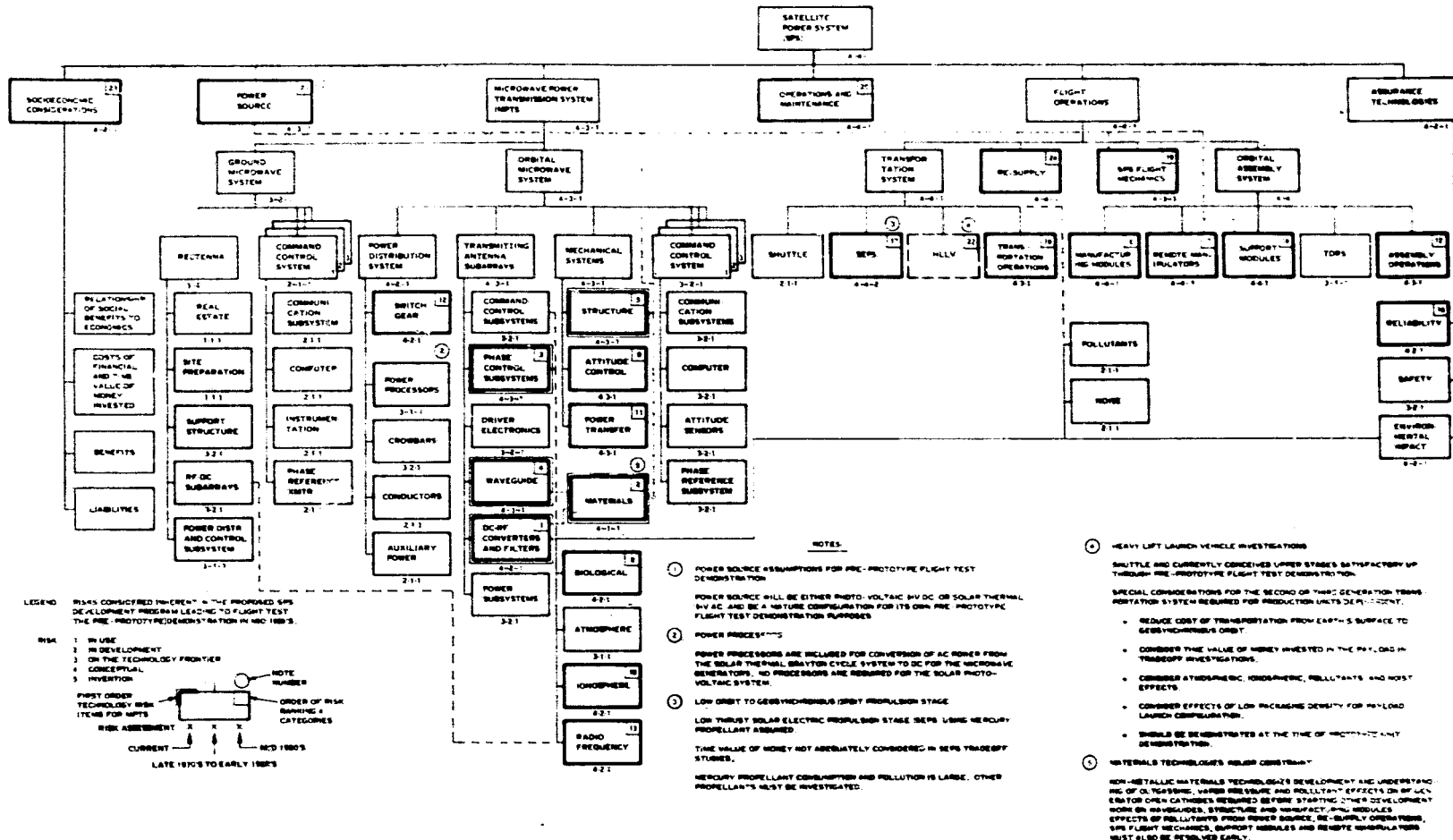
RESOLUTION/STATUS

- TOP THREE TECHNOLOGY RISK AREAS
 - DC-RF CONVERTERS
 - MATERIALS
 - PHASE CONTROL
- TOP THREE ENVIRONMENTAL RISK AREAS
 - BIOLOGICAL
 - IONOSPHERE
 - RFI AND ALLOCATION

		RISK RATING				
		1	2	3	4	5
		IN USE	IN DEVELOPMENT	ON THE TECHNOLOGY FRONTIER	CONCEPTUAL	INVENTION
STATUS ANTICIPATED WITH: a) SPECIFIC MPTS-FUNDED PROGRAM b) OTHER KNOWN PROGRAMS	TECHNOLOGY	FULLY DEVELOPED	PARTLY DEVELOPED	KNOWN BUT NOT DEVELOPED	NOT KNOWN, CHANCE OF IT BECOMING KNOWN IN TIME FOR MPTS IS GOOD	NOT KNOWN, CHANCE OF IT BECOMING KNOWN IN TIME FOR MPTS IS POOR
	HARDWARE	OFF-THE-SHELF ITEM OR PROTOTYPE AVAILABLE HAVING REQUIRED FUNCTION, PERFORMANCE & PACKAGING	FUNCTIONALLY EQUIVALENT HARDWARE IN USE (OPERATIONAL)	FUNCTIONALLY EQUIVALENT HARDWARE IN DEVELOPMENT	NO HARDWARE IN USE OR DEVELOPMENT BUT DEVELOPMENT IS PROBABLE	HARDWARE WILL NOT BE AVAILABLE UNLESS A BREAKTHROUGH OR INVENTION IS DEVELOPED
PROBABILITY OF DEVELOPMENT COMPLETION WITHIN SCHEDULE AND COST		CERTAIN (ALREADY EXIST)	VERY HIGH	HIGH	LOW	VERY LOW

Technology and Hardware Development Risk Rating Definition

LEVEL 5 BREAKDOWN



HIGHLIGHTING THE MOST CRITICAL ITEMS TO MPTS DEVELOPMENT (THE FIRST 5 IN ORDER)

Satellite Power System Technology Risk Assessment

RISK ASSESSMENT

1. DC-RF CONVERTERS AND FILTERS
2. MATERIALS
3. PHASE CONTROL SUBSYSTEMS
4. WAVEGUIDE
5. STRUCTURE
6. MANUFACTURING MODULES
7. REMOTE MANIPULATORS
8. BIOLOGICAL
9. ATTITUDE CONTROL
10. IONOSPHERE
11. POWER TRANSFER
12. SWITCHGEAR
13. RADIO FREQUENCY INTERFERENCE & ALLOCATION
14. SUPPORT MODULES
15. ORBITAL ASSEMBLY OPERATIONS
16. RELIABILITY
17. SOLAR ELECTRIC PROPULSION SYSTEM (SEPS)
18. TRANSPORTATION OPERATIONS
19. SPS FLIGHT MECHANICS (STATIONKEEPING)
20. OPERATIONS AND MAINTENANCE
21. POWER SOURCE
22. HEAVY LIFT LAUNCH VEHICLE (HLLV)
23. SOCIO-ECONOMIC CONSIDERATIONS
24. RE-SUPPLY

SUMMARY AND CONCLUSIONS
INITIAL MPTS STUDY RESULTS - SUBSYSTEMS AND TECHNOLOGY

ISSUES/CONSIDERATIONS

SYSTEM ANALYSIS AND EVALUATION

RESOLUTION/STATUS

- COST INCREASES INVERSELY WITH POWER
- COST INCREASES WITH FREQUENCY
- POWER DENSITY AT EARTH EXCEEDS 20 MILLIWATTS/CM²
FOR GROUND POWER LEVELS ABOVE 5 GW
 - ALLOWABLE POWER DENSITY AT GROUND NEEDS TO
BE DETERMINED FROM IONOSPHERIC IMPACT AND
BIOLOGICAL POINTS OF VIEW

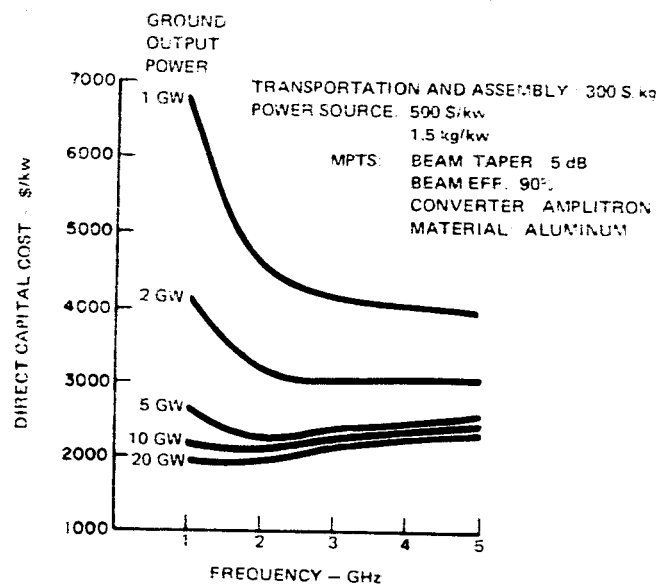
● OVERALL MPTS EFFICIENCY

	<u>CFA APPROACH</u>	<u>KLYSTRON APPROACH</u>
INITIALLY:	54% TO 56%	49% TO 52%
POTENTIAL:	63% TO 67%	56% TO 59%

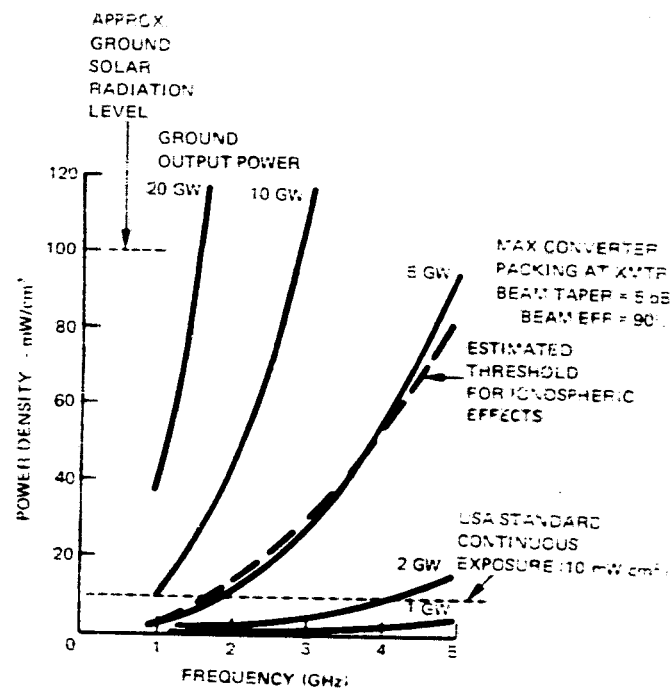
- ALUMINUM RESULTS IN LOWER COST BUT MORE COMPLEX
SYSTEMS THAN DO GRAPHITE COMPOSITES.

SYSTEM ANALYSIS AND EVALUATION

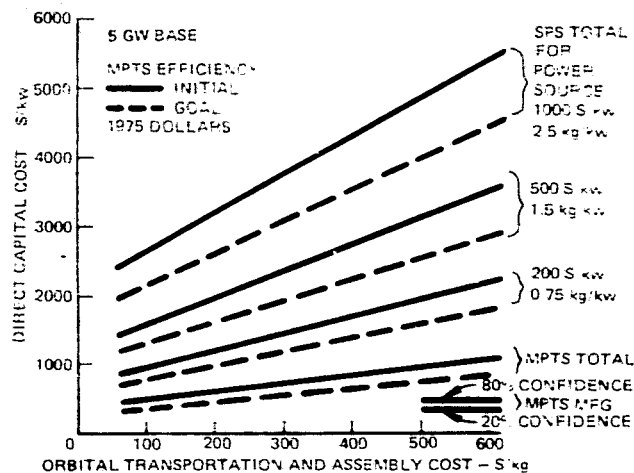
- CAPITAL SPECIFIC COST DECREASES AS GROUND POWER OUTPUT INCREASES.
- AT HIGHER POWER LEVELS, COST IS LOWEST NEAR 2 GHZ.
- FREQUENCY OF 2.45 GHZ IN THE INDUSTRIAL BAND IS THE RECOMMENDED CHOICE.
- SYSTEM CONFIGURATIONS HAVING GROUND BUS POWER LEVELS ABOVE 5 GW EXCEED 20 mW/cm^2 PEAK GROUND POWER DENSITY WHICH IS BEGINNING TO AFFECT THE IONOSPHERE AND SO 5 GW IS CURRENTLY RECOMMENDED AS THE MAXIMUM FOR PLANNING PURPOSES. FURTHER IN-DEPTH ANALYSIS AND TESTING IS REQUIRED TO UNDERSTAND THESE EFFECTS MORE THOROUGHLY AND PERHAPS RELAX THE CONSTRAINT.
- OVERALL MPTS EFFICIENCY IS EXPECTED TO BE ABOUT 54%-56% INITIALLY WITH IMPROVEMENT POTENTIAL TO ABOUT 63%-67% FOR AMPLITRON CONFIGURATIONS; KLYSTRON CONFIGURATIONS WOULD BE 49%-52% TO 56%-59%.
- AMPLITRONS RESULT IN LOWER COST SYSTEMS THAN DO KLYSTRONS.
- ALUMINUM RESULTS IN POTENTIALLY LOWER COST BUT MORE COMPLEX SYSTEMS THAN DO GRAPHITE COMPOSITES.
- DOMINANT COST FACTORS FOR SPS ARE THE POWER SOURCE AND TRANSPORTATION.
- AS A GUIDE, THE POWER SOURCE PARAMETERS SHOULD NOT EXCEED THE COMBINATION OF 350 \$/kW WITH 1.0 kg/kW OR POSSIBLY 250 \$/kW WITH 1.5 kg/kW WHERE THE POWER IS AS DELIVERED TO THE TRANSMITTING ANTENNA.
- AS A GUIDE, TRANSPORTATION AND ORBITAL ASSEMBLY SHOULD NOT EXCEED 200 \$/kg.
- AS A GUIDE, BUILD AND DEPLOY CYCLE FOR SPS SHOULD NOT EXCEED 3 YEARS TO LIMIT INTEREST CHARGES.
- FOR THE ALUMINUM-AMPLITRON CONFIGURATION, NEAR OPTIMUM TRANSMITTING ANTENNA AND RECIEVING ANTENNA WEIGHT IS ABOUT 6×10^6 kg.



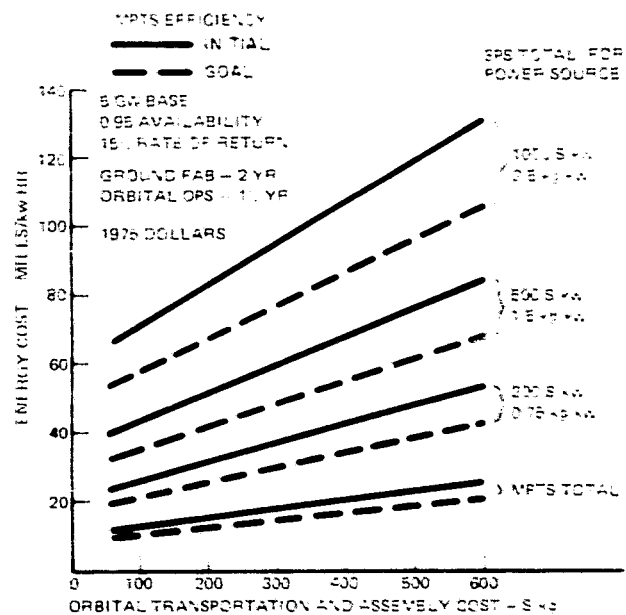
SPS Capital Cost vs
Frequency - 300 \$/kg



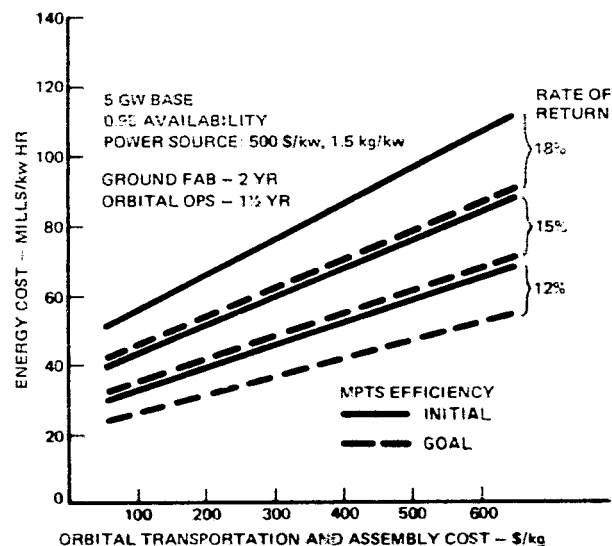
Peak Ground Power
Density vs Frequency



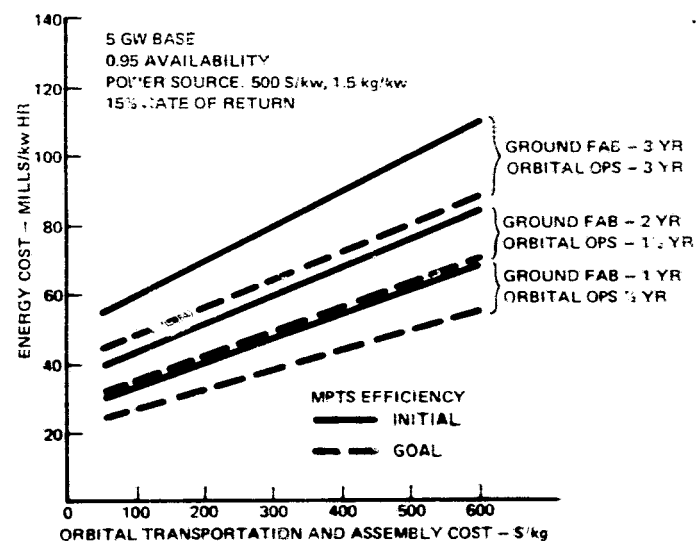
SPS Capital Cost for
Various Power Source
Characteristics



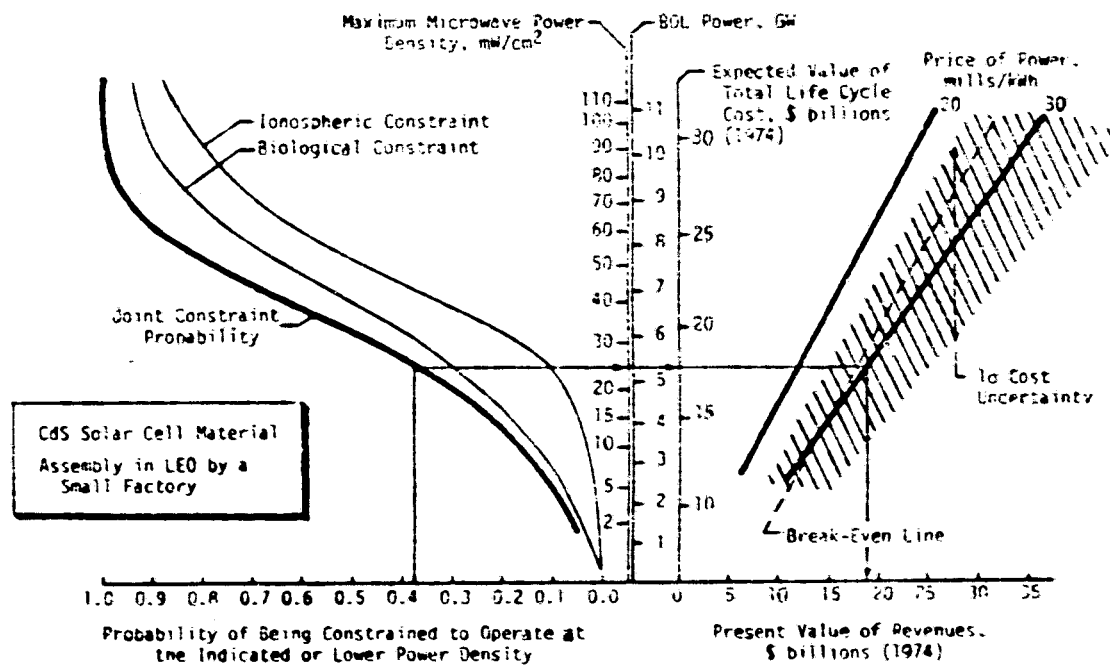
SPS Energy Cost for
Various Power Source
Characteristics



SPS Energy Cost for
Various Rates of
Return



SPS Energy Cost
for Various
Construction Cycles



The Effect of Constraints on Microwave Power Density

OVERALL MPTS EFFICIENCY ESTIMATES

	<u>CROSSED FIELD AMPLIFIER</u>	<u>KLYSTRON</u>
INITIAL SYSTEMS	54 TO 56	49 TO 52
IMPROVEMENT POTENTIAL	63 TO 67	56 TO 59

REF: NASA CR-134886, SECTION 1.2.3

	INITIAL	GOAL	NOMINAL
POWER DISTRIBUTION	96	97	96
DC-RF CONVERTER	85	90	87
PHASE CONTROL	95	97	96
ATMOSPHERE	99	99	99
BEAM COLLECTION	90-95*	90-95*	90-95*
RECTENNA	84	90	87
POWER INTERFACE	<u>93</u>	<u>95</u>	<u>94</u>
TOTAL	54-57	65-68	58-62

*DEPENDS ON TRADEOFF OF COSTS, LAND USE, POWER DENSITY LIMITS. TAPER OF POWER DISTRIBUTION ON ORBIT 5 DB LIMIT IS 90%, 10 DB LIMIT APPROACHES 95%.

MPTS Efficiency Budget

GROUND POWER GW	XMTR TAPER dB	BEAM INTERCEPTION %	TRANSMITTING ANTENNA WT - KGX10 ⁶	TRANSMITTING ANTENNA DIA - km	RECTENNA DIMENSIONS* km	MAX GROUND POWER DENSITY mW/cm ²
5	5	90	6.2	0.8	11 x 15	17
	10	95	8.3	1.0	10 x 13	22
10	5	90	11.9	1.2	8 x 10	68
	10	95	14.3	1.4	7 x 9	87

*M/ JOR AXIS IS FOR ELEVATION ANGLE = 50 DEG

Figure 48 Amplitron-Aluminum MPTS Comparison

TAPER = 5 dB
BEAM EFFICIENCY = 90%

POWER SOURCE - 1.5 kg/kw
- 500 \$/kw
TRANSPORTATION ASSEMBLY - 300 \$/kg

DC-RF CONVERTER	STRUCTURE & WAVEGUIDE MATERIAL	DC-RF CONVERTER WT KG X 10 ⁶	TRANSMITTING ANTENNA TOTAL WT KG X 10 ⁶	MPTS \$/kw	SPS \$/kw
AMPLITRON	ALUMINUM	2.6	6.2	700	2300
	GRAPHITE	2.6	5.0	700	2300
KLYSTRON	ALUMINUM	7.3	12.5	1100	2800
	GRAPHITE	7.3	10.8	1100	2800

Comparison of 5 GW Systems

SUMMARY AND CONCLUSIONS
INITIAL MPTS STUDY RESULTS - SUBSYSTEMS AND TECHNOLOGY

ISSUES/CONSIDERATIONS

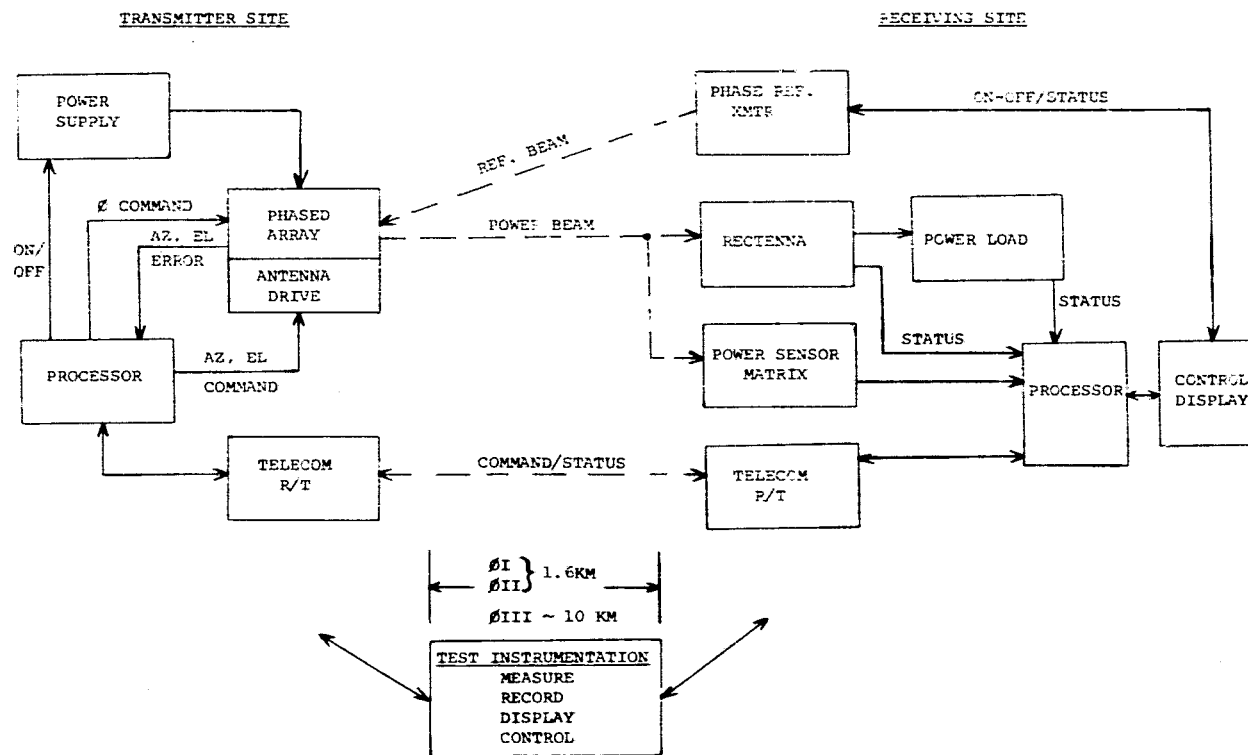
TECHNOLOGY DEVELOPMENT AND TEST PROGRAMS

RESOLUTION/STATUS

- INITIAL TECHNOLOGY DEVELOPMENT NEEDED FOR DC-RF
 - DC-RF CONVERTERS
 - MATERIALS
 - PHASE CONTROL SUBSYSTEM
- TEST PROGRAM TO PROVIDE DATA ON:
 - CONTROLLABILITY
 - RADIO FREQUENCY INTERFERENCE
- INTEGRATED GROUND TEST REQUIRES:
 - TRANSMITTING ANTENNA PHASED ARRAY
 - RECTENNA
- ORBITAL TEST NEEDED TO:
 - DEVELOP AND DEMONSTRATE DC-RF CONVERTERS
 - LEARNING WITH RESPECT TO PROJECTED COSTS AND SCHEDULE
- MODIFIED FACILITIES SUCH AS ARECIBO BEST SUITED TO DETERMINE EFFECTS ON LOWER IONOSPHERE

TECHNOLOGY DEVELOPMENT AND TEST PROGRAMS

- TECHNOLOGY DEVELOPMENT AND GROUND TEST PROGRAM
 - INITIAL TECHNOLOGY DEVELOPMENT IS NEEDED FOR DC-RF CONVERTER, MATERIALS, AND PHASE CONTROL SUBSYSTEM.
 - TEST PROGRAM WILL PROVIDE DATA ON CONTROLLABILITY AND RADIO FREQUENCY INTERFERENCE.
 - TRANSMITTING ANTENNA PHASED ARRAY AND RECTENNA ARE REQUIRED FOR INTEGRATED GROUND TESTING.
 - ROUGH-ORDER-OF-MAGNITUDE COSTS ARE \$4M FOR TECHNOLOGY AND \$23M FOR THE INTEGRATED GROUND TEST.
- TECHNOLOGY DEVELOPMENT AND ORBITAL TEST PROGRAM
 - ORBITAL TEST IS NEEDED TO DEVELOP AND DEMONSTRATE DC-RF CONVERTER STARTUP AND OPERATION, ZERO 'G' ASSEMBLY AND OPERATIONS, AND LEARNING WITH RESPECT TO PROJECTED COSTS AND SCHEDULE.
 - REQUIREMENTS ARE SATISFIED BY A GEOSYNCHRONOUS TEST SATELLITE AND BY A SERIES OF SHUTTLE SORTIE MISSIONS THAT LEAD TO AN ORBITAL TEST FACILITY.
 - A LOW EARTH ORBITAL TEST FACILITY CAN BE SIZED TO DETERMINE THE EFFECTS ON THE UPPER IONOSPHERE OF HIGH MICROWAVE POWER DENSITIES.
 - MODIFIED GROUND BASED FACILITIES SUCH AS AT ARECIBO ARE BEST SUITED TO DETERMINE THE EFFECTS ON THE LOWER IONOSPHERE OF HIGH MICROWAVE POWER DENSITIES.
 - TECHNOLOGY DEVELOPMENT IS NEEDED IN NOT ONLY THE "CRITICAL" AREAS BUT IN ESSENTIALLY ALL MPTS AREAS IN ORDER TO SUPPORT A PROGRESSIVE PROGRAM TO DEMONSTRATE READINESS TO PROCEED TO SIGNIFICANT SCALE FOR A PILOT PLANT OR PROTOTYPE.
 - ROUGH-ORDER-OF-MAGNITUDE COSTS ARE \$318M FOR CRITICAL TECHNOLOGY DEVELOPMENT, AND \$96M FOR THE GEOSATELLITE, AND TO ACCOMPLISH ALL IDENTIFIED OBJECTIVES \$3052M FOR THE SORTIES AND ORBITAL TEST FACILITY.



MPTS Ground Test Functional Block Diagram

Mission Class	Objectives		Microwave Payload	Intermediate Benefits
	Mandatory	Highly Desirable		
Geo-synchronous	<ul style="list-style-type: none"> • dc-rf Converter Starting and Operation • High voltage plasma interaction 	<ul style="list-style-type: none"> • Ionosphere Effects on Pilot Beam • Interferometer Accuracy • Orbital Life Test 	<ul style="list-style-type: none"> • DC-RF Converter • 18 Meter Interferometer • Particle Detectors 	<ul style="list-style-type: none"> • Communications • Bistatic Radar • Ionosphere Data • Observation of LEO Sorties Effects
Low Earth Orbit (LEO) Sorties	<ul style="list-style-type: none"> • Zero "G" Mfg. and Assembly Flow Development - Structure - Microwave - Interface • Operations and Maintenance Development • Initial Verification of Cost and Schedule Projections 	<ul style="list-style-type: none"> • Controllability Demonstration • Thermal Cycling Effects - Large Structures • Preprototype Building Block • Orbital Life Test • Upper Ionosphere Heating Effects 	<ul style="list-style-type: none"> • Build-up to 18M x 18M Power Sub-arrays • Spares to be provided along with Command-Control Sub-array and Orbital Support Equipment • Juxtapositioning to be possible 	<ul style="list-style-type: none"> • Communications • Bistatic Radar - Earth - Planetary • Orbital Microwave Power Transfer • Ionosphere Data

Microwave Orbital Test Program

SUMMARY AND CONCLUSIONS
INITIAL MPTS STUDY RESULTS - SUBSYSTEMS AND TECHNOLOGY

ISSUES/CONSIDERATIONS

ADDITIONAL STUDIES

RESOLUTION/STATUS

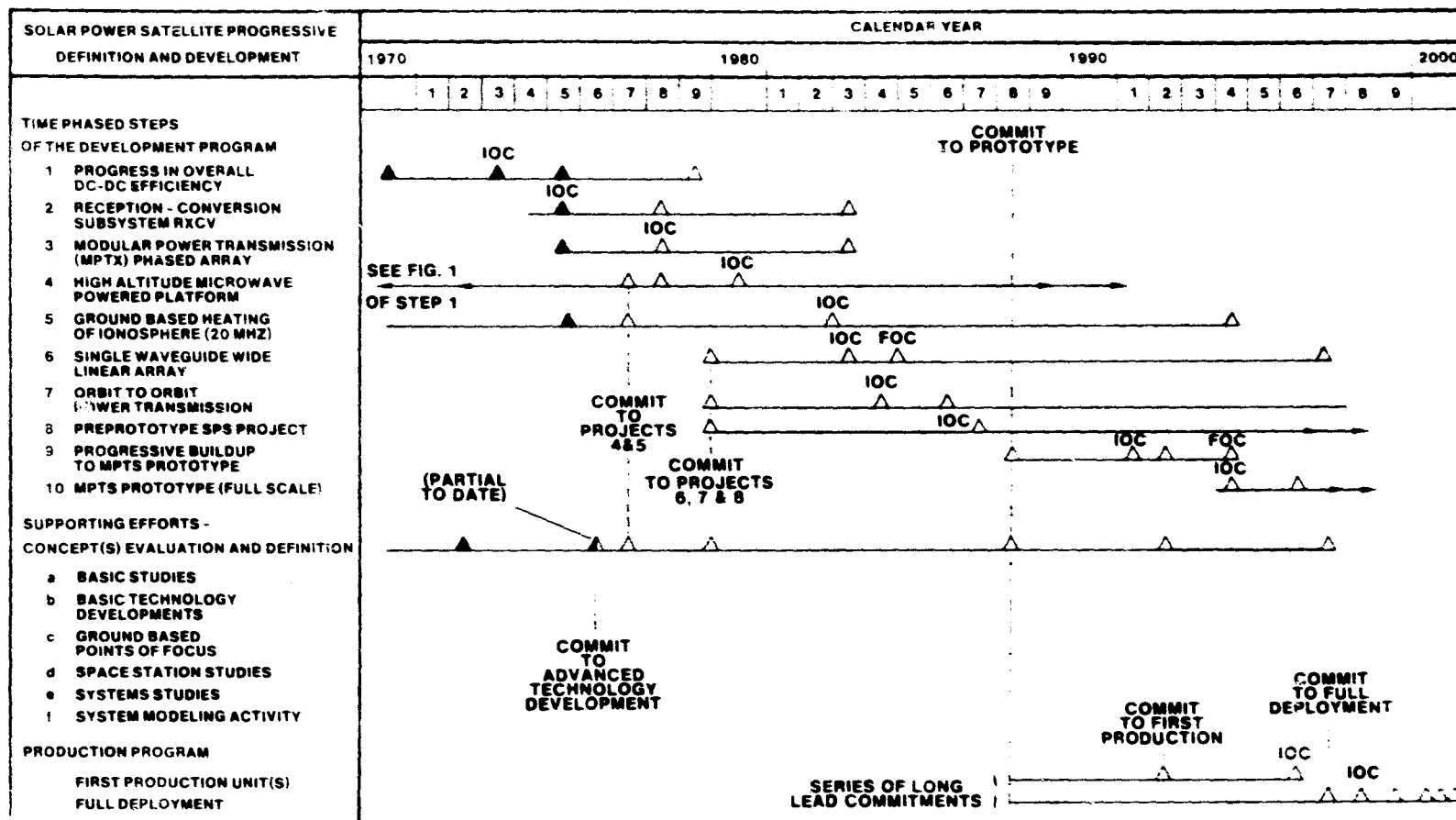
- ANALYZE TRANSIENT THERMAL EFFECTS
- ANALYZE POWER BEAM IONOSPHERIC EFFECTS
 - OTHER USERS
 - MODEL FOR PHASE FRONT CONTROL SIMULATION
- MODEL CLOSED LOOP PHASE FRONT CONTROL TO
BETTER ESTIMATE ERROR BUDGET AND PERFORMANCE
UNDER TRANSIENT CONDITIONS
- DETERMINE SPECIAL REQUIREMENTS FOR MULTIPLE
STATIONS
 - CONTROL
 - FREQUENCY SELECTION
 - INTERFERENCE

ADDITIONAL STUDIES

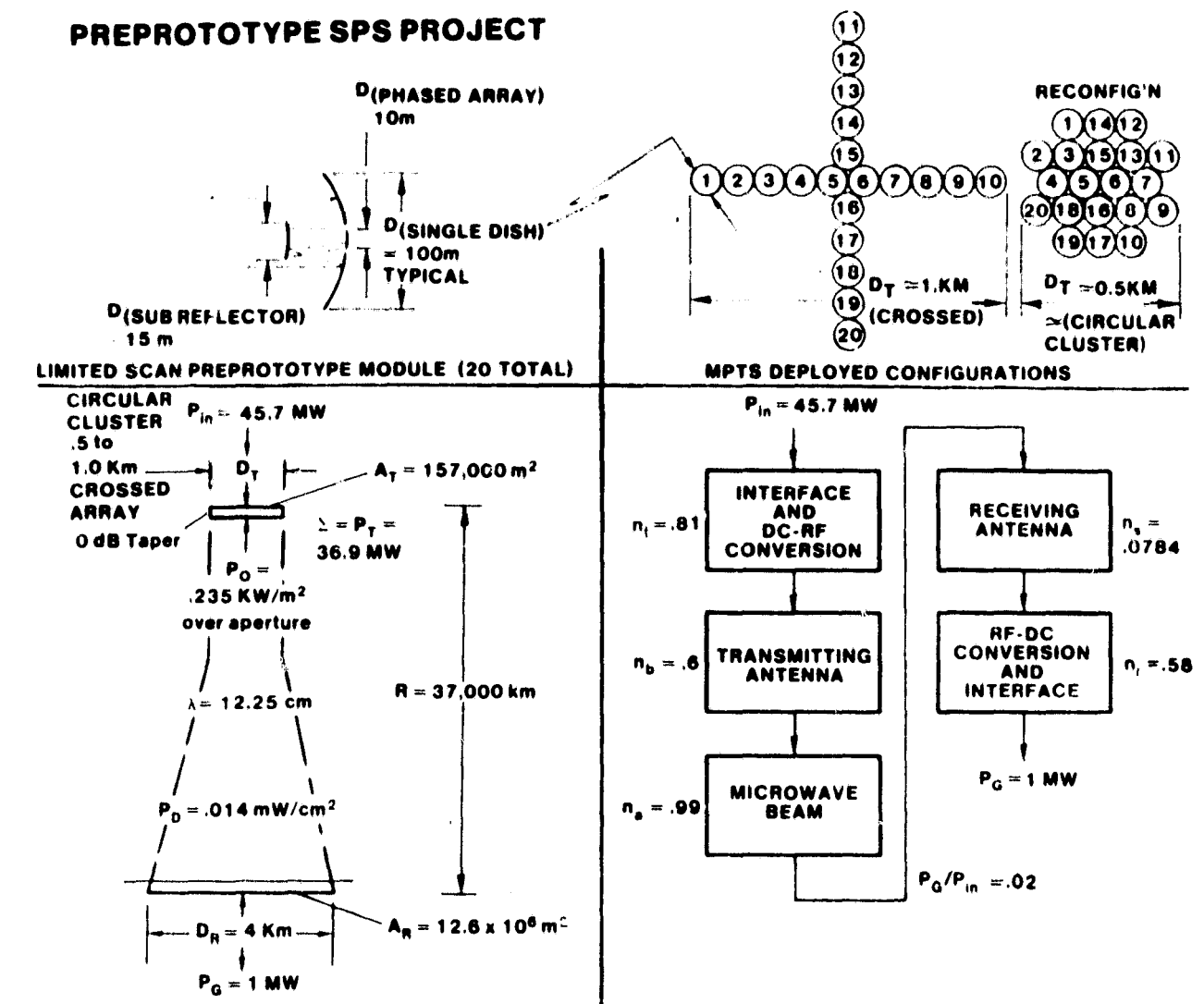
RECOMMENDATIONS FOR EARLY IN-DEPTH STUDIES COMPLEMENTING THE TECHNOLOGY DEVELOPMENT PROGRAMS ARE:

- ANALYZE TRANSIENT THERMAL EFFECTS ON THE TRANSMITTING ANTENNA STRUCTURE, WAVEGUIDE AND ELECTRONICS AS IT PASSES IN AND OUT OF ECLIPSE TO DETERMINE IMPACT ON CONTROLLABILITY AND MATERIALS SELECTION.
- ANALYZE POWER BEAM IONOSPHERIC EFFECTS TO ESTIMATE IMPACT ON OTHER USERS AND PROVIDE A DETAIL MODEL FOR PHASE FRONT CONTROL SIMULATION.
- MODEL CLOSED LOOP PHASE FRONT CONTROL TO BETTER ESTIMATE ERROR BUDGET AND PERFORMANCE UNDER TRANSIENT CONDITIONS.
- DETERMINE SPECIAL REQUIREMENTS FOR MULTIPLE (100) STATIONS RELATING TO SPACING IN ORBIT AND ON THE GROUND, CONTROL, FREQUENCY SELECTION AND INTERFERENCE.
- DETAIL ALTERNATE USES AND INTERMEDIATE BENEFITS OF MPTS AND POTENTIAL IMPACT ON ITS DESIGN AND DEVELOPMENT.
- INVESTIGATE WAYS OF REDUCING TRANSPORTATION AND ASSEMBLY COSTS BY A BETTER (HIGHER LEVEL OF DETAIL) SYNTHESIS OF LAUNCH VEHICLE, ASSEMBLY AND EQUIPMENT TECHNOLOGIES.

PROGRESSIVE DEFINITION AND DEVELOPMENT SATELLITE POWER SYSTEM (SPS)

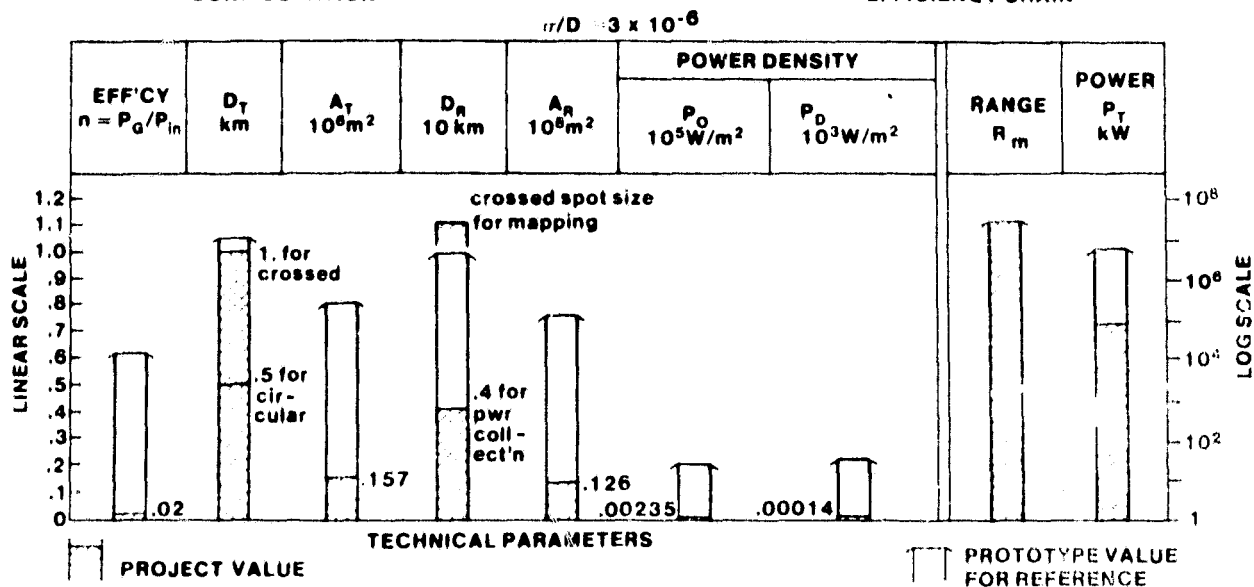


PREPROTOTYPE SPS PROJECT

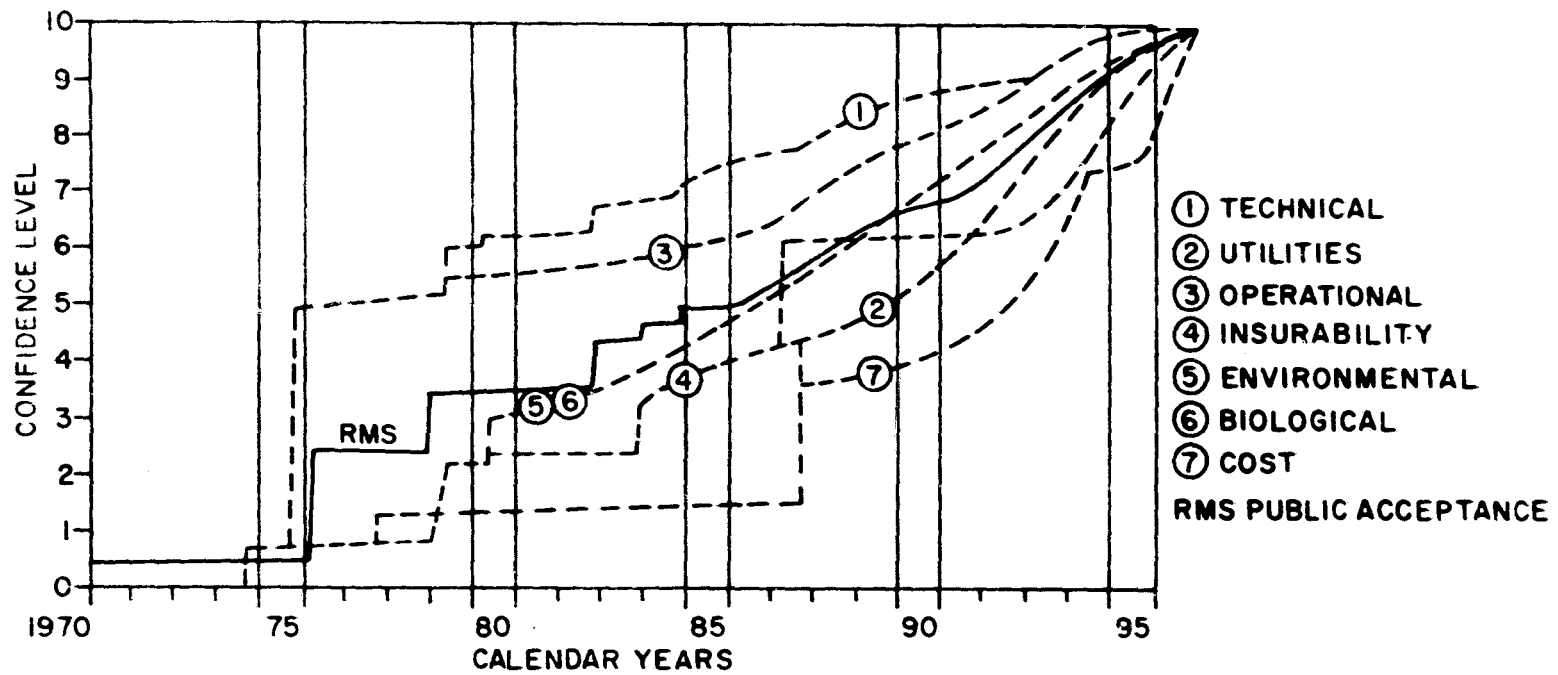


CONFIGURATION

EFFICIENCY CHAIN



CONFIDENCE LEVEL



***Antenna Illumination
and
Beam Shaping
Studies***

***Dr. Erv Nalos,
Boeing***

BEAM PATTERN STUDIES

o ARRAY SIMULATION PROGRAMS

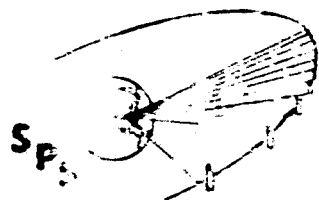
- o RADIALLY SYMMETRIC CIRCULAR ARRAY SIMULATION
- o TILTMAT SUBARRAY SIMULATION
- o MODMAIN MODULE SIMULATION

o PATTERNS STUDIED

- o UNIFORM DISTRIBUTION
NEAR FIELD, FOCUSED/UNFOCUSED BEAM
- o GAUSSIAN TAPER
- o SUPPRESSOR RING
REVERSE PHASE, MULTIPLE RINGS
- o CONTINUOUS PHASE
QUADRATIC PHASE TAPER

o STUDY TRENDS

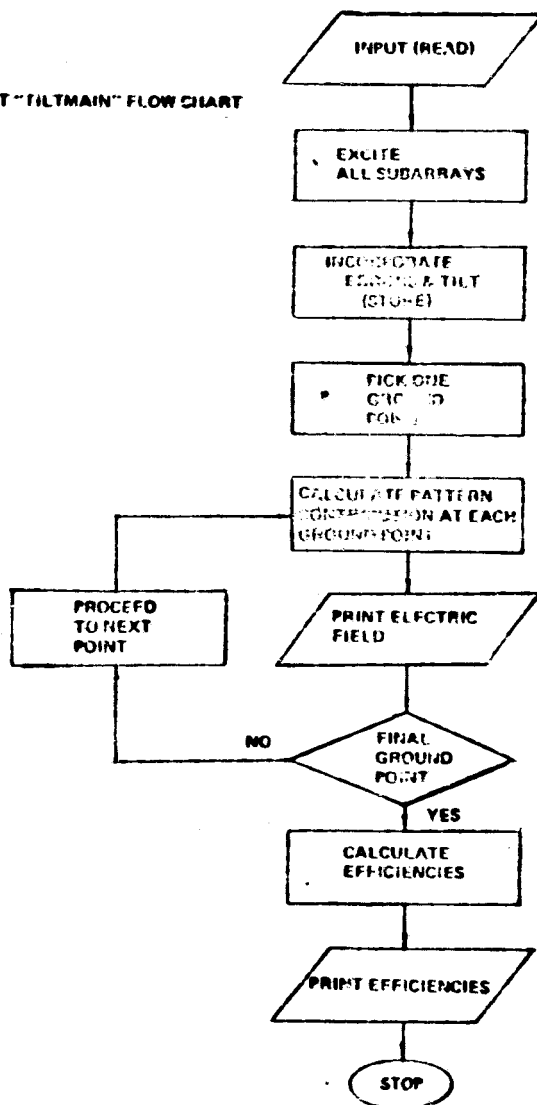
- o NO SIGNIFICANT IMPROVEMENT IN KLYSTRON BASELINE
- o POTENTIAL INCREASE IN POWER WITH CONTROLLED BEAM DEFOCUSING



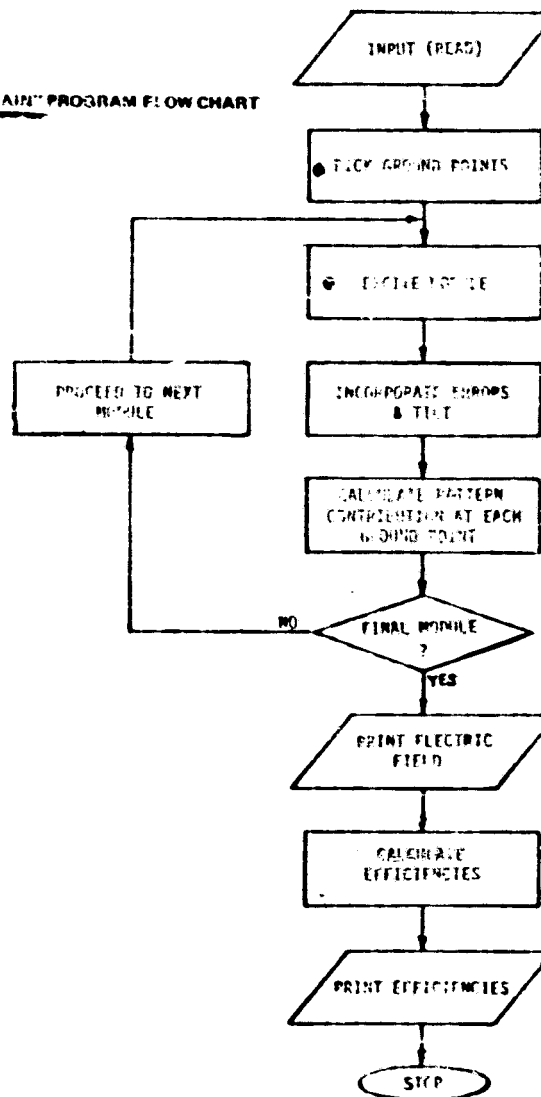
Computer Program Flow Comparison

BOEING

CURRENT "TILTMAN" FLOW CHART

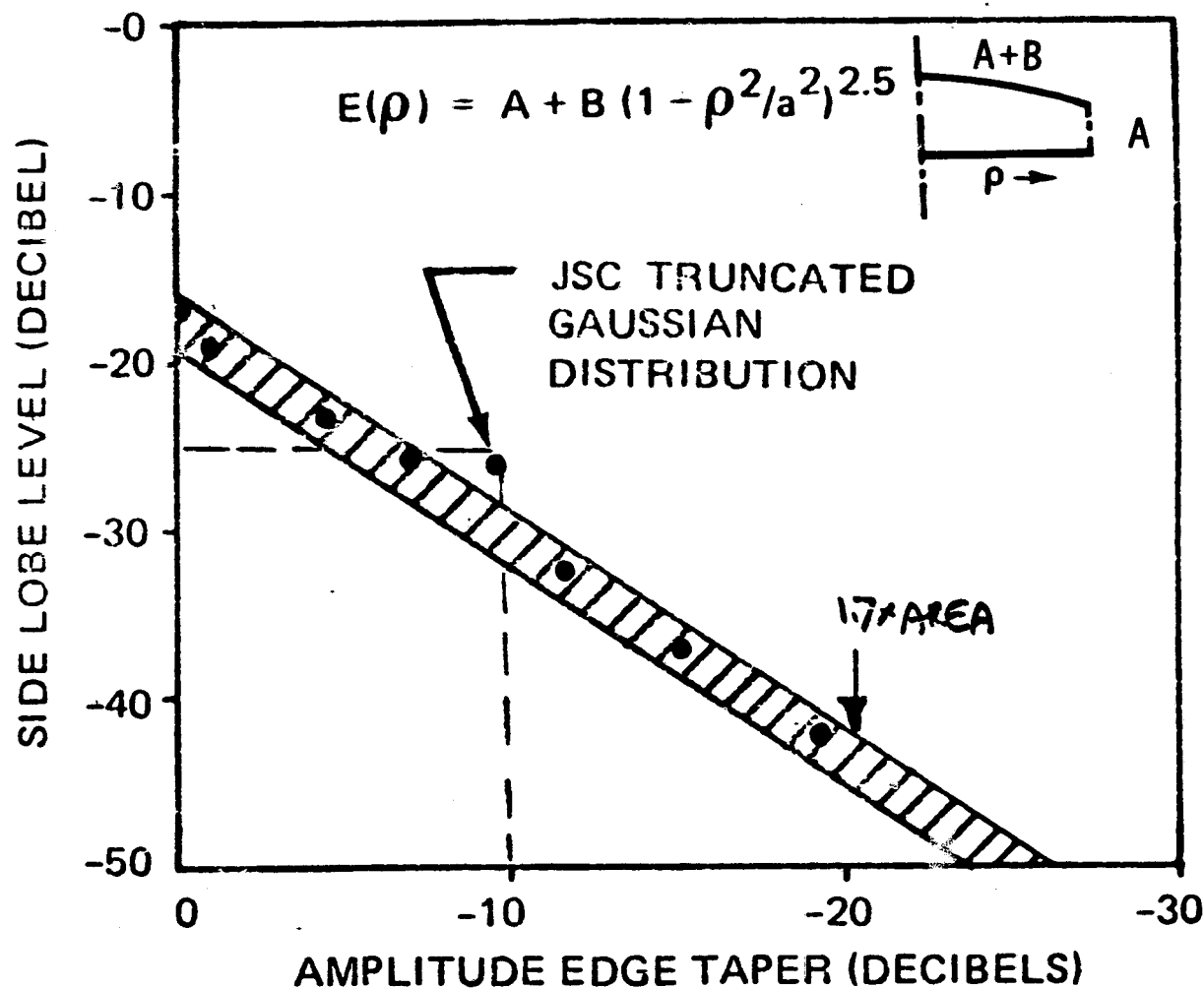


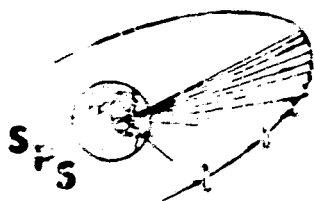
"MOD MAIN" PROGRAM FLOW CHART





Side Lobe Levels Resulting Various Taylor Series Tapers

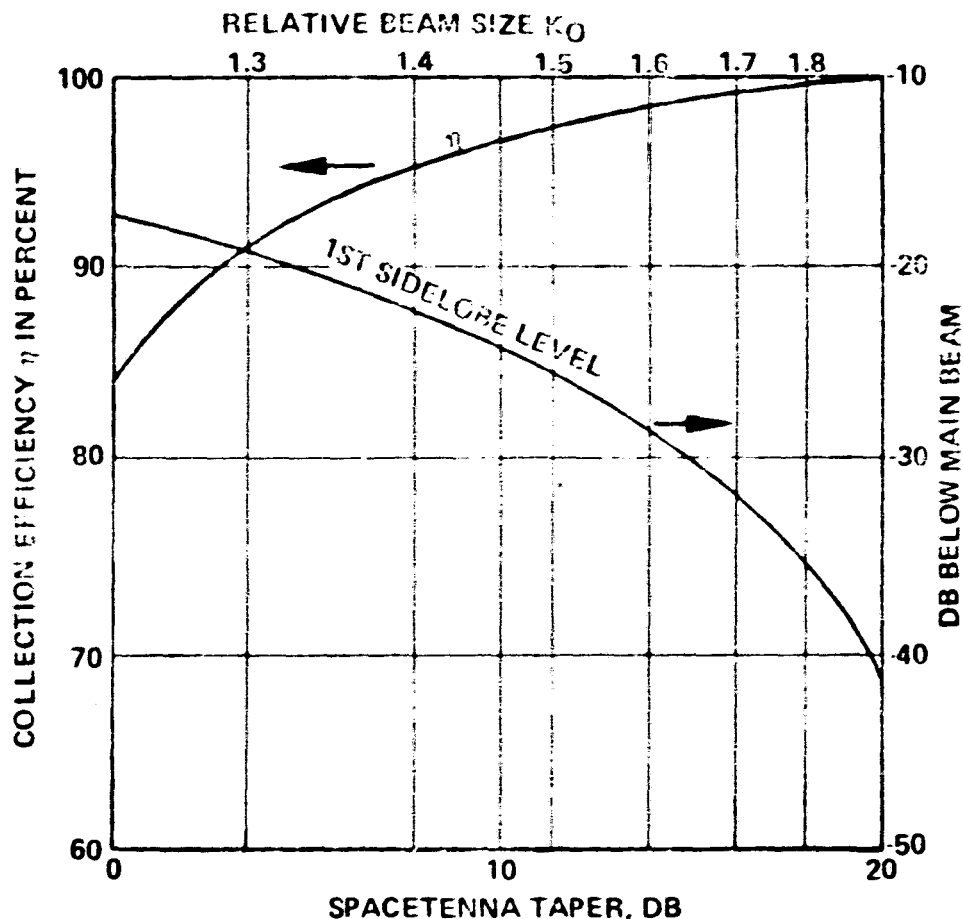




SP-100

Spacenna Illumination Effects for Gaussian Tapers

GOING

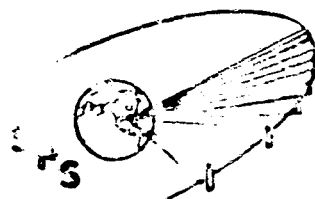


$$K_0 = \frac{2AR}{H\lambda} = (4.6 \times 10^{-7}) AR$$

A = SPACENNA RADIUS

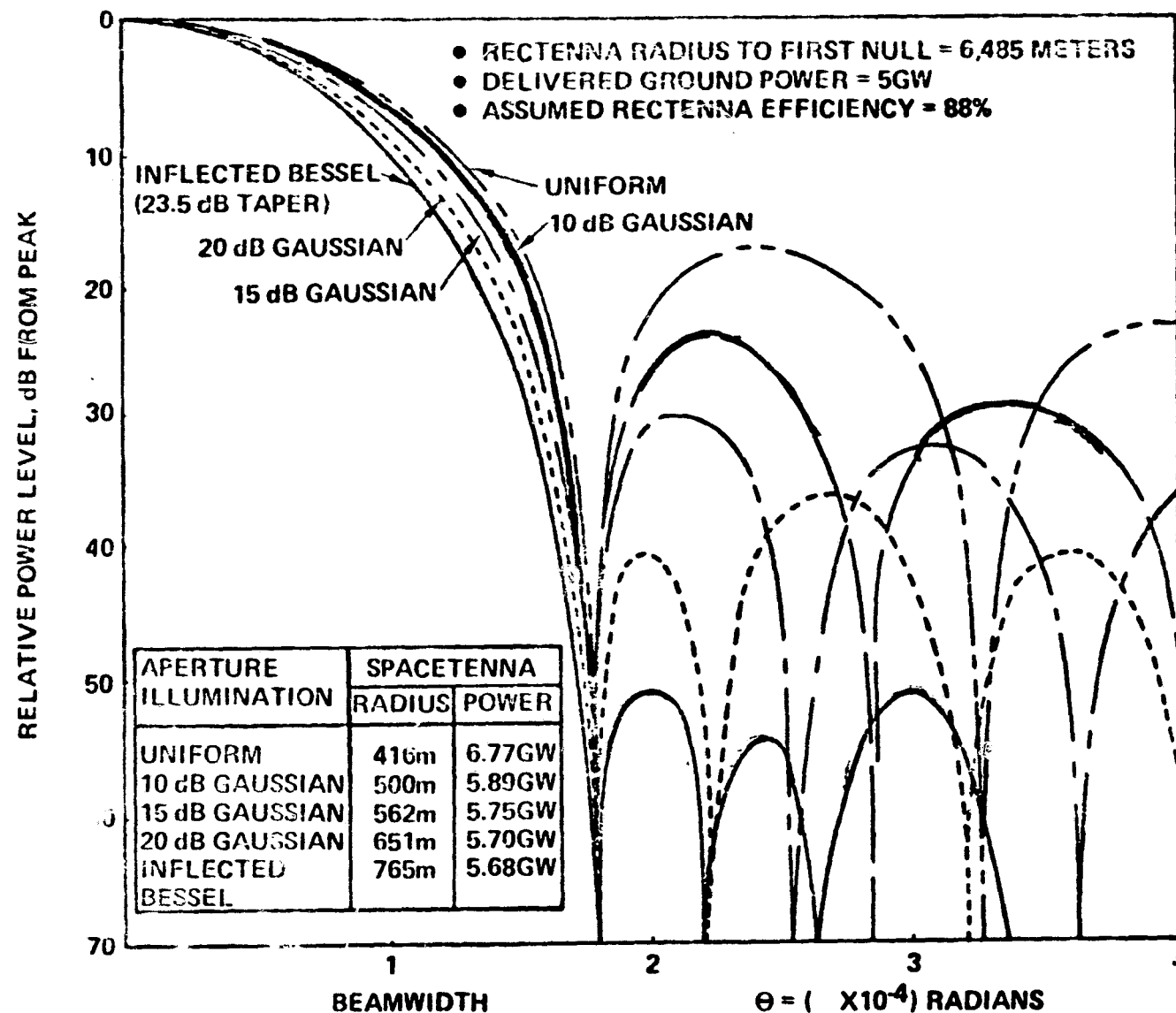
R = BEAM RADIUS AT RECTENNA

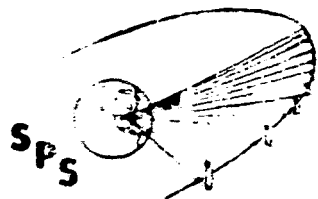
H = RANGE BETWEEN SPACENNA & RECTENNA



Sidelobe Distributions For Fixed Rectenna Constraints

BOEING



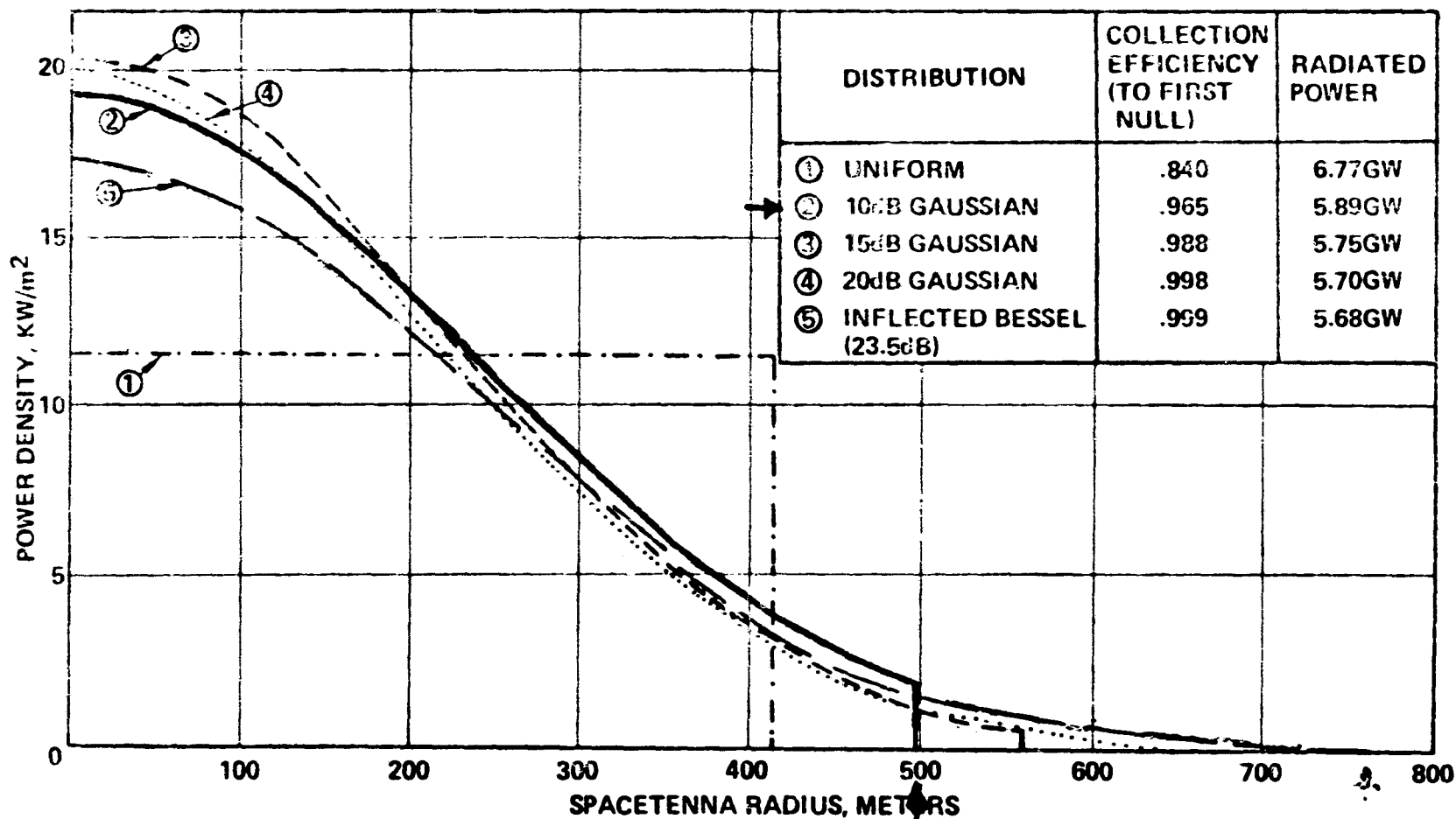


SPS 858

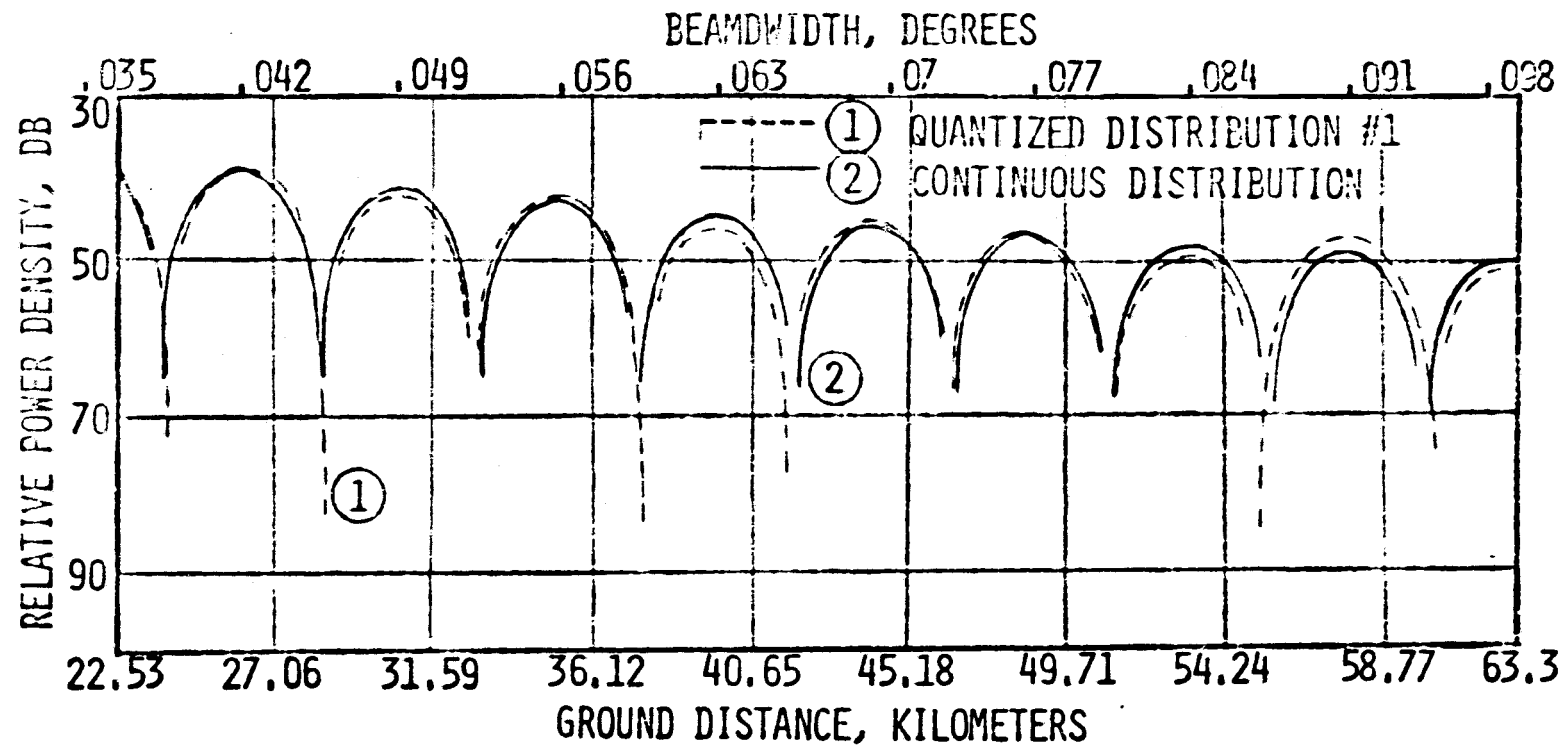
Spacetenna Size and Power Density Required For Fixed Rectenna Size and Power Output

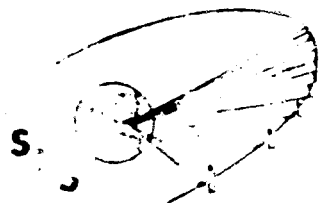
BOEING

- RECTENNA RADIUS TO FIRST NULL = 6,485 METERS
- DELIVERED GROUND POWER = 5GW
- ASSUMED RECTENNA EFFICIENCY = 88%



• COMPARISON OF FURTHER OUT SIDELOBES

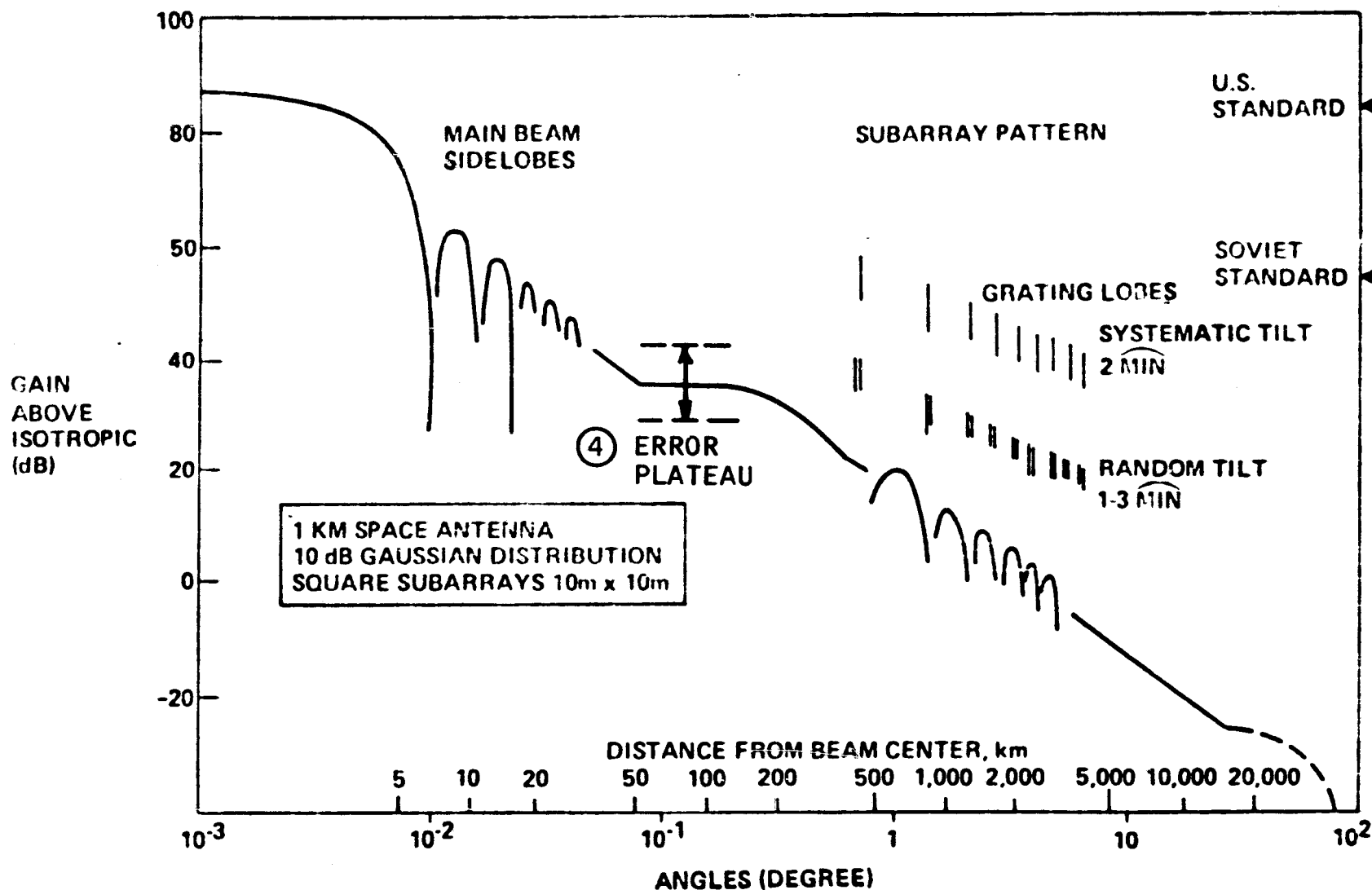




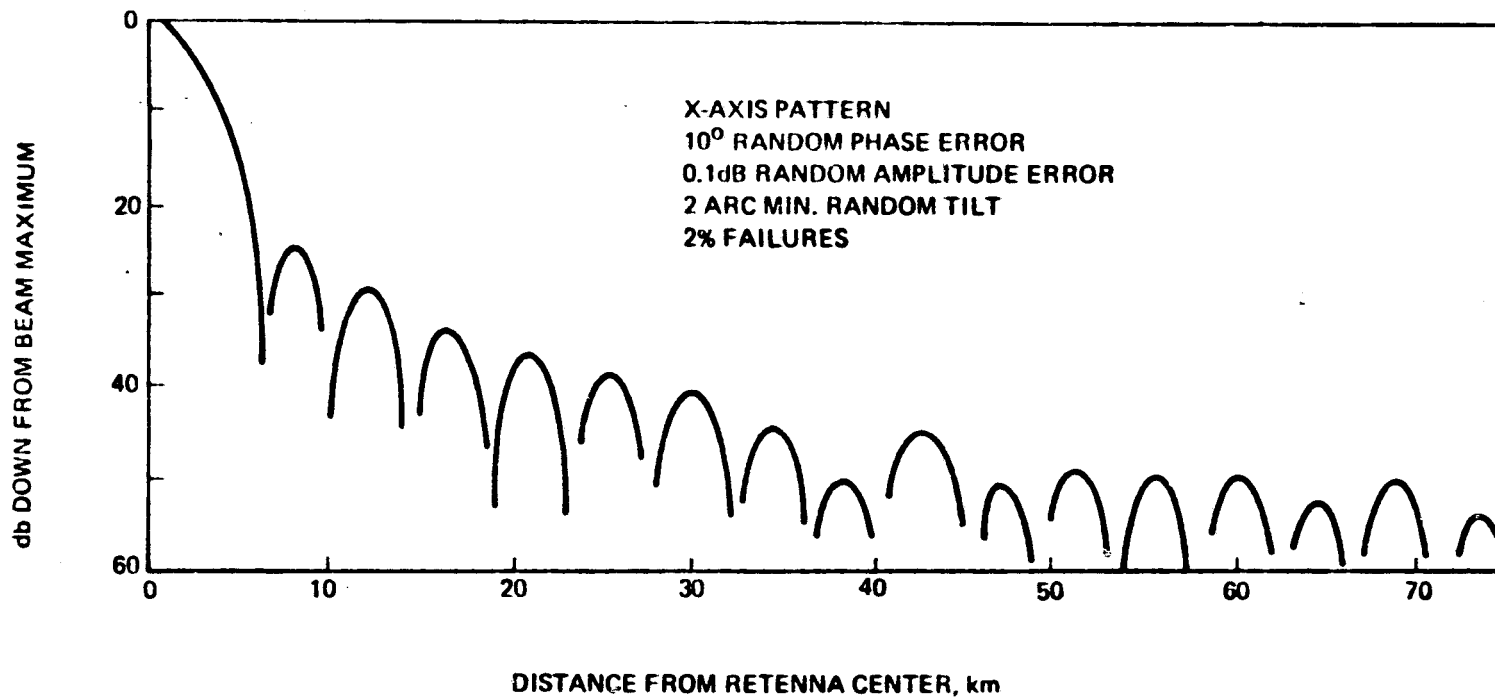
Array Pattern Roll-Off Characteristics

BOEING

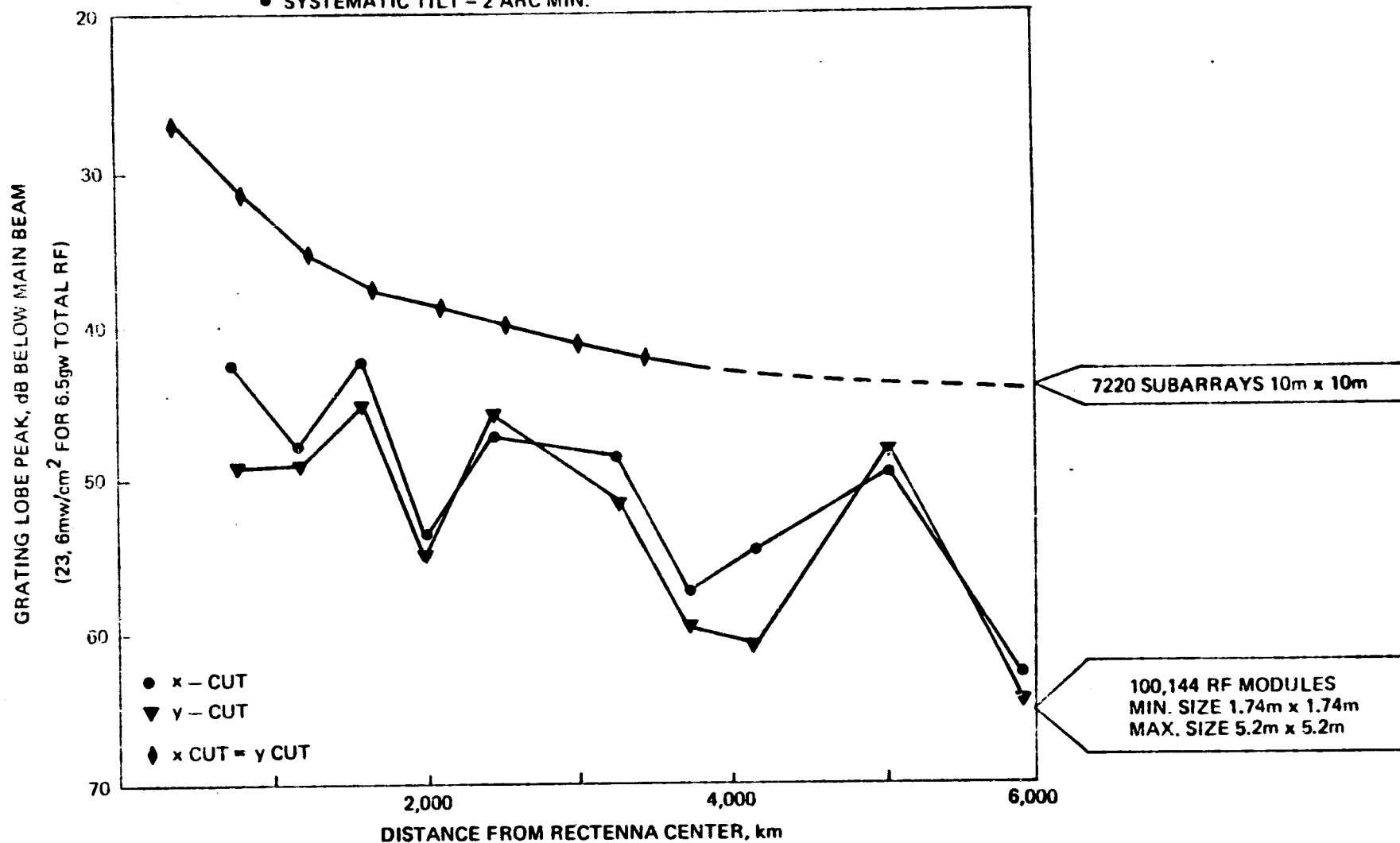
124



Space Antenna Roll-Off Characteristics



- GAUSSIAN ILLUMINATION FUNCTION 9.54 dB TAPER
- ARRAY DIA. = 1 km @ SYNCHRONOUS ORBIT, $F = 2.45$ GHz
- GRATING LOBE 3dB BEAMWIDTH = 5.5 km ($\theta = .0086^\circ$)
- SYSTEMATIC TILT = 2 ARC MIN.



Large Phased Array Simulation of Grating Lobes: Effect of Subarray Size

PEAK GRATING LOBE AMPLITUDES IMPINGING EARTH

SPS REFERENCE DESIGN
3DB BEAMWIDTH = 5.5km

100.144 RF MODULES
MODULE TILT 2 ARC MIN.

LEGEND (Values Below Main Beam)

● 10 $\mu\text{w}/\text{cm}^2$ (Soviet Standard)

● 40-45dB

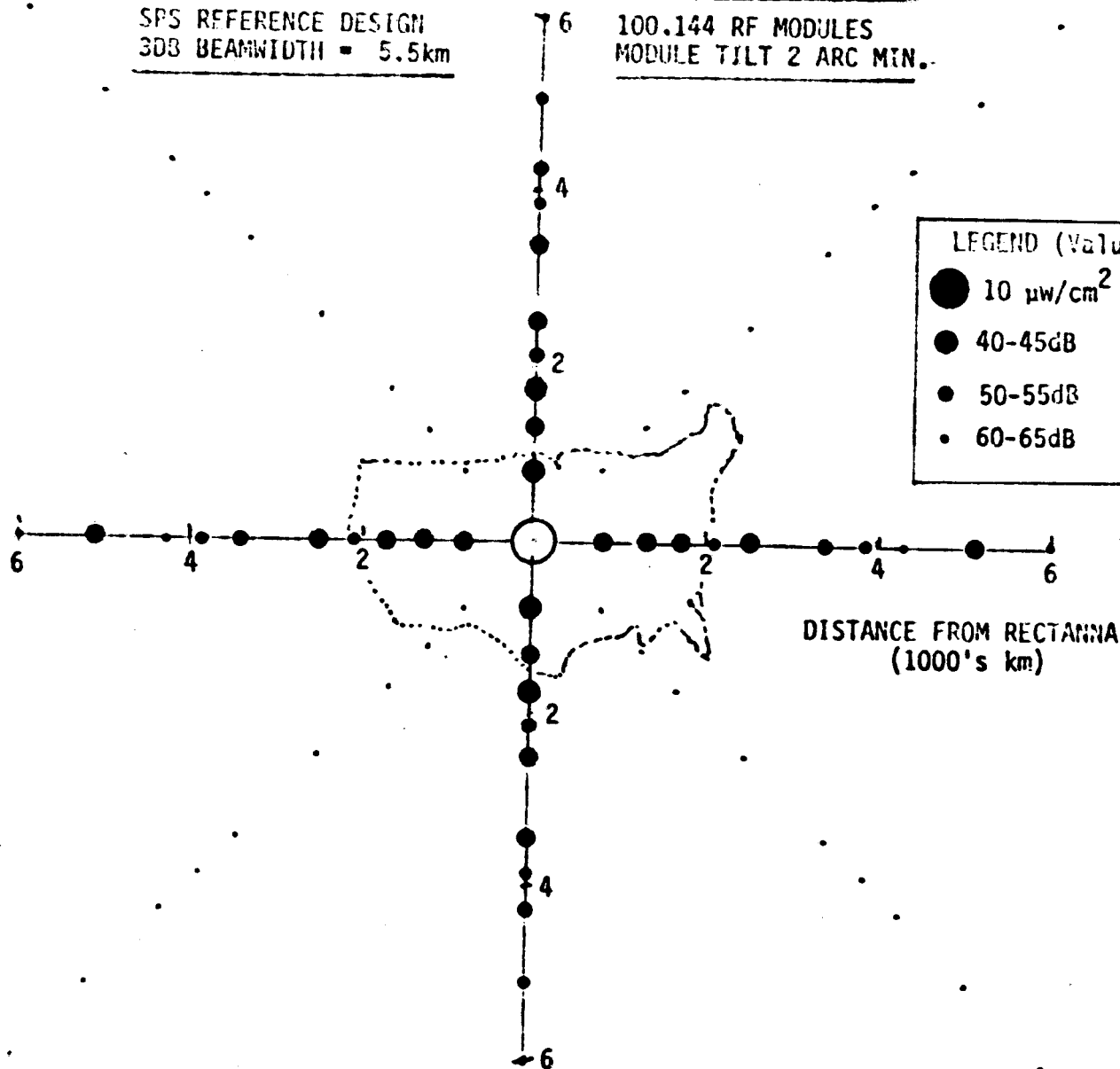
● 45-50dB

● 50-55dB

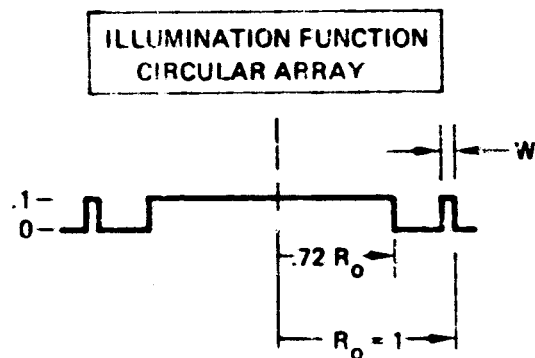
● 55-60dB

● 60-65dB

● <90dB

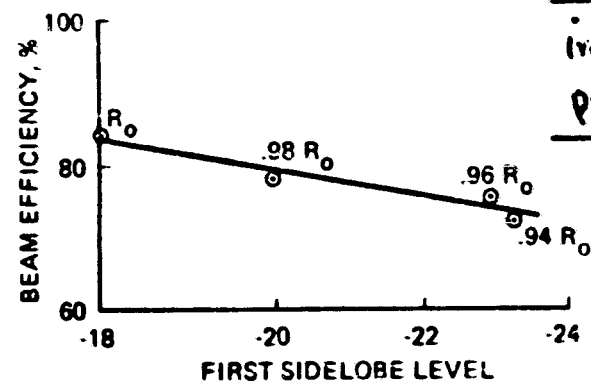


SPS Shaped Beam Synthesis



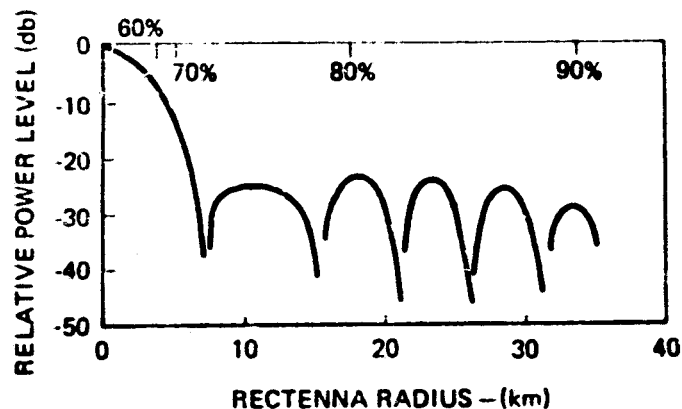
- AMPLITUDE TAPER: UNIFORM WITH SUPPRESSOR RING OF SOME AMPLITUDE
- PHASE OF SUPPRESSOR RING: $\phi = 0, 90^\circ, 180^\circ$ AS INDICATED

EFFECT OF RING WIDTH

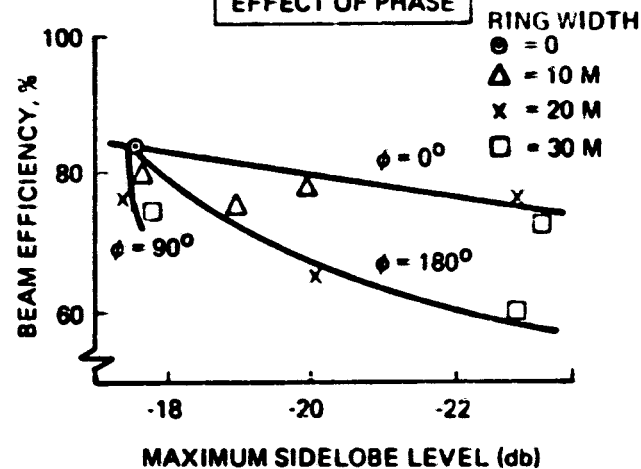


improved sidelobes
poorer efficiency

BEAM PATTERN & EFFICIENCY
 $R = .94 R_0$



EFFECT OF PHASE



SIDE LOBE SUPPRESSOR RING INVESTIGATION

- IN PHASE RINGS

- SIDE LOBES SUPPRESSED BY OUTBOARD RING
- EFFICIENCY REDUCED DUE TO SLOW RING SIDE LOBE ROLLOFF

- OUT OF PHASE RINGS

- S. L. SUPPRESSED BY INBOARD RING
- EFFICIENCY REDUCED DUE TO SLOW RING S. L. ROLLOFF

- QUADRATURE PHASE RING

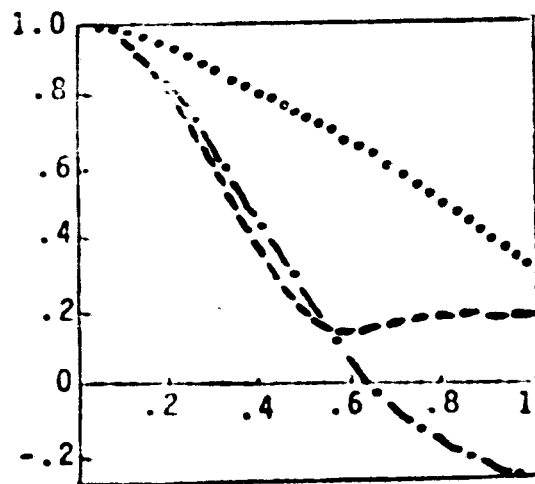
- S. L. NOT SUPPRESSED

- ROLLOFF

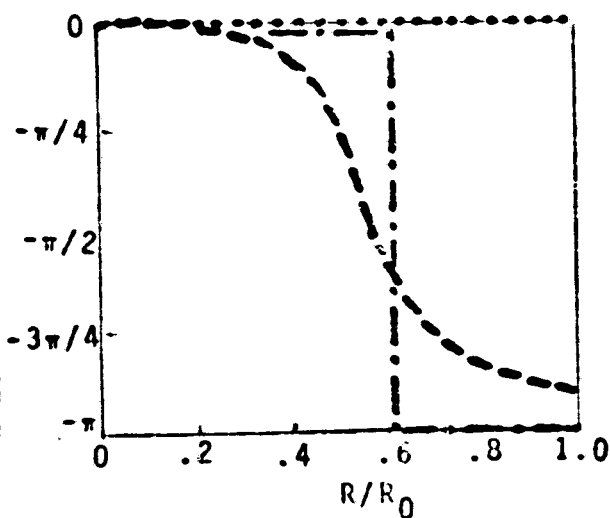
- RINGS: 10dB/DECADE
- REFERENCE DESIGN: 30dB/DECADE
- UNIFORM CIRCULAR APERTURE: 30dB/DECADE

BEAM PATTERN SYNTHESIS

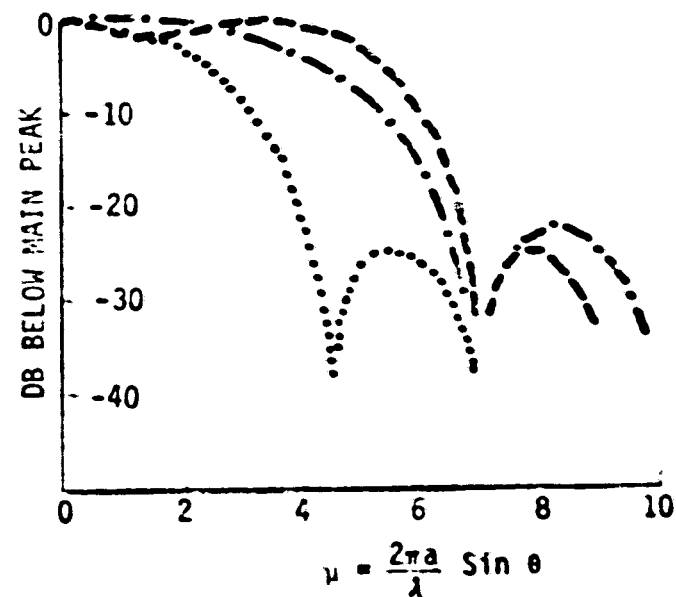
AMPLITUDE TAPER



PHASE TAPER



BEAM SHAPE



LEGEND

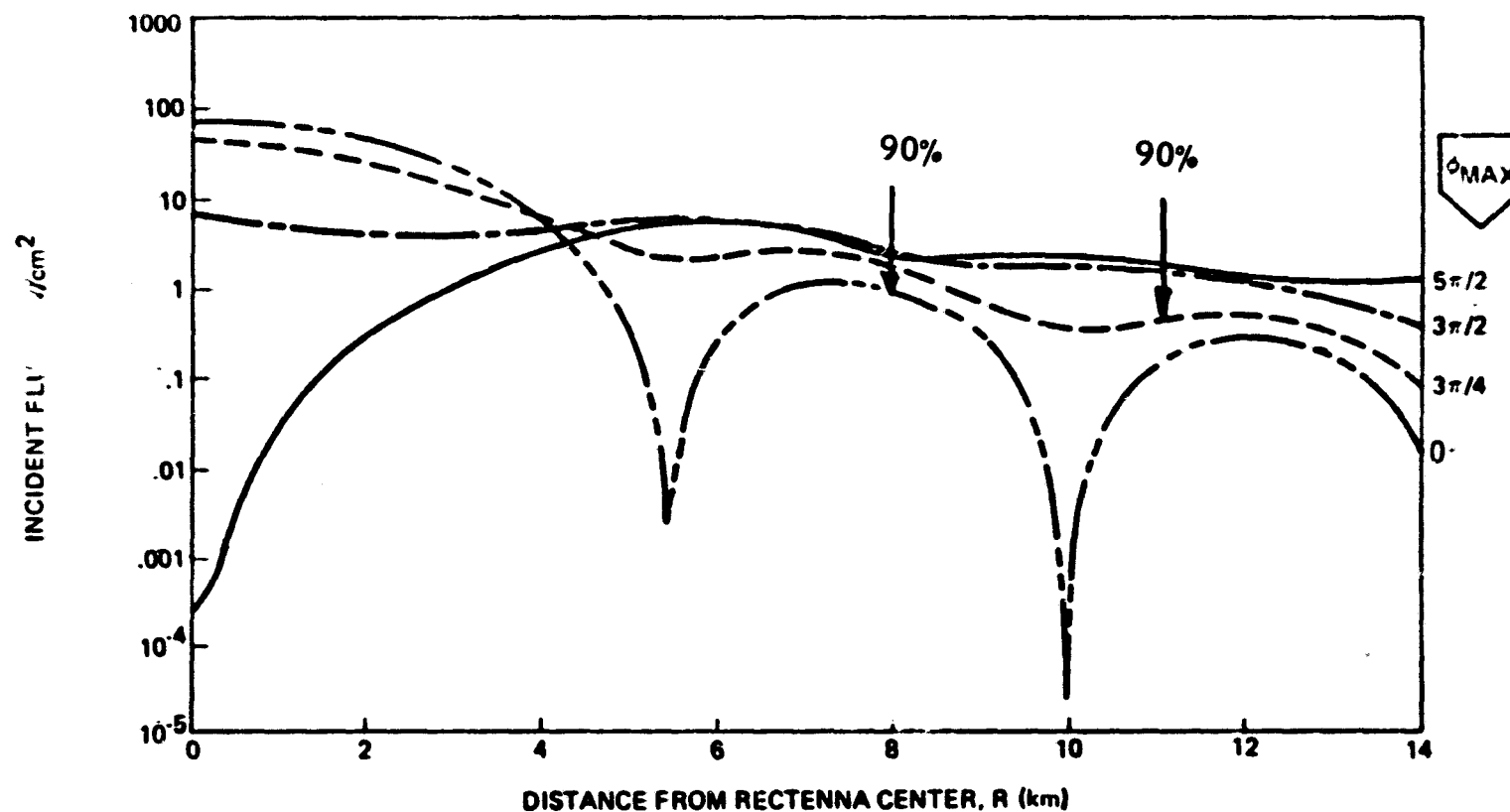
- GAUSSIAN 10DB TAPER
- .-.- REVERSE PHASE MAXIMAL FLATNESS (2 BEAM)
- .-.- CONTINUOUS PHASE SYNTHESIS

SPS Shaped Beam Synthesis

AMPLITUDE TAPER — UNIFORM

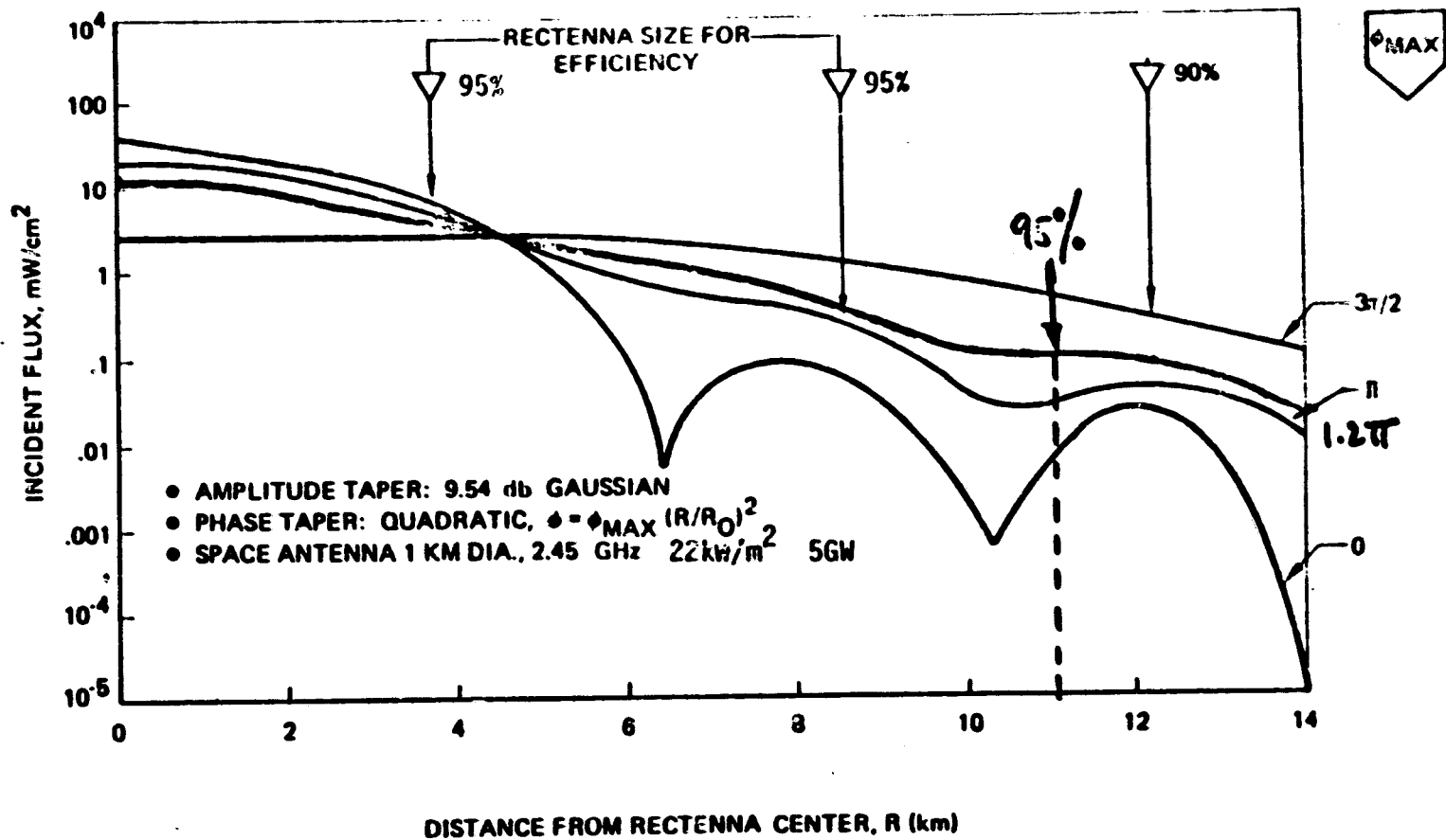
PHASE TAPER — QUADRATIC $\phi = \phi_{\text{MAX}} (R/R_0)^2$

SPACE ANTENNA 1 KM.DIA., 2.45 GHz 22kw/m^2 5GW



SPS Shaped Beam Synthesis

$$\phi = 1.2\pi (R/R_0)^2$$



ALTERNATE SPS DESIGNS USING BEAM DEFOCUSING
 QUADRATIC PHASE TAPER $\phi = \phi_{\text{MAX}}(R/R_0)^2$

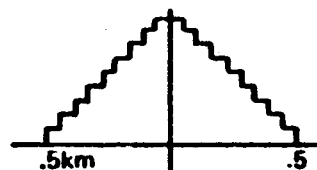
5GW 1KM 22KW/M ²					← KLYSTRON BASELINE 5GW
ϕ_{MAX}	PEAK ON AXIS POWER MW/CM ²	RECTENNA DIAM. KM	POWER FLUCTUATION CR. TO EDGE	EFFIC %	
0	23	10KM	23:1	97	
1.2π	5.8	22	35:1	95	
$3\pi/2$	2.1	28	48:1	92	
10GW 1.4KM 22KW/M ²					← POTENTIAL 10GW KLYSTRON DESIGN
1.2π	23	15.7KM	35:1	95	
2GW 1.5KM 5KW/M ²					← SOLID STATE SPS (BOEING)-2GW
1.2π	20 5.8	6.7 14.7	23:1 35:1	97 95	
4GW 2.1KM 5KW/M ²					← POTENTIAL SPS 4GW DESIGN
1.2π	20	10.5	35:1	95	

ILLUMINATION
FUNCTION

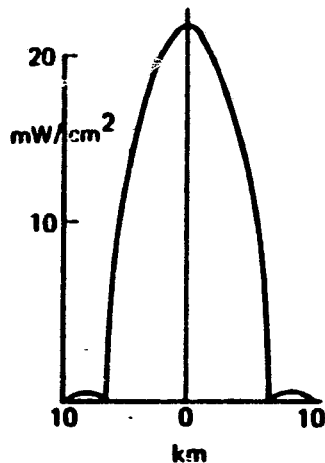
F = 2.45 GH
P = 6.5 GW
D = 1 KM
10M x 10 M
SUBARRAYS
 $k = 2\pi/\lambda$

BEAM SHAPE AT
RECTENNA

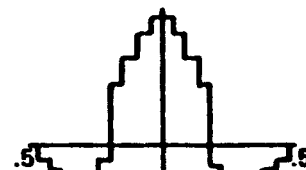
REFERENCE
DESIGN



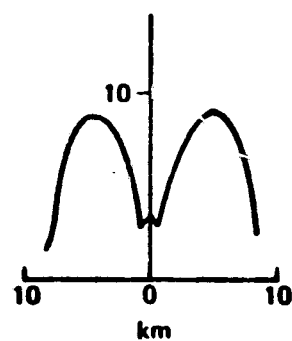
$A = A_1(R) = \text{QUANTIZED}$
10 dB GAUSSIAN TAPER



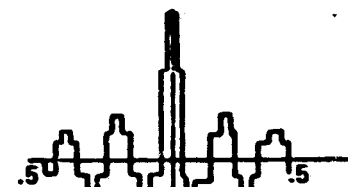
BEAM
SEPARATION
5 km



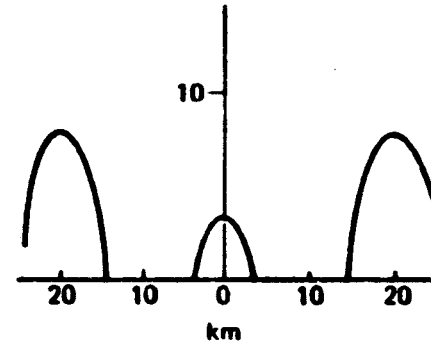
$\theta_1 = 1.5 \times 10^{-4}$ RAD
 $A = A_1(R) \cos(k \times \sin \theta)$



BEAM
SEPARATION
20 km



$\theta_1 = 6 \times 10^{-4}$ RAD



Multiple Beam Large Phased Array Simulation

25

***Antenna Construction
Techniques***

***R. Ried
Lyndon B. Johnson Space Center***

SLOPE & LINE-OF-SIGHT ARE SENSITIVE TO VARIATION IN STRUCTURAL PARAMETERS

VARIATION IN

STRUT LENGTH

JUNCTION
FITTINGS

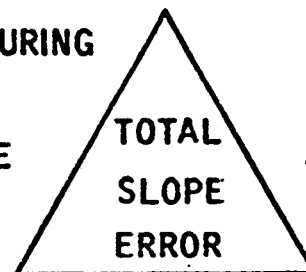
JOINT
TOLERANCE

MEASUREMENT
ACCURACY

TOOLING



MANUFACTURING
&
ASSEMBLY
TOLERANCE



MANEUVERING
&
ENVIRONMENTAL
ACCELERATIONS



FORCES & MOMENTS FROM

ATTITUDE
CONTROL

STATION-
KEEPING

ECLIPSE
PERTURBATIONS

ENVIRONMENT

THERMAL EXPANSION

$CTE \times TEMP \& E \times X-SECTION$

VARIATION IN

COEFFICIENT OF THERMAL EXPANSION

ABSORPTIVITY/EMISSION

RF SYSTEM HEAT DISSIPATION

THERMAL ENVIRONMENT



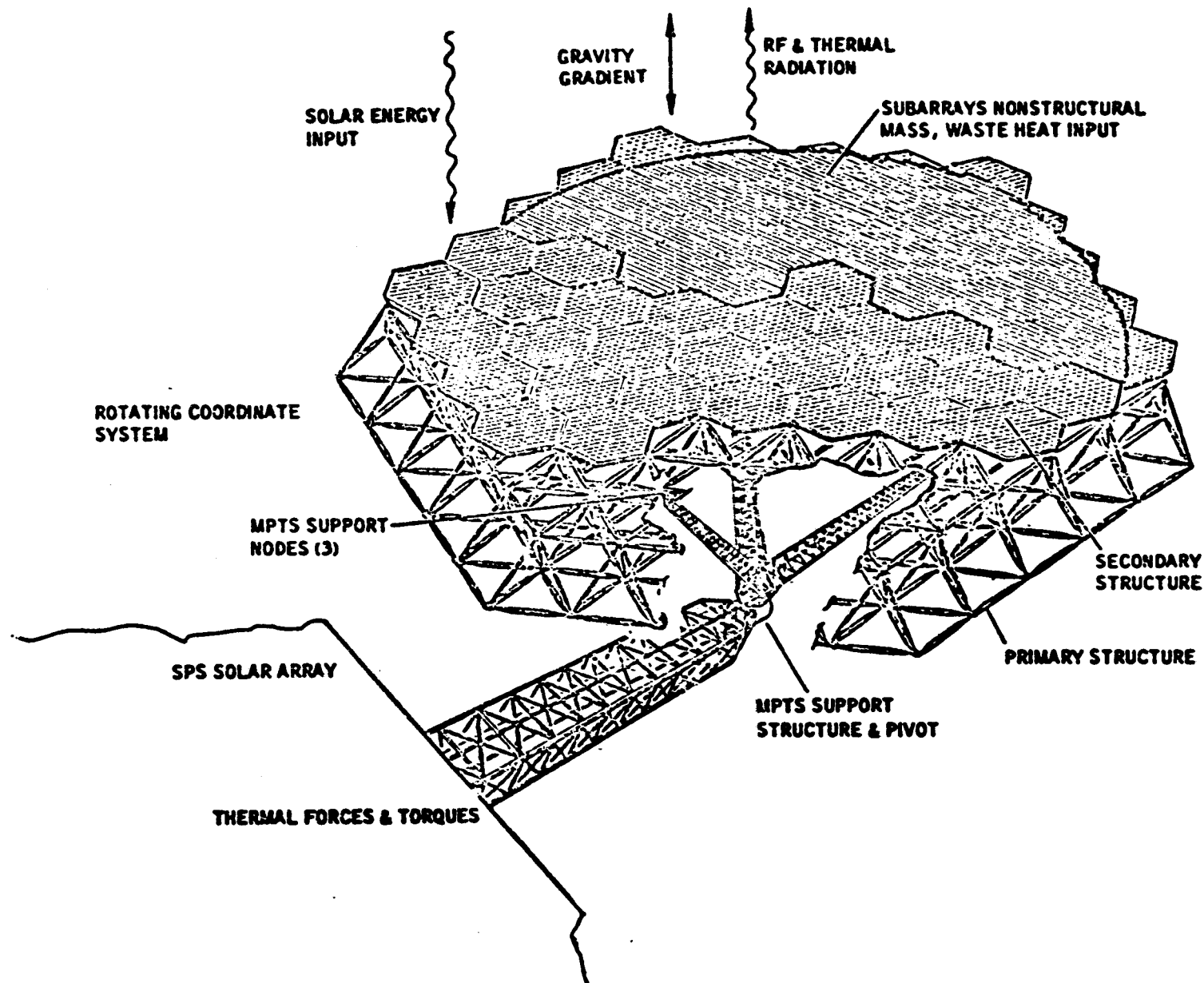
VARIATION IN

MODULUS OF ELASTICITY

STRUT CROSS-SECTIONAL AREA

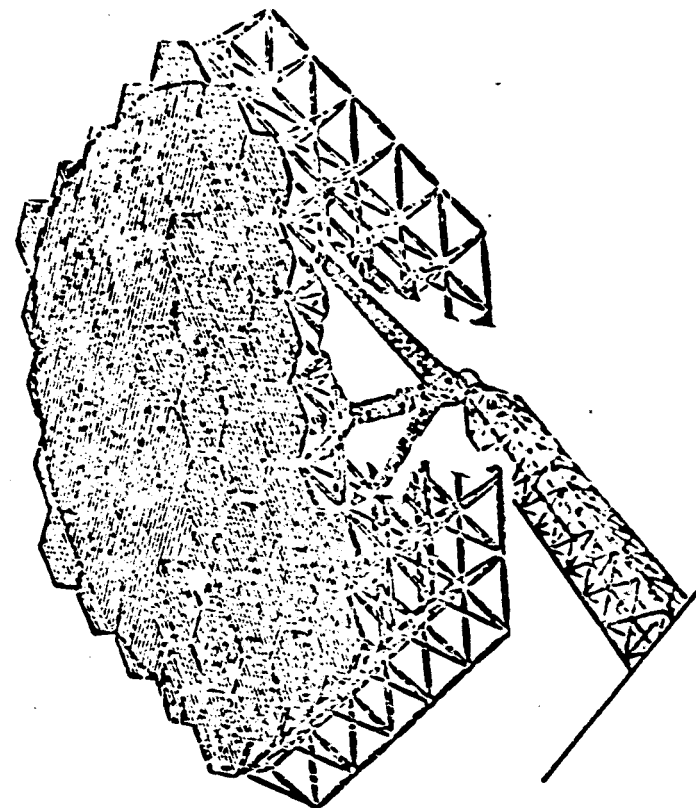
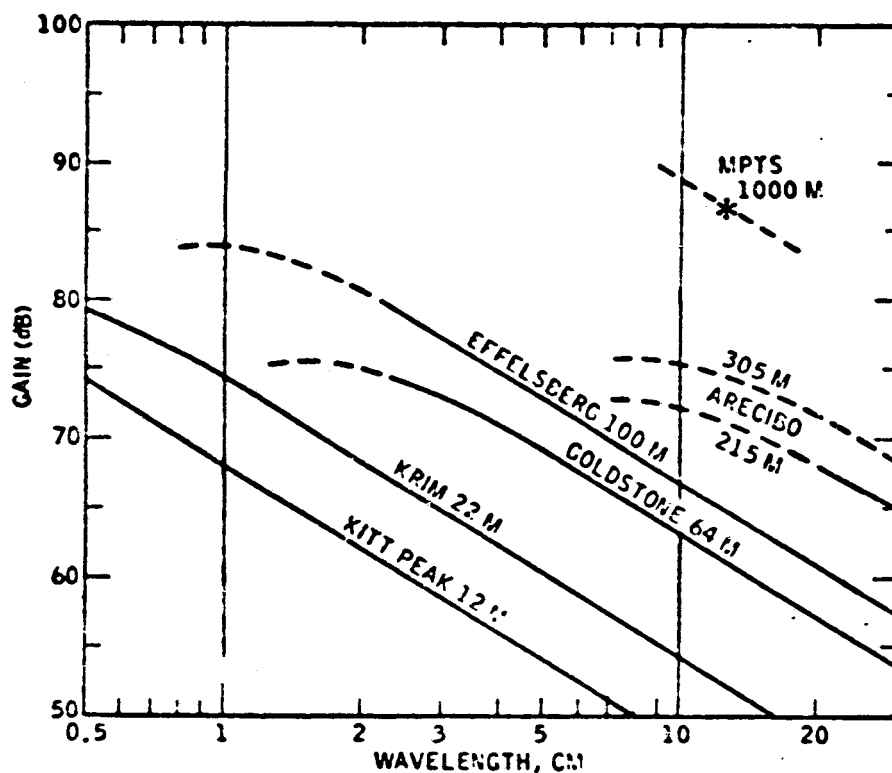


ACHIEVABLE FLATNESS DEPENDS ON MANUFACTURING TOLERANCE & THE OPERATIONAL ENVIRONMENTAL EFFECTS



THE MPTS WILL EXCEED THE GAIN OF THE LARGEST EXISTING MICROWAVE ANTENNAS

GENERAL DYNAMICS
Corvaair Division



ORIGINAL PAGE IS
OF POOR QUALITY

Type of antenna	Planar array
Diameter of aperture.....	1000 m (3281 ft)
Antenna mass	8.58 Mkg (18.92 x 10 ⁶ lb)
Power transmitted (CW).....	5 GW (67 dBW)
Frequency.....	2.45 GHz
Directivity	86 dB
Beamwidth (3-dB).....	31.4 arc sec
Mount — Azimuth range.....	360 degrees
Elevation range.....	+ 10 degrees
Slewing rates (maximum).....	1 arc sec/sec
Mechanical pointing accuracy.....	2 arc minutes
Electronic pointing accuracy.....	6 arc sec
Illumination taper.....	10 dB
Bandwidth — modulation	Not applicable

ACCURACY ERROR BUDGETS

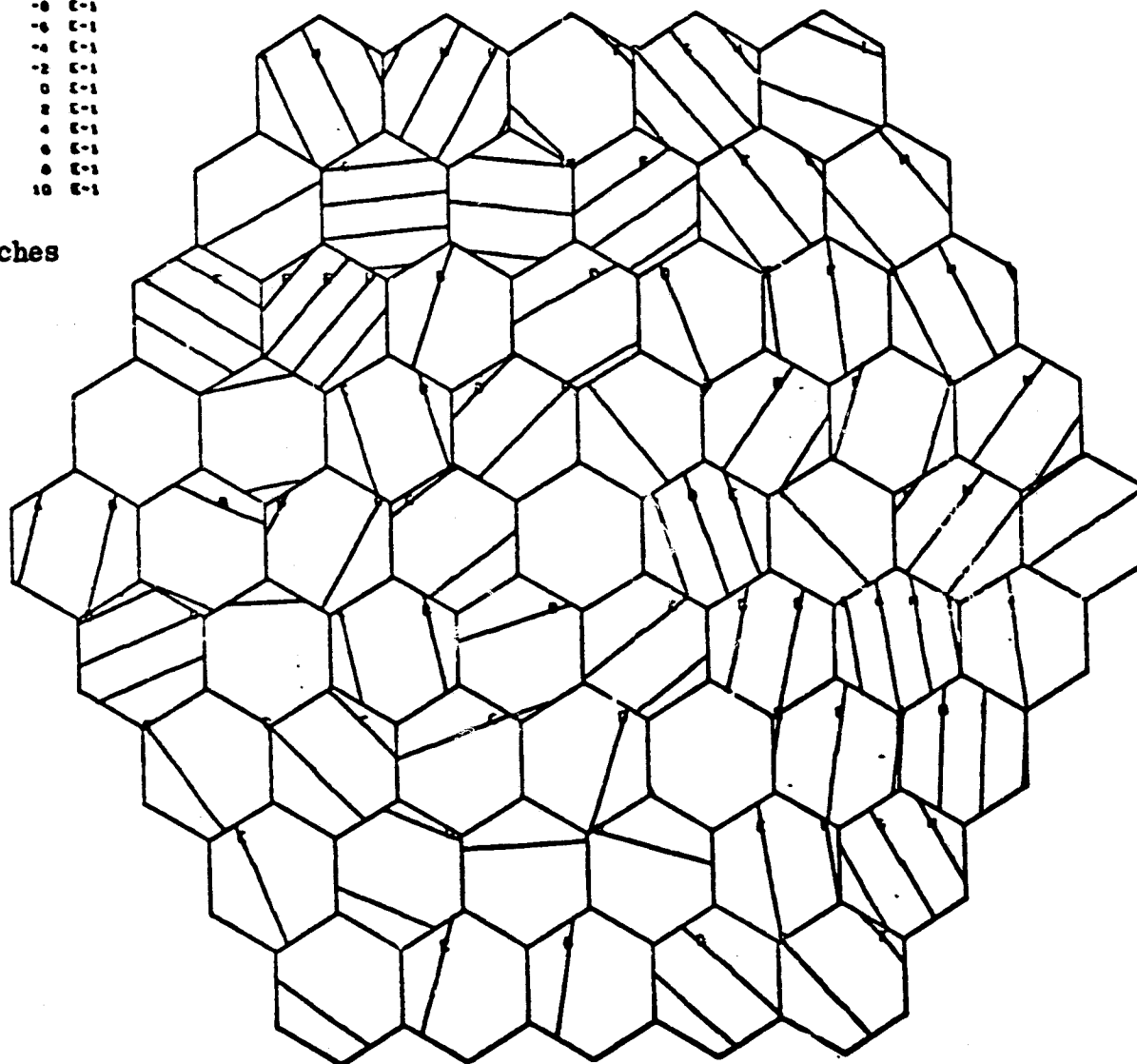
TOTAL BUDGET	SLOPE ERROR RMS ARC MIN <u>2.00*</u>	LOS ERROR MAX ARC MIN <u>2.00*</u>
<u>MANUFACTURING TOLERANCE</u>	<u>1.50</u>	<u>0.00</u>
PRIMARY STRUCTURE	0.64	0.00
PRIMARY/SECONDARY INTERFACE	0.06	0.00
SECONDARY STRUCTURE	1.32	0.00
SUBARRAY INTERFACE	0.32	0.00
<u>MANEUVERING ALLOWANCE</u>	<u>1.10</u>	<u>1.00</u>
PRIMARY DISTORTIONS	0.46	1.00
SECONDARY DISTORTIONS	1.00	0.00
<u>THERMAL ALLOWANCE</u>	<u>0.70</u>	<u>1.00</u>
PRIMARY DISTORTIONS	0.31	1.00
SECONDARY DISTORTIONS	0.63	0.00
<u>ATTITUDE CONTROL SYSTEM</u>	<u>0.00</u>	<u>1.41</u>

* TOTALS BY ROOT-SUM-SQUARE COMBINATION OF UNCORRELATED CONTRIBUTIONS

CONFIGURATION A DEFLECTIONS SIMULATED MANUFACTURING TOLERANCE

CONTOUR LABEL	LEVEL VALUE	
	*	
A	-8	E-1
B	-6	E-1
C	-4	E-1
D	-2	E-1
E	0	E-1
F	2	E-1
G	4	E-1
H	6	E-1
I	8	E-1
J	10	E-1

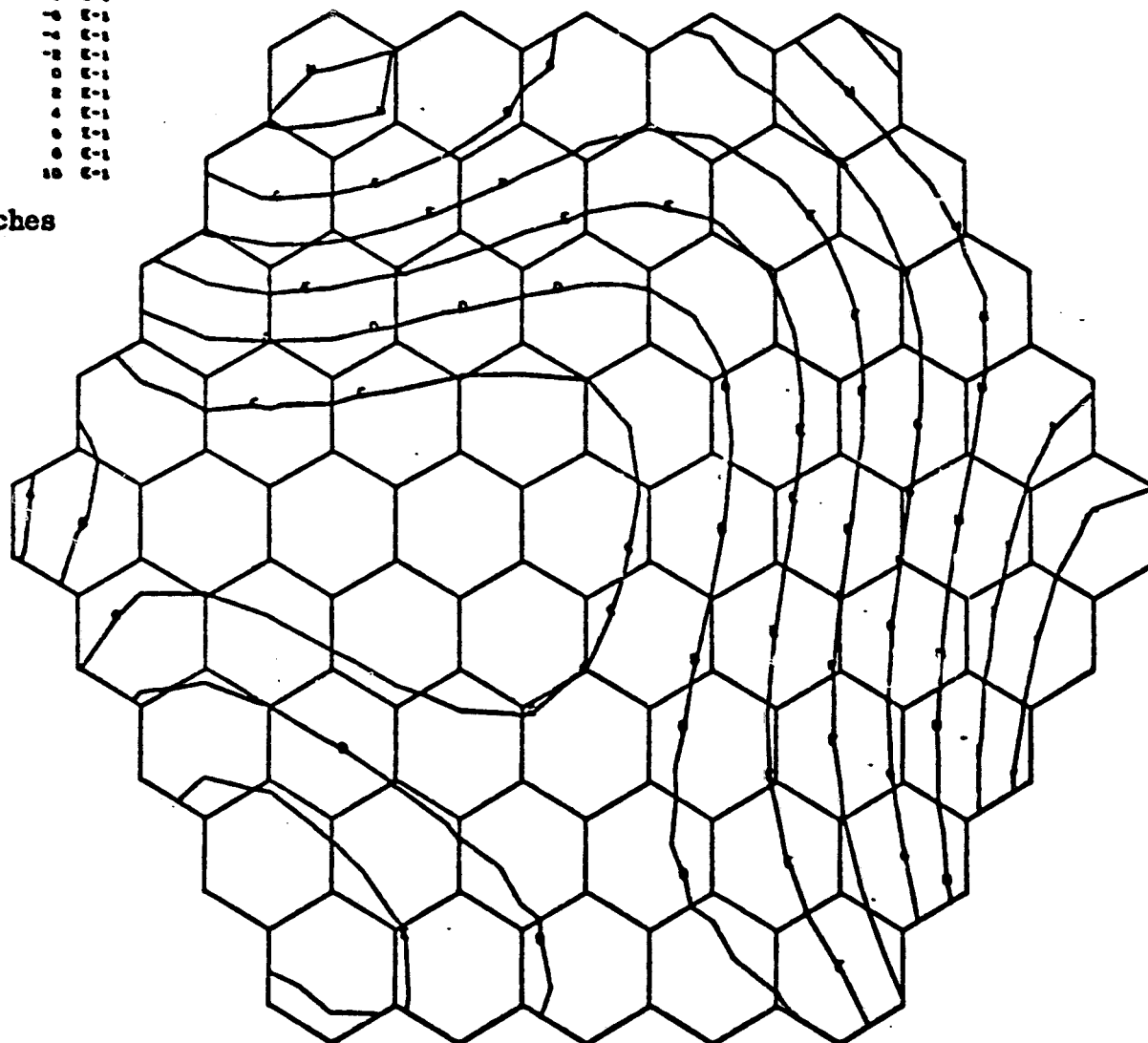
*Inches



CONFIGURATION B DEFLECTIONS SIMULATED MANUFACTURING TOLERANCE

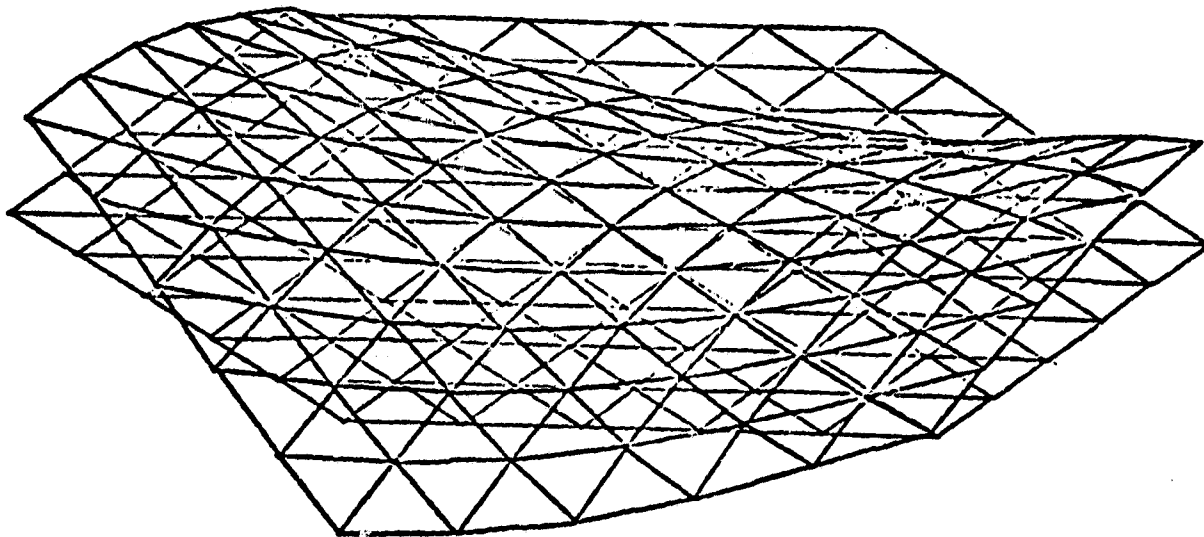
CONTOUR	LEVEL	VALUE
LABEL		
	*	
A	-8	E-1
B	-6	E-1
C	-4	E-1
D	-2	E-1
E	0	E-1
F	2	E-1
G	4	E-1
H	6	E-1
I	8	E-1
J	10	E-1

*Inches

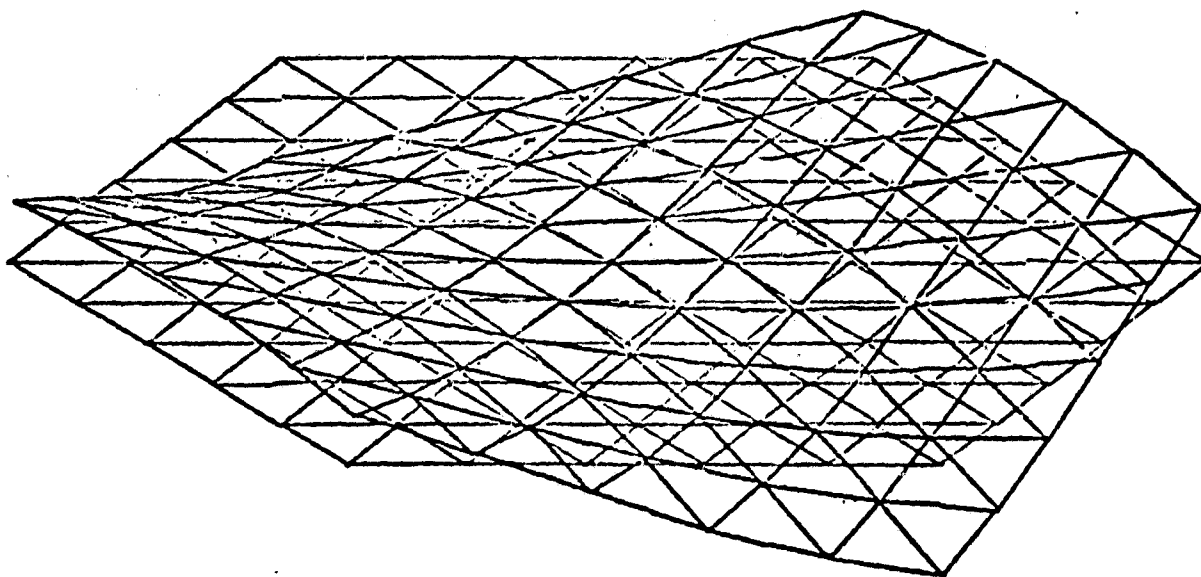


COMPARISON OF SLOPE ERROR FOR CONFIGURATIONS A & B

NUMBER OF CASES	LOADING CONDITION	SIMULATION	<u>RMS (B)</u> <u>RMS (A)</u>
3	LINEAR ACCELERATIONS	ENVIRONMENTAL & CONTROL FORCES	0.9842
3	ROTATIONAL ACCELERATIONS	ENVIRONMENTAL & CONTROL MOMENTS	0.9548
6	RANDOM TEMPERATURE DISTRIBUTIONS	MANUFACTURING TOLERANCE RANDOM CTE x TEMPERATURE	0.8930
1	GAUSSIAN 10-DB TEMPERATURE GRADIENT	AVERAGE CTE EFFECT	1.0203
6	RANDOM & 10-DB TAPER TEMPERATURE DISTRIBUTION	RANDOM CTE & TEMPERATURE TAPER	0.8253
23	STEADY-STATE TEMPERATURES	NONECLIPSE ORBITAL CONDITIONS	1.0112
9	TRANSIENT TEMPERATURES	ECLIPSE ORBITAL CONDITIONS	1.0065
1	UNIFORM TEMPERATURE	RANDOM E x X-SECTION	<u>1.0142</u>
TOTAL 52		AVERAGE	0.9701

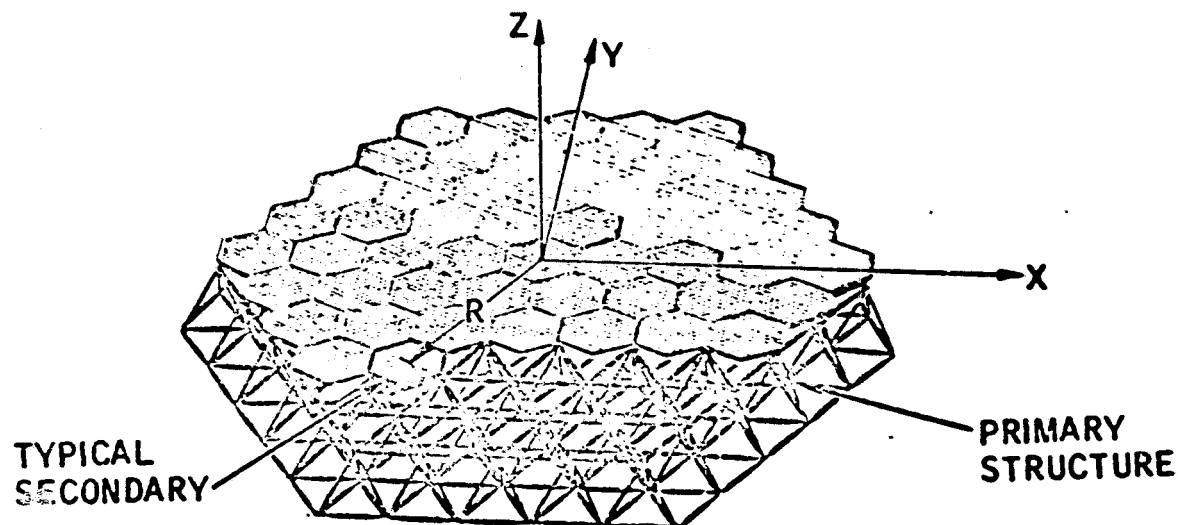


Baseline design, Mode 7, $f = 0.0848$ Hz.



Baseline design, Mode 8, $f = 0.0848$ Hz.

GENERALIZED RMS SLOPE ERROR (ARC MIN)
RESULTING FROM MANEUVERING ACCELERATIONS



ACCELERATION	PRIMARY STRUCTURE		SECONDARY STRUCTURE	OFFSET CG ALLOWANCE	TOTAL RMS SLOPE ERROR
	CONFIG. A	CONFIG. B			
10 ⁻³ G X	0.668	0.653	0.349		0.754
10 ⁻³ G Y	0.668	0.653	0.349		0.754
10 ⁻³ G Z	0.576	0.574	1.697		1.792
1 ARC SEC/SEC ² X	0.302	0.295	0.055	0.409	0.511
1 ARC SEC/SEC ² Y	0.302	0.295	0.055	0.409	0.511
1 ARC SEC/SEC ² Z	0.019	0.017	0.003	0.059	0.062

TYPICAL WASTE HEAT CALCULATION

$$r/R \leq 0.15$$

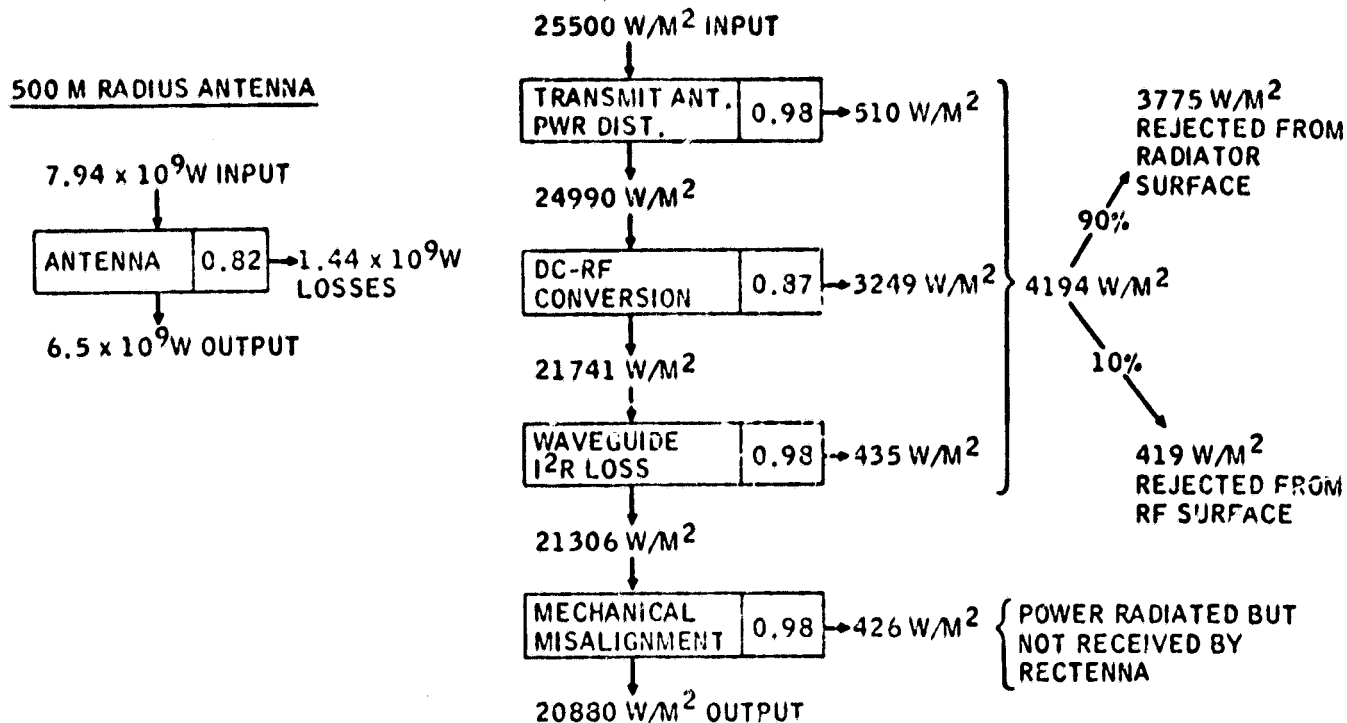
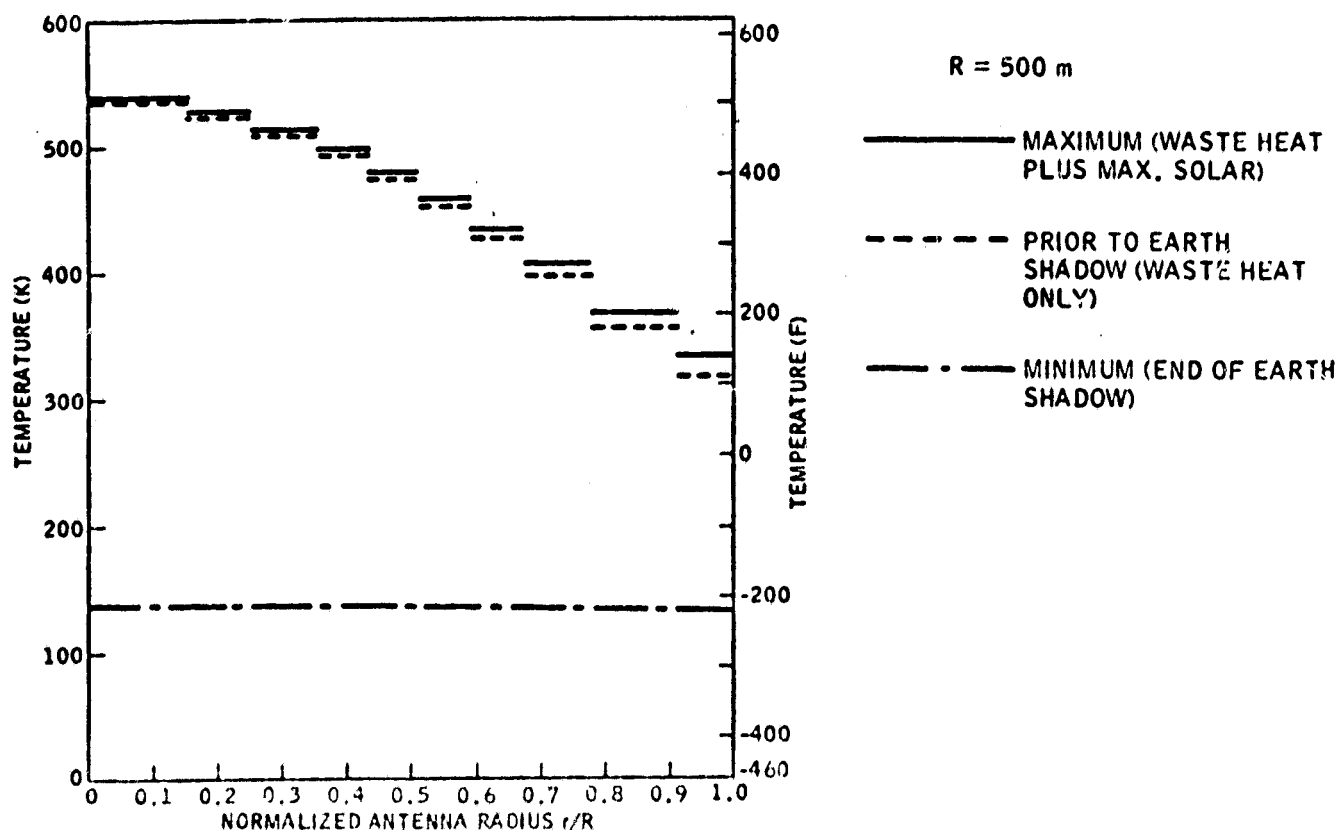


Figure 3-5. Antenna efficiency and waste heat assumptions.



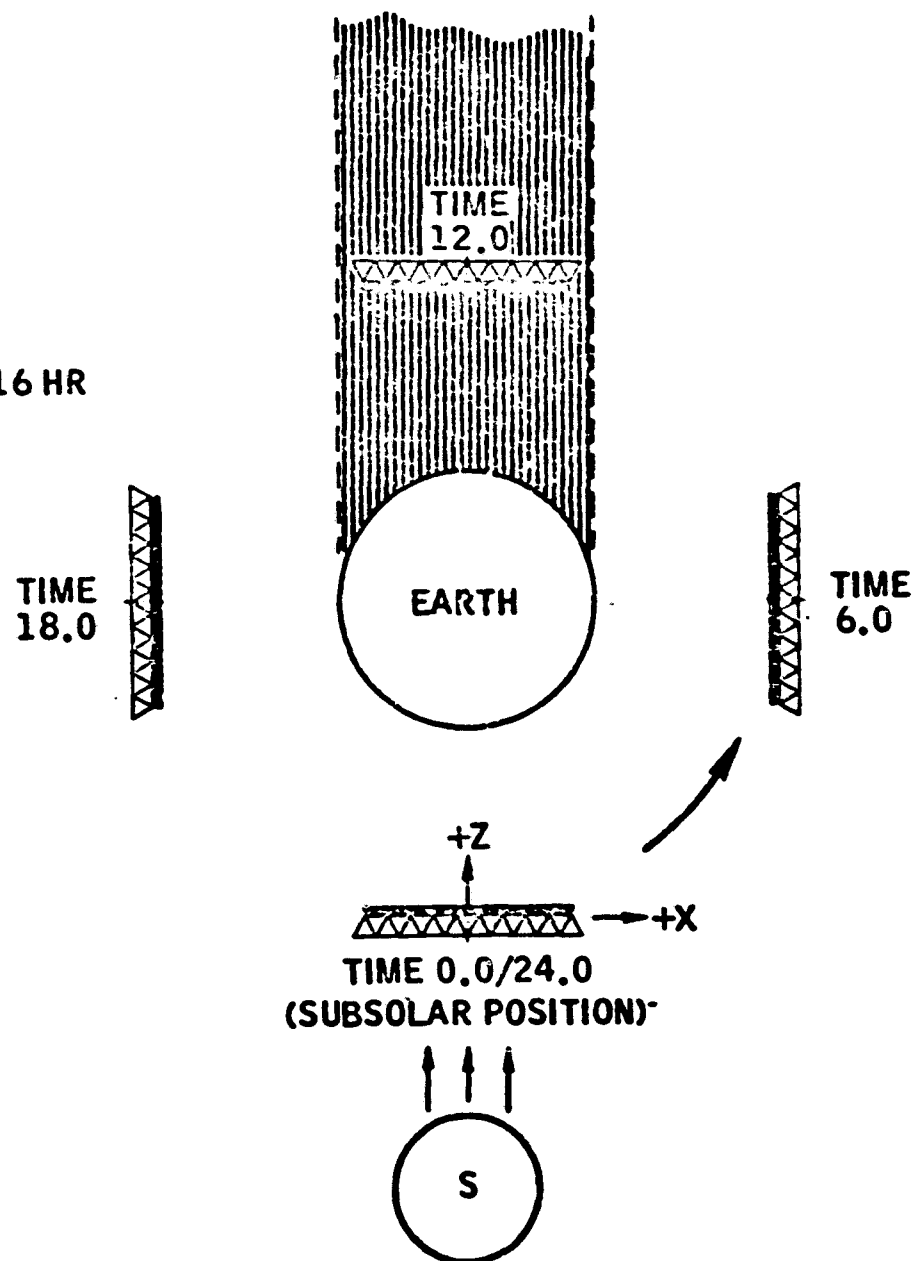
Radiator temperature distribution boundary conditions for thermal analysis.

ORBIT CHARACTERISTICS FOR THERMAL ANALYSIS

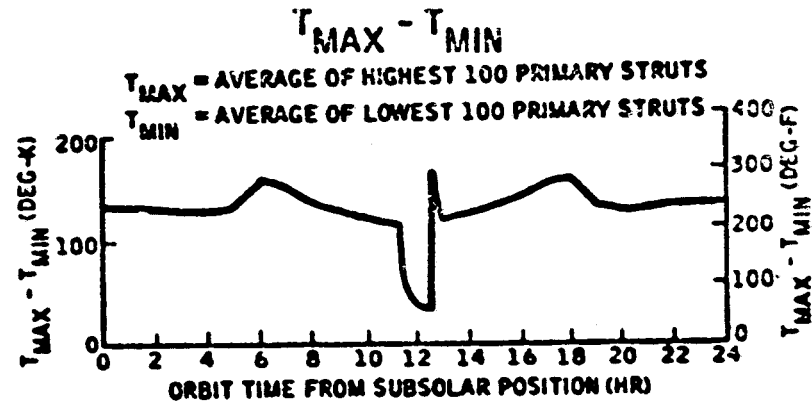
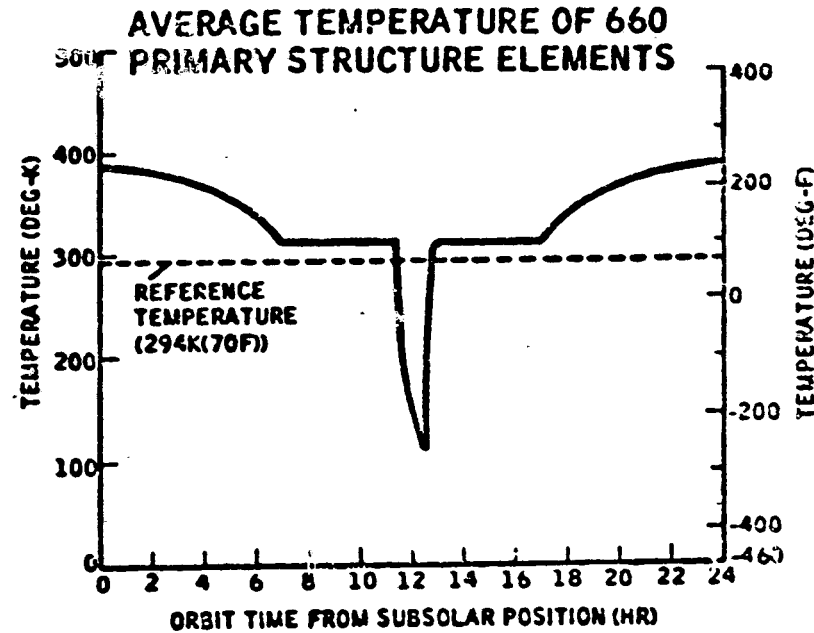
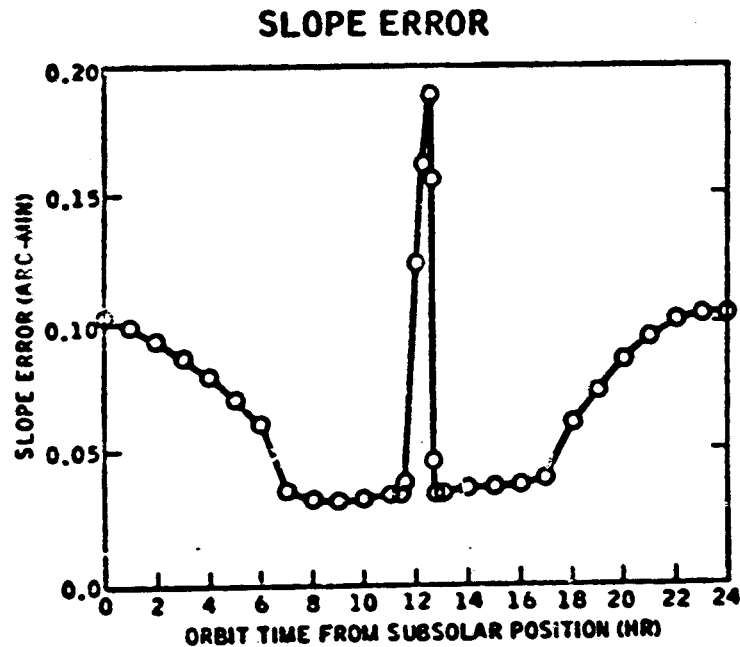
ORBIT ALTITUDE: 19325 NMI

ORBIT PERIOD: ≈ 24.0 HR

MAXIMUM EARTH ECLIPSE TIME: ≈ 1.16 HR



THERMAL SLOPE ERRORS ARE SMALL, BUT OPERATIONAL
TEMPERATURE EXTREMES ARE CRITICAL TO MATERIAL SELECTION



MAXIMUM OPERATING TEMPERATURES OF CURRENT RESINS

- PREDICTED TEMPERATURE EXTREMES IN MPTS ANTENNA (PRIMARY)

82.5K (-312F) TO 505K (449F)

- TYPICAL LONG TERM MAXIMUM OPERATING TEMPERATURES

— THERMOSETTING RESINS

EPOXY	394K (250F)
PHENOLIC	422 - 436K (300 - 325F)
POLYIMIDE	
ADDITION	477K (400F)
CONDENSATION	533 - 561K (500 - 550F)

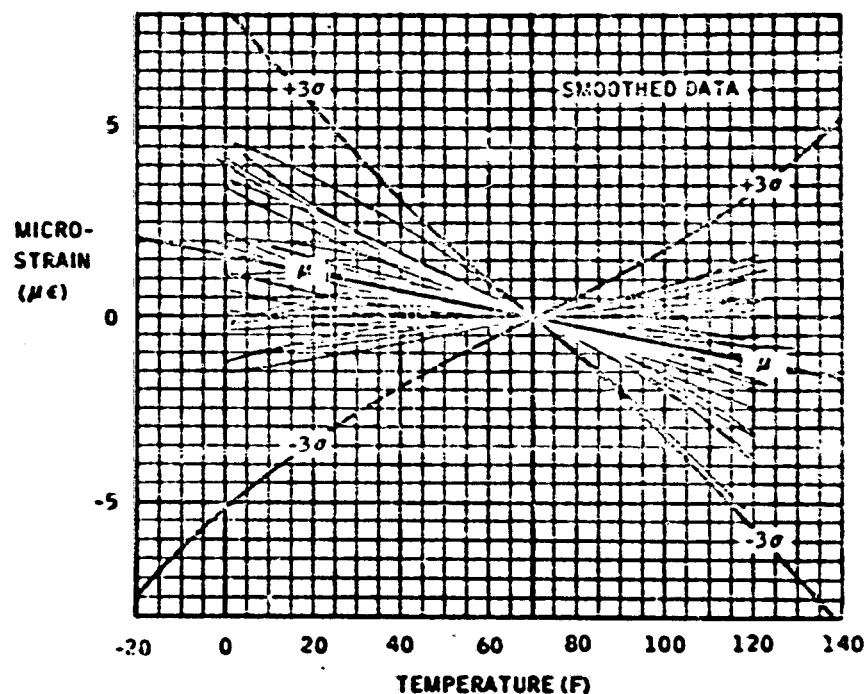
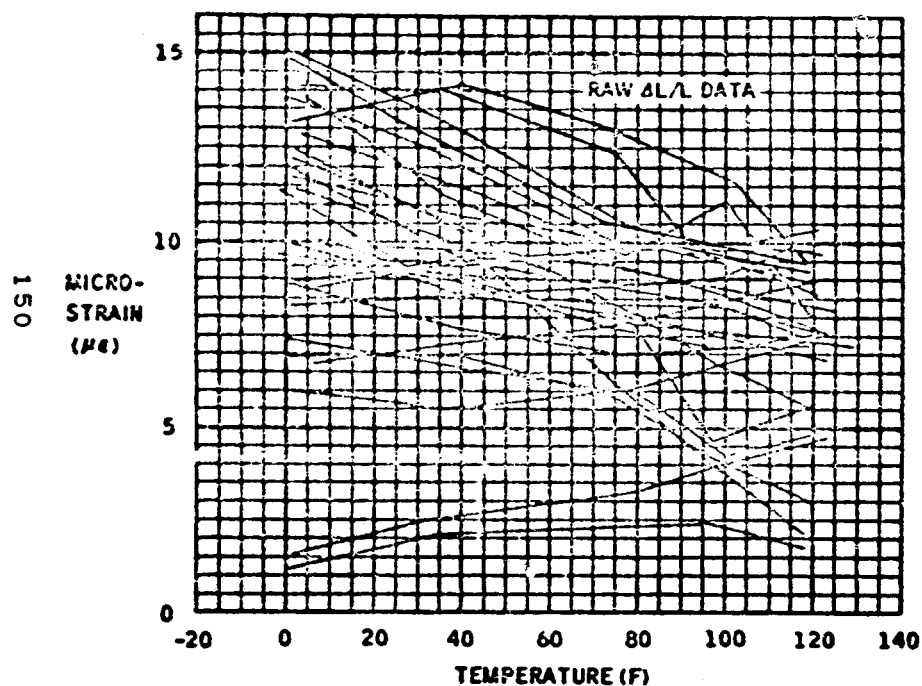
— THERMOPLASTIC RESINS

POLYSULFONE	381K (225F)
POLYIMIDE	589K (600F)

- CURRENT SYSTEMS ARE THEREFORE AVAILABLE BUT MORE TESTING IS REQUIRED TO CHARACTERIZE PROPERTIES OVER THE WIDE TEMPERATURE RANGE.

COMPUTER ANALYSIS OF DATA IS USED TO GENERATE STATISTICAL DISTRIBUTION OF COMPOSITE PROPERTIES

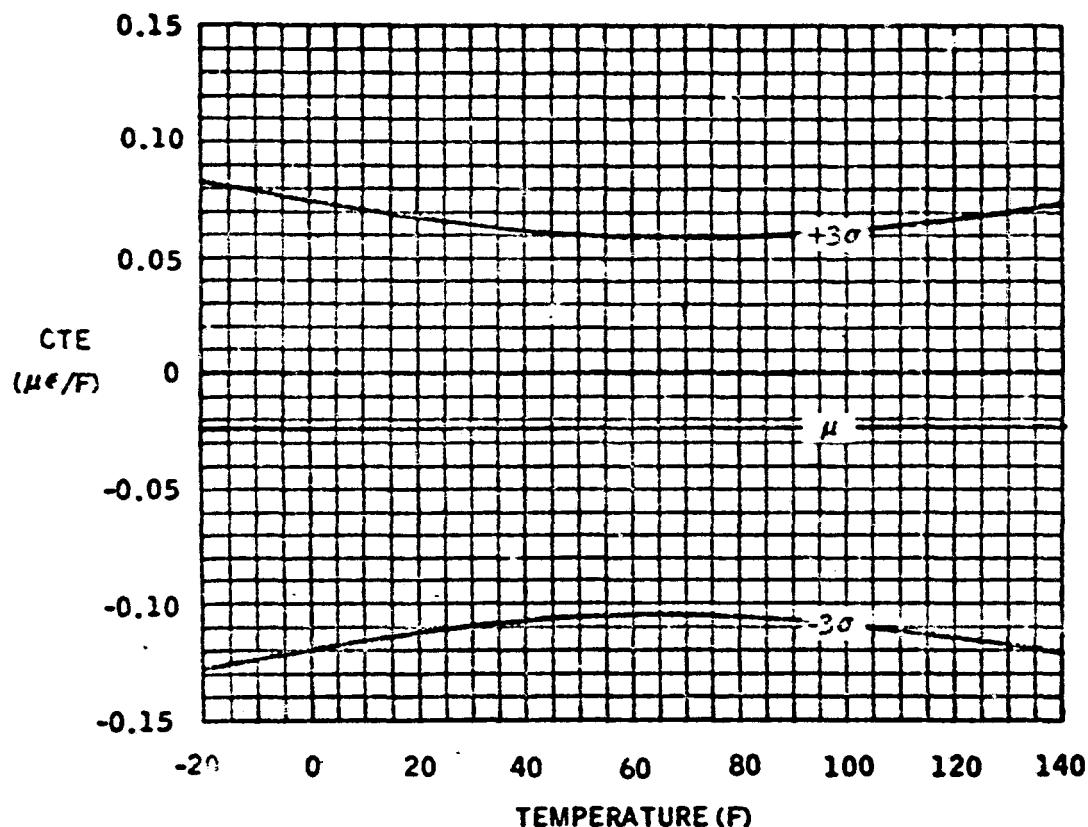
GY-70/X-30 PSEUDOISOTROPIC
(0, 45, 90, 135)_S
29 SPECIMENS



LASER DILATOMETER MEASUREMENT
OF VARIATION IN LENGTH WITH TEMPERATURE

COEFFICIENT OF THERMAL EXPANSION HAS TEMPERATURE DEPENDENCY & RANDOM COMPONENTS

$$CTE = f(T) =$$



$$-2.29 \times 10^{-8}$$

$$+2.71 \times 10^{-8} G$$

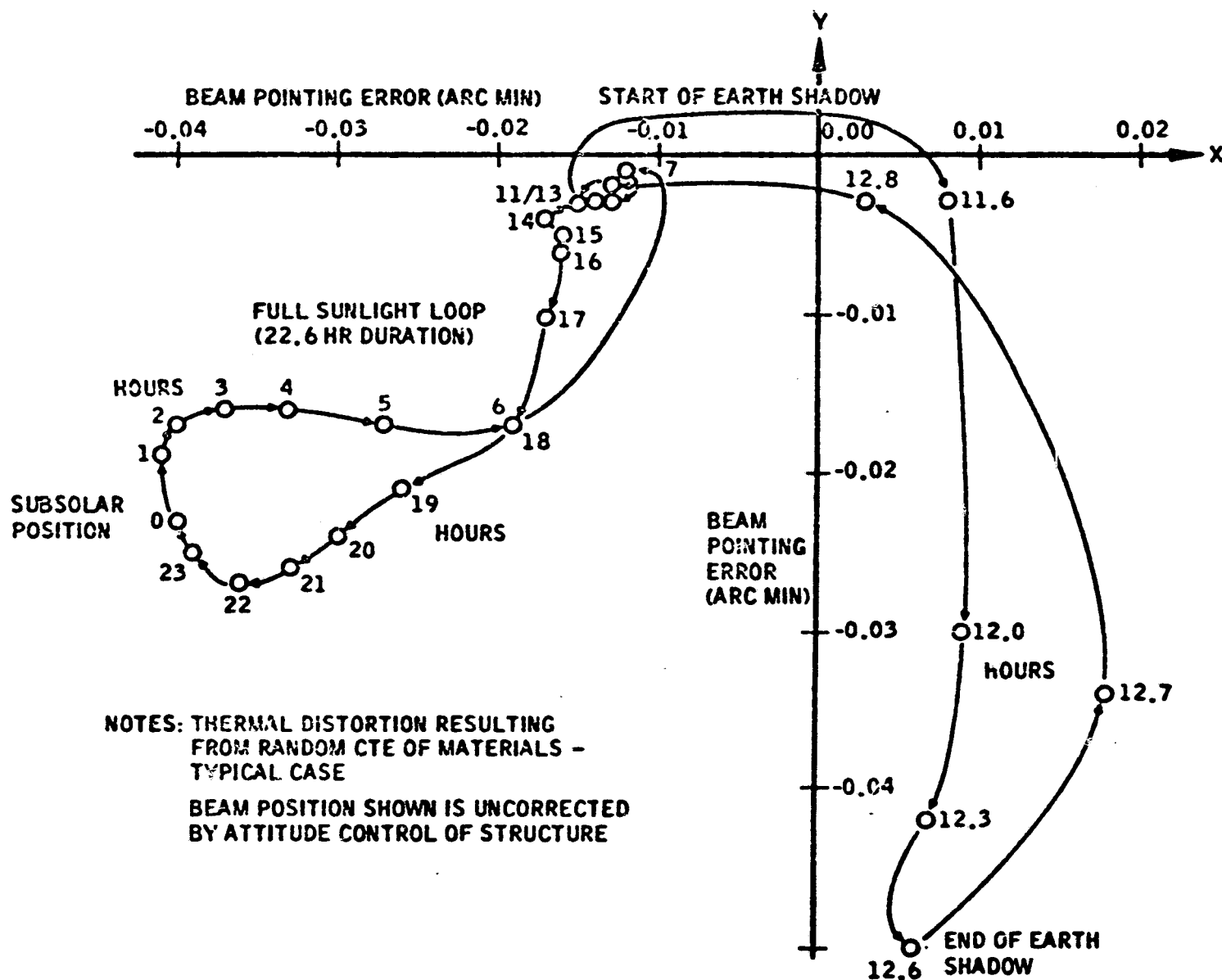
$$-2.30 \times 10^{-12} (T-70)$$

$$+2.52 \times 10^{-10} (T-70) G$$

WHERE G IS A RANDOM
GAUSSIAN VARIABLE WITH
ZERO MEAN & UNIT STANDARD
DEVIATION

(1) 70/X-30 PSEUDO ISOTROPIC
(0, 45, 90, 135)_S

TYPICAL BEAM WANDER OVER 24-HR ORBIT RESULTING FROM THERMAL DISTORTION OF PASSIVE STRUCTURE



INITIAL SLOPE ACCURACY BUDGET

	<u>ARC MIN.</u>	<u>PERCENT EFFICIENCY (LOSS)</u>
REQUIRED SLOPE ACCURACY	3	98.0 (2.0)
RMS SLOPE EQUIVALENT	3	98.0 (2.0)
RMS SLOPE DESIGN GOAL	2	99.0 (1.0)
MANUFACTURING TOLERANCE	1.5	99.5 (0.5)
MANEUVERING ACCELERATIONS	1.1	99.7 (0.3)
THERMAL DISTORTIONS	0.7	99.8 (0.2)

- MANUFACTURING TOLERANCE CAN BE MET WITH STATE-OF-THE-ART TOOLING & ASSEMBLY TOLERANCES.
- ACTUAL SLOPE ERRORS ARE INSIGNIFICANT EXCEPT FOR POSSIBLE OSCILLATIONS AFTER OCCULTATION.
- THERMAL DISTORTIONS ARE SMALL FOR STATE-OF-THE-ART GRAPHITE/EPOXY MATERIAL PROPERTIES.

Subarray Alignment Techniques

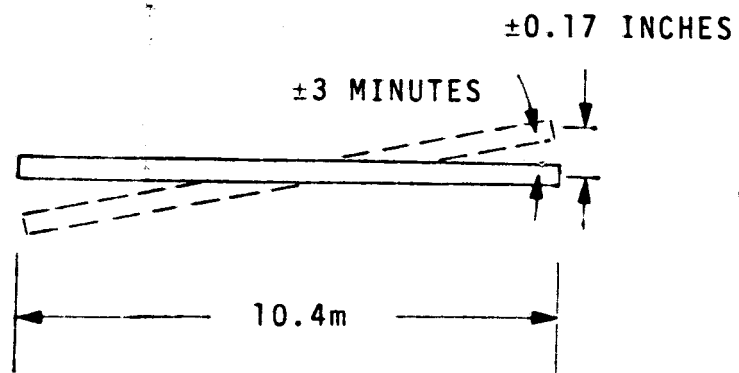
R. Iwasaki
Axiomatix

PRECEDING PAGE BLANK NOT FILMED

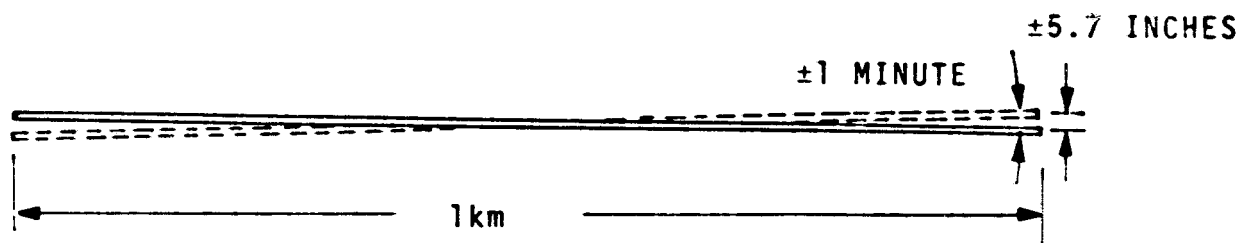
PRECEDING PAGE BLANK NOT FILMED

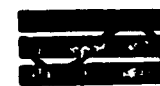
SUBARRAY ALIGNMENTS, BOTH INITIALLY AND REAL-TIME, CAN BE MAINTAINED TO ± 3 MIN BY THE USE OF AZ-E1 MOUNTS AND LASER MEASUREMENT TECHNIQUES.

SUBARRAY



ARRAY





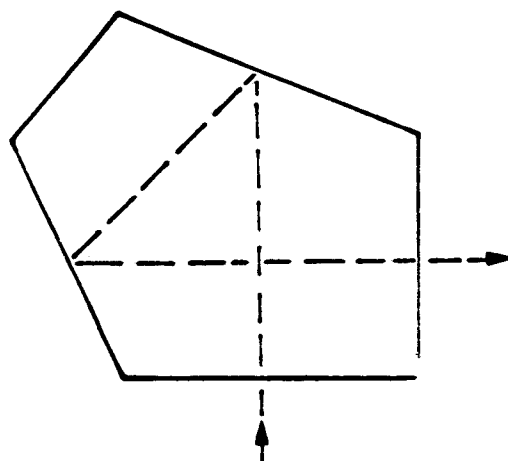
- I LASER BEAM REFERENCE SYSTEM
- II PHOTOCONDUCTIVE SENSORS
- III VARIABLE LENGTH MECHANISMS
- IV THREE POINT SUPPORT
- V MONOPULSE POINTING OF ARRAY

1. COMMERCIALY AVAILABLE FOR CONSTRUCTION APPLICATIONS
2. ROTATING LASER BEAM TO GENERATE OPTICAL REFERENCE PLANE
3. VARIABLE SPEED OF ROTATION
4. PERPENDICULARITY ASSURED BY PENTAPRISM REFLECTOR
5. COLLIMATOR REQUIRED FOR LONG DISTANCES
6. BLOCKAGE "CELLS"
7. REDUNDANCY

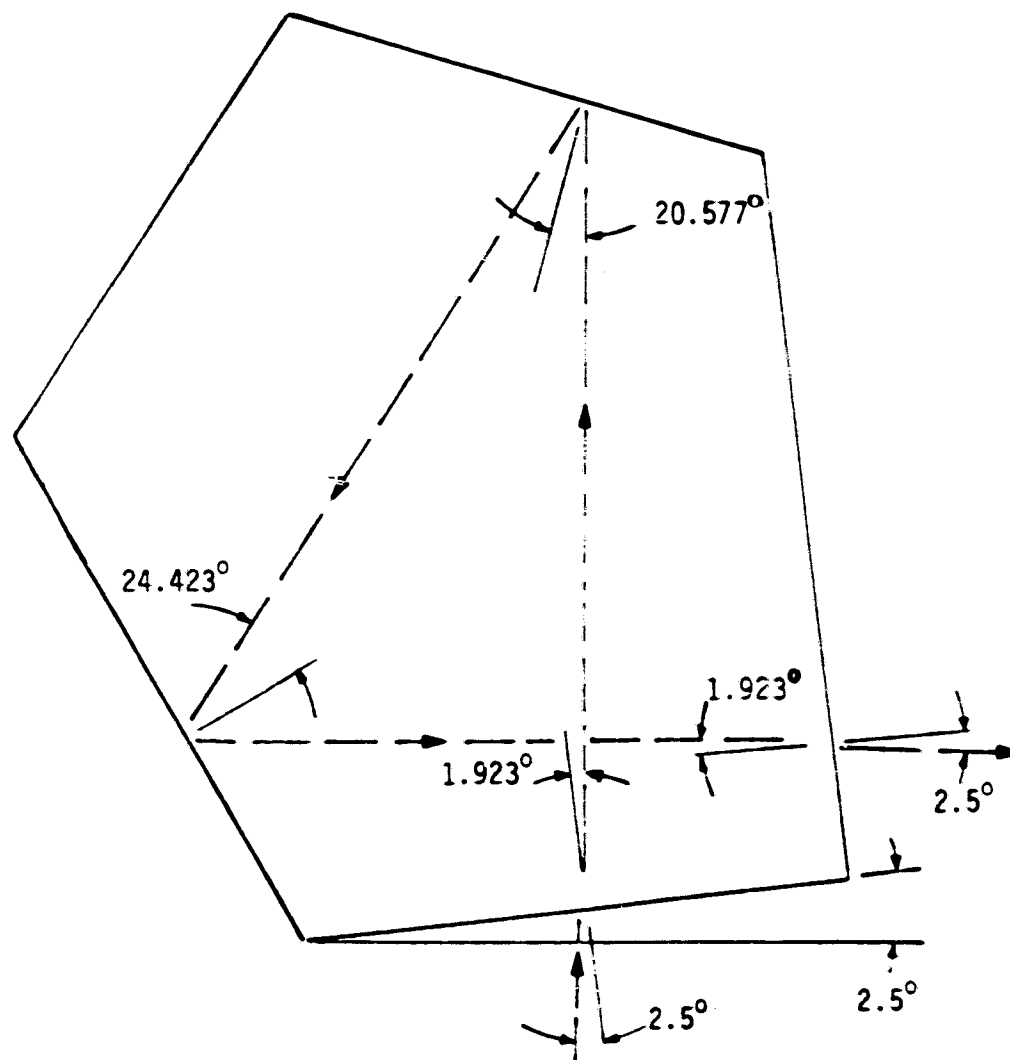
PENTAPRISM COMPENSATION PRINCIPLE

 Axiomatix

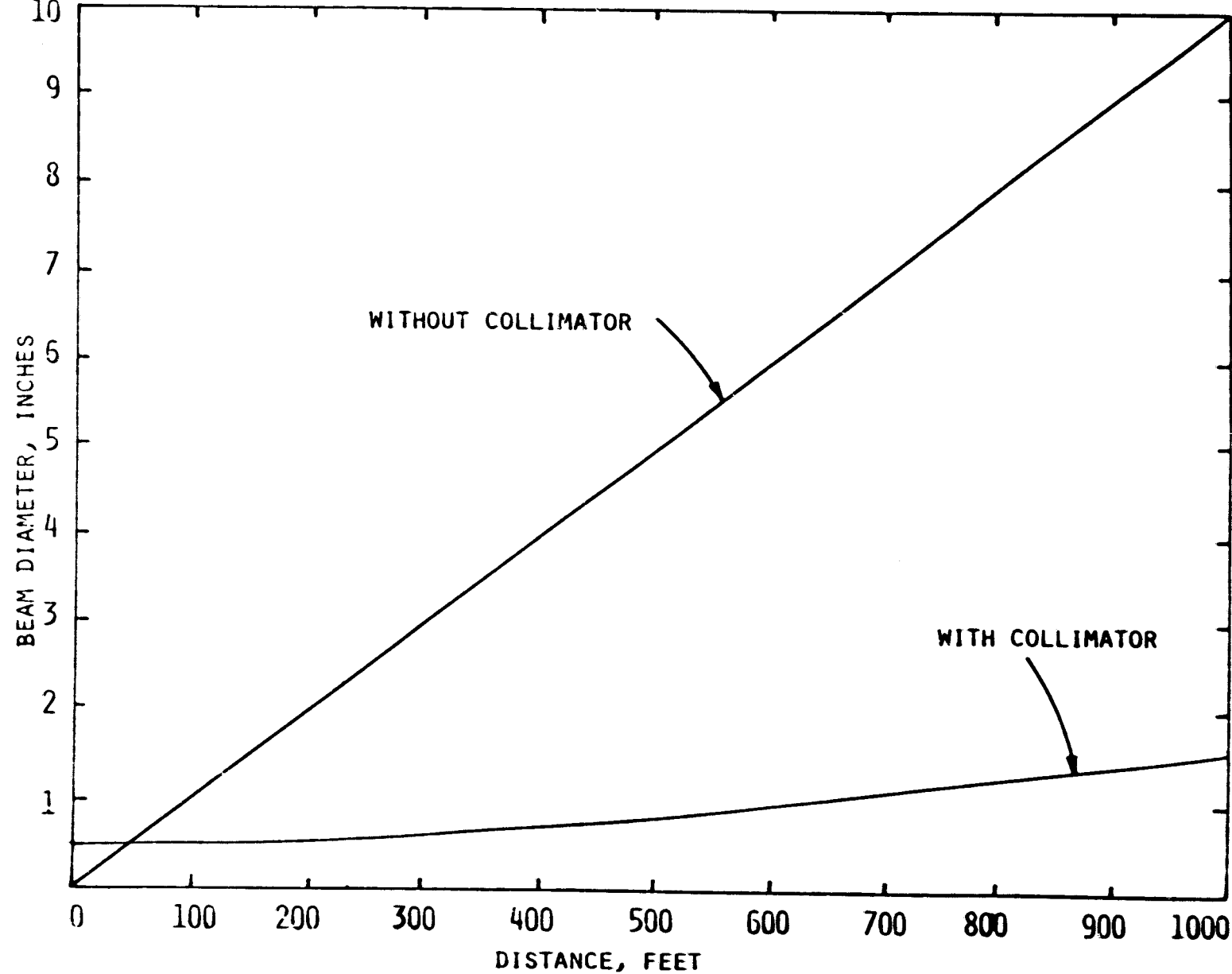
161



PENTAPRISM

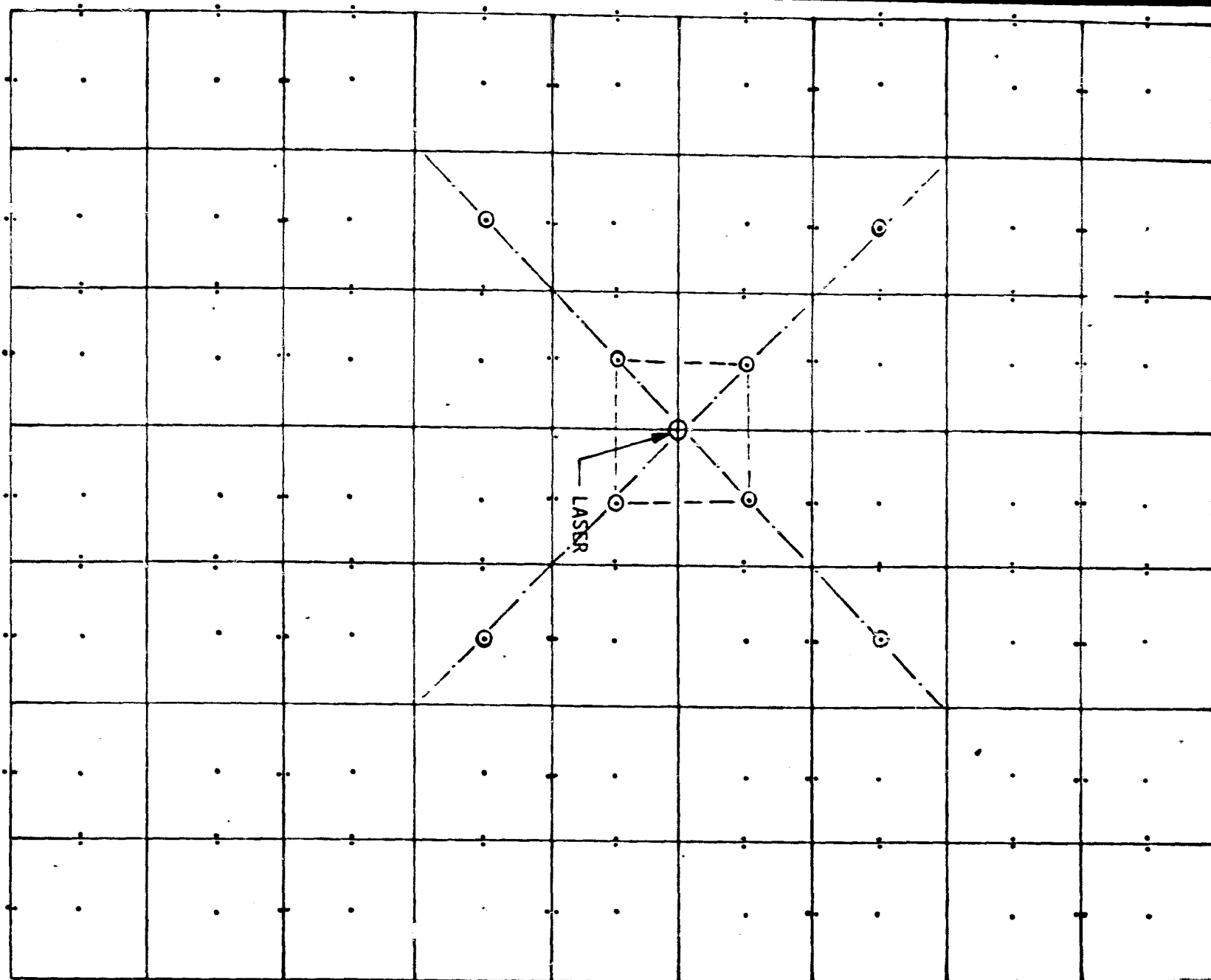


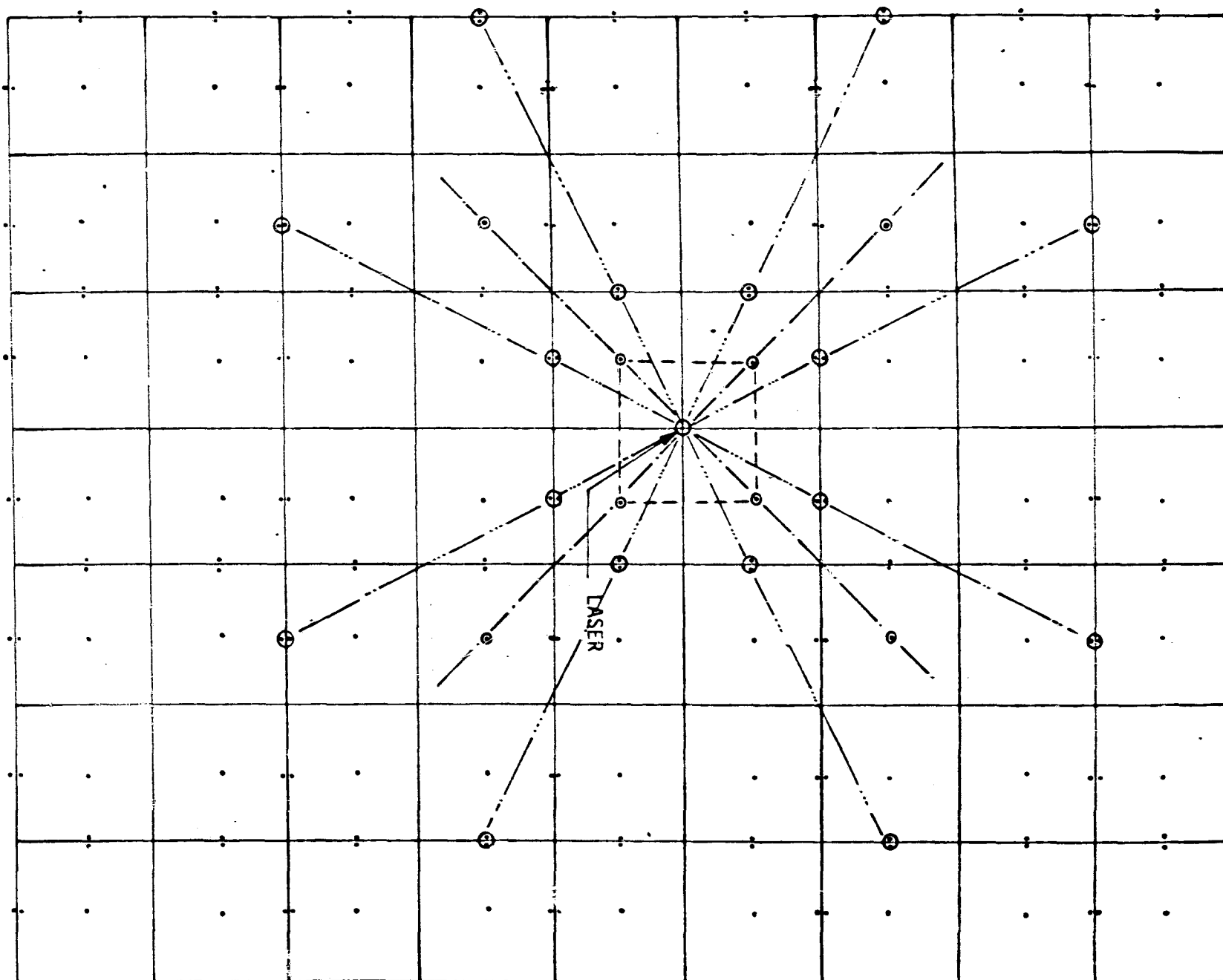
TILTED PENTAPRISM

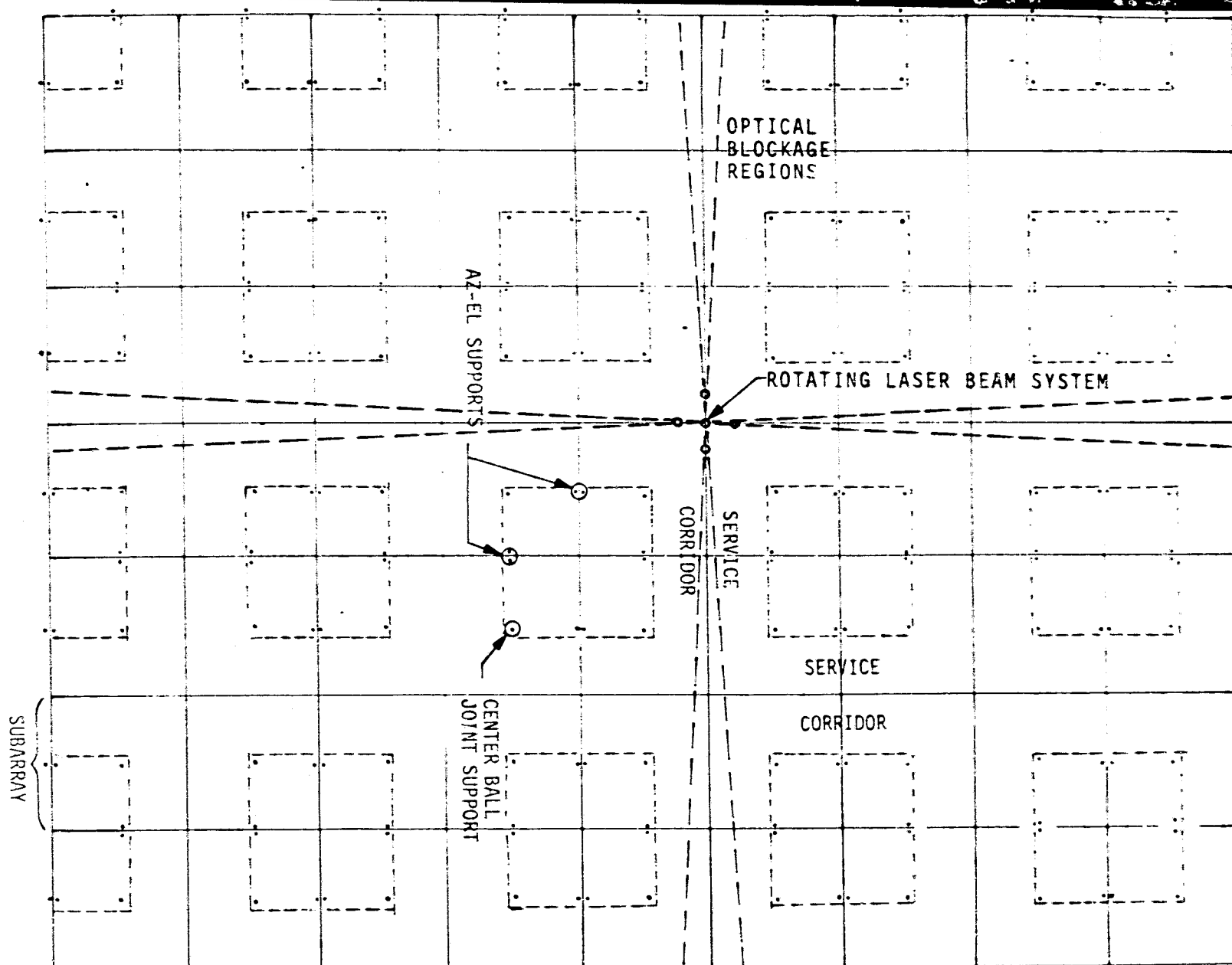


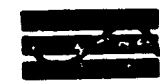
FIRST BLOCKAGE SET

 Axiomatix





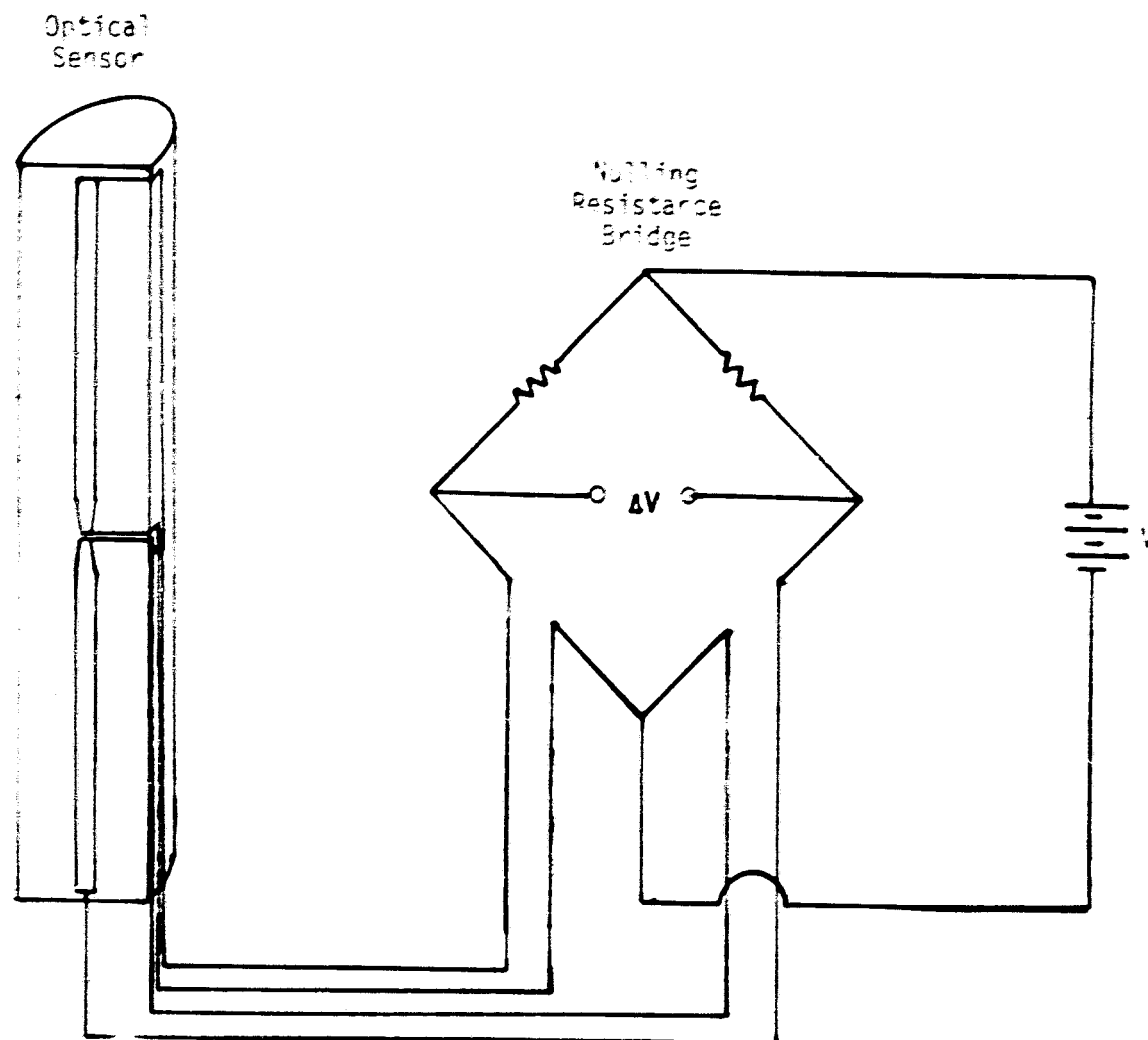


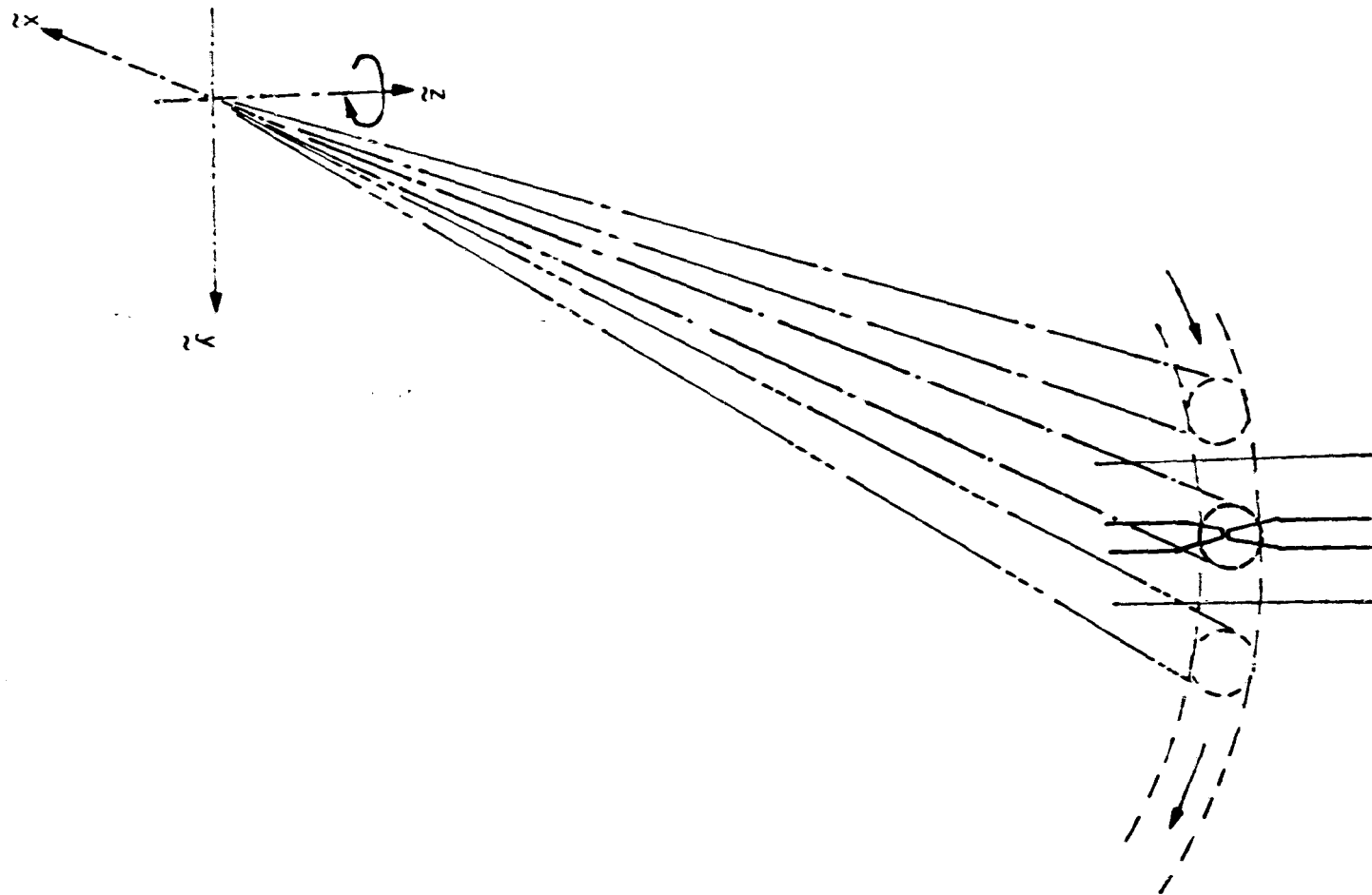


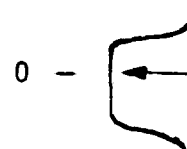
1. HIGH ELECTRICAL SENSITIVITY
2. LOW POWER DISSIPATION
3. DIRECTIONAL POLARITY
4. HIGH DIMENSIONAL RESOLUTION
5. BEAM CENTERING TO ACCOMMODATE BEAM BROADENING
6. REDUNDANCY
7. FOCUSING
8. RFI CONSIDERATIONS
9. REPLACEMENT AND POSITIONING

NULLING RESISTANCE BRIDGE CIRCUIT

 Axiomatix



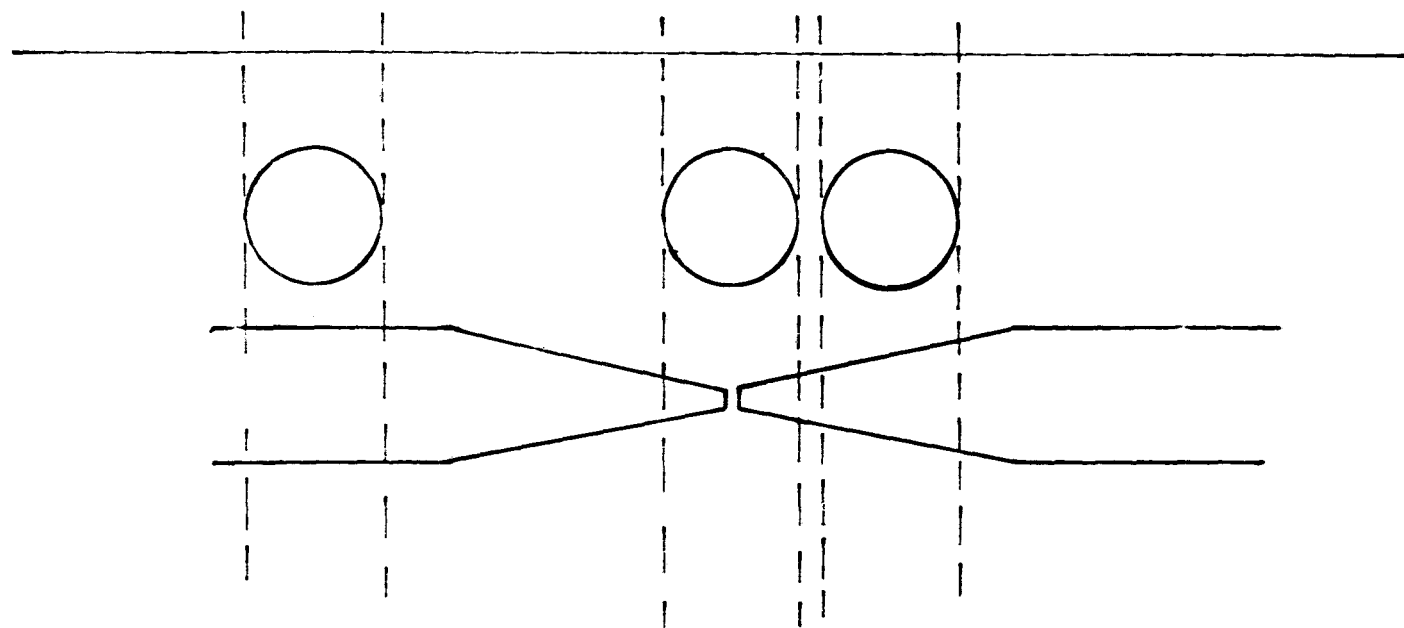


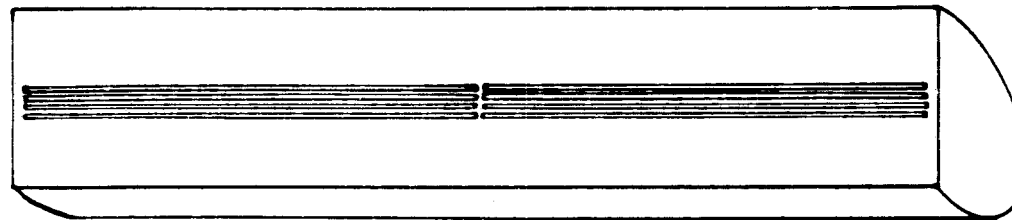


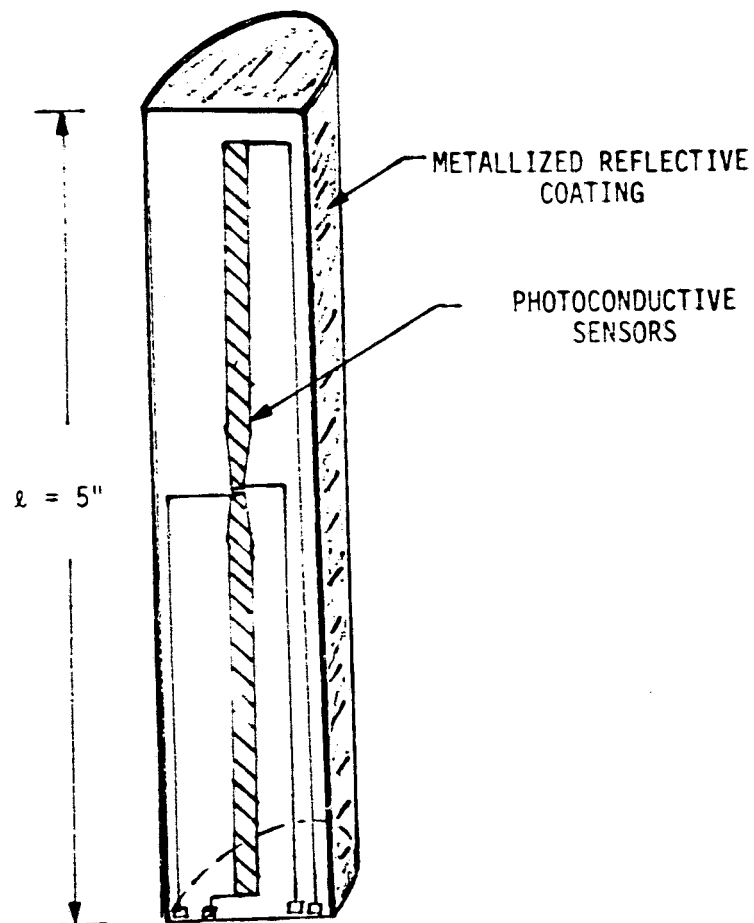
differential
voltage



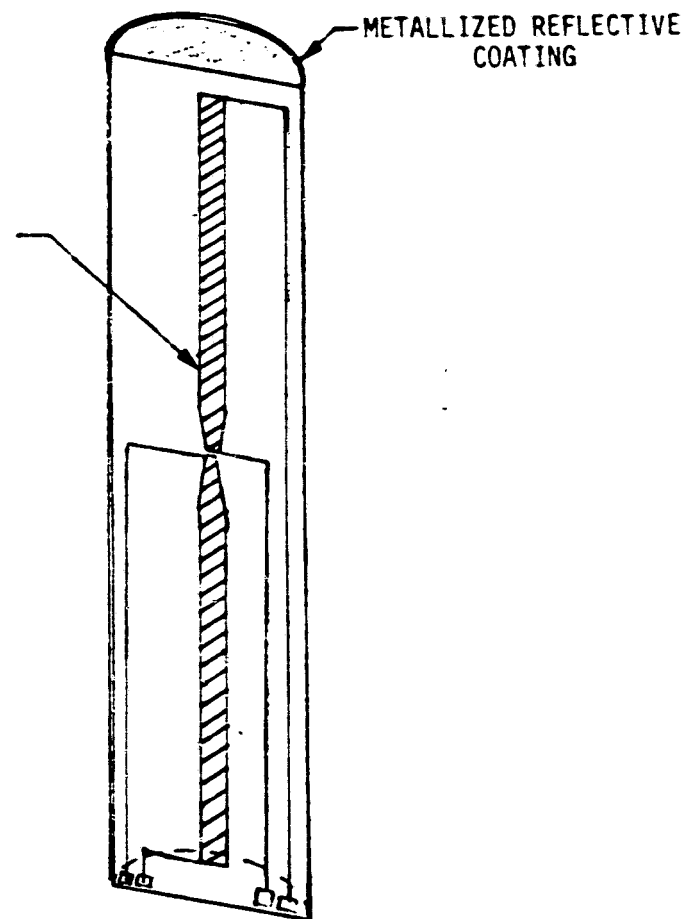
individual
sensor voltages



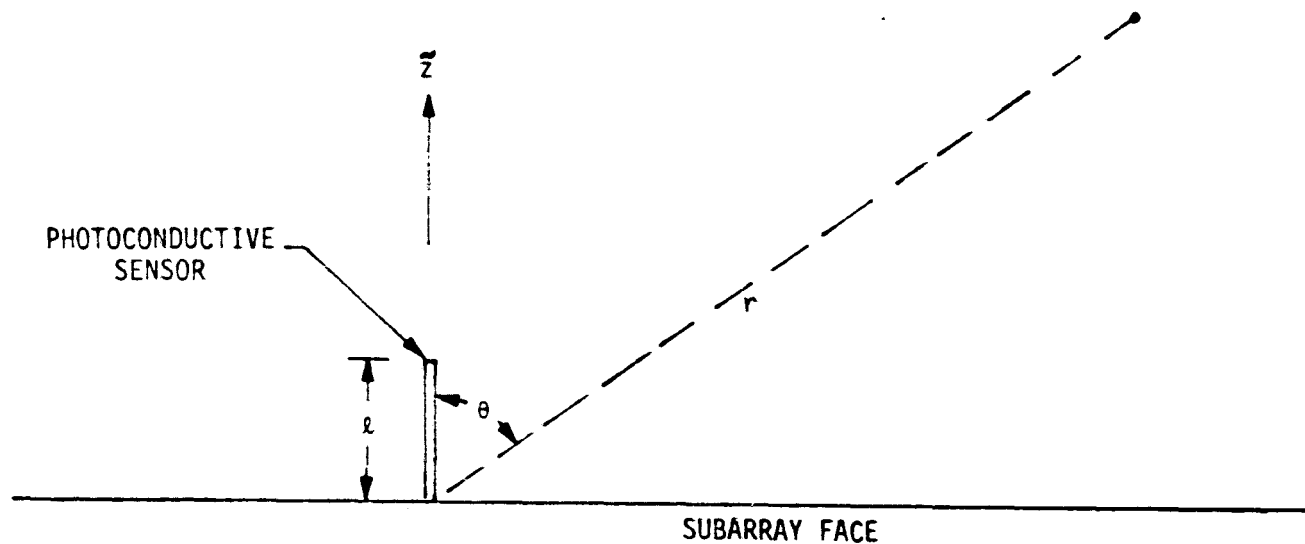




PARABOLIC



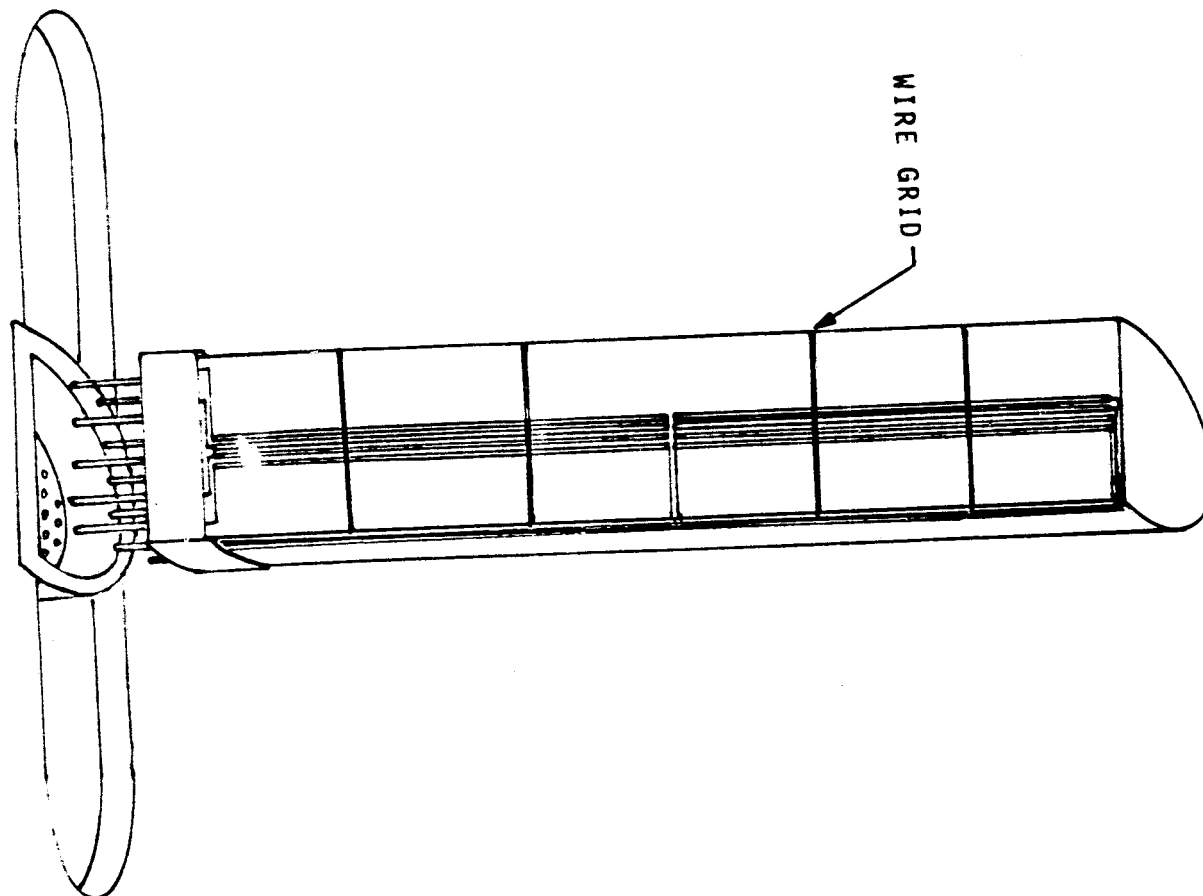
SEMICIRCULAR



$$E_{\theta} = \frac{j n I_m}{2\pi r} e^{-jkr} \left[\frac{\cos(kl \cos\theta) - \cos kl}{\sin\theta} \right]$$

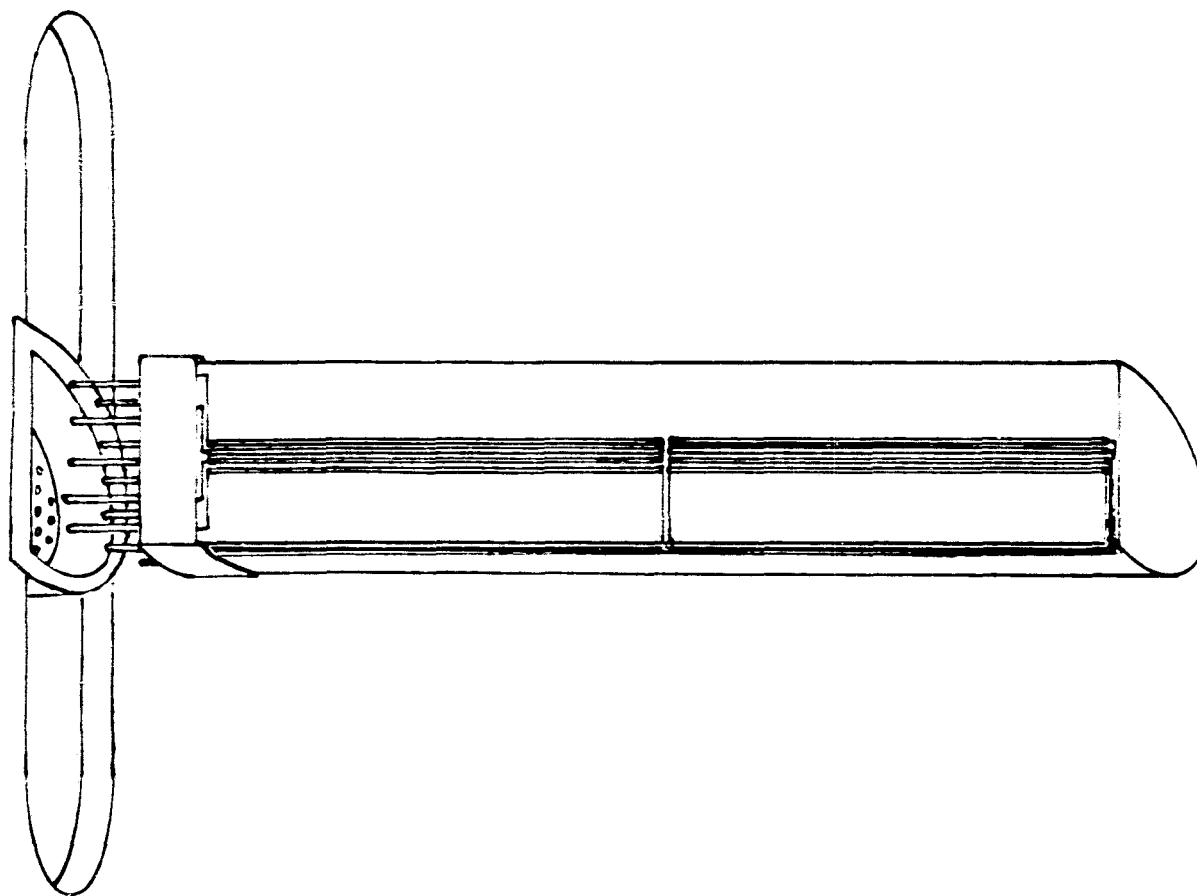
WIRE GRID RFI ELEMENTS

 Axiomatix



REPLACEMENT AND POSITIONING

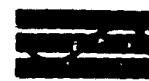
 Axiomatix



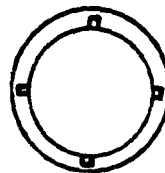
1. BASIC DESIGN
2. REDUNDANCY
3. REMOTE INDIVIDUAL ACCESS
4. HIGH ALIGNMENT RESOLUTION

- WORM SCREW DRIVE
- FORWARD AND REVERSE CAPABILITY
- RELATED TO GARAGE DOOR OPENER

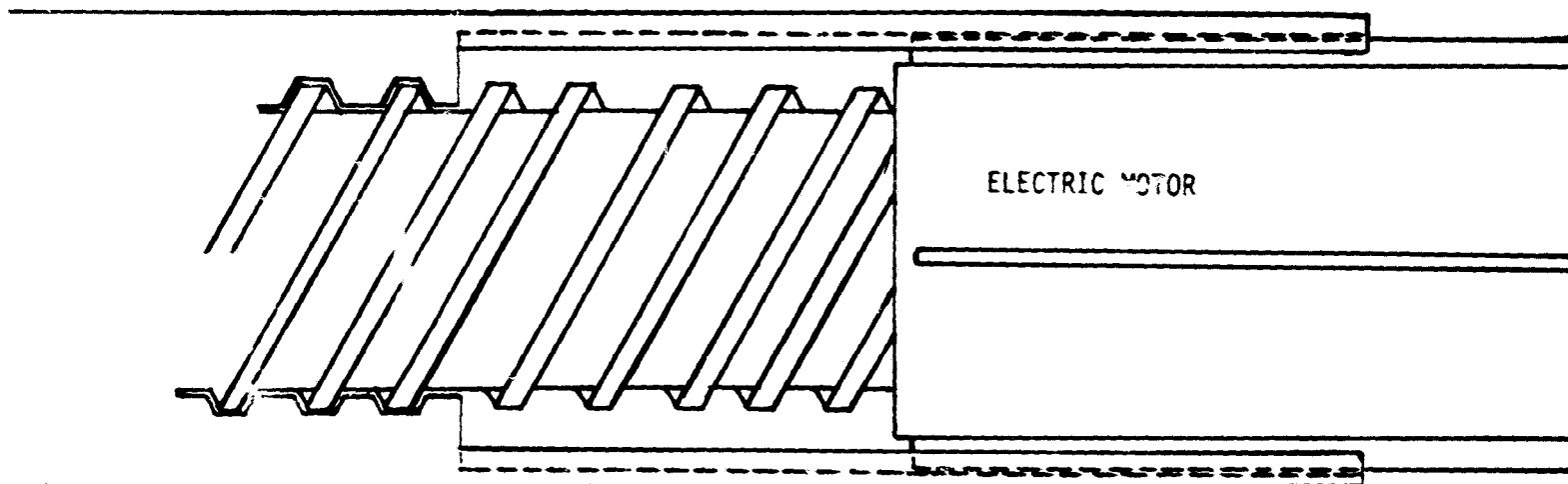
WORM SCREW DRIVE

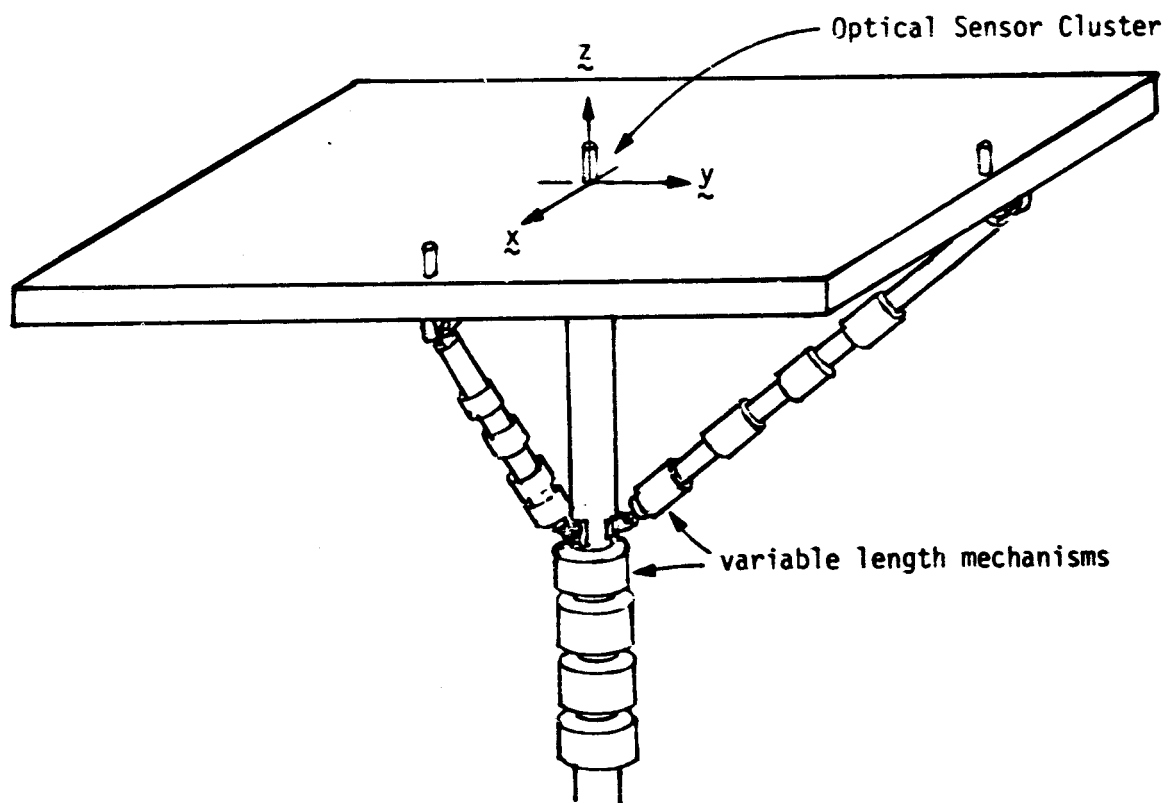


Axiomatix



177



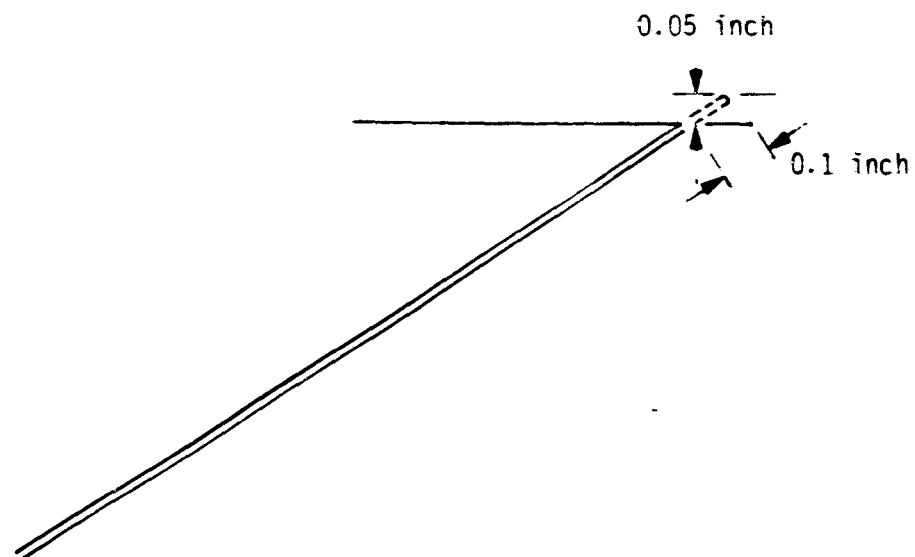
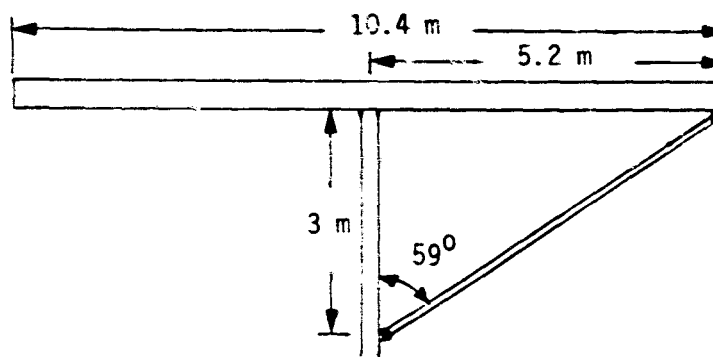


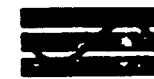
3. REMOTE INDIVIDUAL ACCESS



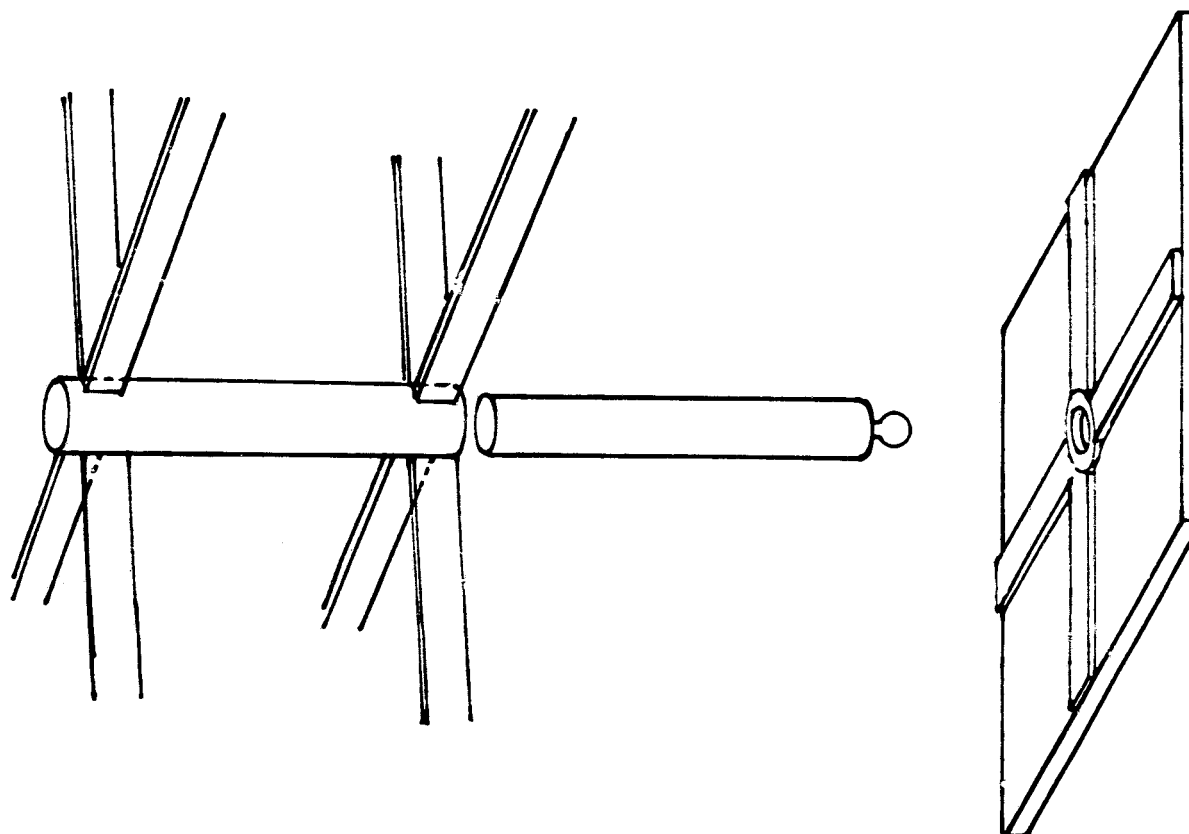
Axiomatix

- 1024 CODED RECEIVER SYSTEMS
NOW COMMERICALLY AVAILABLE
- 7,000 INDIVIDUAL SUBARRAYS
- 21,000 VARIABLE LENGTH MECHANISMS
- CAN BE INDEPENDENTLY CONTROLLED FROM
GROUND STATIONS IF NECESSARY

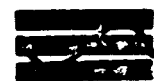




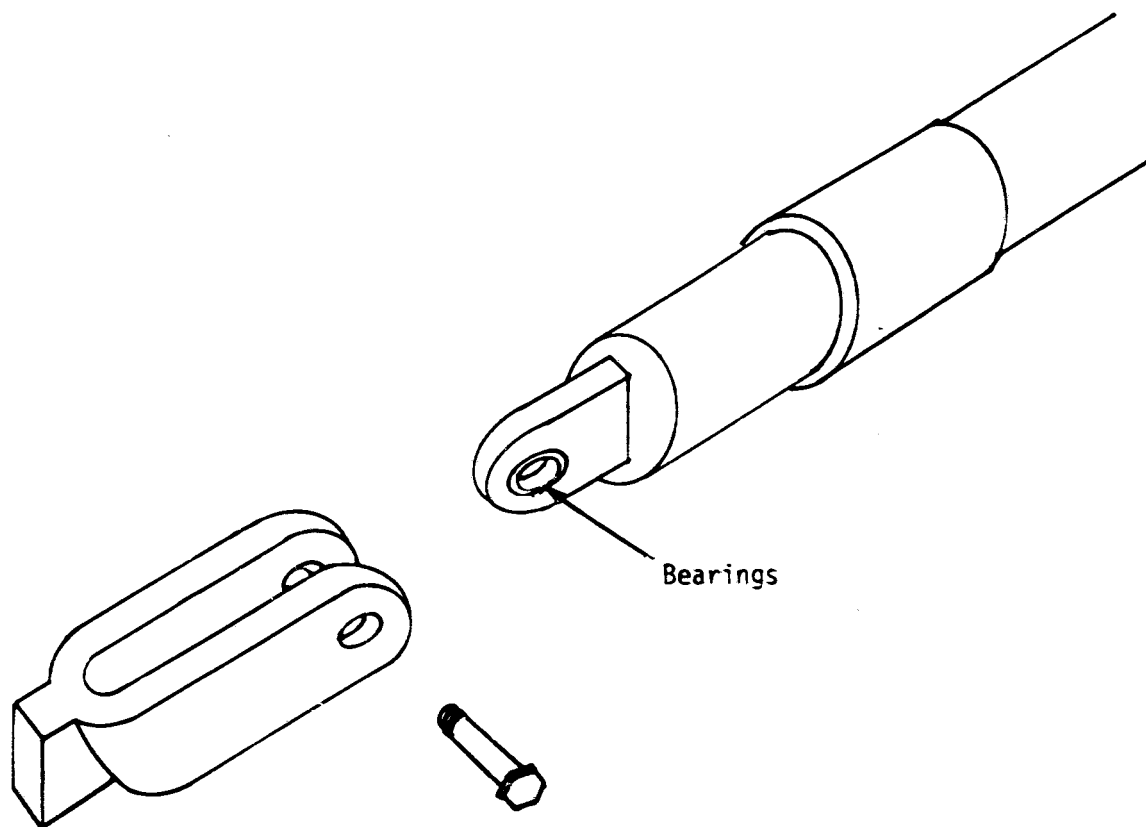
1. SINGLE MOUNTING SUPPORT
2. REPLACEMENT SIMPLICITY
3. MISALIGNMENT COMPENSATION
4. INDEPENDENT ALIGNMENT ADJUSTMENT
5. SERVICE CORRIDORS
6. SUPPLEMENTARY ALIGNMENT VERIFICATION SCHEME

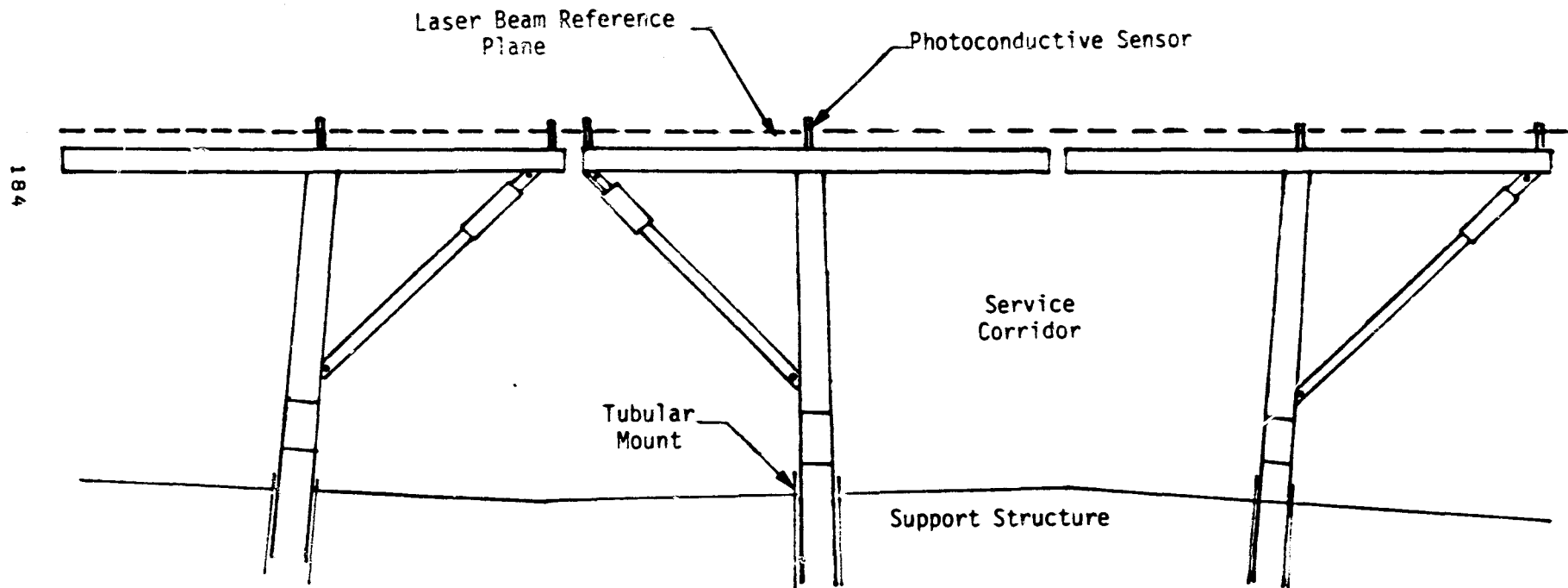


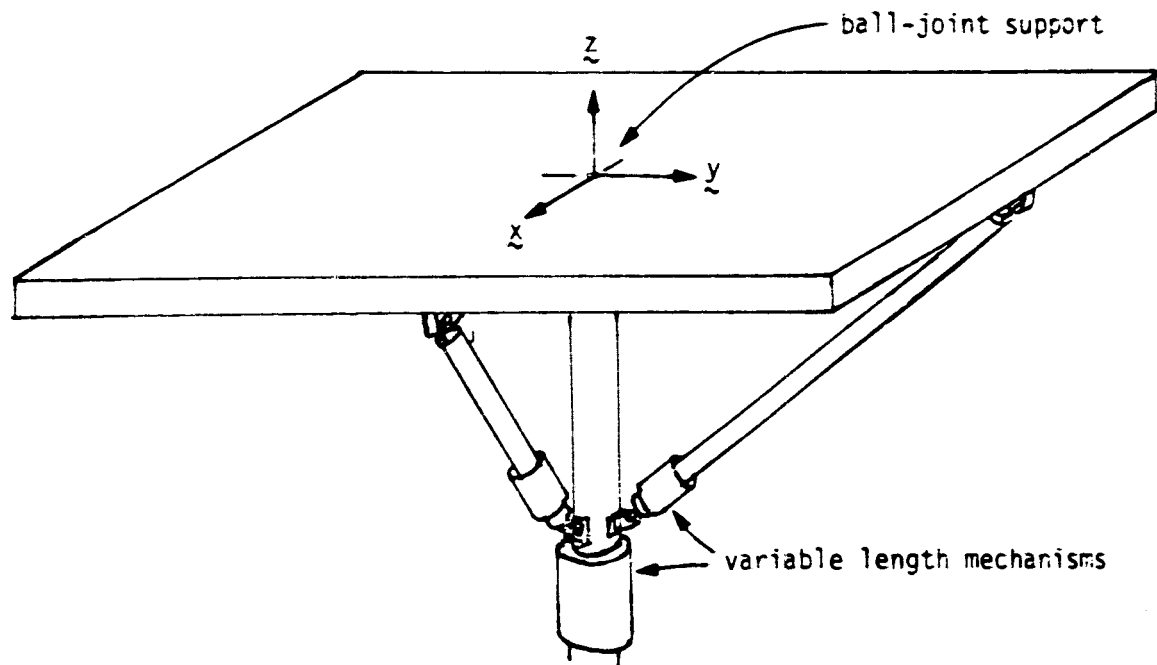
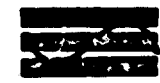
REPLACEMENT SIMPLICITY



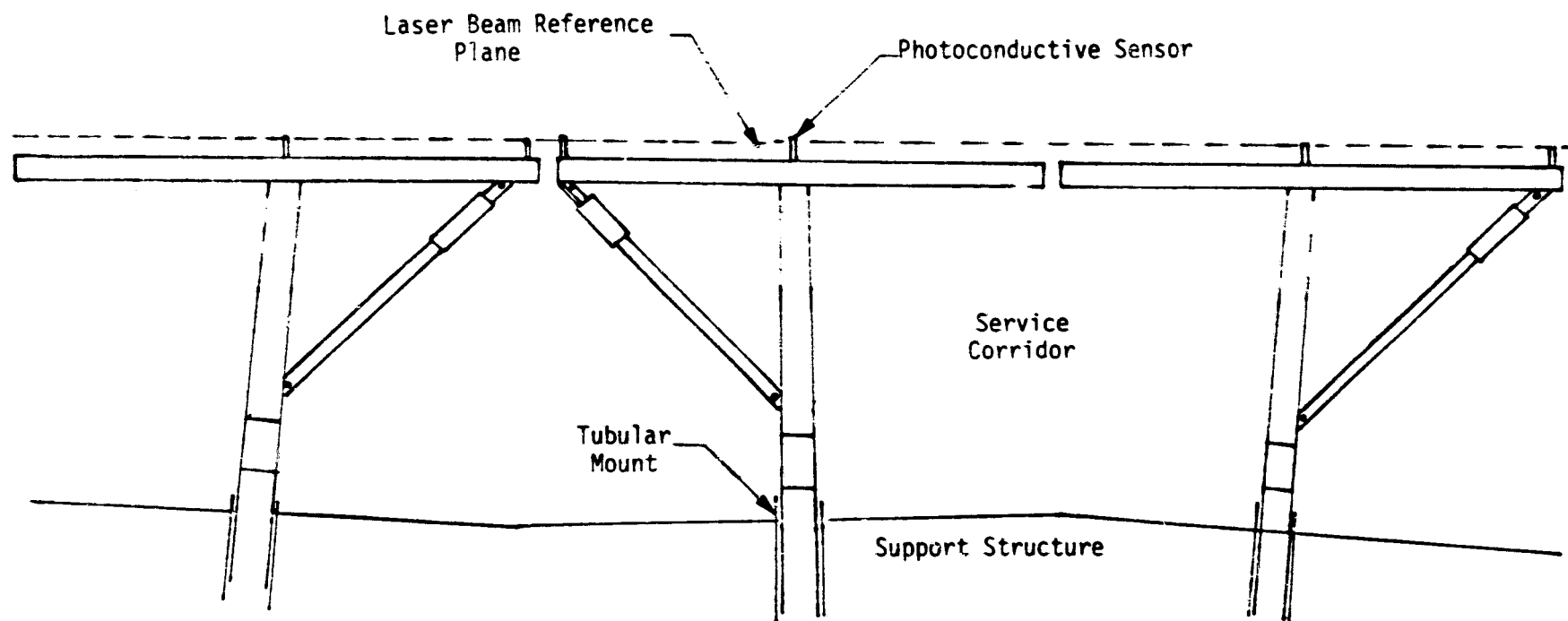
Axiomatix





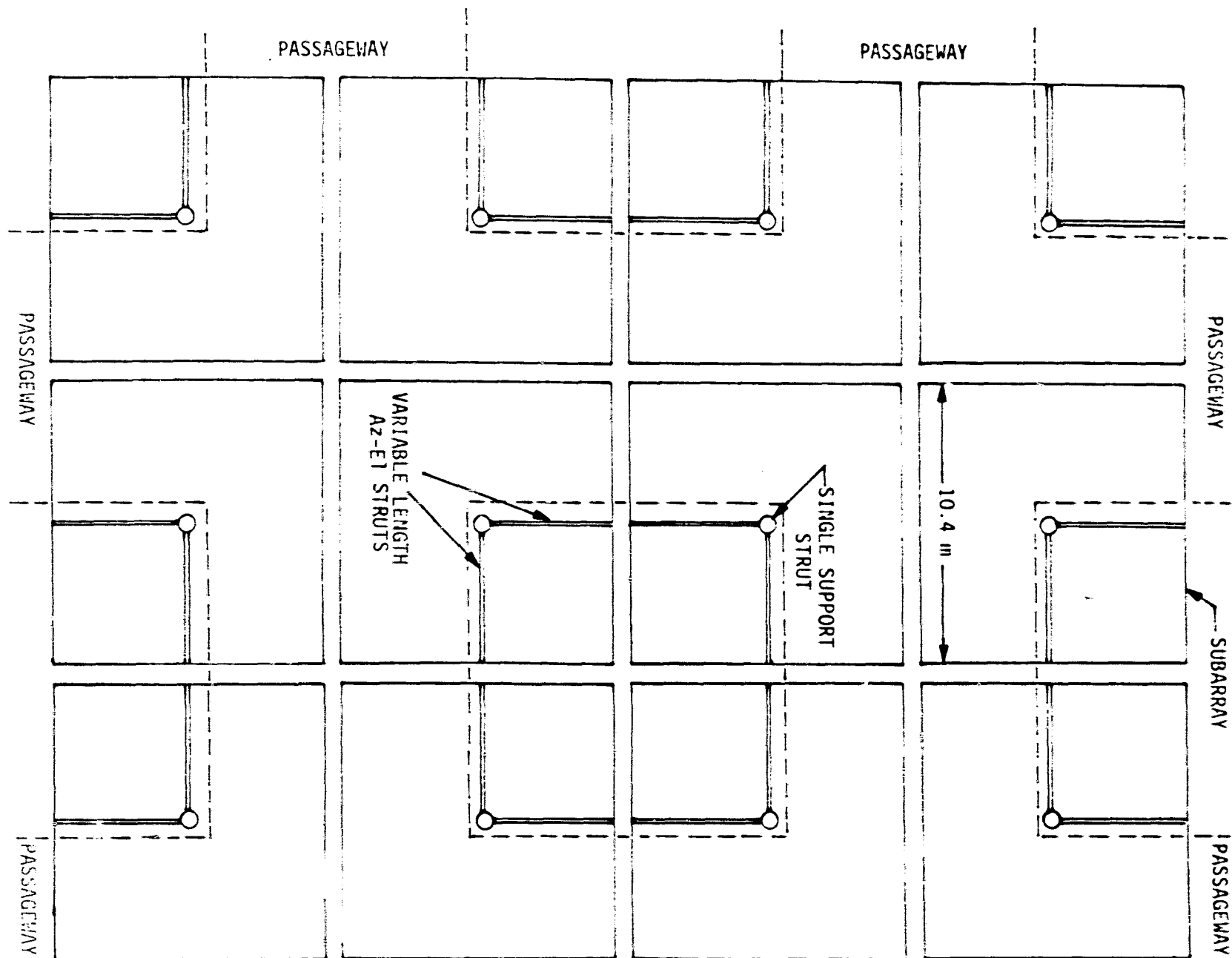


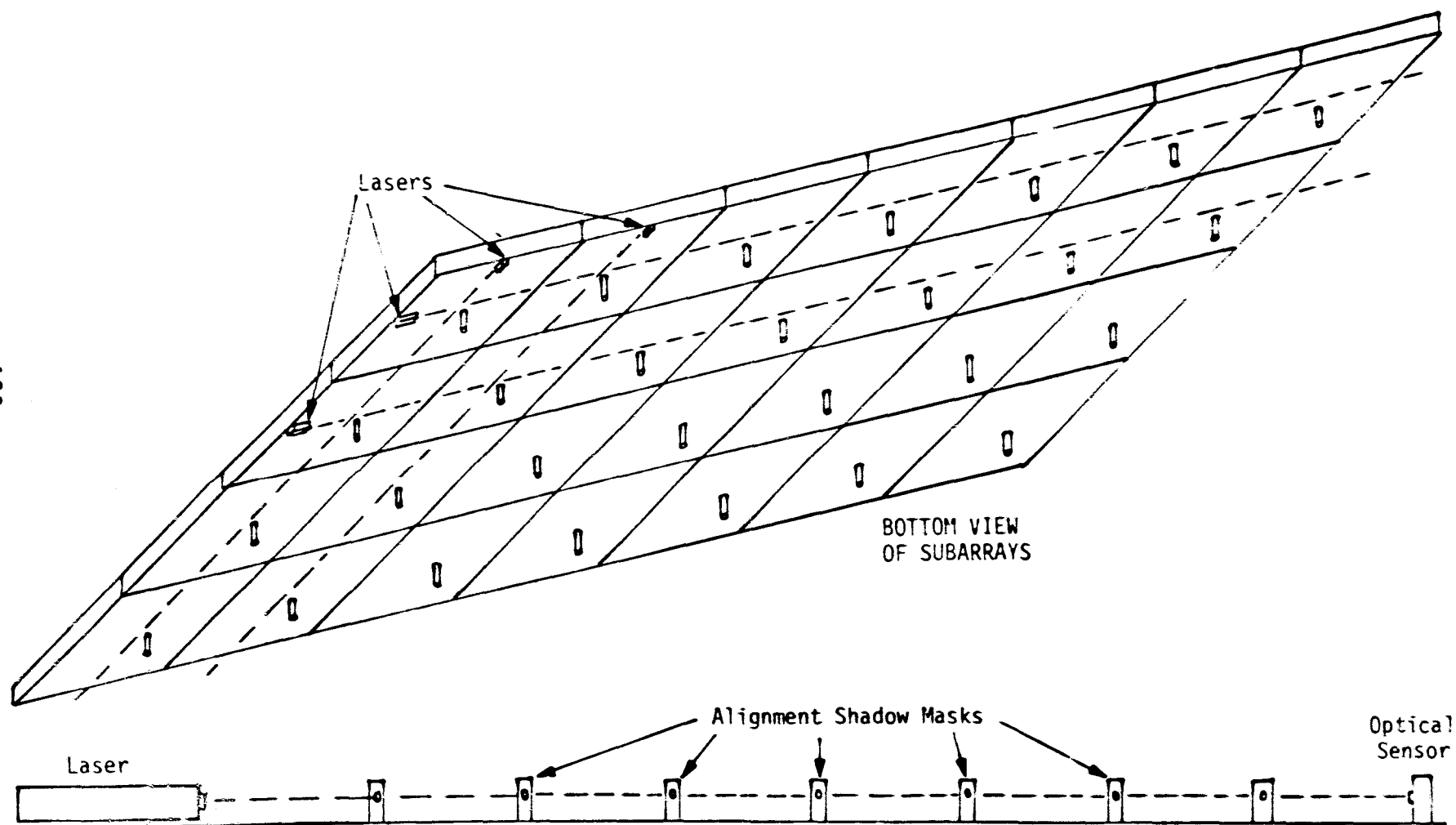
186



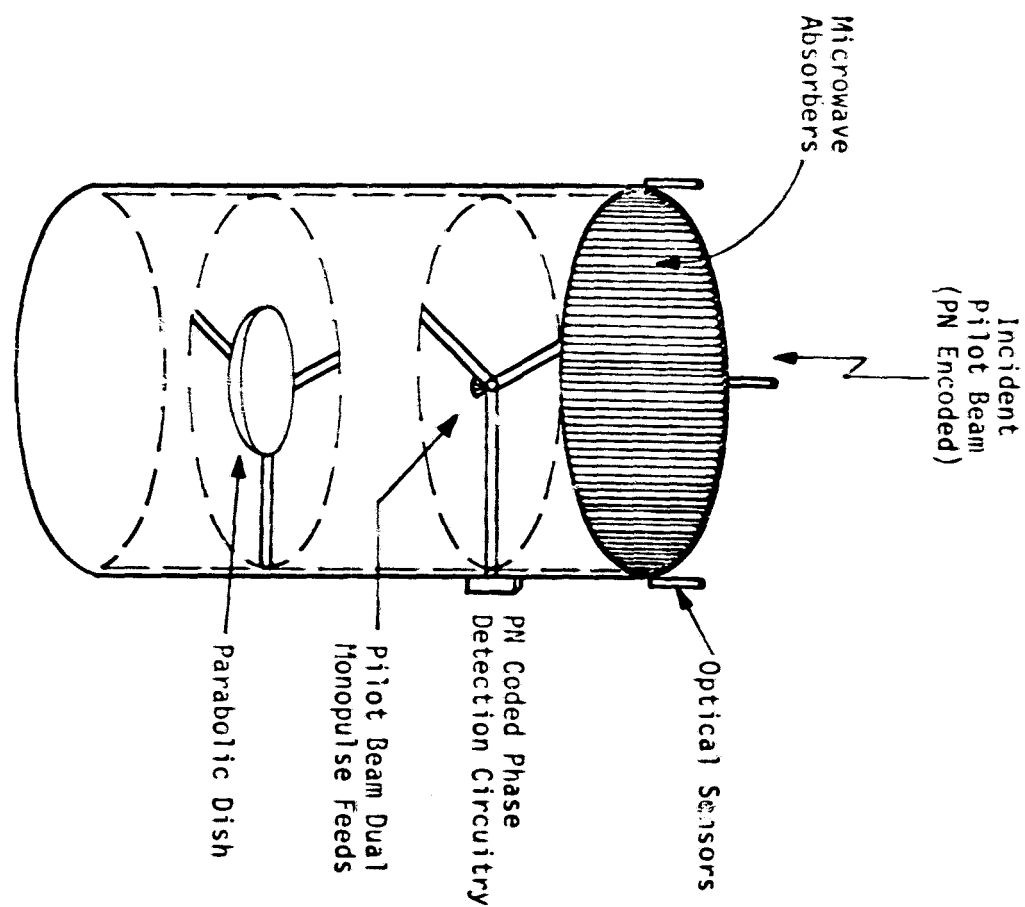
SERVICE CORRIDORS - TOP VIEW

Axiomatix

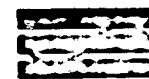




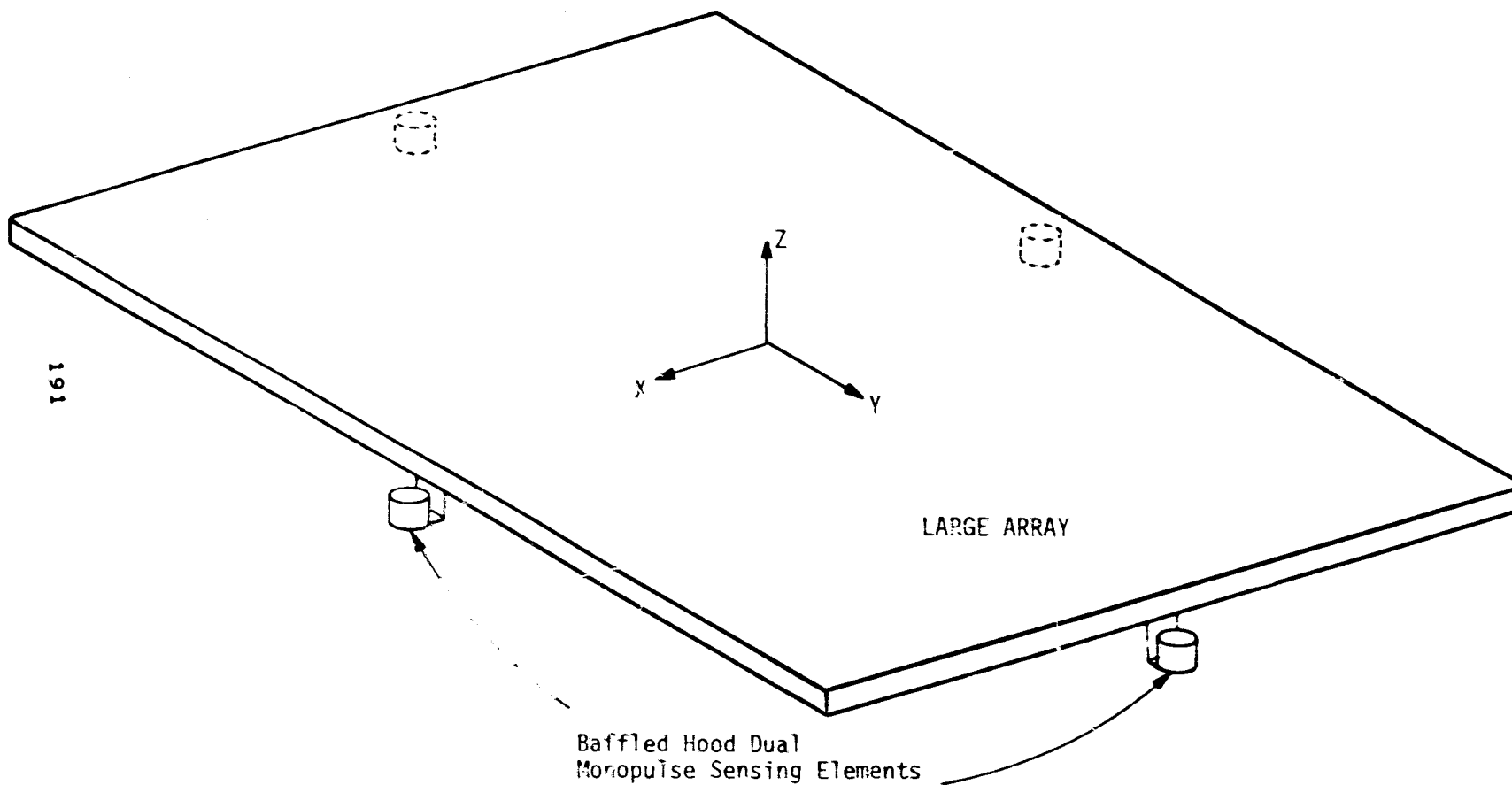
1. TWO AXIS MONOPULSE TRACKING SYSTEM
2. BAFFLED HOOD MONOPULSE ELEMENT
3. ENCODED PILOT BEAM
4. DUAL MONOPULSE SYSTEM FOR POINTING
MONOPULSE ELEMENT



MONOPULSE TRACKING ARRAY



Axiomatix



*Ionospheric Power Beam
Studies*

*W. Gordon
Rice University*

PRECEDING PAGE BLANK NOT FILMED

23 MW/cm²

A POWER DENSITY LEVEL OF 23 MW/cm² HAS ACHIEVED THE STATUS OF A FIRM DESIGN SPECIFICATION BASED ON THEORETICAL CALCULATIONS OF A THRESHOLD FOR MICROWAVE-IONOSPHERE NONLINEAR INTERACTION (THERMAL RUNAWAY).

THERMAL RUNAWAY IS NO LONGER A VALID THEORETICAL CONCEPT ALTHOUGH FOR COMPARABLE POWER DENSITIES ENHANCED ELECTRON HEATING IS OBSERVED TO CHANGE THE ELECTRON TEMPERATURE BY A FACTOR OF TWO OR THREE, BUT NOT BY AN ORDER OF MAGNITUDE.

THERE IS, SO FAR, NO EXPERIMENTAL EVIDENCE TO SUPPORT 23 MW/cm² AS AN UPPER LIMIT.

THE QUESTION TO BE POSED AND ANSWERED IS AT WHAT POWER DENSITIES IS THE IONOSPHERE MODIFIED IN A WAY THAT PRODUCES UNACCEPTABLE COMMUNICATION EFFECTS AND/OR ENVIRONMENTAL IMPACTS?

PRECEDING PAGE BLANK NOT FILMED

ARECIBO TEST RESULTS

CASE 1 HEATING WAVE PENETRATED THE IONOSPHERE

FREQUENCY	OHMIC HEATING AS A FRACTION OF 5 GW SPS HEATING	DIAMETER OF HEATED VOLUME RELATIVE TO SPS HEATED VOLUME	CROSS SECTION FOR FIELD-ALIGNED SCATTER IS LESS THAN
6-10 MHz	1%	3.00	$4 \times 10^{-3} \text{ M}^2$
430 MHz	40%	0.10	$4 \times 10^{-3} \text{ M}^2$
2380 MHz	5%	0.01	10^{-3} M^2

ARECIBO TEST RESULTS

CASE 2 HEATING WAVE REFLECTED BY THE IONOSPHERE (NOT THE SPS CONDITION)

PLASMA INSTABILITIES ARE EXCITED BY THE HF HEATER WAVE LEADING TO FIELD-ALIGNED STRIATIONS THAT SCATTER RADIO WAVES.

FIELD-ALIGNED RADIO-SCATTERING CROSS-SECTIONS UP TO 10^3 m^2 .

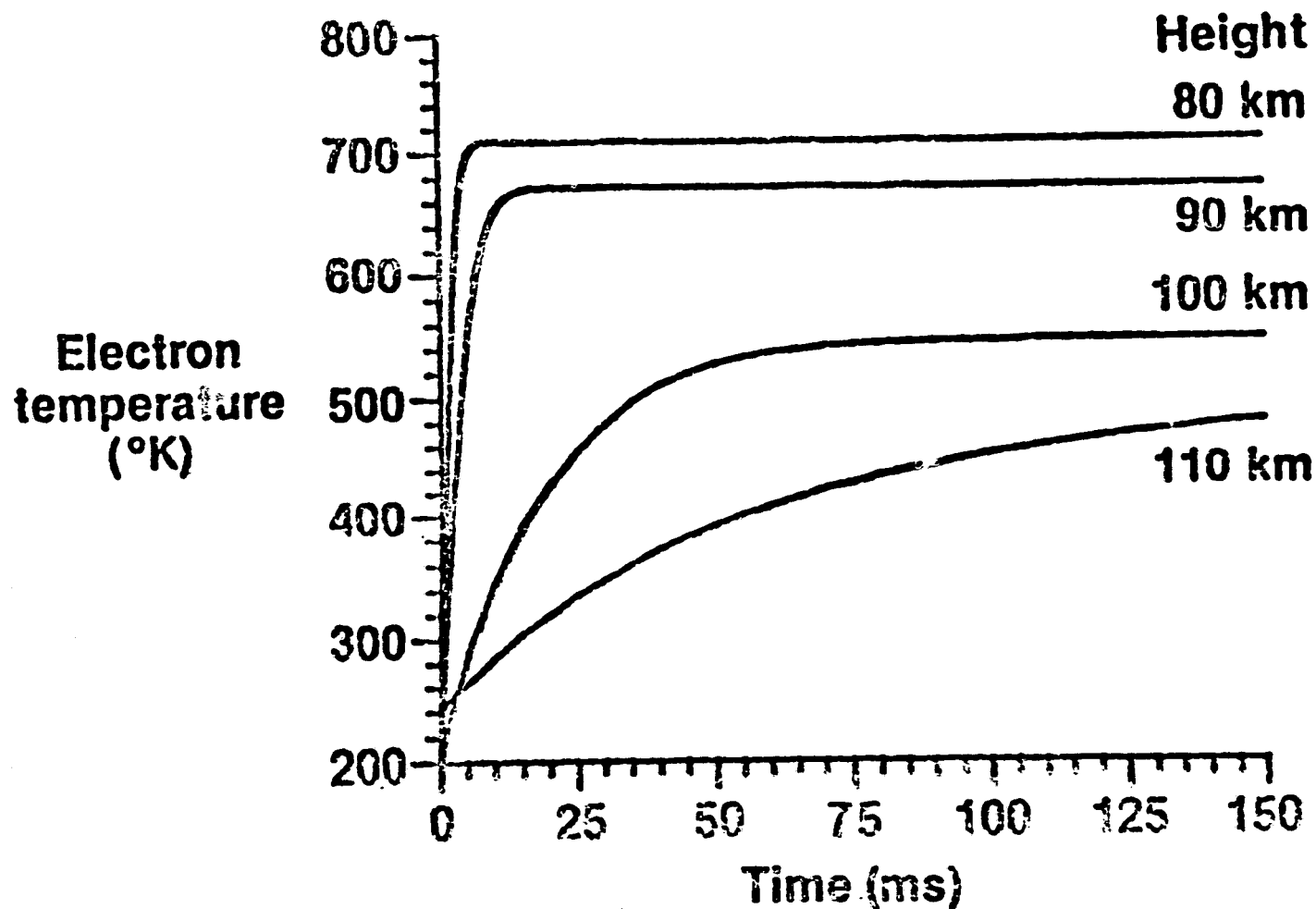
SINCE THE EXCITATION OF THESE INSTABILITIES REQUIRES A MATCHING OF THE HEATER FREQUENCY TO THE IONOSPHERIC PLASMA FREQUENCY, A CONDITION THAT IS NOT MET BY THE SPS, THEY WILL NOT BE EXCITED. NO OTHER INSTABILITIES ARE PRESENTLY KNOWN THAT THE SPS FREQUENCY WILL EXCITE.

THE SIMULTANEOUS ILLUMINATION OF THE IONOSPHERE BY THE SPS FREQUENCY AND A SECOND FREQUENCY SEPARATED BY ABOUT 15 MHz OR LESS COULD PRODUCE THE INSTABILITIES DESCRIBED ABOVE.

ENHANCED ELECTRON HEATING BY THE SPS BEAM

- (1) WILL INCREASE ELECTRON TEMPERATURES BY UP TO A FACTOR OF THREE OR MORE, MOSTLY IN THE LOWER IONOSPHERE.

Power flux = 23 mW/cm²
Frequency = 2450 MHz
Standard midlatitude atmosphere



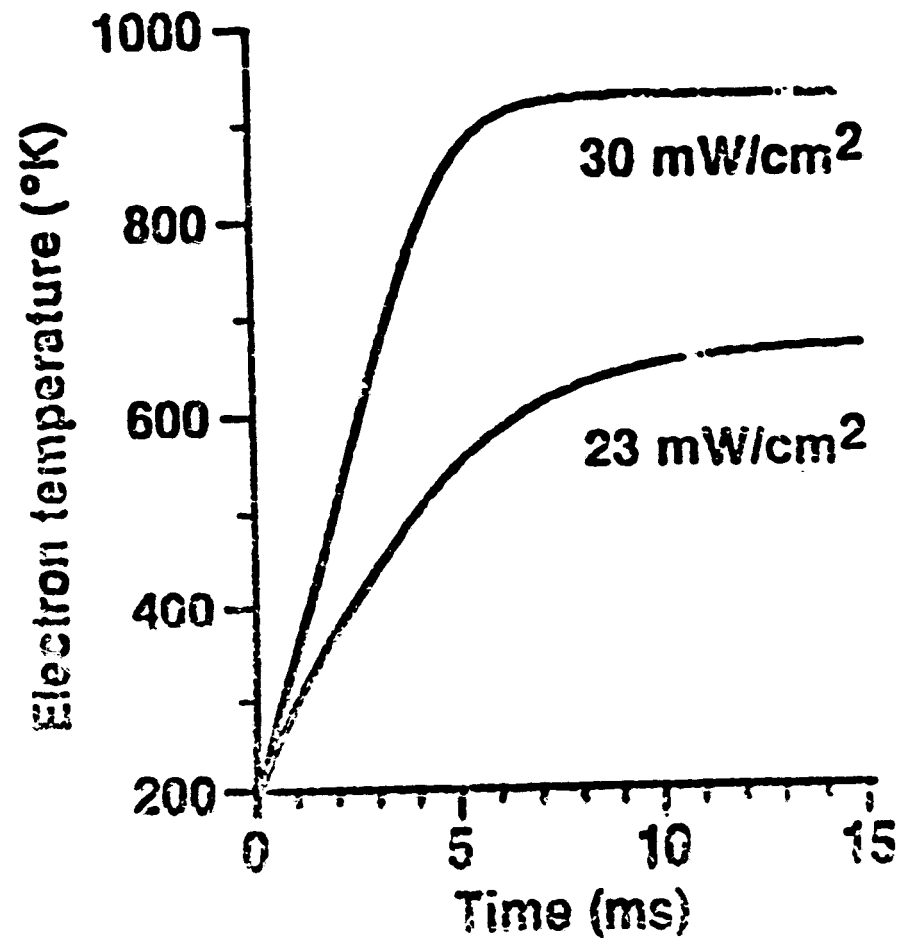
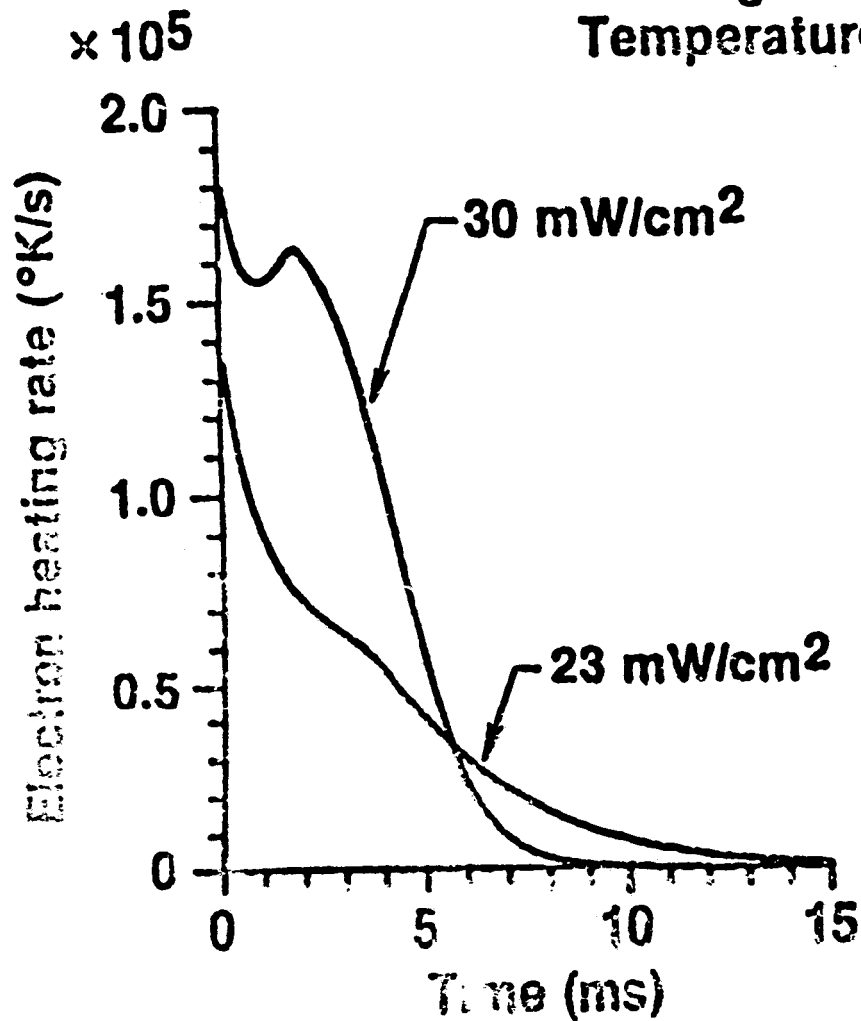
ENHANCED ELECTRON HEATING BY THE SPS BEAM

(2) IS PREDICTED TO BE DEPENDENT ON THE INCIDENT POWER DENSITY.

Frequency = 2450 MHz

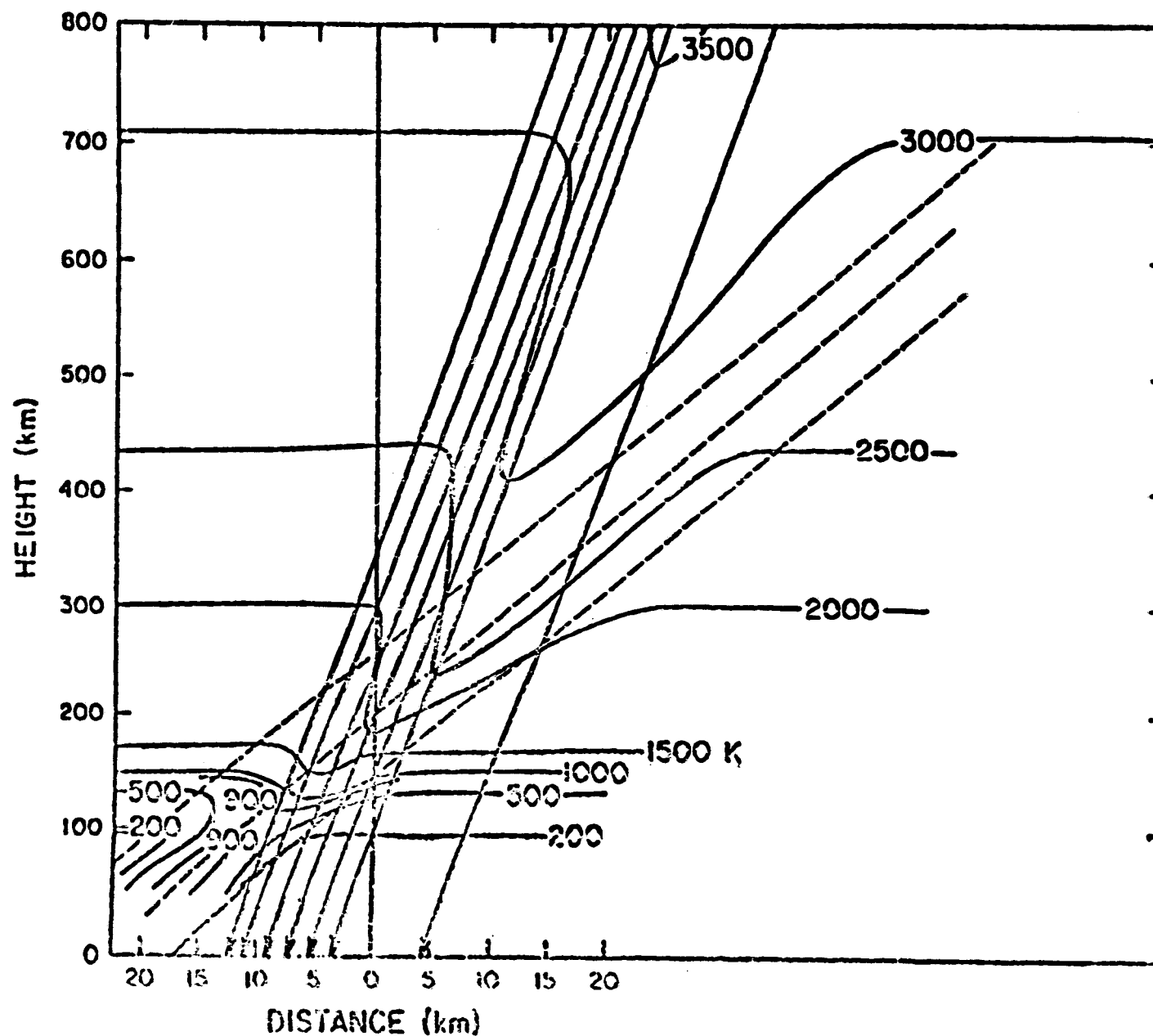
Height = 90 km

Temperature = 187°K.



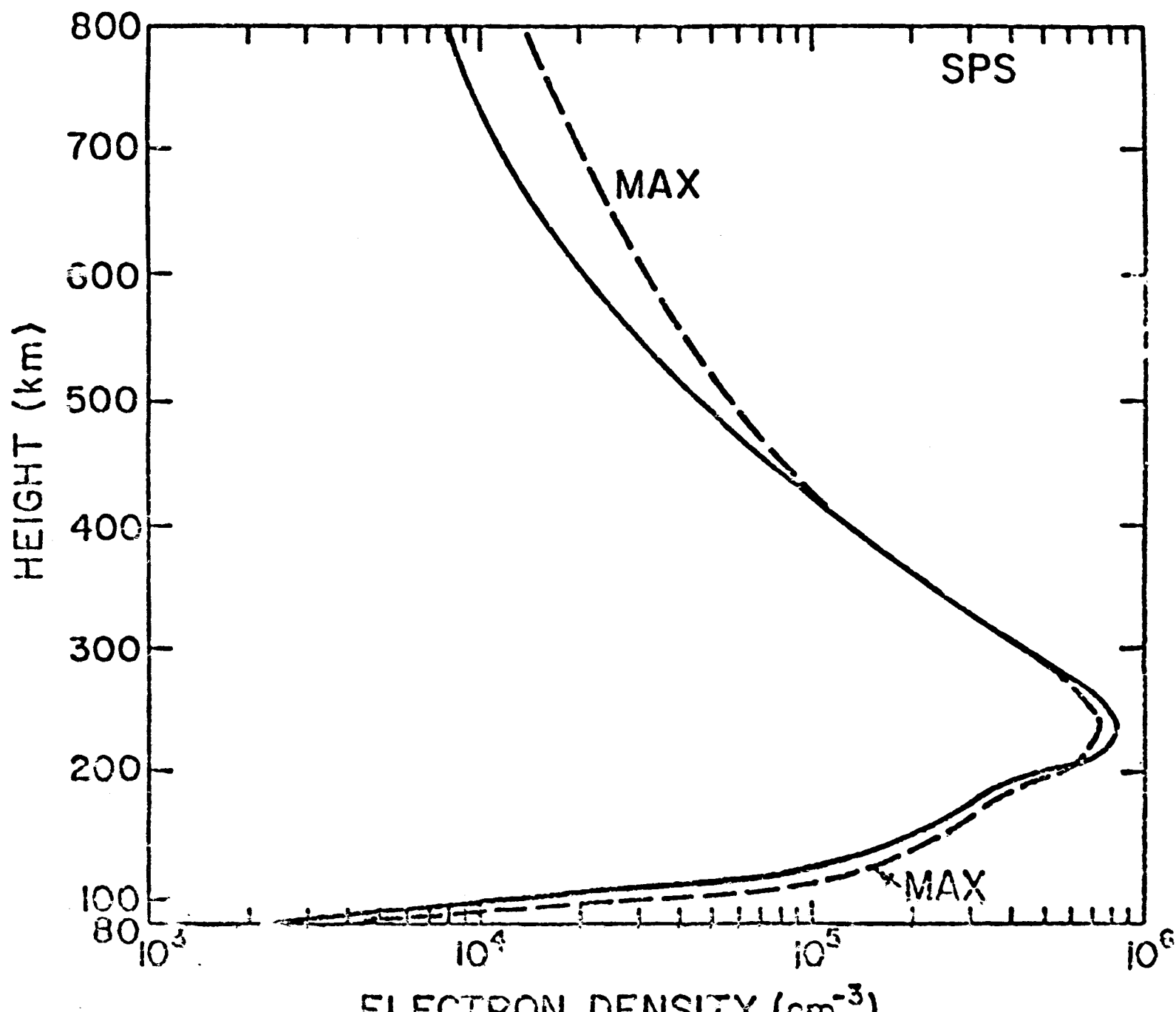
ENHANCED ELECTRON HEATING BY THE SPS BEAM

- (3) WILL INCREASE ELECTRON TEMPERATURES IN AND NEAR THE BEAM BY SMALL FACTORS.

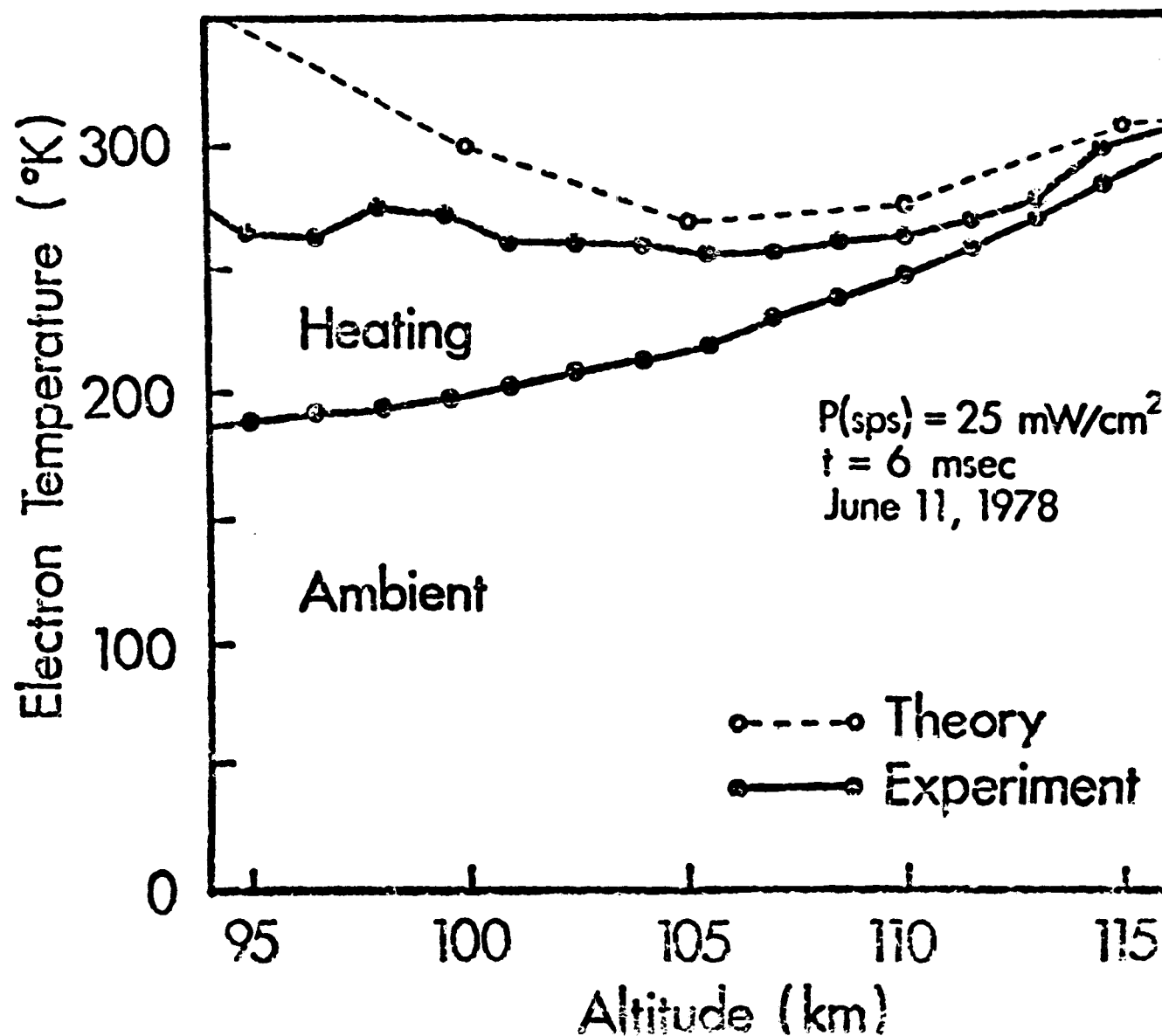


ENHANCED ELECTRON HEATING BY THE SPS BEAM

(4) WILL CHANGE THE ELECTRON DENSITY IN THE BEAM BY SMALL AMOUNTS.



OBSERVATIONS OF ENHANCED ELECTRON HEATING AT ARECIBO ARE CLOSE TO, BUT BELOW,
THE PREDICTED INCREMENTS.



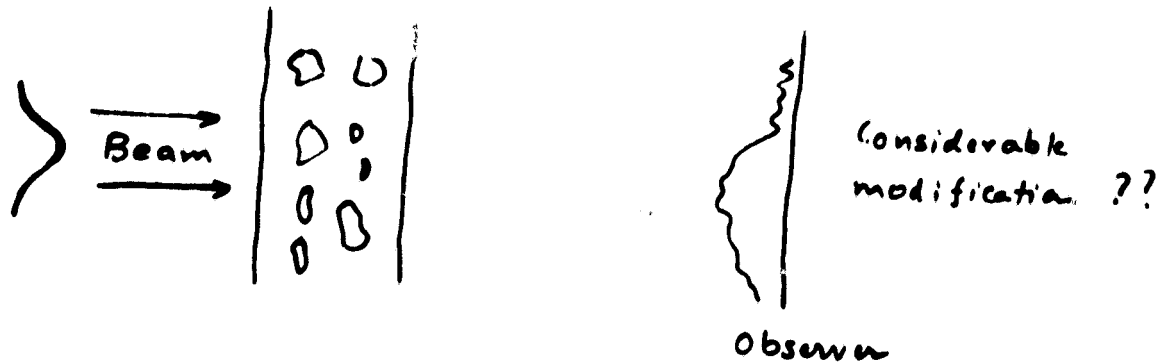
COMPARISON OF 5800 MHz AND 2450 MHz

<u>MEDIUM</u>		<u>2450 MHz</u>	<u>5800 MHz</u>
IONOSPHERE		1 KW	0.25 KW
NEUTRAL ATMOSPHERE AT 60° ELEVATION ANGLE		90 MW	100 MW
RAIN (25mm/HR OVER 20 KM PATH IN BEAM)		45 MW	1.450 GW
HAIL (1.93 cm DIAMETER HAILSTONES, 10 KM PATH THROUGH THE BEAM)	DRY	0.2 GW	1.7 GW
	WET	2.7 GW	4.99 GW

***Ionospheric Perturbations on
Uplink Pilot Beam Signal
(Experimental)***

***Gang and Basu
Emanuel University***

PRECEDING PAGE BLANK NOT FILMED



→ What Modification ?

Beam broadening

Loss of beam intensity

{ Scintillations on
Loss of Temporal and Spatial Coherence of
Intensity & Phase

Beam Wandering

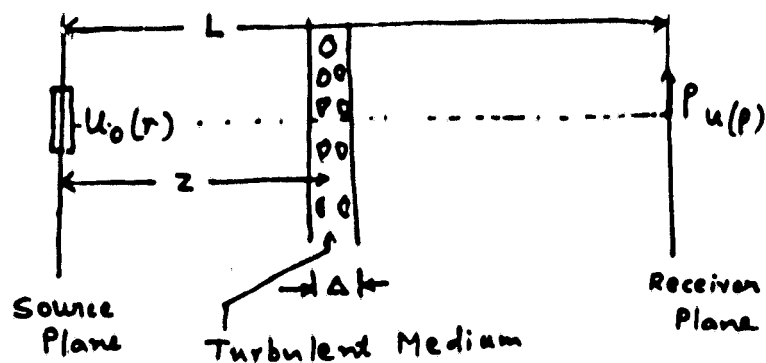
→ Pertinent for what type of Turbulent Medium
What strength of Turbulence ??

PRECEDING PAGE BLANK NOT FILMED

FORMALISM OF THE PROBLEM :

ORIGINAL PAGE IS
OF POOR QUALITY

Huygens - Fresnel Principle



For scale size of turbulent medium large compared to the wavelength of em signal, the electric field of the wave can be approximated by the scalar wave equation

$$\nabla^2 E + k^2 (1 + n_1) E = 0$$

↑ refr index fluctuation

For propagation along the z-direction

$$E = u(r, z) e^{ik_0 z}$$

The field distribution over the receiver plane ($z=L$) can be related to that over the source plane by

$$U(p) = \frac{k}{2\pi i z} \iint_{-\infty}^{+\infty} d^2 r u_0(r) e^{i \frac{k}{2z} (p-r)^2} e^{i S(p, r)}$$

↑ additional phase due to turbulent medium

Spatial coherence of the E field over the receiver plane

$$\langle |U(p)|^2 \rangle = \left(\frac{k}{2\pi z} \right)^2 \iiint_{-\infty}^{+\infty} \iiint_{-\infty}^{+\infty} d^2 r d^2 r' u_0(r) u_0(r') e^{i \frac{k}{2z} (p-r)^2} e^{i \frac{k}{2z} (p-r')^2} \cdot \langle e^{i S(p, r) - i S(p, r')} \rangle$$

$$\langle e^{i S(p, r) - i S(p, r')} \rangle = e^{-\frac{1}{2} D_s(0, r-r')}$$

close to the beam center

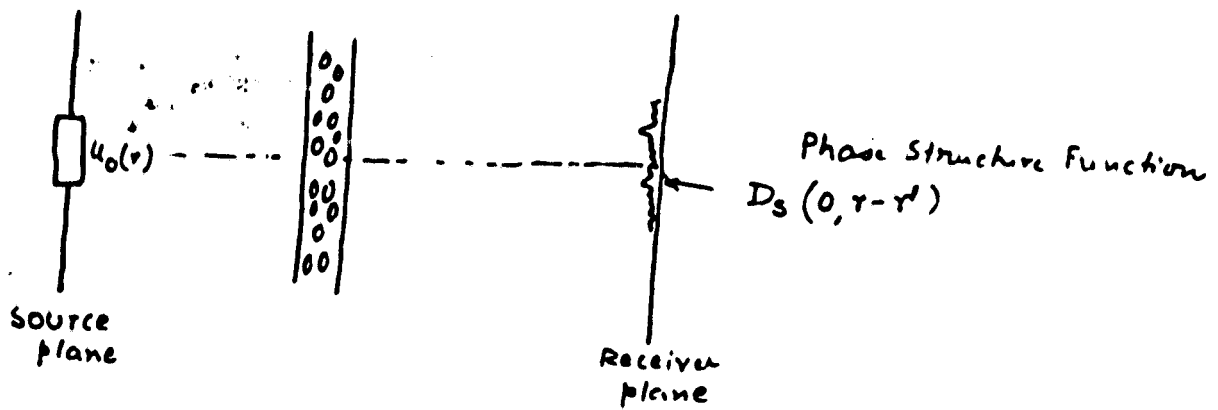
Phase Structure Function for Kolmogorov spectrum $\left[\frac{\phi(K)}{L} = 0.033 C_n^2 K^{-\frac{11}{3}} e^{-\frac{K}{k}} \right]$

$$D_s(0, r-r') = 2.92 k^2 \int_{z_0}^{z_0+\Delta} dz C_n^2(z) \left| \frac{L-z}{L} \right|^{5/3} |r-r'|^{5/3}$$

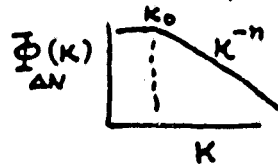
Knowledge of C_n , $K_m = \frac{5.91}{\text{inner scale}}$

For ionosphere $\Phi(K) = C_s K^{-4}$ appropriate for VHF & Microwaves

Fante,
1976



$D_S(r-r')$ ← I. Knowledge of turbulent structure



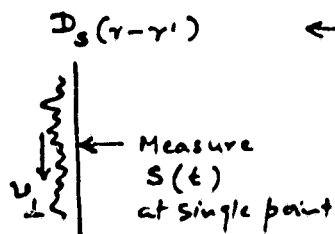
$$\Phi_{\Delta N}(K) = \frac{C_S}{(K^2 + K_0^2)^{\eta/2}}$$

↑
3-dimensional SDF of
integrated of ΔN

For ionosphere $K_0 \rightarrow 2\pi \times 10^{-3} \text{ m}^{-1}$ to $> 2\pi \times 10^{-4} \text{ m}^{-1}$
(typically)

$\eta \rightarrow \sim 4$

$C_S \rightarrow$ very variable
as large as 10^{20} mks in the equatorial region



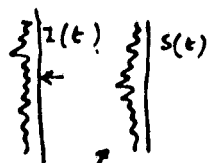
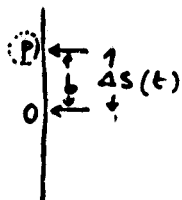
← II. Assume Taylor's hypothesis of "frozen turbulence" with v_{\perp} a constant velocity of inhomogeneities across the ray path.

$$S(r, t + \tau) = S(r - v_{\perp} \tau, t)$$

Obtain $\Phi_S(f) \rightarrow \Phi_S(K)$ Spatial
SDF of phase v_{\perp}

Geostationary source ↔ Doppler shift to be taken out.

$D_S(r-r')$ ← III Obtain $\Delta S(t)$ over variable baselines and compute all spatial harmonics of S



Weak scatterer γ -form

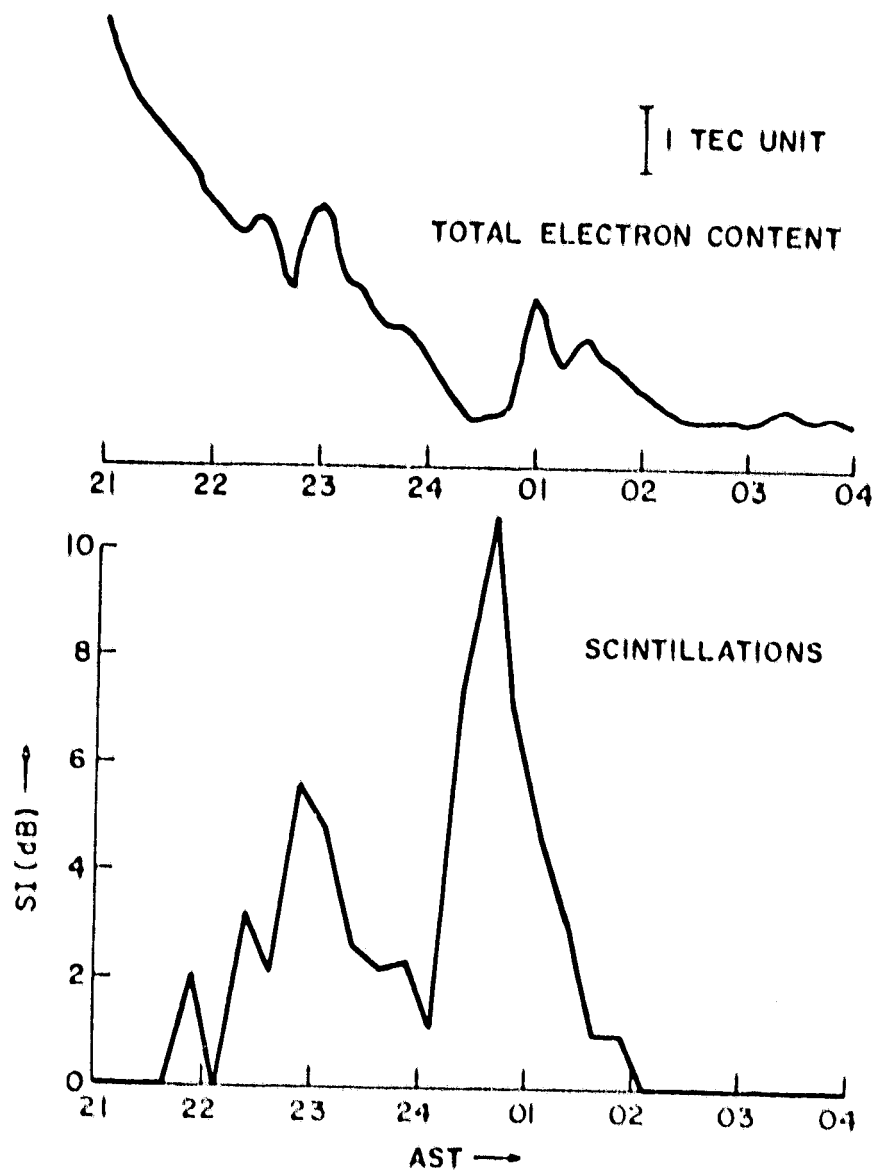
← IV Obtain intensity fluctuations which can be x-formed to phase fluctuations for weak scatter.

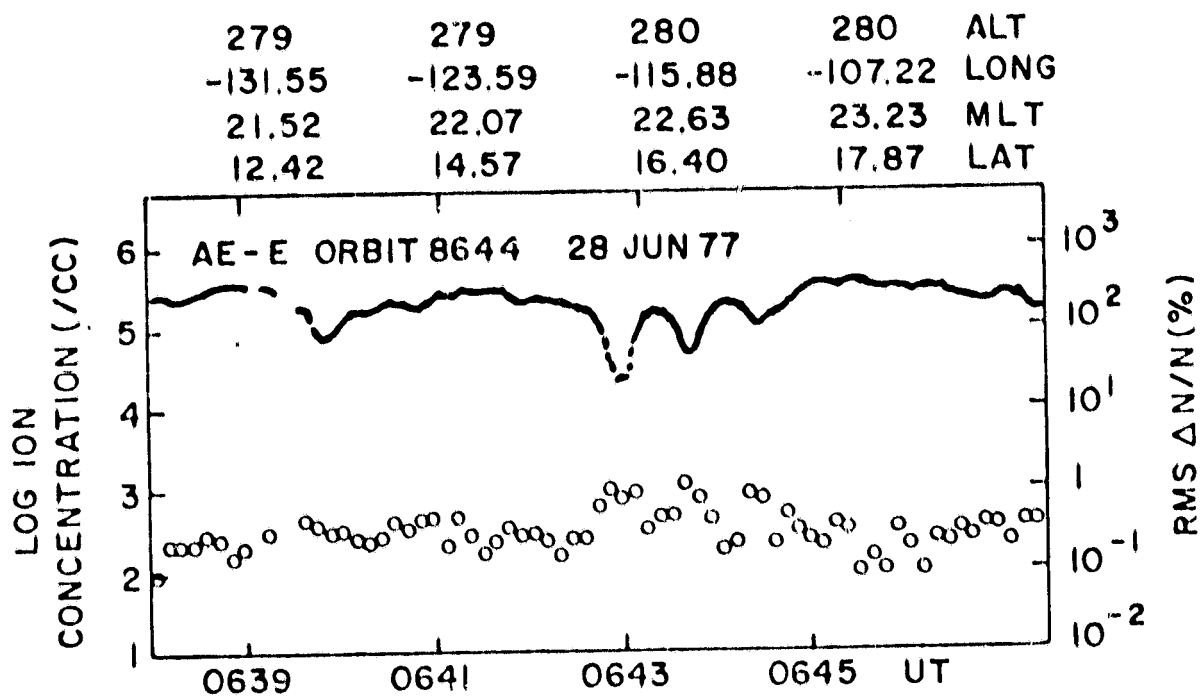
JUNE 28, 1977

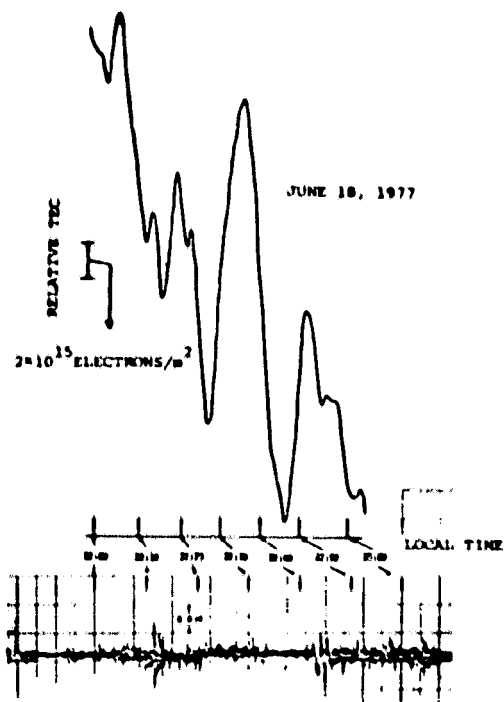
RAMEY, P. R.

SMS-1

137 MHz





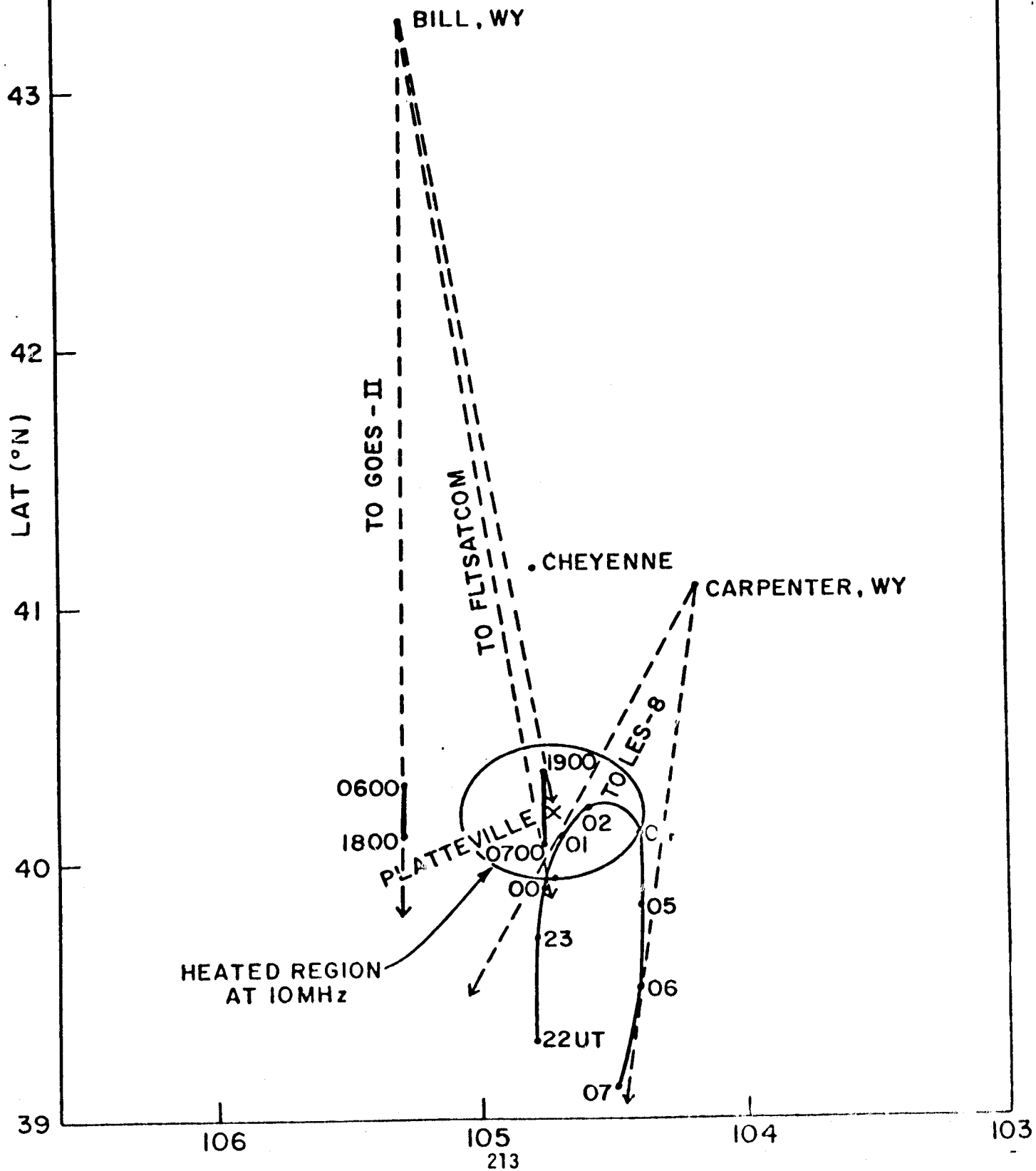


Example of nighttime scintillation (lower) and irregular variation of TEC (upper) observed at Kashima on June 18, 1977.

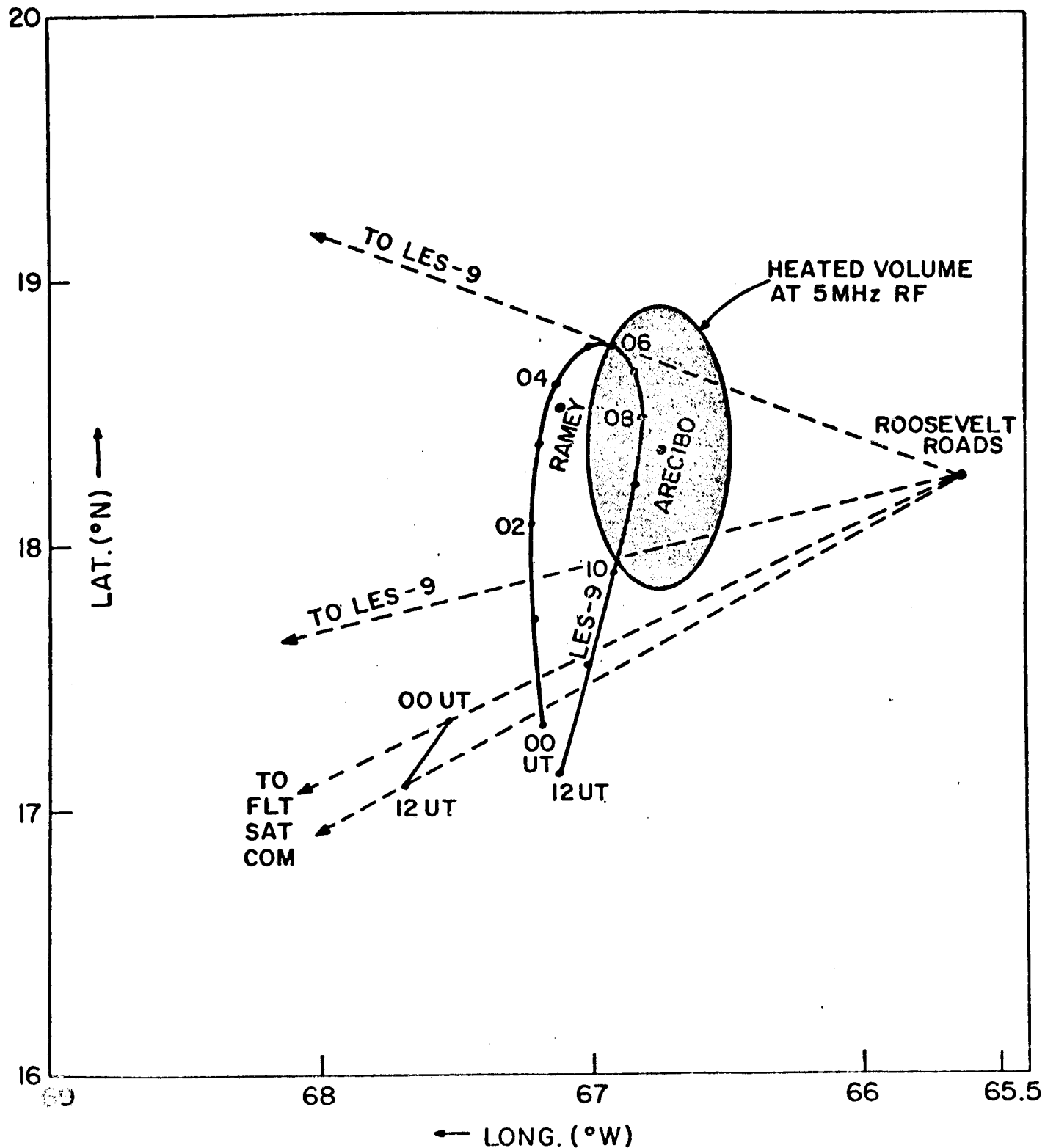
44

SATELLITE POSITIONS FC., MARCH 1, 1980

300km INTERSECTIONS FROM GROUND STATIONS IN WYOMING



SATELLITE POSITIONS FOR DEC. 20, 1979
300km INTERSECTIONS FROM ROOSEVELT ROADS, P. R.



NATURAL IRREGULARITY OBSERVATIONS AT MIDLATITUDES

RAMEY VHF OBS
137 MHz

INTENSITY FLUCTUATIONS : 22 dB

SECOND MOMENT OF INTENSITY : $S_4 = 0.8$

FOR 20 km outer scale $\phi_{rms}^{137 MHz} = 8 \text{ rad}$

BRUTE FORCE EXTRAPOLATION $\phi_{rms}^{2.2 GHz} = 0.5 \text{ rad}$

OVER 1 km $\phi_{rms}^{2.2 GHz} \sim 1^\circ$

JAPANESE OBS
1.7 GHz

INTENSITY FLUCTUATIONS $\rightarrow 2.3 \text{ dB}$

$S_4 = 0.15$

FOR 20 km outer scale $\phi_{rms}^{1.7 GHz} = 3 \text{ rad}$

OVER 1 km $\phi_{rms}^{8.7 GHz} \sim 8^\circ$

*Ionospheric Perturbations on
Uplink Pilot Beam Signal
(Theoretical)
and
Plattville Heating Test Results*

*K. Davis
Batelle Northwest Labs*

*D. Arndt
Lyndon B. Johnson Space Center*

PRECEDING PAGE BLANK NOT FILMED

- POWER BEAM MEDIA MODULATION
 - RECTENNA POWER VARIATIONS
 - OFF-RECTENNA COMPONENTS
 - SIDELobe VARIATIONS
- PILOT BEAM MEDIA MODULATION
 - SPATIAL AND TEMPORAL COMPONENTS
 - SPATIAL CORRELATION
 - INDUCED DOPPLER

ATMOSPHERE MEDIA SIGNAL EFFECTS - APPLICATION AREAS

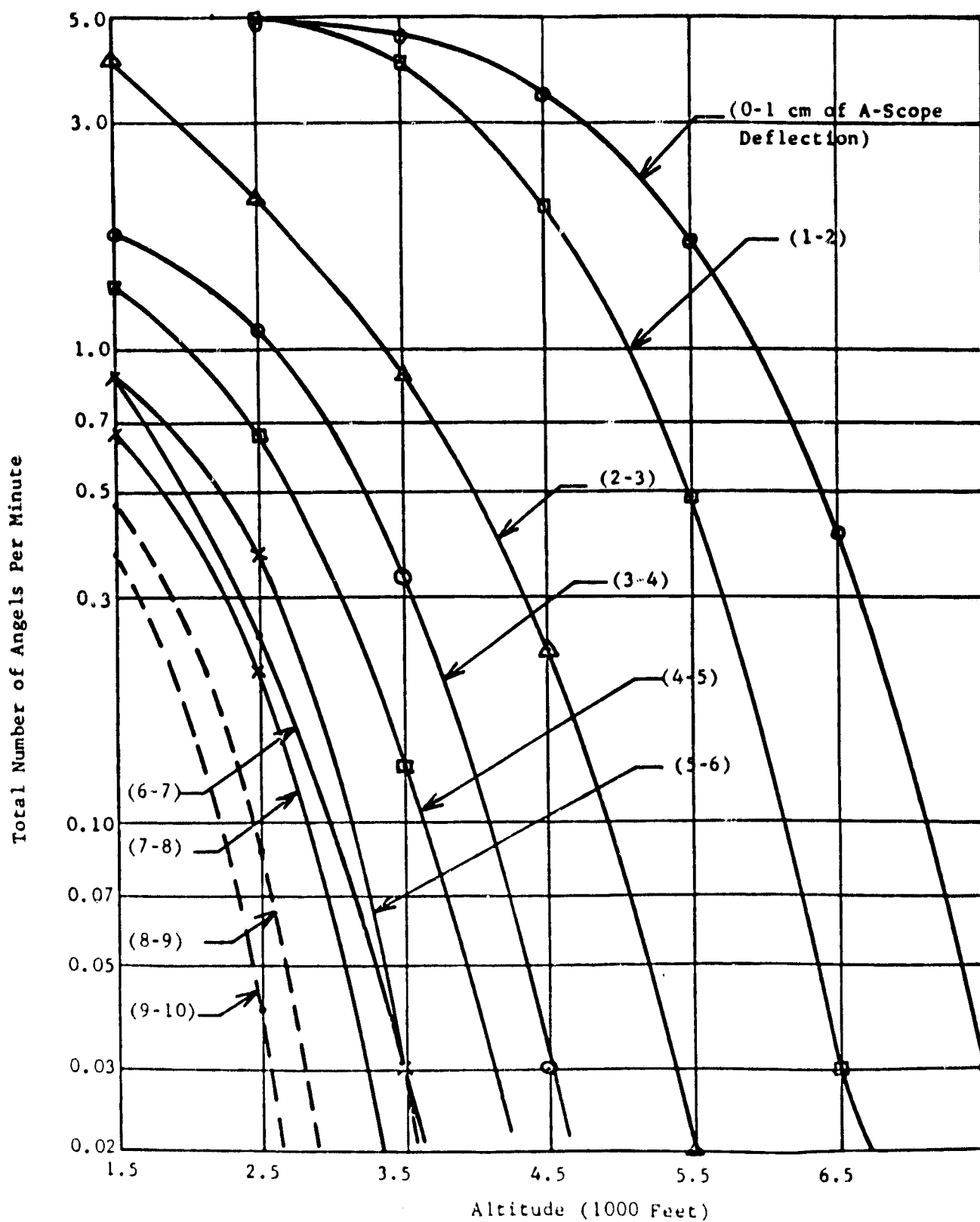


Figure 25. Angel Rate as a Function of Altitude for Various Amplitude Increments.

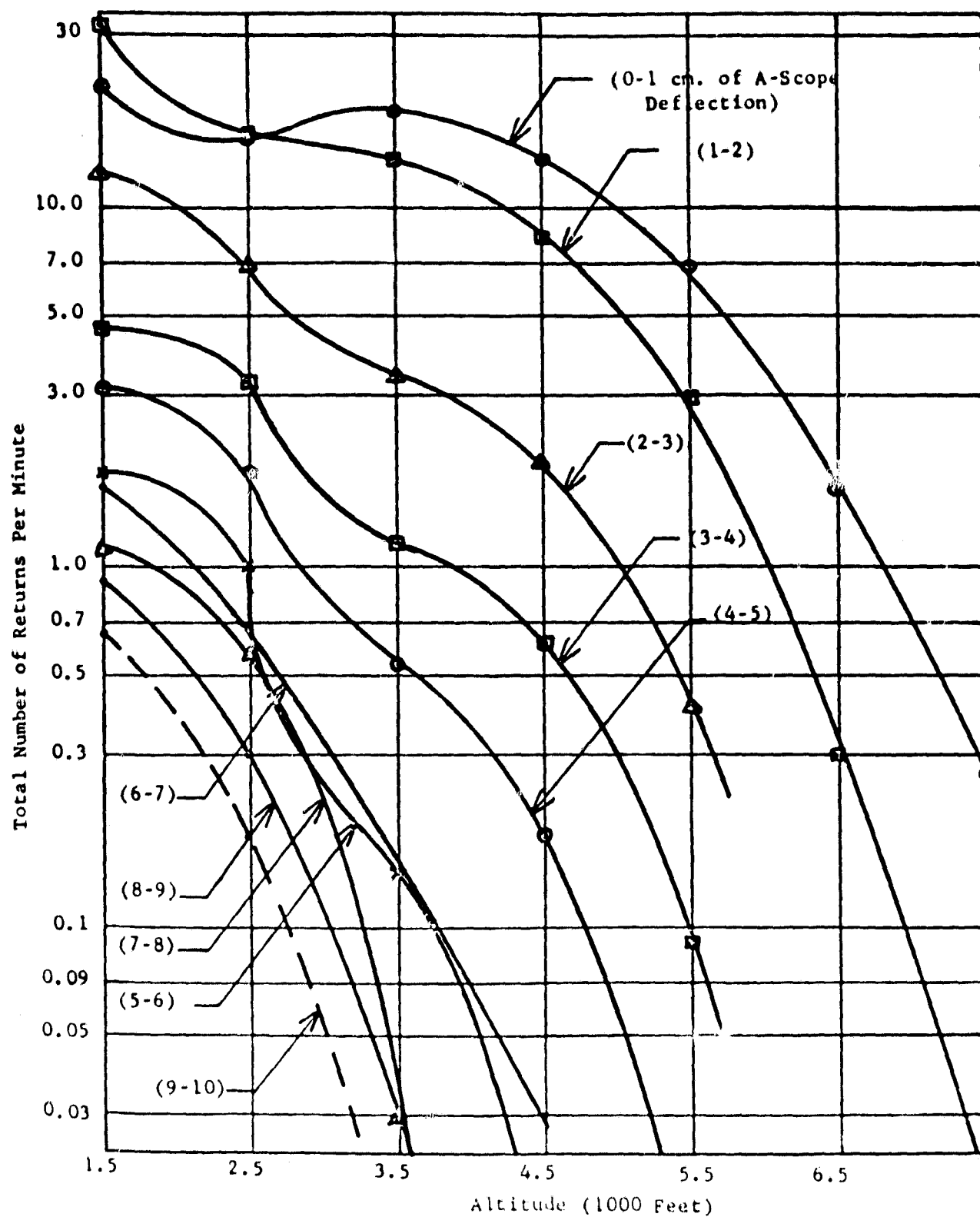


Figure 24. Return Rate as a Function of Altitude for Various Amplitude Increments

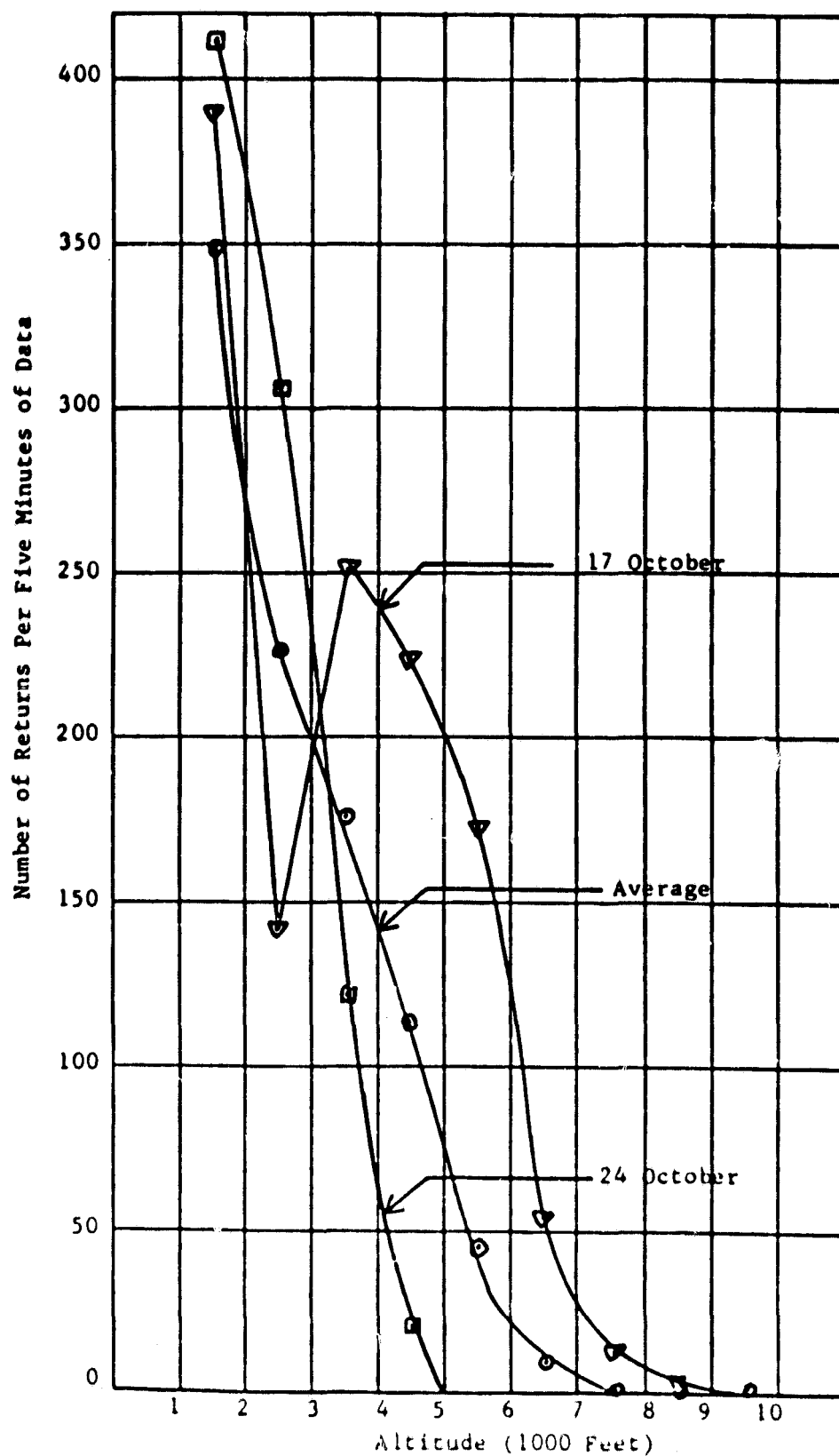


Figure 27. Number of Returns as a Function of Altitude

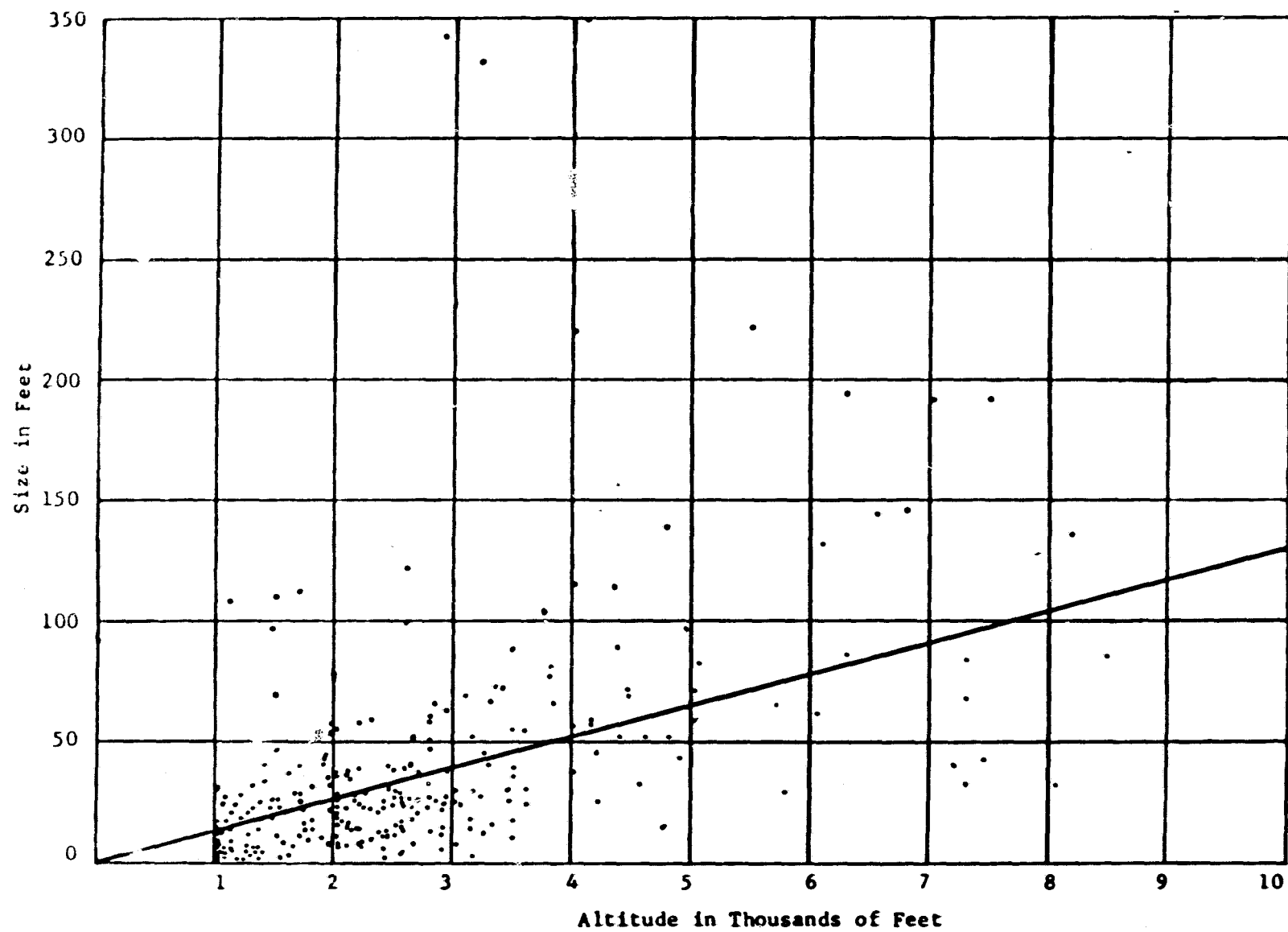


Figure 47. Angel Size Versus Altitude

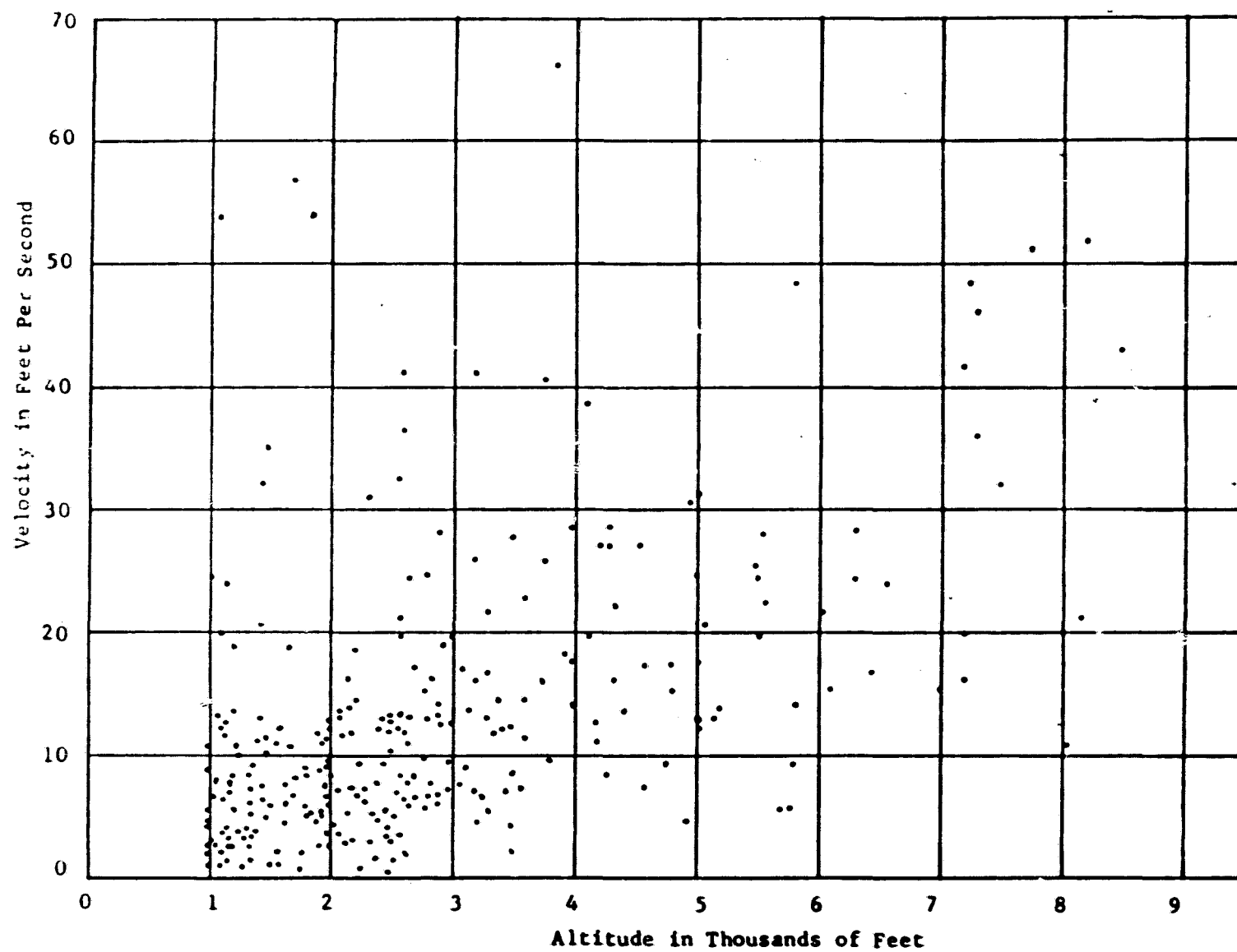


Figure 46. Angel Velocity Versus Altitude

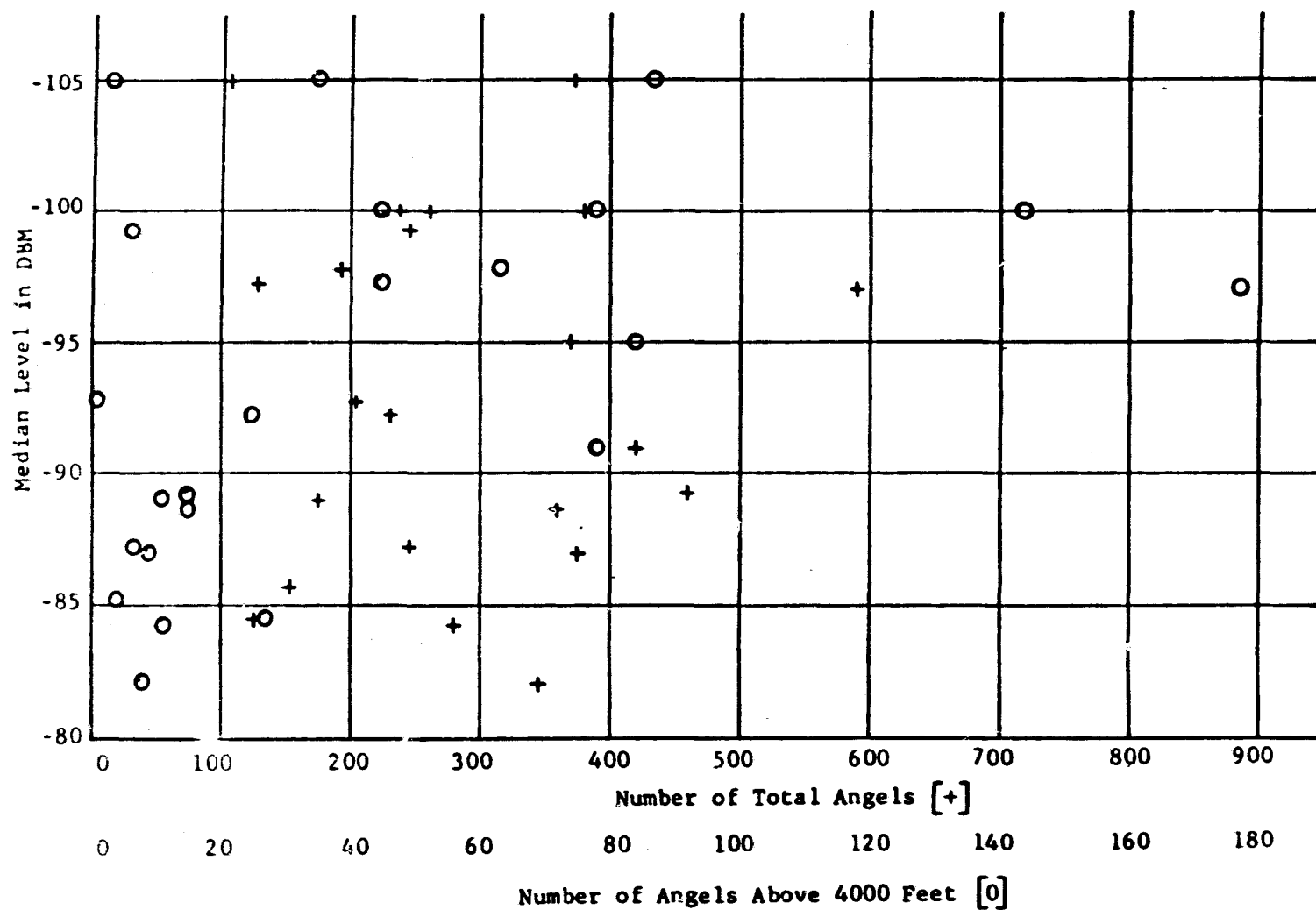


Figure 41. Median Level - Angel Scatter Diagram

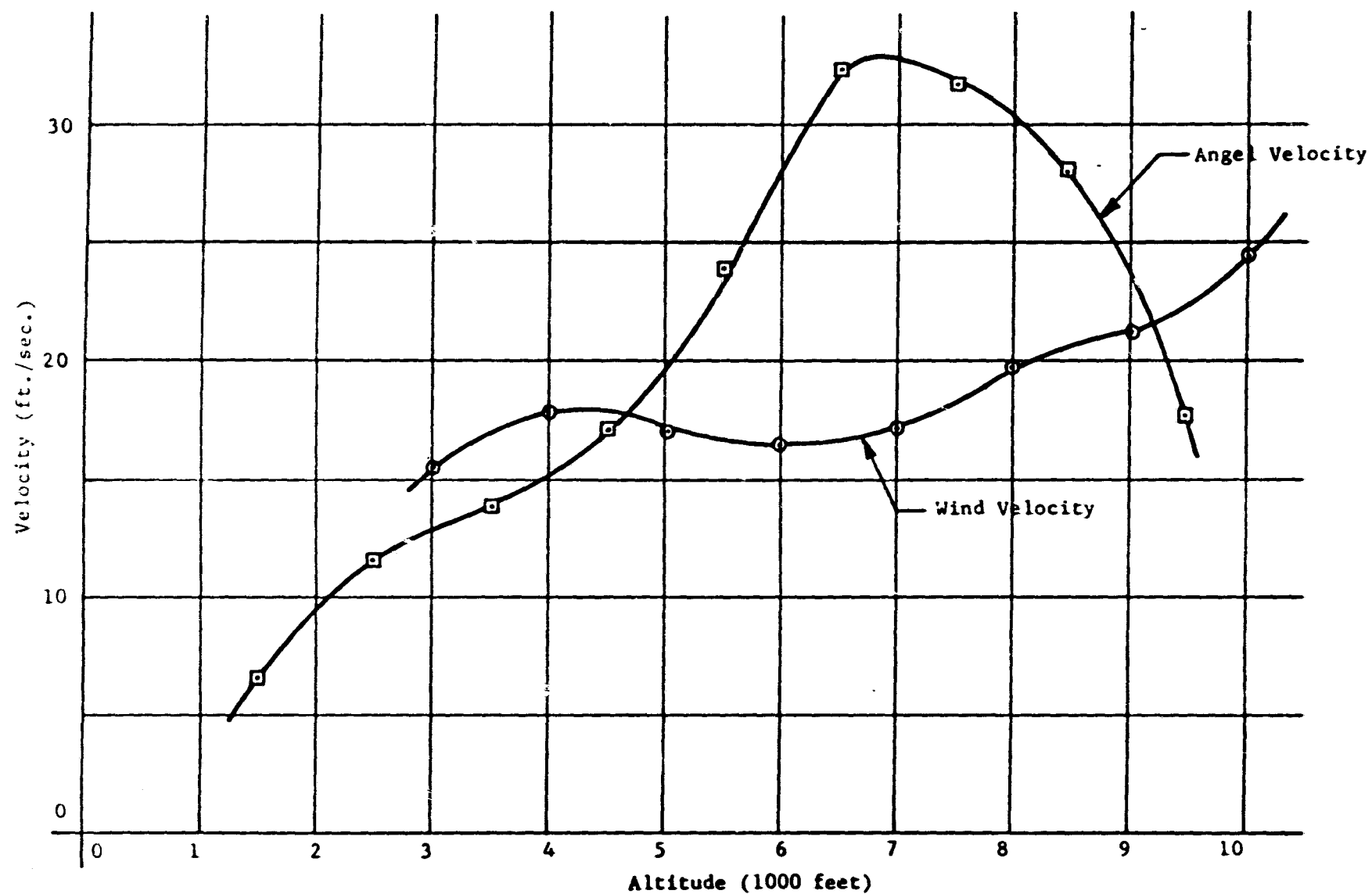
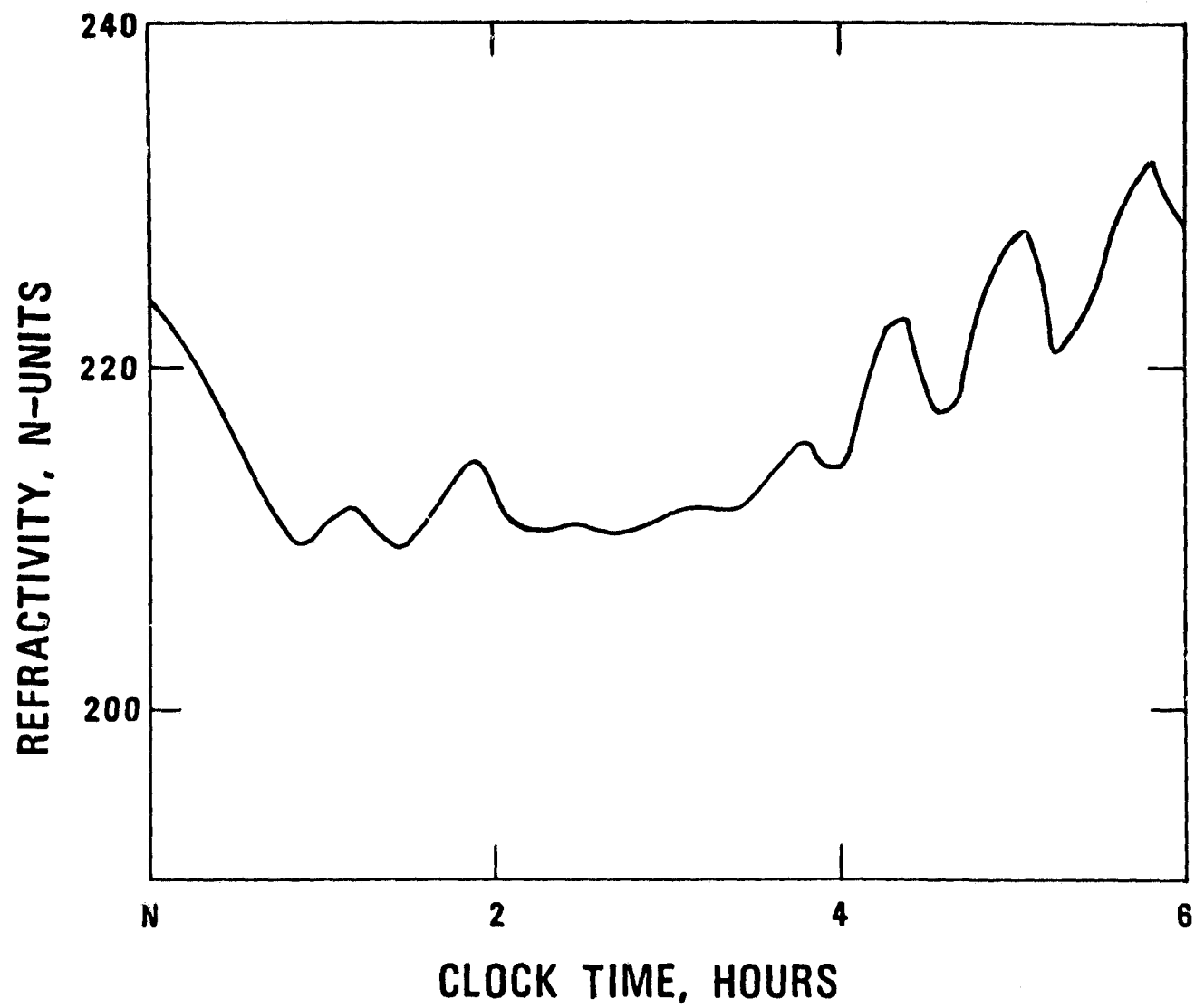


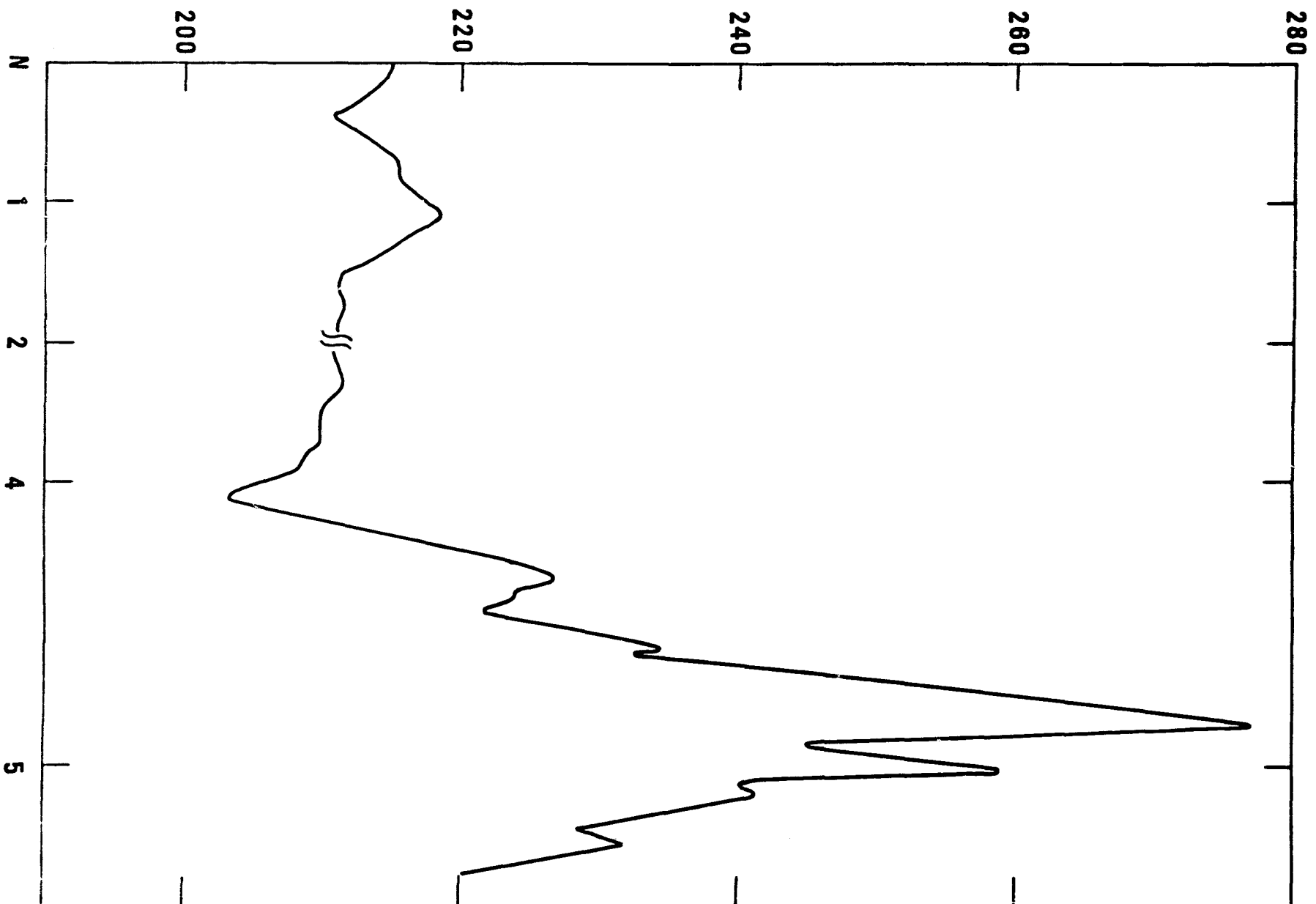
Figure 29. Comparison of Wind and Angel Velocity as a Function of Altitude

- Transmission Frequency 3.6 GHz
- Data Bandwidth 50 MHz
- Transmit Antenna Beamwidth 0.75°
- Carrier Loop Bandwidth 25 Hz
- Link S N 36 dB
- Link Distance 19.2 KM (Avg)
- Elevation Angle Range 23° - 27°

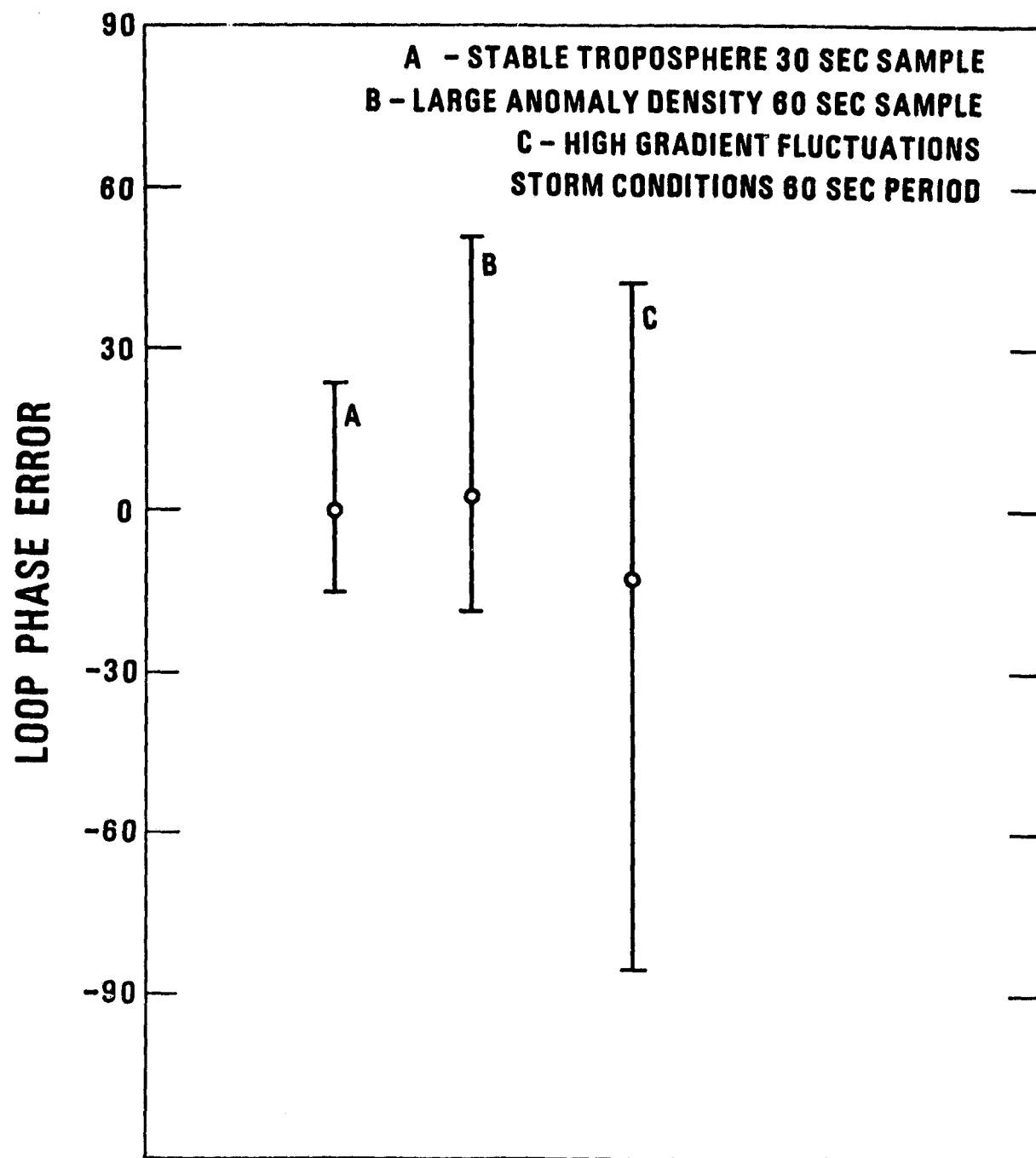
TEST LINK CHARACTERISTICS



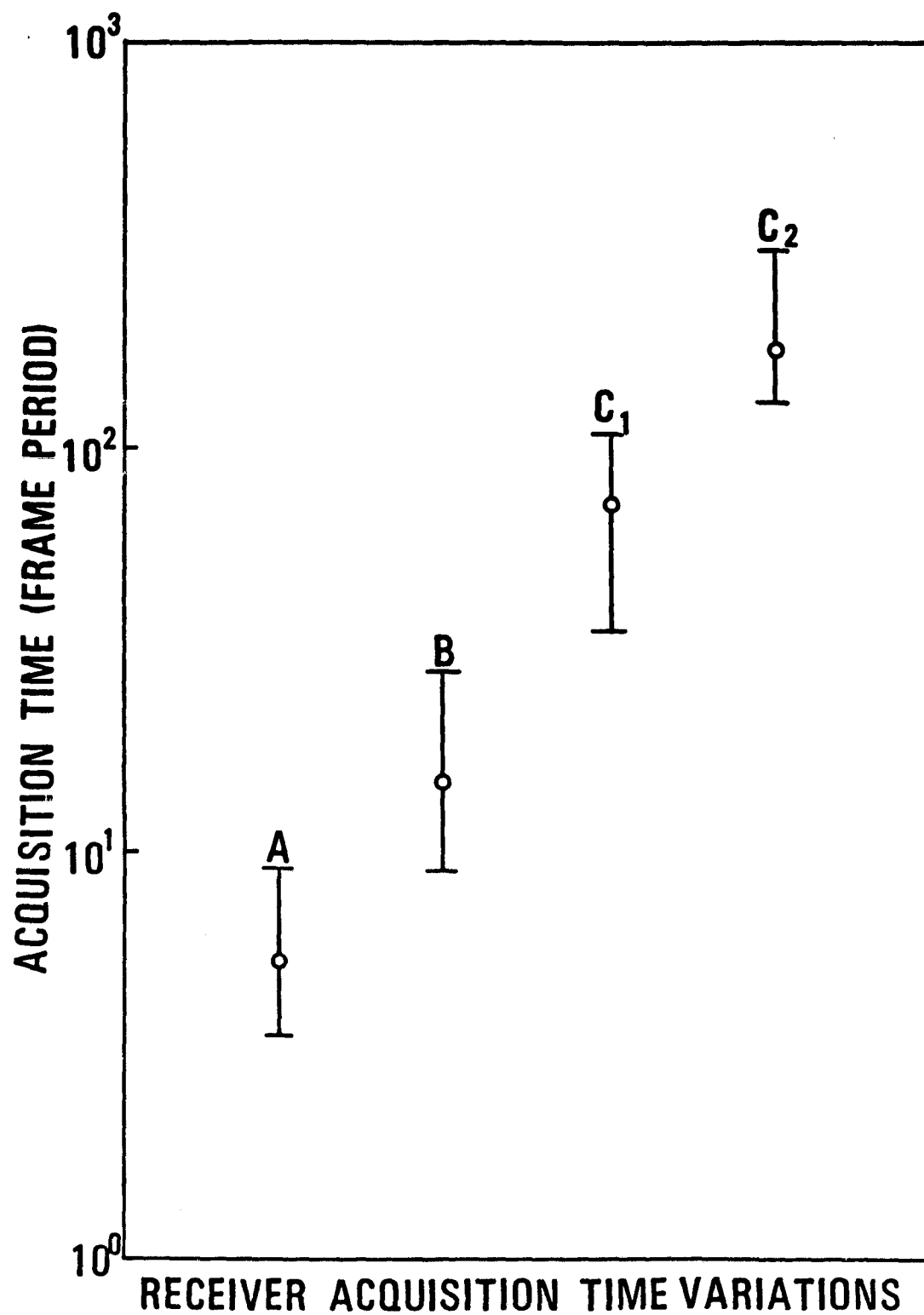
REFRACTIVITY, N-UNITS

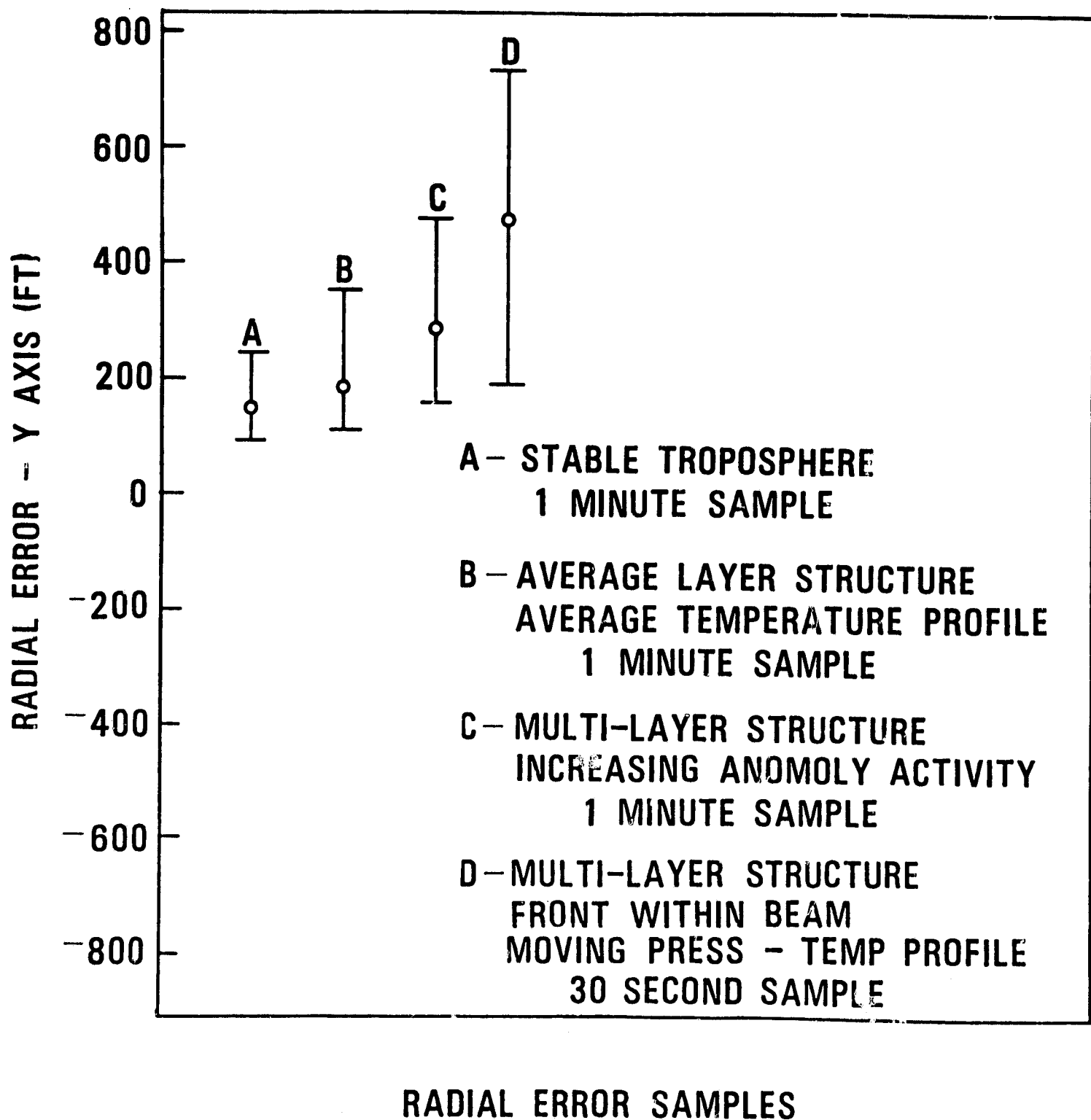


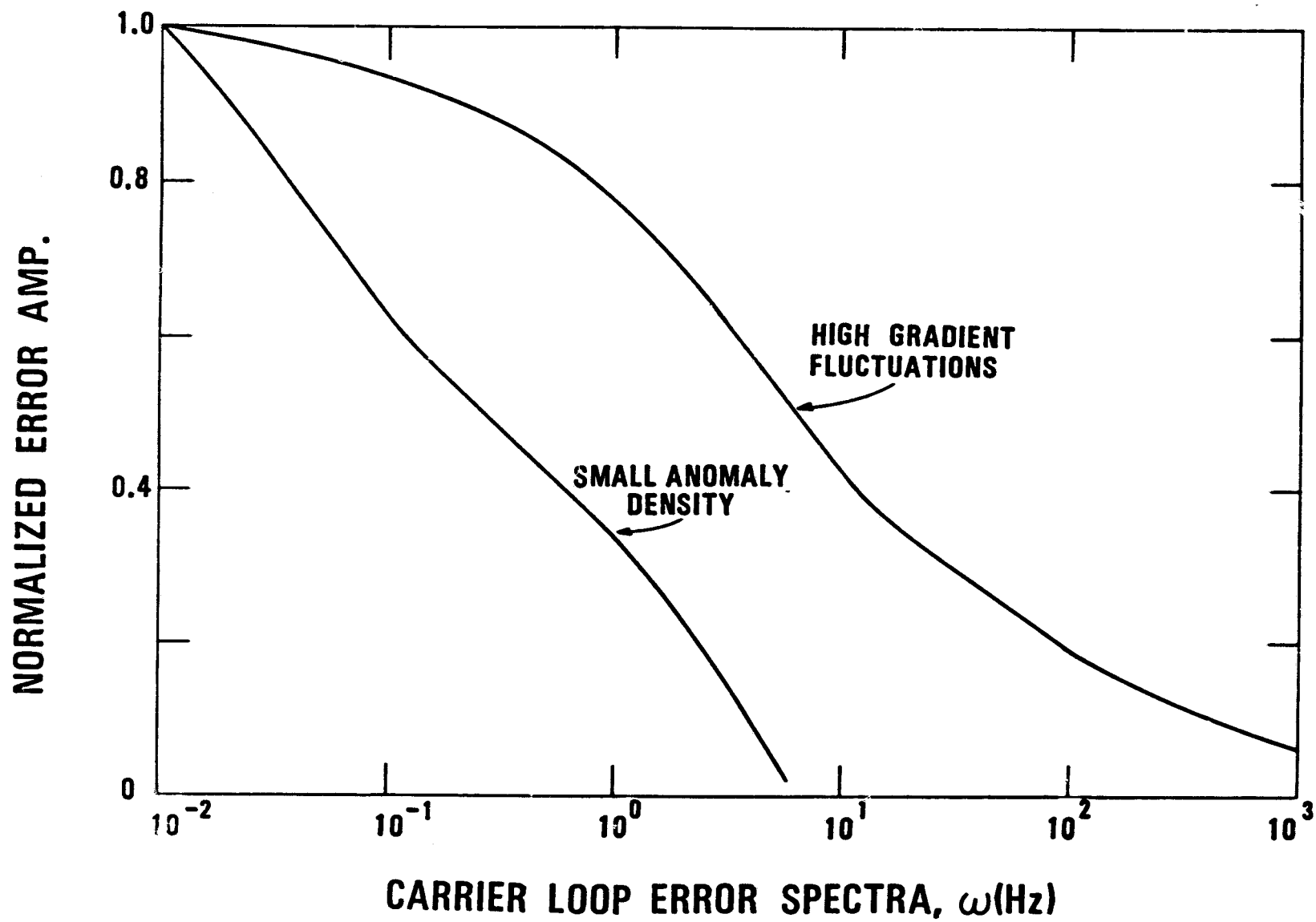
CLOCK TIME, HOURS



TRACK LOOP ERROR DISTRIBUTIONS







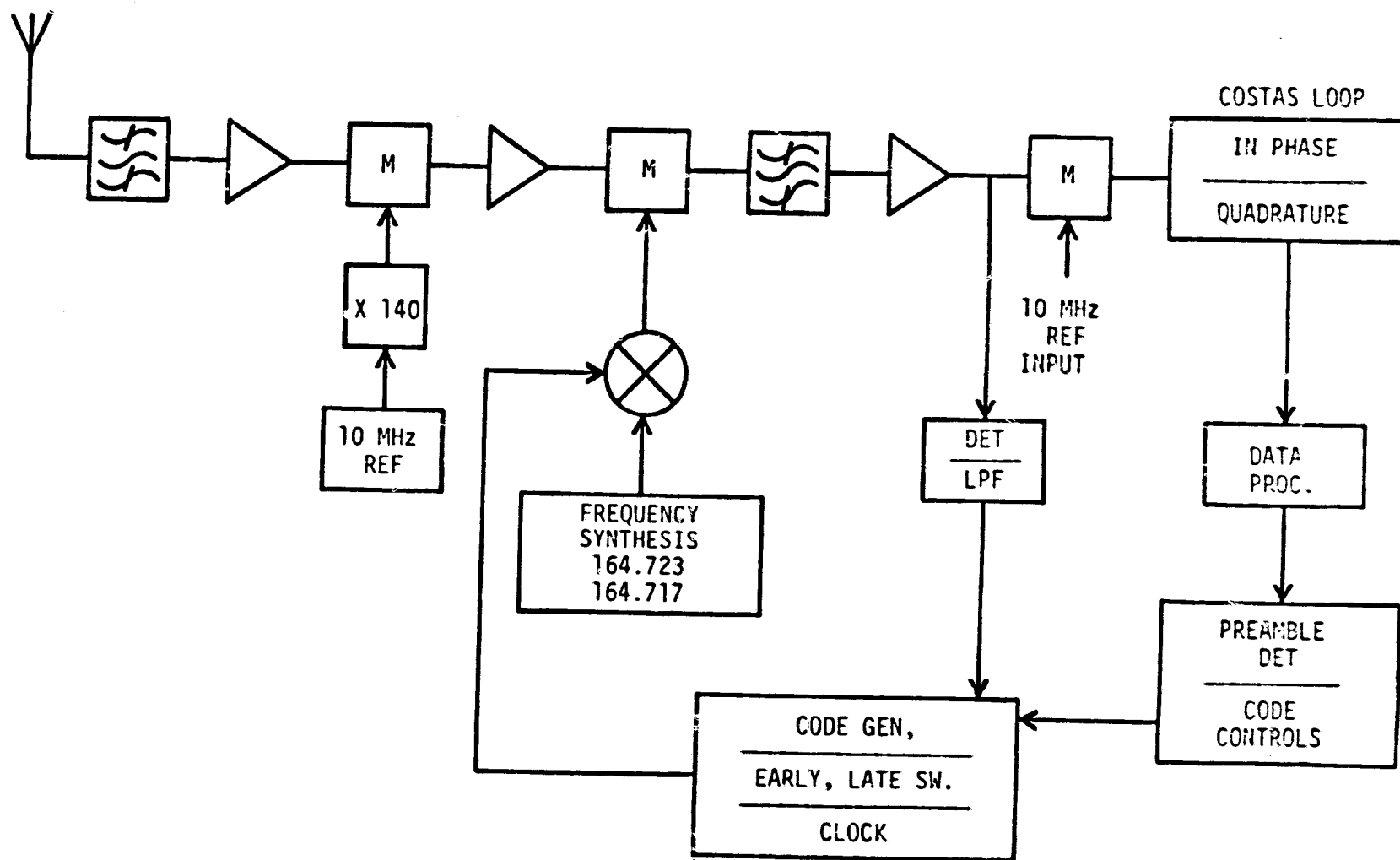
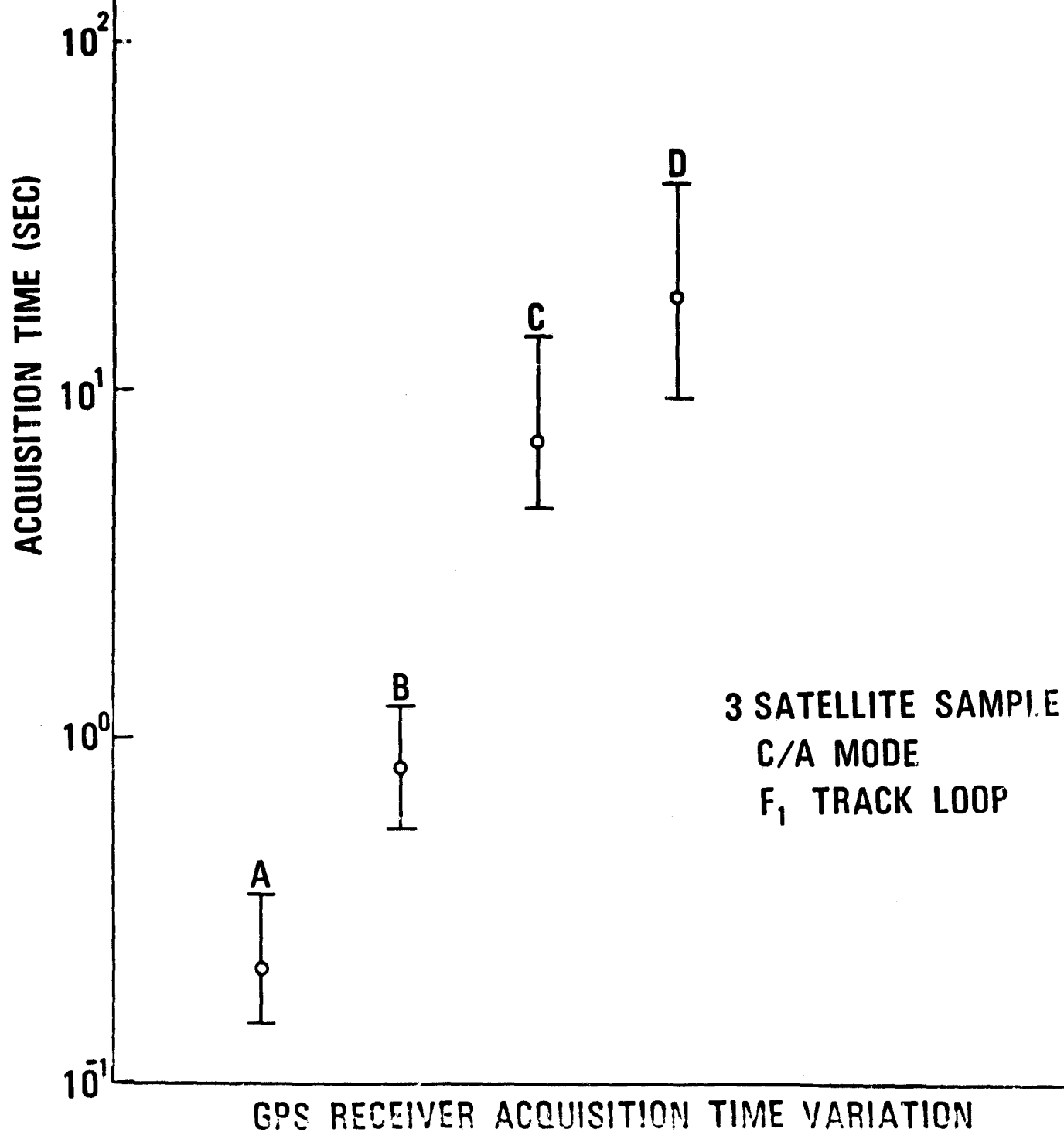


Figure 2. Functional configuration-GPS single channel receiver

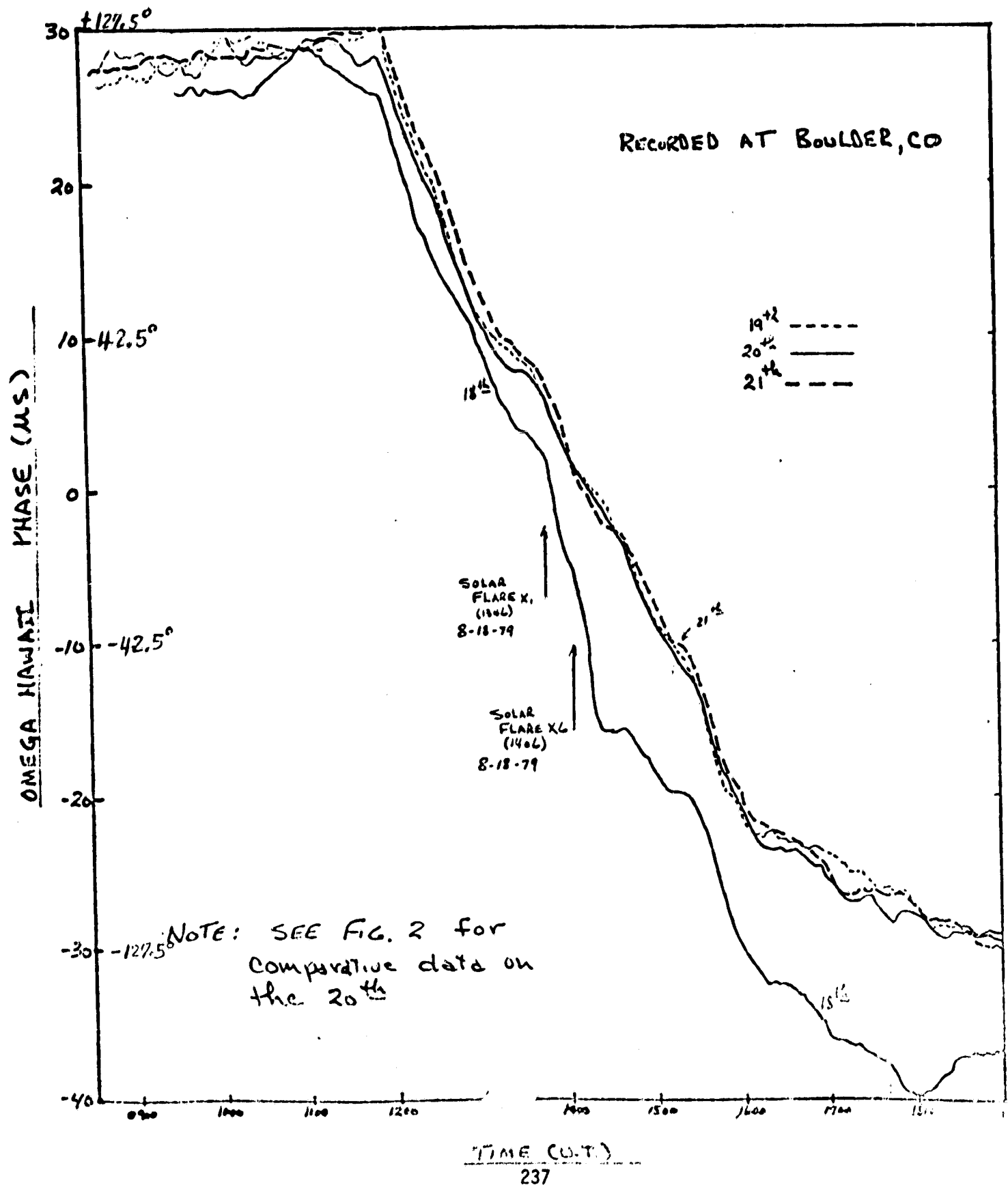
- A - RECEIVER CAPABILITY
- B - AVERAGE IONOSPHERE
- C - DISTURBED IONOSPHERE
- D - DISTURBED IONOSPHERE, STORM FRONT



TELECOMMUNICATIONS EFFECTS EXPERIMENTS
CONDUCTED BY
THE INSTITUTE FOR TELECOMMUNICATION SCIENCES

- UTILIZE PLATTVILLE HEATER TO SIMULATE SPS HEATING OF D&E REGION
- DETERMINE EFFECTS OF HEATING ON SUCH SIGNALS AS
 - LORAN C - 100 KHz
 - OMEGA - 11.8 KHz
 - WWV - 2.5 MHz
 - WWVB - 60 KHz
 - AM BROADCAST - 650 KHz - 1 MHz
- MEASUREMENTS MADE USING MOBILE VAN
 - AMPLITUDE VARIATIONS VS. TIME
 - PHASE VARIATIONS VS. TIME

FIG. 5 OMEGA PHASE FROM FOUR CONSECUTIVE DAYS



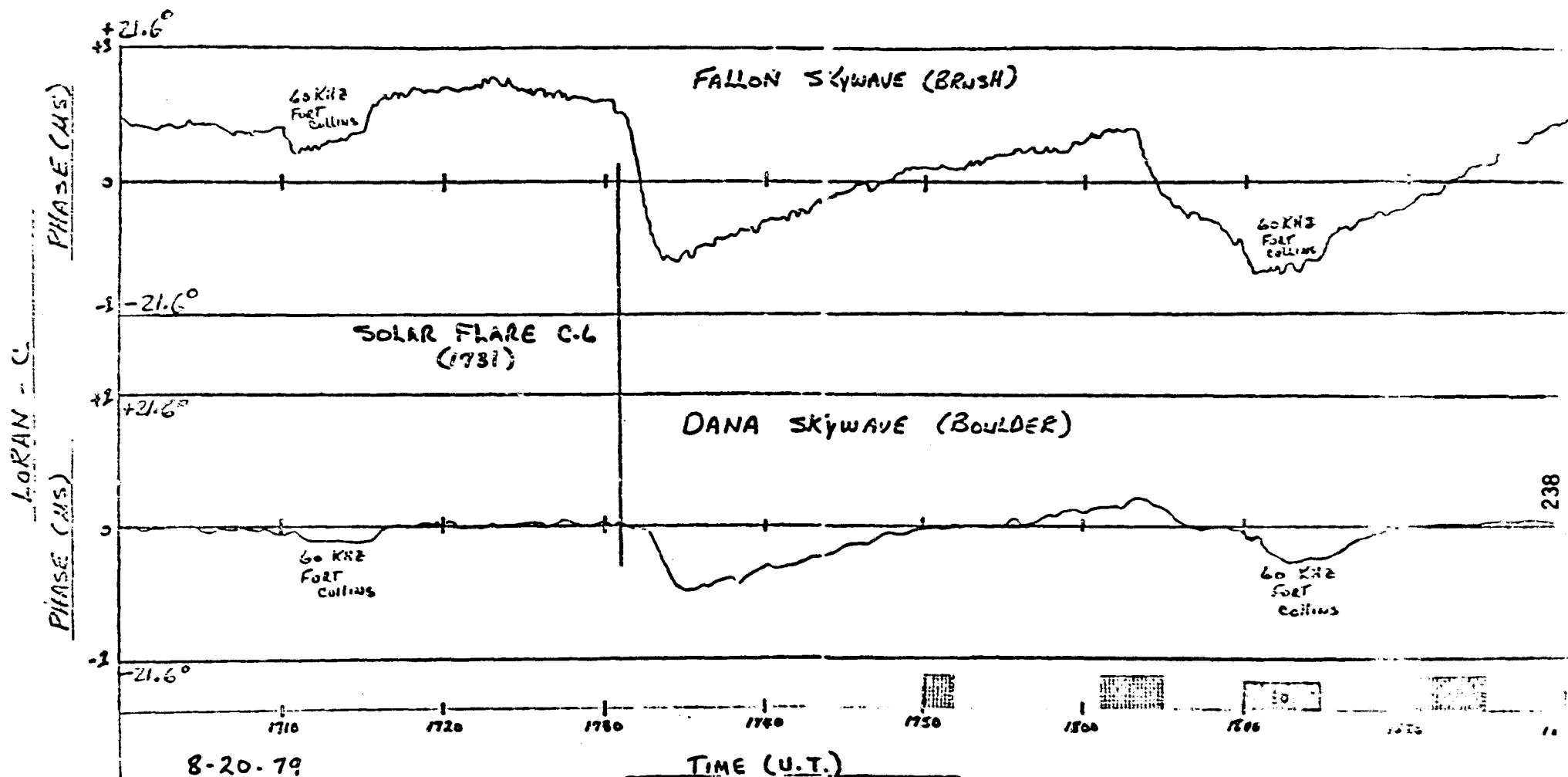


FIG 4 LORAN-C PHASE RECORDED AT BRUSH AND BOULDER

EXPERIMENT RESULTS

- SPS HEATING HAS NO DETECTABLE IMPACTS ON TELECOMMUNICATION/NAVIGATION SIGNALS
 - NO CORRELATION BETWEEN AM/PM VARIATIONS AND HEATING
 - NATURAL PHENOMENON (SOLAR FLARE) RESULT IN AM/PM VARIATIONS ORDERS OF MAGNITUDE GREATER THAN ANY OBSERVED DURING HEATING PERIODS
- PLATTVILLE MAY BE CAPABLE OF HEATING F REGION TO SPS EQUIVALENT LEVELS
 - SCALING MAY BE PROPORTIONAL TO $1/F^3$ INSTEAD OF $1/F^2$
- EVIDENCE HAS BEEN OBTAINED THAT IONOSPHERIC IRREGULARITIES DO NOT FORM IN THE F REGION FOR UNDERDENSE HEATING CONDITIONS

STATUS/RECOMMENDATIONS

- ADDITIONAL TESTS USING THE PLATTVILLE HEATER
 - TESTS PLANNED IN MARCH 1980
 - INVESTIGATE F REGION HEATING EFFECTS
 - BASU AND BASU - SCINTILLATION EXPERIMENTS
 - RECOMMENDED ADDITIONS TO MARCH TESTS
 - APL/UT - ELECTRON DENSITY MEASUREMENTS
 - REQUIRES FUNDING 30K
 - ITS WILL COORDINATE HEATING EXPERIMENTS FOR PROPER NAV. SAT. COVERAGE, ETC.
 - INVESTIGATE POTENTIAL TESTING WITH THE VLA (VERY LARGE ARRAY) AT THE NATIONAL RADIO ASTRONOMY OBSERVATORY NEAR SOCORRIO, N. M.
 - PHASE VARIATIONS OF RADIO STAR SIGNALS DUE TO IONOSPHERIC HEATING



National Aeronautics and
Space Administration

Lyndon B. Johnson Space Center
Houston, Texas 77058



3

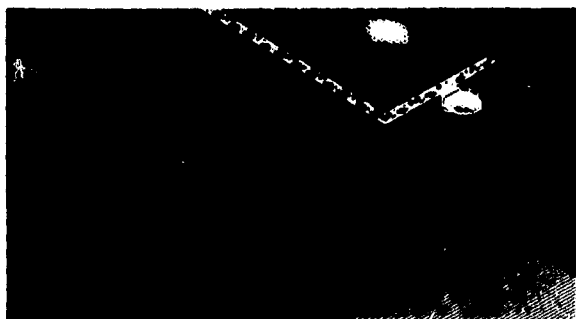
**Phase
Control**



**NASA Solar Power Satellite Workshop on
Microwave Power
Transmission
and Reception**

**Session
Presentations**

**Jan
15-18
1980**



The presentation material herein was used in the Phase Control Session of the Solar Power Satellite Workshop on Microwave Power Transmission and Reception held at the Lyndon B. Johnson Space Center, January 15-28, 1980. The workshop was conducted as part of the technical assessment process of the DOE/NASA Solar Power Satellite Concept Evaluation Program. All aspects of Solar Power Satellite microwave transmission and reception were addressed including studies, analyses, and laboratory investigations. Conclusions from these activities were presented as well as recommended follow-on work. The workshop was organized into eight sessions as follows:

- *General*
- *Microwave System Performance*
- *Phase Control*
- *Power Amplifiers*
- *Radiating Elements*
- *Rectenna*
- *Solid State Configurations*
- *Planned Program Activities*

The material contained herein supplements the workshop papers which were published and distributed at the time of the workshop. Together they are a comprehensive documentation of the numerous analytical and experimental activities in the field of microwave power transmission and reception.

● *Additional information
regarding the workshop
may be obtained by*

contacting: R.H. Dietz
EE4/SPS Microwave Systems
National Aeronautics &
Space Administration
Lyndon B. Johnson Space Center
Houston, Texas 77058
713 483-4507

3

Phase Control Session

contents

- | | |
|------------|---|
| 1 | Active Retrodirective Arrays
Ralph Chernoff/Jet Propulsion Lab |
| 17 | Performance Analyses and Simulation of the
Solar Power Satellite Phase Control System
Dr. W. C. Lindsey/Lincom and C. M. Chie, Lincom |
| 47 | Design and Breadboard Evaluation of the
Solar Power Satellite Reference Phase Control
System Concept
Dr. P. M. Hopkins, Lemsco |
| 67 | Solar Power Satellite Phase Control System Studies
G. Woodcock, Boeing |
| 79 | Solar Power Satellite Fiber Optic Link Assessment
Dr. E. Nalos, Boeing |
| 89 | Ionospheric Effects in Retrodirective Arrays and
Mitigating System Design
Dr. A. K. Nandi, Rockwell International |
| 109 | An Interferometer-Based Phase Control System
Dr. J. Rice, Novar |
| 127 | A Coherent Multitone Technique for Ground Based
Phase Control
Dr. C. M. Chie, Lincom |
| 143 | A Sonic Satellite Power System Microwave Power
Transmission Simulator
J. Ott, Novar |

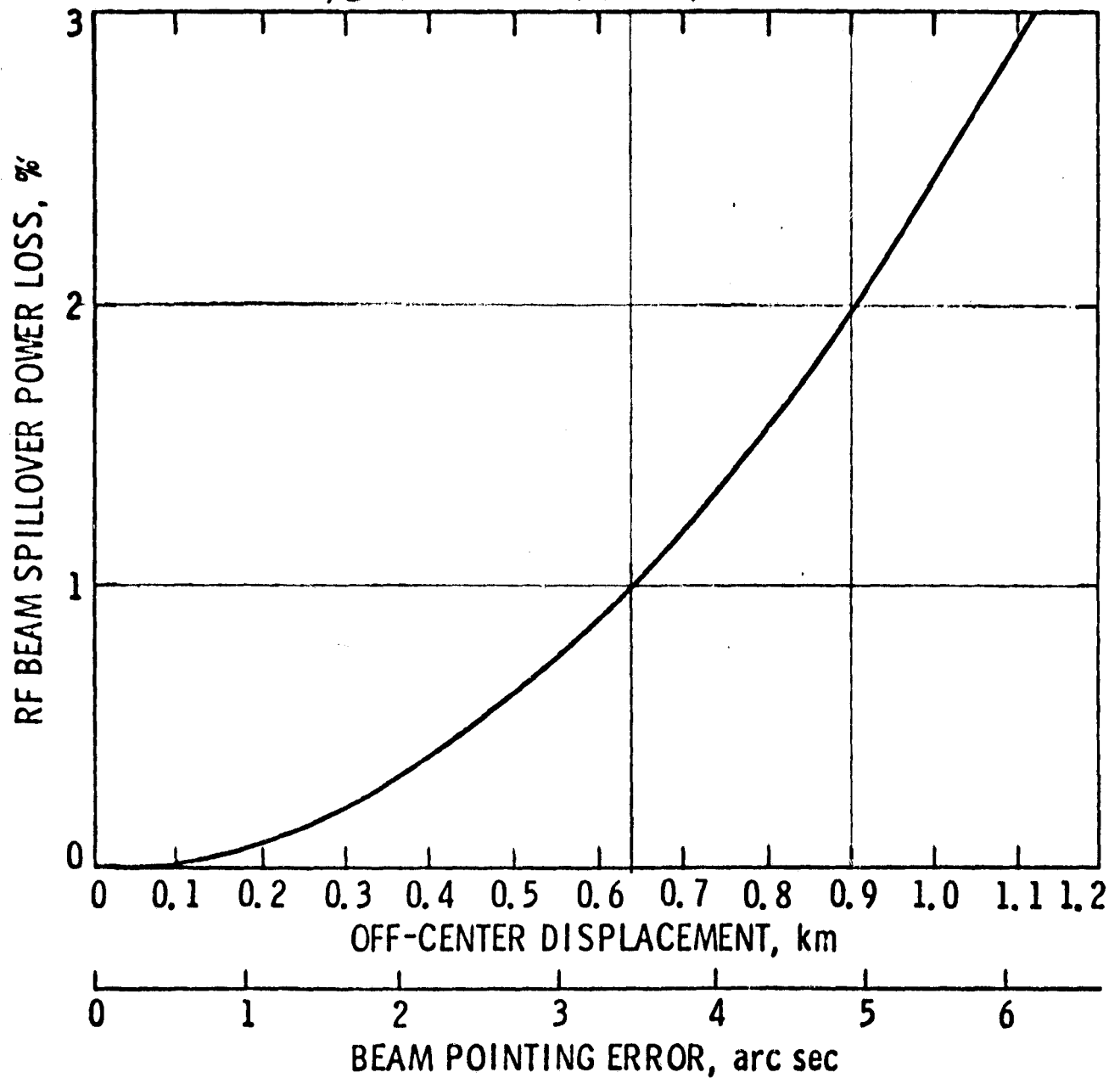
D/

Active Retrodirective Arrays

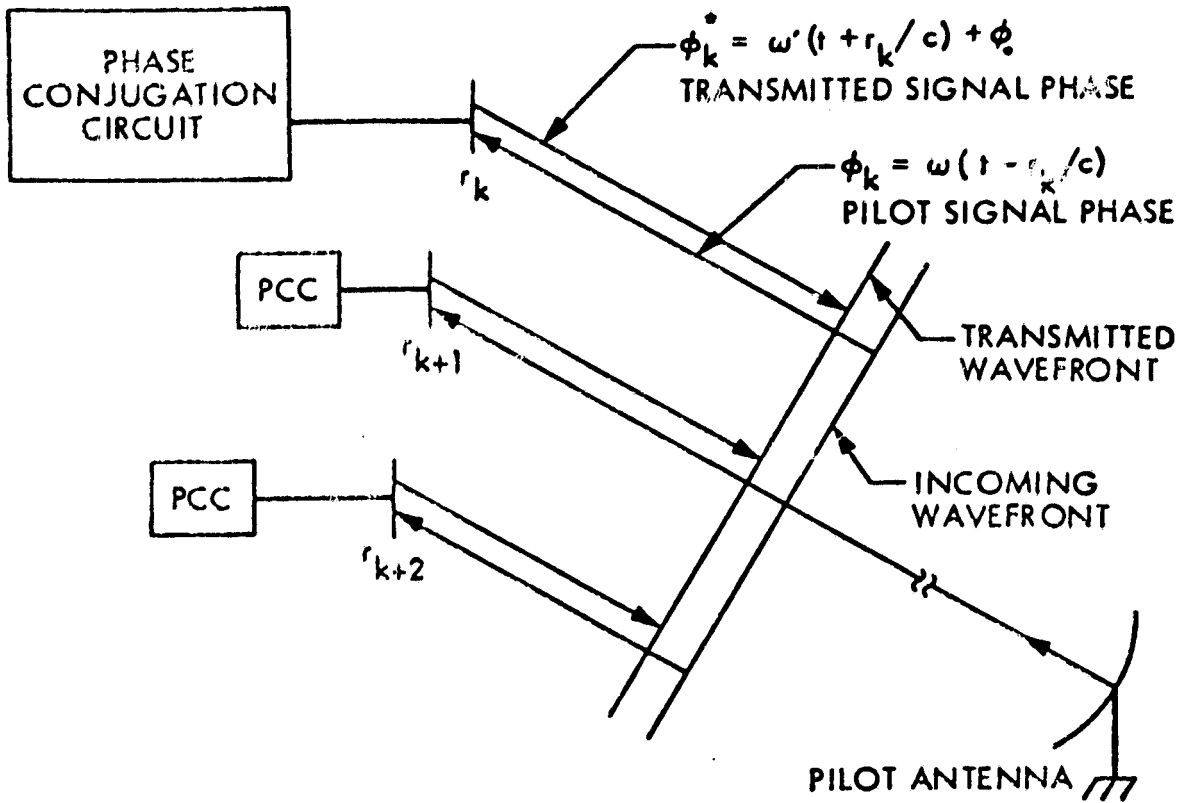
***Ralph Chernoff
Jet Propulsion Lab***

SPS BEAM POINTING LOSS

10 dB GAUSSIAN TAPER

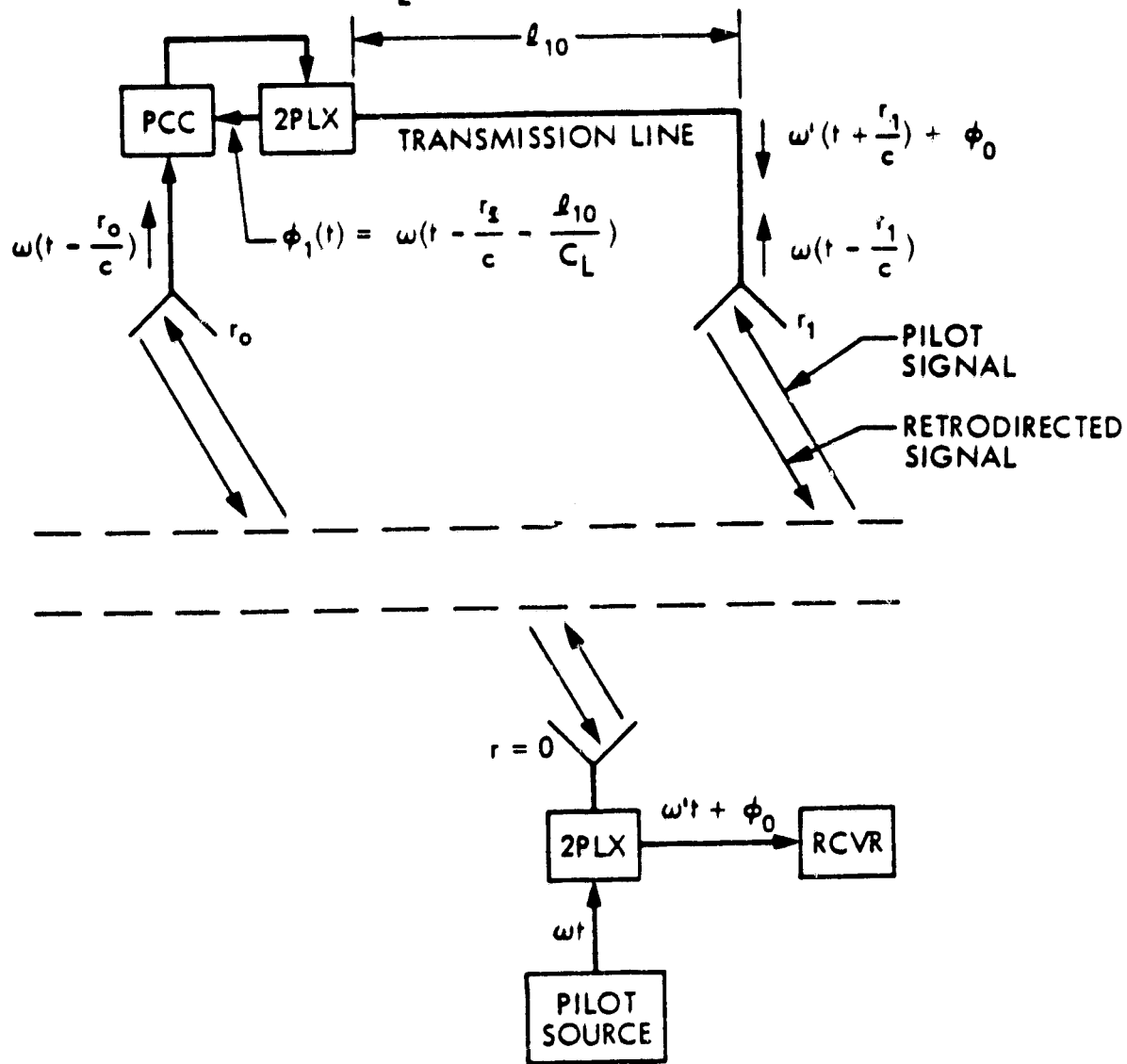


PRECEDING PAGE BLANK NOT FILMED

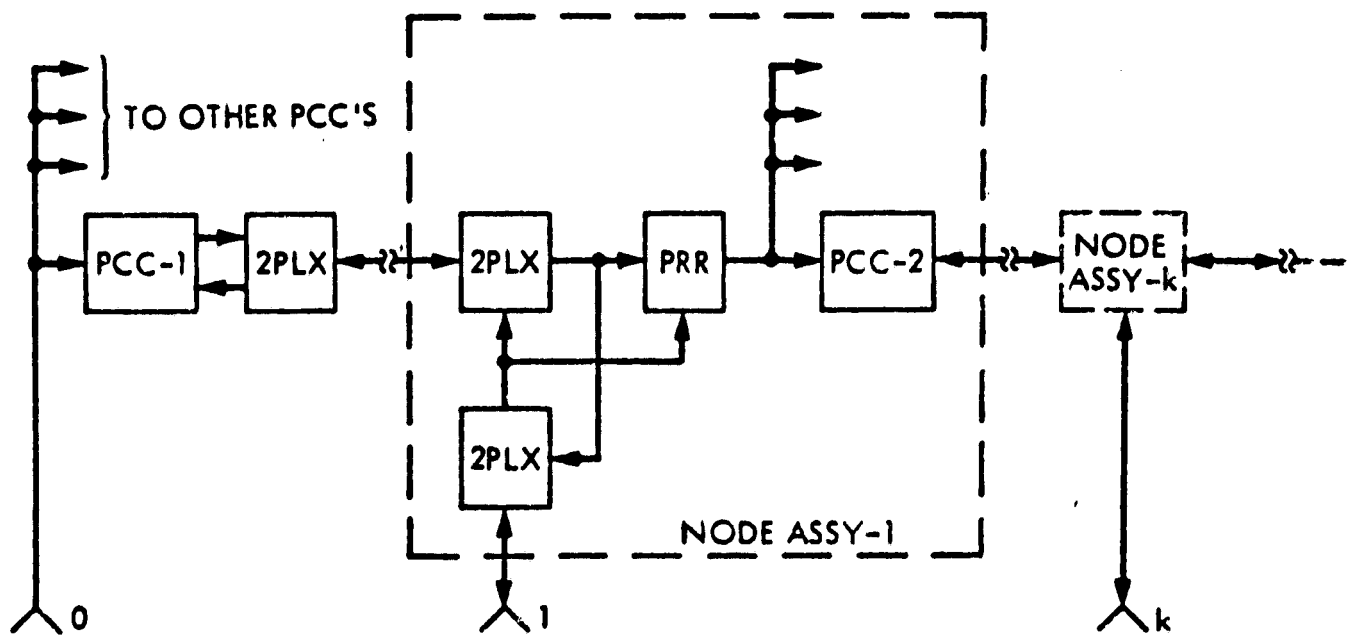


ACTIVE RETRODIRECTIVE ARRAY

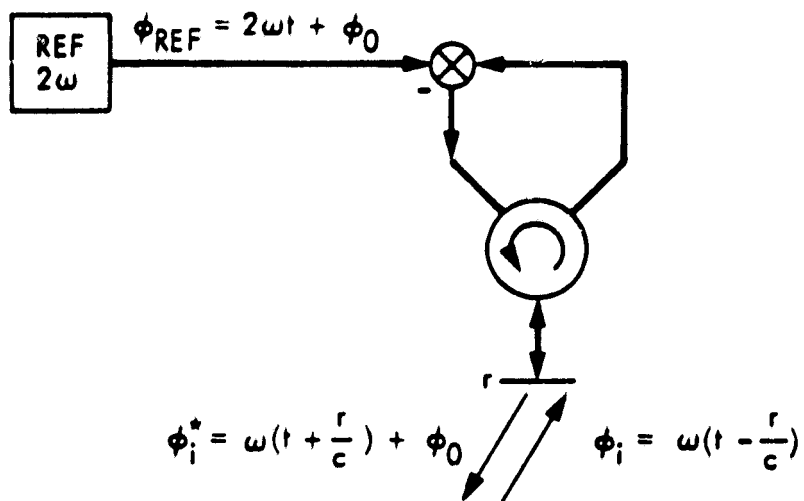
$$|\phi_1(t)|^* = \omega'(t + \frac{r_1}{c} + \frac{d_{10}}{C_L}) + \phi_0$$



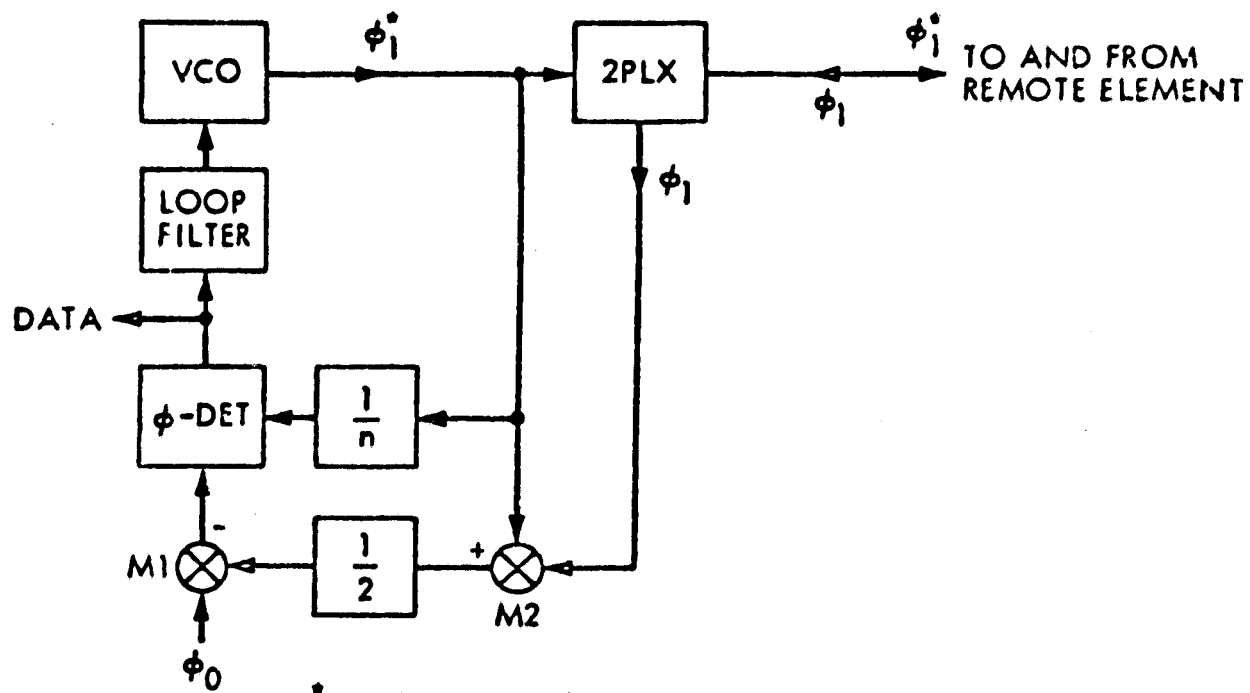
CENTRAL PHASING



TREE STRUCTURE FOR CENTRALLY PHASED ARA



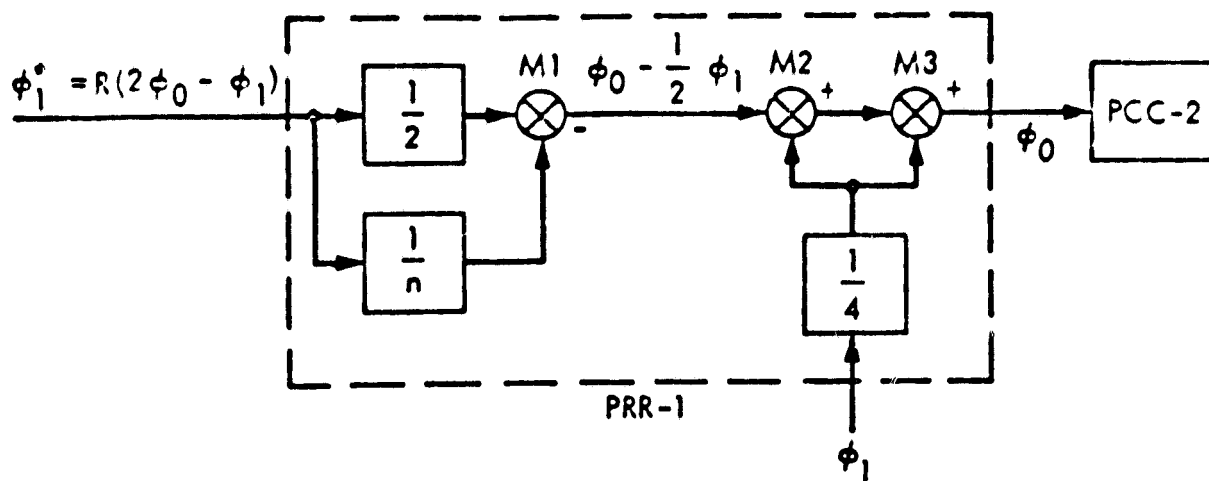
SIMPLE PHASE CONJUGATING CIRCUIT



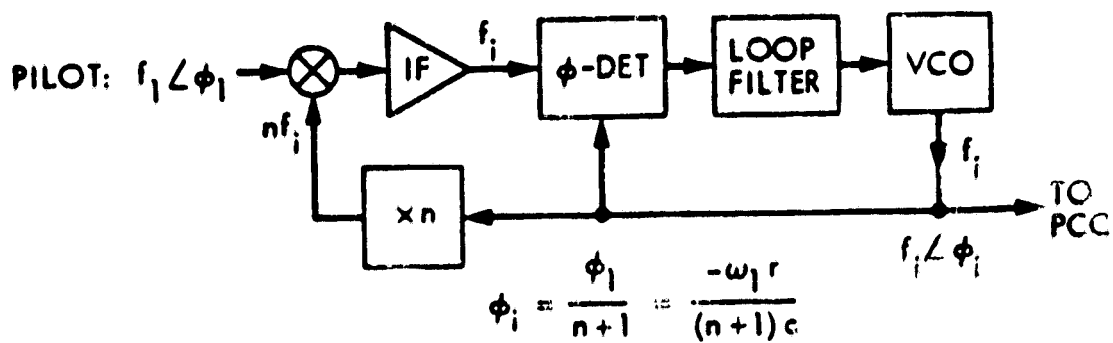
$$\phi_1^* = R(2\phi_0 - \phi_1)$$

$$R = \frac{1}{1 \pm \frac{2}{n}}$$

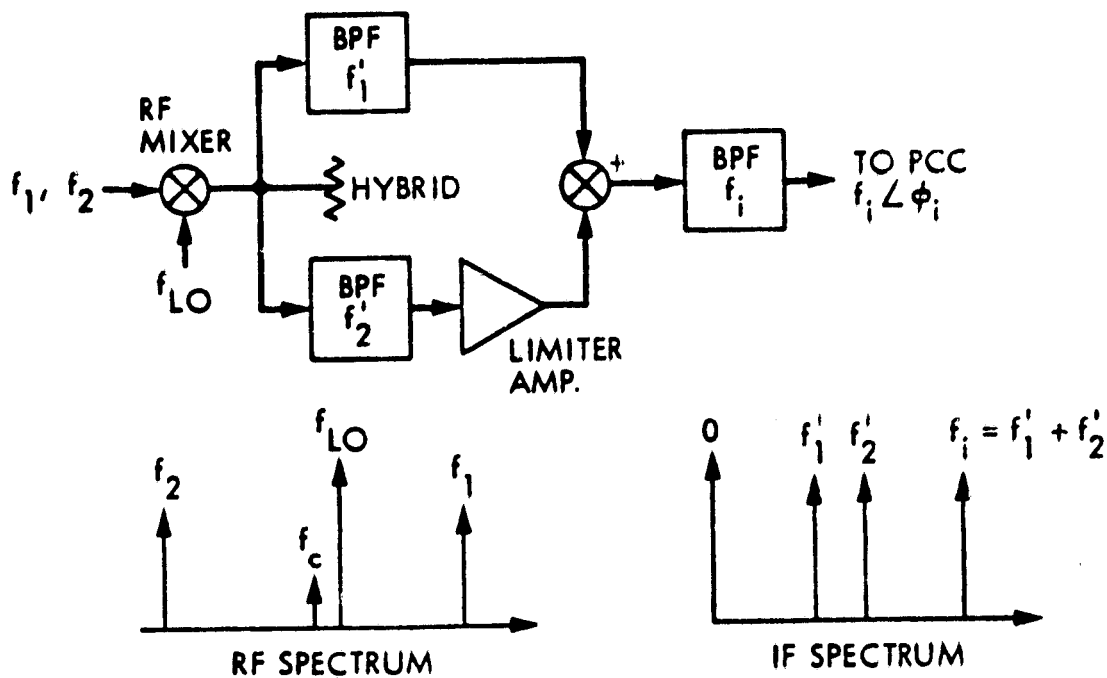
EXACT PCC: PHASE LOCKED LOOP TYPE



PHASE REFERENCE REGENERATOR (PRR) FOR PCC



PHASE LOCKED LOOP RECEIVER
(a)



$$f'_1 = f_1 - f_{LO}$$

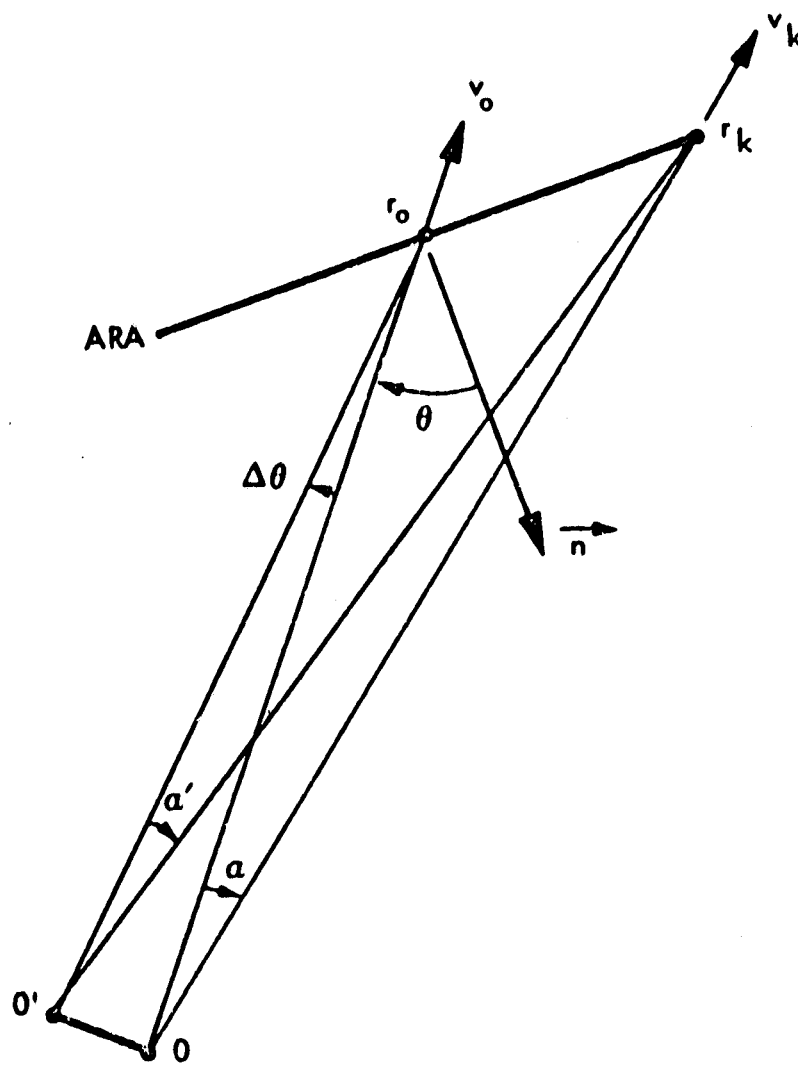
$$f'_2 = f_{LO} - f_2$$

$$f_i = f'_1 + f'_2 = f_1 - f_2$$

$$\phi_i = \phi_1 - \phi_2 = (\omega_2 - \omega_1) \frac{r}{c}$$

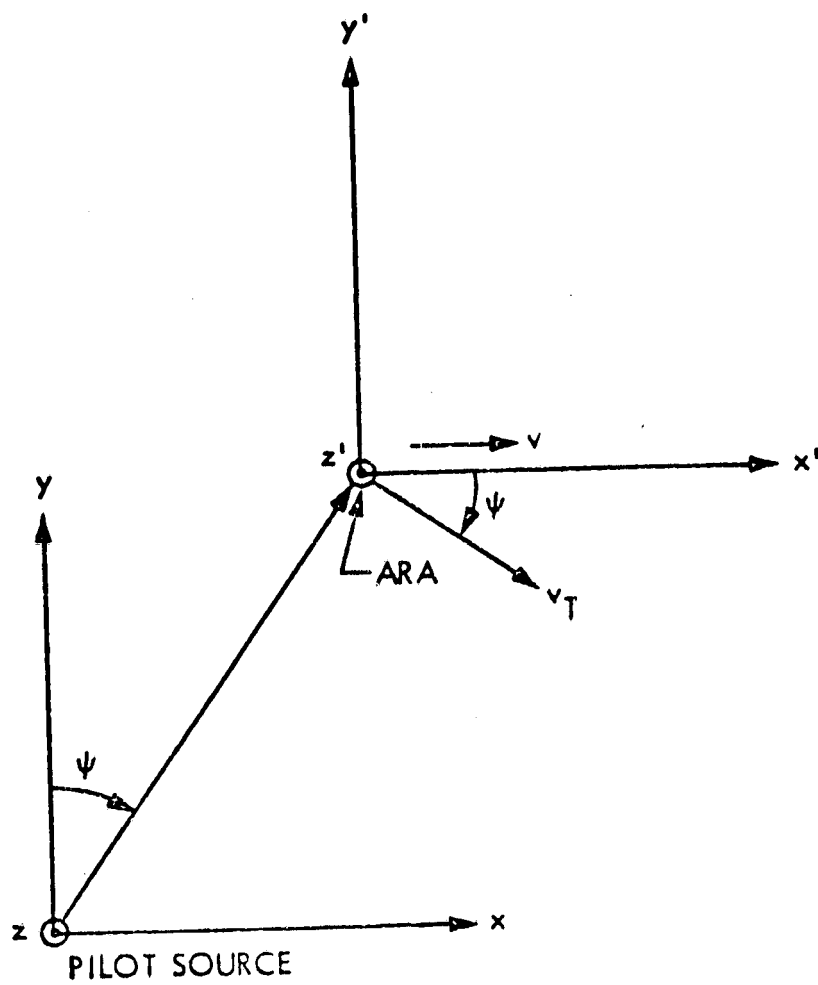
TWO TONE RECEIVER
(b)

ARA RECEIVERS

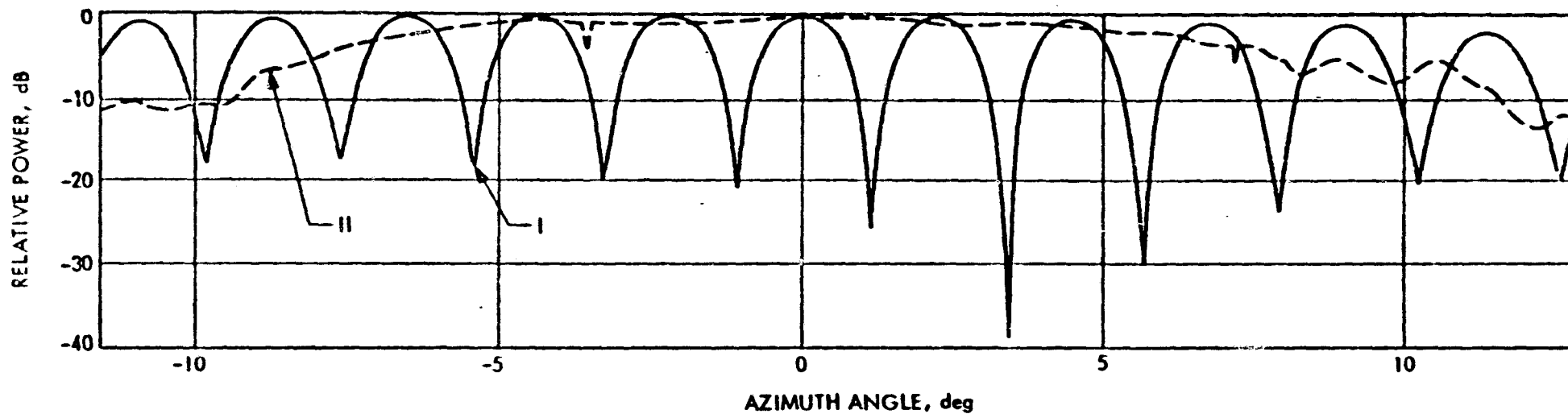


PILOT SOURCE

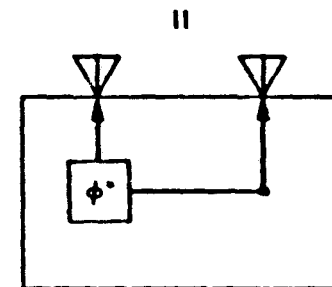
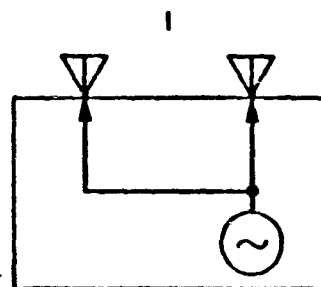
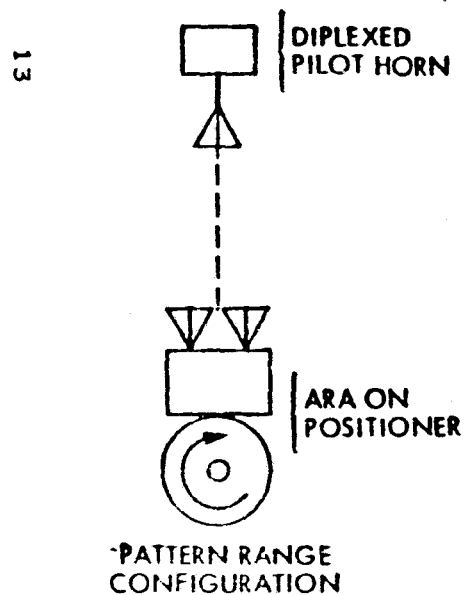
DOPPLER POINTING ERROR



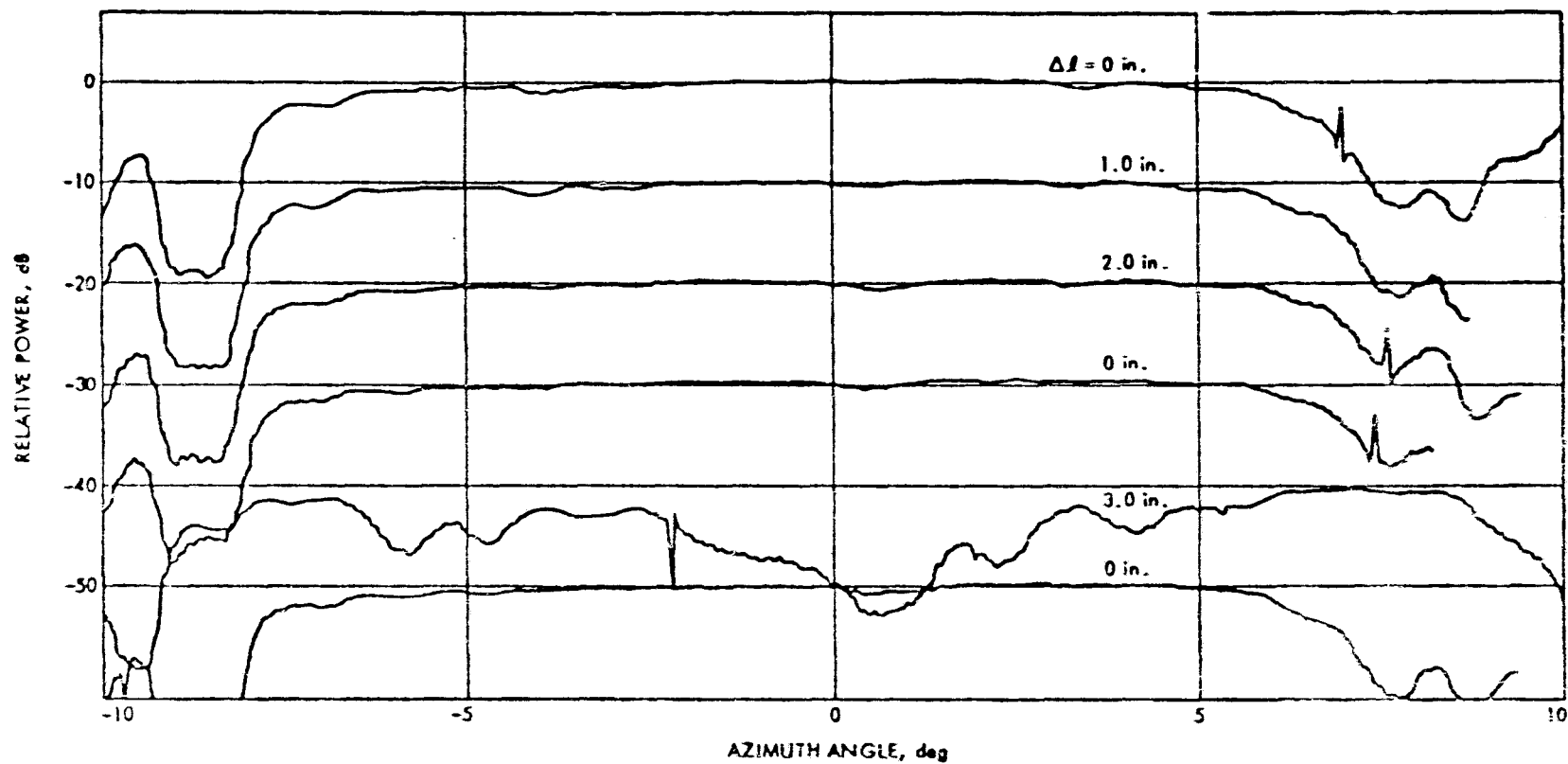
ABERRATION POINTING ERROR



LEGEND:



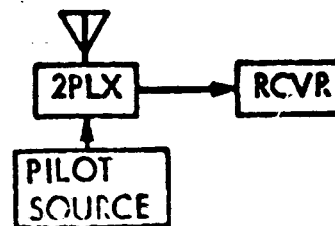
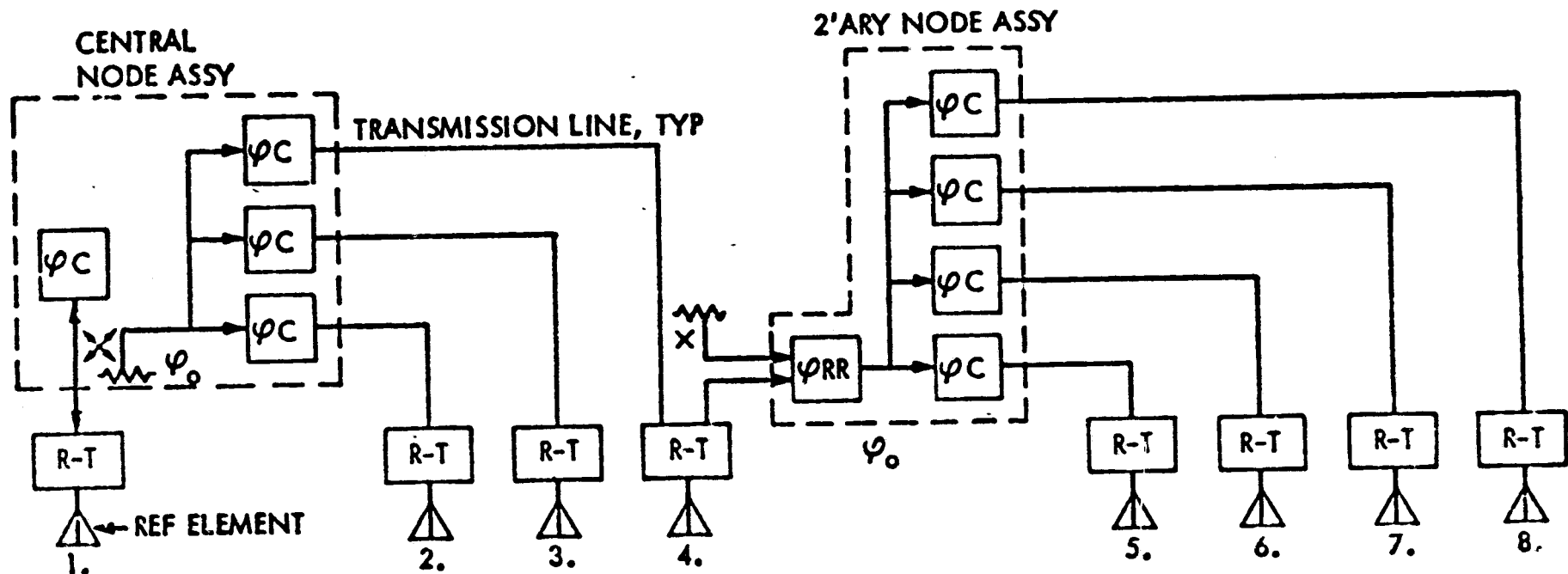
RETRODIRECTIVE ARRAY PATTERN



ARA BREADBOARD: EFFECT OF LINE LENGTH CHANGES

BEAMED RF POWER TECHNOLOGY

8-ELEMENT EXPERIMENTAL ACTIVE RETRODIRECTIVE ARRAY (ARA) BLOCK DIAGRAM



LEGEND:
 R-T = RCVR-XMTR-DIPLEXER ASSY
 ϕC = PHASE CONJUGATOR
 ϕRR = PHASE REFERENCE REGENERATOR
 ϕ_0 = REFERENCE PHASE
 2PLX = DIPLEXER

*Performance Analyses
and
Simulation
of the
Solar Power Satellite
Phase Control System*

*Dr. W. C. Lindsey
Lincom*

*C. M. Chie
Lincom*

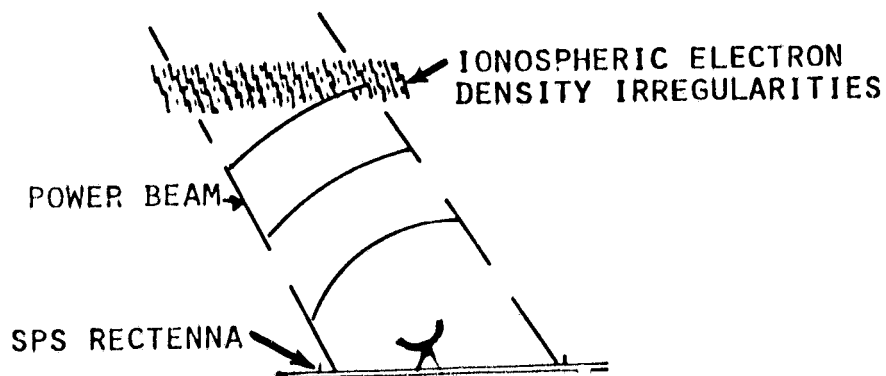
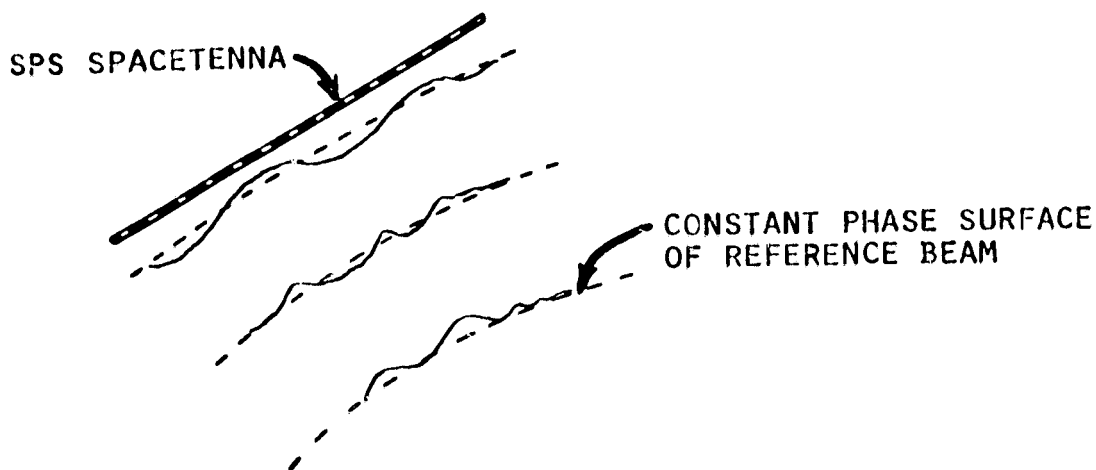
PRECEDING PAGE BLANK NOT FILMED

PERFORMANCE ANALYSIS AND SIMULATION OF
THE SPS REFERENCE PHASE CONTROL SYSTEM

- REFERENCE PHASE CONTROL SYSTEM
- REFERENCE PHASE CONTROL SYSTEM PERFORMANCE
FOUND VIA SOLARSIM
- POWER TRANSPONDER DESIGN AND PERFORMANCE

PRECEDING PAGE BLANK NOT FILMED

KEY PROBLEMS FACED BY THE SPS PHASE CONTROL SYSTEM



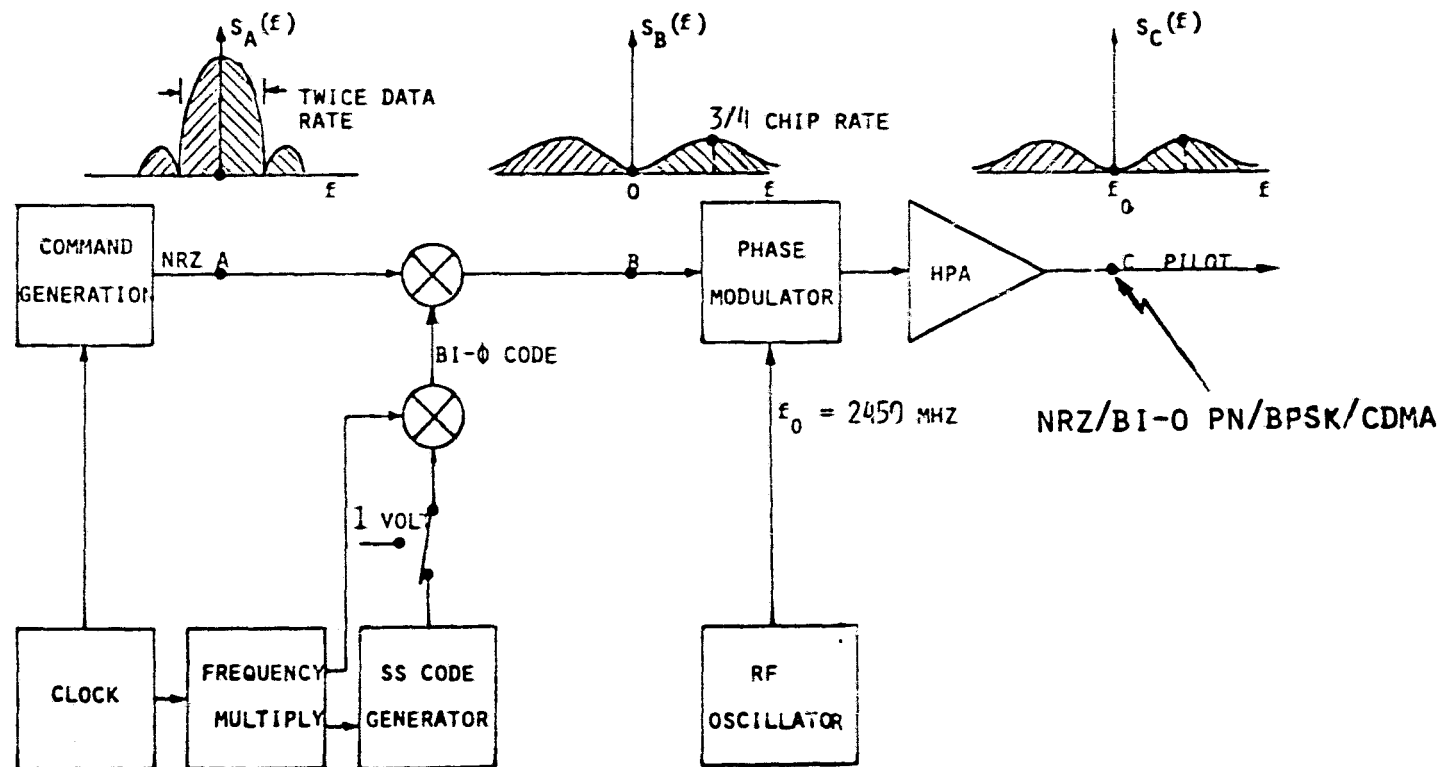
- PATH DELAY VARIATIONS
- IONOSPHERE EFFECTS
- INITIAL BEAM FORMING
- BEAM POINTING
- BEAM SAFING
- PHASE NOISE (HPA)
- INTERFERENCE
- SELF-JAMMING

SPS PILOT SIGNAL DESIGN CONSIDERATIONS

- MAIN CONSIDERATIONS
 - INTERFERENCE
 - IONOSPHERIC EFFECTS
 - BEAM SQUINT
 - ISOLATION OF UP/DOWN LINK
 - PHASE NOISE OF PA's
 - DIPLEXER CHARACTERISTICS
 - SECURITY (AJ MARGIN)
 - COMMANDS
 - AMBIGUITY
 - POWER ROBBING
 - SPS NETWORKING
- MAIN APPROACHES
 - SINGLE-FREQUENCY TONE
 - DOUBLE-FREQUENCY TONE
 - BI- ϕ CODED SPREAD SPECTRUM SIGNAL*

*DESIGN CHOICE

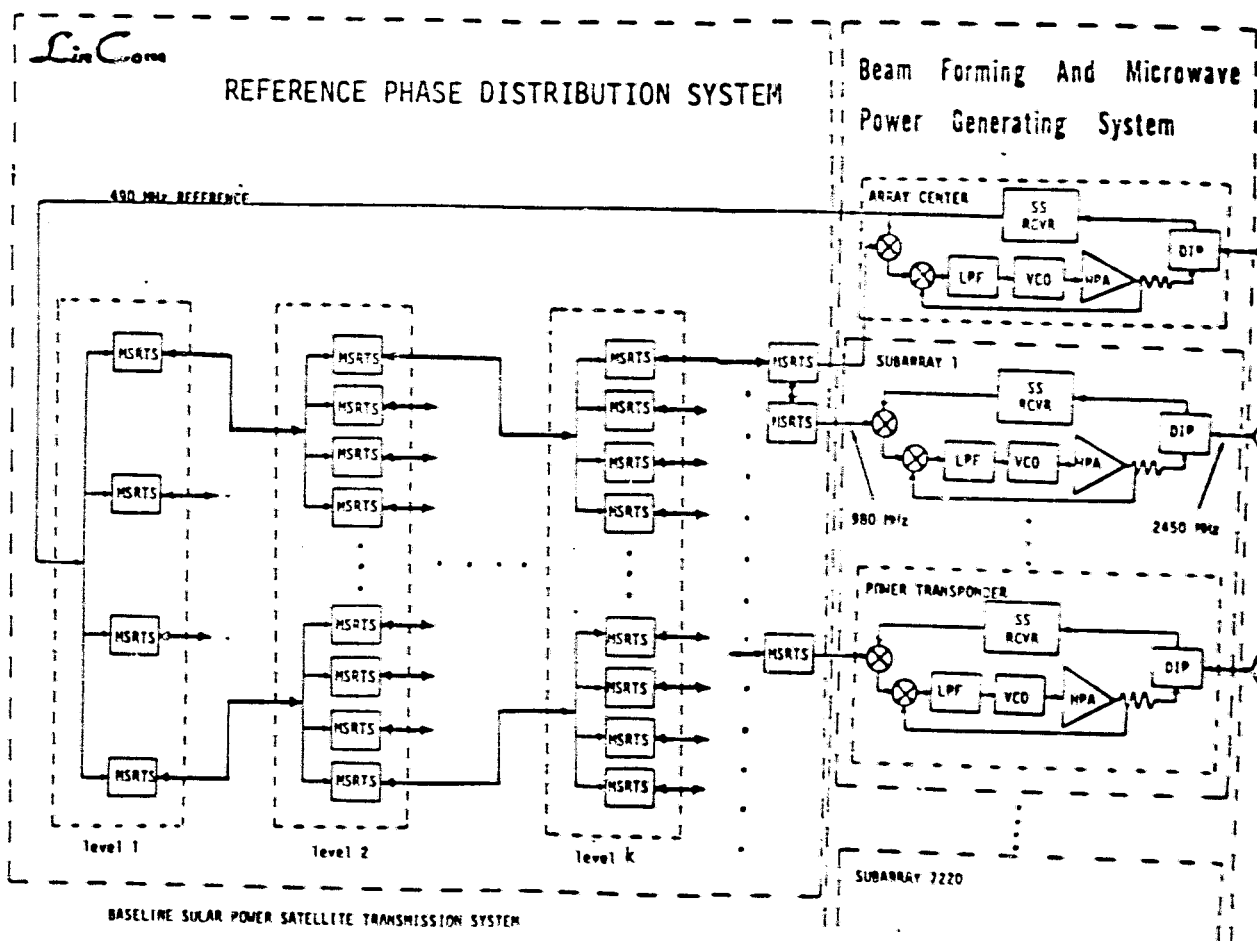
BI- ϕ CODED PILOT TRANSMITTER FUNCTIONAL DIAGRAM



PILOT TRANSMITTER DESIGN PARAMETERS

- SPS WAVEFORM
 - NRZ/BPSK/B1- ϕ PN/CDMA
- EIRP = 93 dBW
- PN CHIP RATE = 10 Mcps
- PN CODE PERIOD = 1 msec
- CODE LENGTH = 4095
 - MAXIMUM LENGTH SEQUENCE
- OPTIMUM CDMA FOR SPS NETWORK
 - BENT FUNCTION SEQUENCE (64)
- GOLD CODES MAY SUFFICE
 - 4097 DIFFERENT SEQUENCES

SPS PHASE CONTROL SYSTEM

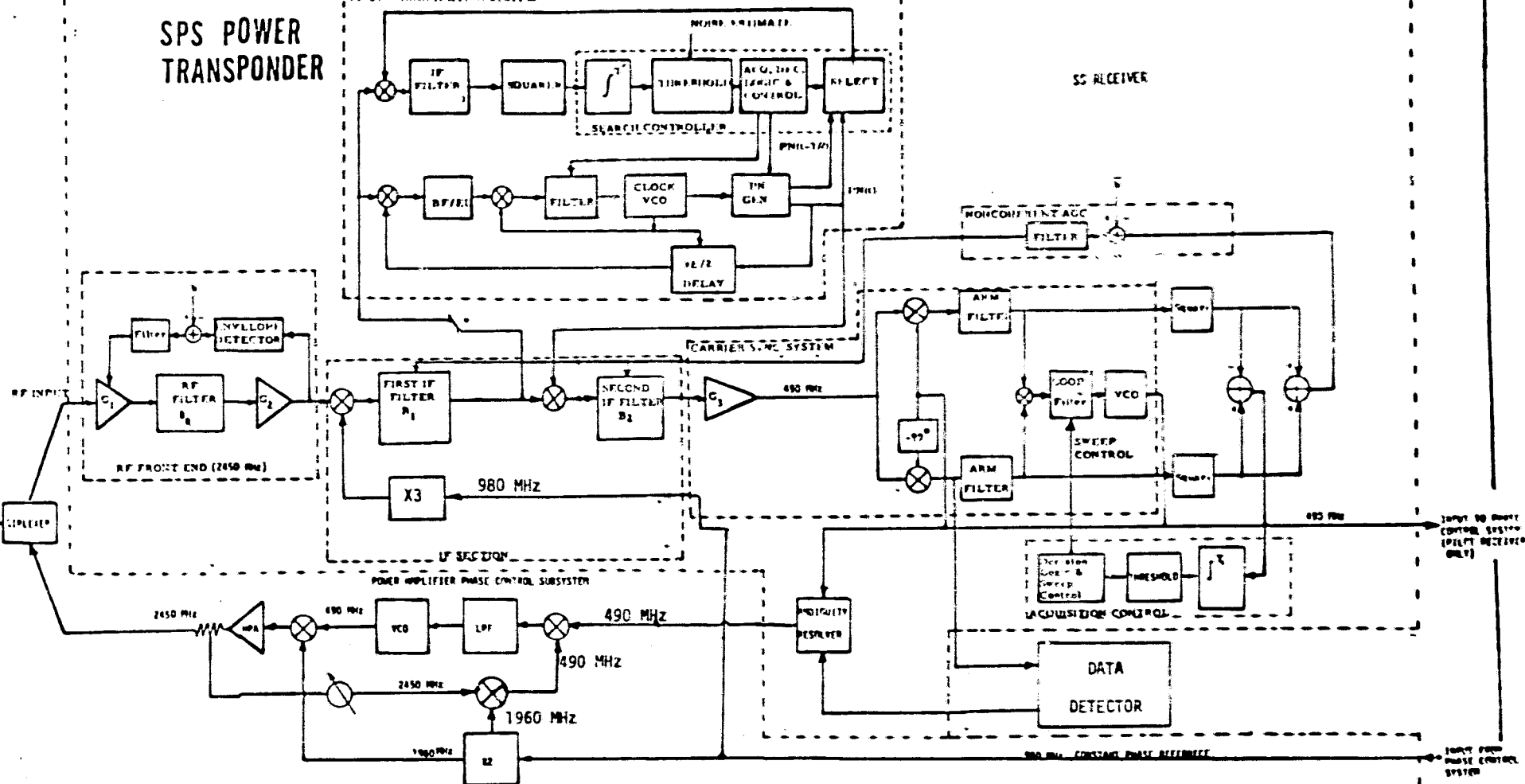


OVERALL SPS POWER TRANSPONDER MODEL

SPS POWER TRANSPONDER

12N SYNCHRONIZATION SYSTEM

SS RECEIVER



SUMMARY OF THE HIGH-LEVEL ELECTRONIC SUBSYSTEMS
REQUIRED IN THE IMPLEMENTATION OF PHASE DISTRIBUTION
SYSTEM, THE BEAMFORMING AND MICROWAVE POWER
GENERATION SYSTEM

(1) NUMBER OF SS RECEIVERS

●COSTAS LOOPS	101,553
●DESPREADERS	101,553

(2) NUMBER OF DIPLEXERS 101,552

(3) NUMBER OF POWER MODULES 101,552

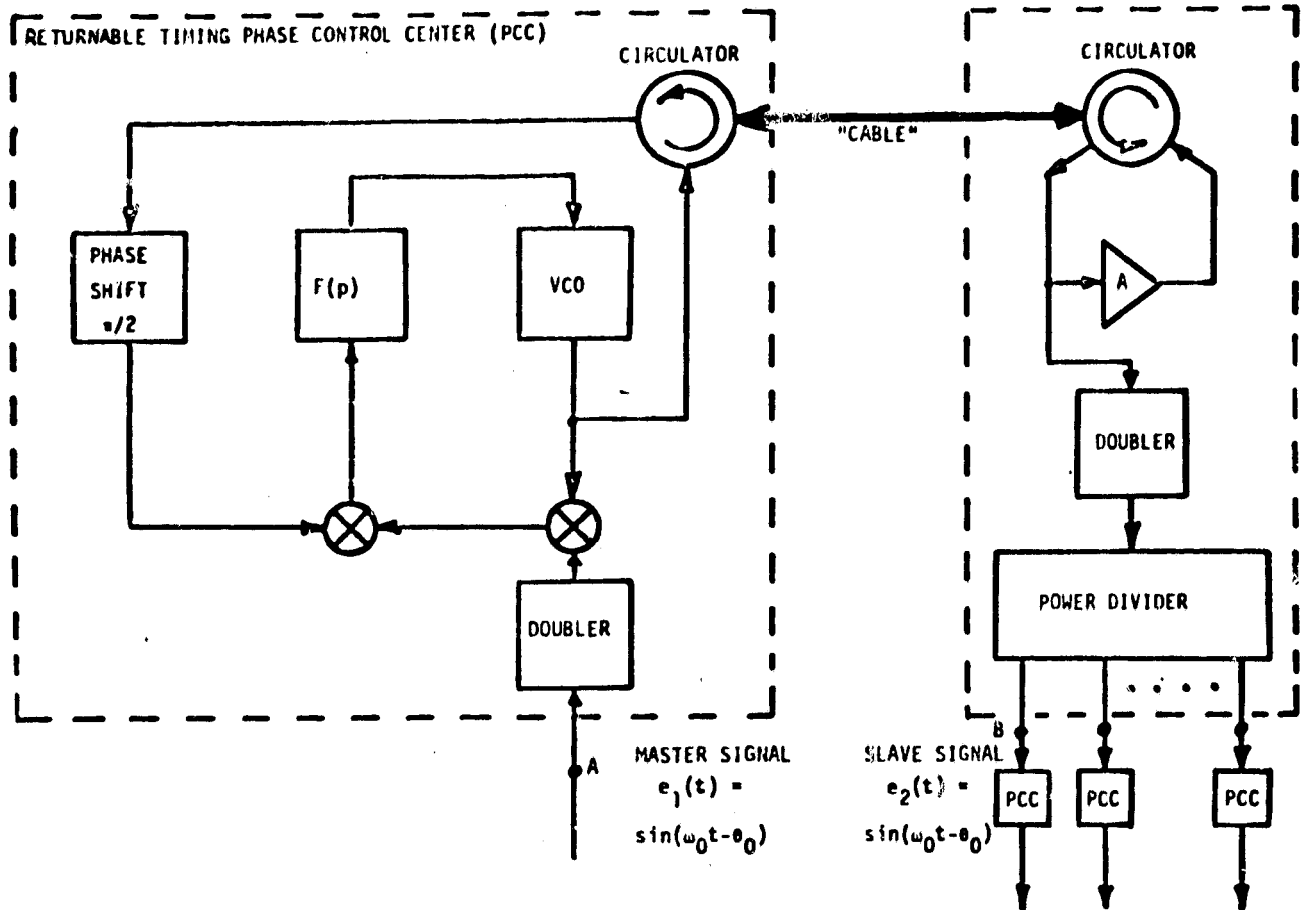
(4) NUMBER OF PHASE CONJUGATOR
MULTIPLIERS 101,552

(5) NUMBER OF 4-WAY POWER SPLITTERS 40,960

(6) NUMBER OF MSRTSS 22,000

(7) APPROXIMATE "CABLE LENGTH"
REQUIRED 120 MILES

RETURABLE TIMING SYSTEM



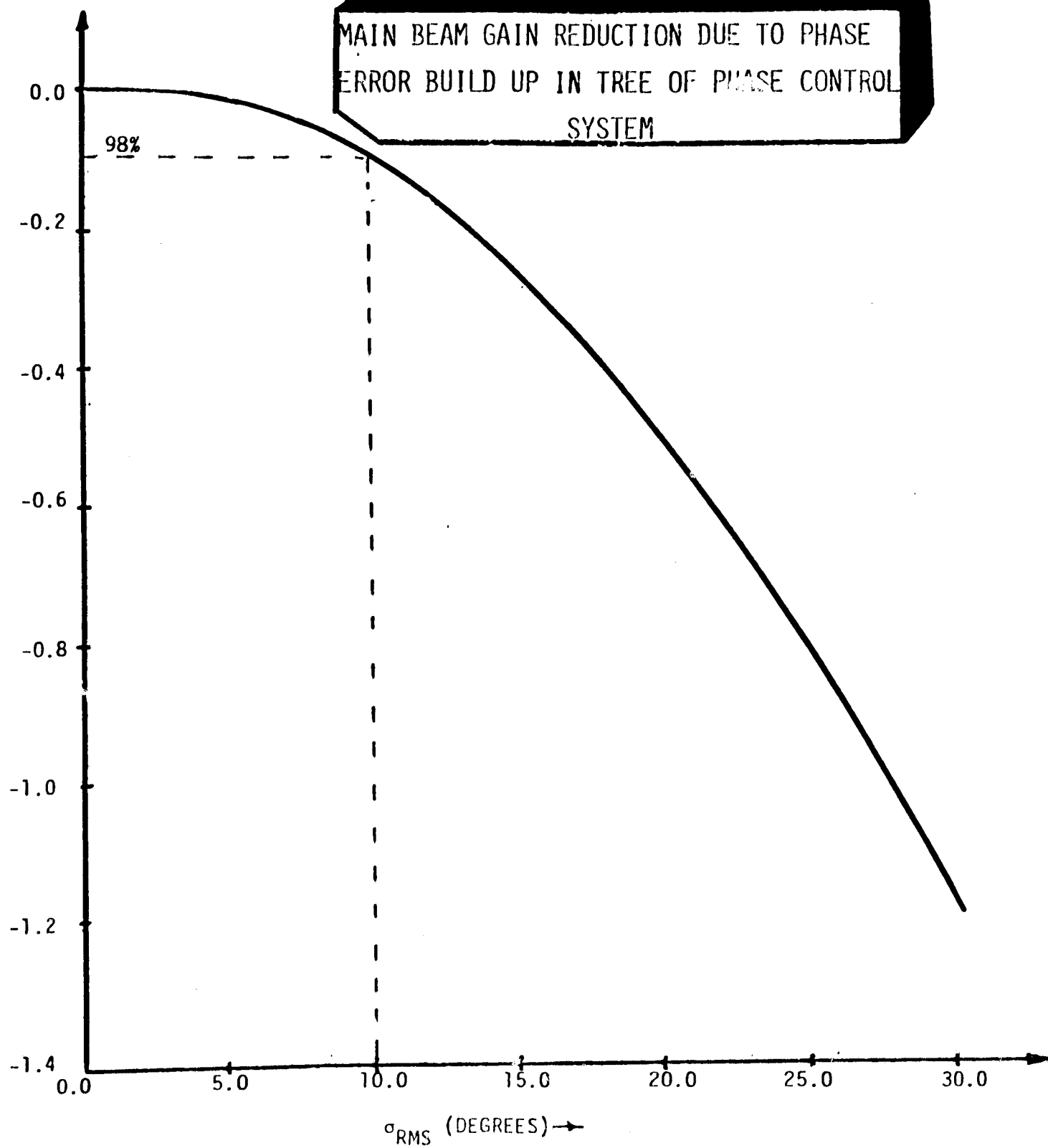
- 4-LEVEL TREE SELECTED
- ADVANTAGES:
 - CONTROLS PHASE BUILD UP AND JITTER
 - MINIMIZES "CABLE LENGTH"

SOLARSIM CAPABILITIES

- ANTENNA ELEMENT COVARIANCE MATRIX
- INDIVIDUAL REALIZATION OF RANDOM POWER PATTERN
- MEAN FAIR FIELD POWER PATTERN
- MEAN BEAM GAIN LOSSES
- RMS POINTING ERROR
- TILT/MECHANICAL ERROR EFFECTS ON GAIN
- EFFECT OF CONJUGATION AT OTHER THAN POWER
MODULE LEVEL
- SIDELobe LEVELS/NULL SHIFTING
- MAIN BEAM POWER TRANSFER EFFICIENCY
- EVALUATE AND PARTITIONING OF PHASE ERROR
BUILD-UP BUDGET
- POWER TRANSPONDER INTERFERENCE SIMULATION
- EVALUATE IONOSPHERIC EFFECTS*

*PRESENTLY UNDER DEVELOPMENT.

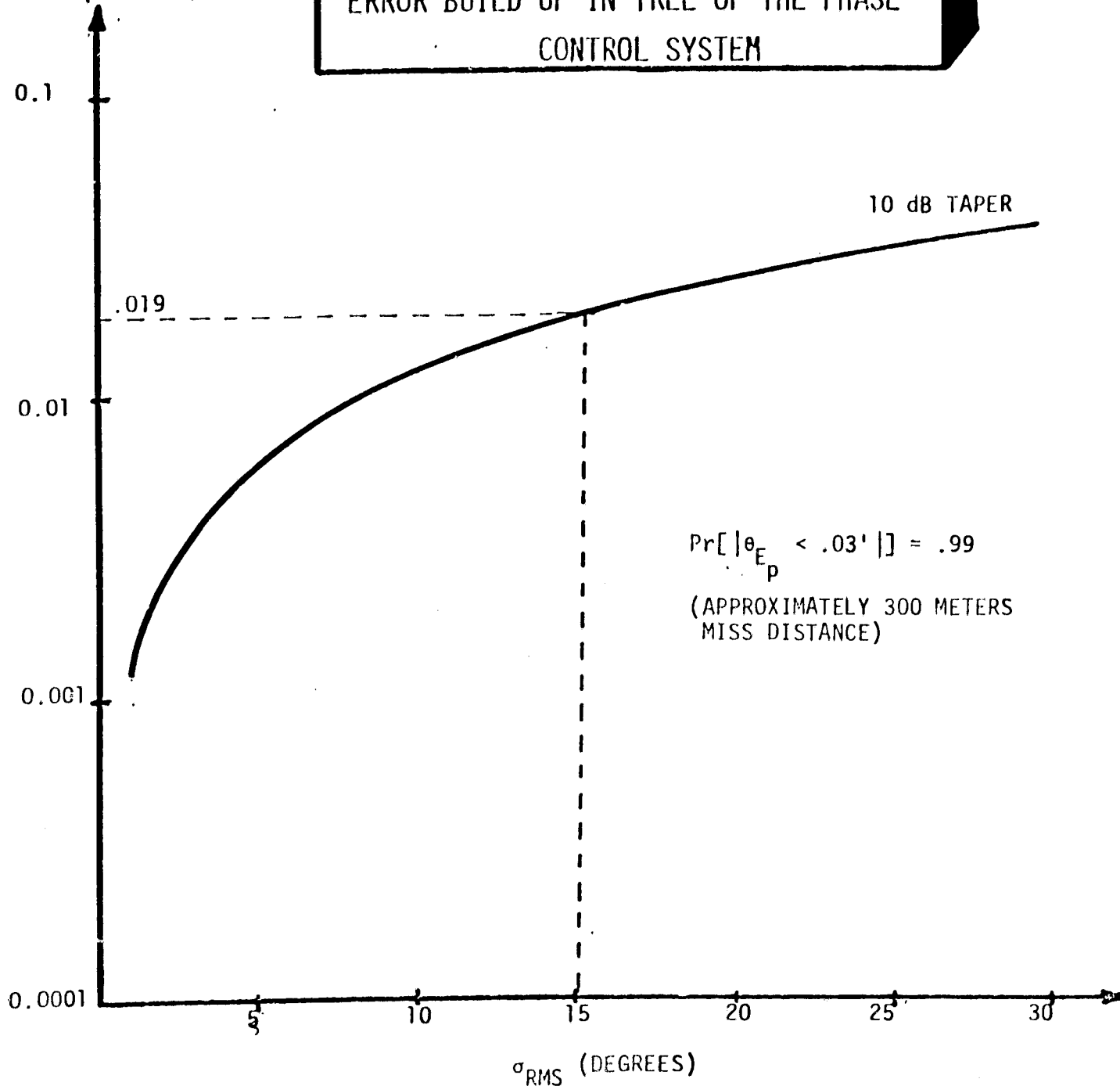
MAIN BEAM GAIN
REDUCTION (dB); G/G_0



LinCom

RMS POINTING ERROR DUE TO THE PHASE
ERROR BUILD UP IN TREE OF THE PHASE
CONTROL SYSTEM

RMS POINTING
ERROR (MINUTES)

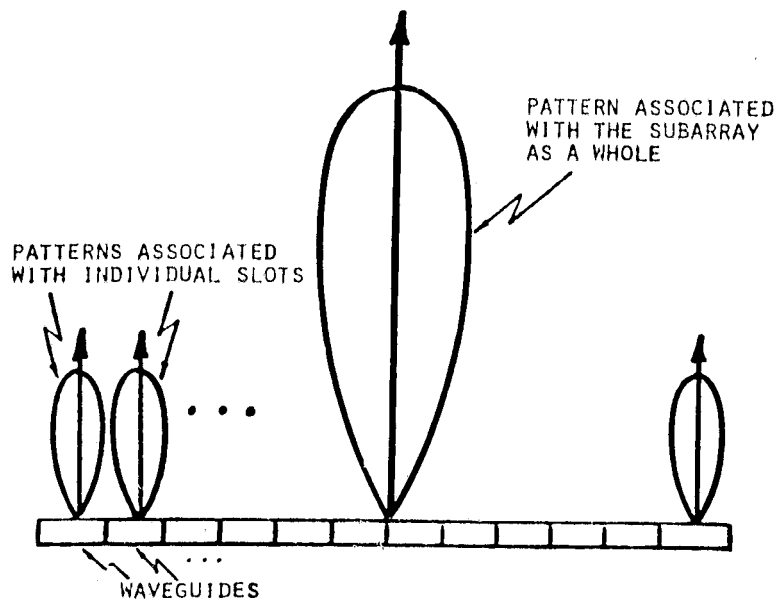
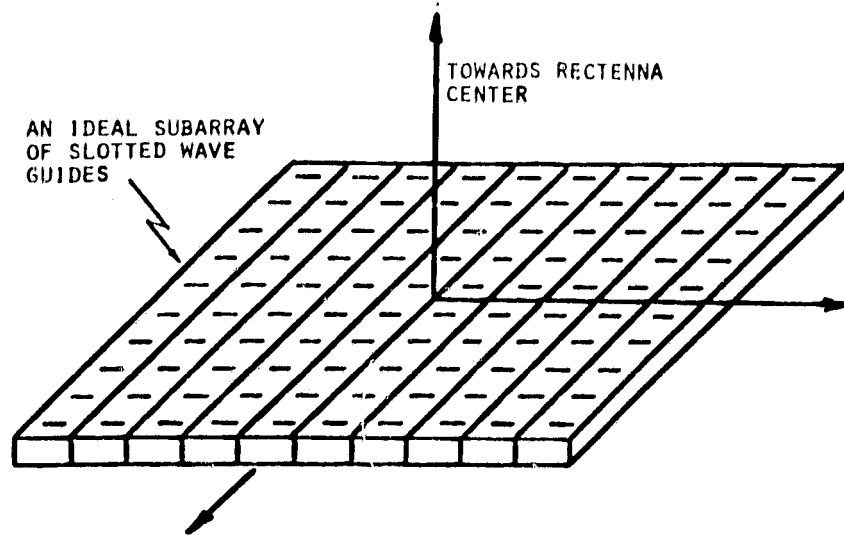


LinCom

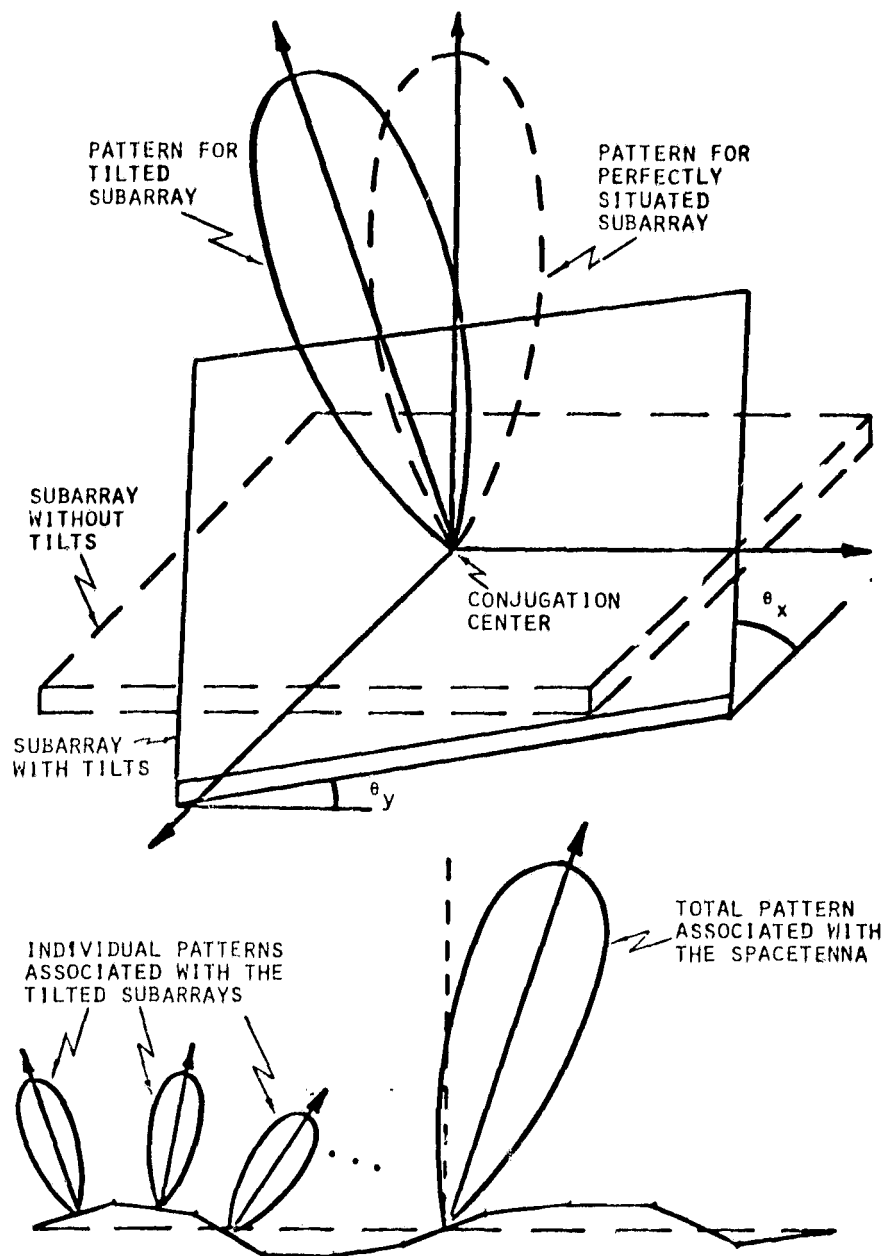
EFFECTS ON FAR FIELD DUE TO:

- SUBARRAY TILT (MECHANICAL POINTING ERROR)
- SUBARRAY SIZE
- SUBARRAY LAYOUT
- CONJUGATION POINT (LOCATION JITTERS)

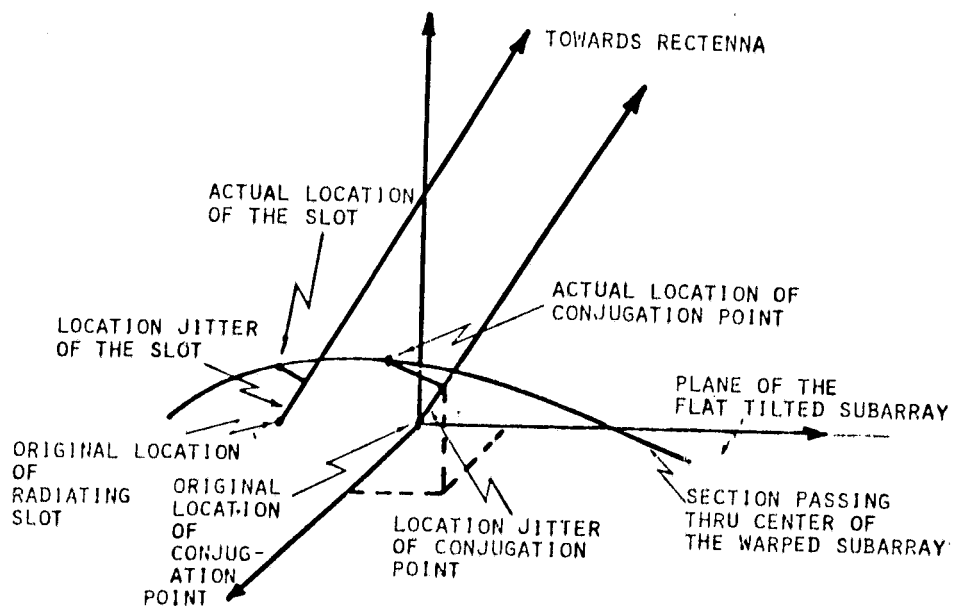
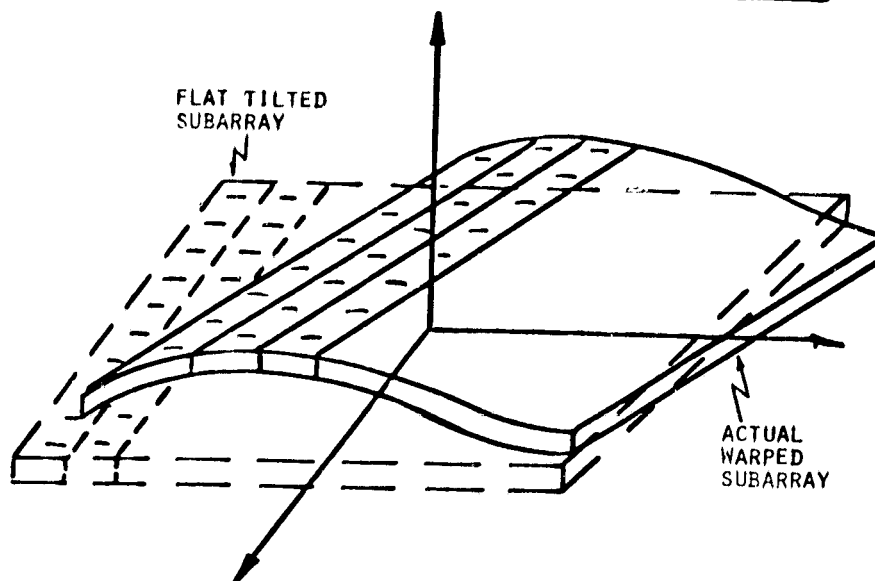
SUBARRAY PATTERN



EFFECT OF MECHANICAL POINTING ERROR



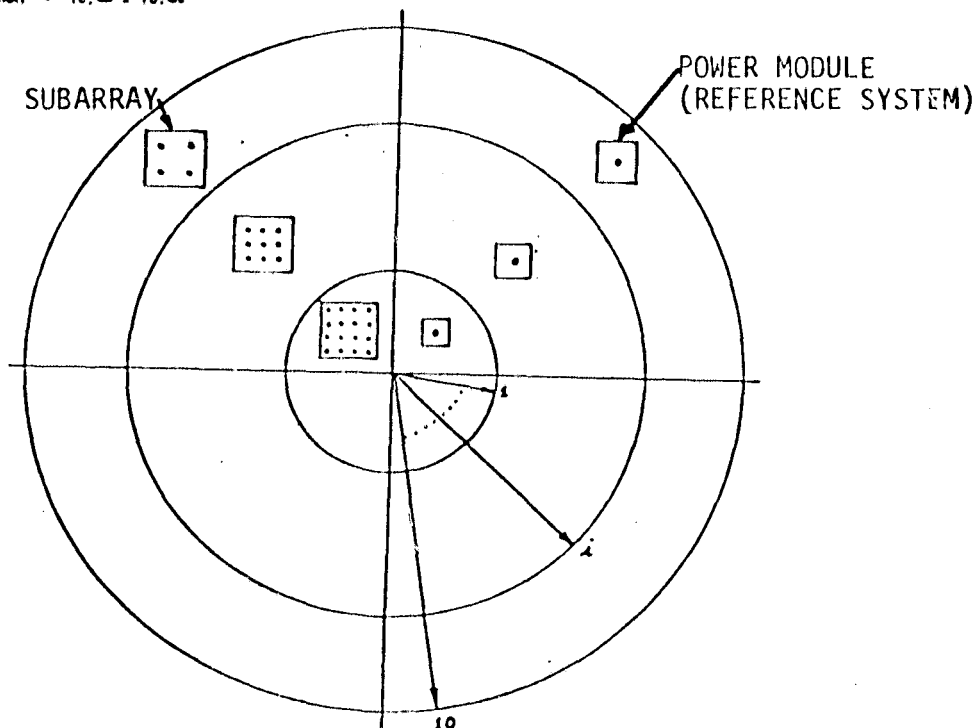
EFFECT OF LOCATION JITTER



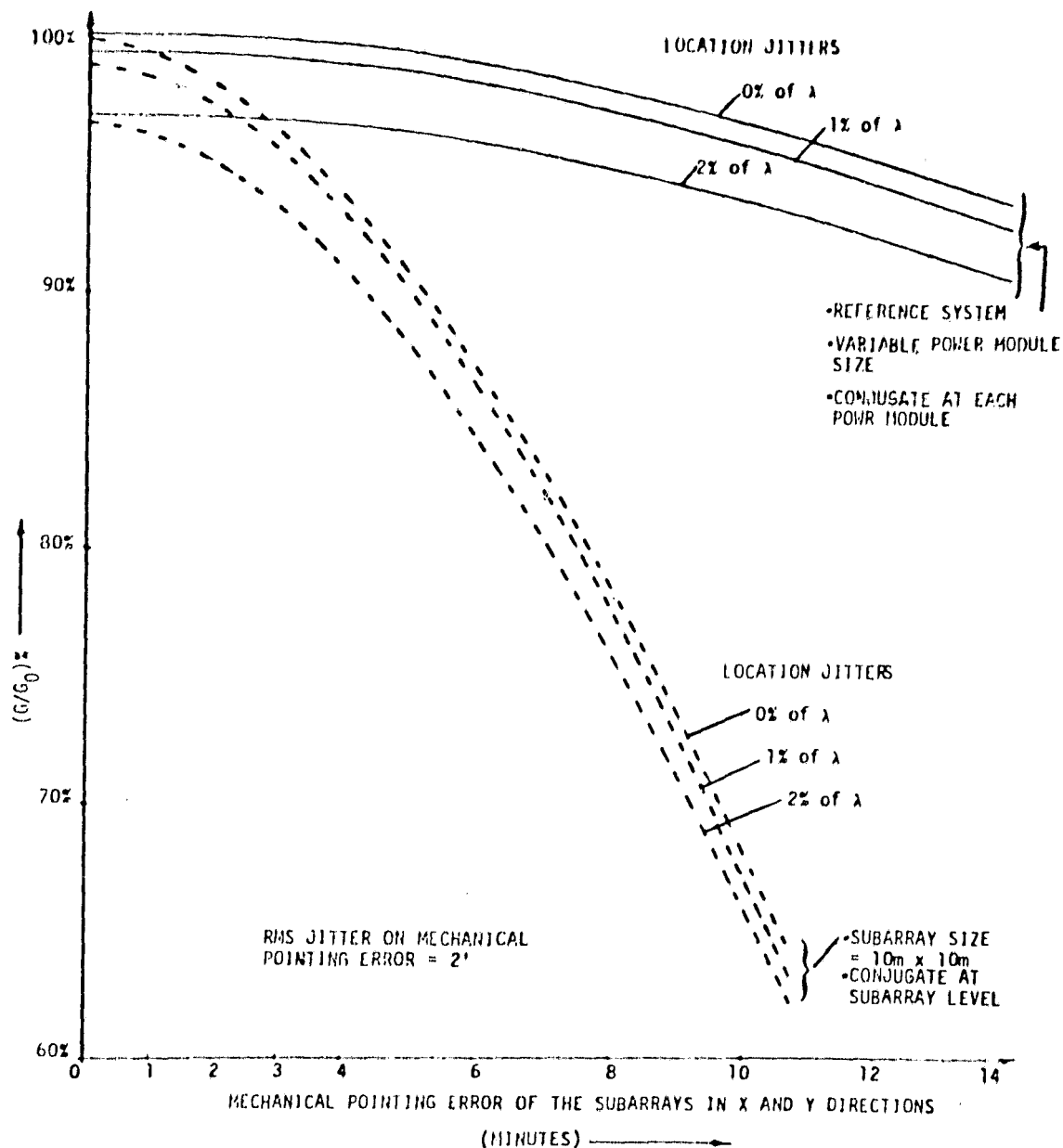
VARIABLE AND FIXED SIZE SUBARRAY GEOMETRY

POWER DENSITY STEP	NUMBER OF SUBARRAYS	NUMBER OF POWER MODULES PER CONJUGATION PT.	TOTAL # OF POWER MODULES PER DENSITY STEP	POWER DENSITY STEP	SIZE OF SUBARRAY	NUMBER OF SUBARRAYS	TOTAL # OF POWER MODULES PER CONJUGATION POINT	# OF POWER MODULES
1	276	36	9936	1	1.73m x 1.73m	9936	1	9936
2	632	30	18960	2	1.89m x 1.89m	18960	1	18960
3	844	24	15456	3	2.12m x 2.12m	15456	1	15456
4	828	20	12560	4	2.32m x 2.32m	12560	1	12560
5	784	16	12544	5	2.6 m x 2.6 m	12544	1	12544
6	500	12	10800	6	3. m x 3. m	10800	1	10800
7	664	9	5976	7	3.46m x 3.46m	5976	1	5976
8	612	8	4896	8	3.67m x 3.67m	4896	1	4896
9	1052	6	6312	9	4.24m x 4.24m	6312	1	6312
10	1078	4	4112	10	5.2 m x 5.2 m	4112	1	4112
TOTAL FOR FULL ARRAY	7220		101552			101552		101552

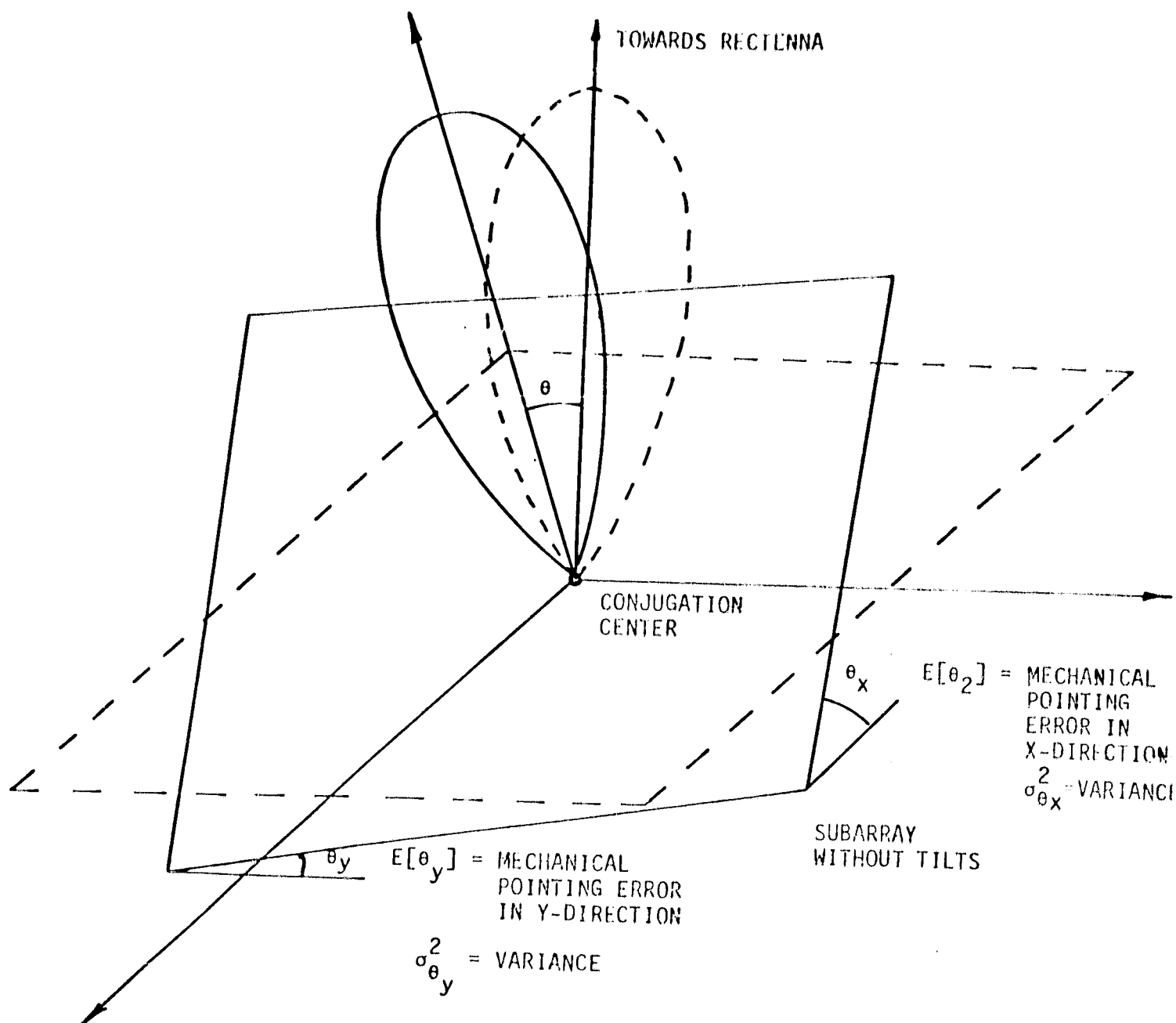
SIZE OF THE SUBARRAY = 10.4m x 10.4m



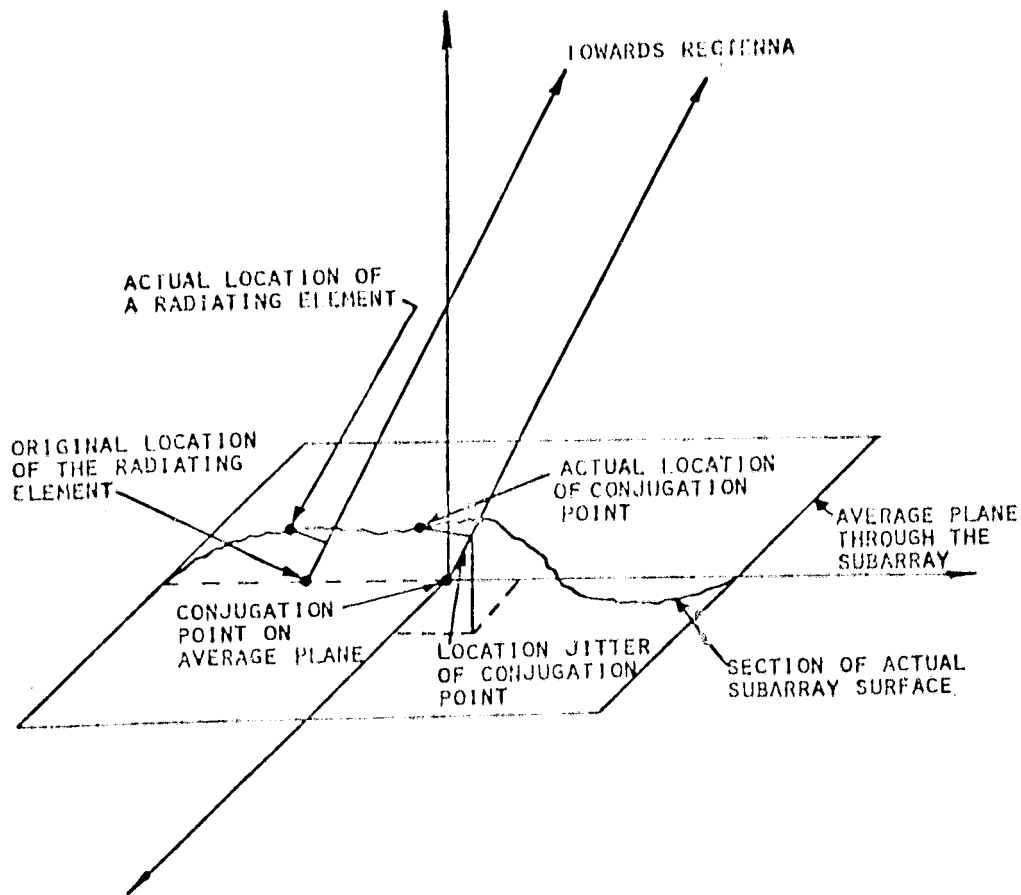
SENSITIVITY TO TILT EFFECTS AS A FUNCTION OF PHASE CONJUGATION LEVEL



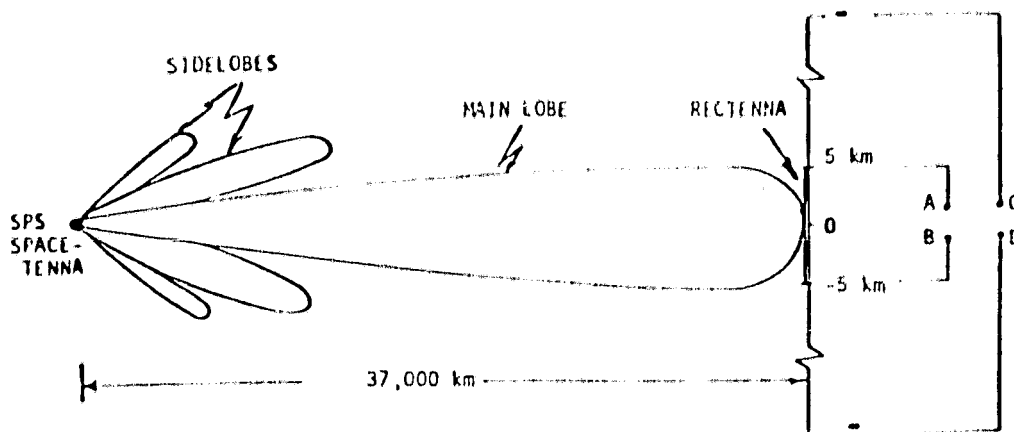
EFFECT OF SUBARRAY MEAN TILT & JITTER



JITTERS ADDED DUE TO LOCATION UNCERTAINTY
OF RADIATING AND CONJUGATION POINTS



POWER TRANSFER EFFICIENCY

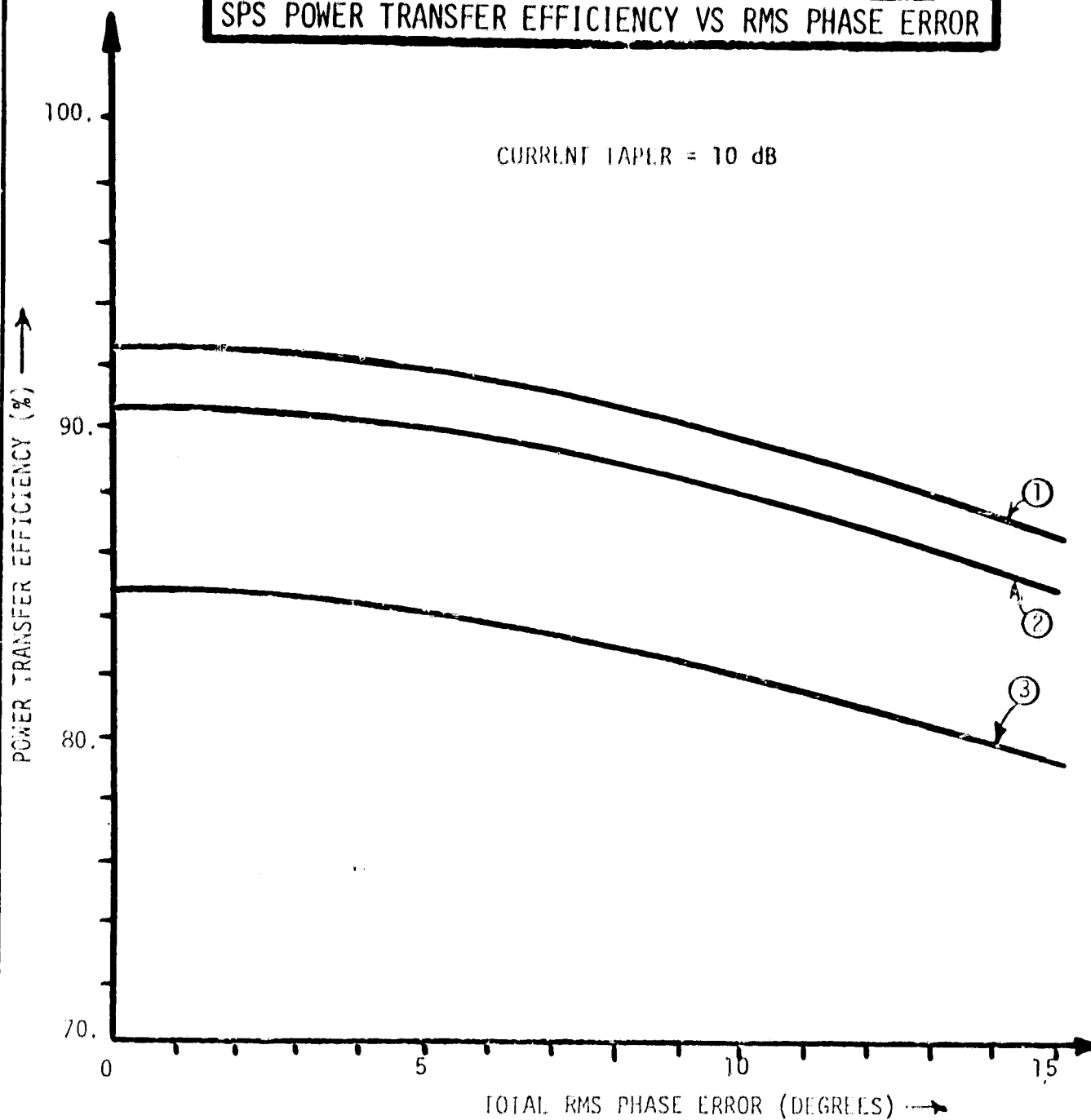


POWER TRANSFER EFFICIENCY = $\frac{\text{POWER RECEIVED BY THE 10 KM DIAMETER RECTENNA}}{\text{TOTAL POWER RADIATED BY THE SPACETENNA}}$

= $\frac{\text{POWER OUTPUT AT TERMINALS A \& B}}{\text{POWER OUTPUT AT TERMINALS C \& D}}$

SPS POWER TRANSFER EFFICIENCY VS RMS PHASE ERROR

CURRENT TAPLR = 10 dB



LEGEND

- ① MECHANICAL POINTING ERROR (MPE) = 0, LOCATION JITTER (LJ) = 0, JITTER ON MECHANICAL POINTING = 0
- ② MPE = 10', LJ = 0, JITTER ON MPE = 2'
- ③ MPE = 10', LJ = 2% of λ , JITTER ON MPE = 2'

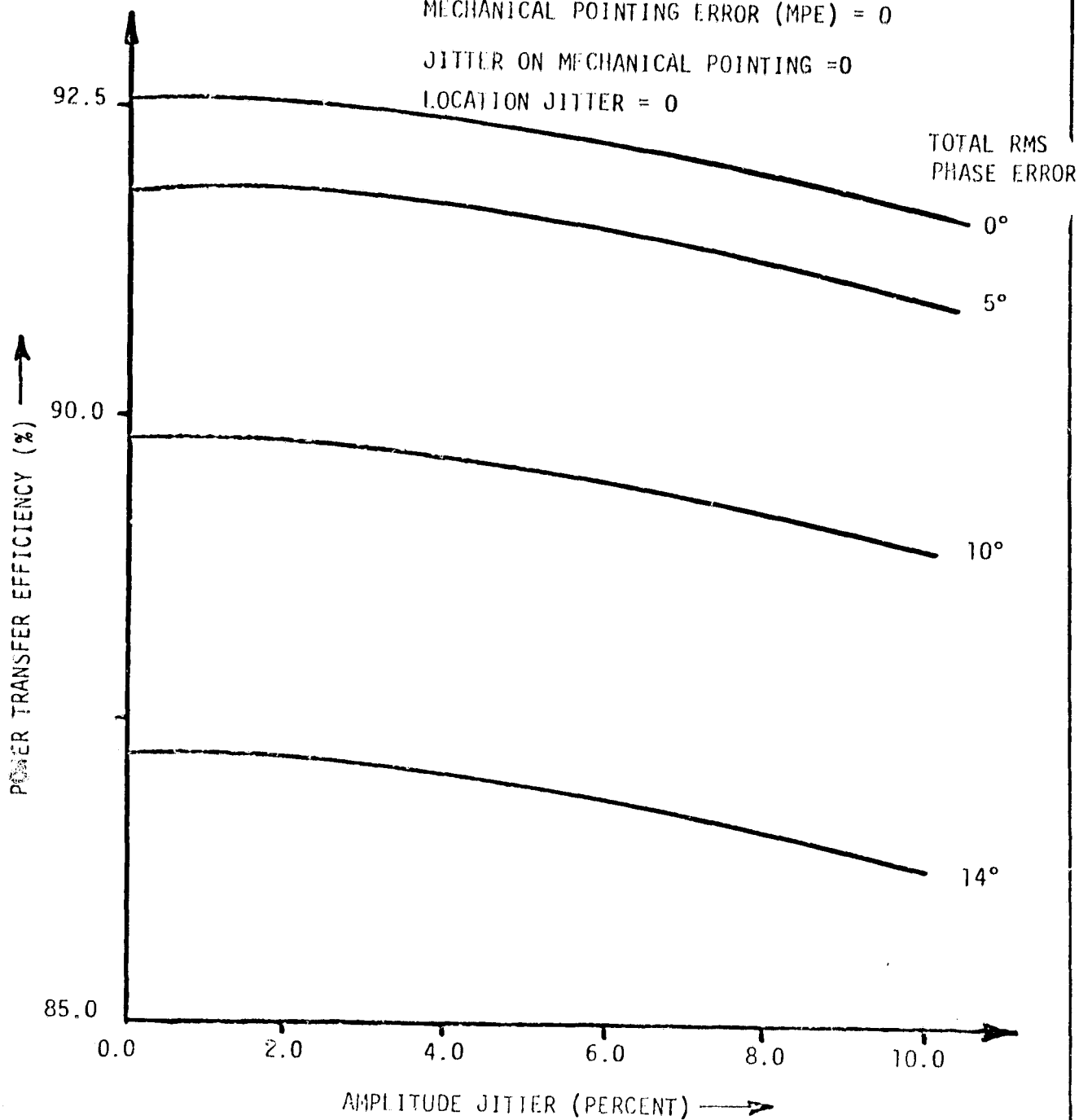
EFFECT OF AMPLITUDE JITTER ON SPS POWER TRANSFER EFFICIENCY

CURRENT TAPER = 10 dB

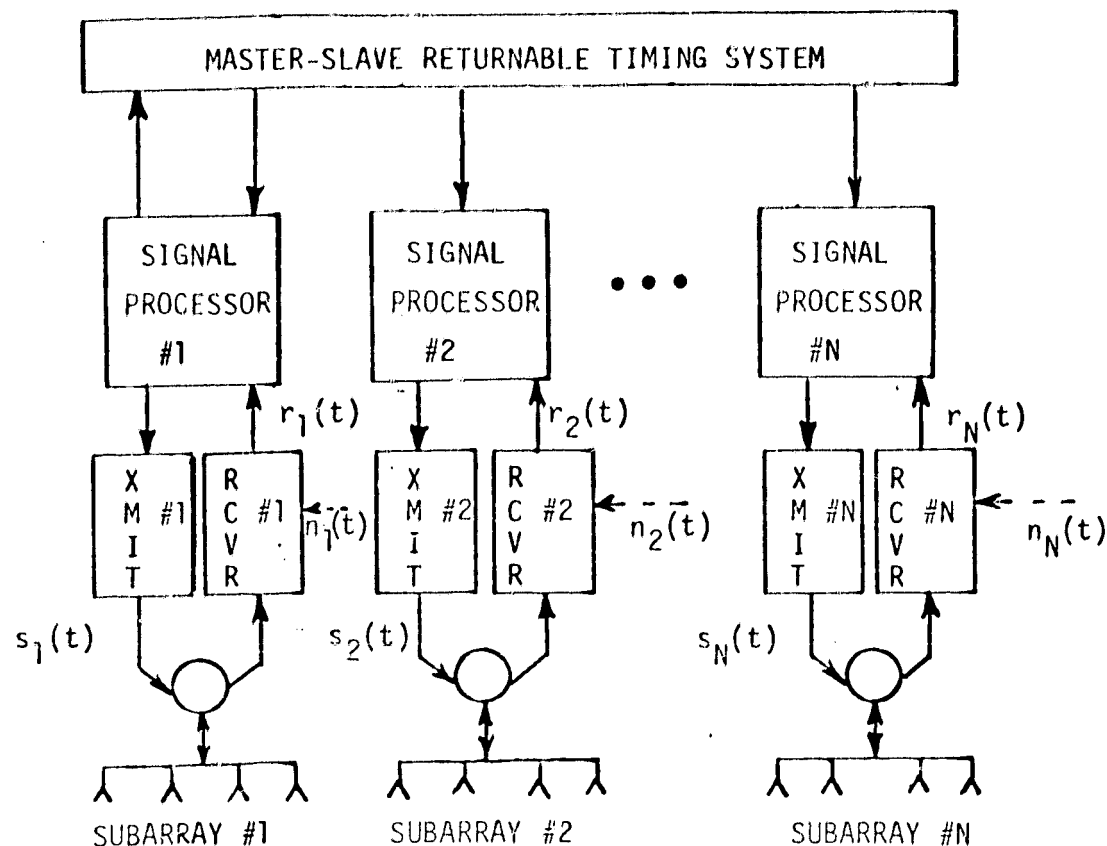
MECHANICAL POINTING ERROR (MPE) = 0

JITTER ON MECHANICAL POINTING = 0

LOCATION JITTER = 0



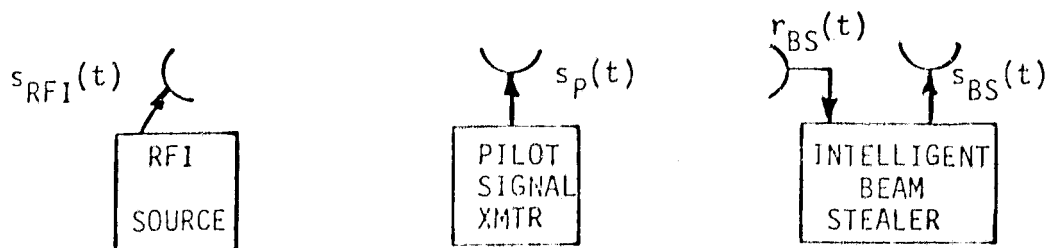
RF SIGNAL SCENARIO



S P A C E T E N N A

I O N O S P H E R E

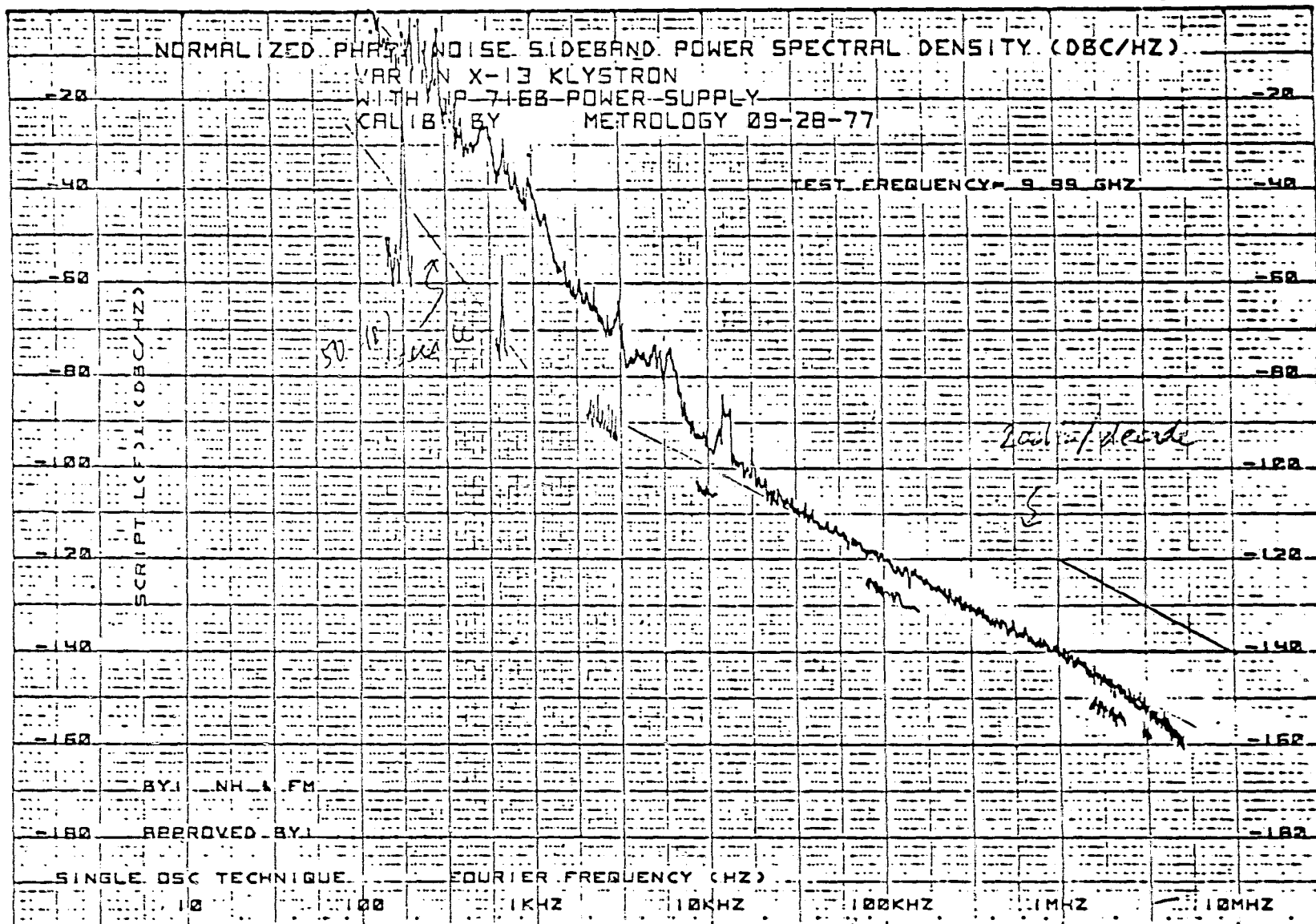
A T M O S P H E R E



79 0255

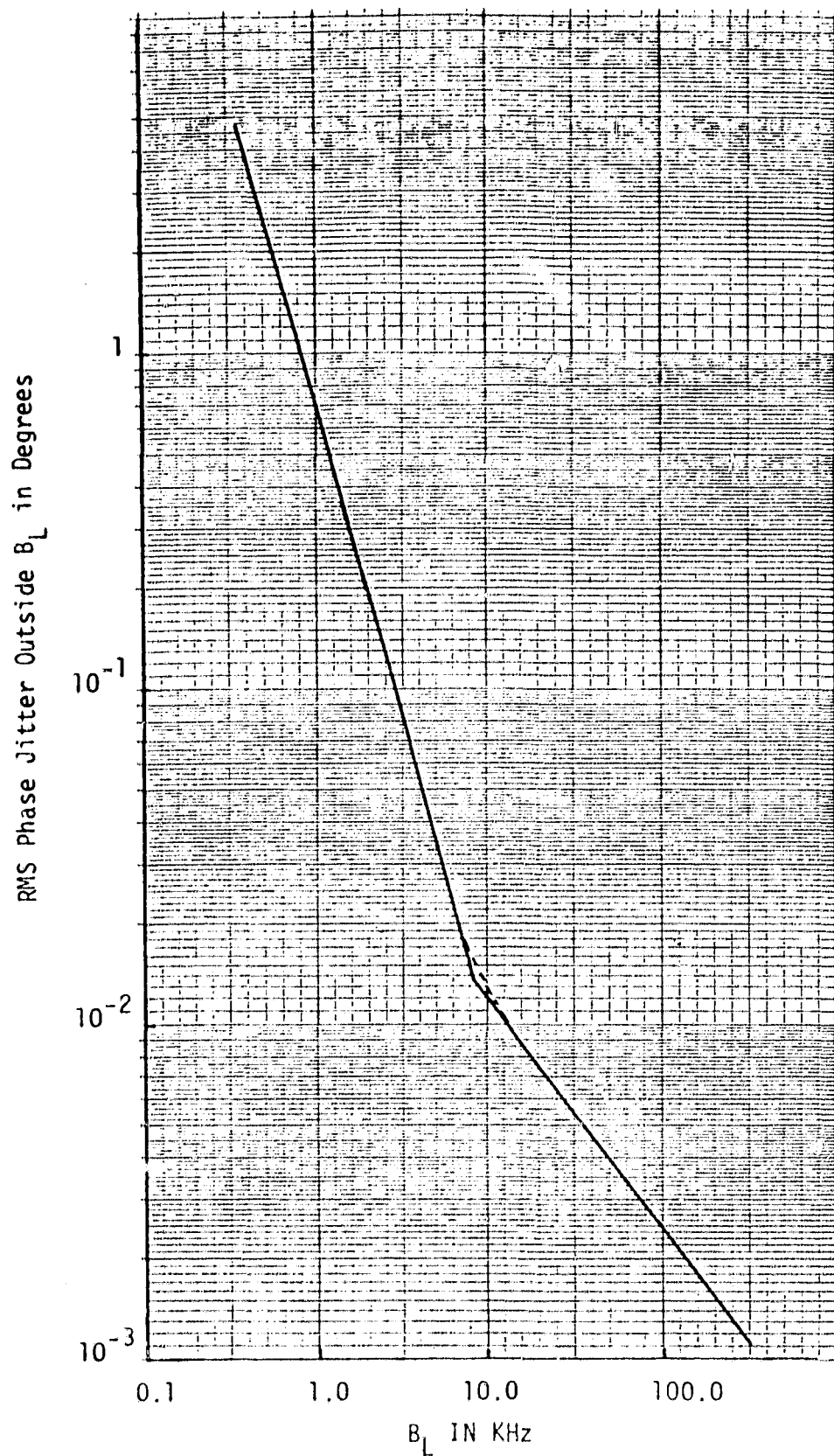
SUMMARY OF PILOT TRANSMITTER
AND POWER TRANSPONDER DESIGN

- EIRP = 93.3 dBW
- PN CHIP RATE ~ 10 Mcps
- RF FILTER 3 dB CUTOFF FREQUENCY ~ 20 MHz
- NOTCH FILTER 3 dB CUTOFF FREQUENCY ~ 1 MHz
- NOTCH FILTER DC ATTENUATION ~ 60 dB
- PN CODE PERIOD ~ 1 msec
- COSTAS LOOP PHASE JITTER ≤ 0.1 DEG FOR 10 HZ
LOOP BANDWIDTH
- CHANNEL DOPPLER IS NEGLIGIBLE
- KLYSTRON PHASE CONTROL LOOP BANDWIDTH
 ≥ 10 kHz



Normalized Phase Noise Sideband Power Spectral Density of a Varian X-13 klystron Tube (courtesy of Dr. Algie Lance, TRW).

ORIGINAL PAGE IS
OF POOR QUALITY



A Plot of rms Klystron Phase Noise Outside a Bandwidth B_L .

*Design and Breadboard
Evaluation of the
Solar Power Satellite
Reference Phase Control
System Concept*

*Dr. P. M. Hopkins
Lemsco*

PRECEDING PAGE BLANK NOT FILMED

OBJECTIVES

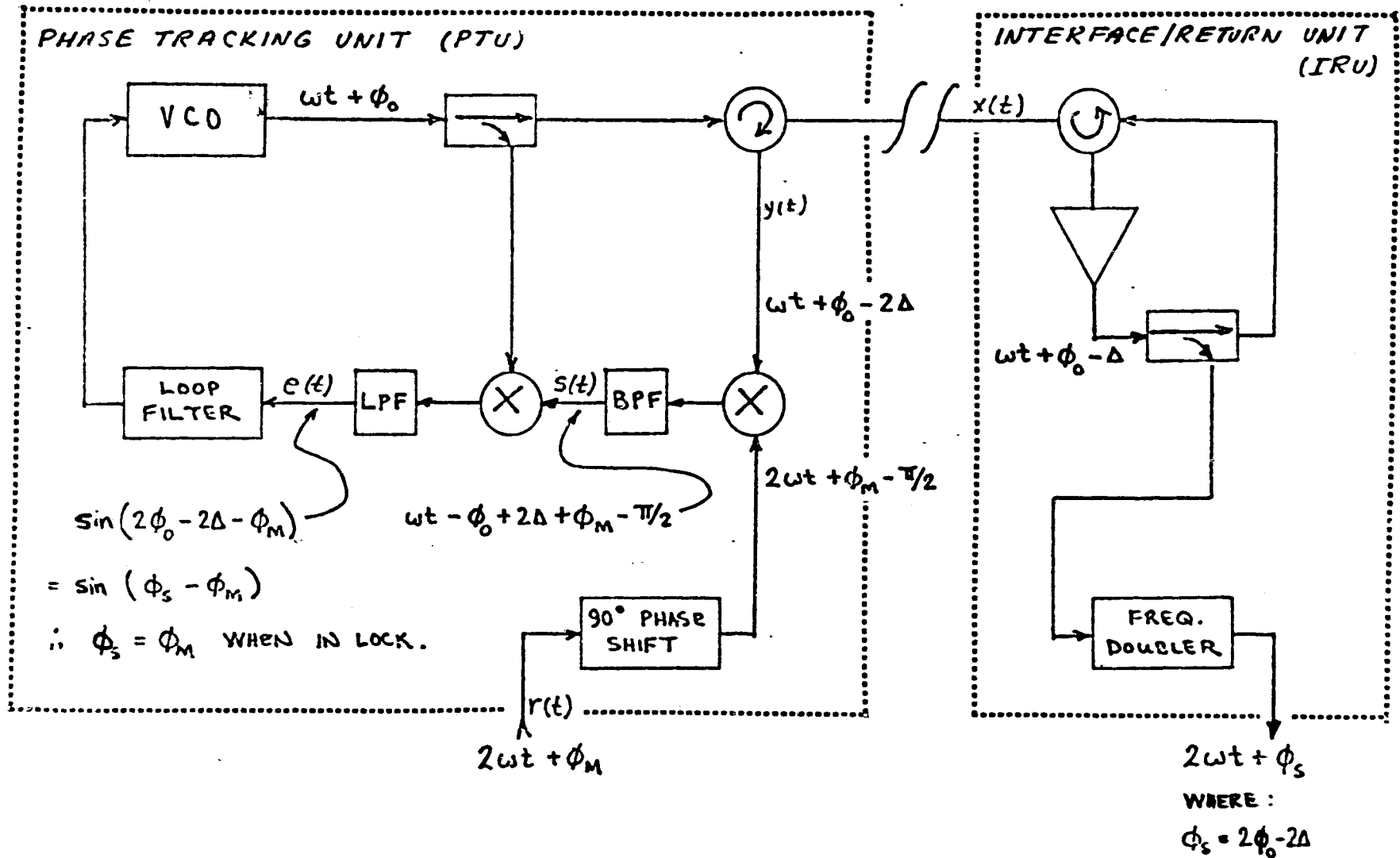
- EVALUATION OF MSRTS CONCEPT
 - FEASIBILITY
 - ACCURACY
 - LIMITATIONS
- EVALUATION OF MICROWAVE POWER TRANSPONDER
 - PHASE CONJUGATION CONCEPT
 - POWER AMPLIFIER NOISE SUPPRESSION
- EVALUATION OF TOTAL SYSTEM PERFORMANCE
 - PILOT TRANSMITTER
 - CENTRAL PILOT RECEIVER
 - MSRTS
 - POWER TRANSPONDER

PRECEDING PAGE BLANK NOT FILMED

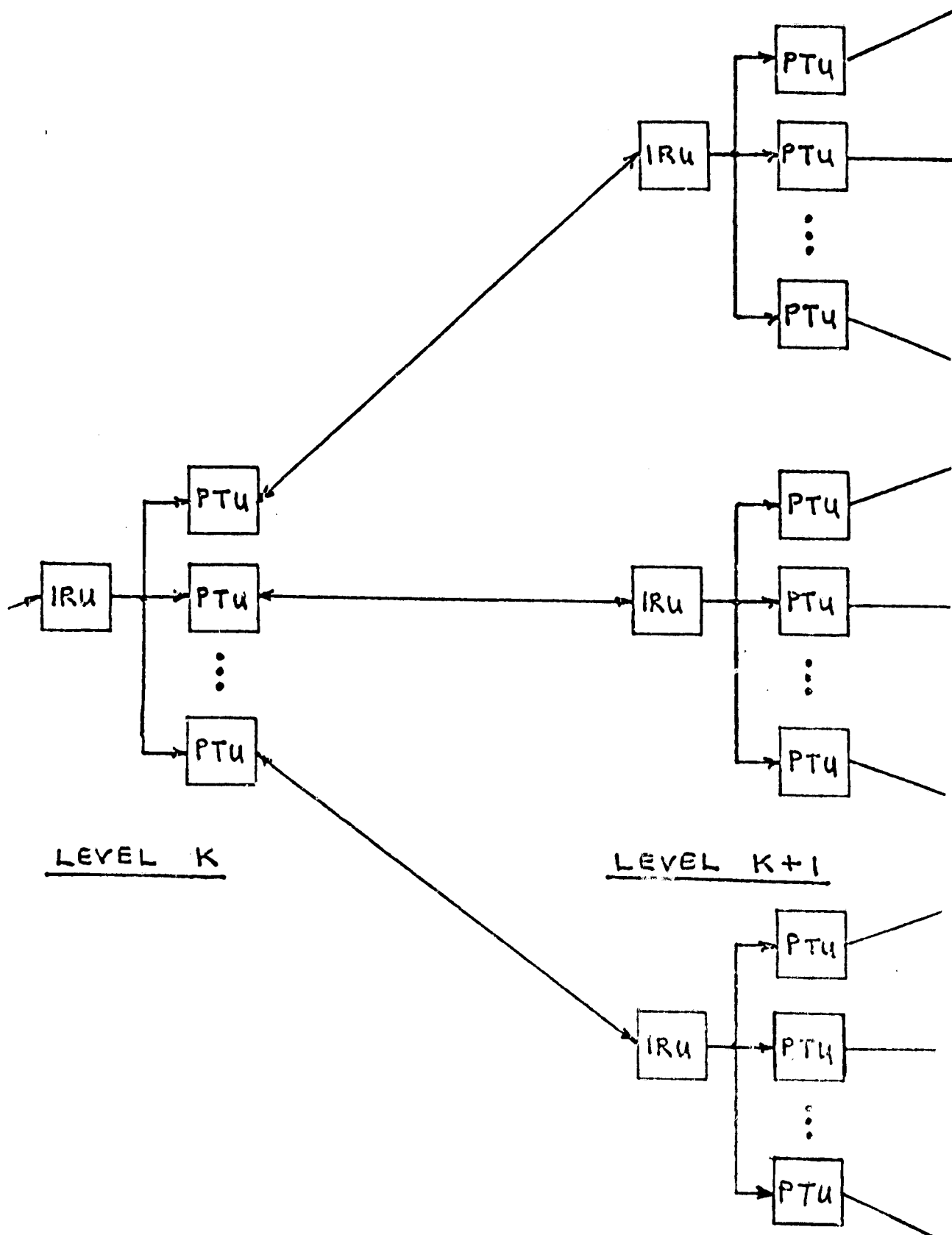
MSRTS BREADBOARD MILESTONES

- DESIGN
- FABRICATE THREE PROTOTYPE UNITS
- TEST THREE-POINT MSRTS
- FABRICATE SIX ADDITIONAL UNITS
- TEST SIX-POINT MSRTS
- INTEGRATE WITH TOTAL SYSTEM

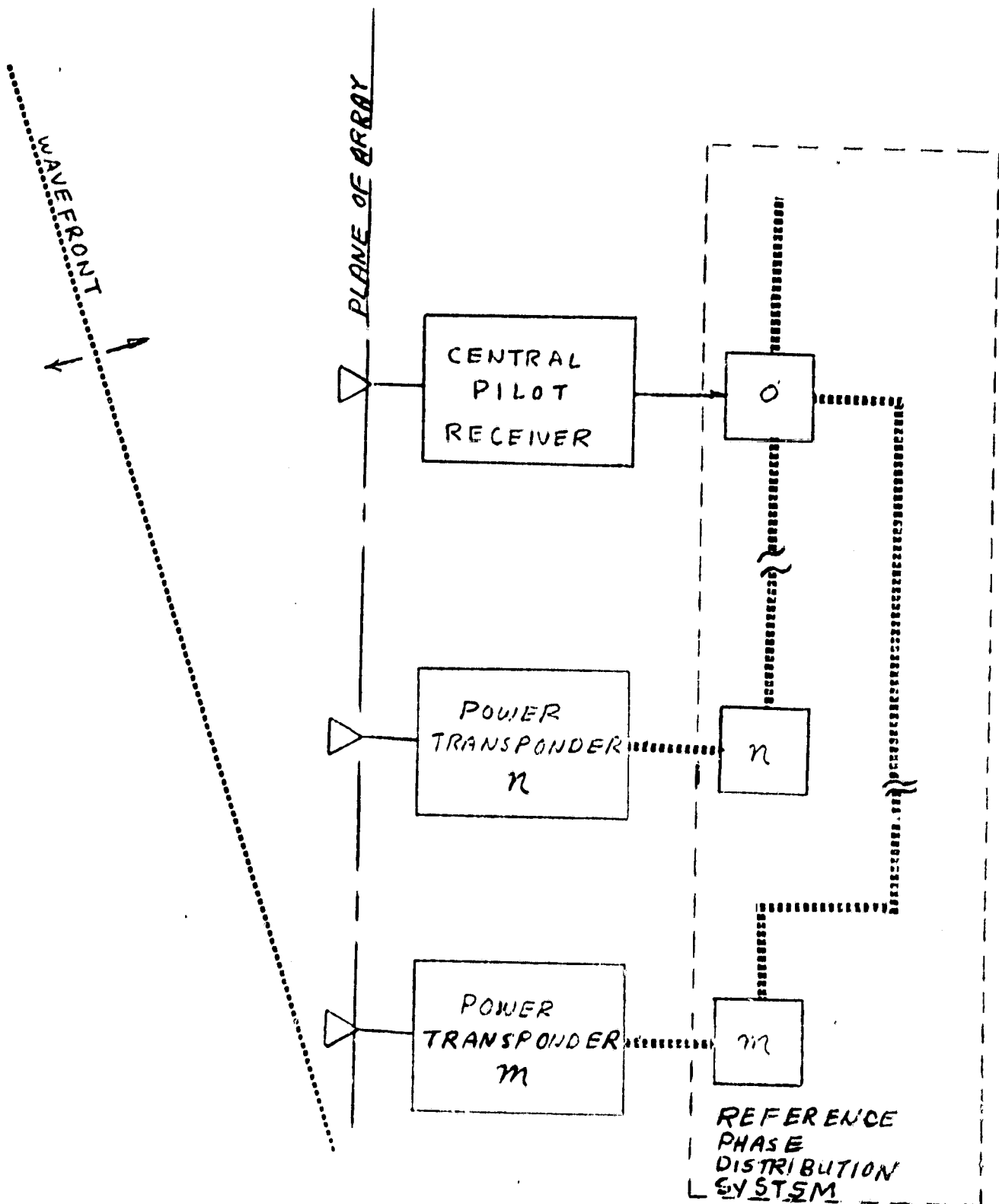
SIMPLIFIED FUNCTIONAL DIAGRAM OF MSRTS



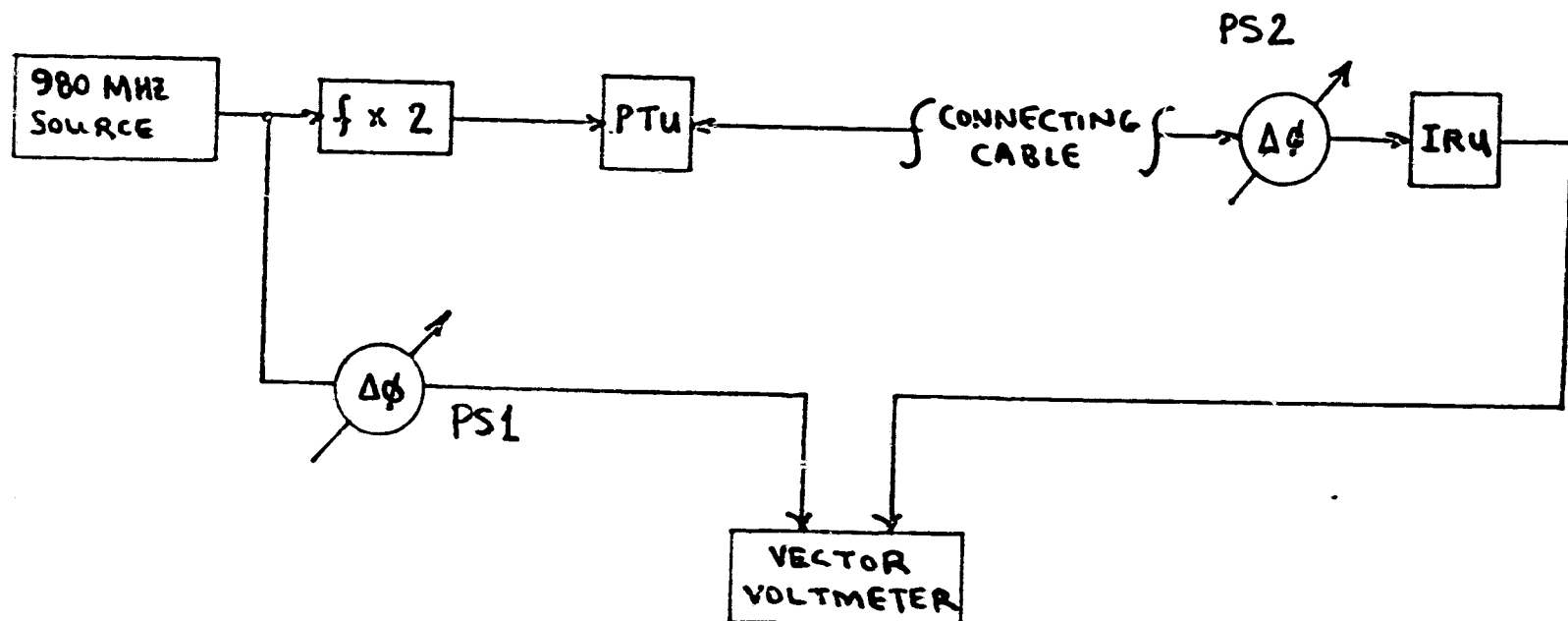
MSRTS ELEMENTS IN SPS DISTRIBUTION NETWORK



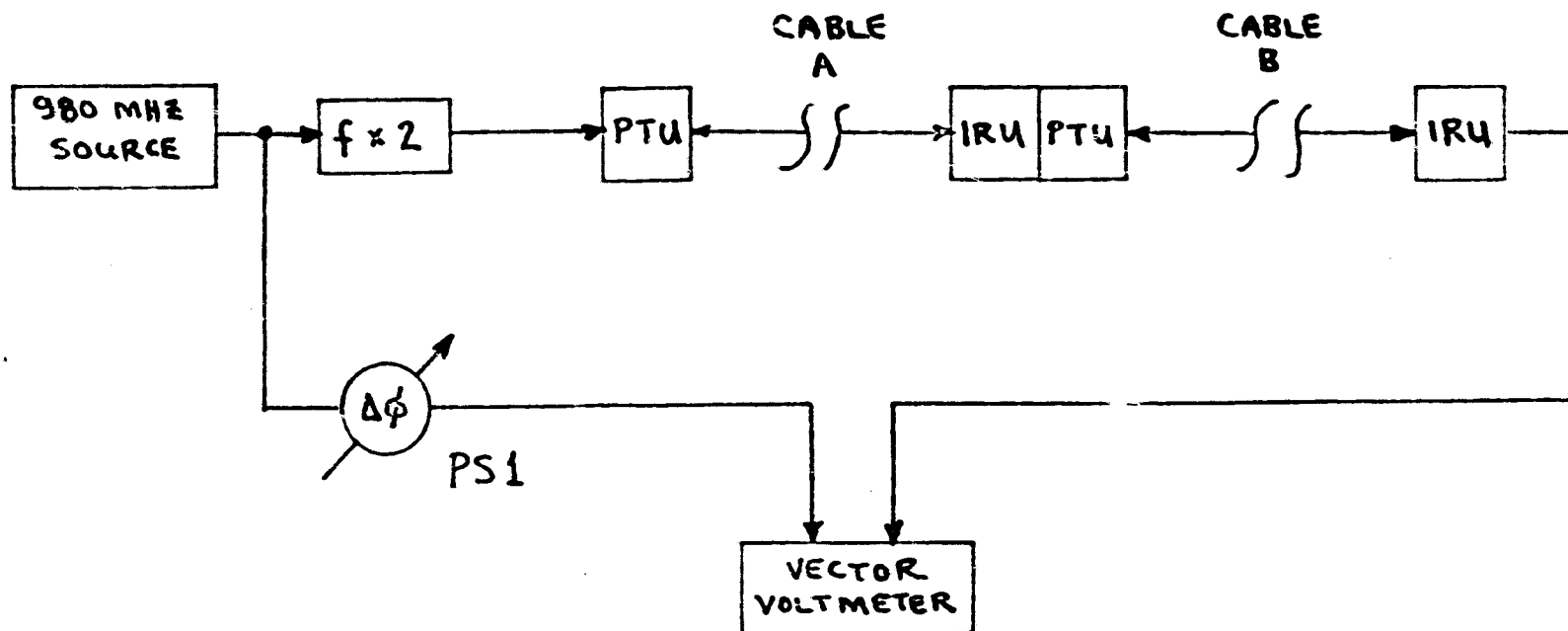
RETRODIRECTIVE ARRAY CONCEPT



TWO NODE TEST CONFIGURATION



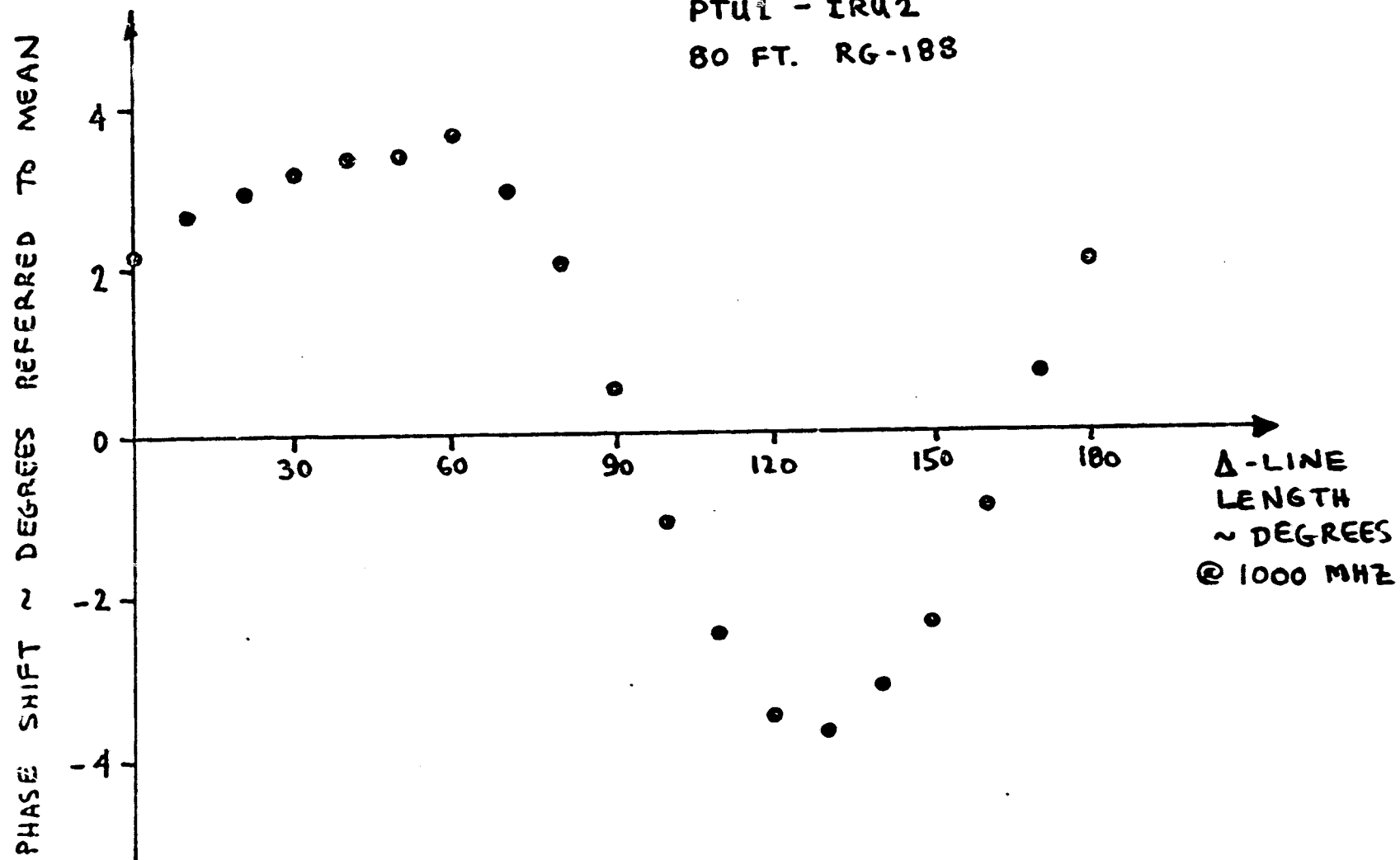
THREE-NODE TEST CONFIGURATION



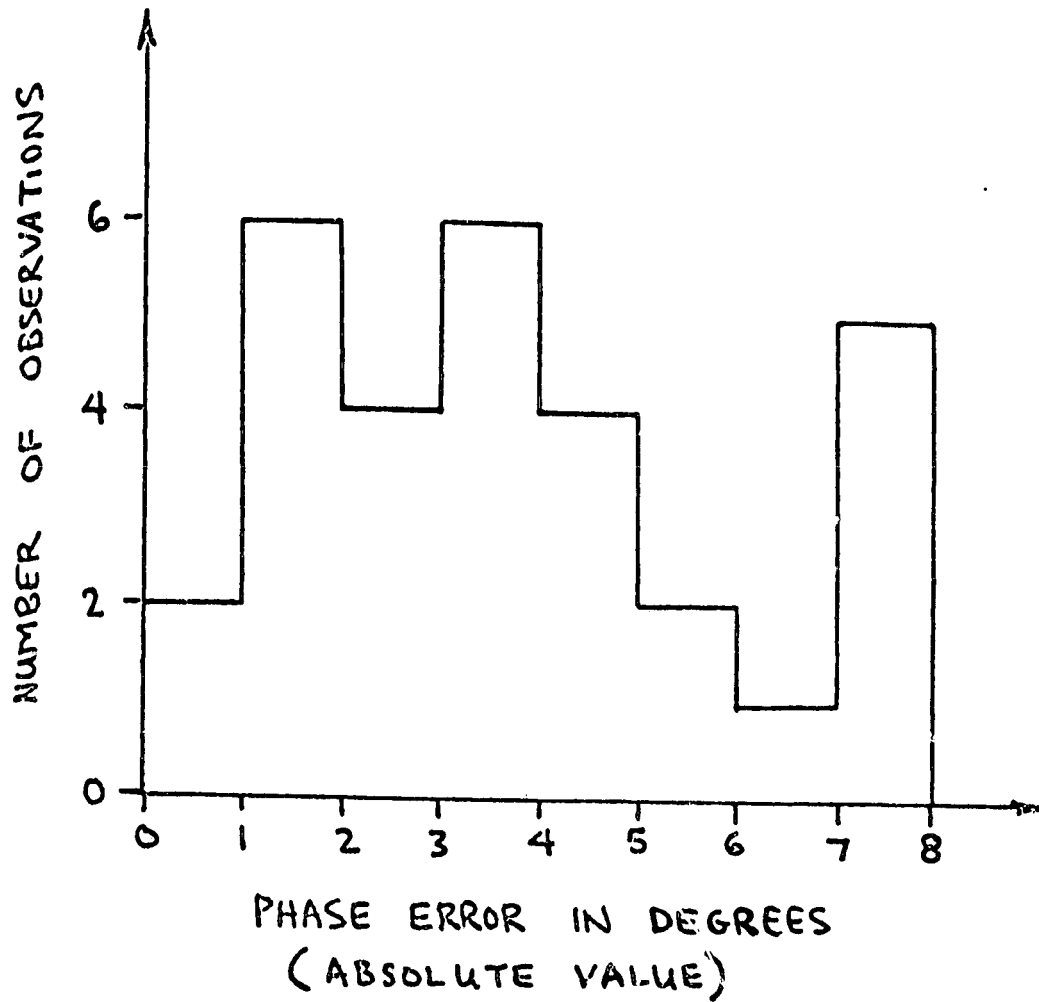
PHASE ERROR VERSUS MINOR LINE LENGTH PERTURBATION: LONG CABLE

PTU1 - IRU2

80 FT. RG-188



HISTOGRAM OF THREE-NODE TEST RESULTS



STD. DEV. OF 30 TRIAL SAMPLE = 4.2 DEGREES

C - 8

CONCLUSIONS FROM THREE-POINT TEST RESULTS

- FEASIBLE IN LABORATORY CONDITIONS
- ACCURACY LIMITED BY COMPONENT IMPERFECTIONS

MSRTS PERFORMANCE LIMITING FACTORS

- POOR ISOLATION IN CIRCULATORS, COUPLERS, AND MIXERS
- VCO PULLING AND SELF-LOCKING TENDENCIES
- INTERMODULATION PRODUCTS IN MIXERS
- EFFECTS OF TEMPERATURE VARIATION
- MECHANICAL EFFECTS; STRESS ON CONNECTORS AND CABLES, VIBRATION EFFECT ON VCO

MICROWAVE POWER TRANSPONDER (MPTX) MILESTONES

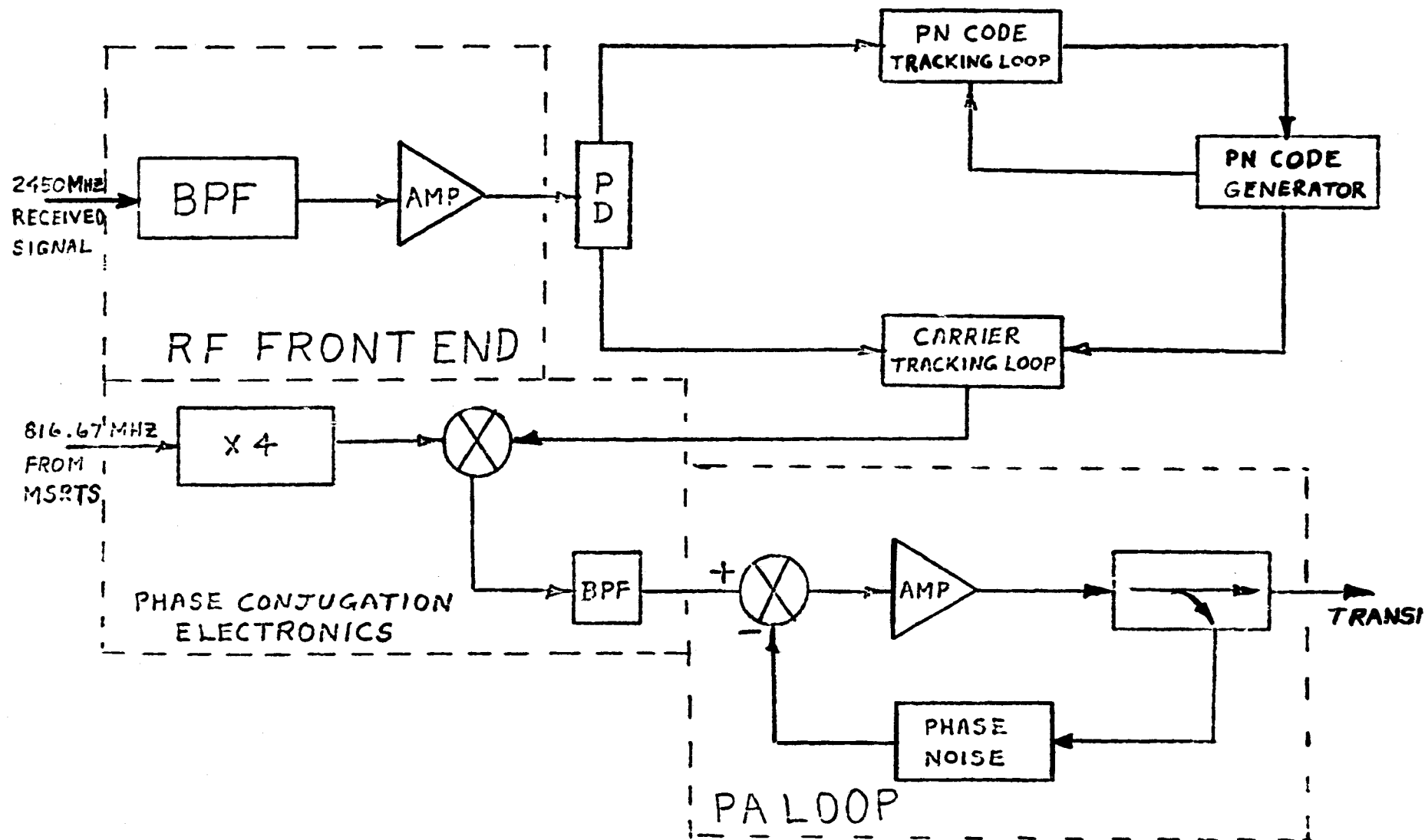
- DESIGN
- FABRICATE MPTX ELEMENTS
 - PILOT TRANSMITTER
 - PILOT RECEIVER
 - TWO TRANSPONDERS
- TEST INDEPENDENTLY
- INTEGRATE WITH MSRTS BREADBOARD

MICROWAVE POWER TRANSPONDER

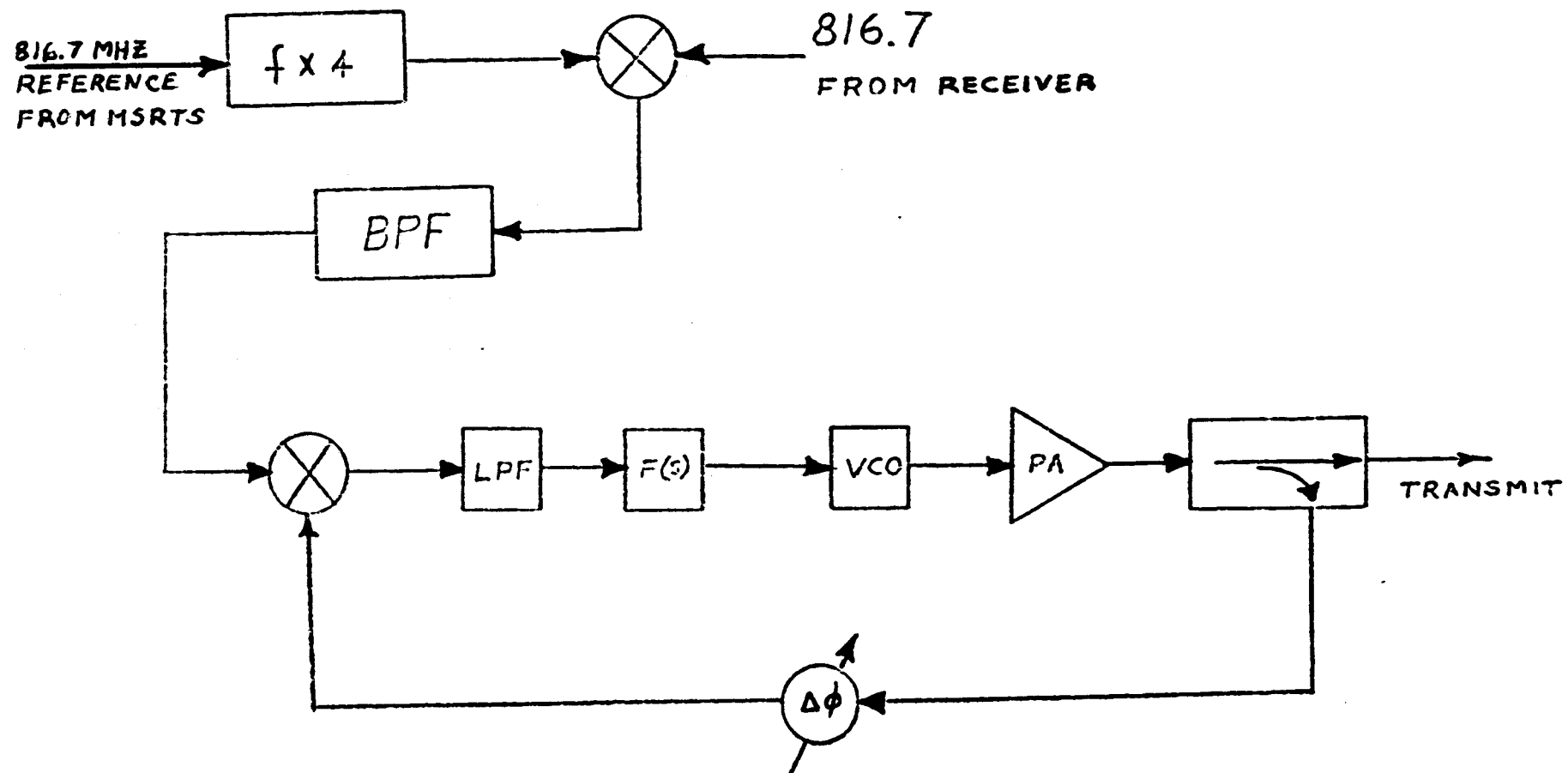
- SPLIT-PHASE, SPREAD SPECTRUM PILOT SIGNAL
- BASEBAND DESPREADER
- PHASE-LOCKED CARRIER RECOVERY LOOP WITH NO PHASE AMBIGUITIES
- PHASE CONJUGATED RETURN SIGNAL
- PHASE-LOCKED NOISE SUPPRESSION LOOP AROUND POWER AMPLIFIER

MICROWAVE POWER TRANSPONDER

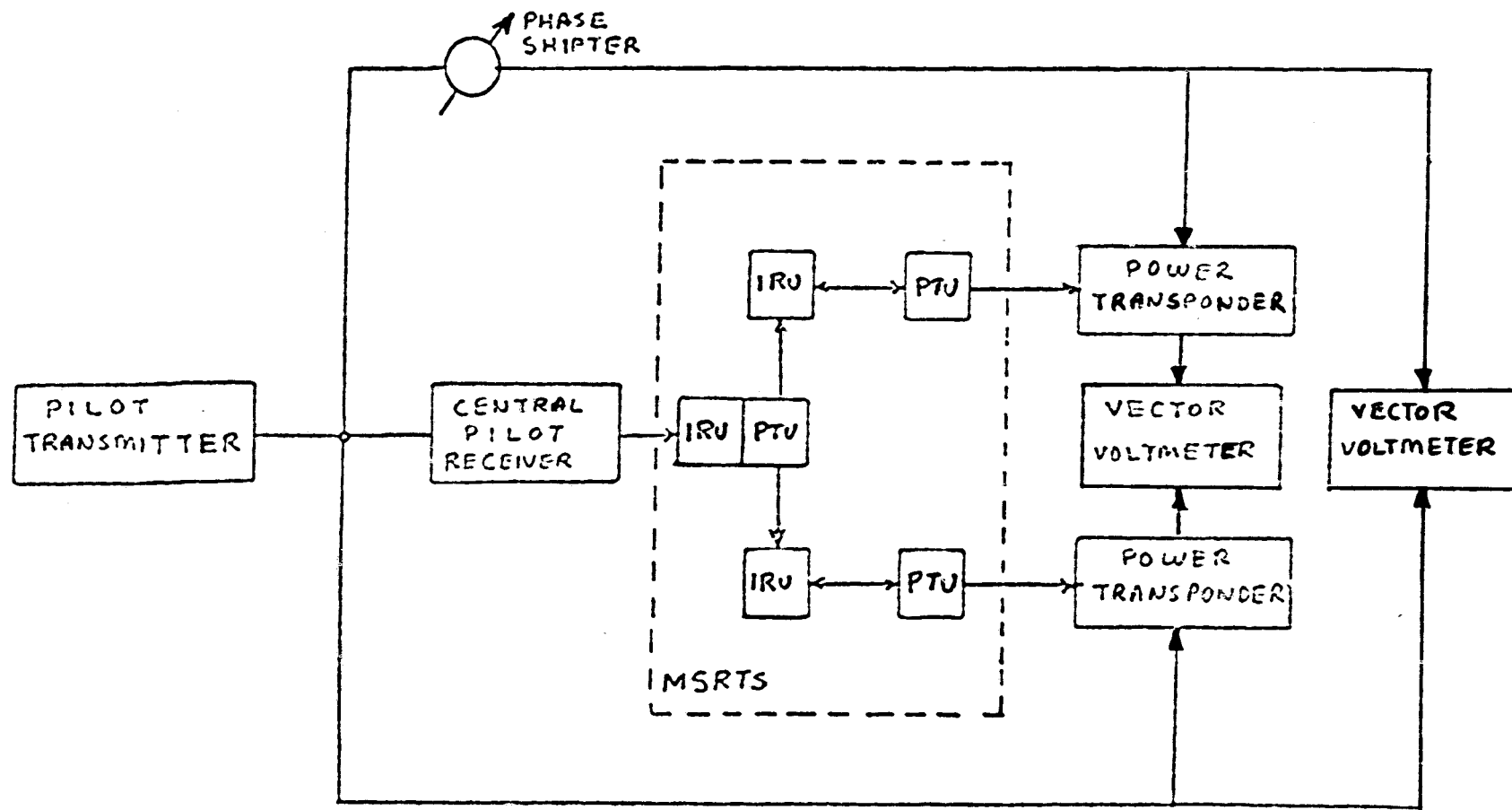
29



TRANSPONDER WITH POWER AMPLIFIER LOOP



BREADBOARD SPS PHASE CONTROL SYSTEM IN TYPICAL TEST CONFIGURATION



PROGRAM MILESTONES/STATUS

- MSRTS BREADBOARD TESTS
 - THREE-POINT TEST COMPLETED
 - SIX-POINT TEST MAY 1980
- MICROWAVE POWER TRANSPONDER DEVELOPMENT
 - PILOT TRANSMITTER APRIL 1980
 - PILOT RECEIVER APRIL 1980
 - KLYSTRON POWER AMPLIFIER MAY 1980
- TOTAL SYSTEM TESTS JUNE-JULY 1980

***Solar Power Satellite
Phase Control System
Studies***

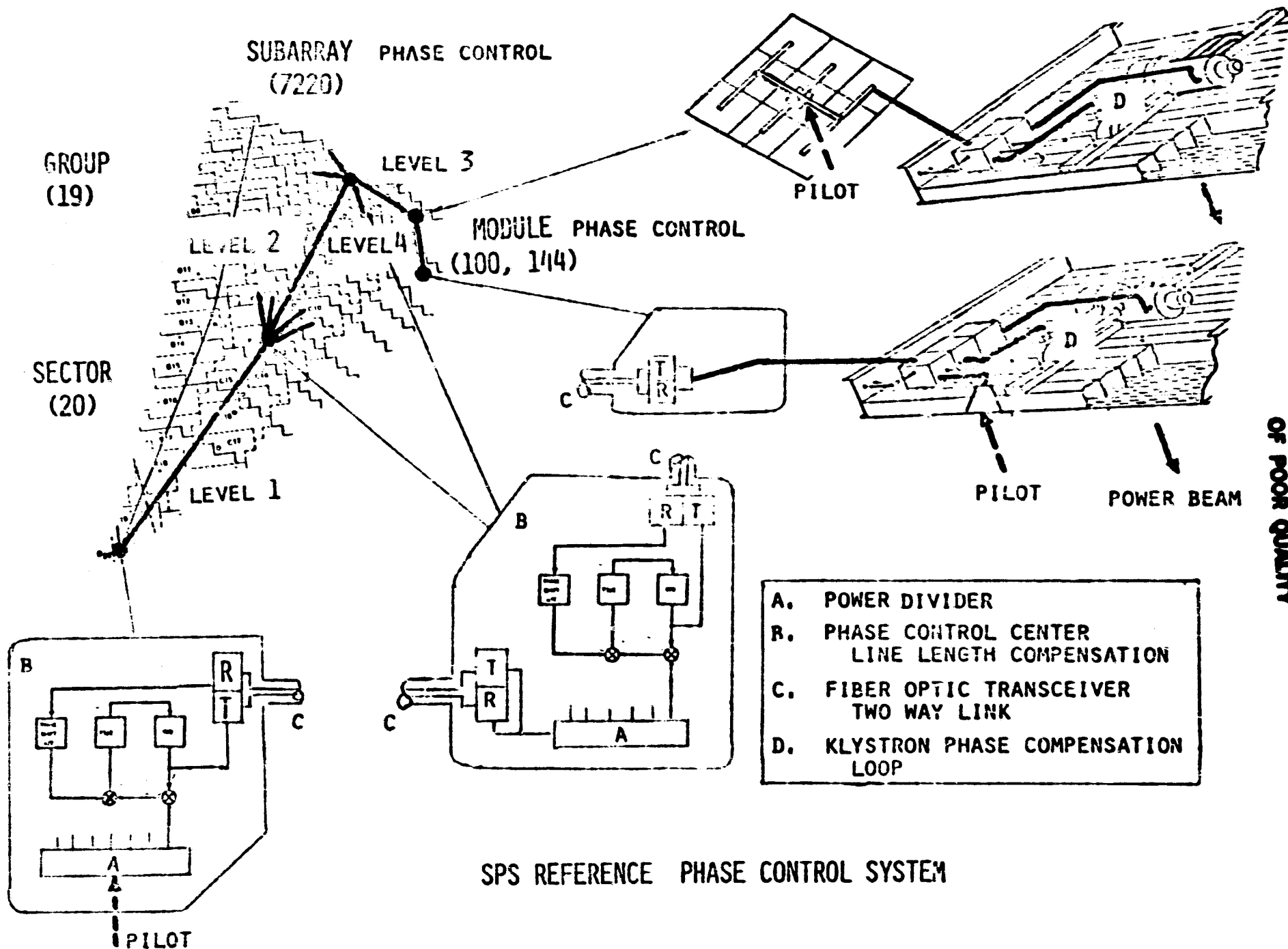
***Gordon Woodcock
Boeing***

PRECEDING PAGE BLANK NOT FILMED

SPS PHASE SYSTEM COMPARISONS

	PILOT BEAM	PHASE CONJUGATION	REF. DISTRIBUTION	FEATURES
JPL	DUAL (DOUBLE) SIDEBAND SUPPRESSED CARRIER DSBSC	EXACT 2 IF DIFFERENCE FREQ.	SERIES TREE CENTRAL PHASING	PHASE LOCK LOOP (PLL)
LIN COM	SPREAD SPECTRUM	EXACT 2 IF FREQ.	4 LAYER TREE MSRTS	PLL TIPS SYSTEM
BOEING/ G.E.	DUAL DSBSC (3-PILOT)	APPROX. 2 IF DIFFERENCE FREQ.	3 LAYER TREE CENTRAL PHASING	NO PLL'S MIXERS ONLY CORRECTS/ SYSTEMATIC ERRORS

PRECEDING PAGE BLANK NOT REPRODUCED



SPS REFERENCE PHASE CONTROL SYSTEM

BOEING SPS

INTRASUBARRAY PHASE CONTROL SYSTEM PRODUCTION COST CHARACTERISTICS

79-377

<u>Subarray Type</u>	<u>Number of Klystrons</u>	<u>Subarrays of This Type</u>	<u>PCR Mass (kg)</u>	<u>PCR Cost (\$)</u>	<u>RPDS Mass (kg)</u>	<u>RPDS Cost (\$)</u>	<u>Length Cable (m)</u>	<u>Cable Mass (kg)</u>	<u>Cable Cost (\$)</u>
1	4	1028	4.4	2240	1.0	595	33	3.7	73
2	6	1052	6.6	3360	1.0	595	49	5.4	108
3	8	612	8.8	4480	1.0	595	61	6.9	138
4	9	664	9.9	5040	1.0	595	72	8.0	160
5	12	900	13.2	6720	1.0	595	95	10.6	212
6	16	784	17.6	8960	1.0	595	132	14.5	290
7	20	628	22.0	11200	1.0	595	167	18.2	365
8	24	644	26.4	13440	1.0	595	197	21.6	433
9	30	632	33.0	16800	1.0	595	232	26.0	522
10	36	276	39.6	20160	1.0	595	296	32.5	649
TOTAL		7220	112 T	\$57M	7 T	\$4M		91 T	\$1M



INTERSUBARRAY PHASE CONTROL SYSTEM
PRODUCTION COST CHARACTERISTICS

79-378

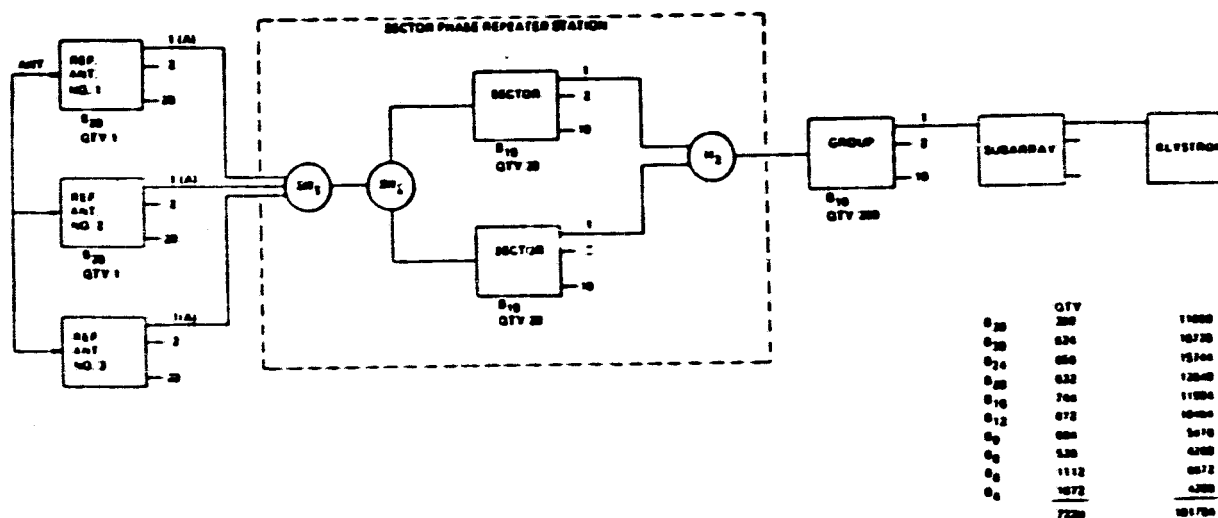
<u>Item</u>	<u>No. Req'd.</u>	<u>Avg. Unit</u>	<u>Per SPS (M)</u>
Master Reference Receiver and Reference Phase Transmitter	3	424K	1.272
Cables	60	4.6K	0.276
Slave Repeaters	400	25.1K	10
Level 2 Cables	380	2.5K	0.95
			<u>\$12.5M</u>

Level 3 cables are common with
area-subarray data harness (see WBS 1.1.3)

BOEING SPS

PHASE DISTRIBUTION NETWORK REDUNDANCY

74-386



PHASE DISTRIBUTION NETWORK BLOCK DIAGRAM WITH FAILURE RATES

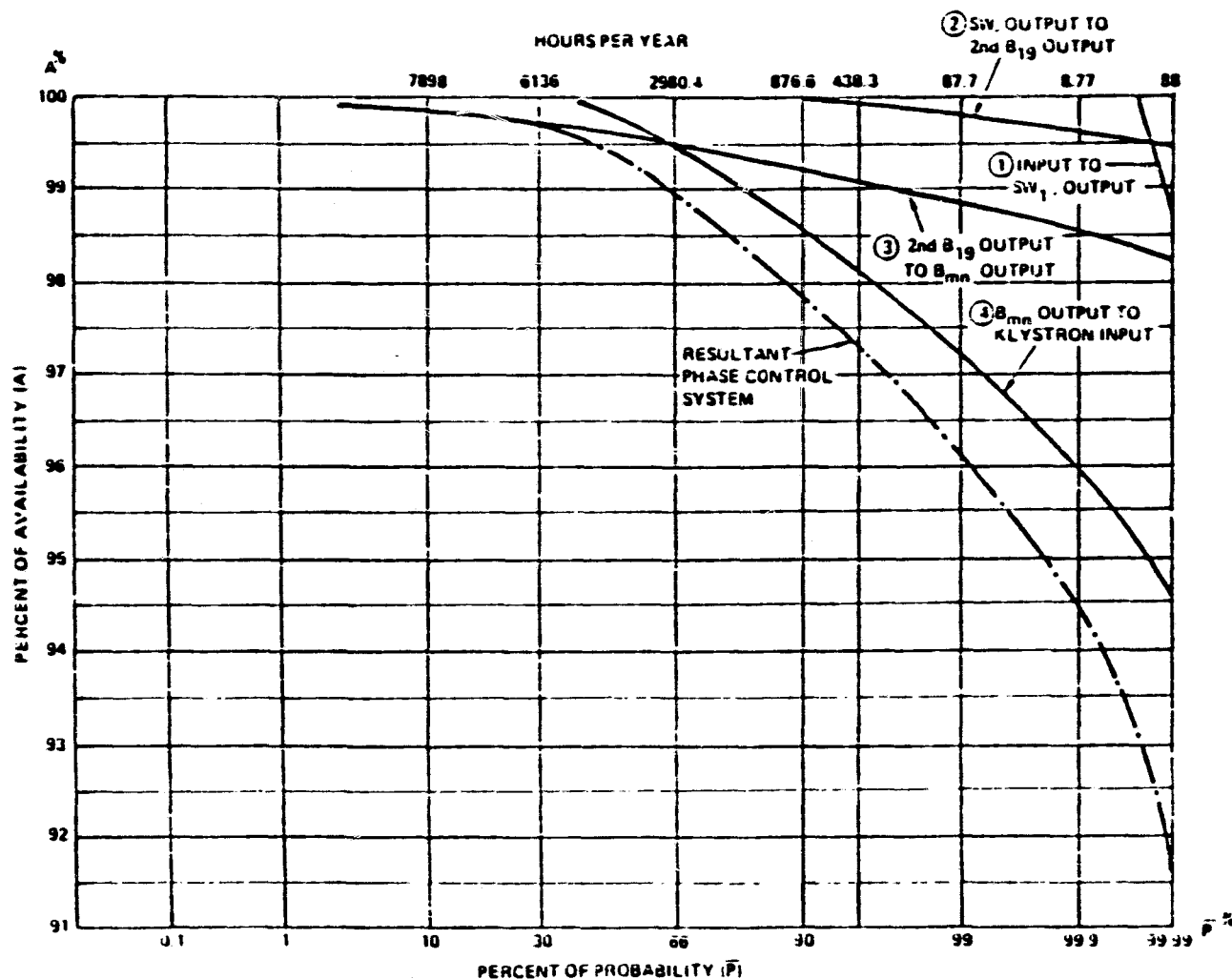
[illegible]

FAILURES ARE SHOWN
IN THE FAILURE PER
100 HRS UNITS

74

PHASE CONTROL SYSTEM AVAILABILITY vs PROBABILITY

79-385



SPACETENNA AVAILABILITY ESTIMATE

79-387

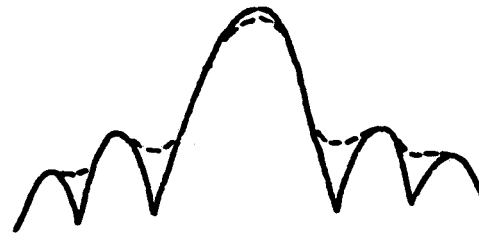
ITEM	MEAN AVAILA- BILITY	MAINTENANCE HOURS, SEMI- ANNUAL REPAIR	IMPACT ON EFFICIENCY
DC DISTRIBUTION REDUNDANT DC-DC CONVERTERS	.995	281	~ 1%
PHASE CONTROL SYSTEM REDUNDANT 1ST 2ND LEVEL RECEIVERS AND CONJUGATORS	.989	620	~ 2.2%
KLYSTRON 25YR. MTBF NO REDUNDANCY	.98	2544	~ 4%
TOTAL MPTS EQUIPMENT	.902	7013	

PHASE CONTROL PERFORMANCE SIMULATION

CORRELATED ERRORS

BEAM STEERING

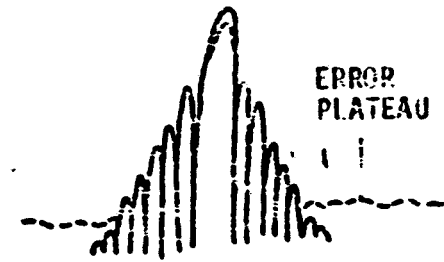
DEFOCUSING



4%/4 BRANCH
REF. DIST. TREE

1% LOSS/24° OF
RADIAL PHASE ERROR
BUILDUP

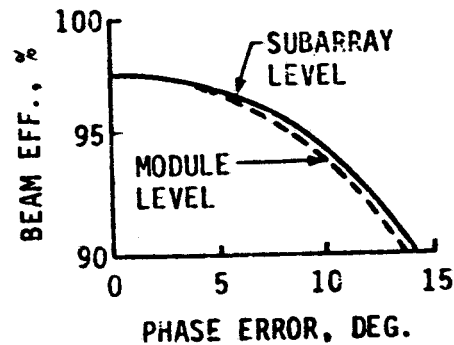
UNCORRELATED



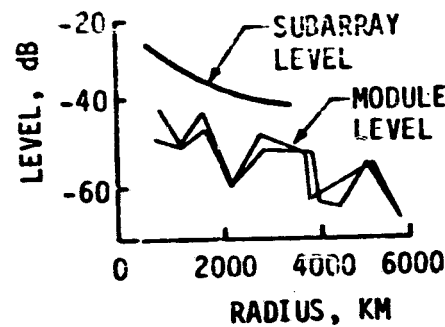
ERROR
PLATEAU

3% LOSS/10° OF
RANDOM PHASE ERROR

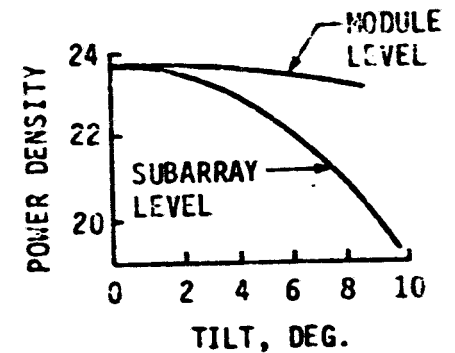
INDEPENDENT OF RANDOM ERROR



EFFECT ON GRATING LOBE LEVEL



EFFECT ON SCAN LOSS



PHASE
ERRORS

PHASE
CONTROL
LEVEL

***Solar Power Satellite
Fiber Optic Link Assessment***

***Dr. Erv Nalos
Boeing***

PRECEDING PAGE BLANK NOT FILMED

SPS FIBER OPTIC LINK ASSESSMENT CONTRACT NAS 9-15636A

TASKS:

- Analyze existing optical fibers for applicability for use in the test with emphasis on phase change effects, attenuation and bandwidth.
- Analyze suitable optical emitters and detectors to determine feasibility of operation and usage at 980 MHz.
- Select and purchase candidate optical fibers and an emitter and detector for testing.
- Test candidate fibers at 60 MHz for phase sensitivity to temperature.
- Design and construct impedance matching system for matching the optical emitter and detector to Boeing laboratory equipment.
- Assemble and test a two way opto-electronic link at 980 MHz consisting of two selected emitters and detector units and a jacket material 2-fiber cable of minimum length of 200 meters.

PRECEDING PAGE BLANK NOT FILMED

SPS TEST-LINK COMPONENT STATUS

DEVICE UNDER CONSIDERATION	TYPE	FEATURES
EMITTER	GaAlAs MULTI-MODE INJECTION LASER DIODE	1) LOW COST 2) HIGH POWER ~500
	GaAlAs SINGLE-MODE INJECTION LASER DIODE	1) HIGH POWER 2) HIGH COUPLING EFF. 3) LOW THRESHOLD 4) LOW DISTORTION ~750 5) NARROW SPECTRAL WIDTH 6) HIGH RELIABILITY
DETECTOR	SILICON AVALANCHE PHOTO DIODE	1) GAIN-BW PRODUCT = 80 GHz 2) HIGH RCVR S/N 3) LOW COST ~100
DEVICE COUPLING NETWORKS	RESONANT CAVITY	1) STABLE 2) HIGH Q
	STRIPLINE NETWORK	1) LOW COST 2) EASY TO MANUFACTURE

SPS FIBER INVESTIGATION RESULTS

o CRITERIA FOR MULTI-MODE, GRADED INDEX FIBERS

REQUIREMENTS FOR TEST	CORNING IVPO ⁽¹⁾	CORNING OVPO ⁽²⁾	TIMES OVPO ⁽²⁾	VALTEC IVPO ⁽¹⁾	GALILEO IVPO ⁽¹⁾	ITT IVPO ⁽¹⁾	NIPPON MULTI- COMPONENT
-----------------------	--------------------------------	--------------------------------	------------------------------	-------------------------------	--------------------------------	----------------------------	-------------------------------

BANDWIDTH ≥ 1 GHz-Km	X	X	X			X	
ATTENUATION ≤ 10 dB/Km	X	X	X	X	X	X	X
UNIQUE DOPANT/ MANUFACTURING TECHNIQUE	X	X	X			X ⁽³⁾	X
AVAILABILITY	X	X	X	X	X	X	X
UNJACKETED	X	X	X	X	X		X
SUGGESTED FOR TEST $\Delta\phi$	•••	•••	••				•

~3/m

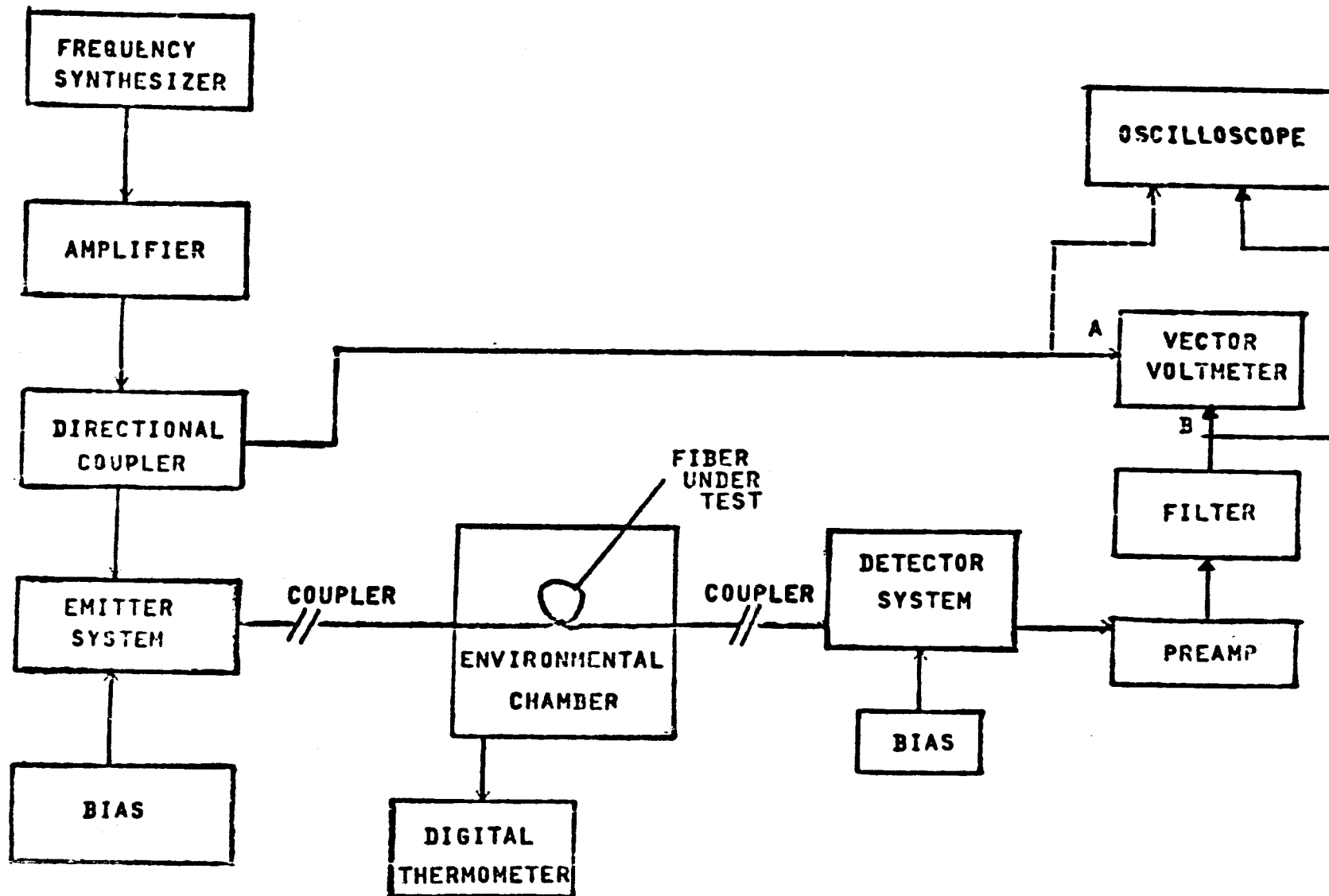
~2/m

o CRITERIA FOR SINGLE-MODE FIBERS

- o SELECTION WILL BE BASED ON AVAILABILITY OF TEST SAMPLES. GENERALLY SUGGESTED THAT A PURE FUSED SILICA FIBER WITH Ge DOPED CORE WILL BE SUPERIOR TO OTHER TYPES.

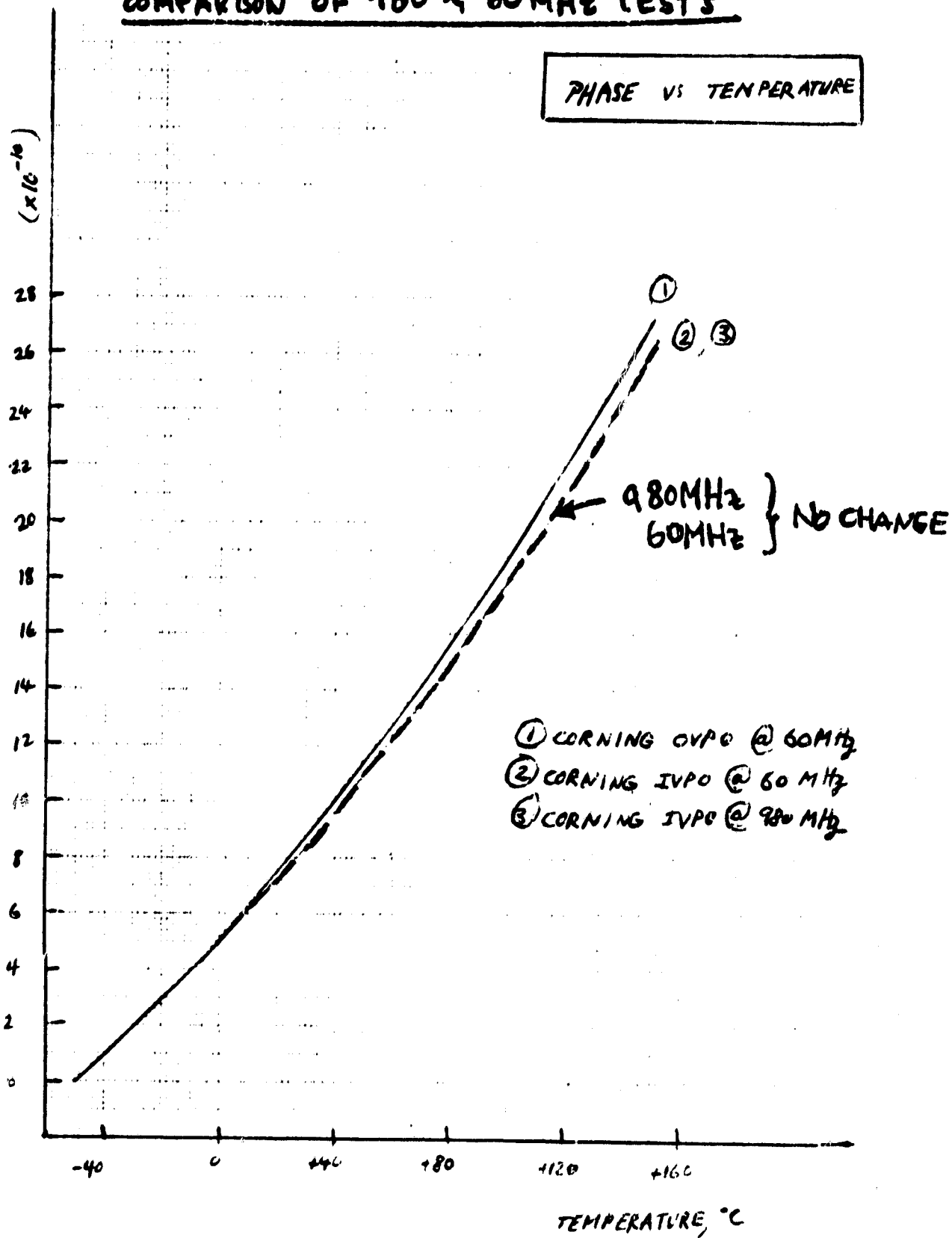
- (1) IVPO - INSIDE VAPOR PHASE OXIDATION PROCESS
- (2) OVPO - OUTSIDE VAPOR PHASE OXIDATION PROCESS
- (3) FIBER HAS TIGHTLY EXTRUDED PLASTIC JACKET

OVEN MEASUREMENTS - 60MHz

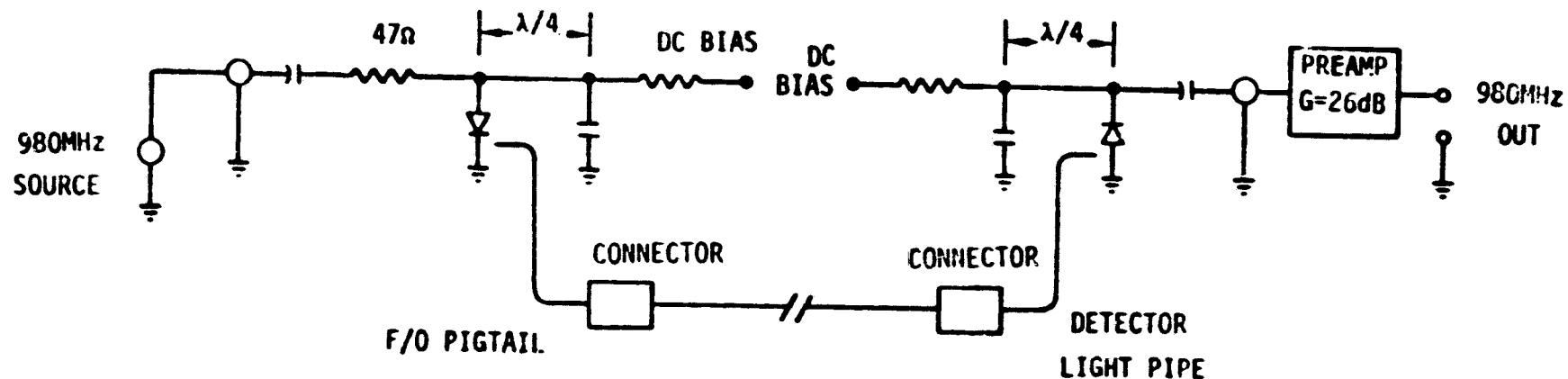


COMPARISON OF 980 & 60 MHz TESTS

CHANGE IN PHASE, DEGREES / 43 METER



SPS 980MHz FIBER OPTIC LINK TEST



98

EMITTER

- o NEC INJECTION LASER DIODE
- o BIAS COUPLED THROUGH QUARTER-WAVE MICROSTRIP
- o $I_{\text{BIAS}} = 88\text{ma DC}$
- o OPTICAL POWER = 437 μwatt @ EMITTER DIGTAIL
- o $V_{980\text{MHz}} = 0.7\text{ VOLTS RMS}$

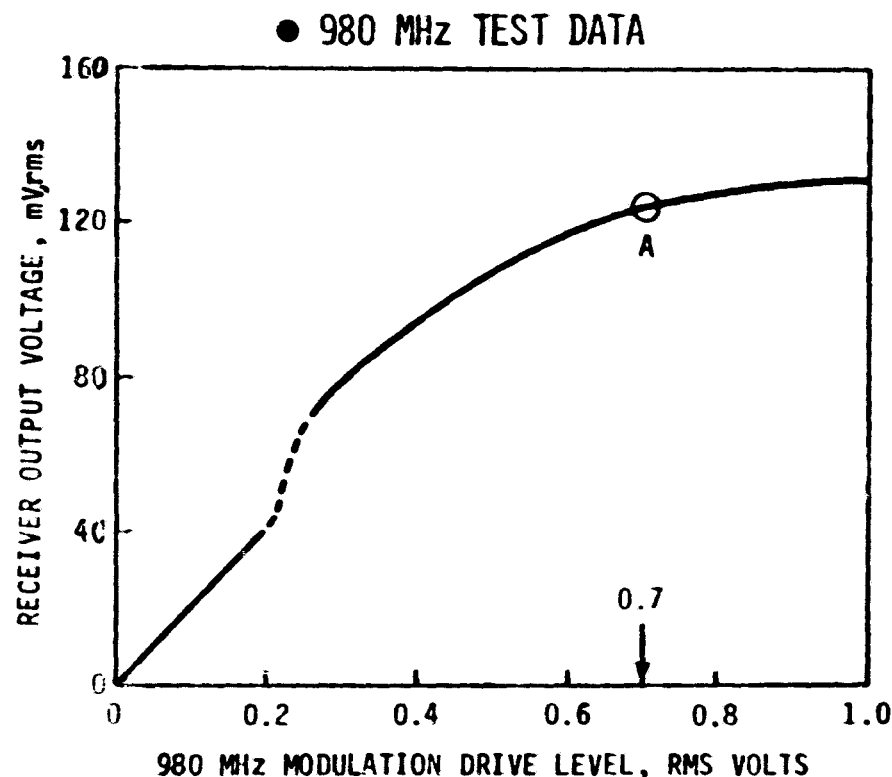
FIBER

- o CORNING IVPO, GRADED INDEX
- o LENGTH = 303 METERS
- o ATTN. = 3.9dB/km
- o BW = 870MHz-km
- o N.A. = 0.218

DETECTOR

- o RCA AVALANCHE PHOTODIODE
- o BIAS COUPLED THROUGH QUARTER-WAVE MICROSTRIP
- o $V_{\text{BIAS}} = 180\text{ VOLTS DC}$
- o OPTICAL POWER = 228 μwatt @ DETECTOR LIGHT PIPE
- o $V_{980\text{MHz}} = 135\text{ mv RMS OUT OF PREAMP}$

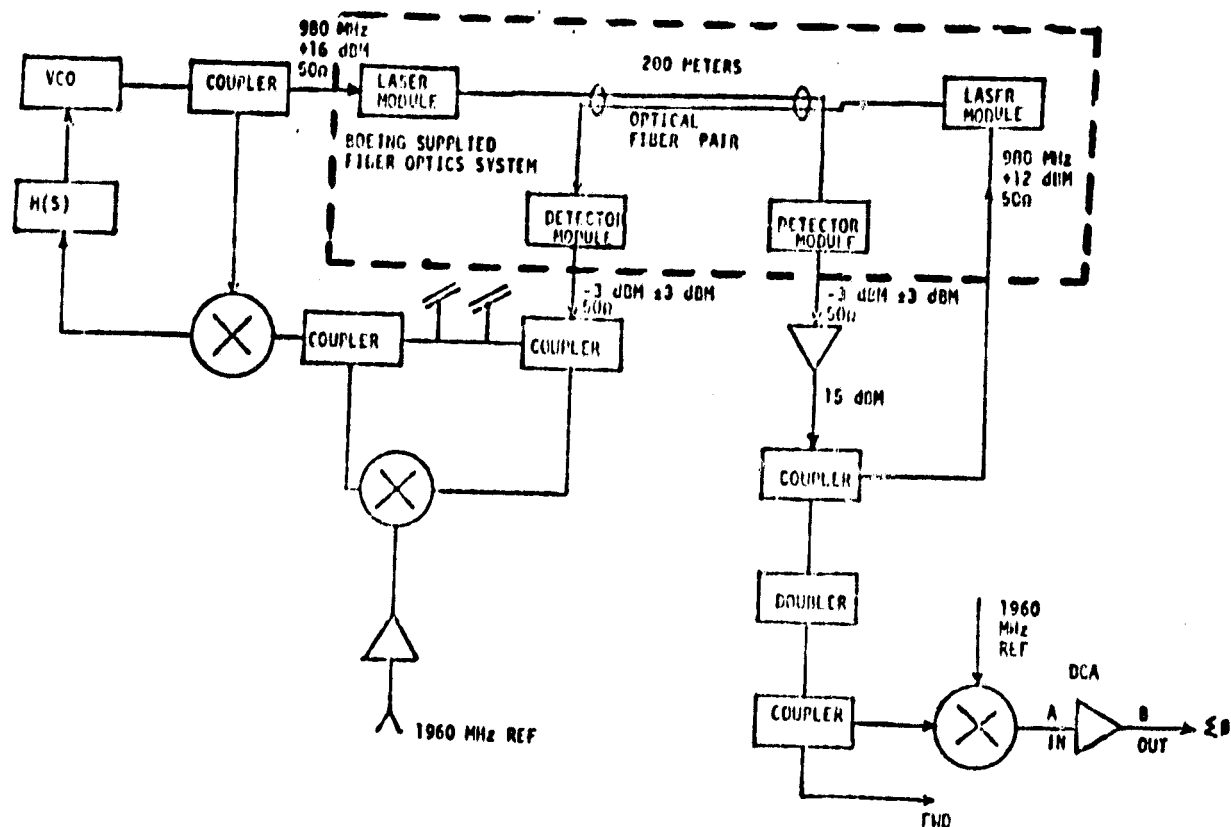
SPS FIBER OPTIC LINK TEST



- POWER EMITTED FROM EMITTER MODULE
= 437 μ WATT = -3.6 DBM (MEASURED)
- LOSSES DUE TO FIBER ATTENUATION
= 3.9 DB/KM \times 0.303 KM = 1.18 DB
- COUPLING LOSS AT EMITTER TO FIBER
= 1.65 DB (MEASURED)
- COUPLING LOSS AT FIBER TO DETECTOR
= 1.0 DB (ESTIMATED)
- ∴ POWER ONTO DETECTOR (AVERAGE)
= -3.6 DBM - 1.0 - 1.65 - 1.18
= -7.43 DBM (181 μ WATT)

- NOISE EQUIVALENT OPTICAL POWER = 331 NWATT RMS = -34.8 DBM (CALCULATED)
- AC RMS EMITTER/DETECTOR RESPONSIVITY PRODUCT = 0.211 (MEASURED)
- AC RMS 980 MHz SIGNAL POWER AT DETECTOR = 0.211 \times 181 μ WATTS = 38.2 μ WATT
= -14.2 DBM (PT. A)
- OPTICAL EQUIVALENT SIGNAL TO NOISE RATIO = -14.2 DBM + 34.8 DBM = 20.6 DB
- POST DETECTION ELECTRICAL S/N (SQUARE WAVE DETECTOR) = 41.2 DB

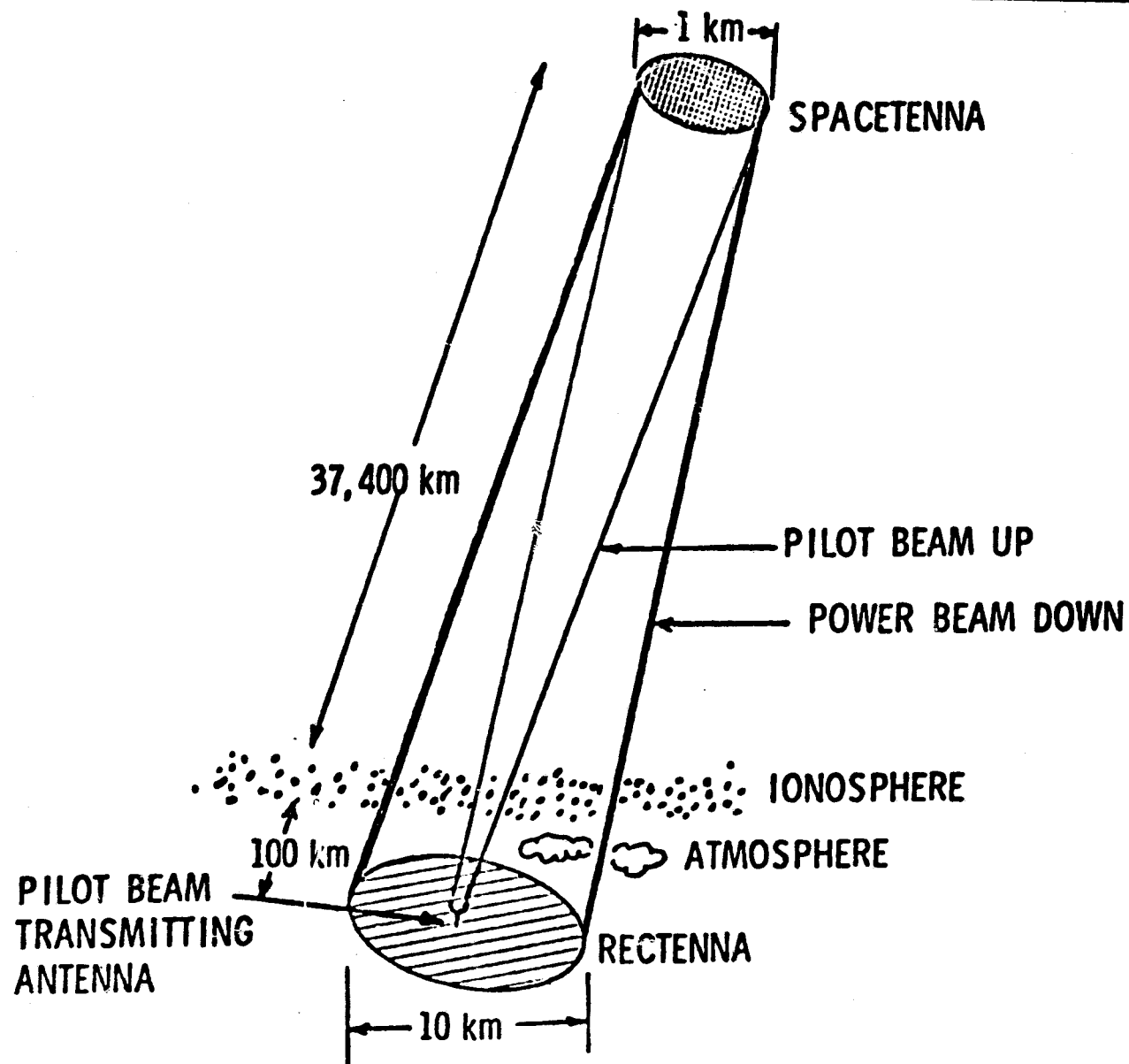
TWO-WAY LINK FOR SPS VERIFICATION



***Ionospheric Effects in
Retrodirective Arrays
and
Mitigating System Design***

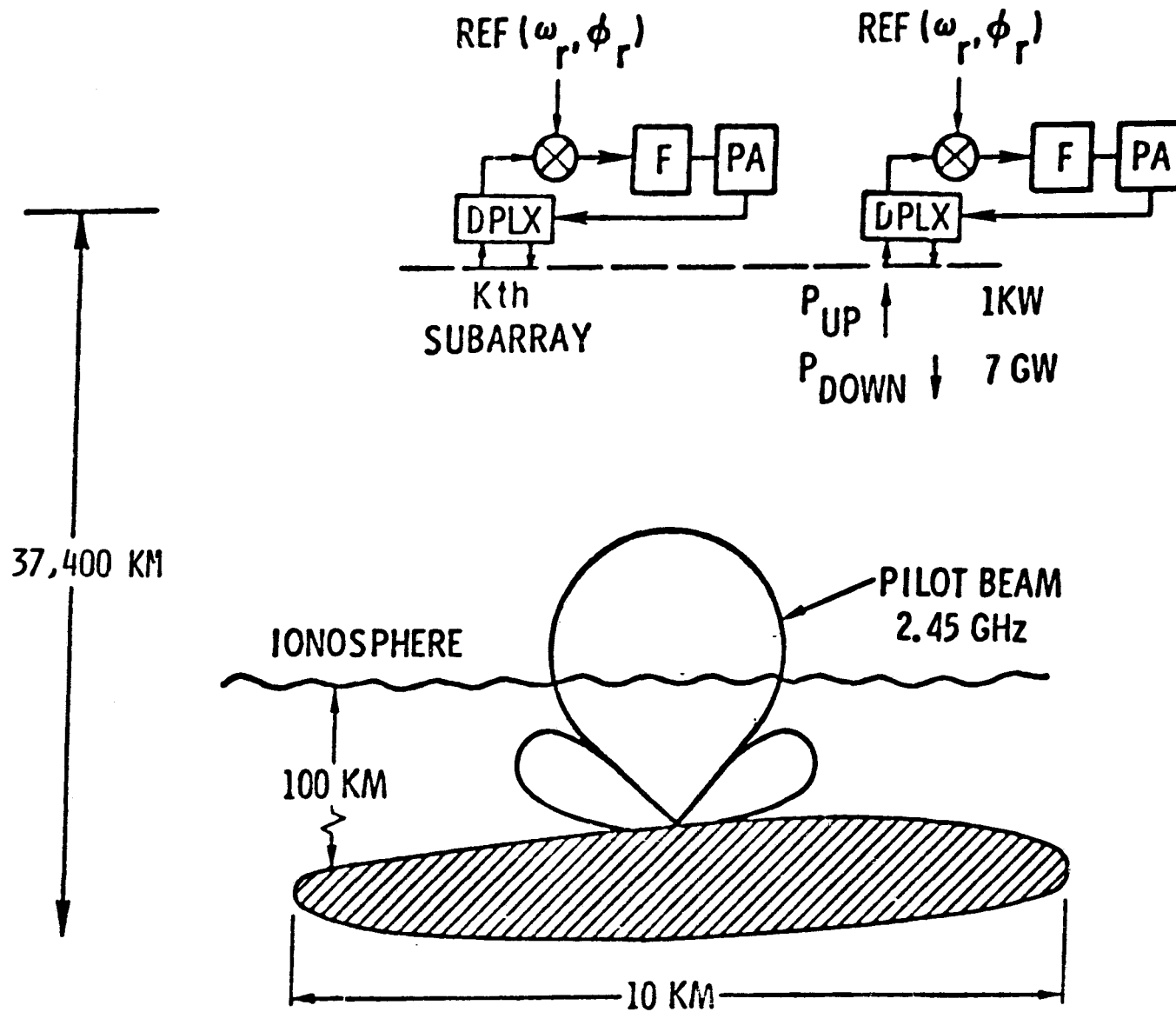
***Dr. A. K. Nandi
Rockwell International***

BASIC UP/DOWN BEAM GEOMETRY



PRECEDING PAGE BLANK NOT FILMED

BASIC SPS POWER FLOW MECHANISM - ACTIVE RETRODIRECTIVE ARRAY



IONOSPHERE CHARACTERIZATIONS

1. STEADY-STATE REGULAR (IDEAL STRATIFIED LAYERS)

⇒ HOMOGENEOUS, DISPERSIVE MEDIUM

2. STEADY-STATE IRREGULAR (LARGE-SCALE WEDGES OR SMALL-SIZE ANOMALIES)

⇒ INHOMOGENEOUS, DISPERSIVE MEDIUM

3. TIME-VARIABLE AND IRREGULAR

⇒ INHOMOGENEOUS, DISPERSIVE AND TIME-VARYING.
MEDIUM

BASIC ASSUMPTIONS REGARDING IONOSPHERE

A. STATIONARY OR SLOWLY-VARYING

B. NO SERIOUS PROBLEMS DUE TO HEATING OF IONOSPHERE
BY DOWNLINK POWER BEAM

IONOSPHERIC EFFECTS ON SINGLE-TONE PILOT BEAM

ASSUME f_U (UPLINK FREQUENCY) $\neq f_D$ (DOWNLINK FREQUENCY)

THE PATH-RELATED PHASE-SHIFT AT f_U ON ONE PARTICULAR LINK

$$\begin{aligned}\phi(f_U) &= 2\pi f_U \frac{L}{C} - \frac{40.5 \times 2\pi}{f_U C} \int_0^L N dl \\ &= 2\pi f_U \frac{L}{C} - \frac{K_U}{f_U}\end{aligned}$$

MULTIPLY BY f_D/f_U AND PHASE CONJUGATE

$$\tilde{\phi}^*(f_D) = -2\pi f_D \frac{L}{C} + K_U \frac{f_D}{f_U^2}$$

DOWNLINK SIGNAL AT TRANSMIT END

$$s^T(t) = \cos \left[\omega_D \left(t + \frac{L}{C} \right) - K_U \frac{f_D}{f_U^2} \right]$$

DOWNLINK SIGNAL AT RECEIVE END

$$s^R(t) = \cos \left[\omega_D t - K_U \frac{f_D}{f_U^2} + \frac{K_D}{f_D} \right] ; K_D = \text{A CONSTANT SIMILAR TO } K_U$$

IONOSPHERIC EFFECTS ON SINGLE-TONE PILOT BEAM (CONT'D)

K_U AND K_D COULD BE DIFFERENT BECAUSE OF

1. TIME VARIATIONS
2. UPLINK/DOWNLINK GEOMETRY

IN GENERAL, THE PAIR $\{K_U, K_D\}$ WILL BE DIFFERENT ON DIFFERENT LINKS BECAUSE OF IONOSPHERE INHOMOGENEITY. A CONSEQUENCE OF THIS IS THAT DOWNLINK BEAM IS NOT PHASE-COHERENT AT PILOT SOURCE!

PROBLEM: NEED TO EVALUATE THE AMOUNT OF PHASE ERROR THAT COULD OCCUR DUE TO WORST-CASE IONOSPHERIC CONDITIONS.

FURTHER COMMENTS ON IONOSPHERIC EFFECTS (SINGLE-TONE SYSTEM)

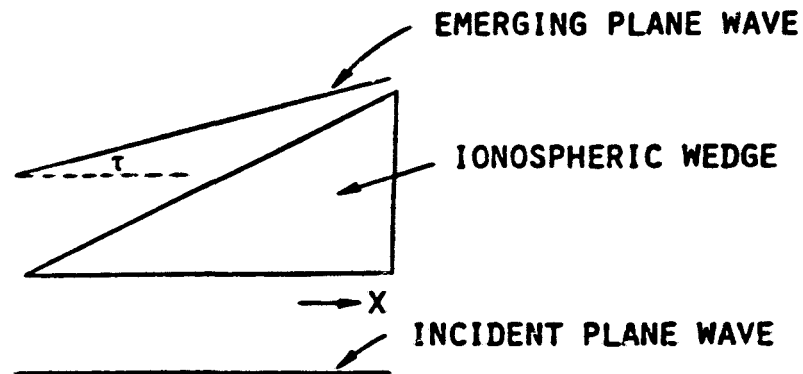
PROBLEM A: IONOSPHERE - INDUCED PHASE ERRORS CAN CAUSE LOSS OF PHASE COHERENCE AT SOURCE.

PROBLEM B: LARGE-SCALE IONOSPHERIC IRREGULARITIES (E.G., WEDGES) CAN CAUSE BEAM POINTING ERRORS.

THE MAGNITUDE OF PROBLEM A NEEDS TO BE EVALUATED UNDER WORST-CASE IONOSPHERIC CONDITIONS.

THE MAGNITUDE OF PROBLEM B CAN BE ESTIMATED BASED ON LIMITED AVAILABLE KNOWLEDGE ON WEDGES. (LAWRENCE, ET AL., PROC. IEEE, JANUARY 1964)

FURTHER COMMENTS ON IONOSPHERIC EFFECTS (SINGLE-TONE SYSTEM) (CONT'D)



τ = TILT ANGLE OF REFRACTED WAVEFRONT

$$= \frac{b}{\omega^2} \frac{d}{dx} \left(\int N dz \right) \text{ RADIANS; } b = 1.6 \times 10^3 \text{ MKS}$$

ASSUME TRANSVERSE GRADIENT = 1% OF $\int N dz$ OVER 10 KM

$$= 10^{-6} \times \int N dz$$

ASSUME $\int N dz = 10^{19}$ (WORST-CASE), $\omega = 2\pi \times 2.5 \times 10^9$

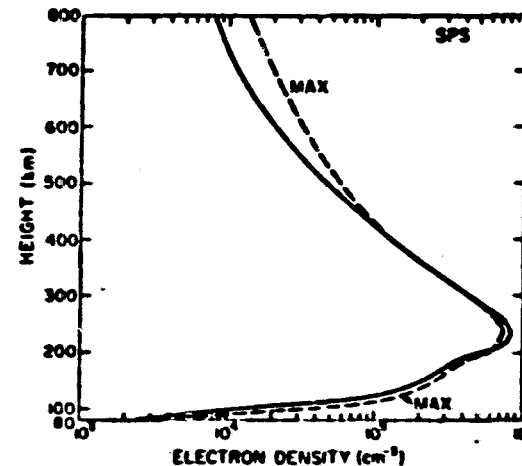
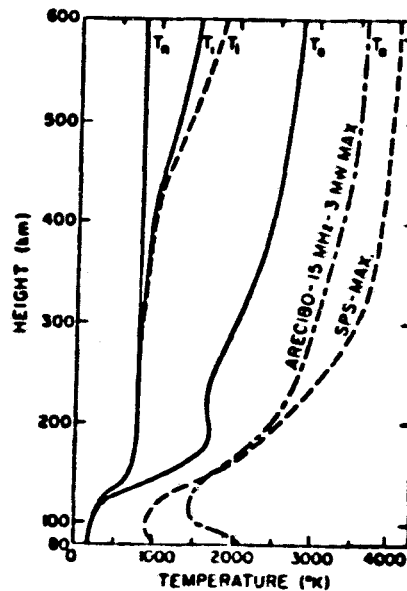
THEN $\tau = 13$ ARC SEC.

FURTHER COMMENTS ON IONOSPHERIC EFFECTS (SINGLE-TONE SYSTEM)
(CONT'D)

- FOR SPS, $|f_U - f_D| \approx 100$ MHz AND τ_U AND τ_D ARE ALMOST EQUAL
- UPLINK (PILOT) BEAM IS BROAD ($\theta_U = 3000$ ARC SEC), THE BENDING ON INCIDENT BEAM WILL GO PRACTICALLY UNDETECTED AT SPACE ANTENNA.
- DOWNLINK (POWER) BEAM IS NARROW ($\theta_D = 30$ ARC SEC), THE BENDING IS APPRECIABLE BUT IONOSPHERE TOO CLOSE TO RECTENNA (≈ 100 KM) TO DO ANY DAMAGE.

REMARKS ON IONOSPHERE HEATING DUE TO POWER BEAM

(REF: PERKINS AND ROBLE (1978), DAVIES (1979))



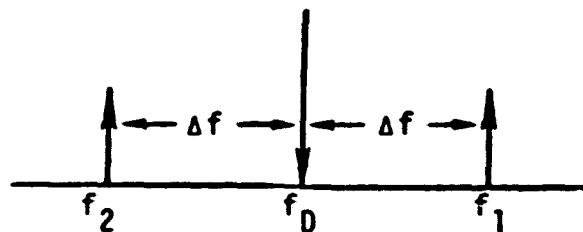
- AT 2.5 GHZ, RESISTIVE HEATING OCCURS IN E-LAYER (DUE TO HIGH COLLISION FREQUENCY) AND THERMAL RUNAWAY OCCURS IN ELECTRON TEMPERATURE 200°K + 1000°K.
- THE ELECTRON DENSITY VS. HEIGHT PROFILE SHOWS ABOUT 3 TIMES INCREASE IN E-LAYER DENSITY (DECREASE IN RECOMBINATION RATE AT HIGHER ELECTRON TEMPERATURE).
- THE INTEGRATED ELECTRON DENSITY COULD CHANGE BY 20%. THIS MAY NOT PRODUCE UNACCEPTABLE BEAM REFRACTION.

REMARKS ON IONOSPHERE HEATING DUE TO POWR BEAM
(CONT'D)

CONCLUSION:

BASED ON PRESENT KNOWLEDGE, THE IONOSPHERE DOES NOT
SEEM TO HURT THE SINGLE-TONE PILOT BEAM SYSTEM BADLY.
SOME MORE STUDY IS REQUIRED.

TWO-TONE PILOT BEAM



- AVERAGE OF THE PHASE AT $f_D \pm \Delta f$ IS DESIRED TO DUPLICATE THE PHASE OF A SINGLE PILOT TONE AT f_0
- PHASE MEASURED AT THE SPACETENNA AT $f_1 = f_D + \Delta f$ AND $f_2 = f_D - \Delta f$ IS

$$\phi_1 = \frac{2\pi f_1 D}{C} - \frac{40}{f_1} \frac{2\pi}{C} \int N dz$$

$$\phi_2 = \frac{2\pi f_2 D}{C} - \frac{40}{f_2} \frac{2\pi}{C} \int N dz$$

$$\bar{\phi} = \frac{\phi_1 + \phi_2}{2} \approx \phi_D ; \left| \frac{\Delta f}{f_D} \right| \ll 1$$

D = DISTANCE TO SPS ~37,400 KM

C = VELOCITY OF LIGHT

N = ELECTRON DENSITY

TWO-TONE PILOT BEAM (CONT'D)

PROBLEMS: THE AVERAGING INDICATED TO OBTAIN $\bar{\phi}$ CAN SOMETIMES GIVE WRONG ANSWERS (OFTEN CALLED π AMBIGUITIES). THIS CAN HAPPEN IF

(I) $\phi_1 - \phi_2 = K 2\pi + \Delta$; $|\Delta| < 2\pi$ AND K IS ODD INTEGER
AND/OR

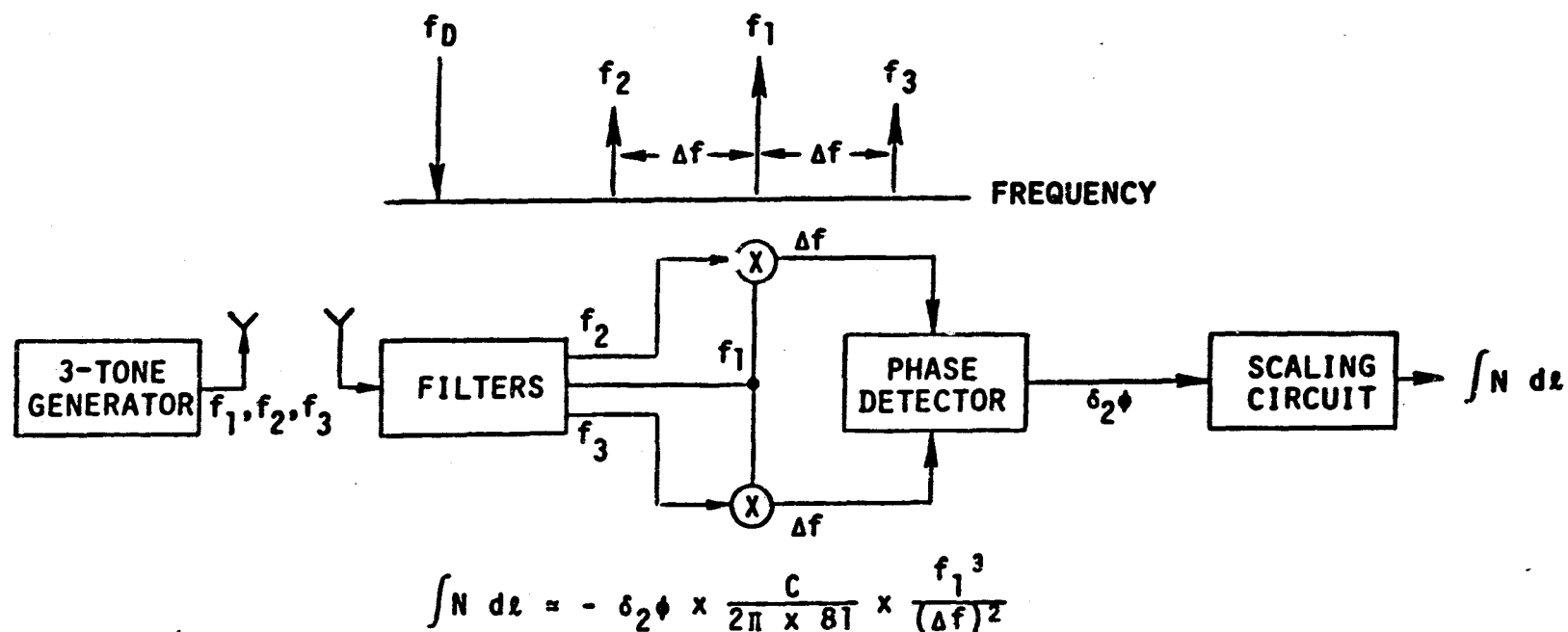
(II) ASYNCHRONOUS DIVIDERS ARE USED

THREE-TONE PILOT BEAM

OBJECTIVE: WISH TO CORRECT FOR IONOSPHERE-INDUCED PHASE SHIFTS ON
(POSSIBLY) ALL LINKS OF INTEREST. NEED TO ESTIMATE
 $\int_0^L N dz$ FIRST.

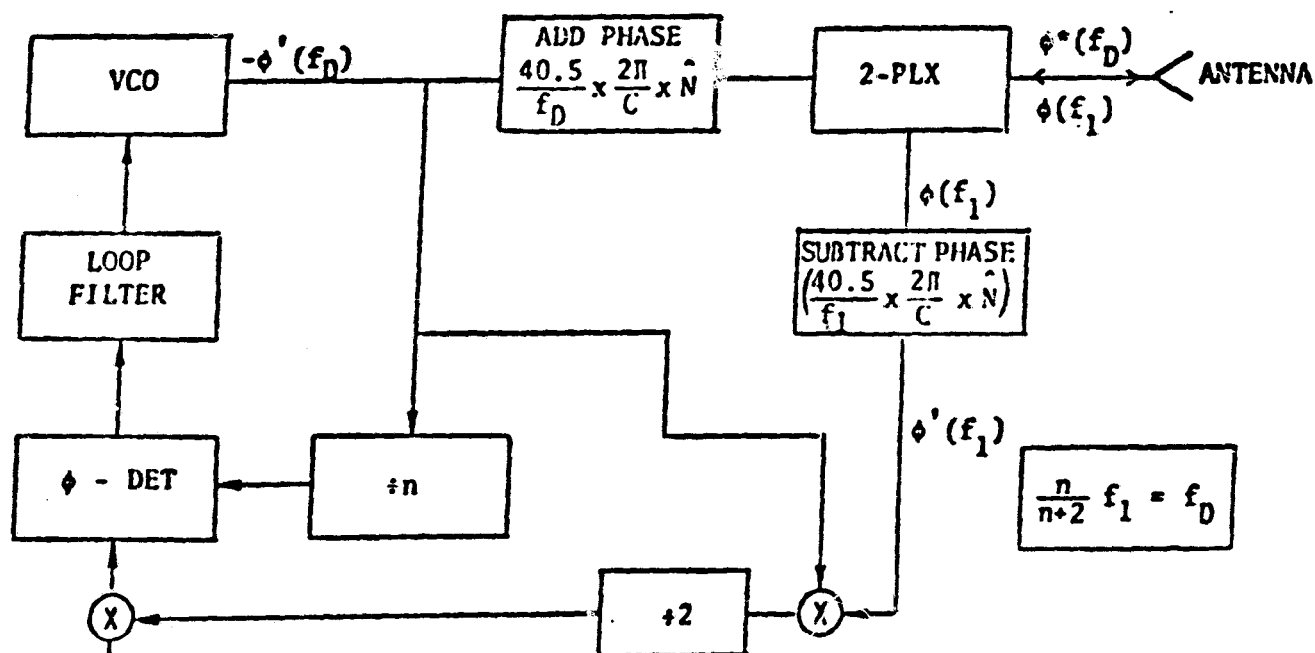
USE COHERENT THREE-TONE TECHNIQUE DUE TO BURNS AND
FREMOUNG TO OBTAIN THIS ESTIMATE \hat{N} .

THREE-TONE PILOT BEAM (CONT'D)



CAUTION: Δf NEEDS TO BE CHOSEN APPROPRIATELY SO THAT $\delta_2 \phi$ CAN BE MEASURED WITHOUT 2π AMBIGUITY FOR $\int N dl \leq 10^{19}$ ELECTRONS/M².

MODIFIED CHERNOFF CONJUGATOR



$$\begin{aligned}\phi_0(f_1) &= \text{Ref Phase} \\ &= \omega_1 \frac{L_0}{C} - \frac{40.5}{f_1} \times \frac{2\pi}{C} \times \int_0^{L_0} N \, dl \\ &= \text{Constant at all subarrays}\end{aligned}$$

$$\phi(f_1) = \omega_1 \frac{L}{C} - \frac{40.5}{f_1} \times \frac{2\pi}{C} \times \int_0^L N \, dl$$

$$\phi^*(f_D) = -\phi'(f_D) + \frac{40.5}{f_D} \times \frac{2\pi}{C} \times \hat{N}$$

$$= \frac{n}{n+2} [2\phi_0(f_1) - \phi'(f_1)] + \frac{40.5}{f_D} \times \frac{2\pi}{C} \times \hat{N}$$

$$= \text{const.} - \omega_D \frac{L}{C} + \frac{40.5}{f_D} \times \frac{2\pi}{C} \left[\hat{N} \left(1 - \frac{f_D^2}{f_1^2} \right) + \frac{f_D^2}{f_1^2} \int_0^L N \, dl \right]$$

THREE-TONE PILOT BEAM
(CONT'D)

COMMENTS:

JUSTIFICATION FOR USE OF SAME \hat{N} FOR UPLINK AND
DOWNLINK PHASE COMPENSATION.

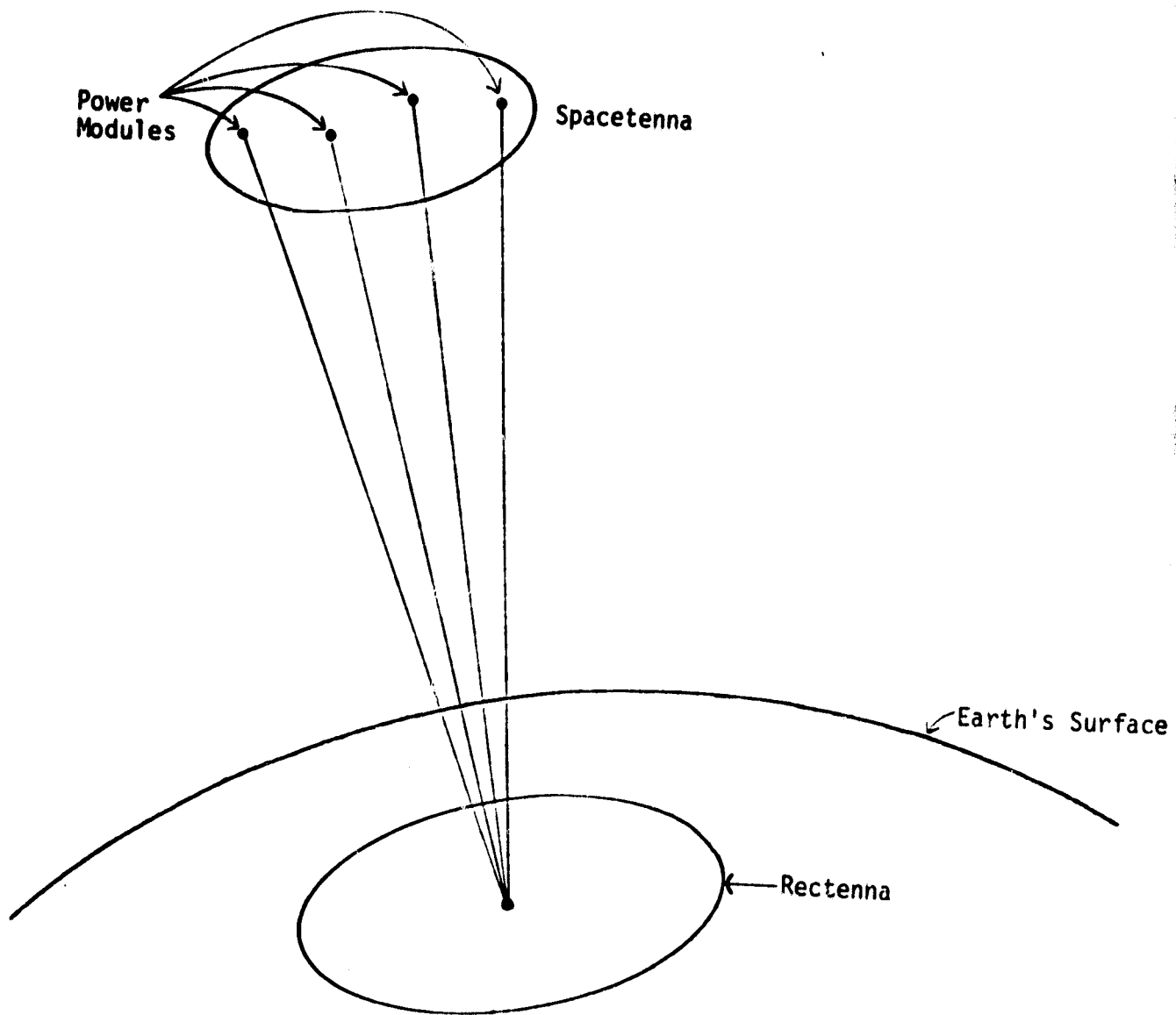
DIVIDER AMBIGUITY PROBLEMS IN THE MODIFIED CONJUGATOR.
(HAS BEEN SOLVED)

REQUIRED AREAS OF FURTHER INVESTIGATION

- A. STATISTICAL ANALYSIS RELATED TO IONOSPHERIC TURBULENCE.
- B. THE PROBLEM OF IONOSPHERE HEATING DUE TO THE DOWNLINK POWER BEAM AND ITS EFFECT ON OVERALL SYSTEM OPERATION.
- C. PERFORMANCE ANALYSIS OF THE RAYTHEON SOLUTION FOR AMBIGUITY RESOLUTION.
- D. IMPLICATION OF CHANGING DIVIDER RATIO N IN CHERNOFF CONJUGATOR.
- E. POSSIBILITY OF SPATIAL AND TEMPORAL FILTERING TO REDUCE IONOSPHERIC EFFECTS.
- F. EFFECTS OF CHANGING THE FREQUENCIES OF PILOT TONES AND THEIR SPACING.
- G. PRACTICAL IMPLEMENTATION OF FIGURE 9. HOW TO INTRODUCE THE IONOSPHERE RELATED PHASE COMPENSATION?
- H. EVALUATION OF BROAD PILOT BEAM CONCEPT.
- I. WAVEFORM DEFINITION IN A MULTI-SATELLITE ENVIRONMENT.

***An Interferometer-Based
Phase Control System***

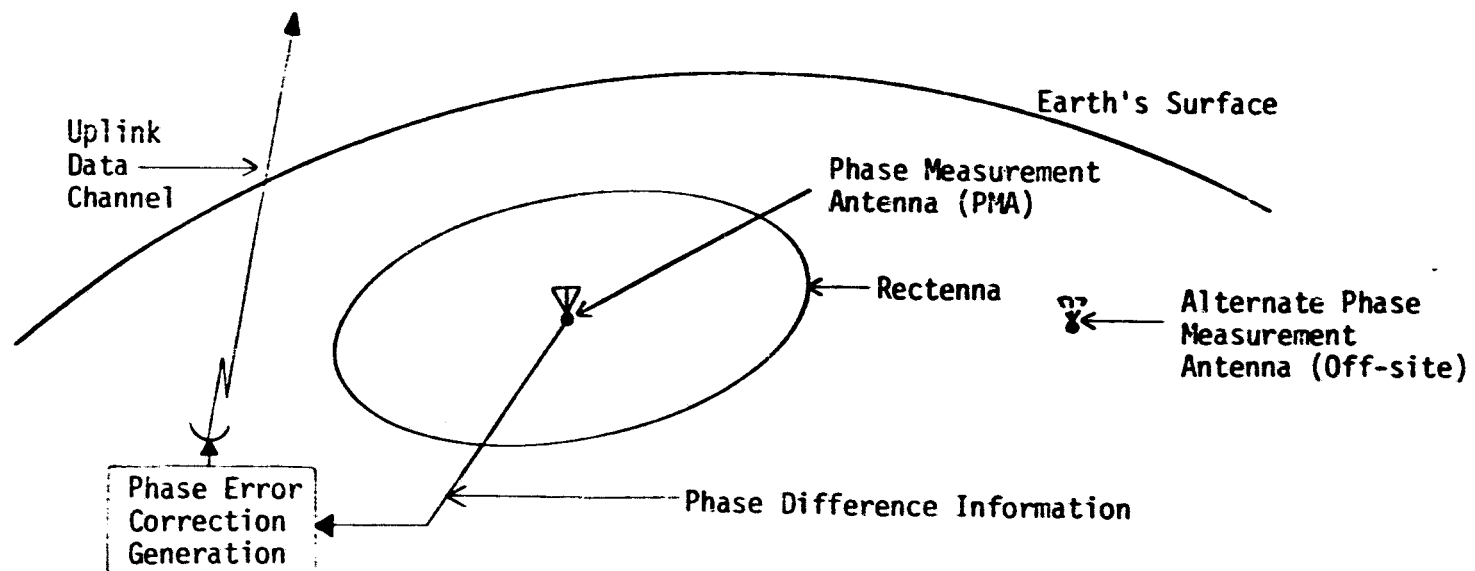
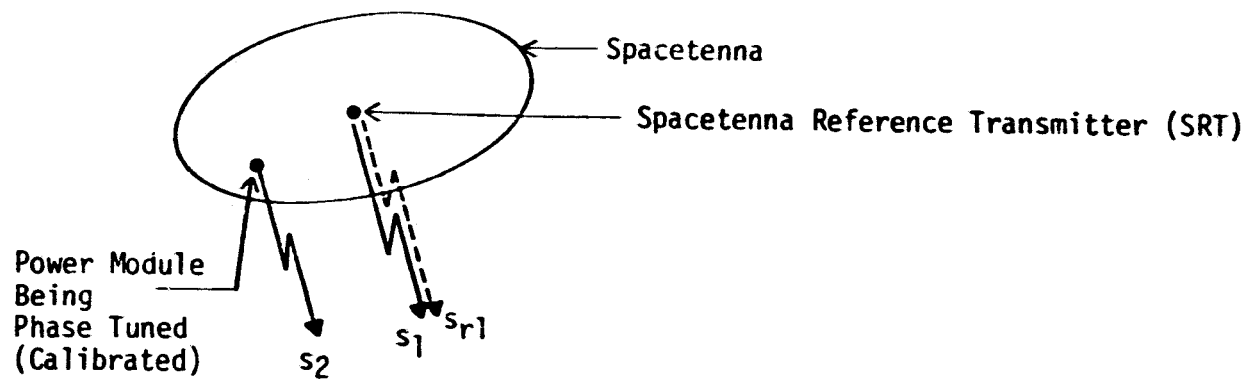
***Dr. J. Rice
Novar***



- IF SIGNALS TRANSMITTED BY EACH POWER MODULE ARRIVE AT CENTER OF RECTENNA IN PHASE -
 - POWER BEAM WILL BE PROPERLY FOCUSED AND POINTED

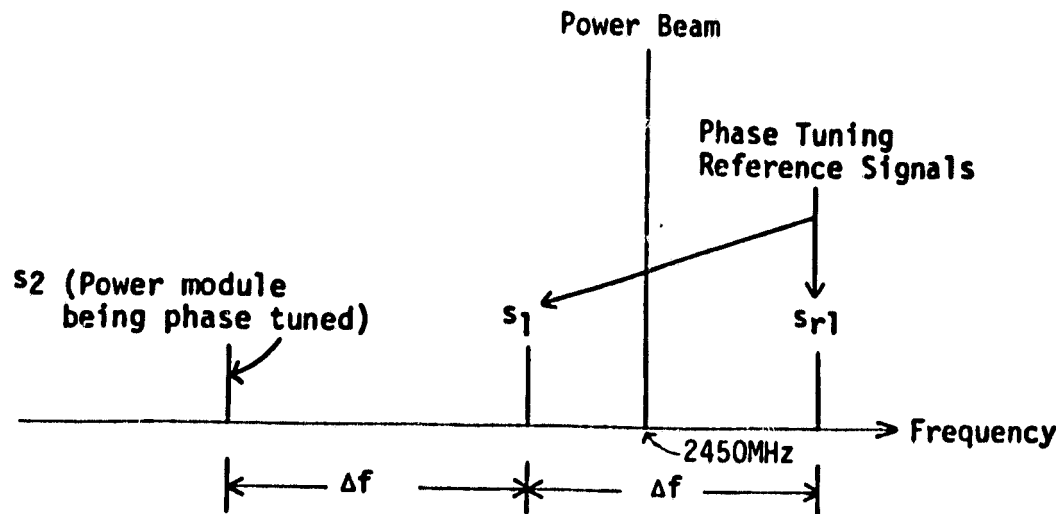
PRECEDING PAGE BLANK NOT FILMED

- A PHASE CONTROL SYSTEM IS NEEDED TO CORRECT FOR EFFECTS OF:
 - SPACETENNA STRUCTURAL DEFORMATIONS
 - PHASE VARIATIONS WITHIN SPACETENNA CIRCUITRY
 - MOTIONS OF THE SOLAR POWER SATELLITE

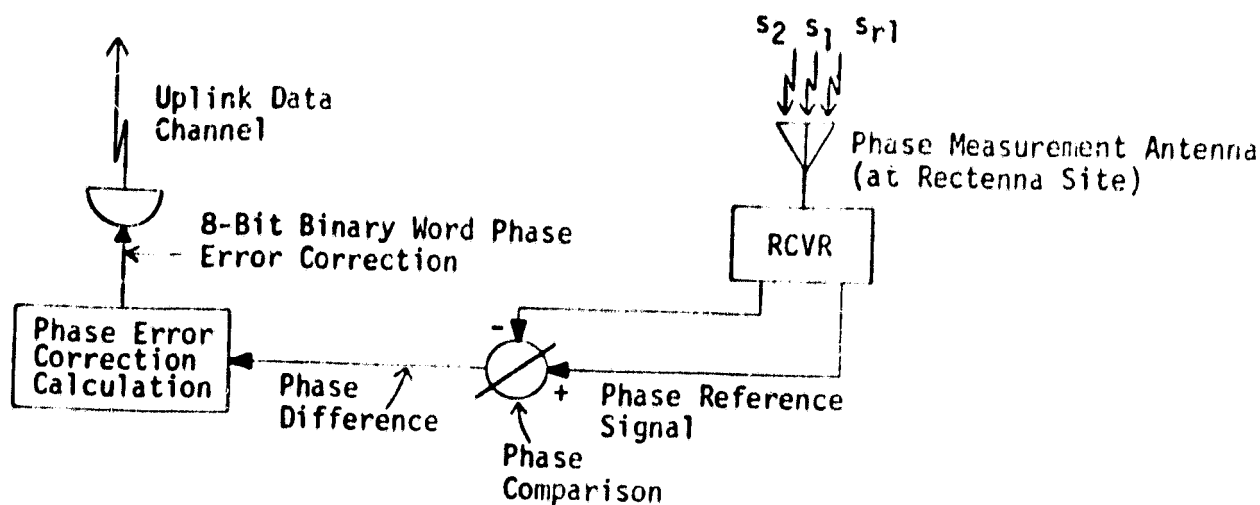


INTERFEROMETRIC PHASE CONTROL SYSTEM

- PHASE MEASUREMENT ANTENNA (PMA) RECEIVES SIGNALS FROM:
 - SPACETENNA REFERENCE TRANSMITTER (SRT)
 - POWER MODULE BEING PHASE TUNED (CALIBRATED)
- PHASE DIFFERENCE INFORMATION DETERMINED
- PHASE ERROR CORRECTION GENERATED
- PHASE ERROR CORRECTION TRANSMITTED TO ON-BOARD POWER MODULE
PHASE CONTROL CIRCUITRY
 - VIA CONVENTIONAL UPLINK DATA CHANNEL

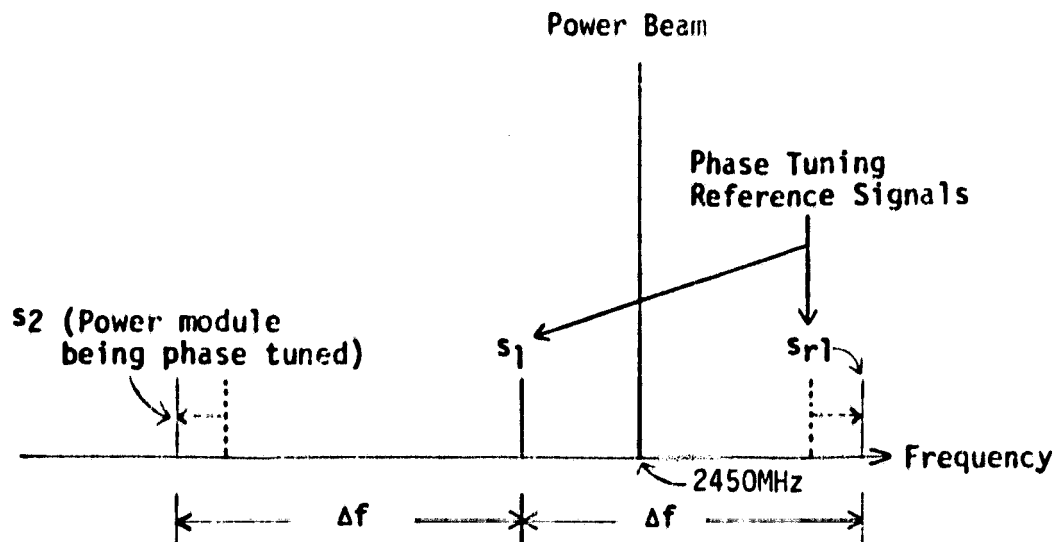


- COHERENT SIGNALS TRANSMITTED FROM SPACETENNA (AT THREE DIFFERENT FREQUENCIES)
 - TWO FROM SPACETENNA REFERENCE TRANSMITTER (S_1 & S_{R1})
 - ONE FROM POWER MODULE BEING PHASE TUNED (S_2)
- BEAT FREQUENCY OF S_1 AND S_2 SAME AS S_1 AND S_{R1}



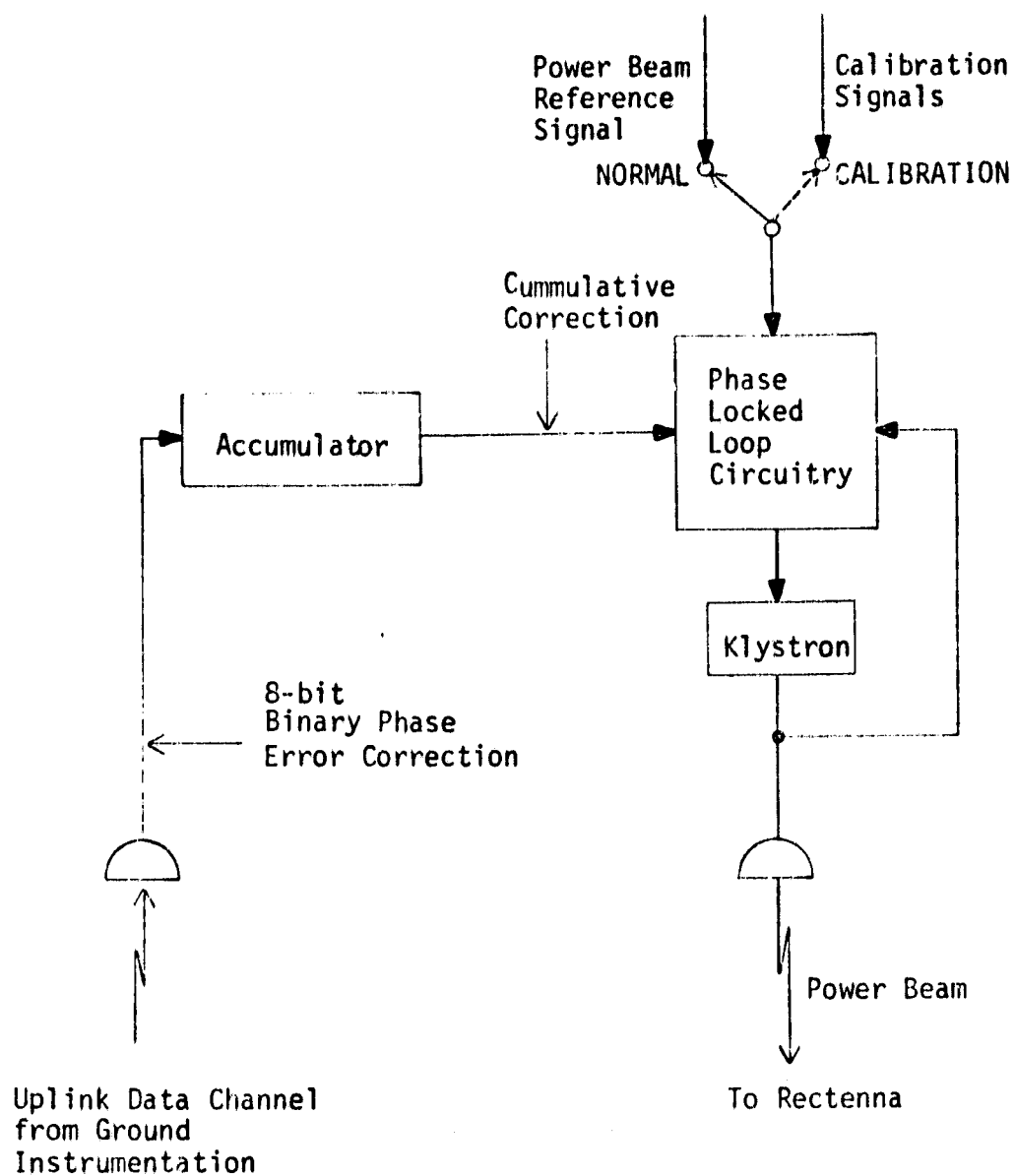
GROUND BASED PHASE CONTROL CIRCUITRY

- TWO DIFFERENCE FREQUENCY SIGNALS DETECTED AT PHASE MEASUREMENT ANTENNA
 - ONE DUE TO s_1 AND s_2
 - OTHER DUE TO s_1 AND s_{r1} (PHASE REFERENCE SIGNAL)
- PHASES OF THE TWO DIFFERENCE FREQUENCY SIGNALS ARE COMPARED
- PHASE DIFFERENCE IS A FUNCTION OF:
 - Z-AXIS DISPLACEMENT IN POWER MODULE BEING PHASE TUNED
 - PHASE BIASES IN PHASE FEED NETWORK OF SPACETENNA



- A SECOND SET OF FREQUENCIES FOR S_{R1} AND S_2 PROVIDES A SECOND PHASE DIFFERENCE MEASUREMENT
- DISTINGUISHES FREQUENCY DEPENDENT FROM FREQUENCY INDEPENDENT PHASE ERRORS IN S_2 .

- PHASE ERROR CORRECTION IS CALCULATED FROM THE TWO PHASE DIFFERENCE MEASUREMENTS
 - 8-BIT BINARY WORD OUTPUT TO SATELLITE
 - RESULTS IN VERY HIGH POINTING ACCURACY
(VERIFIED BY COMPUTER SIMULATION)

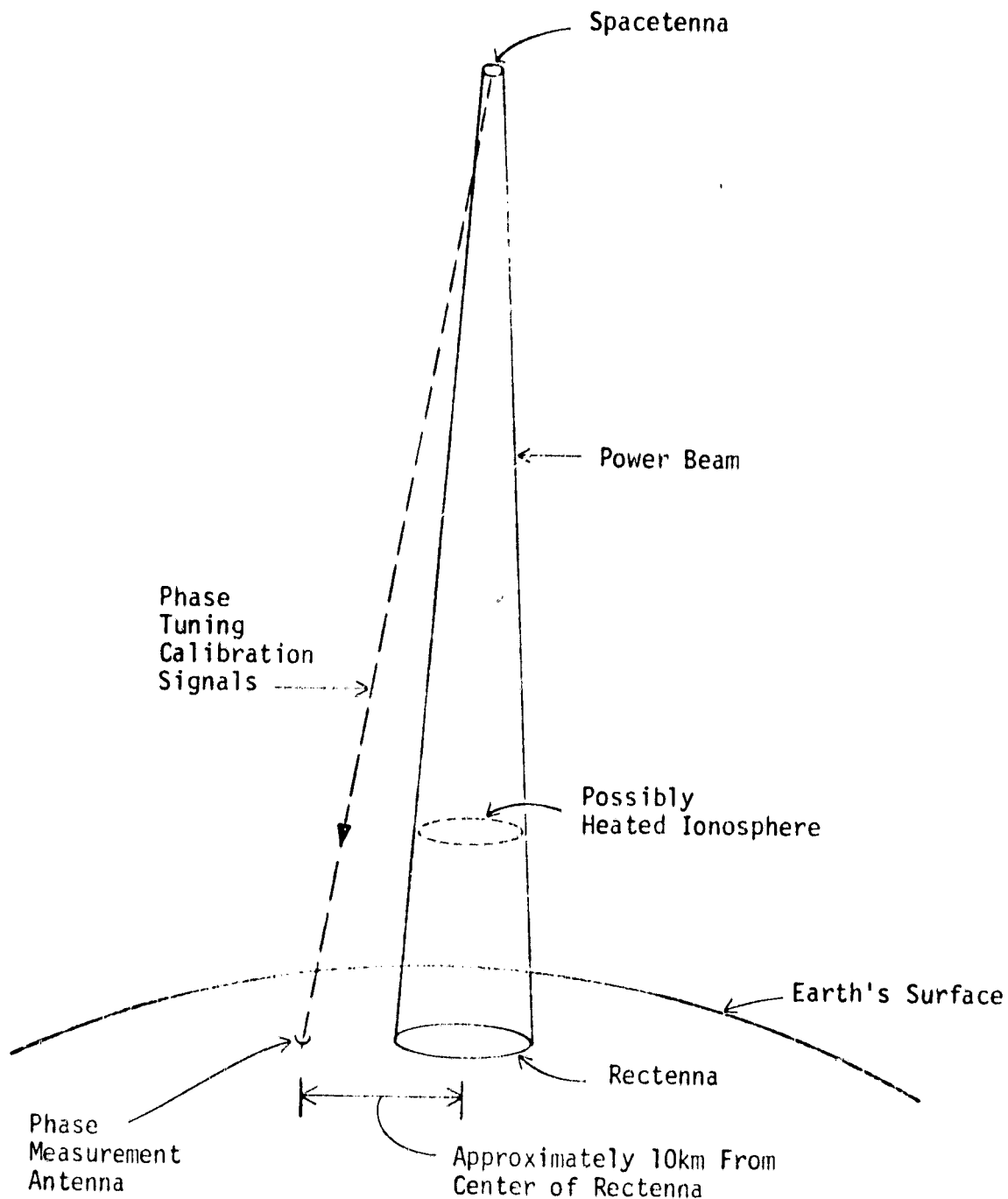


POWER MODULE PHASE CONTROL CIRCUITRY (ON-BOARD)

- CHARACTERISTICS OF INTERFEROMETRIC PHASE CONTROL (IPC)
 - GROUND BASED AND CLOSED LOOP
 - CALIBRATES POWER MODULES SEQUENTIALLY
 - LESS THAN ONE MINUTE FOR COMPLETE CALIBRATION OF SPACETENNA
 - CALIBRATES POWER MODULE AT SLIGHTLY DIFFERENT FREQUENCY FROM POWER BEAM DURING NORMAL POWER TRANSMISSION

• IONOSPHERE MAY BE SUBJECTED TO UNDERTERMINED HEATING
EFFECTS BY POWER BEAM

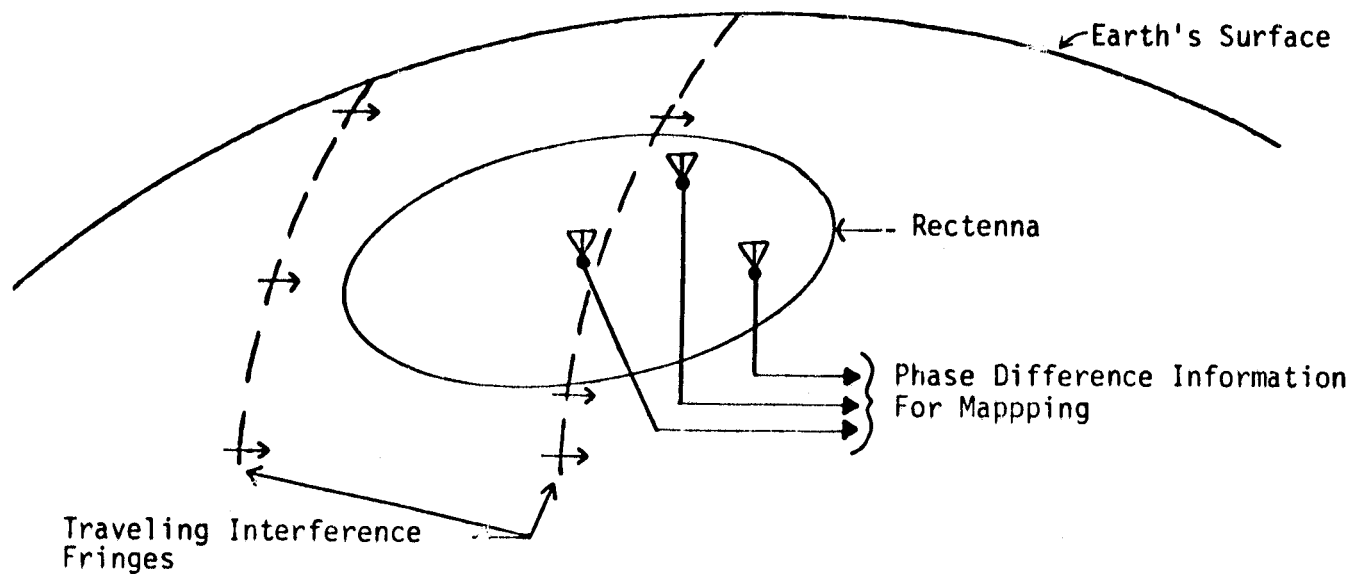
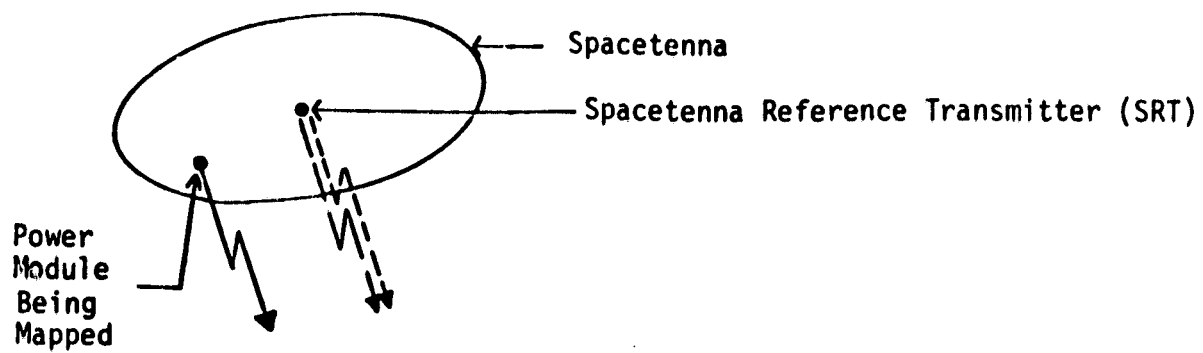
■ A HEATED REGION CAN BE AVOIDED BY MAKING
INTERFEROMETRIC PHASE CONTROL MEASUREMENTS
OFF-SITE FROM RECTENNA



OFF-SITE PHASE MEASUREMENT TO HAVE PHASE TUNING
CALIBRATION SIGNALS AVOID POSSIBLY HEATED IONOSPHERE

- ANY IONOSPHERIC EFFECTS ON PHASE CONTROL CALIBRATION SIGNALS CAN BE MINIMIZED USING:
 - STATISTICAL ERROR REDUCTION TECHNIQUES
 - ▲ TIME AVERAGING
 - ▲ SPATIAL AVERAGING
 - MULTIPLE PHASE MEASUREMENT ANTENNA SITES

- PREDICTION OF SPACETENNA DEFORMATION DYNAMICS
 - LEARNING CURVES, ADAPTIVE MODELING TECHNIQUES
 - ENTIRE SPACETENNA TUNED BY FREQUENT MEASUREMENT OF KEY POWER MODULES
 - OCCASIONAL MEASUREMENTS OF REMAINING POWER MODULES
- MAPPING OF FACE OF SPACETENNA
 - DETERMINES RELATIVE MOTION AND LOCATION OF EACH POWER MODULE
 - TRANSVERSE MODAL ANALYSIS
 - IDENTIFIES DEFECTIVE POWER MODULES
 - ONLY TWO ADDITIONAL EARTH MEASUREMENT ANTENNAS
 - SIMULTANEOUS WITH PHASE CONTROL



MAPPING

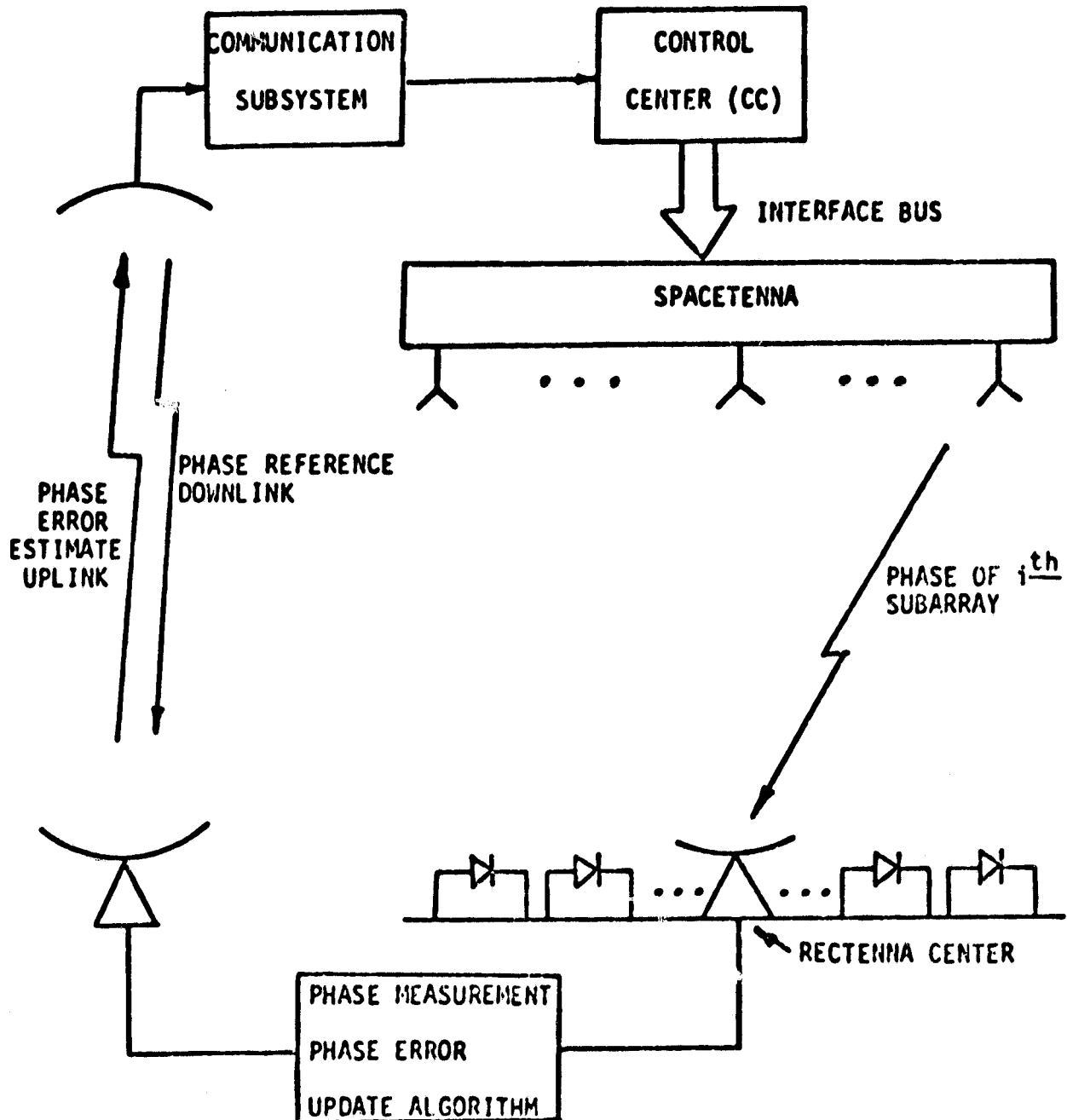
- INTERFEROMETER-BASED PHASE CONTROL AS ADJUNCT TO RETRODIRECTIVE SYSTEM
 - MITIGATES PHASE BIASING PROBLEMS
 - POSSIBLE BACKUP IF ATMOSPHERE/IONOSPHERE OCCASIONALLY PRECLUDES USE OF RETRODIRECTIVE SYSTEM

D8

***A Coherent Multitone
Technique for
Ground Based Phase Control***

***Dr. C. M. Chie
Lincom***

GROUND BASED PHASE CONTROL CONCEPT WITH MAJOR FUNCTIONAL BLOCKS



PRECEDING PAGE BLANK NOT FILMED

GROUND-BASED VS REFERENCE RETRODIRECTIVE PHASE CONTROL SYSTEM

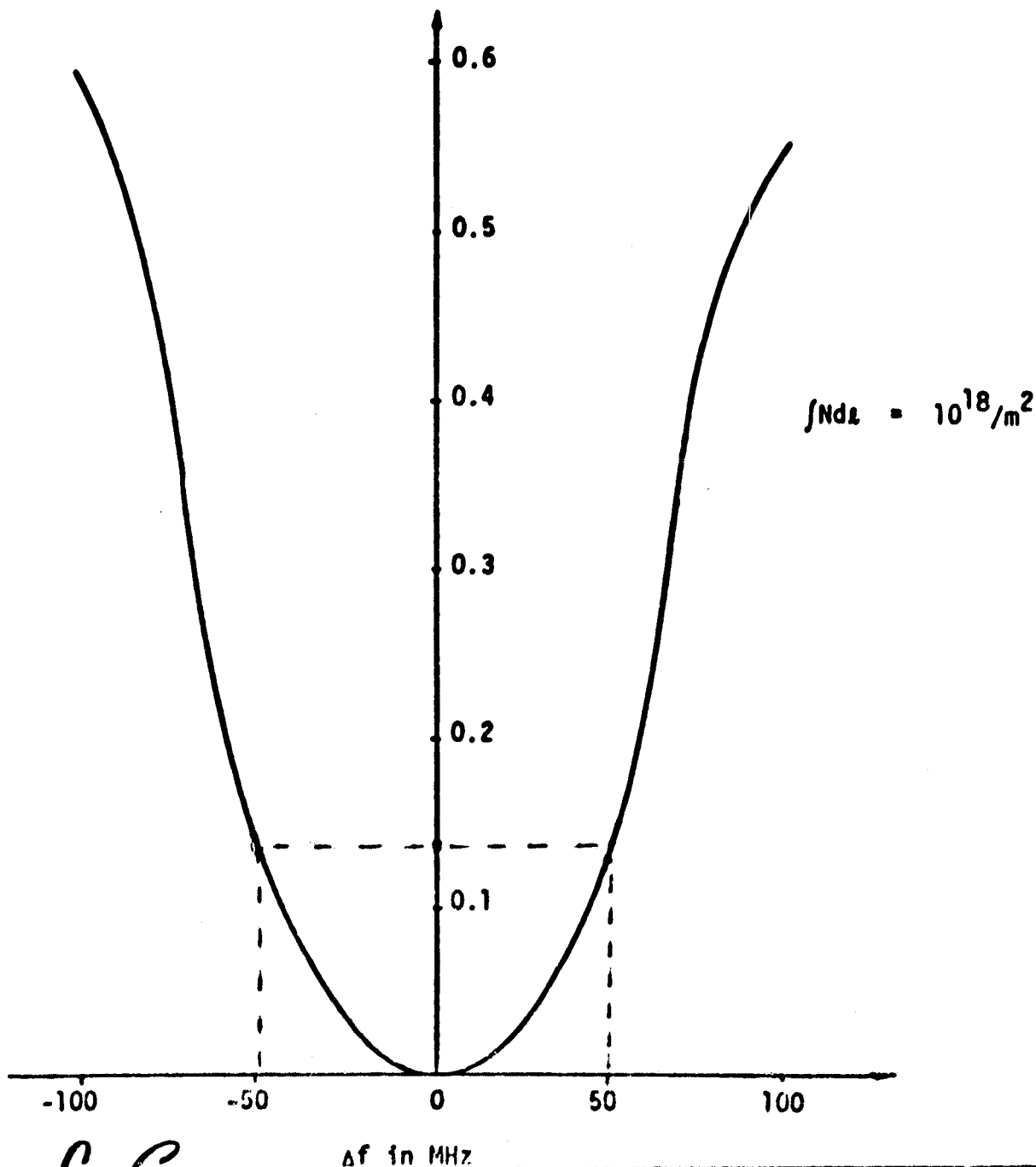
REFERENCE SYSTEM	GROUND BASED SYSTEM
<ul style="list-style-type: none"> •REQUIRES LARGE AMOUNT OF SPACEBORNE ELECTRONICS •COMPLEX SPACEBORNE PROCESSING BUT SIMPLE GROUND SIGNAL PROCESSING •CORRECTS FOR IONOSPHERIC DISTURBANCES WITH CORRELATION TIME MORE THAN 0.25 sec •REQUIRES PN CODE FOR SECURITY •INSTANTANEOUS CORRECTION FOR SPACETENNA MOTION •PERFORMANCE INHERENTLY LIMITED BY THE PHASE ERROR INTRODUCED BY THE PHASE REFERENCE DISTRIBUTION SYSTEM •DOES NOT CORRECT FOR DC PHASE OFFSETS BEYOND THE PHASE CONJUGATION POINT •FAST START-UP 	<ul style="list-style-type: none"> •REQUIRES LESS SPACEBORNE ELECTRONICS •COMPLEX GROUND PROCESSING BUT SIMPLE SPACEBORNE SIGNAL PROCESSING •CORRECTS FOR IONOSPHERIC DISTURBANCES WITH CORRELATION TIME MORE THAN 1.25 sec •SECURITY OF DOWNLINK •SENSITIVE TO RATE OF CHANGE OF POINTING ERROR •PERFORMANCE INHERENTLY LIMITED BY PHASE ERROR INTRODUCED BY THE DIGITAL PHASE SHIFTER •NOT AFFECTED BY DC OFFSETS INTRODUCED ANYWHERE ALONG THE SIGNAL PATH •SLOWER START-UP

MEASUREMENT WAVEFORM DESIGN CONSIDERATIONS

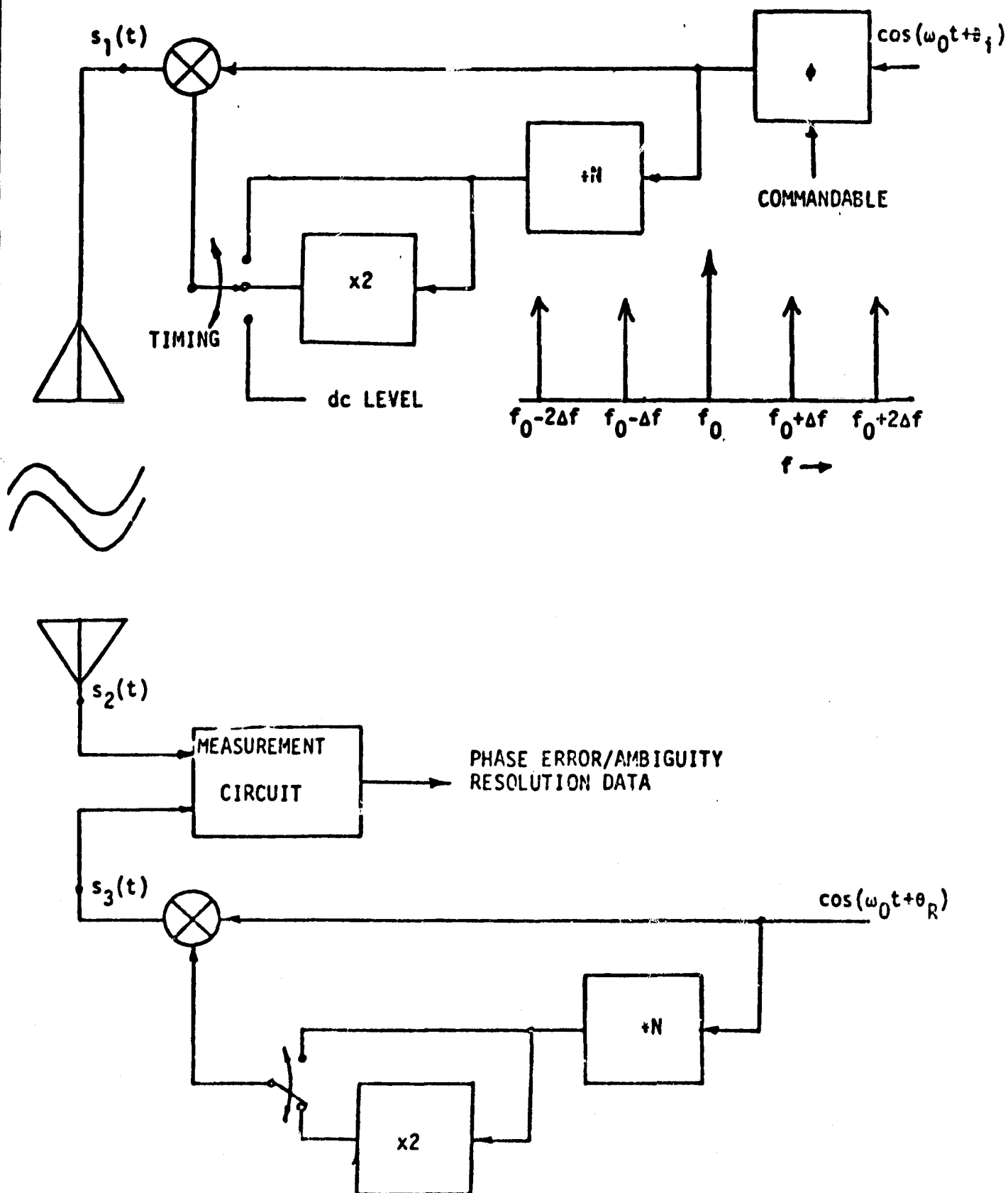
CONSTRAINTS	CONSEQUENCES	COMMENTS
• POWER BEAM INTERFERENCE AT DESIRED FREQUENCY	• SUPPRESSED CARRIER • MULTITONES	• AMBIGUITY RESOLUTION
• MEASUREMENT INTERVAL 10 μ sec/sec	• OPEN LOOP • SIMPLE WAVEFORM	• TDMA OPERATION
• NONLINEAR PHASE SHIFT INTRODUCED BY THE IONOSPHERE	• TONE SEPARATION LIMIT	• 50 MHz
• HPA FREQUENCY RESPONSE	• TONE SEPARATION LIMIT • SUPPRESSED CARRIER GENERATION CAPABILITY	• 5 - 50 MHz

NONLINEAR PHASE SHIFT EXHIBITED BY
THE EQUIVALENT FILTER CHARACTERISTICS
INTRODUCED BY THE IONOSPHERE

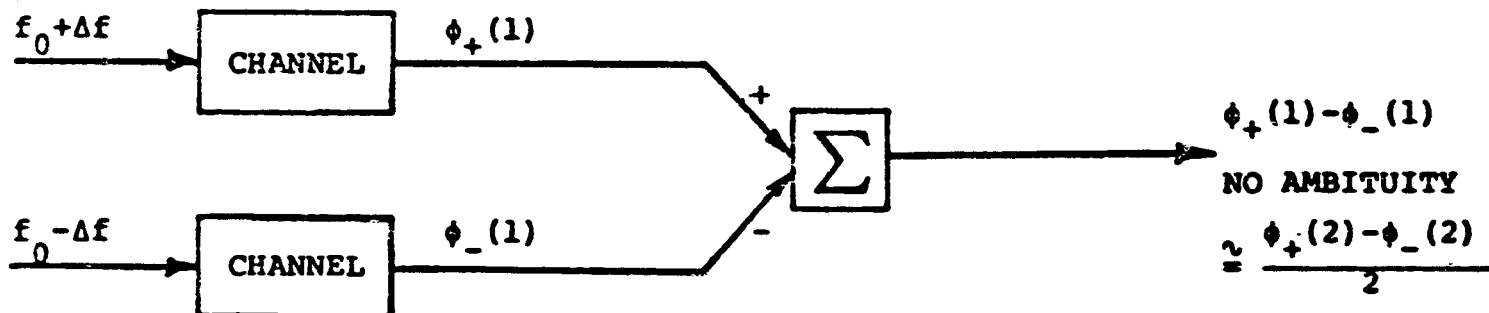
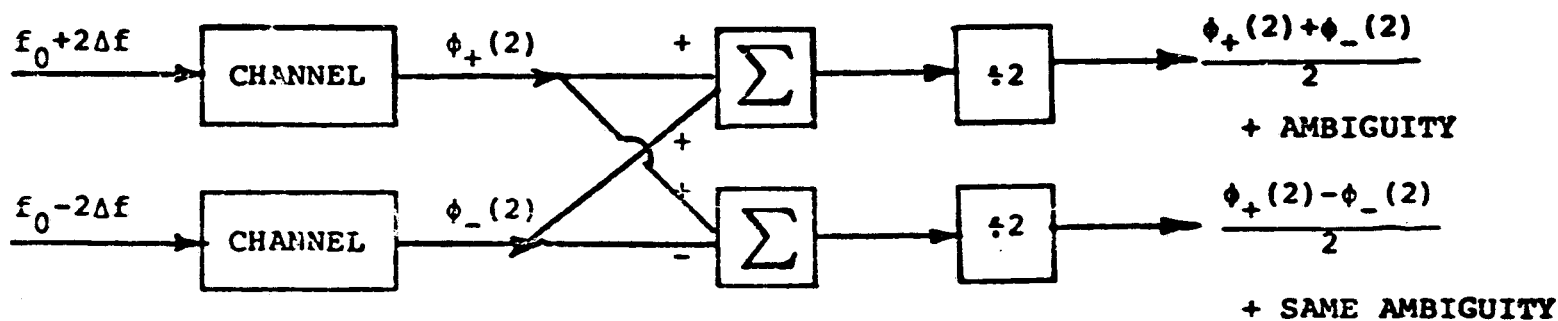
NONLINEAR PHASE SHIFT IN RAD



FOUR-TONE PHASE MEASUREMENT SCHEME



PRINCIPLE OF OPERATION OF 4-TONE TECHNIQUE



• AMBIGUITY IN $\frac{\phi_+(2) + \phi_-(2)}{2}$ RESOLVED BY COMPARING $\frac{\phi_+(2) - \phi_-(2)}{2}$
 AND $\phi_+(1) - \phi_-(1)$

BASELINE SYSTEM CHARACTERISTICS

- SATELLITE BASED FREQUENCY/TIMING SYSTEM
REFERENCE
 - IF AT 490 MHz
- 4-TONE MEASUREMENT SCHEME
 - 2,450 \pm 9.57 MHz AND \pm 19.14 MHz
 - HARDLIMITED SIGNAL (AM/PM SUPPRESSION)
- MEASUREMENT MODE 1 μ s PER SEC PER POWER MODULE
- MINIMUM LOSS IN TOTAL POWER TRANSMITTED
- DOWNLINK PILOT AT 4,900 MHz
- FREQUENCY ALLOCATION -- 2 DOWNLINK, 1 UPLINK

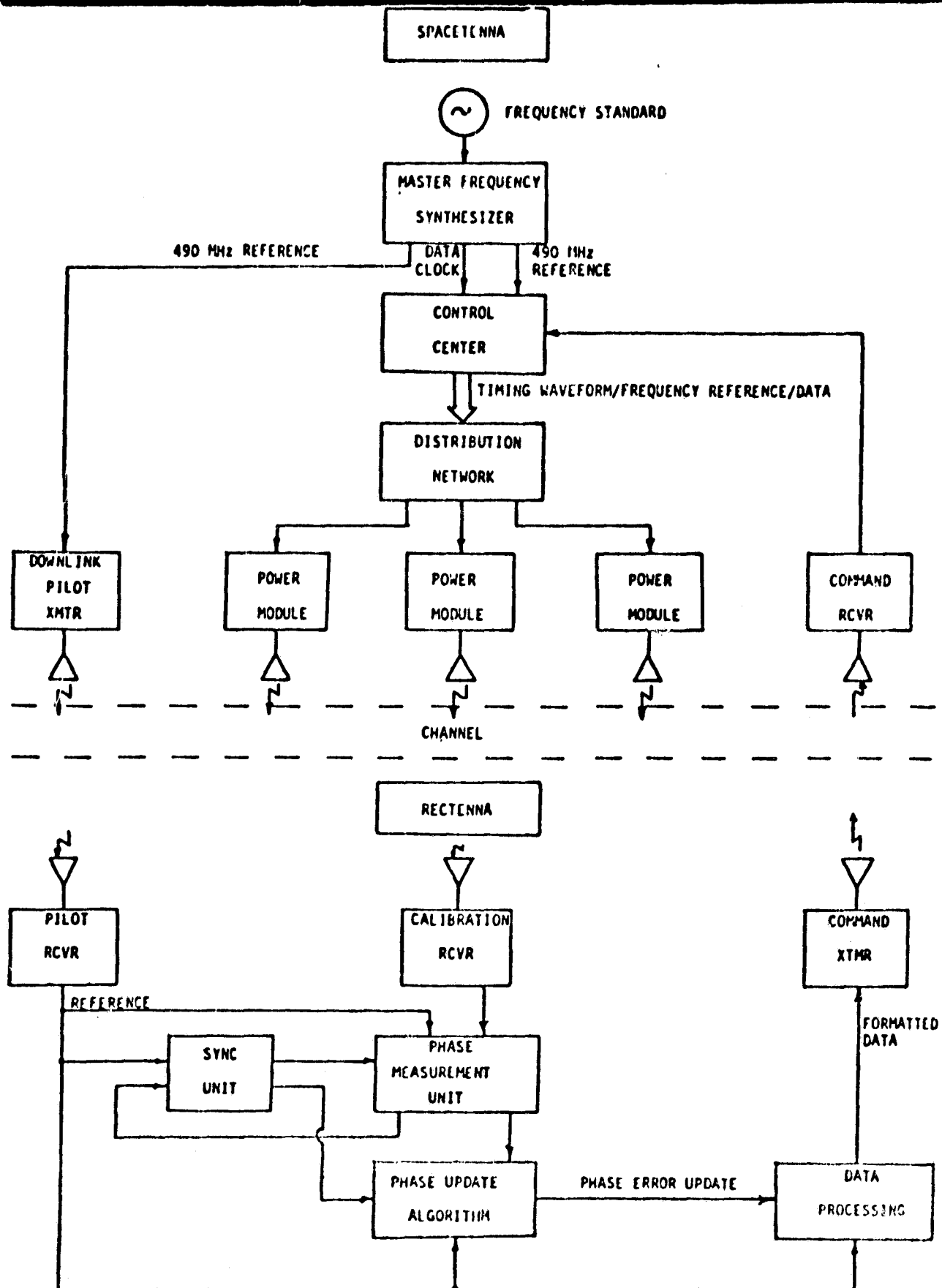
BASELINE FUNCTIONAL SUBSYSTEMS**•SATELLITE**

- TIMING/FREQUENCY REFERENCE GENERATION
- PROCESSING CONTROL CENTER
- DISTRIBUTION NETWORK
- PROCESSING POWER MODULE
- DOWNLINK PILOT TRANSMITTER

•GROUND STATION

- CALIBRATION RECEIVER
- PILOT BEACON RECEIVER
- COMMAND TRANSMITTER
- PHASE MEASUREMENT UNIT
- SYNC UNIT
- PHASE UPDATE ALGORITHM
- DATA PROCESSING

SPS GROUND BASED PHASE CONTROL FUNCTIONAL BLOCK DIAGRAM SHOWING SYSTEM TIMING HIERARCHY

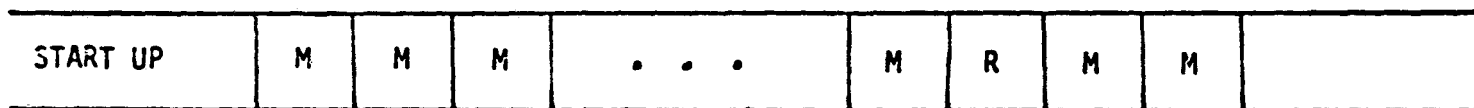


OVERALL SYSTEM TIMING DIAGRAM

- START UP
 - STOP START-UP CYCLE AFTER GROUND ACQUIRES SYNC
- CALIBRATION CYCLE
 - DIVIDES INTO MEASUREMENT MODE AND AMBIGUITY RESOLUTION MODE
 - ONLY PERIODIC AMBIGUITY RESOLUTION REQUIRED
 - MEASUREMENT MODE AND RESOLUTION MODE IDENTIFIED BY OFFSET FREQUENCY

**TIMING DIAGRAM FOR MEASUREMENT AND AMBIGUITY RESOLUTION
ON NORMAL OPERATION**

—|1 sec|—



—| CALIBRATION CYCLE |—

M = PHASE MEASUREMENT MODE

R = AMBIGUITY RESOLUTION MODE

FREQUENCY OFFSET (± 1 Hz)

± 9.57

AMBIGUITY RESOLUTION MODE

SYNC

PM#

PM#

101552

SYNC

1

2

± 19.14

SYNC

PM#

PM#

101552

SYNC

1

2

PHASE MEASUREMENT MODE

LinCom

START UP WAVEFORM

FREQUENCY SHIFT (+MHz)

140

19.14
9.57

SYNC

0

PM#

1

PM#

2

PM#

3

PM#

4

...

PM#

101499

PM#

101550

PM#

101551

PM#

101552

TIME FROM
SYSTEM START UP

1 sec

START-UP WAVEFORM DESIGN

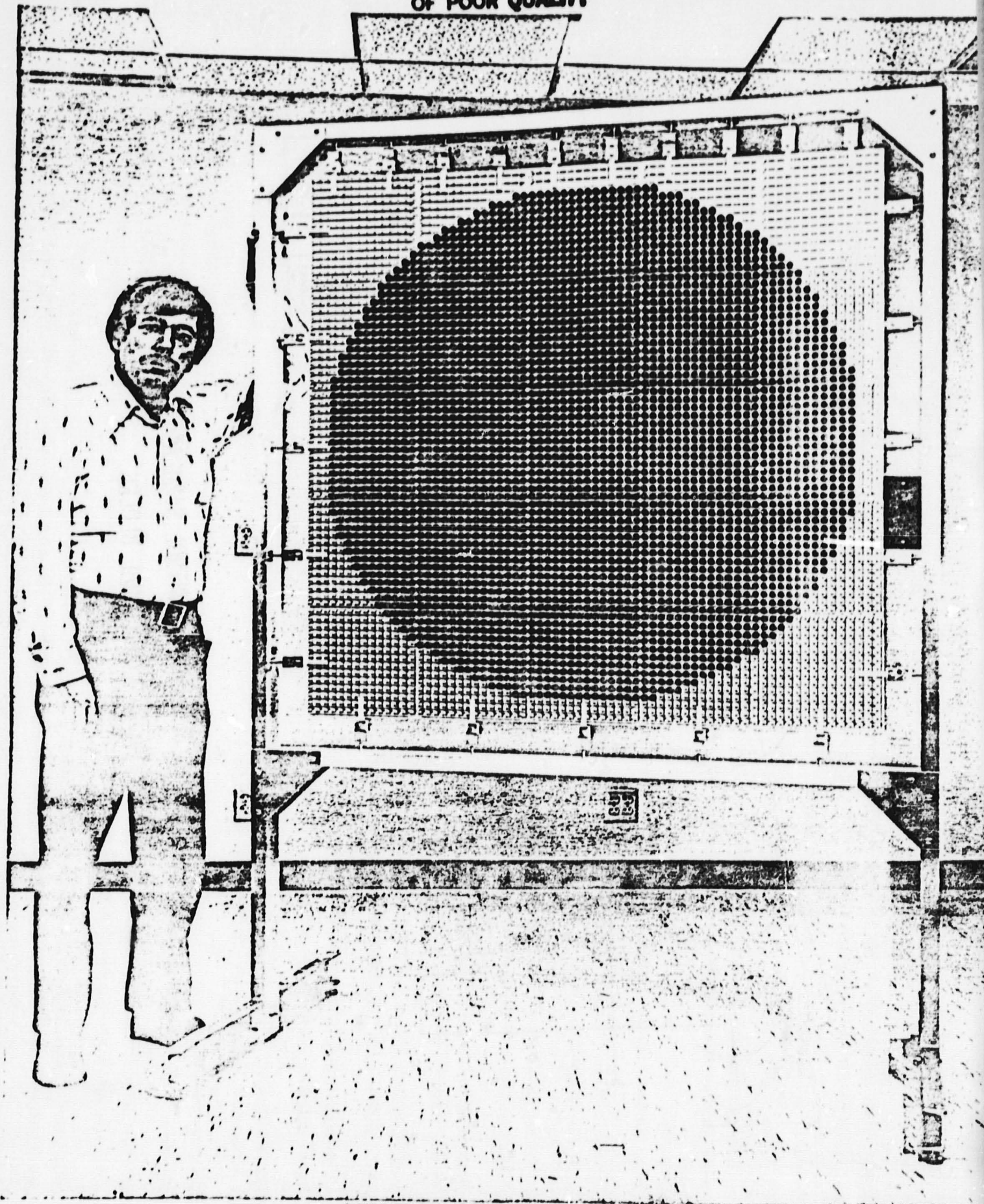
- PROVIDES MEASUREMENT TIME-SLOT SYNC INFORMATION
- 1 SEC FRAME DIVIDED INTO 2+101552 TIME SLOTS
- ALL PM TRANSMIT AT 2,450 MHz FOR 2 TIME SLOTS AT THE START OF THE FRAME TO IDENTIFY PM #1
- 1TH PM TRANSMITS FREQUENCY SHIFTED TONES AT THE 1+2 SLOT. OTHERWISE, TRANSMIT POWER AT 2,450 MHz.
- EVEN NUMBERED PM TRANSMIT SHIFTED TONES AT $2,450 \pm 19.14$ MHz. ODD PM AT $2,450 \pm 9.57$ MHz.
- FRAME CYCLES FOR A PREDETERMINED TIME TO ALLOW SYNC ACQUISITION ON THE GROUND

143
*A Sonic
Satellite Power System
Microwave Power
Transmission Simulator*

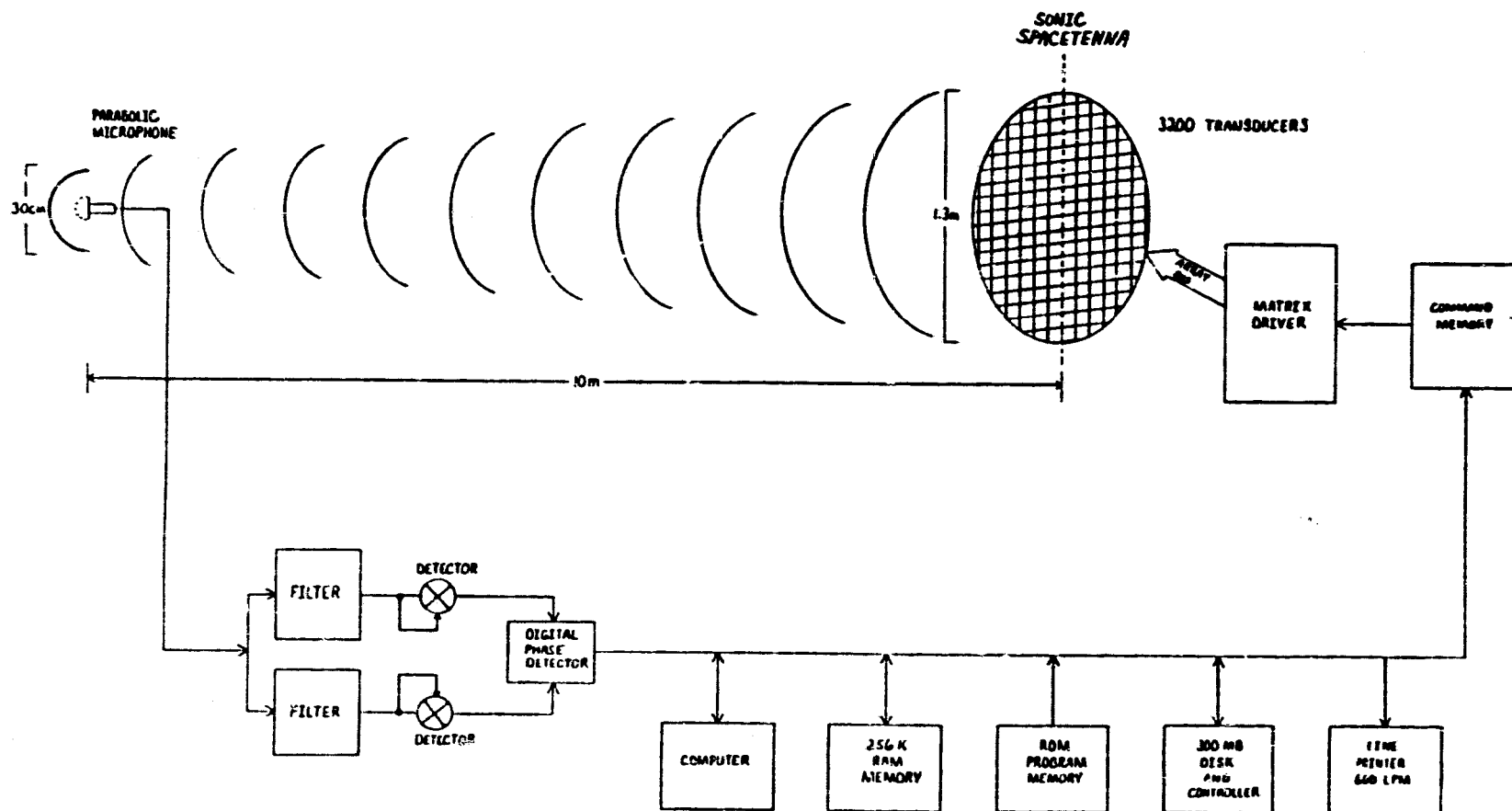
*J. Ott
Novar*

PRECEDING PAGE BLANK NOT FILMED

ORIGINAL PAGE IS
OF POOR QUALITY



PRECEDING PAGE BLANK NOT FILMED



SONIC SPS PHASE CONTROL SIMULATOR
MAJOR FUNCTIONAL BLOCKS

ACOUSTIC SIMULATION OF ELECTROMAGNETICS

• "TELEGRAPHER'S" EQUATIONS

■ ACOUSTIC

$$\frac{\partial p}{\partial z} = -\rho v \frac{\partial u}{\partial t}$$

$$\frac{\partial u}{\partial z} = -K \frac{\partial p}{\partial t}$$

■ ELECTROMAGNETIC

$$\frac{\partial E_x}{\partial z} = -\mu \frac{\partial H_y}{\partial t}$$

$$\frac{\partial H_y}{\partial z} = -\epsilon \frac{\partial E_x}{\partial t}$$

• WAVE EQUATIONS

$$\frac{\partial^2 p}{\partial z^2} = \frac{1}{c_a^2} \frac{\partial^2 p}{\partial t^2}$$

$$\frac{\partial^2 E_x}{\partial z^2} = \frac{1}{c_e^2} \frac{\partial^2 E_x}{\partial t^2}$$

• SIMULATION VALID FOR

- BEAM SHAPE AND SIDE LOBE
- GRATING LOBES
- SCINTILLATION AND FADING CAUSED BY
 - ▲ REFRACTION
 - ▲ DIFFRACTION
 - ▲ OBSTRUCTIONS

STGNIFICANT SONIC SIMULATOR SCALING FACTORS

	SPS	SCALE FACTOR	SIMULATOR
PROPAGATION VELOCITY	3×10^8 M/SEC	10^6	3×10^2 M/SEC
RANGE	3.5×10^7 M	3.5×10^6	10 M
WAVELENGTH	12 CM	4	3 CM
BEAM FREQUENCY	2.45 GHZ	2×10^5	12 KHZ
ONE WAY TRAVEL TIME	.1 SEC	3	.03 SEC
FILTER SETTTLING TIME	10^{-3} MS	10^{-3}	1 MS
TRANSMITTER SOURCES	10^5	31	3,200
SPACETENNA UPDATE TIME*	10 SEC	3×10^{-2}	5 MIN

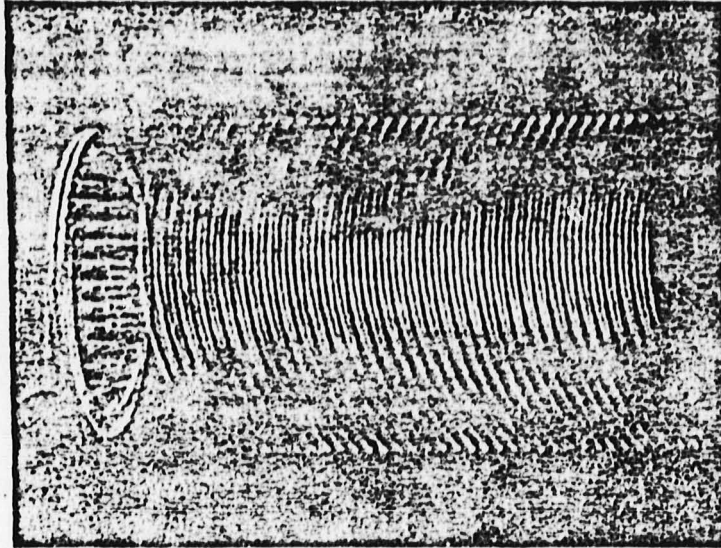
* 100 X FILTER SETTTLING TIME

SONIC SIMULATOR CAPABILITIES

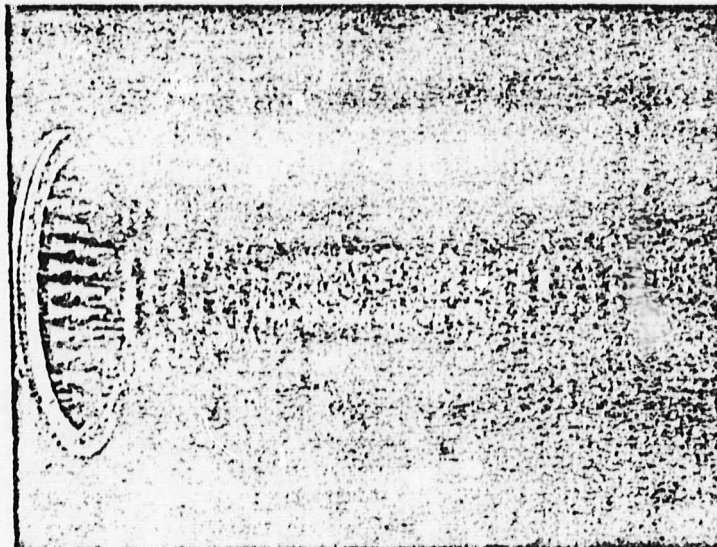
- REAL TIME SIMULATION OF SPS PHASE CONTROL SYSTEM
- SONIC "SPACETENNA" CONTAINS 3200 INDEPENDENT TRANSMITTING ELEMENTS
- COMPUTER-BASED CONTROL OF AMPLITUDE, PHASE AND FREQUENCY OF EACH TRANSMITTER ELEMENT (6° RESOLUTION)
- ELEMENT SPACING OF $.7\lambda$ AT DESIGN FREQUENCY GIVES NO GRATING LOBES
- ANY ILLUMINATION TAPER CAN BE PROGRAMMED
- ELECTRONIC STEERING
- DEMONSTRATE GROUND BASED MODAL VIBRATION PREDICTING
- "SPACETENNA" DESIGNED TO PERMIT MECHANICAL FLEXURE AND SHAPE DISTORTION
- SIMULATOR PROBABLY INSENSITIVE TO LAB'S ACOUSTICS
- PHOTOGRAPHIC RECORDING OF PHASE AND AMPLITUDE PATTERNS WHERE NEEDED

ORIGINAL PAGE IS
OF POOR QUALITY

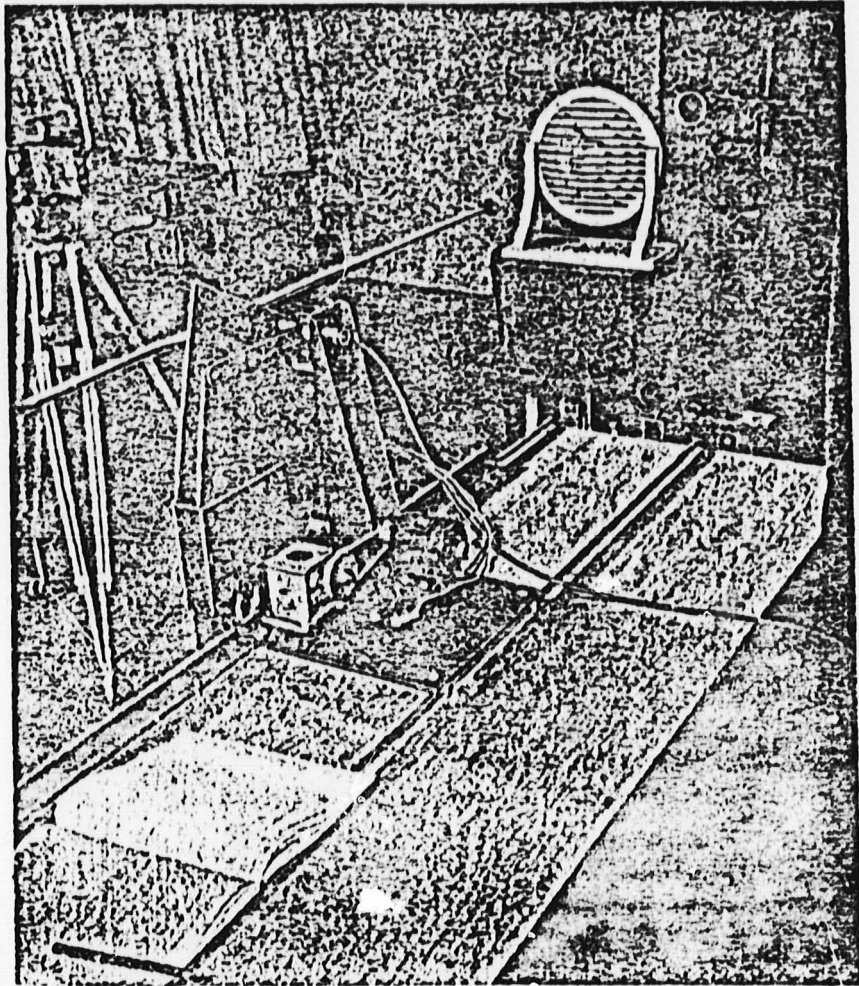
THE BELL SYSTEM TECHNICAL JOURNAL, JULY 1951



An early photo of a sound field in which the scanning strokes were too coarse.

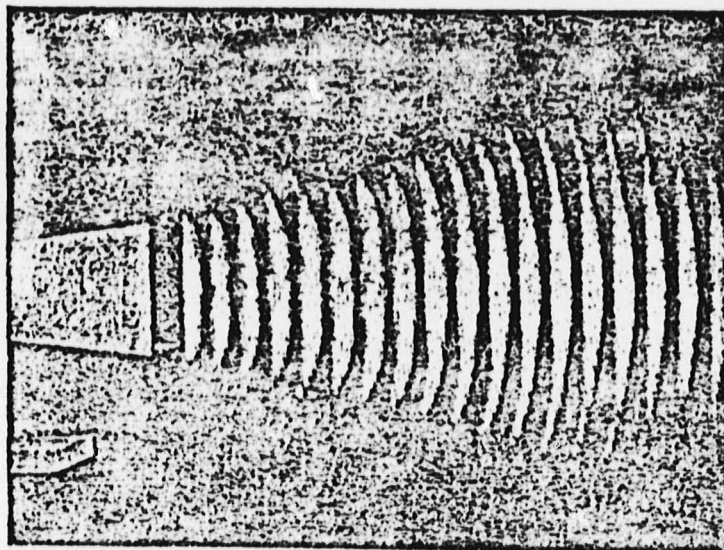


Finer grained scanning produces a smooth pattern of the 10" acoustic lens of Fig. 2. $f = 9$ KC ($\lambda = 1.51"$).

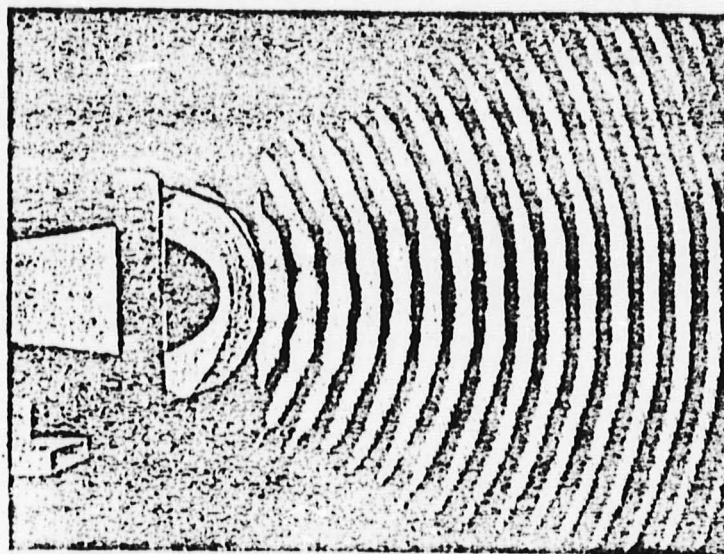


The scanning mechanism set up for photographing the sound field in front of an acoustic lens.

SOUND WAVE AND MICROWAVE SPACE PATTERNS

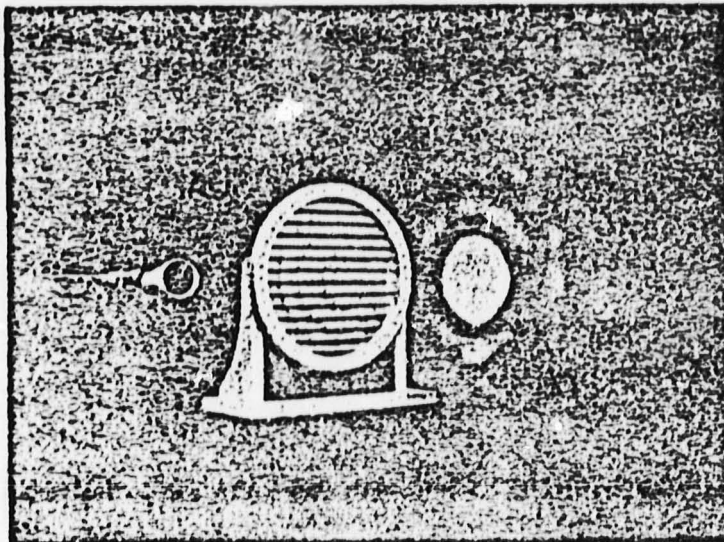


The beam from the 6" aperture horn loud speaker of Fig. 4 has fairly flat wave fronts and a narrow angular coverage. $f = 9$ KC.



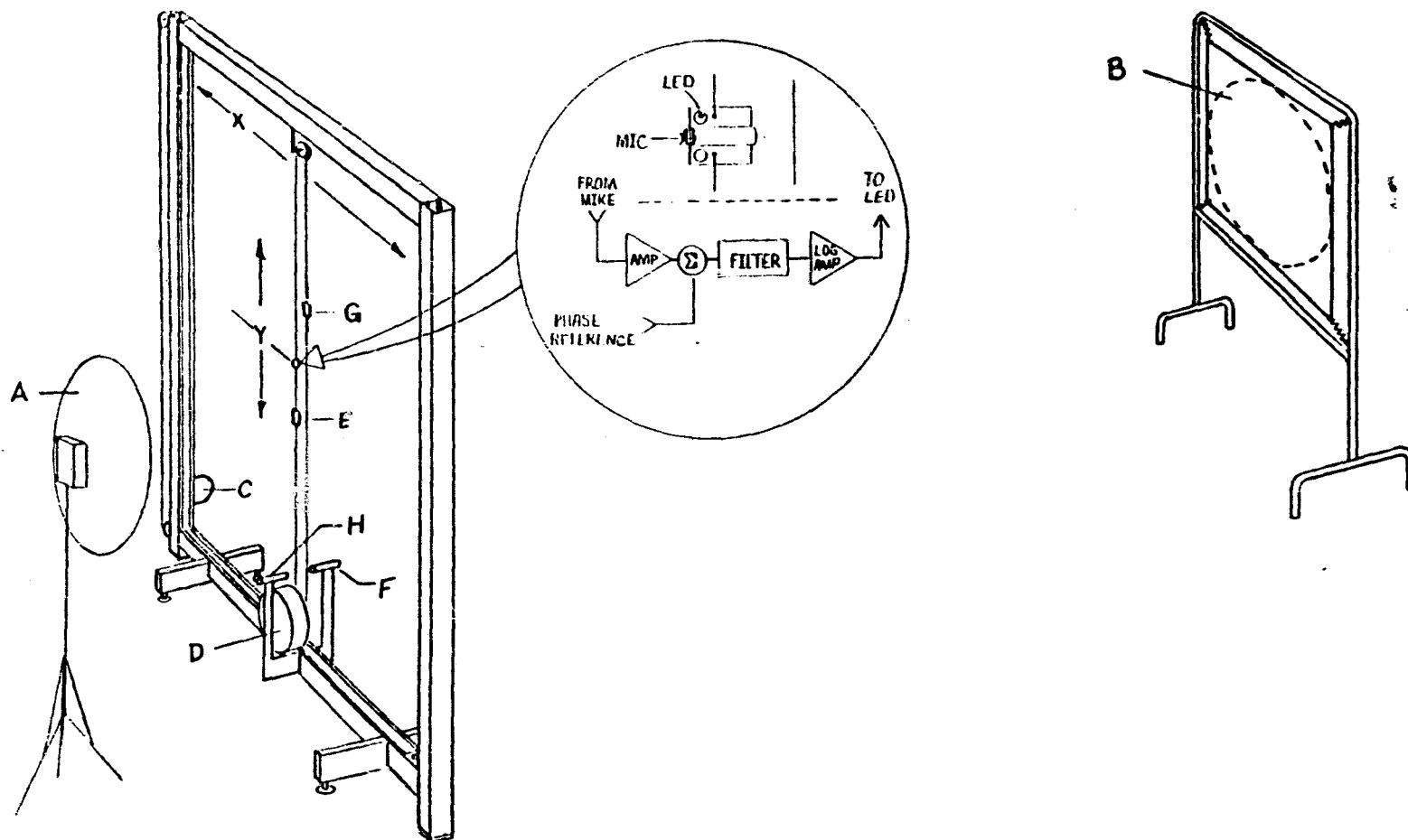
A diverging acoustic lens in the aperture of the horn in Fig. 21 converts the straight line waves into circular waves with their greater angular coverage. $f = 9$ KC.

ORIGINAL PAGE IS
OF POOR QUALITY

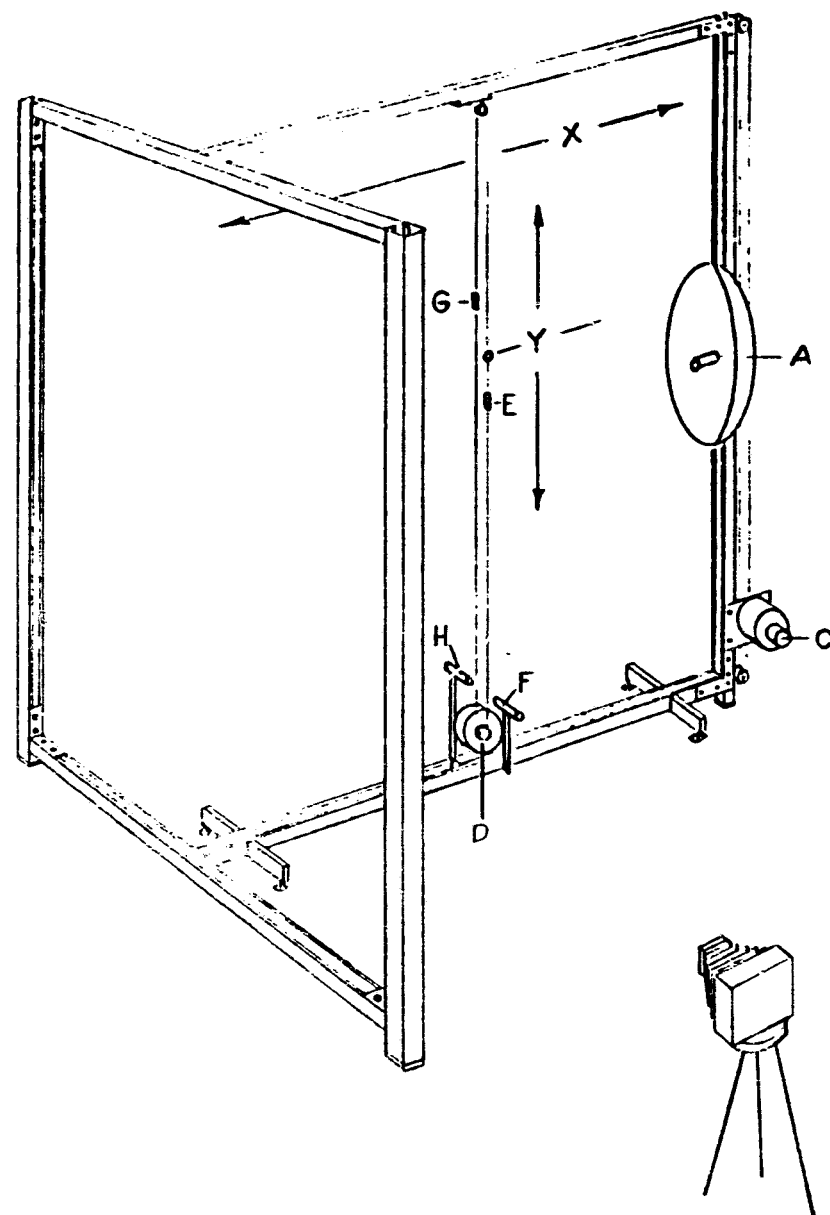
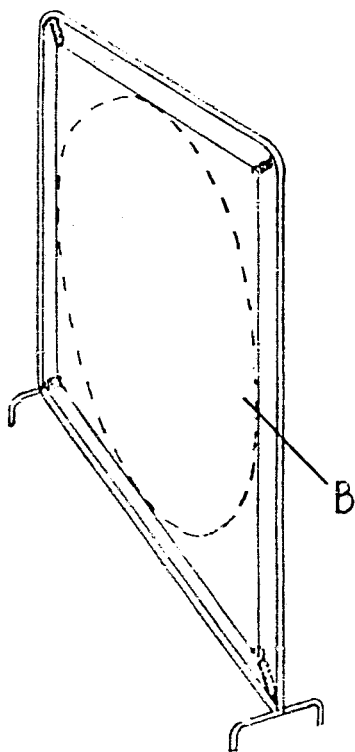


By scanning a plane perpendicular to the axis of radiation, the diffraction rings around the focal spot of the lens of Fig. 3 are portrayed. $f = 9$ KC.

ACOUSTIC-OPTIC CONVERTER DETAIL

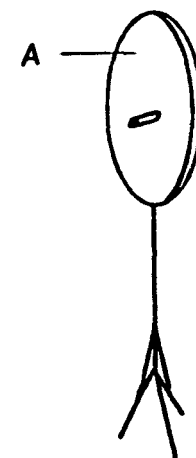
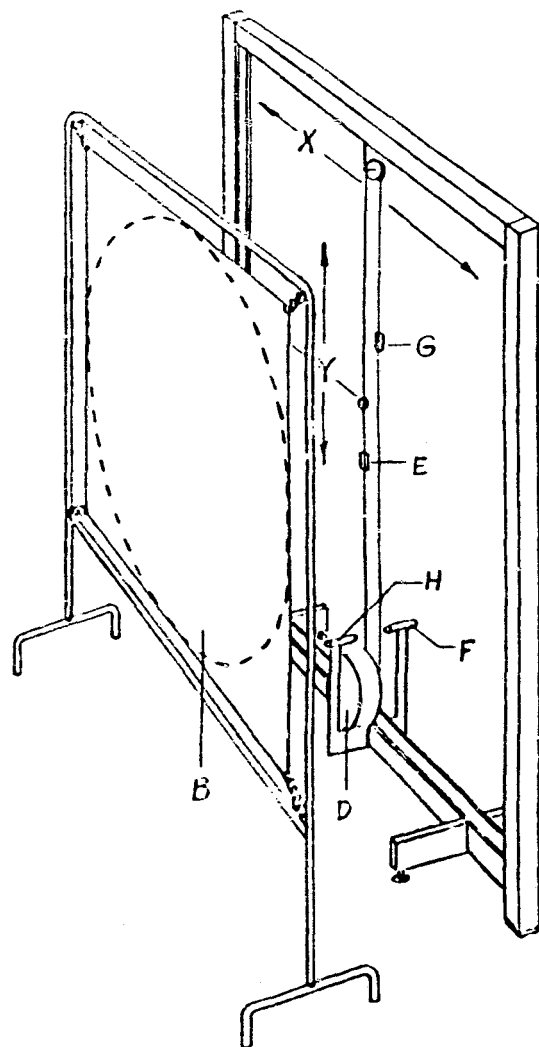


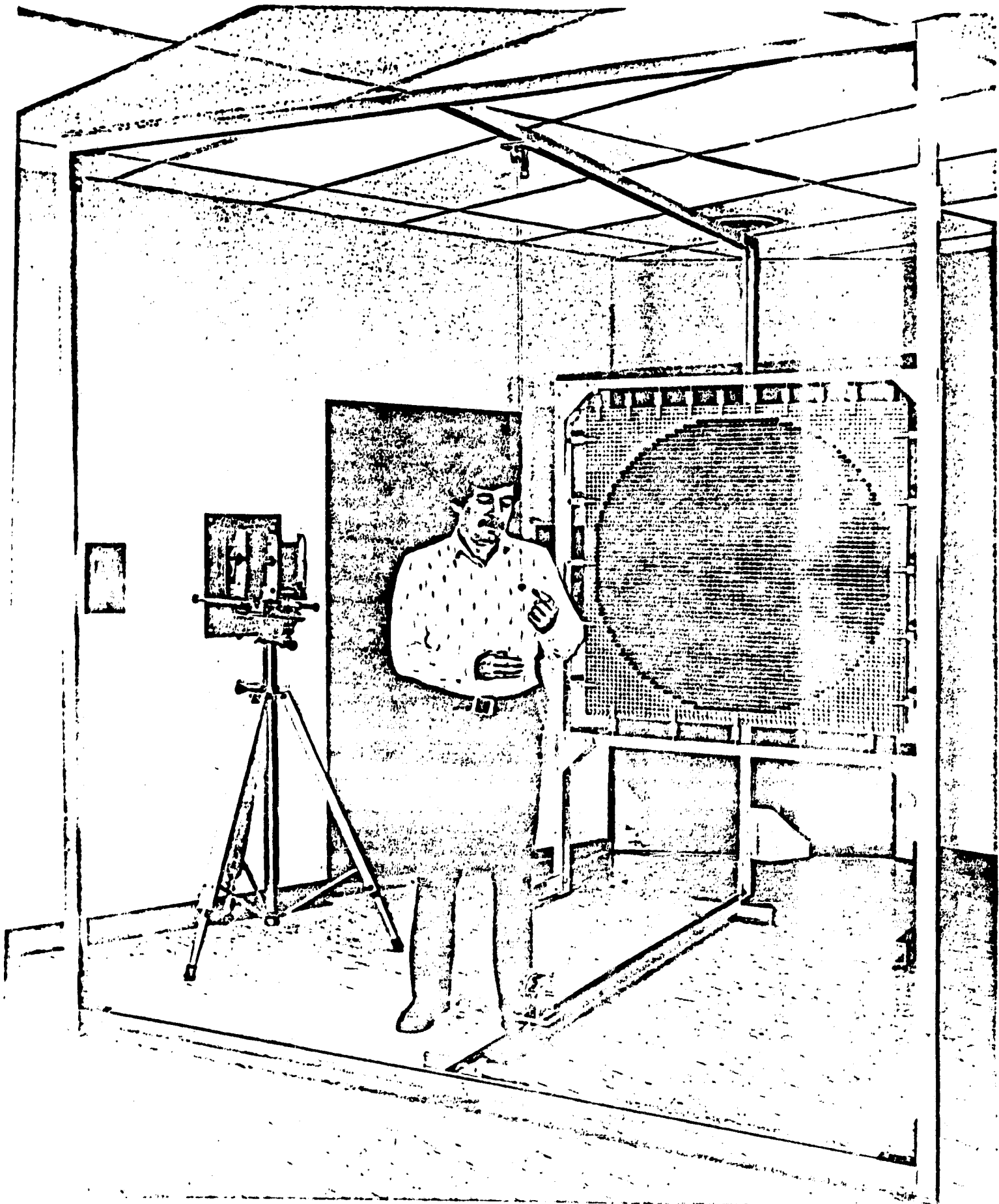
PHOTOGRAPHING FAR-FIELD Z DIMENSION PATTERN



PHOTOGRAPHING CROSS SECTION OF SPACETENNA BEAM

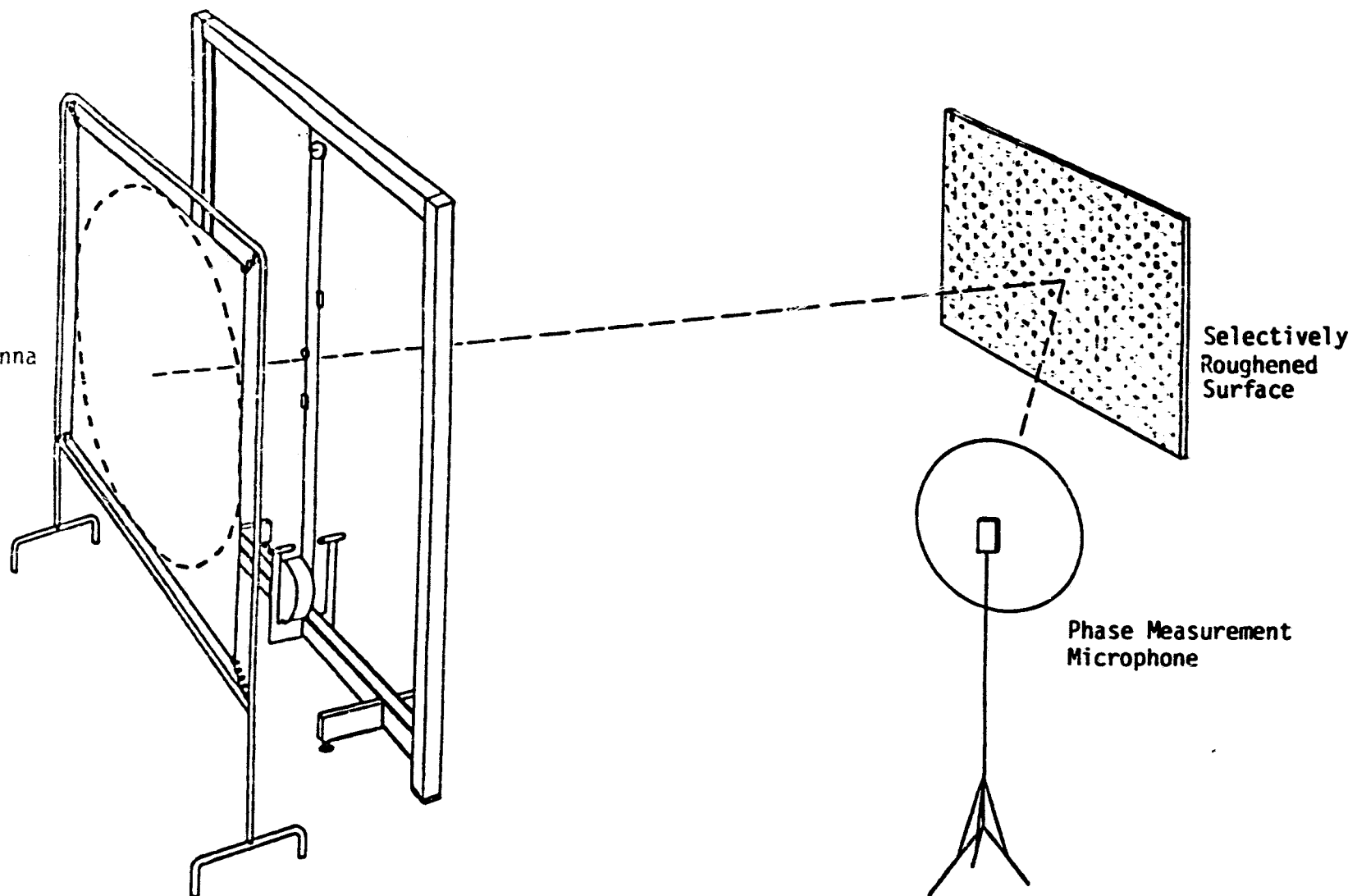
156





MODELS WHICH WILL SIMULATE PROPAGATION EFFECTS

- SCULPTURED REFLECTING SURFACE
- UNEVENLY TENSIONED MYLAR MEMBRANE
- PERFORATED MEMBRANE
- CONTROLLED AIR TURBULENCE (E.G. FAN, HEATER)



SIMULATED PERTURBATION OF SPACETENNA BEAM



National Aeronautics and
Space Administration

Lyndon B. Johnson Space Center
Houston, Texas 77058

175

4

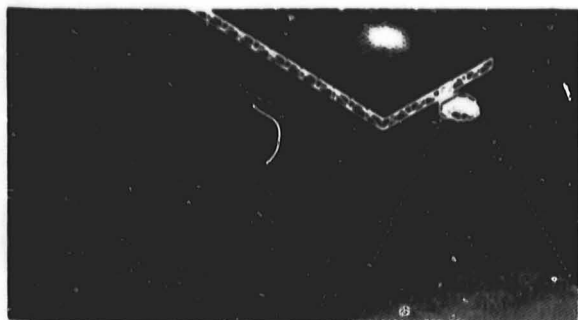
**Power
Amplifiers**



**NASA Solar Power
Satellite**

**Workshop on
Microwave Power
Transmission
and Reception**

**Session
Presentations: Jan
15-18
1980**



The presentation material herein was used in the Power Amplifiers Session of the Solar Power Satellite Workshop on Microwave Power Transmission and Reception held at the Lyndon B. Johnson Space Center, January 15-28, 1980. The workshop was conducted as part of the technical assessment process of the DOE/NASA Solar Power Satellite Concept Evaluation Program. All aspects of Solar Power Satellite microwave transmission and reception were addressed including studies, analyses, and laboratory investigations. Conclusions from these activities were presented as well as recommended follow-on work. The workshop was organized into eight sessions as follows:

- *General*
- *Microwave System Performance*
- *Phase Control*
- *Power Amplifiers*
- *Radiating Elements*
- *Rectenna*
- *Solid State Configurations*
- *Planned Program Activities*

The material contained herein supplements the workshop papers which were published and distributed at the time of the workshop. Together they are a comprehensive documentation of the numerous analytical and experimental activities in the field of microwave power transmission and reception.

- *Additional information regarding the workshop may be obtained by*

contacting: R.H. Dietz
 EE4/SPS Microwave Systems
 National Aeronautics &
 Space Administration
 Lyndon B. Johnson Space Center
 Houston, Texas 77058
 713 483-4507

4

Power Amplifier Session

contents

1	Role of Power Amplifiers in Reference System Dr. Erv Nalos, Boeing
21	Klystron A. D. LaRue, Varian
35	Klystron Efficiency and Cathode Life Dr. Henry Kosmahl, Lewis Research Center
49	Progress Report of the Adapting of the Cross-field Directional Amplifier to the Requirements of the Solar Power Satellite W. C. Brown, Raytheon
95	Summary of Past Activities L. Leopold, Lyndon B. Johnson Space Center

***Role of Power Amplifiers in
Reference Systems***

***Dr. Erv Nalos
Boeing***

C-9



Alternate High Power Klystron Designs

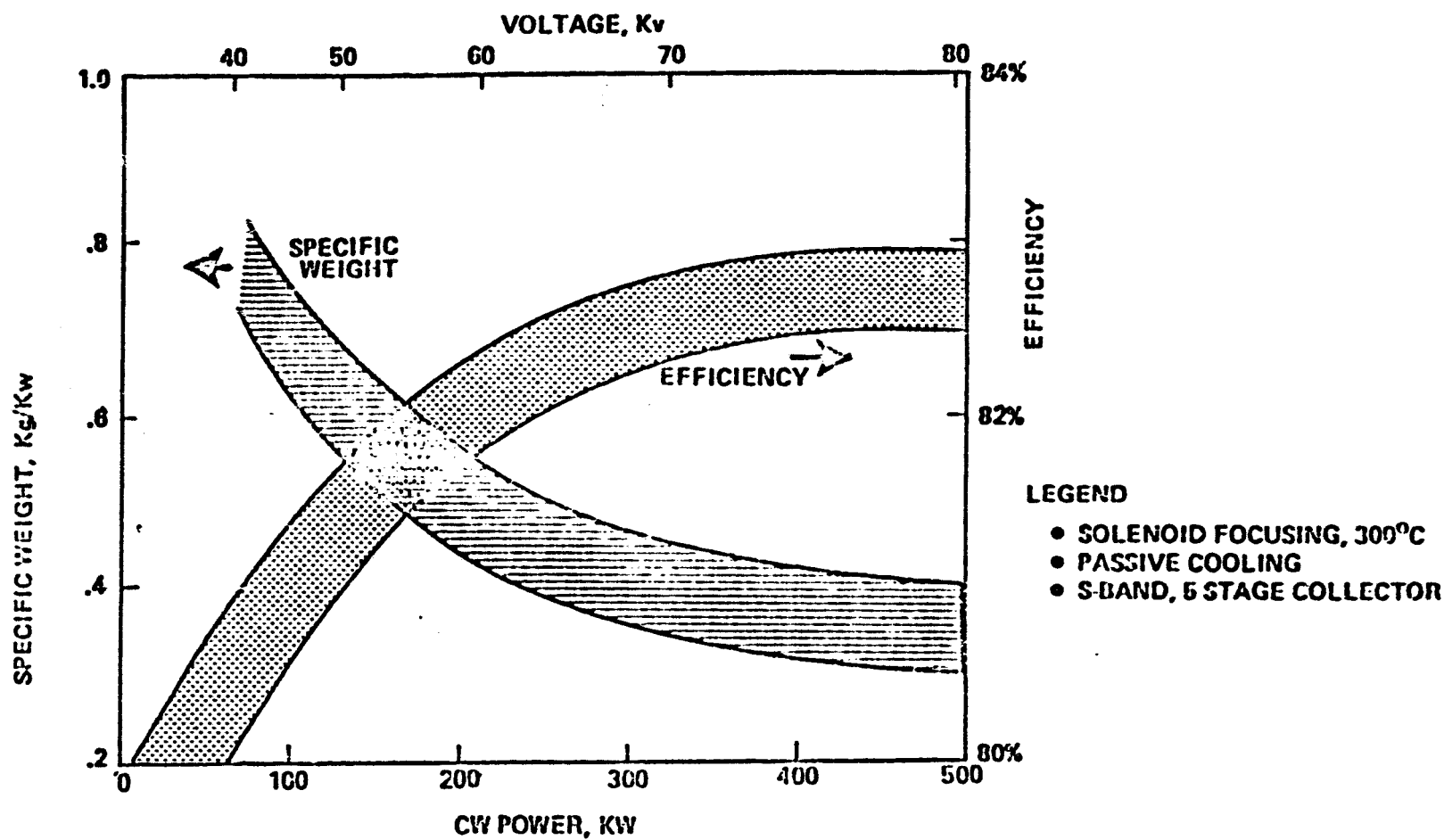
POWER VOLTAGE/CURRENT PERVEANCE $K \times 10^{-6}$ RF SECTION LENGTH $\sim \sqrt{V_0}$	70.6kw 42kv/2.2amps .25 16.5in		250kw 65kv/5amps .30 20.5in		500kw 80kv/8.2amps .36 22.8in	
	WEIGHT, kg	POWER, kw	WEIGHT	POWER	WEIGHT	POWER
TUBE WEIGHT CAVITY, SEALS, BODY ETC. $\sim 1.2 \sqrt{V_0}$	10kg		15kg		16.6kg	
COLLECTOR WEIGHT (EST.) $\sim V_0 I_0$	7.0kg		13.2kg		18.7kg	
SOLENOID (EST.) @ 300°C, 1 KGAUSS, $P \sim R_2 \propto L \sim \sqrt{V_0}$ K	20kg	2kw	24.8kg	2.93kw	27.9kg	3.98kw
HEATER AND REFOCUSING COIL RF LOSSES		1.0kw 4.2kw		1.50kw 14.7kw		2.0kw 29.8kw
RADIATOR AND HEAT PIPES	0	1m	0	1m	0	1m
WEIGHT AND POWER DISSIP'N REQ'D @ 300°C	9.5	14.5	25.3	38.6	47.3	72.0
WEIGHT AND POWER DISSIP'N REQ'D @ 500°C	4.9	9.3	16.7	32.1	33.8	64.9
TOTAL WEIGHT KG	51.4	60.8	95.0	123.7	144	199.8
SPECIFIC WEIGHT KG PER KW	.727	.860	.380	.495	.288	.400
EFFICIENCY INC. SOLENOID	80.51%		82.43%		82.67%	

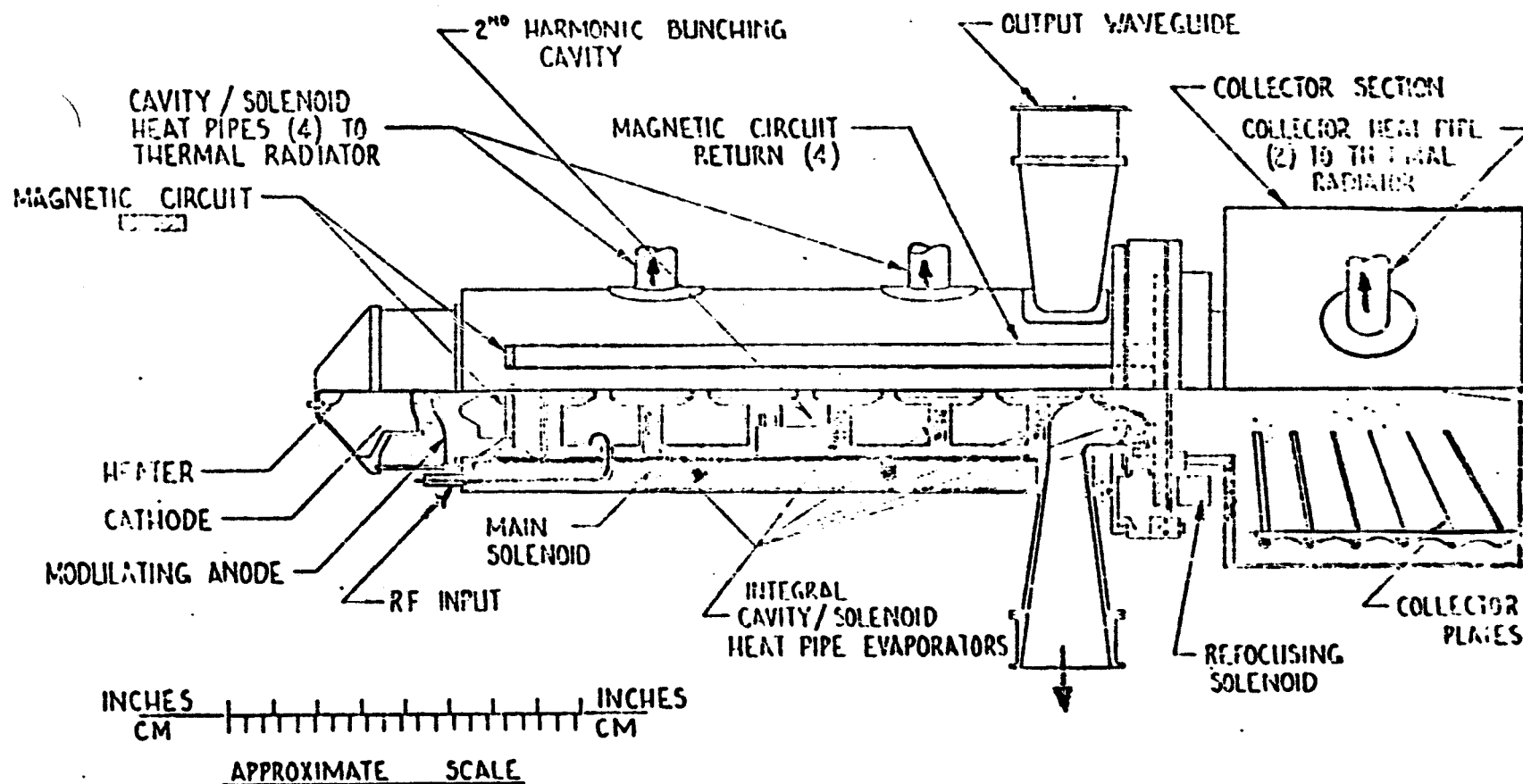
LEGEND:

- SOLENOID FOCUSING, FIVE STAGE COLLECTOR, 45% RECOVERY.
- RF LOSSES AT INPUT, OUTPUT, PLUS 4% INTERCEPTION LOSS TOTAL 4.45% OF $V_0 I_0$
- USEFUL RF OUTPUT = $.7629 V_0 I_0$
- COLLECTOR THERMAL DISSIPATION = $.105 V_0 I_0$
- COLLECTOR POWER RECOVERED = $.0860 V_0 I_0$
- EFFICIENCY = 83.4% EXCLUDING SOLENOID
- HEAT PIPES (I/O METER) + RADIATOR WEIGHT ESTIMATED @ 2.01/1.32kg/kw @ 300°C (BODY AND SOLENOID)
- @ .94/.49kg/kw @ 500°C (COLLECTOR)
- S BAND DESIGN WITH SOLENOID @ 300°C, ID = 3" OD = 4 1/2"

PRECEDING PAGE BLANK NOT FILLED

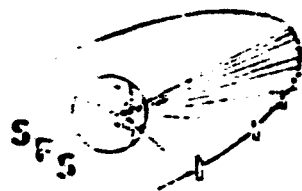
ORIGINAL PAGE IS
OF POOR QUALITY





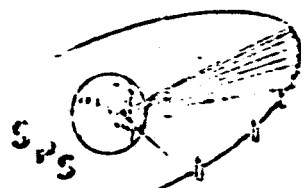
HIGH EFFICIENCY KLYSTRON DESIGN

{ 35%
70kW



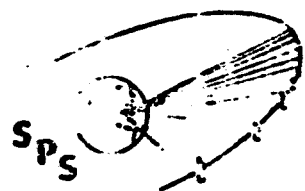
Reference Klystron Design Criteria

POWER LEVEL	70.6 KW	BASED ON A PERVEANCE OF $S = 0.25 \times 10^{-6} = I_0/V_0^{3/2}$ AS DETERMINED TO MAINTAIN HIGH EFFICIENCY @ MAX. VOLTAGE OF 42.1 Kv.
COLLECTOR	5-SEGMENT DEPRESSED COLLECTOR	BASED ON EXPERIMENTAL RESULTS ON COLLECTOR RECOVERY OF $\approx 50\%$, OBTAINED BY UTILIZING AS SMALL REFocusing COIL IN THE COLLECTOR SECTION.
RF DESIGN	SINGLE 2ND HARMONIC BUNCHING SIX CAVITY DESIGN	A DESIGN OPTION RESULTING IN HIGH BASIC EFFICIENCY IN A COMPACT DRIFT TUBE CONFIGURATION. TO OBTAIN A GAIN ABOUT 40 db, RESULTING IN A SOLID STATE DRIVER FEASIBILITY AND LOW POWER PHASE SHIFT REQUIREMENTS (< 10 WATTS)
FOCUSING	SOLENOID (RFF.) PM/PPM (FUTURE)	TO OBTAIN HIGH EFFICIENCY WITH A LOW RISK APPROACH. IF IN THE PROCESS OF SPS DEVELOPMENT, A HIGH POWER SAMARIUM-COBALT PM/PPM DESIGN CAN BE PROVEN WITH GOOD EFFICIENCY, IT SHOULD BE CONSIDERED.
THERMAL DESIGN	HEAT PIPE WITH PASSIVE RADIATORS	TO OBTAIN THE DESIRED CW LEVEL WITH CONSERVATIVE HEAT DISSIPATION RATINGS.
AUXILIARY PROTECTION	MODULATING ANODE	TO PROVIDE RAPID PROTECTION SHUT OFF CAPABILITY AT THE INDIVIDUAL TUBE LEVEL, HOPEFULLY OBTAINING THE NEED FOR CROW-BAR TYPE OF TURN OFF.
CATHODE	COATED POWDER OR METAL MATRIX MEDIUM CONVERGENCE	TO OBTAIN A CATHODE EMISSION OF $< 200 \text{ ma/cm}^2$ TO OBTAIN 30 YEAR LIFE TO EMISSION WEAROUT.
POWER EXTRACTION	2-PORT OUTPUT	RESULTING IN RATING 35kw CW PER EACH WAVEGUIDE OUTPUT, CAPABLE OF OPERATING IN VACUUM WITH RADIATIVE COOLING ONLY AT A TEMPERATURE BELOW 200°C .



Klystron Mass Estimate

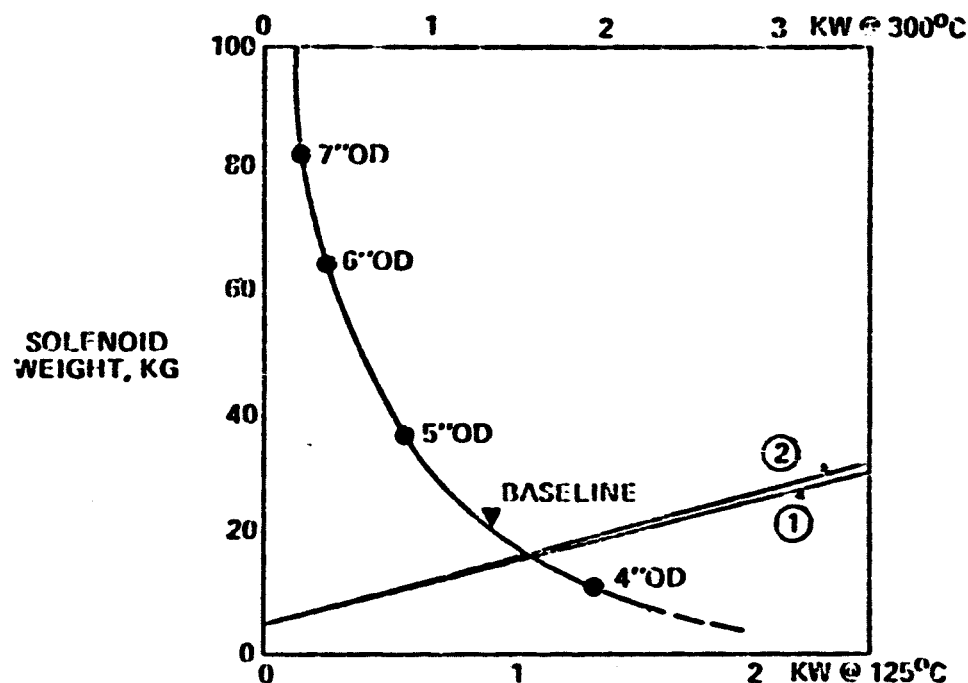
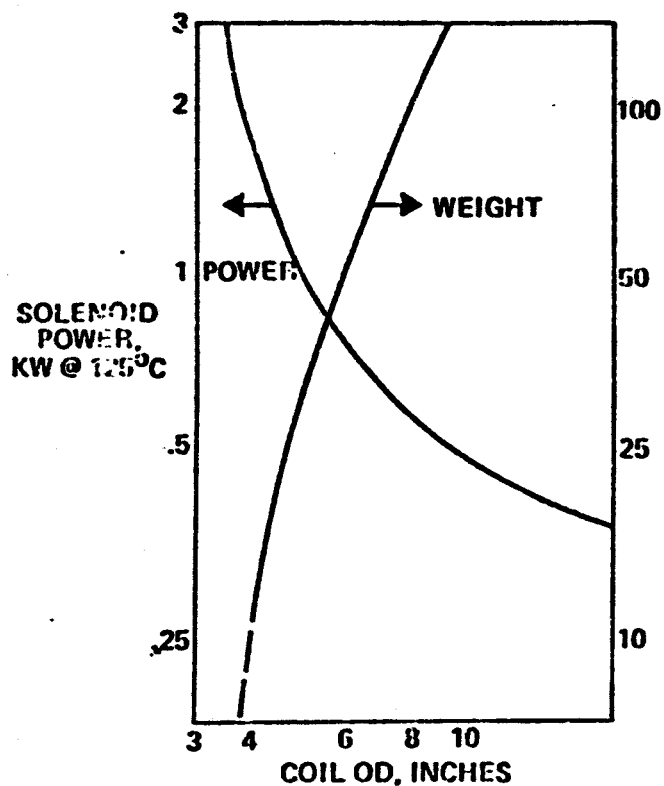
ITEM	MATERIAL	PRINCIPAL DIMENSIONS (CM)	MASS (kg)
SOLENOID	COPPER	OD = 11.4, ID = 7.6, L = 41.9	16.4
WIRE		(75% OF SOLENOID VOLUME)	15.0
INSULATION	ALUMINA	(5% OF SOLENOID VOLUME)	0.4
CAVITIES ASSEMBLY	COPPER	D = 7.6, L = 41.9, Z = 0.95	7.4
POLE PIECES (2)	IRON	D = 15.2, d = 2.5, Z = 1.02	2.8
SOLENOID HOUSING	STEEL	D = 12.7, L = 41.9, Z = 0.32	4.2
COLLECTOR PLATES			4.6
PLATE 1 (LWR)	TUNGSTEN	D = 15.2, d = 5.1, H = 0.3, t = 0.53	1.7
PLATE 2	TUNGSTEN	D = 15.2, d = 5.1, H = 1.0, t = 0.30	1.0
PLATE 3	TUNGSTEN	D = 15.2, d = 5.1, H = 1.3, t = 0.15	0.5
PLATE 4	TUNGSTEN	D = 15.2, d = 5.1, H = 1.5, t = 0.03	0.2
PLATE 5	TUNGSTEN	D = 15.2, d = 5.1, H = 1.8, t = 0.08	0.2
PLATE 6 (UPP)	TUNGSTEN	D = 15.2, d = 5.1, H = 2.0, t = 0.23	1.0
PROBE	TUNGSTEN	D = 2.5, d = 0, H = 3.3, t = 0.15	~
COLLECTOR PLATE ISOLATOR	ALUMINA	OD = 18.3, ID = 15.2, H = 15.5, t = 1.22	2.9
COLLECTOR SECTION COVER	STEEL	D = 20.3, H = 19.1, t = 0.13	2.0
OTHER COMPONENTS:			7.7
REFOCUSING COIL, HEAT PIPES, HI-VOLTAGE CERAMIC SEALS, MODULATING ANODE CONNECTOR, CATHODE CONNECTOR, HEATER, OUTPUT WAVEGUIDES (2), VAC. ION CONNECTOR, CAVITY TUNING PROVISIONS, INTERNAL CABLING, ETC., AND ASSEMBLY AND INSTALLATION HARDWARE.			(48 kg)

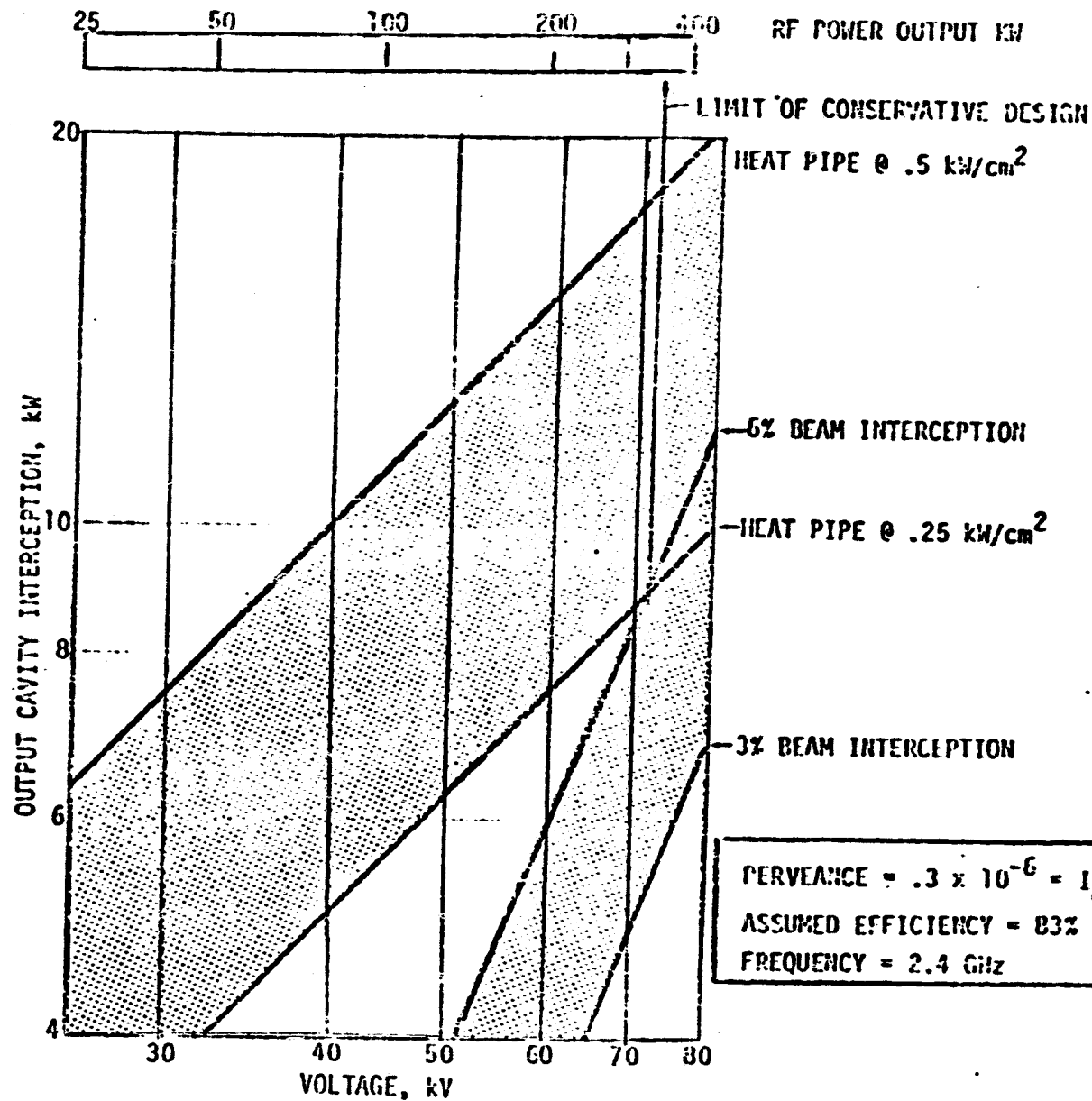


High Power Klystron Solenoid Design Considerations

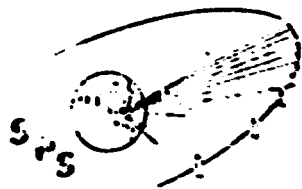
COPPER SOLENOID 3" ID, 1000 GAUSS, 16.5" LONG

- ① ASSUMES POWER GENERATION @ 3.5 kg/kw AND PASSIVE HEAT REJECTION @ 6.2 kg/kw (125°C).
- ② AS ABOVE, WITH 3.86 kg/kw FOR 300°C HEAT REJECTION.

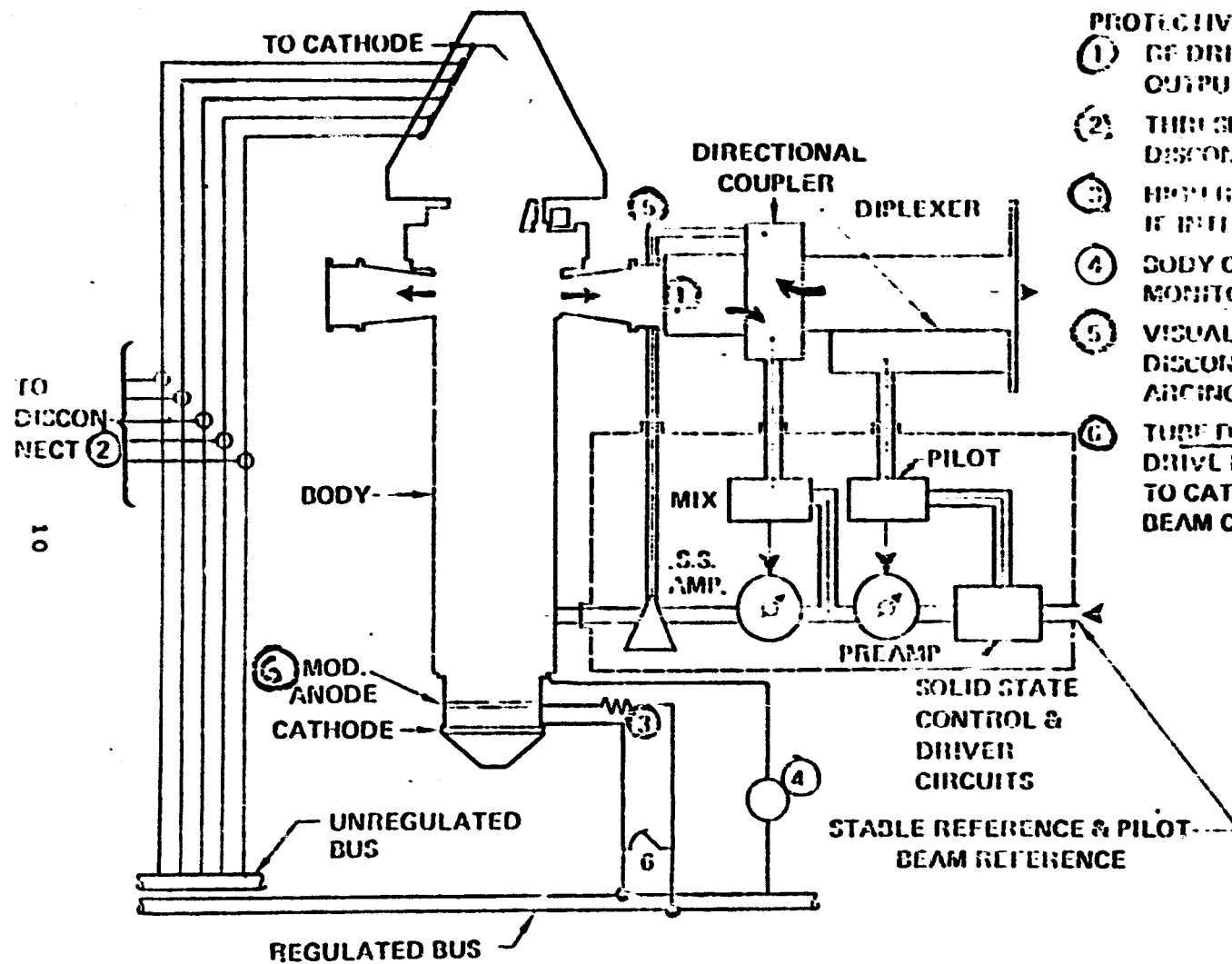




HIGH POWER CW LIMITATION OF HIGH EFFICIENCY KLYSTRON



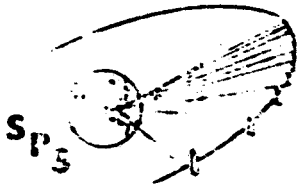
Klystron Protective Devices



PROTECTIVE FEATURES

- ① RF DRIVE SHUT OFF WITH OUTPUT WAVEGUIDE ARCS
- ② THRESHOLD CURRENT DETECTORS DISCONNECT IF INTERNAL ARCS
- ③ HIGH RESISTANCE ARC ON BEARING IF INTERNAL ARCS
- ④ BODY CURRENT METER MONITORS CATHODE EMISSION
- ⑤ VISUAL ARC DETECTOR DISCONNECTS TUBE IF EXTERNAL ARCS
- ⑥ TUBE DISCONNECT DRIVE MOD ANODE VOLTAGE TO CATHODE—REMOVES BEAM CURRENT

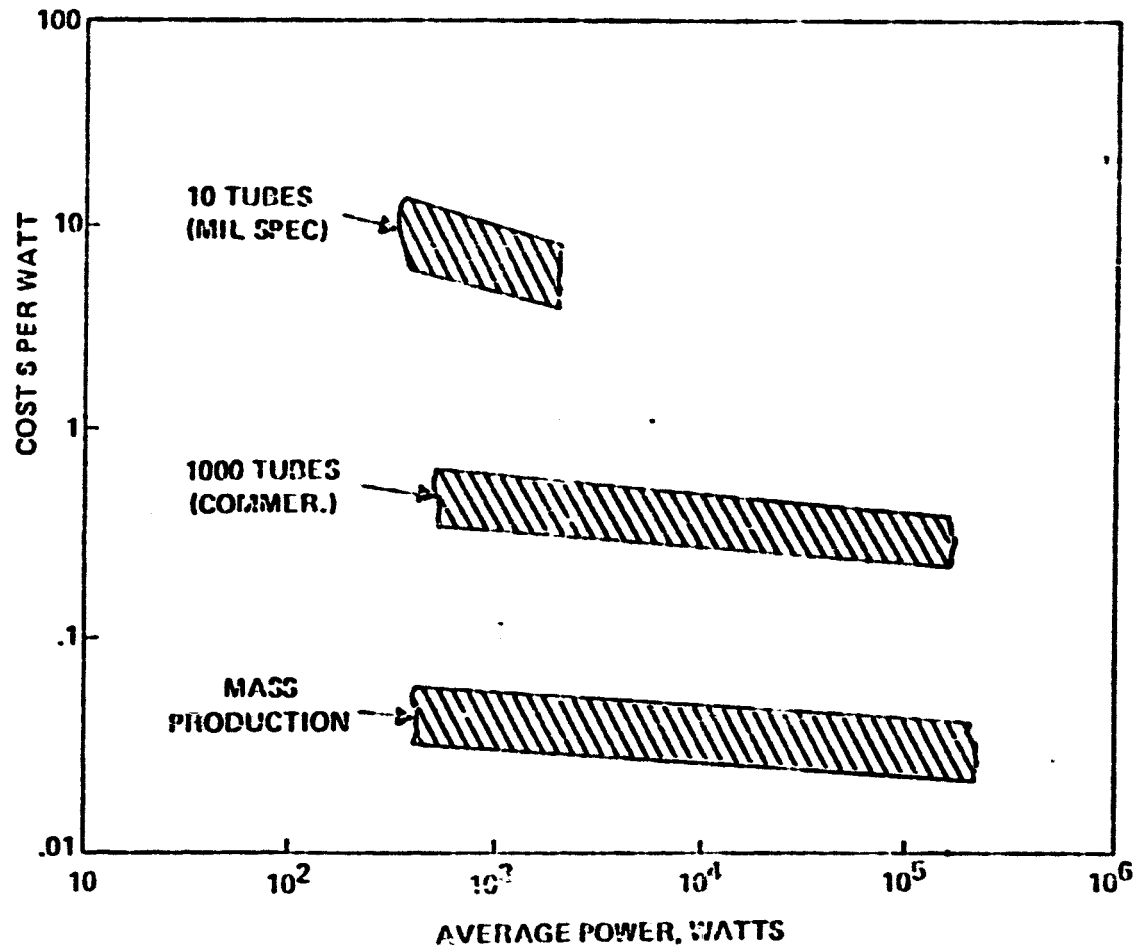
ORIGINAL PAGE IS
OF POOR QUALITY



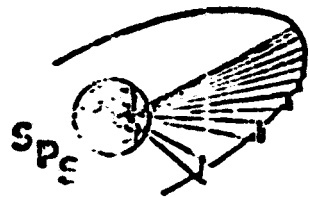
Cost Variations with Power Level and Quantity

SPS-1-51

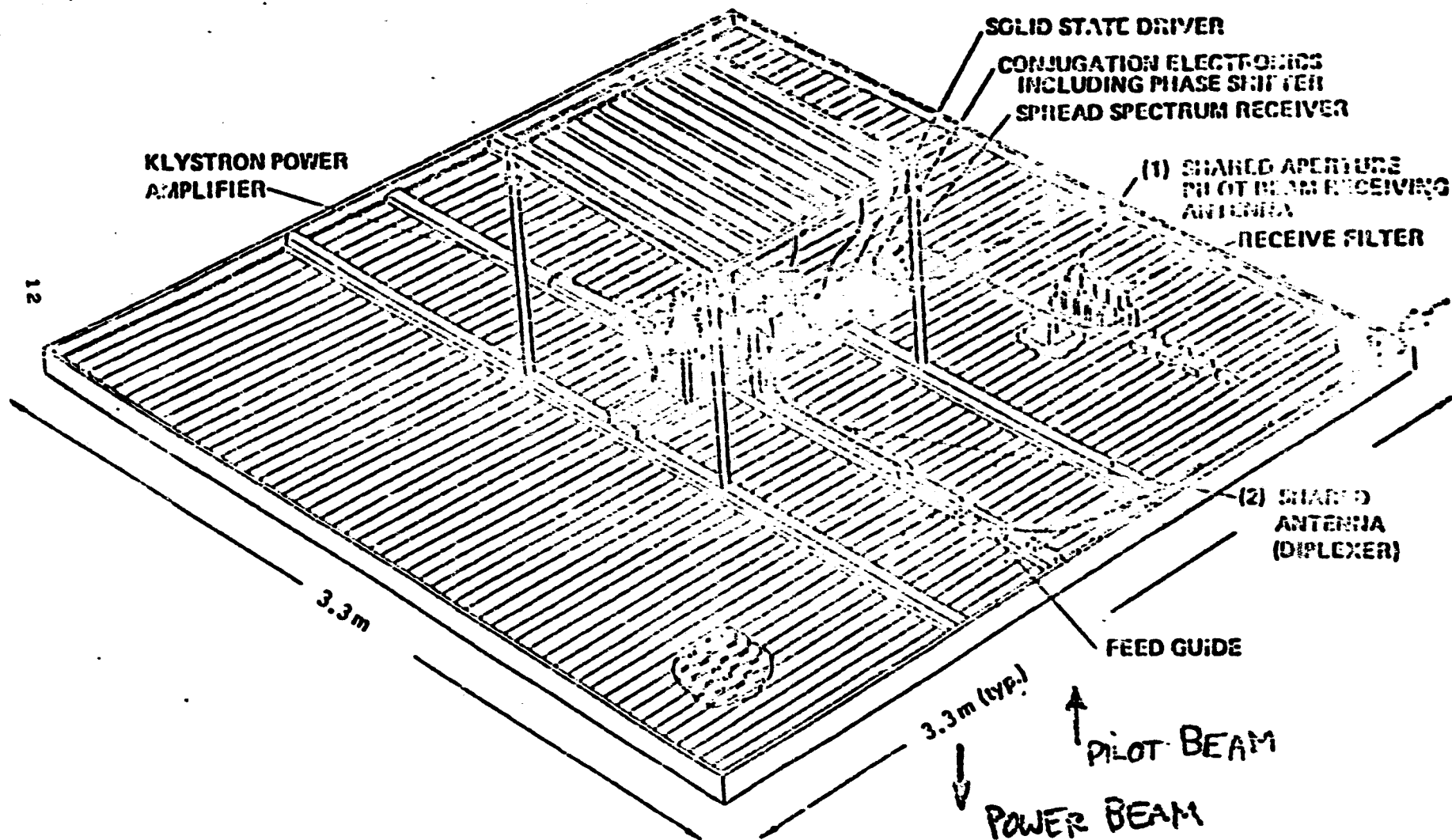
DOING



(D) COST VARIATION WITH POWER LEVEL AND QUANTITY

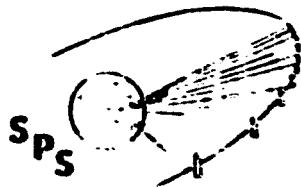


Typical Klystron Module



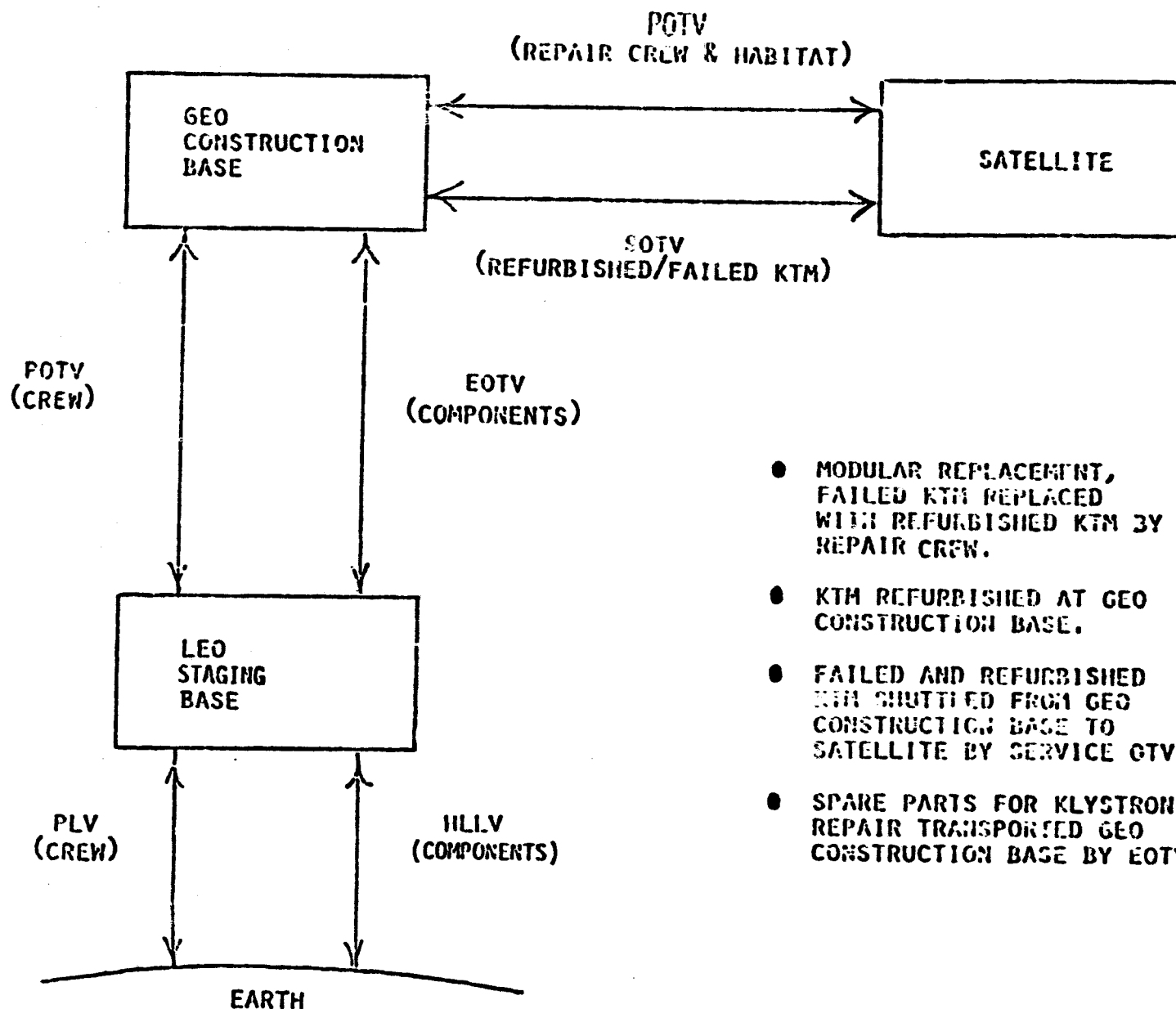
	KLYSTRON BODY <hr/> 300 C 5.2kw	KLYSTRON COLLECTOR <hr/> 500 C 8kw
HEAT PIPE SYSTEM LIQUID METAL	28 LBS	13.5 LBS
PUMPED FLUID SYSTEM DOWTHERM A STEAM LIQUID NAK	10 LBS	18 LBS 5 LBS

KLYSTRON THERMAL CONTROL CONCEPTS

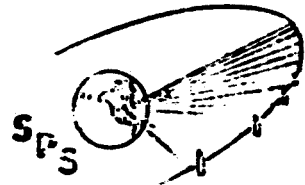


Maintenance and Operations Analysis

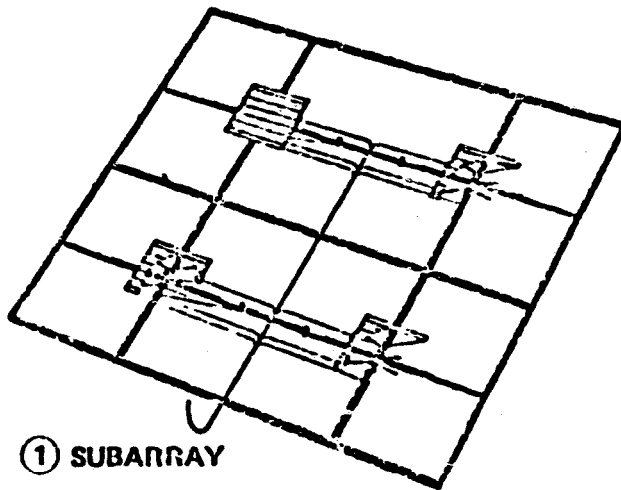
- ITEMS REQUIRING MAINTENANCE
- LEVEL OF REPLACEMENT
- REPLACEMENT CONCEPT
 - EQUIP REQ'D
 - ANTENNA DESIGN IMPACT
- MAINTENANCE SCHEDULE
 - HOW OFTEN
 - HOW RAPIDLY
 - WHEN
- MAINTENANCE MISSION
 - HABITAT LOCATION
 - REFURB LOCATION
 - TRANSPORTATION
- REFERENCE SYSTEM DESCRIPTION
- SATELLITE MAINTENANCE OPERATIONS SUMMARY



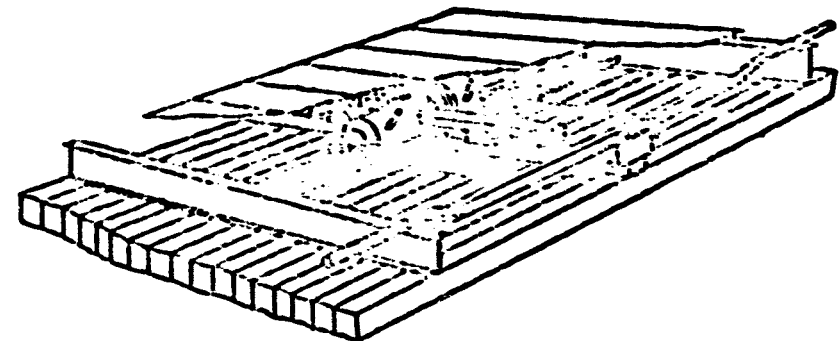
- MODULAR REPLACEMENT, FAILED KTM REPLACED WITH REFURBISHED KTM BY REPAIR CREW.
- KTM REFURBISHED AT GEO CONSTRUCTION BASE.
- FAILED AND REFURBISHED KTM SHUTTLED FROM GEO CONSTRUCTION BASE TO SATELLITE BY SERVICE OTV.
- SPARE PARTS FOR KLYSTRON REPAIR TRANSPORTED GEO CONSTRUCTION BASE BY EOTV.



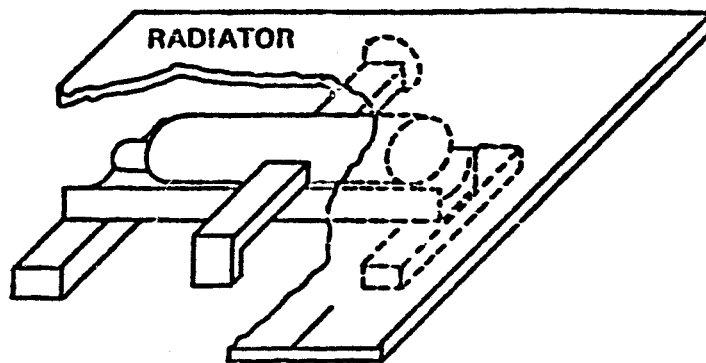
Level of Replacement Options at Satellite



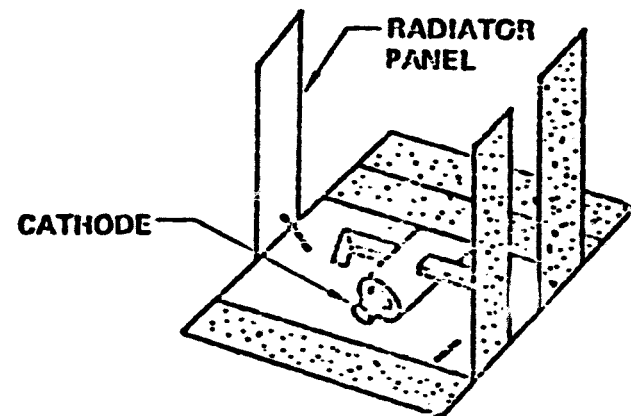
① SUBARRAY



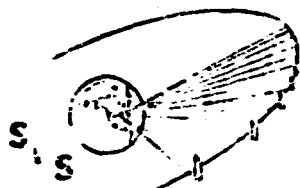
② COMPLETE KLYSTRON MODULE INCLUDING WAVEGUIDE



③ KLYSTRON TUBE PLUS THERMAL CONTROL



④ COMPONENTS

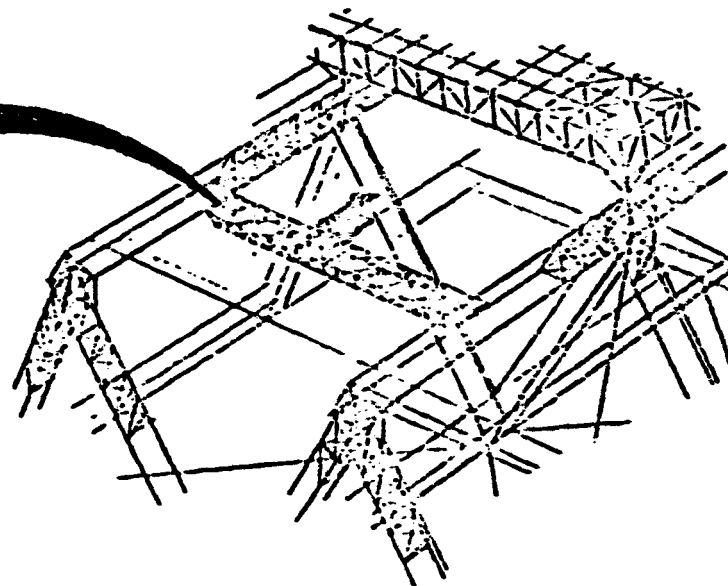
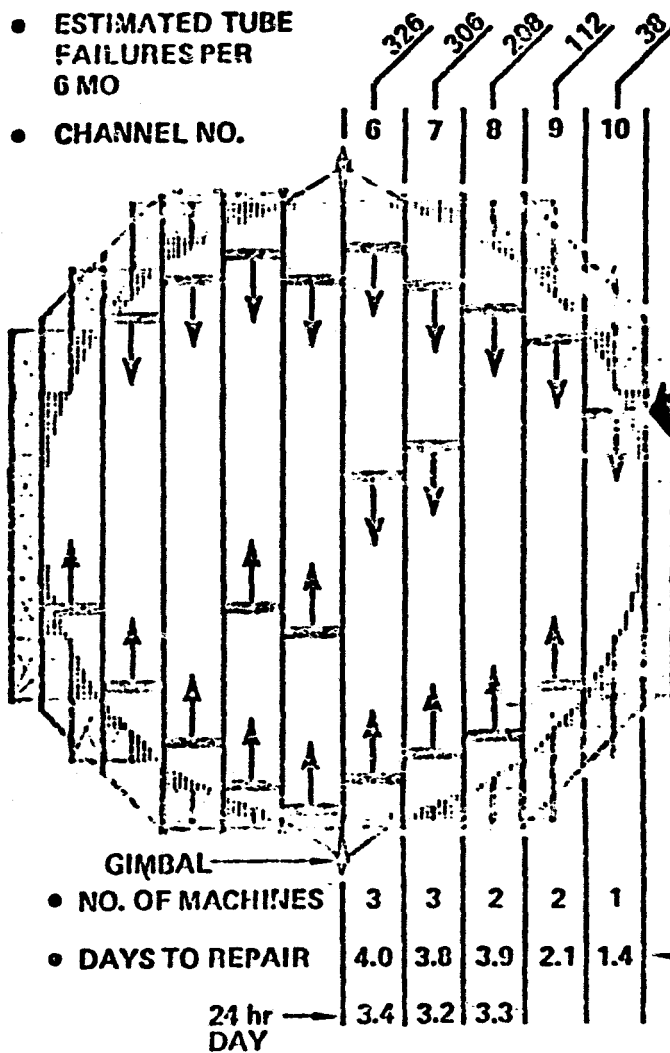


Antenna Maintenance System Installation

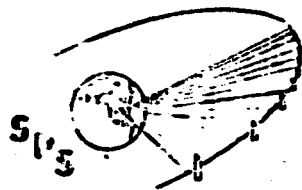
SDRMS

- ESTIMATED TUBE FAILURES PER 6 MO

- CHANNEL NO.



20 hr/DAY
3.5 DAY ALLOWABLE



Vertical Access Maintenance Vehicle

SUBARRAY

MAINTENANCE
VEHICLE

TUBE RACK

CUBIC SECONDARY
STRUCTURE

VERTICAL AND
DIAGONAL MEMBERS
(TELESCOPE)

HORIZ
MEMBERS
(KNEE
JOINTS)

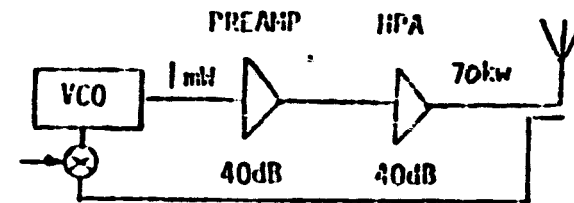
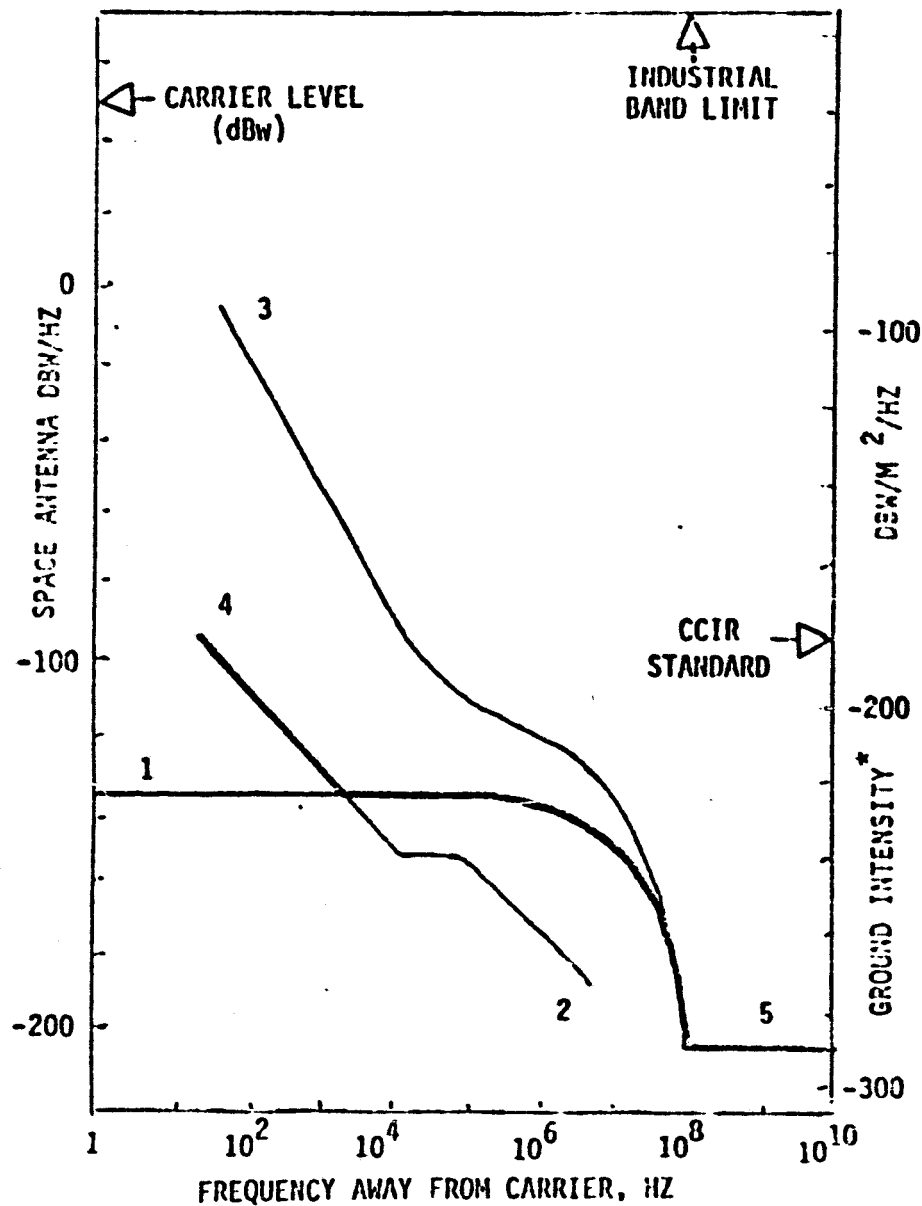
MAINTENANCE
GANTRY

PRIMARY
STRUCTURE
RIDGE BEAM

SECTION A-A

ORIGINAL PAGE IS
OF POOR QUALITY

NOISE SPECTRAL DENSITY ESTIMATE



LEGEND

- 1 KLYSTRON ALONE
(VARIAN 5 CAVITY SPS TUBE ANALYSIS)
 - 2 VCO WITH PHASE LOCKED LOOP
ALONE
 - 3 PREVIOUS ESTIMATE OF
CHAIN WITH PHASE COMPENSATION LOOP
 - 4 POTENTIAL CHAIN PERFORMANCE
WITH PHASE COMPENSATION LOOP
 - 5 THERMAL NOISE AT 2930K
- * 100,000 TUBES,
35dB = KLYSTRON MODULE GAIN
GEO: $4\pi R^2 = -162.4 \text{ dBm}^2$

OUTPUT GAP COOLING

PREFERRED CONCEPT :

- INVERTED MENISCUS INTEGRAL HEAT PIPE(S)
- WATER - OHFC
- 32 W/CM^2 EVAPORATOR FLUX
- SEPARATE TRANSPORT PIPE(S) TO RADIATOR
- MECHANICAL JOINT BETWEEN OUTPUT GAP PIPE(S) & TRANSPORT PIPE(S)

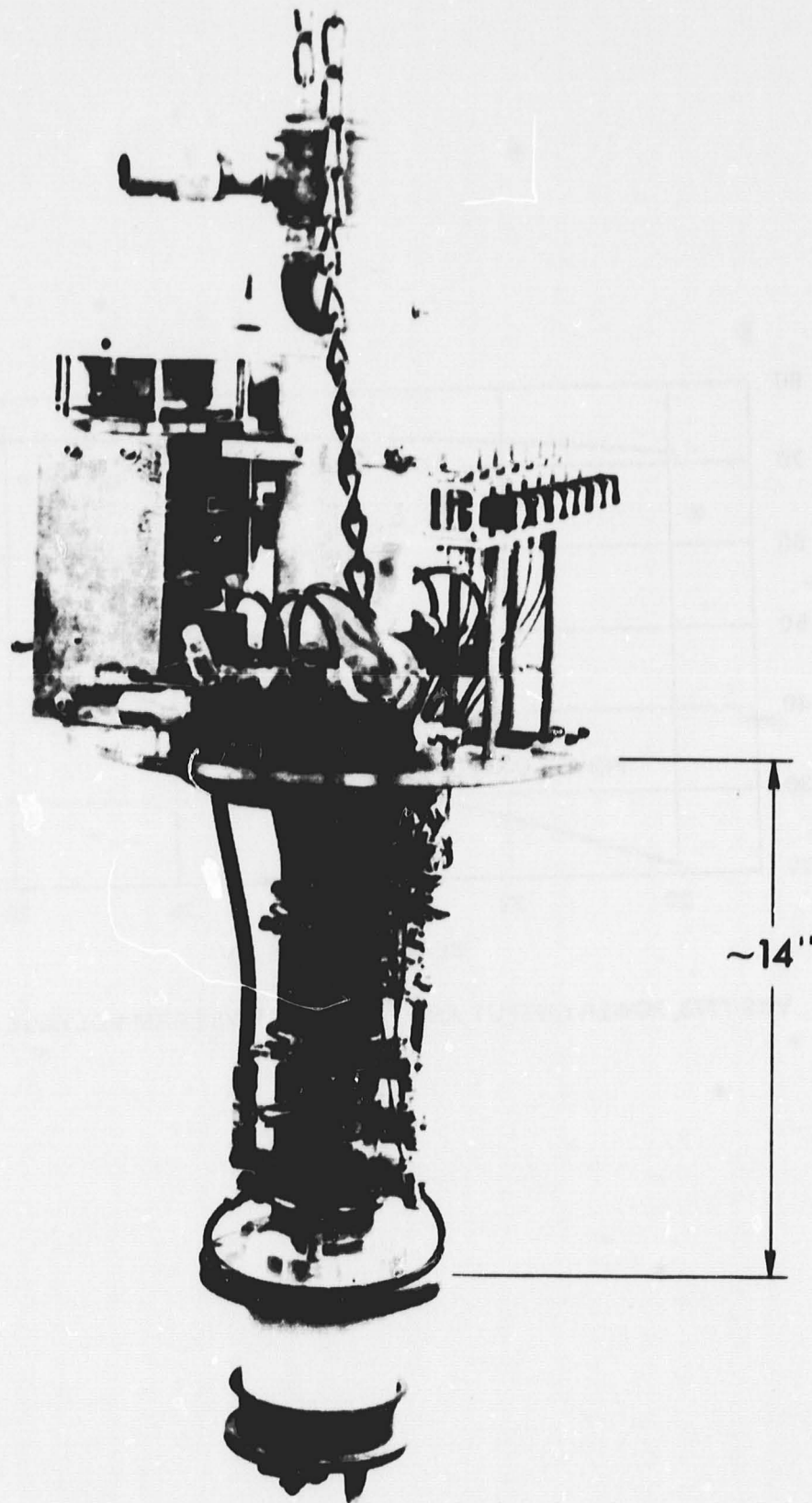
ISSUES :

- OUTPUT GAP / RADIATOR TEMPERATURE
- GAP FABRICATION

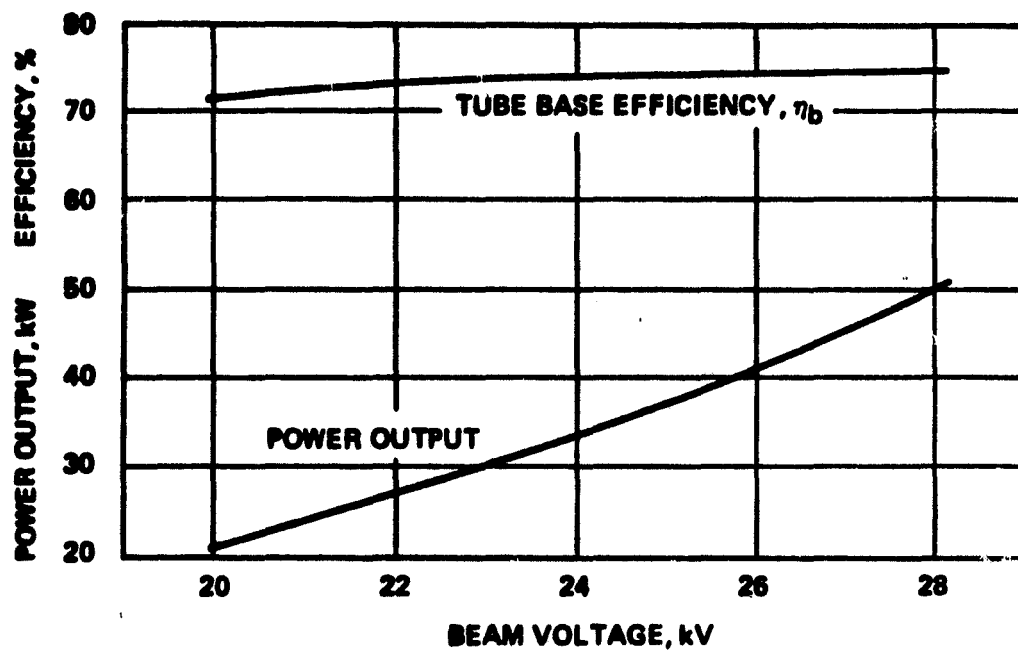
92
Klystron

A. D. LaRue
Varian

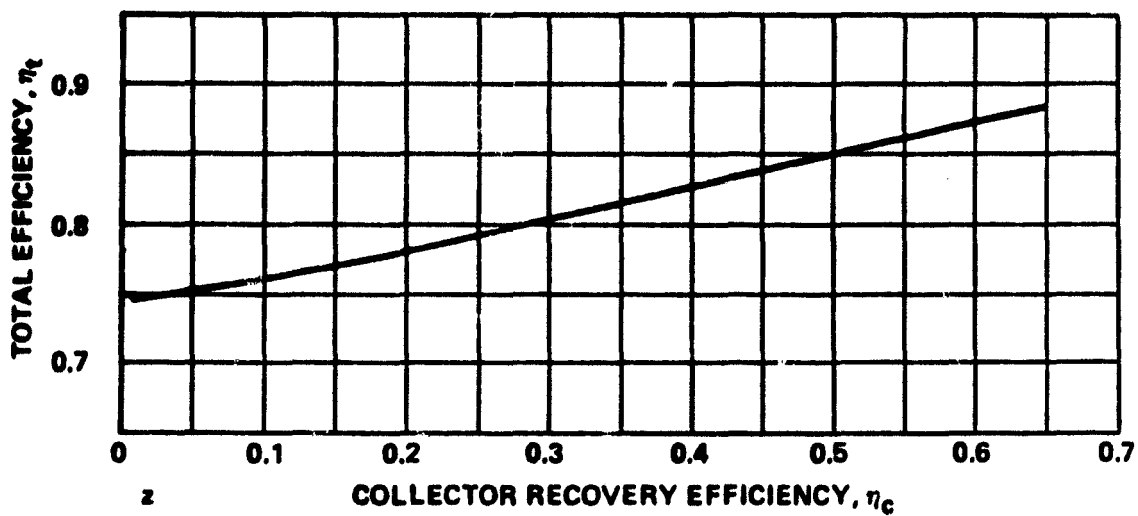
ORIGINAL PAGE IS
OF POOR QUALITY



VKS-7773 EXPERIMENTAL HIGH EFFICIENCY KLYSTRON CW AMPLIFIER
PRECEDING PAGE BLANK NOT FILMED



VKS-7773, POWER OUTPUT AND EFFICIENCY VS BEAM VOLTAGE

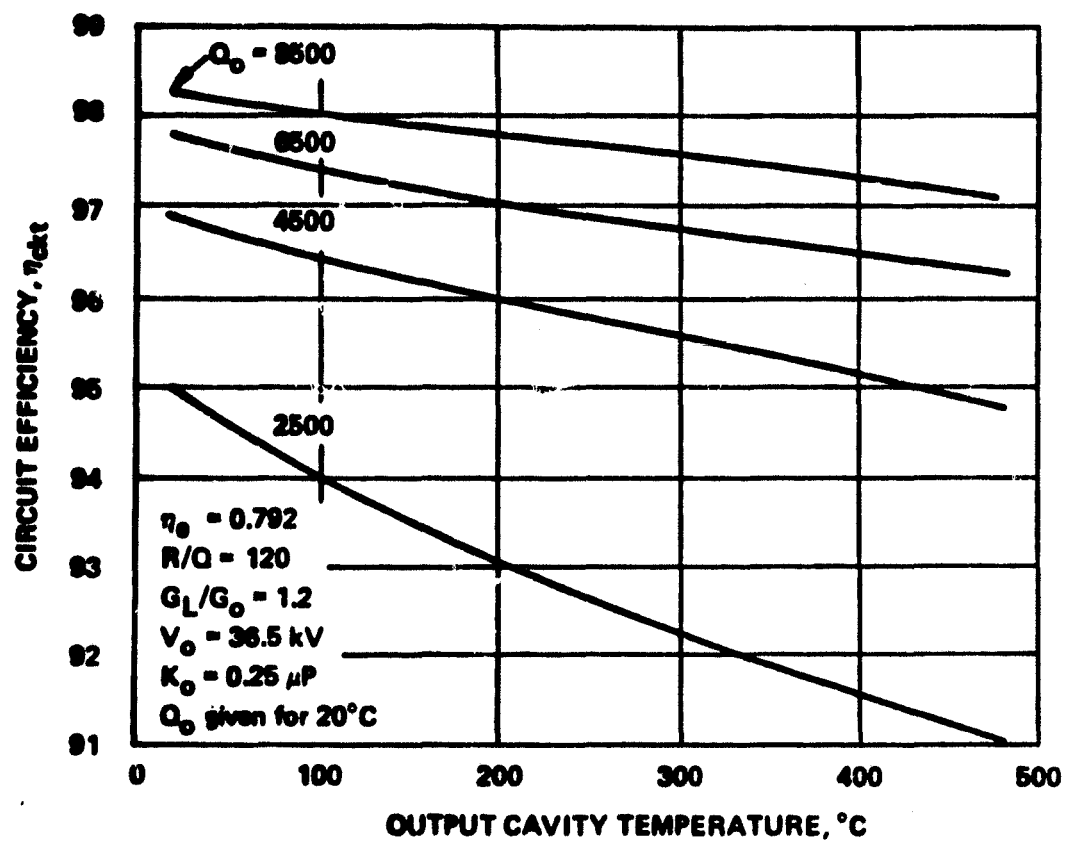


VA-7773, TOTAL EFFICIENCY WITH A DEPRESSED COLLECTOR

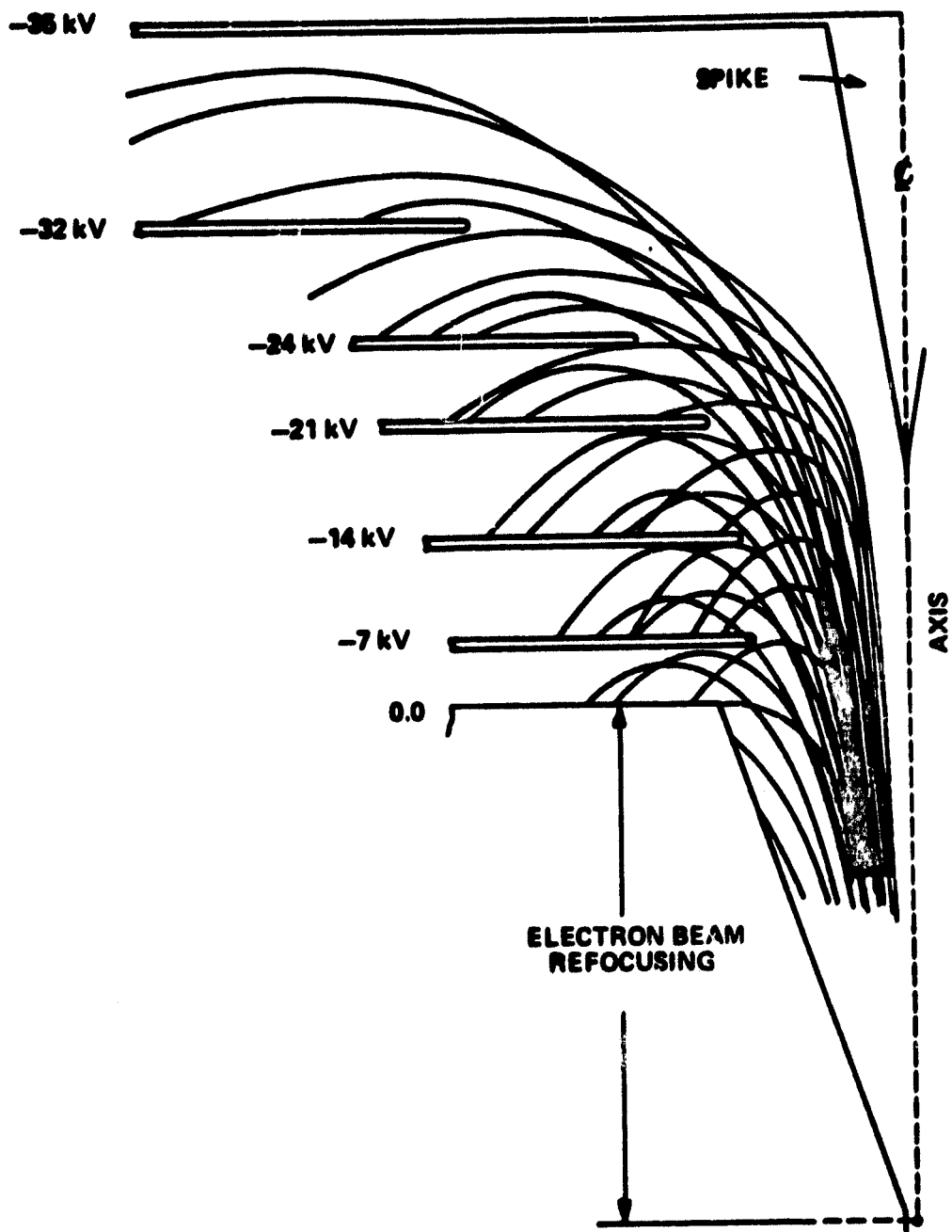
Klystron CW Amplifier Operating Characteristics

	<u>VKS-7773</u>	<u>New Design</u>
Frequency, GHz	2.45	2.45
Tuning, MHz	± 25	Fixed
Beam Voltage, kV	28	35
Mod-Anode Voltage, kV	--	17
Gun μ perveance	0.5	0.85
Beam μ perveance	0.5	0.3
Beam Current, A	2.4	1.96
Power Output, kW	50	52
Base Efficiency, η_b , %	74	77
Collector Efficiency, η_c , %	--	51*
Total Efficiency, η_t , %	--	85*
Saturated Gain, dB	50	50
Brillouin Field, B, Gauss	465	349

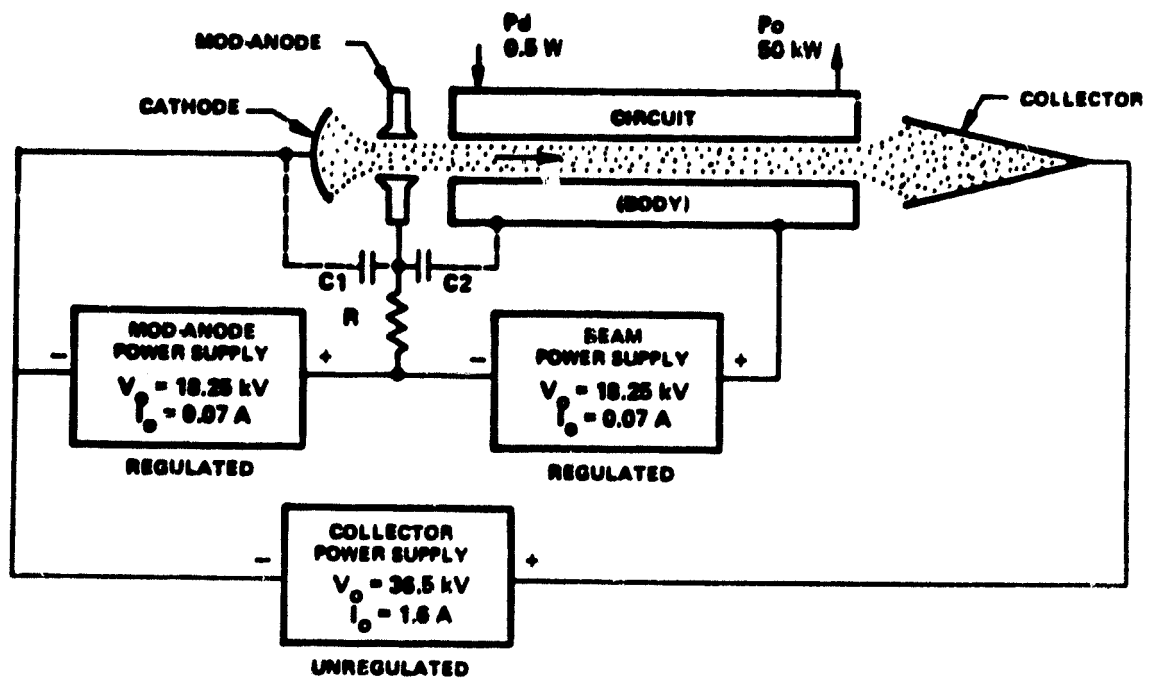
*With depressed collector assembly



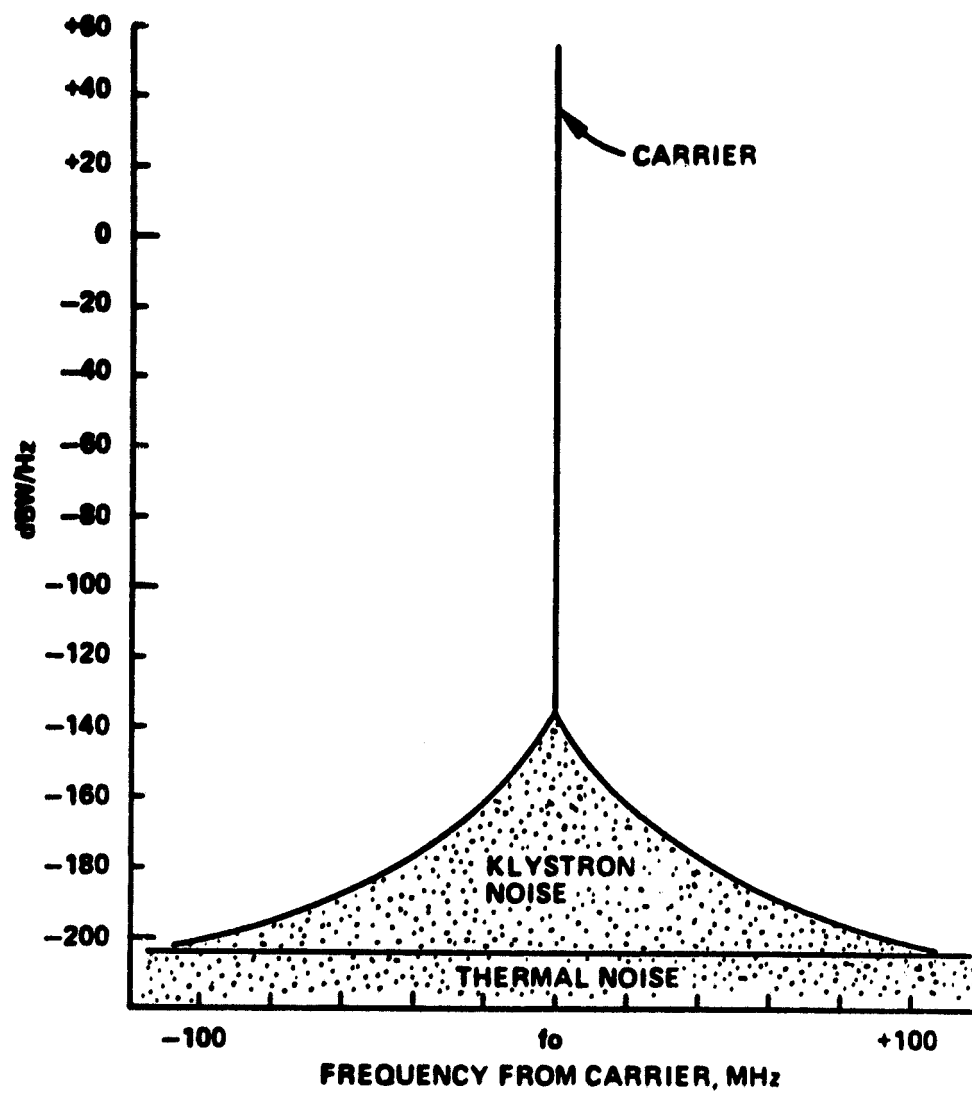
CIRCUIT EFFICIENCY VS OUTPUT CAVITY TEMPERATURE



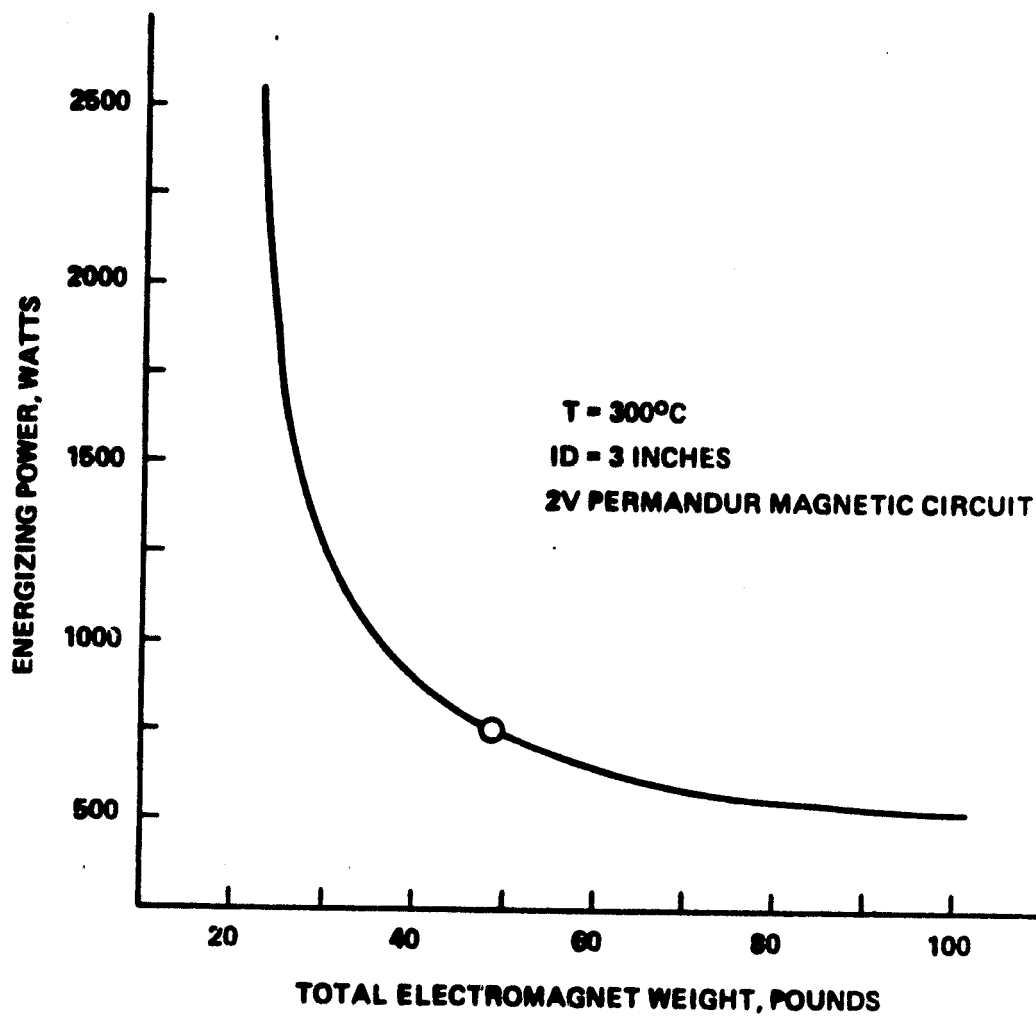
**EXAMPLE OF MULTISTAGE
DEPRESSED ELECTROSTATIC COLLECTOR**



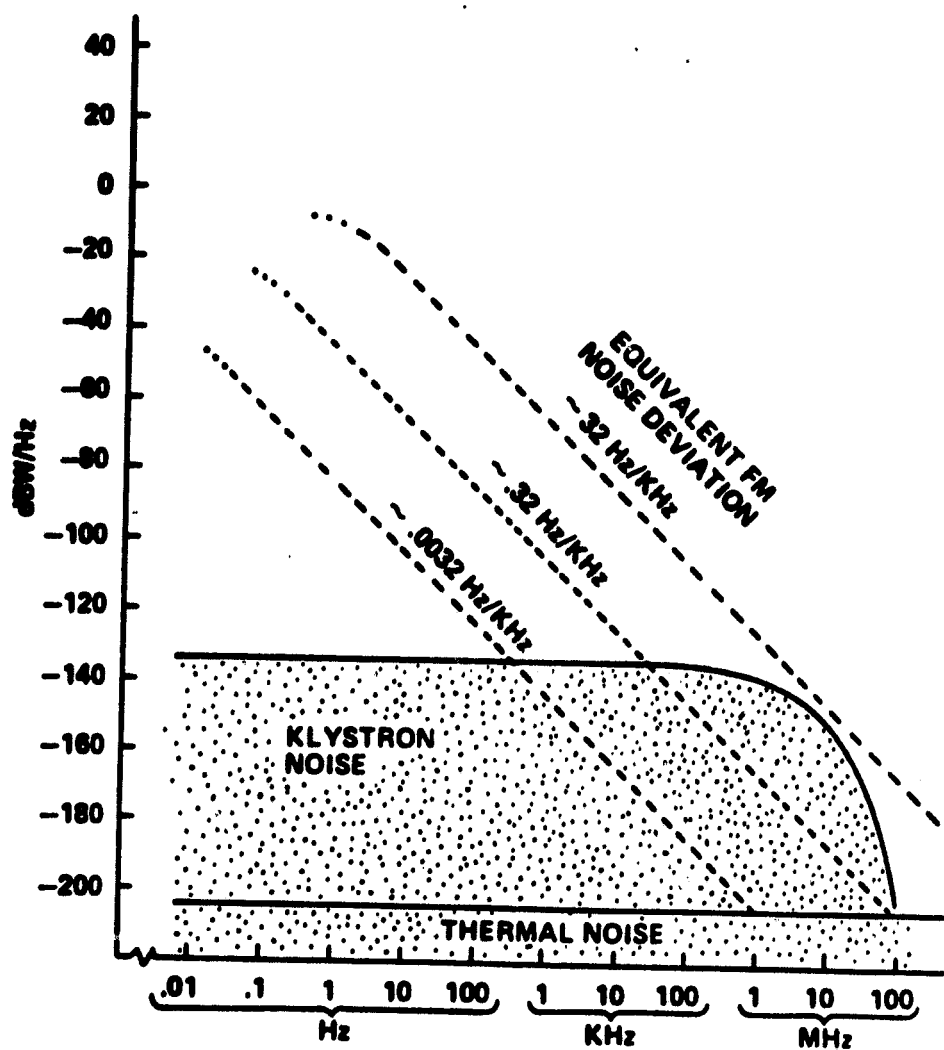
SIMPLIFIED DIAGRAM ILLUSTRATING THE KLYSTRON MOD-ANODE



COMPUTED KLYSTRON NOISE POWER SPECTRAL DENSITY



SPS KLYSTRON ELECTROMAGNET: ESTIMATED WEIGHT VS POWER TRADE-OFF



COMPUTED NOISE POWER SPECTRAL DENSITY FOR
KLYSTRON AND FOR THREE OSCILLATOR DRIVERS

Estimated Attenuation of Harmonic Filters

<u>Harmonic</u>	<u>3 ft Lossy Leaky Wall</u>	<u>Lossy "Tee"</u>	<u>Reactive Stub Array</u>
2nd	60 dB	8 dB	40 dB
3rd	40 dB	10 dB	30 dB
4th	15 dB	12 dB	20 dB
5th	10 dB	14 dB	10 dB
6th	5 dB	16 dB	5 dB

Estimate of Klystron Cooling Requirements

($P_o = 52 \text{ kW}$, $K_o = 0.3 \text{ uP}$)

<u>Klystron Element</u>	<u>Power, Watts</u>	<u>Maximum Temperature</u>
Heater	100	
Electromagnet	750	
RF Driver Cavities	887	
RF Output Cavity	1758	
Subtotal	3495	< 300°C
Collector Plates	6938	> 600°C
Total	10433	

VA-842 Klystron Life Data

Long-Lived VA-842 Klystrons

<u>S/N</u>	<u>Status</u>	<u>Hours</u>	<u>Years</u>
408	Still Running	144,883	16.5
393	Still Running	139,993	16.0
374	Still Running	133,469	15.2
511	Still Running	123,384	14.1
317	Failed 12/75	121,303	13.8
332	Failed 8/76	108,777	12.4
505	Failed 12/74	102,259	11.7

Calculated MTBF (68 tubes) = 37,748 hours

Data from USAF "Electron Inventory Report", 30 June 1979

Advantages of High Efficiency Klystron CW Amplifier for Space Applications

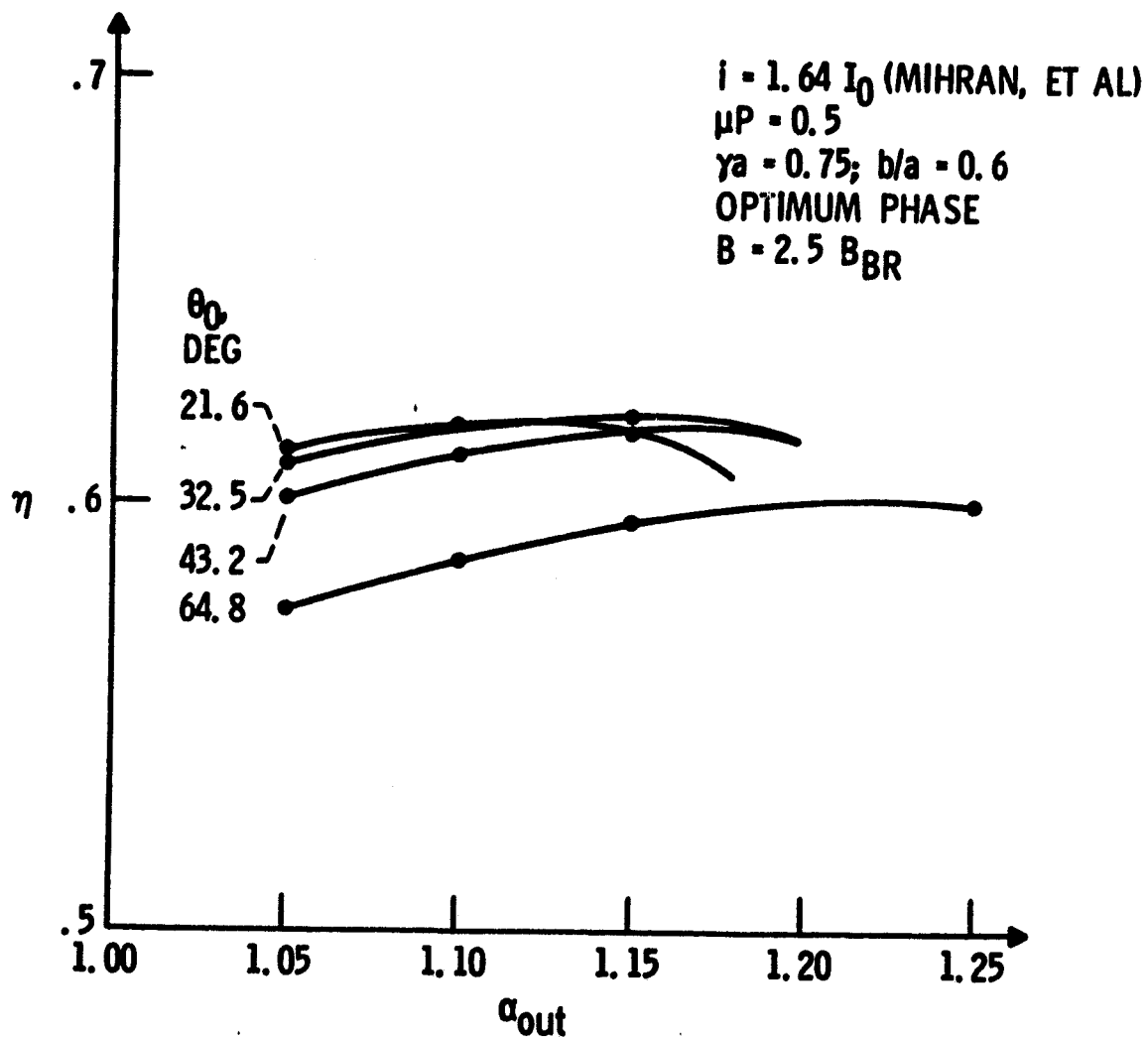
1. High Gain Amplifier, 40 to 50 dB
2. High Power Output, 50 kW or more
3. High Efficiency, ~85% with collector depression
4. Low Noise Output Narrow bandwidth klystron
5. Low Harmonic Output Typically -30 dB or more from carrier
6. Long Life Potential ~16.5 years on record with one klystron type
7. Ease of Control and Protection with Mod-Anode Electron Gun Design

D3

Klystron Efficiency and Cathode Life

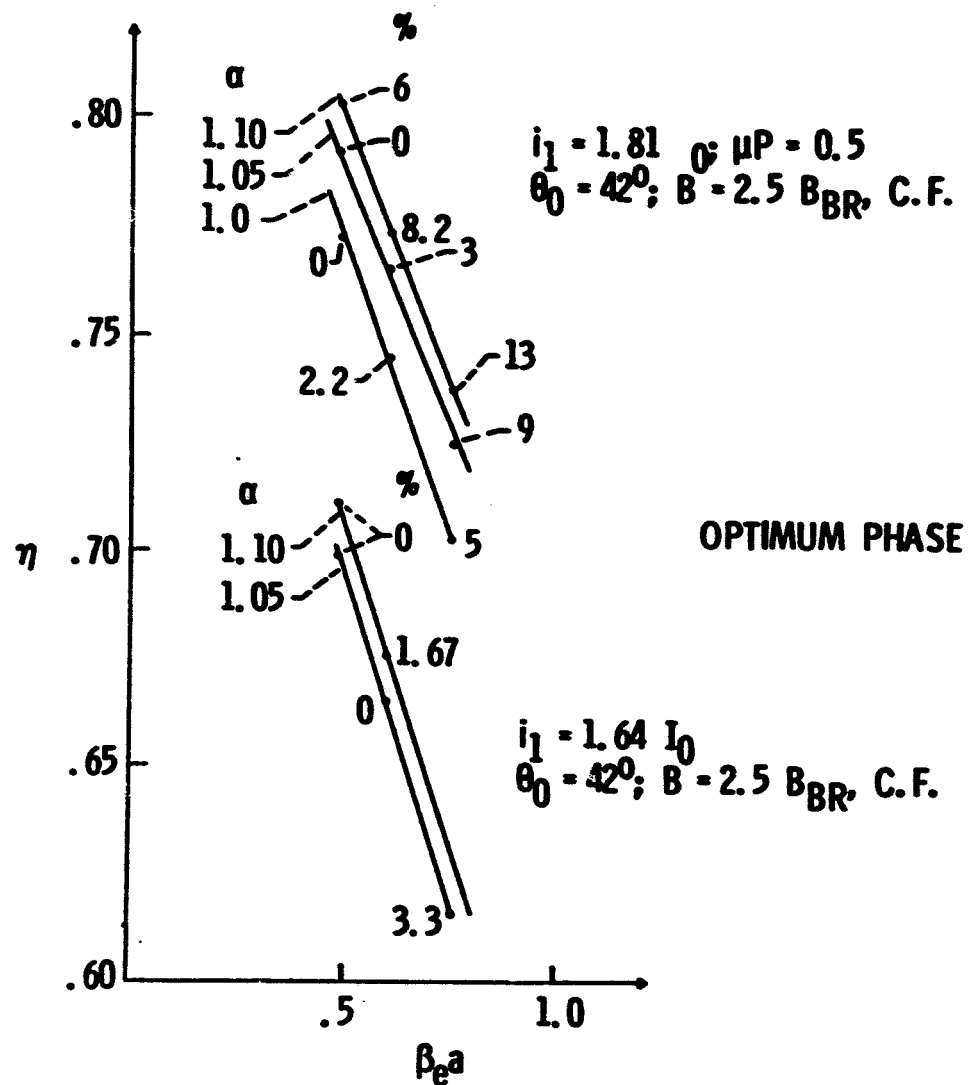
***Dr. Henry Kosmahl
Lewis Research Center***

EFFICIENCY VS OUTPUT VOLTAGE $\alpha = \hat{V}/V_0$ WITH
 OUTPUT GAP ANGLE θ_0 AS PARAMETER
 PHASE ADJUSTED FOR HIGHEST EFFICIENCY

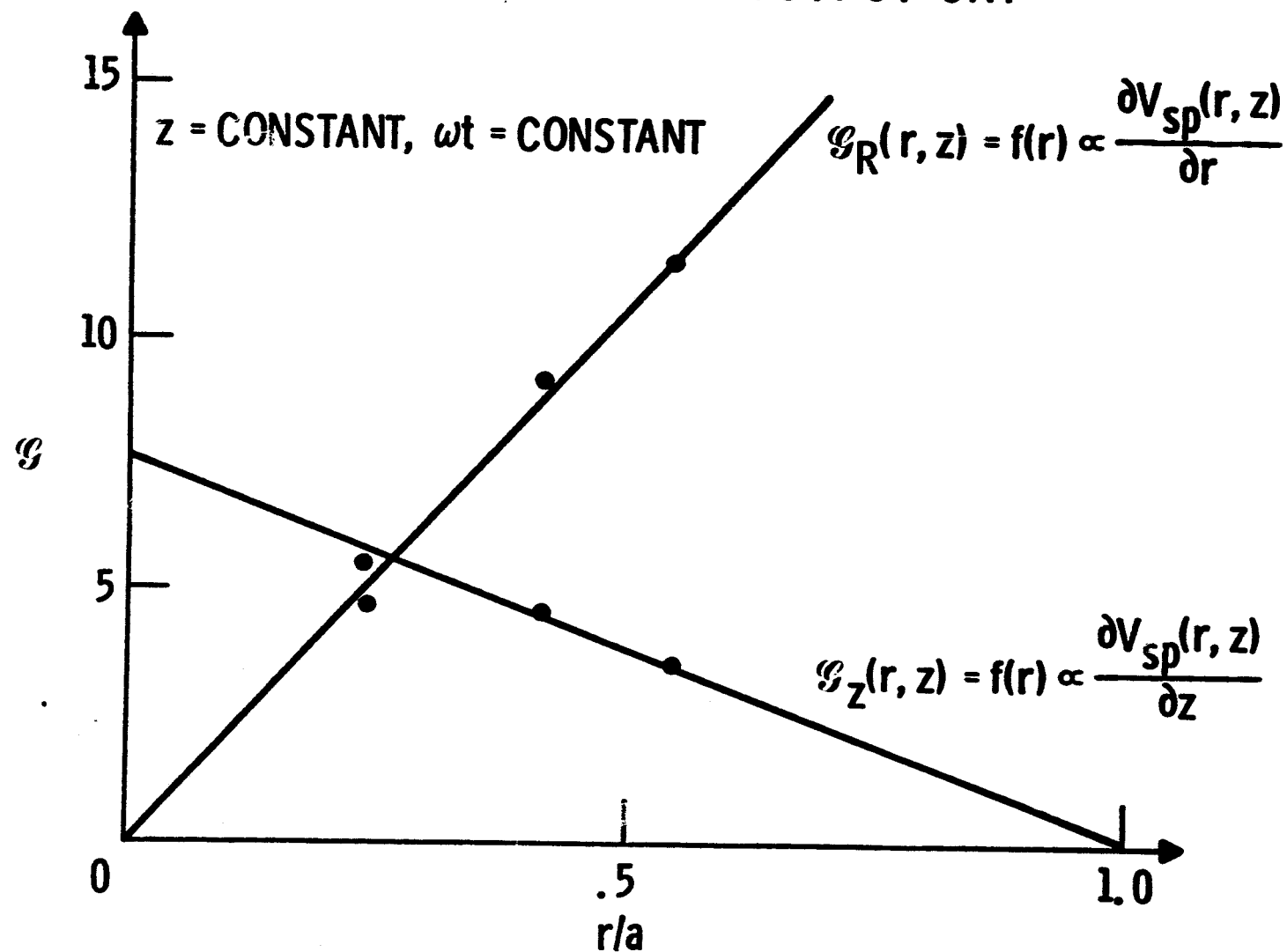


PRECEDING PAGE BLANK NOT FILMED

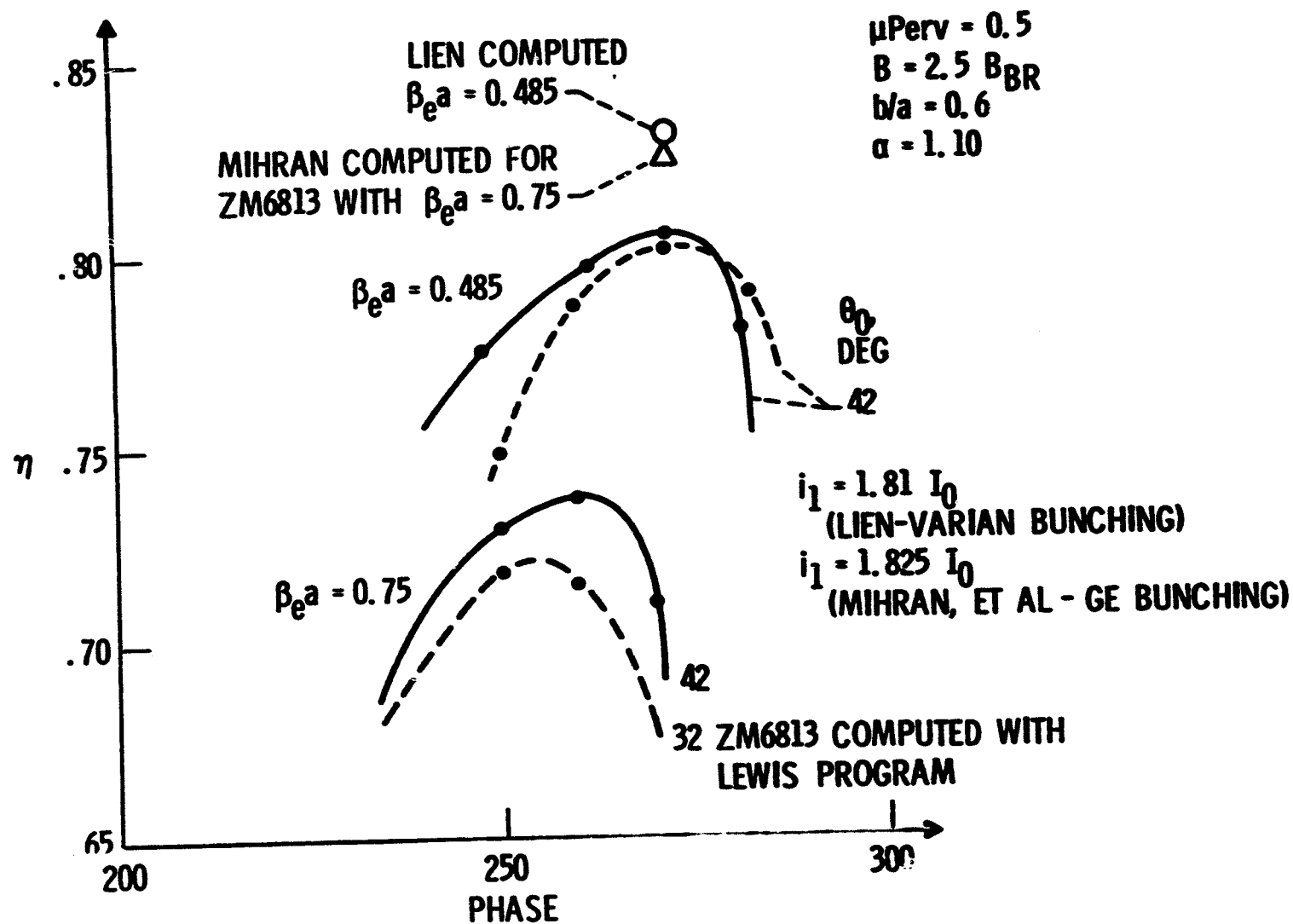
EFFICIENCY VS $\beta_e a$ WITH VOLTAGE SWING α AS PARAMETER
CURRENT INTERCEPTION IS LISTED IN % POINTS



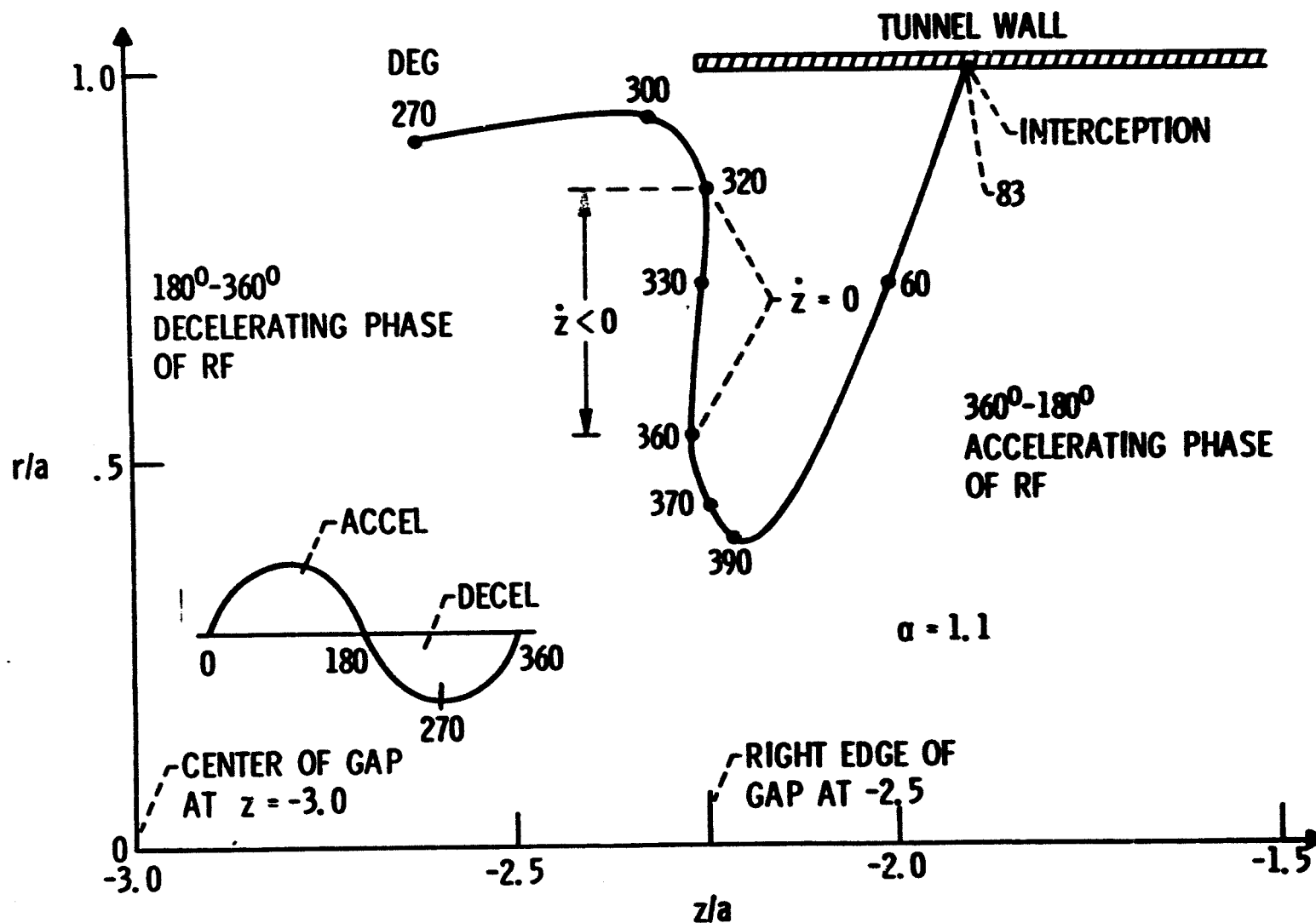
TYPICAL AXIAL AND RADIAL SPACE CHARGE FUNCTIONS OF THE BEAM IN THE OUTPUT GAP



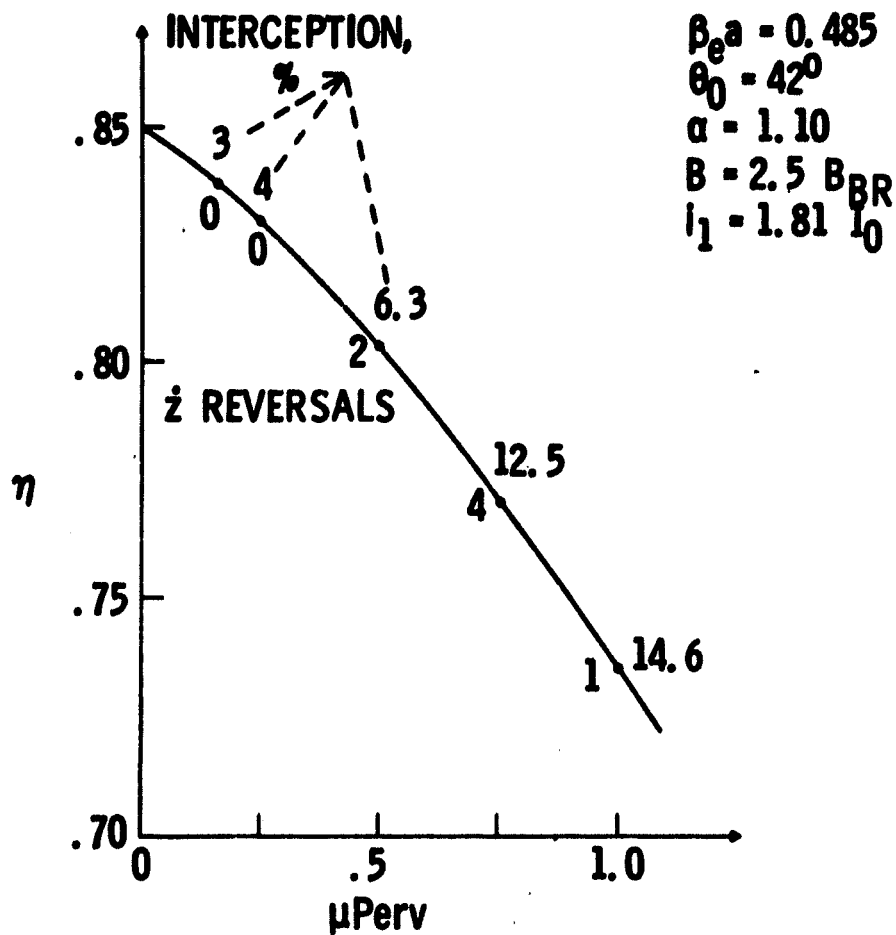
INTERNAL CONVERSION EFFICIENCY COMPUTED WITH LEWIS PROGRAM FOR GE AND VARIAN HIGH EFFICIENCY DESIGNS



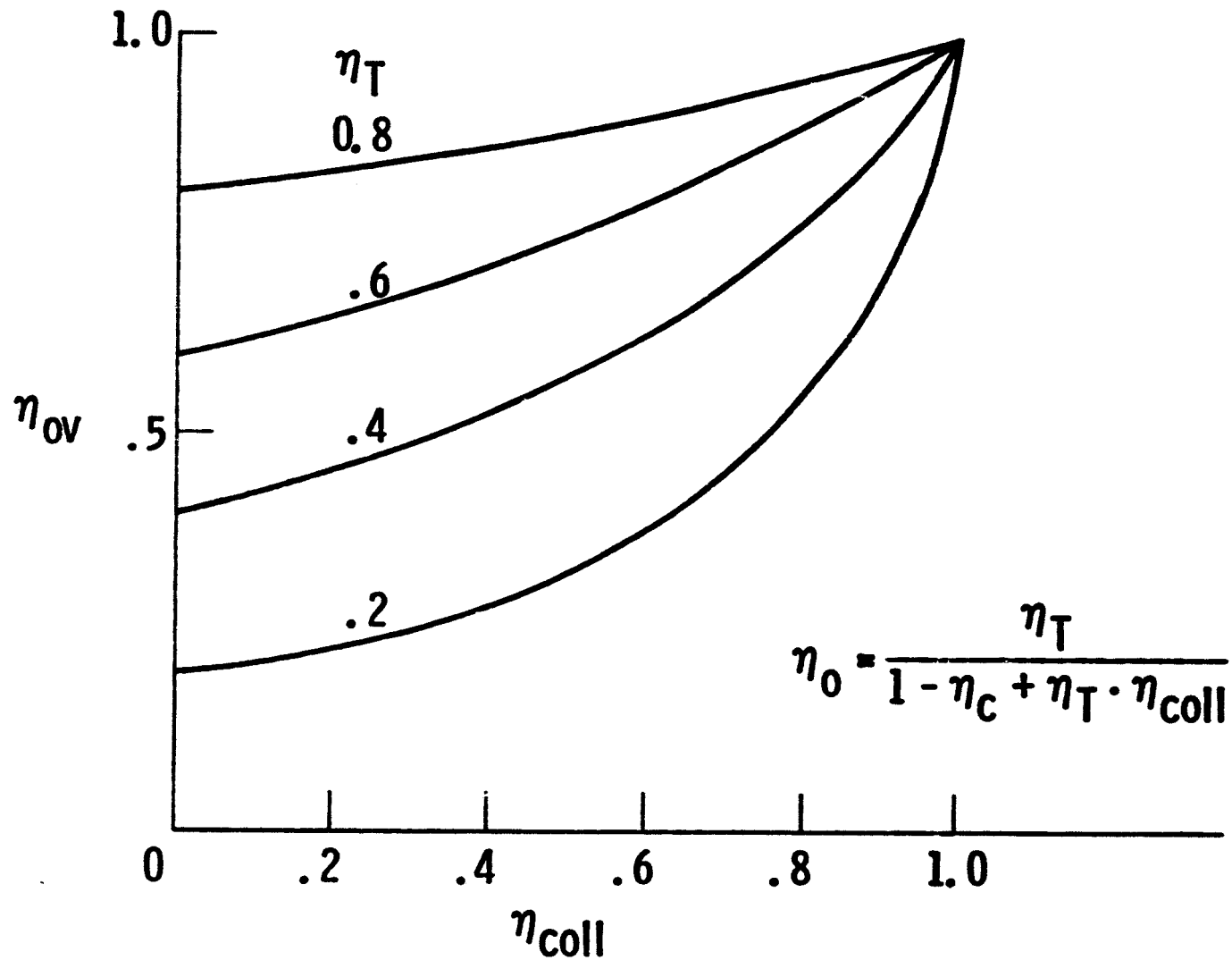
42



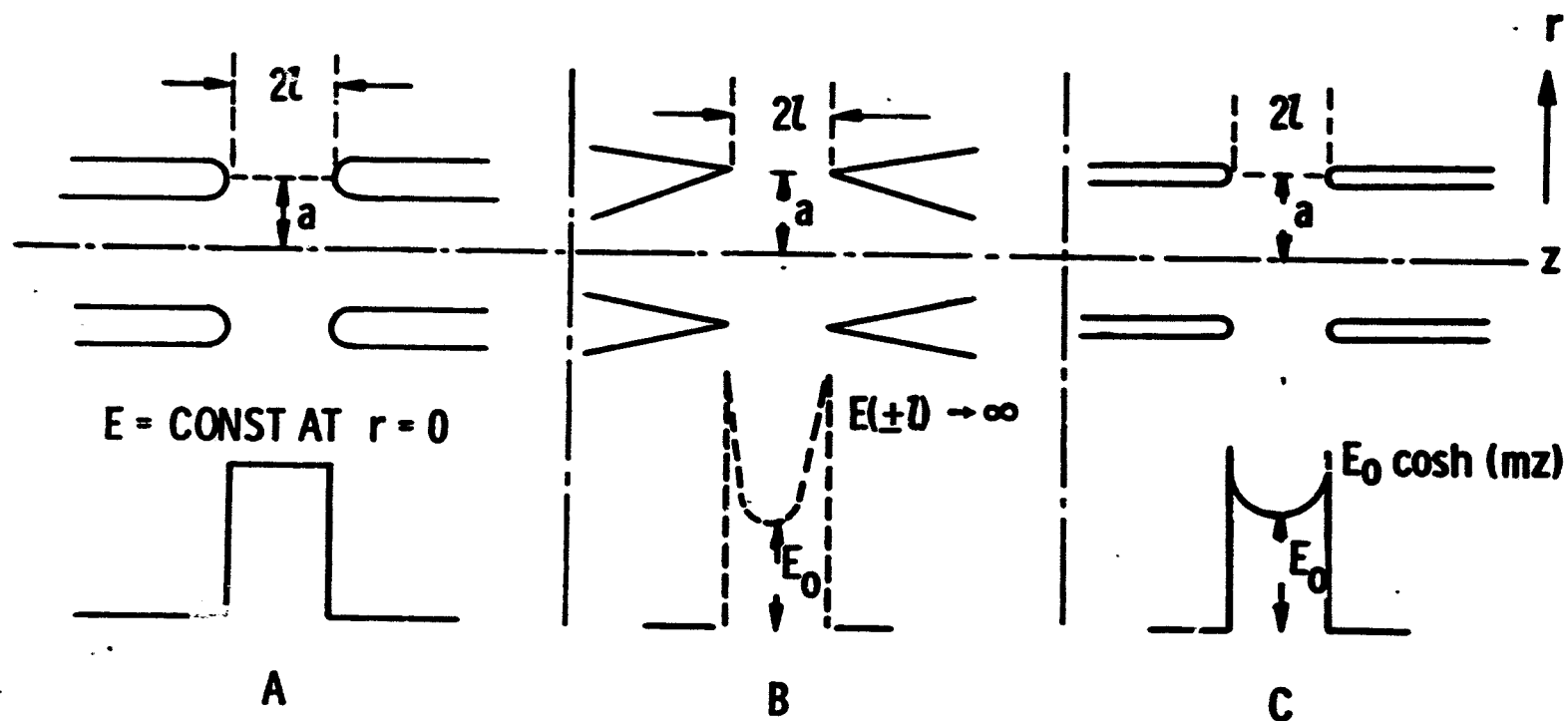
**EFFICIENCY VS PERVEANCE ASSUMING
CONSTANT BUNCHING LEVEL
INTERCEPTIONS & VELOCITY REVERSALS ARE
LISTED AT COMPUTED POINTS**



OVERALL EFFICIENCY VS COLLECTOR EFFICIENCY



ELECTRIC FIELD SHAPE BETWEEN REENTRANT TUNNEL TIPS A - CONSTANT FIELD; B - "KNIFE EDGE" FIELD; C - ACTUAL FIELD



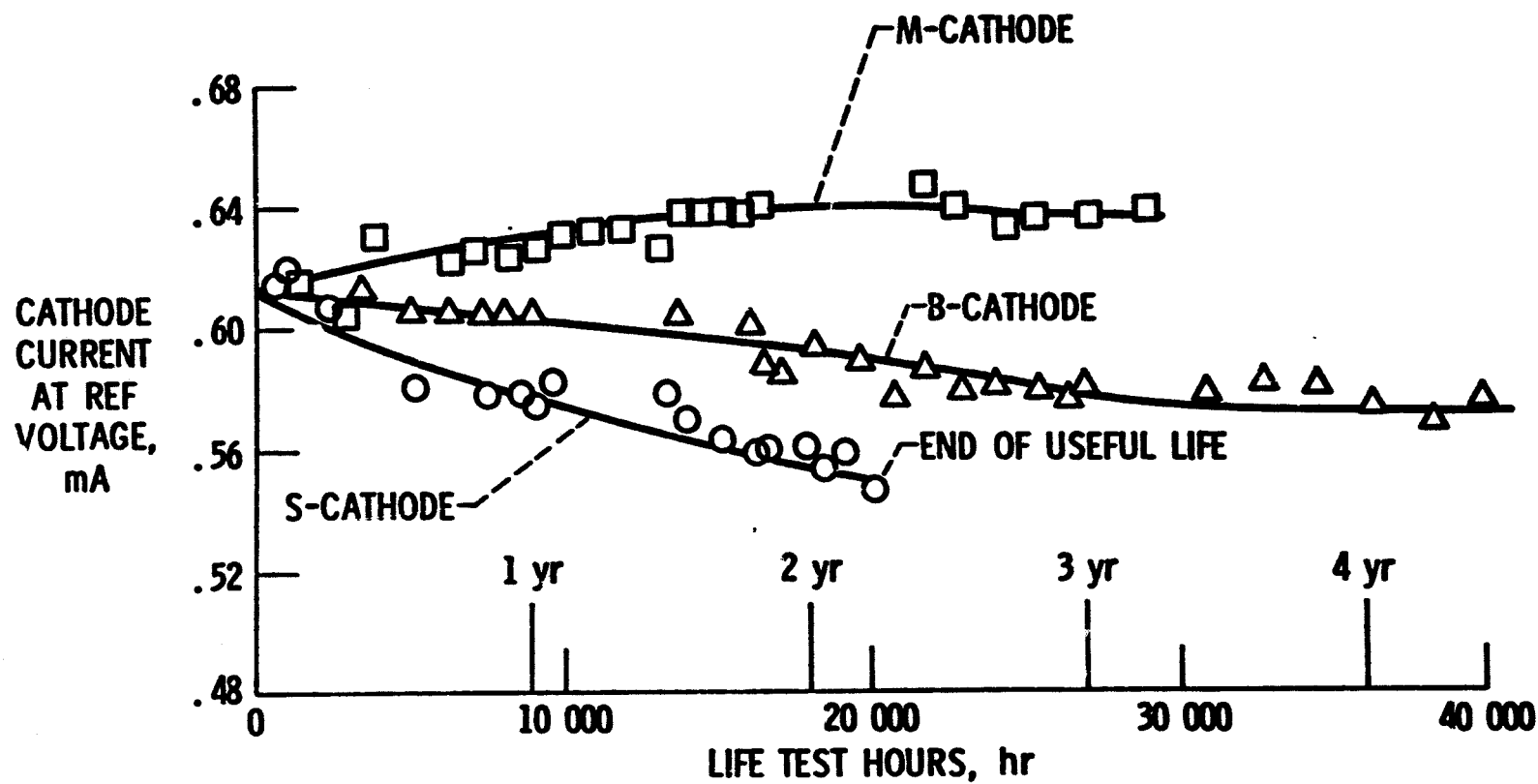
COMPARISON BETWEEN MEASURED & LEWIS COMPUTED EFFICIENCIES & INTERCEPTIONS FOR A VARIAN DESIGN

$$i_1 = 1.81 I_0; \beta_e a = 0.485; \mu_{Perv} = 0.5$$

α	MEASURED (LIEN)		LEWIS COMPUTED	
	η	INT, %	η	INT, %
1.08	0.751	1.9	0.775	1.5
0.953	0.705	1.6	0.709	0.5
0.903	0.681	1.4	0.679	0

LIFE TEST STUDY OF STATE-OF-ART CATHODES

2 A/cm²



$$\frac{V_{\min}}{V_0} = 1 - f(\mu_{\text{perv}}) \cdot \sqrt[3]{\eta_e \cdot \mu_{\text{perv}}}$$

$$\eta_{\text{col}} = \eta_{\text{DC}} \left[1 - \frac{1}{N-1} \frac{f(\mu_{\text{perv}}) \sqrt[3]{\eta_e \cdot \mu_{\text{perv}}}}{2 - f(\mu_{\text{perv}}) \cdot \sqrt[3]{\eta_e \cdot \mu_{\text{perv}}}} \right].$$

$$\eta_{\text{OV}} = \frac{\eta_{\text{CK}} \cdot \eta_e}{1 - \eta_{\text{col}} + \eta_{\text{col}} \left(\eta_e + \frac{P_{\text{INT}}}{P_0} \right) + \frac{P_{\text{SOL}}}{P_0}}$$

*Progress Report on the Adapting
of the Cross-field Directional
Amplifier to the Requirements
of the Solar Power Satellite*

*W. C. Brown
Raytheon*

PRECEDING PAGE BLANK NOT FILMED

OUTLINE OF PRESENTATION

- **CROSSED-FIELD DEVICE FEATURES OF INTEREST IN SPS**
- **OPERATING PRINCIPLES OF AMPLITRON AND MAGNETRON DIRECTIONAL AMPLIFIER**
- **ARCHITECTURAL INTERFACE OF MAGNETRON DIRECTIONAL AMPLIFIER AND SYSTEM**
- **CONTROL OF THE PHASE AND AMPLITUDE OF THE MICROWAVE OUTPUT**
- **SIGNAL-TO-NOISE RATIO PERFORMANCE**
- **DISCUSSION OF POTENTIAL FOR LONG TUBE LIFE**
- **DISCUSSION OF EFFICIENCY**
- **AREAS OF CONCERN NEEDING ADDITIONAL ATTENTION**

OUTLINE OF PRESENTATION

- **CROSSED-FIELD DEVICE FEATURES OF INTEREST IN SPS**

- **OPERATING PRINCIPLES OF AMPLITRON AND MAGNETRON DIRECTIONAL AMPLIFIER**

- **ARCHITECTURAL INTERFACE OF MAGNETRON DIRECTIONAL AMPLIFIER AND SYSTEM**
- **CONTROL OF THE PHASE AND AMPLITUDE OF THE MICROWAVE OUTPUT**
- **SIGNAL-TO-NOISE RATIO PERFORMANCE**
- **DISCUSSION OF POTENTIAL FOR LONG TUBE LIFE**
- **DISCUSSION OF EFFICIENCY**
- **AREAS OF CONCERN NEEDING ADDITIONAL ATTENTION**

- HIGH EFFICIENCY
- HIGH SIGNAL TO NOISE RATIO
- POTENTIAL LIFE OF 50 YEARS OR MORE
- LOW RATIO OF MASS TO MICROWAVE POWER OUTPUT
- ACCURATE CONTROL OF THE PHASE AND AMPLITUDE OF THE MICROWAVE POWER OUTPUT
- POTENTIAL TO PERFORM THE BULK OF THE SYSTEM POWER CONDITIONING REQUIREMENTS
- MINIMAL X-RAY RADIATION
- ONLY ONE VOLTAGE AND TWO TERMINALS REQUIRED FOR NORMAL MICROWAVE TUBE OPERATION
- SIMPLICITY OF CONSTRUCTION
- HIGH DEGREE OF MATURATION IN PRODUCTION AND COST

- High Efficiency: Overall efficiencies in excess of 85% have been demonstrated in an off-the-shelf magnetron used for industrial microwave heating and in certain laboratory models of the amplatron. An efficiency in excess of 80% at power levels (3 kW) low enough to utilize passive cooling has also been obtained.
- High Signal to Noise Ratio: Random noise level in a 1 MHz band down 100 dB or more at frequencies above and below carrier frequency by more than 10 MHz. The noise level may be lower because instrumentation is the limitation.

- Potential Life of 50 Years or More: Such life is possible by operating at low emission current densities that allow the low operating temperatures that have a proven association with extremely long life of carburized thoriated tungsten cathodes.
- Low Ratio of Mass to Microwave Power Output: The current estimate by the author is 0.4 kilograms per kilowatt of microwave power at the tube output. This includes the weight of the passive radiator but not the buck-boost coils which are considered a power conditioning function.

- Accurate Control of the Phase and Amplitude of the Microwave Power Output: By use of a set of phase and amplitude references and a set of phase and amplitude sensors the phase can be controlled to within ± 1 degrees and amplitude to within $\pm 3\%$.
- Potential to Perform the Bulk of the System Power Conditioning Requirements: The buck-boost coils necessary for output amplitude control of the magnetron can take on the added function of adjusting the input of the microwave system to operate at the optimum output voltage for the solar array.

- Minimal X-Ray Radiation: The crossed-field tube energy conversion mechanism generates negligible radiation, permitting maintenance functions during operation of the SPS.
- Only One Voltage and Two Terminals Required for Normal Microwave Tube Operation: Auxiliary power is required for a few seconds to heat up the cathode and initiate emission.

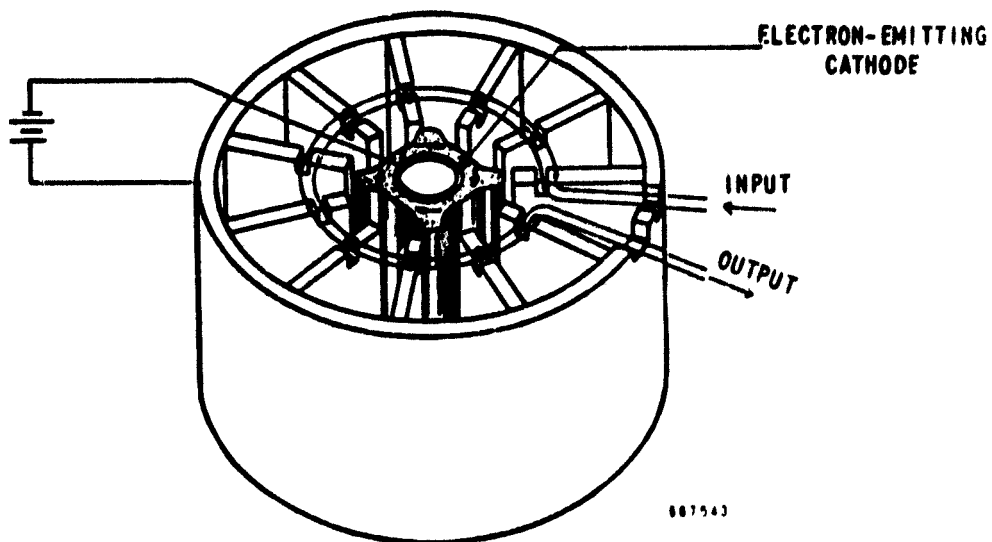
- Simplicity of Construction: The crossed-field device, particularly in its magnetron form, is very simple in construction.
- High Degree of Maturation in Production and Cost: Currently, more than two million magnetrons that closely resemble a similar tube for the SPS are manufactured annually for the microwave oven.

OUTLINE OF PRESENTATION

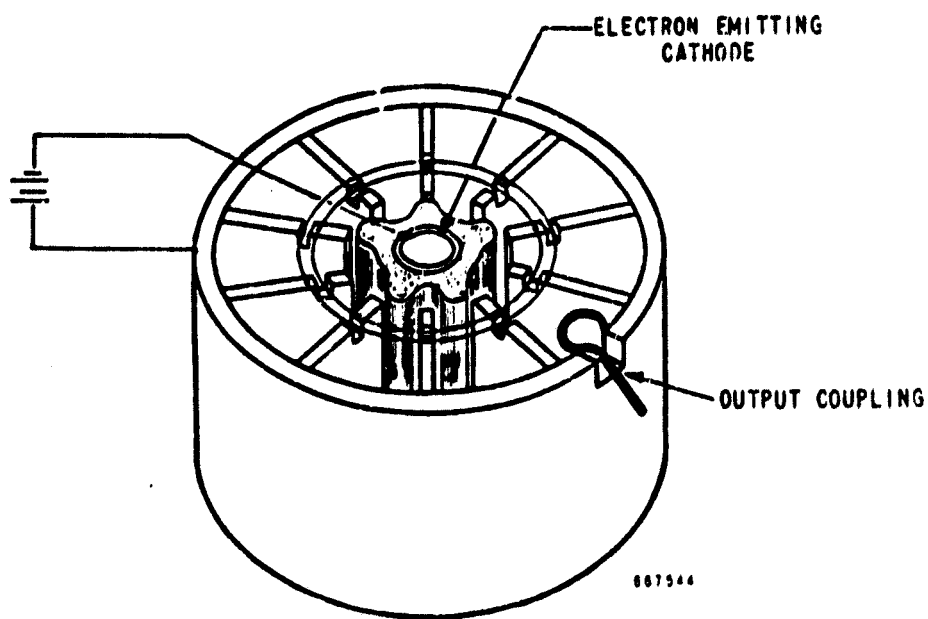
- **CROSSED-FIELD DEVICE FEATURES OF INTEREST IN SPS**

- **OPERATING PRINCIPLES OF AMPLITRON AND MAGNETRON DIRECTIONAL AMPLIFIER**

- **ARCHITECTURAL INTERFACE OF MAGNETRON DIRECTIONAL AMPLIFIER AND SYSTEM**
- **CONTROL OF THE PHASE AND AMPLITUDE OF THE MICROWAVE OUTPUT**
- **SIGNAL-TO-NOISE RATIO PERFORMANCE**
- **DISCUSSION OF POTENTIAL FOR LONG TUBE LIFE**
- **DISCUSSION OF EFFICIENCY**
- **AREAS OF CONCERN NEEDING ADDITIONAL ATTENTION**

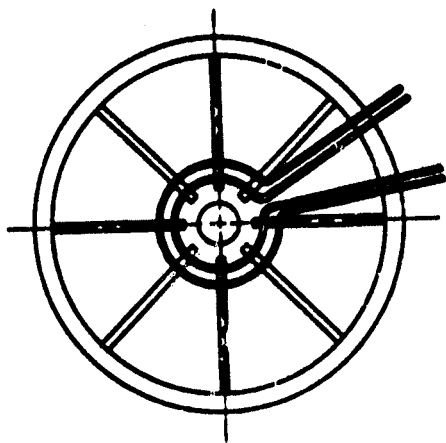


a

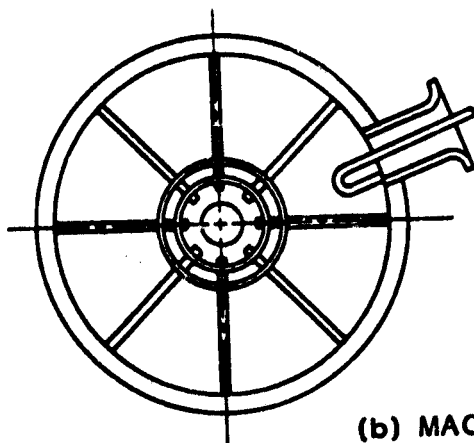
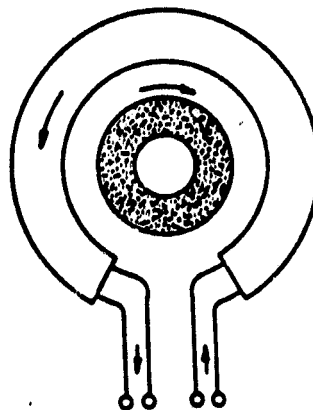


b

**DIAGRAM ILLUSTRATING THE BASIC DIFFERENCES OF CONSTRUCTION
AND OPERATION BETWEEN THE AMPLITRON AND THE MAGNETRON**

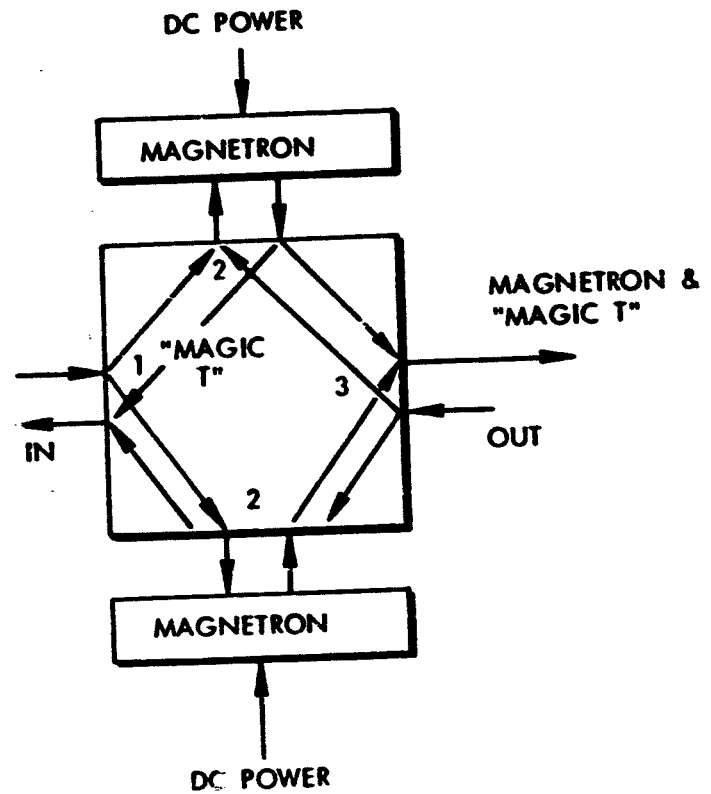
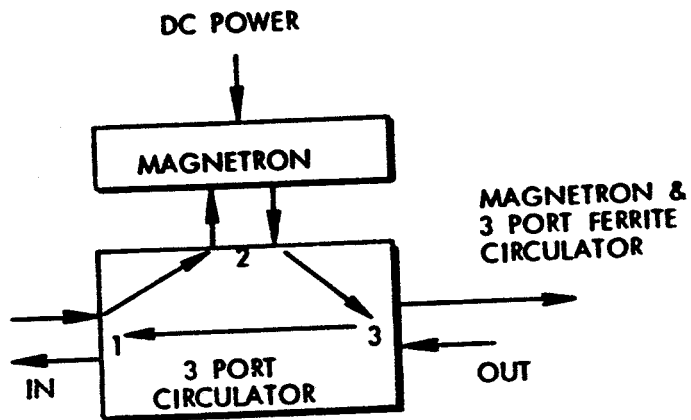
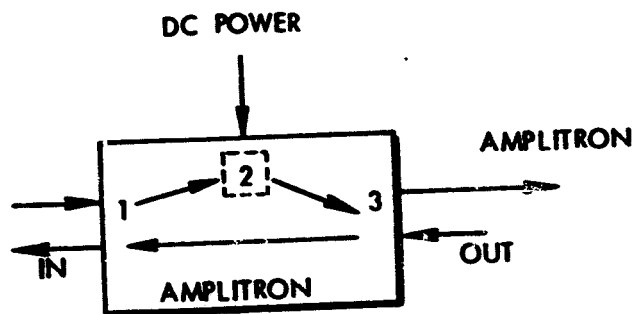


(a) AMPLITRON



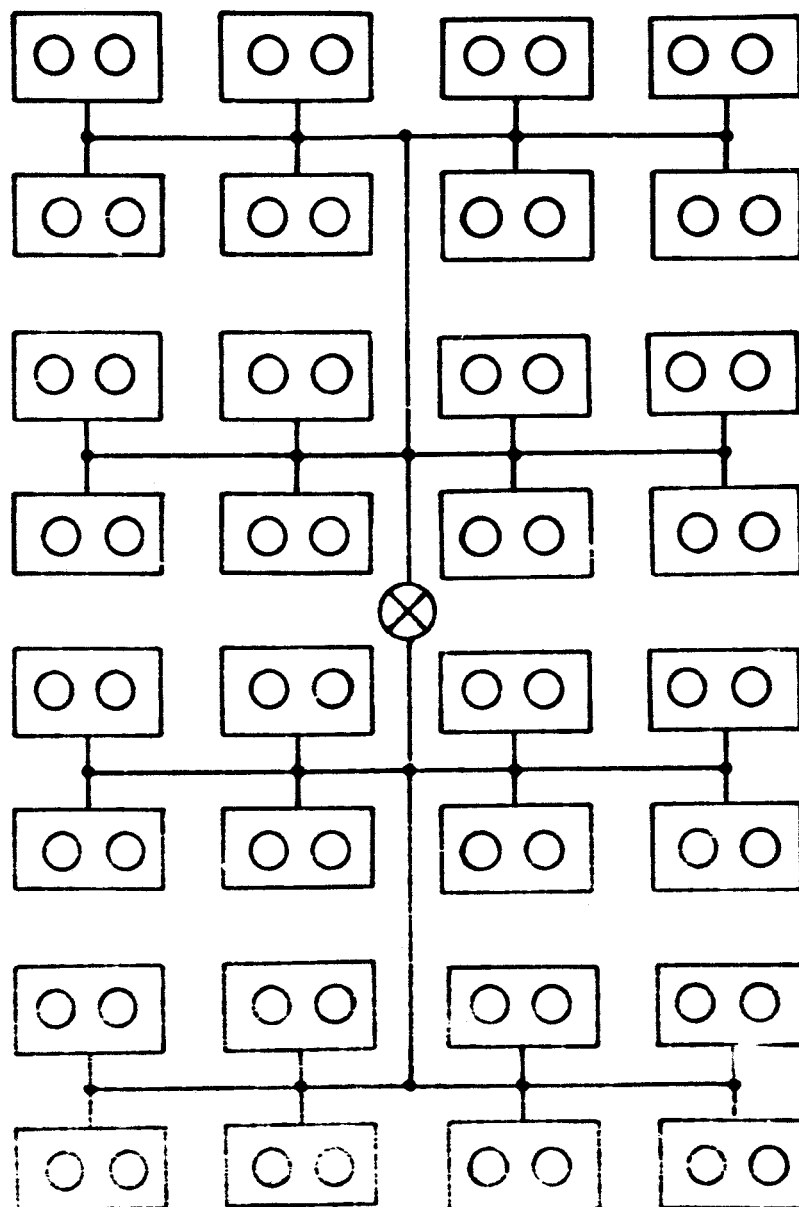
(b) MAGNETRON

DIRECTIONAL AMPLIFIER APPROACH



OUTLINE OF PRESENTATION

- **CROSSED-FIELD DEVICE FEATURES OF INTEREST IN SPS**
- **OPERATING PRINCIPLES OF AMPLITRON AND MAGNETRON DIRECTIONAL AMPLIFIER**
- **ARCHITECTURAL INTERFACE OF MAGNETRON DIRECTIONAL AMPLIFIER AND SYSTEM**
- **CONTROL OF THE PHASE AND AMPLITUDE OF THE MICROWAVE OUTPUT**
- **SIGNAL-TO-NOISE RATIO PERFORMANCE**
- **DISCUSSION OF POTENTIAL FOR LONG TUBE LIFE**
- **DISCUSSION OF EFFICIENCY**
- **AREAS OF CONCERN NEEDING ADDITIONAL ATTENTION**

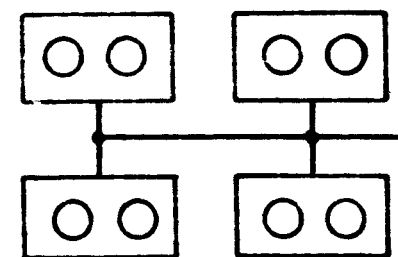


**SCHEMATIC OF SUBARRAY
MADE FROM SUBSECTIONS**

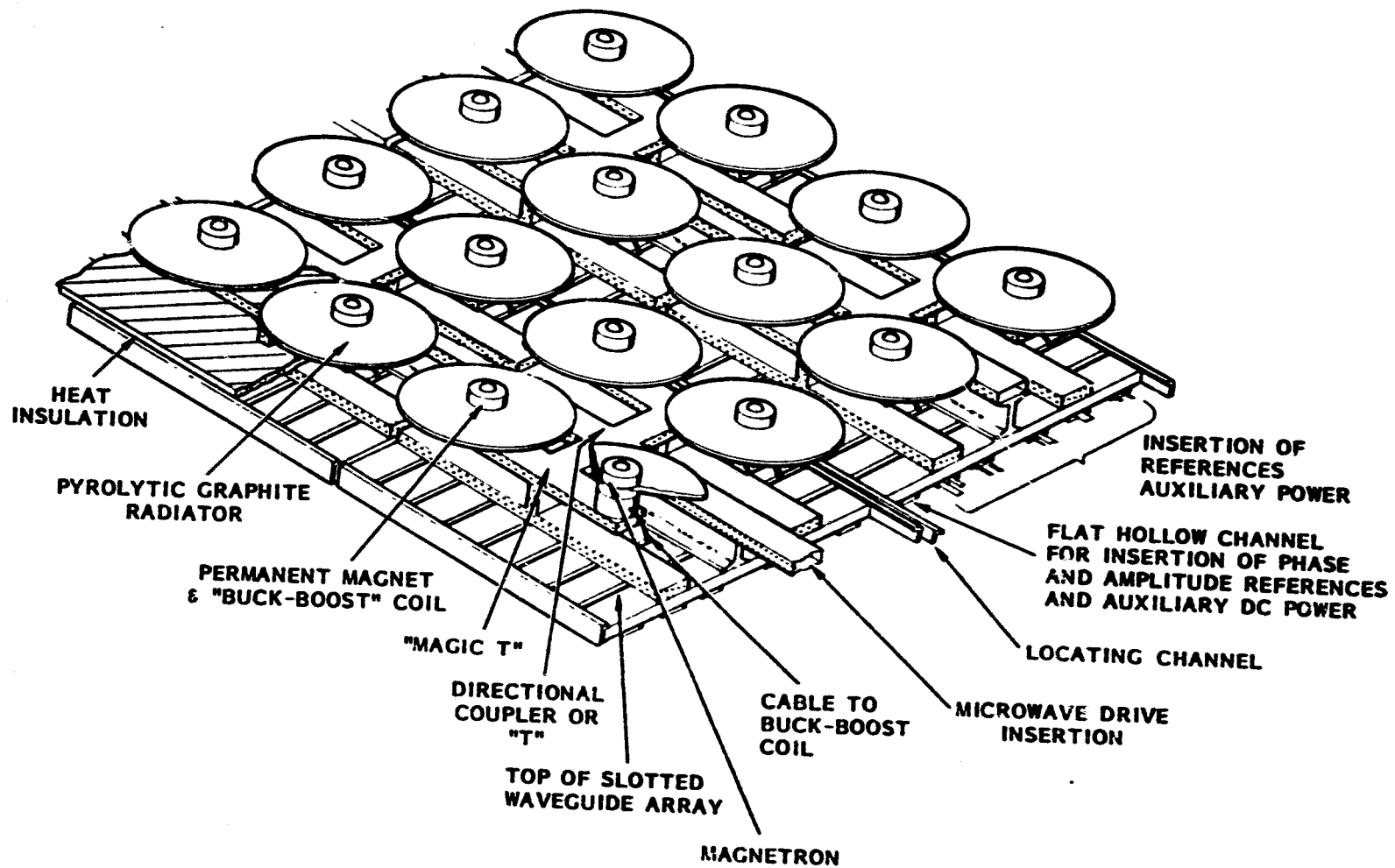
⊗ SOURCE OF RF DRIVE,
PHASE AND AMPLITUDE
REFERENCES, AND
AUXILIARY DC POWER

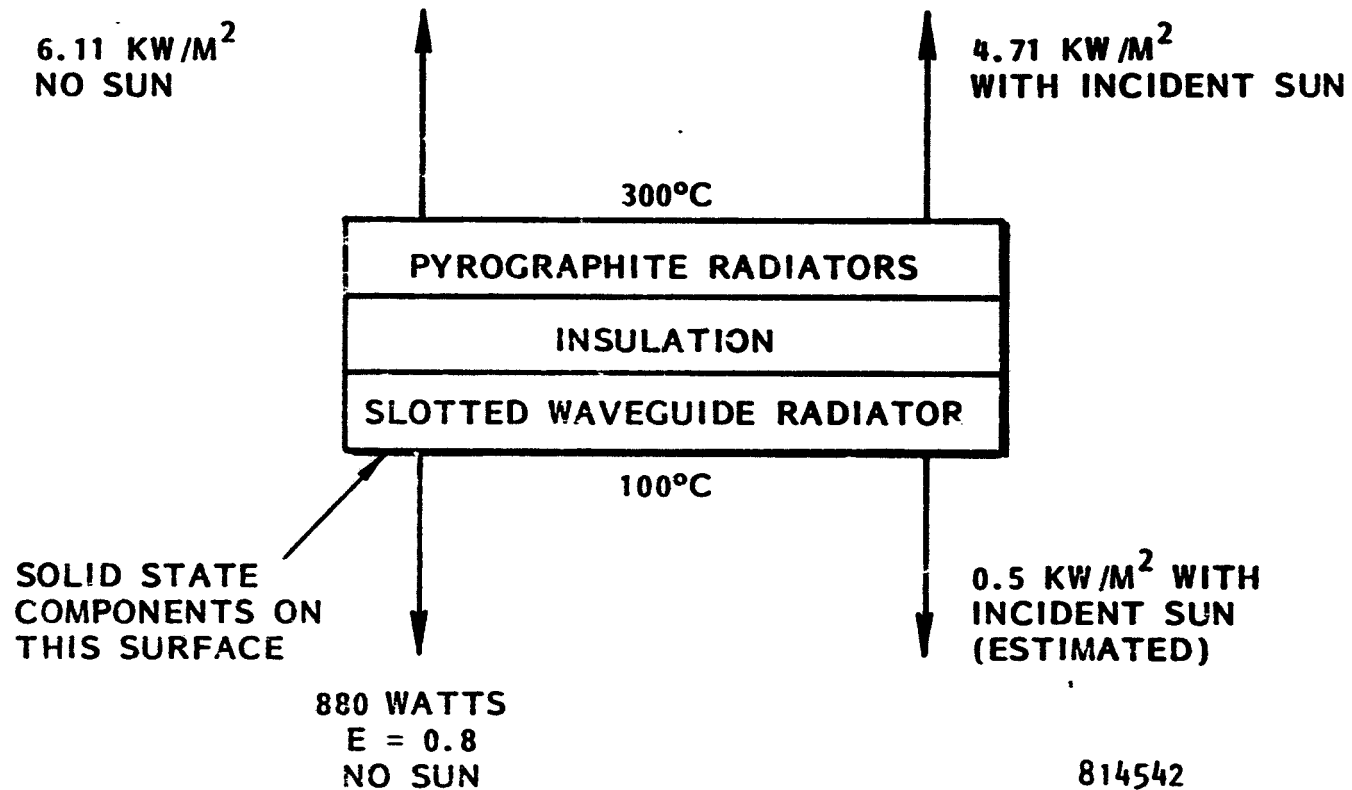
○ MAGNETRON

 RADIATING UNIT -
"MAGIC-T" MAGNETRON
DIRECTIONAL AMPLIFIER



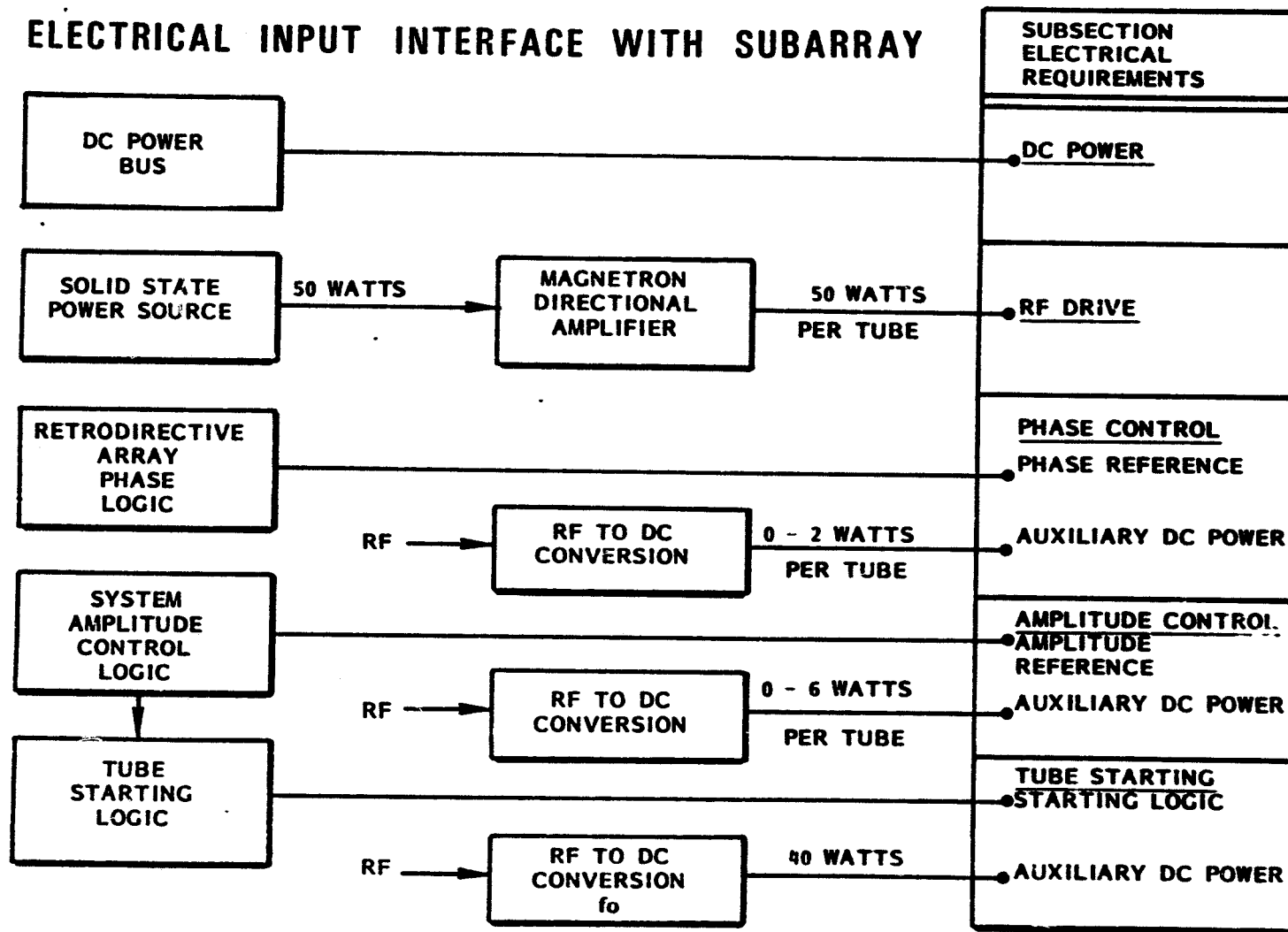
SUBSECTION





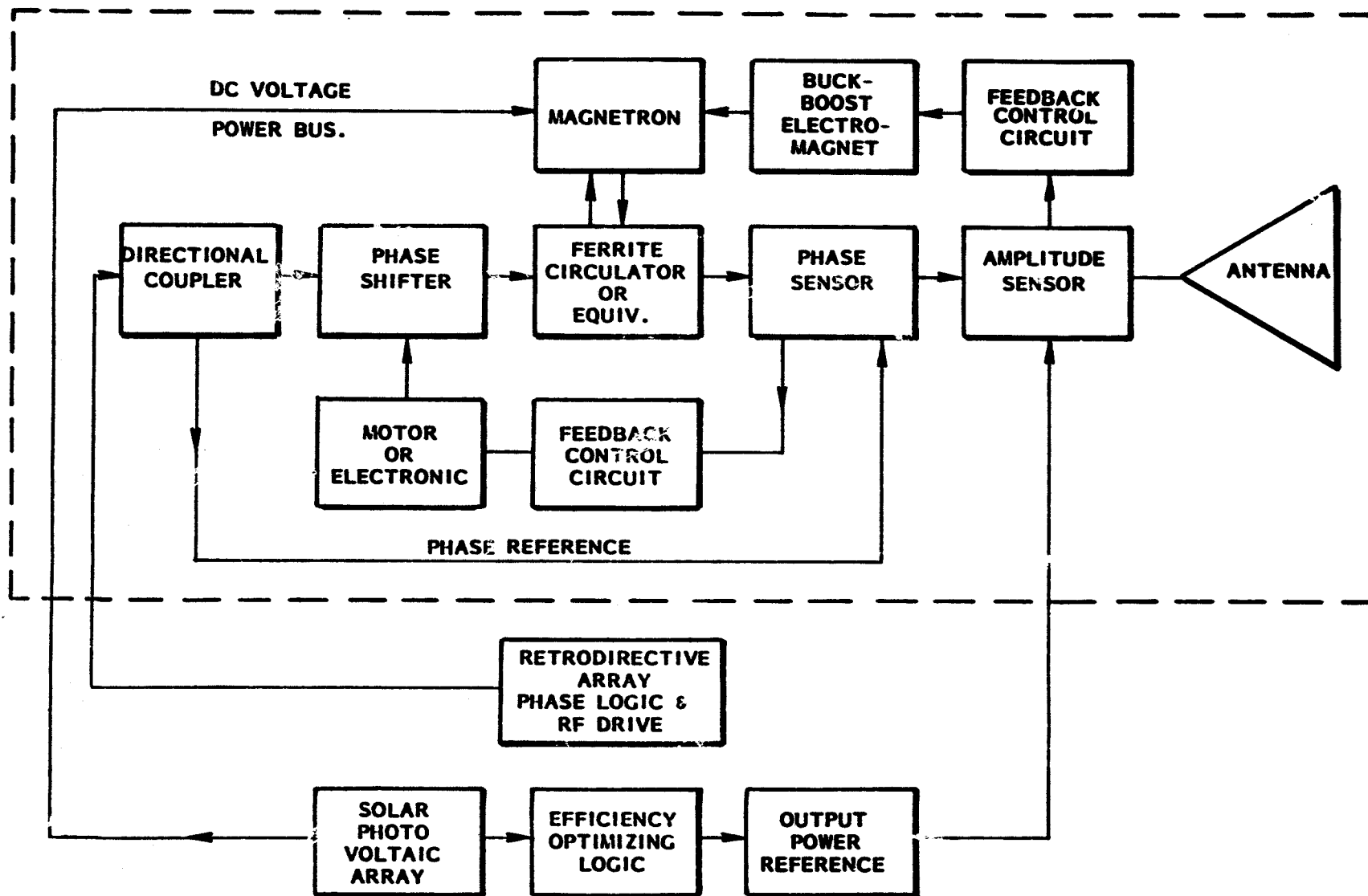
Thermal Interfaces in Subsection

ELECTRICAL INPUT INTERFACE WITH SUBARRAY

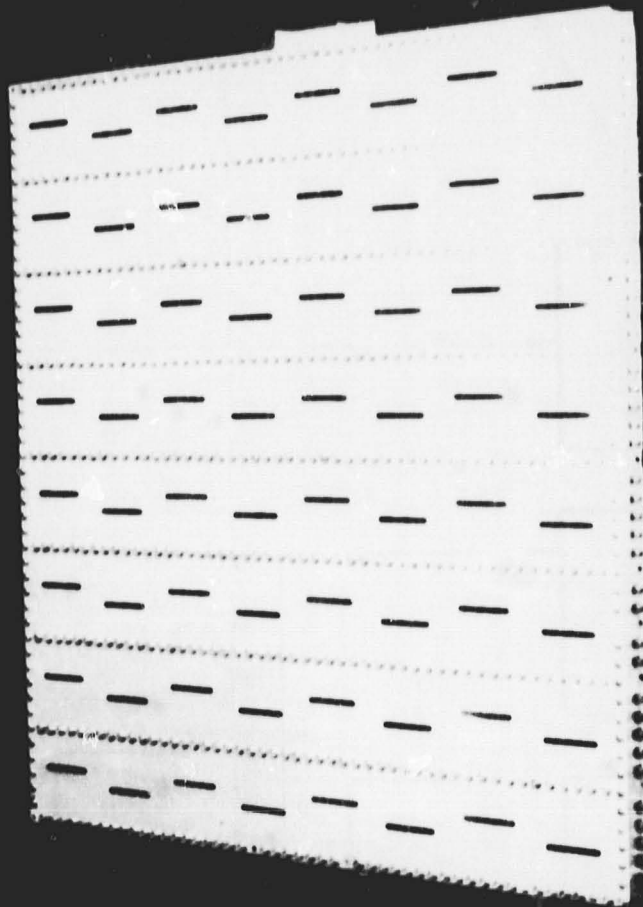


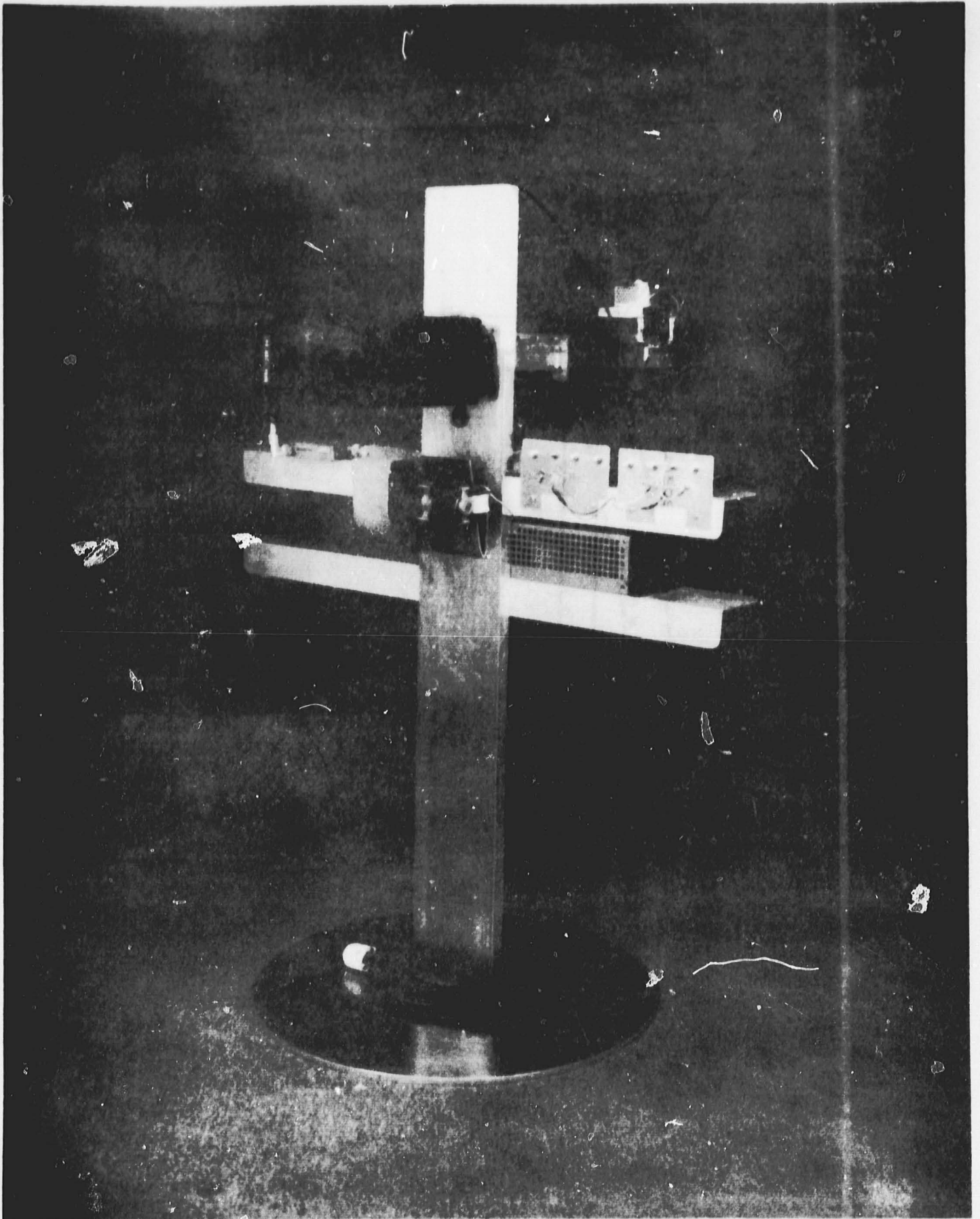
OUTLINE OF PRESENTATION

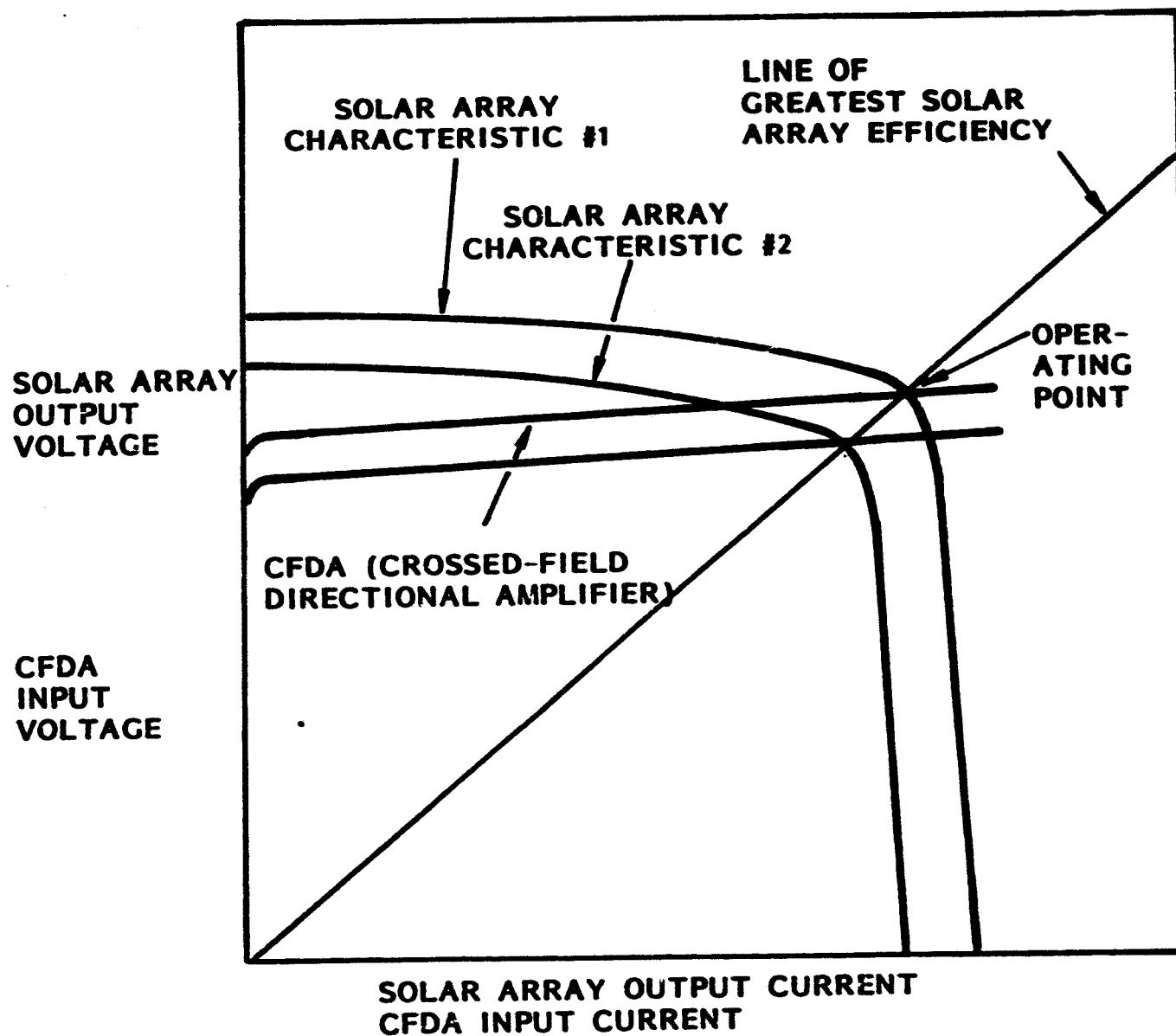
- CROSSED-FIELD DEVICE FEATURES OF INTEREST IN SPS
- OPERATING PRINCIPLES OF AMPLITRON AND MAGNETRON DIRECTIONAL AMPLIFIER
- ARCHITECTURAL INTERFACE OF MAGNETRON DIRECTIONAL AMPLIFIER AND SYSTEM
- CONTROL OF THE PHASE AND AMPLITUDE OF THE MICROWAVE OUTPUT
- SIGNAL-TO-NOISE RATIO PERFORMANCE
- DISCUSSION OF POTENTIAL FOR LONG TUBE LIFE
- DISCUSSION OF EFFICIENCY
- AREAS OF CONCERN NEEDING ADDITIONAL ATTENTION

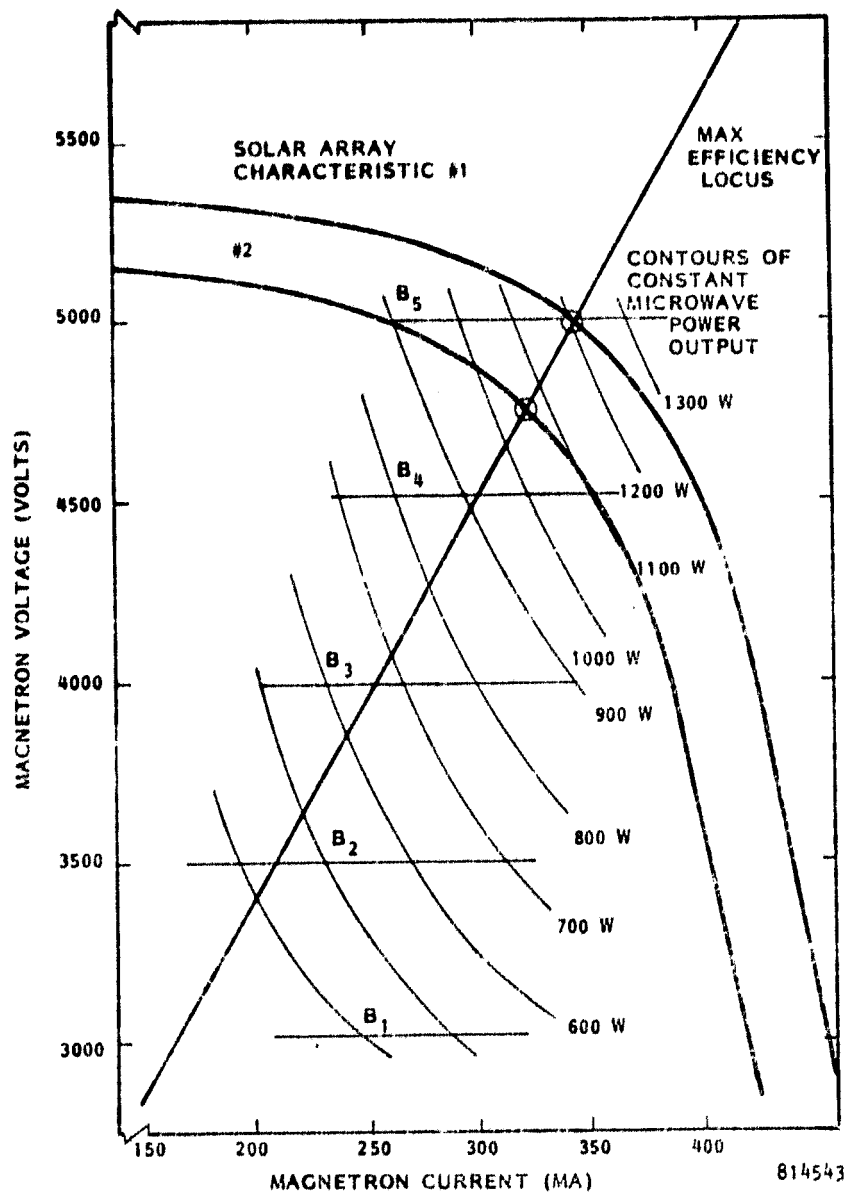


ORIGINAL PAGE
OF POOR QUALITY









814543

PHASE AMPLITUDE TRACKING

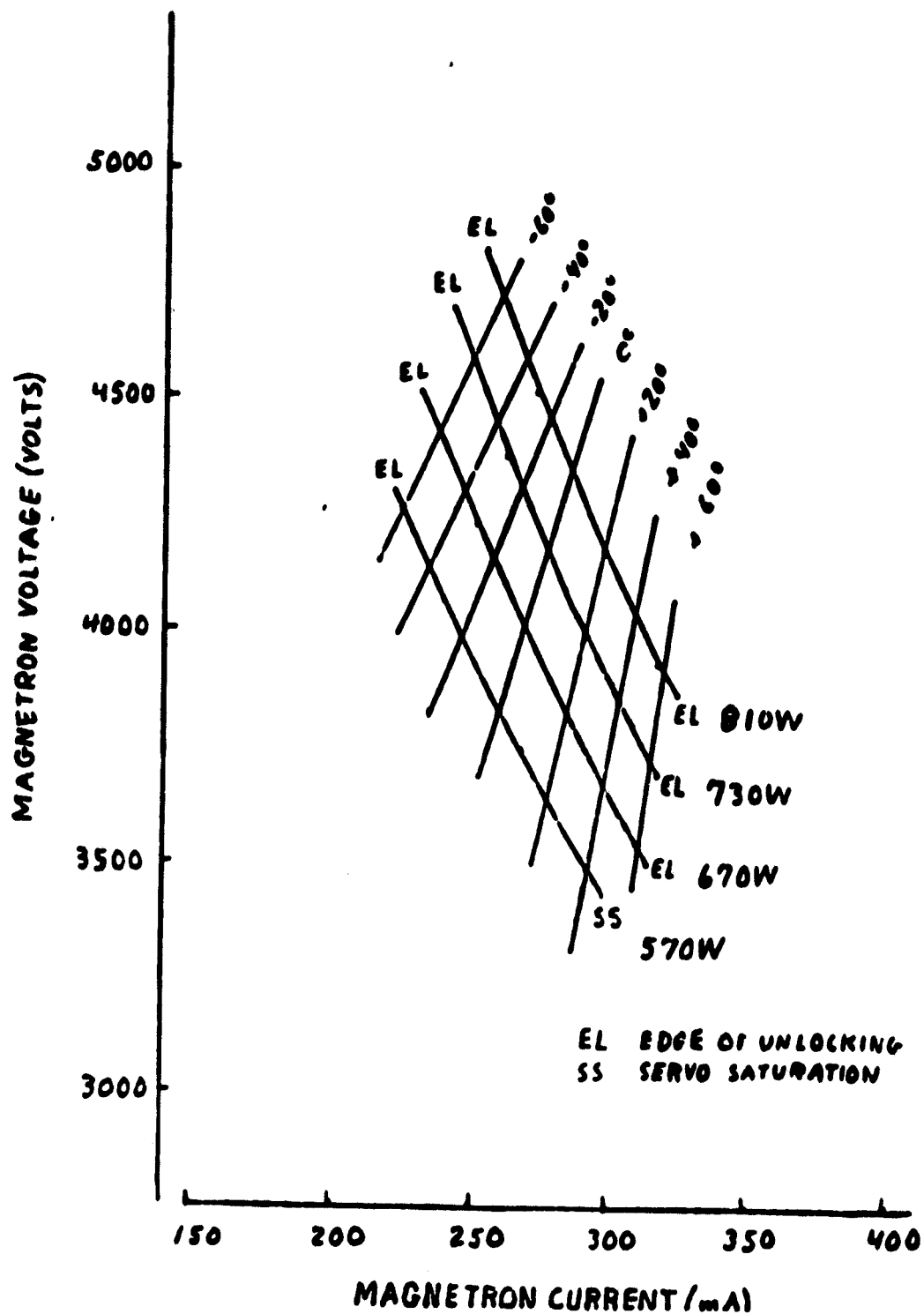
1-10-80

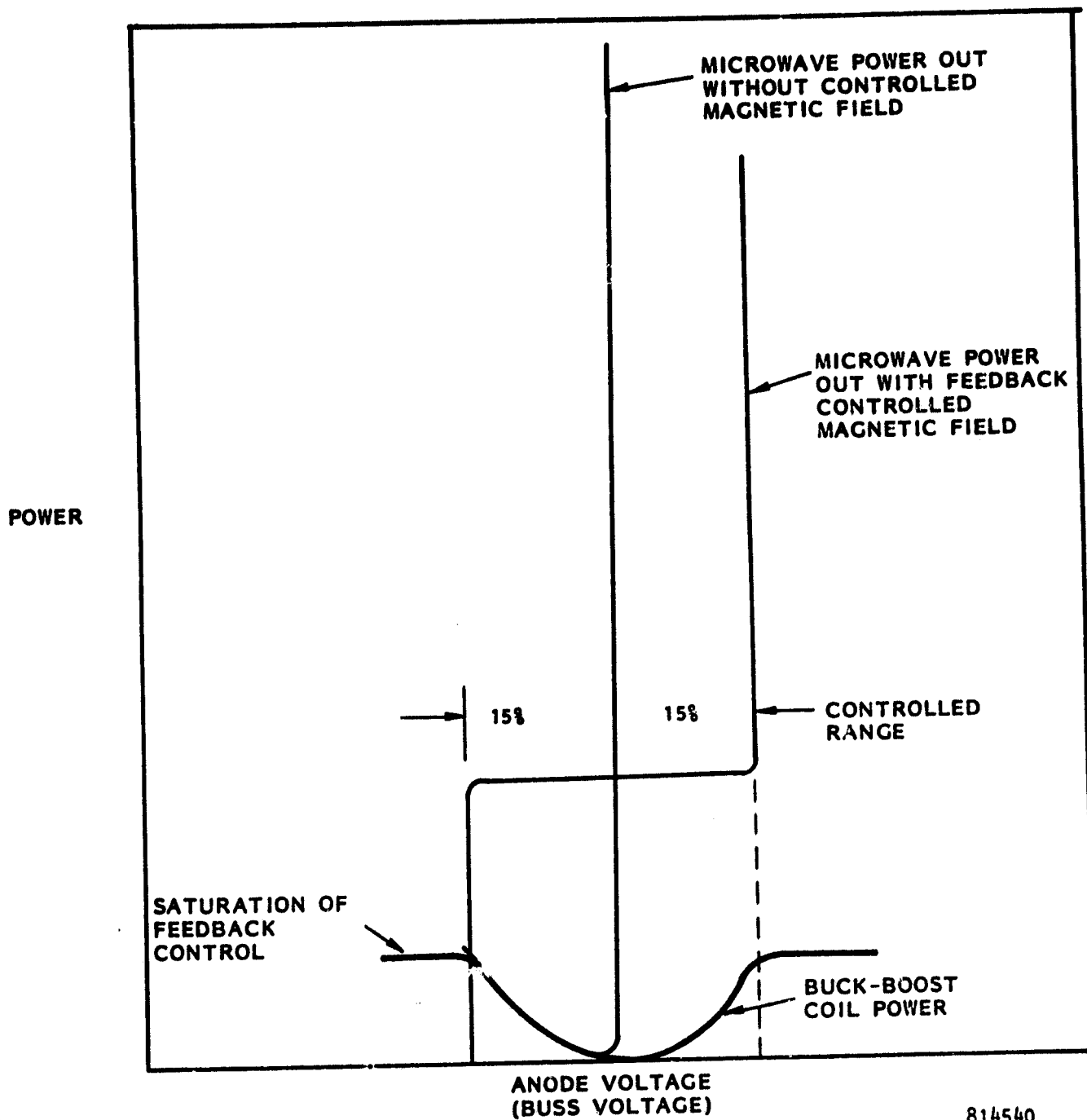
TUBE #12

$P_H = 10 \text{ WATTS}$

$FREQ = 2.45 \text{ GHz}$

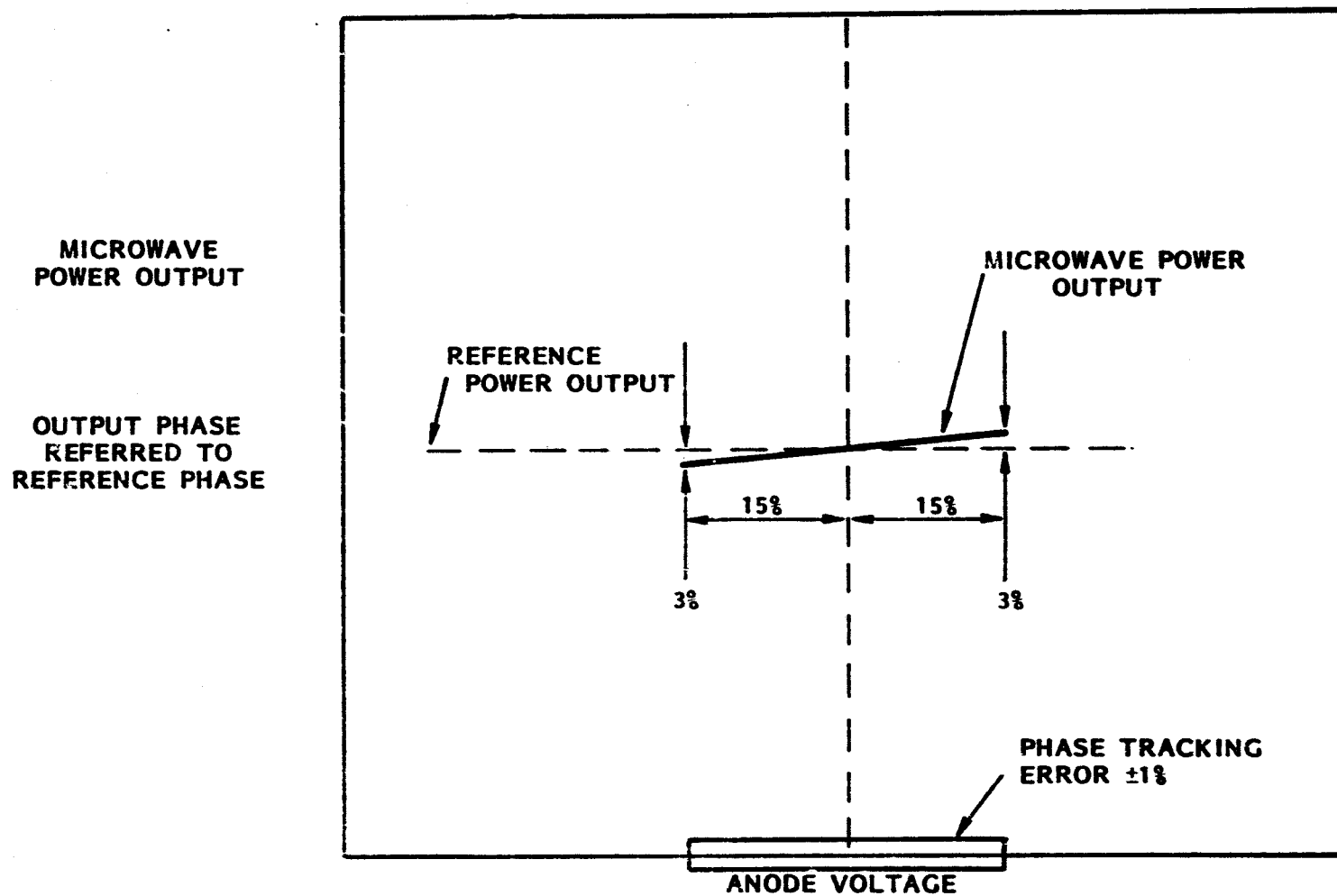
$P_{TH} = 0$





814540

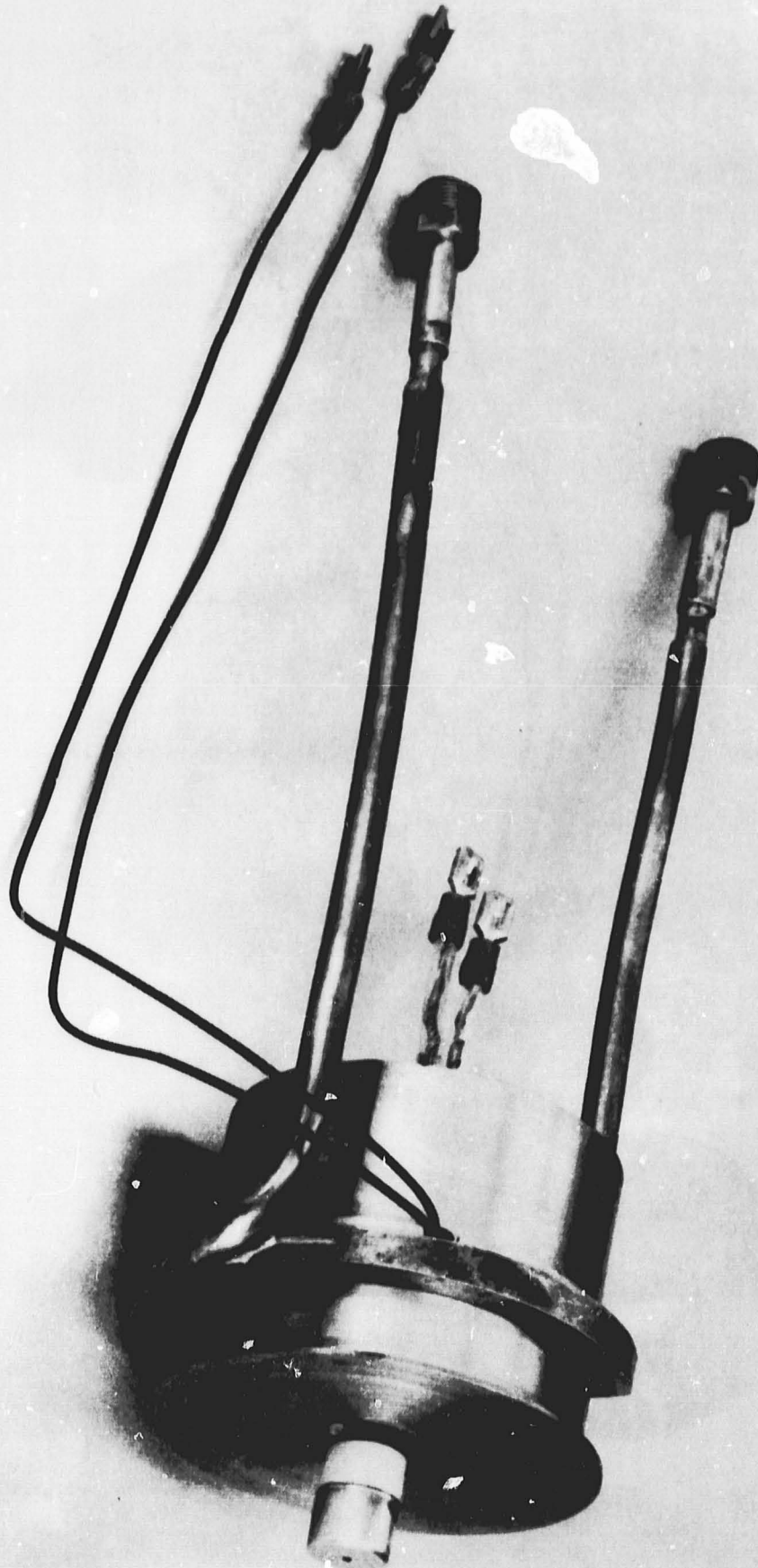
Control of Power Output by Means of Buck-Boost Coil



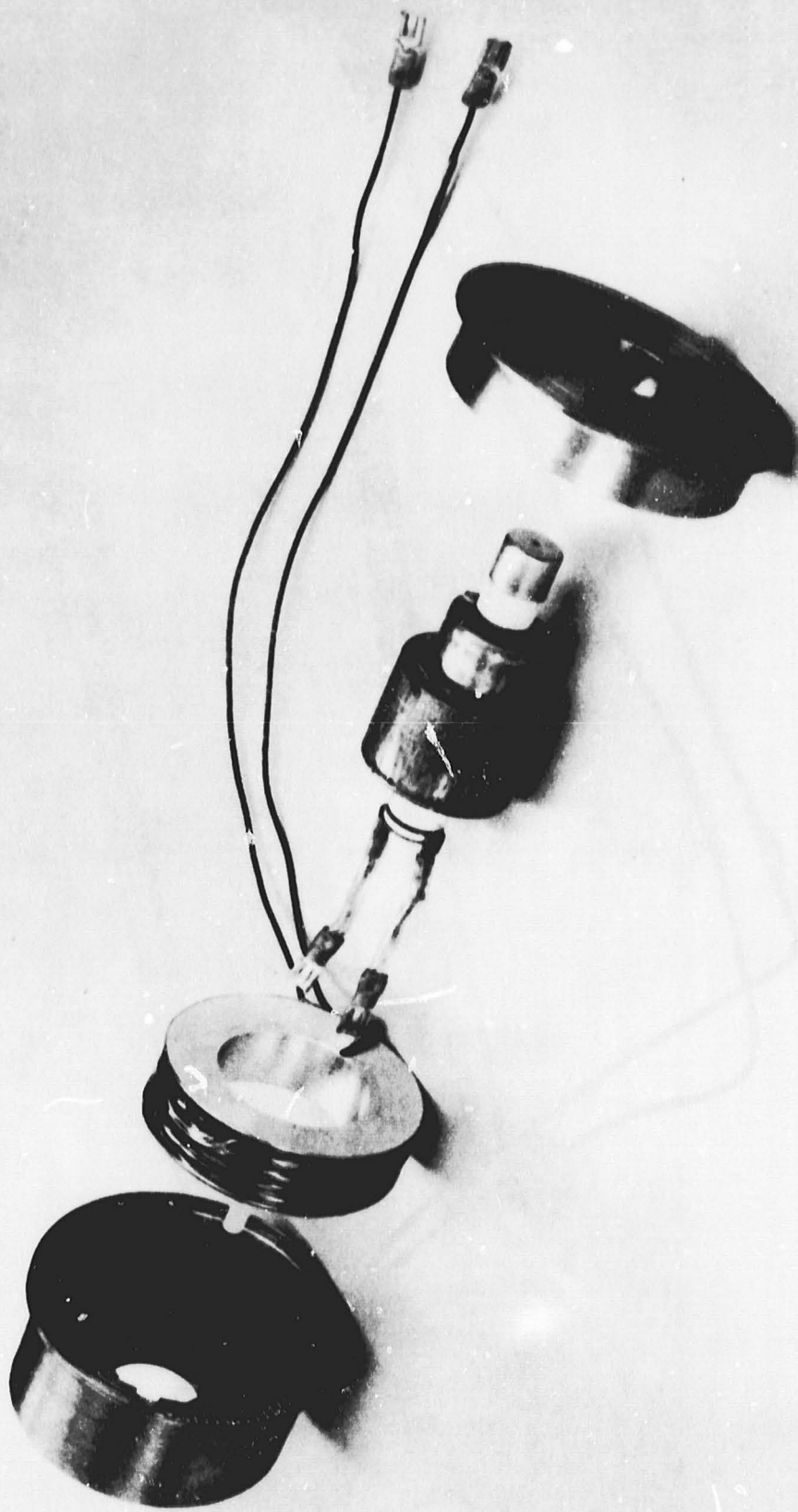
814541

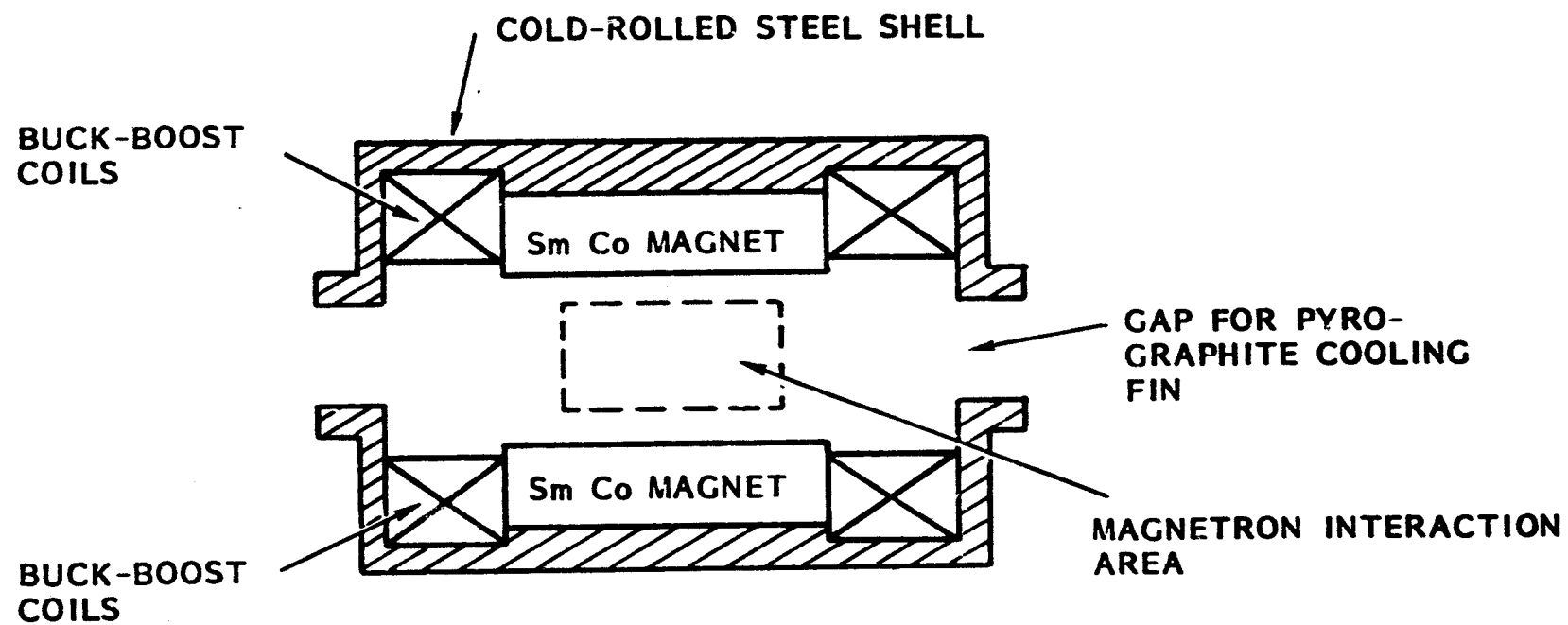
Objective Phase and Amplitude Tracking Errors of Microwave Output of Magnetron Directional Amplifier.

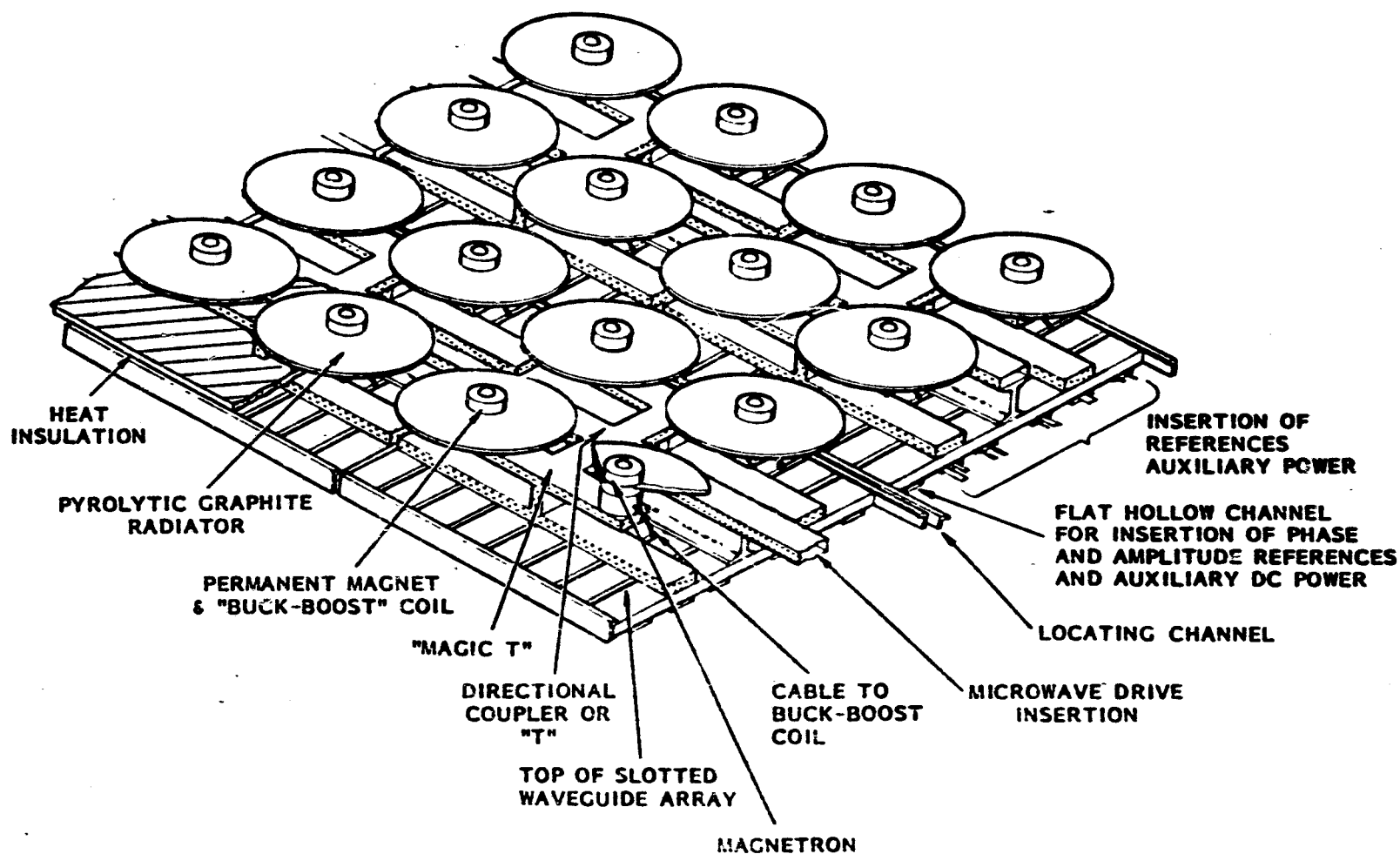
ORIGINAL PAGE IS
OF POOR QUALITY



ORIGINAL PAGE IS
OF POOR QUALITY





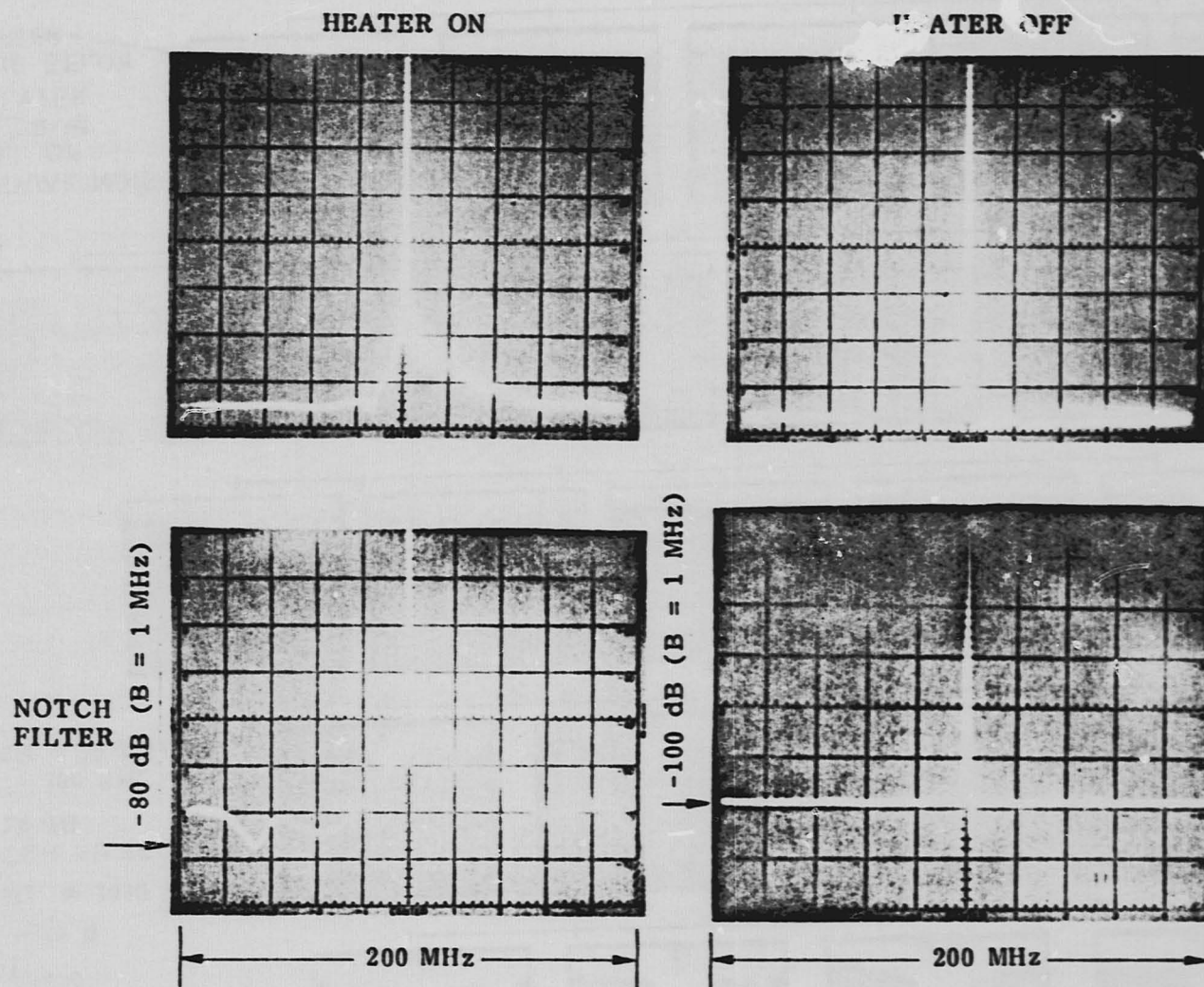


**ESTIMATED MASS OF POWER MODULES
FOR 7.4 GIGAWATTS OF RADIATED POWER
FROM 1 KM DIAMETER ANTENNA**

TUBES (85% EFFICENCY) AND RADIATING FINS	2.25 x 10 ⁶ KG
SLOTTED WAVEGUIDES AND OTHER MASS IN POWER MODULES	1.48 x 10 ⁶ KG
THERMAL INSULATING BLANKETS	<u>1.00 x 10⁶ KG</u>
TOTAL MASS	4.73 x 10 ⁶ KG

OUTLINE OF PRESENTATION

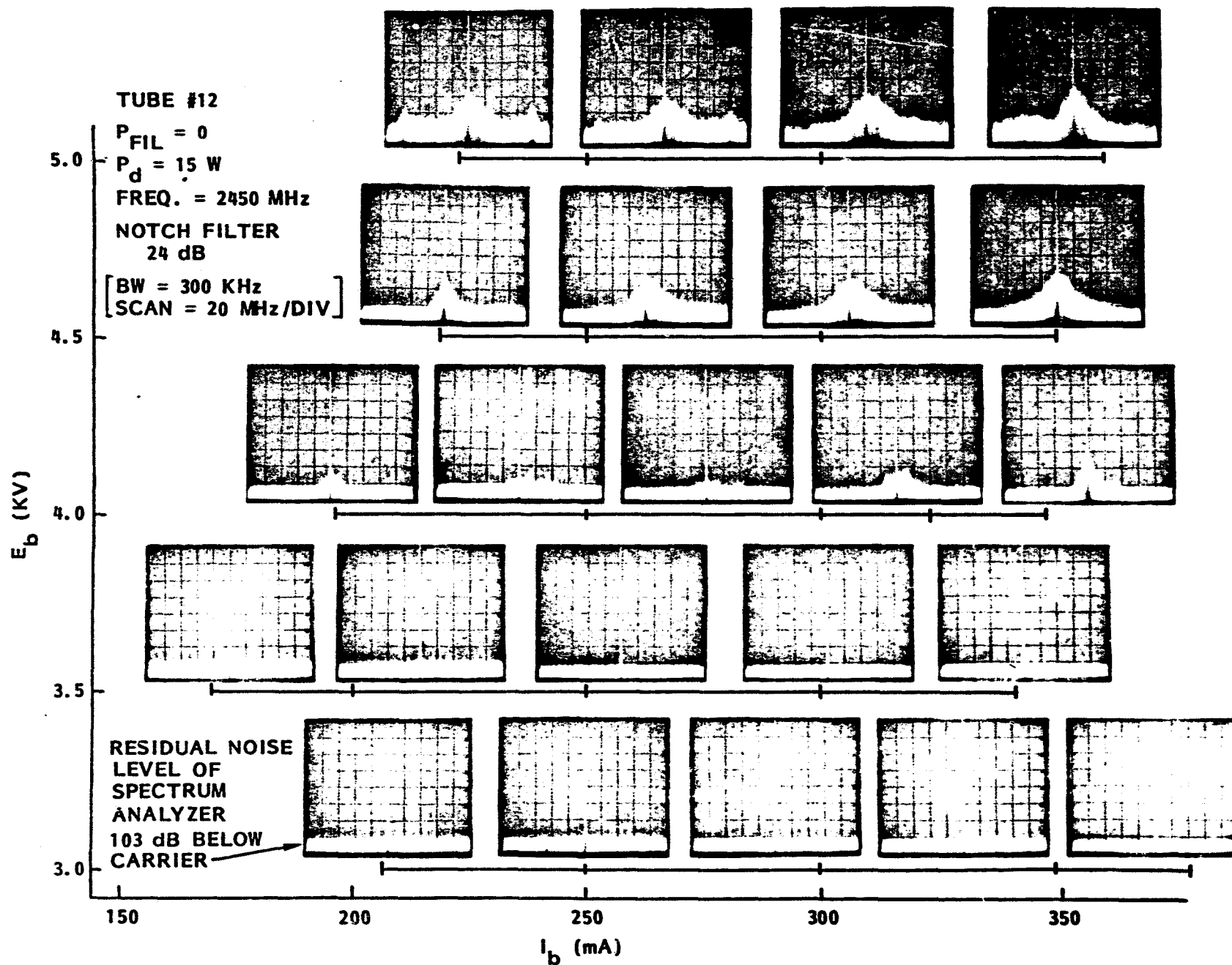
- **CROSSED-FIELD DEVICE FEATURES OF INTEREST IN SPS**
- **OPERATING PRINCIPLES OF AMPLITRON AND MAGNETRON DIRECTIONAL AMPLIFIER**
- **ARCHITECTURAL INTERFACE OF MAGNETRON DIRECTIONAL AMPLIFIER AND SYSTEM**
- **CONTROL OF THE PHASE AND AMPLITUDE OF THE MICROWAVE OUTPUT**
- **SIGNAL-TO-NOISE RATIO PERFORMANCE**
- **DISCUSSION OF POTENTIAL FOR LONG TUBE LIFE**
- **DISCUSSION OF EFFICIENCY**
- **AREAS OF CONCERN NEEDING ADDITIONAL ATTENTION**



Spectrum of Locked Magnetron.

ORIGINAL PAGE IS
OF POOR QUALITY

SIGNAL TO NOISE AS A FUNCTION OF VOLTAGE AND CURRENT



SIGNAL TO NOISE AS A FUNCTION OF DRIVE LEVEL

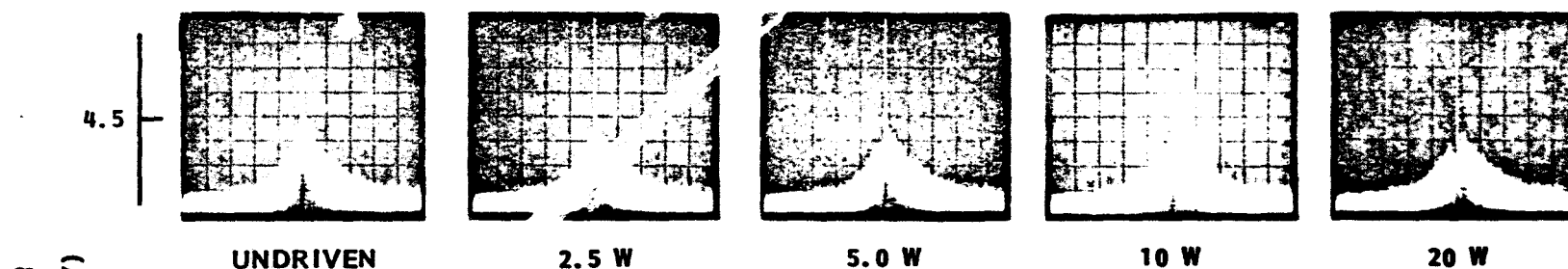
TUBE #12

FREQ. = 2450 MHz

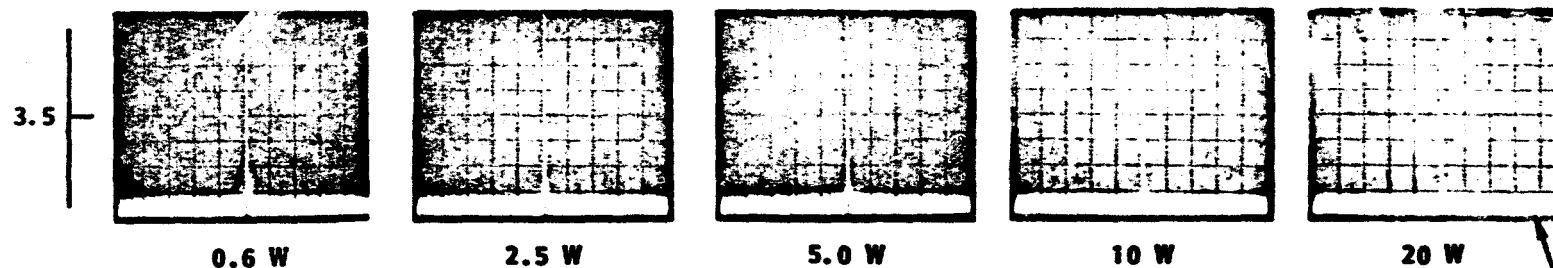
$P_{FIL} = 0$

NOTCH FILTER 24 dB

[BW = 300 KHz
SCAN 20 MHz/DIV]



$P_o = 890 \text{ W}$ $I_b = 300 \text{ mA}$

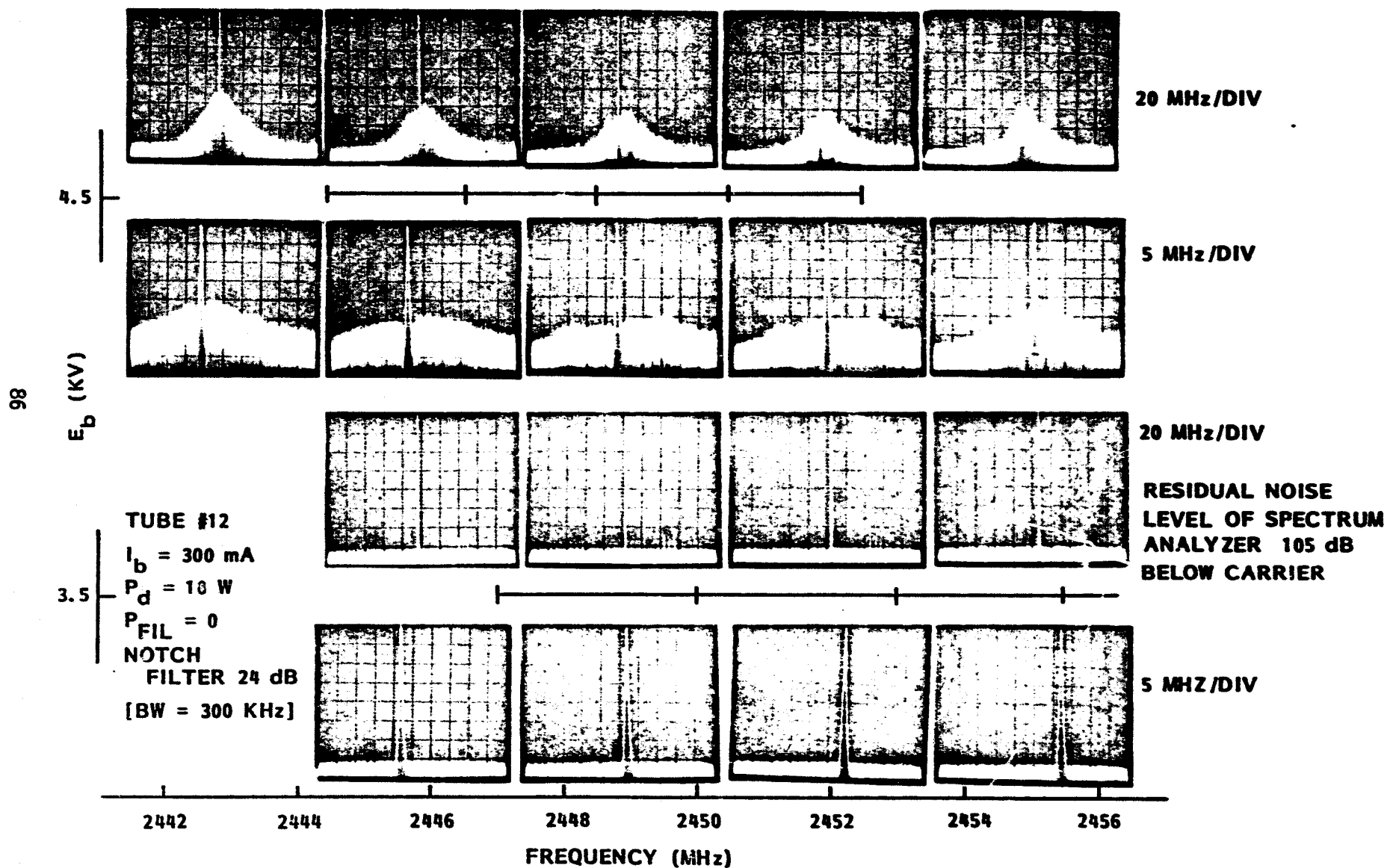


$P_o = 530 \text{ W}$ $I_b = 250 \text{ mA}$

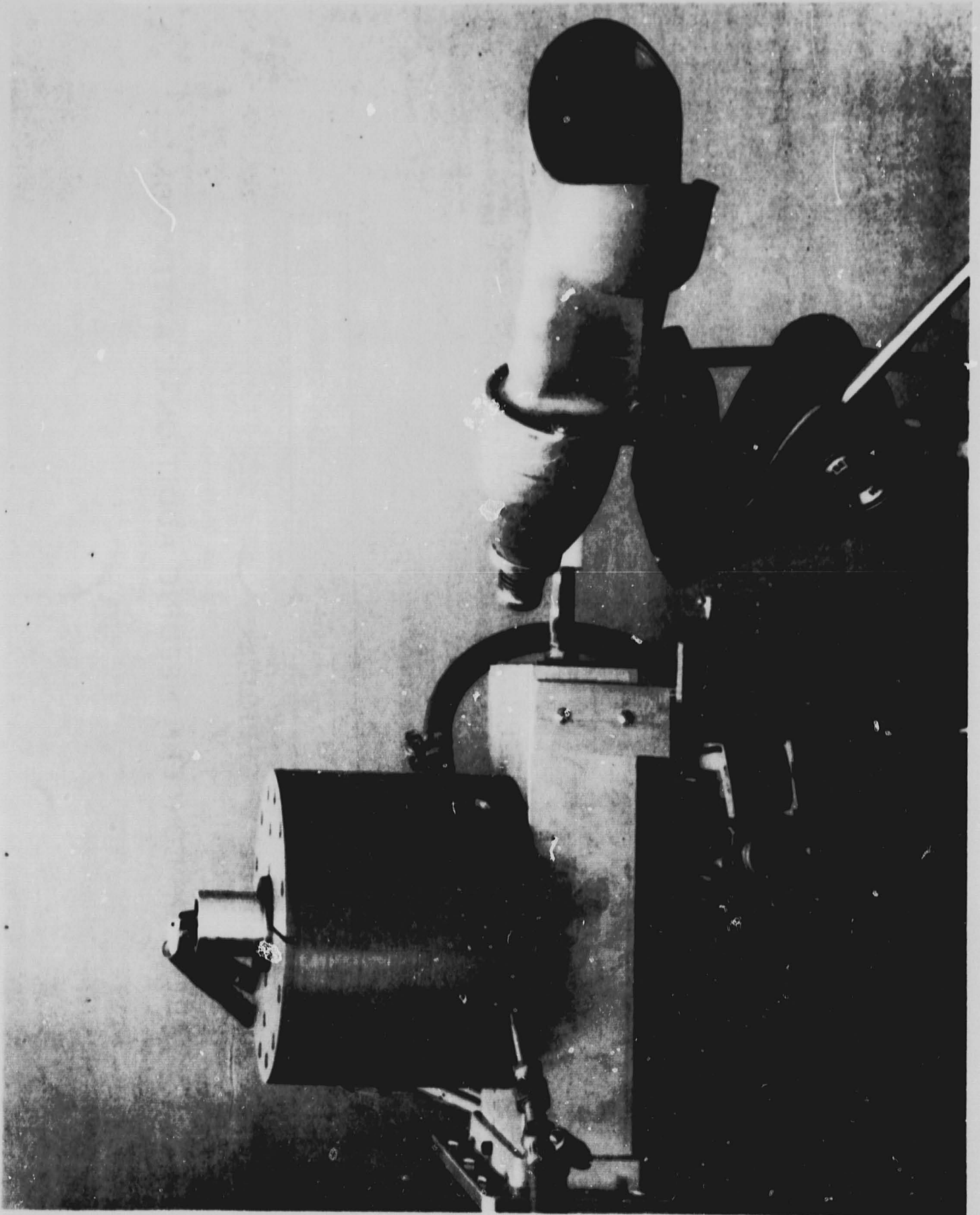
DRIVE LEVEL.

RESIDUAL NOISE LEVEL
OF SPECTRUM ANALYZER
135 dB BELOW CARRIER

SIGNAL TO NOISE AS A FUNCTION OF FREQUENCY DEVIATION

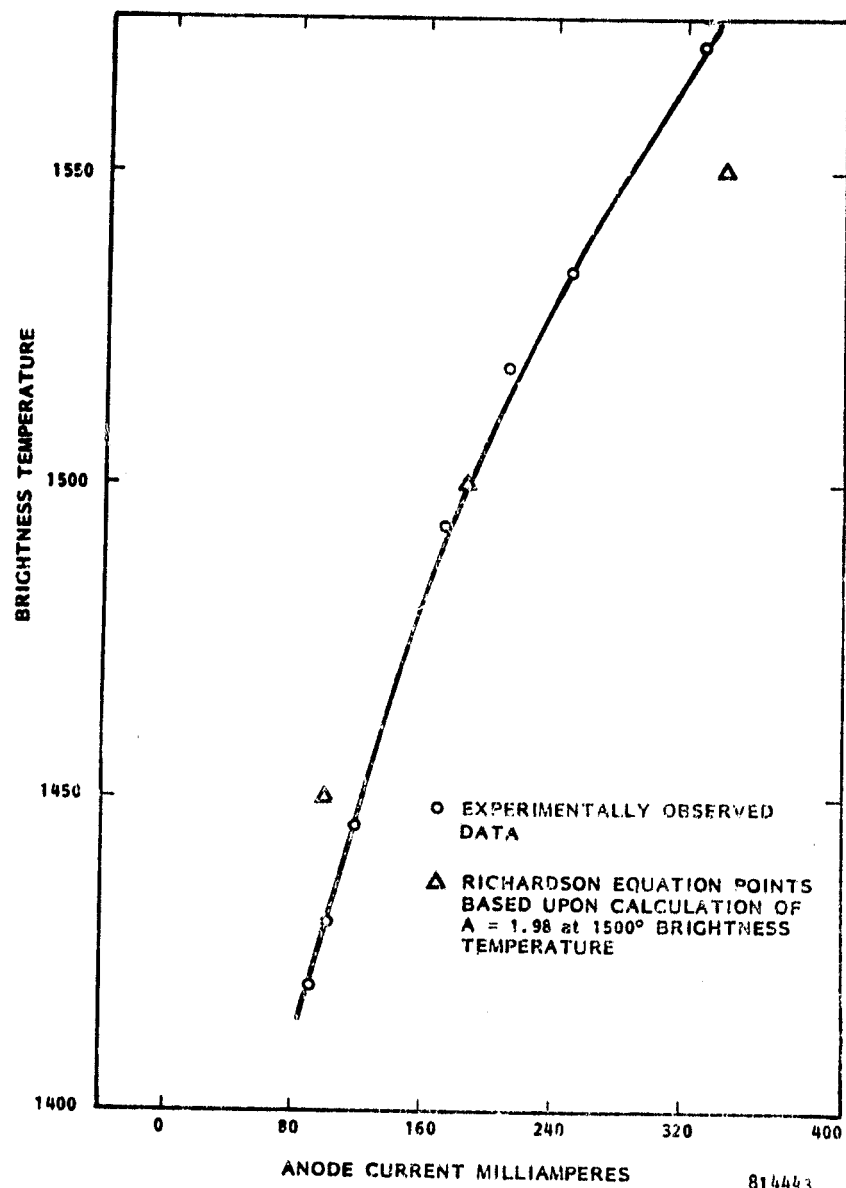


ORIGINAL PAGE IS
OF POOR QUALITY



OUTLINE OF PRESENTATION

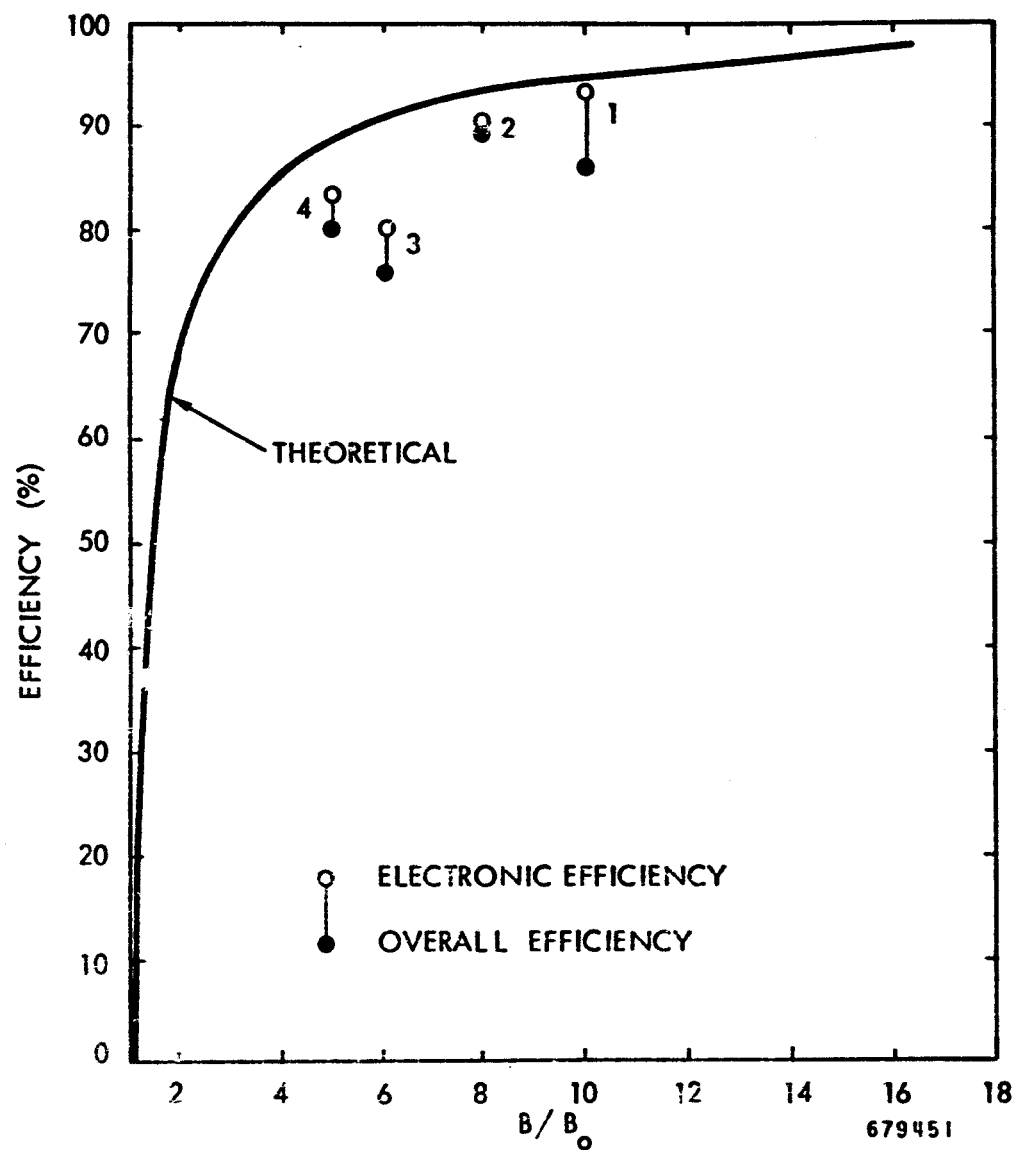
- **CROSSED-FIELD DEVICE FEATURES OF INTEREST IN SPS**
- **OPERATING PRINCIPLES OF AMPLITRON AND MAGNETRON DIRECTIONAL AMPLIFIER**
- **ARCHITECTURAL INTERFACE OF MAGNETRON DIRECTIONAL AMPLIFIER AND SYSTEM**
- **CONTROL OF THE PHASE AND AMPLITUDE OF THE MICROWAVE OUTPUT**
- **SIGNAL-TO-NOISE RATIO PERFORMANCE**
- **DISCUSSION OF POTENTIAL FOR LONG TUBE LIFE**
- **DISCUSSION OF EFFICIENCY**
- **AREAS OF CONCERN NEEDING ADDITIONAL ATTENTION**



814443

OUTLINE OF PRESENTATION

- **CROSSED-FIELD DEVICE FEATURES OF INTEREST IN SPS**
- **OPERATING PRINCIPLES OF AMPLITRON AND MAGNETRON DIRECTIONAL AMPLIFIER**
- **ARCHITECTURAL INTERFACE OF MAGNETRON DIRECTIONAL AMPLIFIER AND SYSTEM**
- **CONTROL OF THE PHASE AND AMPLITUDE OF THE MICROWAVE OUTPUT**
- **SIGNAL-TO-NOISE RATIO PERFORMANCE**
- **DISCUSSION OF POTENTIAL FOR LONG TUBE LIFE**
- **DISCUSSION OF EFFICIENCY**
- **AREAS OF CONCERN NEEDING ADDITIONAL ATTENTION**

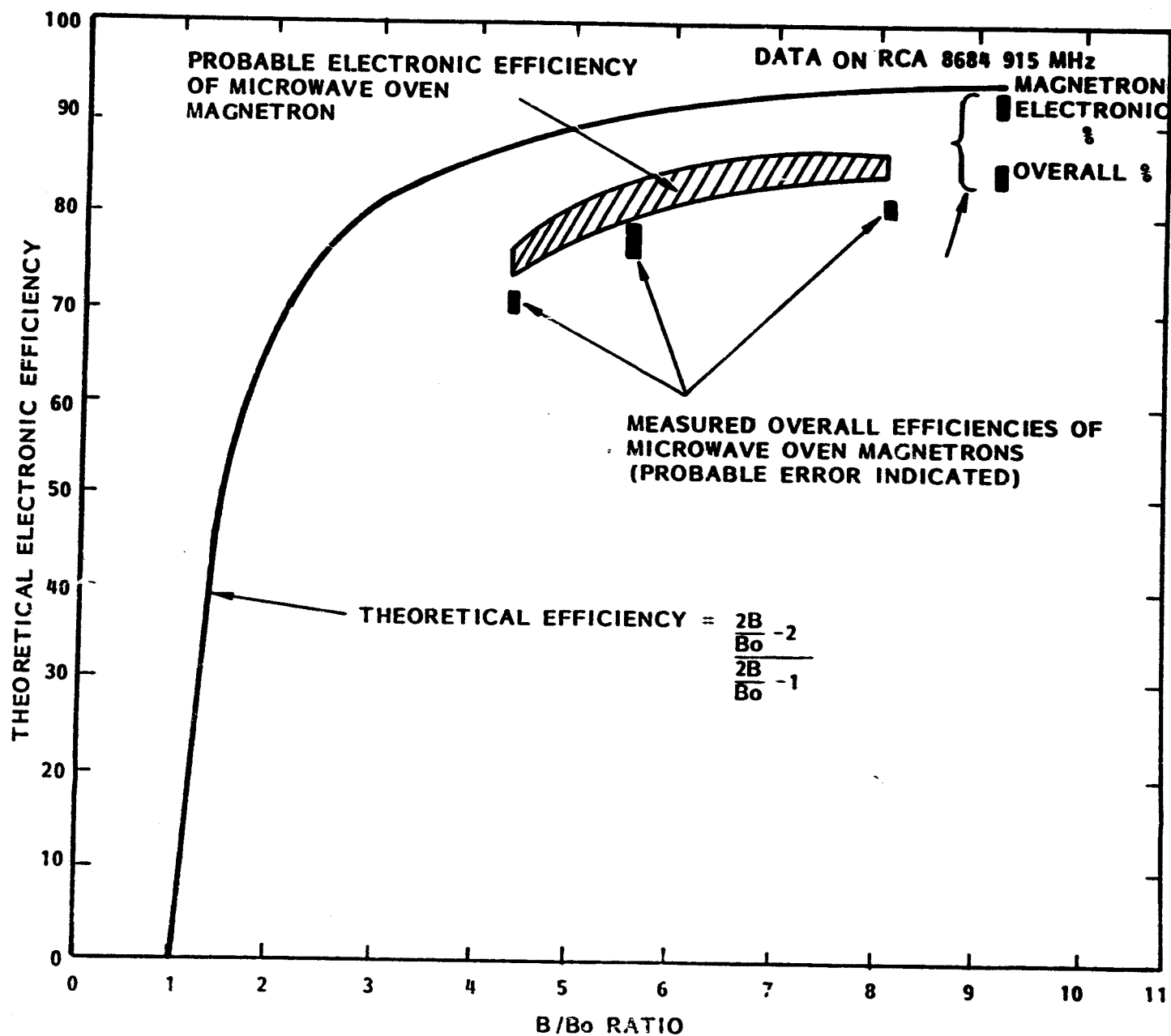


1. 8684 MAGNETRON
915 MHz; 25 kW CW
SHELF ITEM

2. 1220 AMPLITRON
500 MHz; LOW POWER
RESEARCH ITEM

3. 849 AMPLITRON
3000 MHz; 200-400 kW CW
NOT A SHELF ITEM

4. 622 AMPLITRON
3000 MHz; 3 MW PULSED
SHELF ITEM



OUTLINE OF PRESENTATION

- **CROSSED-FIELD DEVICE FEATURES OF INTEREST IN SPS**
- **OPERATING PRINCIPLES OF AMPLITRON AND MAGNETRON DIRECTIONAL AMPLIFIER**
- **ARCHITECTURAL INTERFACE OF MAGNETRON DIRECTIONAL AMPLIFIER AND SYSTEM**
- **CONTROL OF THE PHASE AND AMPLITUDE OF THE MICROWAVE OUTPUT**
- **SIGNAL-TO-NOISE RATIO PERFORMANCE**
- **DISCUSSION OF POTENTIAL FOR LONG TUBE LIFE**
- **DISCUSSION OF EFFICIENCY**
- **AREAS OF CONCERN NEEDING ADDITIONAL ATTENTION**

AREAS OF CONCERN NEEDING ADDITIONAL ATTENTION

- **COMPATIBILITY OF OPERATION AT HIGH EFFICIENCY AND LONG CATHODE LIFE WITH HIGH SIGNAL TO NOISE RATIO.**
- **PHASE AND AMPLITUDE CONTROL ARE CURRENTLY BEING INVESTIGATED WITH USE OF FERRITE CIRCULATOR. FOR SPS APPLICATION EITHER A FERRITE CIRCULATOR THAT WILL OPERATE AT HIGH TEMPERATURES IS REQUIRED, OR PHASE AND AMPLITUDE CONTROL MUST BE ADAPTED TO THE "MAGIC" ARRANGEMENT.**
- **A FRICTIONLESS PHASE SHIFTER THAT WILL OPERATE IN A HIGH TEMPERATURE ENVIRONMENT AT THE 50 WATT LEVEL MUST BE DEvised.**

23

Summary of Past Activities

***L. Leopold
Lyndon B. Johnson Space Center***

SOLAR POWER SATELLITE

RELATED ACTIVITIES

PHOTOKLYSTRON

- o OSCILLATES AT RADIO FREQUENCIES WHEN ILLUMINATED BY LIGHT.
- o NO EXTERNAL ACCELERATING BIAS VOLTAGE IS NECESSARY TO CONTINUE OSCILLATION.
- o ENERGY TO SUSTAIN OSCILLATION IS DERIVED SOLELY FROM PHOTO-ELECTRONS.
- o EFFICIENCY OF 1% HAS BEEN DEMONSTRATED. ULTIMATE EFFICIENCY OF 10% APPEARS POSSIBLE.
- o MODES OF OSCILLATIONS IN THE FREQUENCY RANGE FROM 8 TO 240 MHz HAVE BEEN REACHED.
- o OUTPUT VOLTAGES ARE 2.0 VOLTS RMS ACROSS A 50 OHM LOAD.
- o BECAUSE OF THE UNIQUE SOLAR ENERGY TO POWER CONVERSION, THE PHOTOKLYSTRON IS A POSSIBLE CANDIDATE FOR FURTHER INVESTIGATION.

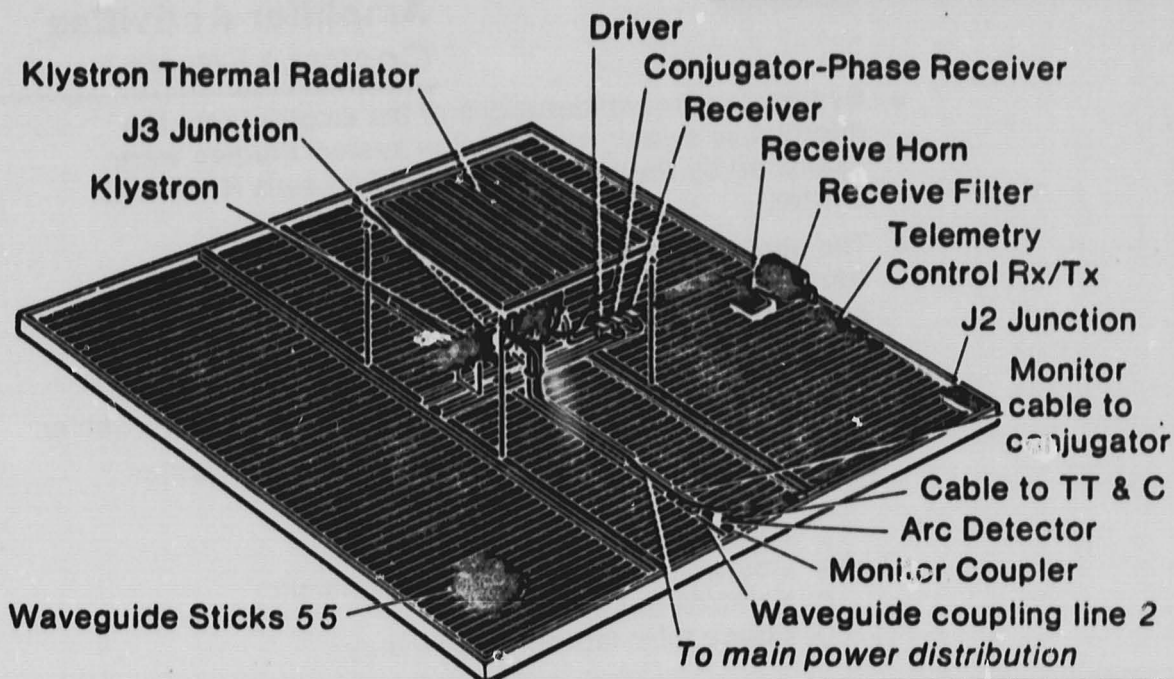
SOLAR POLAR SATELLITE

RELATED ACTIVITIES

GYROCOM

- o DEVELOPED IN THE USSR
- o THE OUTPUT IS ONE MEGAWATT CW AT 180 MHz.
- o BASED ON RECENT COMPUTER ANALYTICAL RESULTS INDICATING HIGH GAIN, LOWER POWERS AND HIGH EFFICIENCIES, THE GYROCOM IS A POSSIBLE CANDIDATE FOR FURTHER INVESTIGATION.

ORIGINAL PAGE IS
OF POOR QUALITY



- A The klystron power amplifier has the attractive features of high gain (40 - 50 dB), low drive power required from the phase control system, high power (50-70 kW), low noise characteristics, and fewer tubes per antenna requiring phase control.
- B Cathode lifetime and its maintenance implications is a major concern for the SPS.
- C Efficiencies of 75% at S-band and a power output of 50 kW have already been recorded. The application of depressed collectors have increased tube efficiencies. It appears likely that 85% can be achieved.
- D A heat pipe cooling system is required for heat rejection.

NASA**Solar Power
Satellite**

**History of Power
Amplifier Activities
*Contract Efforts***

- System level considerations of the amplatron for the microwave power transmission system studies were examined by Raytheon for the NASA Lewis Research Center.
- The study of the klystron for the microwave power transmission system studies was conducted by Shared Applications, Inc. for Raytheon.
- The VKS-7773 CW klystron evaluation program was undertaken by Varian for the NASA Johnson Space Center.
- Various design features of the klystron were studied by Varian for Boeing, these include:
 - A Klystron design for the SPS
 - B Characteristics of the 70 kW design
 - C Klystron failure modes
 - D Space tube factory and facilities

NASA**Solar Power
Satellite**

**Power Amplifier Conclusions
*Amplatron***

- Projected performance of amplitrons is less attractive for SPS applications because of low power (5kW), low gain (7dB), higher noise levels, high drive power required from the phase control system, and more tubes per antenna requiring phase control. The amplatron is less complex and passive cooling techniques appear to be within the state-of-the-art.

Magnetron

- Because of recent projections in performance characteristics (low noise, high efficiency, and moderate gain), magnetrons warrant continued investigation. The magnetron is also less complex and hence the maintenance implications appear to make it more attractive.

NASA**Solar Power
Satellite**

**History of Power
Amplifier Activities
Contract Efforts**

- Varian served as a consultant on klystron applications to the SPS system for Rockwell.
- The development of a possible SPS amplifron was undertaken by Raytheon for NASA Lewis Research Center.
- The study and design of the magnetron for possible application to the SPS was preformed by Raytheon for JPL.
- The exploration of the possible integraton of the magnetron with SPS microwave system was completed by Raytheon for Marshall Space Flight Center

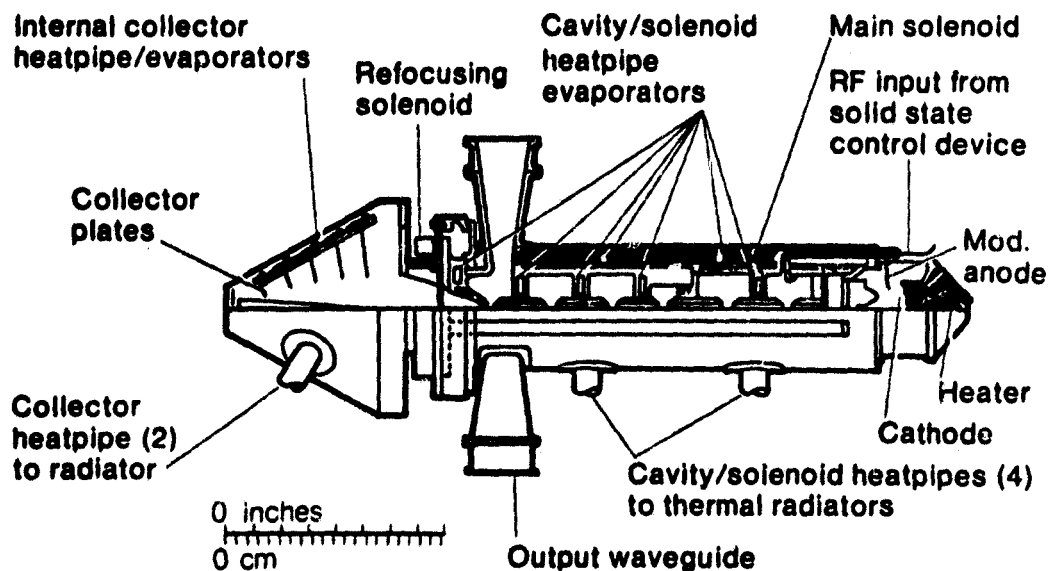
NASA**Solar Power
Satellite**

**Remaining Issues —
Power Amplifiers
tube**

- 1 High dc-rf conversion efficiency (85%)
 - 2 Reliability
 - 3 Amplifier rf (noise, harmonics, filtering requirements)
 - 4 Other operating parameters (temperature, gain)
 - 5 Thermal cooling capability
 - 6 Specific weight
 - 7 High volume manufacturing techniques
 - 8 Precision manufacturing
 - 9 Design for ease of maintenance
 - 10 Design for power supply/PA for stable operation
 - 11 Depressed collectors
 - 12 Investigation of circuit protection devices
 - 13 Package consideration during launch and transportation
 - 14 Metals and materials research: magnets, cathodes
-

NASA**Solar Power
Satellite****Features of
Power Amplifiers**

Item	Amplifon	Klystron	Solid State
Power	5 kW with 10 ⁴ tubes	50 - 250 kW with 10 ⁴ tubes	1 - 3 W (5-10 W)
Efficiency	85 - 90%	80 - 85%	80%
Cathode	Cold pure metal (avail life data 10,000 hrs.)	Thermionic oxide/matrix (avail life data 50,000 hrs.)	
Gain	7 dB	40 dB	20 dB
Voltage	20 kV	40 - 65 kV	12 to 20 V
Spurious signal AM (Typ.)	-100 dB/kHz 10 MHz from carrier	-125 dB/kHz 5 kHz away from carrier	unknown
M T B F	Comparable to klystron	Comparable to amplifon	approx. 100 years
Thermal dissipation	Concentrated interaction region	Distributed, collector can run 500-700°C, require heat pipes	100-125° C passive
Specific cost	~20/kW	~20 to ~40/kW	unknown
Specific weight	0.4 kg/kW	0.4 to 0.8 kg/kW	0.01 to 0.03 kg/kW
Array interface	Series operation no feed waveguides	Power adjusts to voltage changes, corporate feed	Device to antenna element

NASA**Solar Power
Satellite****70 kW Klystron**

- A** Based on present assumptions of microwave system requirements and projected performance of various microwave power amplifiers, the klystron offers a feasible approach for SPS microwave power generation. The amplitron appears to be less suitable, and the magnetron should continue to be investigated to better understand its performance characteristics relative to SPS applications.
 - B** Based on SPS microwave system applications, it is desirable to have maximum power output and gain consistent with other microwave system parameters.
-

H3



National Aeronautics and
Space Administration

Lyndon B. Johnson Space Center
Houston, Texas 77058



5

**Radiating
Elements**



**NASA Solar Power
Satellite**

**Workshop on
Microwave Power
Transmission
and Reception**

**Session
Presentations**

**Jan
15-18
1980**

C - 10



The presentation material herein was used in the Radiating Elements Session of the Solar Power Satellite Workshop on Microwave Power Transmission and Reception held at the Lyndon B. Johnson Space Center, January 15-28, 1980. The workshop was conducted as part of the technical assessment process of the DOE/NASA Solar Power Satellite Concept Evaluation Program. All aspects of Solar Power Satellite microwave transmission and reception were addressed including studies, analyses, and laboratory investigations. Conclusions from these activities were presented as well as recommended follow-on work. The workshop was organized into eight sessions as follows:

- *General*
- *Microwave System Performance*
- *Phase Control*
- *Power Amplifiers*
- *Radiating Elements*
- *Rectenna*
- *Solid State Configurations*
- *Planned Program Activities*

The material contained herein supplements the workshop papers which were published and distributed at the time of the workshop. Together they are a comprehensive documentation of the numerous analytical and experimental activities in the field of microwave power transmission and reception.

● *Additional information regarding the workshop may be obtained by*

contacting: R.H. Dietz

EE4/SPS Microwave Systems

National Aeronautics &

Space Administration

Lyndon B. Johnson Space Center

Houston, Texas 77058

713 483-4507

5

Radiating Elements Session contents

- | | |
|-----------|---|
| 1 | Reference System Description and
Testing and Evaluation of "Thick Wall
Waveguide Element"
Dr. Erv Nalos, Boeing |
| 15 | Resonant Cavity Radiator
K. Schroeder, Rockwell International |
| 31 | Construction and Evaluation of a "Thin Wall
Waveguide Element"
W. Brown, Raytheon |
| 39 | Microwave Measurement Techniques, Problems
and Potential Solutions in Ultra High
Accuracy Antenna
Kozakoff, Georgia Tech Experiment Station |

①

***Reference System Description and
Testing and Evaluation of "Thick
Wall Waveguide Element"***

***Dr. Erv Nalos
Boeing***

SUBARRAY LOSSES DUE TO DIMENSIONAL TOLERANCES

<u>COMPONENT DIMENSION</u>	<u>TOLERANCE</u>	<u>EFFECT</u>	<u>MAIN BEAM POWER DEGRADATION</u>
SUBARRAY SURFACE UNIFORMITY	± 50 MILS RMS	SCATTERING FROM PHASE VARIANCE	0.50% (1)
SUBARRAY TILT	0.1" AVERAGE	SUBARRAY PATTERN GAIN REDUCTION	0.50% (1)
GAP BETWEEN SUBARRAYS	$\pm .25$ " AVERAGE	ARRAY FILLING LOSS (AREA LOSS)	0.13%
RADIATING WAVEGUIDE LENGTH	± 30 MILS	MISMATCH LOSS	0.02% (2)
RADIATING WAVEGUIDE WIDTH	± 3 MILS	MISMATCH LOSS	0.12
FEED WAVEGUIDE LENGTH	± 30 MILS	MISMATCH LOSS	0.02% (2)
FEED WAVEGUIDE WIDTH	± 3 MILS	MISMATCH LOSS	0.03%
RADIATING SLOT OFFSET	± 6 MILS	SCATTERING FROM AMPLITUDE VARIANCE	0.10 (4)
TOTAL			1.42%

LEGEND: ALL LOSSES ARE ADDITIVE.

(1) INDEPENDENT OF SUBARRAY SIZE.

(2) INDEPENDENT OF STICK LENGTH.

(3) REFERRED TO AVERAGE STICK LENGTH OF $16.7 \lambda = 2.76$ METERS.

(4) ASSUMES MEAN SLOT OFFSET ERROR IS ZERO.

SPS ANTENNA ELEMENT EVALUATION CONTRACT NAS 9-15636C

TASKS:

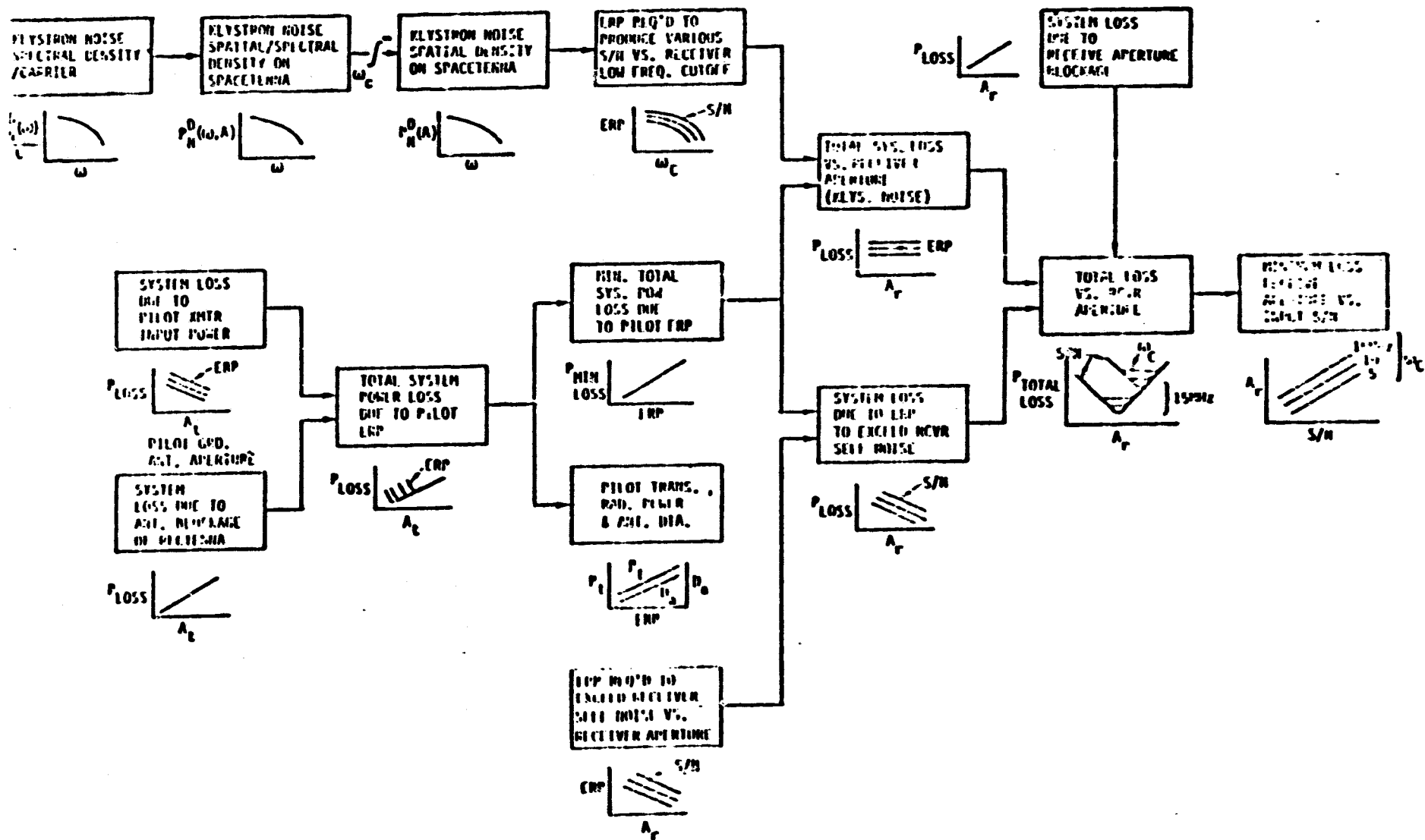
● RECEIVING TECHNIQUES EVALUATION

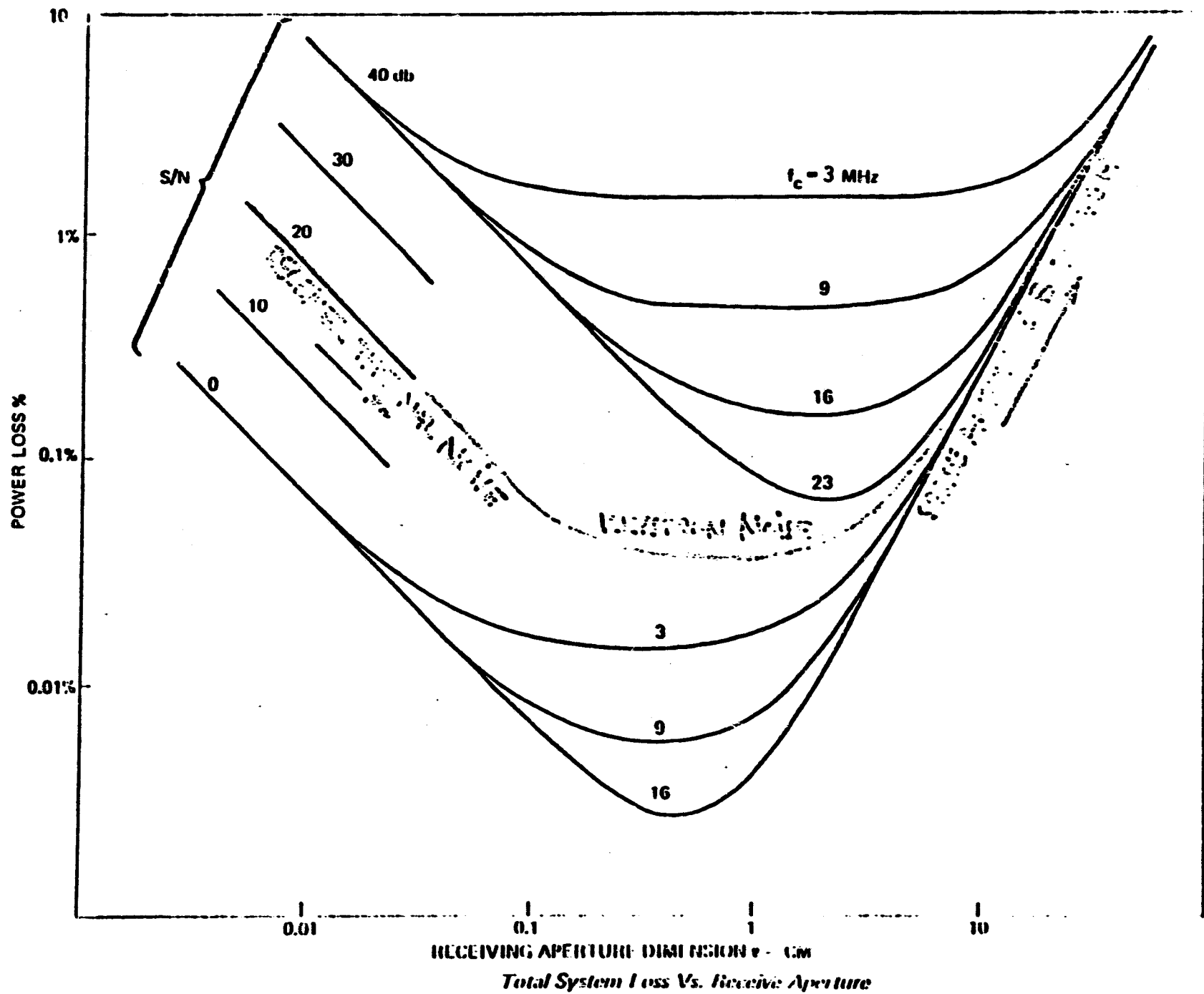
- Conduct shared antenna versus separate receiving antenna analysis to determine feasible pilot beam budget and receiving antenna constraints due to power module.
- Design and select a pilot beam receiving antenna compatible with waveguide array having minimum impact on power beam radiation efficiency.
- Evaluate pilot-beam receive-antenna techniques compatible with power beam array to allow simultaneous transmission/reception of an S-Band carrier and the anticipated pilot-beam spread-spectrum signal.

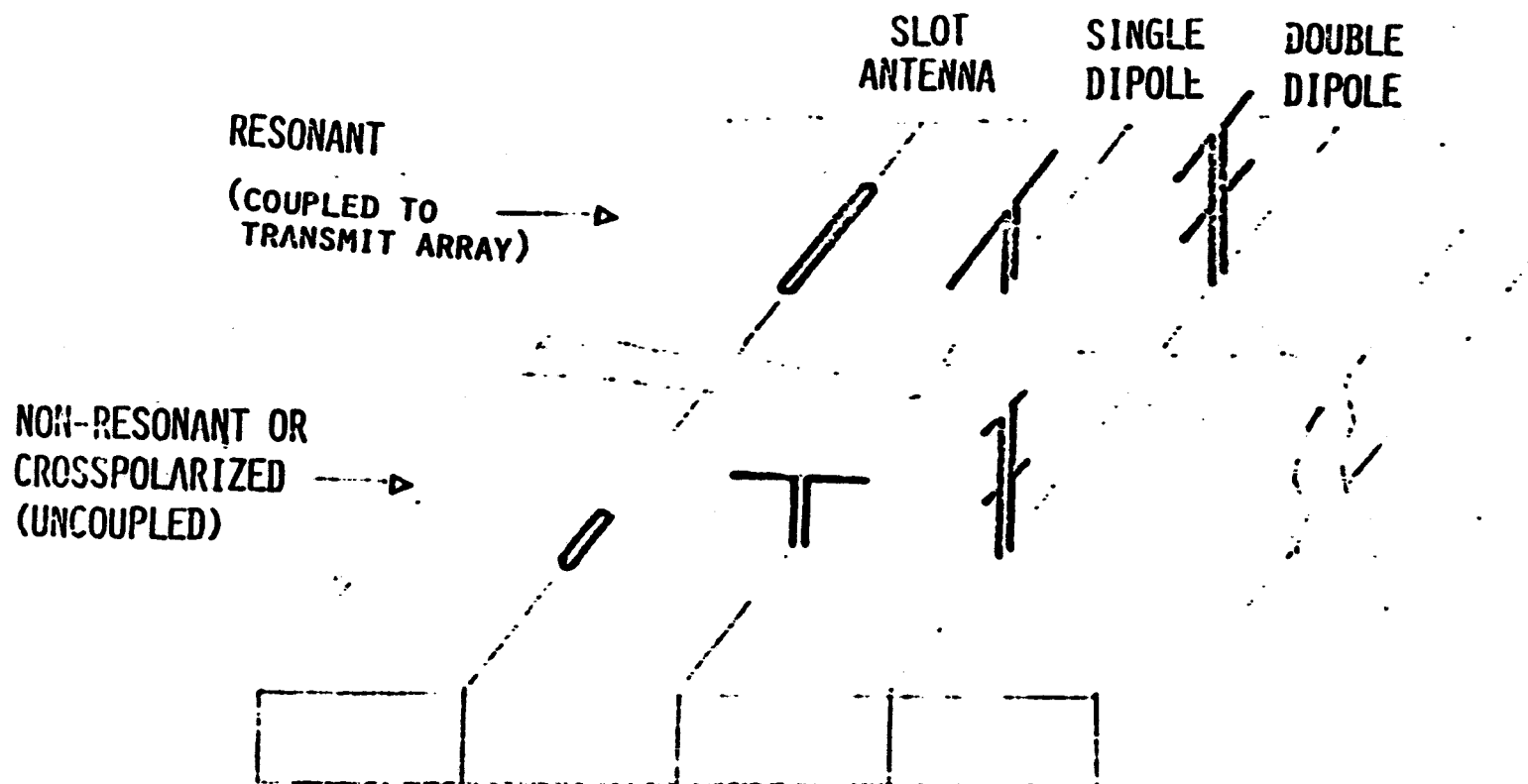
● POWER MODULE ANTENNA EVALUATION

- Define and apply mechanical and structural assembly methods to minimize mechanical tolerance errors and distortions in the power module antenna evaluation.
- Build full-scale half-module 10-stick array, utilizing single stick measurements based on analytical and experimental slot design parameters. Iterate single stick design until desired impedance characteristics are obtained. Develop and experimentally verify feed-line slot design using variable geometry slots. Utilize this technique to build a feed line with minimum reflections when connected to waveguide stick.
- Measure (1) antenna patterns, (2) impedance and return loss, and (3) swept transmission amplitude and phase on 200-foot antenna range to provide data base for design of a receive antenna system. Control mutual coupling with edge mirrors and show by varying mirror extent validity of the technique for eliminating edge effects on impedance and pattern.

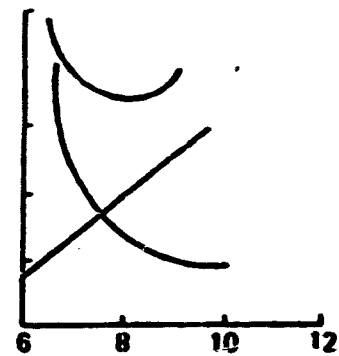
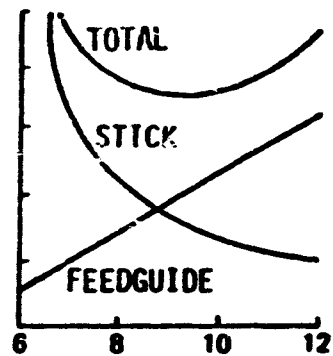
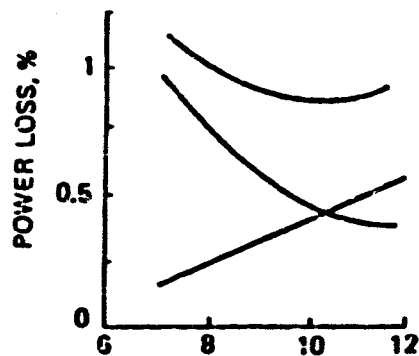
PILOT LINK ANALYSIS FLOW CHART



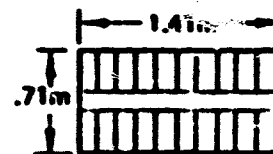
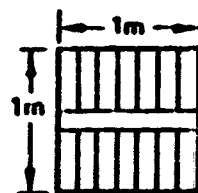
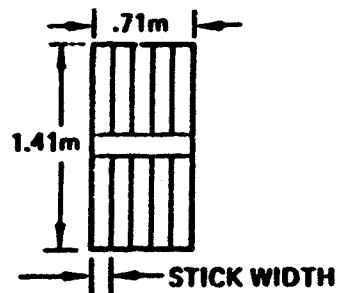




POTENTIAL SPS PILOT-LINK RECEIVING ANTENNA CONFIGURATIONS.
THE DOUBLE DIPOLE CONFIGURATIONS AFFORD PARTIAL NOISE
CANCELLATION.



STICK WIDTH - cm

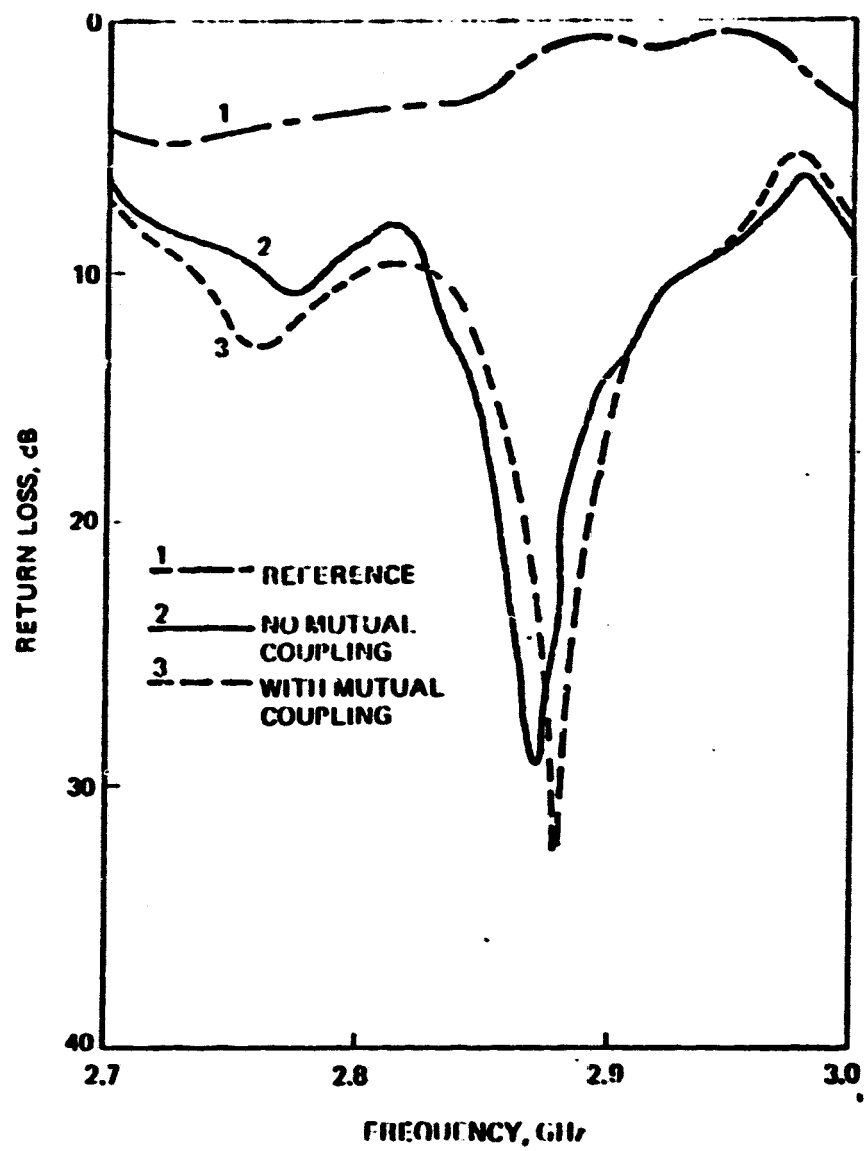


- NOT SENSITIVE TO MODULE ASPECT RATIO
- NOT VERY SENSITIVE TO WAVEGUIDE SIZE
- STICK STANDING WAVES SUGGEST END FEEDING PREFERABLE

RF Module P^2R Optimization

MODULE 12R LOSSES

- NOT SENSITIVE TO MODULE ASPECT RATIO
- NOT VERY SENSITIVE TO WAVEGUIDE SIZE
- STICK STANDING WAVES SUGGEST END FEEDING PREFERABLE



Effect of Mutual Coupling -- Two Stick Measurement

ANALYTICAL EXPRESSION¹

$$\frac{Y}{Y_0} = \frac{4 S_E S_H (1 - jw)}{b \lambda^2 [1 + w^2] + \left(\frac{\lambda}{2a}\right)^2} \cos^2 \left(\frac{\pi}{2} \sqrt{1 + \frac{\lambda^2}{2a^2}} \right) \sin^2 \left(\frac{\pi x}{b} \right)$$

WHERE

$$w = \sum_{m=1}^{\infty} \sum_{n=1}^{\infty} \left[\frac{\sin \left[\frac{\pi g m}{S_E} \right]}{\frac{\pi g m}{S_E}} \right]^2 \left[\frac{\cos \left[\frac{\pi n \lambda}{2 S_H} \right]}{1 + \left[\frac{n \lambda}{S_H} \right]^2} \right]^2 \frac{\left[\left(\frac{n \lambda}{S_H} \right)^2 - 1 \right]}{\sqrt{\left(\frac{n \lambda}{S_H} \right)^2 + \left(\frac{m \lambda}{S_E} \right)^2}}$$

$l = \%$ THE NUMBER OF NEIGHBORING SLOTS CONSIDERED IN THE 'z' PLANE

$k = \%$ THE NUMBER OF NEIGHBORING SLOTS CONSIDERED IN THE 'y' PLANE

$a =$ GUIDE I.D. WIDTH

$b =$ GUIDE I.D. HEIGHT

$S_E =$ SLOT 'z' PLANE SPACING

$S_H =$ SLOT 'y' PLANE SPACING

$x =$ SLOT OFFSET

$\lambda =$ SLOT WIDTH

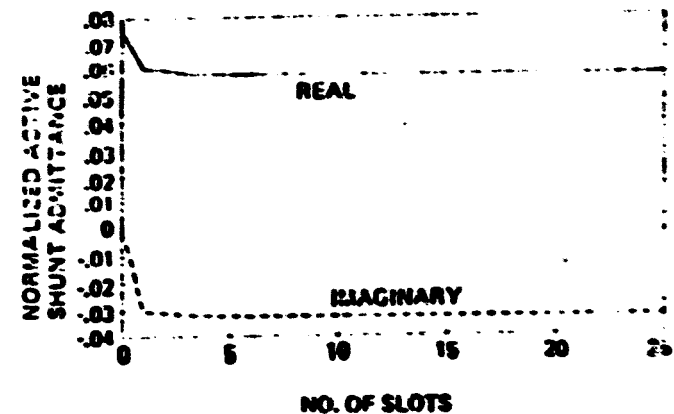
$g =$ SLOT SHUNT ADMITTANCE

$Y_0 =$ GUIDE CHARACTERISTIC

1. MODIFICATION OF STARK'S DIPOLE EXPRESSION TO SLOTS

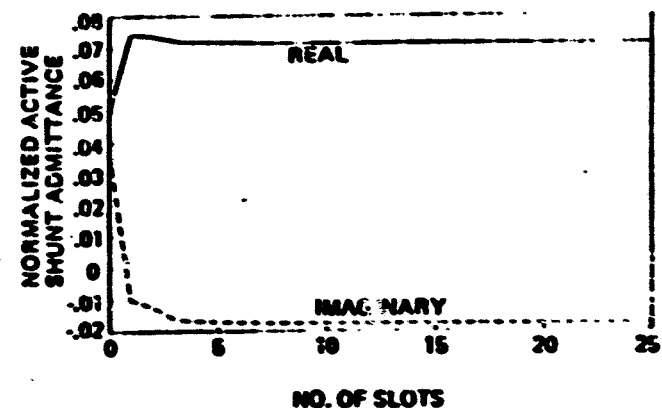
SINGLE STICK

$\frac{Y}{Y_0}$



TWO STICKS

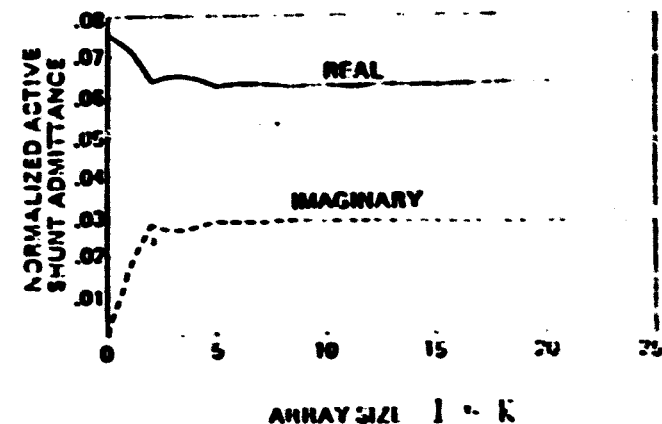
$\frac{Y}{Y_0}$



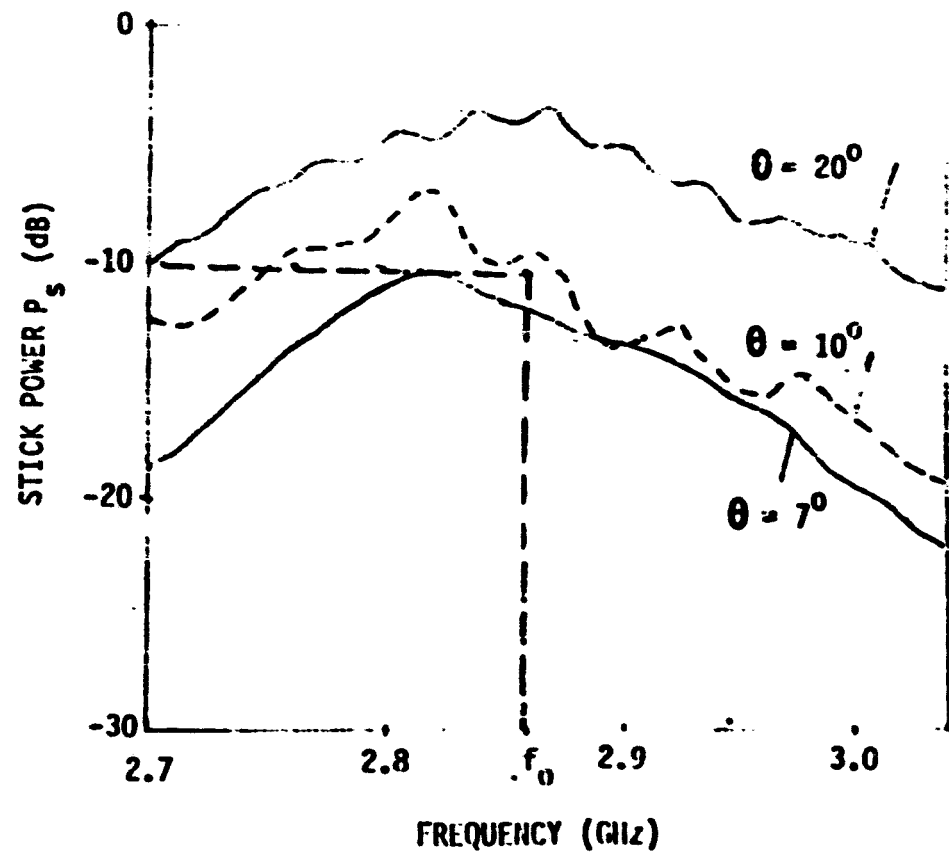
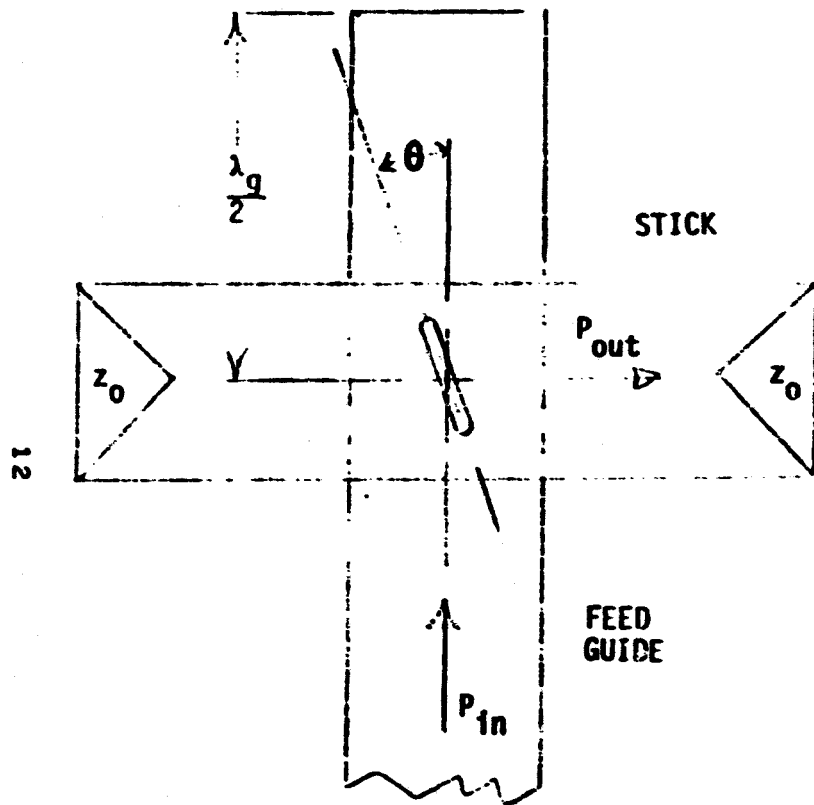
SQUARE ARRAY

$I \times K$

$\frac{Y}{Y_0}$

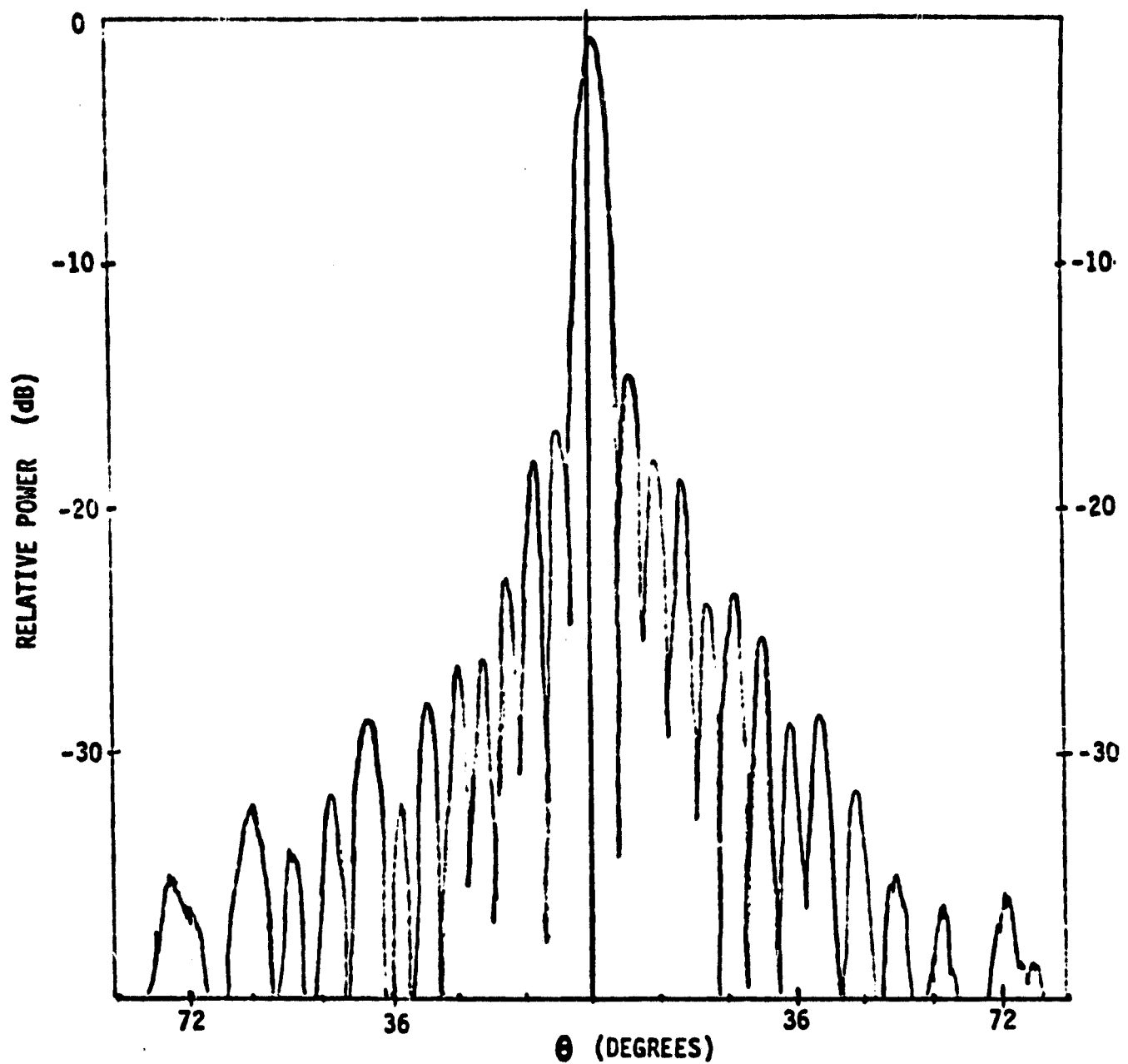


DETERMINATION OF COUPLING SLOT ORIENTATION



- COUPLING SLOT LENGTH ADJUSTED FOR RESONANCE AT 2.86GHz
- FOR A 10 STICK ARRAY, DESIRE A SINGLE STICK POWER OF -10DB
- FROM ABOVE DATA, OPTIMAL SLOT OFFSET IS ABOUT $8^\circ \rightarrow 10^\circ$

SINGLE STICK H-CUT MEASURED PATTERN



- 18 SLOT STICK IN WR 284 WAVEGUIDE
- TEST FREQUENCY 2.86 GHz
- SEPARATION BETWEEN STICK AND ILLUMINATOR OF $4.75 D^2/\lambda$

Resonant Cavity Radiator

***K. Schroeder
Rockwell International***

PRECEDING PAGE BLANK NOT FILMED

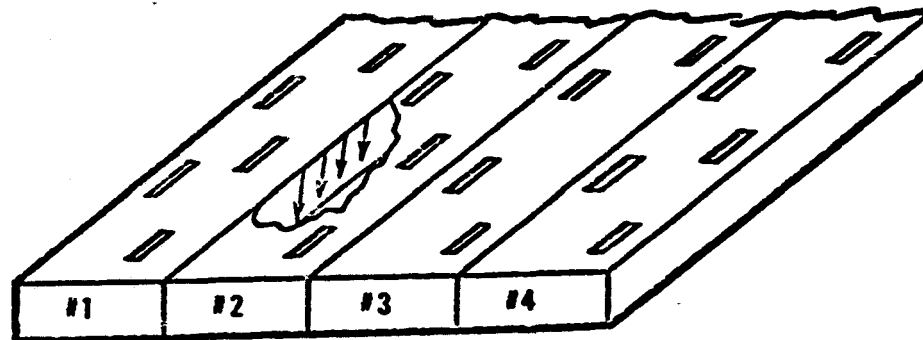
SPS MICROWAVE SYSTEMS WORKSHOP
RADIATING ELEMENTS
THE RESONANT CAVITY RADIATOR (RCR)

- o CREATED BY REMOVING SIDEWALLS FROM MULTIPLE WAVEGUIDE
STANDING WAVE SLOT ARRAY
- o SLOT SPACINGS & COUPLING SAME AS IN STANDING WAVE RADIATOR
(SWR) ARRAY
- o WEIGHT OF RCR IS REDUCED AS COMPARED TO SWR
- o STRUCTURE CAN BE SIMPLIFIED
- o EFFICIENCY MAY BE IMPROVED, IF HIGHER ORDER MODES CAN
BE AVOIDED

PRECEDING PAGE BLANK NOT FILMED

SPS MICROWAVE SYSTEMS WORKSHOP
THE RESONANT CAVITY RADIATOR

TYPICAL TE_{10} SWR ARRAY



SPS MICROWAVE SYSTEMS WORKSHOP
THE RESONANT CAVITY RADIATOR

ANALYTICAL EXPRESSION FOR CONDUCTION LOSSES

$$\alpha_c = \frac{2.8738 \times 10^{-4}}{b \sqrt{1 - \left(\frac{m\lambda}{2a}\right)^2}} \left[1 + \frac{2b}{a} \frac{m\lambda^2}{2a} \right] \frac{\text{dB}}{\text{meter}}$$

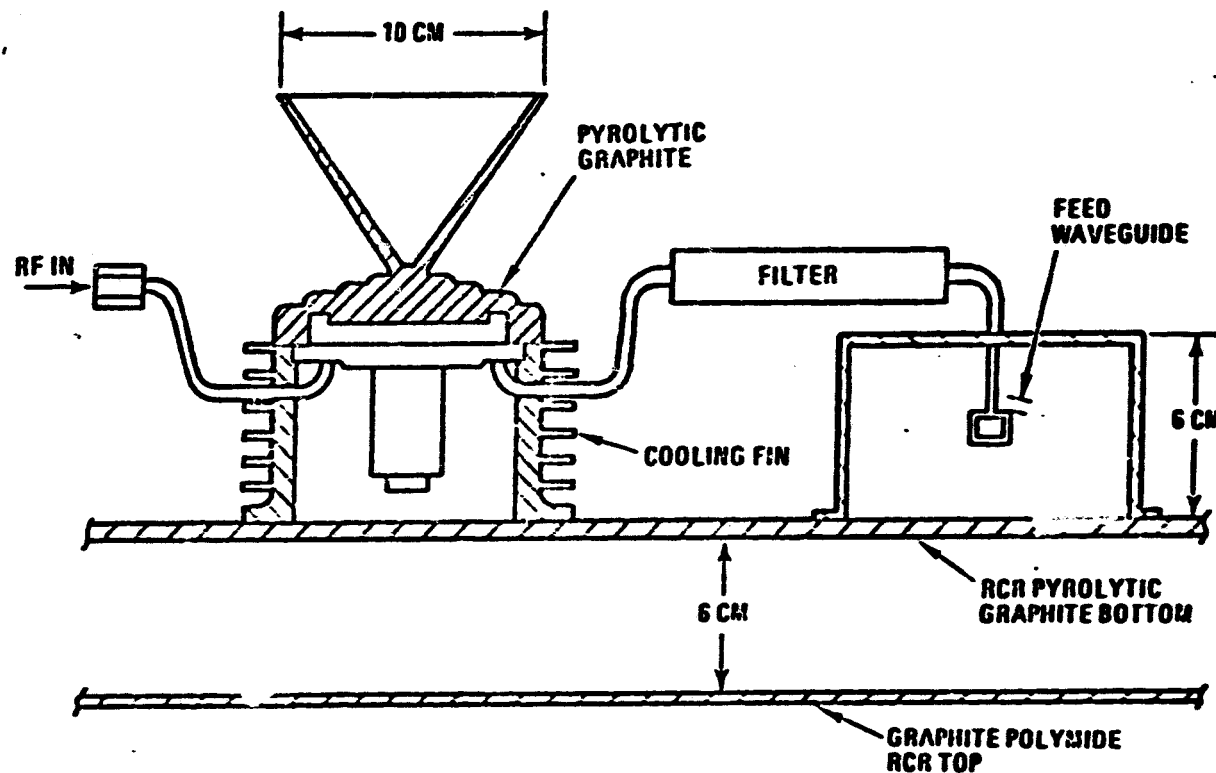
SPS MICROWAVE SYSTEMS WORKSHOP
THE RESONANT CAVITY RADIATOR

THEORETICAL POWER SAVING OF RCR OVER CONVENTIONAL
STANDING WAVE TE₁₀ SLOTTED ARRAYS

Mode	(ac) dB/Meter	Loss Differential for 2.5m (dB)	Power Savings 5-GW/Base
TE _{1,0}	8.068×10^{-3}	-	
TE _{2,0}	7.193×10^{-3}	.00218	2.51×10^6
TE _{3,0}	6.901×10^{-3}	.00291	3.35×10^6
TE _{4,0}	6.755×10^{-3}	.00328	3.77×10^6
TE _{5,0}	6.668×10^{-3}	.00350	4.02×10^6
TE _{6,0}	6.609×10^{-3}	.00364	4.19×10^6
TE _{7,0}	6.567×10^{-3}	.00375	4.3×10^6
TE _{8,0}	6.530×10^{-3}	.003845	4.42×10^6
TE _{10,0}	6.490×10^{-3}	.00394	4.53×10^6

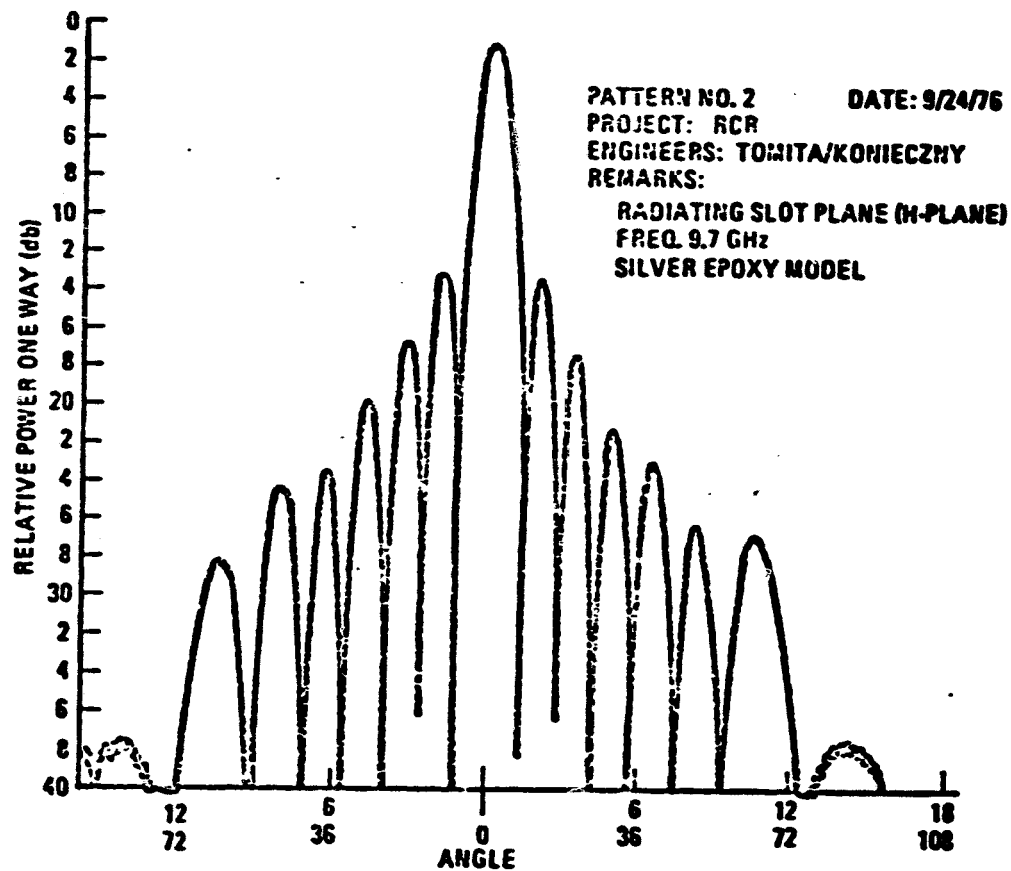
SPS MICROWAVE SYSTEMS WORKSHOP
THE RESONANT CAVITY RADIATOR

MAGNETRON MODIFIED HEAT SINK
(INPUT-OUTPUT CONNECTIONS MAY BE DIFFERENT)



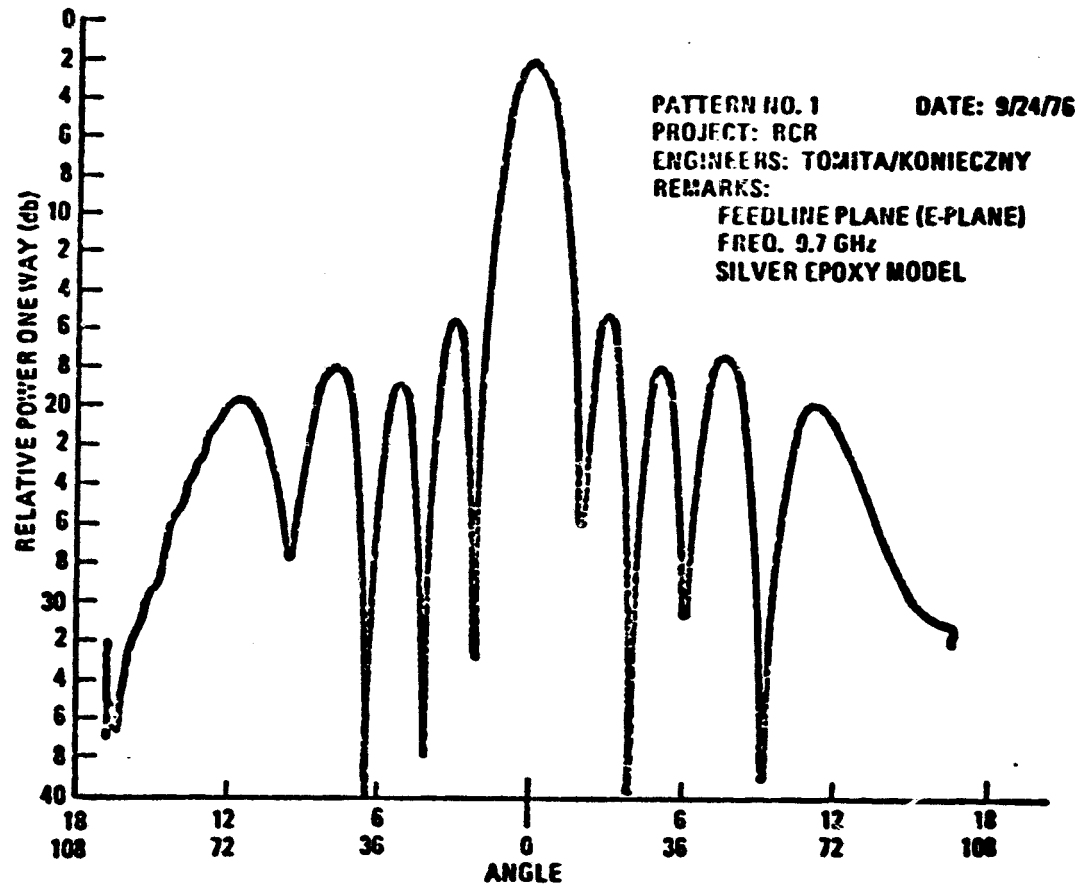
SPS MICROWAVE SYSTEMS WORKSHOP
THE RESONANT CAVITY RADIATOR

RCR H-PLANE PATTERN



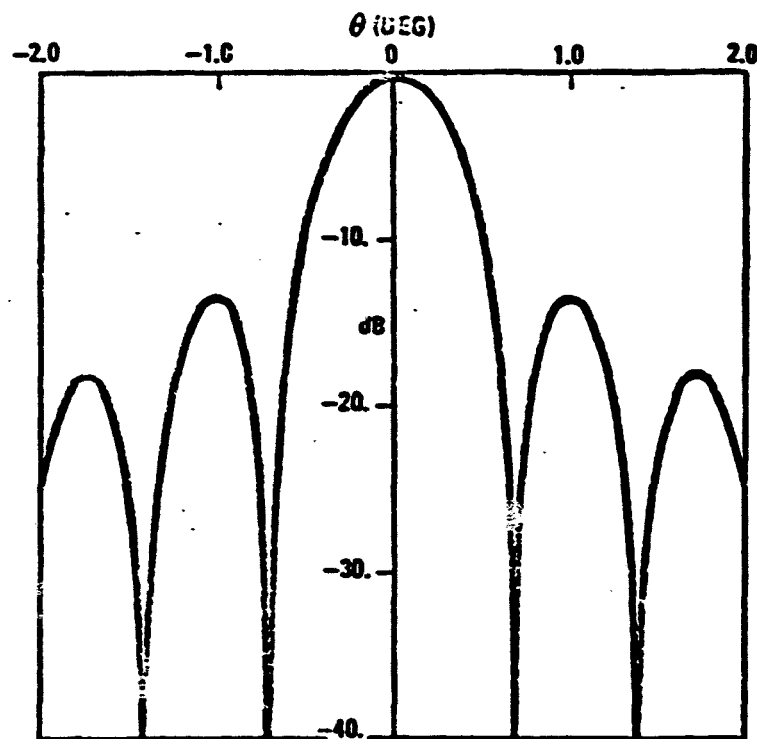
SPS MICROWAVE SYSTEMS WORKSHOP
THE RESONANT CAVITY RADIATOR

RCR E-PLANE PATTERN



SPS MICROWAVE SYSTEMS WORKSHOP
THE RESONANT CAVITY RADIATOR

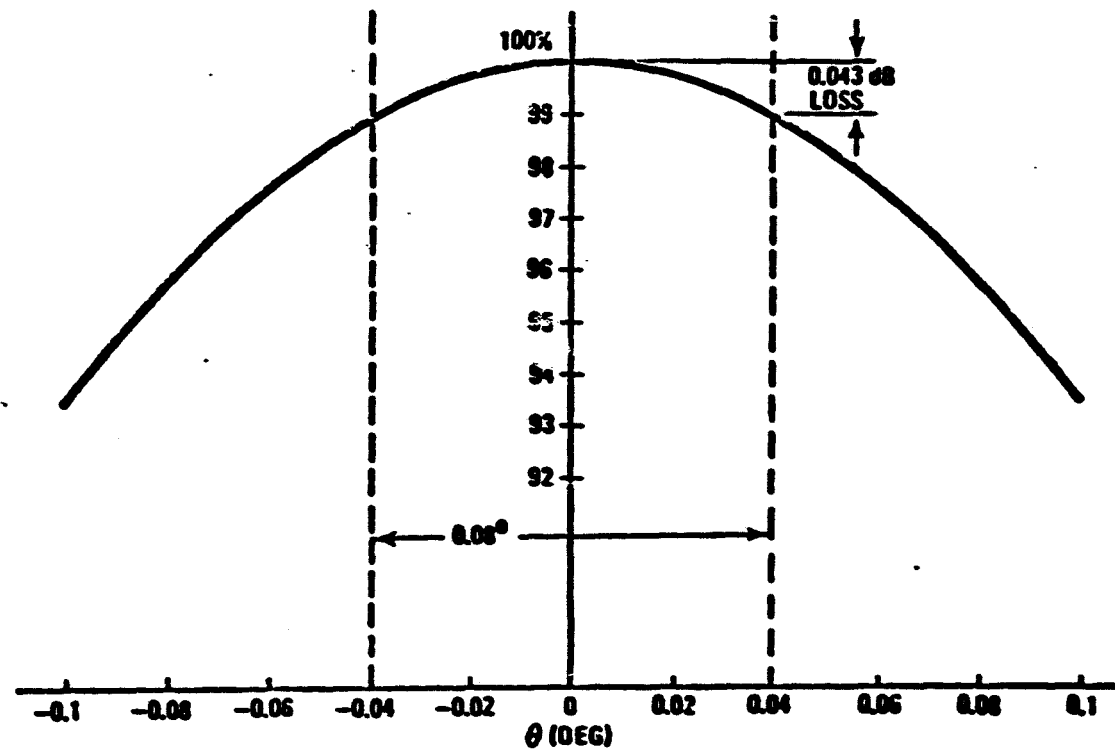
FAR-FIELD RADIATION PATTERN
(10-METER SQUARE SUBARRAY)



SPS MICROWAVE SYSTEMS WORKSHOP

THE RESONANT CAVITY RADIATOR

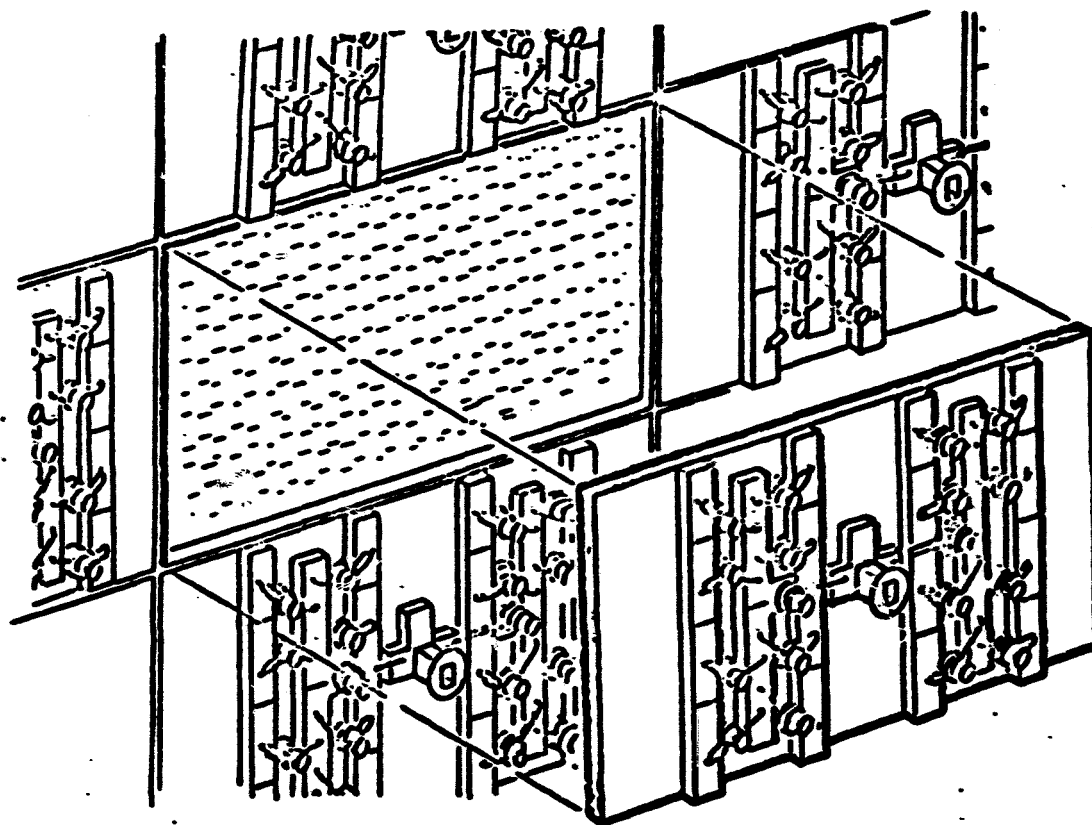
10-METER SQUARE ELEMENT FACTOR



SPS MICROWAVE SYSTEMS WORKSHOP

THE RESONANT CAVITY RADIATOR

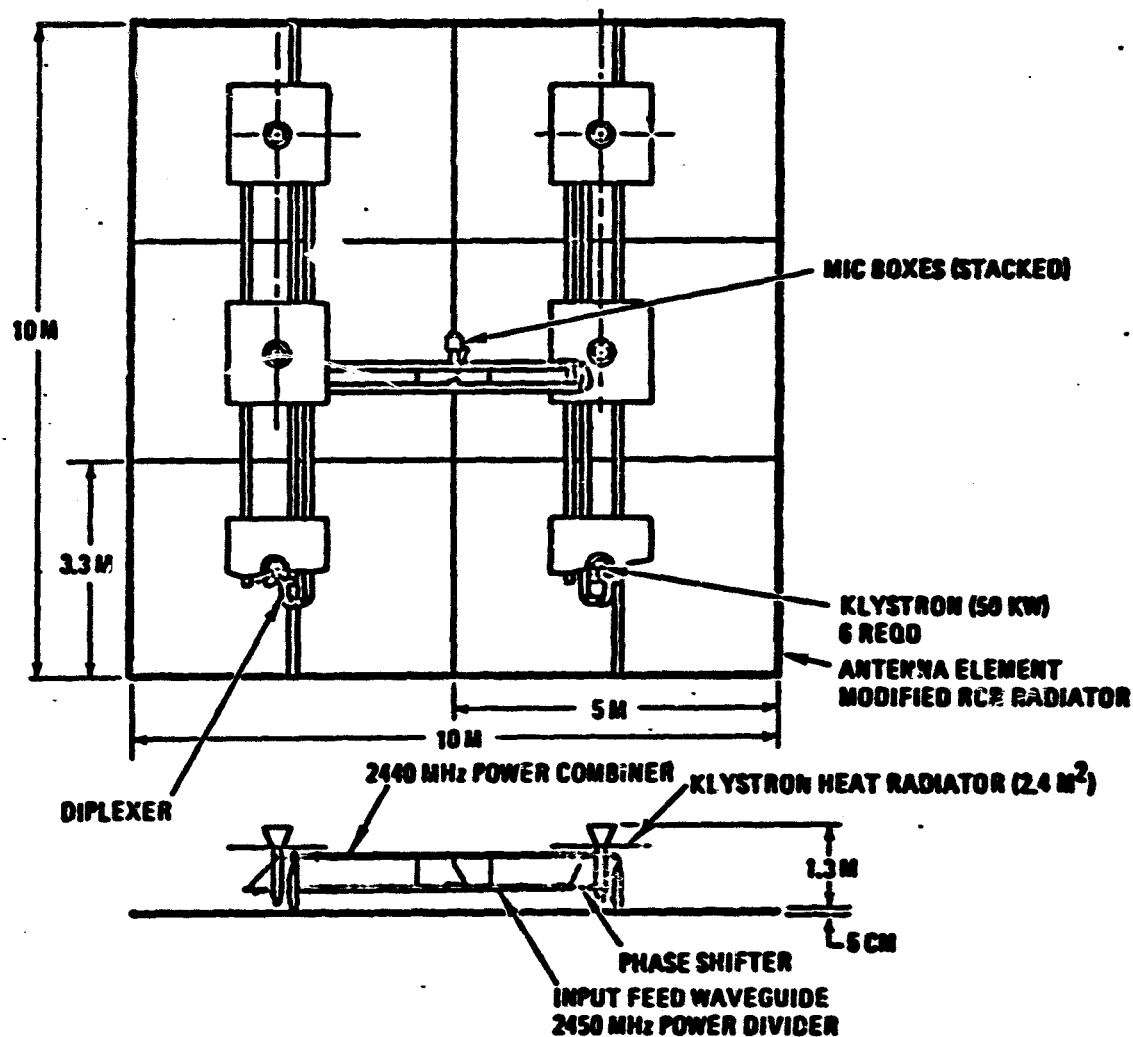
RCR ELEMENT MAINTENANCE



SPS MICROWAVE SYSTEMS WORKSHOP

THE RESONANT CAVITY RADIATOR

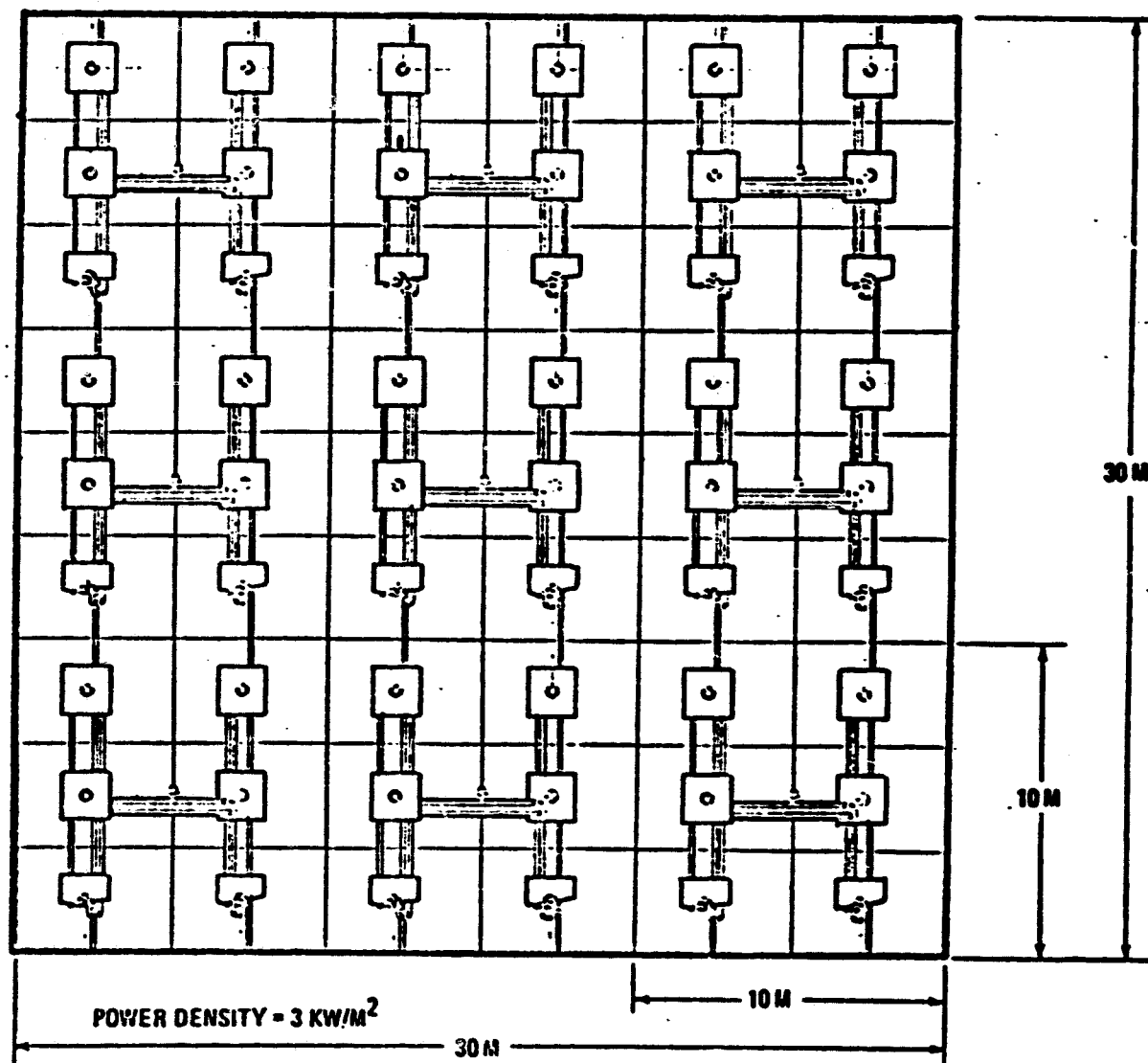
LOW-DENSITY 10-METER-SQUARE SUBARRAY



28

SPS MICROWAVE SYSTEMS WORKSHOP
THE RESONANT CAVITY RADIATOR

LOW-DENSITY 30-METER-SQUARE LAYOUT ARRAY

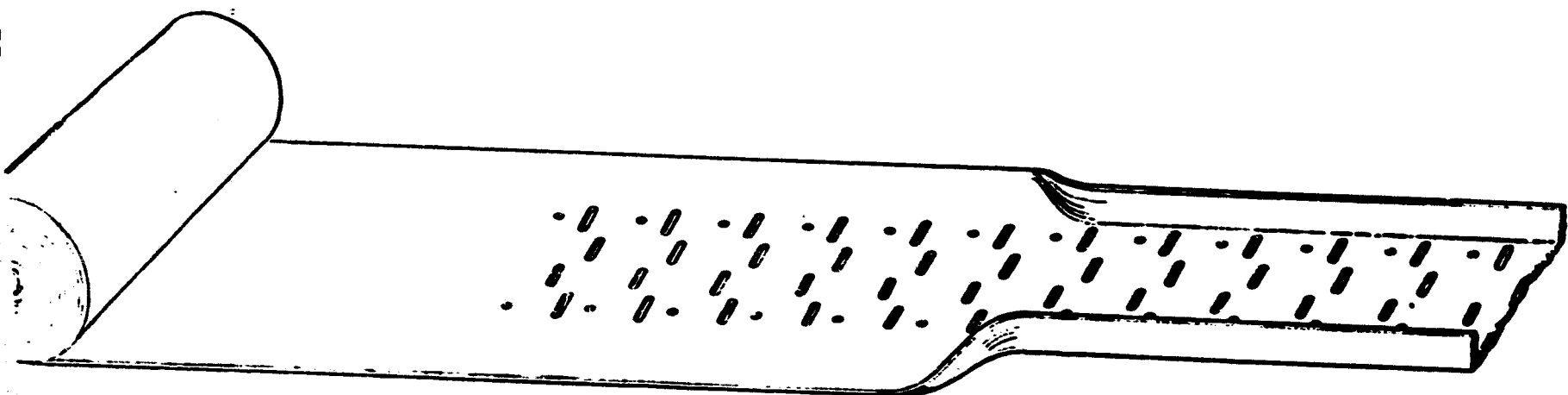
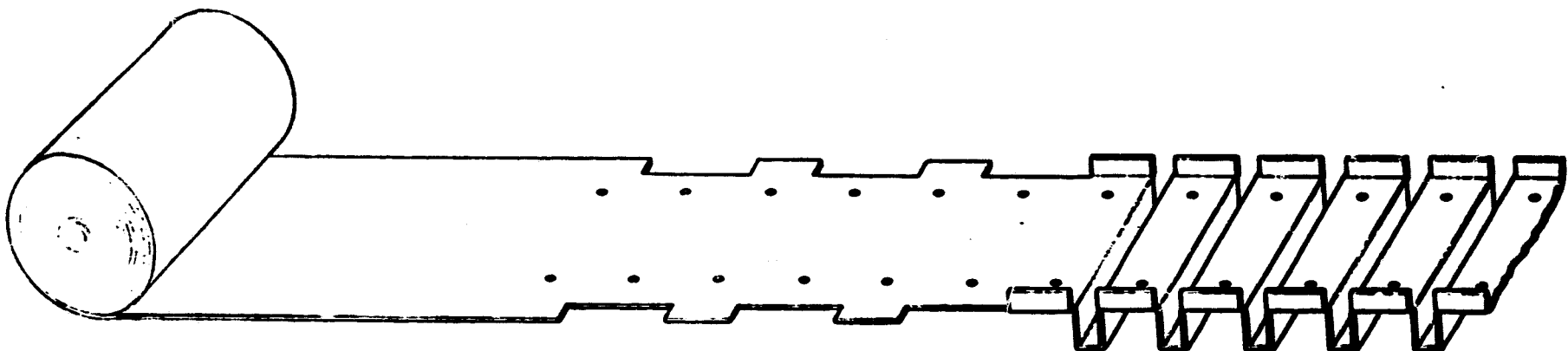


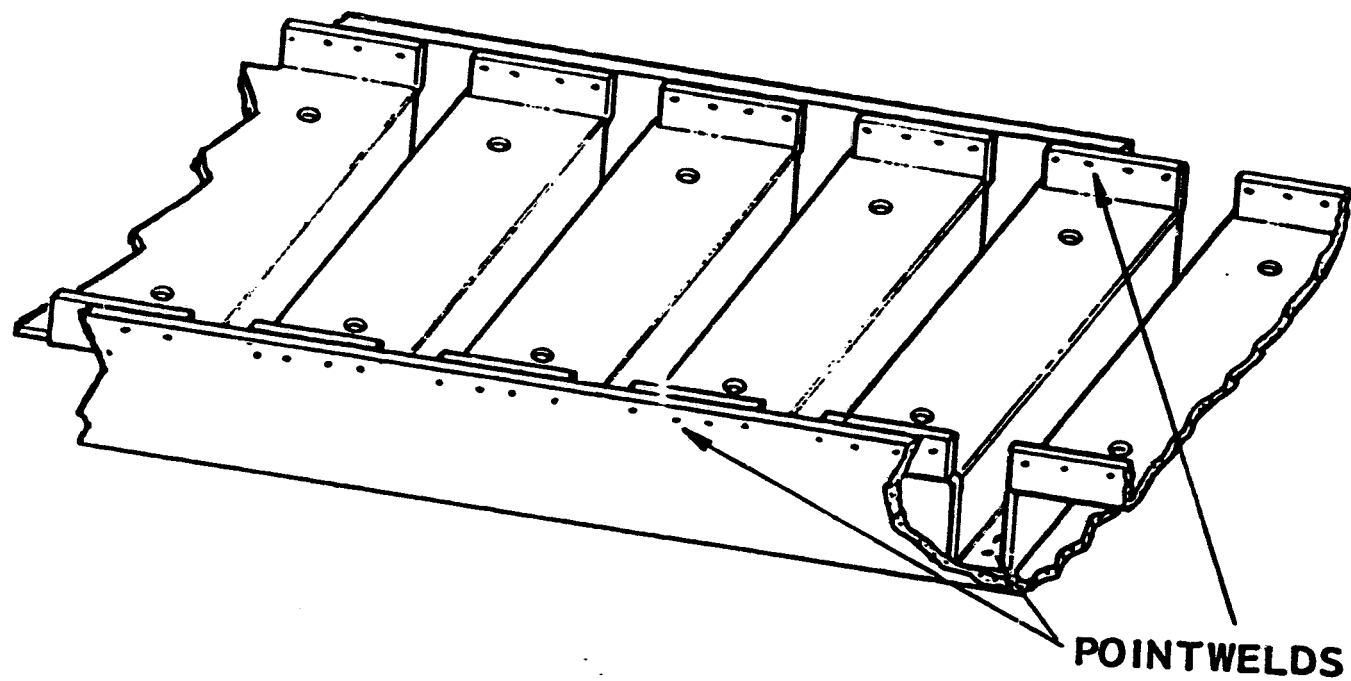
*Construction and Evaluation of a
"Thin Wall Waveguide Element"*

omit
to
P39

*W. Brown
Raytheon*

PRECEDING PAGE BLANK NOT FILMED





Matrix Array Amp
on Main Me

. 1 Phase Information
. Array #1

Col Row		1	2	3	4	5	6	7	8
1	Phase Amp	105 .53	100 .57	109 .67	110 .70	103 .64	96 .61	93 .62	105 .62
2	Phase Amp	104 .61	84 .51	80 .59	82 .67	91 .71	94 .72	79 .59	90 .40
3	Phase Amp	94 .45	80 .58	88 .63	89 .71	85 .64	85 .58	94 .56	106 .56
4	Phase Amp	105 .61	79 .56	80 .60	73 .73	80 .73	89 .69	72 .65	94 .40
5	Phase Amp	120 .50	81 .60	86 .59	76 .72	70 .68	85 .52	84 .58	120 .50
6	Phase Amp	96 .68	80 .53	74 .57	83 .68	92 .72	90 .69	79 .60	91 .39
7	Phase Amp	89 .49	73 .60	83 .67	82 .69	80 .61	86 .60	91 .54	104 .55
8	Phase Amp	100 .59	86 .60	90 .53	93 .63		96 .70	88 .57	160 .45

Overall array is an 8 x 8 matrix

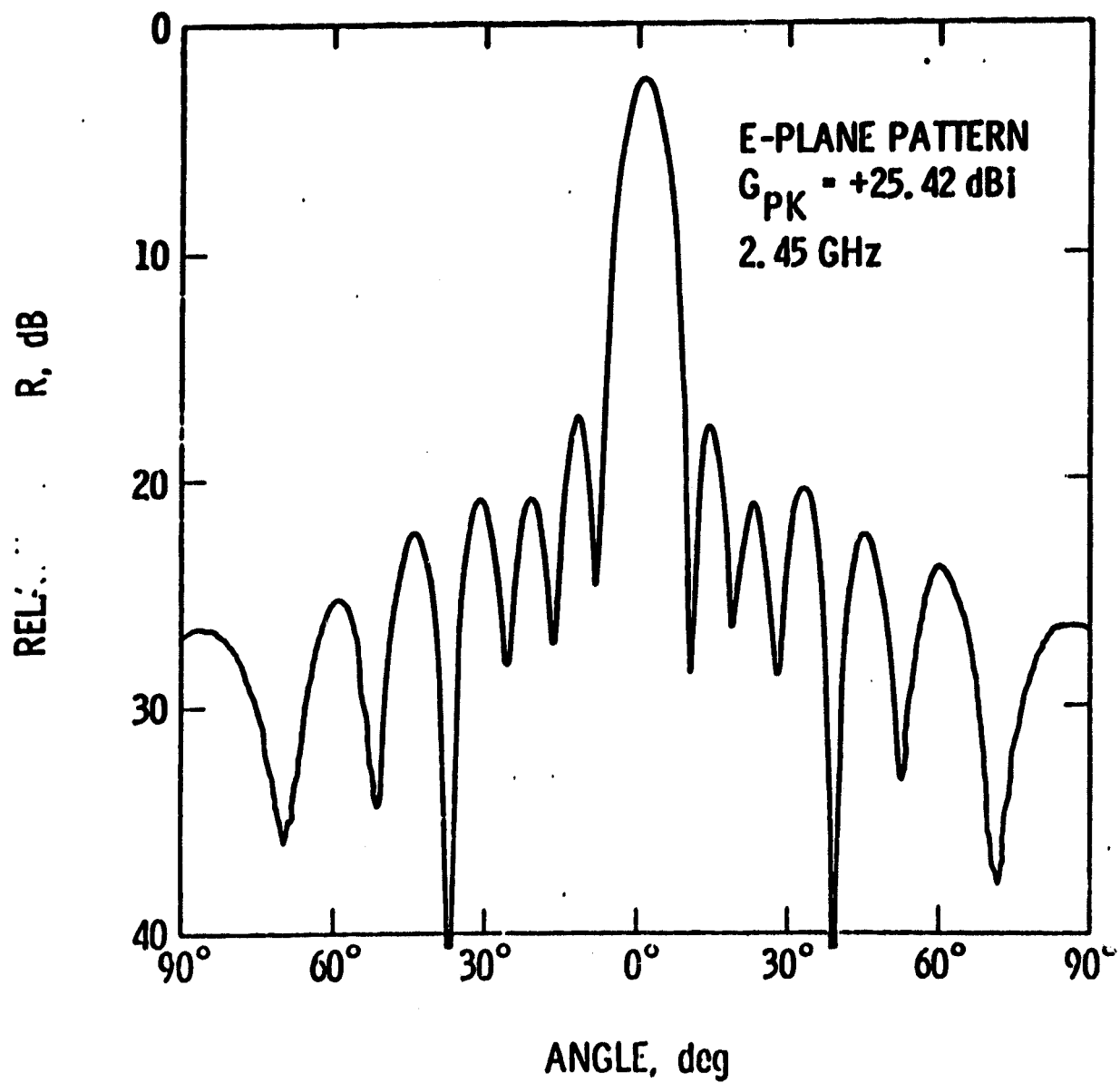
"Internal" array is a 6 x 6 matrix

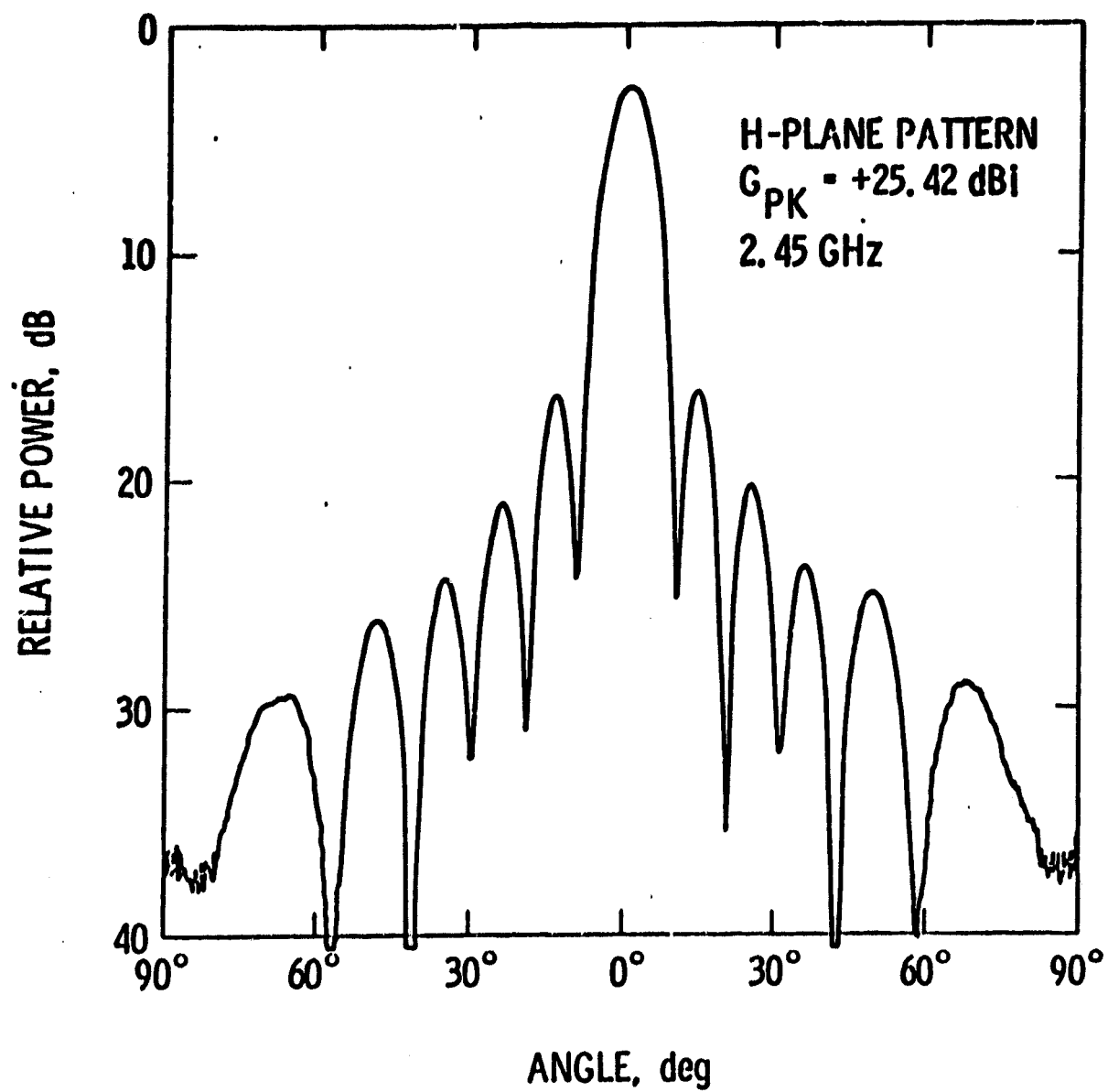
Test data obtained by dipole probe placed in front of each radiating slot.

RMS of phase deviation of internal array is 6.22°.

RMS of phase deviation of overall array is 8.89°.

RMS of amplitude variation of internal array is 0.0628 from a mean value of 0.627.





***Microwave Measurement Techniques,
Problems and Potential Solutions in
Ultra High Accuracy Antenna***

***D. J. Kozakoff
Georgia Tech Experiment Station***

PRECEDING PAGE BLANK NOT FILMED

SUMMARY

OBJECTIVES/DEFINITIONS

ERROR BUDGET(S)

FAR-FIELD MEASUREMENT TECHNIQUES

GROUND REFLECTION RANGE

ELEVATED RANGE

ANTENNA POSITIONER FACTORS

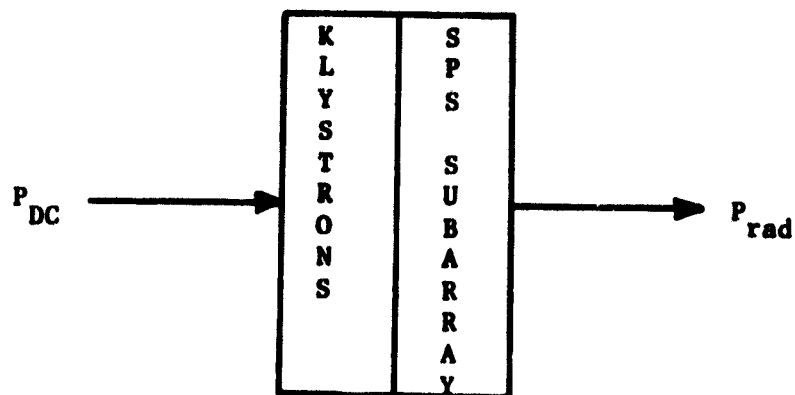
MEASUREMENT ELECTRONICS

NEAR-FIELD MEASUREMENT TECHNIQUES

CONCLUSIONS

PRECEDING PAGE BLANK NOT FILMED

DEFINITION OF RADIATION EFFICIENCY η

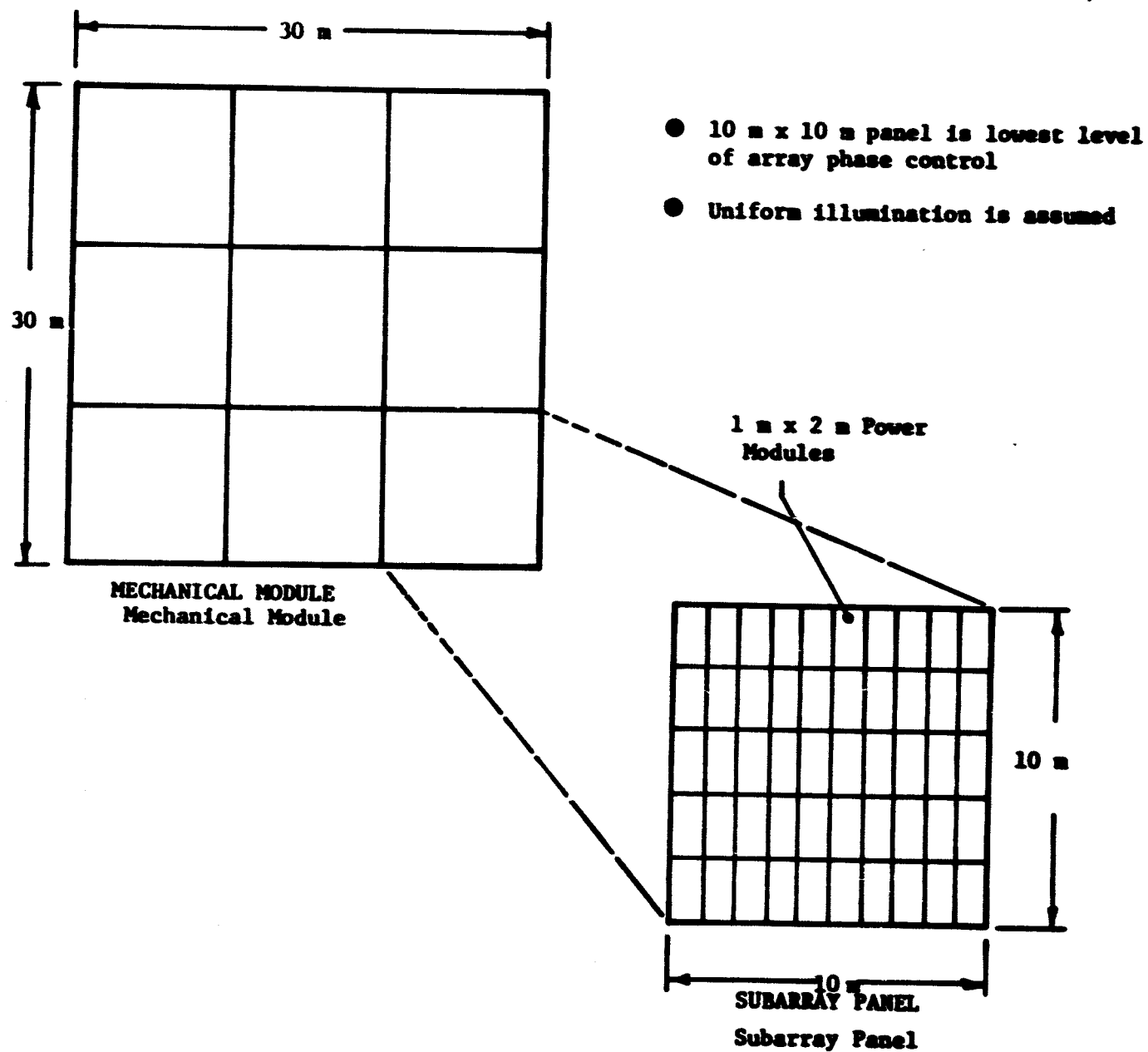


$$\eta = \frac{P_{rad}}{P_{DC}} ; \text{ where } P_{rad} = \text{RF Power in Main Beam}$$

OBJECTIVES OF STUDY

1. QUANTIFY PROBLEM AREAS IN MEASURING SUBARRAY POWER IN THE TRANSMIT BEAM AND RADIATION EFFICIENCY TO 1% (0.04 dB) ACCURACY GOAL.
2. EVALUATE PERFORMANCE POTENTIAL OF FAR-FIELD ELEVATED AND GROUND REFLECTION RANGES, AND NEAR-FIELD TECHNIQUES, TO ACHIEVING MEASUREMENT OBJECTIVES.
3. IDENTIFY STATE-OF-THE-ART PERFORMANCE OF CRITICAL COMPONENTS OR DEVICES ASSOCIATED WITH VIABLE MEASUREMENT TECHNIQUES.
4. IDENTIFY SPECIALIZED AND/OR UNIQUE FACILITIES REQUIRED.

SPS ANTENNA SUBARRAY CONFIGURATION



MEASUREMENTS ERROR BUDGET

ERROR SOURCE	COMPONENTS	ALLOWABLE VALUE	COMMENTS
ANTENNA RANGE	FIELD UNIFORMITY QUADRATIC PHASE ERROR EXTRANEIOUS REFLECTIONS STANDARD GAIN ANTENNA UNCERTAINTY ATMOSPHERIC EFFECTS AXIAL RATIO	0.036 dB	AN ADEQUATE GAIN STANDARD HAS NOT YET BEEN IDENTIFIED REFERENCE RECEIVER MUST BE NORMALIZE EFFECTS OF ATMOSPHERE
STRUCTURAL/ ENVIRONMENTAL	SPS ANTENNA RIGIDITY/ STABILITY POSITIONER ERROR WIND LOADING/THERMAL	0.01 dB	 WIND LOADING/THERMAL CAN BE CONTROLLED BY RADOME OVER TEST ANTENNA
TRANSMITTER	AMPLITUDE STABILITY FREQUENCY STABILITY	0.01 dB	PHASE LOCKED TECHNIQUES AND TEMPERATURE STABILIZATION MUST YIELD AMPLITUDE STABILITY OF 0.007 dB
RECEIVER	PRECISION ATTENUATOR UNCERTAINTY REFERENCE INPUT PHASE/ AMPLITUDE ERRORS SIGNAL TO NOISE RATIO FREQUENCY STABILITY DYNAMIC RANGE DETECTOR LINEARITY VSWR	0.01 dB	ATTENUATOR CALIBRATED TO 0.005 dB S/N RATIO MUST EXCEED 40 dB DETECTOR CALIBRATION CAN EXCEED 0.005 dB VSWR KEPT BELOW 1.05 dB

TOTAL RSS = 0.04 dB

REQUIREMENTS FOR FAR-FIELD ANTENNA RANGES

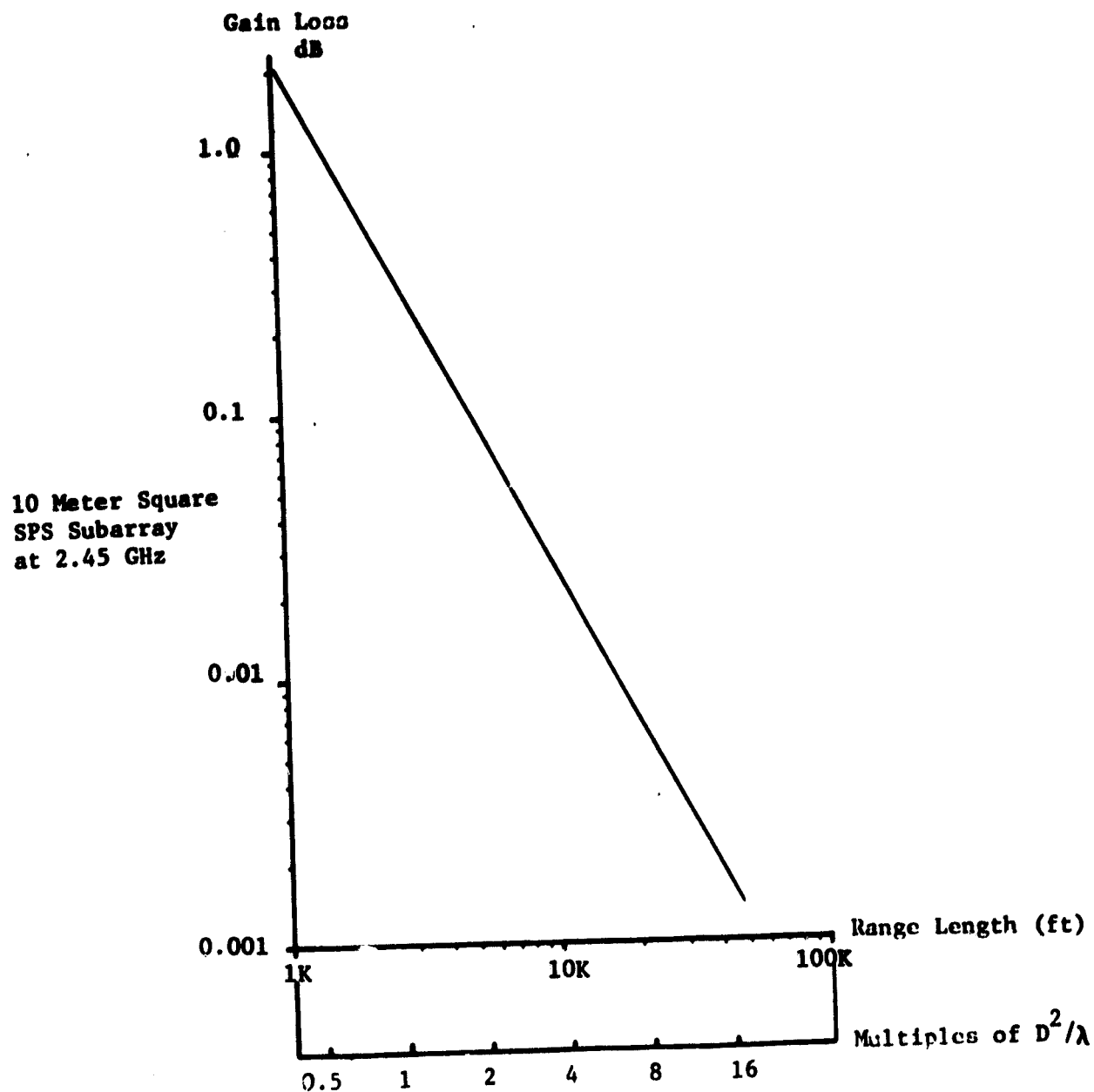
MINIMUM QUADRATIC PHASE ERROR

MINIMUM EXTRANEJUS REFLECTIONS

UNIFORM WAVEFRONT

ADEQUATE GAIN REFERENCE

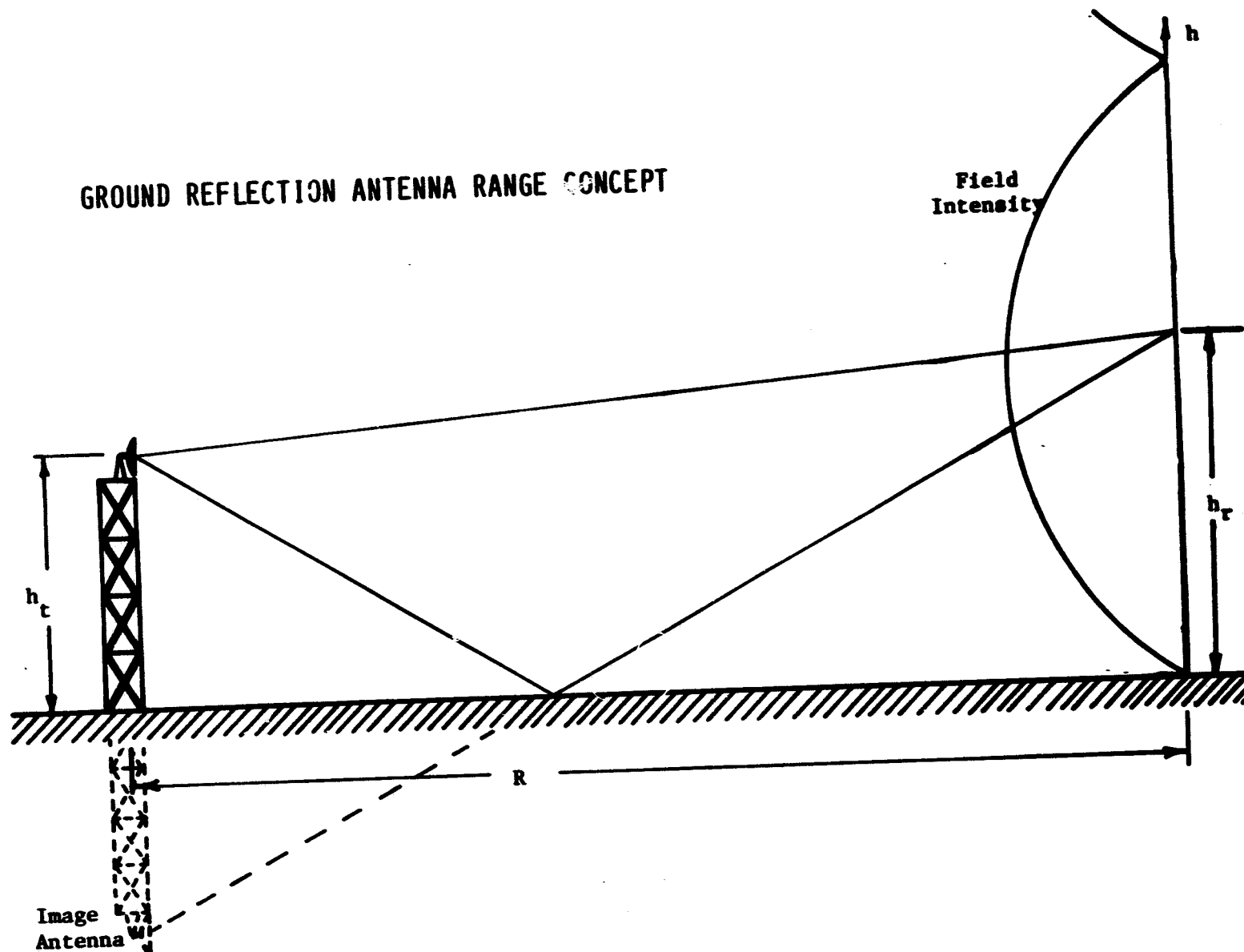
GAIN LOSS DUE TO QUADRATIC PHASE ERROR



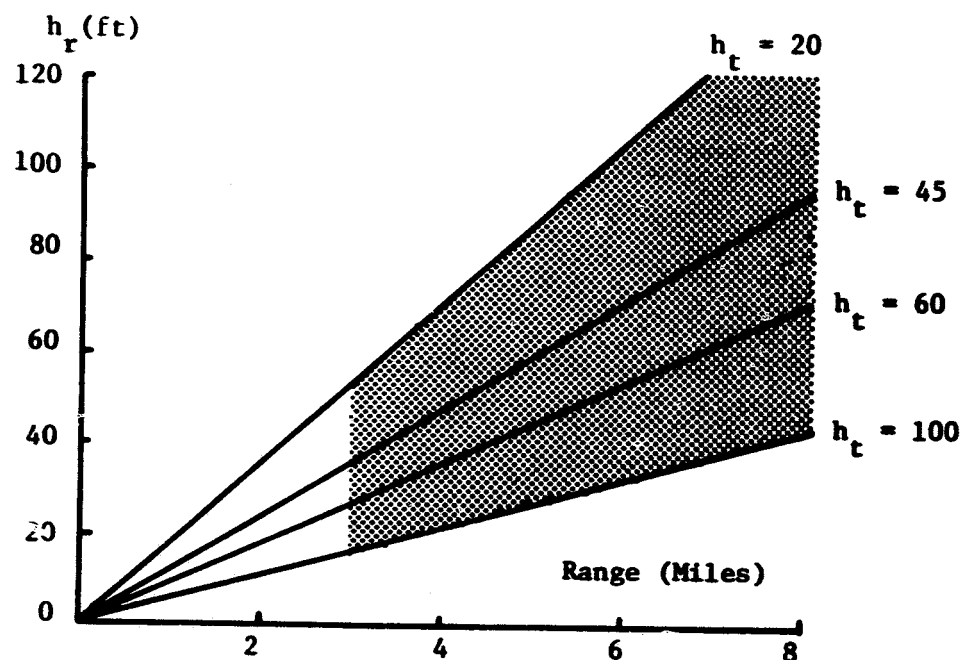
ANTENNA RANGE MEASUREMENTS ERROR SUB-BUDGET

<u>ERROR COMPONENT</u>	<u>ALLOWABLE VALUE</u>	<u>COMMENTS</u>
Field Uniformity	0.015 dB	Maximum amplitude taper at edge of SPS subarray approx. 0.04 dB
Quadratic Phase Error	0.010 dB	Requires range greater than $6 D^2/\lambda$
Standard Gain Antenna Uncertainty	0.020 dB	Gain standard needs to be developed
Atmospheric Effects	0.005 dB	Atmospheric effects cancelled by reference
VSWR	0.005 dB	VSWR loss calibrated out
Extraneous Reflections	0.025 dB	Extraneous reflections -57 dB down
<hr/>		
RSS Subtotal	0.037 dB	

GROUND REFLECTION ANTENNA RANGE CONCEPT



GROUND REFLECTION RANGE RELATIONS

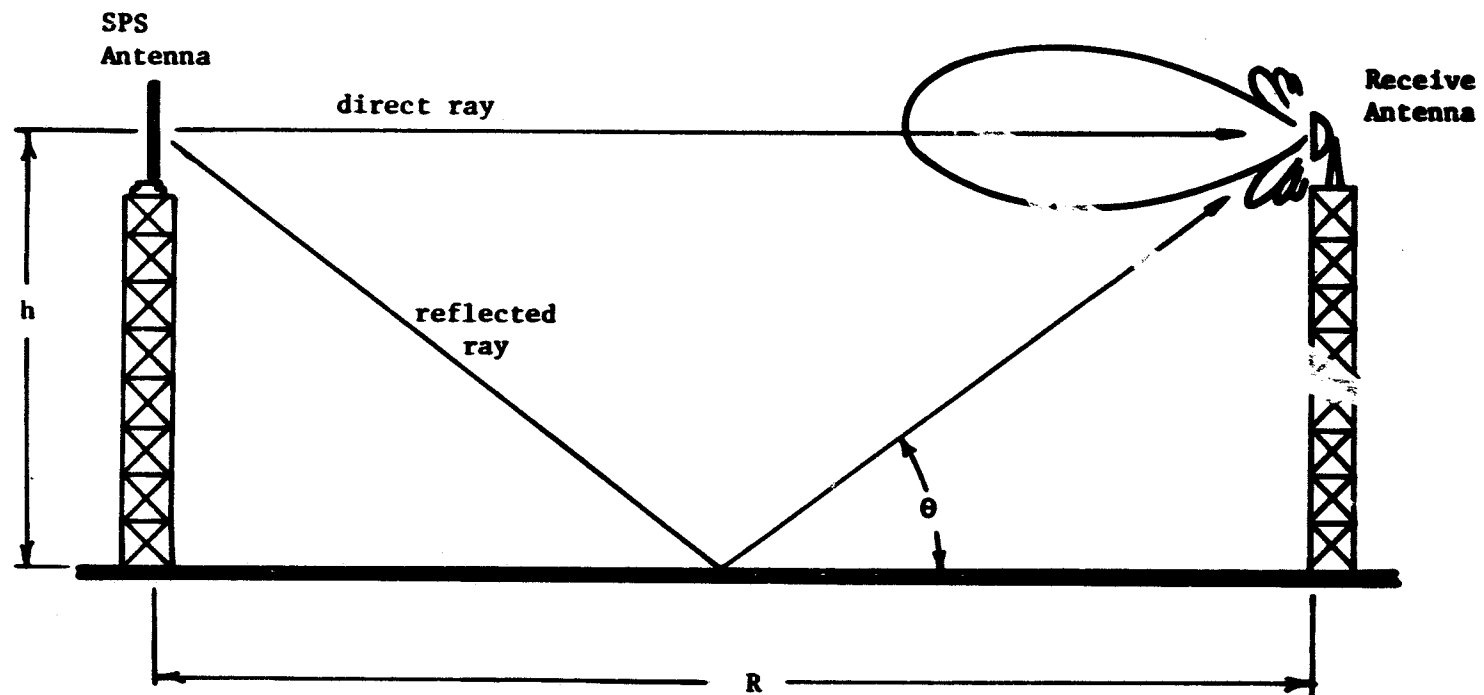


NOTE: Darkened area is allowable operating region for SPS subarray pattern measurements.

h_r = Receive Antenna Height

h_t = Transmit Antenna Height

ELEVATED ANTENNA RANGE CONCEPT



ELEVATED ANTENNA RANGE RELATIONS FOR EQUAL TRANSMIT AND RECEIVE ANTENNA HEIGHTS

Antenna Height h (feet)	Antenna Diameter (feet)	Half Power Beamwidth (degrees)	1st Null Position (degrees)	Required Range R (miles)	Comments
100	4	7.0	9.3	0.23	"h" is Highest Practical Tower Height
	8	3.5	4.7	0.46	
	12	2.3	3.1	0.70	
	15	1.85	2.5	0.87	
600	4	7.0	9.3	1.39	Mountain Top to Mountain Top Range
	8	3.5	4.7	2.76	
	12	2.3	3.1	4.20	
	15	1.85	2.5	7.04	

ANTENNA POSITIONER FACTORS

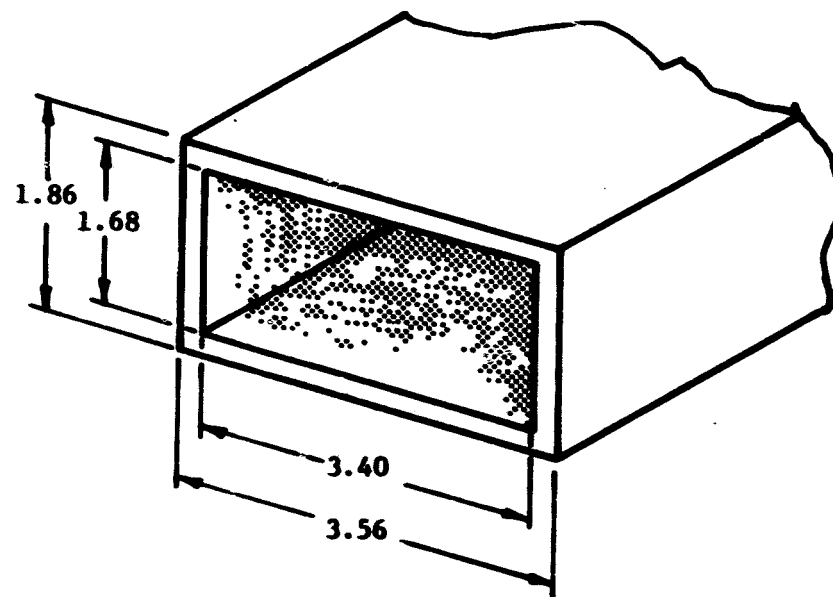
ANTENNA WEIGHT/LOADING

POSITIONING ACCURACY

POSITIONER SCAN LIMITS

WAVEGUIDE WEIGHT ESTIMATES

WR 340 (RG 112/u)
2.2 - 3.3 GHz



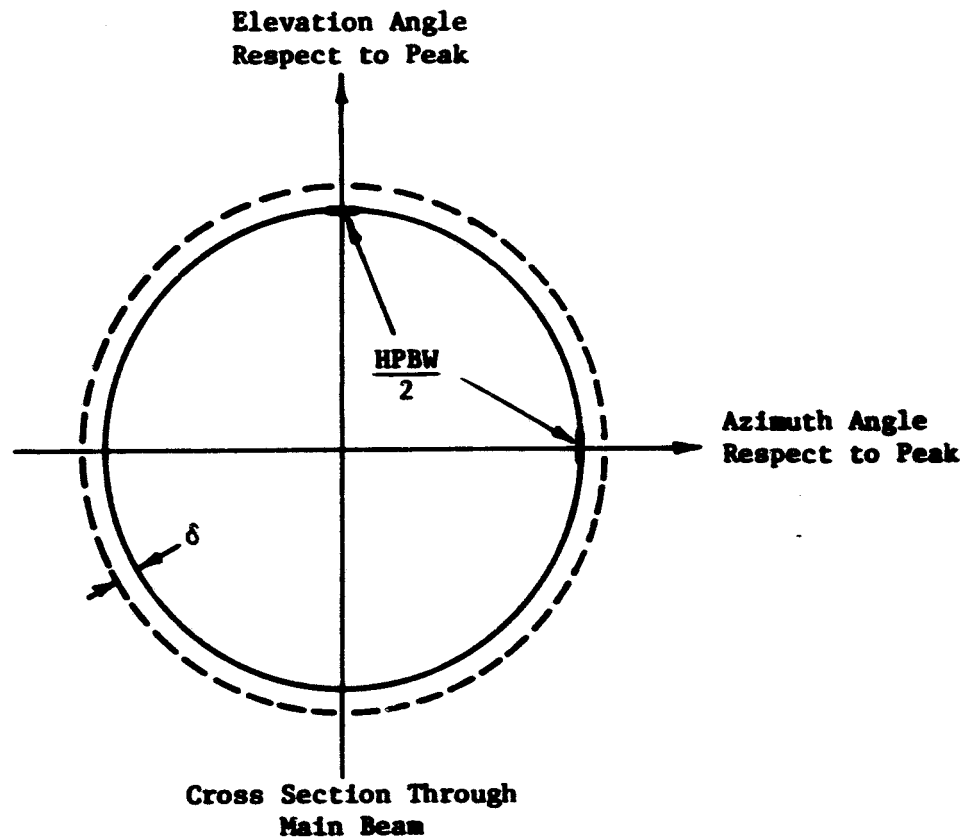
Material	Density lbs/in ³	Waveguide in ³ per ft	Waveguide lbs per ft
Copper	0.3180	10.915	3.1818
Aluminum	0.0979	10.915	0.9795

ESTIMATES OF MINIMUM SUBARRAY WEIGHT

Subarray Size (M)	Subarray Size (ft)	No. of WR340 Waveguides*	Total Length of WR340 (ft)	Total Aluminum Waveguide Wt. (tons)	Total Est. Aluminum Array Wt. (tons)	Total Copper Waveguide Wt. (tons)	Total Est. Copper Array Wt. (tons)
1	3.281	11.059	36.273	0.02	0.025	0.058	0.08
3	9.843	33.177	326.546	0.16	0.225	0.520	0.73
7	22.966	77.413	1,777.859	0.87	1.225	2.828	3.98
10	32.808	110.590	3,628.284	1.78	2.5	5.772	8.0
30	98.425	331.770	32,654.560	15.99	22.5	51.95	73.09
70	229.659	774.131	177,785.936	87.07	122.5	282.84	397.92
100	328.084	1,105.901	362,828.441	177.69	250	577.22	812.08

* Outer width = 3.56 inches = 0.2967 ft.

QUANTIFICATION OF RDP SAMPLE ACCURACY REQUIRED



Assuming power in the main beam is proportional to beam area, the δ corresponding to 1% power change is:

$$\pi \left(\frac{HPBW}{2} + \delta \right)^2 = 1.01 \pi \left(\frac{HPBW}{2} \right)^2$$

or

$$\delta = 0.005 \left(\frac{HPBW}{2} \right)$$

SUBARRAY PATTERN MEASUREMENT CRITERIA AT 2.45 GHz

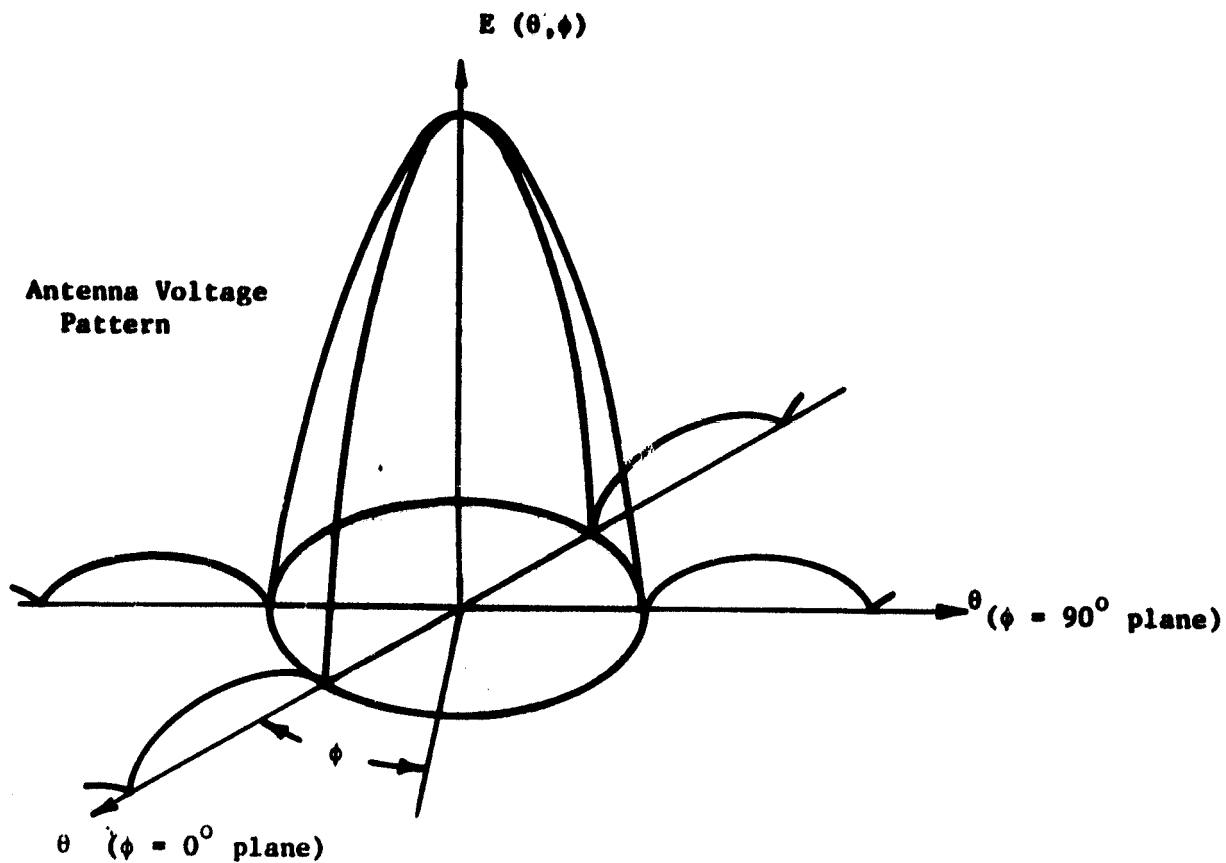
Subarray Size (M)	Subarray Size (wavelengths)	Subarray HPBW* (deg)	Pattern δ for 1% Power Change (deg)	ENCODER Requirement (Bits)**	Data Array Size for ± 1.5 Degrees Square Raster***	Total Data Array Size (words)	Comments
1	8.167	6.24	0.016	16	188x188	35.344K	
3	24.502	2.081	0.0052	18	577x577	332.929K	
7	57.172	0.892	0.0022	19	1,364x1,364	1.86K	
10	81.67	0.624	0.0016	19	1,875x1,875	3.516M	Encoder Quantification to 0.00097 degrees
30	245.02	0.208	0.00052	21	5,770x5,770	33.293M	Encoder not Available
70	571.72	0.0892	0.00022	22	13,637x13,637	185.968M	Encoder not Available
100	816.7	0.0624	0.00016	23	18,750x18,750	351.562M	Encoder not Available

* Uniform illumination

** Quantification to approximately $\delta/2$

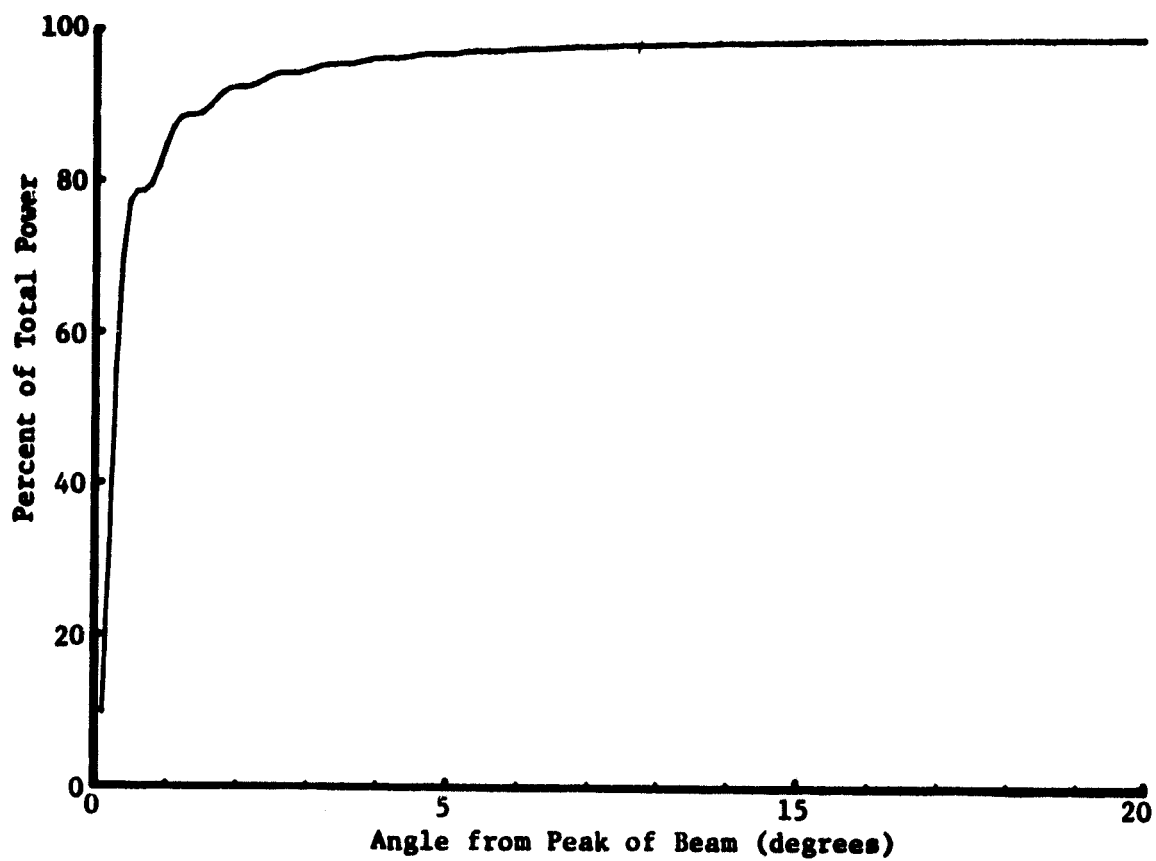
*** Sampled at $\delta/2$

Definition of Antenna Beam Parameters



$$\text{Fractional Beam Power} = \frac{\int_0^{\pi/2} \int_0^{2\pi} E^2(\theta, \phi) \sin\theta \, d\phi \, d\theta}{\int_0^{\pi} \int_0^{2\pi} E^2(\theta, \phi) \sin\theta \, d\phi \, d\theta} \times 100$$

FRACTIONAL BEAM POWER FOR SPS SUBARRAY PATTERN



- Approximately 89% of Total Power Within $\pm 1.5^\circ$
- Over 99% of Radiated Power Within $\pm 20^\circ$

ANTENNA POSITIONER REQUIREMENTS
FOR 10- BY 10- METER SUBARRAYS

WEIGHT

FOR SUBARRAY CONSTRUCTED OF STANDARD
WR-340 ALUMINUM WAVEGUIDE (0.98 LBS/FT),
NO KLYSTRONS

2.5 TONS

FOR LIGHT WEIGHT PROTOTYPE WAVEGUIDE
(11.8 LBS/M²), PLUS 50 VARIAN 4K3SK
KLYSTRONS AT 85 LBS EACH

2.7 TONS

ENCODER

TO PROVIDE 0.0018 - DEG. RESOLUTION
REQUIRED FOR 1% POWER MEASUREMENT ACCURACY

19 BITS

SCAN LIMITS

COMPATIBLE WITH MAIN LOBE BEAM POWER
PATTERN INTEGRATION

±1.5 - DEGREES
(AZIMUTH AND
ELEVATION)

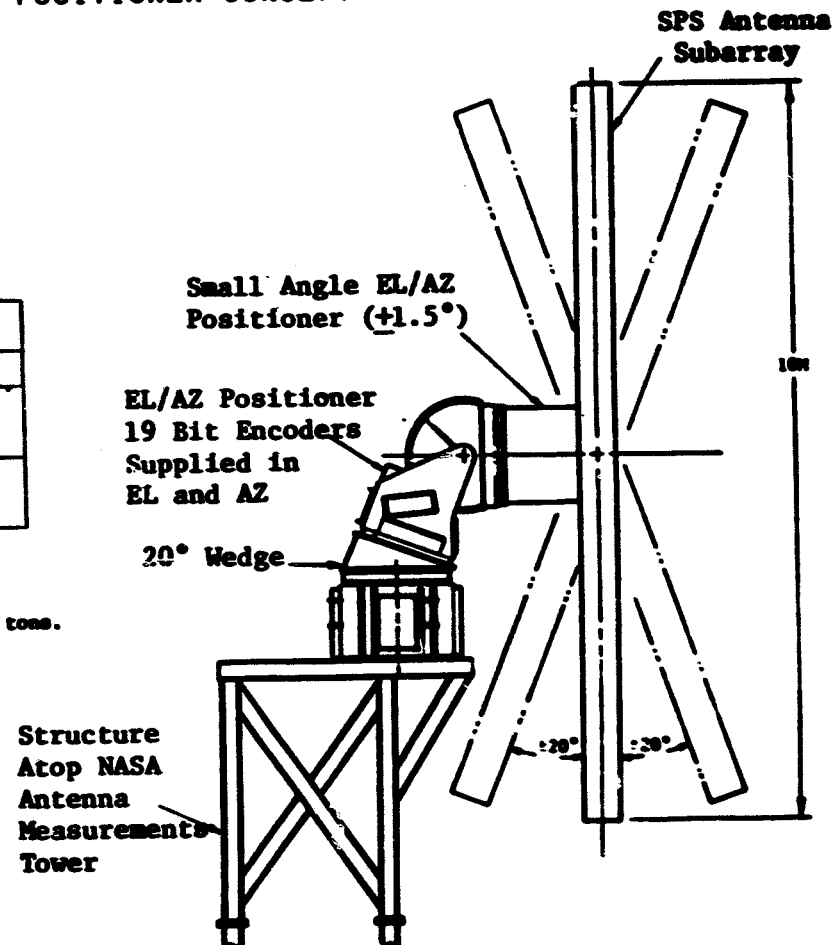
STATE-OF-THE-ART POSITIONER CONCEPT

Positioner Performance

Scientific Atlasca Series**	Maximum Moment (Kft-lb)	Estimated Moment Arm [*] (ft)	Maximum Subarray Wt.	
			Klbs	Tons
85	150	9.5	15.8	7.9
45	75	7.5	10	5

* Elevation over azimuth plus SNAP configuration.

** NOTE: the series 85 has a maximum vertical load limit of 25 tons.



MEASUREMENT ELECTRONICSS FACTORS

STABILITY

LINEARITY

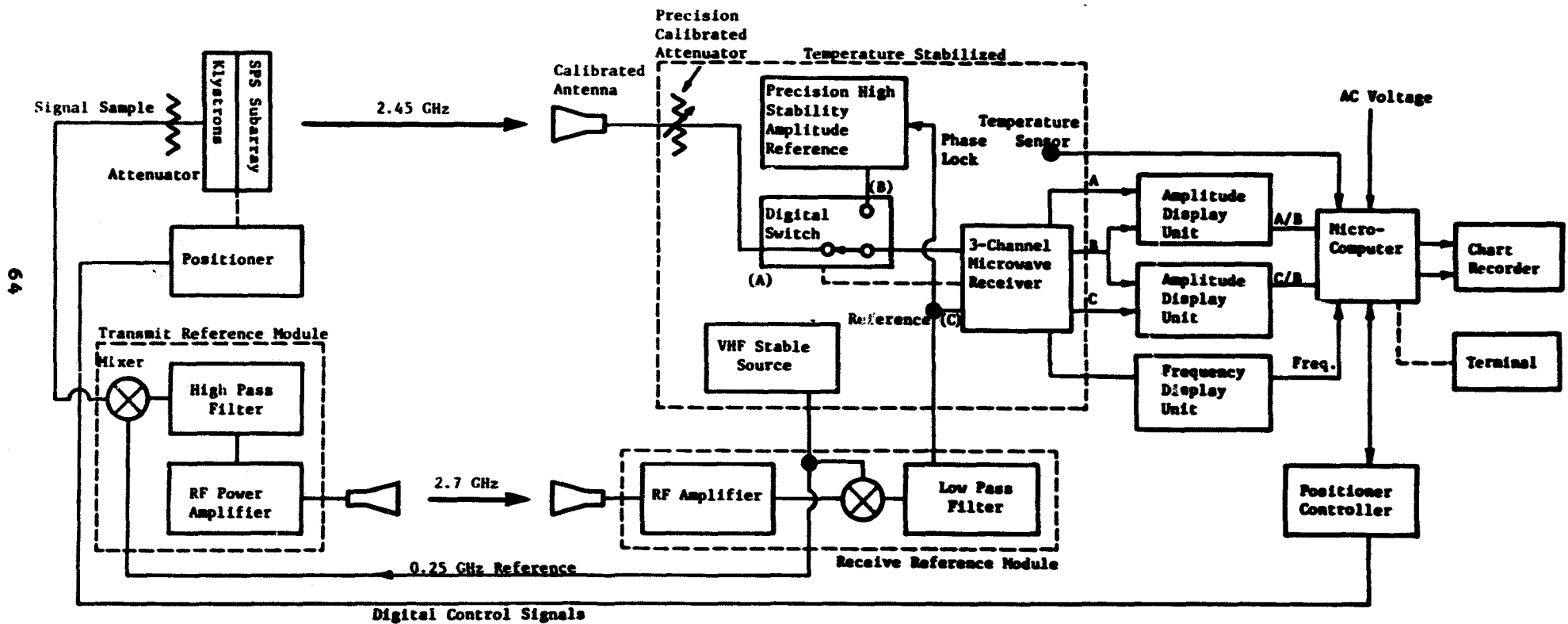
ACCURACY

ERROR SUB-BUDGET FOR RECEIVER ELECTRONICS

ERROR SOURCE	STATE-OF-THE-ART PERFORMANCE (1)	SPS ERROR BUDGET	COMMENTS
LINEARITY	0.05 dB/10 dB	0.005 dB	MICROCOMPUTER CALIBRATION REQUIRED
IF AMPLIFIER DRIFT	0.05 dB/°C	0.002 dB	TEMP. STABILIZATION AND MICROCOMPUTER CALIBRATION REQUIRED
CABLE LOSSES	0.2%/°C	0.002 dB	PRECISION AMPLITUDE REFERENCE WILL NORMALIZE CABLE LOSS VARIATIONS
CROSSTALK	0.1 dB FOR 40 DB DIFFERENCE BETWEEN CHANNELS	0.003 dB	MICROCOMPUTER COMPENSATION REQUIRED
AMPLITUDE RESOLUTION	0.1 dB OVER 80 DB DYNAMIC RANGE (2)	0.001 dB	17 BIT PARALLEL BCD RECEIVER OUTPUTS REQUIRED FOR 0.001 DB RESOLUTION
S/N RATIO	0.01 dB FOR S/N = 60 DB	0.005 dB	NARROW IF BW REQUIRED TO EXTEND DYNAMIC RANGE
LINE VOLTAGE VARIATION	0.02 dB FOR 1% CHANGE IN LINE VOLTAGE	0.001 dB	VOLTAGE REGULATION AND MICROCOMPUTER COMPENSATION REQUIRED
PRECISION IF/ RF ATTENUATORS	+ 0.2 dB FOR 10 DB STEPS	0.005 dB	MICROCOMPUTER COMPENSATION MAY BE REQUIRED
VSWR	0.15 dB FOR VSWR OF 1.3:1	0.002 dB	ALL VSWR'S MAINTAINED BELOW 1.05 AND/OR CALIBRATED OUT
RSS TOTAL		0.01 dB	

- NOTES: (1) DATA BASED ON S/A 1711 AND 1770 RECEIVERS
- (2) DATA BASED ON S/A 1832A AMPLITUDE DISPLAY UNIT

ANTENNA MEASUREMENT EQUIPMENT BLOCK DIAGRAM



KEY DEVELOPMENT ITEMS

PRECISION ATTENUATOR

GAIN STANDARD

STABLE OSCILLATOR (AMPLITUDE AND PHASE)

COMPUTERIZED NORMALIZATION

N E A R - F I E L D R A N G E

USEFUL FOR TESTING AT INTERMEDIATE POWER LEVELS

PLANAR SCANNER APPROACH CAN BE IMPLIMENTED INDOORS

TECHNIQUE MAY BE APPLICABLE TO FULL 30-METER MODULE TESTING

REQUIREMENTS FOR NEAR-FIELD RANGES

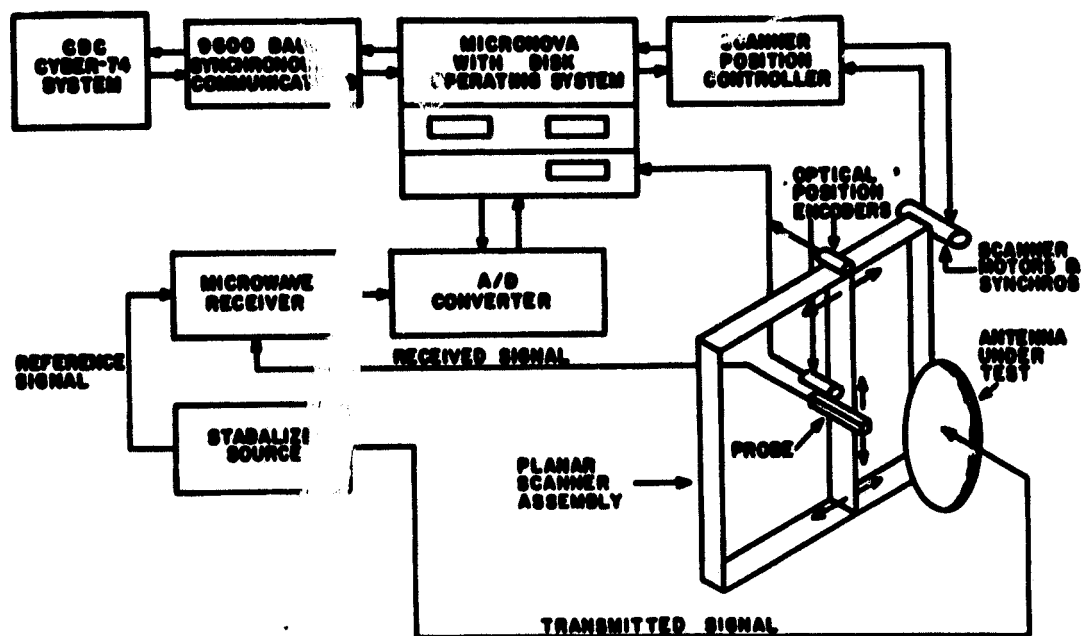
PRECISION SCANNER MECHANISM

CALIBRATED FIELD PROBE

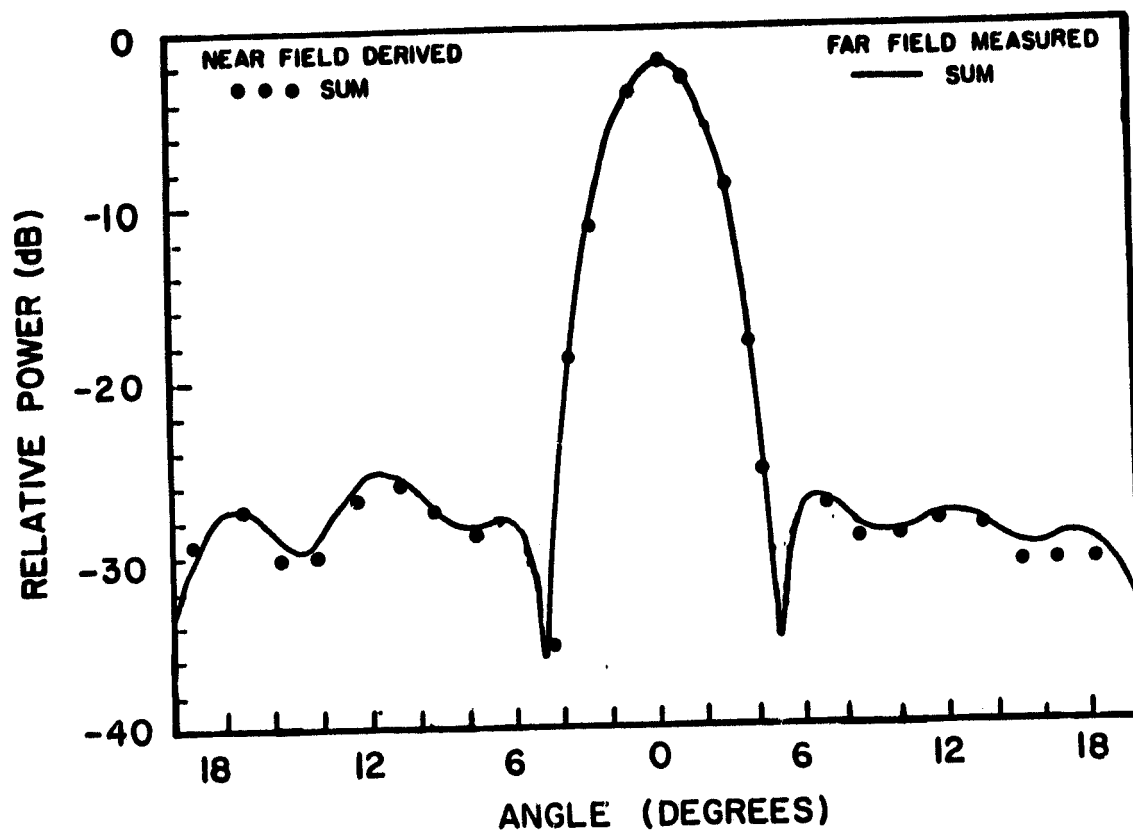
**MUST MEASURE AMPLITUDE AND PHASE OF BOTH
POLARIZATIONS**

COMPUTER PROCESSOR

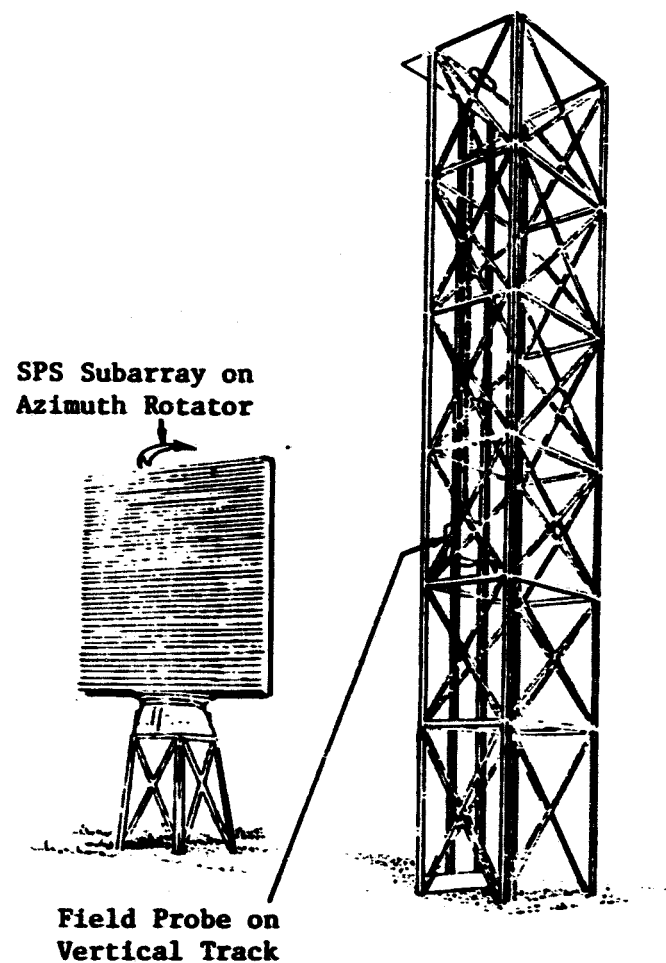
NEAR-FIELD MEASUREMENTS EQUIPMENT BLOCK DIAGRAM



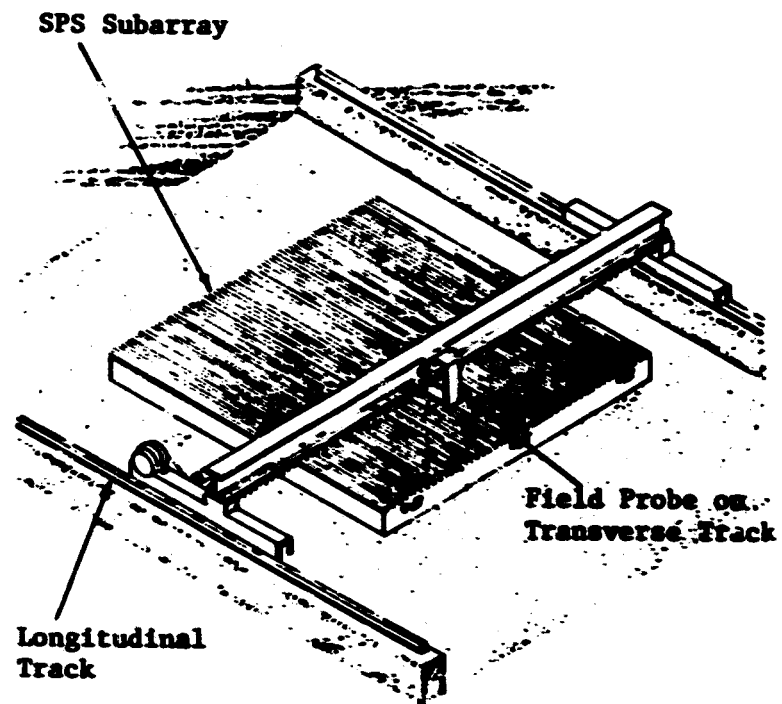
NEAR FIELD DERIVED AND FAR FIELD MEASURED SUM PATTERNS OF A MONOPULSE ANTENNA



NEAR FIELD MEASUREMENT TECHNIQUES



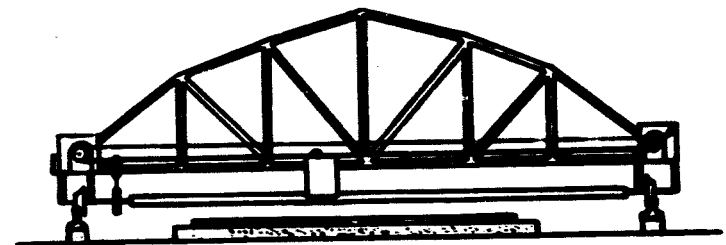
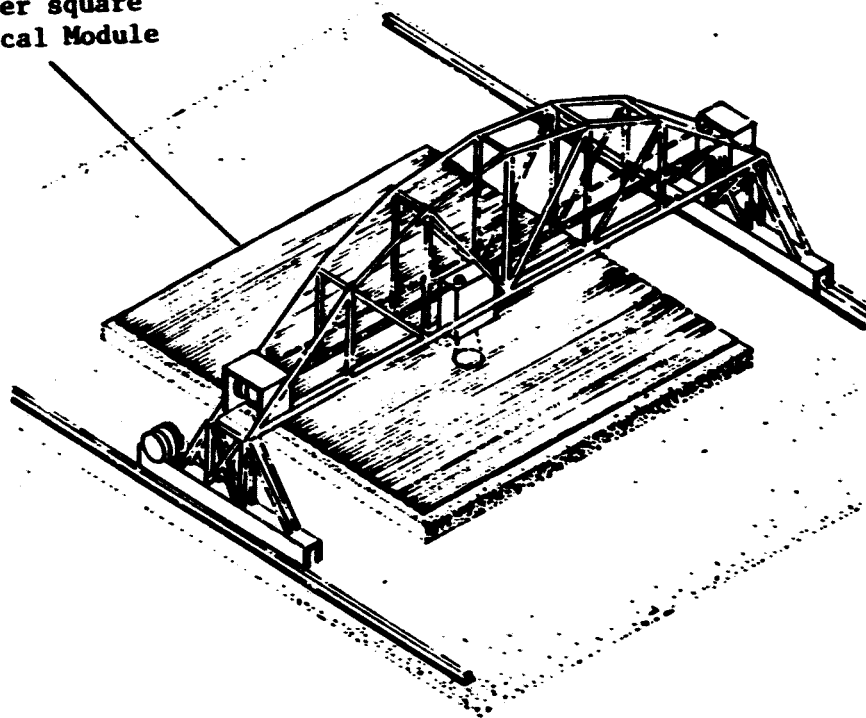
Cylindrical Scanner Concept



Planar Scanner Concept

PLANAR SCANNER CONCEPT FOR MECHANICAL MODULE NEAR-FIELD MEASUREMENTS

30-meter square
Mechanical Module



C O N C L U S I O N S

ELEVATED RANGES CAN MEET ALL KNOWN REQUIREMENTS

**MANY POTENTIAL SITES HAVING RANGES GREATER THAN 3 MILES
ARE AVAILABLE**

FULL HIGH POWER TESTING CAN BE PERFORMED

**THE ELECTRONICS REQUIREMENTS HAVE BEEN FULLY INVESTIGATED. ERROR
BUDGETS INDICATE ACHIEVABLE ADVANCES IN STATE-OF-THE-ART ARE REQUIRED
IN SEVERAL AREAS**

**NEAR-FIELD TECHNIQUES ARE APPLICABLE FOR TESTING AT INTERMEDIATE
POWER LEVELS**

**INDOOR TESTING OF FULL 30 BY 30-METER MECHANICAL MODULES ARE
POSSIBLE**



National Aeronautics and
Space Administration

Lyndon B. Johnson Space Center
Houston, Texas 77058



6

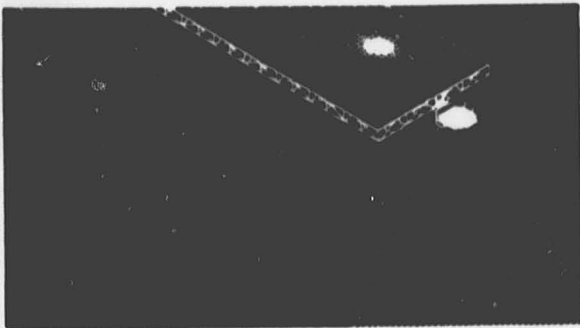
Rectenna



NASA Solar Power Satellite Workshop on
Microwave Power Transmission and Reception

Session
Presentations

Jan
15-18
1980



The presentation material herein was used in the Rectenna Sessir Satellite Workshop on Microwave Power Transmission and Reception held at the Lyndon B. Johnson Space Center, January 15-28, 1980. The workshop was conducted as part of the technical assessment process of the DOE/NASA Solar Power Satellite Concept Evaluation Program. All aspects of Solar Power Satellite microwave transmission and reception were addressed including studies, analyses, and laboratory investigations. Conclusions from these activities were presented as well as recommended follow-on work. The workshop was organized into eight sessions as follows:

- *General*
- *Microwave System Performance*
- *Phase Control*
- *Power Amplifiers*
- *Radiating Elements*
- *Rectenna*
- *Solid State Configurations*
- *Planned Program Activities*

The material contained herein supplements the workshop papers which were published and distributed at the time of the workshop. Together they are a comprehensive documentation of the numerous analytical and experimental activities in the field of microwave power transmission and reception.

- *Additional Information regarding the workshop may be obtained by contacting: R.H. Dietz*

EE4/SPS Microwave Systems
National Aeronautics &
Space Administration
Lyndon B. Johnson Space Center
Houston, Texas 77058
713 483-4507

6

Rectenna Session *contents*

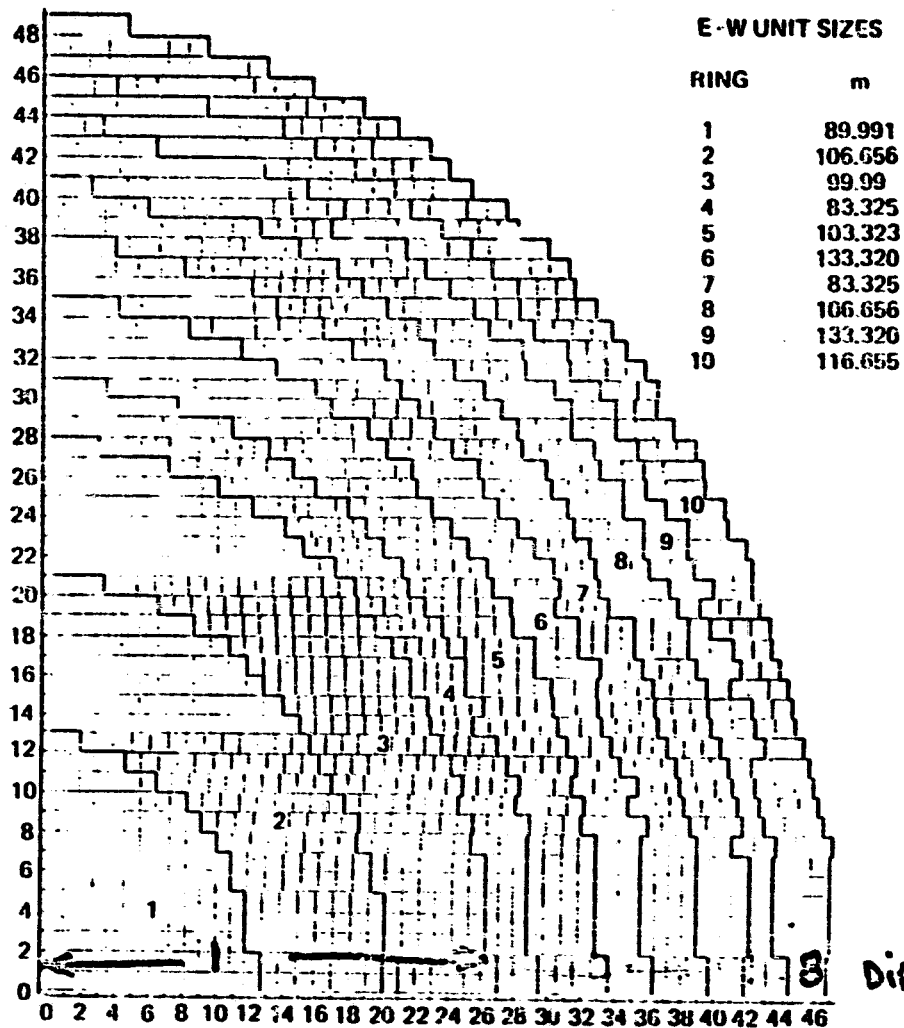
1	Reference System Description Dr. Erv Nalos and G. Woodcock, Boeing
23	Micro Aspects R. Gutmann, Rensselaer Polytechnic Institute
77	Macro Aspects A. Few, Rice University
119	Analytic Array J. Ott, Novar Corp
159	Large Array Measurement Results D. Dickinson, Jet Propulsion Lab

Reference System Description

*Dr. Erv Nalos and
G. Woodcock
Boeing*

PRECEDING PAGE BLANK NOT FILLED

3

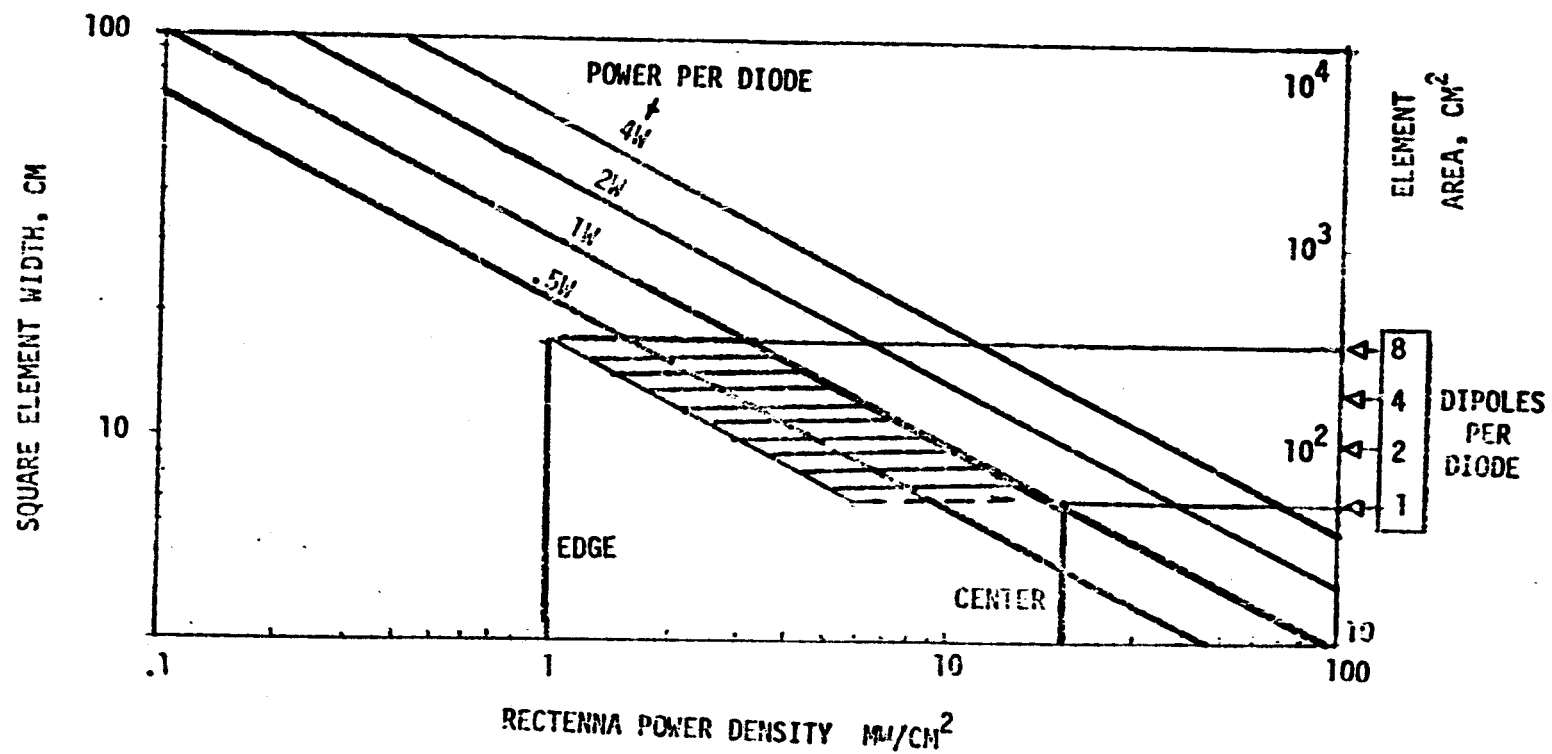


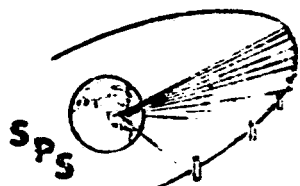
DIPLES/DIODE

Rectenna Ring and Unit Boundary Map

ORIGINAL PAGE IS
OF POOR QUALITY.

RECTENNA POWER DENSITY CONSIDERATIONS





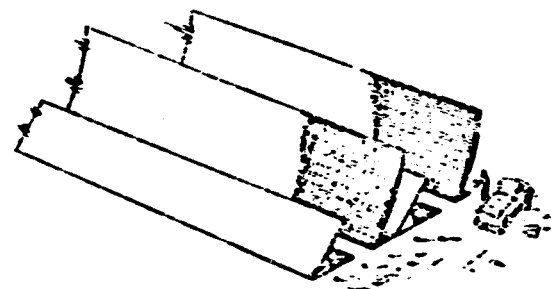
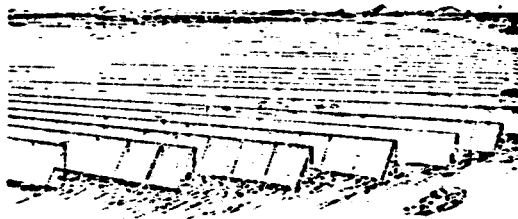
Potential Rectenna Configurations

BOEING

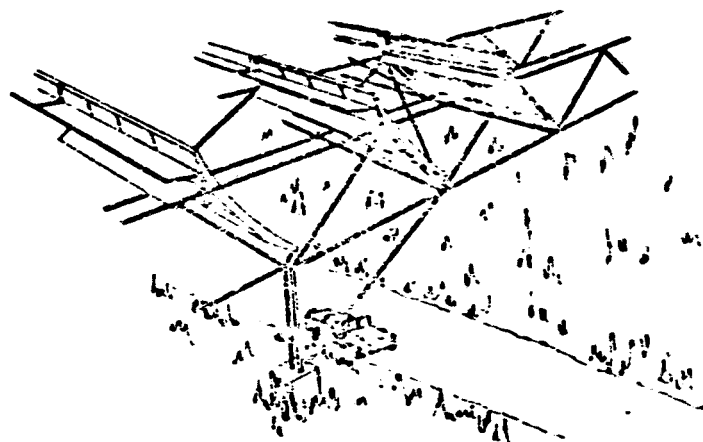
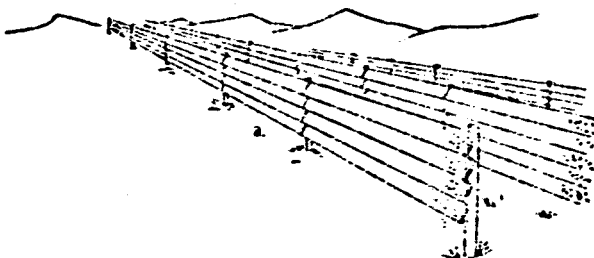
NON-CONCENTRATING

CONCENTRATING

GROUND
LOCATION



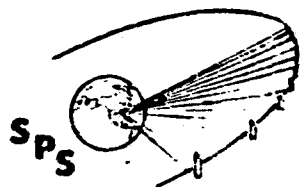
ELEVATED



Ⓐ FLAT RECTENNA

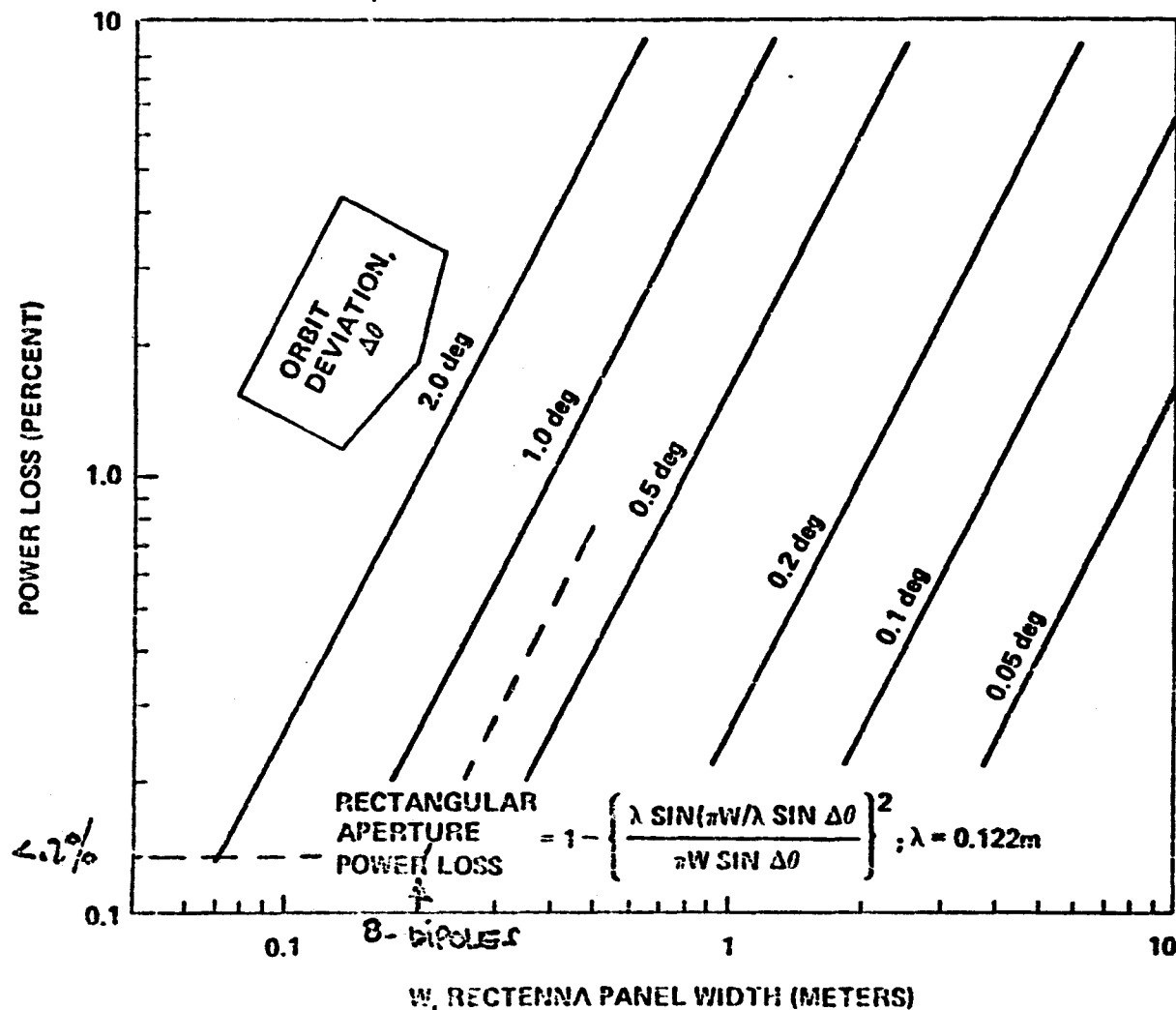
Ⓑ CYLINDRICAL PARABOLA

ORIGINAL PAGE IS
OF POOR QUALITY

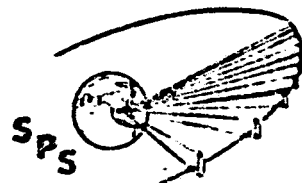


Power Loss Due to SPS Orbit Deviation

BOEING

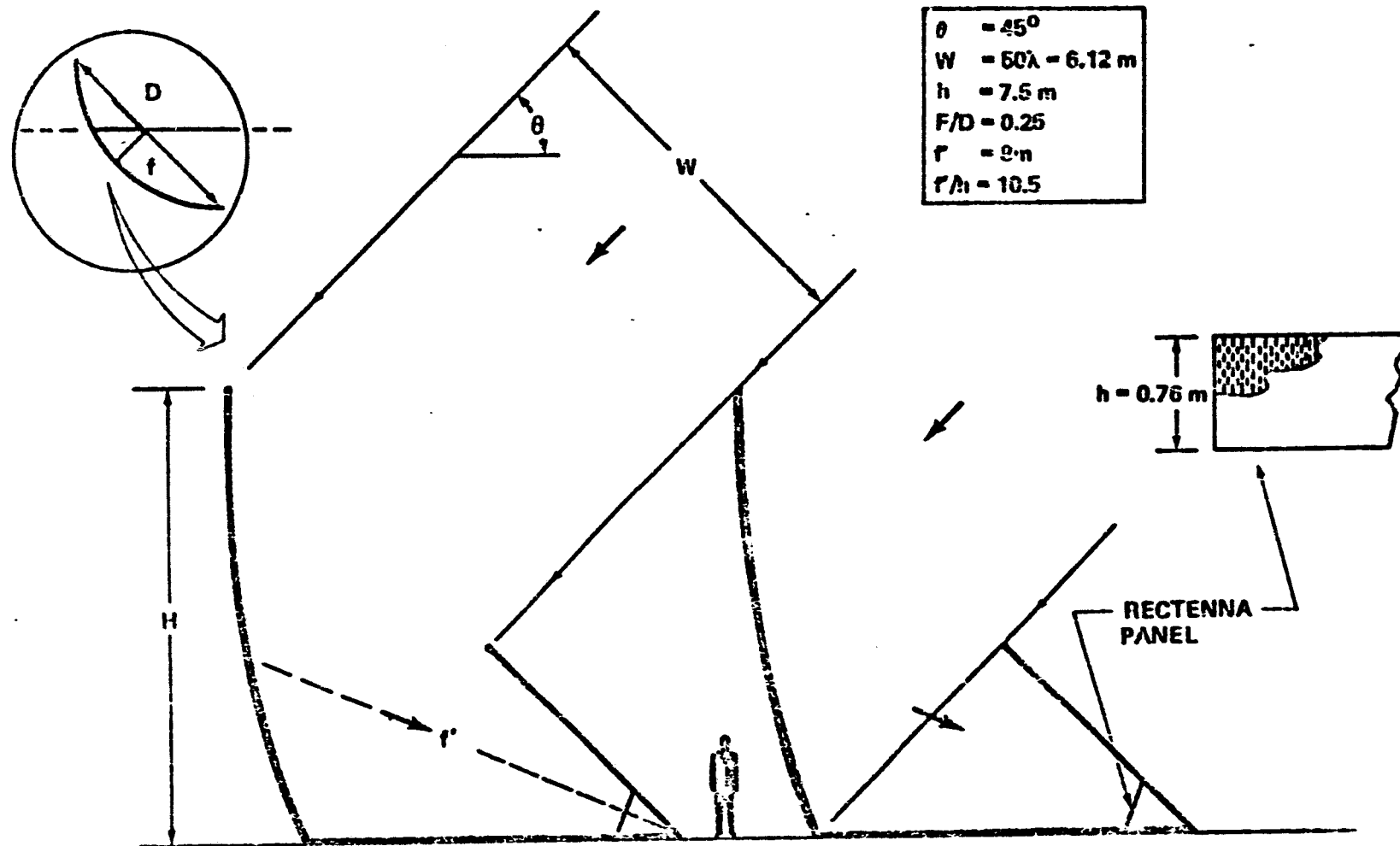


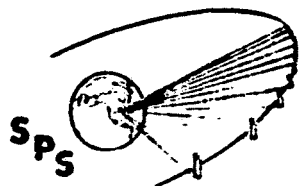
RECEIVED
JAN 12 1968



Hogline Rectenna Configuration for SPS

BOEING





Potential Rectenna Configurations for Efficient Rectification

BOEING

CENTER
(23 mW/cm²)

EDGE
(0.85 mW/cm²)

1 x 2

(a)

6 x 6

(b)

3 x 12

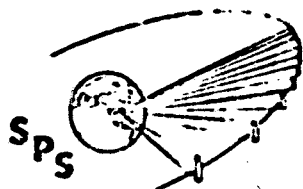
2 x 4

1 x 8

2 x 2

1 x 4

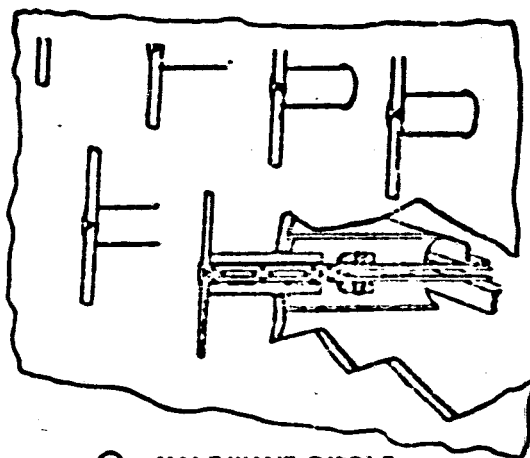
NUMBER OF MODULES (75 cm ² EACH)		2	36	36	8	8	4	4
PANEL SIZE, m	y	w _x 0.037	0.52	0.26	0.17	0.087	0.17	0.087
	x	w _y 0.17	0.52	1.04	0.35	0.7	0.17	0.35
AREA, m ²		A 0.015	0.27	0.27	0.06	0.06	0.03	0.03
POWER PER DIODE		P 3.45	2.3	2.3	2.04	2.04	2.04	2.04
OPTICAL CONCENTRATION		NO	NO	NO	4:1	4:1	8:1	8:1
MATCHING LOSSES		LOW	HIGH	HIGH	MED	MED	LOW	LOW
LOSS FOR ORBIT STABILITY OF 0.5 deg x 0.1 deg	L _x	0	0.4%	0.1%	0.7%	0.7%	1.6%	1.6%
	L _y	0	0	0.1%	0.2%	0.8%	0	0.2%
	TOTAL	0	0.4%	0.2%	0.9%	1.5%	1.6%	1.8%



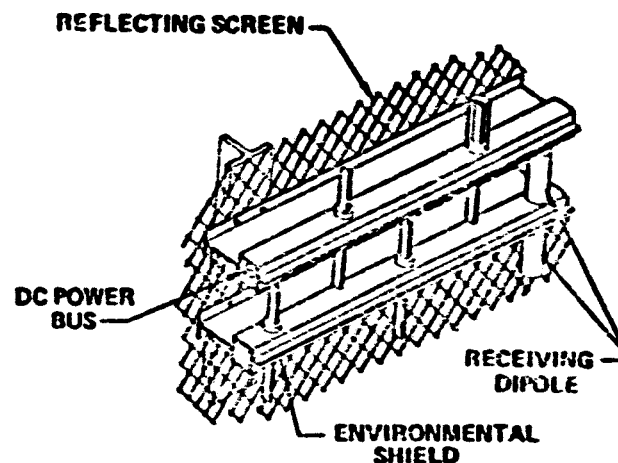
Rectenna Receiving Element Options

BOEING

SINGLE RADIATOR
PER DIODE

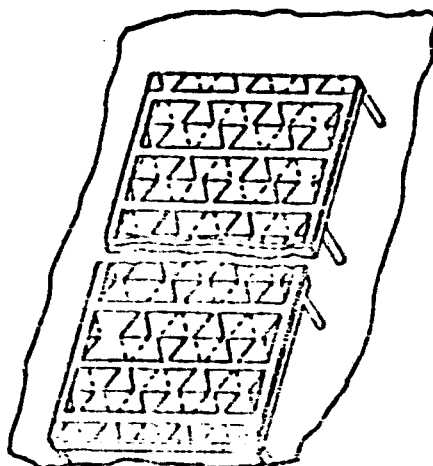


(B) HALF WAVE DIPOLE

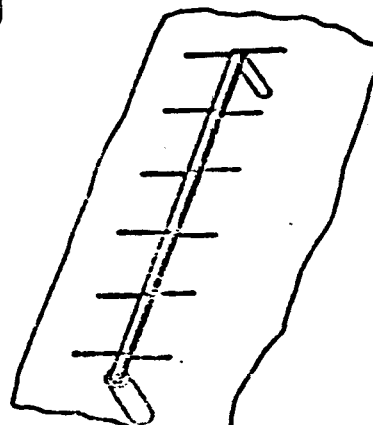


(b) MODIFIED HALF-WAVE DIPOLE

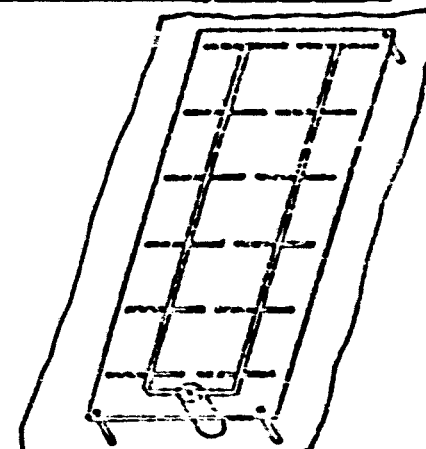
MULTIPLE
RADIATORS
PER DIODE



(C) HALF-WAVE DIPOLE STRIPLINE



**(d) AIR DIELECTRIC
TRANSMISSION-LINE
FEED**



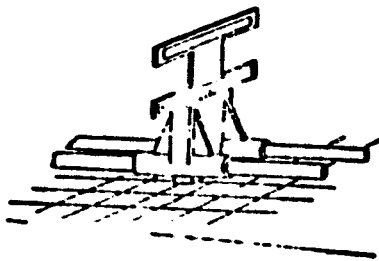
**(e) FULL WAVELENGTH DIPOLE
STRIPLINE**

HIGH EFFICIENCY
LOW NOISE

Rectenna Collecting Element Options

MULTIELEMENT

YAGI



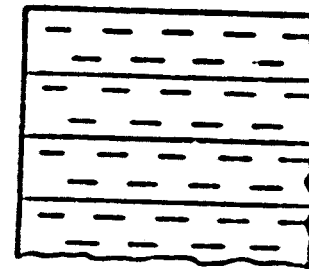
3-ELEMENT

MULTIELEMENT
& CONCENTRATOR

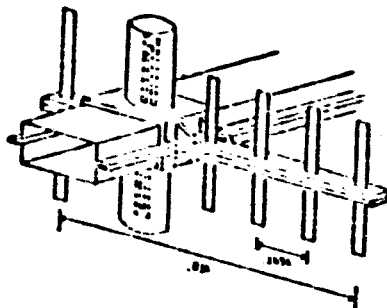


PARABOLIC TROUGH

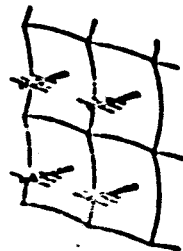
WAVEGUIDE



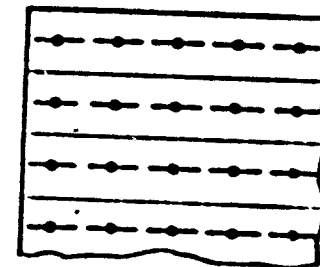
SLOTTED WAVEGUIDE



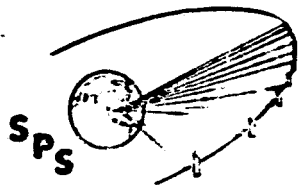
6 ELEMENT



PARABOLIC HORN



WAVEGUIDE FED
DIPOLES



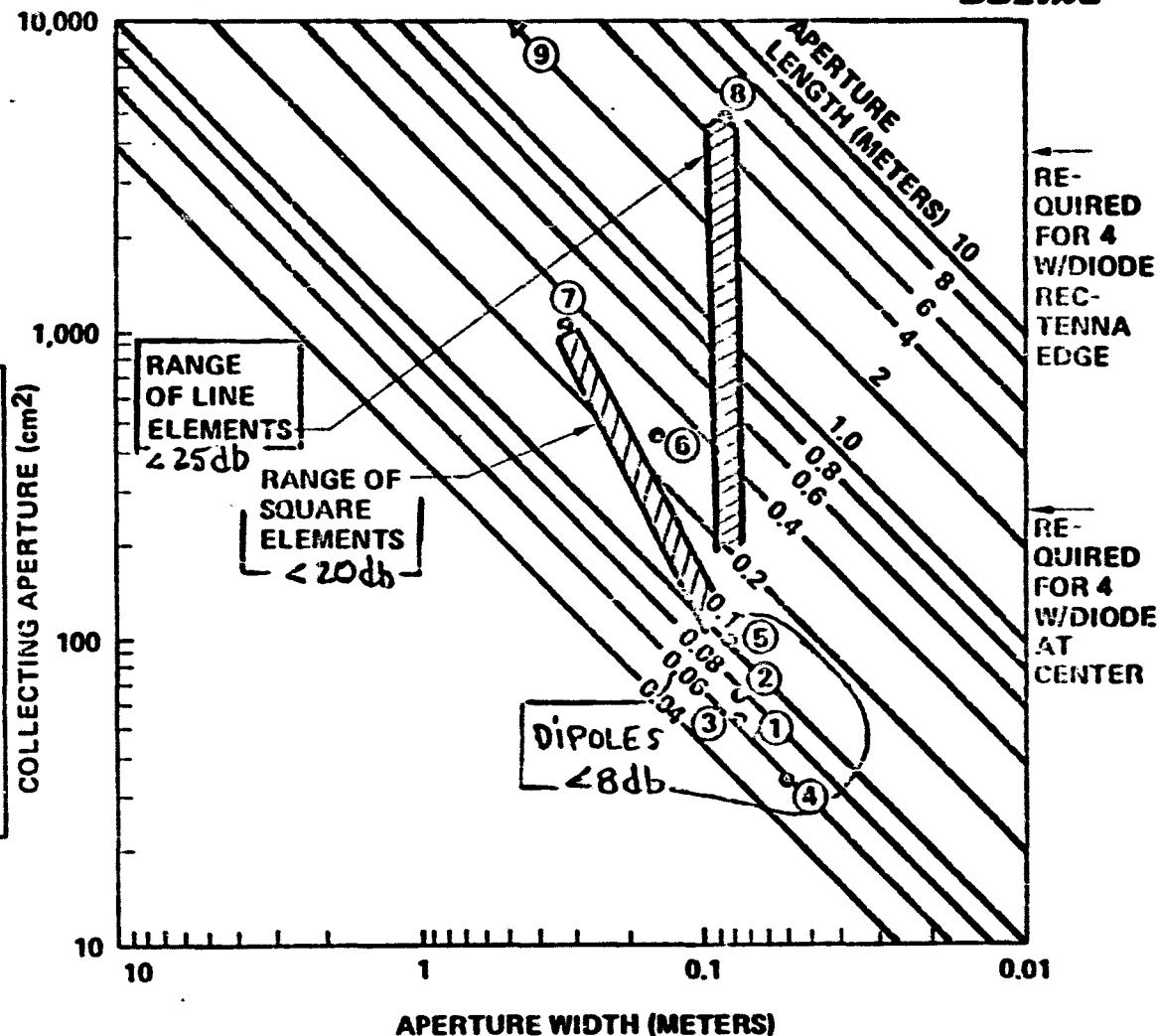
Capture Area of Different Types of Rectenna Elements

SPS-2134

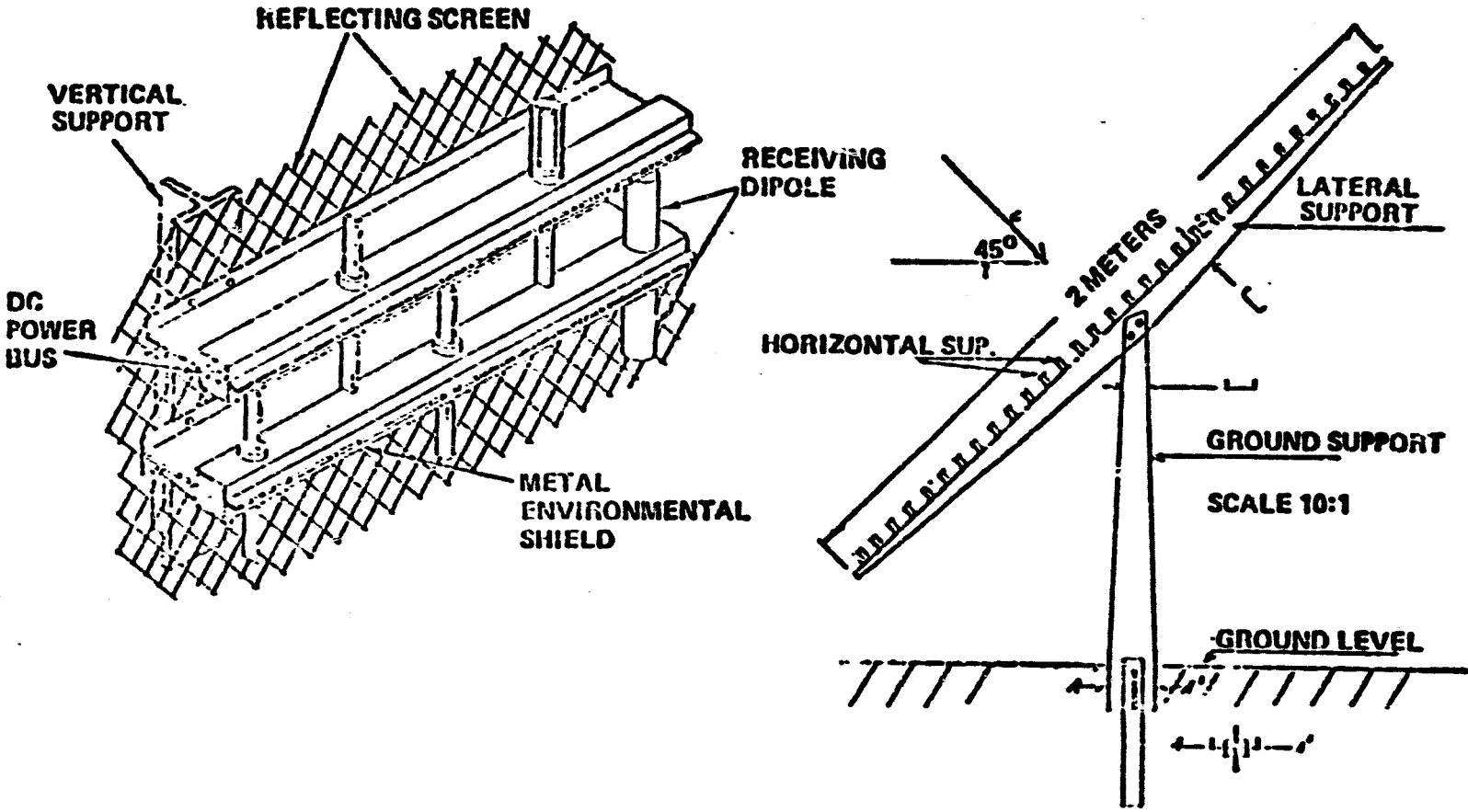
BOEING

LEGEND:

- ① BASELINE DIPOLE CELL ($\lambda/2$)
- ② DIPOLE IN AIR DIELECTRIC (λ)
- ③ DIPOLE IN STRIPLINE (λ)
- ④ DIPOLE IN STRIPLINE ($\lambda/2$)
- ⑤ POTENTIAL DIPOLE CELL LIMIT
- ⑥ RECTENNA CAVITY ELEMENT (2 x 3 SLOTS, TYPICAL)
- ⑦ LIMIT OF YAGI ELEMENT
- ⑧ MAXIMUM WAVEGUIDE STICK LENGTH (30g)
- ⑨ TYPICAL CAVITY RADIATOR (ROCKWELL)



RECTENNA RF BASELINE



12

ORIGINAL PAGE IS
OF POOR QUALITY

LOW COST RECTENNA ELECTRICAL AND MECHANICAL DESIGN

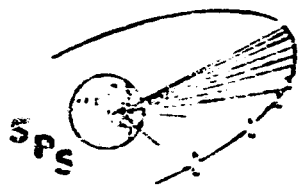
- ENVIRONMENTAL SHIELD IS USED AS THE HORIZONTAL STRUCTURAL LOADING BEARING MEMBER

- ENVIRONMENTAL SHIELD IS THE CONDUIT FOR THE DC POWER BUS

THE DC POWER BUSES ALSO FORM THE MICROWAVE CIRCUITS FOR STORAGE OF ENERGY DURING THE RECTIFICATION PROCESS AND FOR FILTERING OF HARMONICS

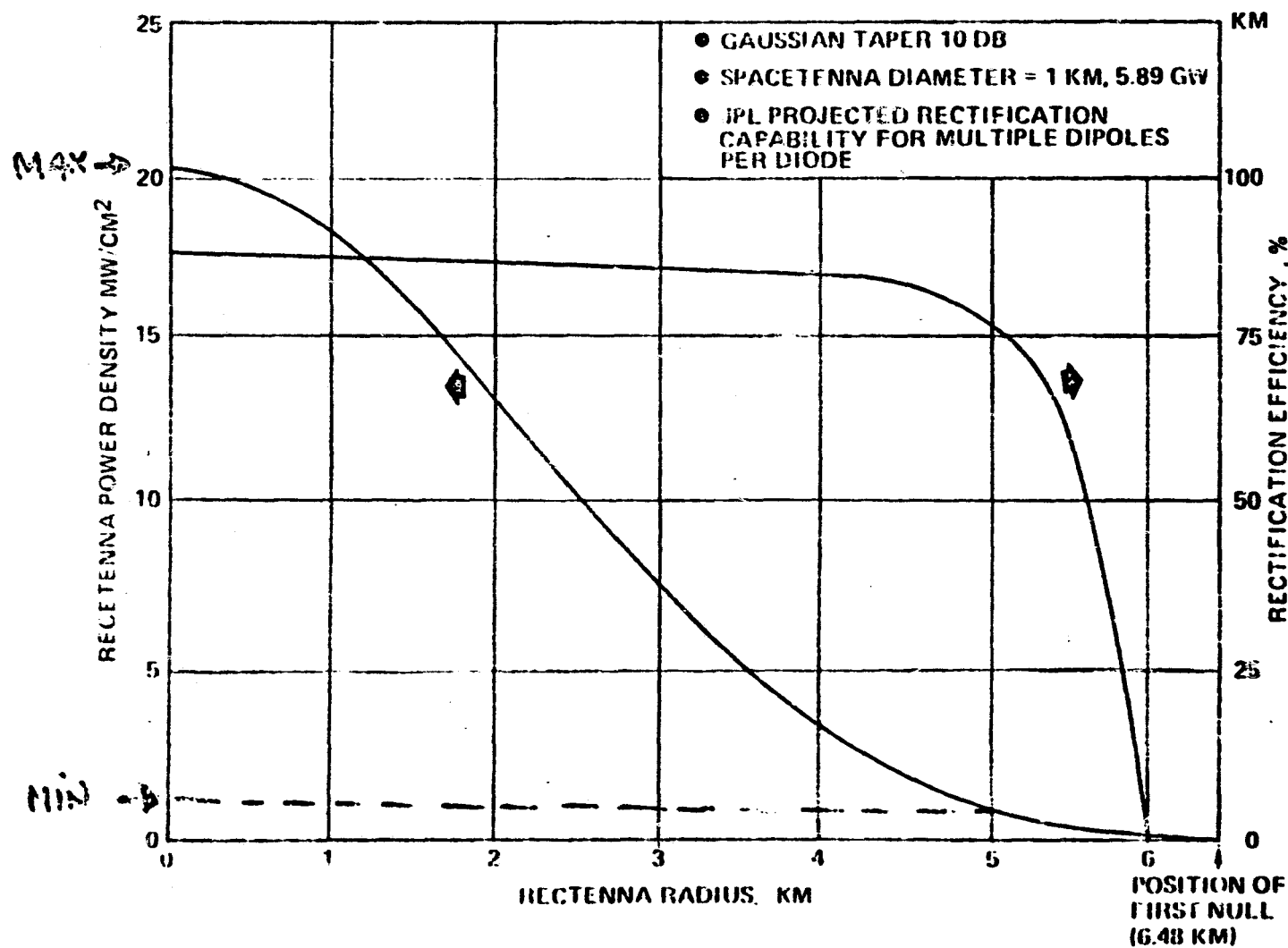
- THE DESIGN LENDS ITSELF TO HIGH SPEED, FULLY AUTOMATED CONSTRUCTION

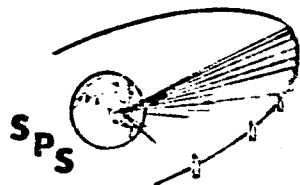
THE DESIGN USED LOW COST MATERIALS



Rectenna Power Density and Rectification Efficiency

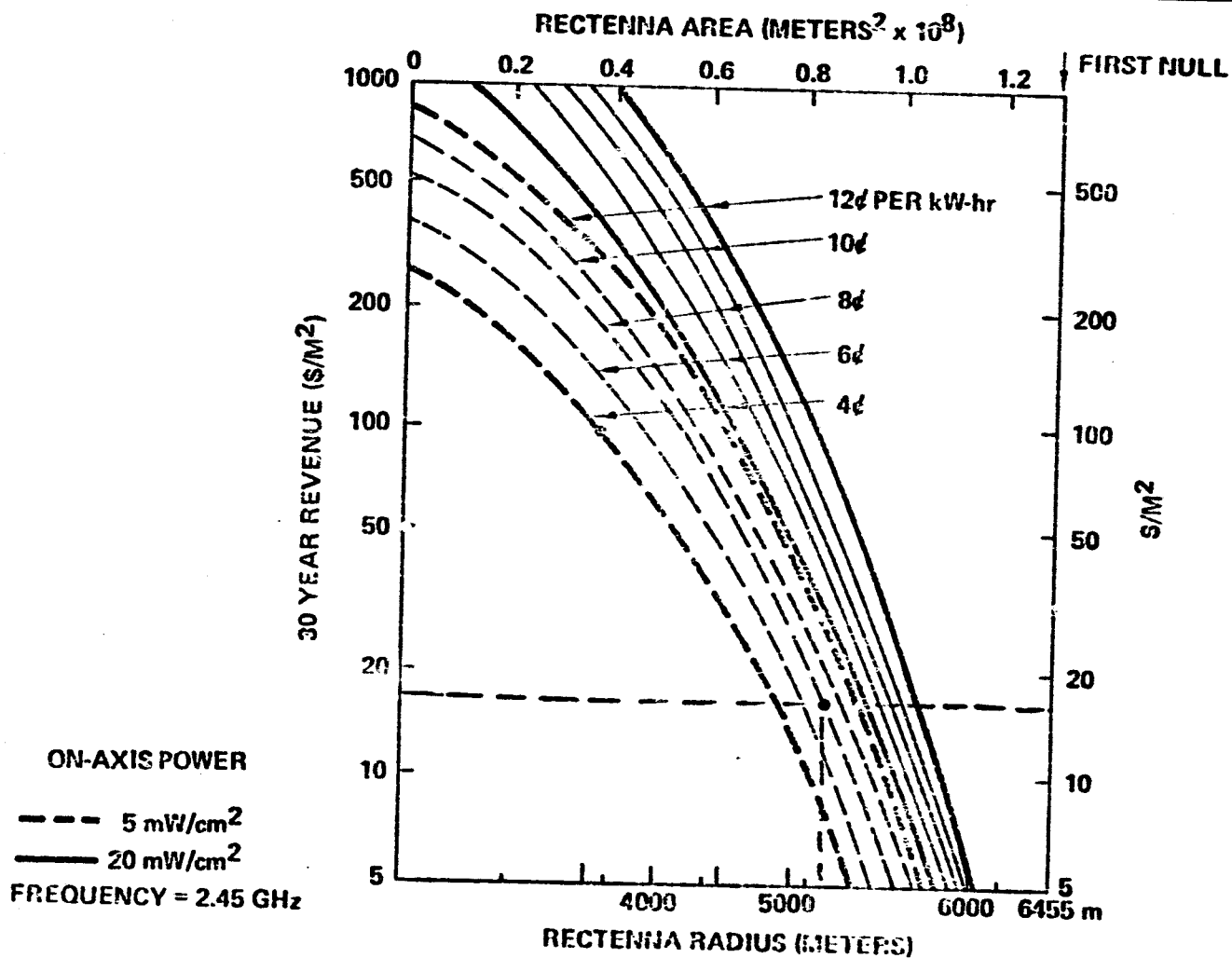
BOEING

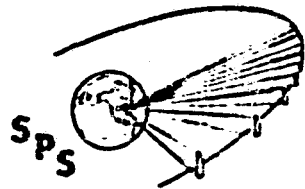




Optimum Rectenna Dimension for Given Rectenna Cost

BOEING

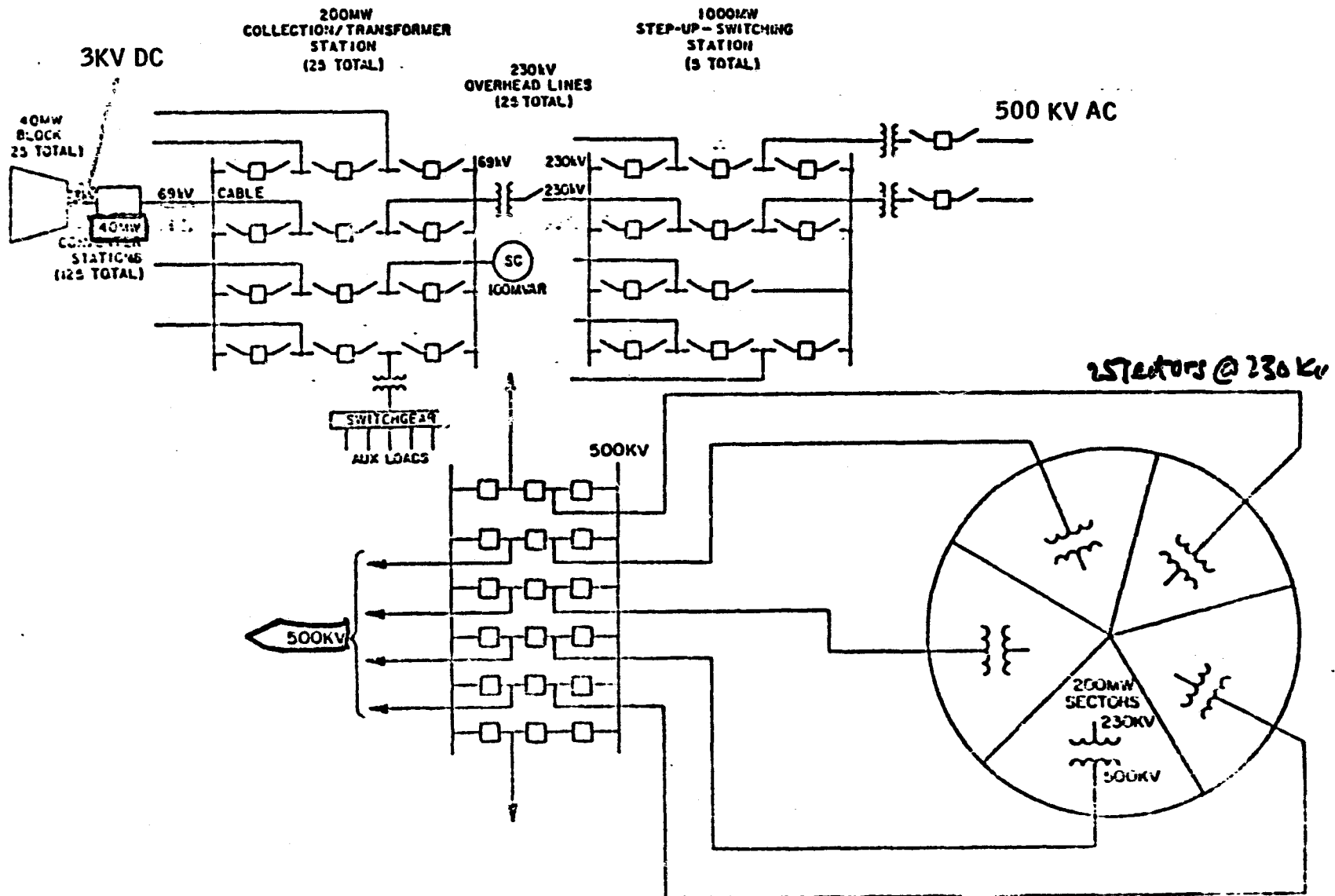




GRID CONNECTION APPROACH

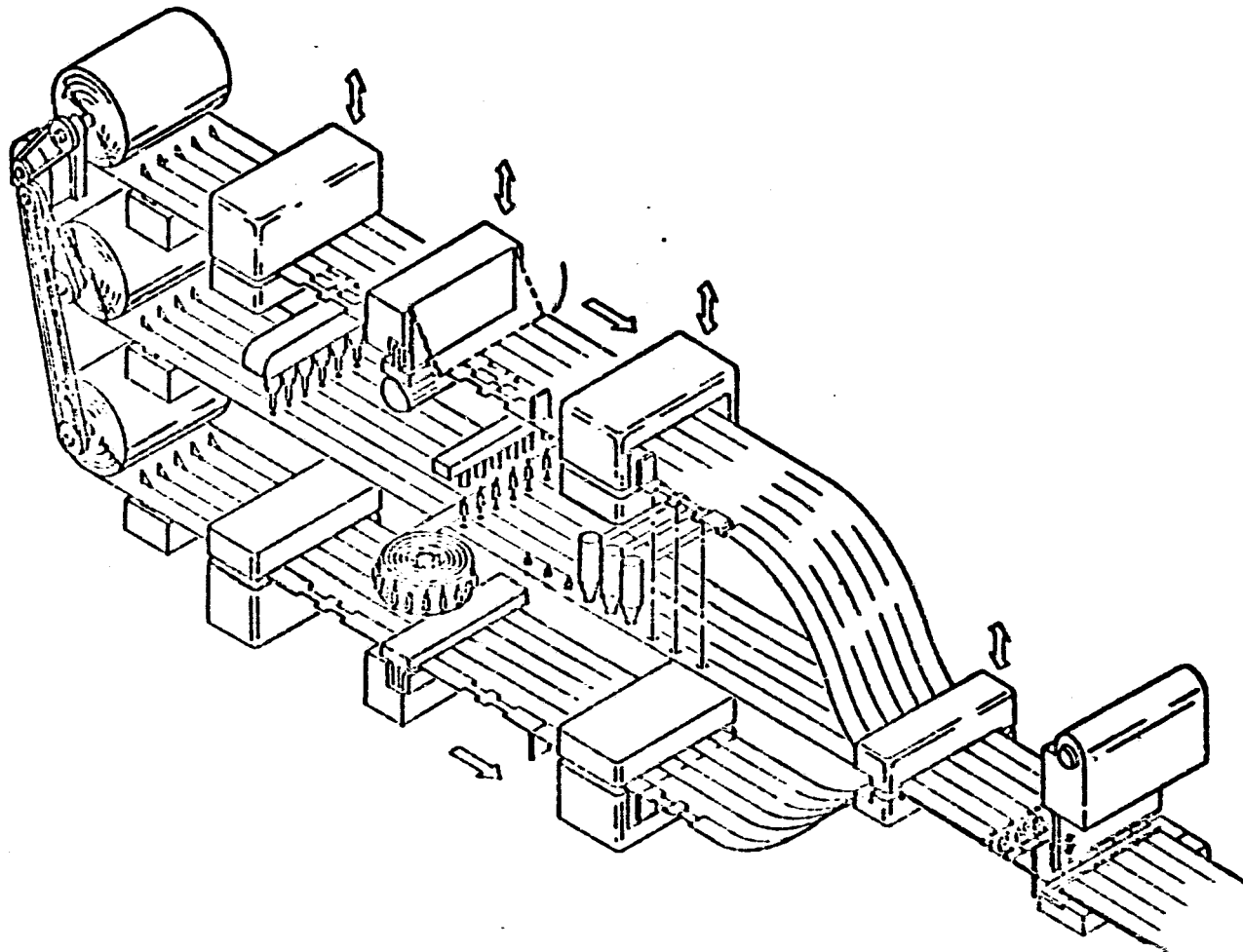
AC POWER COLLECTION

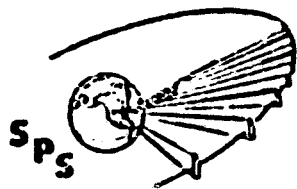
BOEING



ORIGINAL PAGE IS
OF PHOTO ALTY

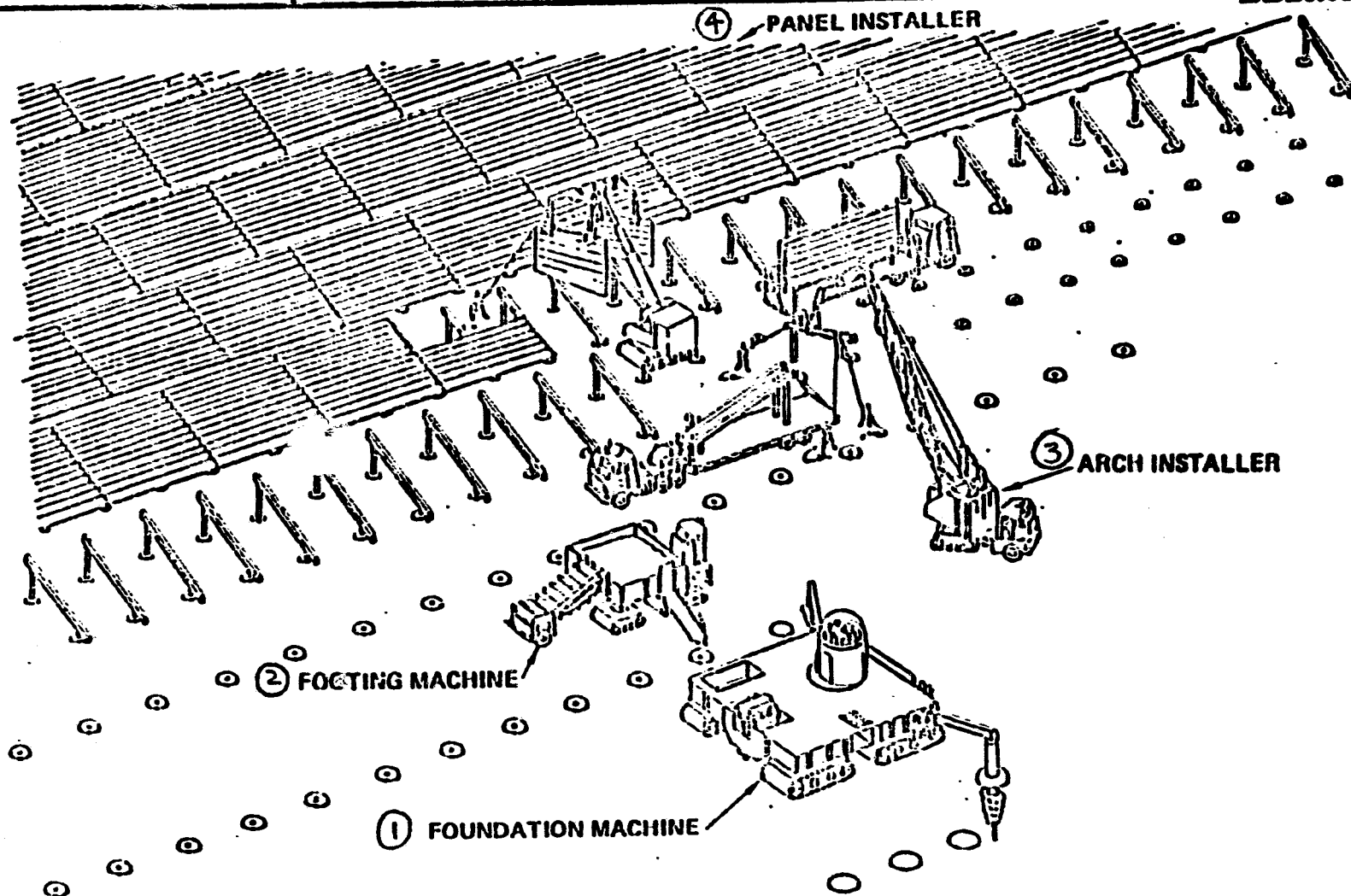
DIPOLE MACHINE



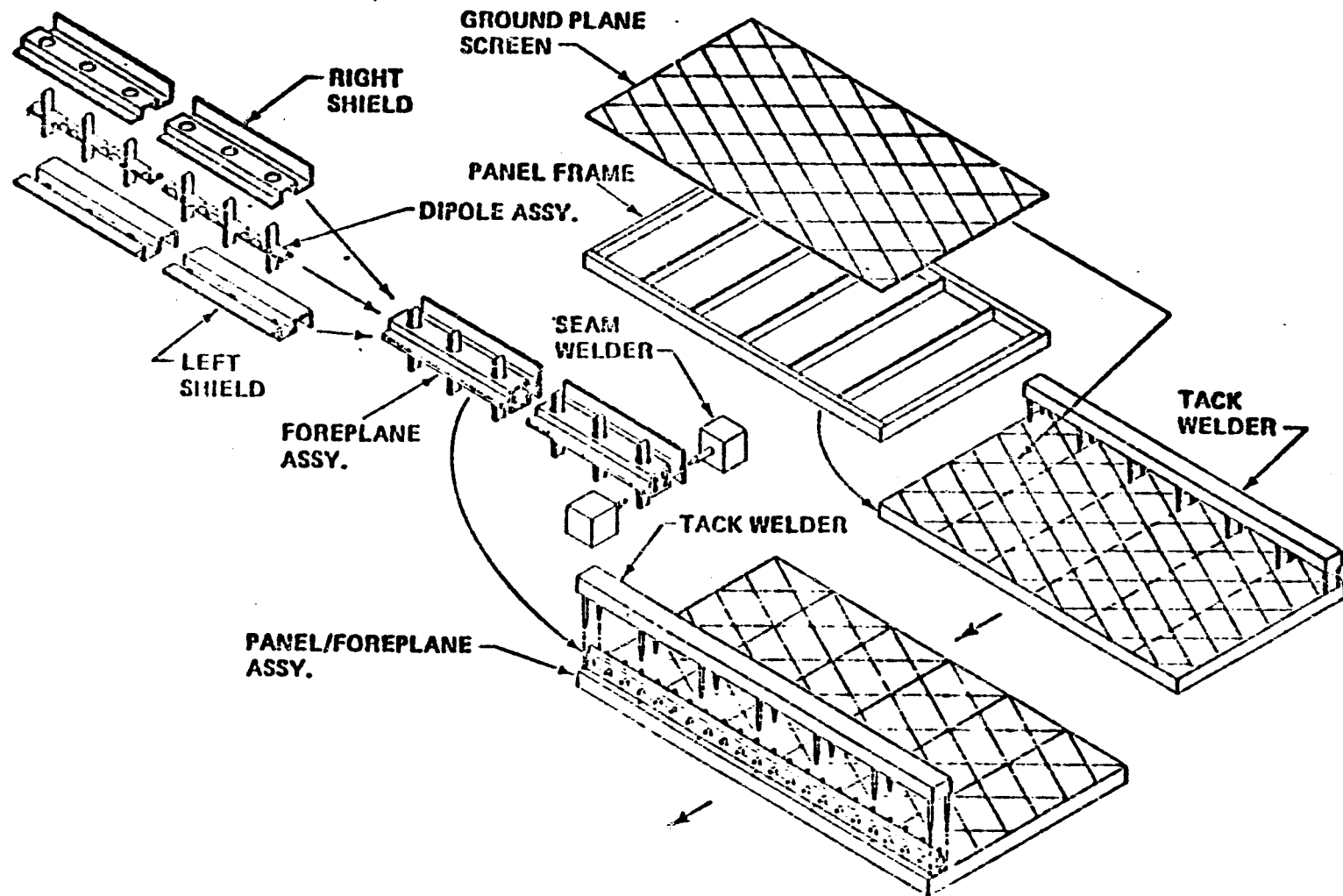


Rectenna Construction Concept

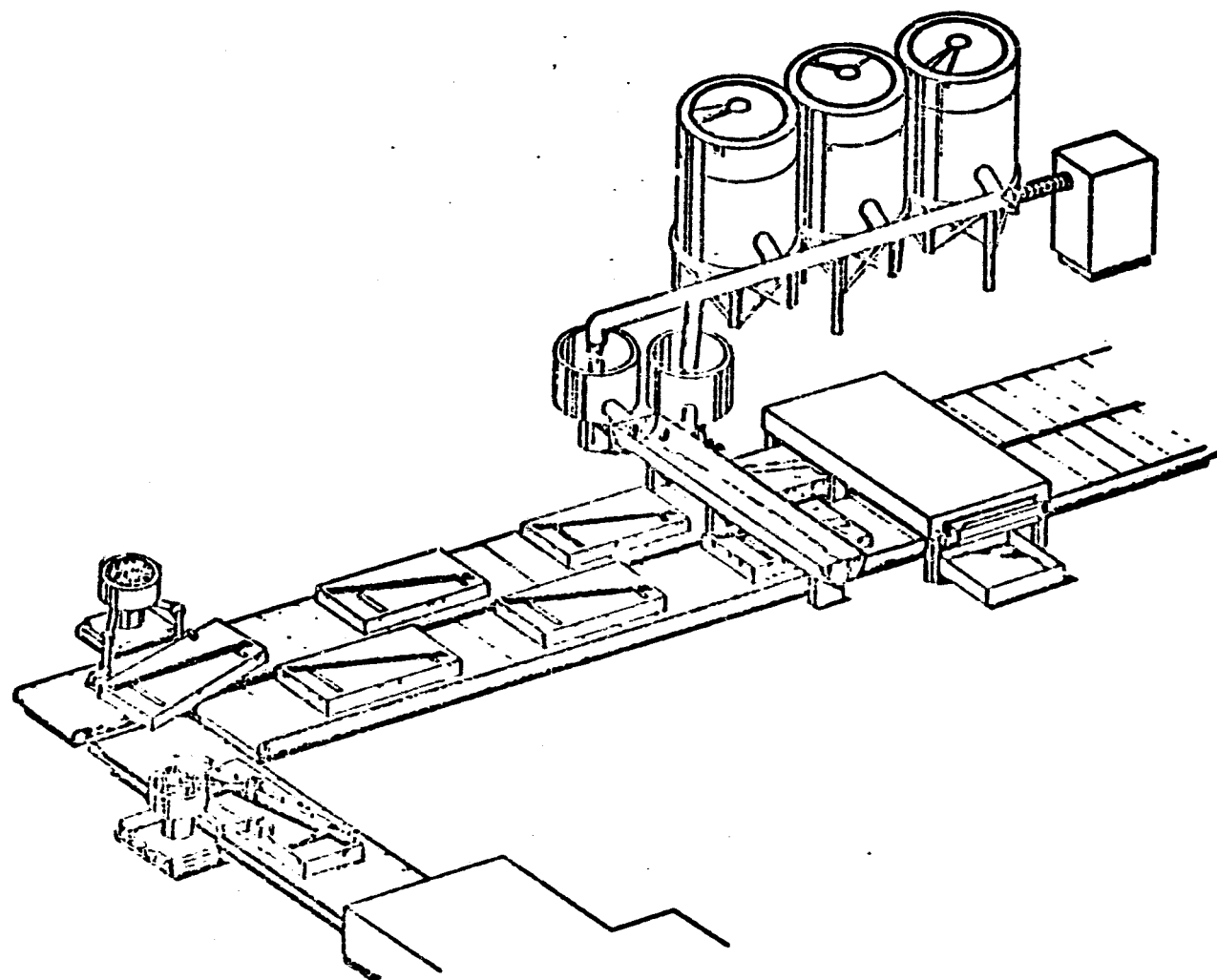
BOEING

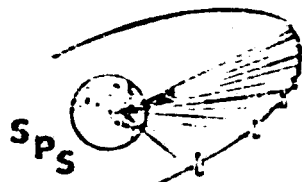


RECTENNA PANEL FABRICATION SEQUENCE



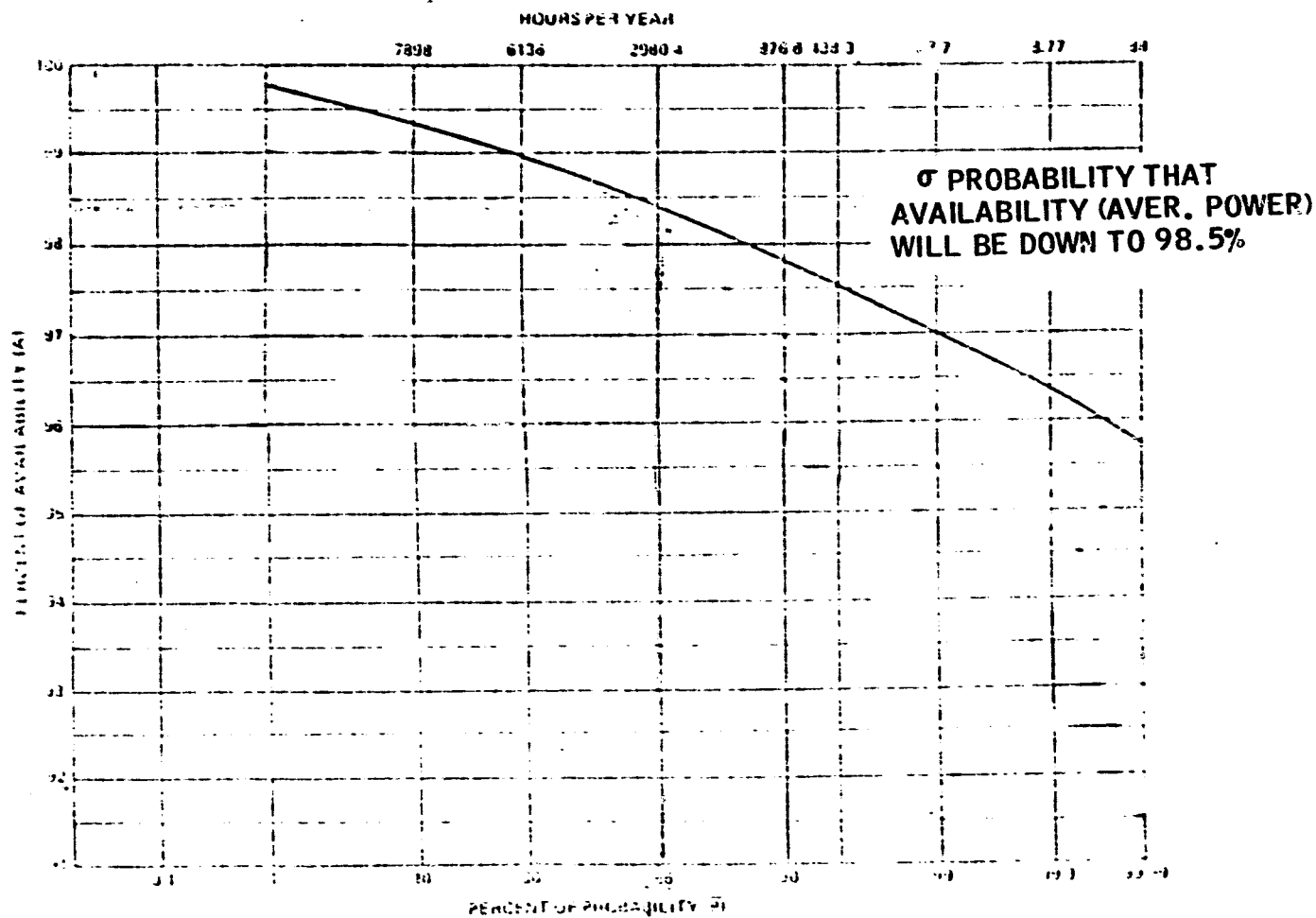
ARCH CASTING FACTORY





DC POWER COLLECTION SYSTEM AVAILABILITY vs PROBABILITY

BOEING



D2

Micro Aspects

*R. Gutmann
Rensselaer Polytechnic Institute*

PRECEDING PAGE BLANK NOT FILMED

ORGANIZATION OF PRESENTATION

- PROGRAM OVERVIEW
 - TASKS
 - KEY ACCOMPLISHMENTS
- PARALLEL-SERIES COMBINING ANALYSIS
 - APPROACH TAKEN
 - CLOSED FORM MODEL
 - COMPUTER SIMULATION MODEL
 - CONCLUSIONS
- DIRECTIONAL RECEIVING ELEMENT
 - YAGI-UDA ELECTRICAL DESIGN
 - PRINTED CIRCUIT EVALUATION
 - EIGHT DESIGNS EVALUATED
 - CONCLUSIONS

PRECEDING PAGE BLANK NOT FILMED

PARALLEL-SERIES COMBINING ANALYSIS

- DEVELOP BASIC FUNDAMENTALS FOR PARALLEL-SERIES COMBINING OF DC POWER FROM RECTENNA ELEMENTS (INTO BASIC 10 KW TO 300 KW POWER MODULES)
- DEVELOP A MODEL OF RECTENNA ELEMENT OPERATION THAT CAN BE USED IN CALCULATION OF EFFECT OF POWER DENSITY SPATIAL VARIATIONS ON PARALLEL-SERIES COMBINING EFFICIENCY
- PERFORM PRELIMINARY EVALUATION OF SPS POWER MODULE SIZE CONSTRAINTS FOR BASELINE RECTENNA
- DELINEATE AREAS FOR FURTHER WORK TO QUANTIFY POWER COMBINING DEGRADATION WITH POWER DENSITY FLUCTUATIONS

DIRECTIONAL RECTENNA ELEMENTS

- DEVELOP LIST OF CHARACTERISTICS WITH RELATIVE WEIGHTS IN EACH CATEGORY
- PERFORM PRELIMINARY LIST OF BASIC ANTENNA ELEMENTS TO DELINEATE SMALL NUMBER (~3) OF MOST PROMISING ALTERNATIVES
- PERFORM DETAILED COMPARISON OF MORE PROMISING ANTENNA ELEMENTS FOR A MORE DIRECTIONAL RECTENNA
- PERFORM PRELIMINARY EVALUATION OF RECTENNA ELEMENT PRODUCTION TECHNIQUES WITH MORE PROMISING ELEMENTS
- PERFORM A PRELIMINARY COST COMPARISON OF MORE PROMISING ELEMENTS AND COMPARE TO BASELINE RECTENNA ELEMENT (INCLUDING PERFORMANCE FACTORS)

KEY ACCOMPLISHMENTS - POWER COMBINING EVALUATION

- COMPUTER MODEL OF BASELINE TYPE CONVERSION CIRCUITRY USING AVAILABLE NON LINEAR PROGRAM
- CLOSED FORM MODELS OF CONVERSION CIRCUITRY DEVELOPED
- POWER COMBINING INEFFICIENCIES FOR SERIES AND PARALLEL COMBINING EVALUATION
- IMPACT OF POWER COMBINING INEFFICIENCIES ON POWER MODULE SIZING INITIATED

KEY ACCOMPLISHMENTS - DIRECTIONAL RECEIVING ELEMENTS

- PRINTED CIRCUIT IMPLEMENTATION EVALUATION
- ELECTRICAL DESIGN OF YAGI-UDA ELEMENTS WITH TRADEOFF OF GAIN, F/B RATIO AND SIZE
- DEMONSTRATED DIRECTIONAL RECEIVING ELEMENTS LOWER OVERALL RECTENNA COSTS (BASELINE TYPE OR PRINTED CIRCUIT IMPLEMENTATION)

PARALLEL-SERIES COMBINING ANALYSIS

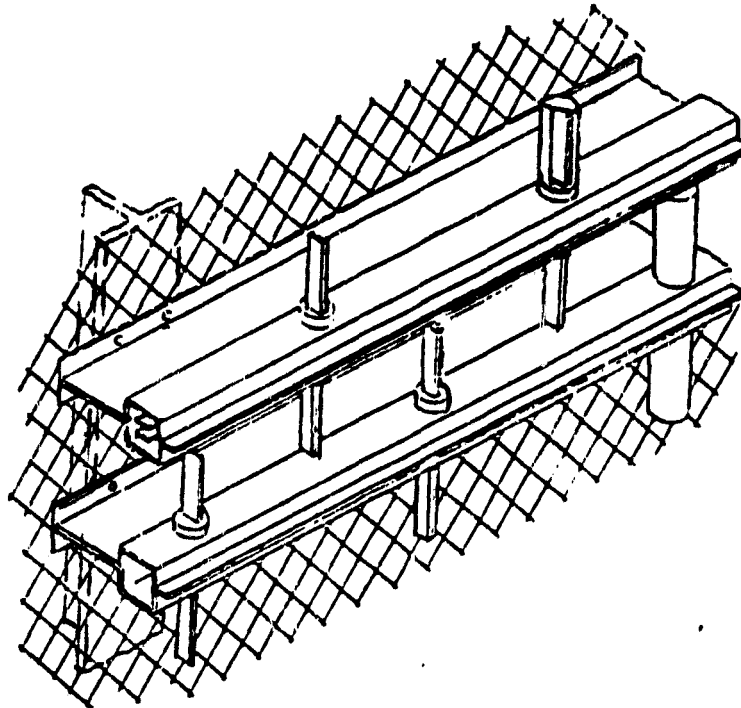
ASSUMPTIONS AND UNDERLYING TENETS

- PARALLEL-SERIES COMBINING ANALYSIS USING LOAD LINE TECHNIQUE
- COMPUTER SIMULATION OF BASELINE RECTIFIER CRUCIAL
- USE OF STANDARDIZED COMPUTER PROGRAMS PREFERRED
- ENHANCED UNDERSTANDING OF RECTIFIER FUNDAMENTALS DESIRABLE
- SYSTEM POWER DENSITY VARIATIONS NEED FURTHER QUANTIFICATION

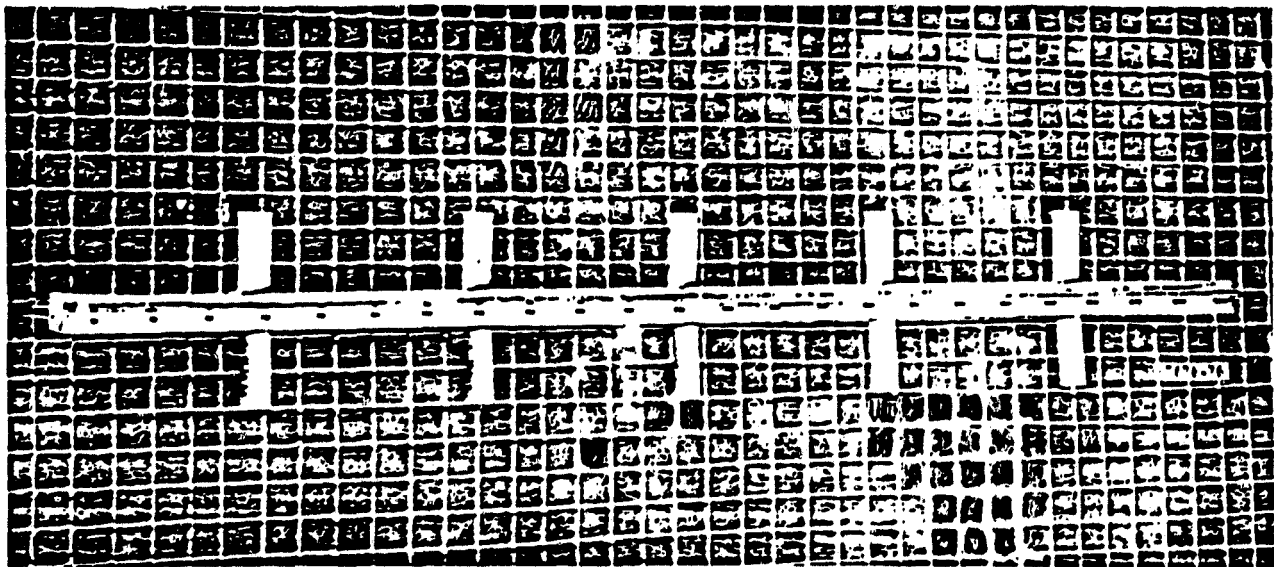
APPROACH TAKEN

- USE OF SPICE 2 TRANSIENT ANALYSIS PROGRAM
- DEVELOPMENT OF BASELINE TYPE POWER RECTIFIER MODEL
- DEVELOPMENT OF CLOSED FORM RECTIFIER MODEL
- EMPHASIS ON HARMONIC AMPLITUDE AND PHASE AS WELL AS TRANSIENT WAVEFORMS
- INITIATION OF FUNDAMENTAL PARALLEL AND SERIES COMBINING INVESTIGATION

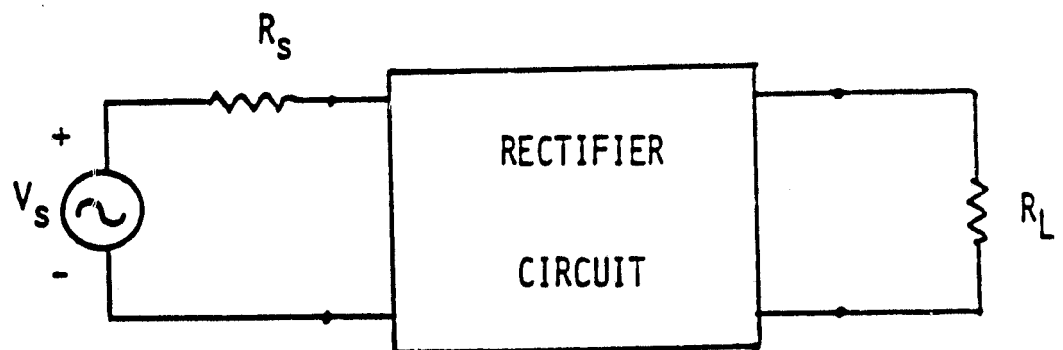
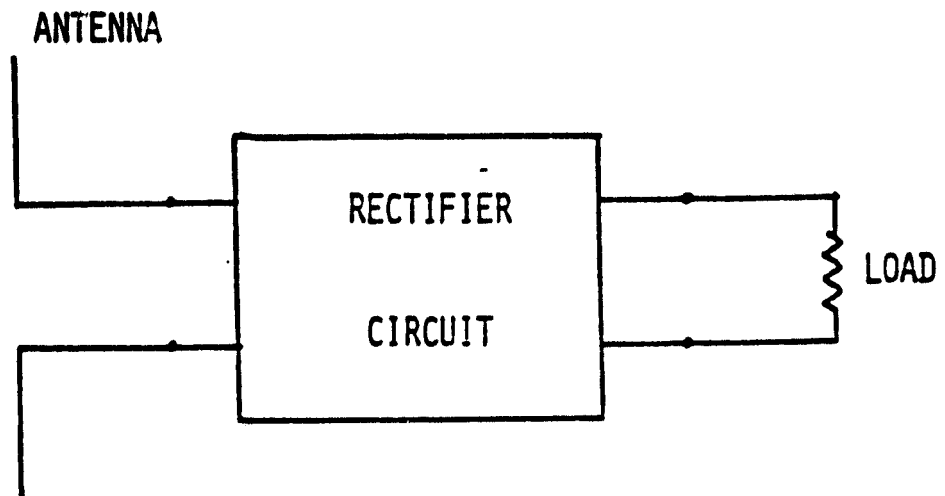
ORIGINAL PAGE IS
OF POOR QUALITY



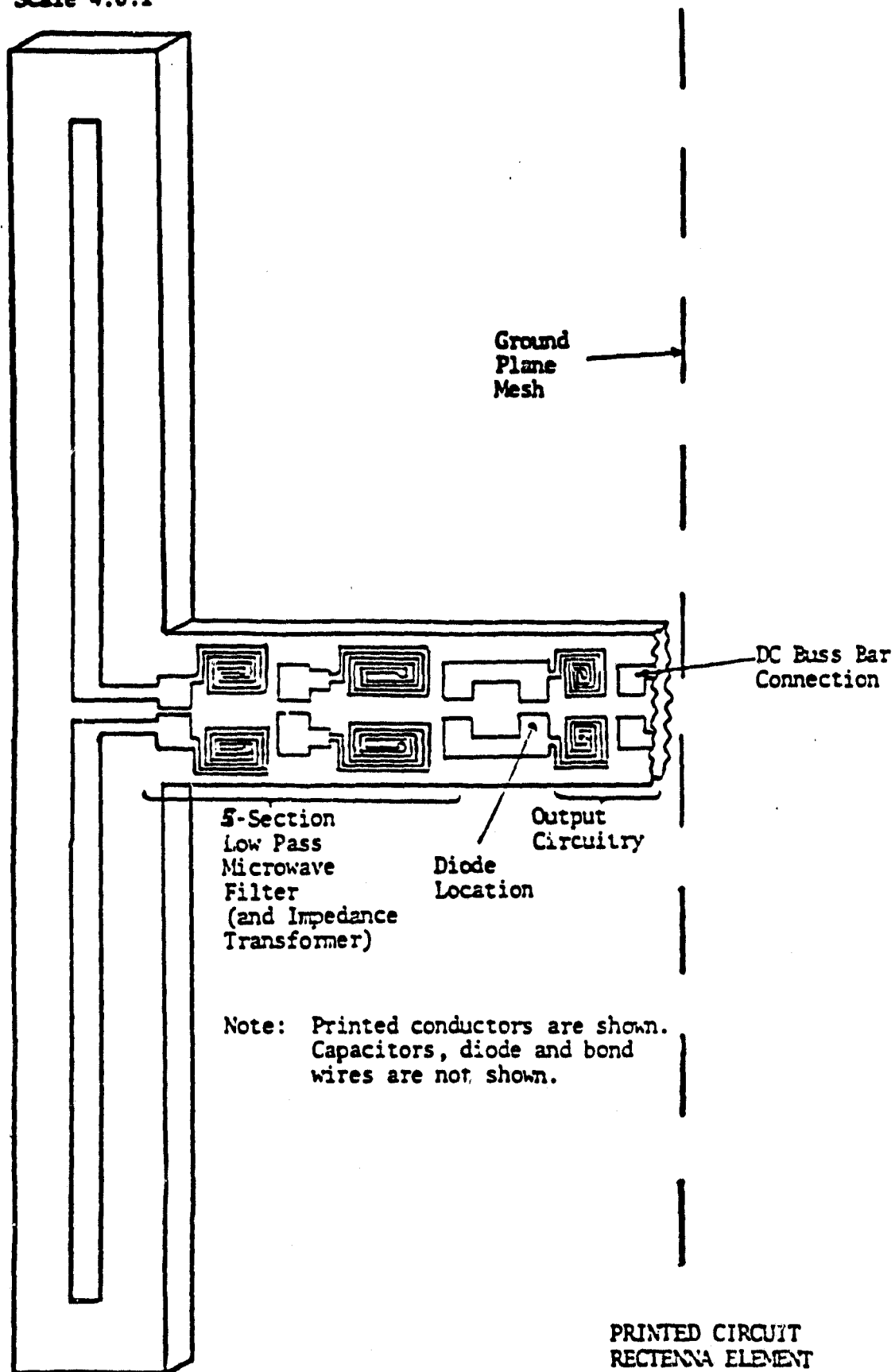
Proposed design of Rectenna motivated by environmental protection and cost considerations.

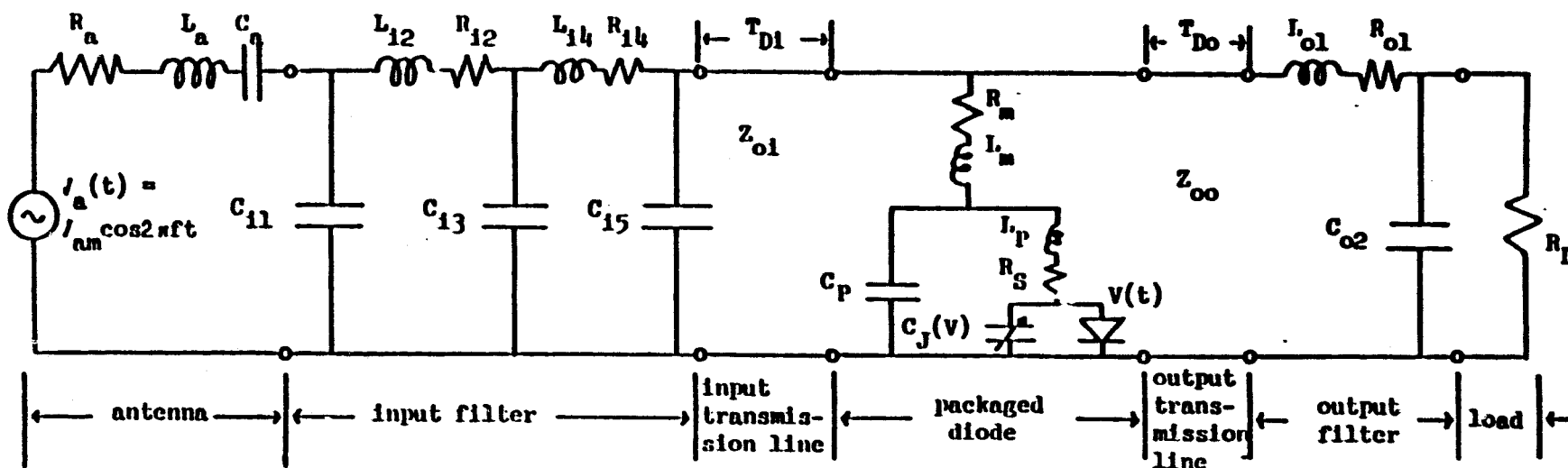


Physical construction of two-plane rectenna. With the exception of covers (white teflon sleeves in photograph) this is the same five element foreplane that was electrically tested. Reflecting plane made from hardware cloth is representative of what could be used in SSPS rectenna.



Scale 4.0:1





Source Parameters

$$f = 2.45 \times 10^9 \text{ Hz (2.45 GHz)}$$

$$V_{am} = 25 \text{ V (1.04 W input)}$$

Input Filter Parameters

$$\begin{aligned} C_{11} &= 1.40 \text{ pF} & C_{13} &= 2.09 \text{ pF} \\ I_{12} &= 5.70 \text{ nH} & I_{14} &= 5.70 \text{ nH} \\ R_{12} &= 0.66 \text{ ohms} & R_{14} &= 0.66 \text{ ohms} \\ & & C_{15} &= 1.40 \text{ pF} \end{aligned}$$

Output Filter Parameters

$$\begin{aligned} I_{01} &= 10.4 \text{ nH} \\ R_{01} &= 1.20 \text{ ohms} \\ C_{02} &= 10.75 \text{ pF} \end{aligned}$$

Diode Parameters ($T = 300^\circ \text{K}$)

$$\begin{aligned} \phi &= 0.8 \text{ eV} \\ n &= 1.0 \\ C_J(0) &= 0.7 \text{ pF} \\ I_s &= 10.0 \text{ nA} \\ R_s &= 0.50 \text{ ohm} \end{aligned}$$

Input Transmission Line

$$\begin{aligned} Z_{01} &= 75 \text{ ohms} \\ T_{01} &= 51 \text{ pS} \end{aligned}$$

Output Transmission Line

$$\begin{aligned} Z_{00} &= 75 \text{ ohms} \\ T_{00} &= 0 \text{ pS} \end{aligned}$$

Diode Package and Mount

$$\begin{aligned} L_p &= 0.3 \text{ nH} \\ C_p &= 0.2 \text{ pF} \\ L_m &= 0.5 \text{ nH} \\ R_m &= 0.25 \text{ ohm} \end{aligned}$$

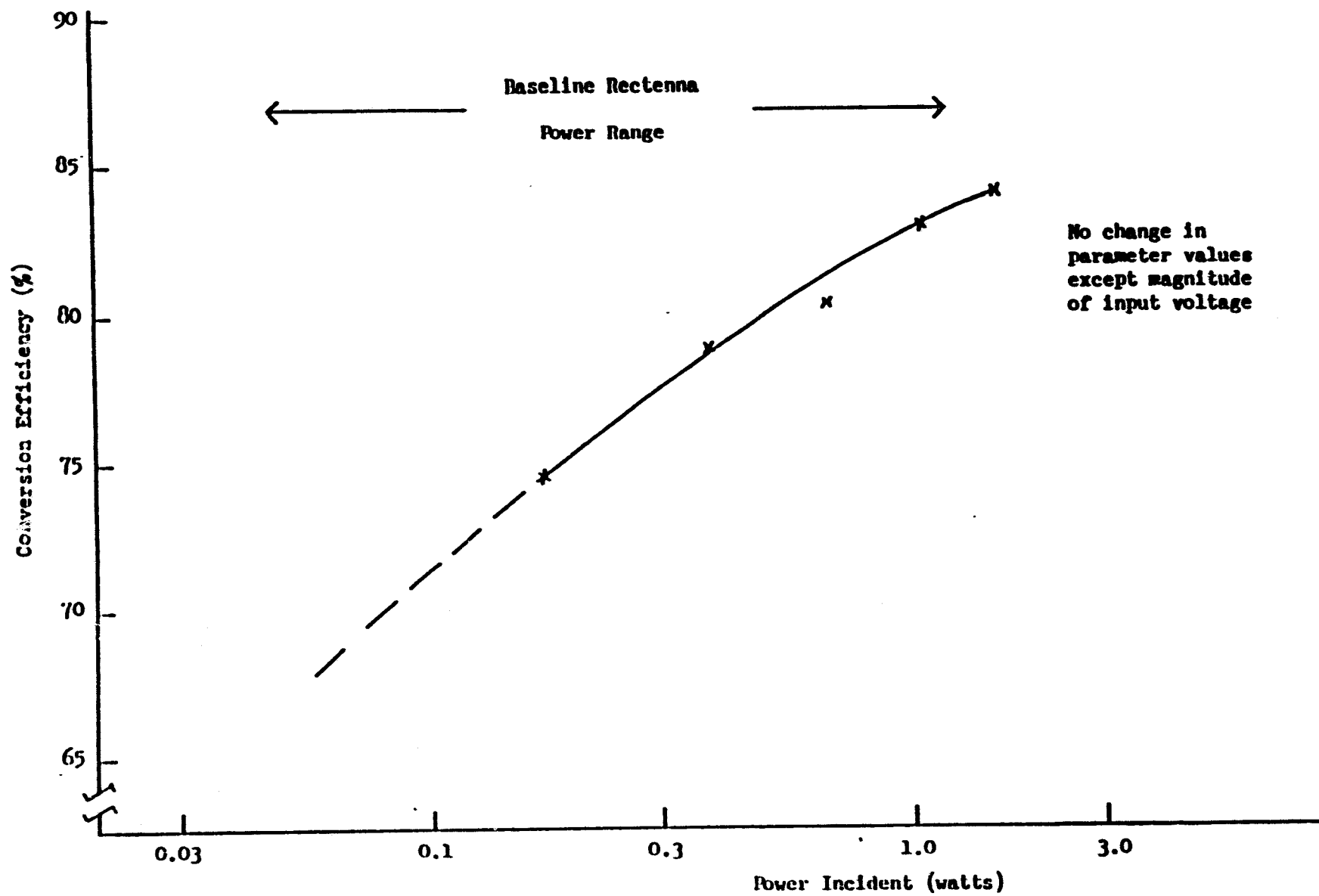
Load

$$R_L = 75 \text{ ohms}$$

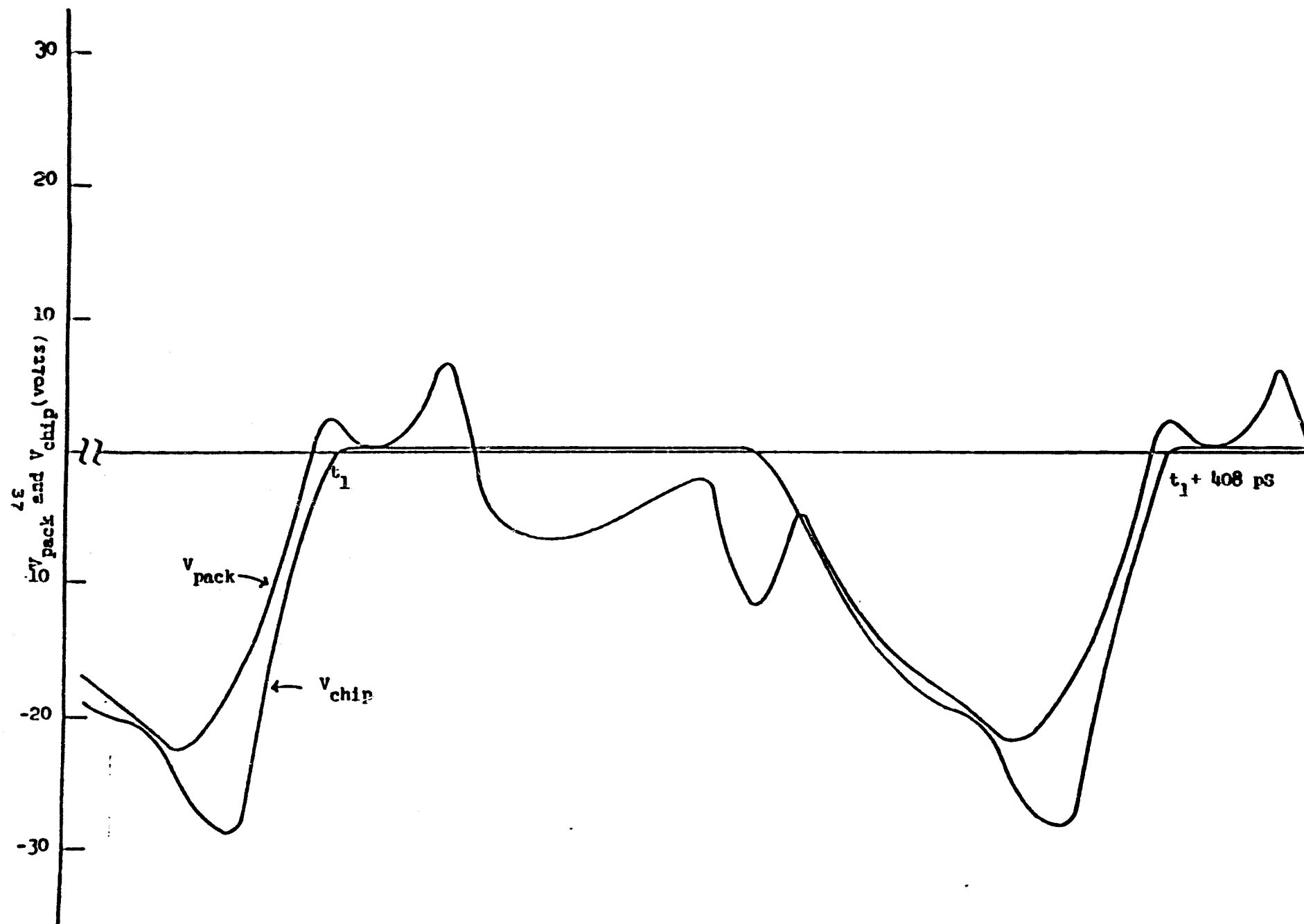
Antenna Parameters

$$\begin{aligned} R_a &= 75 \text{ ohms} \\ L_a &= 0 \text{ nH} \\ C_a &= 3 \text{ pF} \end{aligned}$$

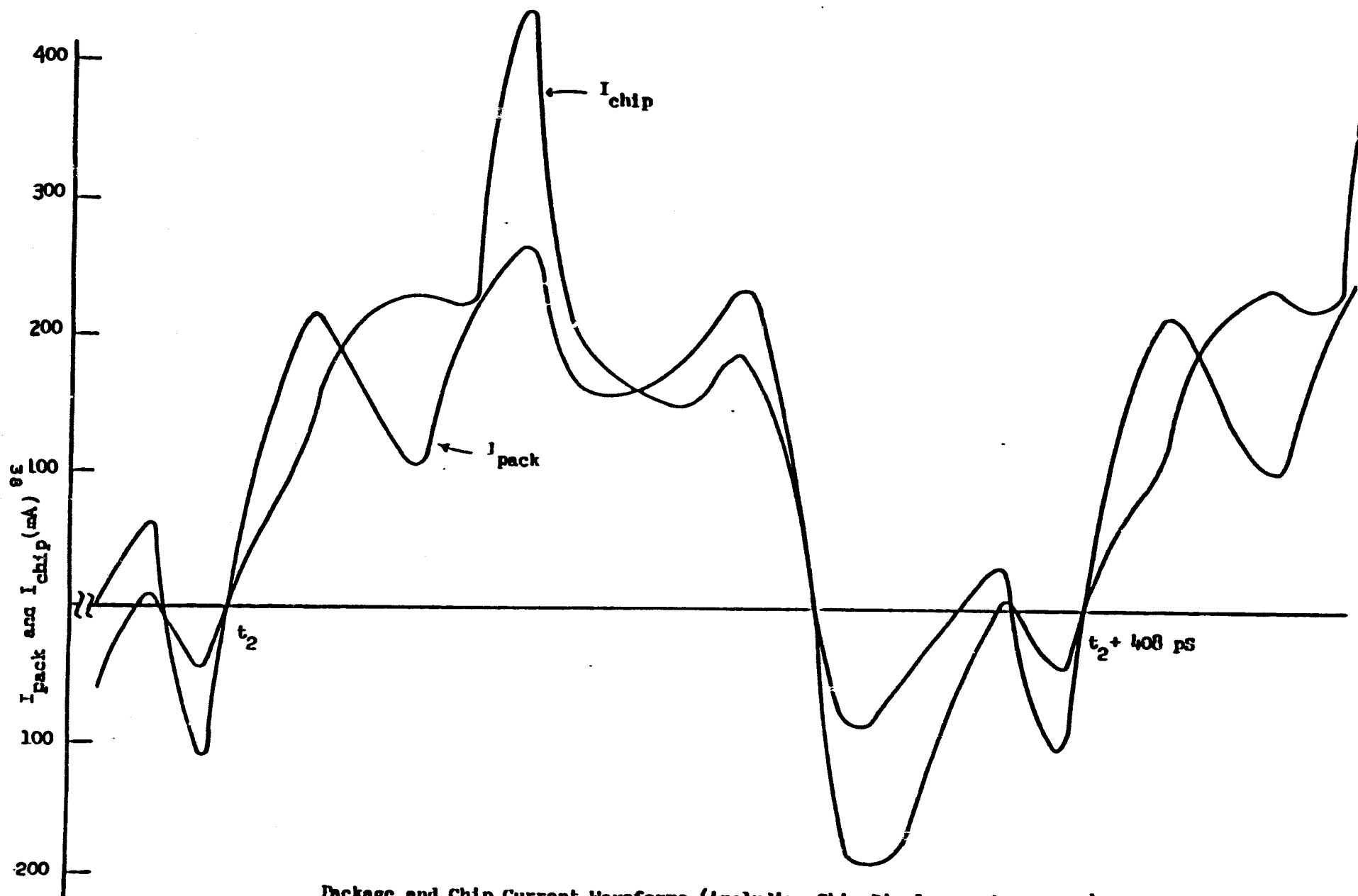
Computer Simulation Model for Baseline Type RF to DC Conversion Circuitry



Conversion Efficiency of Computer Simulation Model

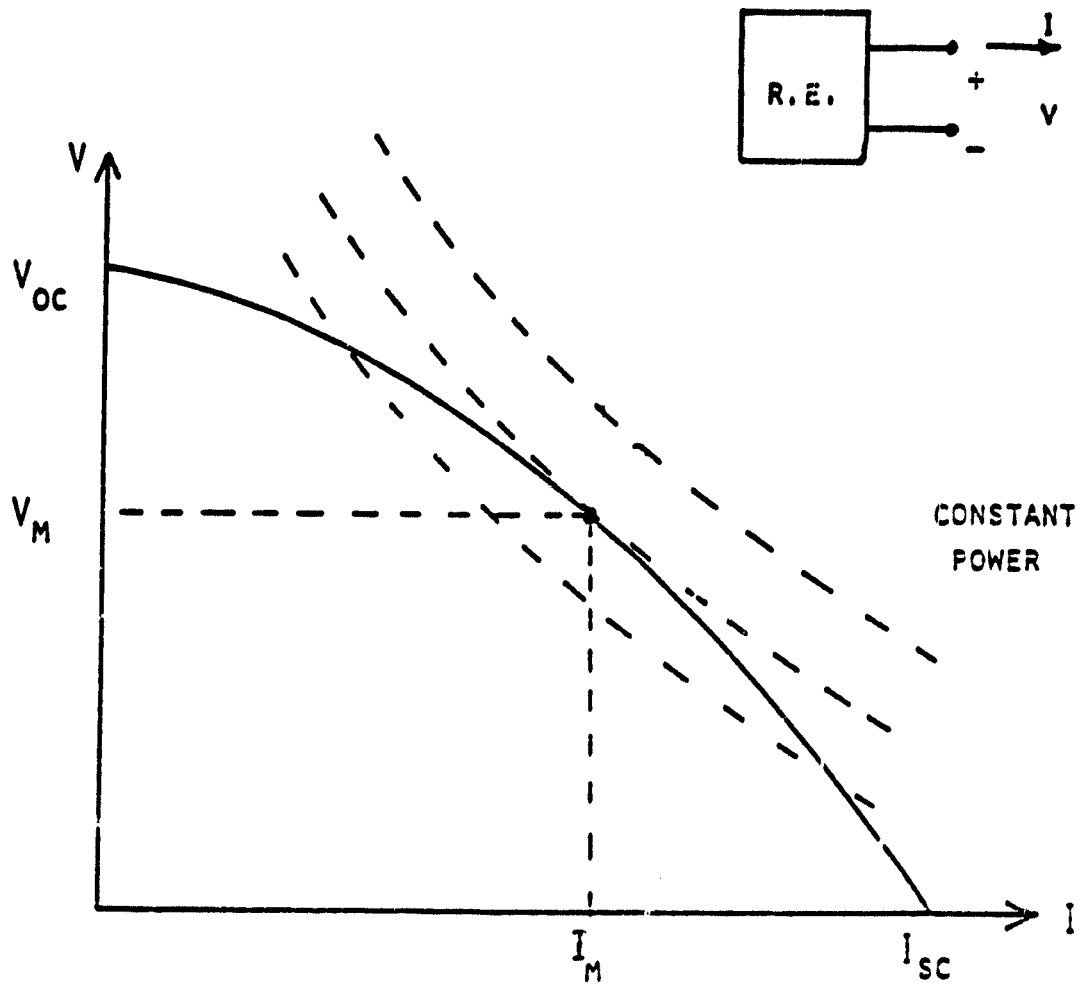


Package and Chip Voltage Waveforms of Computer Simulation Model at 1W Level



Package and Chip Current Waveforms (including Chip Displacement Current)
of Computer Simulation Model at 1W Level

MAXIMUM POWER CONDITION



$$V = f(I, \theta) \quad I = h(V, \theta)$$

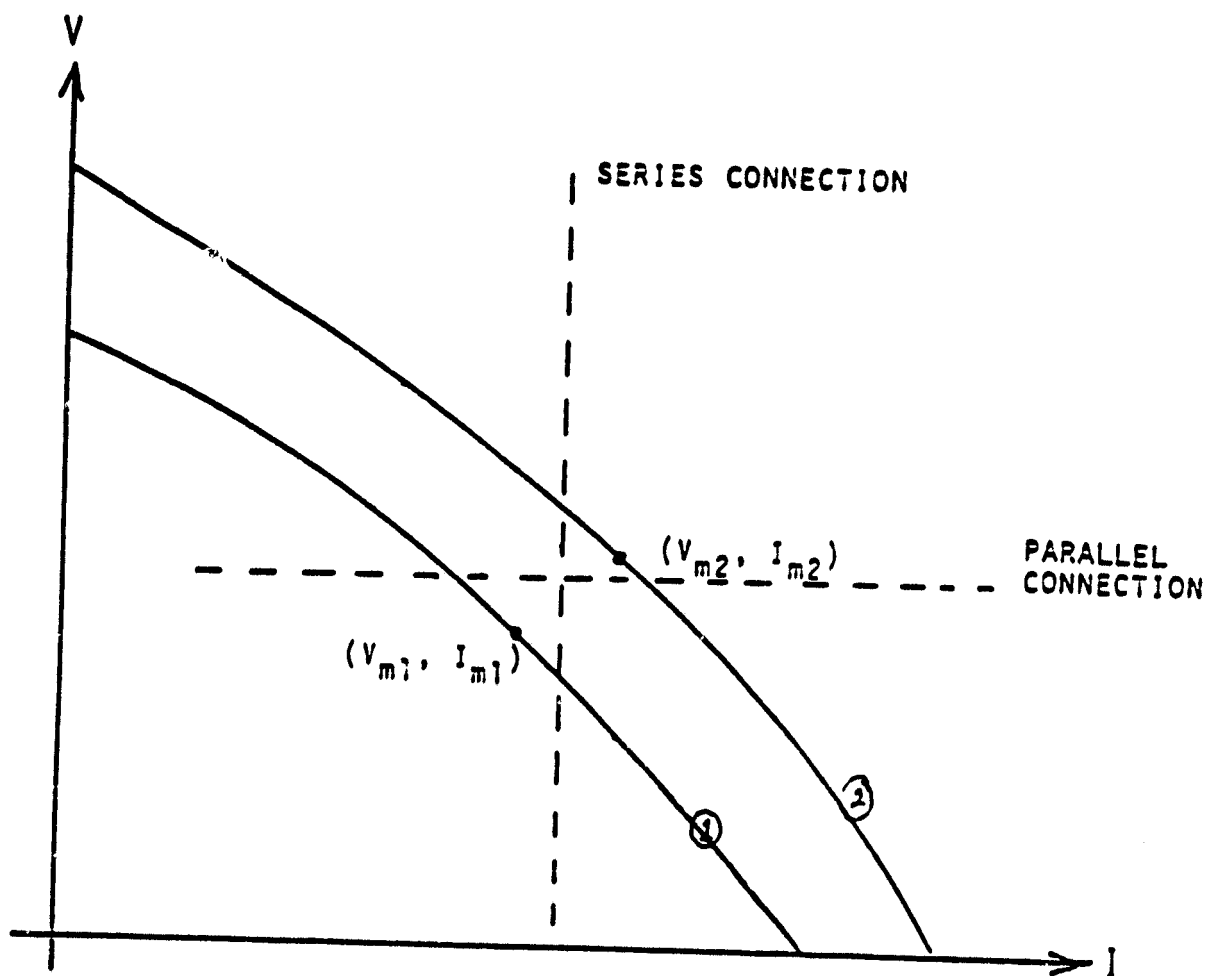
$$P = I \cdot V = I f(I, \theta) = V h(V, \theta)$$

MAXIMUM POWER CONDITION:

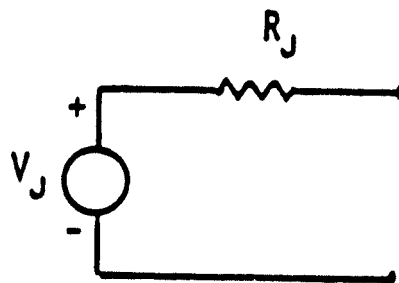
$$\frac{V_M}{I_M} = -f'(I_M, \theta) = r(I_M, \theta)$$

$$R_L = r_m$$

INTERCONNECTION OF ELEMENTS



RELATIVE POWER LOSS



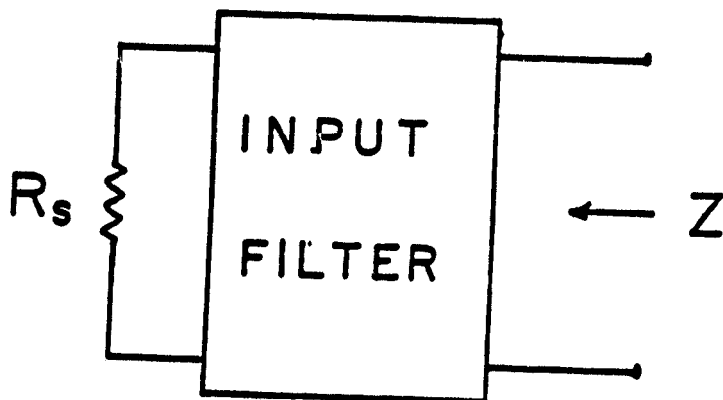
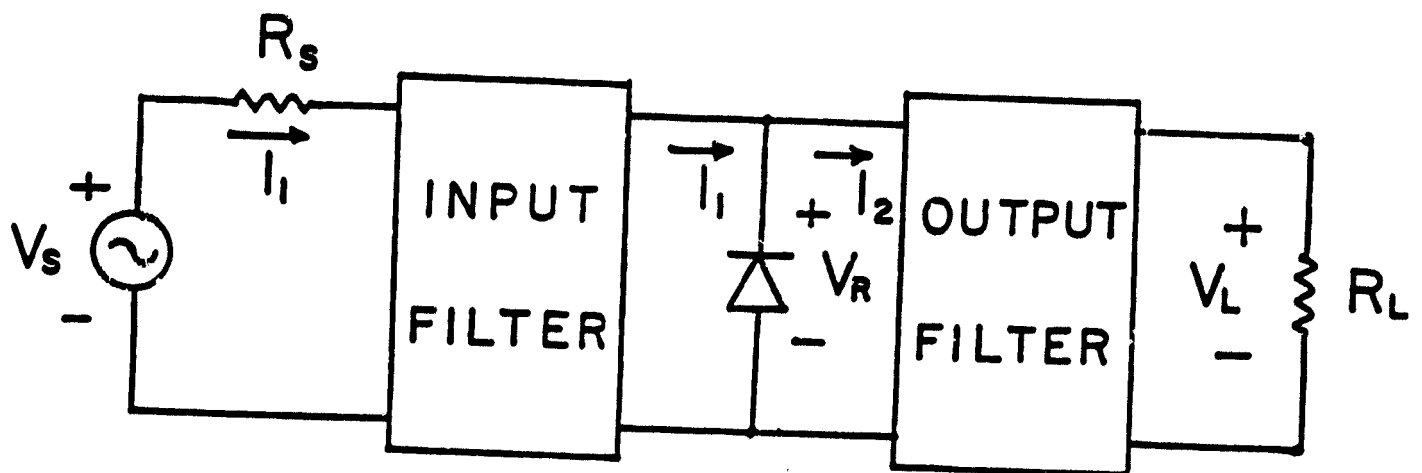
$$J = 1, 2, 3, \dots, N$$

SERIES CONNECTION:

$$\frac{\Delta P_S}{P_{MAX}} = \frac{\sum V_J^2 / R_J - (\sum V_J)^2 / \sum R_J}{\sum V_J^2 / R_J}$$

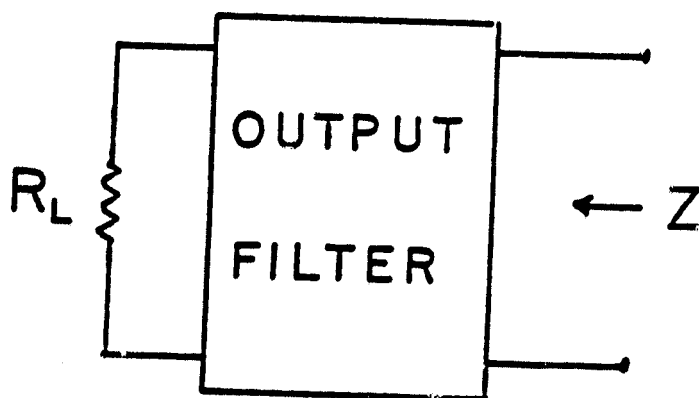
PARALLEL CONNECTION:

$$\frac{\Delta P_P}{P_{MAX}} = \frac{\sum V_J^2 / R_J - (\sum 1/R_J)(\sum V_J / R_J + \sum 1/R_J)^2}{\sum V_J^2 / R_J}$$



$$Z = R_s \text{ at } \omega$$

$$Z = \infty \text{ at } 0, 3\omega, \dots$$

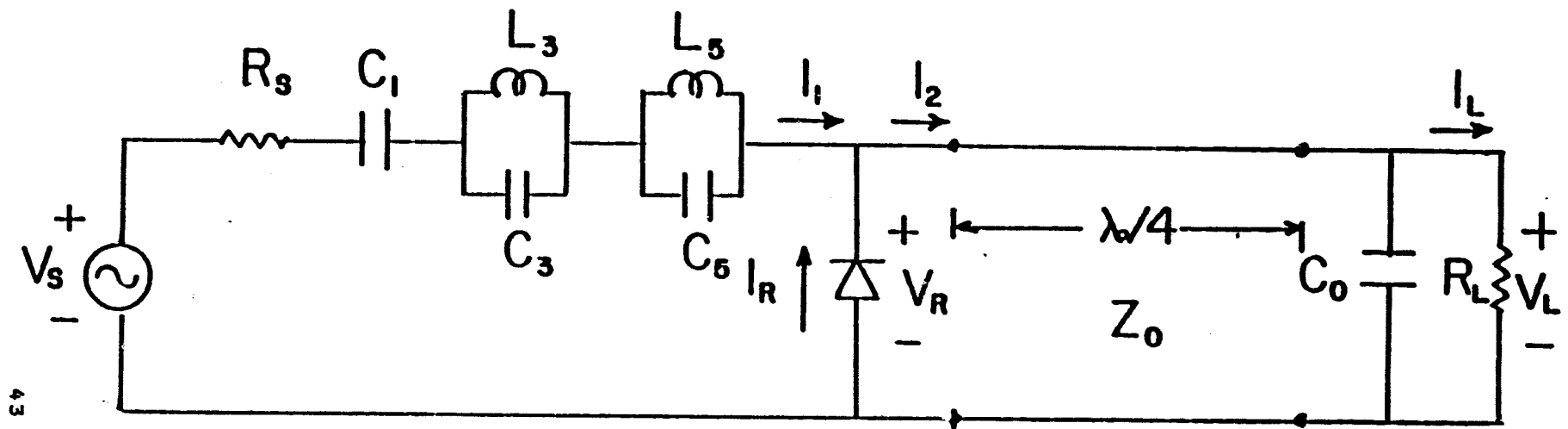


$$Z = R_L \text{ at } 0$$

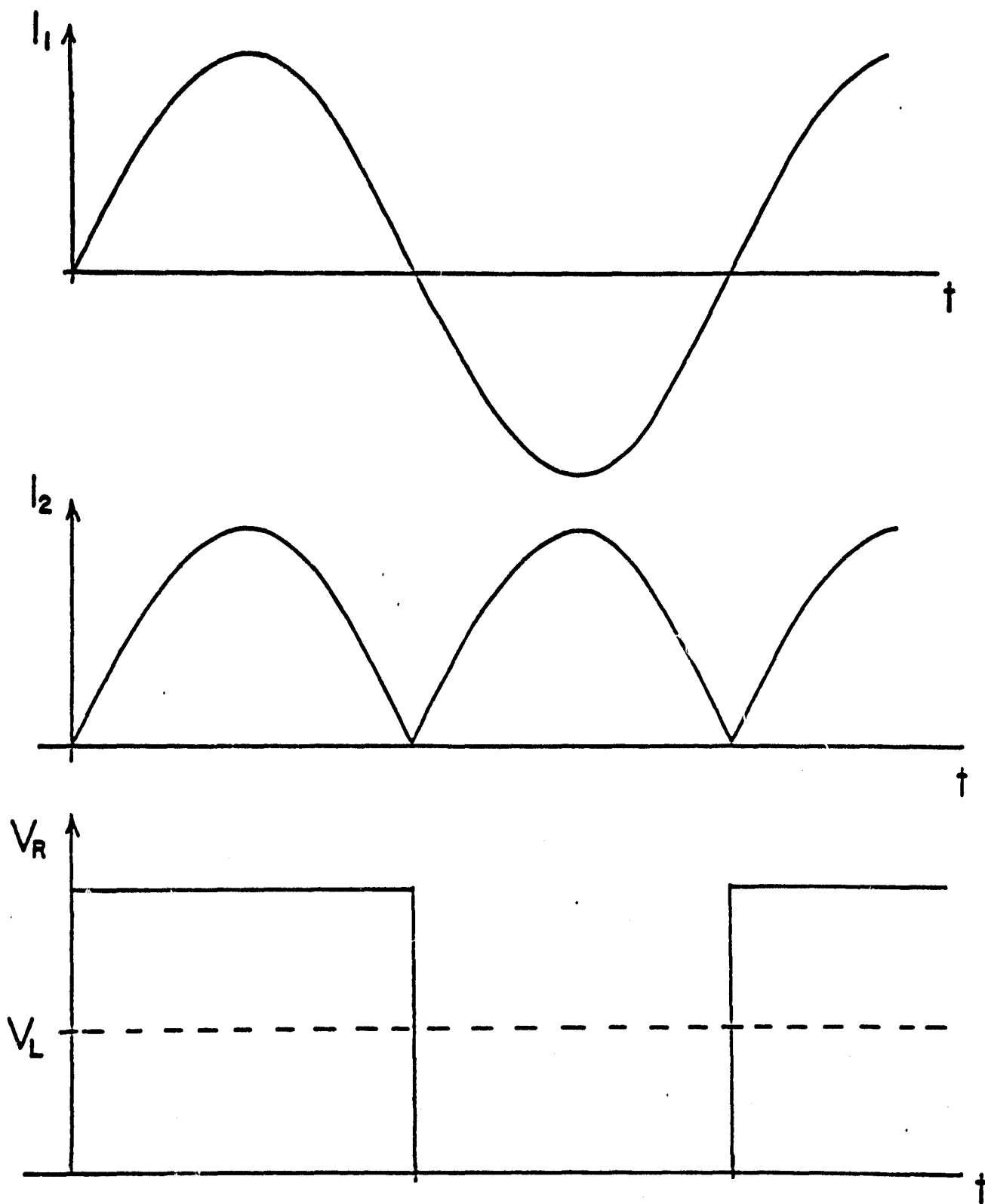
$$Z = 0 \text{ at } 2\omega, 4\omega, \dots$$

$$Z = \infty \text{ at } 3\omega, 5\omega, \dots$$

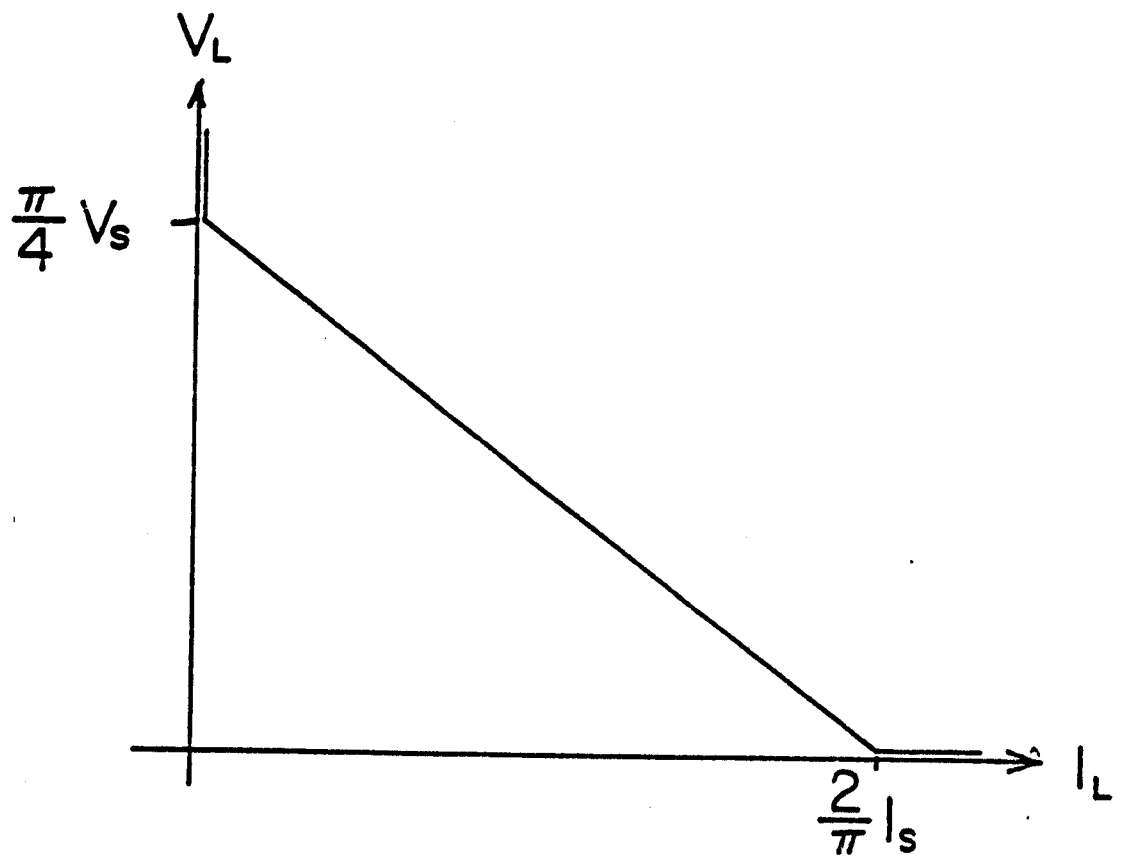
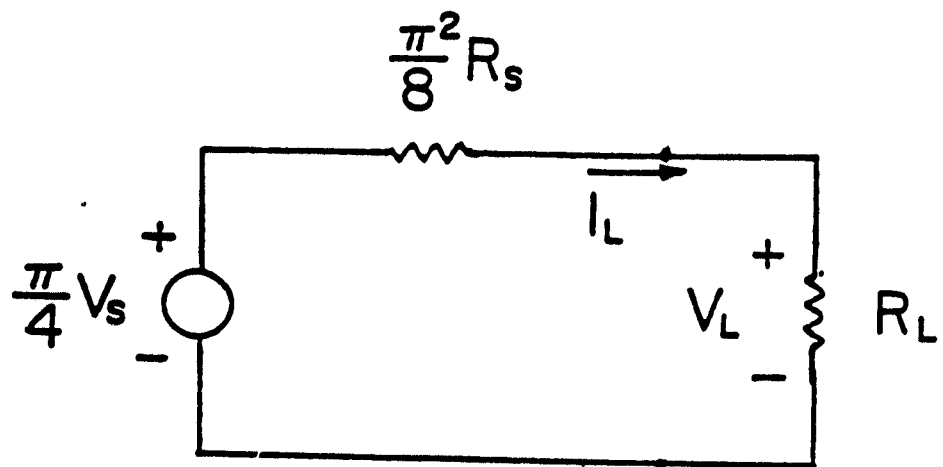
CHARACTERISTICS OF INPUT AND OUTPUT
FILTERS FOR HIGH EFFICIENCY RECTIFICATION



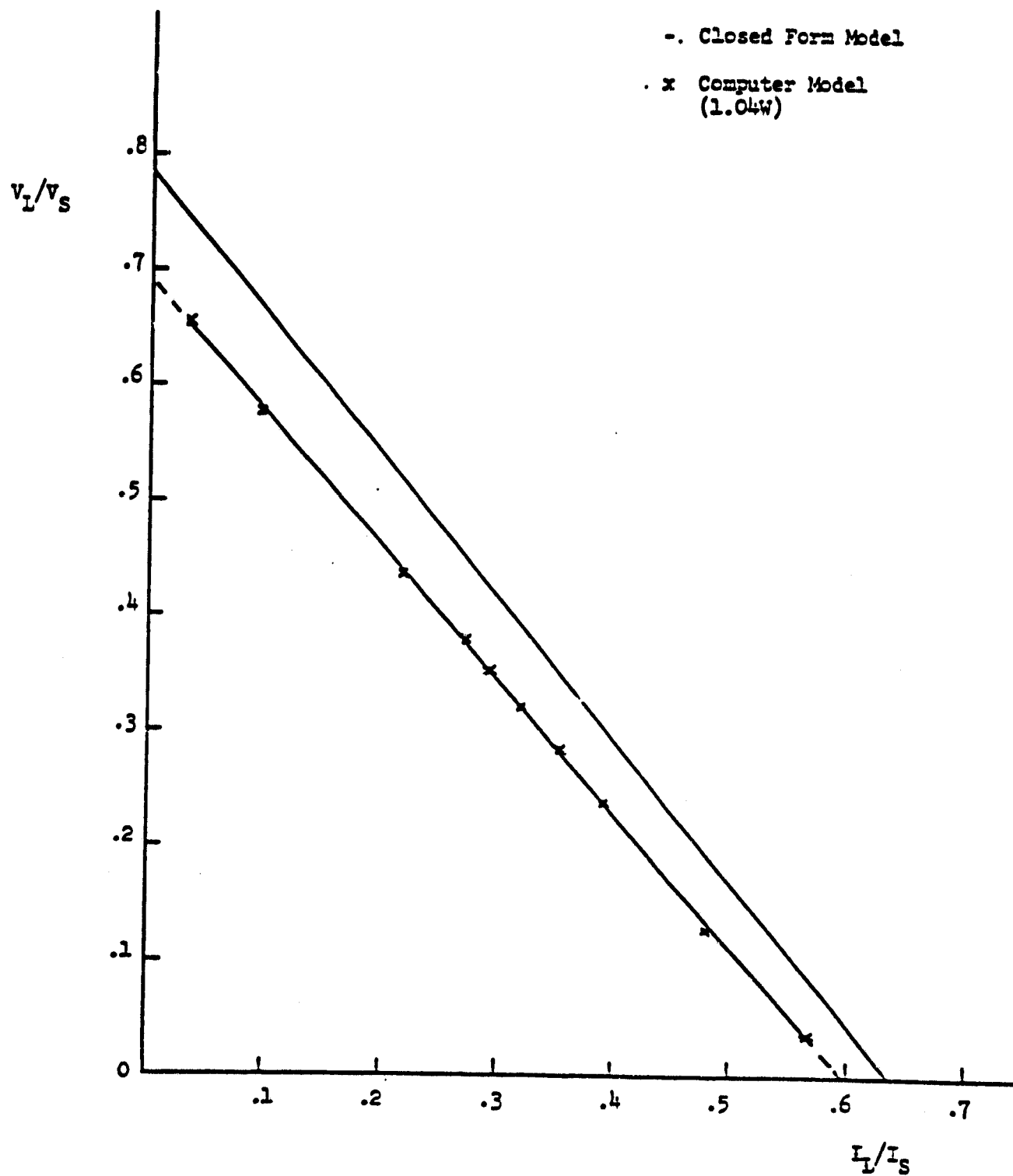
REALIZATION OF HIGH EFFICIENCY RECTIFIER

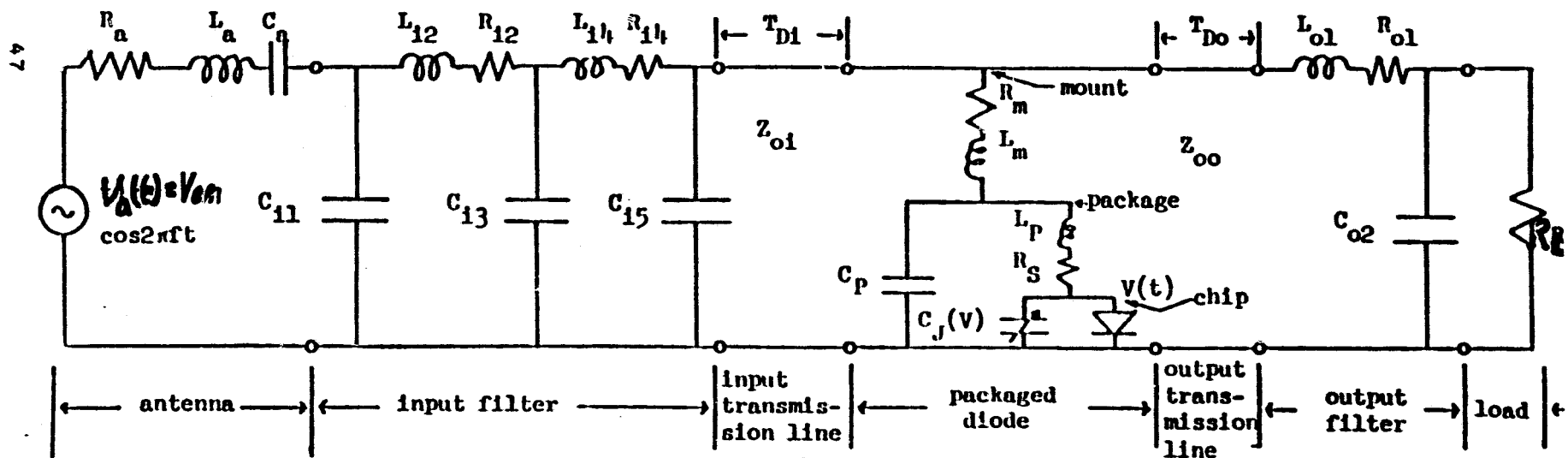
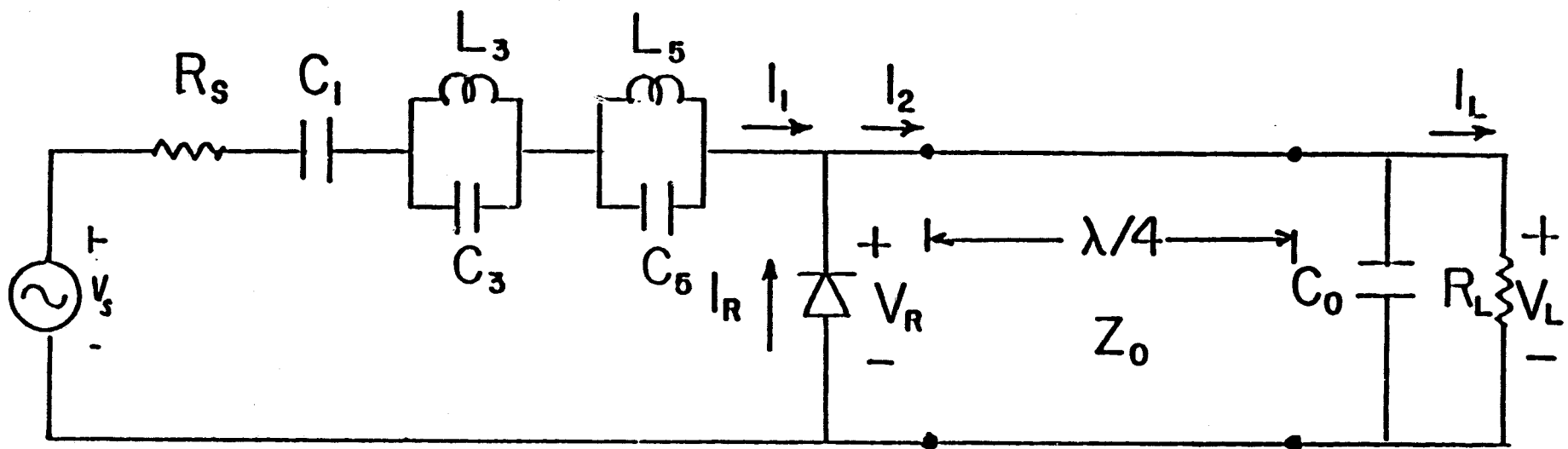


CURRENT AND VOLTAGE WAVEFORMS IN
HIGH EFFICIENCY RECTIFIER



EQUIVALENT CIRCUIT OF HIGH
EFFICIENCY RECTIFIER

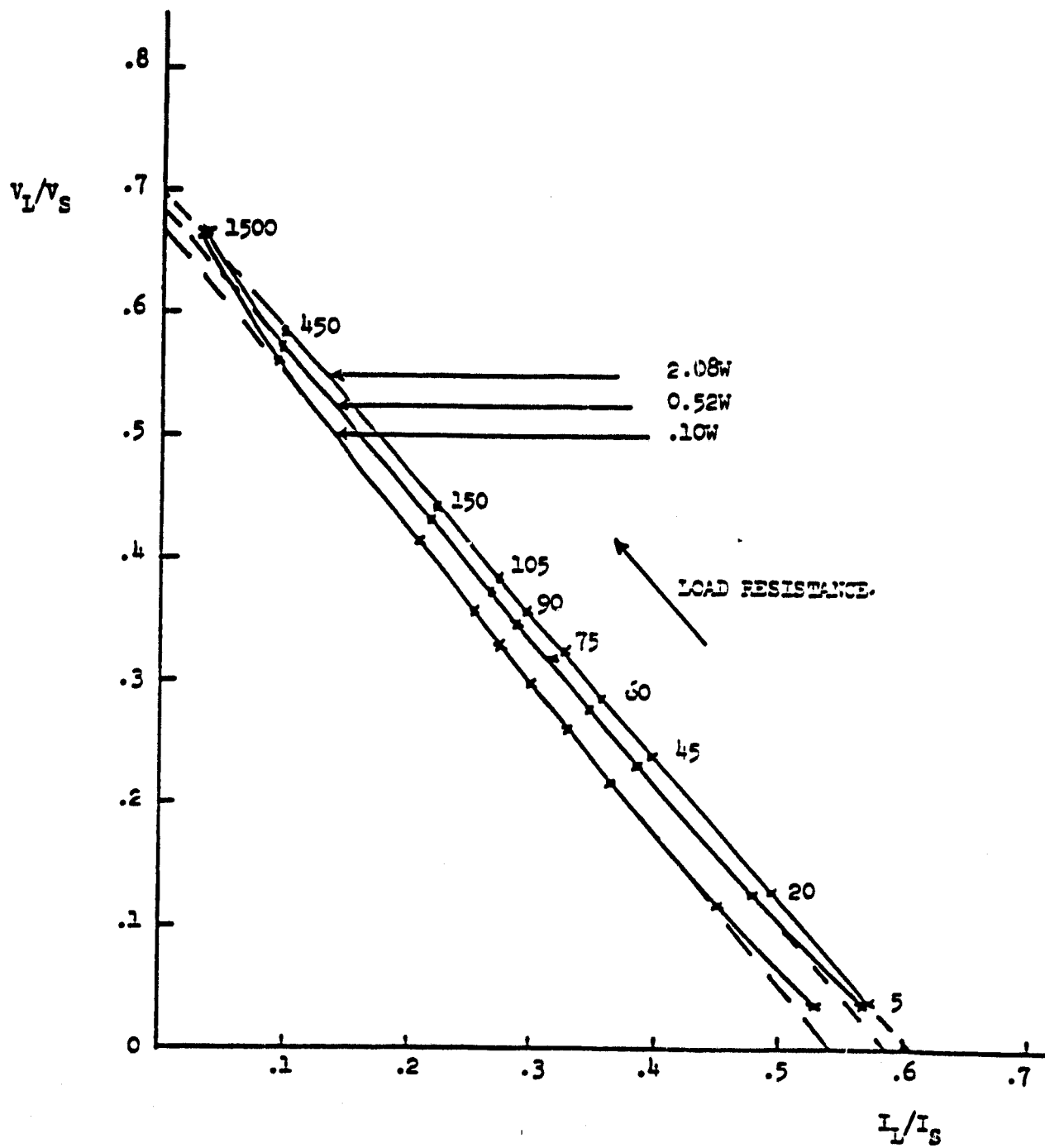


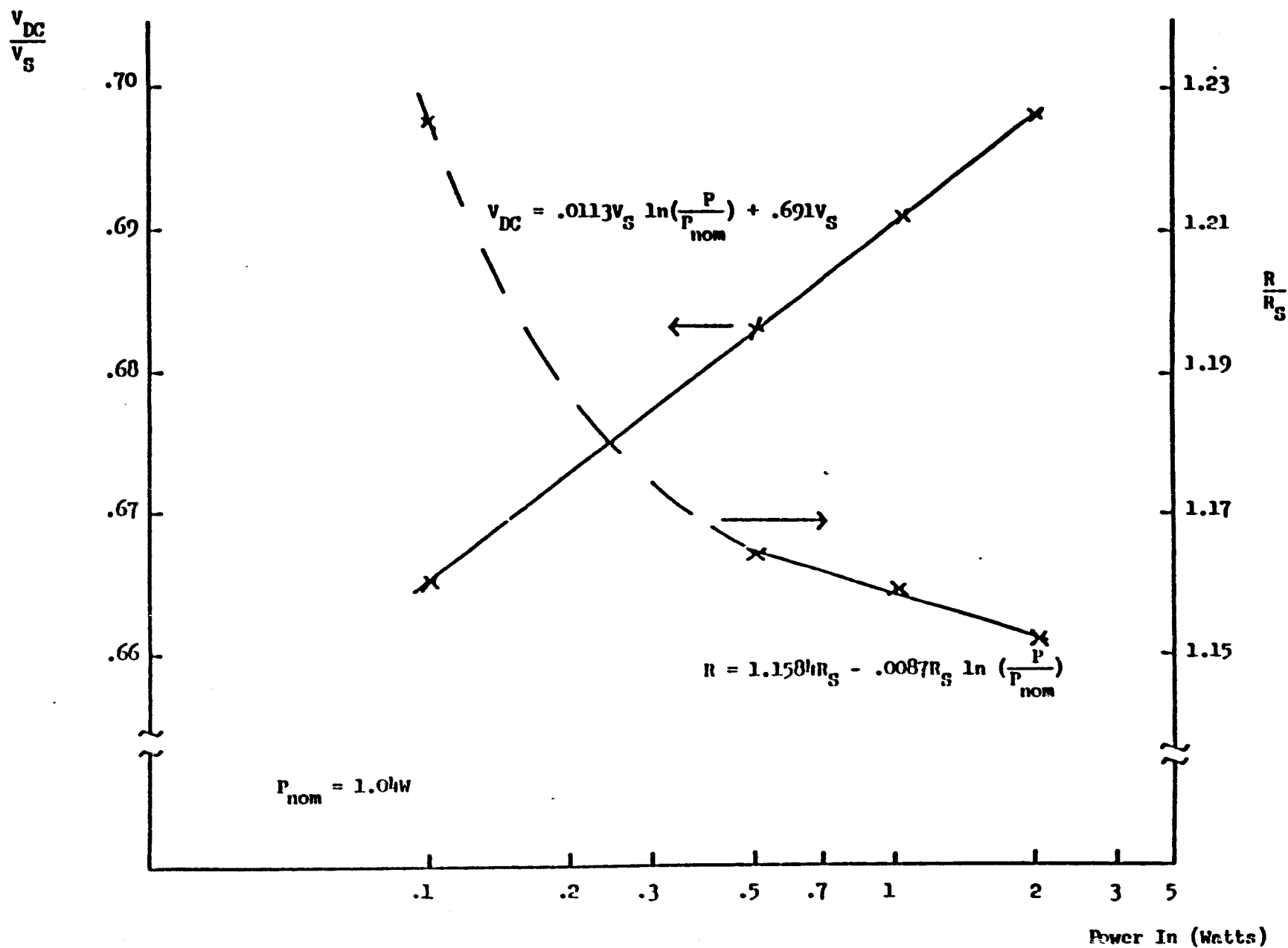


Equivalent Circuit Models for Microwave Rectifier

(A) Ideal Circuit Model

(B) Realistic Circuit Model of Baseline Rectifier





Power Distributions (discrete probability density functions)

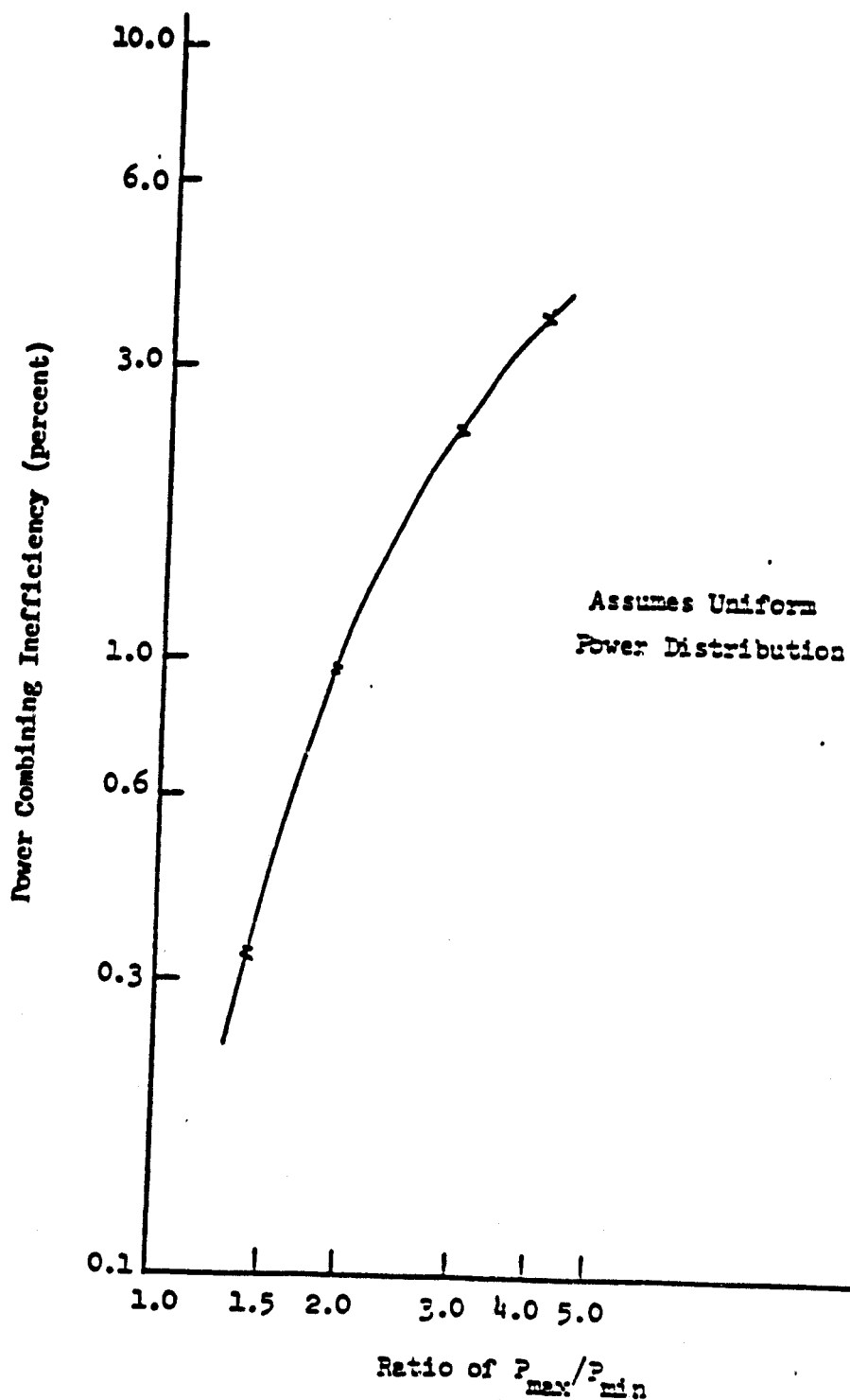
$$\frac{P}{P_{nom}}$$

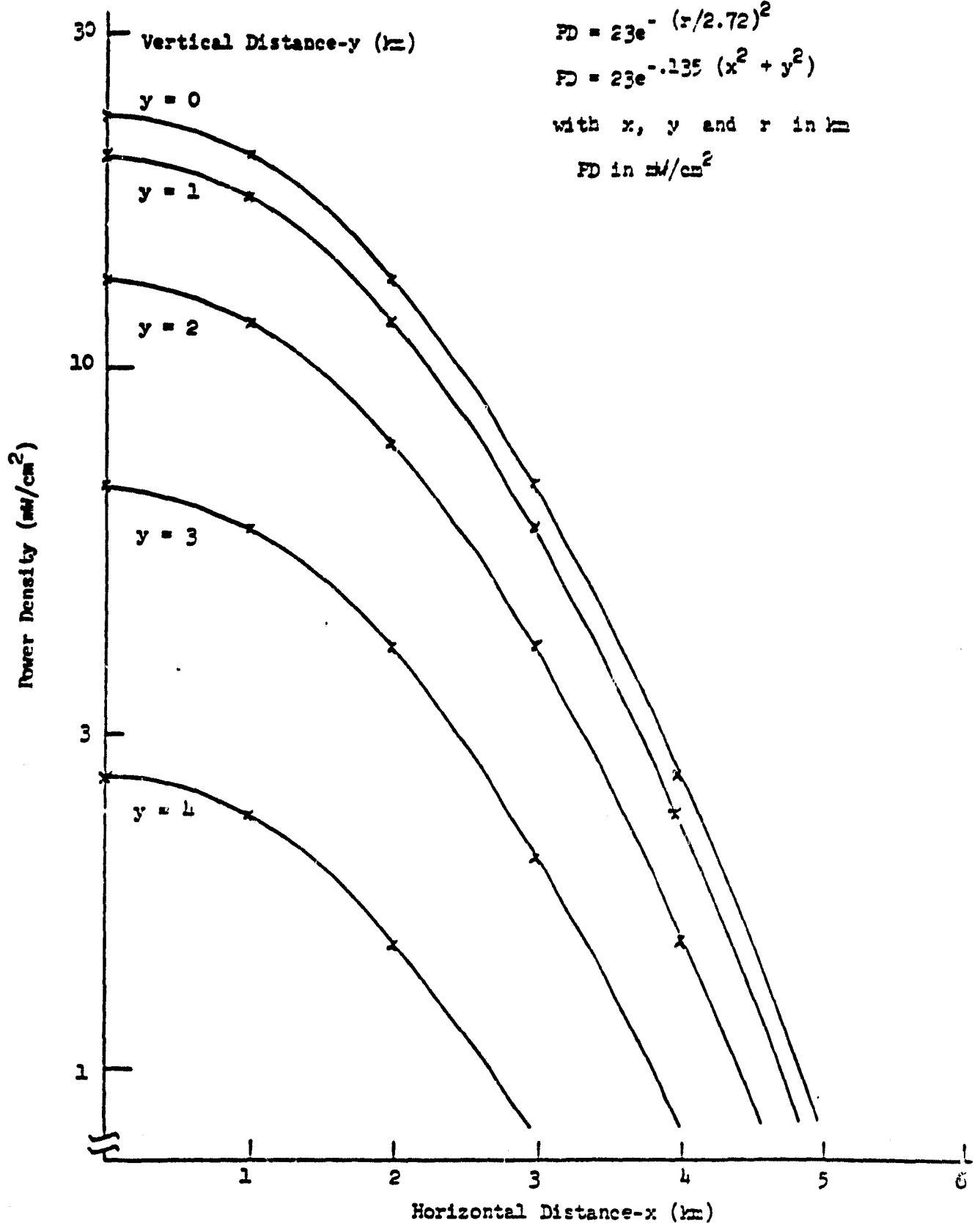
	.5	.6	.7	.8	.9	1.0	1.1	1.2	1.3	1.4	1.5	1.6	1.7	1.8	1.9	2.0
Relative Number																
Case 1	.1	-	-	-	-	.9	-	-	-	-	-	-	-	-	-	-
Case 2	.3	-	-	-	-	.7	-	-	-	-	-	-	-	-	-	-
Case 3	.5	-	-	-	-	.5	-	-	-	-	-	-	-	-	-	-
Case 4	.1	-	-	-	-	-	-	-	-	-	-	-	-	-	-	.9
Case 5	.3	-	-	-	-	-	-	-	-	-	-	-	-	-	-	.7
Case 6	.5	-	-	-	-	-	-	-	-	-	-	-	-	-	-	.5
Case 7	.7	-	-	-	-	-	-	-	-	-	-	-	-	-	-	.3
Case 8	.9	-	-	-	-	-	-	-	-	-	-	-	-	-	-	.1
Case 9	$\frac{1}{16}$	$\frac{1}{16}$	$\frac{1}{16}$	$\frac{1}{16}$	$\frac{1}{16}$	$\frac{1}{16}$	$\frac{1}{16}$	$\frac{1}{16}$	$\frac{1}{16}$	$\frac{1}{16}$	$\frac{1}{16}$	$\frac{1}{16}$	$\frac{1}{16}$	$\frac{1}{16}$	$\frac{1}{16}$	$\frac{1}{16}$
Case 10	$\frac{1}{10}$	$\frac{1}{10}$	$\frac{1}{10}$	$\frac{1}{10}$	$\frac{1}{10}$	$\frac{1}{10}$	$\frac{1}{10}$	$\frac{1}{10}$	$\frac{1}{10}$	$\frac{1}{10}$	-	-	-	-	-	-

Power Combining Inefficiency (percent)

	Computer Simulation Model		Closed Form Model
	Series Combining	Parallel Combining	(Series and Parallel)
Case 1	.88	.86	.81
Case 2	2.31	2.24	2.12
Case 3	3.13	3.04	2.86
Case 4	2.61	2.52	2.43
Case 5	7.31	7.07	6.77
Case 6	10.83	10.51	10.00
Case 7	12.05	11.75	11.05
Case 8	7.68	7.51	6.92
Case 9	3.98	3.87	3.67
Case 10	2.62	2.55	2.40

Power Combining Inefficiency versus Power Range (Ratio of P_{\max}/P_{\min}) assuming Uniform Power Distribution.





Power Beam Taper Used in Power Combining Evaluation (Horizontal Distance is Parallel to DC Combining Buss or East-West while Vertical Distance is Parallel to Narrow Dimension of Rectenna Slat or North-South).

Row y in km	Radial Range for Specified Power Density Range				No. of Elements per Row	Power Output per Row (kW)	Power Combining Inefficiency	Size of Rectenna : for 1 MW Module (m)
	1-3 mW/cm ²	3-9 mW/cm ²	9-18 mW/cm ²	other				
Radial (y = 0)	3.9-4.8 km	2.6-3.9 km	1.4-2.6 km	0-1.4 km (18-23 mW/cm ²)	11,500	1.2	2.5%	56.3
					16,700	5.0	2.5%	13.5
					15,400	10.4	1.1%	6.5
					18,000	18.9	0.2%	3.6
y = 1	3.7-4.7 km	2.4-3.7 km	0.9-2.4 km	0-0.9 km (18-20 mW/cm ²)	12,800	1.3	2.5%	52.0
					16,700	5.0	2.5%	13.5
					19,200	13.0	1.1%	5.2
					11,500	11.0	<0.1%	6.1
y = 2	3.3-4.4 km	1.7-3.3 km	0-1.7 km (9-13 mW/cm ²)		14,100	1.4	2.5%	48.2
					20,500	6.2	2.5%	10.9
					21,800	12.0	0.4%	5.6
y = 3	2.4-3.8 km		0-2.4 km (3-7 mW/cm ²)		18,000	1.8	2.5%	37.5
					30,800	7.7	1.6%	8.8
y = 4	0-2.7 km				34,600	3.5	2.5%	19.3

Fig. 3 Power Module Characteristics with Row Combining

EXAMPLE OF IMPACT ON RECTENNA BUSSING

A) BASELINE EDGE TAPER:

1 MW/CM² AT 4.7 KM RADIUS
3 MW/CM² AT 4.0 KM RADIUS
OR 3:1 IN POWER DENSITY OVER 700 M

BASELINE RECTENNA:

50 CM²/RECTENNA ELEMENT
7.8 CM BETWEEN ELEMENTS

ROW DC COMBINING:

9000 ELEMENTS YIELDING 900 W NOMINALLY
POWER COMBINING INEFFICIENCY 2.5%

B) BASELINE MIDDLE TAPER:

3 MW/CM² AT 4.0 KM
9 MW/CM² AT 2.7 KM
OR 3:1 IN POWER DENSITY OVER 1300 M

BASELINE RECTENNA:

SAME AS ABOVE

ROW DC COMBINING:

16,700 ELEMENTS YIELDING 5000 W NOMINALLY
POWER COMBINING INEFFICIENCY 2.5%

DIRECTIONAL RECTENNA ELEMENTS

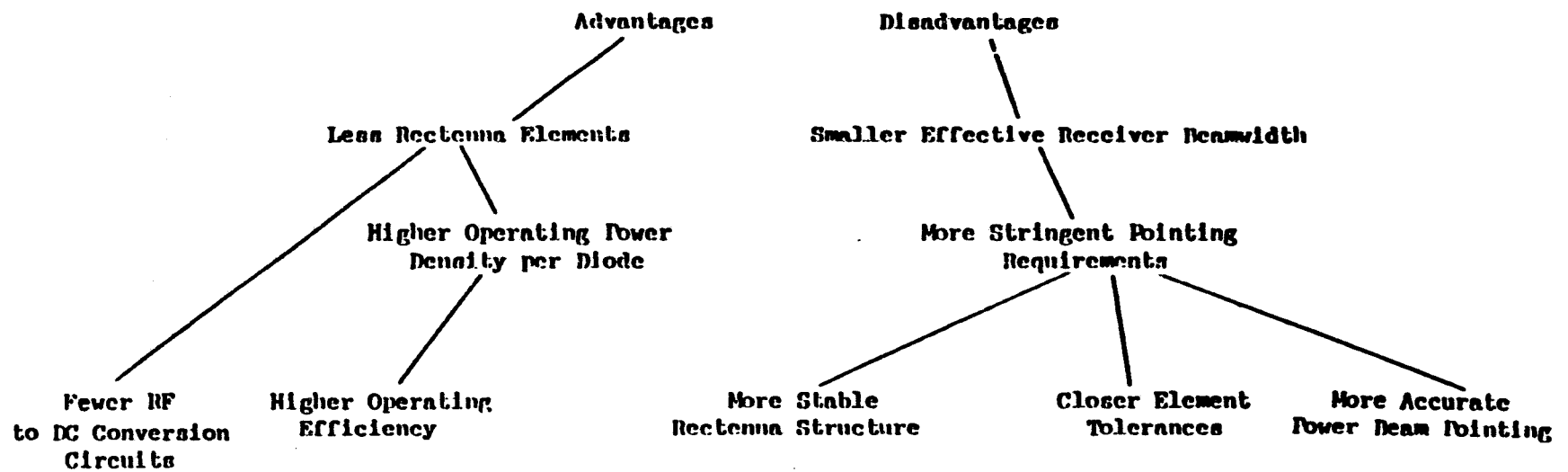
ASSUMPTIONS AND UNDERLYING TENETS

- O BASELINE RECTENNA DEMONSTRATED CAPABILITY OF ADEQUATE ELECTRICAL PERFORMANCE**
- O PROJECTED PER ELEMENT COST SIGNIFICANT AND LARGE UNCERTAINTY**
- O PROJECTED RECTENNA STRUCTURE COST LARGE**
- O GAAs SCHOTTKY RECTIFIER CAPABLE OF INCREASED POWER LEVELS**
- O ORBIT CONSIDERATIONS INDICATE MORE DIRECTIONAL RECEIVING ELEMENT POSSIBLE**
- O PRINTED CIRCUIT IMPLEMENTATION WORTH CONSIDERING IN DEPTH**

APPROACH TAKEN

- 0 DELINEATE LIST OF DESIRABLE CHARACTERISTICS
- 0 FOCUSED ON THREE BASIC DESIGNS (HALF-WAVE DIPOLE, YAGI, HOGLINE)
- 0 EVALUATE PERFORMANCE PENALTY WITH PRINTED CIRCUIT IMPLEMENTATION
- 0 COMPARED 5 ALTERNATIVES USING CHARACTERISTIC LISTED
- 0 ARRIVED AT PRELIMINARY DESIGNS OF YAGI AND HOGLINE DIRECTIONAL RECTENNAS
- 0 INITIATED CONSIDERATION OF ARRAYING HALF WAVE DIPOLES AND YAGI

**More Directional,
Higher Gain Elements**



Advantages and disadvantages of a higher gain, more directional element receiving

Rectenna Element Beamwidth Requirements

Orbit Considerations

Zero inclination orbit

$c = .02 \longrightarrow \pm 2.75^\circ$ in azimuth

$c = .04 \longrightarrow \pm 5.14^\circ$ in azimuth

elevation angle variations appreciably smaller

Small but finite inclination orbit

azimuth angle variations relatively unchanged

elevation angle variations increase

Conclusion (subject to quantification of orbits and more detailed analysis)

azimuth angle variation $\pm 3^\circ$ to 5°

elevation angle variation ± 0.5 to 1.0°

(assuming no refraction effects nor rectenna misalignment or settling problems)

Baseline Rectenna (Data from R.M.Dickinson JPL)

For small variations in c plane, power pattern $\propto \cos \theta$

$\pm 5.73^\circ \longrightarrow 0.5\%$ power reduction (-0.022 dB)

$\pm 8.11^\circ \longrightarrow 1.0\%$ power reduction (-0.044 dB)

$\pm 11.48^\circ \longrightarrow 2.0\%$ power reduction (-0.088 dB)

H plane pattern similar

Conclusion

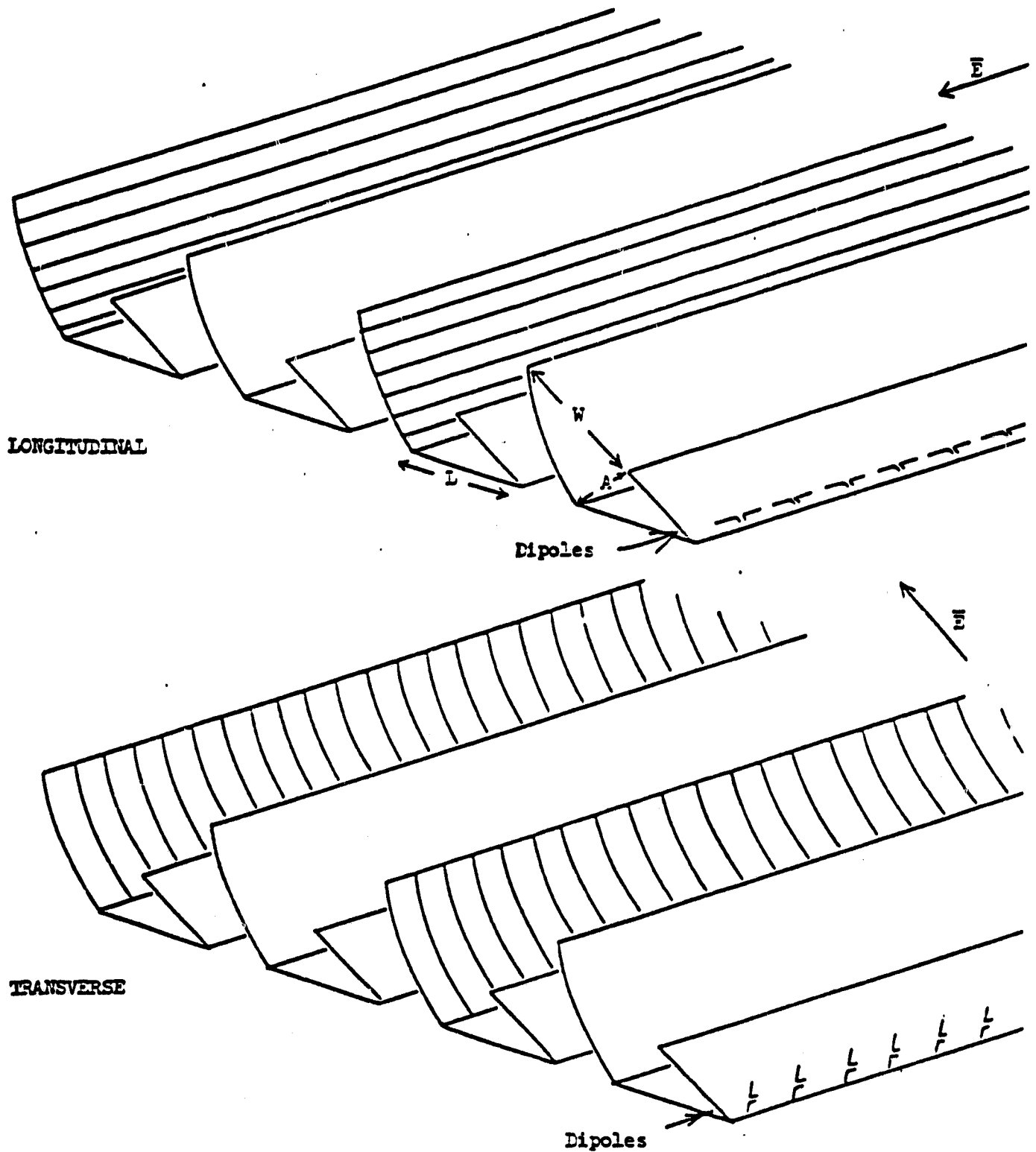
If 1% power reduction permitted under worse cases, azimuth beamwidth can be reduced by factor of 2 and elevation beamwidth by a factor of 10.

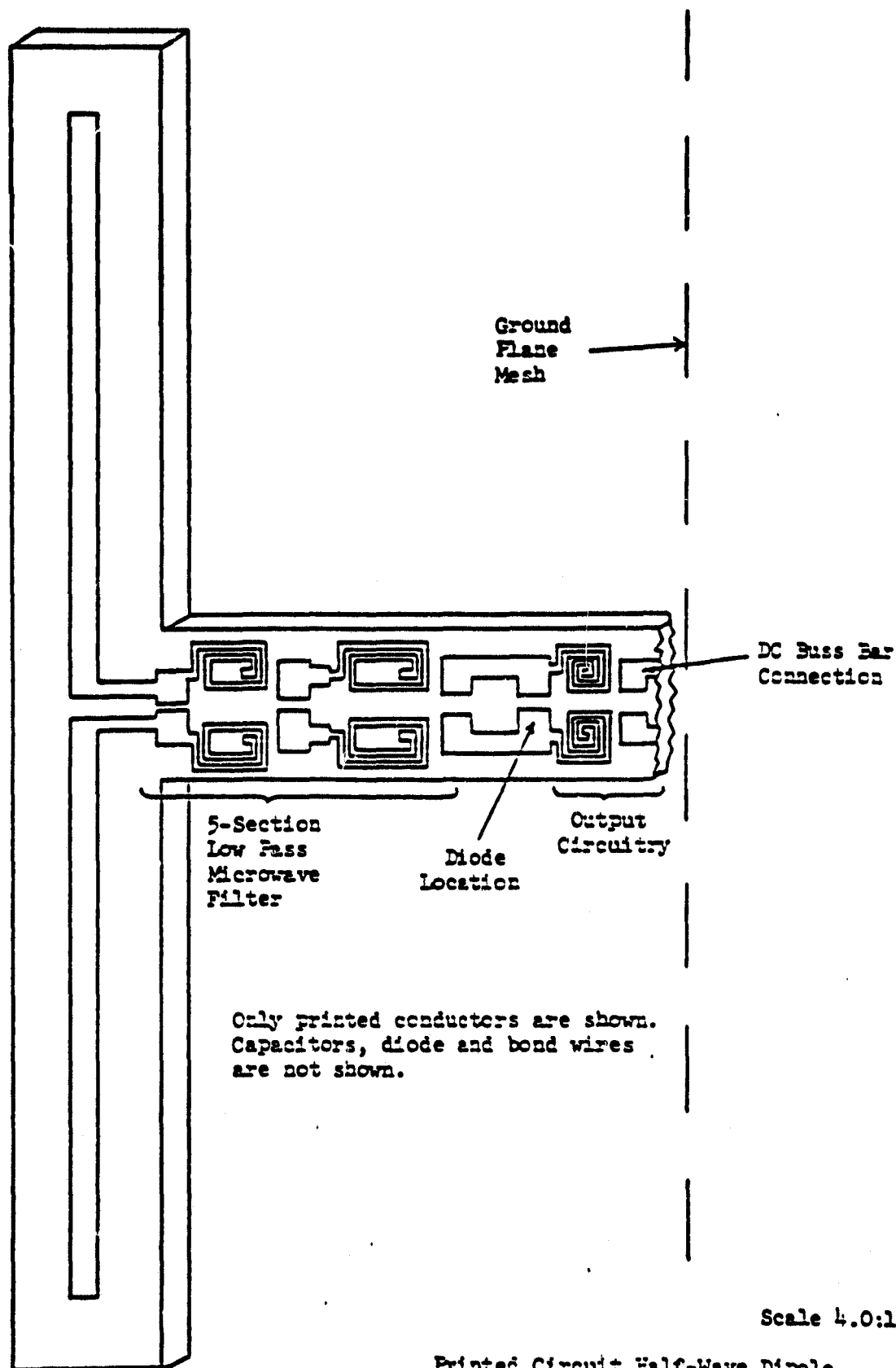
Characteristic	Relative Weight (1 to 5 with 5 most important)	Baseline Di- pole Rectenna	Printed Circuit Dipole Implemen- tation	Yagi Printed Circuit	Yagi with Baseline Construction	Hogline
<u>Electrical Emphasis</u>						
capable of efficient reception	5	5	5	4	4	3
conversion efficiency with Schottky rectifier	5	5	3	4	5	4
controllable directivity	3	2	2	3	3	4
controllable radiation impedance	2	2	4	3	2	4
amenable to analysis and modeling	2	4	4	3	3	3
harmonic radiation characteristics	3	3	3	2	2	4
cross polarization considerations	1	4	4	2 or 4 ^a	2 or 4 ^a	3
combining network compatibility	4	5	4	4	4	3 or 5 ^a
<u>Manufacturing Emphasis</u>						
low cost raw material usage	5	3	4	4	3	4
low manufacturing complexity	4	4	5	5	4	4
lack of manufacturing tolerances	3	5	5	4	4	3
structural implications	4	3	3	3	3	3
single building block for rectenna	2	2	2	2	2	2
terrain tolerance	3	3	3	3	3	2
<u>System Considerations</u>						
multiple land use feasibility	4	3	3	4	4	2
interference implications	2	2	4	4	2	3
environmental protection	3	3	3	3	3	4

^a polarization dependent

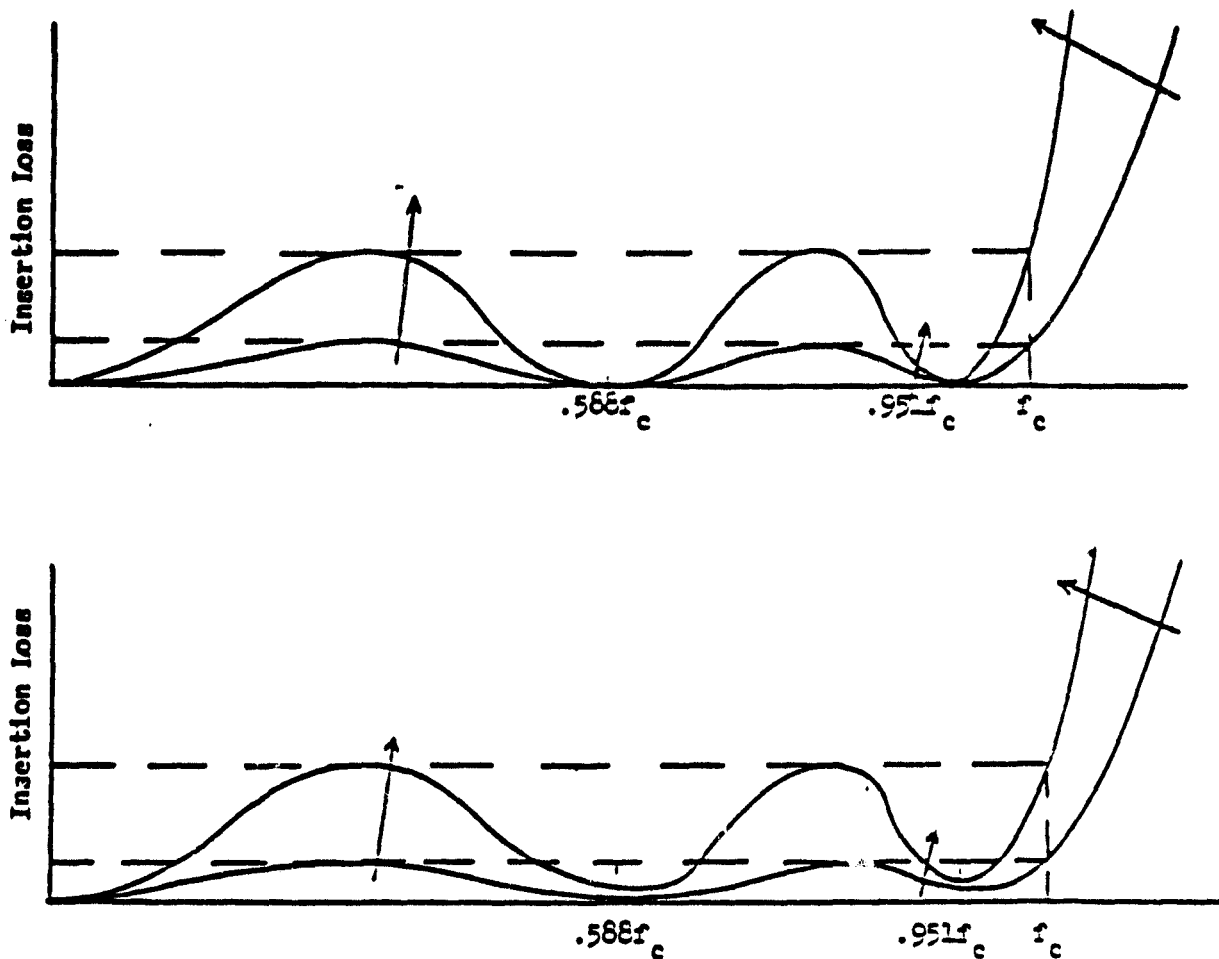
1 to 5 with 5 most favorable

Hogline Parabolic Reflector Conductor Requirements and Dipole
Alignment for Longitudinal and Transverse Polarization





Printed Circuit Half-Wave Dipole Rectenna Element (Ref. 5)



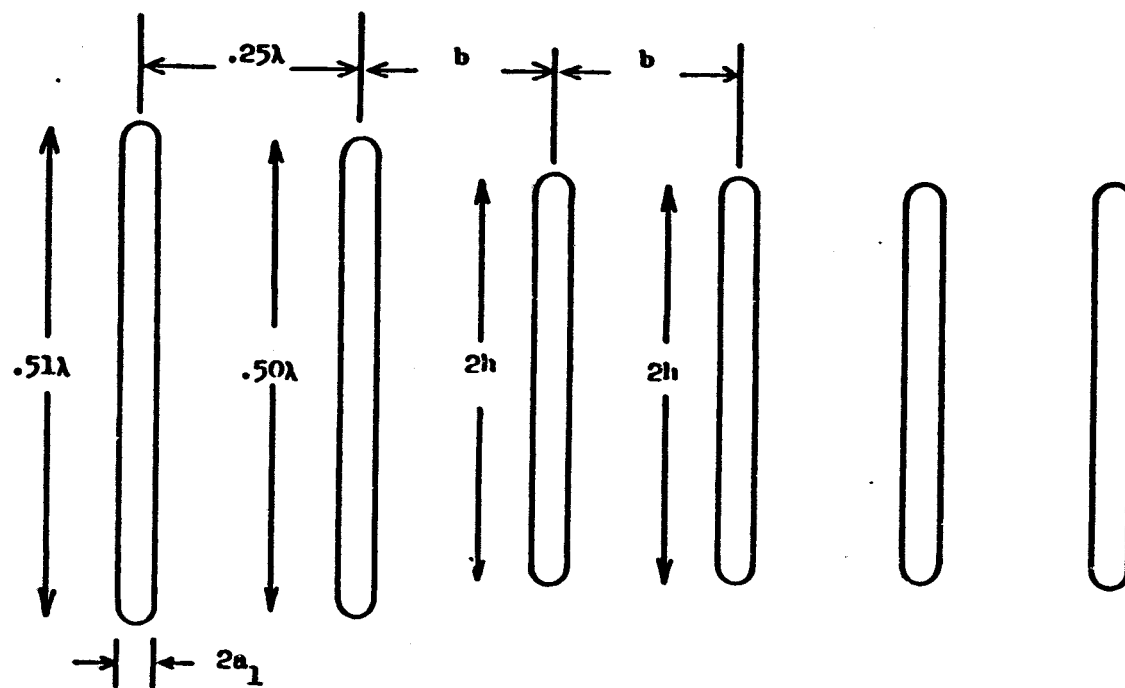
Insertion Loss vs. Frequency for $N=5$ Chebyshev Filters. Arrows in direction of increasing ripple factor.

(A) Lossless Elements

(B) Finite Q Elements

Note: $.951f_c = 2.45 \text{ GHz}$ or $f_c = 2.576 \text{ GHz}$

Concept of Chebyshev Input Filter Design



$$a_1 = a_2 = \dots = .00337\lambda$$

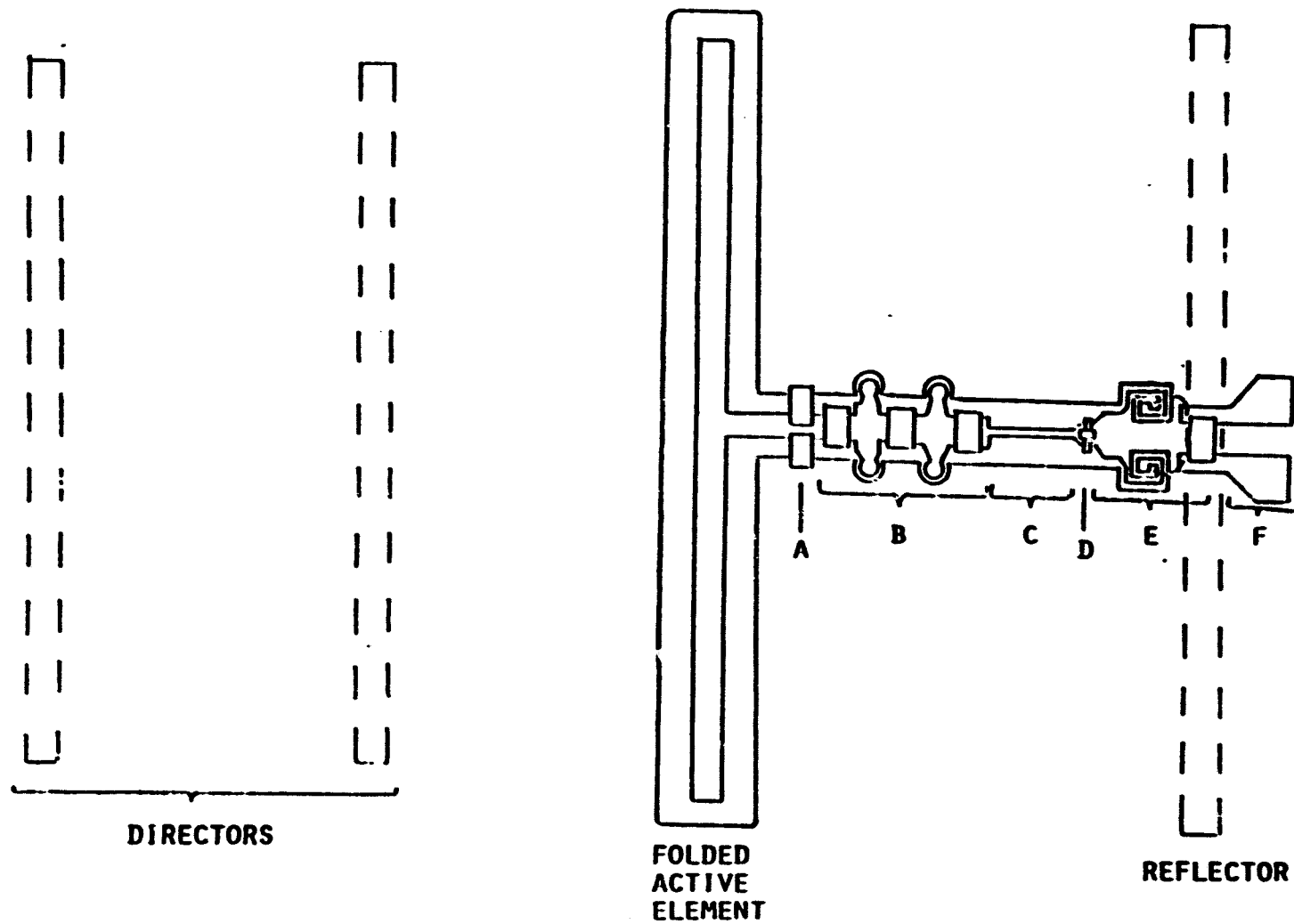
A Yagi-Uda Array with Directors of Constant Length, Radius and Spacing (after Ref. 11)

Expected Optimal Performance of Yagi-Uda Receiving Elements

	<u>Gain (wrt Isotropic) dB</u>	<u>F/D Ratio dB</u>	<u>Receiving Element* Reduction Factor</u>
3 Element-Low F/D ratio	11	5	2.82
3 Element-Moderate F/D ratio	10	15	2.24
3 Element-High F/D ratio	8.5	25	1.50
6 Element-Low F/D ratio	14	5	5.62
6 Element-Moderate F/D ratio	13	15	4.47
6 Element-High F/D ratio	11.5	25	2.82

* Relative to 6.5 dB Isosine Half-Wave Dipole.

YAGI PRINTED CIRCUIT RECTENNA ELEMENT



- A BLOCKING CAPACITOR
- B N=5 INPUT FILTER
- C HARMONIC PHASING TRANSMISSION LINE

- D SCHOTTKY DIODE CHIP
- E N=2 OUTPUT FILTER-TRANSFORMER
- F DC BUSS CONNECTOR

ORIGINAL PAGE IS
OF POOR QUALITY

EIGHT RECTENNA ELEMENT DESIGNS

Printed Circuit Implementation

Half-wave Dipole

3 element Yagi with Ground Plane

3 element Yagi without Ground Plane

6 element Yagi without Ground Plane

Baseline Type Construction

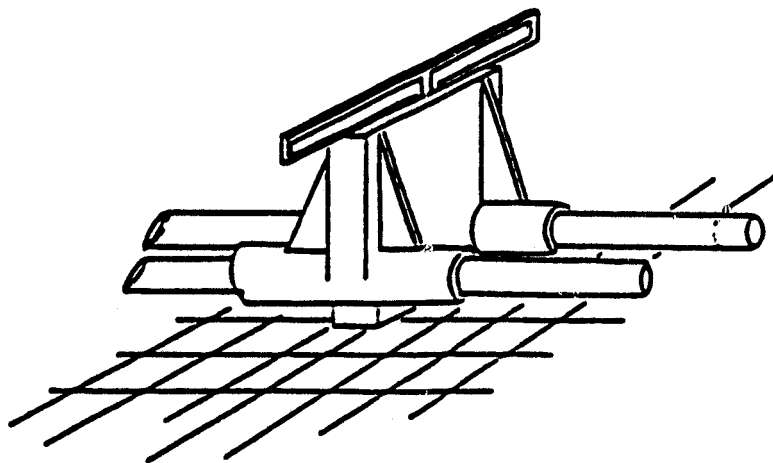
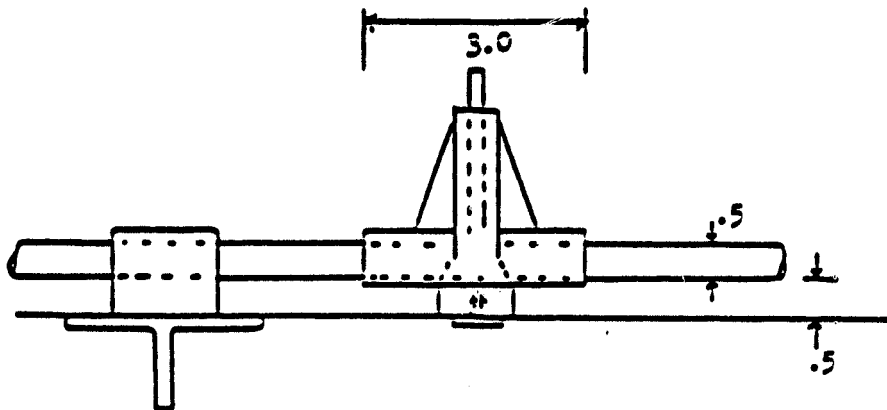
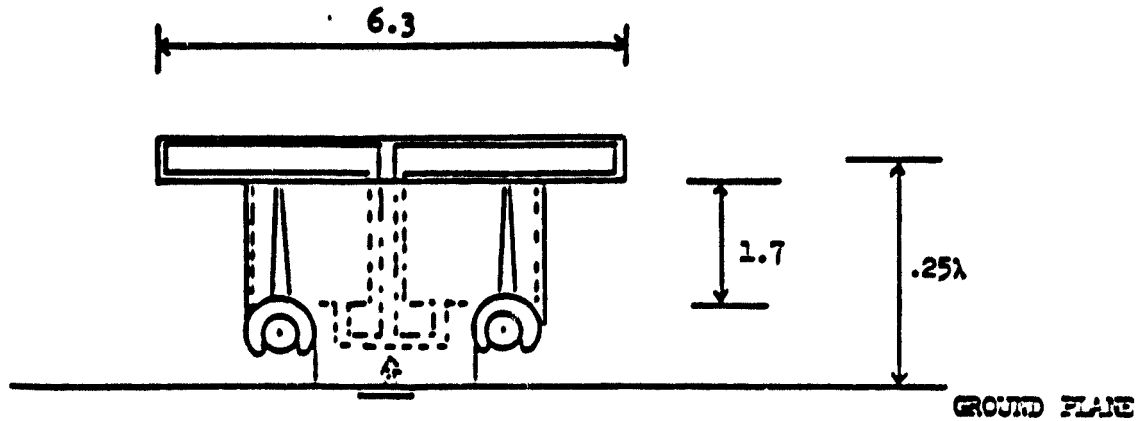
Half-wave Dipole

3 element Yagi with Ground Plane

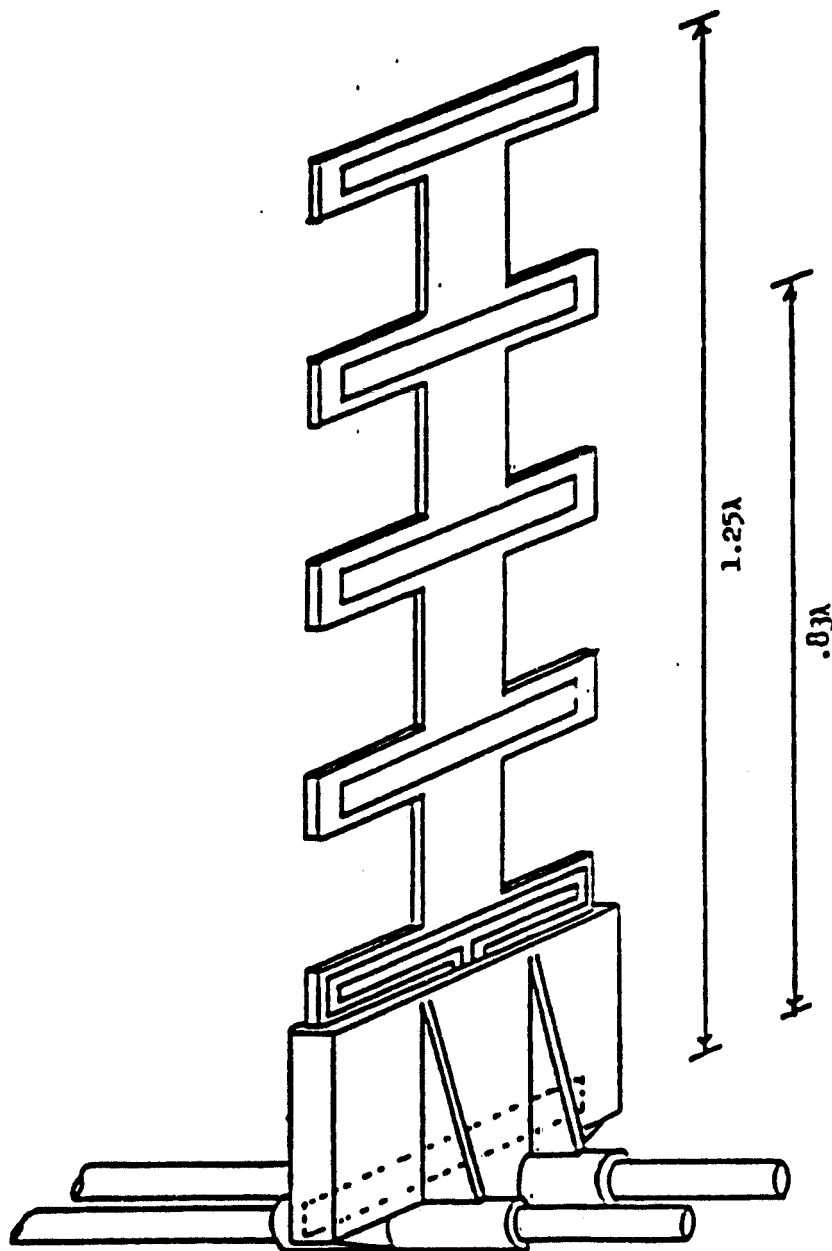
3 element Yagi without Ground Plane

6 element Yagi without Ground Plane

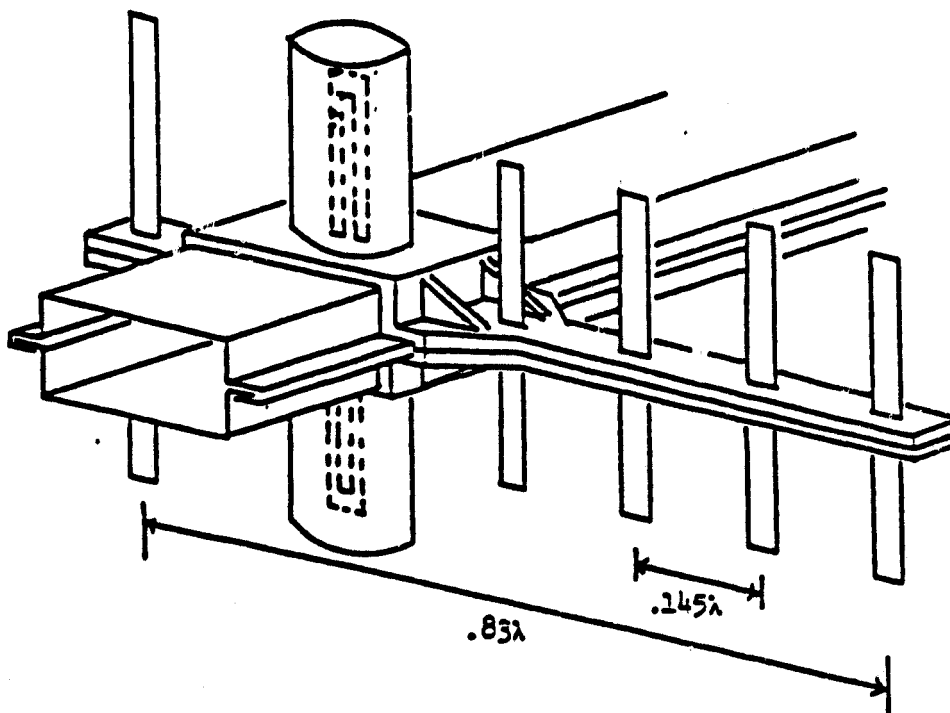
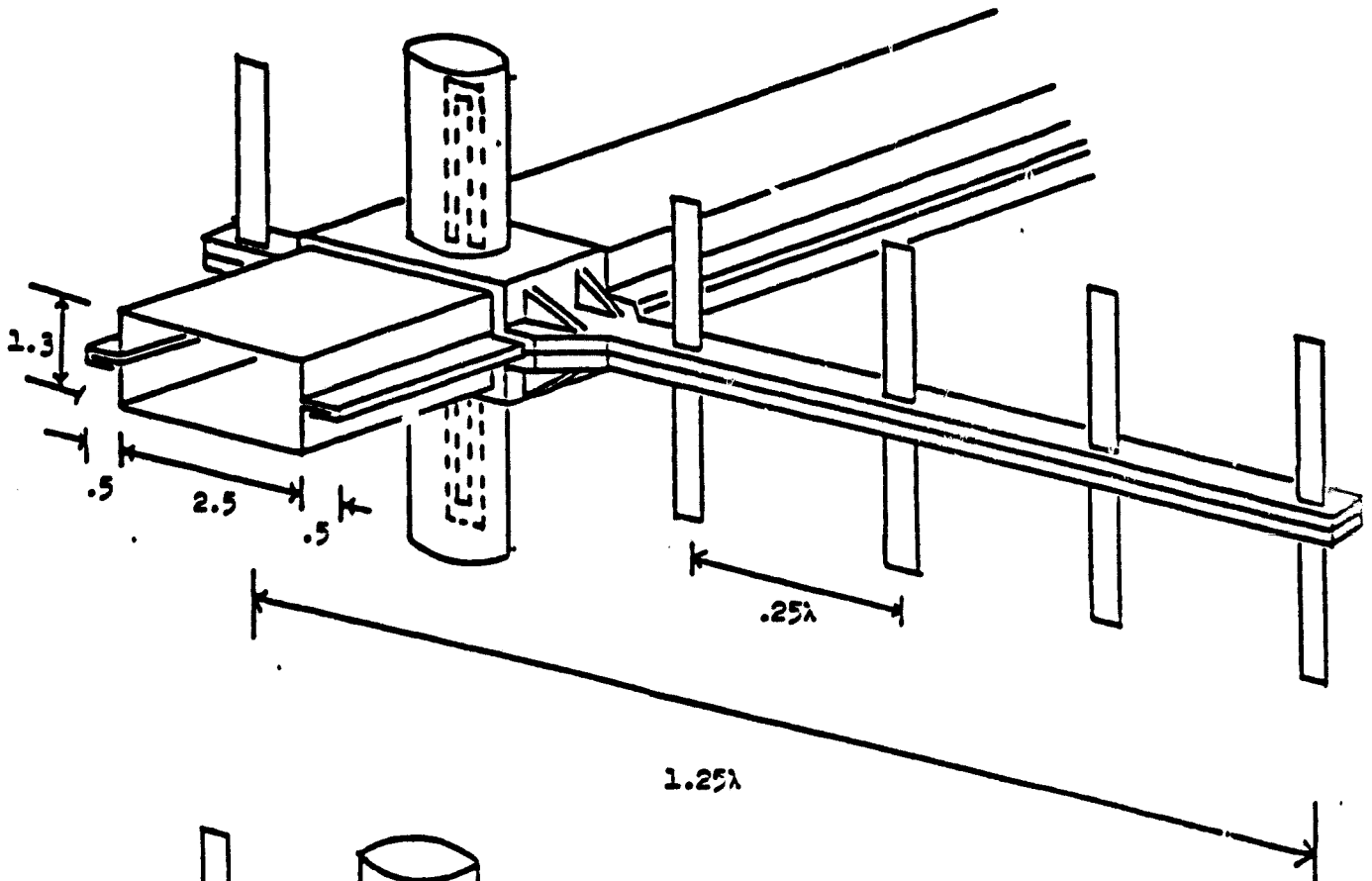
Printed Circuit Half-Wave Dipole
(all dimensions in centimeters)



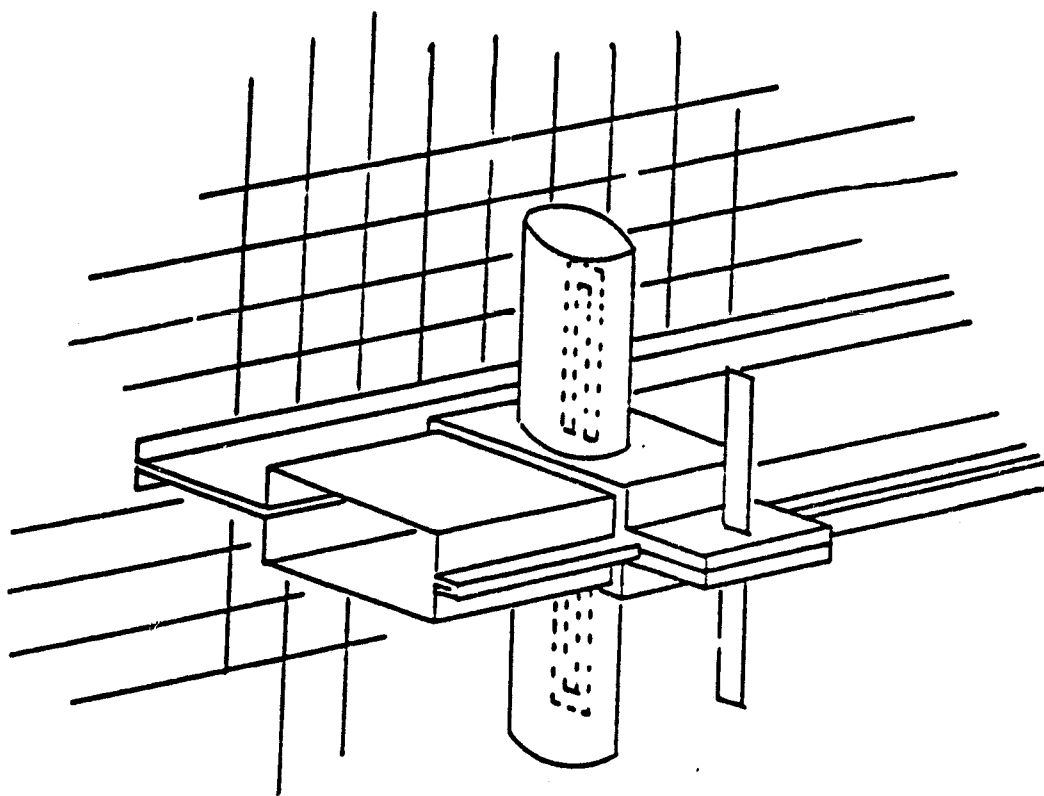
Six Element Printed Circuit Yagi-Uda without Ground Plane



Six Element Baseline Construction Yagi-Uda without
Ground Plane (all dimensions in centimeters)



Designs 1 and 3
given in Table 2-7.



Rectenna Element Density Used in Cost Estimates

	Half-wave Dipole with ground plane	<u>3 element Yagi</u> with ground plane	without ground plane	<u>5 element Yagi</u> without ground plane smaller size	larger size
Gain with respect to isotropic (dB)	6.5	10.2	8.4	11.11	12.7
Gain ratio with respect to isotropic	4.4	10.4	6.8	12.7	18.4
Effective Area, A_e (cm ² /element)	52	123	81	150	218
Element Density (No. of elements/m ²)	192	81	123	67	46
Density Reduction Factor	1	2.37	1.56	2.87	4.17
Element Spacing (cm) (on triangular grid)	7.8	11.9	9.7	13.2	15.9
Rows of Elements/m	14.9	9.7	11.9	8.8	7.3

$$A_e = \frac{GA^2}{4\pi} \quad \begin{array}{l} \text{-- } G \text{ is the gain ratio with respect to isotropic.} \\ \text{-- } A_e \text{ is the effective area of the rectenna element.} \end{array}$$

The half-wave dipole with ground plane had all other parameters derived from the element spacing, the reverse of what is done here for the Yagi elements.

A. PCB Implementation

(costs are given in $\$/m^2$)

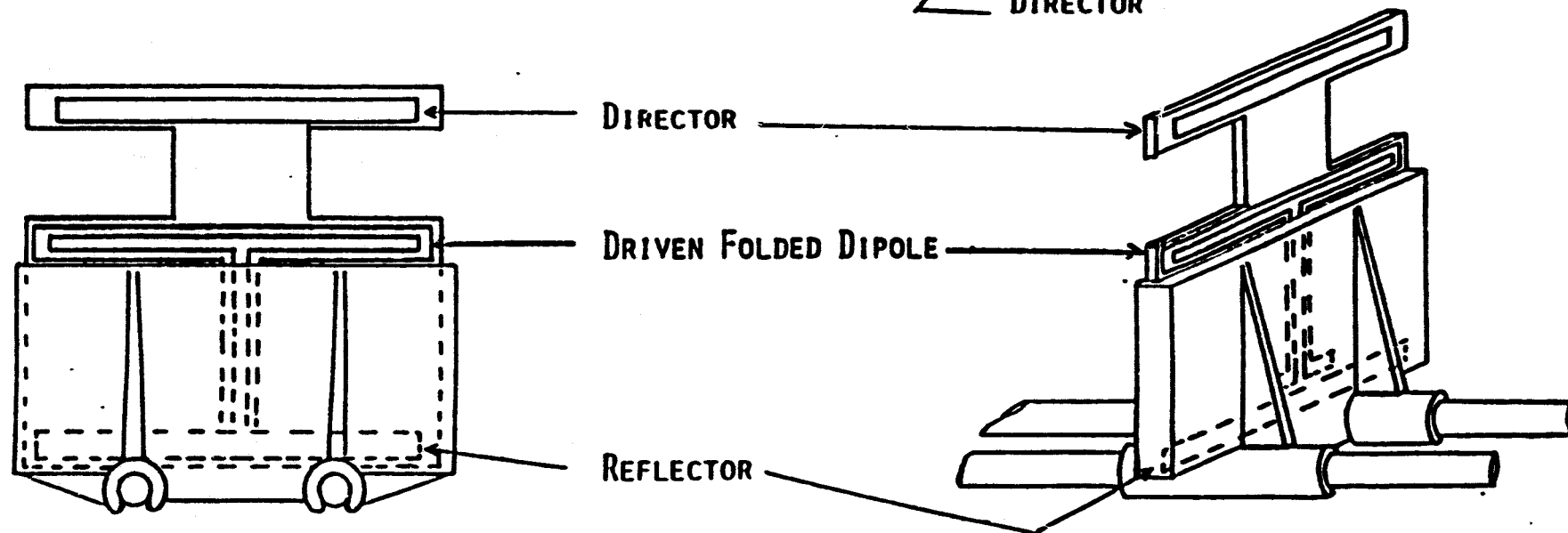
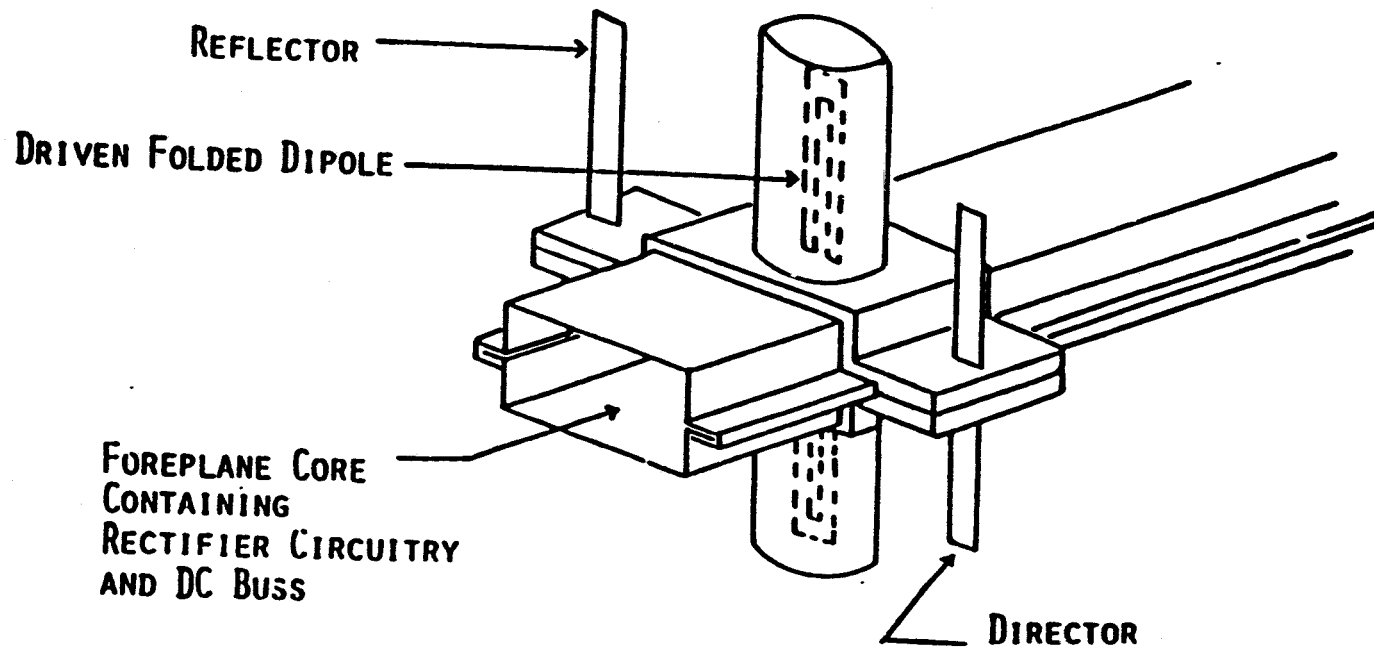
	<u>Half-wave Dipole</u>	<u>3 element Yagi</u> with ground plane	<u>without ground plane</u>	<u>6 element Yagi</u> without ground plane (average size)
Element Density ($\frac{\text{elem.}}{m^2}$)	192	81	123	57
Socket	\$.92	\$.39	\$1.12	\$.52
DC buss bar	2.78	1.81	2.23	1.55
PCB (less diode)	.24	.24	.42	.44
Ground Plane	<u>1.91</u>	<u>1.91</u>	<u>.00</u>	<u>.00</u>
Cost/ m^2	\$5.85	\$4.35	\$3.77	\$2.51
Diodes at \$.01 each	<u>\$1.92</u>	<u>\$.81</u>	<u>\$1.23</u>	<u>\$.57</u>
Total Cost/ m^2	\$7.77	\$5.16	\$5.00	\$3.08

B. Baseline Type Construction

(costs are given in $\$/m^2$)

	<u>Half-wave Dipole</u>	<u>3 element Yagi</u> with ground plane	<u>without ground plane</u>	<u>6 element Yagi</u> without ground plane
Element Density ($\frac{\text{elem.}}{m^2}$)	192	81	123	57
Foreplane Core	\$3.13	\$1.47	\$2.09	\$1.09
Aluminum Shield/ Structural Member	2.14	1.40	.92	.64
Yagi-Uda Additions	.00	.30	.71	.76
Ground Plane	<u>1.91</u>	<u>1.91</u>	<u>.00</u>	<u>.00</u>
Cost/ m^2	\$7.18	\$5.08	\$3.72	\$2.49
Diodes at \$.01 each	<u>1.92</u>	<u>.81</u>	<u>1.23</u>	<u>.57</u>
Total Cost/ m^2	\$9.10	\$5.89	\$4.95	\$3.06

Table 2-10 Overall Cost Estimates



Three Element Yagi-Uda Receiving Array
(A) Baseline Construction
(B) Printed Circuit Construction

CONCLUSIONS

- MORE DIRECTIONAL YAGI-UDA RECEIVING ELEMENTS CAN REDUCE RECTENNA COST SIGNIFICANTLY

<u>RECEIVING ELEMENT</u>	<u>RECTENNA COST (BASELINE TYPE CONSTRUCTION)</u>
HALF-WAVE DIPOLE	\$710 x 10 ⁶
3 ELEMENT Y-U WITH GROUND PLANE	\$460 x 10 ⁶
3 ELEMENT Y-U WITHOUT GROUND PLANE	\$390 x 10 ⁶
6 ELEMENT Y-U WITHOUT GROUND PLANE	\$240 x 10 ⁶

- PRINTED CIRCUIT IMPLEMENTATION DOES NOT APPEAR TO LOWER COST APPRECIABLY ALTHOUGH MORE STRUCTURAL WORK NEEDED
- POWER COMBINING INEFFICIENCY SIMILAR FOR SERIES AND PARALLEL COMBINING
- POWER COMBINING INEFFICIENCY WILL AFFECT DC BUSS NETWORK (AND POSSIBLY POWER BEAM TAPER AND/OR EDGE RECTENNA ELEMENT DESIGN)
- CLOSED FORM MODEL CAN BE USED FOR ACCURATE POWER COMBINING CALCULATIONS

D3
Macro Aspects

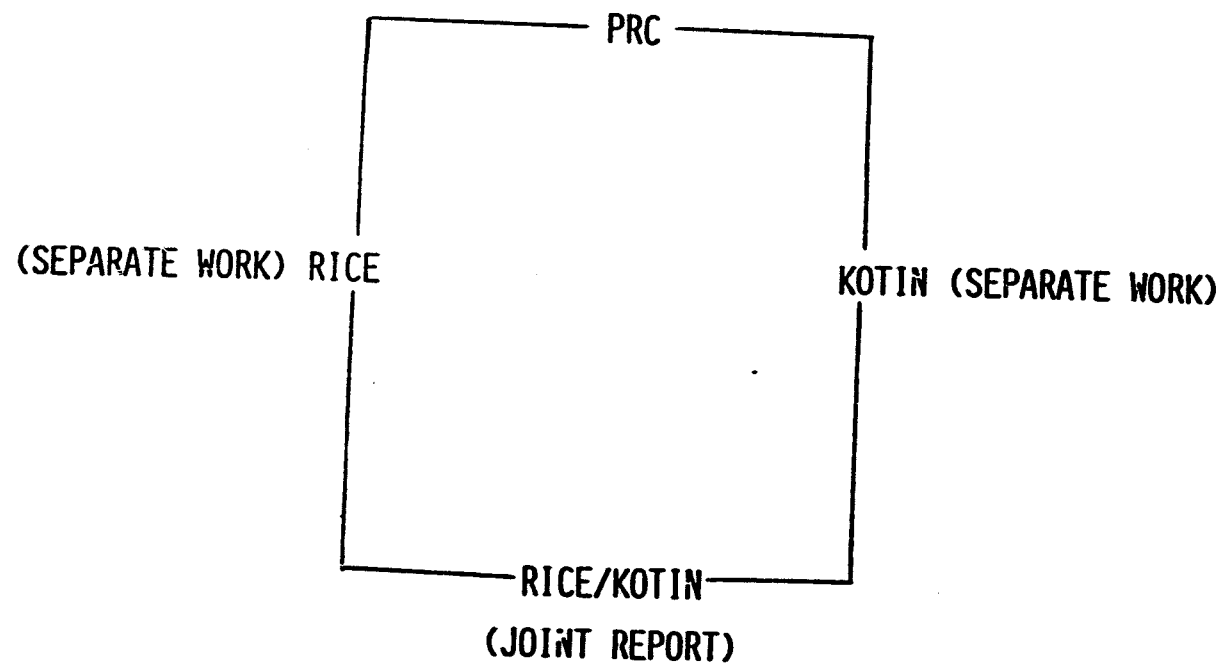
*A. Few
Rice University*

PRECEDING PAGE BLANK NOT FILMED

PRECEDING PAGE BLANK NOT FILMED

- RECTENNA SITING STUDIES
BLACKBURN - RICE UNIVERSITY
- OFFSHORE RECTENNA STUDIES
FREEMAN - RICE UNIVERSITY
- METEOROLOGICAL IMPACTS OF RECTENNA OPERATIONS
ORVILLE - SOUTH DAKOTA SCHOOL OF MINES
- LIGHTNING HAZARD TO THE RECTENNA
FEW - RICE UNIVERSITY

TEAM ORGANIZATION



CLASSIFICATION APPROACH

CLASSIFICATION BASED UPON

SEVERITY OF THE IMPACTS

DEDICATED LAND AREAS

SEVERE CLIMATIC CHARACTERISTICS

CHARACTERIZATION OF THE VARIABLES

ABSOLUTE EXCLUSION VARIABLE

POTENTIAL EXCLUSION VARIABLE

DESIGN VARIABLE

ADJACENCY VARIABLE

CLASSIFICATION OF THE VARIABLES

INDIAN RESERVATIONS
NATIONAL FOREST
PRIME AGRICULTURAL
FLYWAYS OF WATERFOWL
SEISMIC HAZARDS
40 DEGREE LATITUDE
DAYS OF HAIL PER YEAR
SHEET RAINFALL
ACID RAINFALL
BIRD MIGRATORY CORRIDORS
SNOWFALL
WATER AVAILABILITY
RAILROAD
LIGHTNING DENSITY
TIMBERED AREAS
WETLAND AREAS
WILD AND SCENIC RIVERS
CLASS I AIR QUALITY AREAS
ICING

POTENTIAL EXCLUSION
POTENTIAL EXCLUSION
POTENTIAL EXCLUSION
POTENTIAL EXCLUSION
DESIGN ?
DESIGN
DESIGN
DESIGN
DESIGN
POTENTIAL EXCLUSION
DESIGN
POTENTIAL EXCLUSION
ADJACENCY
DESIGN
POTENTIAL EXCLUSION
POTENTIAL EXCLUSION
DESIGN
POTENTIAL EXCLUSION
DESIGN

[illegible]

CLASSIFICATION OF VARIABLES

<u>VARIABLE</u>	<u>CLASSIFICATION</u>	<u>REFINEMENT STATUS</u>
LAND AREAS	INFORMATIONAL	BETTER RESOLUTION
WATER AREAS (INLAND)	ABSOLUTE EXCLUSION	BETTER RESOLUTION
NATIONAL RECREATION AREAS	ABSOLUTE EXCLUSION	BETTER RESOLUTION
MILITARY RESERVATIONS	ABSOLUTE EXCLUSION	OLD VARIABLE
STANDARD METROPOLITAN STATISTICAL AREAS	ABSOLUTE EXCLUSION	OLD VARIABLE
POPULATION (NON-SMSA)	ABSOLUTE EXCLUSION	BETTER RESOLUTION
WETLANDS	ABSOLUTE EXCLUSION	OLD VARIABLE
TOPOGRAPHY UNACCEPTABLE	ABSOLUTE EXCLUSION	OLD VARIABLE
NAVIGABLE WATERWAYS	ABSOLUTE EXCLUSION	OLD VARIABLE
	ADJACENCY	
INTERSTATE HIGHWAYS	ABSOLUTE EXCLUSION	OLD VARIABLE/BETTER RES.
	ADJACENCY	
HABITATS OF E.S.	ABSOLUTE EXCLUSION	OLD VARIABLE/EXPANDED
EMC (KOTIN)	ABSOLUTE EXCLUSION	NEW VARIABLE
	POTENTIAL EXCLUSION	

CLASSIFICATION OF THE VARIABLES

DUST STORM AREAS

DESIGN

NEW VARIABLE

MAXIMUM WINDS

DESIGN

NEW VARIABLE

TORNADO AREAS

DESIGN

NEW VARIABLE

CLASSIFICATION OF VARIABLES - OFFSHORE

<u>VARIABLE</u>	<u>CLASSIFICATION</u>	<u>REFINEMENT STATUS</u>
CONTINENTAL SHELF	INFORMATIONAL	NEW VARIABLE
NAVIGATION LANES	ABSOLUTE EXCLUSION	NEW VARIABLE
DEDICATED OCEAN AREAS	ABSOLUTE EXCLUSION	NEW VARIABLE
OCEAN HAZARD AREAS	ABSOLUTE EXCLUSION	NEW VARIABLE
UNCONSOLIDATED MUD	ABSOLUTE EXCLUSION	NEW VARIABLE
SANDY BOTTOMS	DESIGN	NEW VARIABLE
IRREGULAR BATHYMETRY	ABSOLUTE EXCLUSION	NEW VARIABLE
DESIGNATED MARINE SANCTUARY	ABSOLUTE EXCLUSION	NEW VARIABLE
NOMINATED MARINE SANCTUARY	POTENTIAL EXCLUSION	NEW VARIABLE
BIRD MIGRATION ROUTES	POTENTIAL EXCLUSION	NEW VARIABLE
MAJOR FISHING AREAS	POTENTIAL EXCLUSION	NEW VARIABLE
OFFSHORE PRODUCTION AREAS	POTENTIAL EXCLUSION?	NEW VARIABLE
HURRICANE CORRIDORS	ABSOLUTE EXCLUSION	NEW VARIABLE
RECREATIONAL AREAS	POTENTIAL EXCLUSION?	NEW VARIABLE
HEIGHT AND FORCE OF TIDES	POTENTIAL EXCLUSION	NEW VARIABLE
TSUNAMI RISK	DESIGN	NEW VARIABLE
EXTREME ICING CONDITIONS	DESIGN	NEW VARIABLE
SHEET RAINFALL	DESIGN	NEW VARIABLE

STATUS OF OFFSHORE VARIABLE COLLECTION

DATA IN HAND AND READY TO MAP

CONTINENTAL SHELF
NAVIGATION LANES
OCEAN HAZARD AREAS
UNCONSOLIDATED MUD
SANDY BOTTOMS
BIRD MIGRATION ROUTES
DEDICATED OCEAN AREAS

DATA IN HAND BUT NEEDING ADDITIONAL STUDY

FISHING AREAS
HURRICANE CORRIDORS
IRREGULAR BATHYMETRY

DATA FORTHCOMING BUT NOT IN HAND

OFFSHORE PRODUCTION AREAS
DEDICATED MARINE SANCTUARIES
NOMINATED MARINE SANCTUARIES

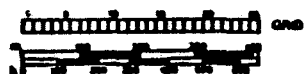
PROBLEM AREAS

RECREATIONAL AREAS
HEIGHT AND FORCE OF TIDES
TSUNAMI RISK
EXTREME ICING CONDITIONS
SHEET RAINFALL

DATA ANALYSIS

1. DETERMINATION OF VARIABLES
 - . ABSOLUTE EXCLUSION
 - . POTENTIAL EXCLUSION
 - . DESIGN
 - . ADJACENCY
2. DATA GATHERING
 - . DESCRIPTION OF METHODS AND SOURCES
3. VALIDITY CHECK ON VARIABLES
 - . AGGREGATION PROBLEMS
 - . BOUNDARY PROBLEMS
 - . TEMPORAL PROBLEMS
4. DATA PROCESSING
 - . MAPPING
 - . ENCODING
 - . STORAGE/DISPLAY
5. SPATIAL ANALYSIS
 - . VARIABLE COMBINATIONS
 - . EXCLUSION AREAS
6. VALIDITY CHECK ON EXCLUSION AREAS
 - . OVER-DETERMINATION
 - . UNDER-DETERMINATION
7. DOCUMENTATION

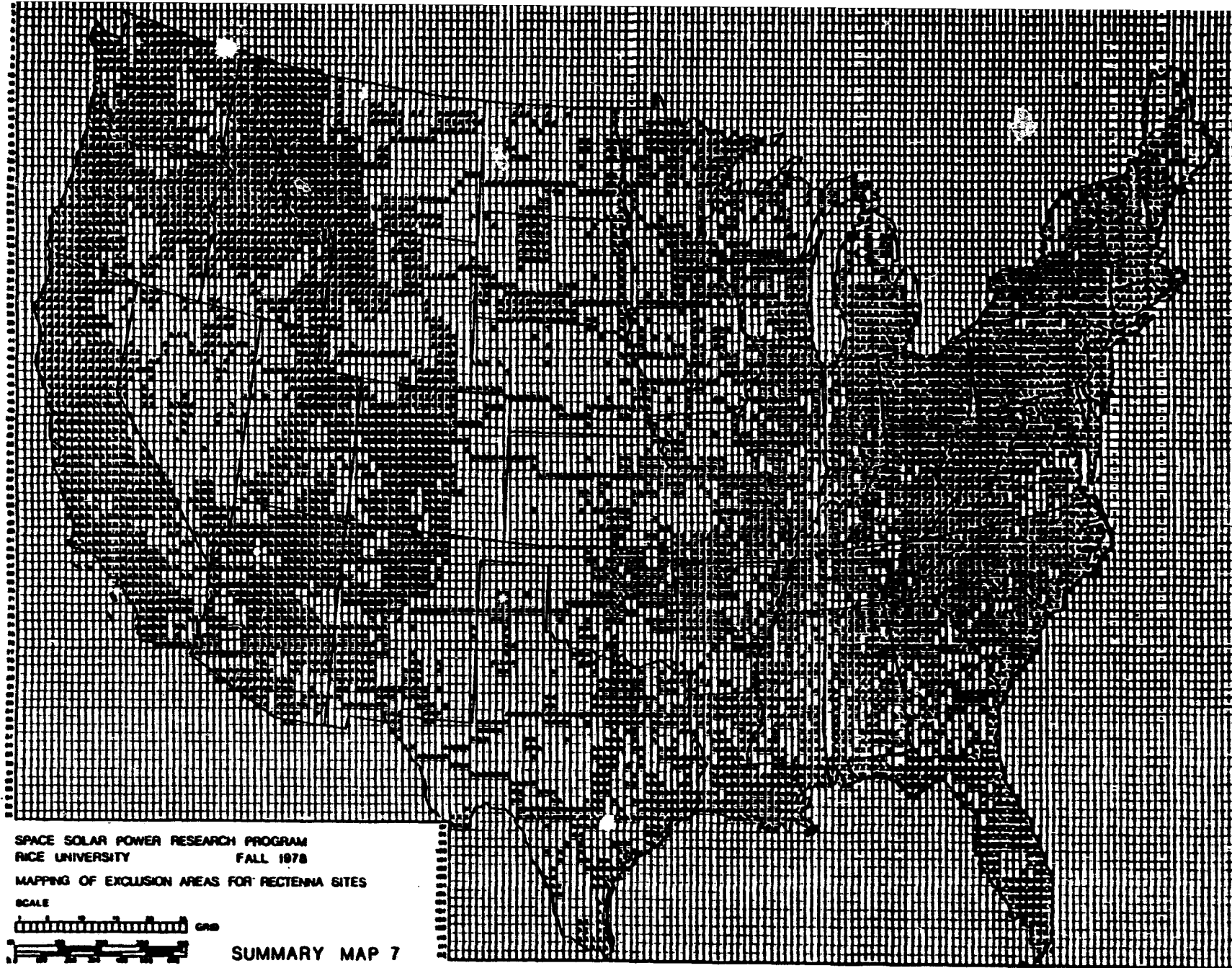
SPACE SOLAR POWER RESEARCH PROGRAM
 RICE UNIVERSITY FALL 1978
 MAPPING OF EXCLUSION AREAS FOR RECTENNA SITES
 SCALE



SEISMIC HAZARDS

• Major Damage / Moderate Damage

ORIGINAL PAGE IS
 OF POOR QUALITY



06

100-443887-100

- BRUTE FORCE OR TRADITIONAL STRUCTURAL TECHNIQUES ARE TOO COSTLY COMPARED TO LAND SITE
- INNOVATIVE CONCEPTS ARE BEING STUDIED

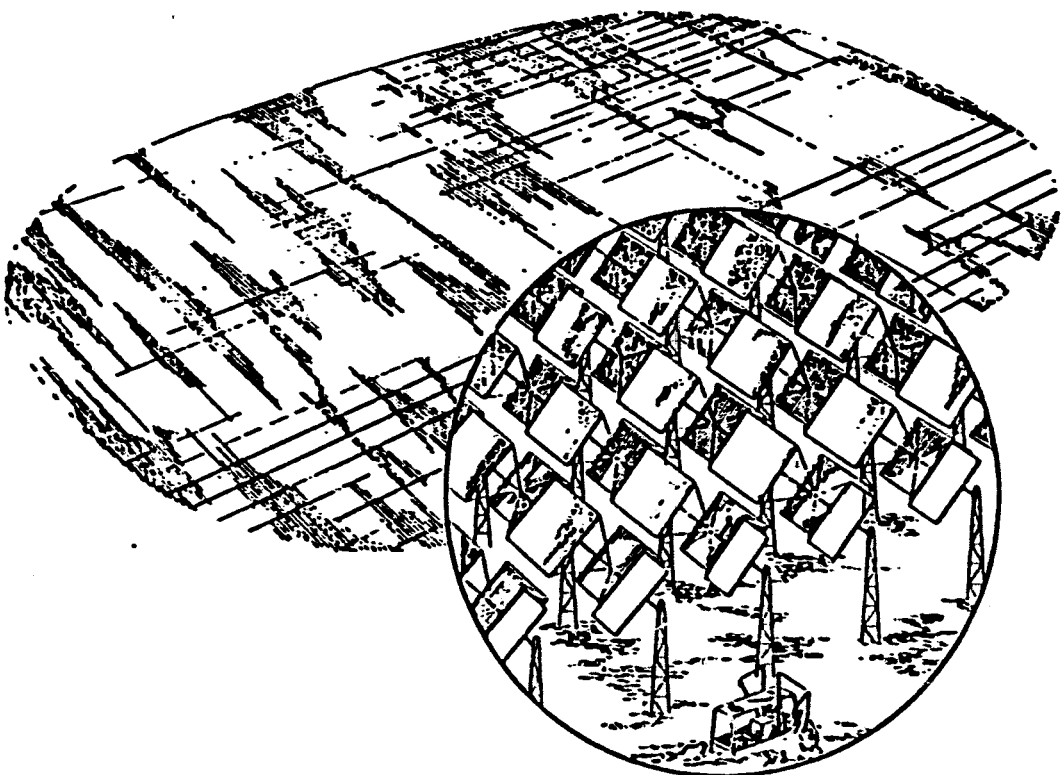
OFFSHORE RECTENNA
STUDY OBJECTIVES

TO ESTABLISH A PRACTICAL PRELIMINARY DESIGN AND COST ESTIMATE FOR A
5 GW OFFSHORE RECTENNA.

THE STUDY WILL BE CONDUCTED JOINTLY BY RICE UNIVERSITY AND BROWN
AND ROOT DEVELOPMENT INC. AND ARTHUR D. LITTLE .INC.

THE STUDY WILL TAKE 7 MONTHS STARTING MAY 19, 1979.

ORIGINAL PAGE IS
OF POOR QUALITY



SITE SELECTION GUIDELINES

1. CAPABLE OF SERVING NEW YORK AND BOSTON METROPOLITAN AREAS (APPROXIMATELY 200 MILES OUTER LIMIT).
2. AVOID SHIPPING LANES.
3. MAXIMIZE DISTANCE FROM SHORE BUT DO NOT EXCEED 40 MILES OUT.
4. AVOID RECREATIONAL BOAT TRAFFIC AREAS.
5. AVOID HEAVY FISHING AREAS.
6. AVOID HAZARDOUS AREAS SUCH AS SHOALS OR RIP TIDES.
7. STAY ON THE CONTINENTAL SHELF.
8. AVOID PETROLEUM EXPLORATION AND WASTE DISPOSAL AREAS.

SITE III (FAVORED SITE)

GENERAL DATA

- LOCATION: 40° 59' N, 70° 44' W
- DISTANCE TO N.Y.: 280 KM
- DISTANCE TO BOSTON: 121 KM
- DISTANCE TO MARTHA'S VINEYARD: 30 KM
- SEABED: COARSE SAND AND SCATTERED GRAVEL
- WATER DEPTH: 50 M
- TIDAL CURRENTS: ABOUT 1 KM/HR
- ANNUAL TIDES: 1.1 M

SEVERE ENVIRONMENTAL DESIGN DATA

STORM WINDS:

- EXTREME WIND SPEEDS: 67 m/sec (150 MPH)
(SUSTAINED HURRICANE STORM WIND 1 MINUTE)
- WINTER STORM WINDSPEEDS: 31.3 m/sec (70 MPH)
- THREE SECOND GUST VELOCITY: 85 m/sec (188 MPH)

STORM WAVES:

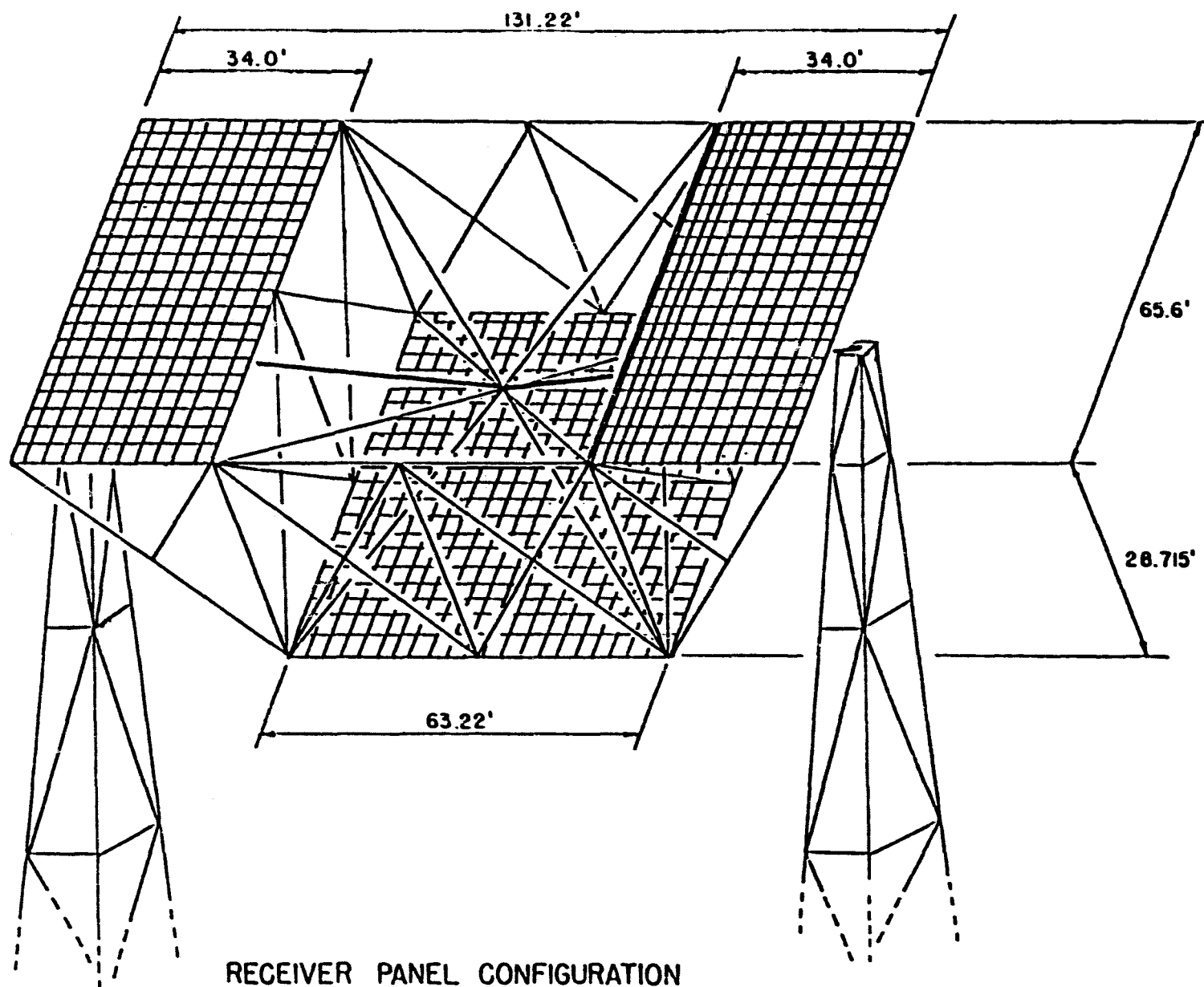
- 100 YEAR RECURRENCE MAXIMUM WAVE HEIGHT:
26.5 m (87,0 FT)
- SIGNIFICANT STORM WAVE HEIGHT:
13.6 m (44.6 FT)
- STORM SURGE TIDE: 1 m

ICING

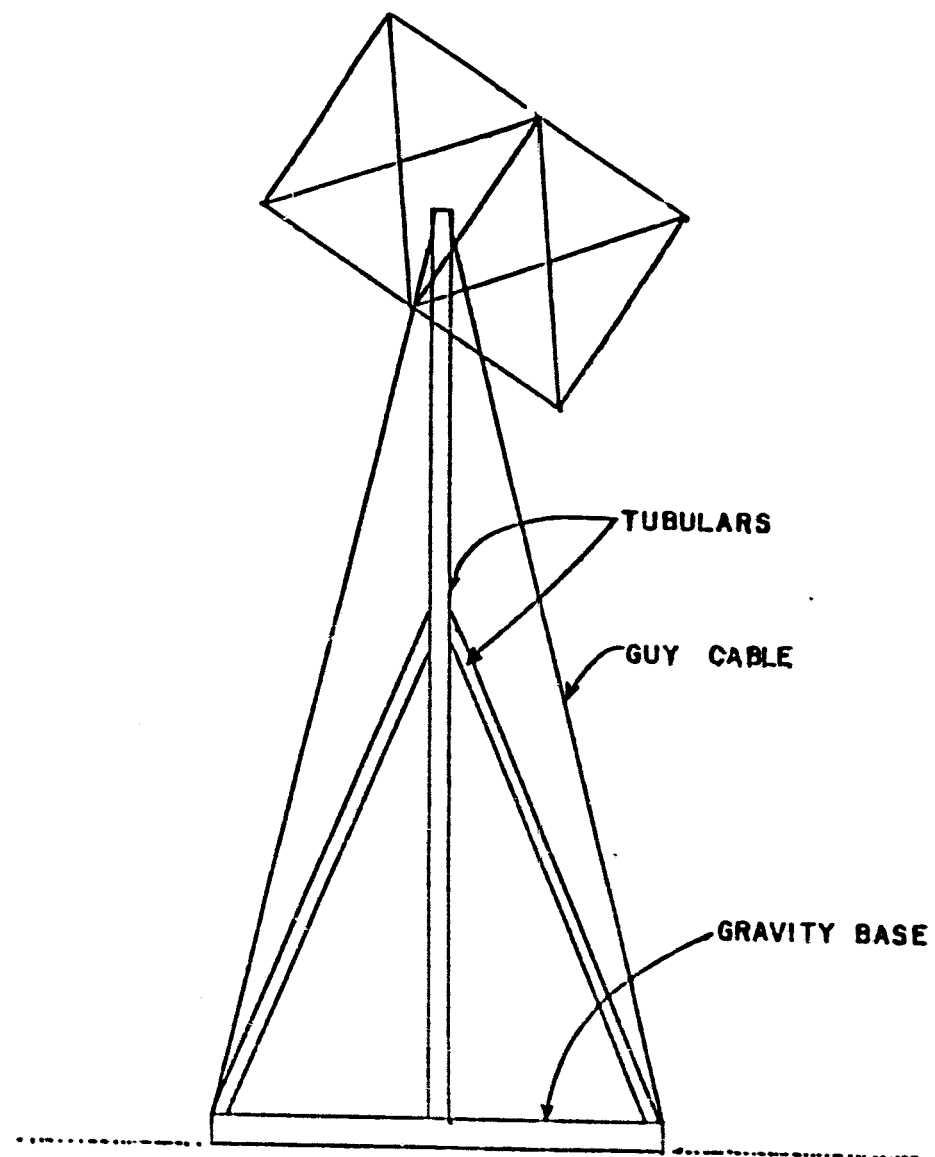
- AVERAGE MONTHLY FREQUENCY OF MODERATE SUPERSTRUCTURE
ICING: DECEMBER, 12.5%; JANUARY, 22,5%; FEBRUARY, 15%.
- ESTIMATED ICING, LESS THAN 1.3 CM

SNOW

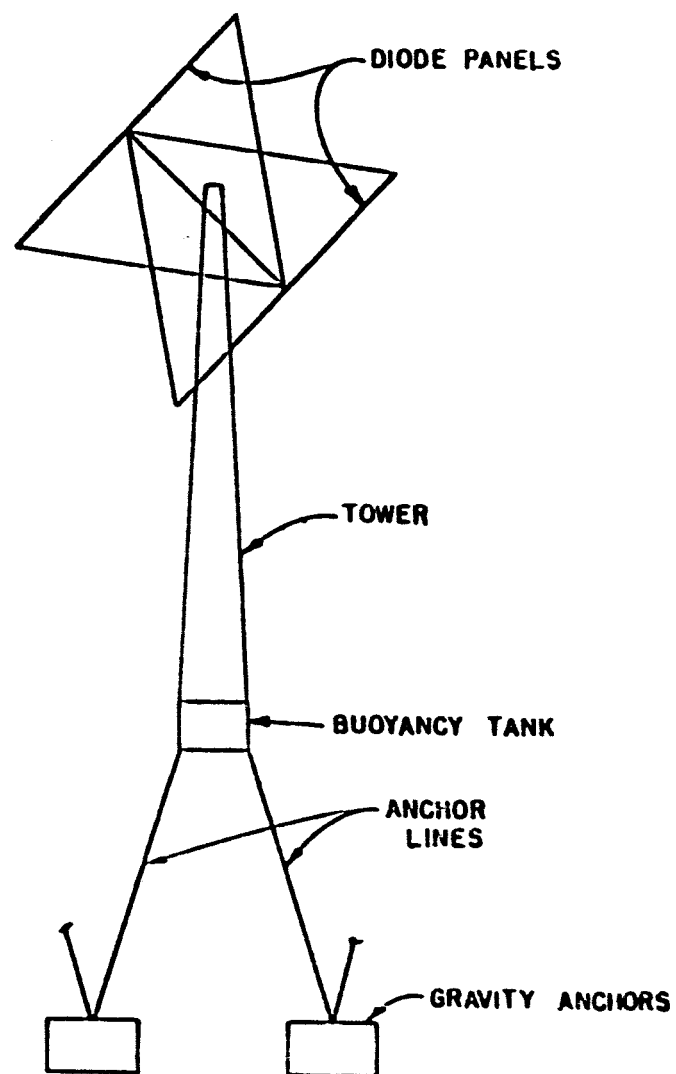
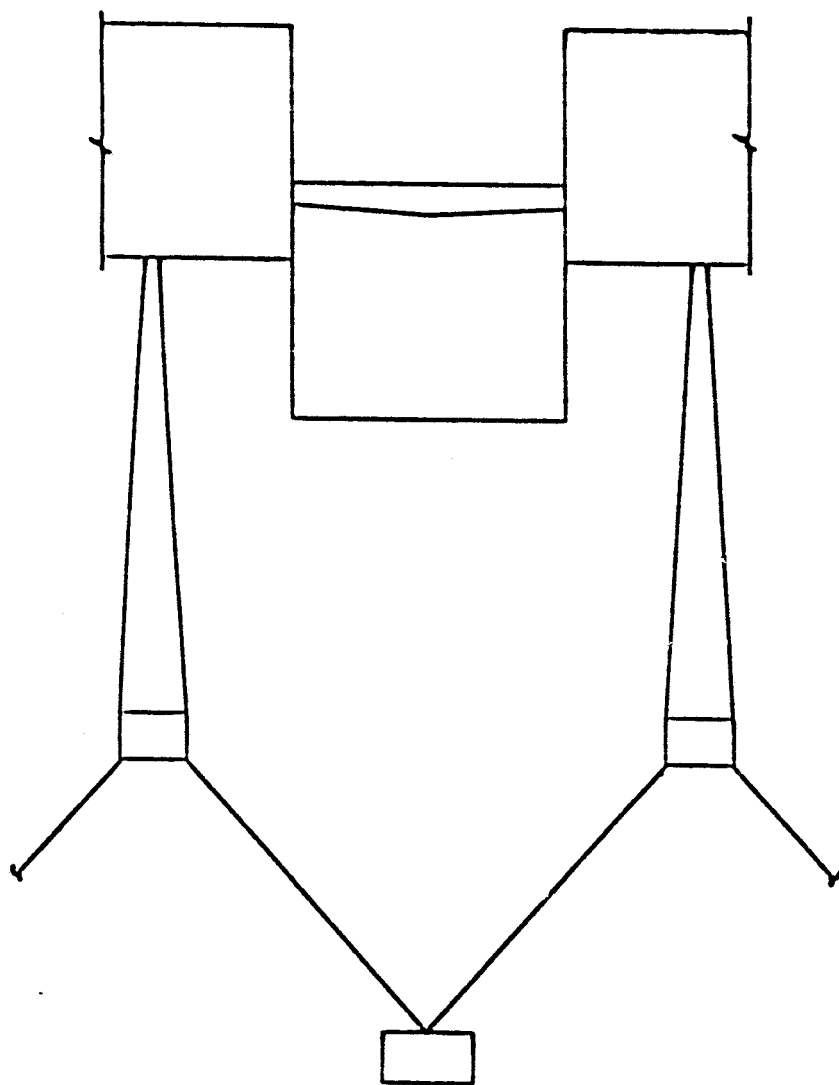
- WEIGHT: 65KG/M²



RECEIVER PANEL CONFIGURATION



GRAVITY STRUCTURE



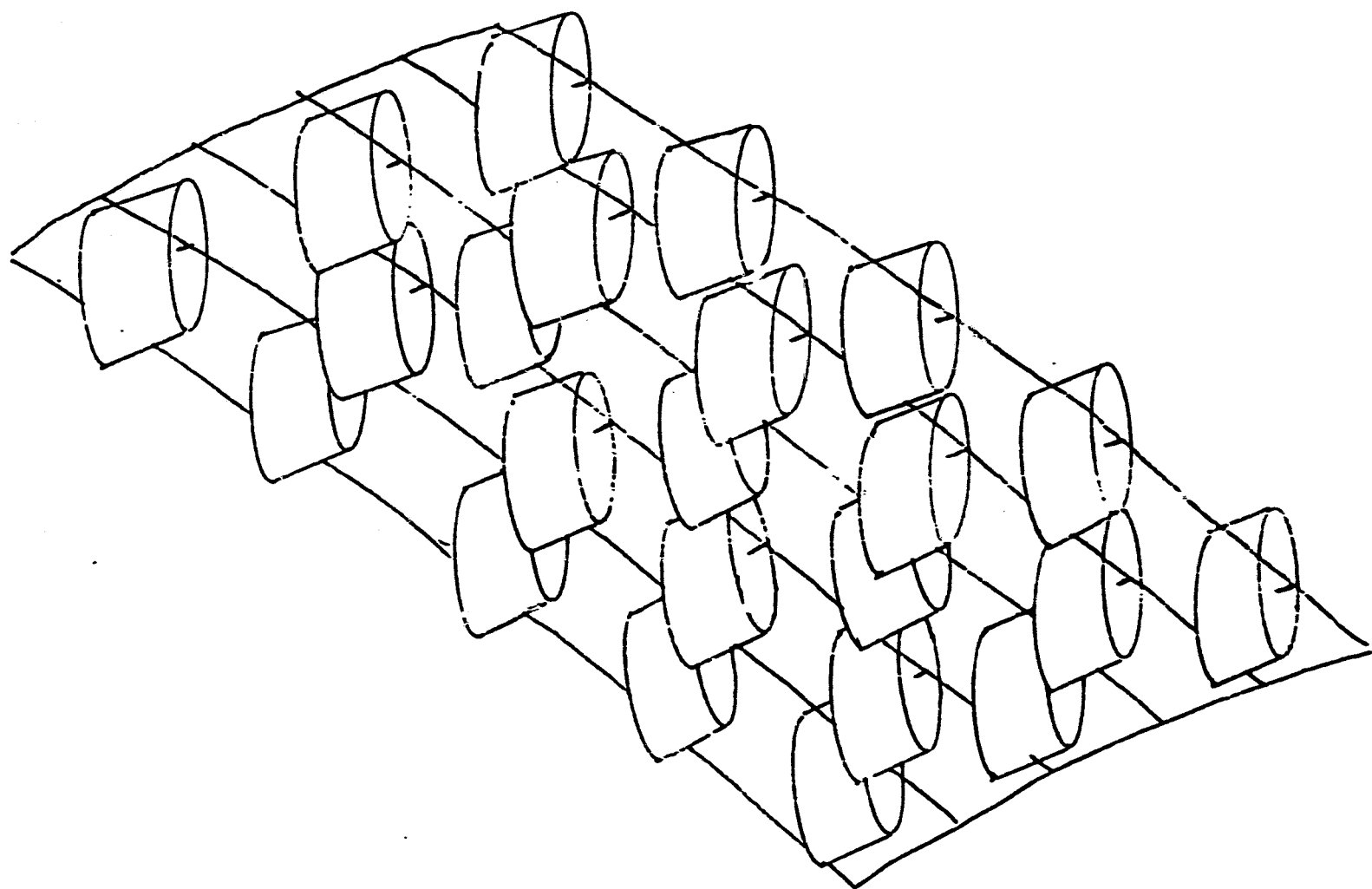
OFFSHORE RECTENNA STRUCTURAL COMPONENTS

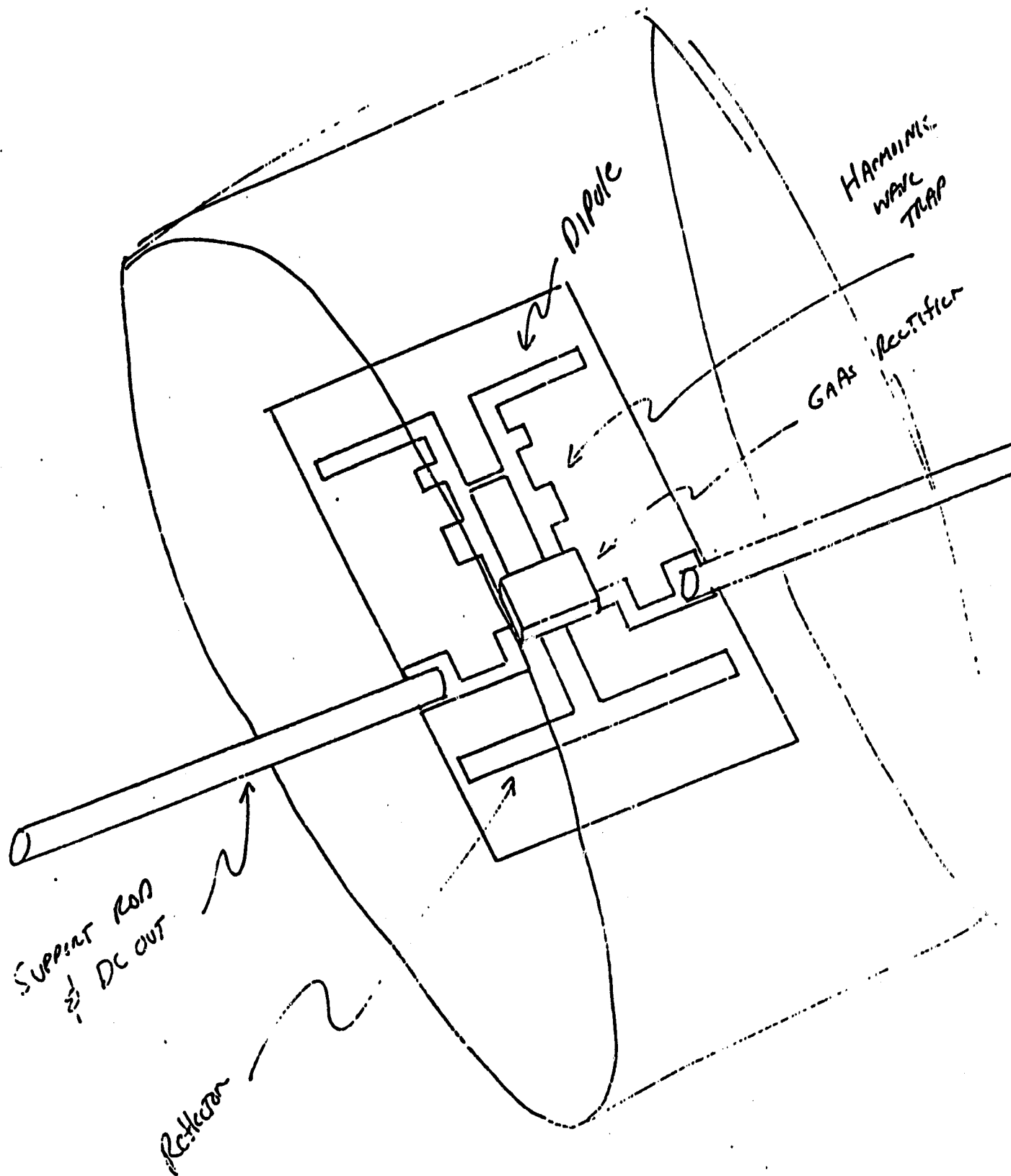
ICING TEST RESULTS-MONOPOLE

- WITH NO COVER THE REFLECTION COEFFICIENT ASYMPTOTICALLY APPROACHES 0.5 AT AN ICE THICKNESS OF ABOUT 0.5 CM.
- A 1 CM RADIUS COVER ON THE ACTIVE ELEMENT REDUCES THE REFLECTION COEFFICIENT TO 0.1 - THICKER COVER YIELDS NO SIGNIFICANT ADVANTAGE.
- RAINWATER IS AS BAD AS ICE.

ICING TEST RESULTS-DIPOLE

- 2 MM ICE ON THE GROUND PLANE GIVES A REFLECTION COEFFICIENT OF 0.3.
- TESTS OF COVER REQUIRED NOT YET COMPLETE.





RECTENNA-RELATED METEOROLOGICAL EFFECTS OF SPS OPERATION
WORKSHOP HELD CHICAGO 23-25 AUGUST 1978

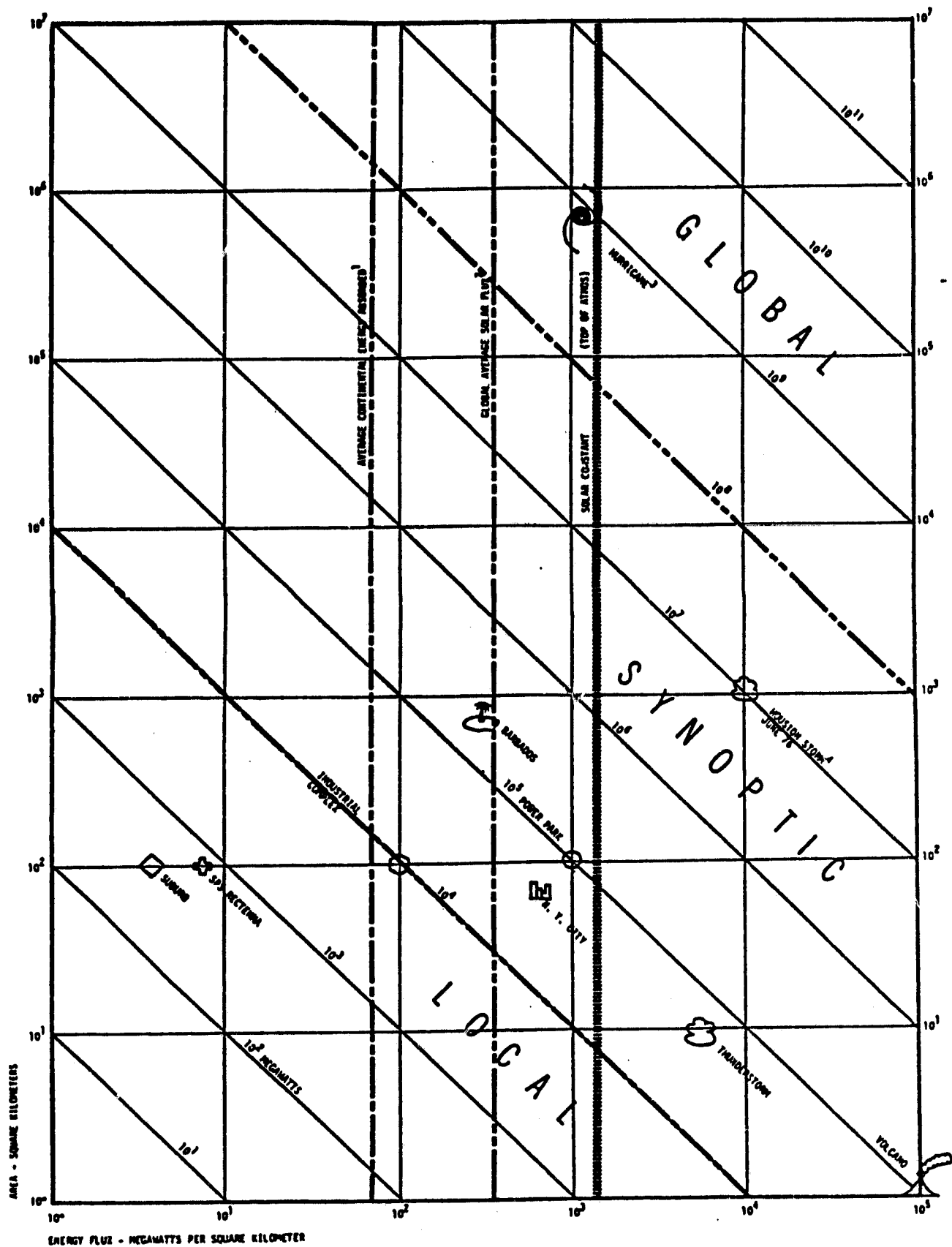
PROBLEM AREAS CONSIDERED

- RECTENNA WASTE HEAT
- MICROWAVE PROPAGATION
- ATMOSPHERIC ELECTRICITY

REF: LEE, J. L., D. M. ROTE, AND H. D. ORVILLE, WORKSHOP ON METEOROLOGICAL EFFECTS OF SATELLITE POWER SYSTEM RECTENNA OPERATION, BULL. AM. METEORO. SOC., 60, 1333-1337, 1979.

RECTENNA WASTE HEAT

- ESTIMATED WASTE HEAT $6.5 - 9.5 \text{ W/m}^2$
- COMPARE TO MAXIMUM SOLAR FLUX 850 W/m^2 OR MAXIMUM NET FLUX 75 W/m^2
PERTURBATION $\sim 10\%$
- COMPARE TO OTHER MAN-MADE PERTURBATIONS
CITY (CINCINNATI IN 1971) 25 W/m^2
- ALBEDO CHANGES
SMALL 5% CHANGE IN ALBEDO PRODUCES MAXIMUM SOLAR FLUX ABSORPTION CHANGE
 40 W/m^2
- CONCLUSIONS: ALBEDO CHANGES ARE OF GREATER CONCERN THAN WASTE HEAT AND
EFFECTS ARE COMPARABLE TO OTHER LARGE-SCALE HUMAN ACTIVITIES.



Atmospheric Heating

MICROWAVE PROPAGATION

- REFRACTIVE TURBULENCE IN THE BOUNDARY LAYER. NO SERIOUS DELETERIOUS EFFECTS.
- SCATTERING AND ATTENUATION BY THUNDERSTORMS AND SQUALL LINES.
AN AREA THAT REQUIRES ADDITIONAL RESEARCH.
- REFRACTIVE TURBULENCE ASSOCIATED WITH JET STREAMS.
ADDITIONAL RESEARCH INDICATED.
- REFRACTIVE TURBULENCE AT STABLE LAYERS WITH HIGH GRADIENTS IN HUMIDITY.
ADDITIONAL RESEARCH INDICATED.

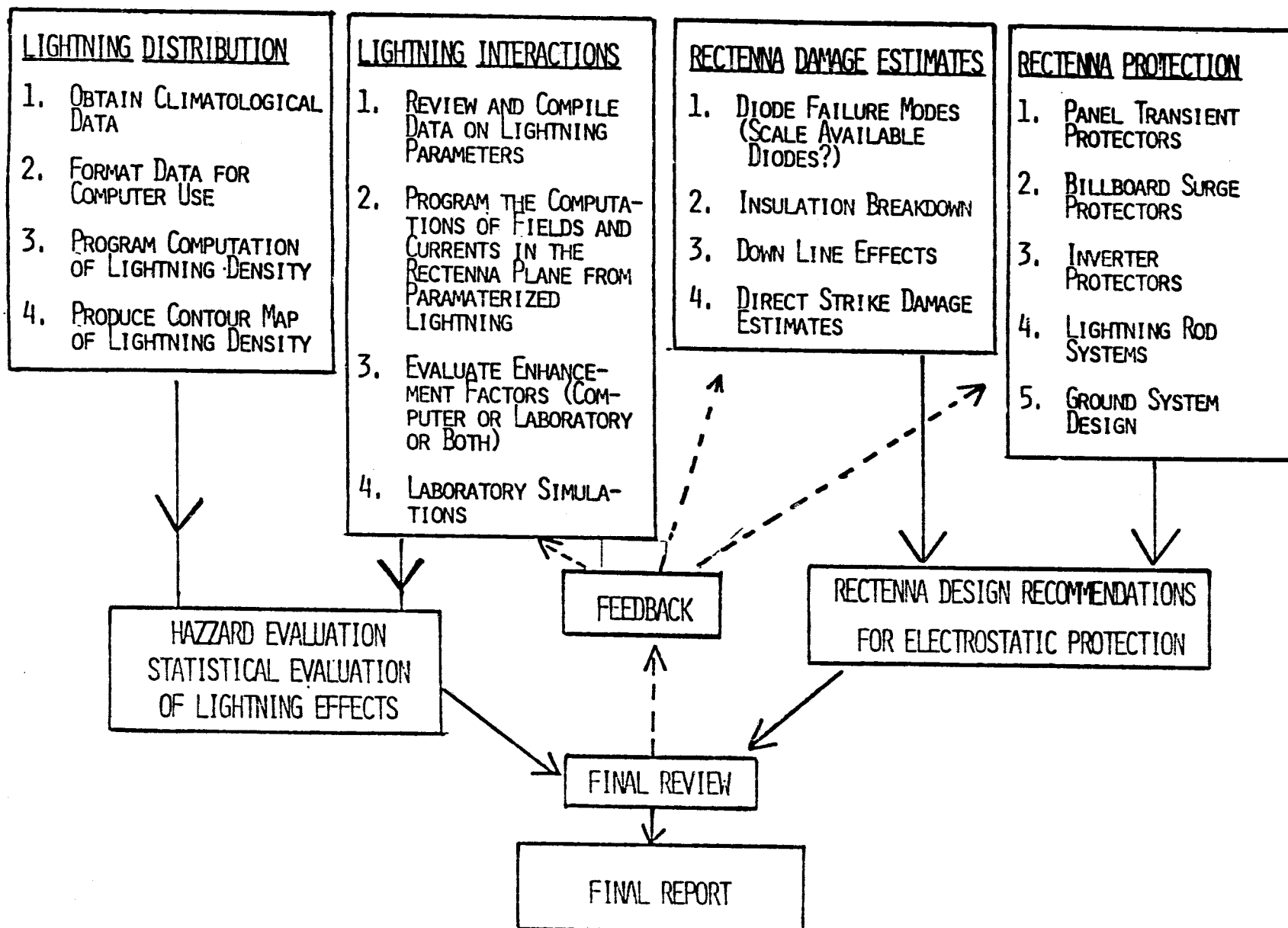
ATMOSPHERIC ELECTRICITY

- DIRECT MICROWAVE INTERACTION WITH NORMAL ATMOSPHERIC ELECTRICAL PARAMETERS. NONE EXPECTED BELOW IONOSPHERE.
- RECTENNA MODIFICATION OF ELECTRODE LAYER WILL HAPPEN BUT MAGNITUDE AND CONSEQUENCES UNKNOWN.
- RECTENNA INTERACTIONS WITH ELECTRICAL STORMS. POSSIBLE ENHANCEMENT OF CLOUD TO GROUND LIGHTNING OVER INTRACLOUD LIGHTNING. POSSIBLE ENHANCEMENT OF CLOUD ELECTRIFICATION VIA ION ENTRAINMENT.
- MICROWAVE INTERACTIONS WITH CLOUD MICROPHYSICAL PROCESSES. POSSIBLE BUT PROBABLY SMALL.

OBJECTIVES

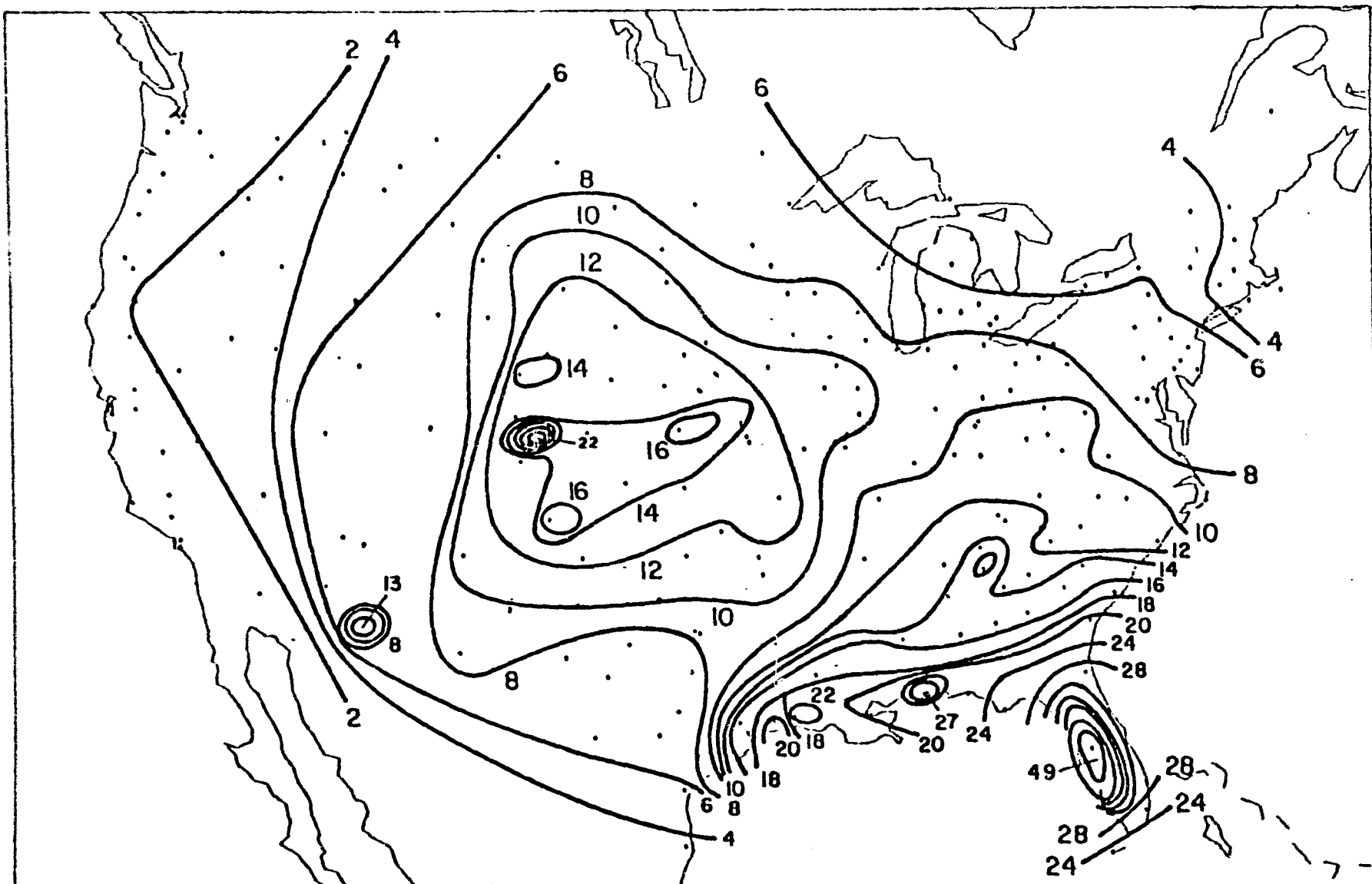
The objectives of Part II of this study is to evaluate the hazard posed by lightning flashes to ground on the SPS rectenna and to make recommendations for a lightning protection system that will provide sufficient protection to the rectenna. For purposes of this study, the SPS rectenna design is based upon the data supplied to us by Rockwell International in July, 1978.

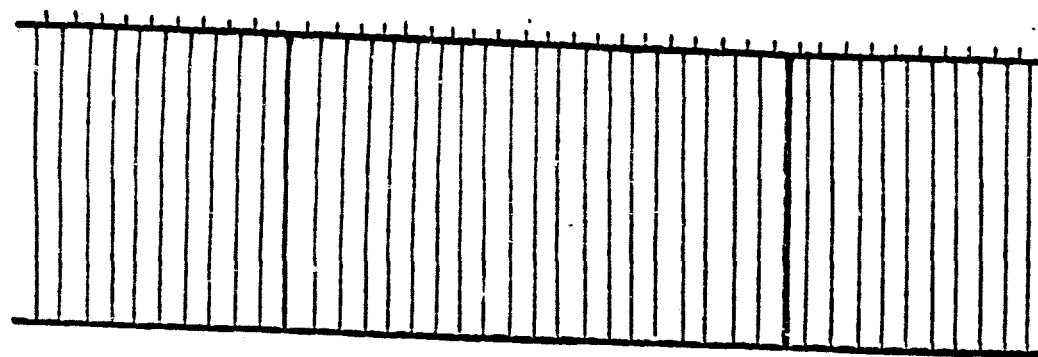
RECTENNA ELECTROSTATIC PROTECTION



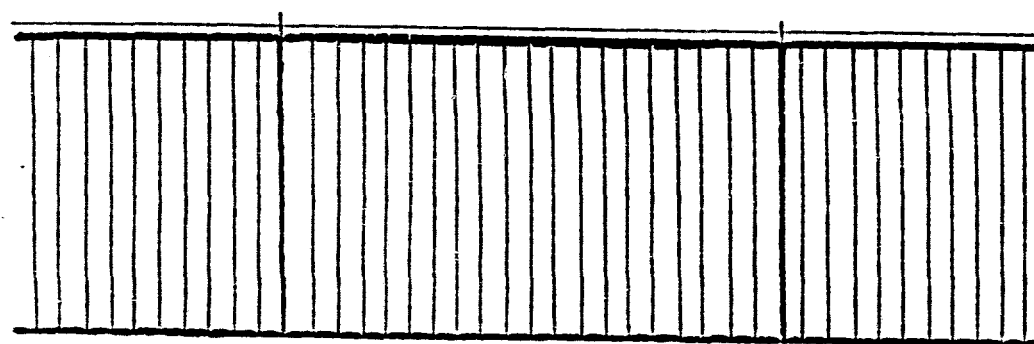
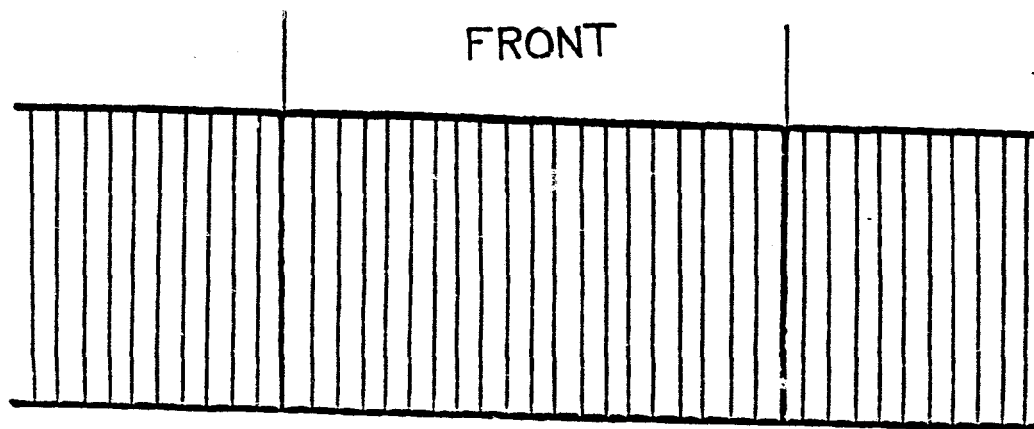
Recommendation and Conclusion Summary

1. The very high lightning flash density in many parts of the United States and the large size of the SPS rectenna require us to incorporate lightning protection systems in the rectenna design.
2. A distributed lightning protection system is described in this report that will protect the rectenna components from direct lightning strike damage and will, in addition, provide reduced induced lightning effects in the power and control circuits.
3. The proposed lightning protection system should be incorporated as a structural member of the rectenna support system; viewed as such the lightning protection system will not appreciably increase the total material requirements for the rectenna unless materials are used that are incapable of safely conducting lightning currents.
4. The lightning protection design places the conducting elements so that the microwave shadow cast by protection systems falls along the upper edge of the billboard on which it is mounted (and the lower edge of the next billboard to the north); these areas are highly marginal with respect to collection efficiency so the protection elements produce very little, if any, additional power loss to the rectenna as a whole.
5. Individually the microwave diodes are self-protecting with respect to "average" lightning and those near the center of the rectenna are safe from extreme lightning. However, the series connection of the diodes to form 40,000 V strings creates a protection requirement for the string. Standard surge protection practices are necessary for the string.
6. Electric power industries usually attribute 10% of the cost of power transmission equipment to lightning protection requirements. If this factor is not already included in cost-estimates, it should be added.



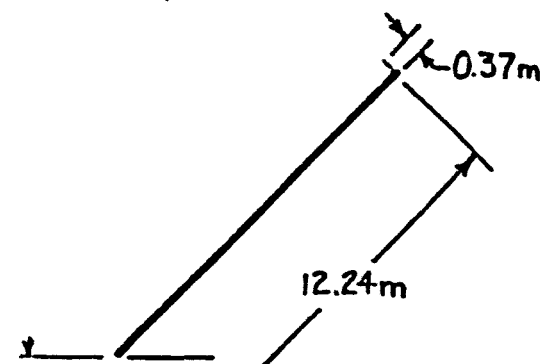


FRONT

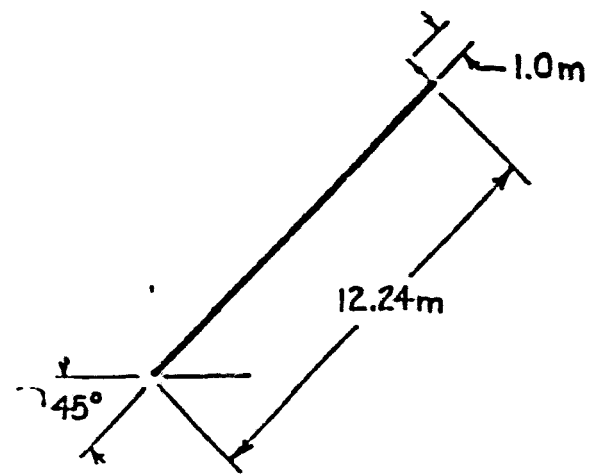
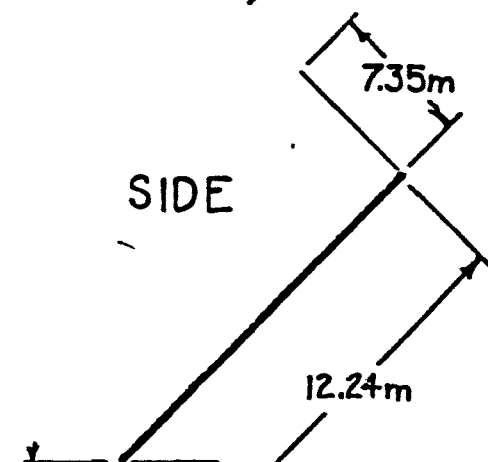


0.74m PANEL
TYP.

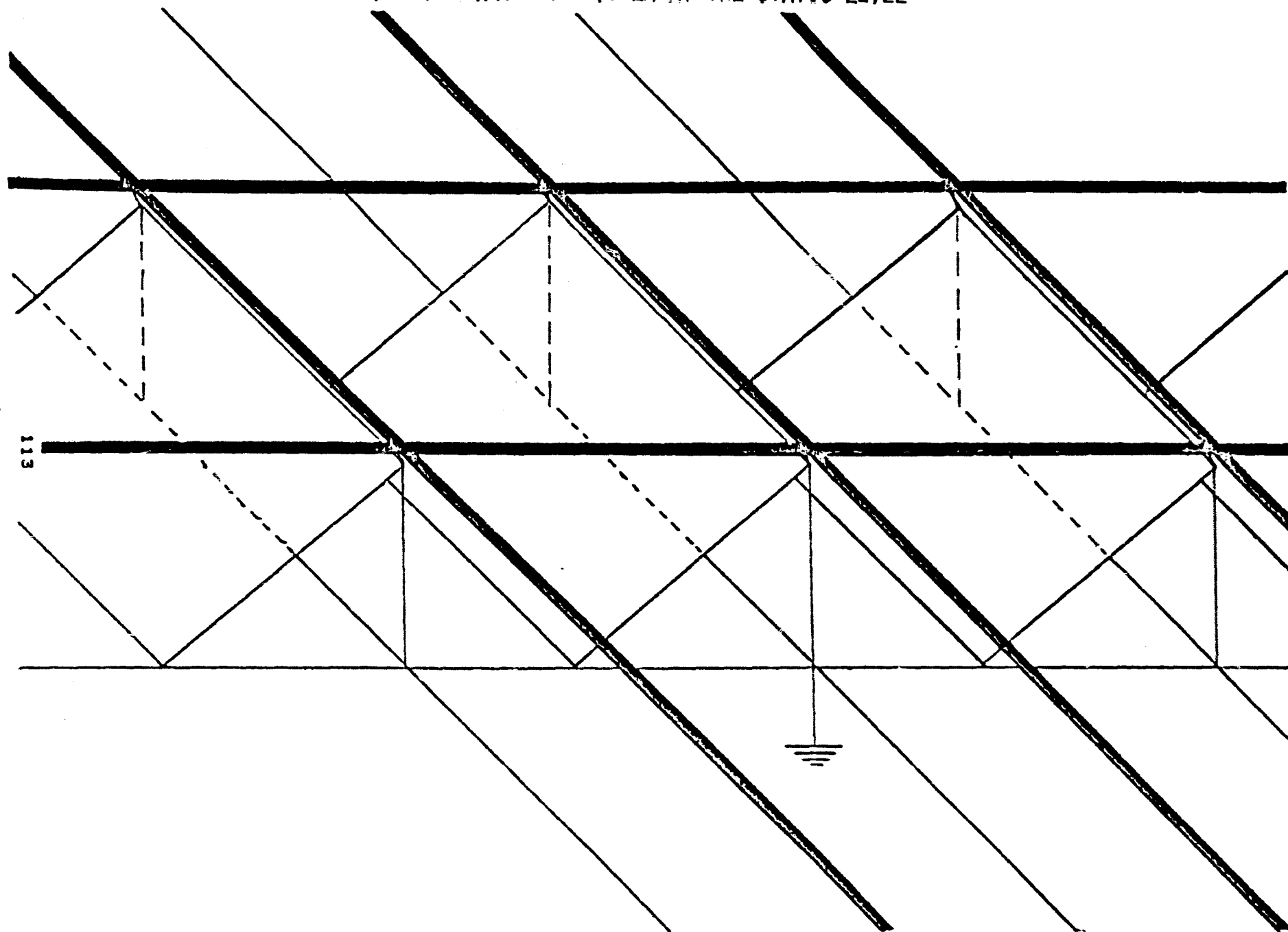
— "BILLBOARD" $n-1$ — — "BILLBOARD" n — — "BILLBOARD" $n+1$ —



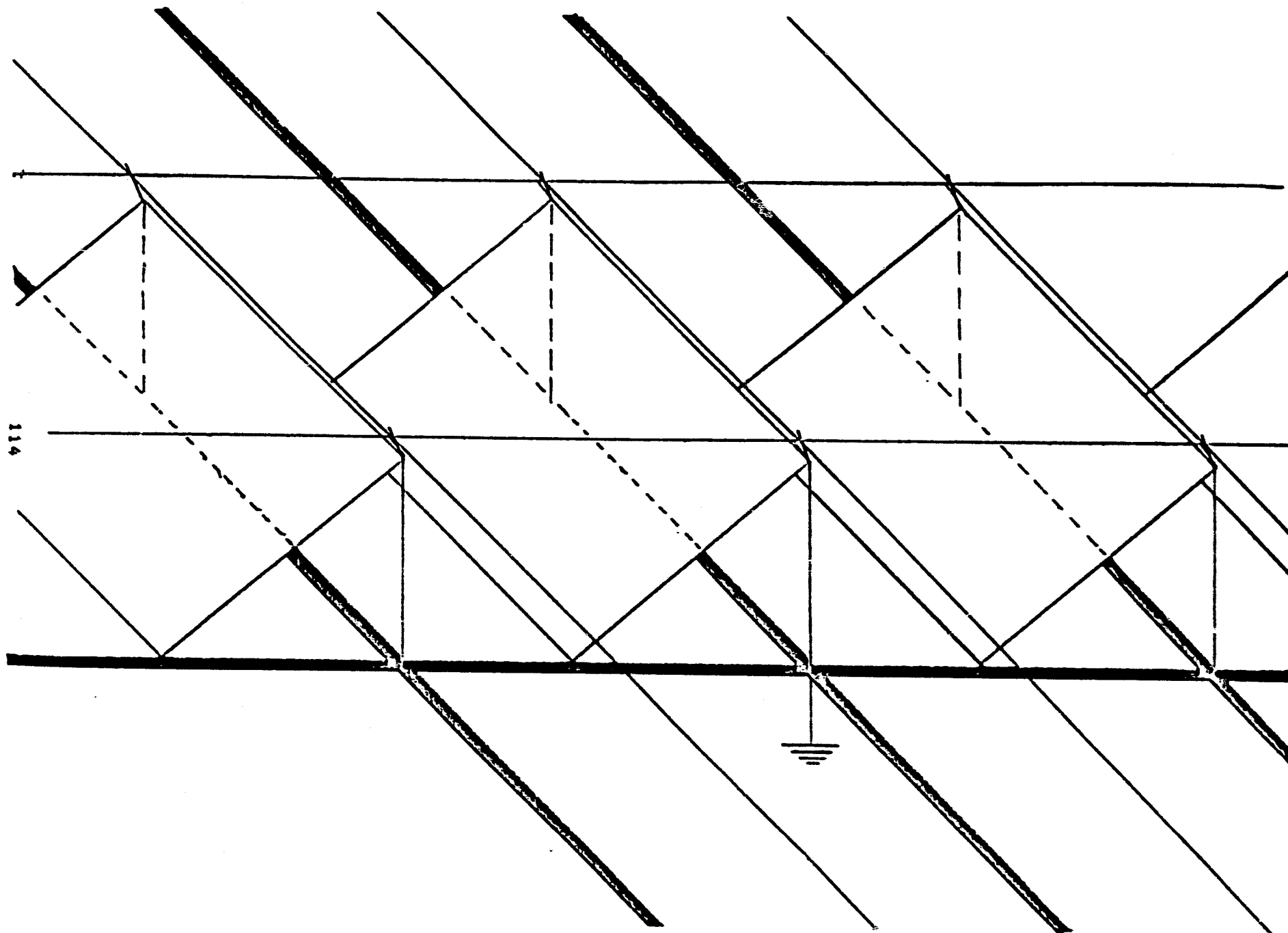
SIDE



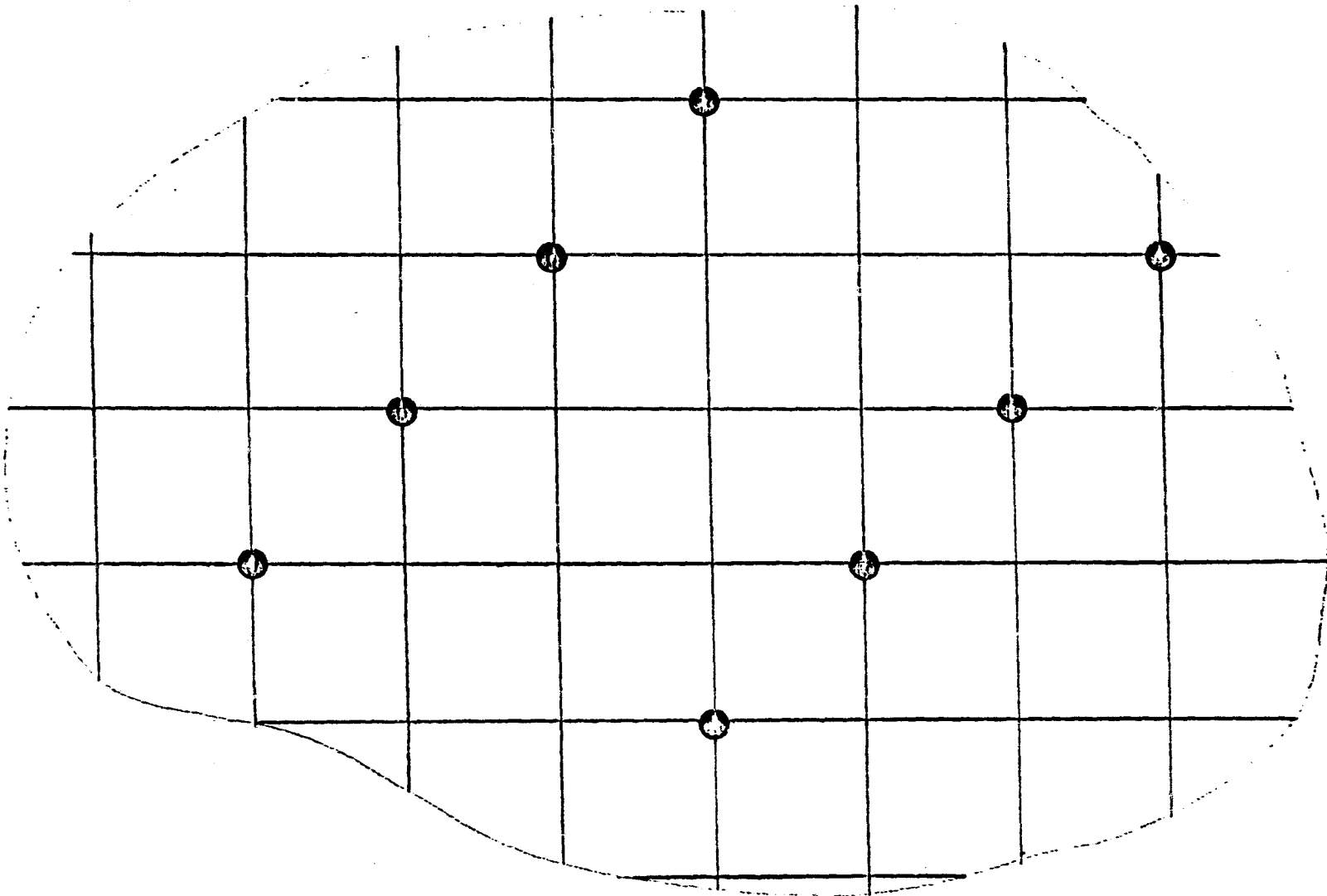
THE PRIMARY GROUNDING SYSTEM AT THE STATIC LEVEL

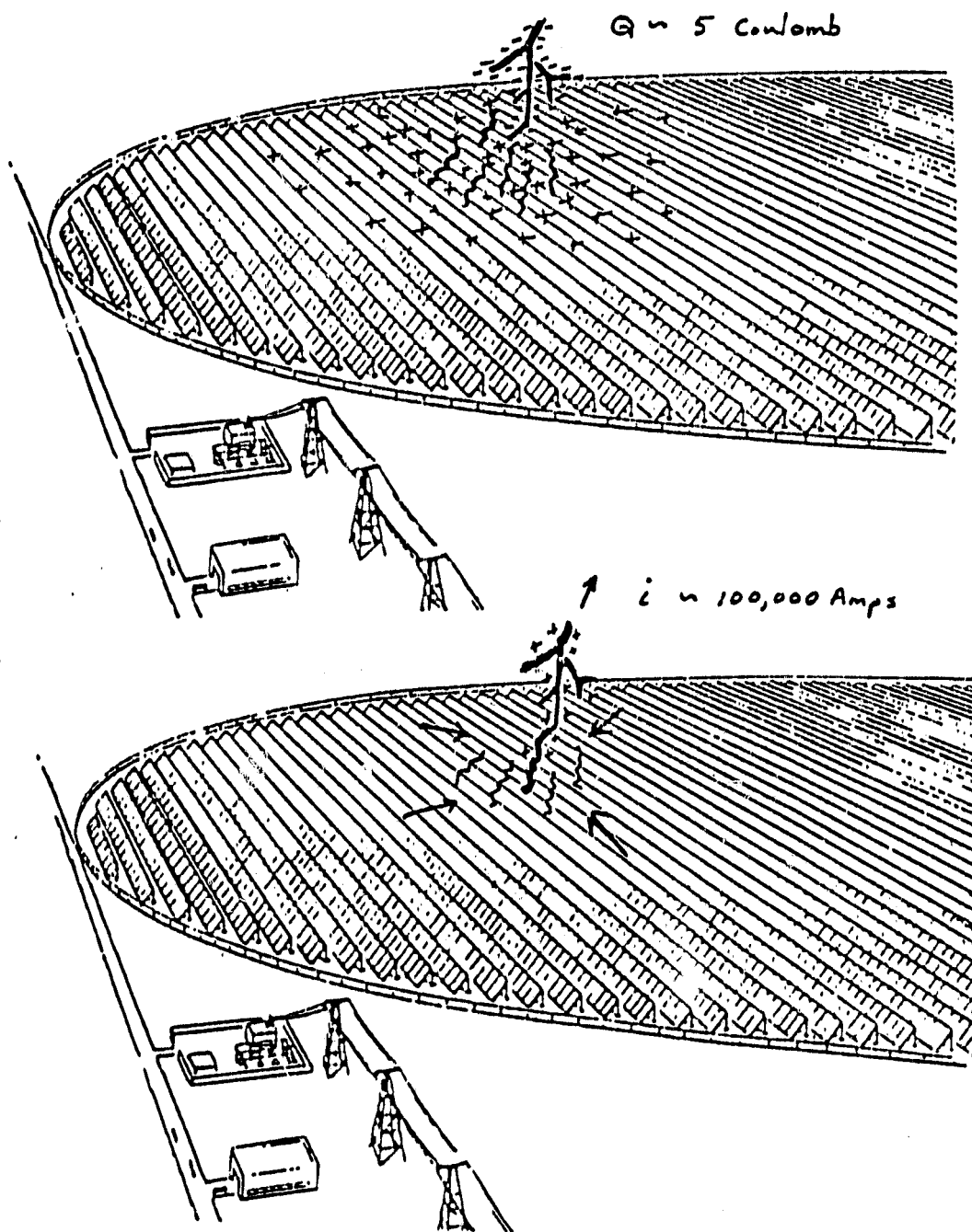


THE SURFACE-LEVEL GROUNDING NETWORK



PLACEMENT OF EARTH GROUNDS





LOCATION OF LINE CHARGES SIMULATING BILLBOARD

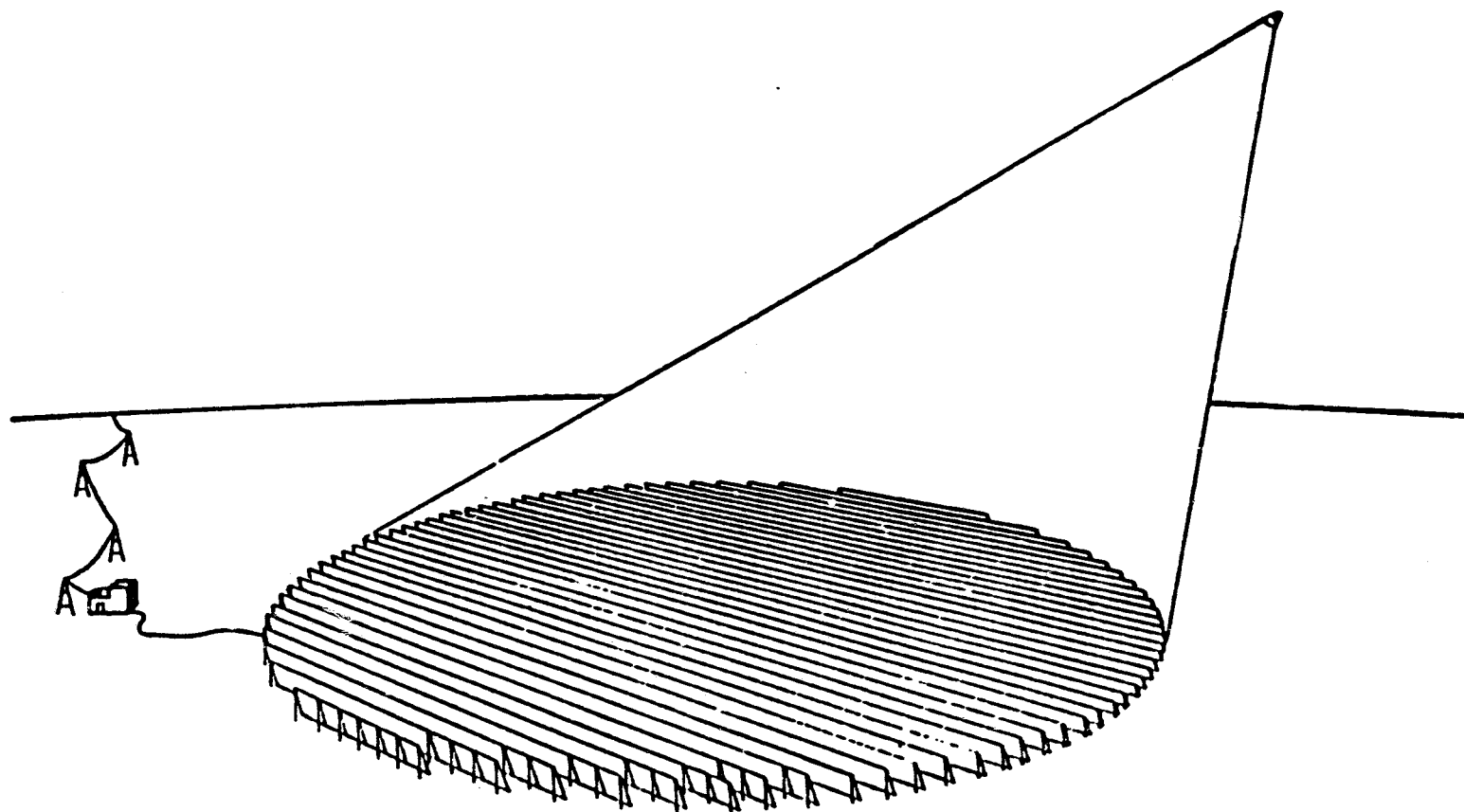
Analytic Array

*J. Ott
Novar*

PRECEDING PAGE BLANK NOT FILMED

PRECEDING PAGE BLANK NOT FILMED

121



SPS RECTENNA

TWO MATHEMATICAL MODELS DEVELOPED

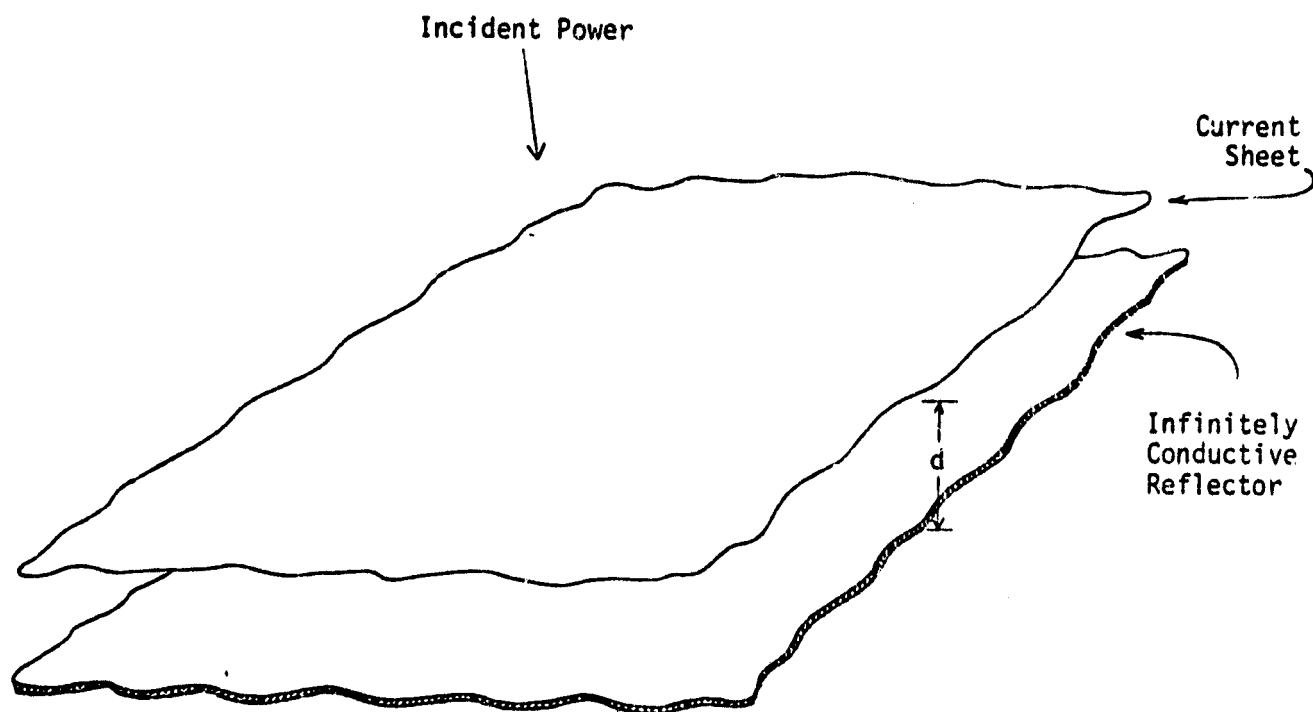
- DERIVED FROM MAXWELL'S EQUATIONS
- QUANTIFY SEVERAL CONDITIONS FOR TOTAL ABSORPTION
- PROVIDE VALUES FOR SCATTERING LOSSES DUE TO DEVIATIONS IN EACH CONDITION

RESULTS OF STUDY

- TOTAL ABSORPTION (NO SCATTERING) IS THEORETICALLY POSSIBLE
- SEVERAL IMPROVEMENTS IN THE RECTENNA DESIGN ARE INDICATED
- THE NATURE OF RECTENNA SCATTERING AND ATMOSPHERIC EFFECTS INVESTIGATED

1st MODEL

- BASED ON CURRENT SHEET EQUIVALENCY OF A LARGE PLANAR ARRAY ABOVE A REFLECTOR



CURRENT SHEET RECTENNA MODEL

- MAXWELL'S EQUATIONS SOLVED TO GIVE GENERAL EXPRESSIONS FOR THE FIELDS ABOVE AND BELOW THE CURRENT SHEET
- BOUNDARY CONDITIONS SATISFIED AT
 - REFLECTOR SURFACE
 - CURRENT SHEET
- EXPRESSIONS FOR WAVES AT SURFACE OF CURRENT SHEET SOLVED FOR POWER REFLECTION COEFFICIENTS

MAXWELL'S EQUATIONS IN PHASOR NOTATION

$$\nabla \times \underline{E} = -j\omega \underline{H}$$

$$\begin{aligned} \nabla \times \underline{H} &= \underline{J} + j\omega \epsilon' \underline{E} = j\omega \left(\epsilon' + \frac{\sigma}{j\omega} \right) \underline{E} \\ &= j\omega \epsilon \underline{E} \quad (\epsilon = \epsilon' - j\epsilon'') \end{aligned}$$

$$\nabla \cdot \underline{E} = 0 \quad (\text{CHARGE-FREE REGION})$$

$$\nabla \cdot \underline{H} = 0$$

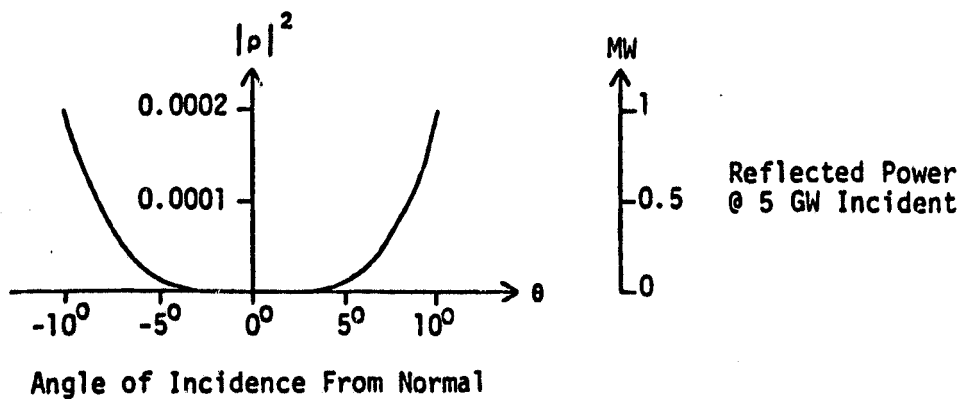
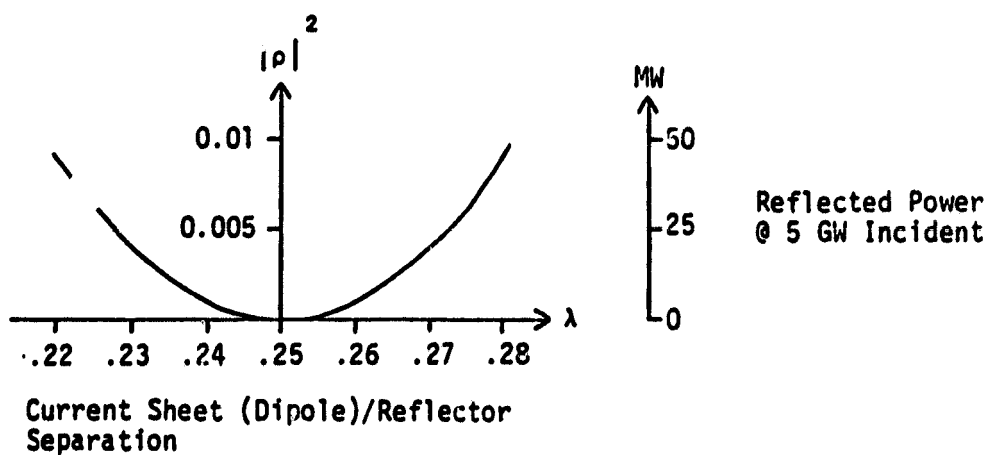
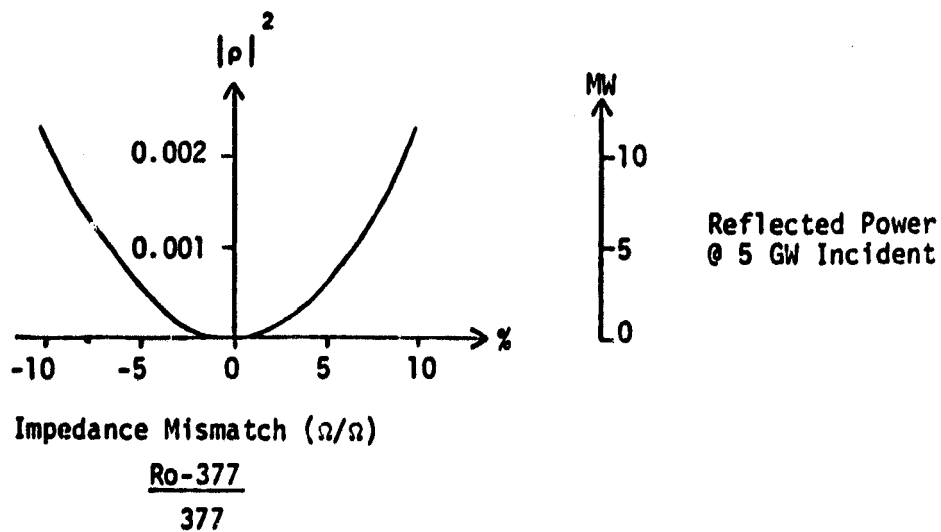
$$|p_{\parallel}|^2 = \frac{\left(\frac{\sqrt{\mu}}{R_0} \cos \theta - 1\right)^2 + \cot^2 \left(\frac{2\pi}{\lambda} d \cos \theta\right)}{\left(\frac{\sqrt{\mu}}{R_0} \cos \theta + 1\right)^2 + \cot^2 \left(\frac{2\pi}{\lambda} d \cos \theta\right)}$$

$$|p_{\perp}|^2 = \frac{\left(\frac{\sqrt{\mu}}{R_0} \sec \theta - 1\right)^2 + \cot^2 \left(\frac{2\pi}{\lambda} d \cos \theta\right)}{\left(\frac{\sqrt{\mu}}{R_0} \sec \theta + 1\right)^2 + \cot^2 \left(\frac{2\pi}{\lambda} d \cos \theta\right)}$$

POWER REFLECTION COEFFICIENTS

MODEL PREDICTS

- CONDITIONS FOR TOTAL ABSORPTION AT NORMAL INCIDENCE OF POWER BEAM ($\theta = 0$)
 - IMPEDANCE OF CURRENT SHEET MATCHED TO FREE SPACE ($R_0 = \sqrt{\frac{\mu}{\epsilon}} = 377\Omega$)
 - QUARTER-WAVE SEPARATION BETWEEN CURRENT SHEET AND REFLECTOR ($d = \frac{\lambda}{4}$)



POWER REFLECTION COEFFICIENT AND REFLECTED POWER LEVEL
OF THE CURRENT SHEET RECTENNA MODEL AS A FUNCTION OF
VARIOUS PARAMETERS

MODEL FURTHER PREDICTS

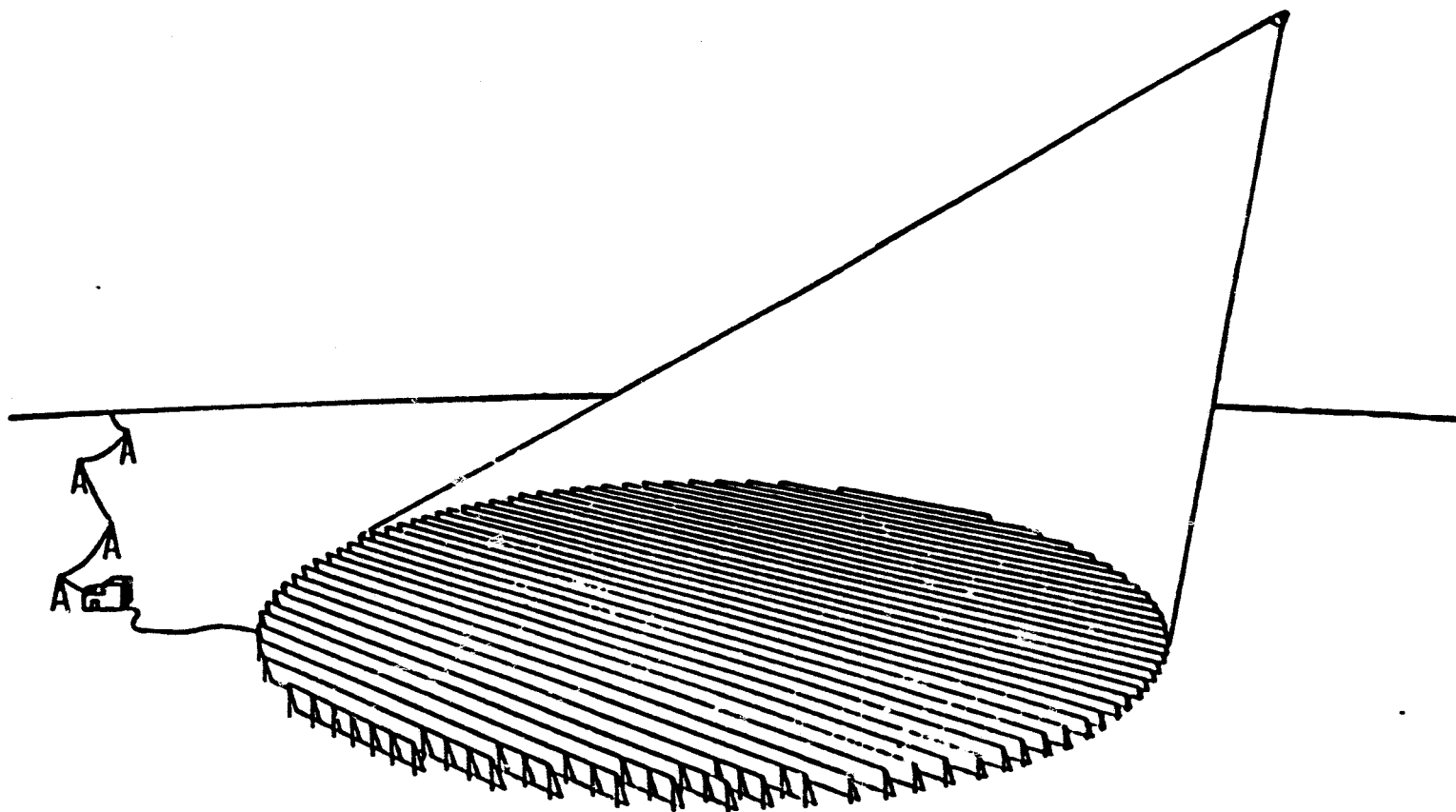
- TOTAL ABSORPTION FOR BEAM ANGLES OFF NORMAL INCIDENCE

CONDITIONS FOR TOTAL ABSORPTION FOR BEAM ANGLES OFF NORMAL INCIDENCE

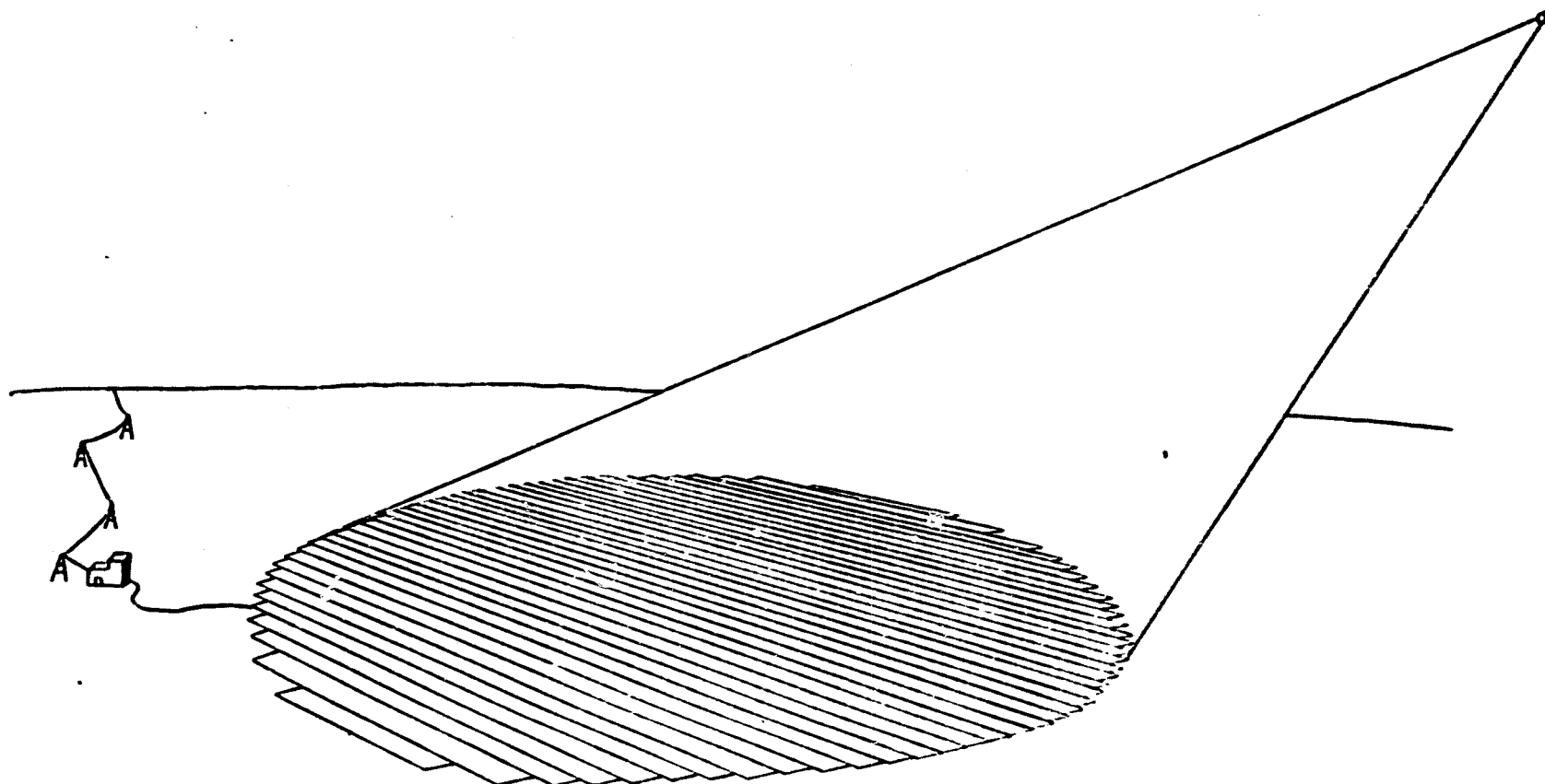
$$d = (2m-1) \frac{\lambda}{4} \sec \theta \text{ FOR } m = 1, 2, 3, \dots$$

$$R_o = \sqrt{\frac{A}{\epsilon}} \cos \theta \text{ FOR PARALLEL POLARIZATION}$$

$$R_o = \sqrt{\frac{A}{\epsilon}} \sec \theta \text{ FOR PERPENDICULAR POLARIZATION}$$



REFERENCE SYSTEM RECTENNA



CONFORMAL RECTENNA

CONFORMAL RECTENNA

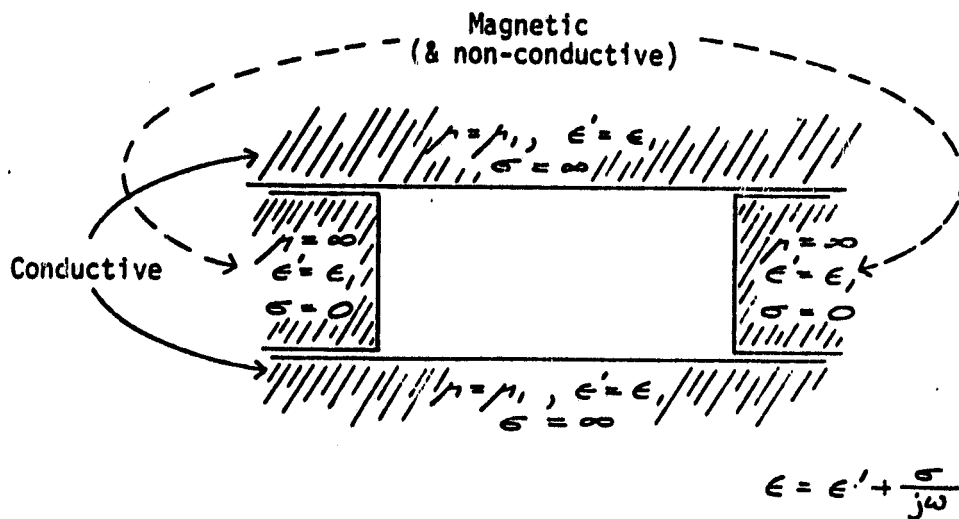
- CONFORMS TO TERRAIN
- MUCH LESS EXCAVATION REQUIRED
- POTENTIAL FOR BEING ABLE TO BE SUSPENDED ABOVE FARMS, BUILDING, ETC.
- ANTICIPATE LESS SCATTERING THAN WITH BILLBOARD DESIGN

2ND MODEL

- QUANTIFIES THE ELECTROMAGNETIC MODES IN THE IMMEDIATE VICINITY OF A RECTENNA ELEMENT
- GIVES LIMITS OF ELEMENT SPACING WHICH PERMIT TOTAL BEAM ABSORPTION
- PREDICTS A SUBSTANTIAL REDUCTION IN THE NUMBER OF ELEMENTS NEEDED FOR TOTAL ABSORPTION

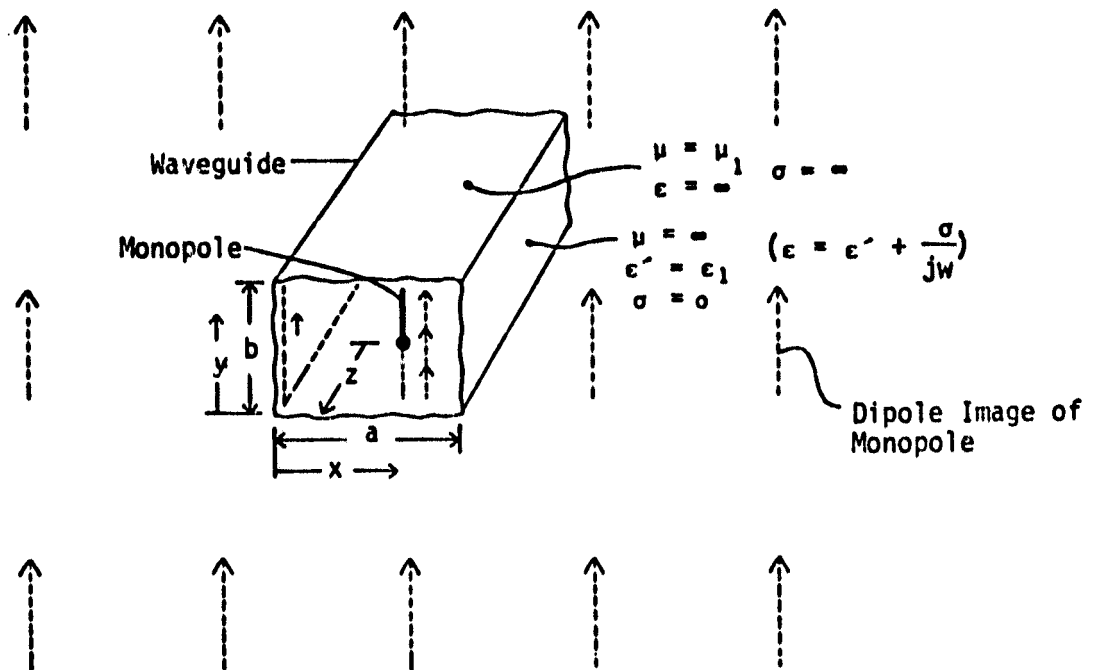
2ND MODEL WILL DESCRIBE A
WAVEGUIDE WITH SPECIAL PROPERTIES

• MIXED-WALL WAVEGUIDE

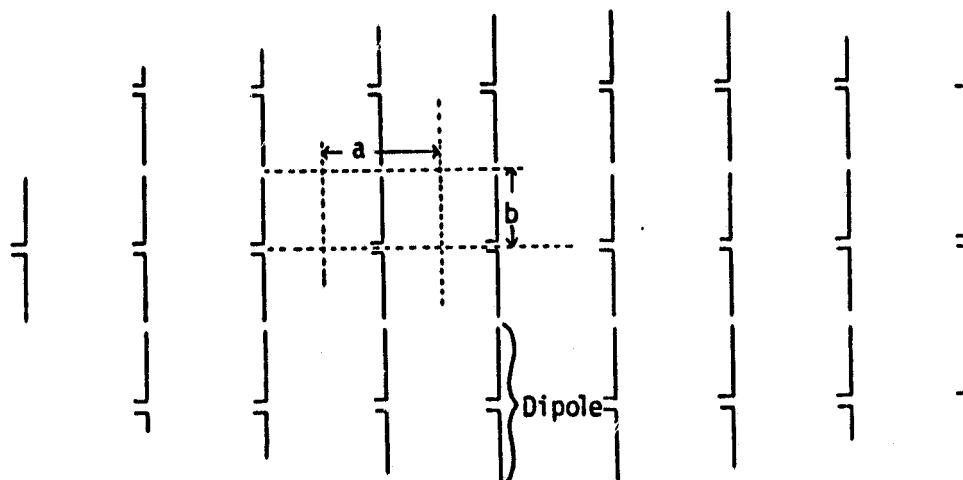


C-12

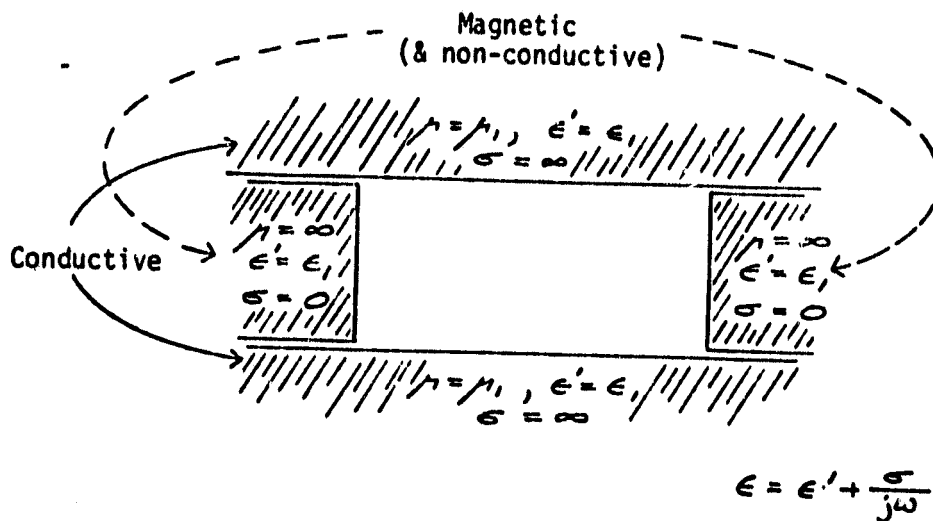
- MONOPOLE IN MIXED-WALL WAVEGUIDE PRODUCES AN INFINITE ARRAY OF IMAGE DIPOLES WITH CURRENTS OF IDENTICAL MAGNITUDE AND PHASE
- CONVERSELY:
 - AN INFINITE ARRAY OF IDENTICAL DIPOLES WITH CURRENTS OF IDENTICAL MAGNITUDE AND PHASE CAN BE REPLACED BY A MONOPOLE IN A MIXED-WALL WAVEGUIDE
 - CURRENTS OF IDENTICAL MAGNITUDE AND PHASE ARE GENERATED BY A NORMAL-INCIDENCE POWER BEAM
 - ▲ IN A LARGE AREA ABOUT A DIPOLE
 - ALLOWING THE PORTION OF THE RECTENNA ARRAY IN THAT LARGE AREA ABOUT THE DIPOLE TO BE MODELED BY AN INFINITE ARRAY



IMAGING PROPERTIES OF MIXED-WALL WAVEGUIDE WITH MONOPOLE



SECTION OF INFINITE ARRAY OF DIPOLES MODELED BY A MONOPOLE IN A "MIXED-WALL" WAVEGUIDE

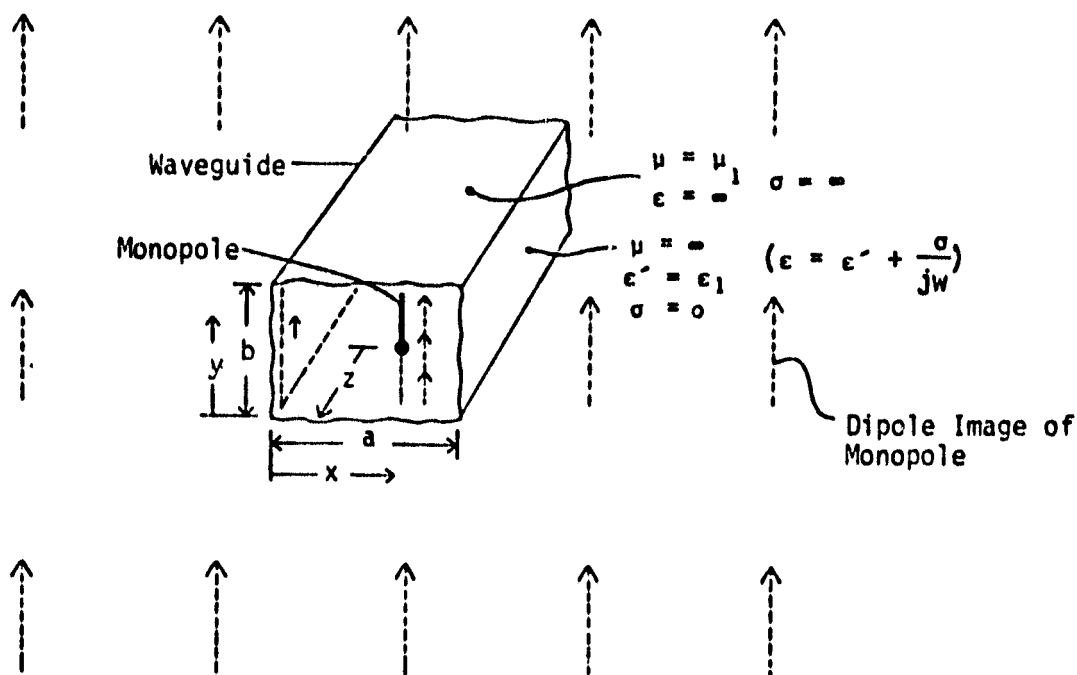


MIXED-WALL WAVEGUIDE WILL SUPPORT TEM MODE

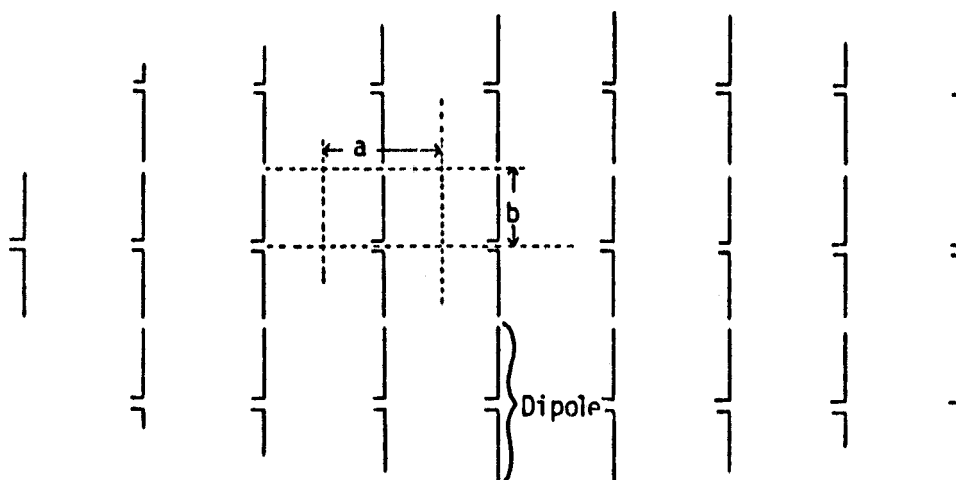
- DOWN TO ZERO FREQUENCY (D.C.)
(SIDE WALLS ARE NON-CONDUCTIVE)
- MIXED-WALL WAVEGUIDE IS EQUIVALENT TO
STRIP LINE FOR TEM

HIGHER ORDER MODES

- WANT HIGHER ORDER MODES TO BE NON-PROPAGATING (EVANESCENT) SO THAT ONLY TEM IS PROPAGATED
 - SO THAT THE PROPAGATING FIELD IN THE WAVEGUIDE IS THE SAME AS THAT OF THE POWER BEAM - A PLANE (TEM) WAVE
 - ALLOW US TO DESCRIBE NEAR FIELDS AROUND DIPOLE IN ARRAY
 - IF OTHER MODES PROPAGATE, THAT IS SCATTERING
-
- SOLVING MAXWELL'S EQUATIONS AND RESULTING WAVE EQUATIONS IN A MIXED-WALL WAVEGUIDE GIVES MODE EQUATIONS IN TERMS OF "a" AND "b" DIMENSIONS OF WAVEGUIDE



IMAGING PROPERTIES OF MIXED-WALL WAVEGUIDE WITH MONOPOLE



SECTION OF INFINITE ARRAY OF DIPOLES MODELED BY A MONOPOLE IN A "MIXED-WALL" WAVEGUIDE

- FOR HIGHER ORDER MODES TO BE NON-PROPAGATING:

$$a < \lambda$$

$$b < \lambda/2$$

$$H_z = 0 + \sum_{m=1}^{\infty} \sum_{n=0}^{\infty} A_{mn} \sin \frac{m\pi}{a} x \cos \frac{n\pi}{b} y e^{-\alpha_{mn} z}$$

$$E_z = 0 + \sum_{f=0}^{\infty} \sum_{g=1}^{\infty} B_{fg} \cos \frac{f\pi}{a} x \sin \frac{g\pi}{b} y e^{-\alpha_{fg} z}$$

$$E_x = 0 + \sum_{m=1}^{\infty} \sum_{n=0}^{\infty} \frac{-j\omega\mu m\pi}{k_{c,mn}^2} A_{mn} \sin \frac{m\pi}{a} x \sin \frac{n\pi}{b} y e^{-\alpha_{mn} z} \\ + \sum_{f=0}^{\infty} \sum_{g=1}^{\infty} \frac{-\alpha_{fg} f\pi}{k_{c,fg}^2} B_{fg} \sin \frac{f\pi}{a} x \sin \frac{g\pi}{b} y e^{-\alpha_{fg} z}$$

$$E_y = \sqrt{\frac{\mu}{\epsilon}} K_0 e^{-j\beta_{00} z} + \sum_{m=1}^{\infty} \sum_{n=0}^{\infty} \frac{j\omega\mu n\pi}{k_{c,mn}^2} A_{mn} \cos \frac{m\pi}{a} x \cos \frac{n\pi}{b} y e^{-\alpha_{mn} z} \\ + \sum_{f=0}^{\infty} \sum_{g=1}^{\infty} \frac{\alpha_{fg} g\pi}{k_{c,fg}^2} B_{fg} \cos \frac{f\pi}{a} x \cos \frac{g\pi}{b} y e^{-\alpha_{fg} z}$$

$$H_x = K_0 e^{-j\beta_{00} z} + \sum_{m=1}^{\infty} \sum_{n=0}^{\infty} \frac{\alpha_{mn} m\pi}{k_{c,mn}^2} A_{mn} \cos \frac{m\pi}{a} x \cos \frac{n\pi}{b} y e^{-\alpha_{mn} z} \\ + \sum_{f=0}^{\infty} \sum_{g=1}^{\infty} \frac{j\omega\epsilon g\pi}{k_{c,fg}^2} B_{fg} \cos \frac{f\pi}{a} x \cos \frac{g\pi}{b} y e^{-\alpha_{fg} z}$$

$$H_y = 0 + \sum_{m=1}^{\infty} \sum_{n=0}^{\infty} \frac{-\alpha_{mn} n\pi}{k_{c,mn}^2} A_{mn} \sin \frac{m\pi}{a} x \sin \frac{n\pi}{b} y e^{-\alpha_{mn} z} \\ + \sum_{f=0}^{\infty} \sum_{g=1}^{\infty} \frac{j\omega\epsilon f\pi}{k_{c,fg}^2} B_{fg} \sin \frac{f\pi}{a} x \sin \frac{g\pi}{b} y e^{-\alpha_{fg} z}$$

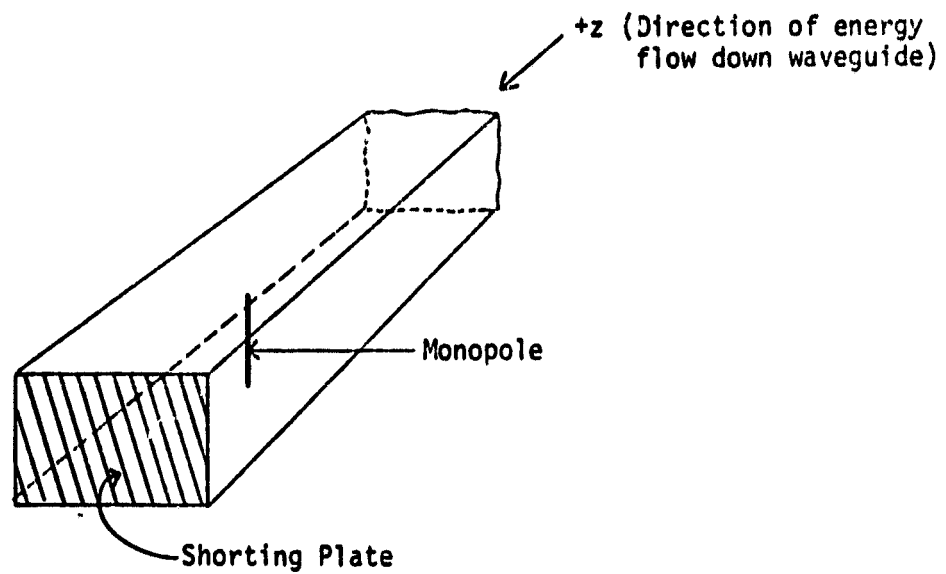
$$\gamma'_{mn} = \alpha_{mn} + j\beta_{mn} = \sqrt{k^2 - \left(\frac{m\pi}{a}\right)^2 - \left(\frac{n\pi}{b}\right)^2} = \sqrt{k^2 - k_{c,mn}^2}$$

$$\gamma'_{fg} = \alpha_{fg} + j\beta_{fg} = \sqrt{k^2 - \left(\frac{f\pi}{a}\right)^2 - \left(\frac{g\pi}{b}\right)^2} = \sqrt{k^2 - k_{c,fg}^2}$$

$$\beta_{00} = k = \frac{2\pi}{\lambda}$$

ELECTROMAGNETIC FIELD EQUATIONS FOR A MIXED-WALL WAVEGUIDE

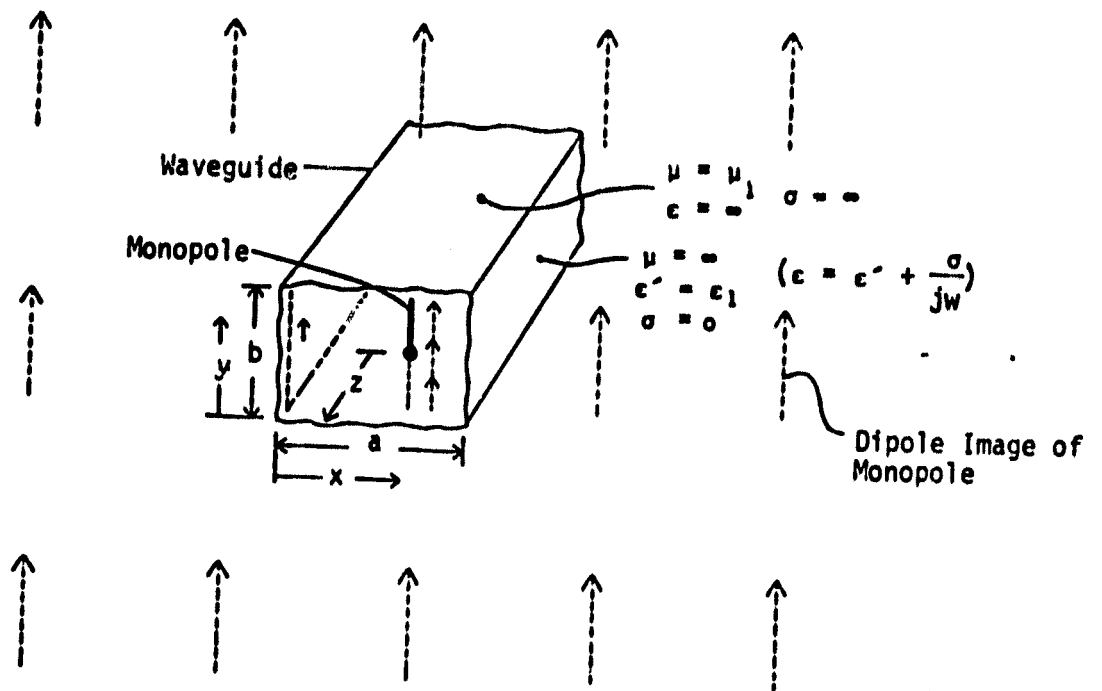
Equations shown are for total "+z directed" portion of the field components in a mixed-wall waveguide. With appropriate sign changes, equations express the "-z directed" components.



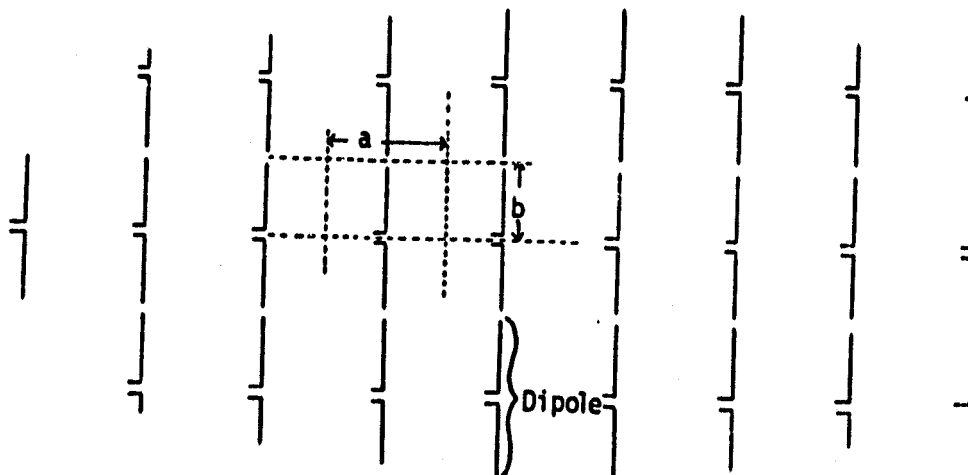
MONOPOLE IN MIXED-WALL WAVEGUIDE
BACKED BY SHORTING PLATE

TOTAL ABSORPTION OF PLANE WAVE IN MIXED-WALL WAVEGUIDE WITH MONOPOLE AND SHORTING PLATE IS EXPECTED BECAUSE:

- TEM MODE IS PROPAGATED IN MIXED-WALL WAVEGUIDE
 - MIXED-WALL WAVEGUIDE DIMENSIONS ARE SUCH THAT ALL OTHER MODES ARE BEYOND CUT-OFF (EVANESCENT) (REACTIVE)
 - IDEAL SHORTING PLATE IN WAVEGUIDE GENERATES A REFLECTED WAVE
 - FIELDS IN NEIGHBORHOOD OF MONOPOLE ARE SUM OF ALL MODES OF THE WAVES TRAVELLING TOWARD IT FROM BOTH DIRECTIONS
 - EQUATIONS DESCRIBING FIELDS IN NEIGHBORHOOD OF MONOPOLE ARE OF SAME FORM AS THOSE IN CONVENTIONAL WAVEGUIDES WITH PROBE AND SHORTING PLATE
-
- THESE EQUATIONS ESTABLISH MATCHING REQUIREMENTS ON THE MONOPOLE AND LOAD IMPEDANCES AND SPACING OF MONOPOLE FROM SHORTING PLATE SO THAT NO TEM WAVE TRAVELS BACK UP THE WAVEGUIDE TOWARD THE SOURCE
-
- ▲ MONOPOLE TO SHORTING PLATE DISTANCE EXPECTED TO BE APPROXIMATELY $\lambda/4$
-
- IT IS WELL-KNOWN THAT A PROBE IN A CONVENTIONAL WAVEGUIDE BACKED BY A SHORTING PLATE CAN ABSORB ALL INCIDENT POWER



IMAGING PROPERTIES OF MIXED-WALL WAVEGUIDE WITH MONOPOLE



SECTION OF INFINITE ARRAY OF DIPOLES MODELED BY A MONOPOLE IN A "MIXED-WALL" WAVEGUIDE

- FOR PROPAGATION OF ONLY A PLANE WAVE IN WAVEGUIDE

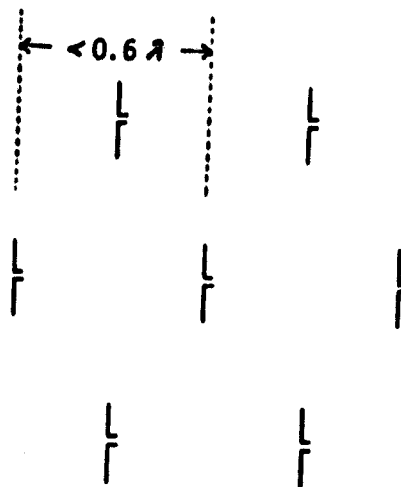
$$a < \lambda$$

$$b < \frac{\lambda}{2}$$

- SEPARATION OF CENTERS OF DIPOLES IN RECTENNA
ARRAY (RECTANGULAR GRID CONFIGURATION)

$$a \times 2b$$

- THEREFORE EQUIVALENT ALLOWABLE SEPARATION OF
CENTERS OF DIPOLES (RECTANGULAR GRID CONFIGURATION)
IS $< \lambda$



TRIANGULAR GRID CONFIGURATION
-REFERENCE SYSTEM

- EXISTENCE OF NON-EVANESCENT HIGHER ORDER MODES =
EXISTENCE OF GRATING LOBES
- GRATING LOBE ANALYSIS SHOWS -

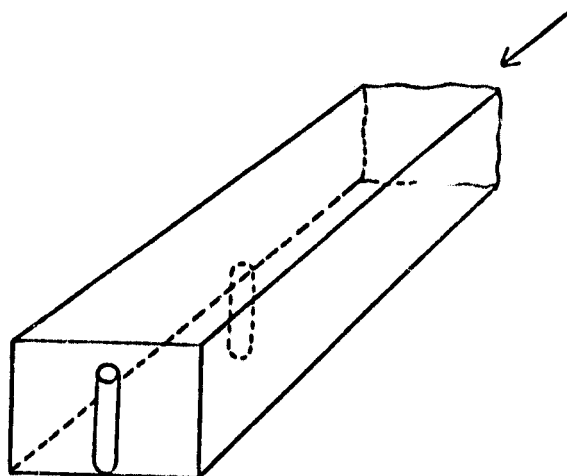
MAXIMUM SEPARATION OF DIPOLE CENTERS FOR TRI-
ANGULAR GRID CONFIGURATION TO AVOID GRATING
LOBES:

$$< 1.15\lambda$$

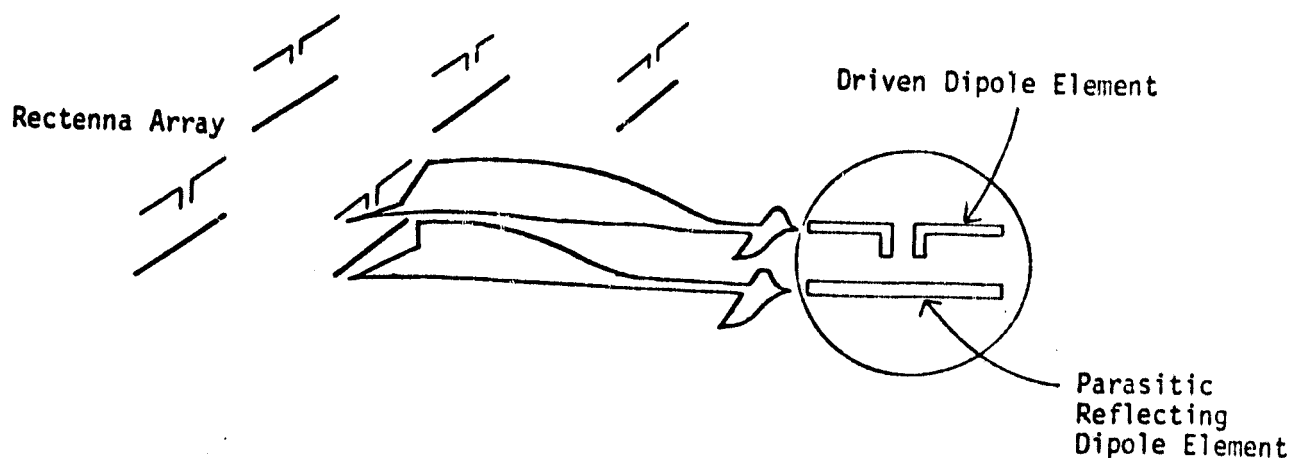
NUMBER OF DIPOLE-DIODE
ELEMENTS REQUIRED
(NORMAL INCIDENCE)

REFERENCE SYSTEM DESIGN	18 BILLION
TRIANGULAR GRID CONFIGURATION WITH MAXIMUM ALLOWABLE DIPOLE SPACING	4.5 BILLION
RECTANGULAR GRID CONFIGURATION WITH MAXIMUM ALLOWABLE DIPOLE SPACING	5.2 BILLION

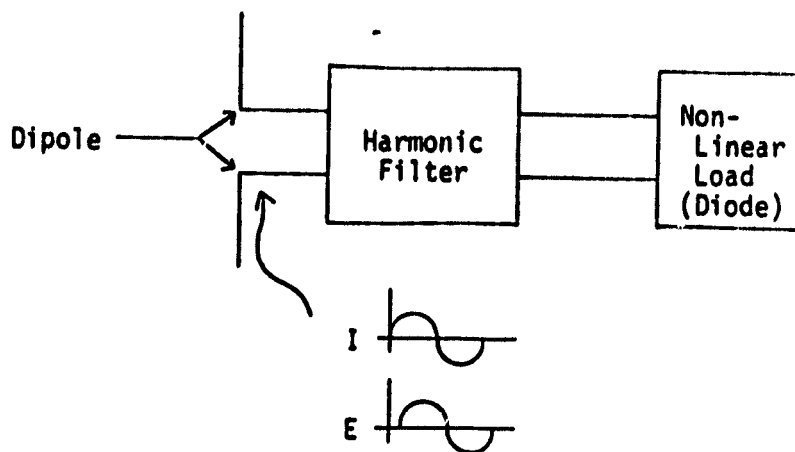
- GREATER DIODE EFFICIENCY IS INDICATED WHEN THE NUMBER
OF RECTENNA DIPOLE ELEMENTS IS REDUCED SINCE THE POWER
PER DIODE IS HIGHER.



TOTAL ABSORPTION OF POWER IN
MIXED-WALL WAVEGUIDE WITH PARASITIC REFLECTING MONOPOLE
IS INDICATED

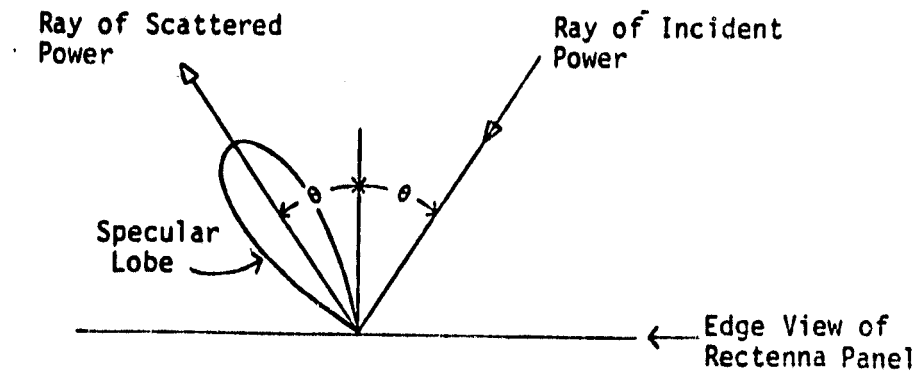


RECTENNA WITH PARASITIC REFLECTING
DIPOLE ELEMENTS



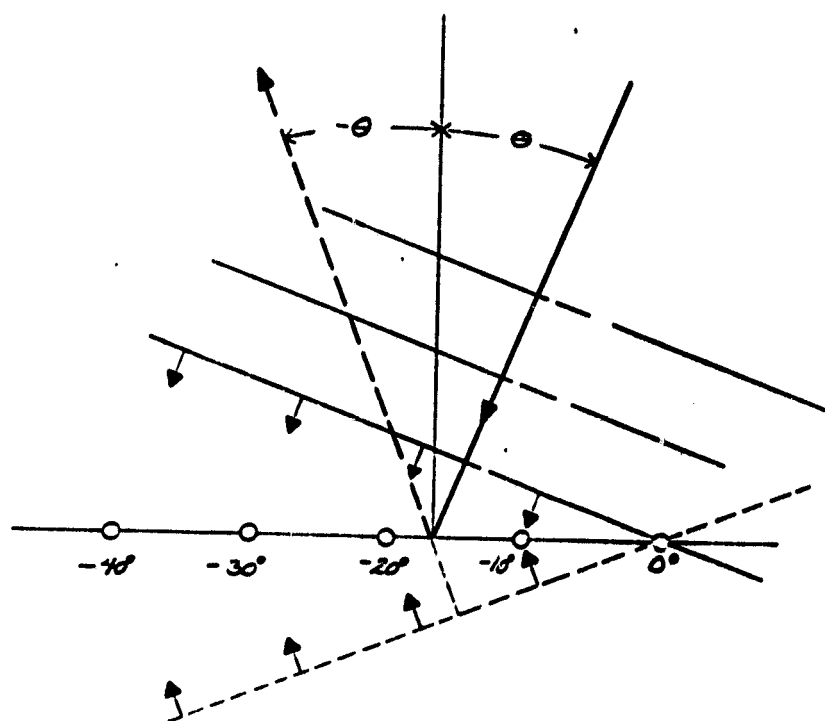
RECTENNA ELEMENT HARMONIC FILTER

- PRESENTS LINEAR LOAD AT DIPOLE TERMINALS
- AS LONG AS CURRENT AND VOLTAGE AT DIPOLE TERMINALS ARE SINUSOIDAL AND NOT IN QUADRATURE, RECTENNA CAN BE TOTALLY ABSORBING

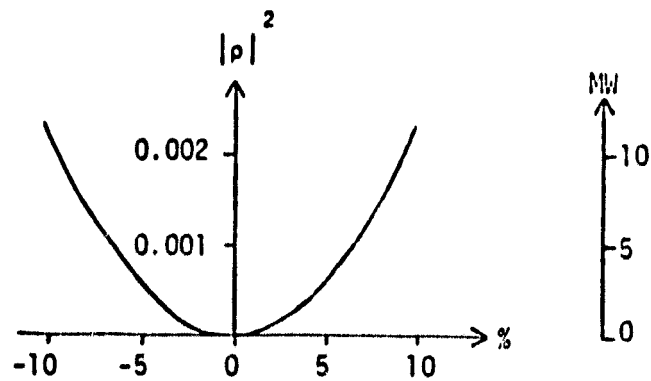


DEPICTION OF SPECULAR SCATTERING FROM RECTENNA

- SPECULAR IS THE PREDOMINANT FORM OF SCATTERING
AT THE FUNDAMENTAL FREQUENCY OF POWER BEAM



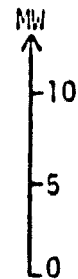
SPECULAR REFLECTION



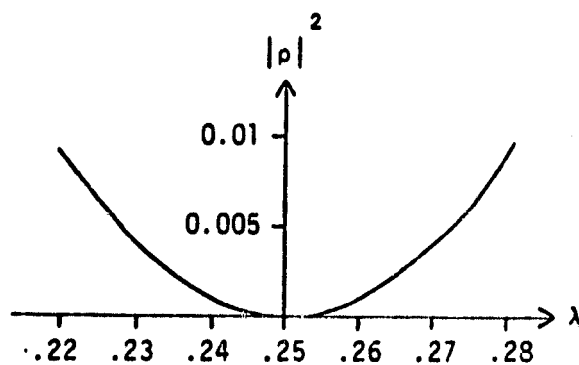
Impedance Mismatch (Ω/Ω)

Ro-377

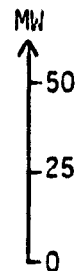
377



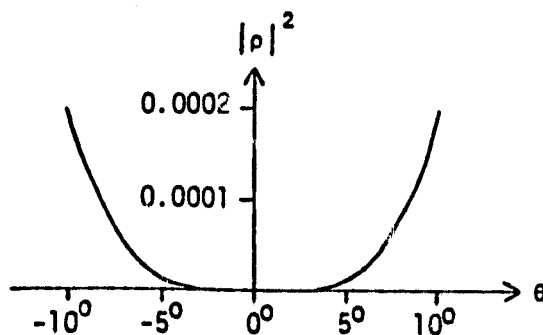
Reflected Power
@ 5 GW Incident



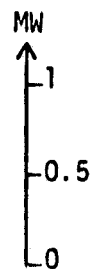
Current Sheet (Dipole)/Reflector
Separation



Reflected Power
@ 5 GW Incident



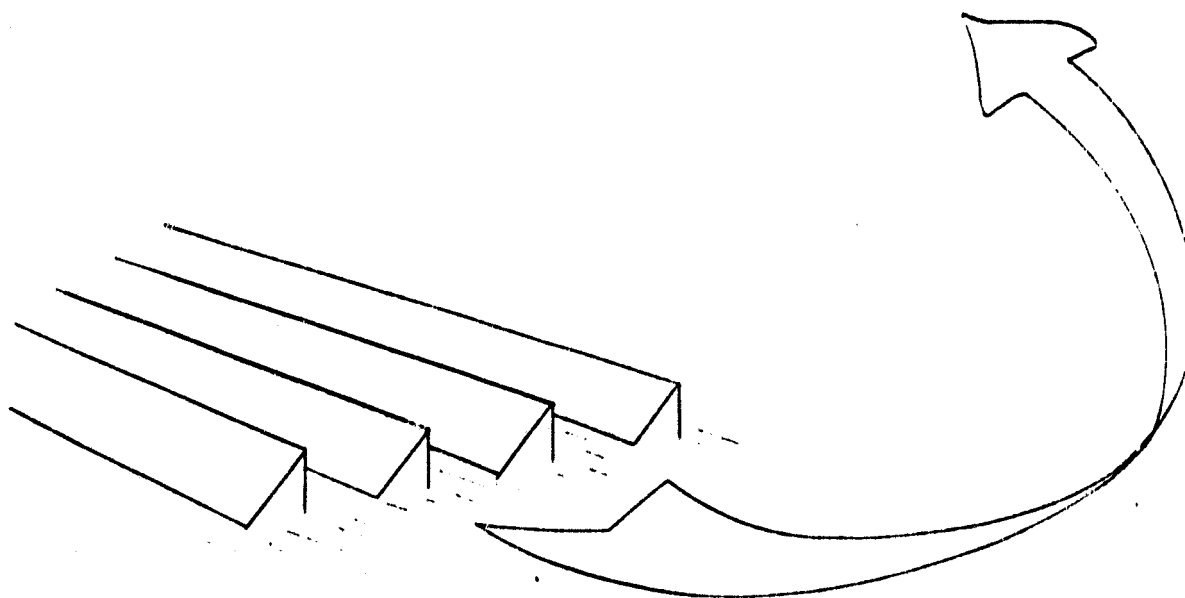
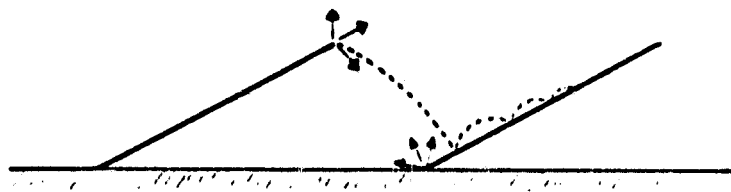
Angle of Incidence From Normal

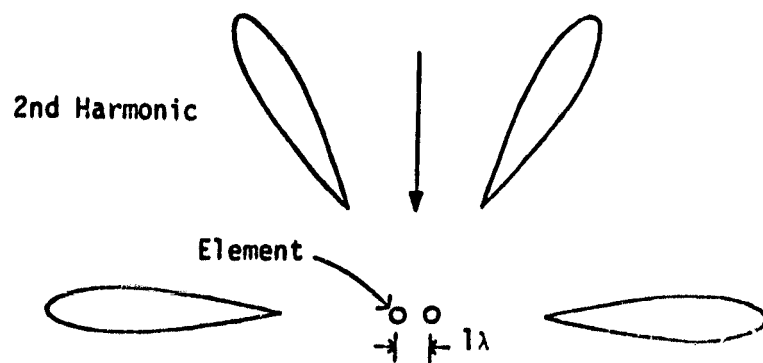


Reflected Power
@ 5 GW Incident

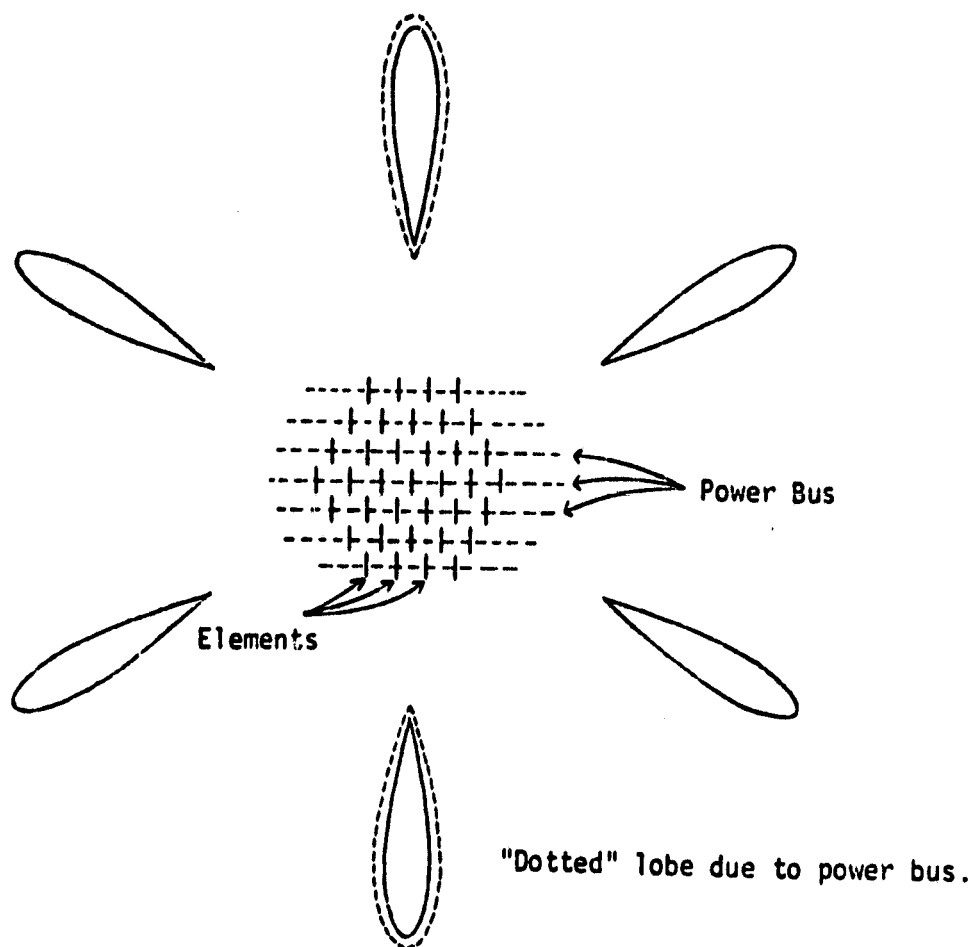
POWER REFLECTION COEFFICIENT AND REFLECTED POWER LEVEL
OF THE CURRENT SHEET RECTENNA MODEL AS A FUNCTION OF
VARIOUS PARAMETERS

"VENETIAN BLIND" SCATTERING SOURCES





GRATING LOBE NATURE OF HARMONIC
SCATTERING FROM A RECTENNA
(ELEVATION EXAMPLE)



GRATING LOBE NATURE OF HARMONIC
SCATTERING FROM A RECTENNA
(AZIMUTH EXAMPLE)

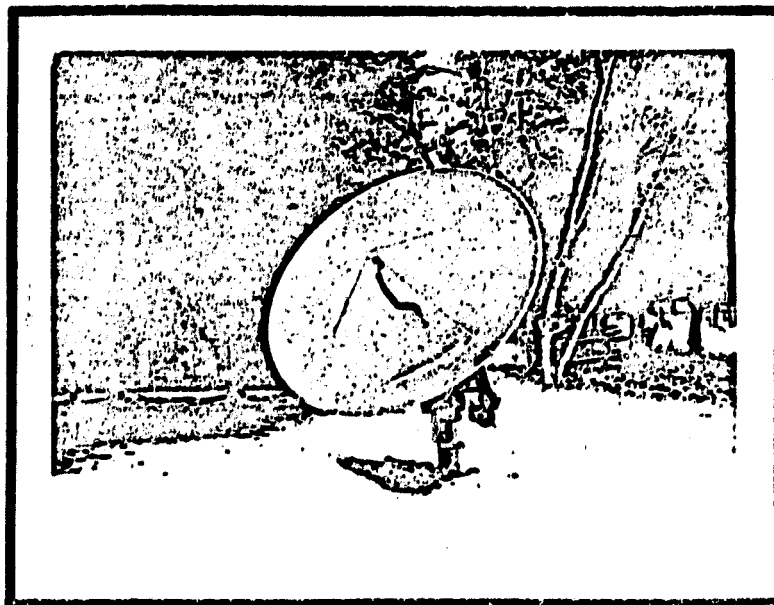
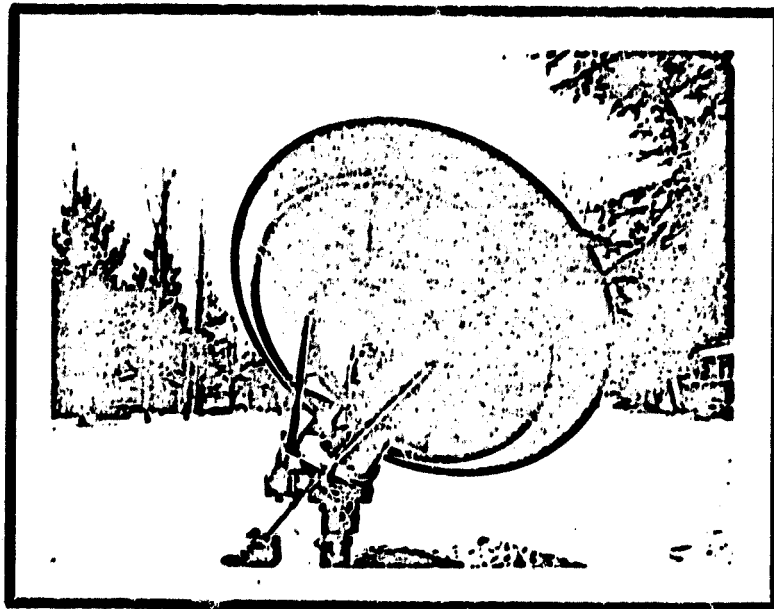
ATMOSPHERIC EFFECTS

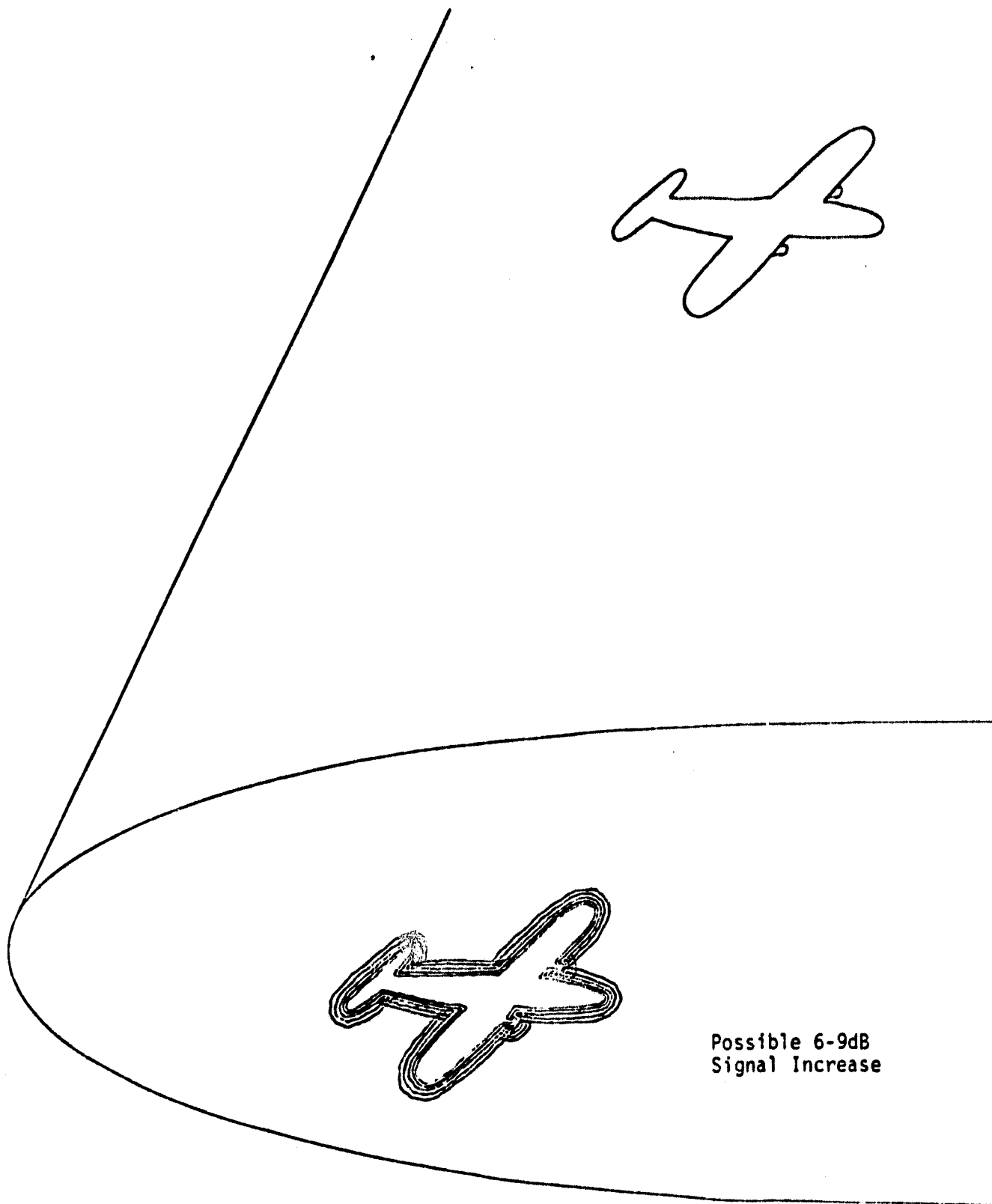
- DEPOLARIZATION PRODUCES SCATTERING IN A RECTENNA
 - DEPOLARIZED SIGNAL MAY PASS THROUGH SOME REFLECTOR DESIGNS
 - DEPOLARIZATING EVENTS UP TO 20 dB (1% SCATTERED) HAVE BEEN OBSERVED AT C-BAND WITH 10 METER APERTURES
- AMPLITUDE FLUCTUATIONS CAUSE SCATTER:
 - BY CAUSING DISRUPTION IN THE RECTENNA ILLUMINATION
 - BY RECTENNA TERMINAL IMPEDANCE CHANGES FROM CHANGING RF LEVELS AT THE DIODES

EXISTING EARTH-SPACE PROPAGATION MEASUREMENTS

- DATA TO DATE SHOWS A MAXIMUM OF 0.1dB AMPLITUDE FLUCTUATIONS
(WOULD CAUSE INSIGNIFICANT SCATTERING)
- FACTORS WHICH IMPAIR APPLICATION OF PREVIOUS EARTH STATION MEASUREMENTS TO SPS
 - SIGNIFICANT APERTURE AVERAGING IN ALL STUDIES FOUND
($5000 \lambda^2$ MIN FOR DATA VS $1 \lambda^2$ FOR SPS)
 - DATA AT C & S BAND FROM MODULATED SIGNALS
(PANCHROMATIC VS MONOCHROMATIC FOR SPS)
 - PRESENT SOLAR MAXIMUM PROVIDES OPPORTUNITY TO EXAMINE WORST-CASE
NATURAL IONOSPHERIC EFFECTS

ORIGINAL PAGE IS
OF POOR QUALITY





Possible 6-9dB
Signal Increase

DIFFRACTION ENHANCEMENT AT RECTENNA
CAUSED BY OBJECT FLYING THROUGH THE
POWER BEAM

DIFFRACTED SIGNAL ENHANCEMENT

- RECTENNA DIODE SHOULD HAVE TOLERANCE TO SPOT-TRANSIENT SIGNAL ENHANCEMENT CAUSED BY LARGE OBJECTS FLYING OVER RECTENNA
- POSSIBLE SIGNAL INCREASE UP TO 9dB DEPENDS ON SIZE, HEIGHT, SHAPE
- FAST AIRCRAFT HAZARD TO RECTENNA DIODES FROM OVERVOLTAGE TRANSIENTS
- SLOWER OBJECTS MAY CAUSE DIODE OVERHEATING E.G. HELICOPTER

D5

Large Array Measurement Results

*R. Dickinson
Jet Propulsion Lab*

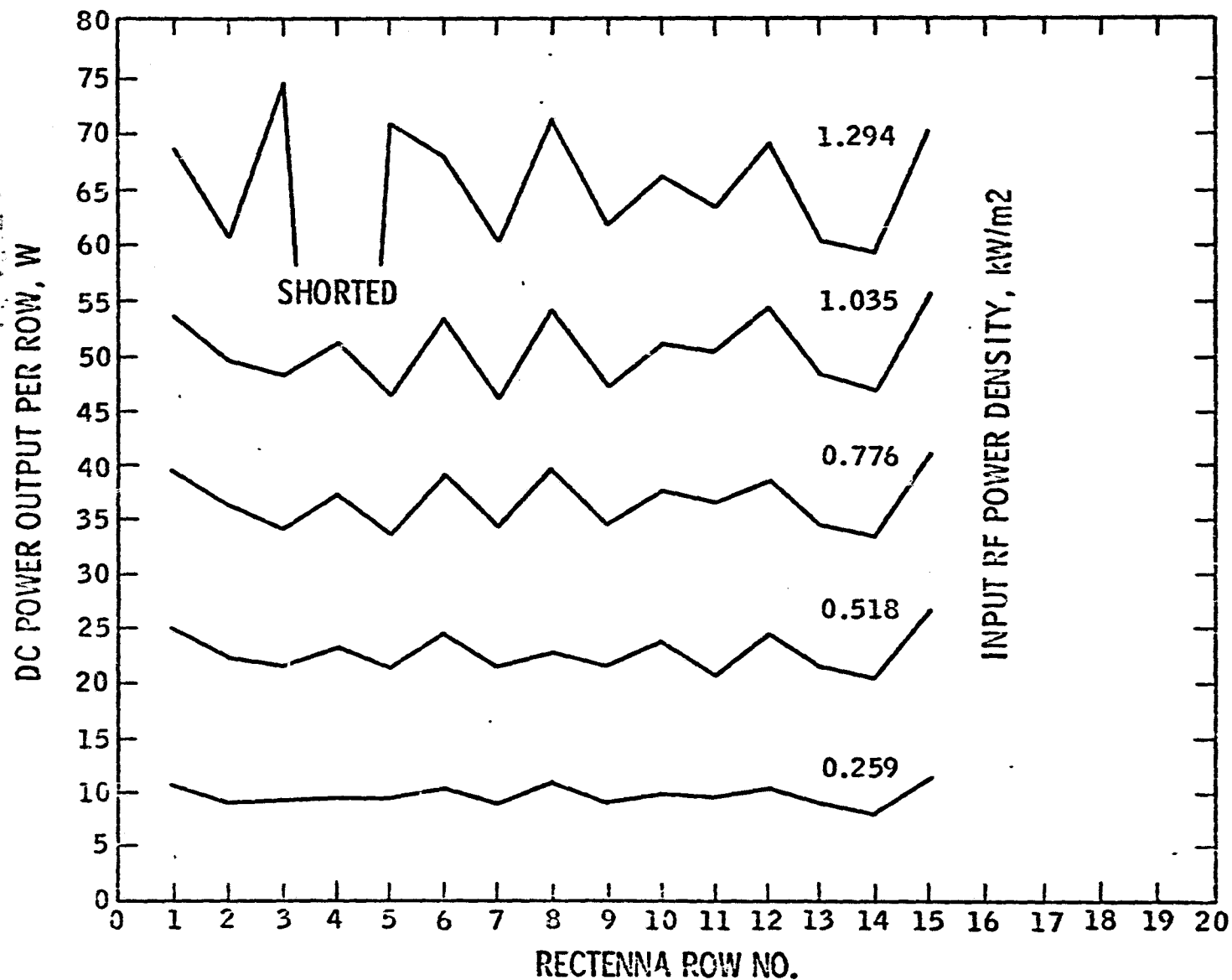
PRECEDING PAGE BLANK NOT FILMED

SUMMARY OF STUDY

- THEORETICAL ABSORPTION = 100% (NO SCATTER)
- SIGNIFICANT REDUCTION IN NUMBER OF ELEMENTS
- GROUND CONFORMING PANELS
- PARASITIC REFLECTORS
- CHARACTER AND CAUSES OF SCATTERING
- ATMOSPHERIC EFFECTS

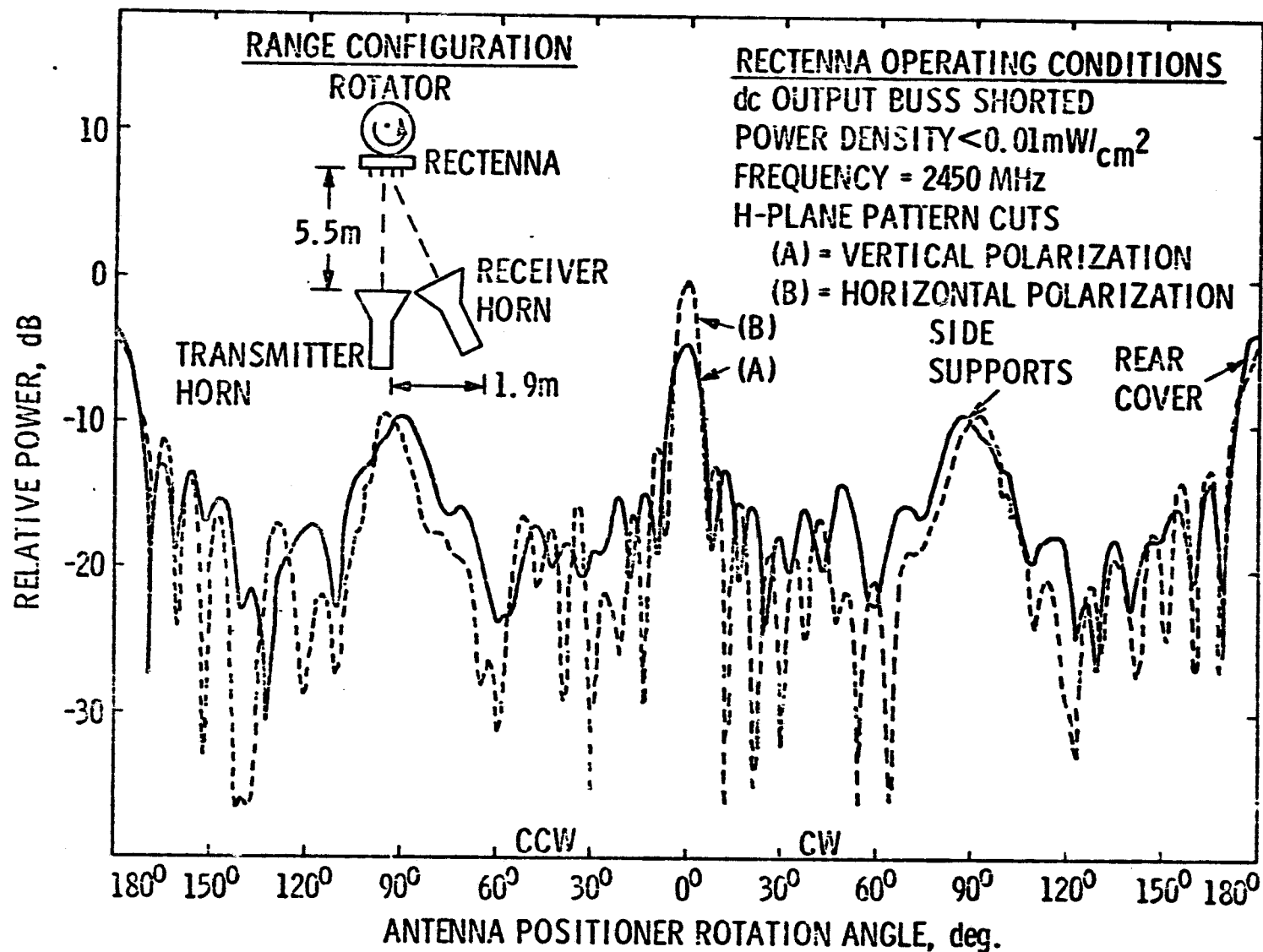
PRECEDING PAGE BLANK NOT FILMED

DC POWER OUTPUT FOR EACH ROW IN THE SUBARRAY



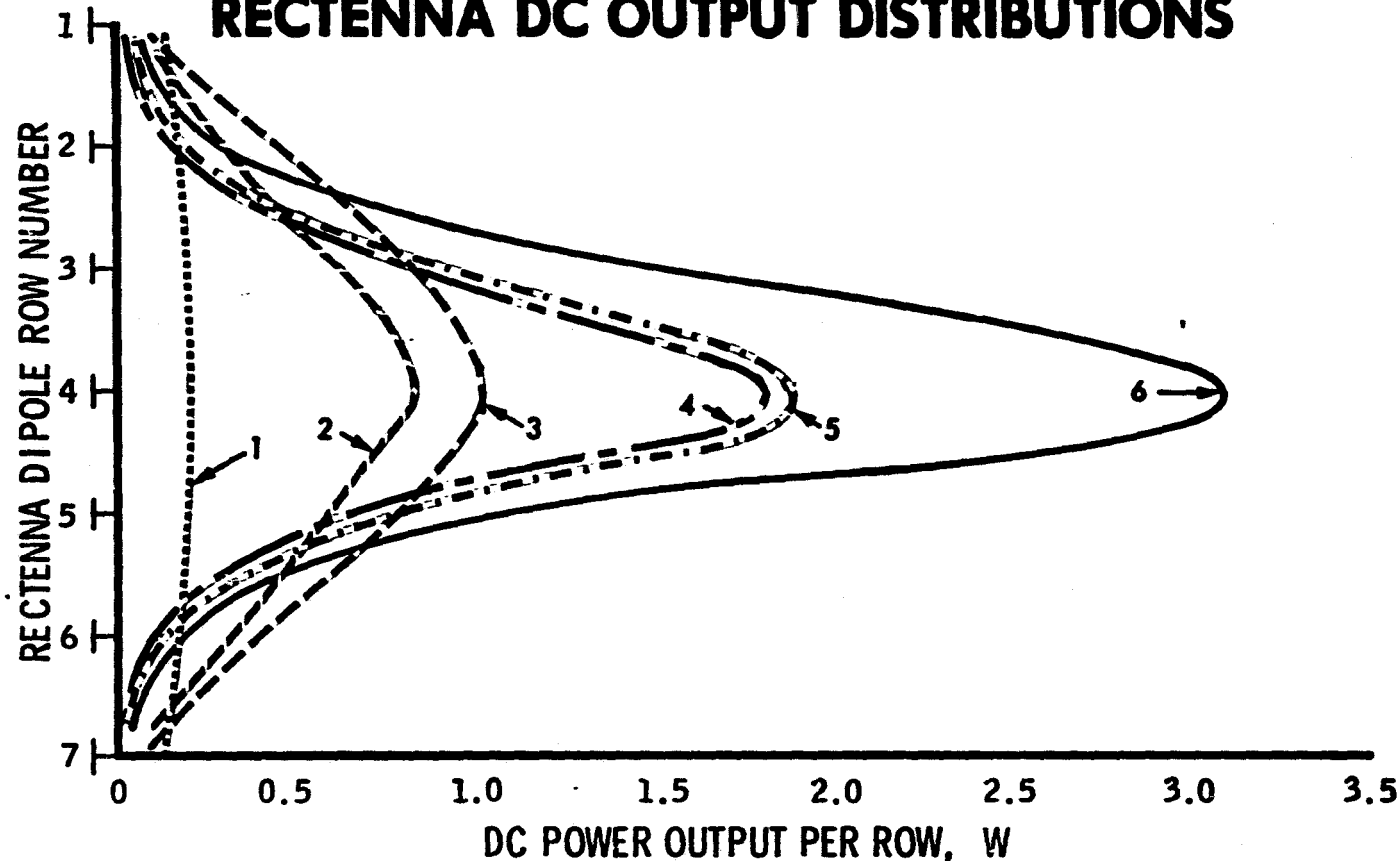


BEAMED RF POWER TECHNOLOGY RECTENNA BISTATIC PATTERNS





BEAMED RF POWER TECHNOLOGY RECTENNA DC OUTPUT DISTRIBUTIONS

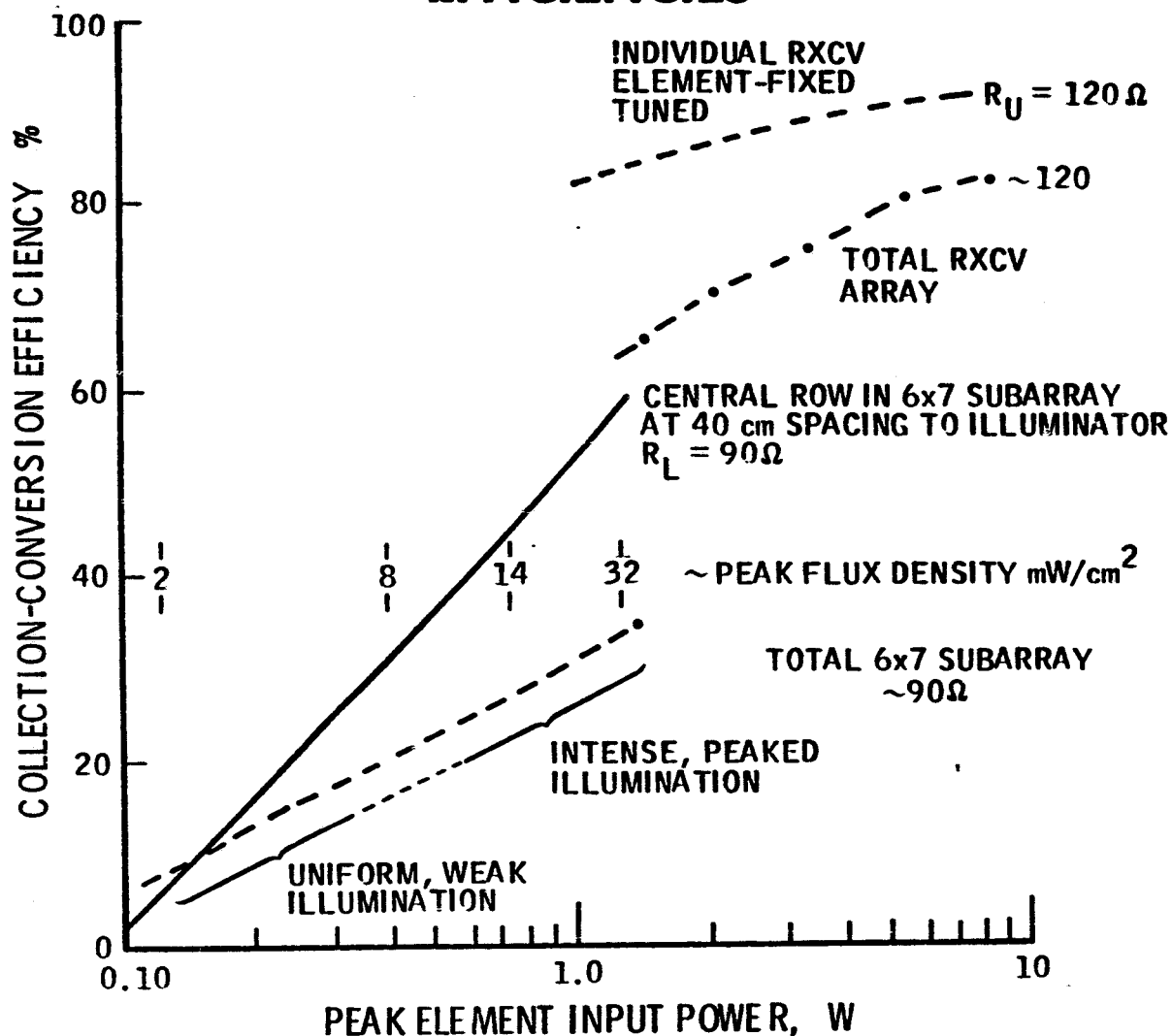


SUBARRAY OPERATING CONDITIONS & PERFORMANCE AT 2.45 GHz

CURVE	ILLUMINATOR SPACING, cm	LOAD RESISTANCE Ω	PEAK FLUX DENSITY mW/cm^2	TOTAL DC POWER OUTPUT, W	COLLECTION-CONVERSION EFFICIENCY %
1	80	15	2	1.29	7.4
2	40	7.5	8	2.9	16.7
3	40	15	8	3.63	21
4	20	15	14	3.51	27
5	20	7.5	32	3.97	19.8
6	20	15	32	6.1	36



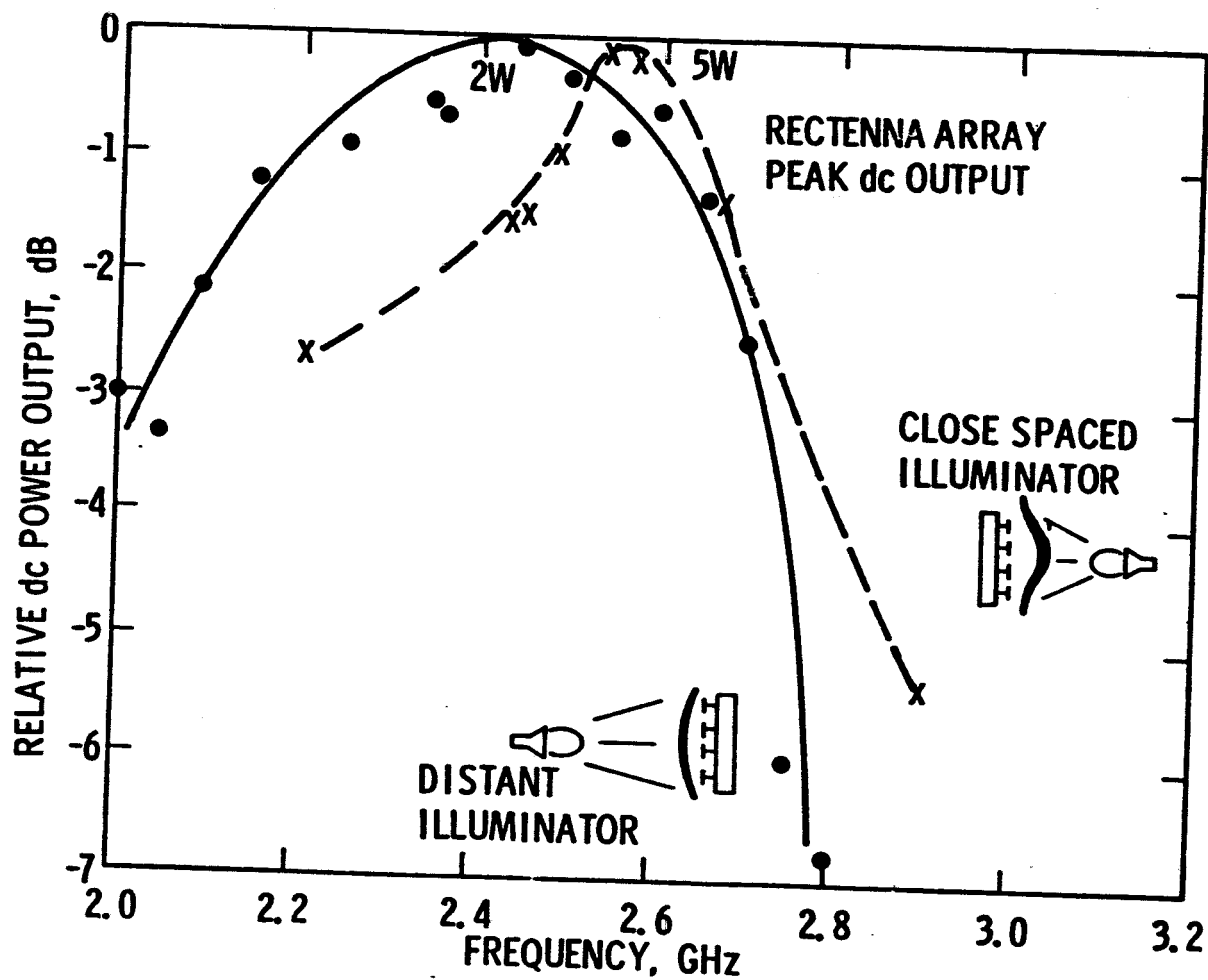
BEAMED RF POWER TECHNOLOGY RECTENNA ELEMENT, ROW AND ARRAY EFFICIENCIES





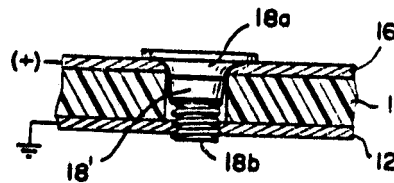
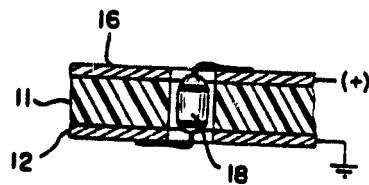
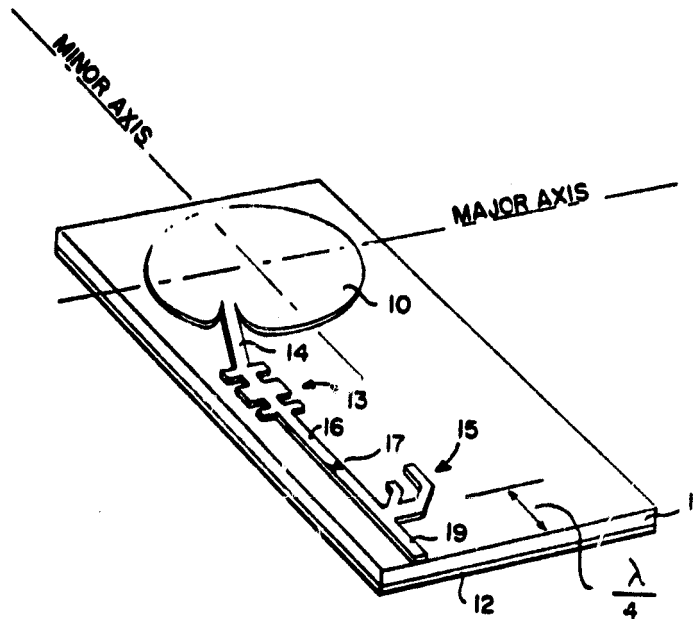
BEAMED RF POWER TECHNOLOGY

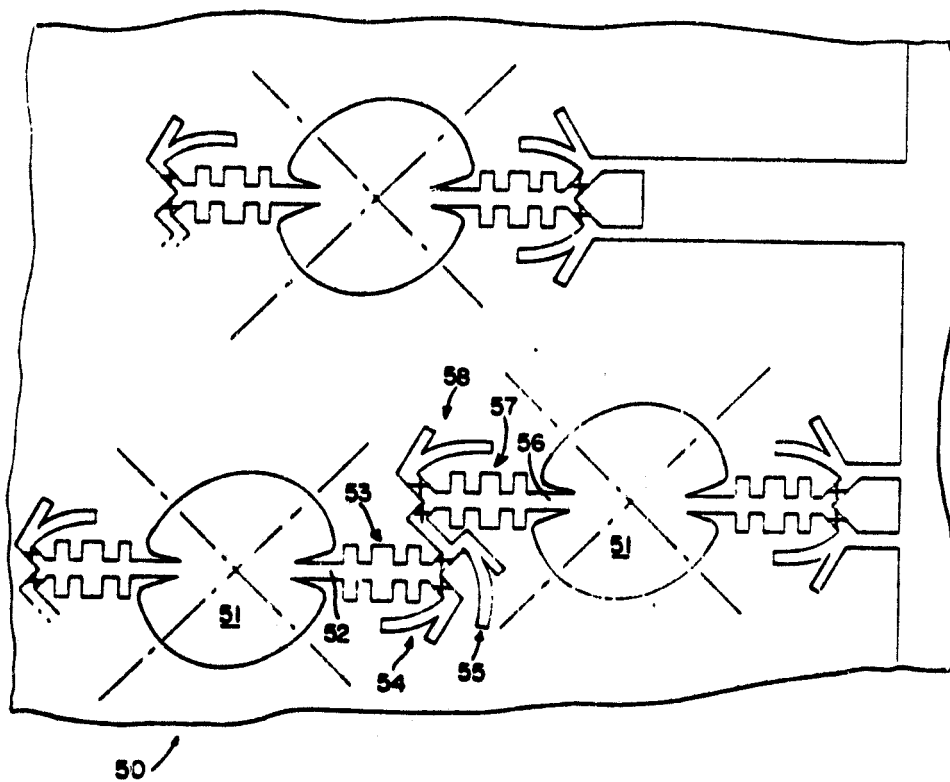
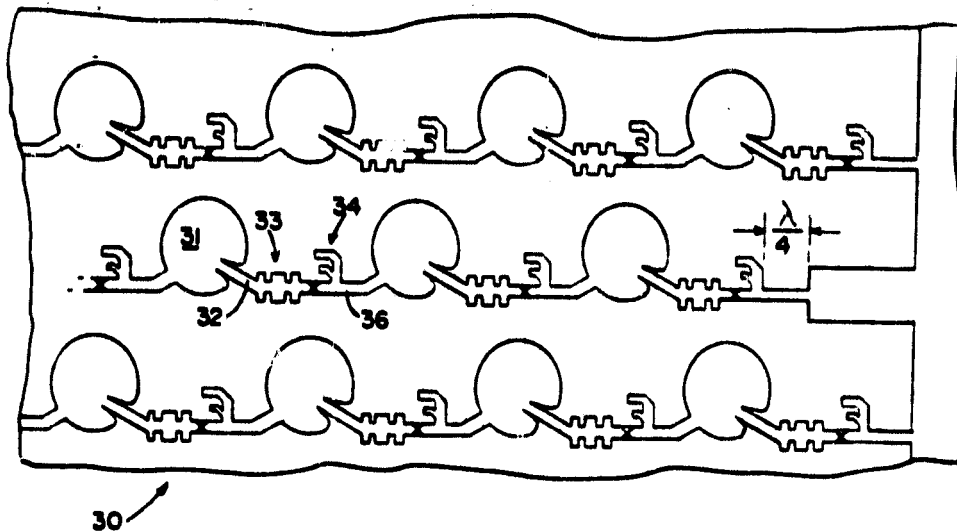
RECTENNA BANDWIDTH

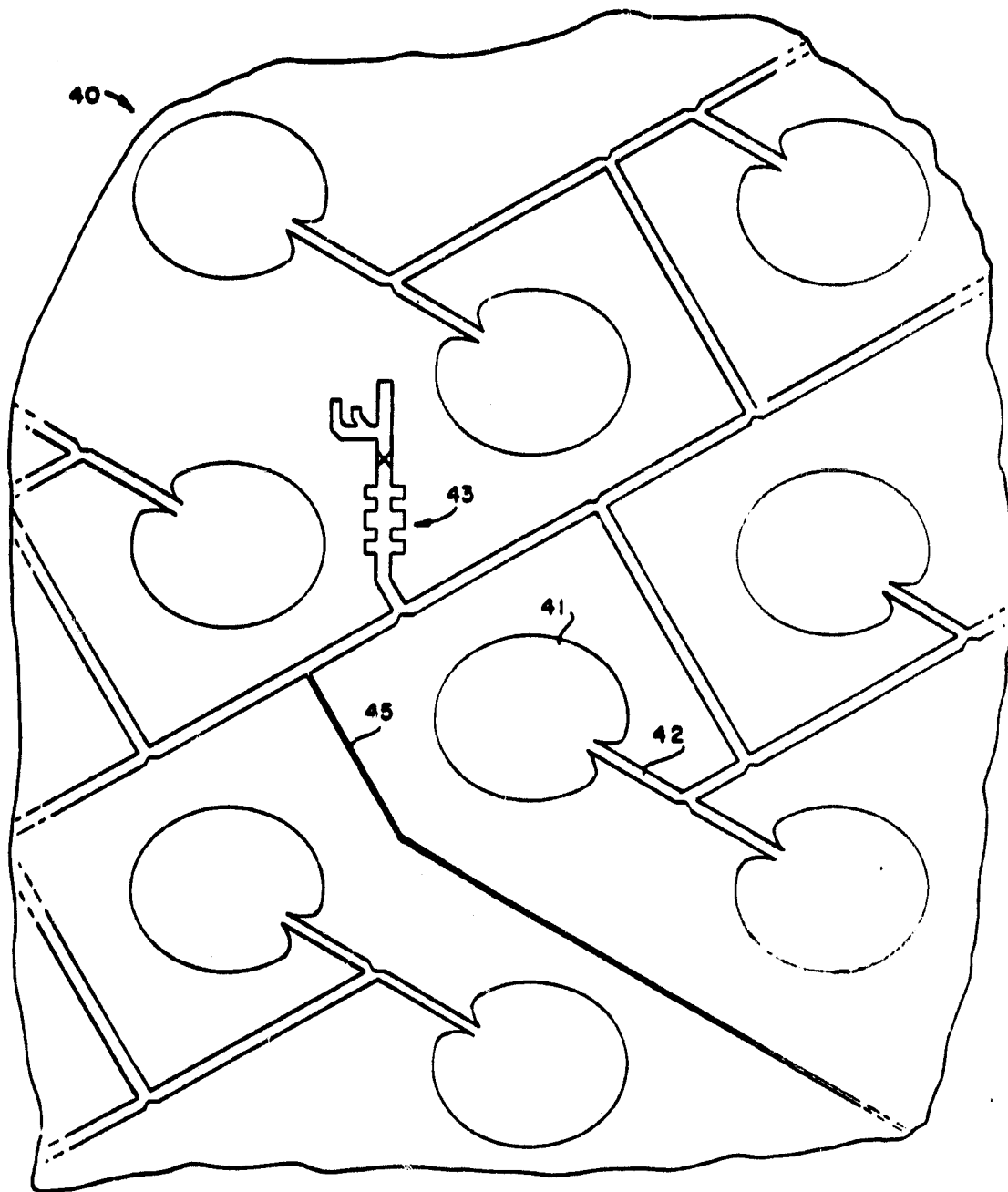


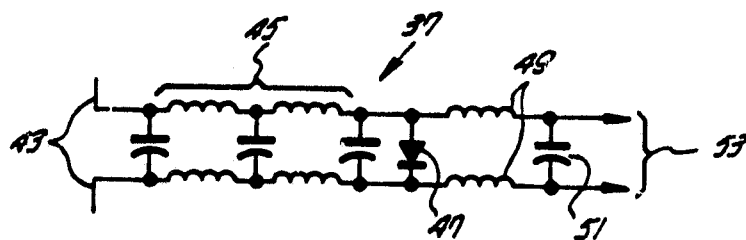
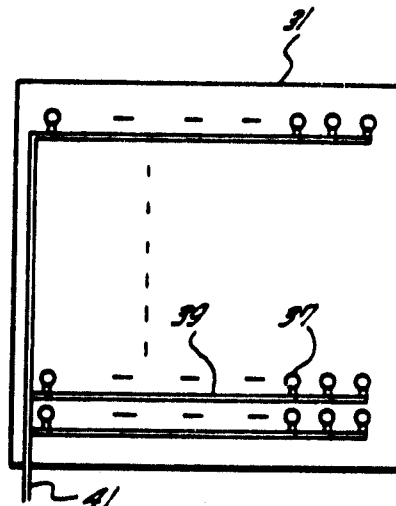
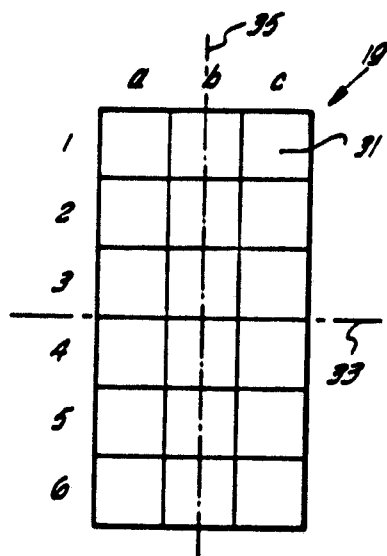
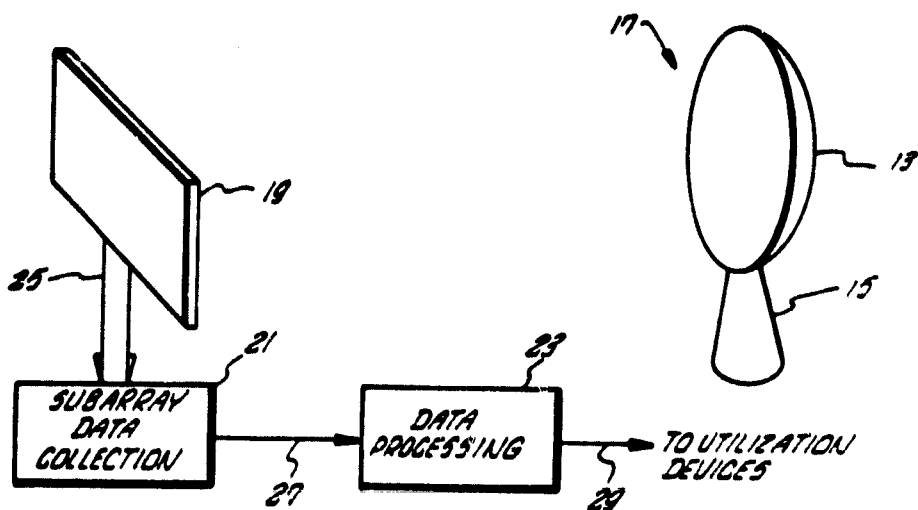
R. M. DICKINSON

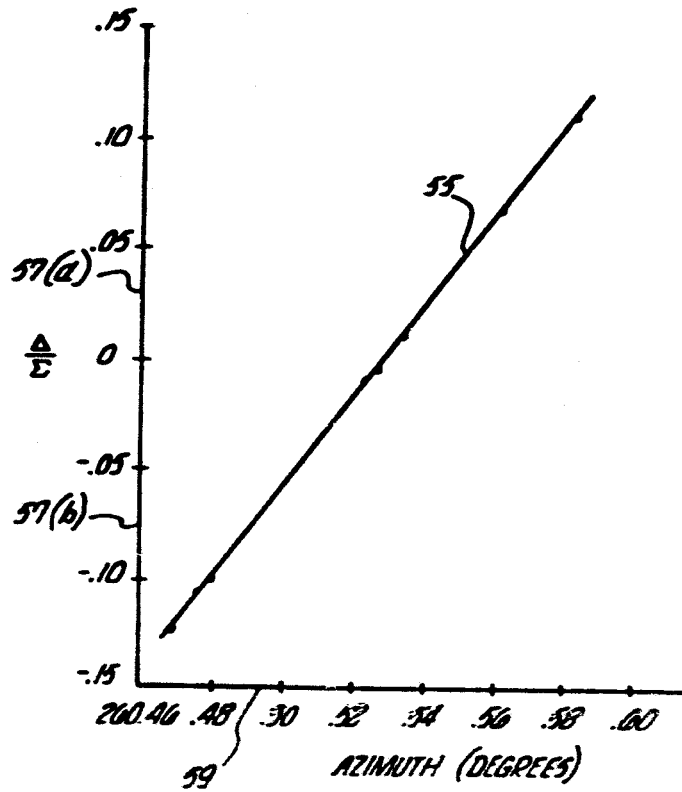
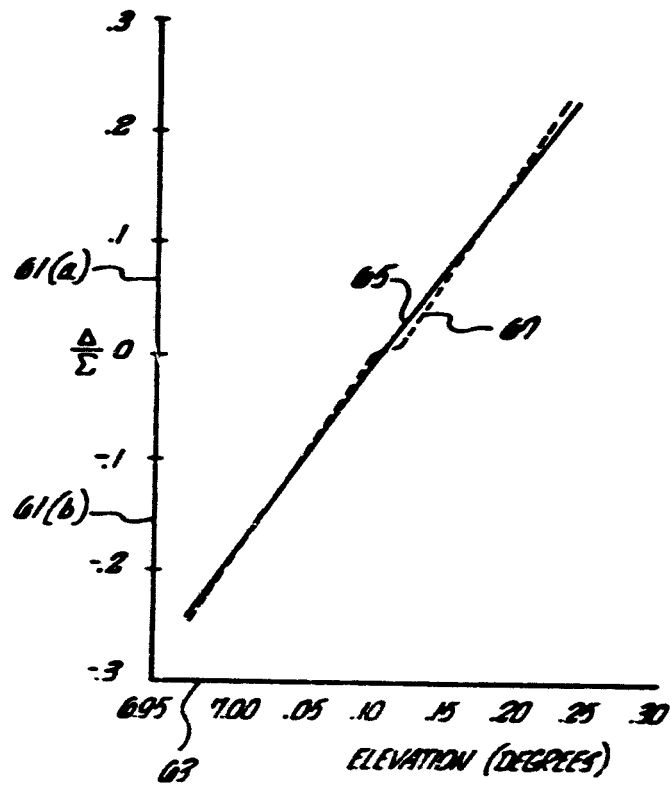
SPS ASSESSMENT REVIEW













The presentation material herein was used in the Solid State Configurations Session of the Solar Power Satellite Workshop on Microwave Power Transmission and Reception held at the Lyndon B. Johnson Space Center, January 15-28, 1980. The workshop was conducted as part of the technical assessment process of the DOE/NASA Solar Power Satellite Concept Evaluation Program. All aspects of Solar Power Satellite microwave transmission and reception were addressed including studies, analyses, and laboratory investigations. Conclusions from these activities were presented as well as recommended follow-on work. The workshop was organized into eight sessions as follows:

- *General*
- *Microwave System Performance*
- *Phase Control*
- *Power Amplifiers*
- *Radiating Elements*
- *Rectenna*
- *Solid State Configurations*
- *Planned Program Activities*

The material contained herein supplements the workshop papers which were published and distributed at the time of the workshop. Together they are a comprehensive documentation of the numerous analytical and experimental activities in the field of microwave power transmission and reception.

● *Additional information regarding the workshop may be obtained by contacting: R.H. Dietz*

EE4/SPS Microwave Systems
National Aeronautics &
Space Administration
Lyndon B. Johnson Space Center
Houston, Texas 77058
713 483-4507

7

Solid State Configurations Session contents

1	MSFC Solid State Activity W. Finell, Marshall Space Flight Center
23	Reference System with Solid State Antenna and Power Combining Dr. Erv Nalos, Boeing
71	Solid State Systems Concepts K. Schroeder and Petroff, Rockwell International
129	Analysis of Solid State S-Band D. Weir, RCA
159	Solid State Sandwich Concept O. Maynard, Raytheon

21
MSFC
Solid State Activity

Pb.

W. Finnell
Marshall Space Flight Center

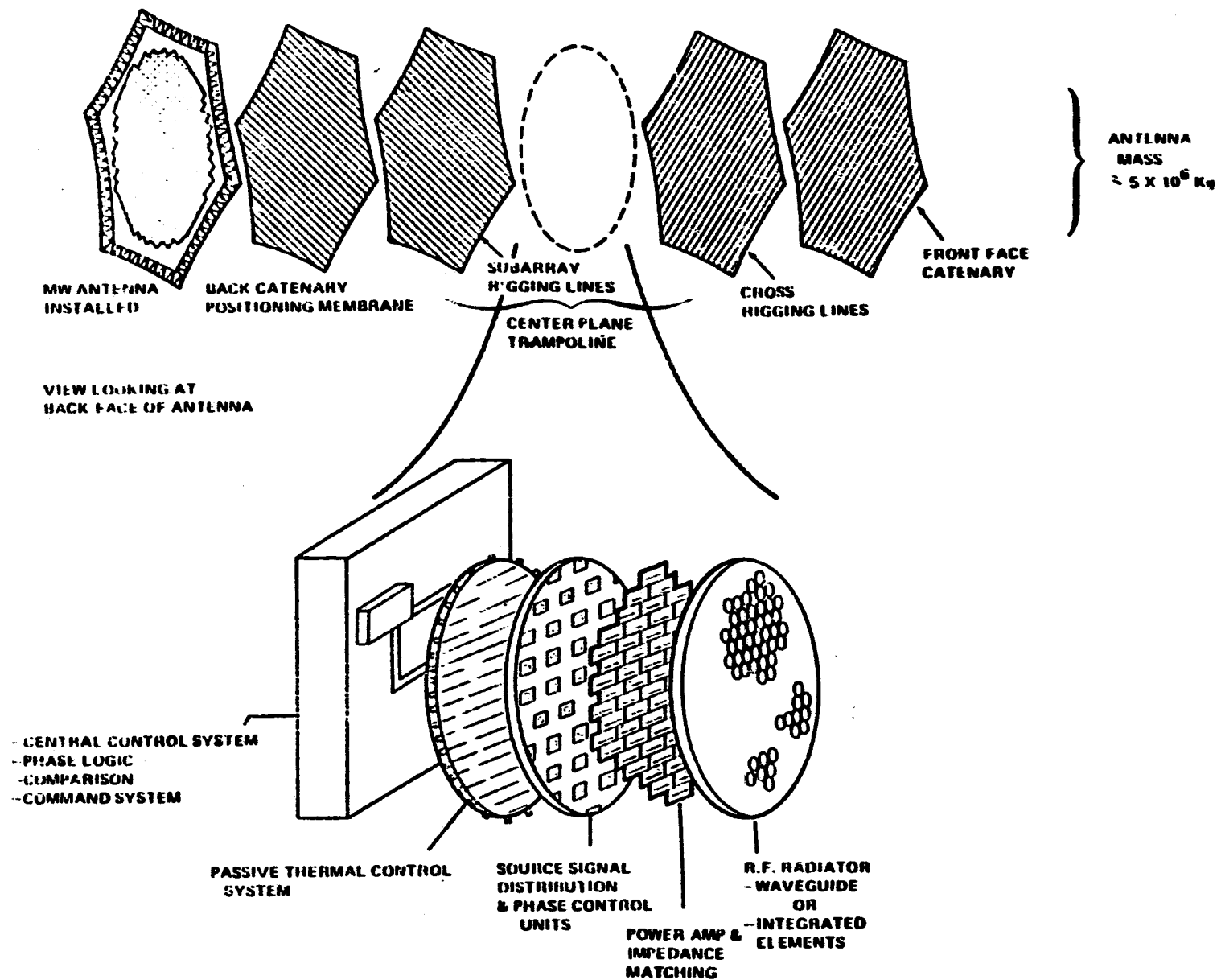
MSFC SOLID STATE ACTIVITY

WHY SOLID STATE

- o HIGHER RELIABILITY THAN TUBES
(- 10^6 HOURS VS. 10^4 HOURS)**
- o TECHNOLOGY BASE**
- o POTENTIAL FOR LOW COST**
- o SYSTEM COSTS OPTIMIZES AT LOWER POWER OUTPUT
AT UTILITIES (1.0-1.5 GW)**
- o POTENTIAL FOR REDUCING FRONT END COST**
- o MORE EASILY ADAPTABLE TO FLIGHT/GROUND TEST**
- o START-UP - SHUT-DOWN**

PRECEDING PAGE BLANK NOT FILMED

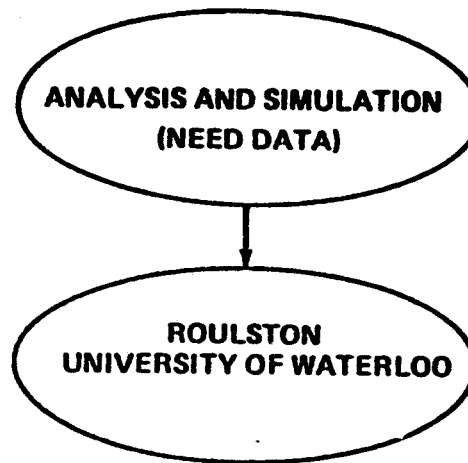
MSFC SOLID STATE ANTENNA USING ROCKWELL SUSPENSION FRAME STRUCTURE



MSFC SOLID STATE ACTIVITY

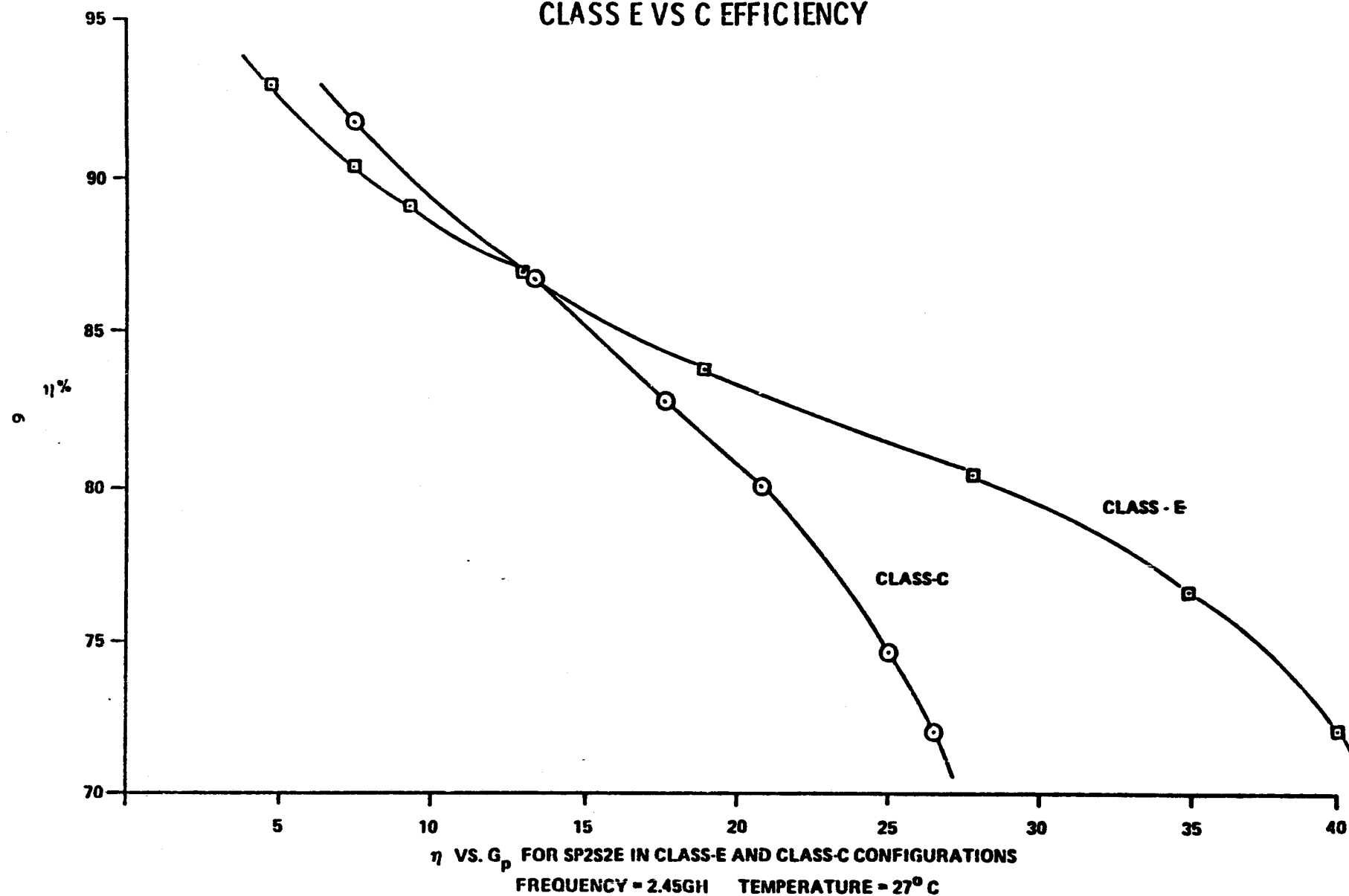
CAN WE HAVE A SOLID STATE DEVICE THAT MEETS SPS REQUIREMENTS?

HOW DO WE GET THERE?

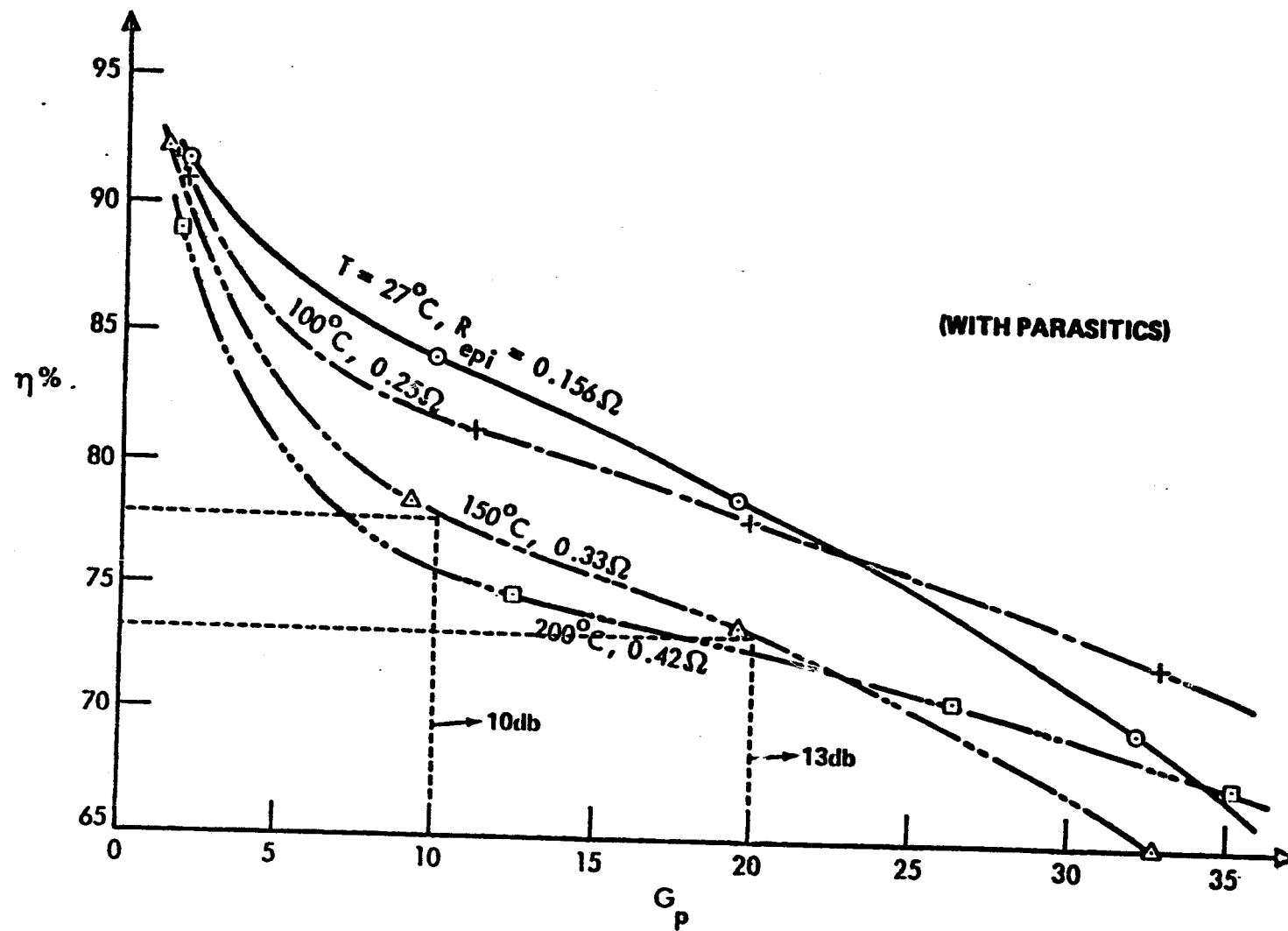


- DEVICE PERFORMANCE PREDICTIONS**
- DEVICE OPTIMIZATION**
- DESIGN DATA**

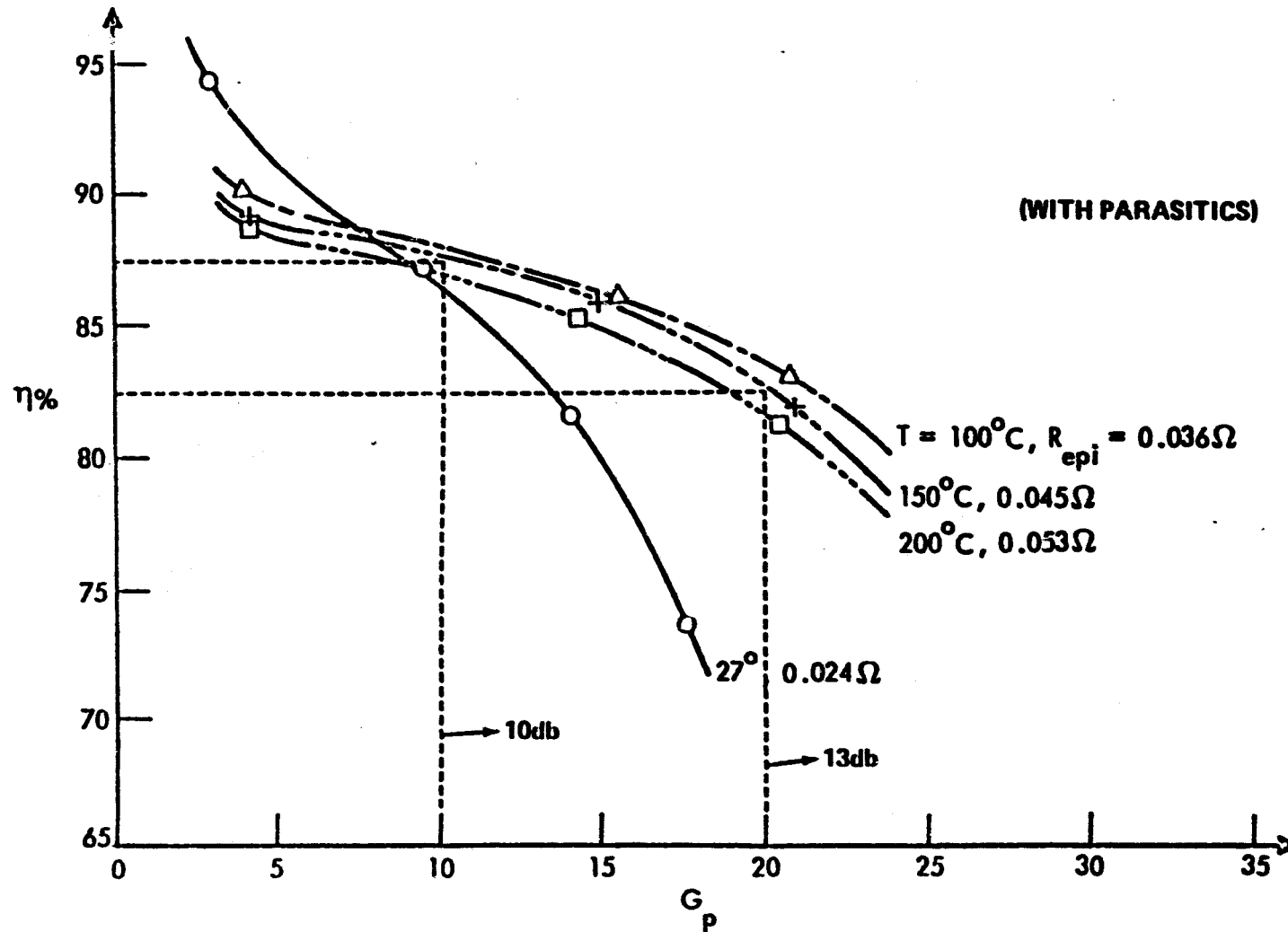
MSFC SOLID STATE ACTIVITY CLASS E VS C EFFICIENCY



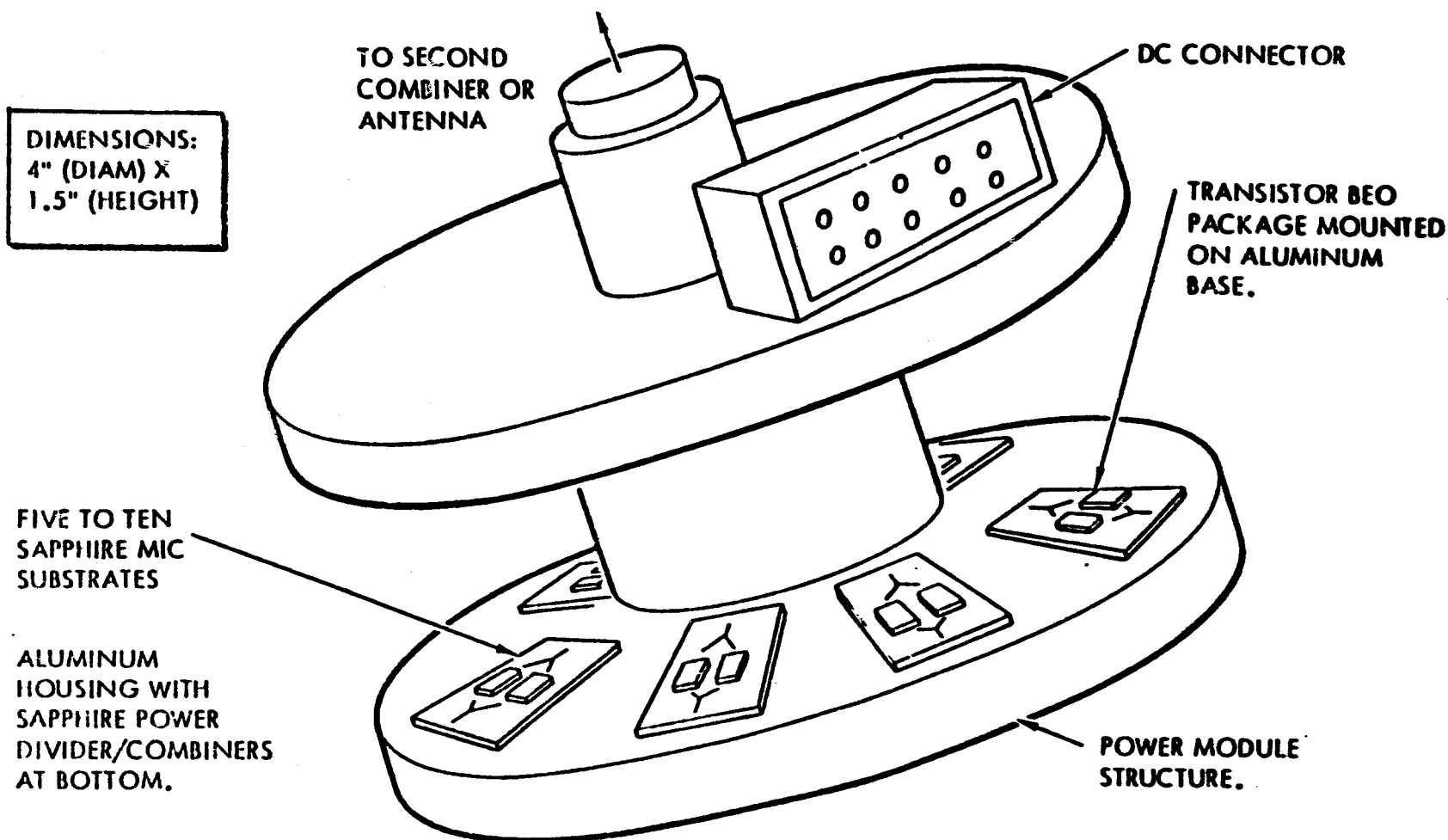
MSFC SOLID STATE ACTIVITY
HIGH TEMPERATURE STUDY (SILICON, 2.45 GHz)
BIPOLE-WATAND



MSFC SOLID STATE ACTIVITY
HIGH TEMPERATURE STUDY (GaAs, 2.45 GHz)
BIPOLE-WATAND

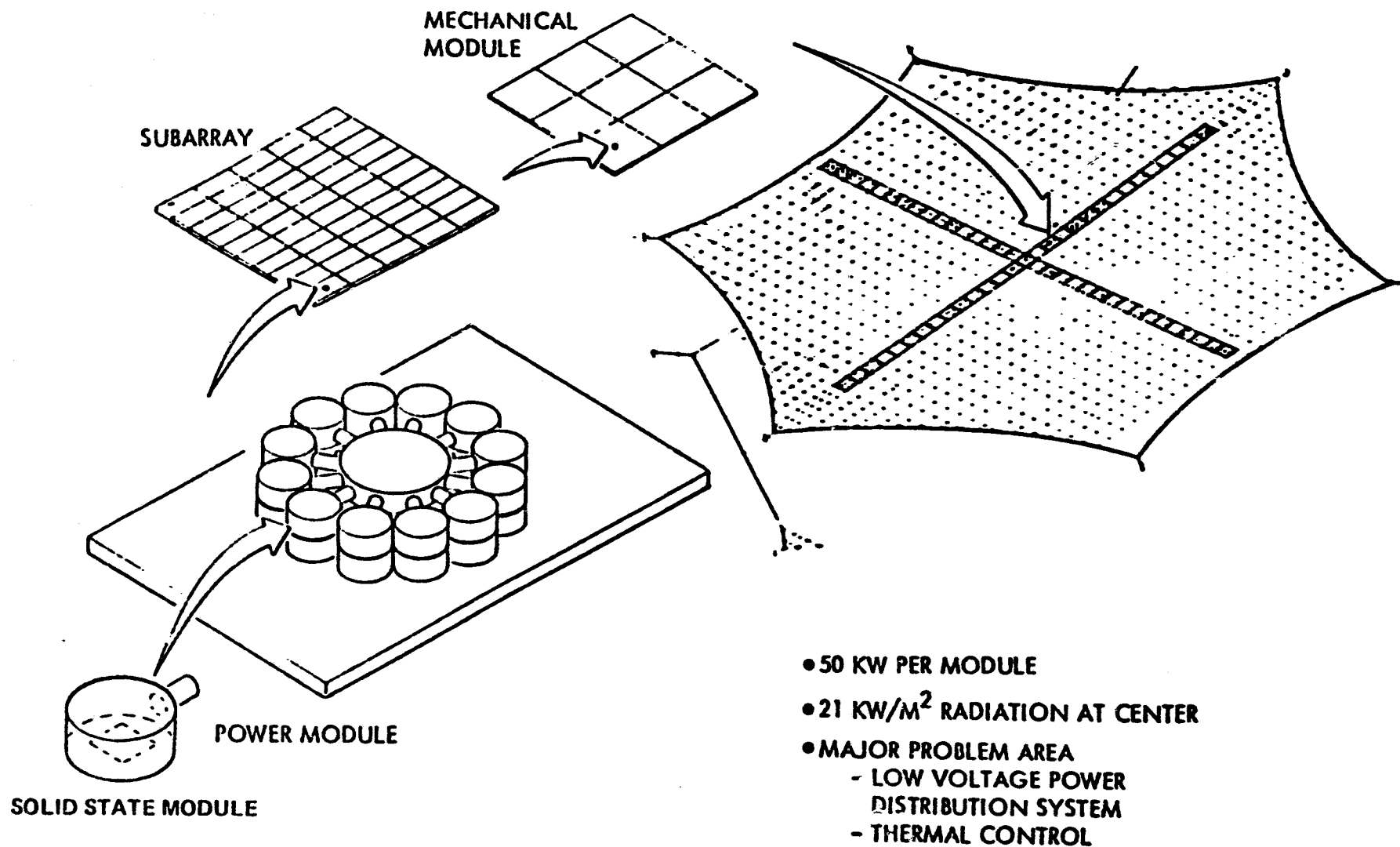


MSFC SOLID STATE ACTIVITY MODULE AMPLIFIER CONFIGURATION



POWER MODULE BASE TEMPERATURE: 275°C TO 285°C (GAUSSIAN)
(PRELIMINARY CALCULATIONS) 160°C TO 170°C (UNIFORM-LARGER ARRAY)

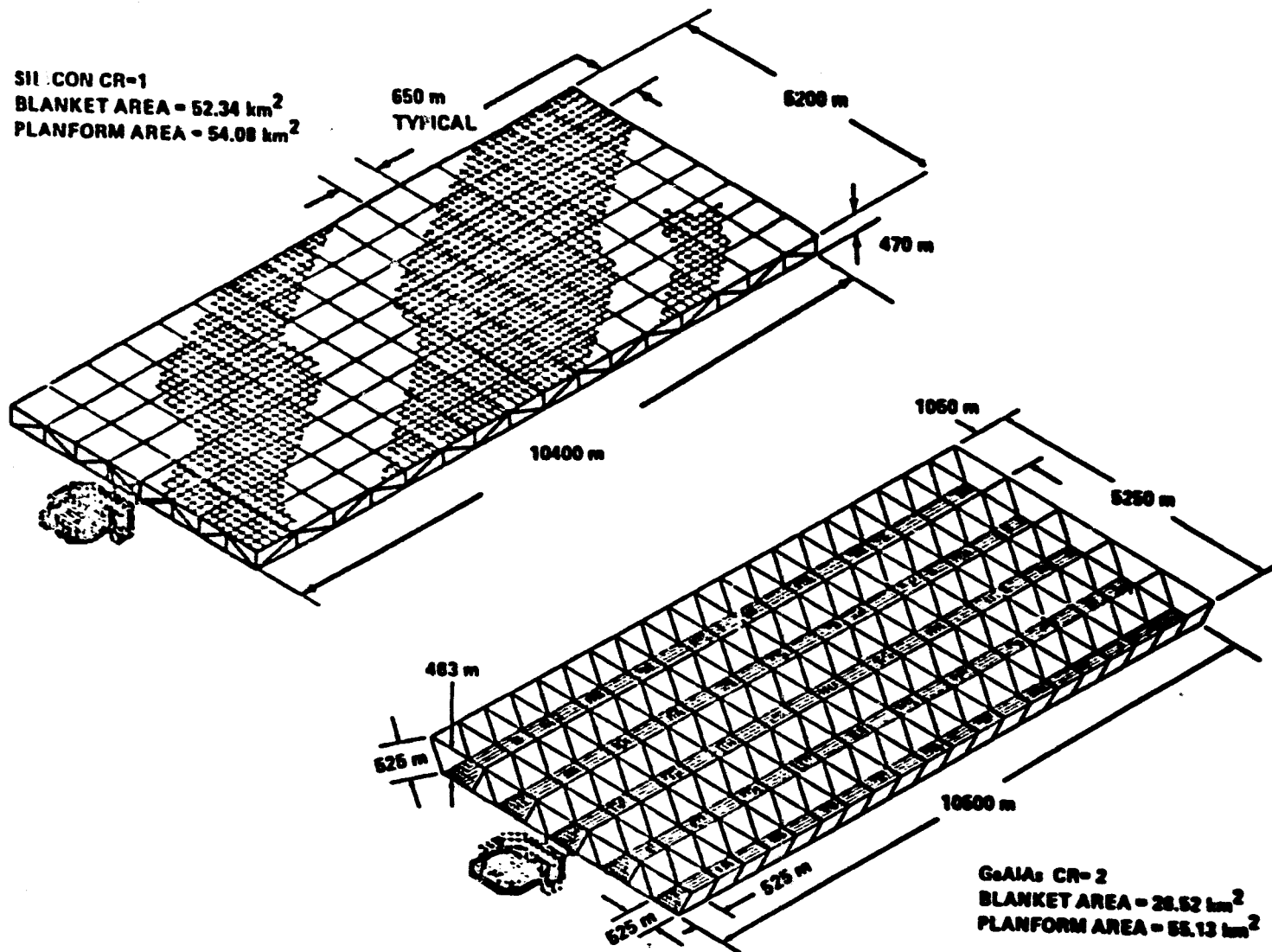
MSFC SOLID STATE ACTIVITY SOLID STATE ANTENNA CONCEPT



**MSFC SOLID STATE ACTIVITY
SOLID-STATE MASS PROPERTY IMPACTS**

	<u>Δ MASS, 10^6 KG</u>	
	<u>MINIMUM</u>	<u>MOST LIKELY</u>
POWER DISTRIBUTION (40 KV TO 40 V CONVERTERS)	4.0	8.0
THERMAL (RADIATORS)	5.5 (150°C)	13.0 (60°C)
SOLAR ARRAY	<u>1.0</u>	<u>1.0</u>
Δ MASS	10.5	22.0
30% GROWTH	<u>3.1</u>	<u>6.6</u>
TOTAL Δ MASS	13.6	28.6

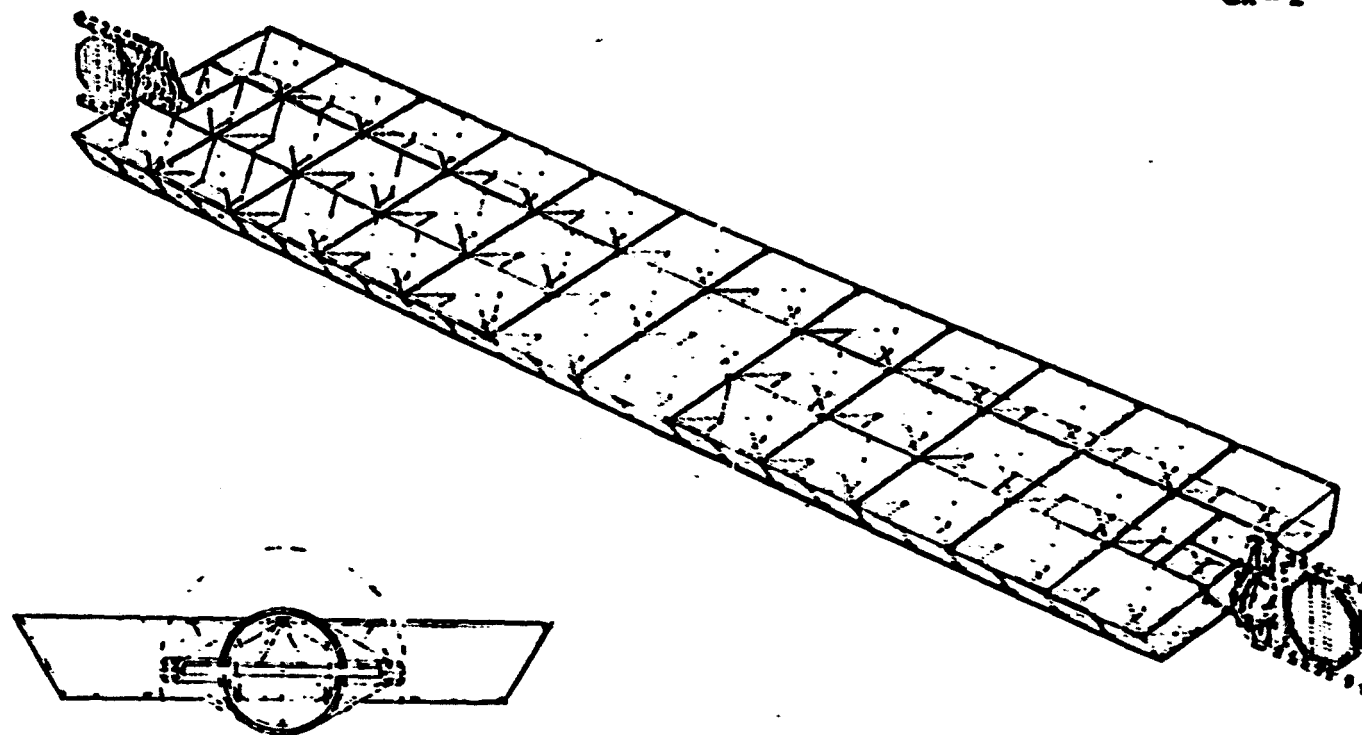
LARGE MASS INCREASES
DRIVE TOWARD NEW
SOLID-STATE CONCEPTS



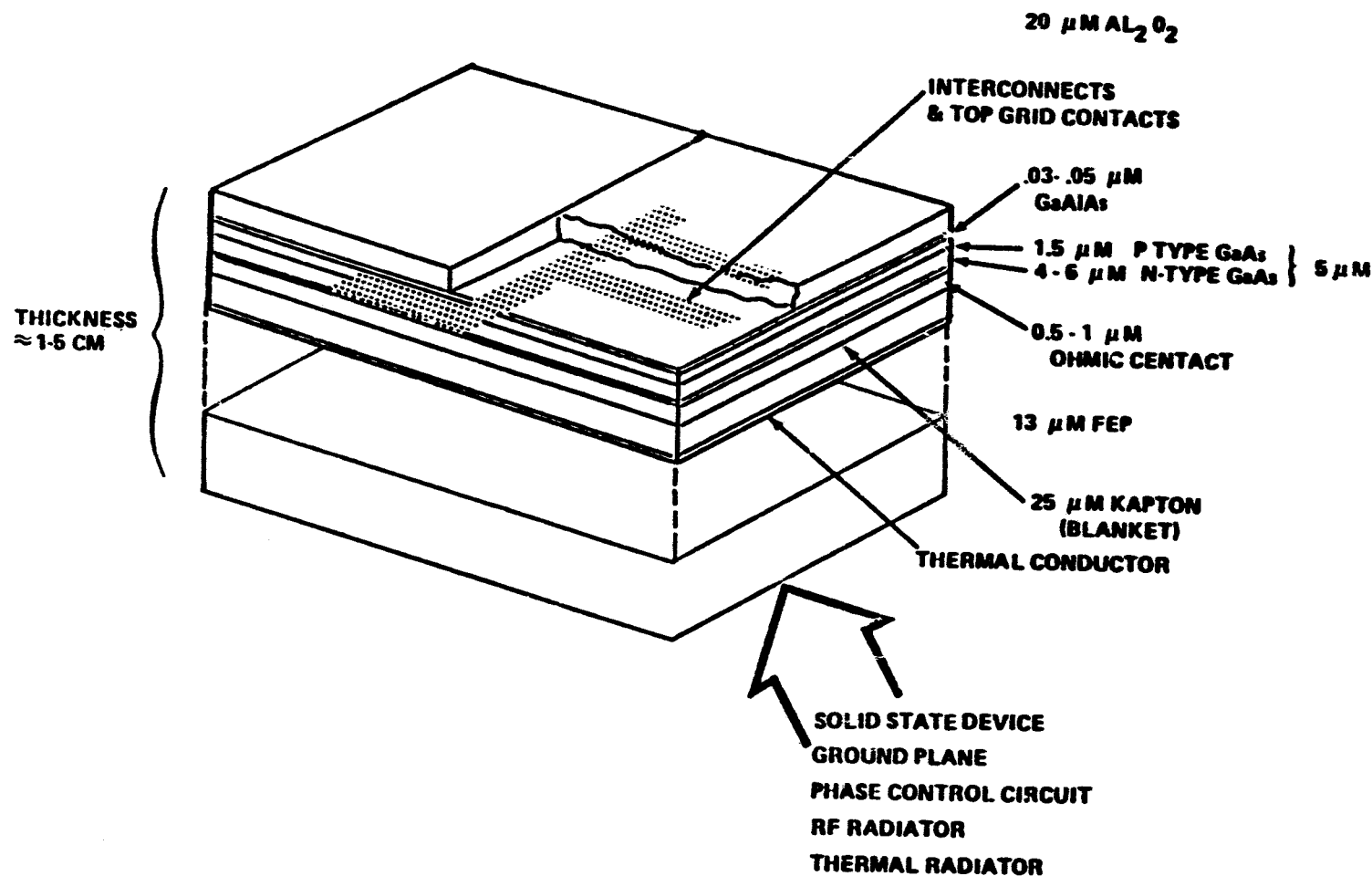
SPS Reference System - Satellite Configuration

SOLID STATE SATELLITE CONCEPT

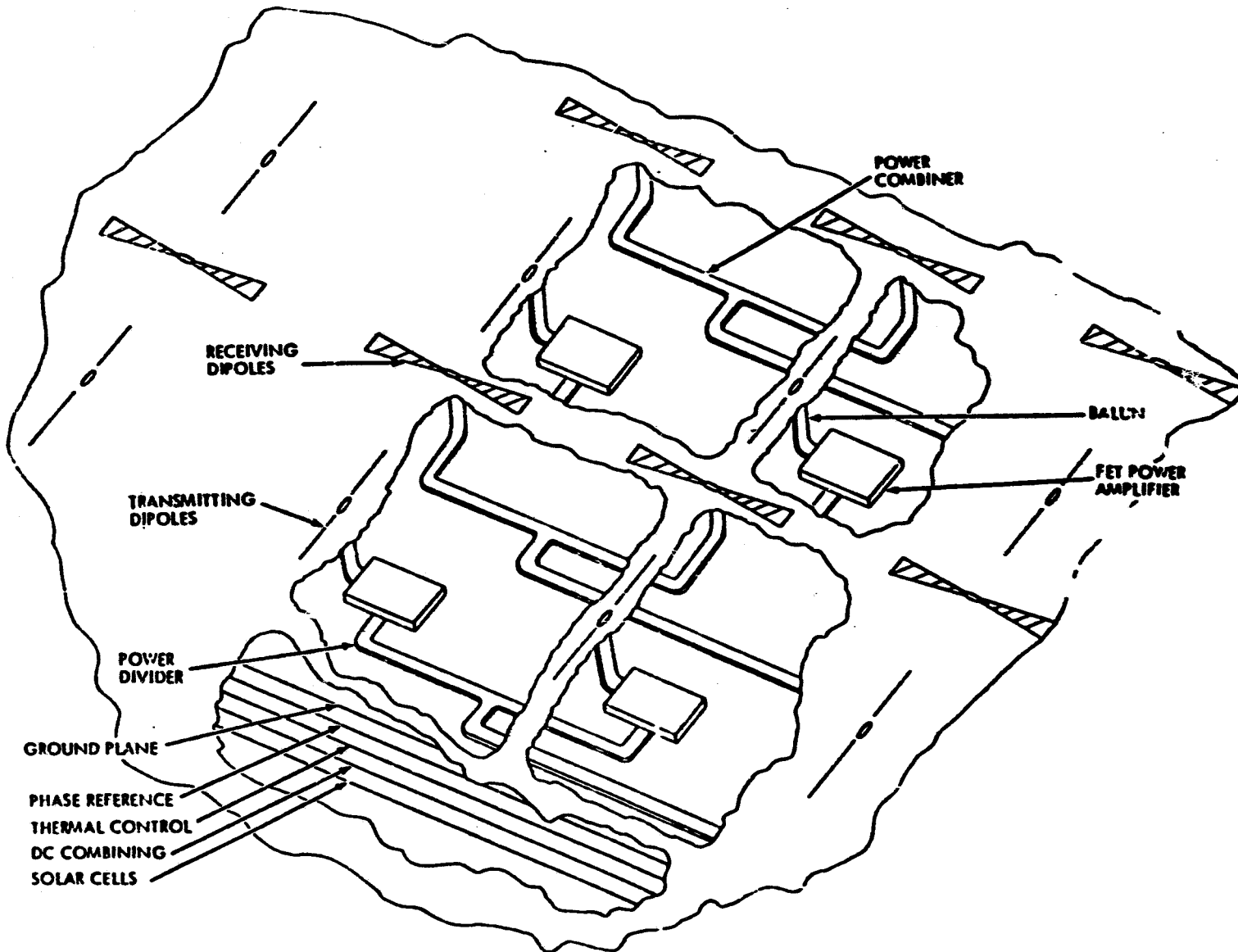
CR-2



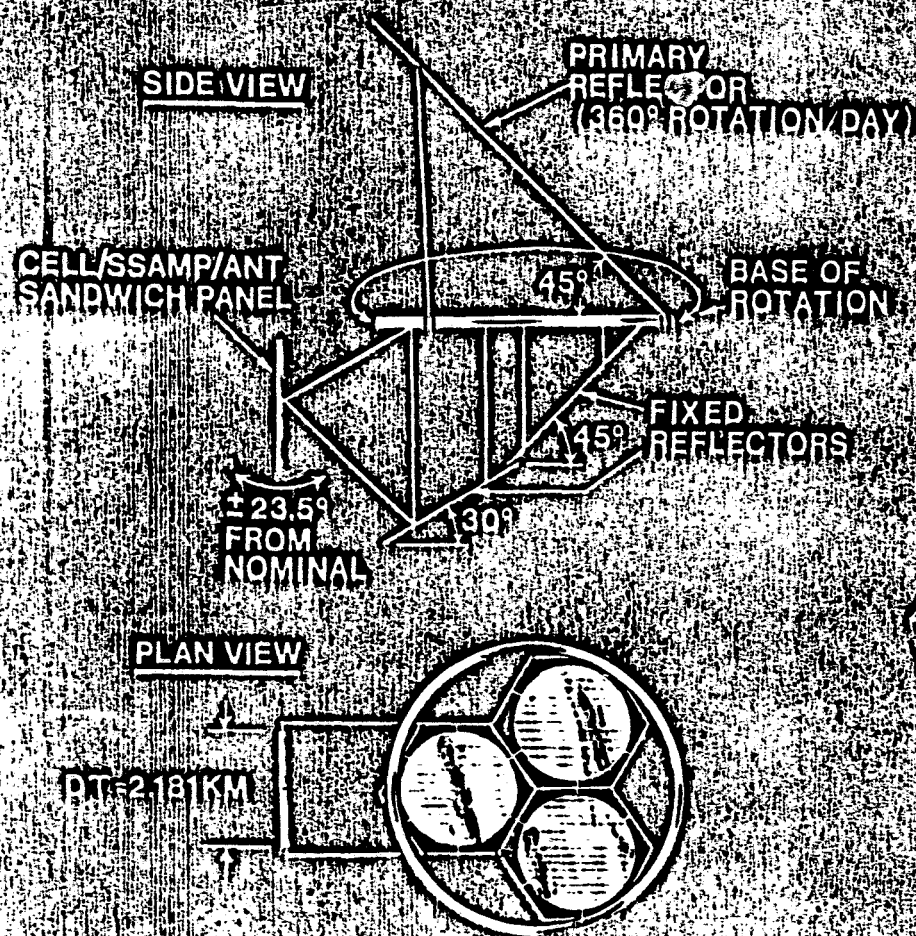
MSFC SOLID STATE ACTIVITY SOLID STATE SOLAR CELL SANDWICH (CANDIDATE CONCEPT)



SPACETENNA - DIPOLE CONCEPT



SOLID STATE SOLAR CELL SANDWICH CONCEPT



ORIGINAL PAGE IS
OF POOR QUALITY

SOLID STATE SOLAR CELL SANDWICH CR-4 CONCEPT

SIDE VIEW

10.5 x 7.5 km

SUPPORT
STRUCTURE

1.8 km DIA SOLAR
ARRAY AND
ANTENNA

2.5 x 1.6 km

2.5 x 1.6 km

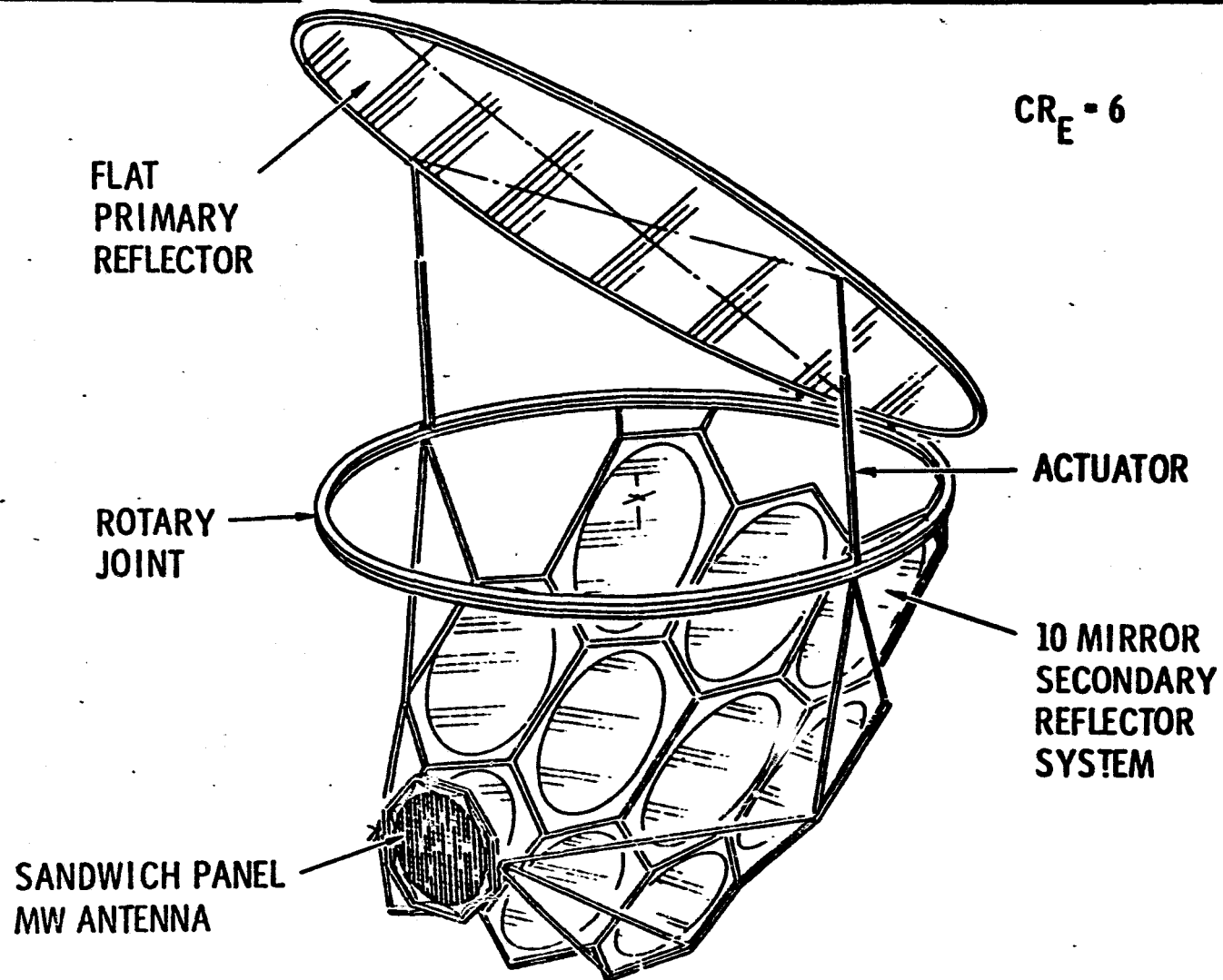
PLAN VIEW

8.2 x 1.7 km

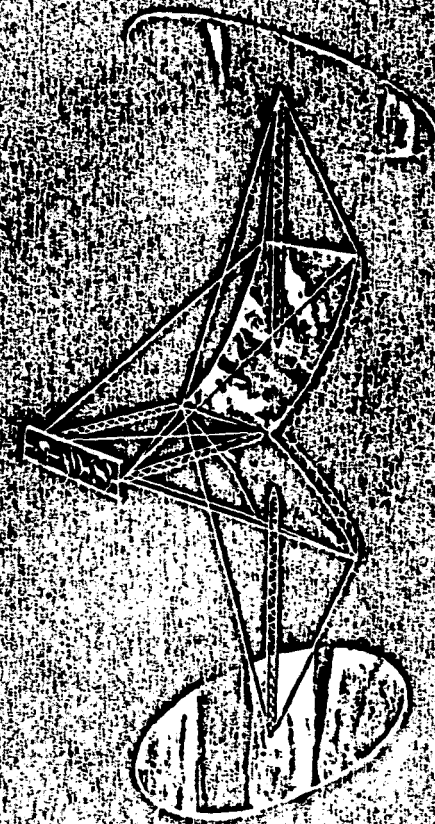
8.2 x 1.8 km

ORIGINAL PAGE IS
OF POOR QUALITY

INTEGRATED CONCEPT



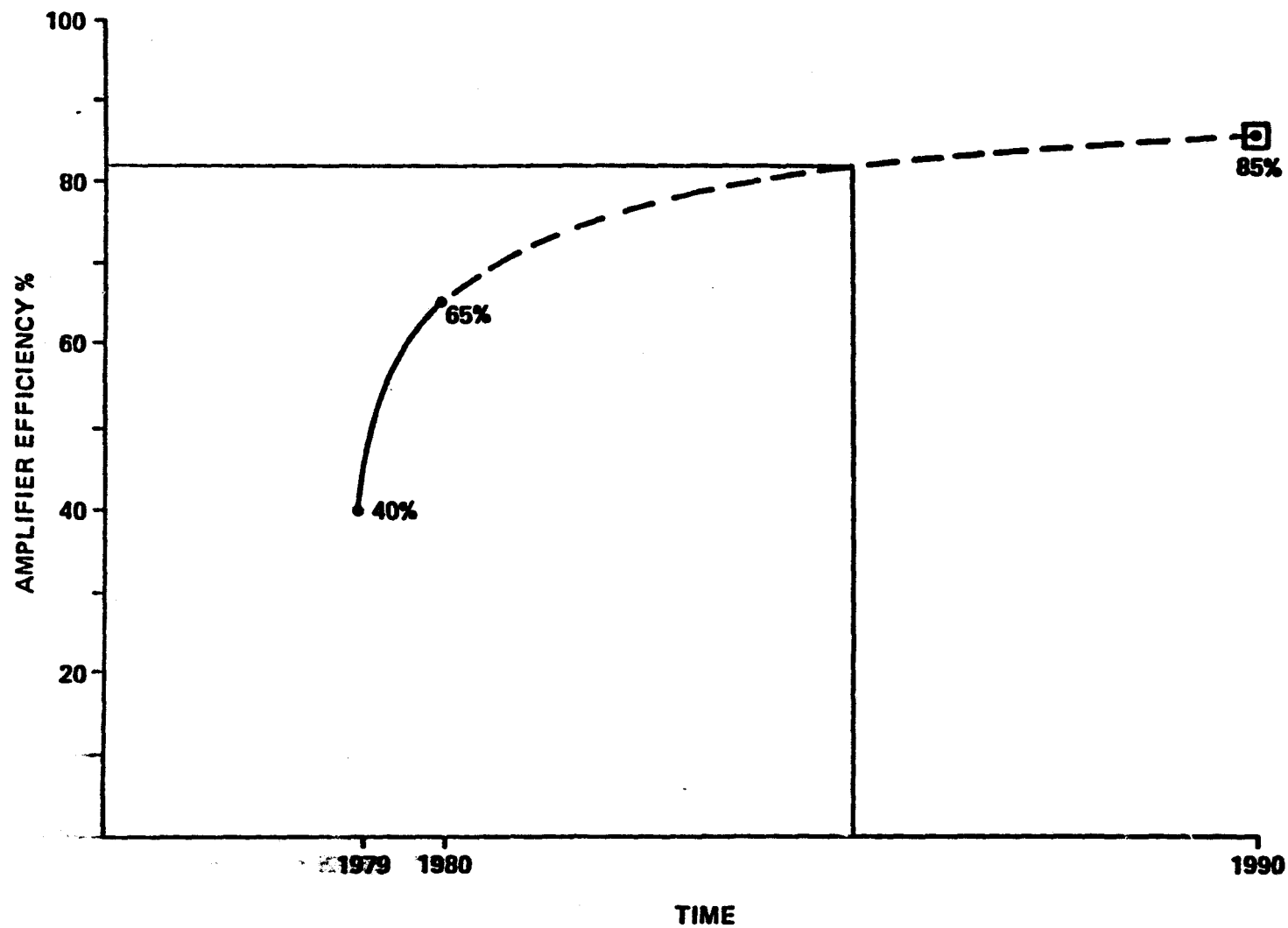
SPS DOUBLE PARABOLIC CONCENTRATOR FOR SANDWICH ANTENNA



R. BELEW
MARCH 479

ORIGINAL PAGE IS
OF POOR QUALITY

PROJECTED EFFICIENCY



SOLID STATE CONCLUSIONS

1. Solid state SPS concepts have not had the same depth of systems definition as the reference concept; however, preliminary results indicate the following.
 - a. The system sizing parameters optimize such that lower power is delivered to the utility grid.
 - b. The transmit antenna is larger primarily because of the thermal limitations.
 - c. The rectenna land requirement is smaller.
 - d. Weight per delivered kilowatt is projected to be more.
 - e. Maintenance projections are better because of the higher reliability.
2. Type of Power Amplifier - Based on studies to date, the GaAs FET is the preferred solid state power amplifier.
3. Antenna Unit Costs - Solid state antennas will have high parts count similar to the solar array, and therefore unit costs are a critical item.
4. Mitigating Designs - Conceptual designs have to some degree mitigated the issues of thermal and low voltage power distribution.
5. Items of Concern - Techniques of phase distribution, (possibly to more points on the array), and power distribution (on the end mounted configuration more DC-to-DC converters are required) are major items of concern in the solid state concept.
6. Technology - Associated technology development is more likely for solid state due to the advancing technology base.
7. Continued Investigation - Based on current findings, continued investigation of solid state concepts and issues is warranted.

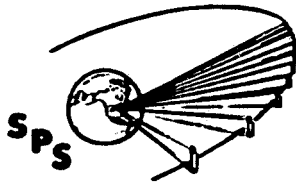
SOLID STATE ISSUES

- o Efficiency
- o Operating Temperature
- o Low Voltage Distribution
- o Harmonic Noise Suppression
- o Power Combining
- o Subarray Size
- o Monolithic Technology
- o Life Time
- o Mutual Coupling
- o Amplifier gain
- o Input to Output Isolation
- o Charge Particle and UV Radiation Effects

D2

***Reference System with Solid State
Antenna and Power Combining***

***Dr. Erv Nalos
Boeing***



Why Solid-State?

BOEING

- RELIABILITY
- LOWER MASS/AREA
- DEVELOPMENT ON SMALL HARDWARE ITEMS

BUT



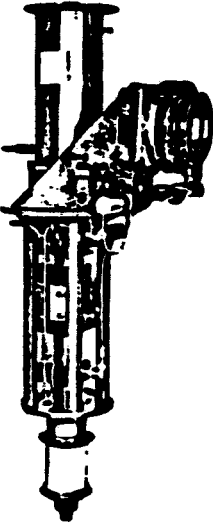
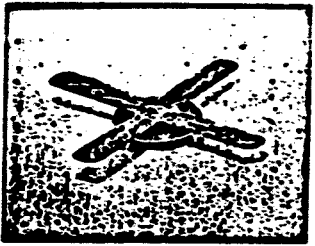
- TEMPERATURE LIMITS
- LOW VOLTAGE, LOW POWER
- EFFICIENCY?
- COST??
- COMPLEXITY??

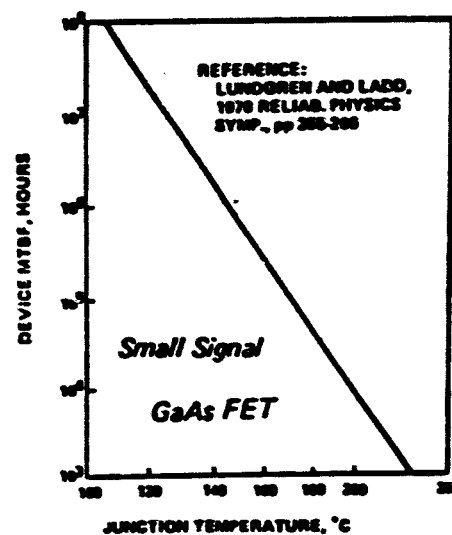
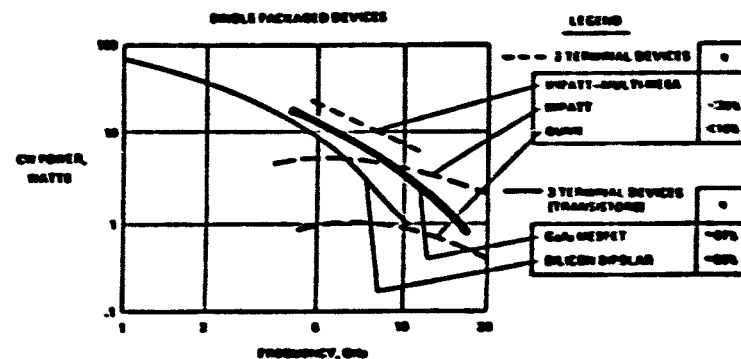
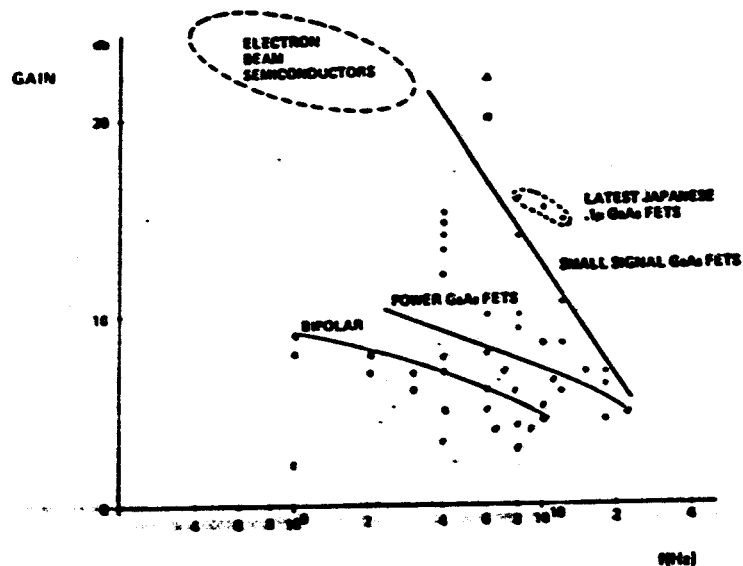
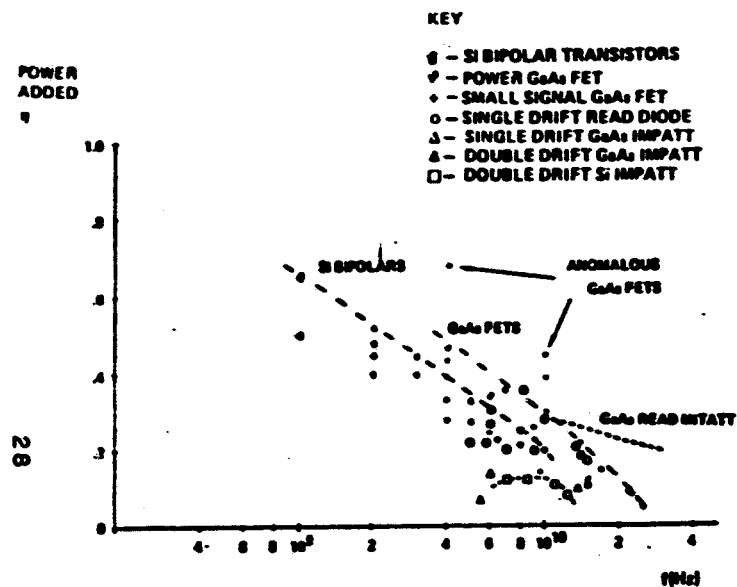
PRECEDING PAGE BLANK NOT FILMED

- 1) ADEQUATE EFFICIENCY (TYPICALLY $> .8$)
- 2) ADEQUATE GAIN (TYPICALLY > 10 DB)
- 3) LOW COST/POWER (TYPICALLY $\approx .1$ \$/WATT)
- 4) LOW MASS/POWER (TYPICALLY $< .1$ KG/KW)
- 5) ACCEPTABLE NOISE CHARACTERISTICS
 - A) CLOSE IN SPECTRUM (SHOULD HAVE MINIMAL SPREAD, RAPID FALLOFF)
 - B) WIDEBAND NOISE (MUST MEET CCIR REQUIREMENTS)

ANY SPS MICROWAVE POWER AMPLIFIER MUST SATISFY THESE
NECESSARY BUT NOT SUFFICIENT REQUIREMENTS.

DC-RF Converter Features

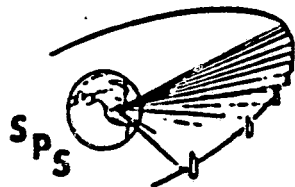
DEVICE  PROPERTY 	KLYSTRON 	CROSSED FIELD AMPLIFIER		SOLID STATE TRANSISTOR
		AMPLITRON	INJECTION LOCKED MAGNETRON	FET 
POWER (CW) VOLTAGE EFFICIENCY MTBF (1935) NO. OF OUTPUT DEVICES PER ANTENNA TEMPERATURE CATHODE SATURATION GAIN	50-70 KW 40 Kv >80% >10 YEARS 10^5 300-500°C THERMIONIC 40db	5 KW <20 Kv >85% >10 YEARS 10^6 300-500°C COLD OR THERMIQNIC <10 db		1-5 WATTS 10-20 V 75% >>100 YEARS $>10^9$ 100-130°C NONE 10 db





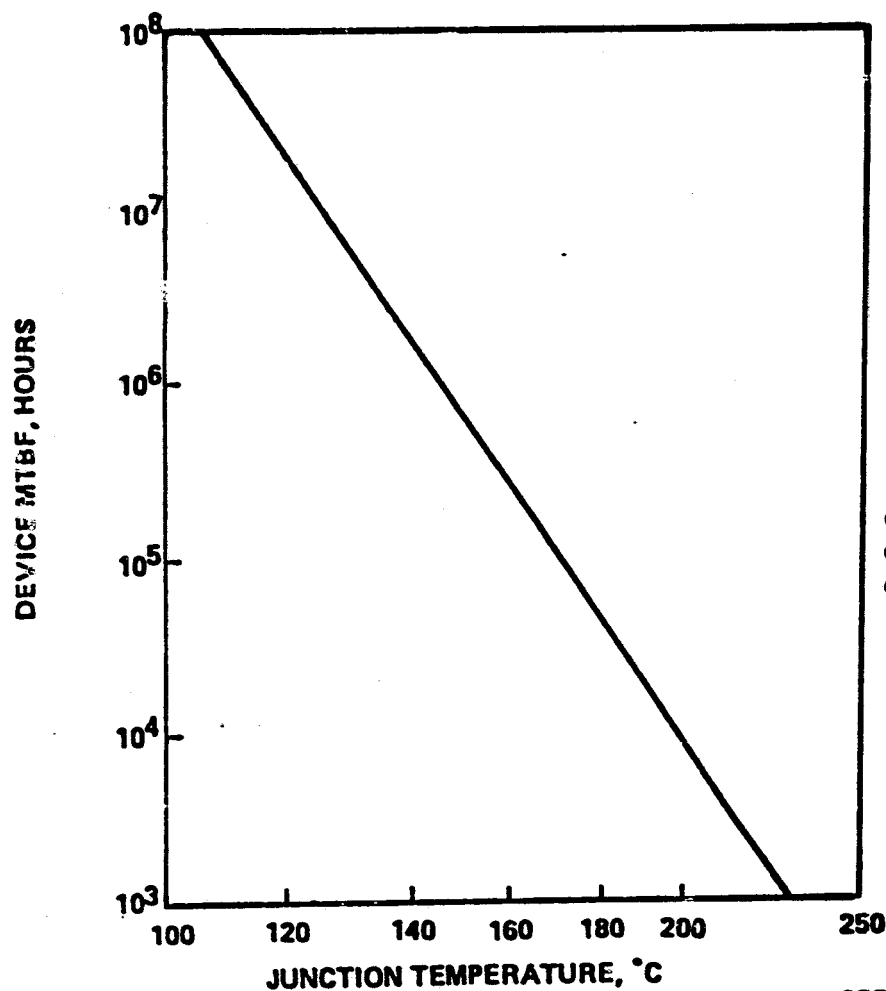
CHARACTERISTICS OF VARIOUS AMPLIFIER CLASSES

		MAXIMUM POWER-ADDED EFFICIENCY FOR SINE WAVE OUTPUT	TYPICAL EFFICIENCY VALUES ACHIEVED	TYPICAL FREQUENCY USED	DUTY CYCLE AT MAXIMUM EFFICIENCY	ACTIVE DEVICE SATURATED ?	ACTIVE DEVICE CUT OFF ?
AMPLIFIER CLASS							
A		.5	.3	4 GHz	1.0	No	No
B		.785	.5	4 GHz	.5	No	Yes
C (unsaturated)		.896	.6	2.5 GHz	.3	No	Yes
29 Switched Mode Ampli- fiers	D	1.0	.9	10 MHz	.5	Yes	Yes
	E	1.0	.9	100 MHz	.5	Yes	Yes
	F	1.0	.9	10 MHz	.5	Yes	Yes
	S	1.0	.8	100 KHz	Variable <<1	Yes	Yes
	Multivoltage	1.0	.8	10 MHz	Variable	Yes	Yes
G		.818	.7	100 KHz	Variable	No	Yes



Solid State Device Lifetime

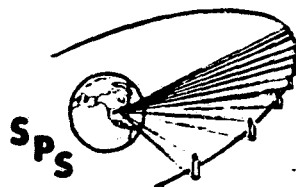
BOEING



- SMALL SIGNAL GaAs FET
- RF POWER ON DURING TEST
- LOG NORMAL FAILURE DISTRIBUTION

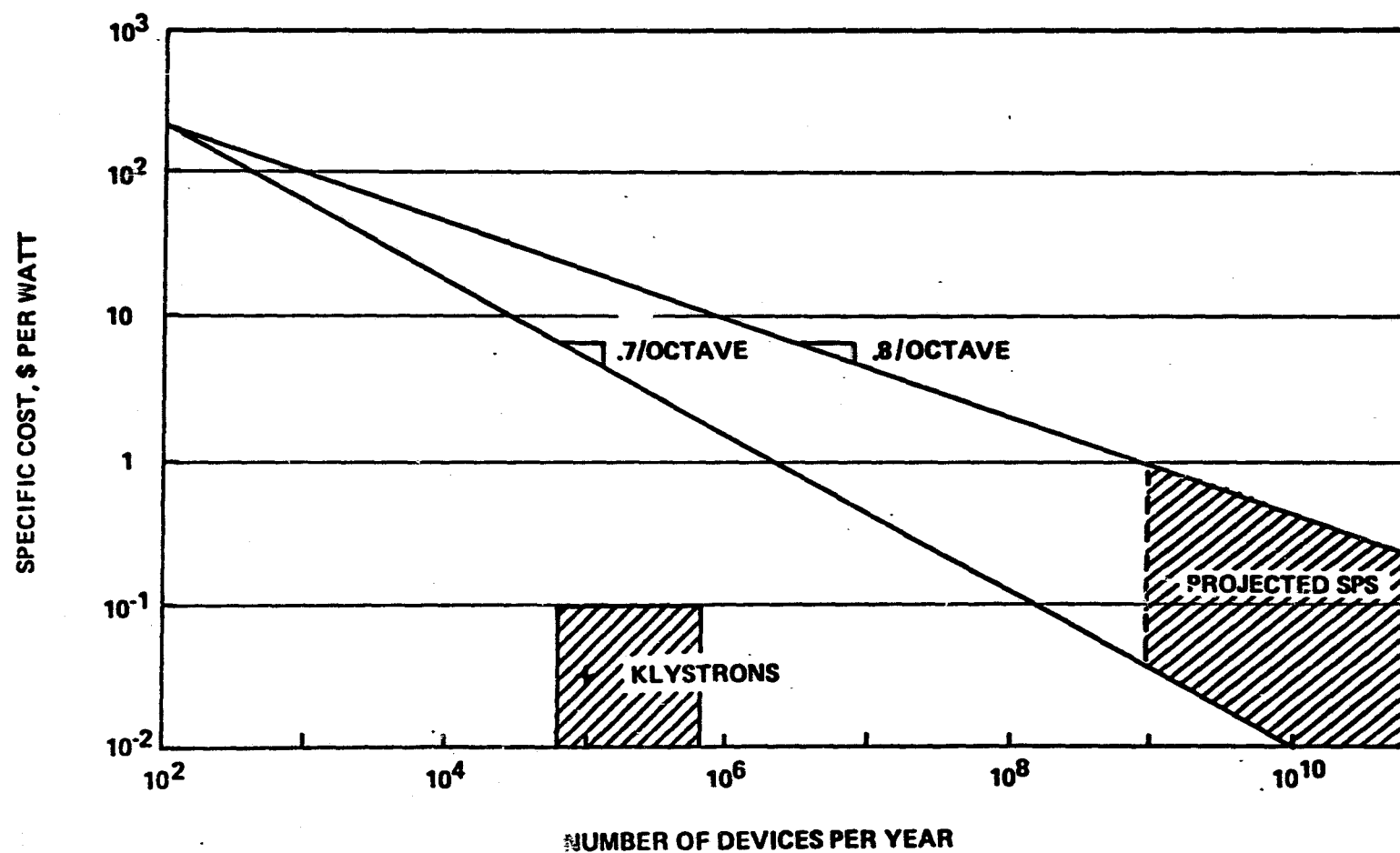
$$\sigma = 1$$

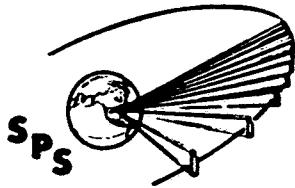
REFERENCE: LUNDGREN AND LADD, PROCEEDINGS OF
IEEE 1978 RELIABILITY PHYSICS SYMPOSIUM



Solid State Device Mature Industry Costing

BOEING





COMBINER MODULE CONCEPT FEATURES

BOEING

- **ADAPTABLE TO ANTENNA-MOUNTED SYSTEM**
- **THERMALLY EFFICIENT**
 - GOOD HEAT PATHS
 - RADIATE FROM BOTH SIDES
- **EFFICIENT COMBINING OF LOW-POWER (~5-WATT) DEVICES**
 - ATTAINS ADEQUATE POWER DENSITY
- **HIGH GAIN, PHASE-STABILIZED**

NASA

Solid State Combiner-Radiator Module

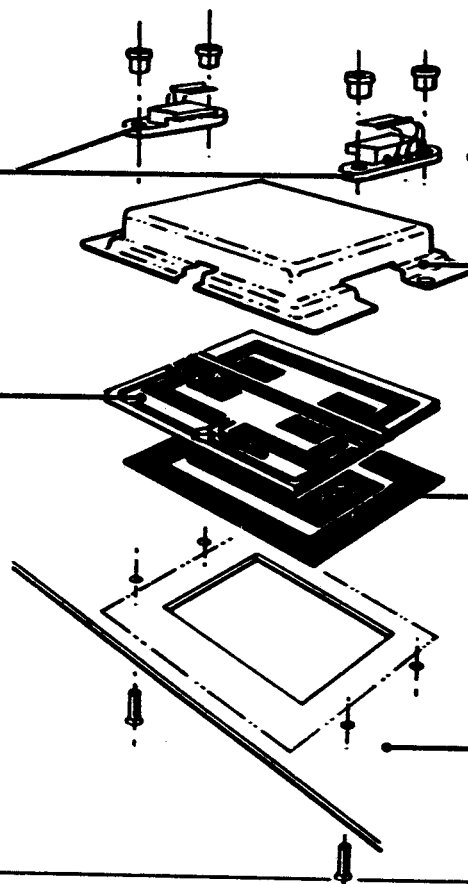
Power Amplifiers

Cavity

Antenna Circuit

Radiator

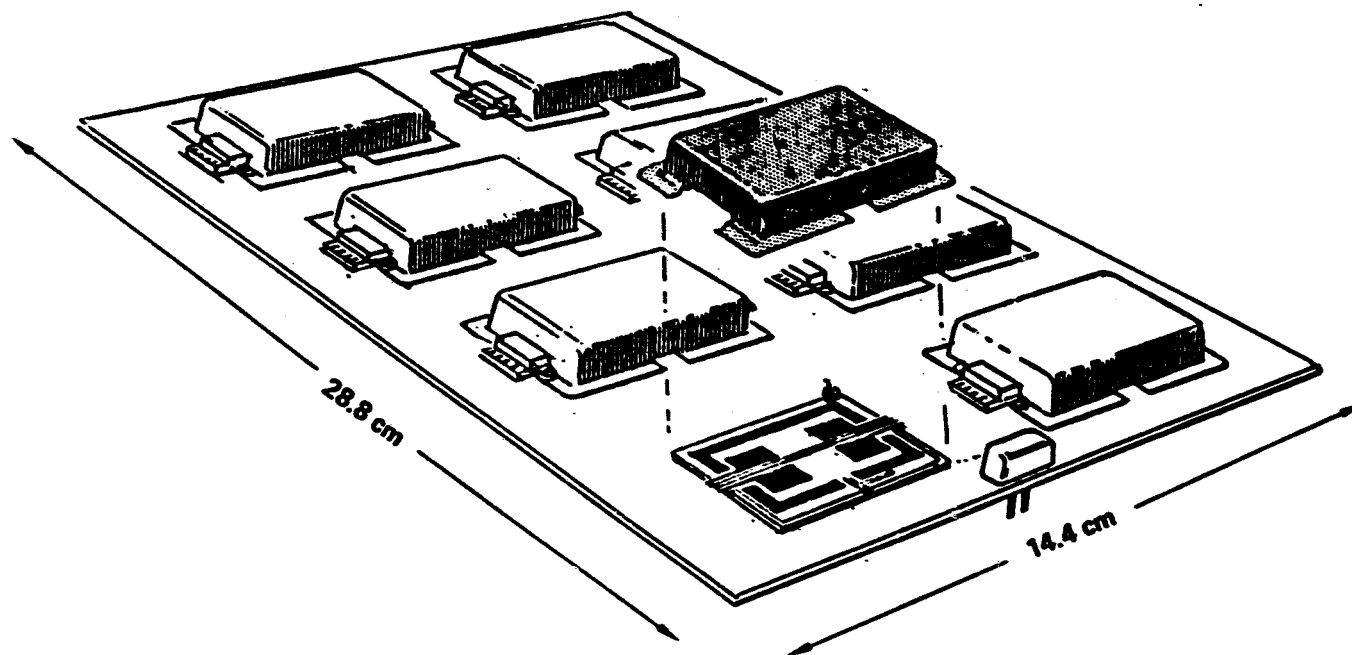
Base Plate

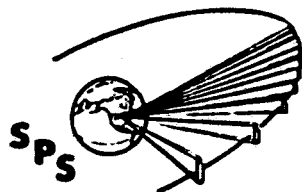


<u>COMPONENT</u>	<u>MASS PER UNIT AREA</u> <u>(KG M⁻²)</u>
7.5 MILS ALUMINUM (FRONT SIDE AVERAGE)	.52
20 MILS ALUMINA	1.99
7.5 MILS ALUMINUM (BACK SIDE AVERAGE)	.52
5 MILS AL EQUIVALENT FOR RADIATION SHIELDING	.35
5 MILS AL EQUIVALENT FOR PHASE FEED	.35
5 MILS AL EQUIVALENT FOR INTERSUBARRAY STRUCTURE	<u>.35</u>
TOTAL	4.07

BOEING
SPS

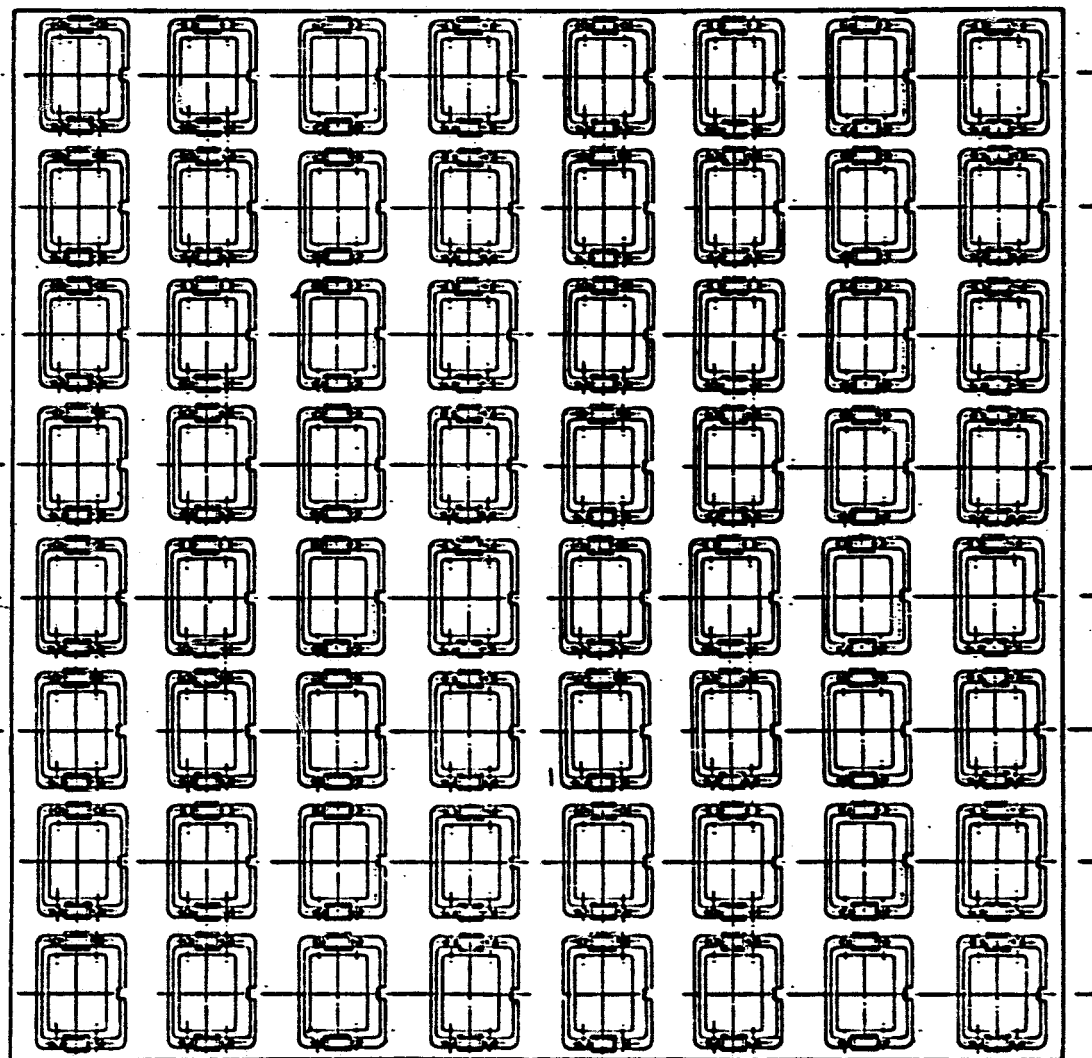
Integration of Modules into Antenna Panel



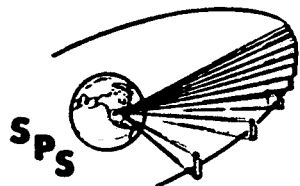


64-Module Panel Layout

BOEING

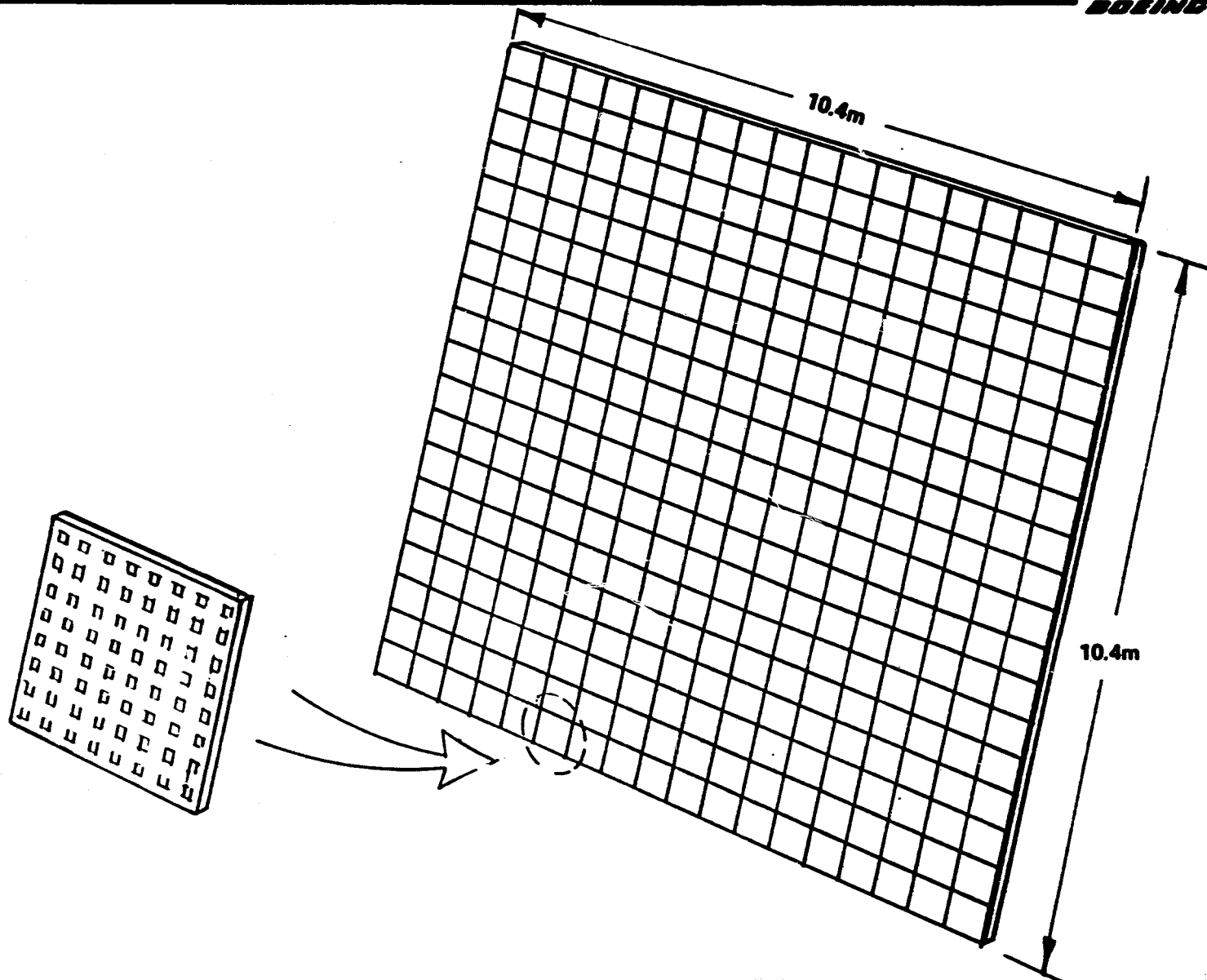


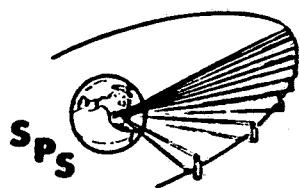
**SECONDARY
TREE PHASE
FEED**



Subarray Assembly (324 Panels; 20, 736 Modules)

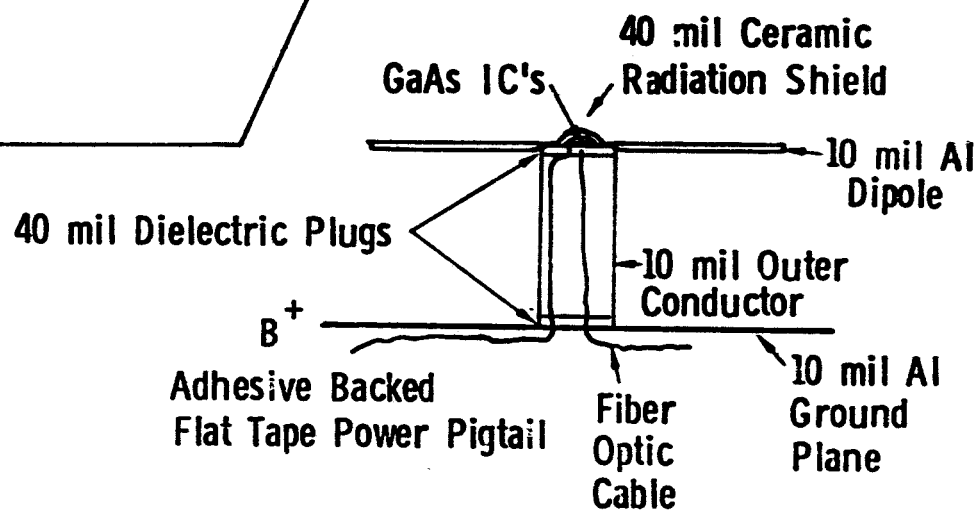
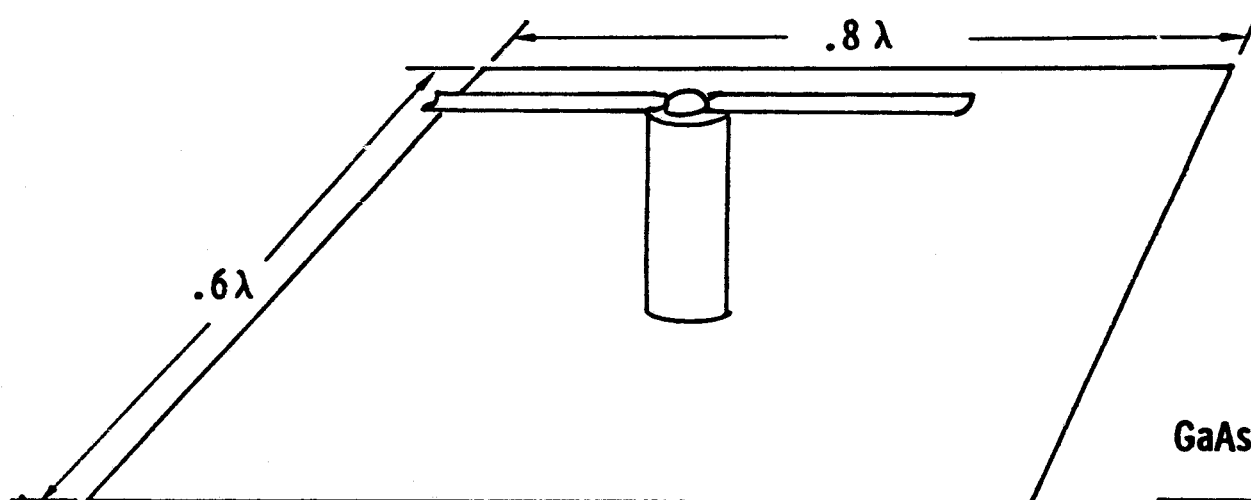
BOEING

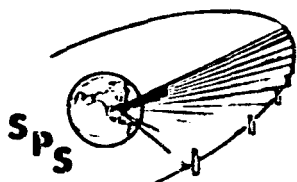




SOLID STATE DIPOLE RADIATOR MODULE

BOEING



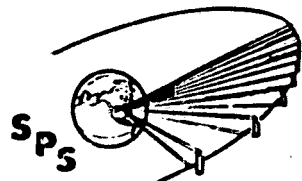


LOW POWER DIPOLE RADIATOR MODULE MASS STATEMENT

BOEING

ITEM	MASS PER MODULE* (kg/m ⁻²)	MASS/AREA (g)
10 MIL AL GROUND PLANE	4.93	.686
CERAMIC SHIELD	.7	.097
DIPOLE AND SUPPORT; 10 mil Al	3.75	.522
DIELECTRIC PLUG	.7	.097
CHIPS, METALLIZATIONS, BENDING, ETC.	.5	.070
TOTAL	11.08	1.472

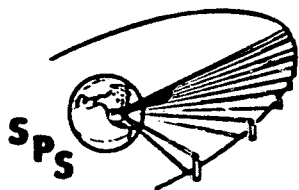
* .6 λ x .8 λ



SOLID STATE TRANSMITTING ANTENNA QUANTIZATION

BOEING

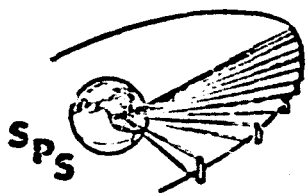
STEP	OUTSIDE RADIUS (m)	STEP AREA (m ²)	NUMBER OF SUBARRAYS	MODULE TYPE	MODULE POWER (W)	(P/A) _{RF} (Kw m ⁻²)	(M/P) _{RF} (kg km ⁻¹)	STEP MODULE MASS (T)	NO. FETS (M)
1	124.8	48,970	456	High Power 4-FET, Cavity Radiator (4.06 kgm ⁻²)	28.7	5.50	.742	200	37.82
2	249.6	146,830	1,360	"	24.0	4.45	.917	600	112.80
3	322.4	130,820	1,208	Reduced Power 4-FET Cavity Radiator (3.58 kgm ⁻²)	19.2	3.56	1.006	468	100.20
4	384.8	138,640	1,280	"	16.0	2.97	1.207	496	108.17
5	457.6	192,680	1,784	2-FET Cavity Radiator (3.06 kgm ⁻²)	12.8	2.37	1.289	590	73.99
6	520.0	191,680	1,776	2 FET Dipole (1.47 kgm ⁻²)	12.8	1.78	.826	582	55.24
7	561.6	141,390	1,312	"	9.6	1.33	1.101	208	40.81
8	582.4	74,795	696	"	8.5	1.18	1.244	110	21.65
9	644.8	238,950	2,208	1 FET Dipole (1.47 kg m ⁻²)	6.4	.89	1.652	351	34.34
10	707.2	264,880	<u>2,448</u>	"	4.3	.59	2.476	<u>389</u>	<u>38.07</u>
	TOTALS		14,528					3,694	621.09



SOLID STATE TRANSMITTING ANTENNA COSTS

BOEING

<u>ITEM</u>	<u>COST ESTIMATING RELATION</u>	<u>COST (\$M)</u>
MODULE MASS	\$70 kg ⁻¹	258.6
MODULE POWER	\$.1 w ⁻¹	330.3
HOOKUP	\$.15 FET ⁻¹	<u>93.2</u>
TOTAL MODULE ASSOCIATED COSTS		682.1
SUBARRAY, STRUCTURE	\$65 kg ⁻¹	47.2
MASTER REFERENCE RECEIVER 3X	500K ea	1.5
SLAVE REPEATERS (800)	25K ea.	20.0
LEVEL 1 CABLES (112)	9.2K ea	1.1
LEVEL 2 CABLES (760)	5.0K ea	3.8
LEVEL 3 CABLES (58,112)	\$800 ea.	46.5
PCR's (58,112)	\$560 ea.	32.5
QUADRANT - PANEL CABLES (81 x 58,112)	\$45 ea	21.2
PCV's (58,112)	\$350 ea	20.3
PANEL PHASE SLAVE REPEATER (81 x 58,112)	\$15 ea	7.6
PANEL CKT BREAKER (81 x 58,112)	\$10 ea	4.7
TOTAL NON-MODULE COSTS		<u>206.4</u>
TOTAL SOLID STATE TRANSMITTING ANTENNA "RF SYSTEM" COSTS		888.5



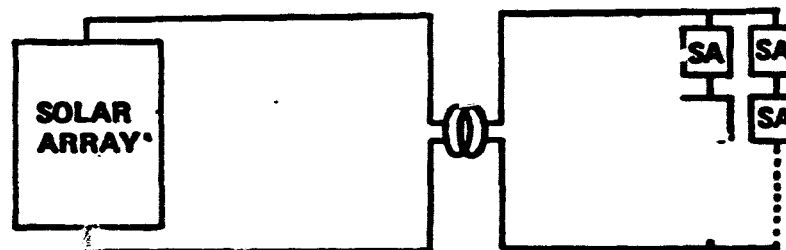
Solid State Power Supply Options

BOEING

● DIRECT HIGH VOLTAGE DC

REQUIRES SUBARRAYS IN SERIES
CONNECTION TOPOLOGY A PROBLEM

HIGH E-FIELDS NEAR ADJACENT SUBARRAYS
MAY CAUSE ARCS, WILL SUSTAIN THEM

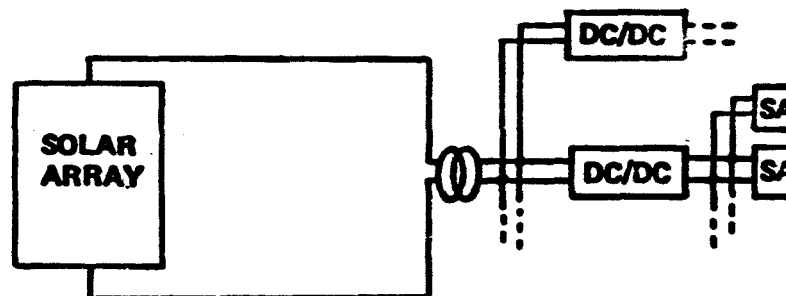


● DC-DC CONVERSION ON MPTS

PERFORMANCE PENALTIES

DC-DC CONVERTERS $\approx 1\text{kg/kw}$
POWER LOSSES IN CONVERTERS

SERIES/PARALLEL CONNECTIONS WITHIN
SUBARRAYS STILL REQUIRED



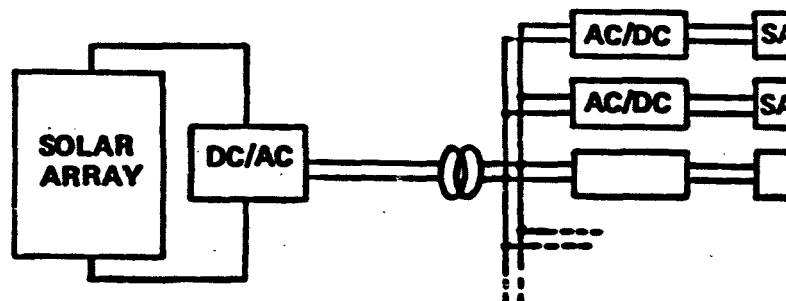
● AC POWER DISTRIBUTION

CONVERT

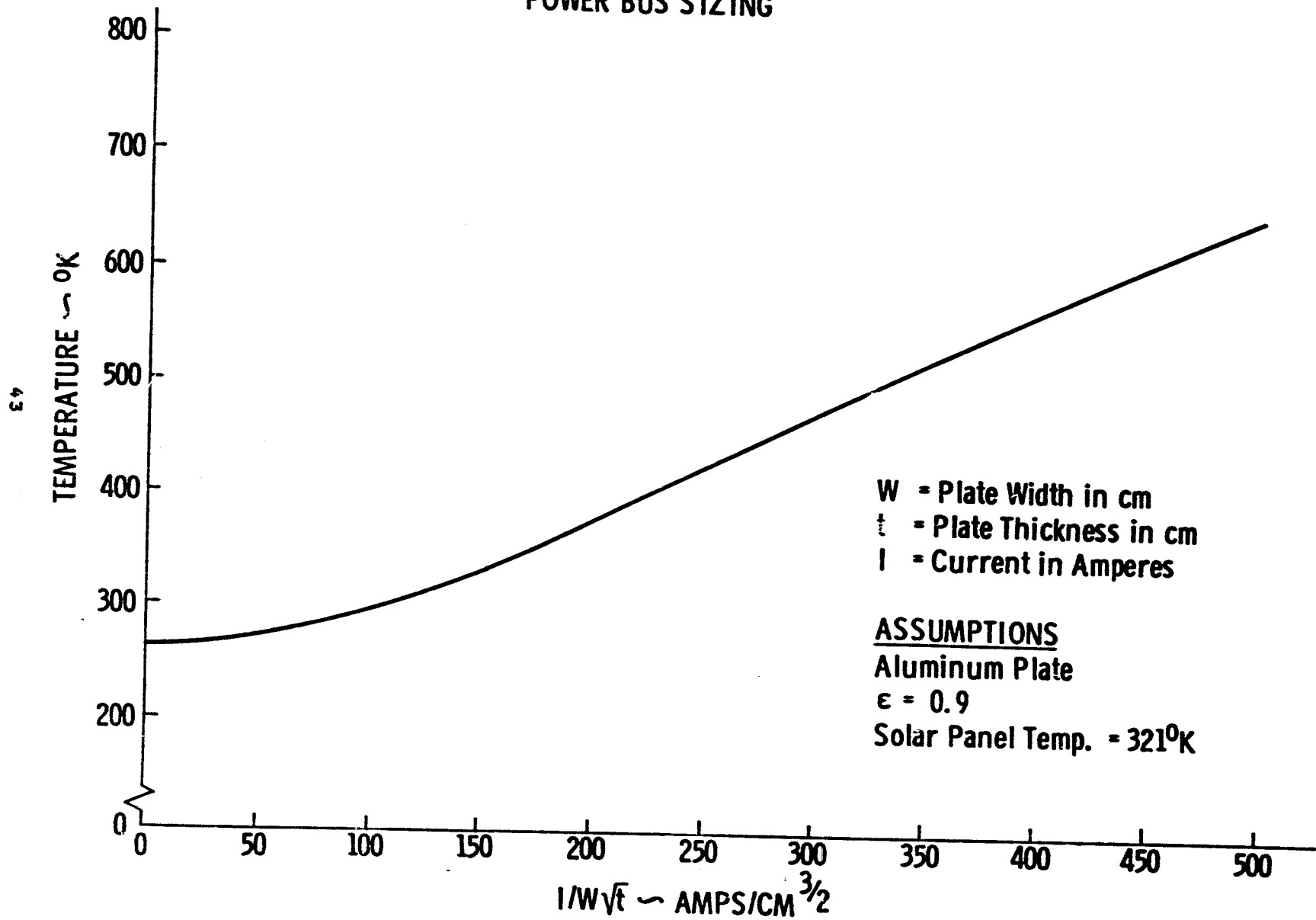
DC/AC ON SOLAR ARRAY

AC/DC AT SUBARRAY

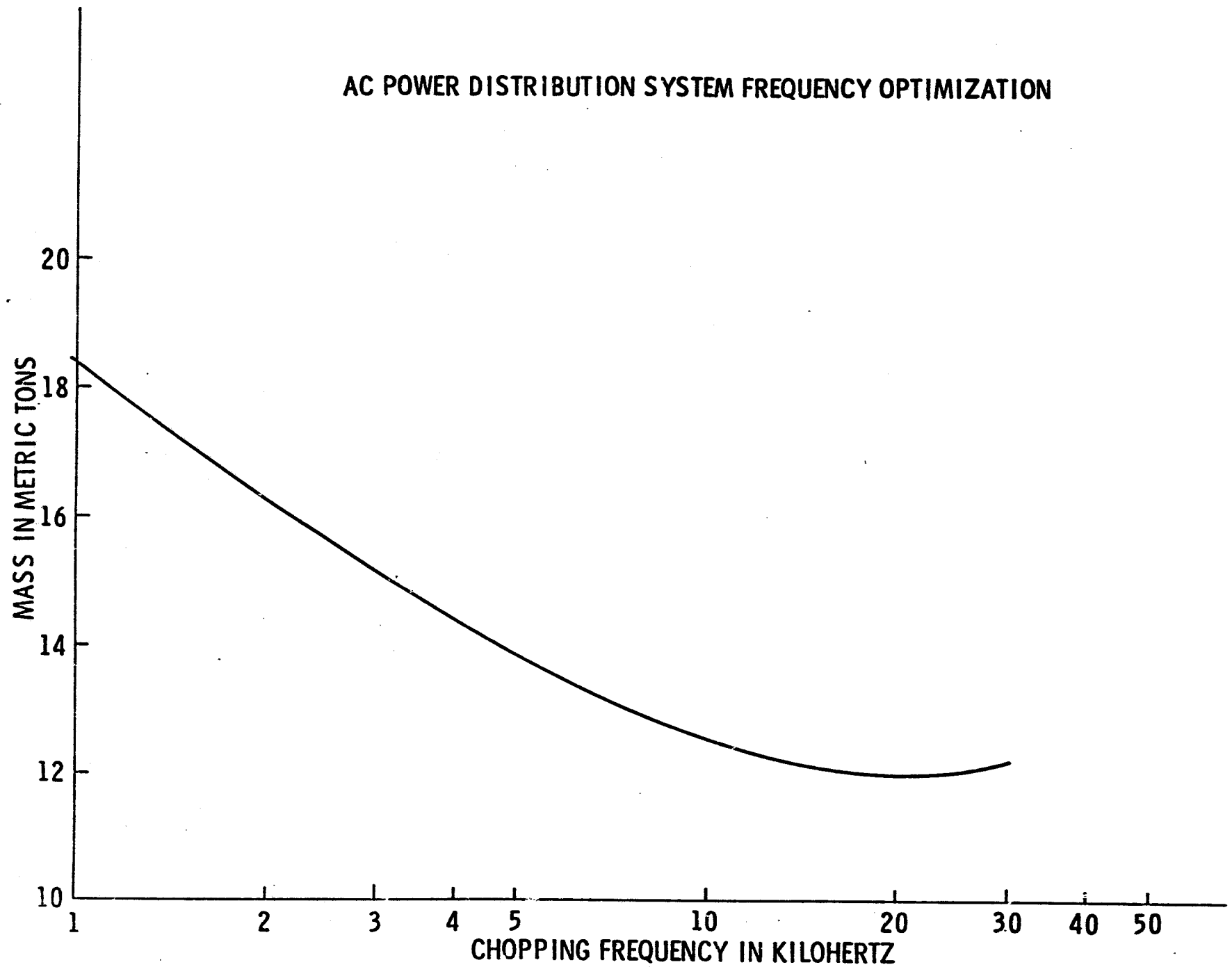
REQUIRES S/P TO SOME EXTENT ON SUBARRAY



POWER BUS SIZING



AC POWER DISTRIBUTION SYSTEM FREQUENCY OPTIMIZATION



AC POWER DISTRIBUTION SUMMARY
2.5 GW SATELLITE, FREQUENCY = 10 KHz, $T_c = 100^\circ\text{C}$
Operating Voltages Array 11 KV, Main Bus 100 KV

SYSTEM ELEMENT	MASS (MT)	I^2R LOSS (MW)
Non P-Max Power Loss Penalty	-	-
Acquisition Buses	19.7	46.0
DC/AC Converters	4,146.5	135.2
Main Buses	257.2	115.0
Switchgear	203.3	-
AC/DC Converters	5,175.9	164.4
TOTAL	9,802.6	406.6

Array Power = 4,760.6 MW
 System Efficiency = 90.3%
 System Losses = 9.7%
 Array Area = 28.53 km²
 Array Mass = 12,119.0

Mass (Array + Pwr Dist) = 21,921.6 MT

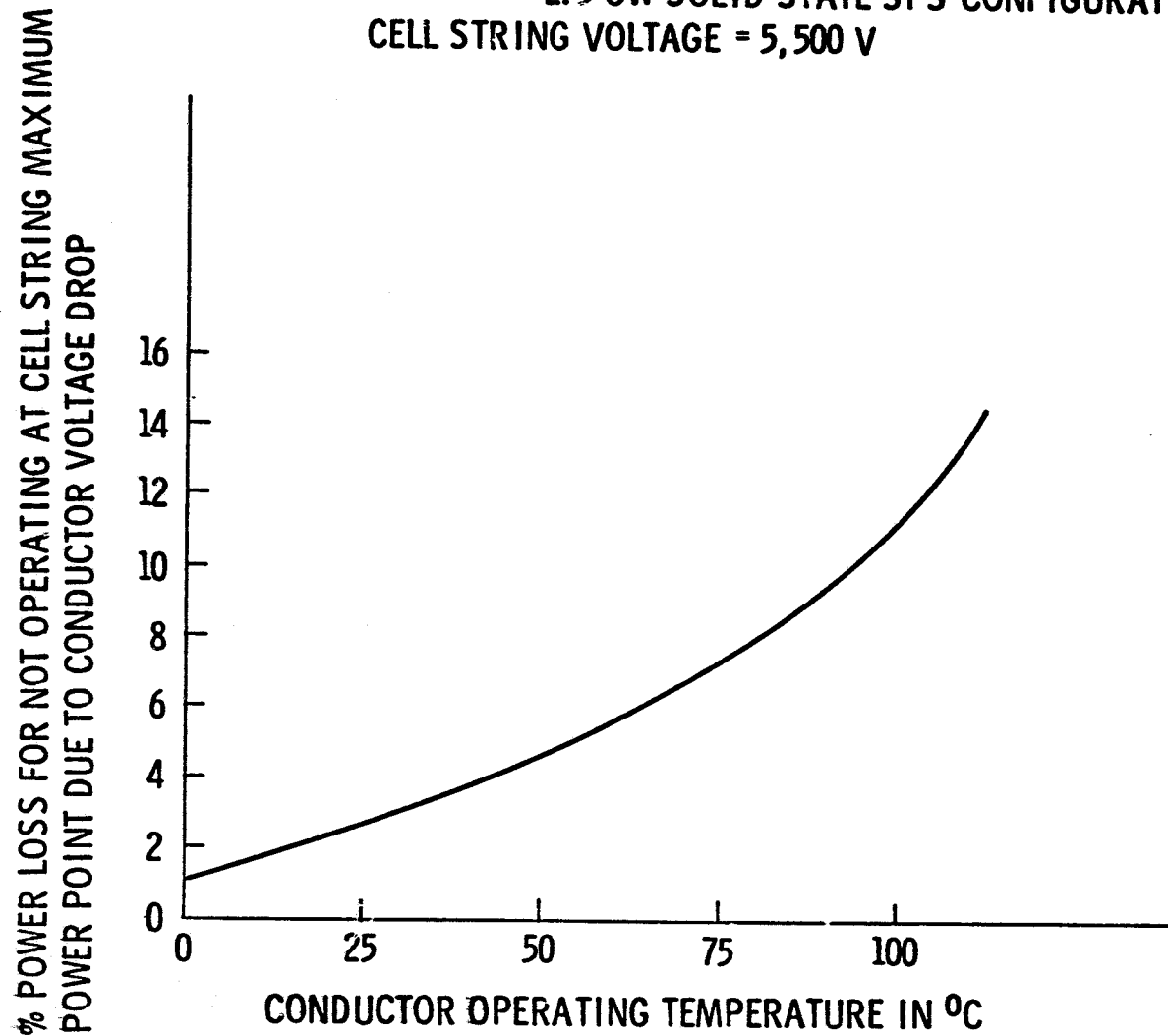
DC POWER DISTRIBUTION - 44 KV
2.5 GW SATELLITE. 100% POWER PROCESSING
T_C = 100°C, DELIVERED POWER = 4,300 MW to DC/RF CONVERTERS

SYSTEM ELEMENT	MASS IN METRIC TONS	LOSSES IN MEGAWATTS
Non-P-Max Power Loss Penalty	-	24.2
Acquisition Buses	19.8	11.3
Main Buses	401.0	264.1
Switchgear	85.7	-
DC/DC Converters	7,239.6	253.2
TOTAL	7,746.1	552.8

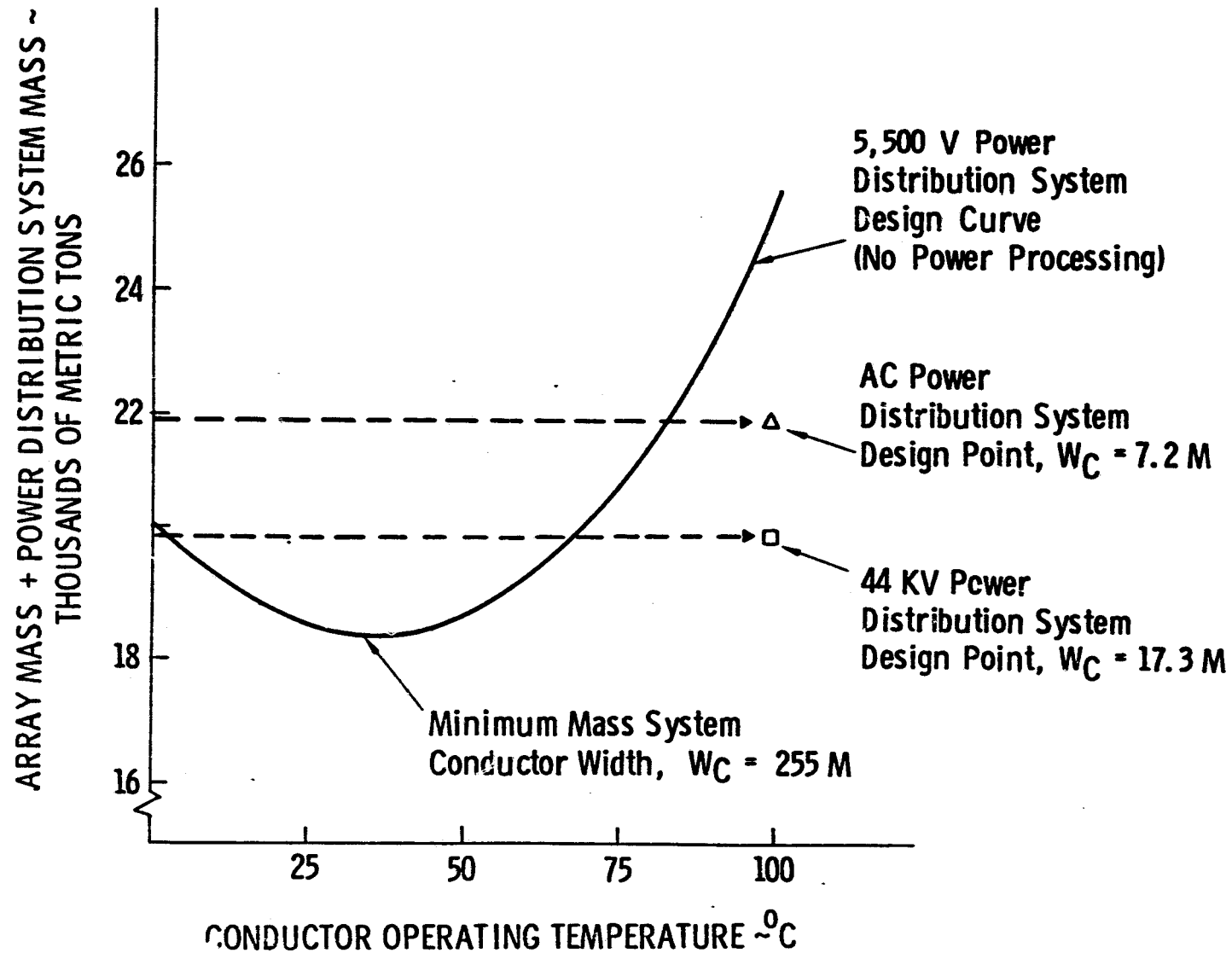
Array Power (MW) = 4,852.8
 Array Area (KM²) = 29.09
 Array Mass (MT) = 12,356.0
 System Efficiency = 88.6%
 Mass (Array + Pwr. Dist) (MT) = 20,102.1

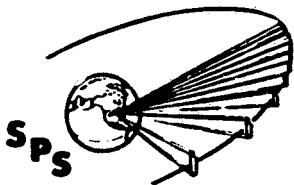
ARRAY MISMATCH LOSSES

2.5 GW SOLID STATE SPS CONFIGURATION
CELL STRING VOLTAGE = 5,500 V



POWER DISTRIBUTION SYSTEM ANALYSIS FOR 2.5 GW SPS

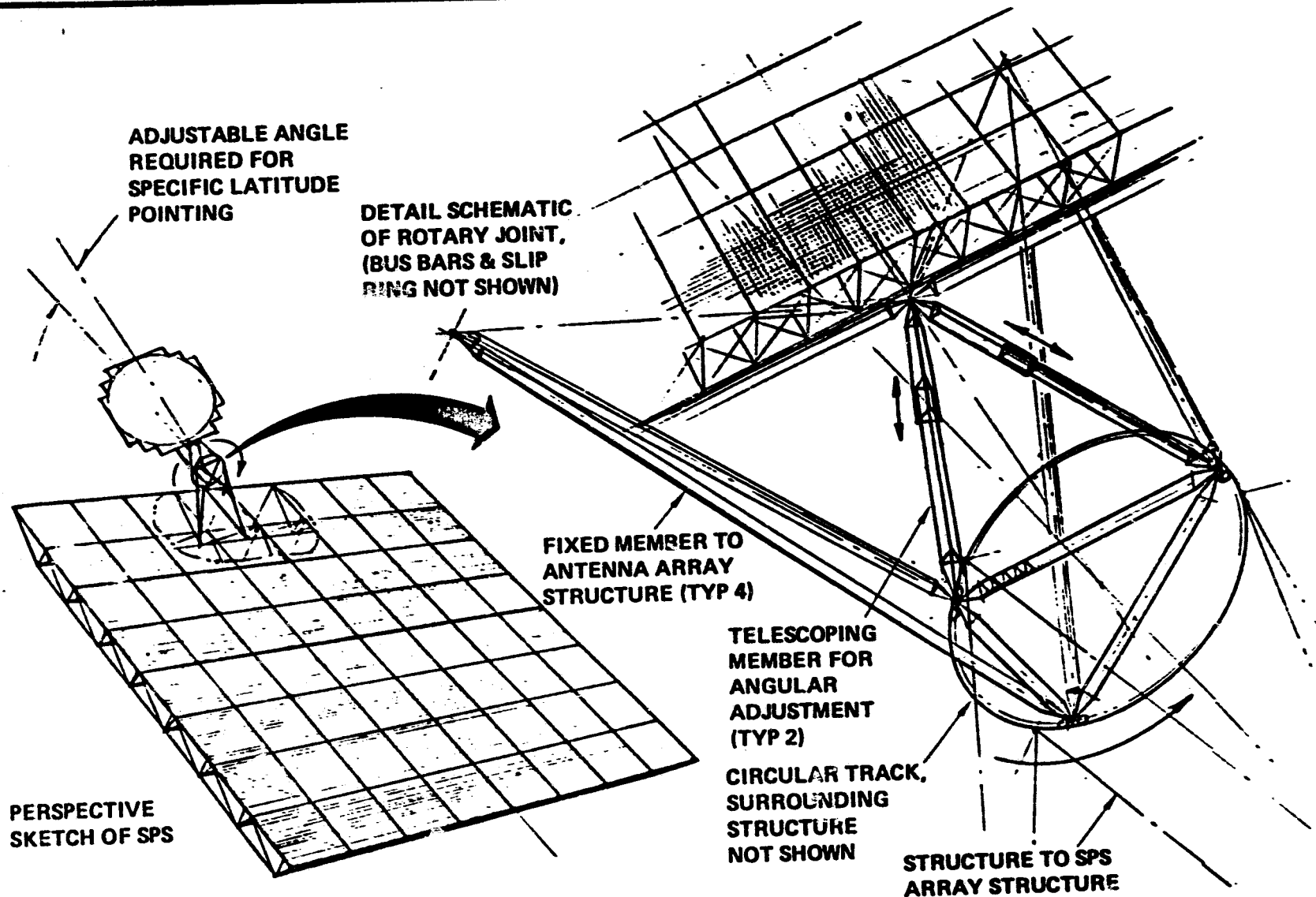




Antenna Array Angular Adjustment Concept 2.5 GW Solid-State SPS

BOEING

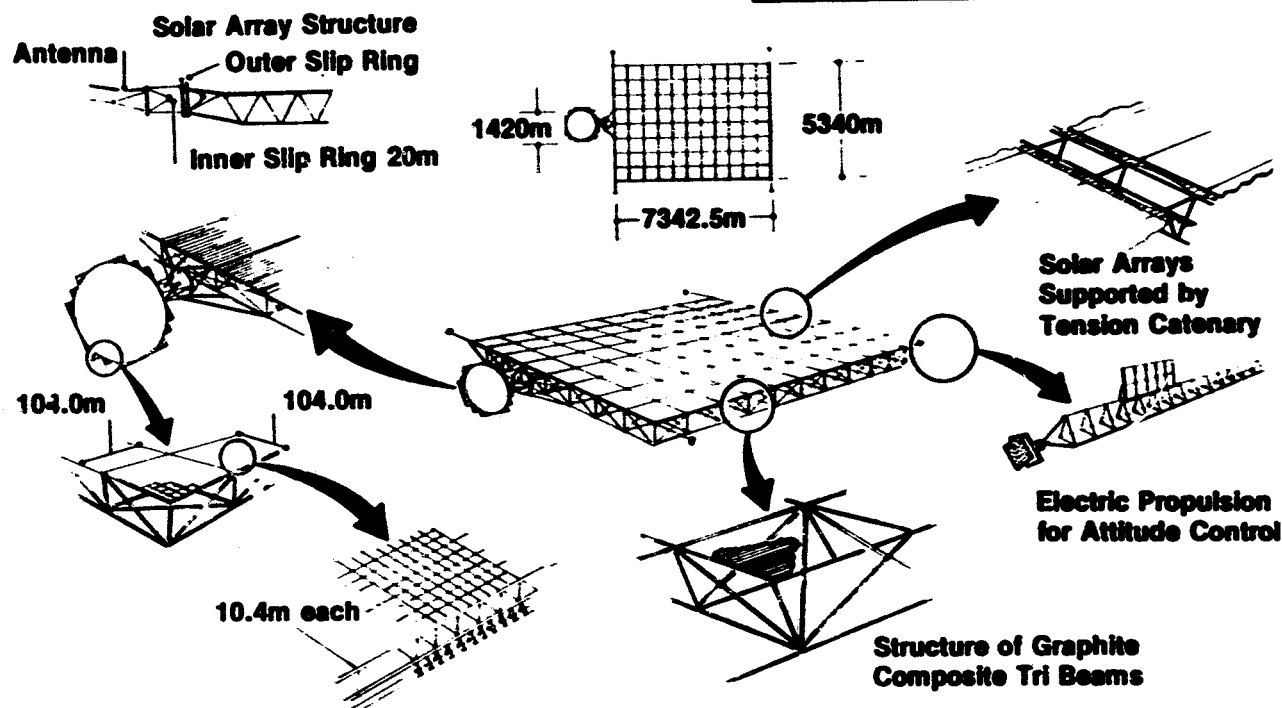
49

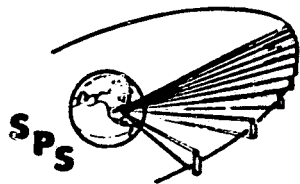


NASA

Solar Power Satellite

2.5 GW Solid State Configuration Separate Antenna



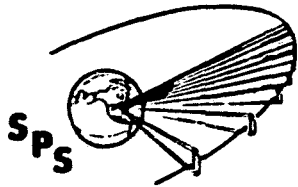


SOLID STATE SPS EFFICIENCY & SIZING

BOEING

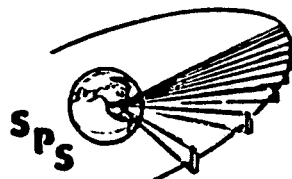
<u>ITEM</u>	<u>EFFICIENCY</u>	<u>MEGAWATTS</u>	
Array Mismatch			
Array Mismatch	.965	6050	Ideal Array Output
Main Bus I ² R	.729	5838	
Antenna Distr	.97	4256	Total Antenna Input
DC-RF Conversion	.8	4128	
Waveguide I ² R	N/A	3303	Total RF Radiated Power
Ideal Beam	.965	3303	
Inter-Subarray Losses	.976	3187	
Intra-Subarray Losses	N/A	3110	
Atmosphere Loss	.98	3110	
Intercept	.95	3048	
Rectenna RF-DC	.89	2896	Incident on Rectenna
Grid Interface	.97	2577	
	<u>.413</u>	<u>2500</u>	Net to Grid

TOTAL ARRAY OUTPUT 6050 MW
 TOTAL SOLAR ARRAY AREA = 33.8 km²



SOLID STATE SPS MASS & COST SUMMARY

	<u>MASS (MT)</u>	<u>ESTIMATING BASIS</u>	<u>BOEING (COST (\$M))</u>
1.1 SPS	<u>35,204</u>		<u>4,541</u>
1.1.1 ENERGY CONVERSION	<u>22,087</u>		<u>2,350</u>
1.1.1.1 STRUCTURE	<u>2,851</u>	Detailed Estimate	<u>275</u>
1.1.1.2 CONCENTRATORS	(0)	Not Required	(0)
1.1.1.3 SOLAR BLANKETS	14,409	Scaled from Reference	1,355
1.1.1.4 POWER DISTRIB.	4,400	Detailed Estimate	530
1.1.1.5 THERMAL CONTROL	(0)	Allocated to Subsystems	(0)
1.1.1.6 MAINTENANCE	427	Scaled from Reference	190
1.1.2 POWER TRANSMISSION	<u>6,365</u>		<u>1,134.5</u>
1.1.2.1 STRUCTURE	<u>460</u>	Scaled from Reference	<u>38</u>
1.1.2.2 TRANSMITTER	4,480	Detailed Estimate	888.5
SUBARRAYS			
1.1.2.3 POWER DISTR. & COND.	1,262	Scaled from 1.1.1.4	124
1.1.2.4 PHASE DISTR.	25	Scaled from Reference	51
1.1.2.5 MAINTENANCE	20	Docking Ports Only	20
1.1.2.6 ANTENNA MECH. POINTING	118	Scaled by Mass x Area	13
1.1.3 INFO MGMT & CONTROL	<u>145</u>	Scaled from Ref.	<u>73</u>
1.1.4 ATT. CONT. & STA. KP.	<u>146</u>	Scaled From Ref	<u>110</u>
1.1.5 COMMUNICATIONS	<u>0.2</u>	Same as Ref.	<u>8</u>
1.1.6 INTERFACE	<u>113</u>	Est. Based on Simplification	<u>46.3</u>
1.1.7 GROWTH & CONTINGY.	<u>6,348</u>	Same % as Reference	<u>819</u>

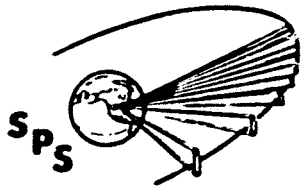


SPS-3071

2.5 GW SOLID STATE SATELLITE SYSTEM RECURRING COSTS

BOEING

<u>ITEM</u>	<u>COST (\$M)</u>
SATELLITE	3,722
LESS IMPLICIT AMORTIZATION	<u>327</u>
	3,395
CONSTRUCTION AND SUPPORT	664
SPACE TRANSPORTATION	2,154
GROUND TRANSPORTATION	20
RECTENNA	1,290
MISSION CONTROL	10
MGMT AND INTEGRATION	385
MASS GROWTH (17% Net Hardware)	<u>577</u>
TOTAL DIRECT OUTLAY	8,505



SOLID-STATE RECOMMENDATIONS

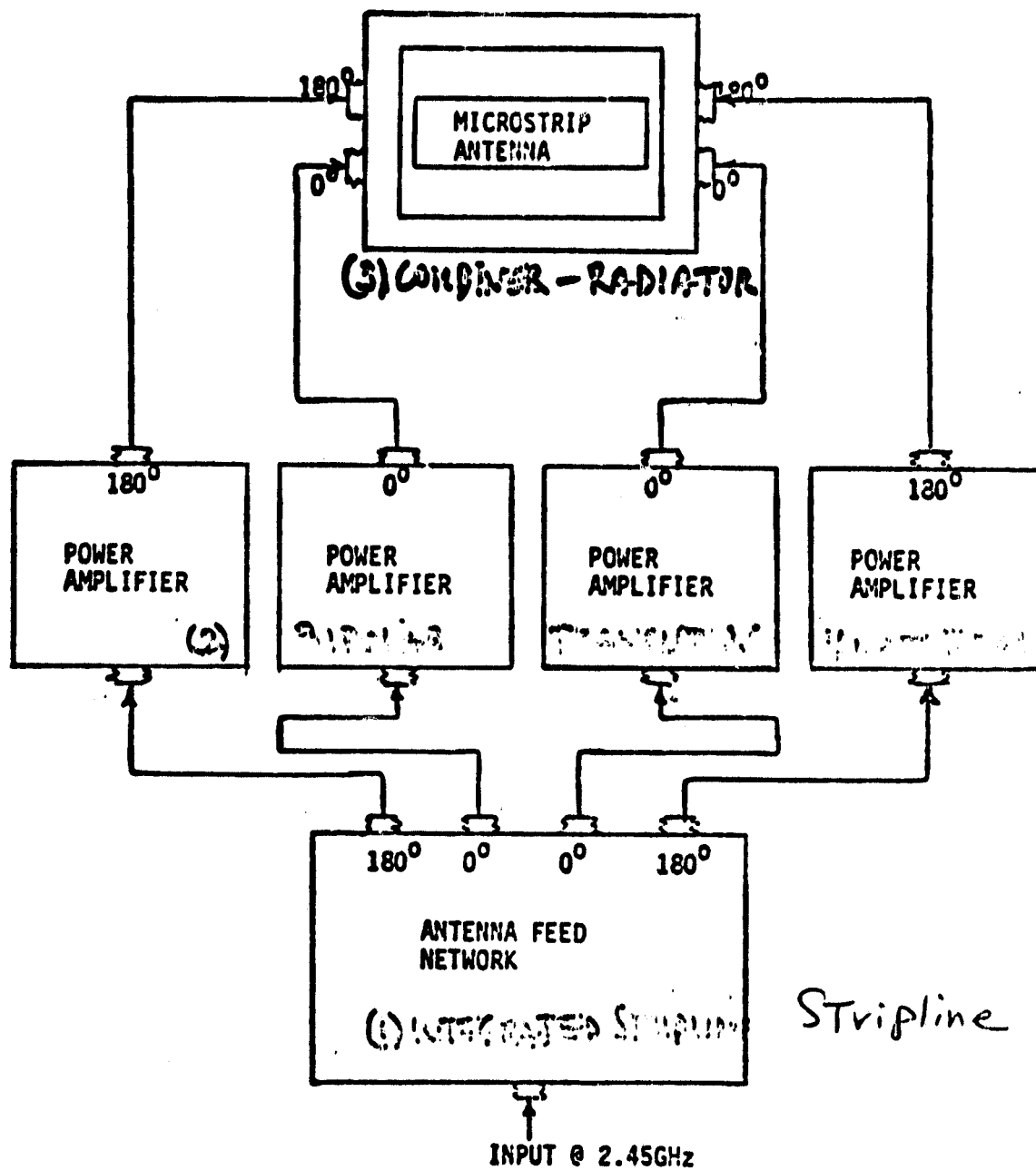
BOEING

- o EXAMINE BEAM TAILORING
 - . Square Up Beam
 - . Open Power Constraint
- o TRY FOR HIGHER DISTRIBUTION VOLTAGE
- o INVESTIGATE "INTERMEDIATE" POWER MODULE OF LOWER MASS/POWER
- o CONDUCT NOISE & HARMONICS ANALYSIS
- o INCREASE DESIGN DETAIL
- o PROVIDE SYSTEM DESCRIPTION/COST DOCUMENT

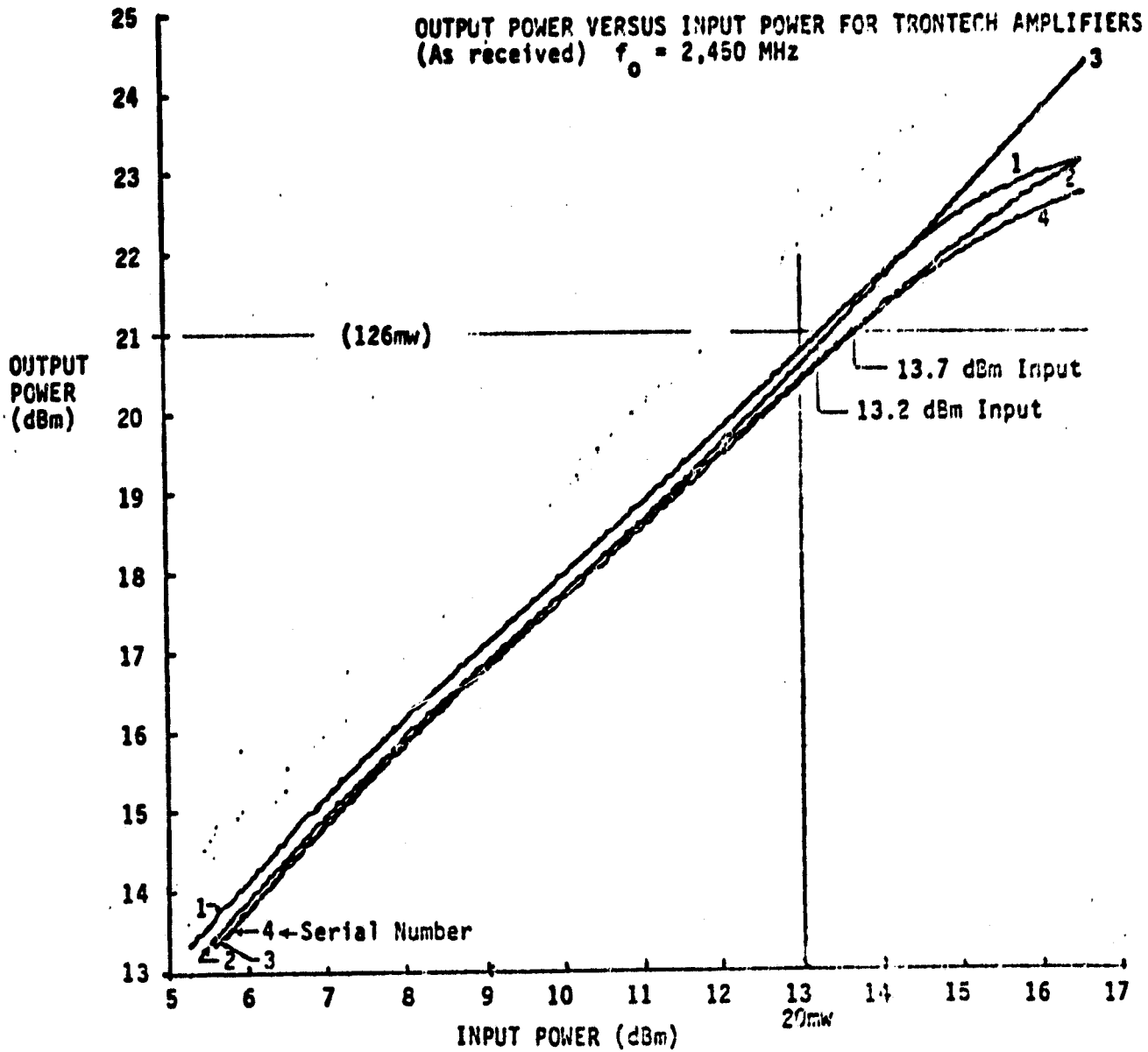
SPS SOLID STATE ANTENNA POWER COMBINER CONTRACT NAS 9-15636B

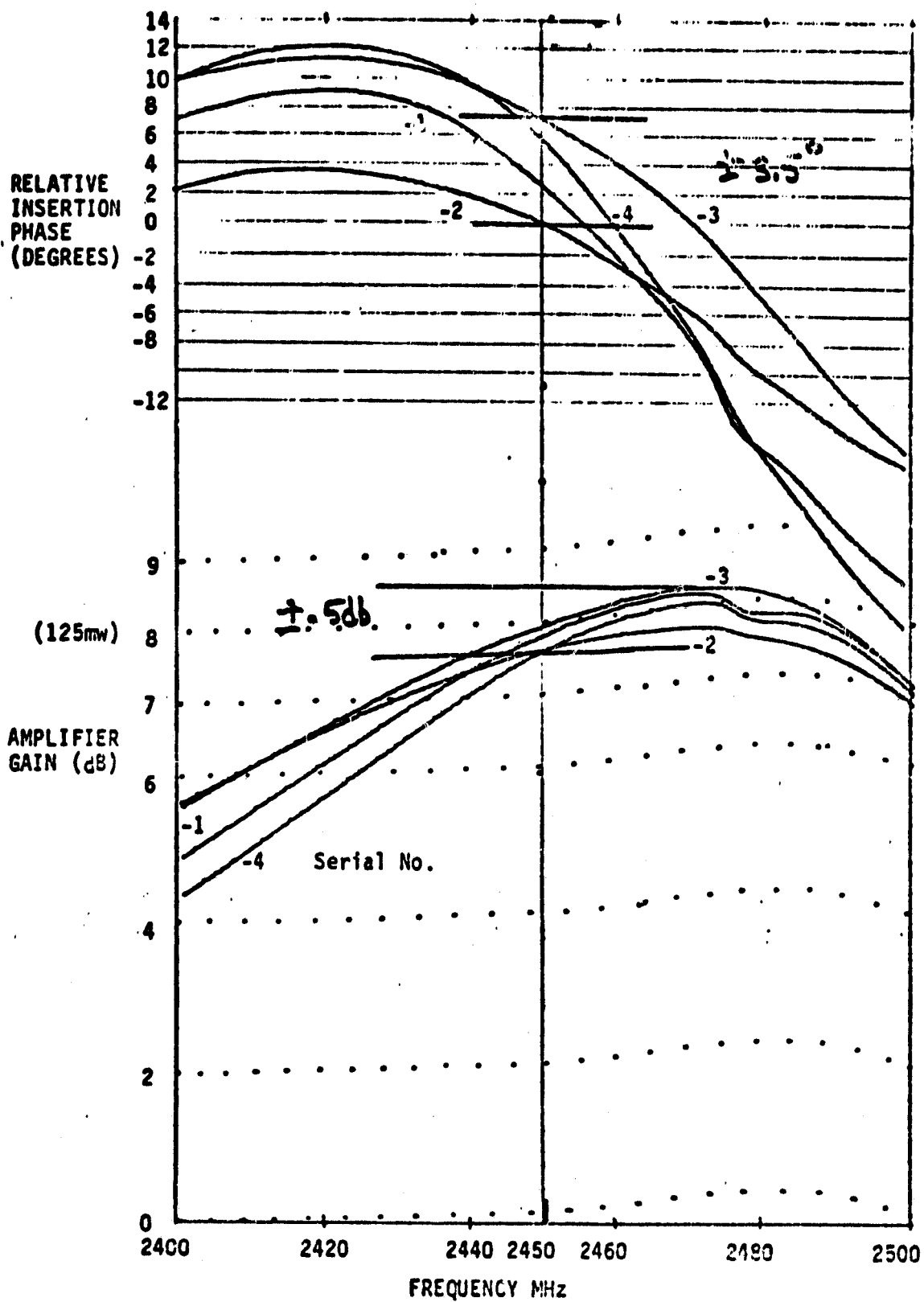
TASKS:

- Specify, purchase and bench test four solid state power amplifiers for adequate phase and amplitude response to verify suitability for power combiner module test.
- Incorporate four power amplifiers into a four-feed combiner module. Refine the four combining antenna design in terms of substrate size, cavity size, slot width, slot spacing and slot feed mechanism to properly match the amplifiers to the module. The designed minimum combined power output will be one-half watt.
- Demonstrate via antenna range measurement the efficiency of the power combining antenna utilizing a 0° - 180° feed system. Demonstrate via antenna range measurement the efficiency of the power combining antenna driven by the four solid-state amplifiers. Range of accuracies of approximately $\pm .5$ dB will be applied.



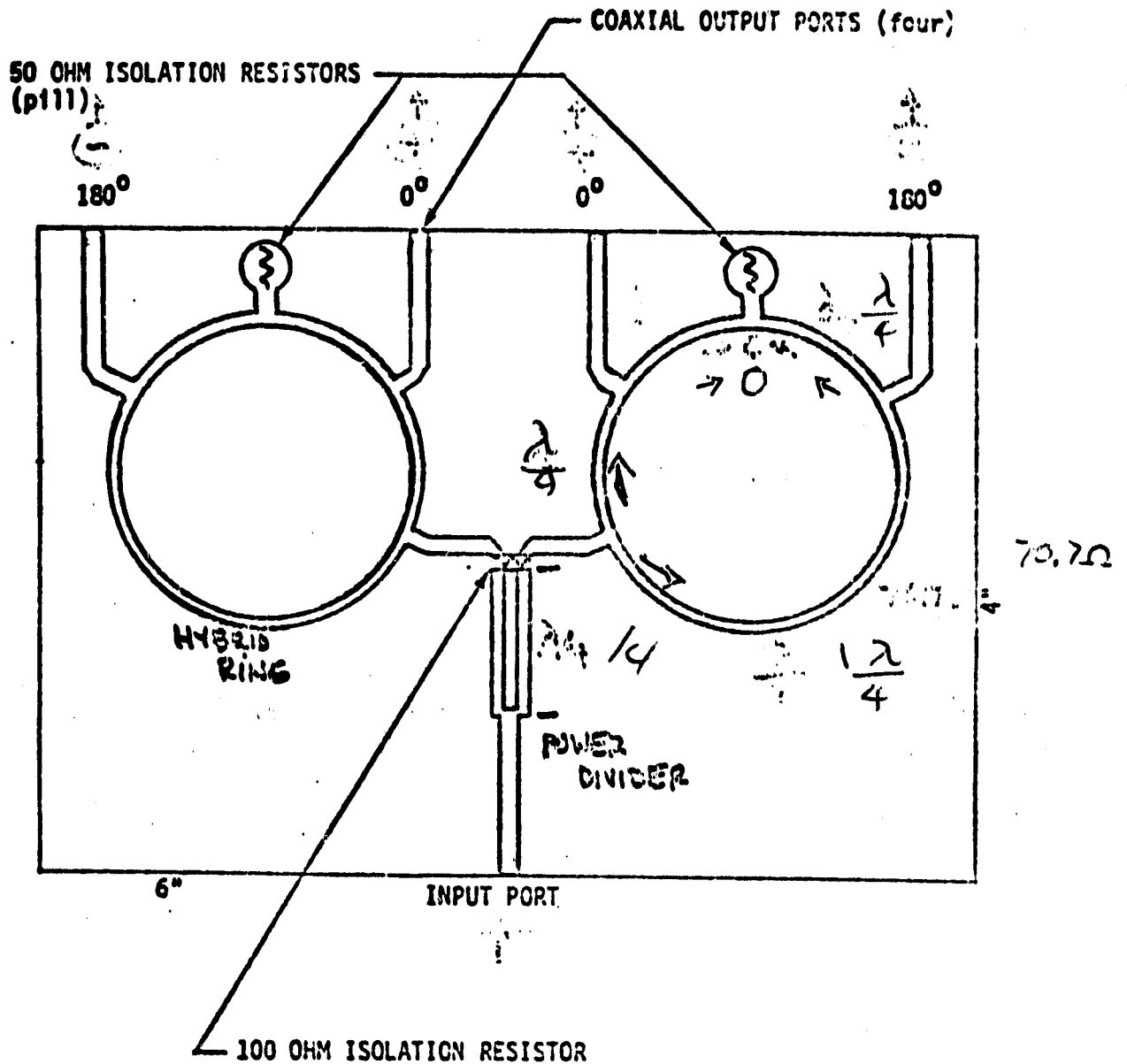
POWER COMBINING ANTENNA, FEED NETWORK & POWER AMPLIFIER
BLOCK DIAGRAM





LARGE SIGNAL GAIN AND RELATIVE INSERTION PHASE FOR TRONTECH AMPLIFIERS
(As Received) $P_{in} = +13 \text{ dBm}$ ($\approx 20\text{mw}$)

ORIGINAL PAGE 19
OF POOR QUALITY



COPPER CLAD TETRAON BLANK SCOTCHCARD STRIPLINE

APPROXIMATE METALIZATION PATTERN OF INTEGRATED STRIPLINE
ANTENNA FEED

- ALL THREE UNITS COMPLETED AND TESTED - - - - EXCELLENT PERFORMANCE.
- TWO REQUIRED FOR TESTS, ONE SPARE.
- MEASURED RESULTS:

<u>SERIAL NUMBER</u>	<u>PHASE BALANCE</u>	<u>LOSS BALANCE</u>	<u>INSERTION LOSS</u>	<u>ISOLATION & RETURN LOSS</u>
001	$\pm .75^{\circ}$	$\pm .03$ dB	.154 dB	> 25 dB
002	$\pm .39^{\circ}$	$\pm .03$ dB	.189 dB	> 25 dB
003	$\pm .81^{\circ}$	$\pm .015$ dB	.172 dB	> 25 dB
<u>GOAL</u>	<u>$< \pm 1^{\circ}$</u>	<u>$< .05$ dB</u>	<u>$< .2$ dB goal</u>	<u>> 20 dB</u>

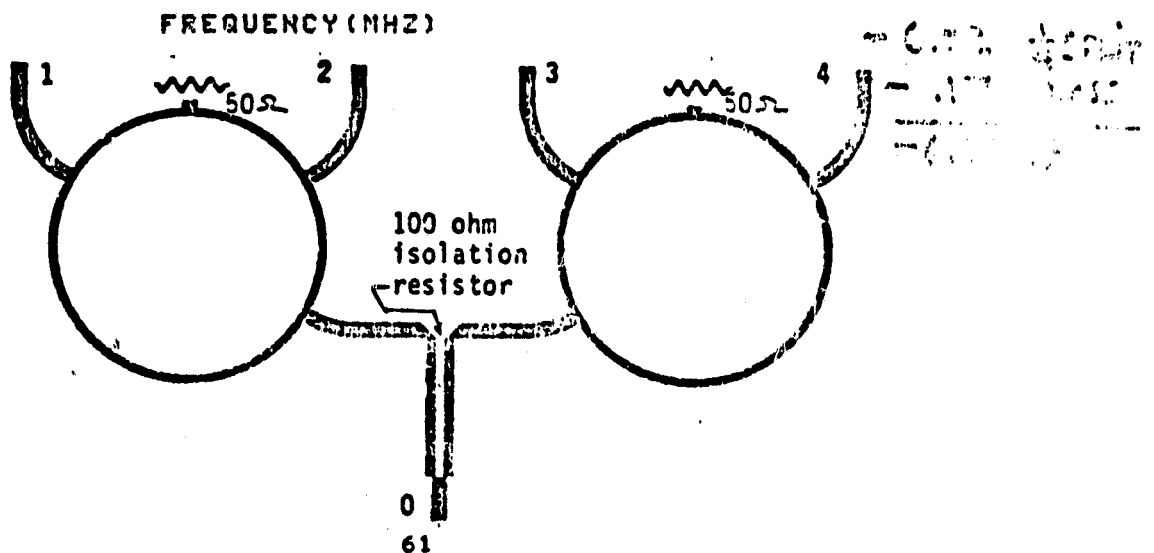
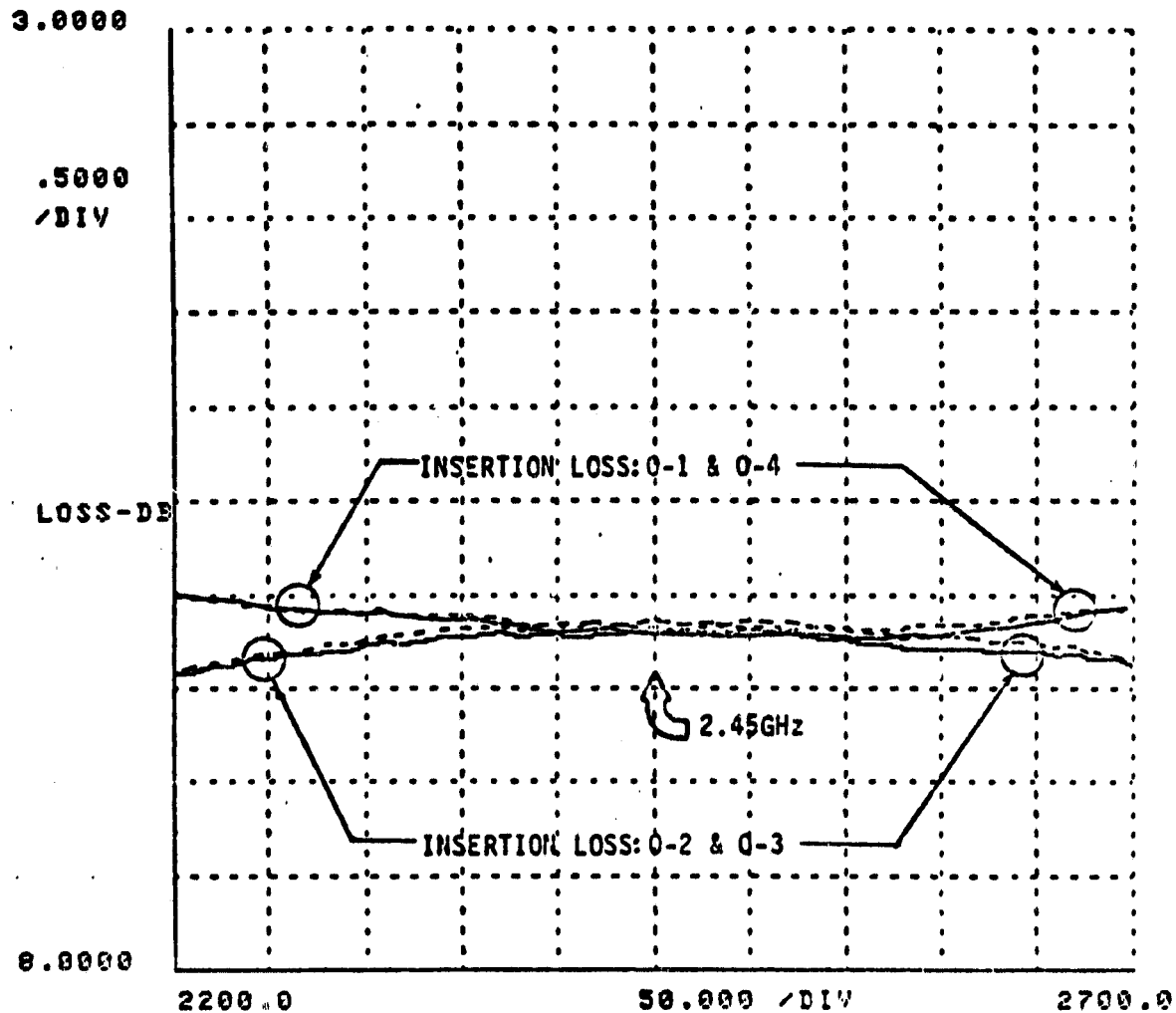
THE BOEING CO. GWF

SEPTEMBER 10, 1979

SPS SOLID-STATE ANTENNA MODULE FEED
NETWORK

2.45 GHZ

SER. #01



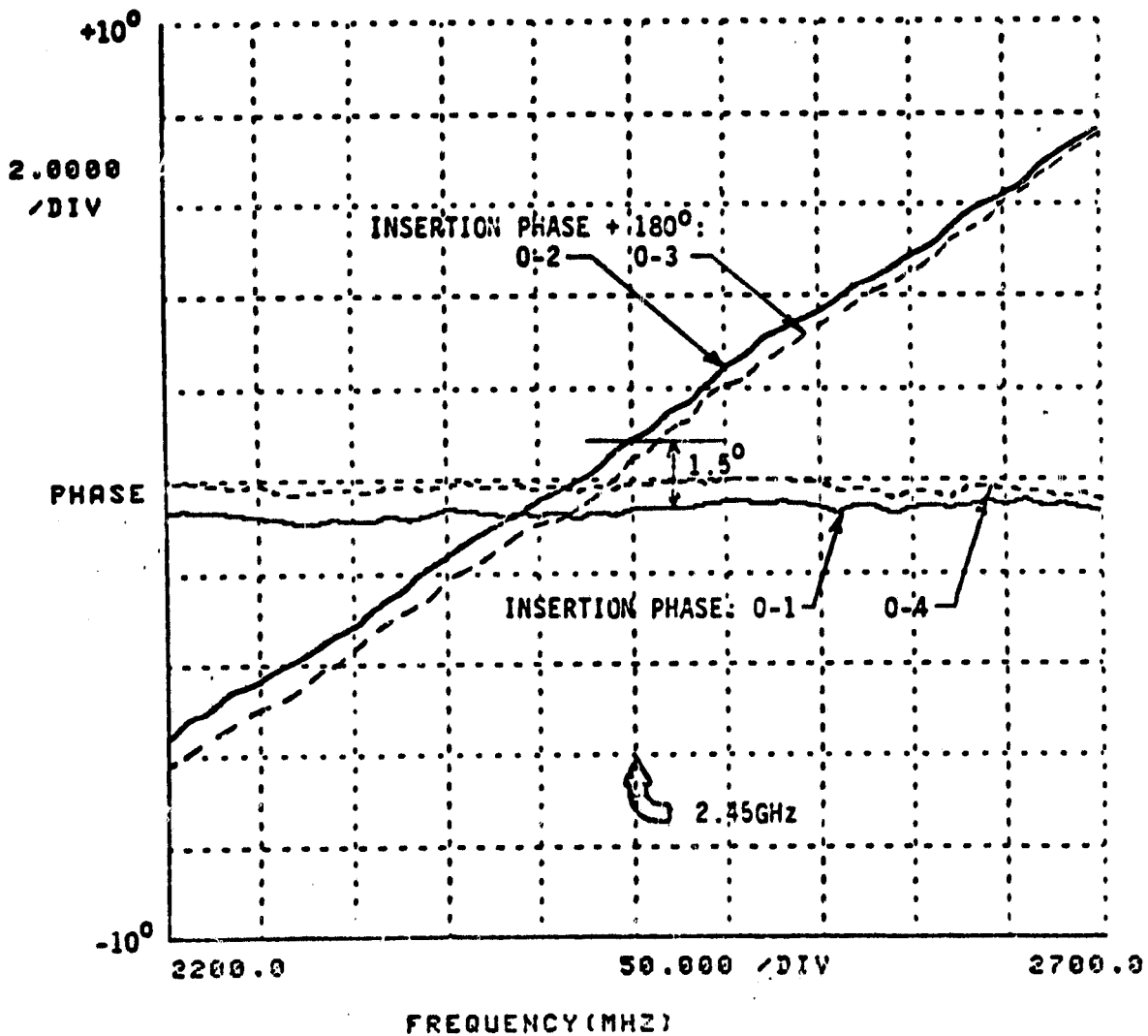
THE BOEING CO. GWF

SEPTEMBER 10, 1979

SPS SOLID-STATE ANTENNA MODULE FEED
NETWORK

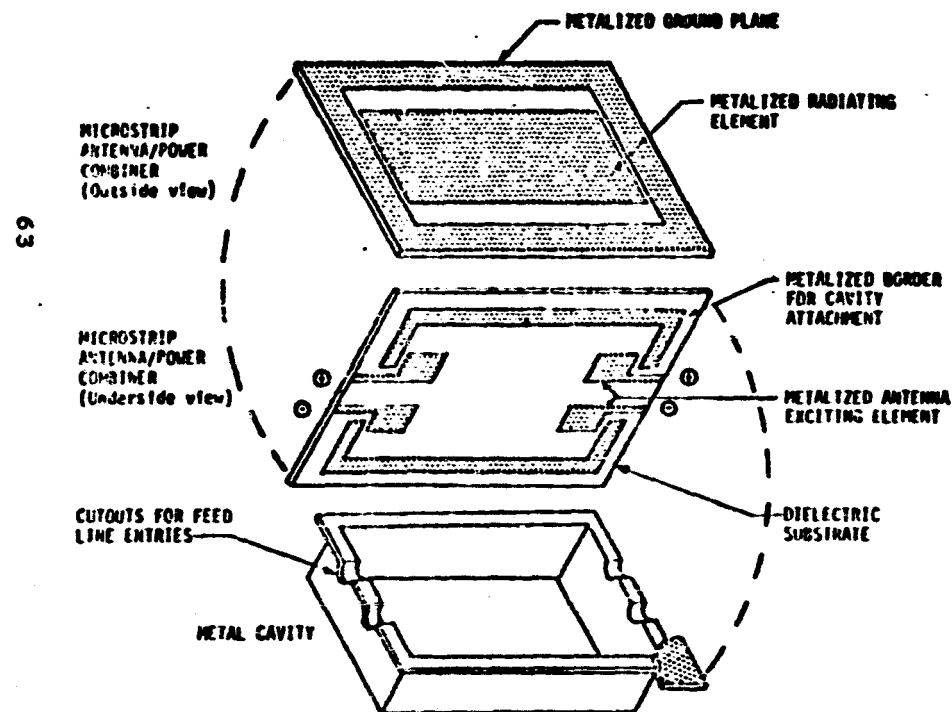
2.45 GHZ

SER. #01



POWER COMBINING MICROSTRIP ANTENNA

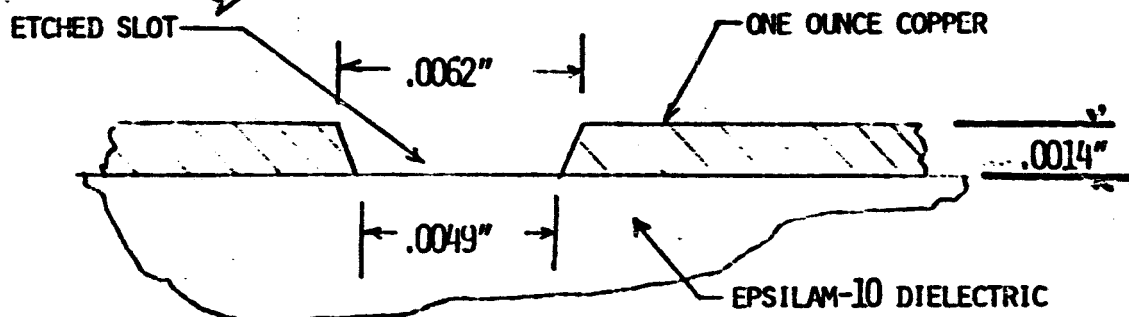
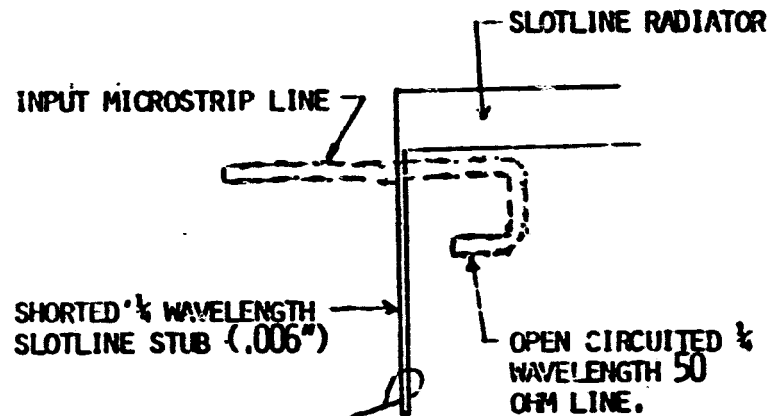
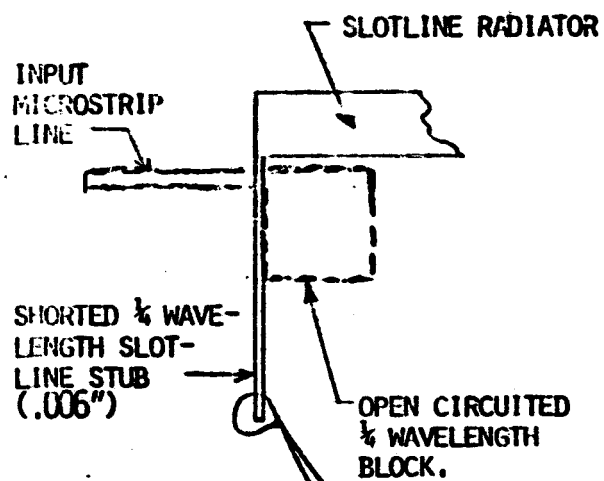
BOEING PROPRIETARY



REPRODUCTION OF
 • SLOTLINE ANTENNA
 • ETCHING

ORIGINAL METHOD

REVISED METHOD

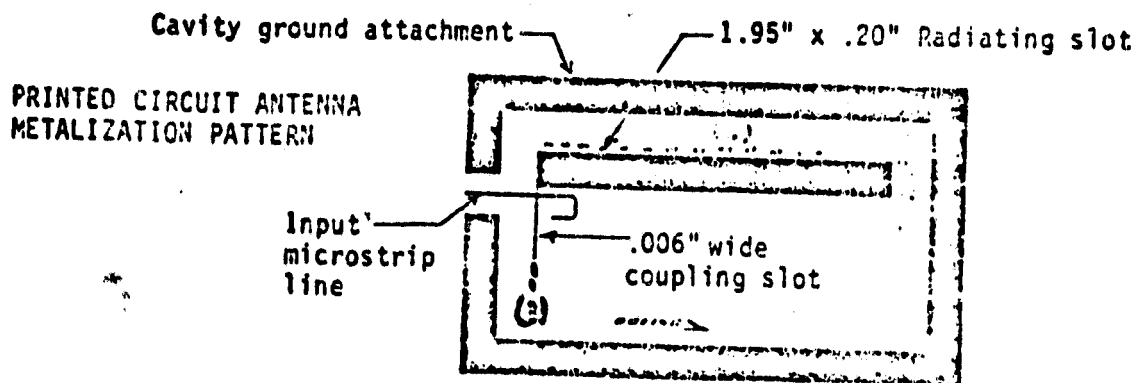
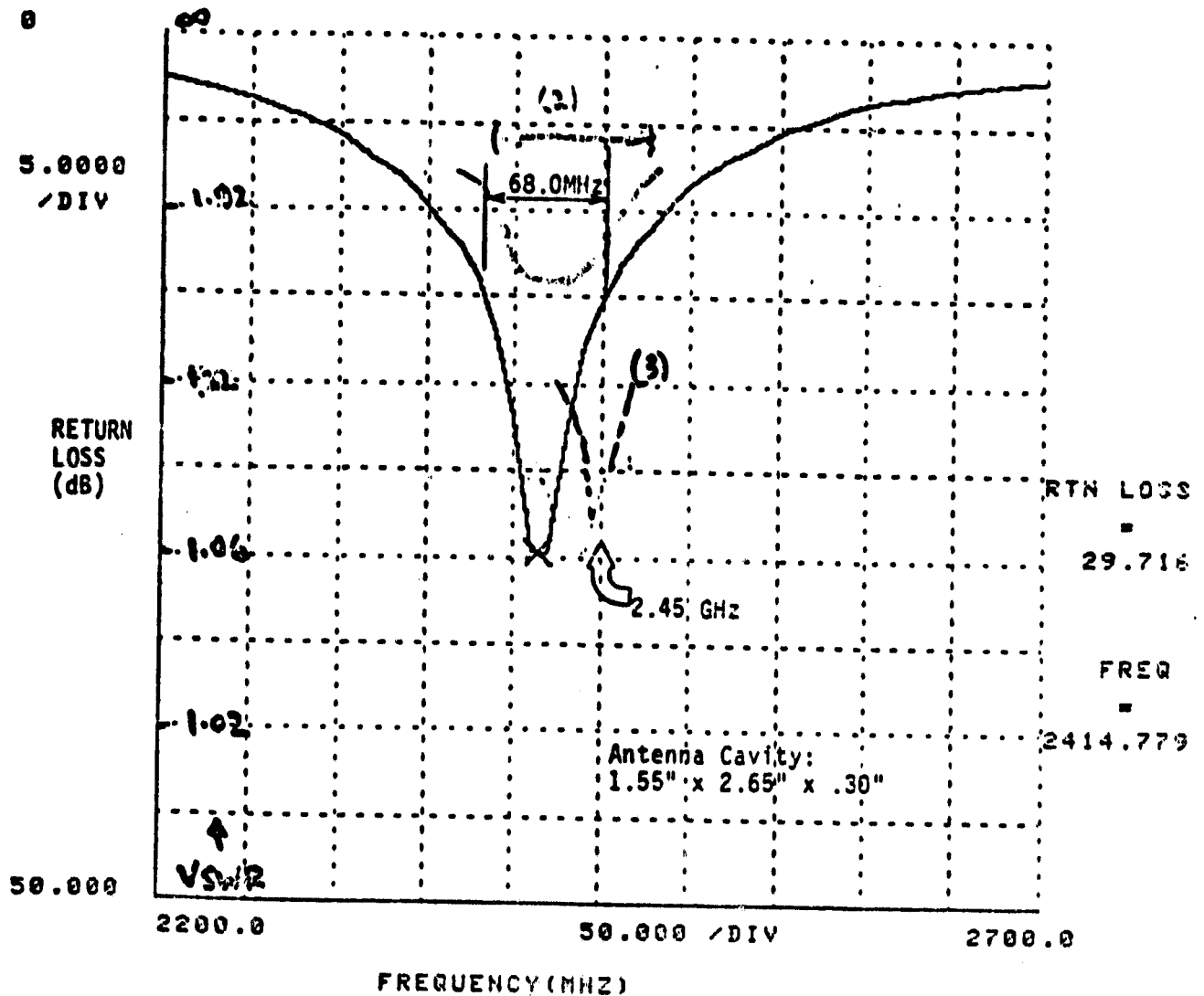


ORIGINAL PAGE IS
 OF POOR QUALITY

THE BOEING CO. GWF

OCTOBER 15, 1979

SPS SOLID STATE MODULE DEVELOPMENT
SINGLE FEED ANTENNA, SHORT OFF-SET = .39"



**EVOLUTION OF A SLOTLINE ANTENNA
(METALIZATION PATTERN)**

**Fig. 2
DUAL FEED ANTENNA**

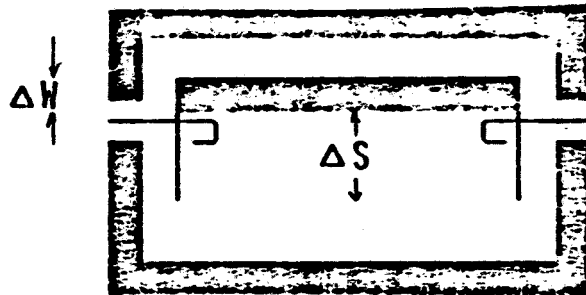
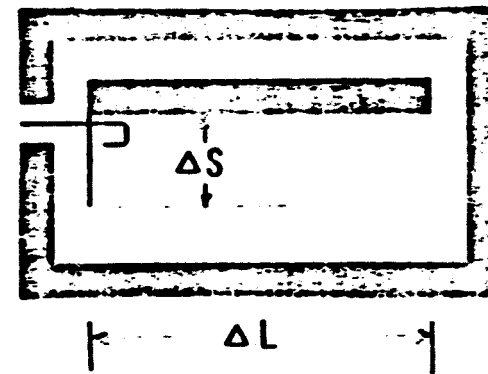
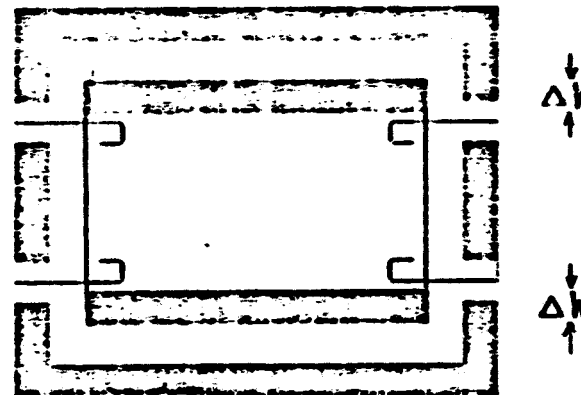


**Fig. 1
SINGLE FEED ANTENNA**



FOUR FEED ANTENNA

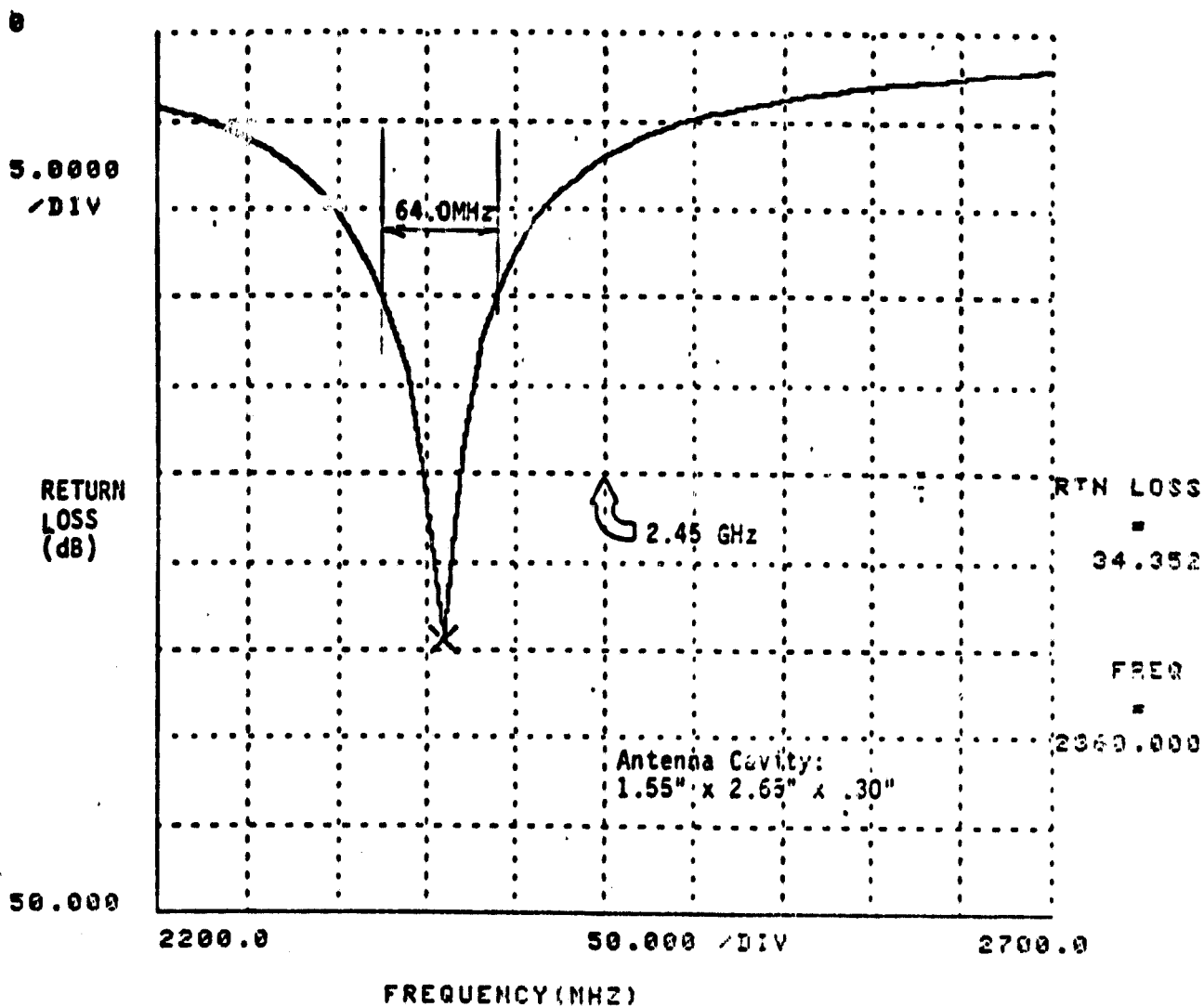
Fig. 3



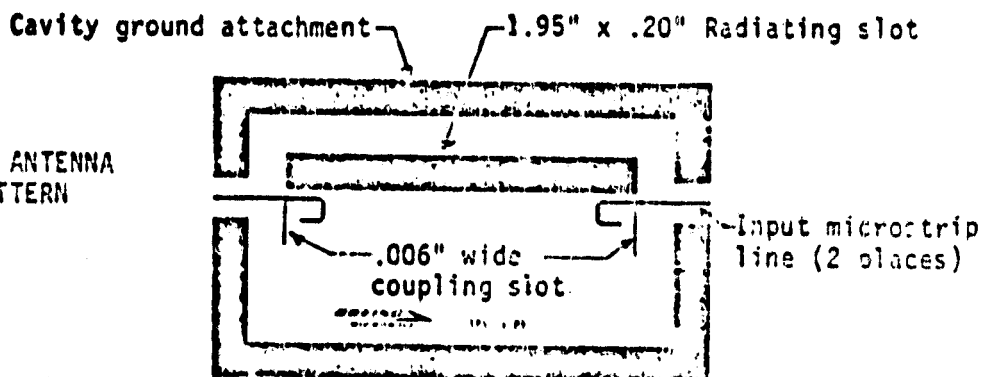
- $\Delta S \rightarrow$ COUPLING MATCH
- $\Delta L \rightarrow$ FREQUENCY
- $\Delta W \rightarrow$ BANDWIDTH

OCTOBER 15, 1979

SPS SOLID STATE MODULE DEVELOPMENT
TWO FEED ANTENNA, SHORT OFF SET = .31"

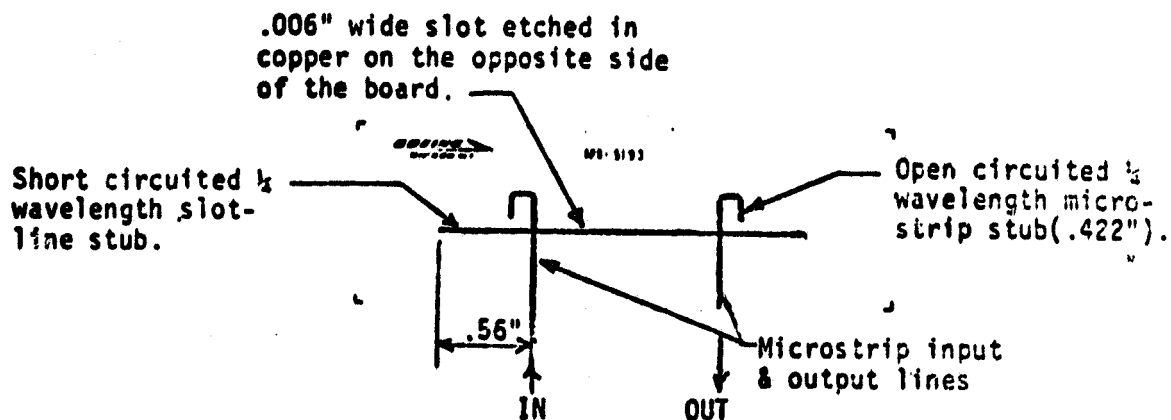
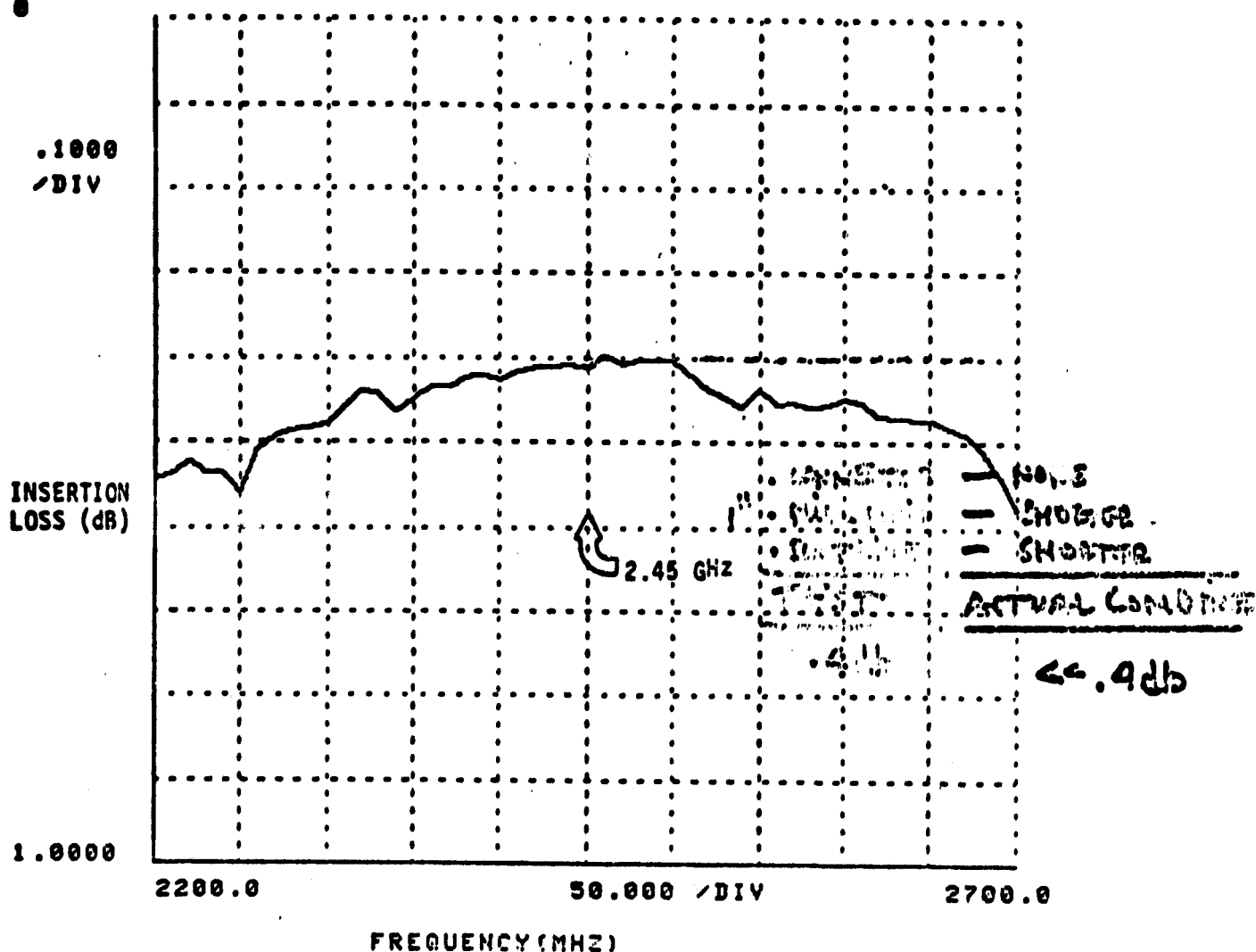


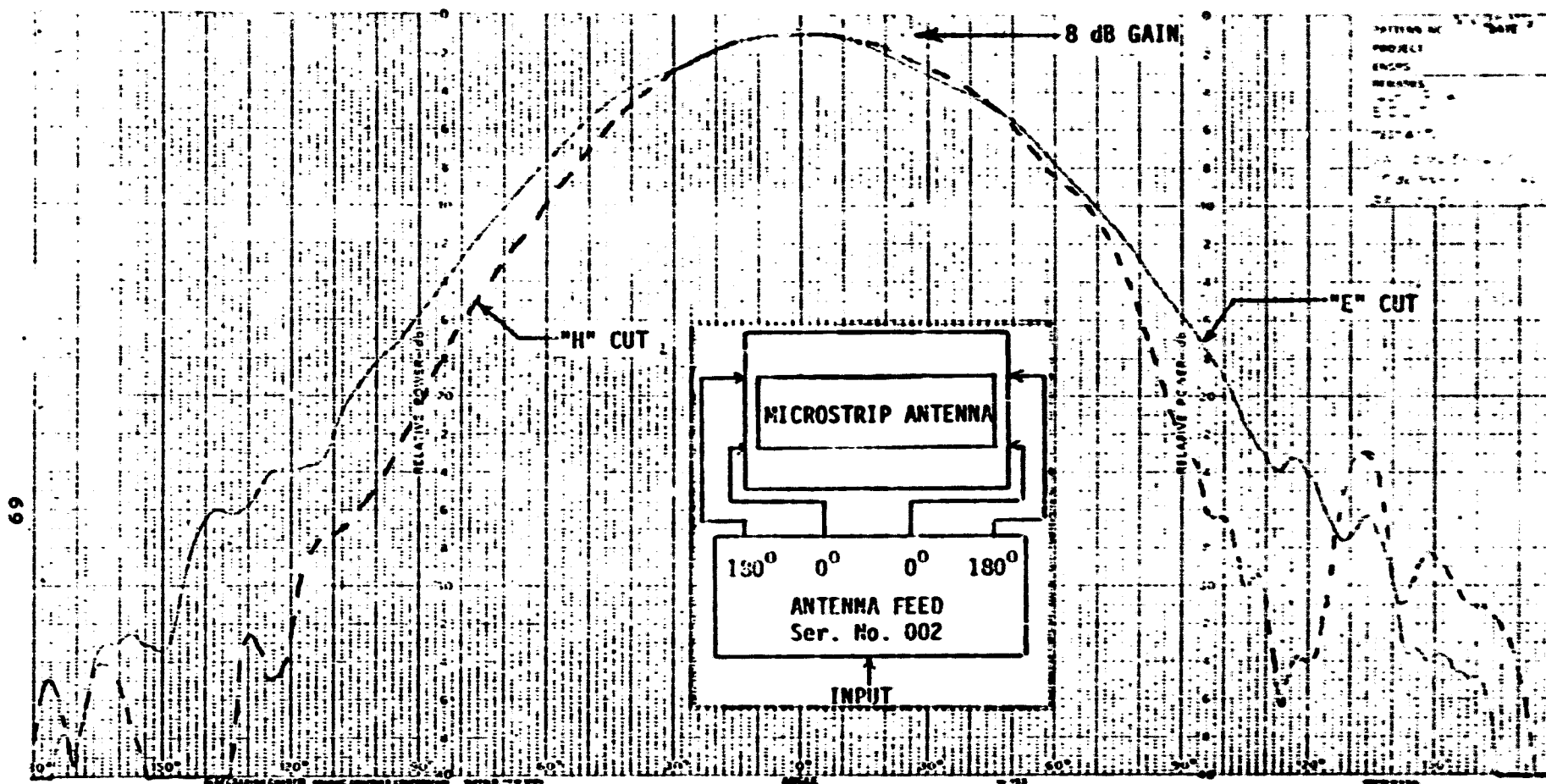
PRINTED CIRCUIT ANTENNA
METALIZATION PATTERN



OCTOBER 15, 1979

SPS SOLID STATE MODULE DEVELOPMENT
 MICROSTRIP-SLOTLINE-MICROSTRIP THRU TEST





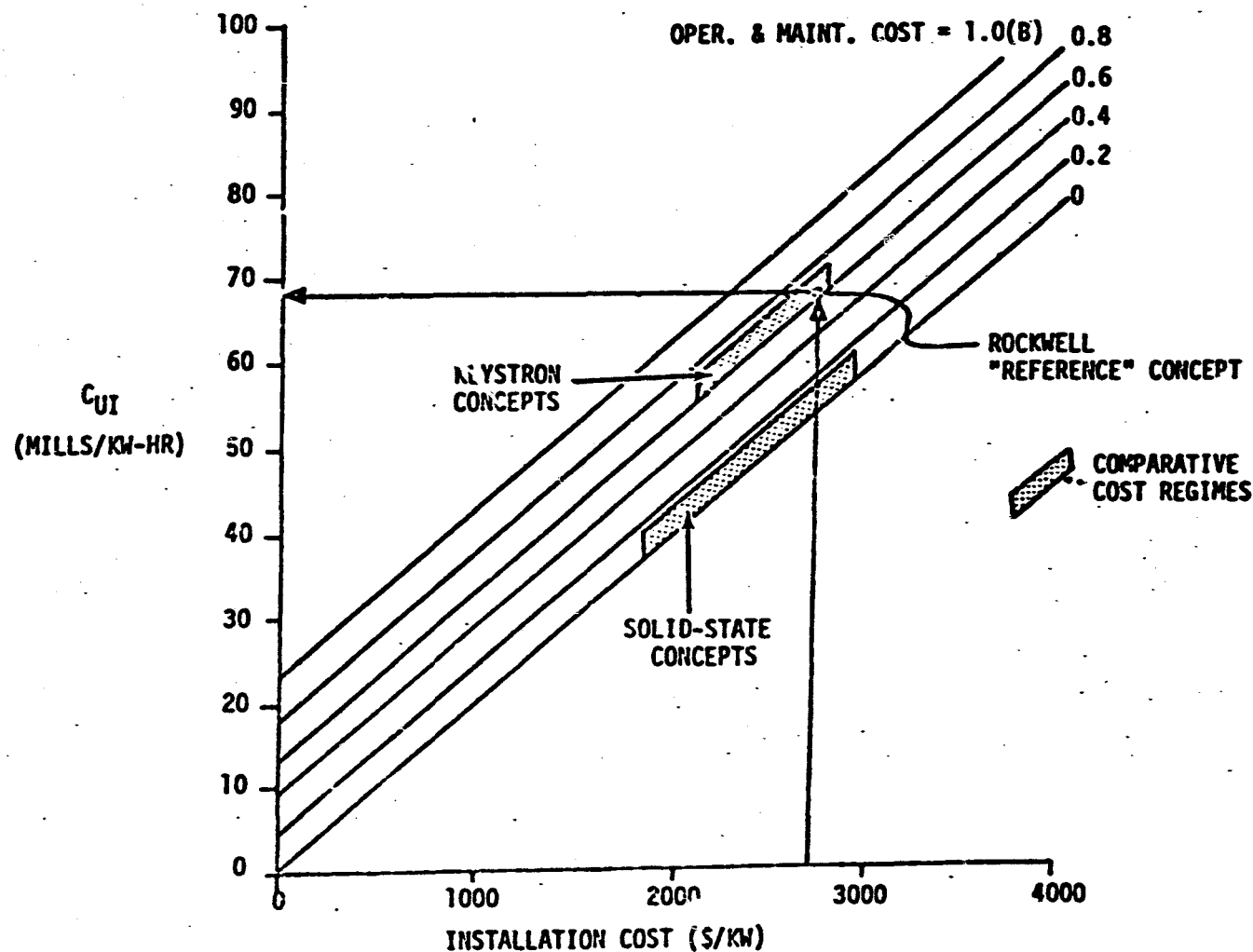
ANTENNA RANGE GAIN PATTERN FOR THE FIRST POWER COMBINING MICROSTRIP ANTENNA
(FEED NETWORK NO. 2)

Solid State Systems Concepts

***K. Schroeder and Petroff
Rockwell International***

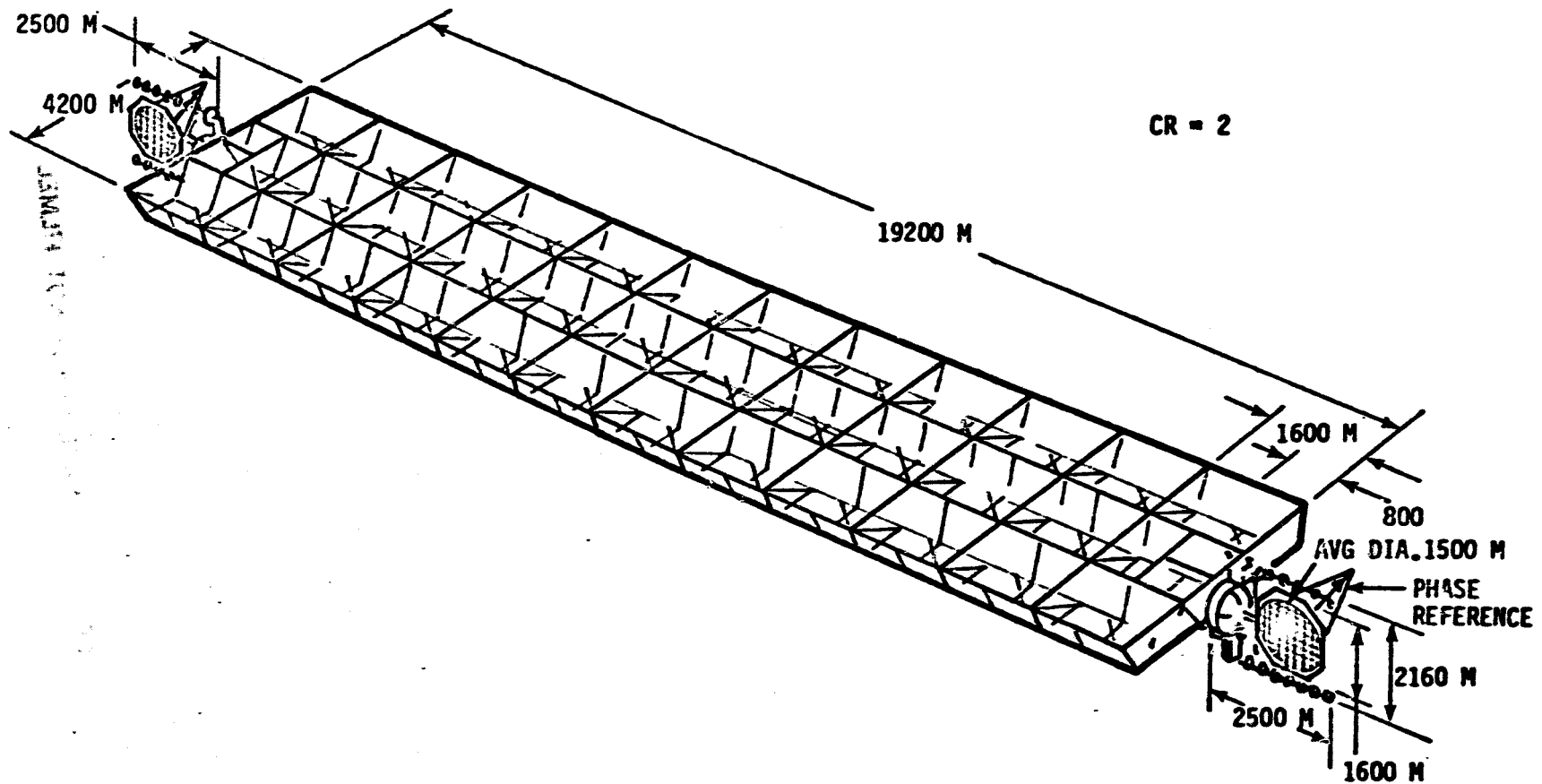
PRECEDING PAGE BLANK NOT FILMED

SIMPLIFIED UTILITY INTERFACE POWER COST RELATIONSHIP



PRECEDING PAGE BLANK NOT FILMED

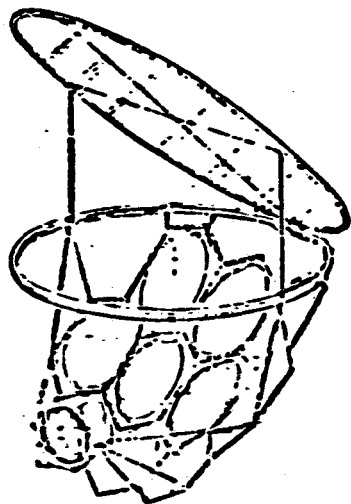
END-MOUNTED SOLID STATE CONCEPT



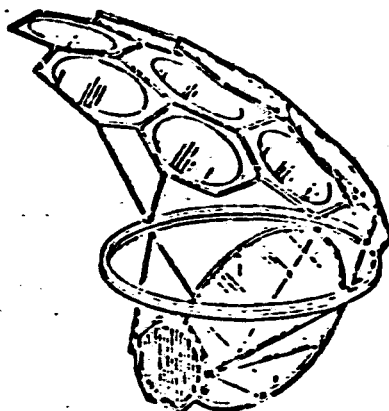
END-MOUNTED SOLID-STATE CONCEPT CHARACTERISTICS

- o GaAs SOLAR ARRAY
- o GEOMETRIC CR = 2.0
- o DUAL END-MOUNTED MICROWAVE ANTENNAS
- o AMPLIFIER BASE TEMPERATURE = 125°C
- o AMPLIFIER EFFICIENCY = 0.8
- o ANTENNA POWER TAPER = 10dB
- o ANTENNA DIAMETER = 1.35 km
- o POWER AT UTILITY INTERFACE = 2.61 GW PER ANTENNA
(5.22 GW TOTAL)
- o RECTENNA BORESIGHT DIAMETER = 7.51 km PER RECTENNA

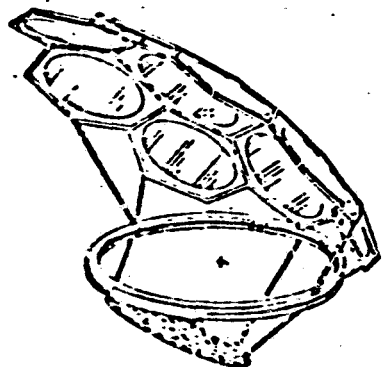
ALTERNATIVE SOLID STATE SANDWICH CONCEPTS



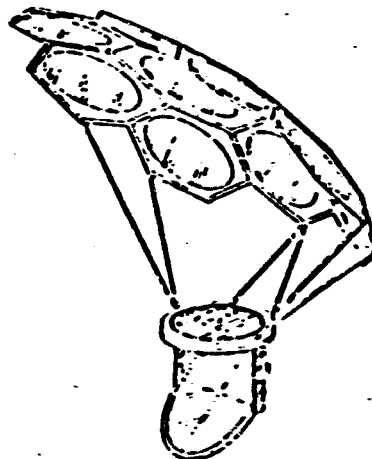
(1) FLAT PRIMARY/FACETED SECONDARY



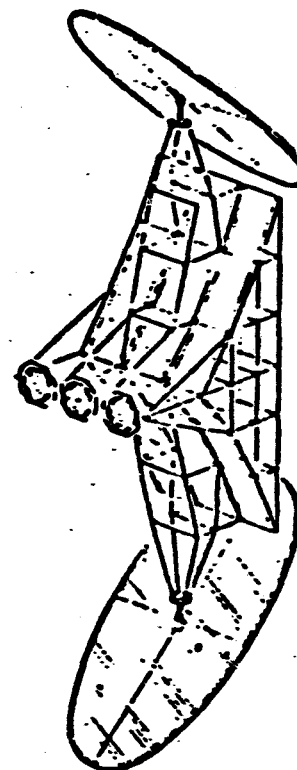
(2) FLAT SECONDARY/
FACETED PRIMARY



(3) INCLINED ANTENNA/
SINGLE FACETED REFLECTOR

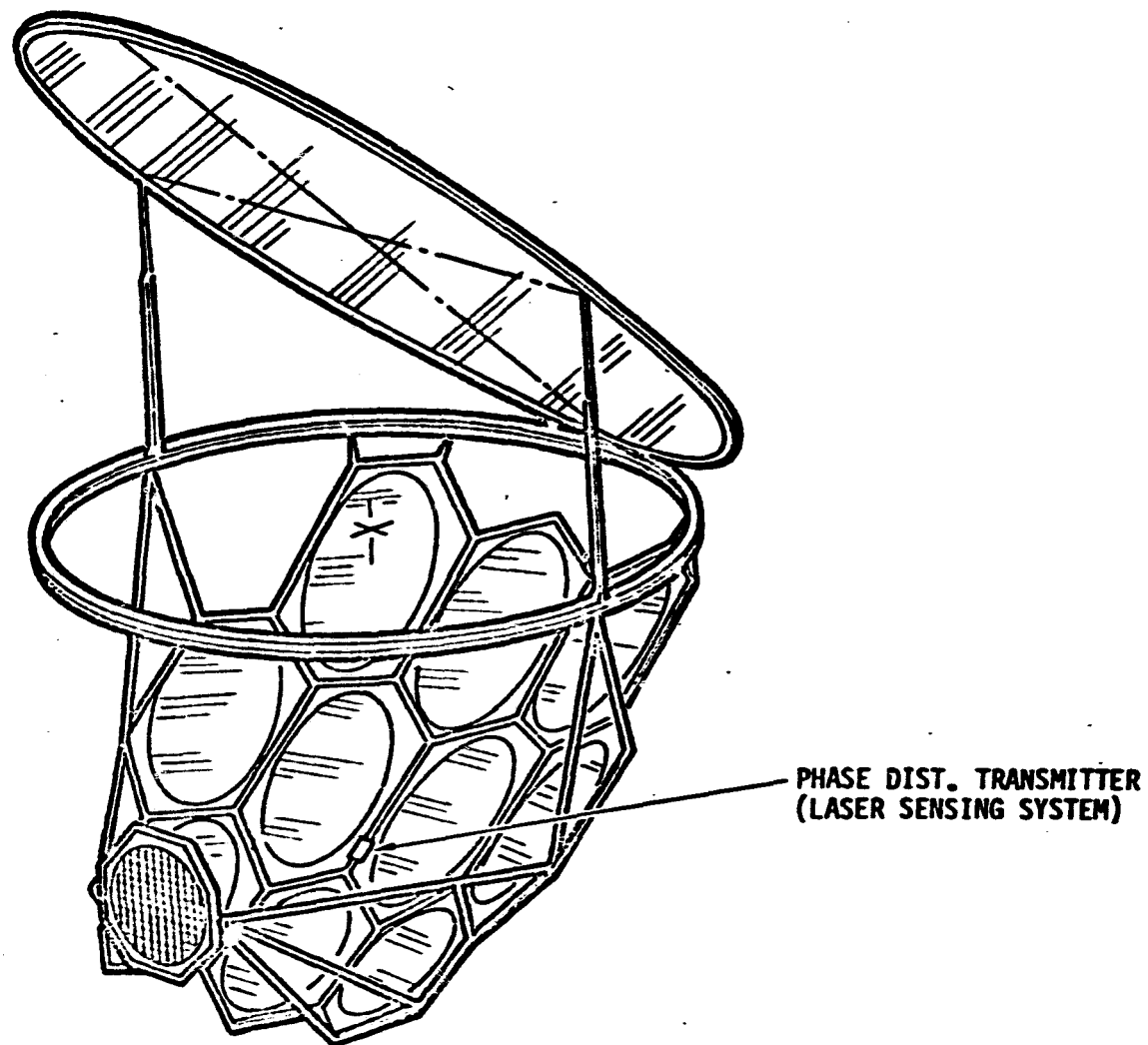


(4) RF REFLECTOR/SINGLE
MULTI-FACETED REFLECTOR



(5) MULTI-ANTENNA CONCEPT

SOLID STATE SANDWICH CONCEPT RECOMMENDED FOR POINT DESIGN



SOLID STATE SANDWICH CONCEPT
COMPARISON OF 0 dB AND 10 dB ANTENNA POWER TAPER

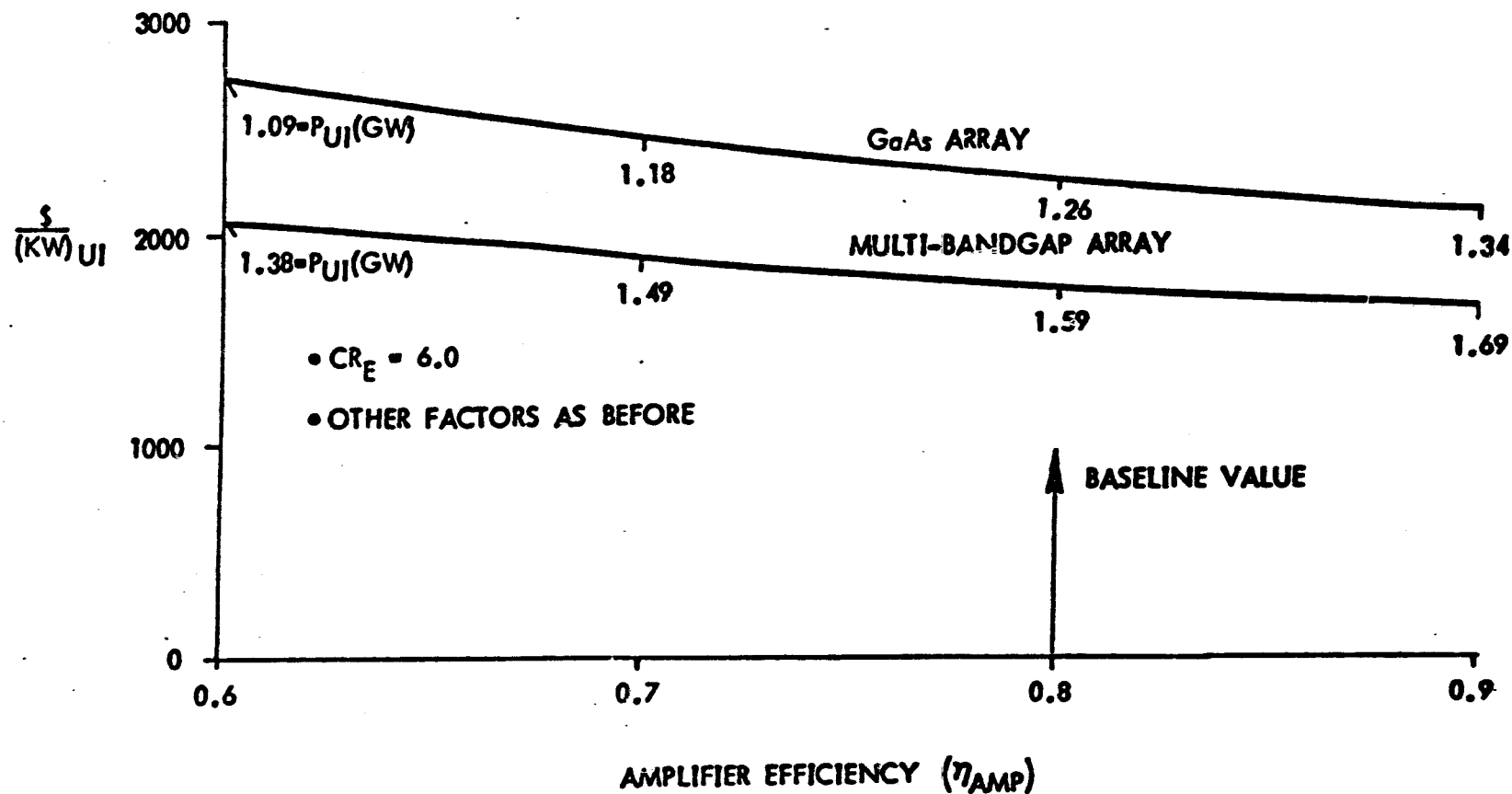
	0 dB	10 dB
TYPE OF SOLAR ARRAY	MBG	MBG
MAXIMUM EFFECTIVE CONCENTRATION RATIO	6.0	6.0
AMPLIFIER EFFICIENCY	0.8	0.8
MAX. ANTENNA POWER DENSITY (W/M ²)	1.235	1.235
ANTENNA DIAMETER (KM)	1.578	2.049
TOTAL TRANSMITTED POWER (GW)	2.418	1.588
POWER AT UTILITY INTERFACE (GW)	1.591	1.127
RECTENNA BORESIGHT DIAMETER (KM)	5.600	4.929
TOTAL SATELLITE MASS (10 ⁶ KG)	10.13	13.30
COST DATA (\$)		
• SATELLITE	0.796	0.963
• CONSTRUCTION OPERATIONS	0.079	0.096
• TRANSPORTATION	0.598	0.798
• RECTENNA	0.935	0.763
• TOTAL COST (INCL. MGMT & CONTINGENCY)	2.789	3.030
INSTALLATION COST (\$/KW) _{UI}	1.759	2.689

RECOMMENDED SOLID-STATE SANDWICH CONCEPT CHARACTERISTICS

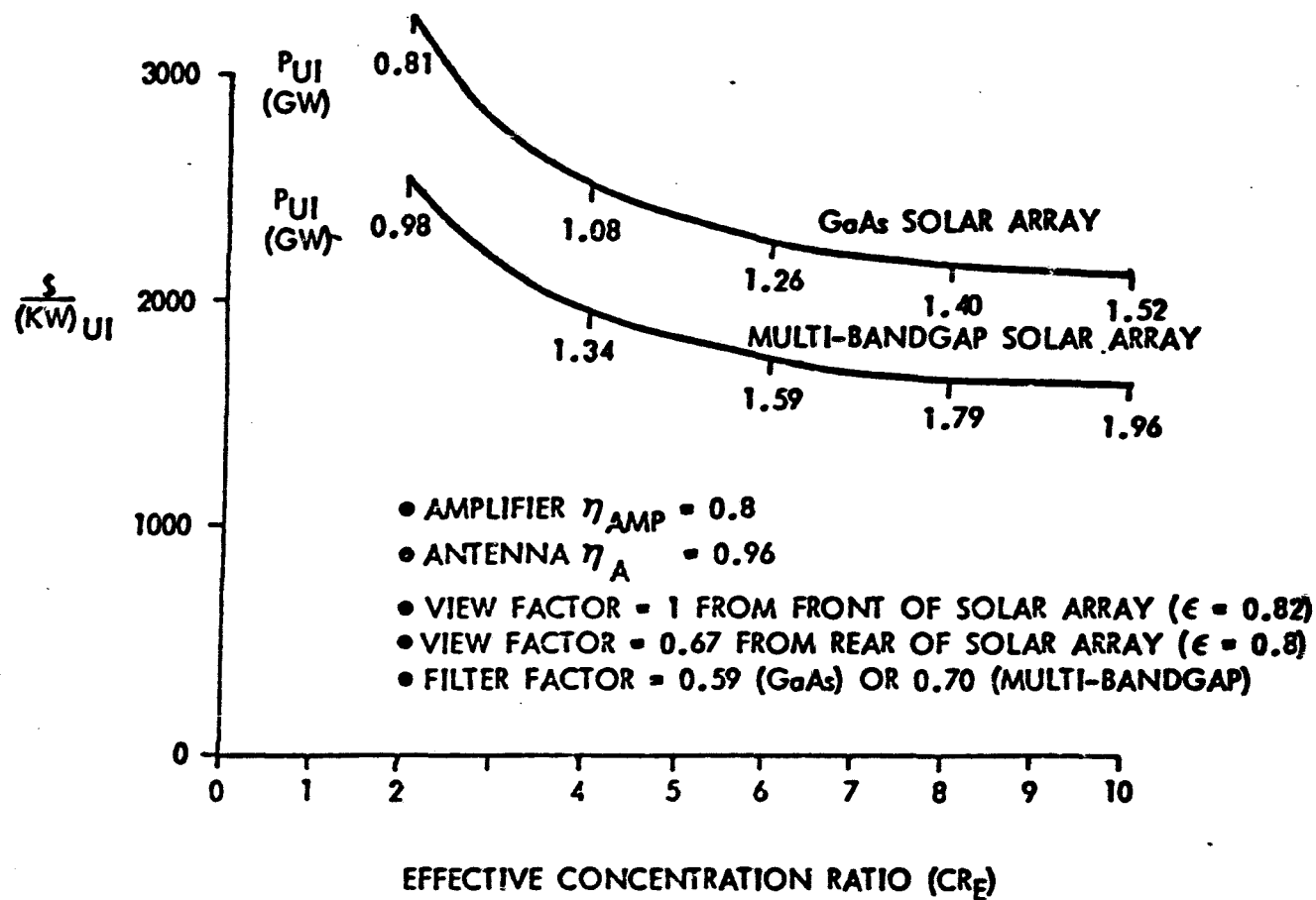
CHARACTERISTIC	SECONDARY	PRIMARY
SOLAR ARRAY TYPE	MULTI-BANDGAP	GaAs
EFFECTIVE CR	5 to 6	6
SOLAR ARRAY TEMPERATURE (°C)	200	200
AMPLIFIER BASE TEMPERATURE (°C)	125	125
AMPLIFIER EFFICIENCY	0.8	0.8
ANTENNA TAPER RATIO (dB)	0	0
ANTENNA DIAMETER (km)	1.64 TO 1.58	1.77
POWER AT UTILITY INTERFACE (GW)	1.47 TO 1.54	1.26
RECTENNA BORESIGHT DIAMETER (km)	5.39 TO 5.68	5.10

SOLID STATE SANDWICH CONCEPT

EFFECT OF AMPLIFIER EFFICIENCY ON INSTALLATION COST

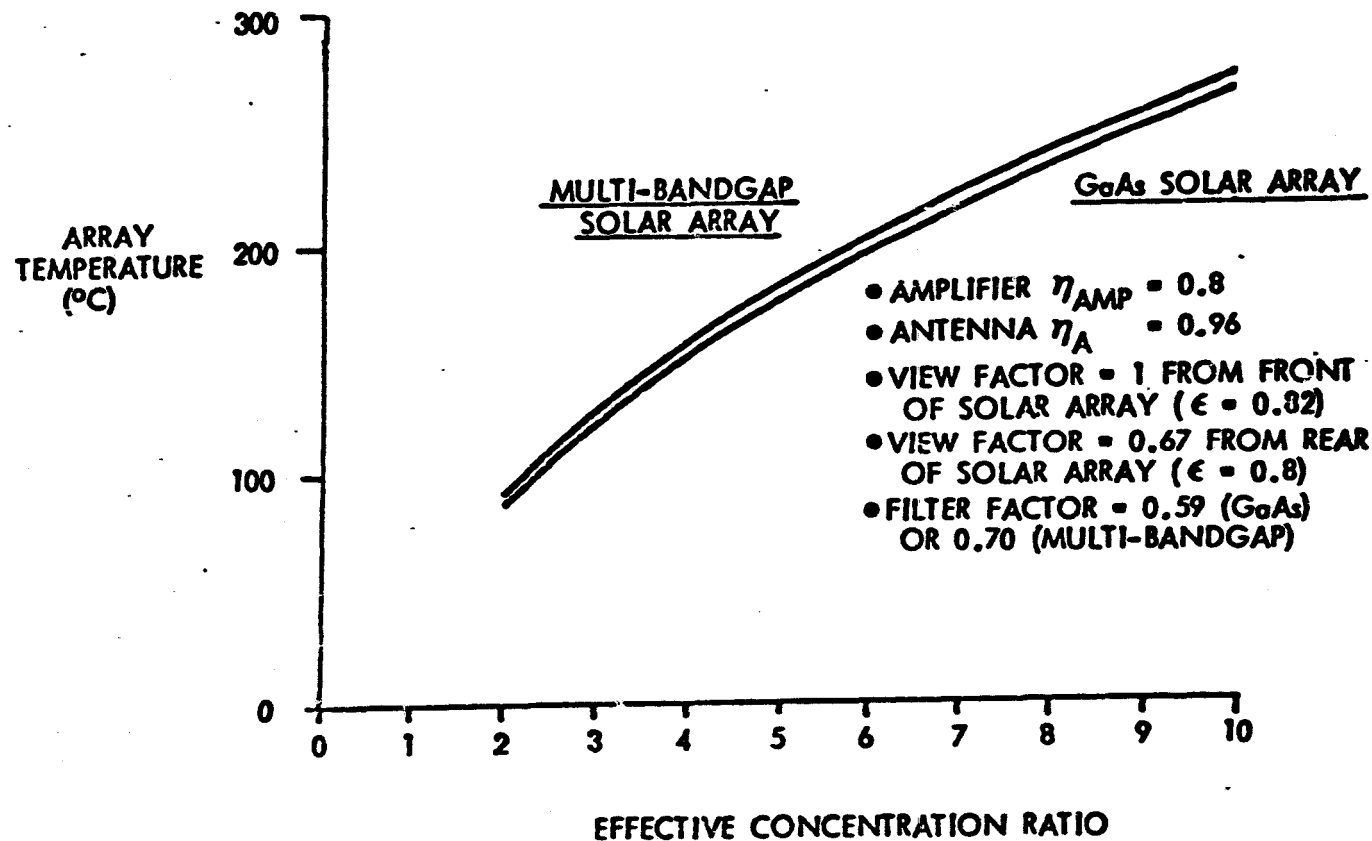


SOLID STATE SANDWICH CONCEPT EFFECT OF CR_E ON INSTALLATION COST

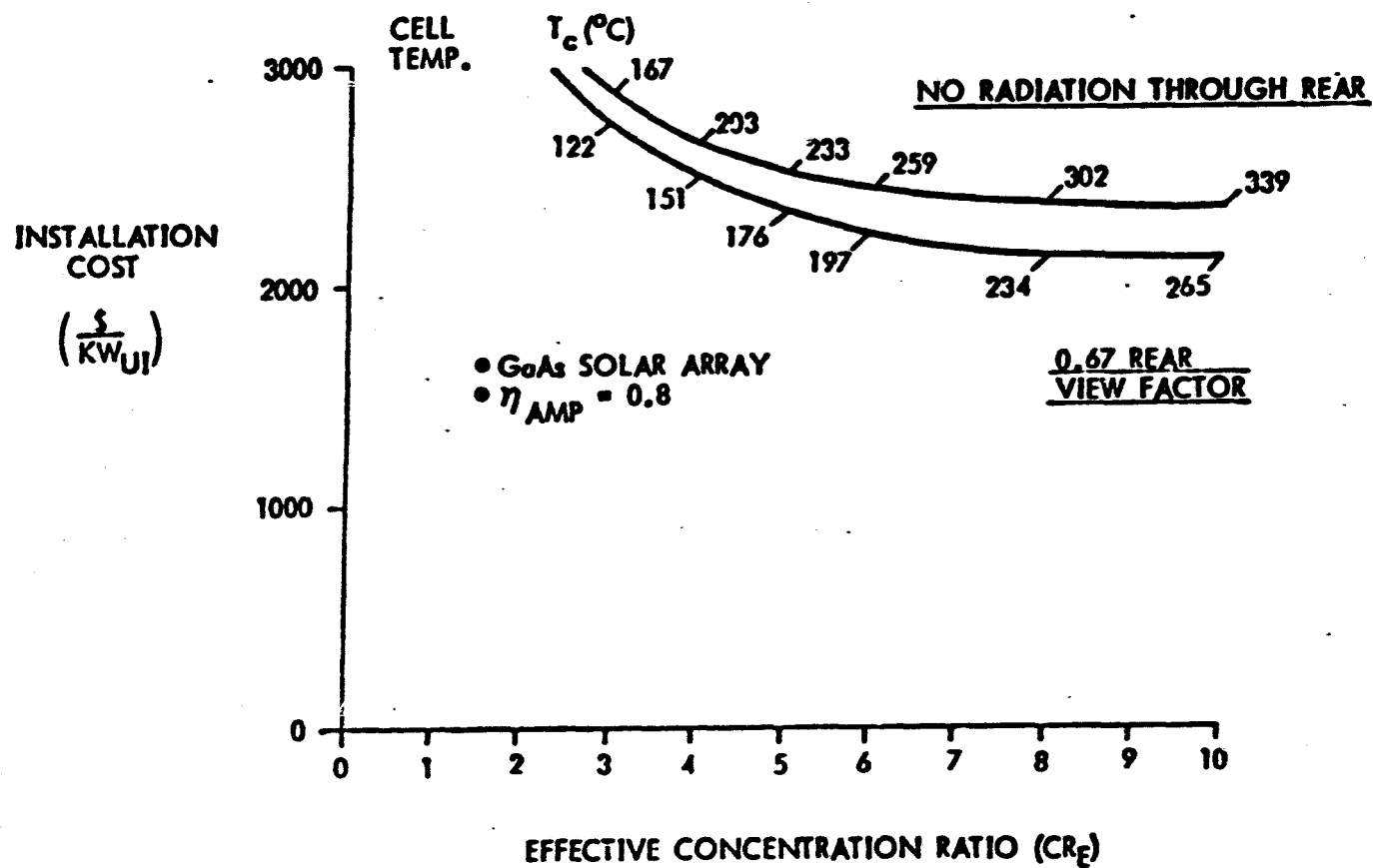


SOLID STATE SANDWICH CONCEPT

EFFECT OF CR_E ON ARRAY TEMPERATURE



SOLID STATE SANDWICH CONCEPT IMPACT OF SOLAR ARRAY THERMAL RADIATION CHARACTERISTICS



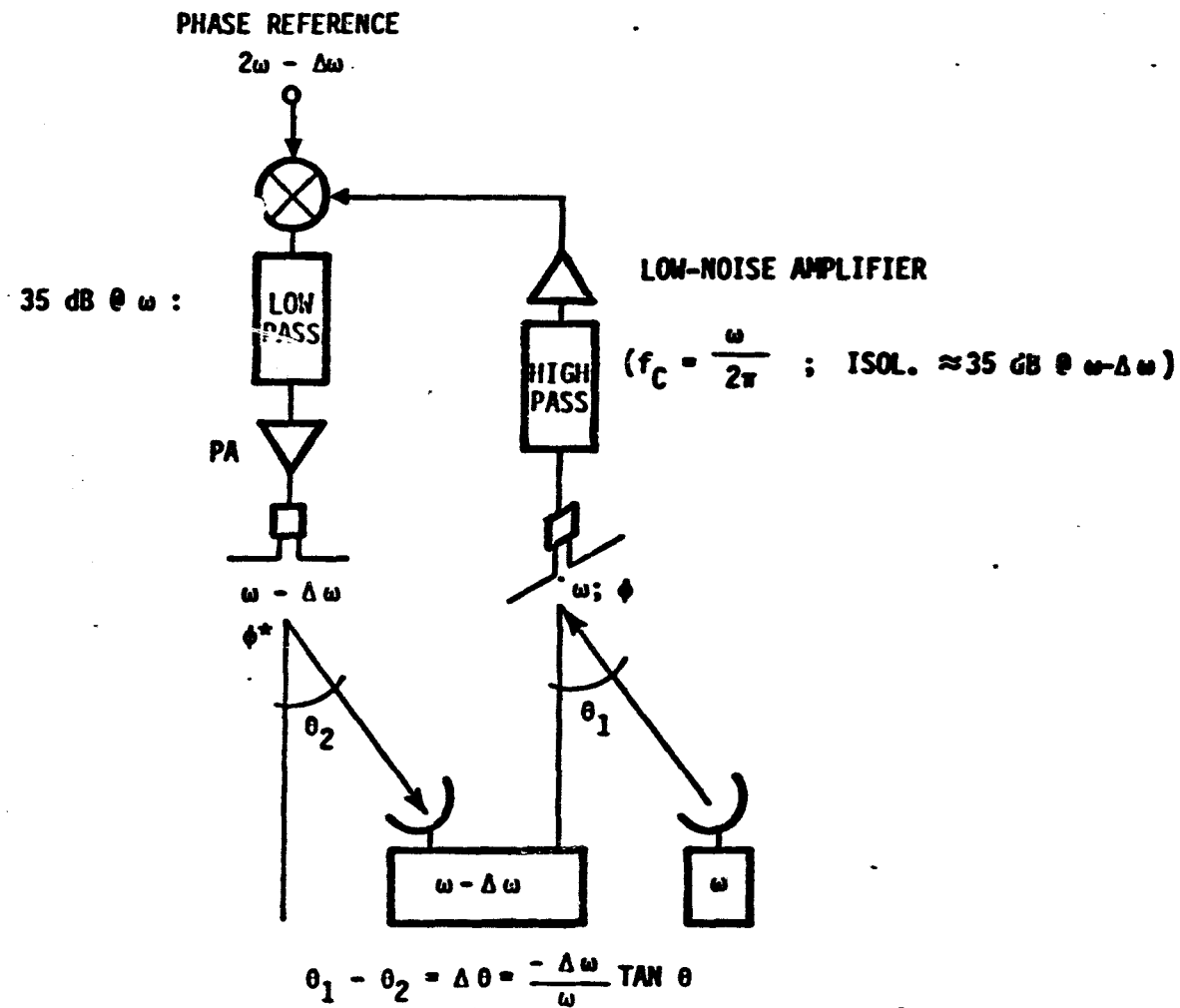
NOMINAL CHARACTERISTICS OF GaAs SANDWICH CONCEPT

UNIFORM ILLUMINATION	
EFFECTIVE (CR_E)	= 6.0
SOLAR CELL TEMPERATURE	= 200°C
SOLAR CELL EFFICIENCY	= 0.151
AMPLIFIER EFFICIENCY	= 0.8
AMPLIFIER BASE TEMPERATURE	= 125°C
ANTENNA OHMIC EFFICIENCY	= 0.96
SOLAR CELL PACKAGING FACTORS	= 0.3547
POWER TRANSMITTED/UNIT AREA	= 773.9 W/m ²
ANTENNA DIAMETER	= 1.77 KM
ANTENNA AREA	= 2.46 KM ²
TOTAL TRANSMITTED POWER	= 1.92 GW
POWER AT UTILITY INTERFACE	= 1.26 GW
RECTENNA DIAMETER	= 4.99 KM
RECTENNA AREA	= 19.6 KM ²

PRELIMINARY MASS PROPERTIES OF
RECOMMENDED SOLID STATE SANDWICH CONCEPTS ($CR_E = 6$)

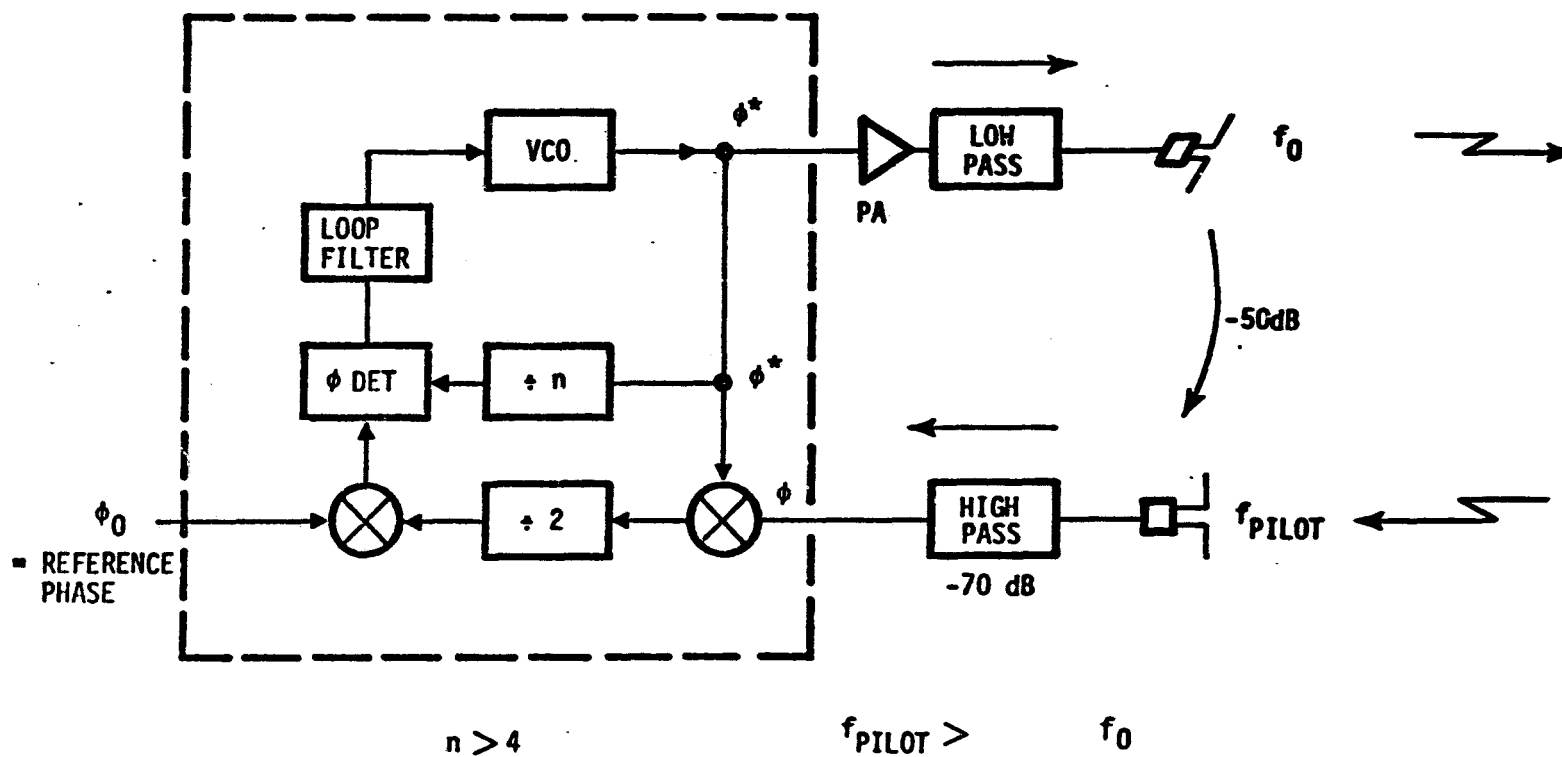
SUBSYSTEM	GaAs ARRAY (10^6 KG)
PRIMARY AND SECONDARY STRUCTURE	3.77
MICROWAVE ARRAY AND SOLAR CELLS	4.674
REFLECTORS	1.24
INFORMATION MGMT & CONTROL	0.68
ACS	0.11
25% CONTINGENCY	2.87
TOTAL	14.3

SIMPLE SINGLE-TONE CONJUGATOR

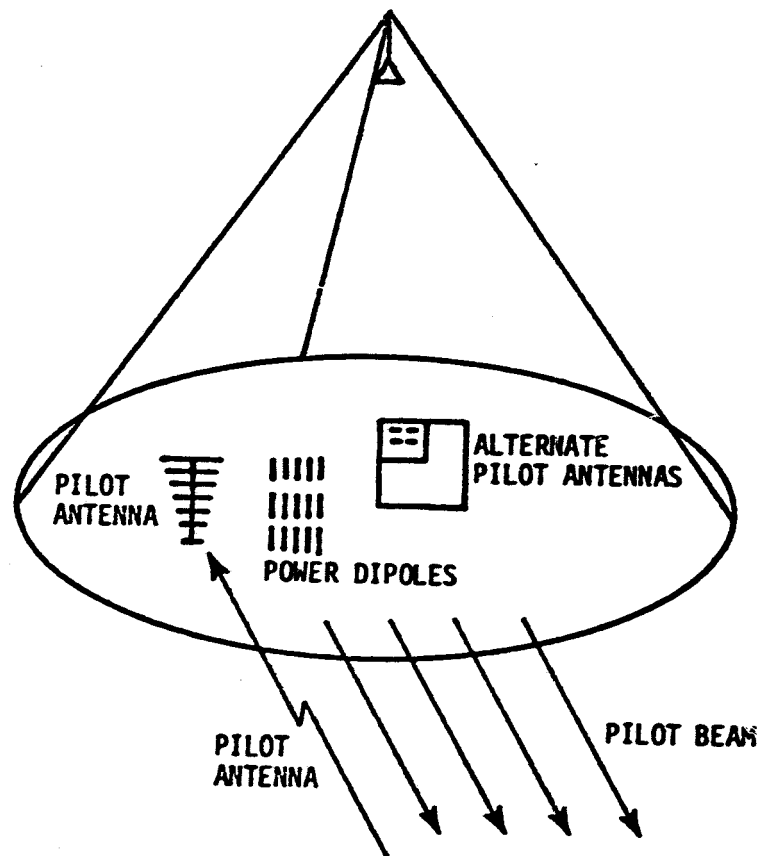


SINGLE PILOT CIRCUIT DIAGRAM

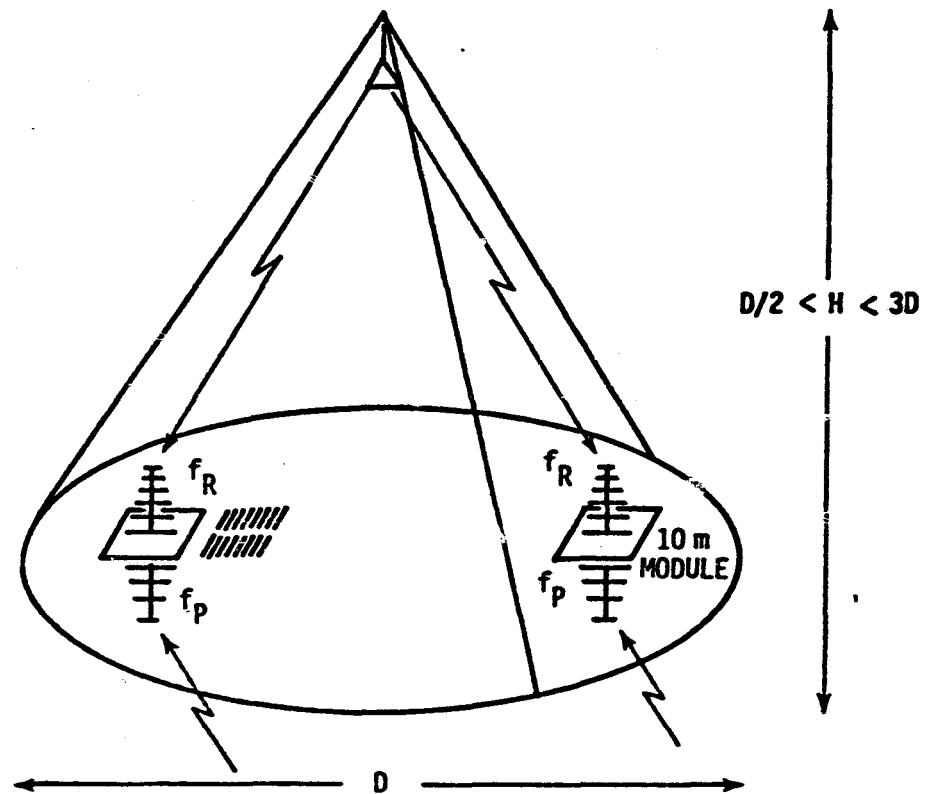
SIMPLIFIED CONJUGATOR FOR DEMONSTRATION
(AFTER CHERNOFF)



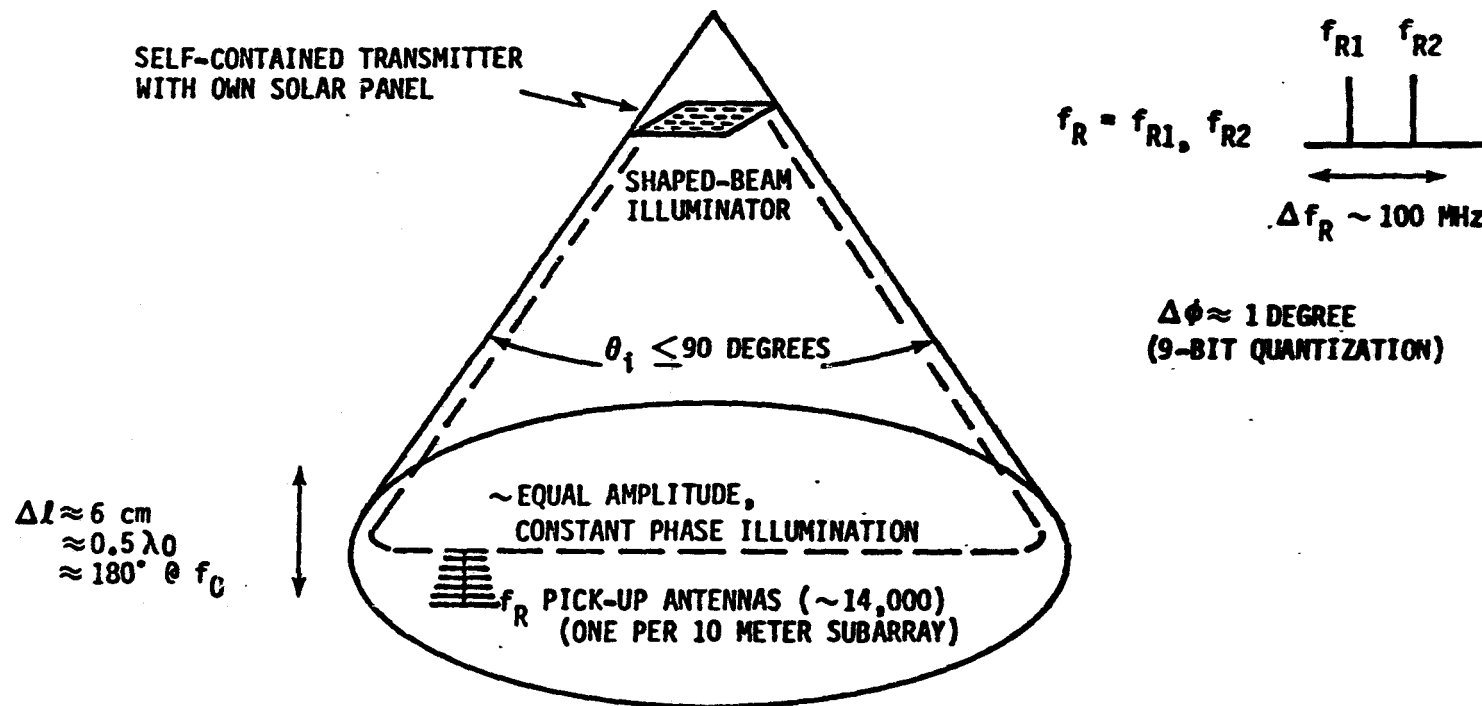
SPACETENNA TOTAL VIEW (BOTTOM)



SPACETENNA TOTAL VIEW (TOP)



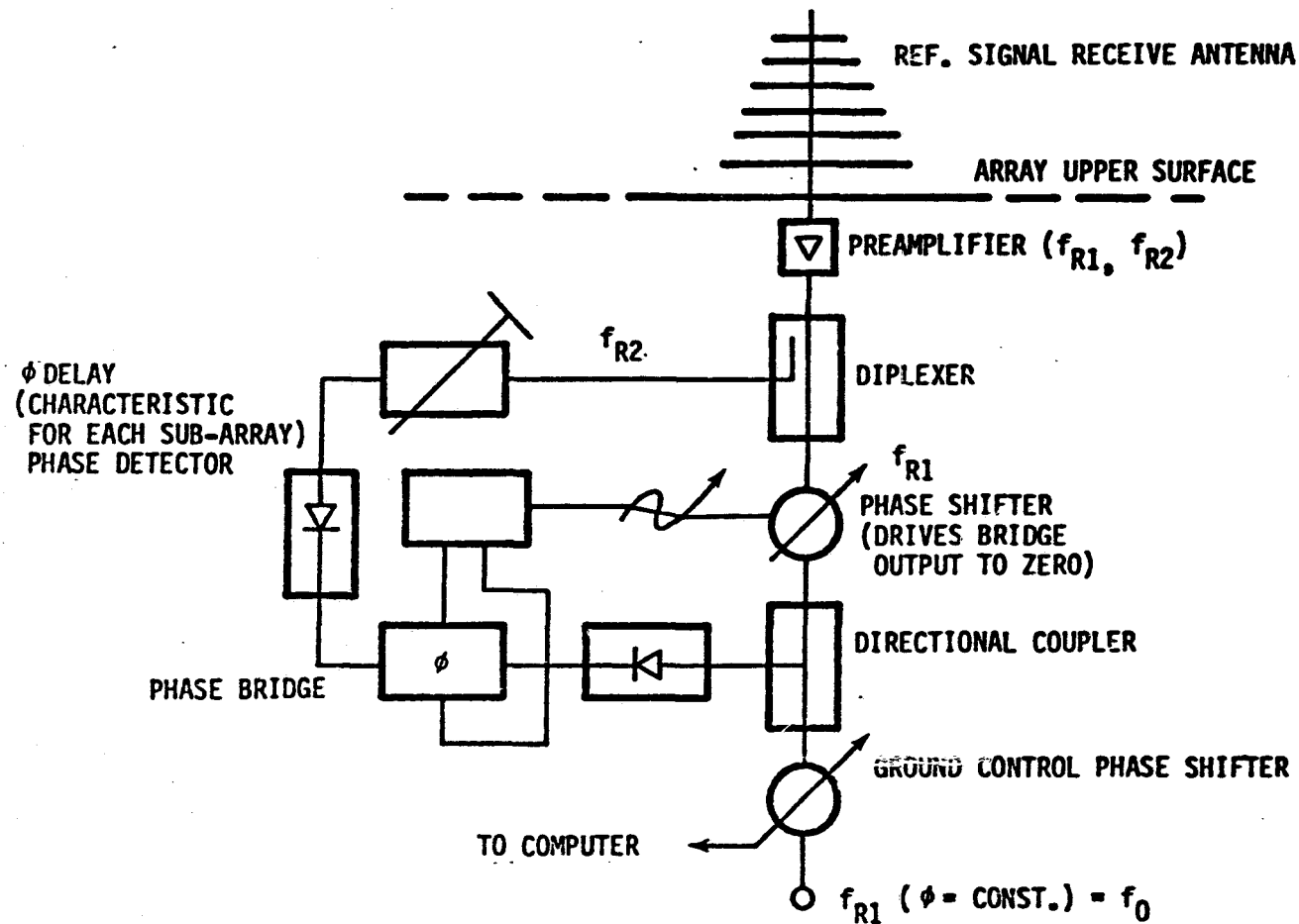
PHASE REFERENCE SIGNAL DISTRIBUTION SYSTEM



NOTE: PICK-UP ANTENNA ORTHOGONALLY POLARIZED WITH RESPECT TO POWER BEAM
TOTAL ISOLATION $I_T \geq 40 + 60 \text{ dB} \geq 100 \text{ dB}$

CROSS POL FRONT-TO-BACK RATIO (CAN BE MADE $> 100 \text{ dB}$)

REFERENCE SIGNAL CONTROL LOOP



PILOT SYSTEM LINK BUDGET

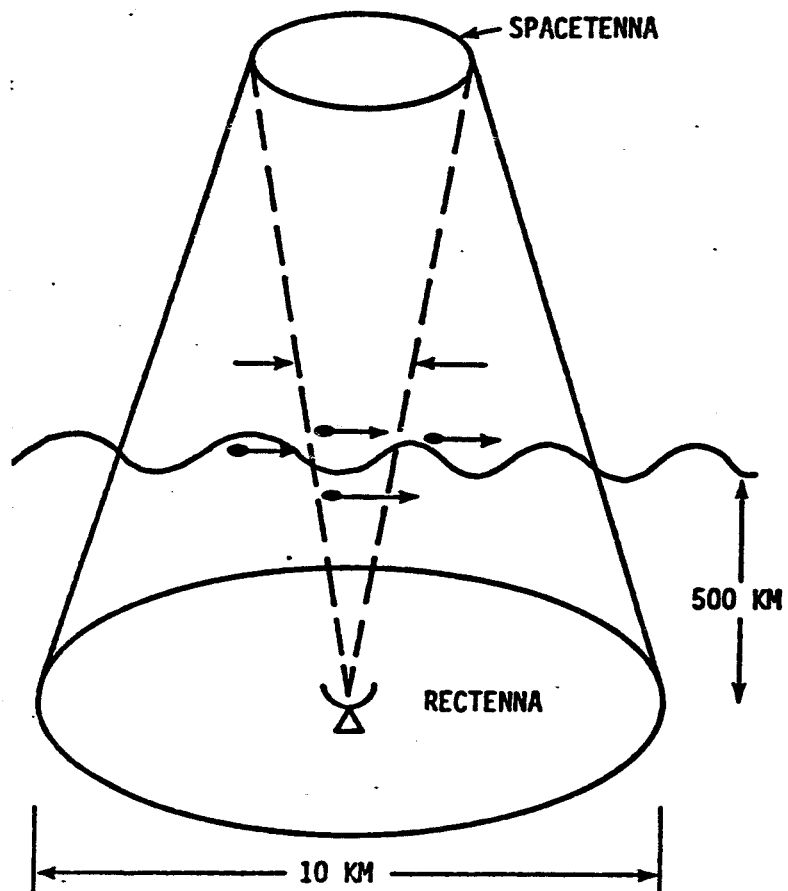
● GROUND SIGNAL ERP	100 dBW	
● SPACE LOSS	<u>-192 dB</u>	
● POWER AT SPACETENNA	- 92 dBW	
● PILOT ANTENNA RECEIVE GAIN	18 dB	-74 dBW
● ISOLATION TO POWER DIPOLE	20 dB	(INCLUDES DIPOLE GAIN)
● POWER DIPOLE OUTPUT	-10 dBW	
● CROSS POLARIZATION ATTENUATION	<u>30 dB</u>	
● PILOT TO POWER SIGNAL RATIO	-34 dB	
● NOTCH FILTER ATTENUATION (RELATIVE TO TWO PILOT SIGNALS SYMMETRICAL TO CARRIER)	+70 dB	
● NET PILOT SIGNAL TO POWER SIGNAL RATIO	<u>+36 dB</u>	
● PILOT-TO-THERMAL NOISE RATIO (ASSUMING 3dB NOISE FIGURE AND 3dB NOTCH FILTER LOSS)	<u>~+37 dB</u>	(THERMAL NOISE \approx -117dBW FOR 500MHZ PILOT WIDTH)

PILOT GROUND SYSTEM SUMMARY

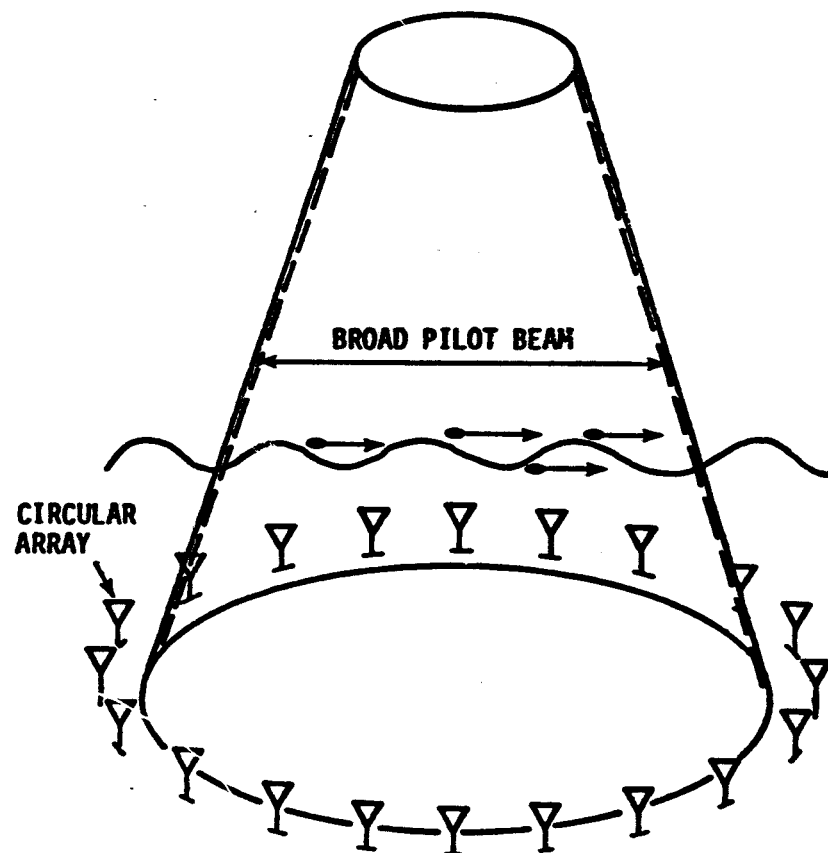
- CIRCULAR ARRAY OF LOW-GAIN ELEMENTS AT 3.14 METER
($\approx 25 \lambda$) SPACING; ELEMENTS FED IN PHASE
- 10,000 PILOT ARRAY ELEMENTS OF 10 DB GAIN EACH
- MINIMUM 50dB ARRAY GAIN
- 10 WATT SOLID-STATE TRANSMITTER AT EACH ELEMENT
- PHASE DISTRIBUTION USING FIBER OPTICS
- BEAM STEERED TO SATELLITE LOCATION BY TIME DELAY COMPENSATION
AT EACH ELEMENT
- TOTAL ERP: 100 dBw

PILOT BEAM GROUND SYSTEM LAYOUT

NO BEAM SYMMETRY



BEAM SYMMETRY



IONOSPHERIC EFFECTS
RANDOMLY FLUCTUATING PERTURBATIONS

- o DISTURBANCES (LOCAL VARIATIONS IN ELECTRON DENSITY) MOVE Laterally THROUGH IONOSPHERE, PERPENDICULAR TO BEAMS
- o DISTURBANCES RANGE IN SIZE FROM 5 TO 100 METERS*) AND MOVE AT RATES OF UP TO 100 METERS/SEC.*)
- o REGION OVER WHICH SUCH VARIATIONS OCCUR CAN BE AS LARGE AS 5KM WIDE AT 500 KM ALTITUDE
- o 5 METER DISTURBANCE MOVING ACROSS 5 METER PILOT BEAM IN 0.1 SECONDS CAN CAUSE BEAM JITTER. MULTIPLE PILOT LOCATIONS ON GROUND CAN OVERCOME THIS PROBLEM, BUT INCREASE COMPLEXITY DURING ONBOARD PROCESSING.
- o BROAD NEAR-FIELD PILOT BEAM (I.E. USING SIMILAR APERTURE AS RECTENNA) PRODUCES UP/DOWNLINK BEAM SYMMETRY, ELIMINATES PROBLEM

*) SPECIFIC PARAMETERS VARY GREATLY FROM SITE TO SITE, MAKING RESEARCH PROGRAM MANDATORY

ALTERNATE BEAM STEERING SYSTEMS
(BACK-UP TO RETRODIRECTIVE BASELINE)

- ON-BOARD PHASE MONOPULSE, USING ~ 24 METER PORTION OF TOTAL ARRAY; ON-BOARD COMPUTATION; PHASE SHIFTERS AT DISTRIBUTION SYSTEM INPUTS.
- ON-BOARD AMPLITUDE MONOPULSE
- ON-BOARD CONICAL SCAN, AVERAGING PILOT DIRECTION OVER A NUMBER OF SCANS. (THIS MAY BE GOOD SOLUTION TO ELIMINATE SHORT-TERM BEAM JITTER)

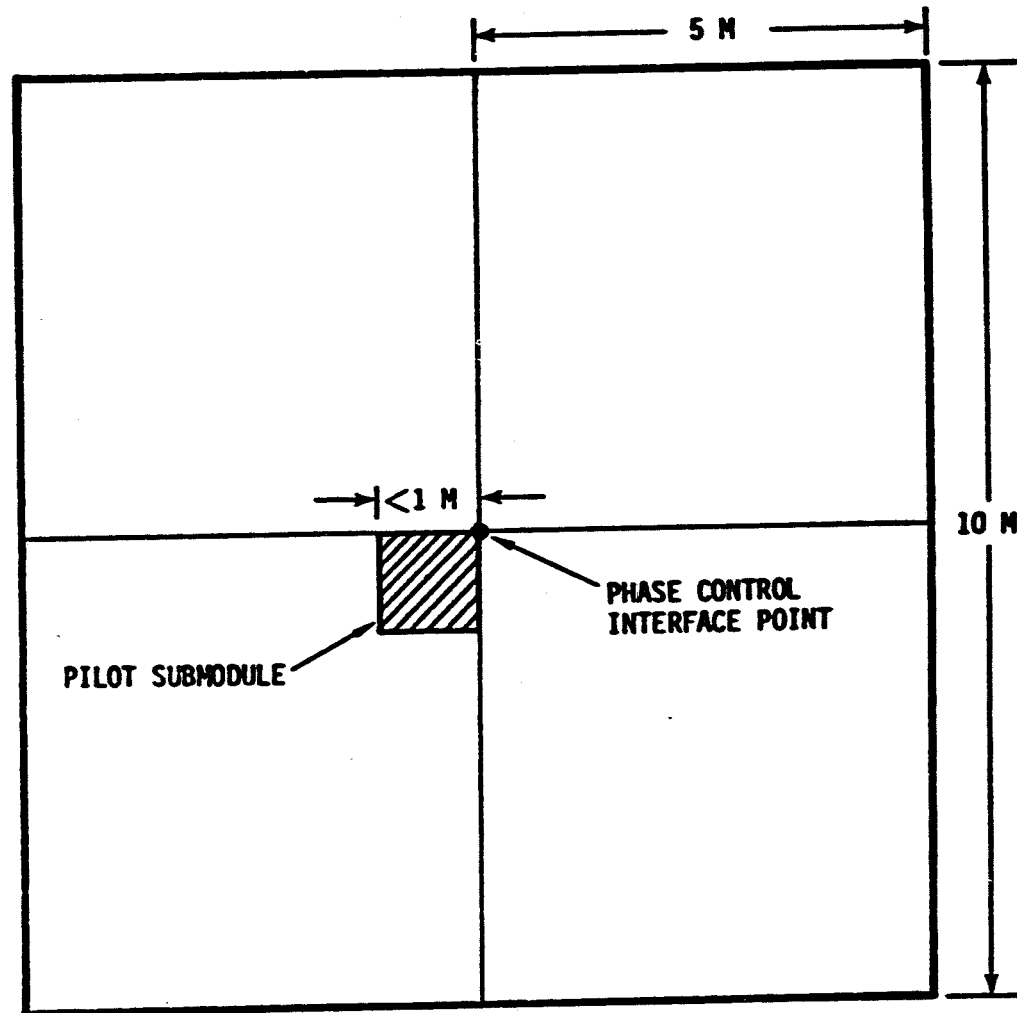
ALTERNATE APERTURE SENSING SYSTEMS
(BACK-UP TO RF DISTRIBUTION LINK)

- DUAL 8-MICRON LASERS SCANNING TOTAL ARRAY STRUCTURE SURFACE ONCE A SECOND TO DETECT STRUCTURAL DEFORMATIONS AND/OR VARIATIONS IN REFERENCE SIGNAL TRANSMITTER LOCATION; CALCULATION OF REQUIRED PHASE COMPENSATION (MODULO 2π)
- NEON/HELIUM LASER WITH WIDEBAND MODULATOR; PERFORMING SAME FUNCTION AS ABOVE
- MIRRORS AT EACH SUBARRAY CENTER TO ENHANCE LASER SIGNAL RETURN, AND PROVIDE PRECISE TIME REFERENCE FOR SCANNING RASTER
- OTHER OPTICAL APPROACHES: "STARING SYSTEM"

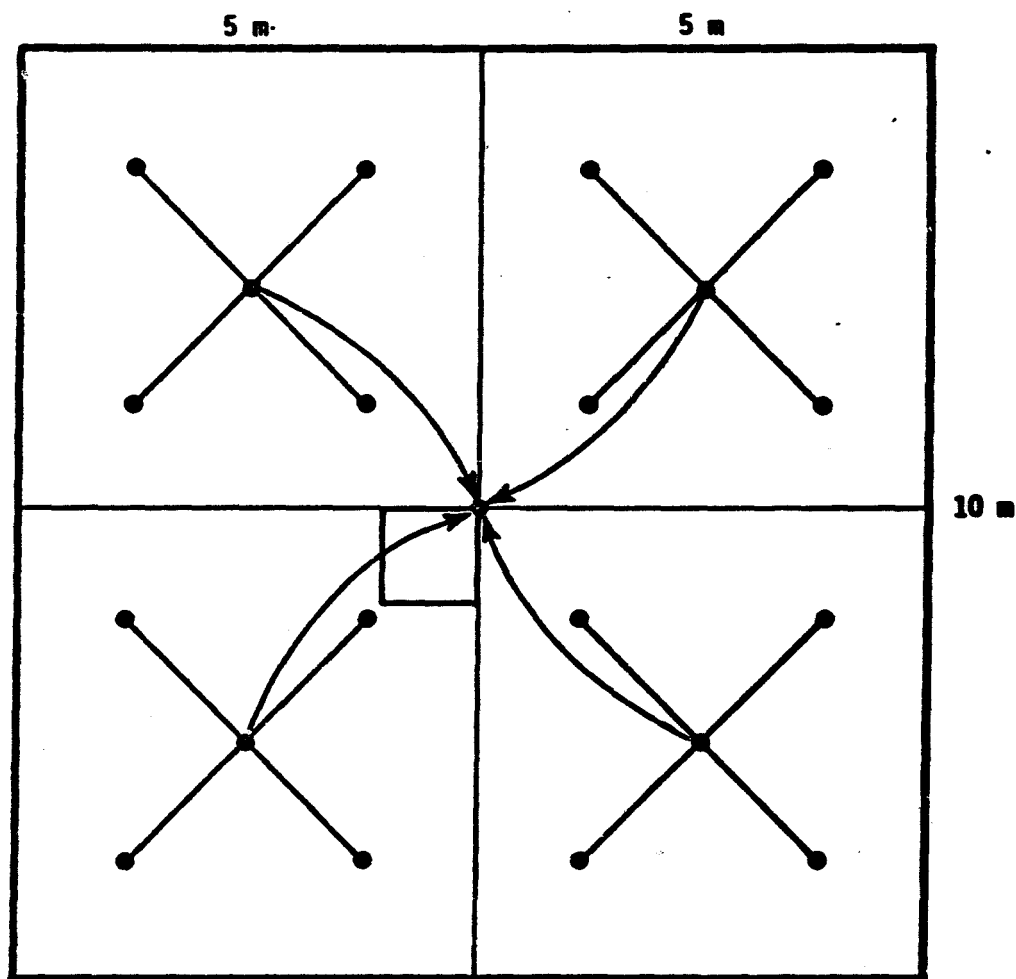
BASIC SOLID STATE CONCEPT

- 10m x 10m SUBARRAY, CONJUGATED + GROUND CONTROL
- ALL ELEMENTS WITHIN 10 x 10 SUBARRAY ARE IN PHASE
- TRANSPORTATION MODULE SIZE: 5m x 5m
- FIRST LEVEL RF SIGNAL DISTRIBUTION (FROM CONJUGATION NETWORK) INTER-CONNECTED IN SPACE AT JUNCTION OF 5m x 5m MODULE
- FIRST & SECOND LEVEL DISTRIBUTION (NON-ISOLATED) = "REAR" LAYER
- THIRD, FOURTH & FIFTH LEVELS = SECOND LAYER
- SIXTH & SEVENTH LEVEL (ISOLATED) HYBRID DIVIDERS = THIRD LAYER
- GROUND PLANE BETWEEN THIRD LAYER & AMPLIFIERS/DIPOLES
- ALL RF DISTRIBUTION LINES USE HI-TEMP SUB-MIN. COAX
- D.C. DISTRIBUTION IN BACK OF REAR RF DISTRIBUTION LAYER

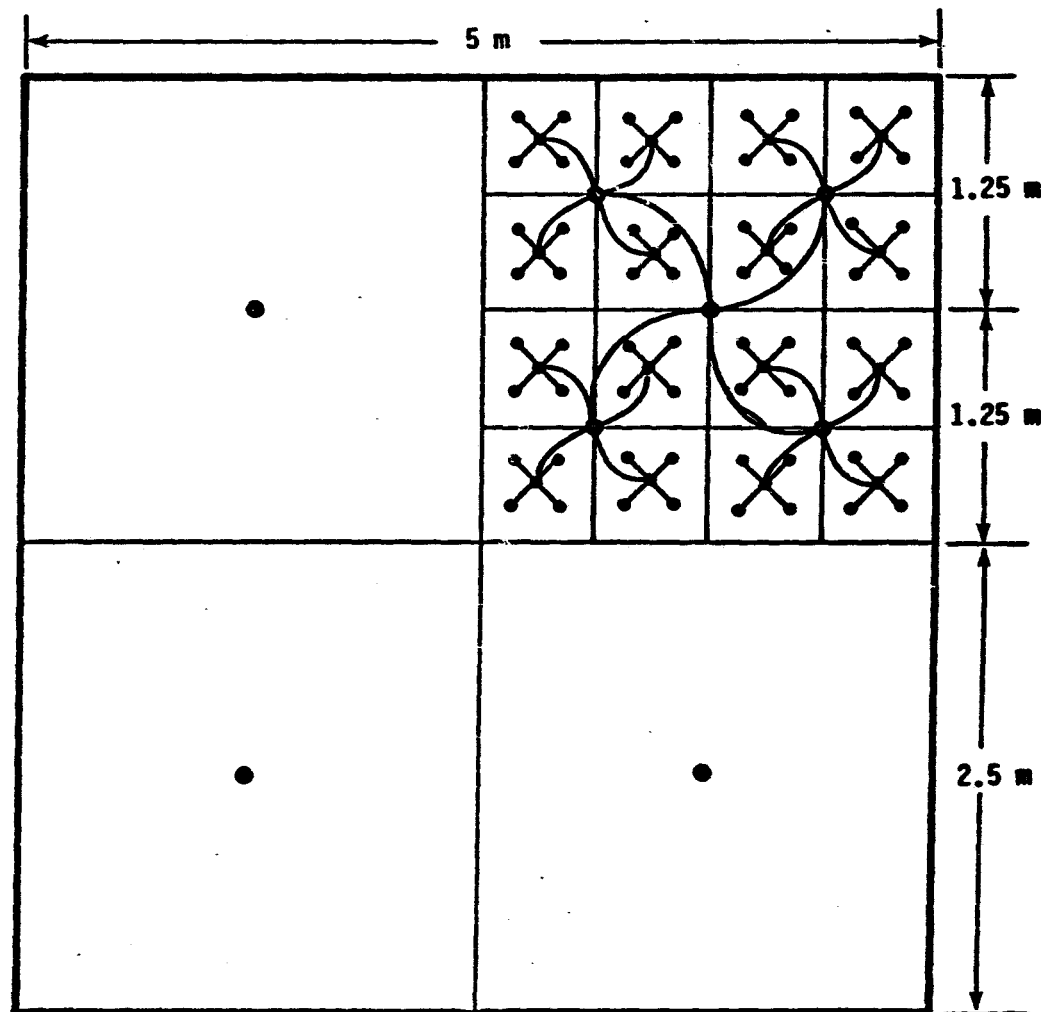
SUBARRAY LAYOUT



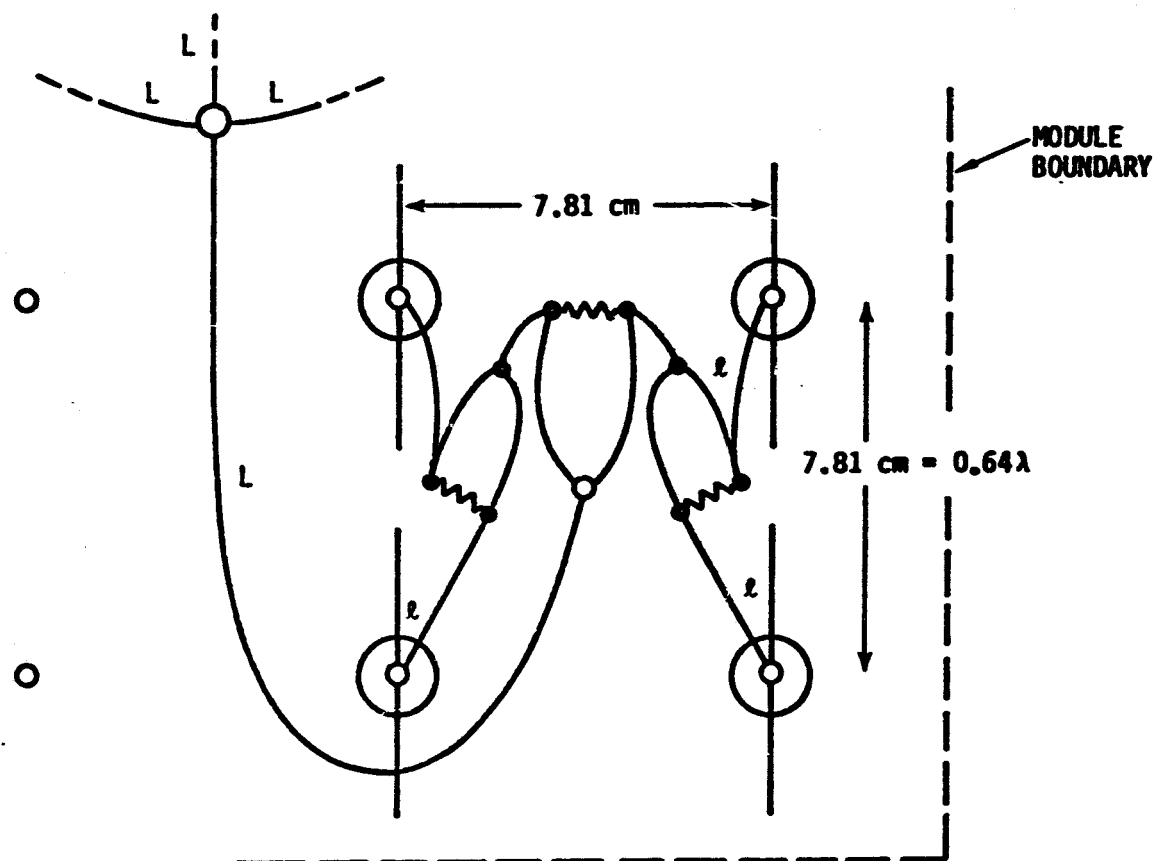
FIRST & SECOND LEVEL SUBARRAY SIGNAL DISTRIBUTION



THIRD, FOURTH & FIFTH LEVEL SIGNAL DISTRIBUTION



HYBRID (ISOLATED) DIVIDER DETAIL FOR SIXTH & SEVENTH LEVEL



CONJUGATED SIGNAL DISTRIBUTION SYSTEM PARAMETERS

LEVEL	1	2	3	4	5	6	7
SPLITTING LOSS (dB)	6	12	18	24	30	36	425
"ELEMENT" NUMBER	4	16	64	256	1024	4096	16,384
AMPLIFIER GAIN (dB)	43	-	-	-	-	-	-
"CABLE"*) LENGTH (M)	3.54	1.77	0.885	.44	.22	.11	.055
SUM OF LENGTHS	14.14	28.23	56.57	113.14	228.27	452.55	905

*) FROM CENTER TO NEXT DISTRIBUTION POINT

ANTENNAS FOR PILOT & REFERENCE SIGNAL RECEPTION

o HELIX

ADVANTAGE: SIMPLE, DEPLOYABLE; HIGH-GAIN, SMALL DIAMETER

DISADVANTAGE: CIRCULAR POLARIZATION

o DISC-ON-ROD:

ADVANTAGE: DEPLOYABLE; HIGH-GAIN; SMALL DIAMETER; ANY POLARIZATION

DISADVANTAGE: MORE COMPLEX THAN HELIX

o YAGI:

ADVANTAGE: SIMPLE, HIGH-GAIN; DEPLOYABLE

DISADVANTAGE: NARROW BAND

o DIPOLE ARRAY:

ADVANTAGE: ARBITRARY GAINS, BANDWIDTH; NEEDS NO DEPLOYMENT

DISADVANTAGE: SHADOWING/INTERFERENCE FROM POWER SYSTEM

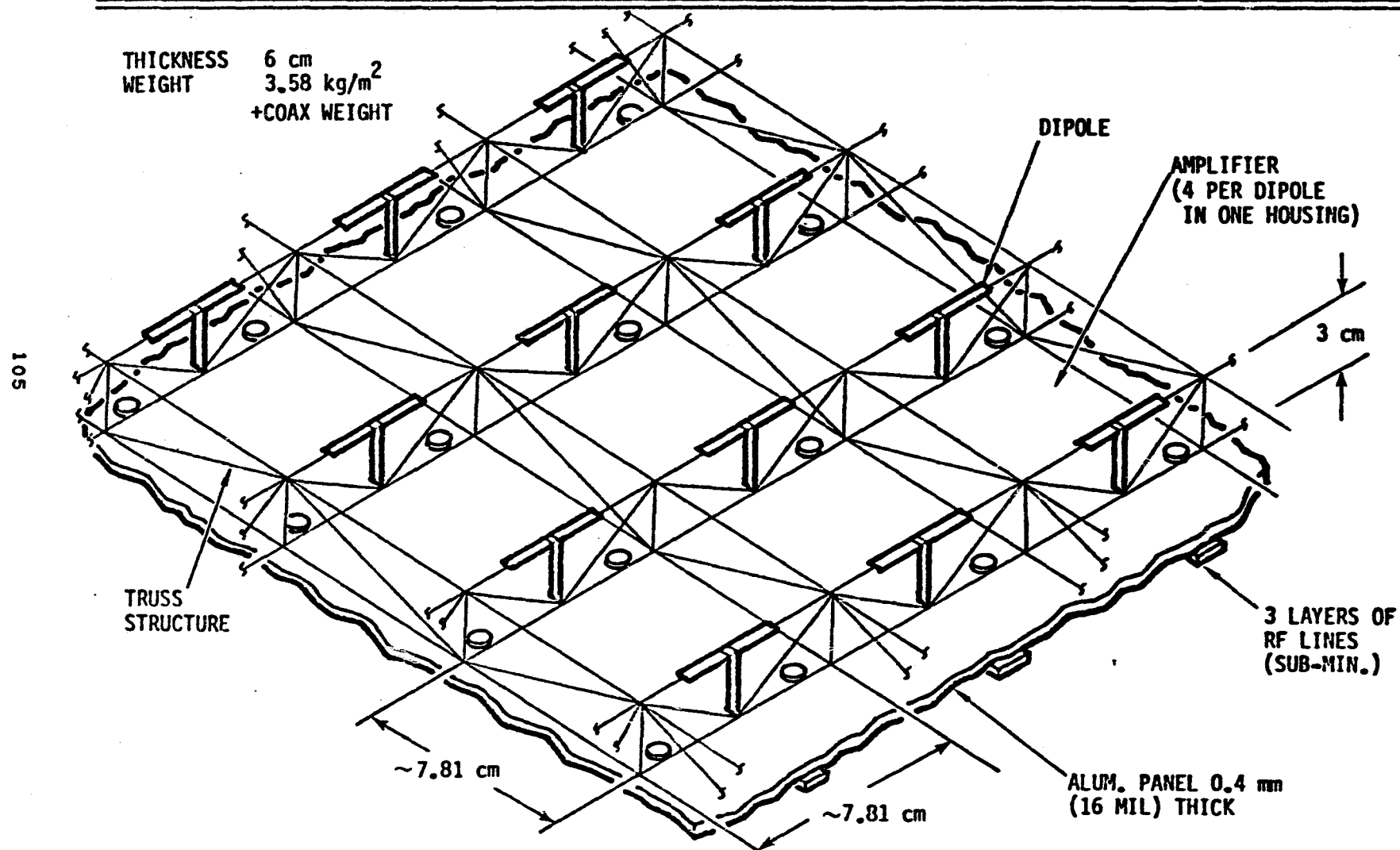
o SLOT ARRAY:

ADVANTAGE: EASIER TO FEED THAN DIPOLE ARRAY

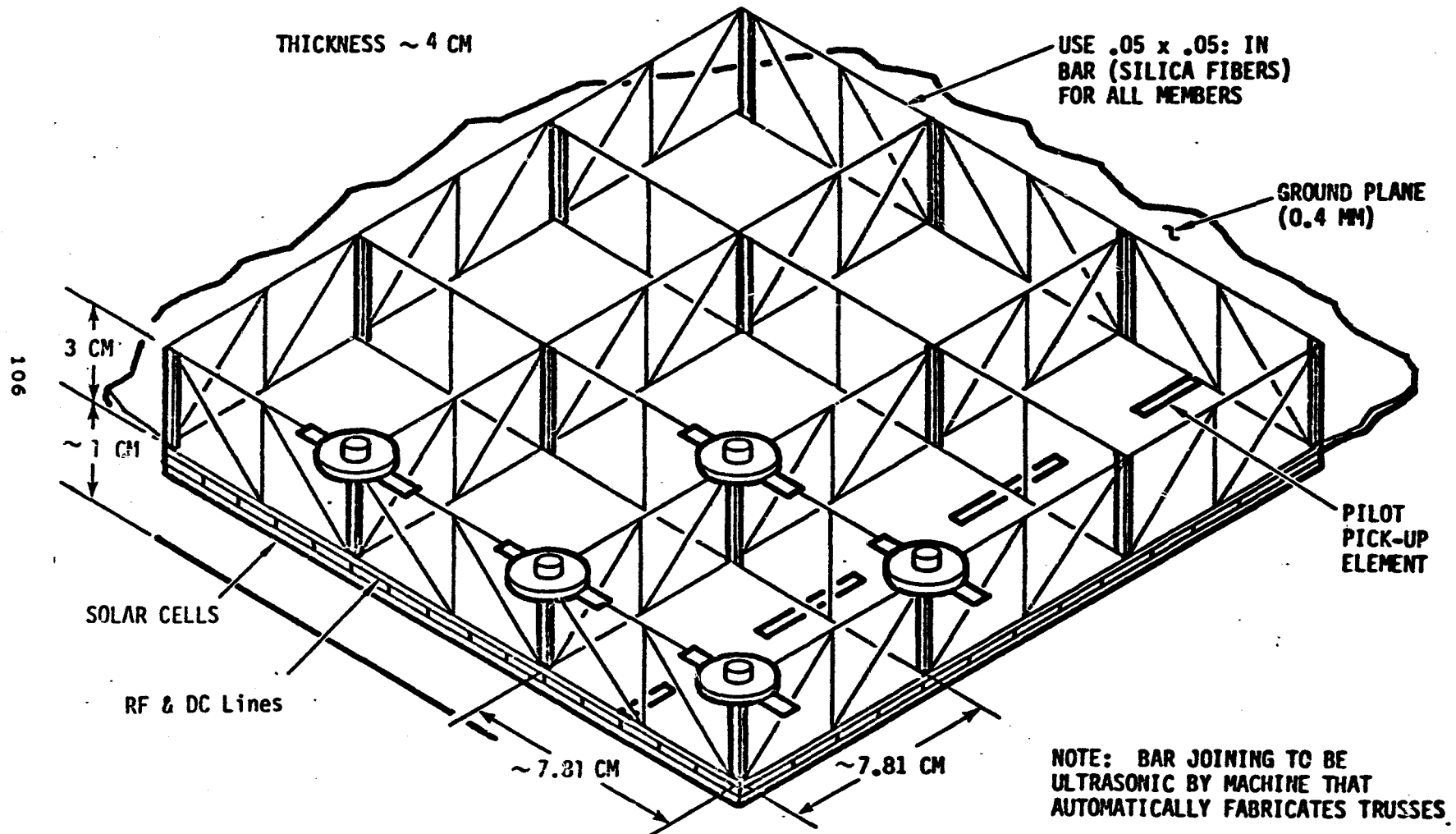
DISADVANTAGE: NARROW BAND; REDUCES THERMAL EMISSIVITY

o MICROSTRIP ARRAYS: TOO NARROW BAND; TOO MUCH AREA

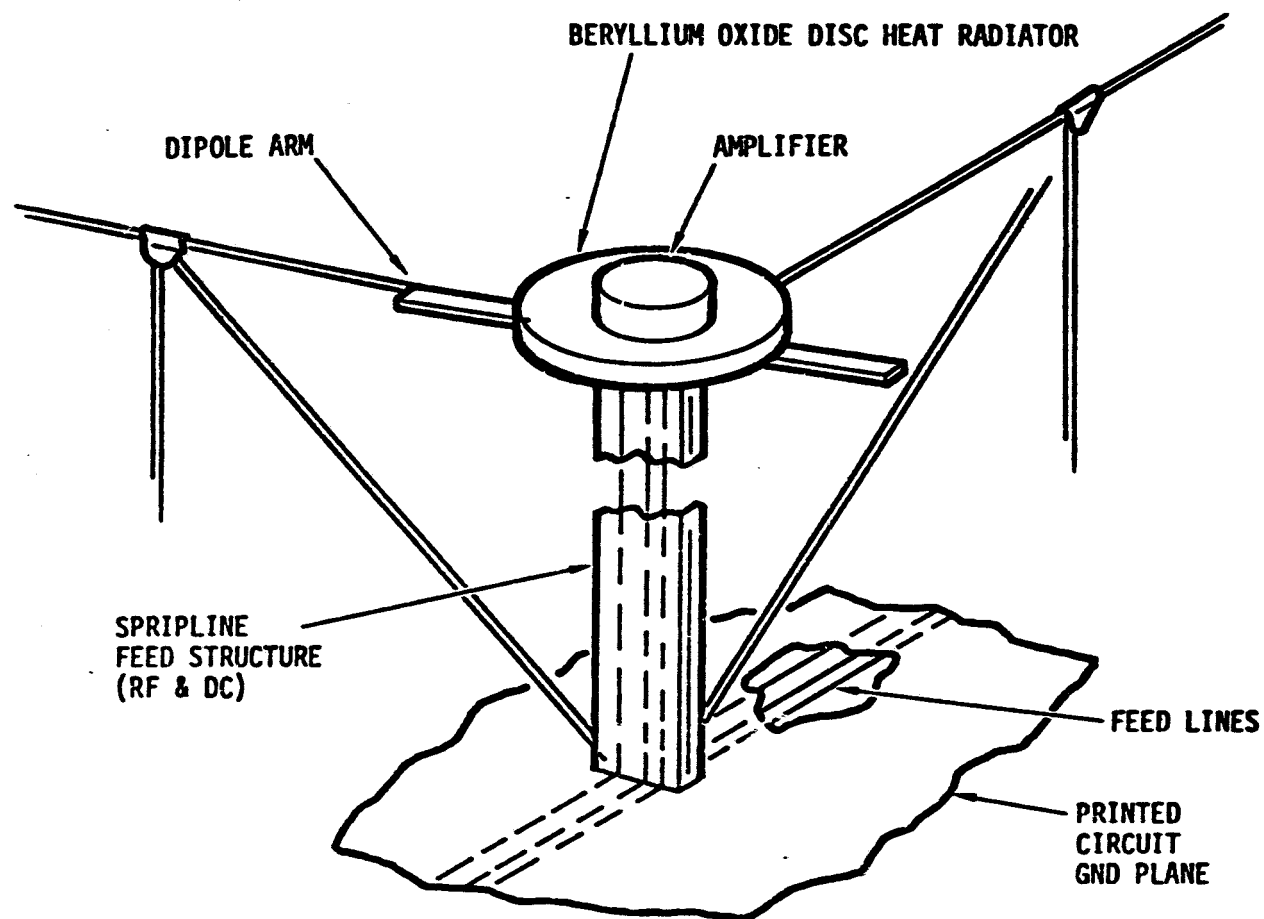
END-MOUNTED ANTENNA WITH DIPOLES OVER GROUND PLANE



SANDWICH ANTENNA WITH DIPOLES OVER GROUND PLANE



DIPOLE AND STRIPLINE FEED DETAIL

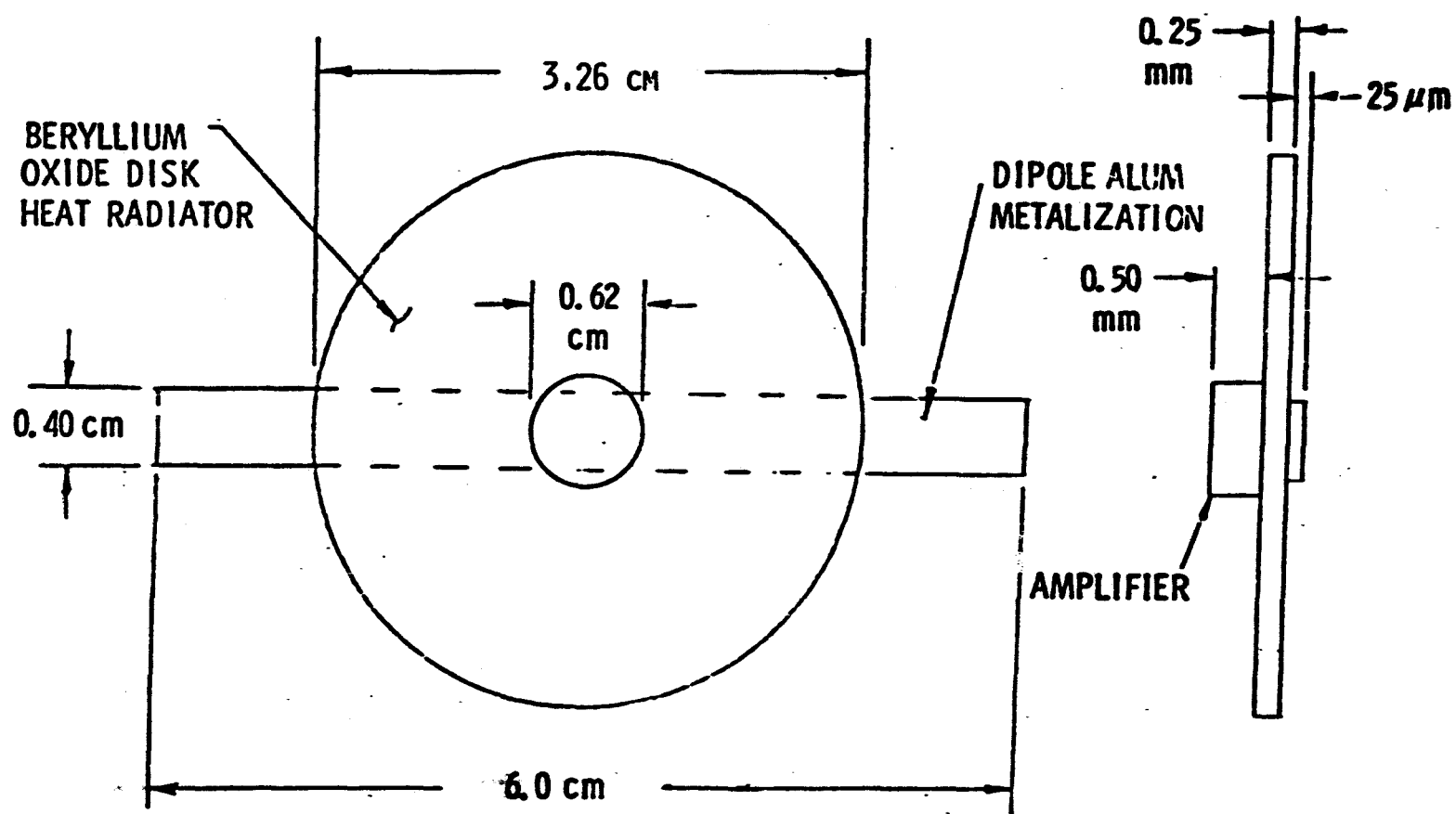


ANTENNA DETAIL FOR GaAs SANDWICH CONCEPT

TYPE-DIPOLE WITH DIPOLE MOUNTED AMPLIFIERS

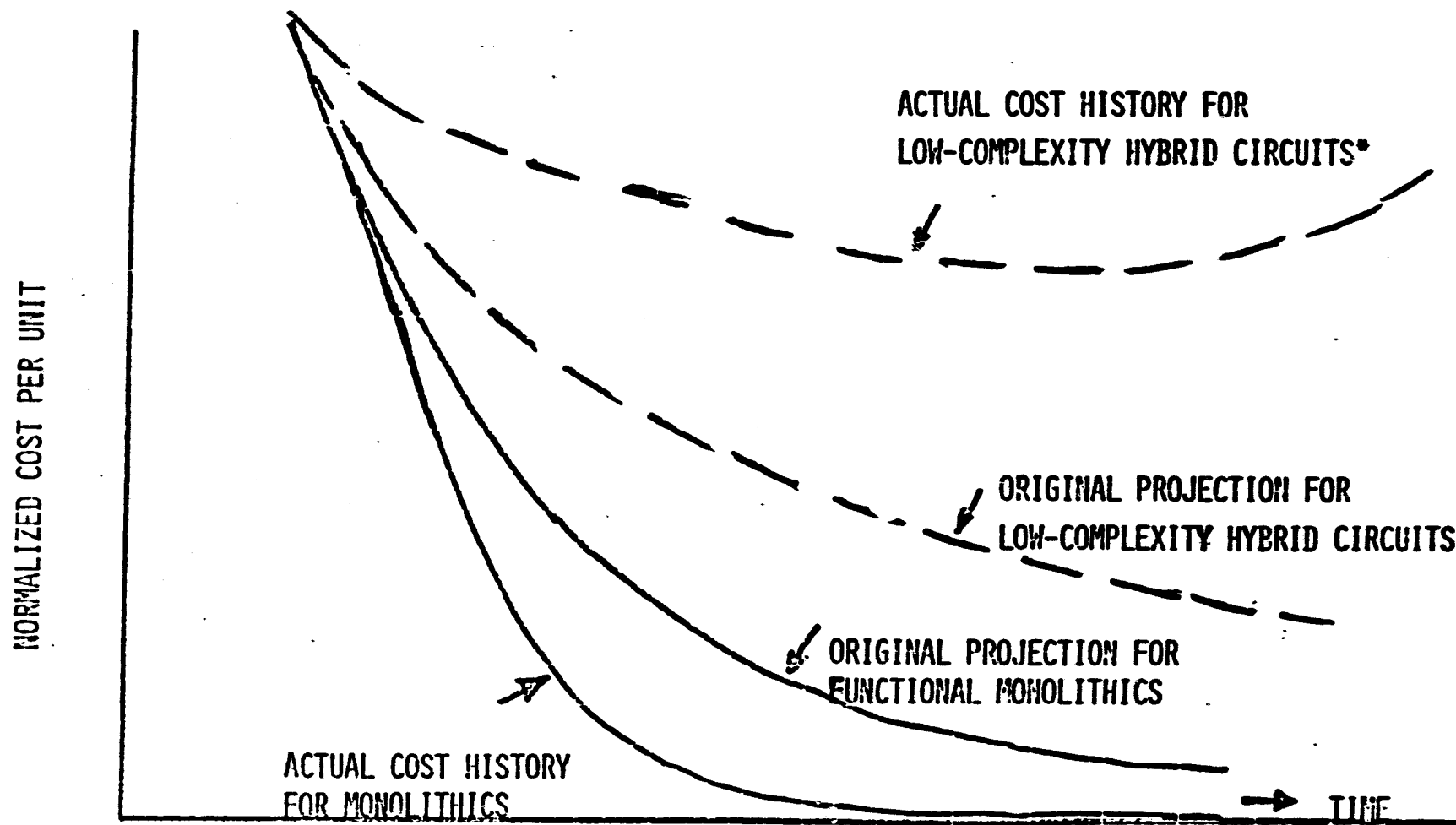
ELEMENT SPACING	= 7.81 cm
NO. ELEMENTS/M ²	= 164 ELEMENT/M ²
OUTPUT POWER/DEVICE	= 4.95 WATTS
HEAT DISSIPATED/DEVICE	= 1.24 WATTS
GROUND-PLANE TO DIPOLE LENGTH	= 3.05 cm
BERLOX DISC DIAMETER	= 3.26 cm
BERLOX DISC AREA	= 8.4 cm ²
BERLOX DISC THICKNESS	= 0.0254 cm
BERLOX DISC VOLUME	= 0.213 cm ³
DISC/ANTENNA AREA RATIO	= 0.138

DIPOLE AND HEAT RADIATOR DETAIL



SOLID-STATE COST TRENDS
HYBRIDS VS. MONOLITHICS

011



SOLID STATE POWER AMPLIFIER ANALYSIS

OBJECTIVE

- **DETERMINE DEVICE FABRICATION PARAMETERS FOR POWER CONVERSION EFFICIENCY $\geq 80\%$**

APPROACH

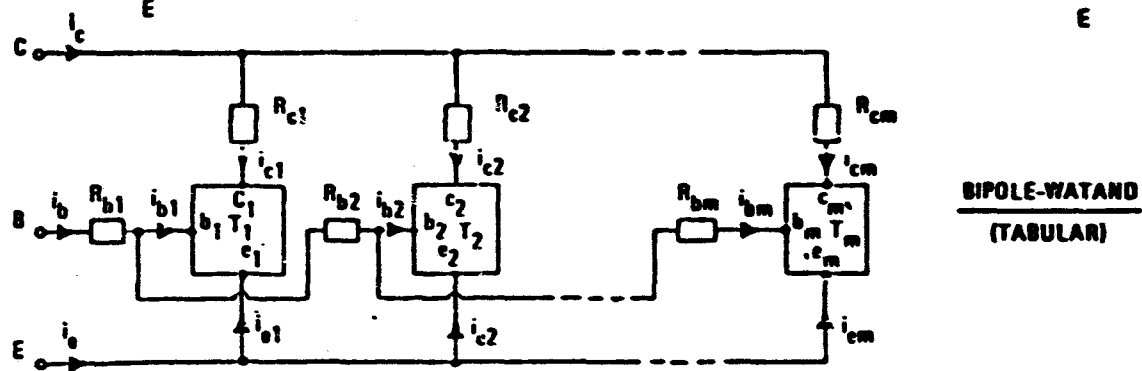
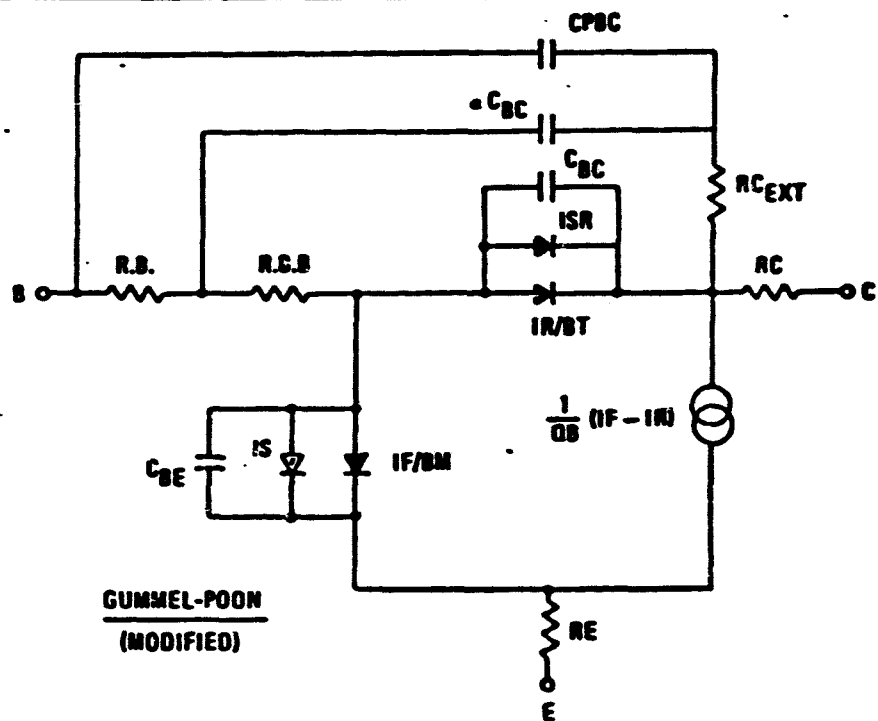
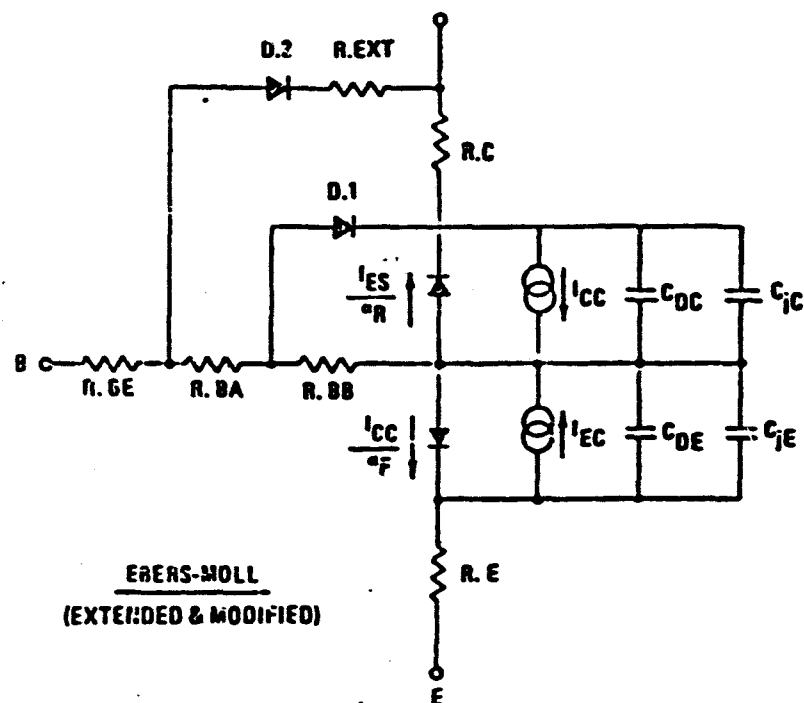
- **DEVICE MODELING AND CIRCUIT SIMULATION**

RESULT TO DATE

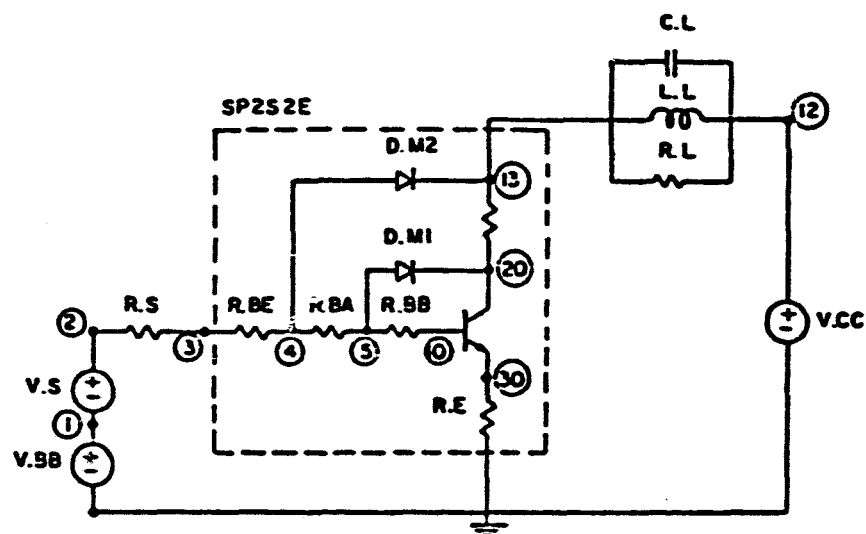
- **SILICON AND GaAs BIPOLAR TRANSISTORS IN CLASS C AND E CIRCUITS OPERATING IN A TEMPERATURE RANGE OF 27°C TO 200°C**
- **SCHOTTKY BARRIER GaAs FETs IN CLASS C/B CIRCUITS - CLASS E ANALYSIS IN PROGRESS**

NOTE: STUDY DONE BY D. J. ROULSTON, UNIVERSITY OF WATERLOO, ONTARIO, CANADA

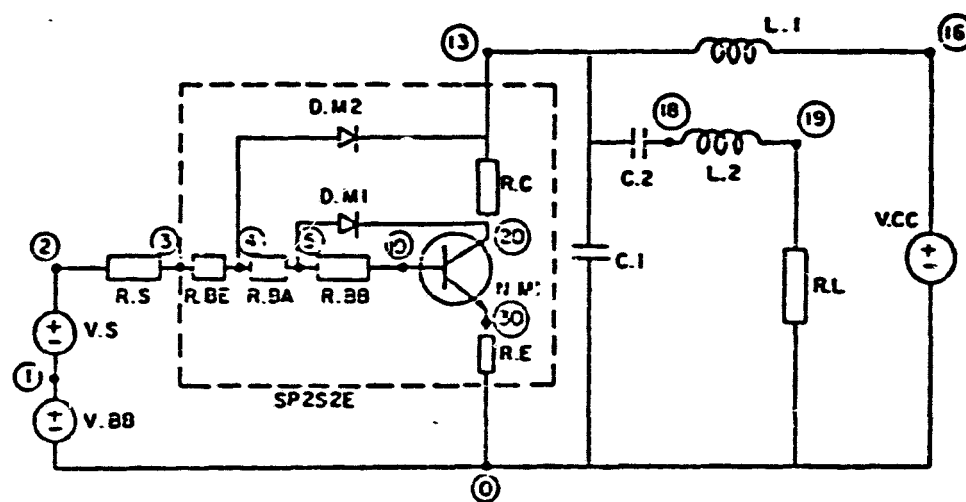
TRANSISTOR MODELS USED IN THIS STUDY



EXTERNAL CIRCUITS USED WITH TRANSISTOR MODELS

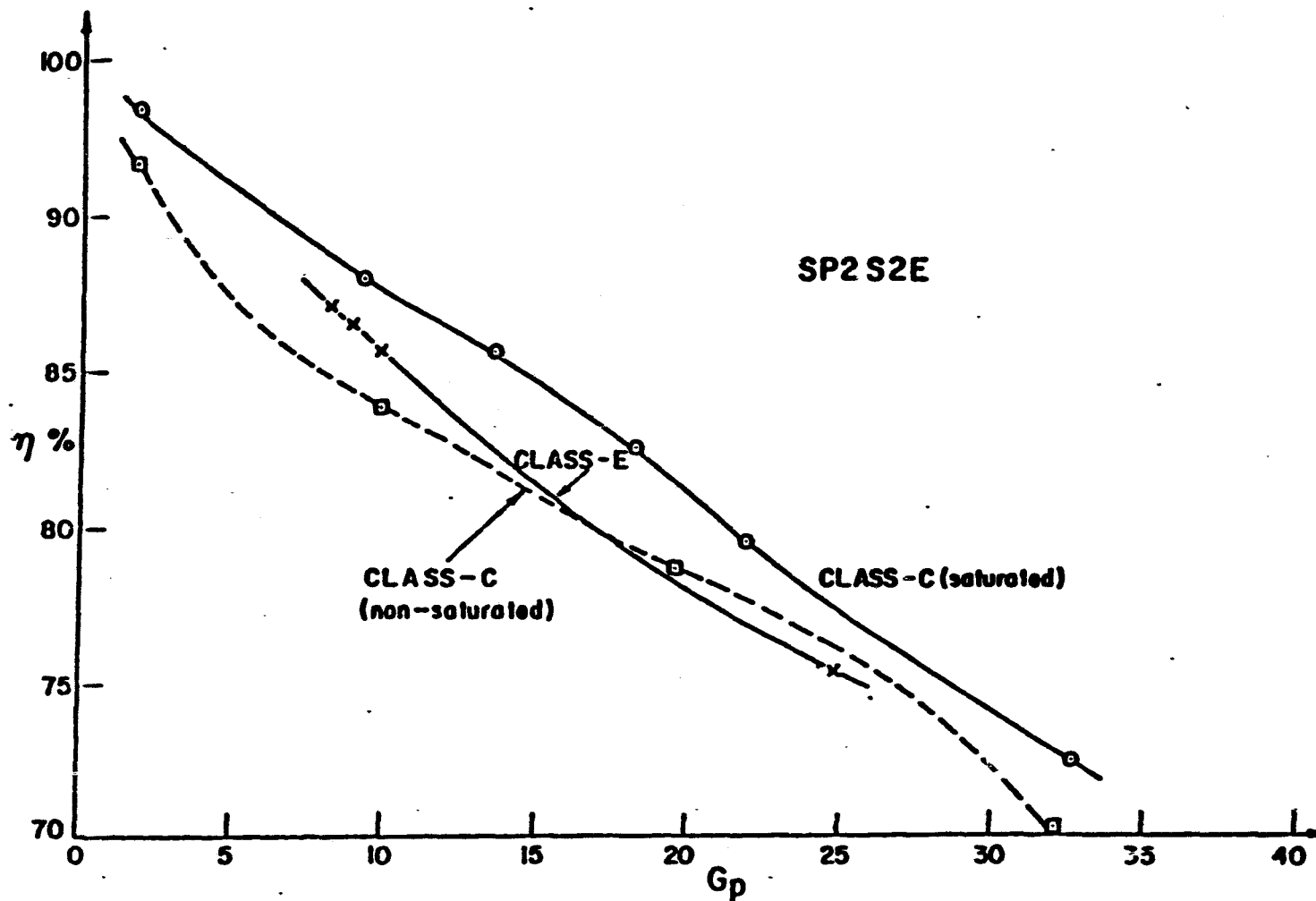


CLASS C CIRCUIT

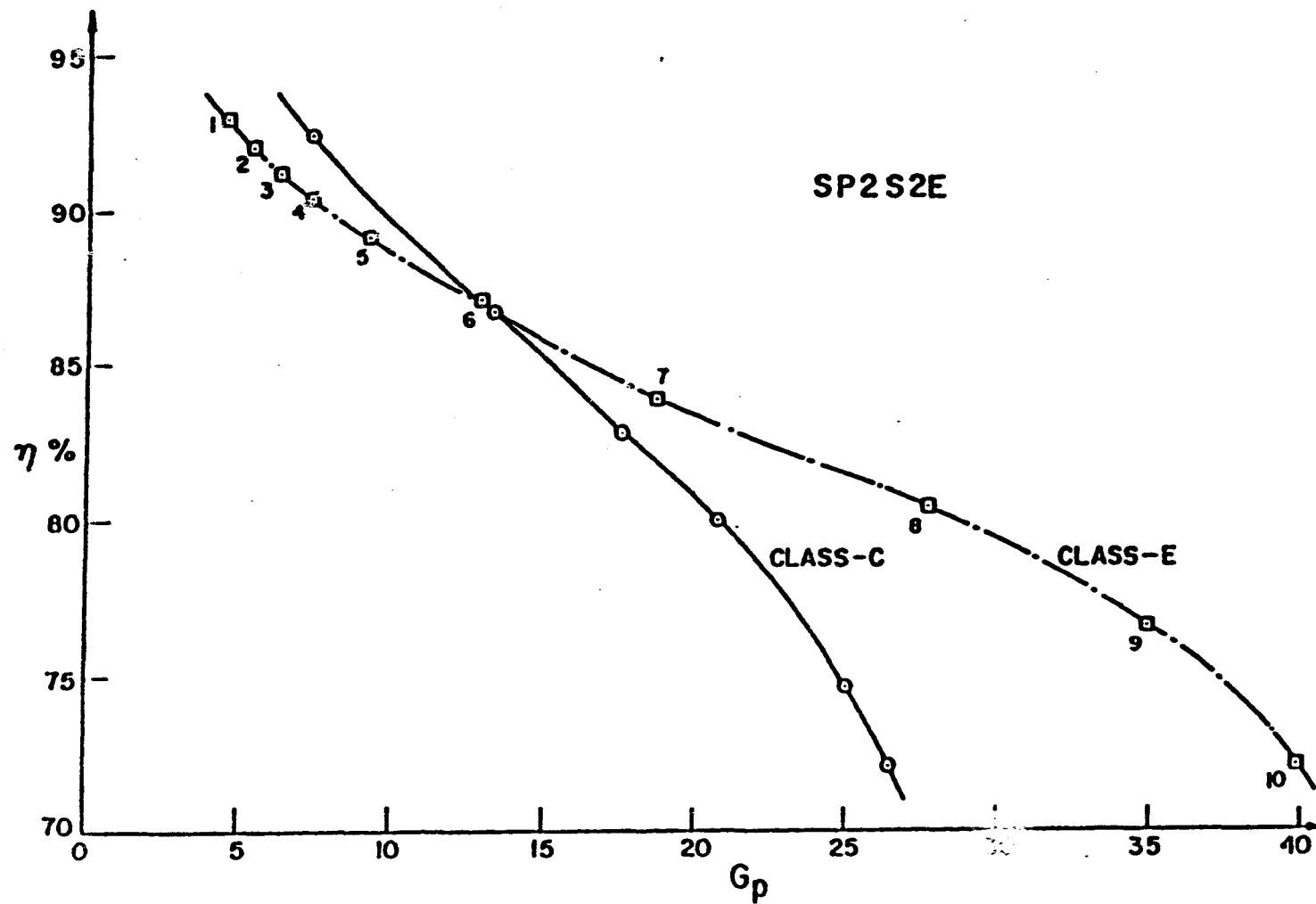


CLASS E CIRCUIT

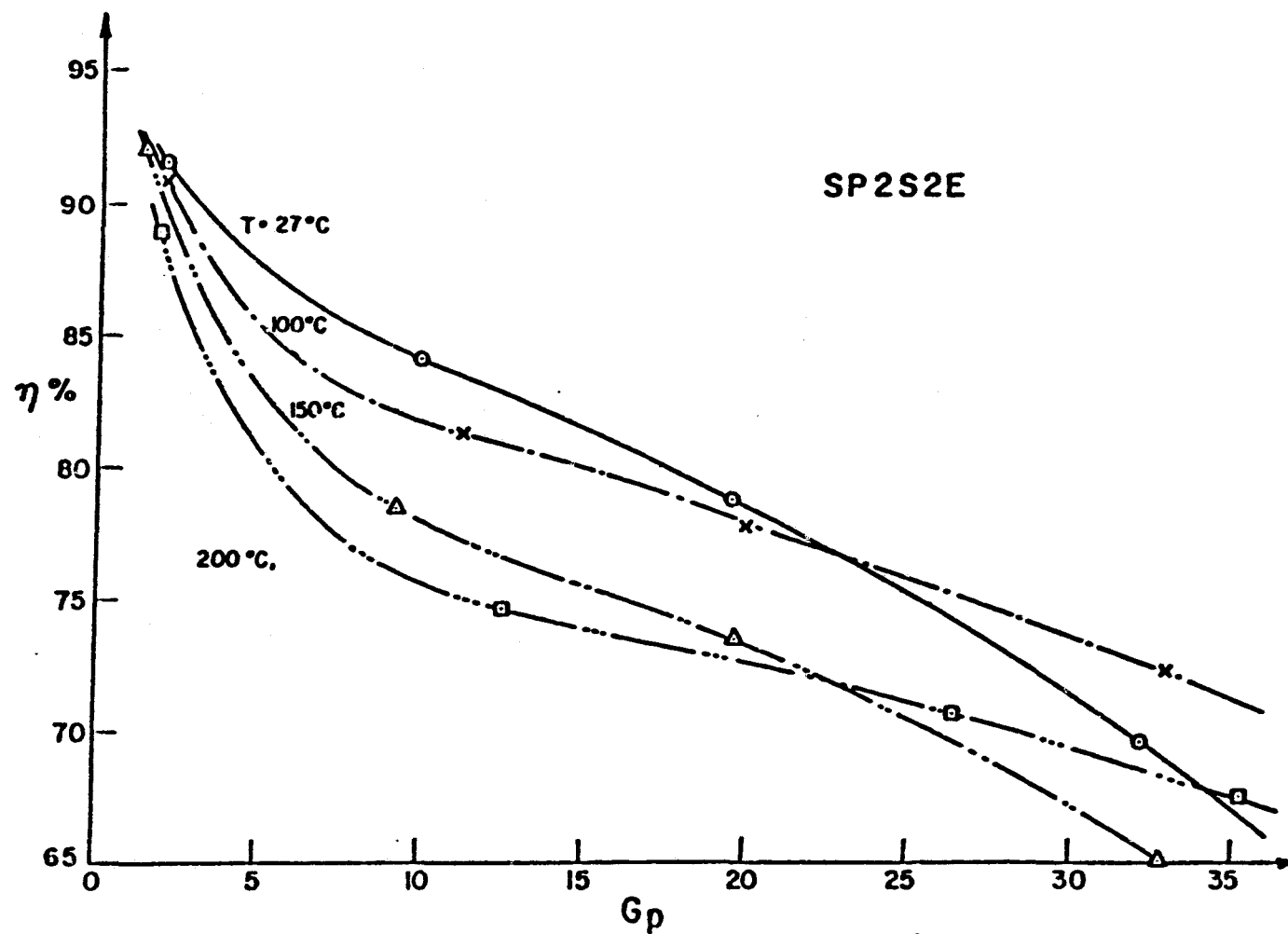
EFFICIENCY vs. GAIN AT 2.45 GHZ AND 27°C
SILICON HIGH POWER (≈ 20 WATTS) DESIGN



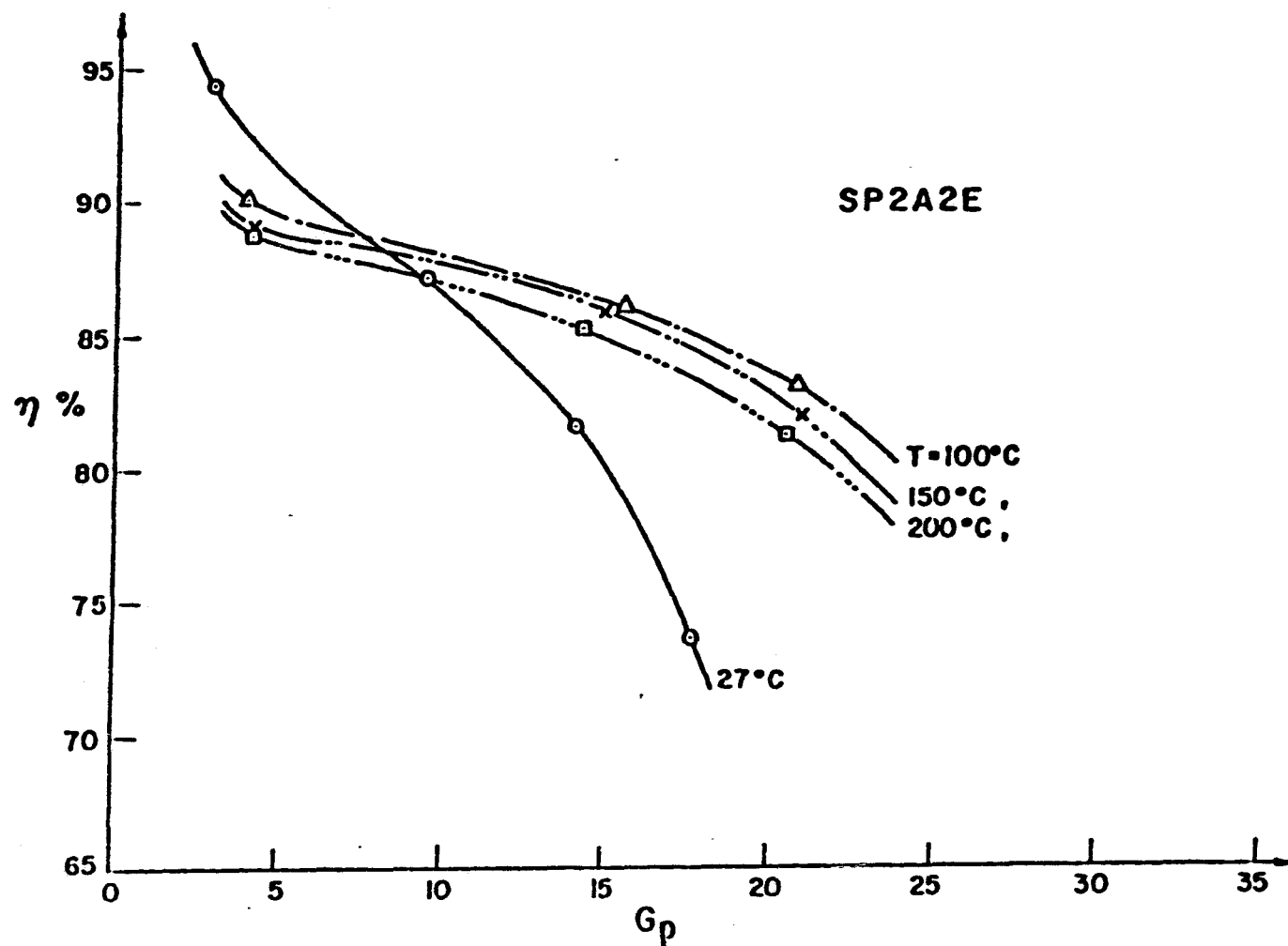
EFFICIENCY vs. GAIN AT 2.45 GHZ AND 27°C
SILICON LOW POWER (≈10 WATTS) DESIGN



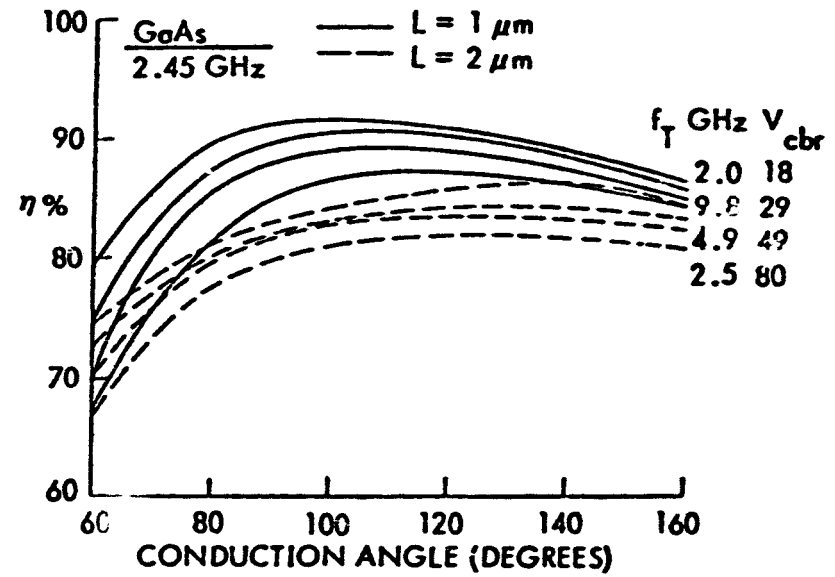
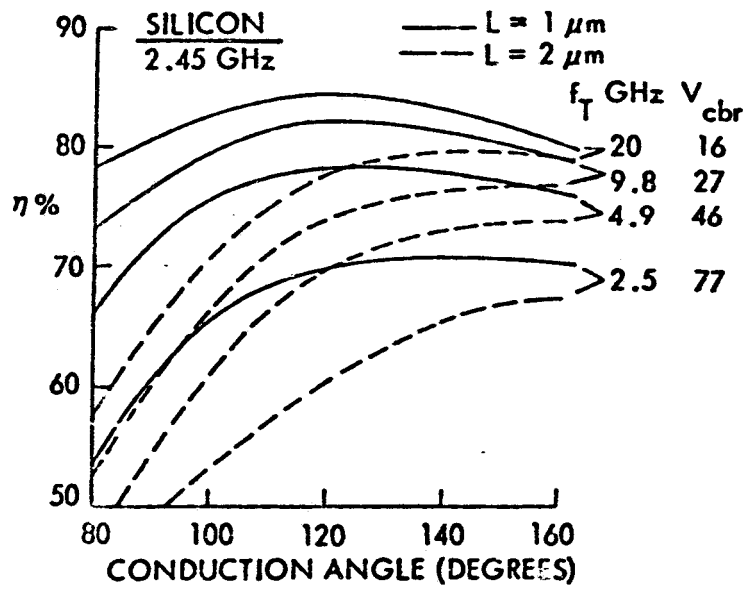
RESULTS OF HIGH TEMPERATURE STUDY FOR THE SILICON TRANSISTOR AT 2.45 GHZ



RESULTS OF HIGH TEMPERATURE STUDY FOR THE
GaAs TRANSISTOR AT 2.45 GHZ



EFFICIENCY OF CLASS C AMPS VS CONDUCTION ANGLE



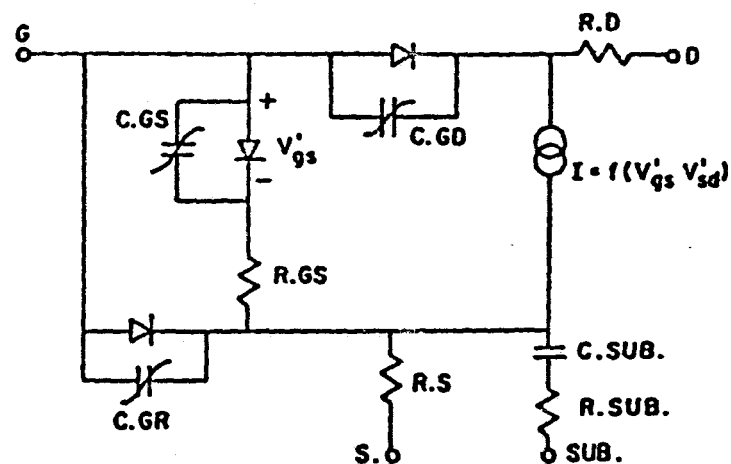
RESULTS OF BIPOLAR TRANSISTOR STUDY

- POWER CONVERSION EFFICIENCY OF 80% APPEARS FEASIBLE
- GaAs ACHIEVES HIGHER EFFICIENCIES THAN SI AT HIGH TEMPERATURES
- GaAs EFFICIENCY LESS SENSITIVE WITH RESPECT TO MODE OF OPERATION
- DESIRABILITY OF CLASS C VS CLASS E CIRCUIT NOT CONCLUSIVE

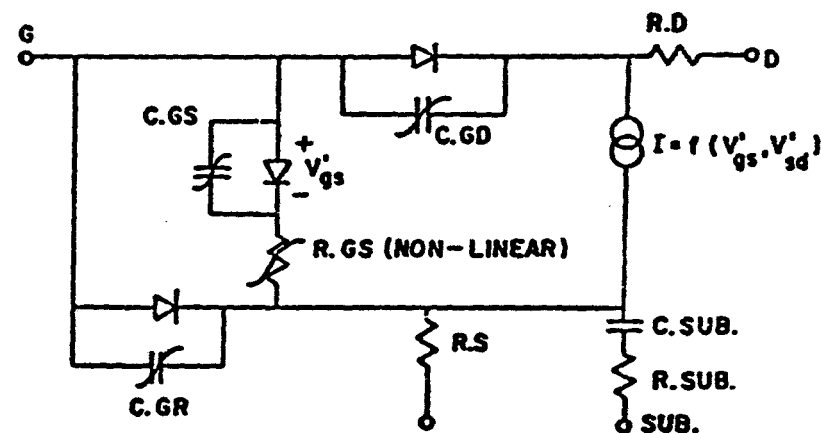
COMMENTS:

EXPERIMENTAL VERIFICATION REQUIRES SUBSTANTIAL DEVELOPMENT OF GaAs
BIPOLAR TECHNOLOGY.

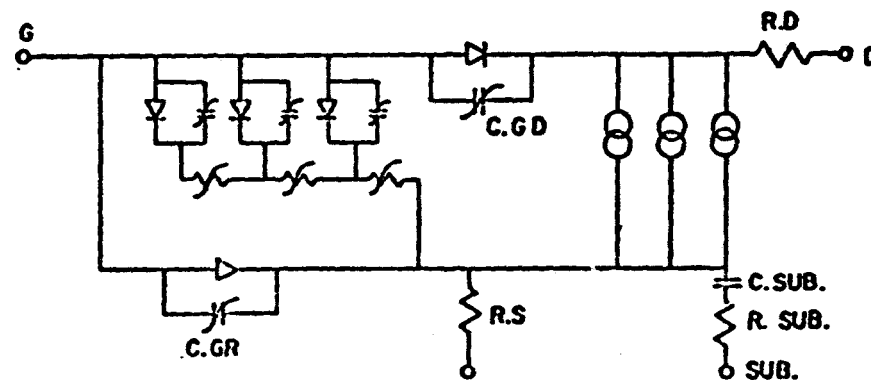
FET MODELS USED IN THIS STUDY



CONSTANT CHANNEL RESISTANCE

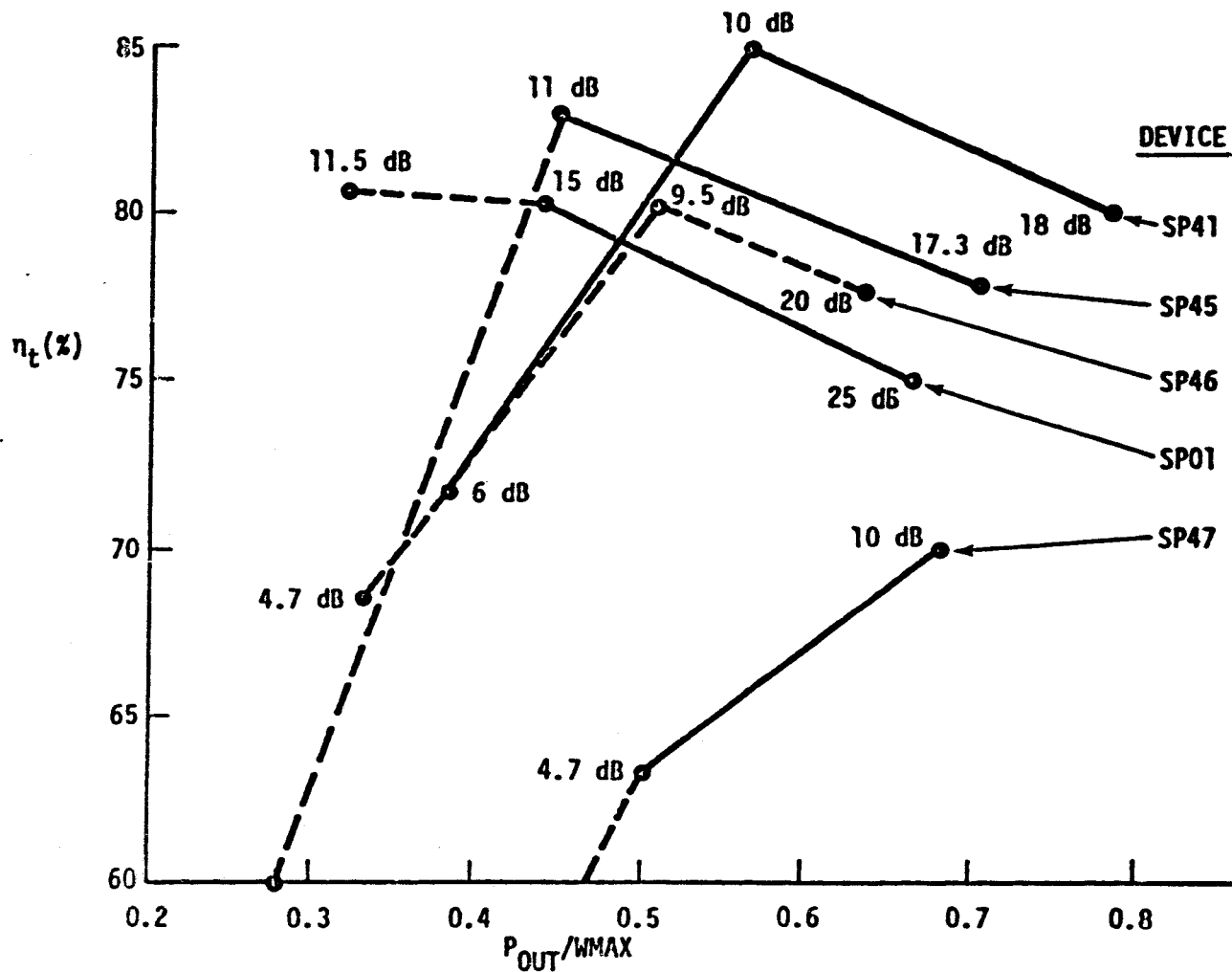


NON LINEAR CHANNEL RESISTANCE

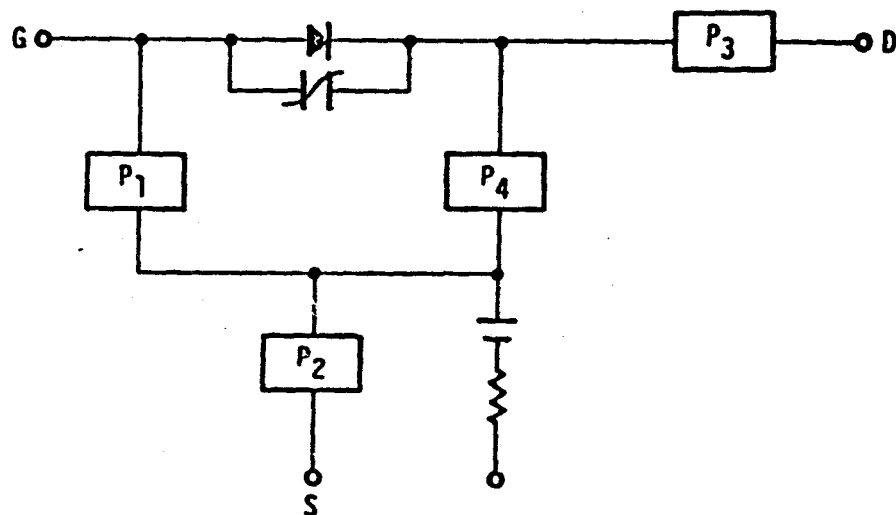


MULTISECTION NON LINEAR CHANNEL RESISTANCE

TOTAL EFFICIENCY vs POUT/WMAX FOR SINUSOIDAL DRIVE AT 2.45 GHZ FOR FIVE DIFFERENT FETs



INTERNAL DISTRIBUTION OF POWER LOSSES



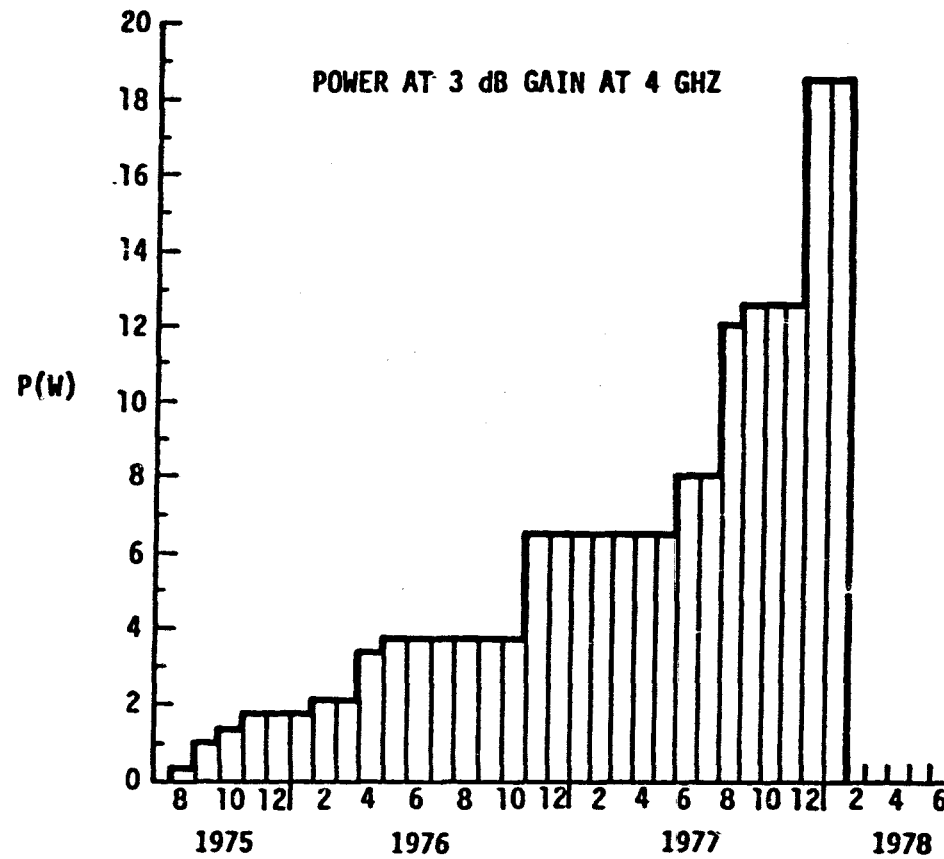
DEVICE: SP41

θ_c	80°	120°	180°
N_o	87.6	92	81.2
N_t	72.2	84.6	80
G_p (dB)	6.1	10.3	18
P_c/P_{max}	.37	.55	.77
$(P_1/P_t)\%$	60	2.3	3.4
$(P_2/P_t)\%$	11.1	5.5	1.6
$(P_3/P_t)\%$	11.1	14.1	9.5
$(P_4/P_t)\%$	17.7	57.6	85.5

RESULTS OF GaAs FET STUDY TO DATE

- POWER CONVERSION EFFICIENCY OF 80% APPEARS POSSIBLE
- TRADE-OFF BETWEEN EFFICIENCY AND OUTPUT POWER MAY BE REQUIRED
- POWER OUTPUT DEPENDS ON ACHIEVABLE TRANSISTOR BREAKDOWN VOLTAGE LIMIT,
AND ABILITY TO CONSTRUCT MULTI-CELL DEVICES

PROGRESS OF POWER GaAs FETs AS A FUNCTION OF TIME*



*IEEE TRANSACTIONS VOL MTT-27, NO. 5, MAY 1979 PP. 367-378

CONCLUSIONS

- EFFICIENCIES OF 80% APPEAR POSSIBLE FOR WIDELY DIFFERENT TRANSISTOR STRUCTURES
- VARIATIONS ON STANDARD CLASS C AND E HIGH EFFICIENCY CIRCUITS SHOULD BE INVESTIGATED
- SEVERAL ADDITIONAL TRANSISTOR STRUCTURES (BIPOLAR HETEROJUNCTION, VERTICAL FETs) SHOULD BE INVESTIGATED TO ESTABLISH AVAILABLE TRADE-OFFS W. R. T. POWER LEVELS OBTAINABLE, COMPARATIVE EFFICIENCIES, GAIN LEVELS
- EXPERIMENTAL VERIFICATION CAN BE STARTED WITH PRESENTLY AVAILABLE TRANSISTOR TYPES

POWER AMPLIFIER DEVELOPMENT OUTLINE

OBJECTIVE:

- DEMONSTRATE THAT HIGH EFFICIENCY OPERATION CAN BE ACHIEVED WITH OFF THE SHELF GaAs POWER FETs
- SHOW THAT OFF THE SHELF PERFORMANCE CAN BE IMPROVED BY OPTIMIZING THE DEVICE WITH RESPECT TO EFFICIENCY LIMITING PARAMETERS

GOALS:

- OFF THE SHELF GaAs FETs

POWER ADDED EFFICIENCY: 50%

POWER 5 WATTS

GAIN 8 dB

- OPTIMIZED FETs

POWER ADDED EFFICIENCY: 65%

POWER 10 WATTS

GAIN 10 dB

POWER AMPLIFIER DEVELOPMENT OUTLINE (CONTINUED)

- TRADE-OFFS BETWEEN EFFICIENCY, POWER LEVEL AND GAIN WILL BE STUDIED
- SUBCONTRACTOR FOR POWER AMPLIFIER DESIGN AND FABRICATION -- RCA

SCHEDULE:

- DEVELOPMENT TO BE COMPLETED JUNE 1980 INCLUDING TESTING AND FREE SPACE TRANSMISSION DEMONSTRATION

54
Analysis of Solid State S-Band

***D. Weir
RCA***

PRECEDING PAGE BLANK NOT FILMED

SECRET

**SOLID STATE DEVICE TECHNOLOGY
for
SOLAR POWER SATELLITE**

PRECEDING PAGE BLANK NOT FILMED

- **ANALYSIS OF SOLID STATE S-BAND TRANSMITTERS FOR SOLAR POWER SATELLITE**
- **RESULTS OF "SPS SOLID STATE AMPLIFIER" WORK FOR ROCKWELL INTERNATIONAL**
- **SOLID STATE TECHNOLOGY FORECAST**

"Page missing from available version"

TREAN

DEVICE CONSIDERATIONS

- o Two device types were considered: MESFET and JFET.
- o Power output versus efficiency tradeoff: size, conduction angle.
- o Power saturation: Schottky barrier breakdown limits voltages.
- o Designs: 4 watts; 80% efficiency; 45° conduction angle.
- o Thermal Analysis: Device Mounting - JFET: 14°C/W; MESFET: 7°C/W
- o Device Mounting: Thermal analysis, impedance matching, mounting costs.
- o Life Expectancy: Thermal, radiation, test results, indicate positive.
- o Experimental Results: Power output 3 W, 58% efficiency, 6.8 dB gain.

TRCA

REFERENCE SYSTEM - SOLID STATE VERSION

• ASSUMPTIONS:

- 2.45 GHz - Geostationary Orbit - maximum 23 mW/cm²
- 10 dB taper - Goal: 5 GW to power grid

• LIMITING PARAMETERS:

- SS device operating voltages - power distribution weight vs. overall eff.
- Power per device - power density vs. eff. (combining losses)
- Thermal constraints - life forecasts required

• DESIGN APPROACH

- Parametric - Nomograph

• SAMPLE DESIGN FOR OPTIMUM

- 3 GW; 1.2 KM; 7 KM; 123 Wλ²; Passive Cooling

• CONCLUSIONS

- While potentially feasible, not superior to tubes; (specific power) W/Kg

"SMART"
MICROWAVE SYSTEM DESIGN

- o ASSUMPTIONS: 2.45 GHz - Geostationary Orbit - 23 mW/cm² max.
Goals: Maximize Watts/KG vs. Reference System
Minimize \$/Watts vs. Reference System
- o SOLID STATE DEVICE LIMITING PARAMETERS SAME.
- o APPROACH:
 - Build solar collector and microwave transmitter back-to-back.
 - Design for uniform illumination.
 - Parametric - Nomograph.
- o SAMPLE DESIGN:
 - Family of designs possible.
 - Reflectors used to gather and direct solar energy.
 - Additional designs possible if solar concentrator used.
- o CONCLUSIONS:
 - Optimized for solid state devices.
 - Limiting parameters no longer impact system design.
 - The question: reflector system complexity vs. SS design simplicity.

TREAT

MODULE CONSIDERATIONS

- o MODULE DESIGN & TRADEOFF LIMITED TO "SMART" CONCEPT.
- o POWER PER MODULE LIMITED BY SOLAR INTENSITY:
- o 1.3λ GRID, 3 W/MODULE, 50 W CLUSTER (16), 30 dB - SINGLE REFERENCE.
- o HIGH Q DESIGN - BETTER EFFICIENCY.
- o PATCH DESIGN - MECHANICAL SIMPLICITY.
- o CONCLUSIONS:
 - 1 Gram/Watt Possible - Compared to 1.56 Gram/Watt for Tube.
 - CONSIDERABLE FREEDOM IN DESIGN OF ANY ARRANGEMENT.

TRC/M

Conclusions

- A Solid State Transmitter for SPS Appears Viable.
- While a "Reference System" Type Solid State Transmitter is Possible, Numerous Advantages can be had by Considering a Solar/Microwave Integrated Approach.
- Solid State Device and Module Projections fit the Solar/Microwave Integrated Approach.
- Solid State offers Longer Life, Greater Reliability, and Considerable Flexibility in System Design.

REAL

Recommendations

- o Further System Studies are Required to Develop and Establish a Reference Design Oriented Toward Solid State
- o Uniform Illumination Beam Systems Should be Included
- o Large Signal Analysis of Microwave Circuits at SPS Frequency Including Waveform Examination is Required
- o Ultimately Special New SPS Devices Will be Needed to Meet the SPS Efficiency Requirements

REAL

PROGRAM SUMMARY

NAME: SPS Solid State Amplifier

SPONSOR: Rockwell International, Electronics Systems Group

CONTRACT NO. A9EA-766939-910

CONTRACTOR: RCA Laboratories, Princeton, NJ 08540

PERIOD: 15 Sept. 79 - 15 May 80

SIZE: \$100K

SCOPE:

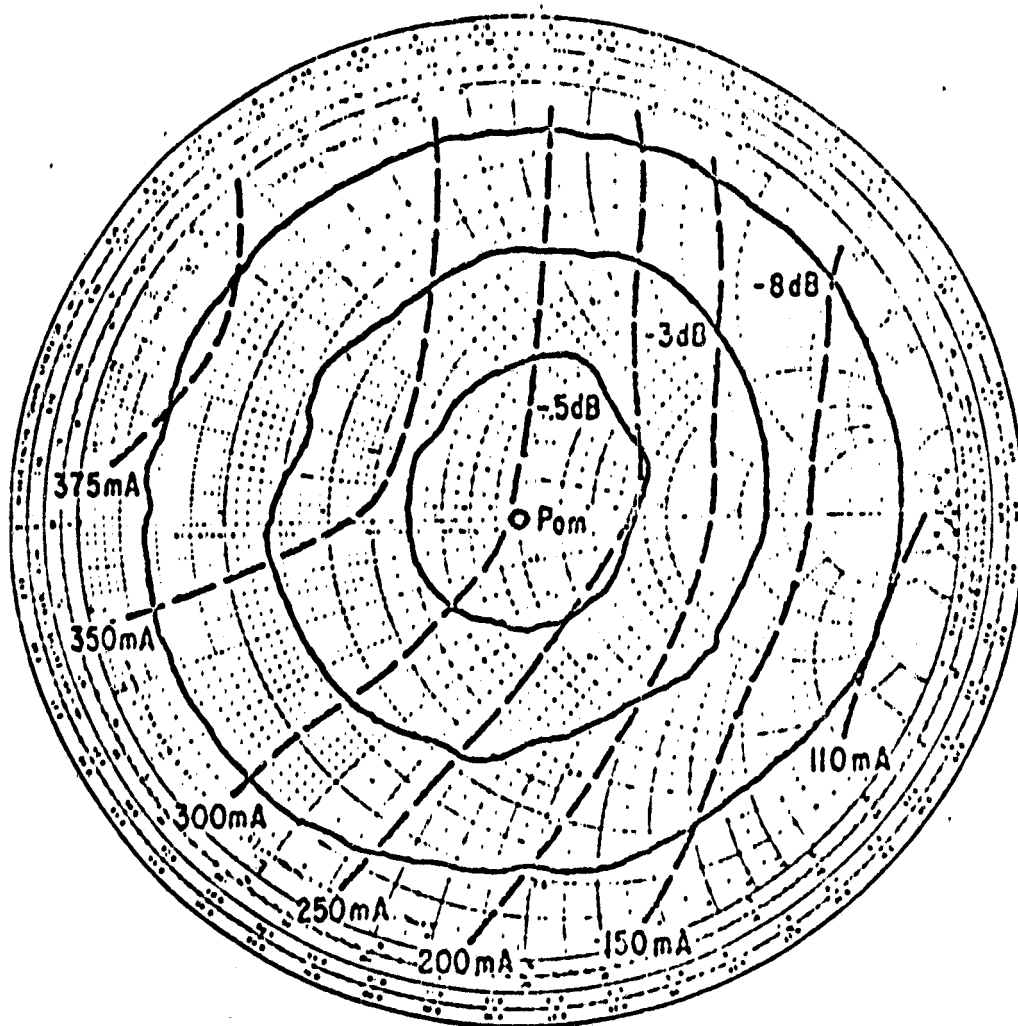
- o Optimize SPS type performance from existing GaAs devices.
- o Develop better understanding of device parameters affecting efficiency.
- o Deliver operating amplifiers for test.

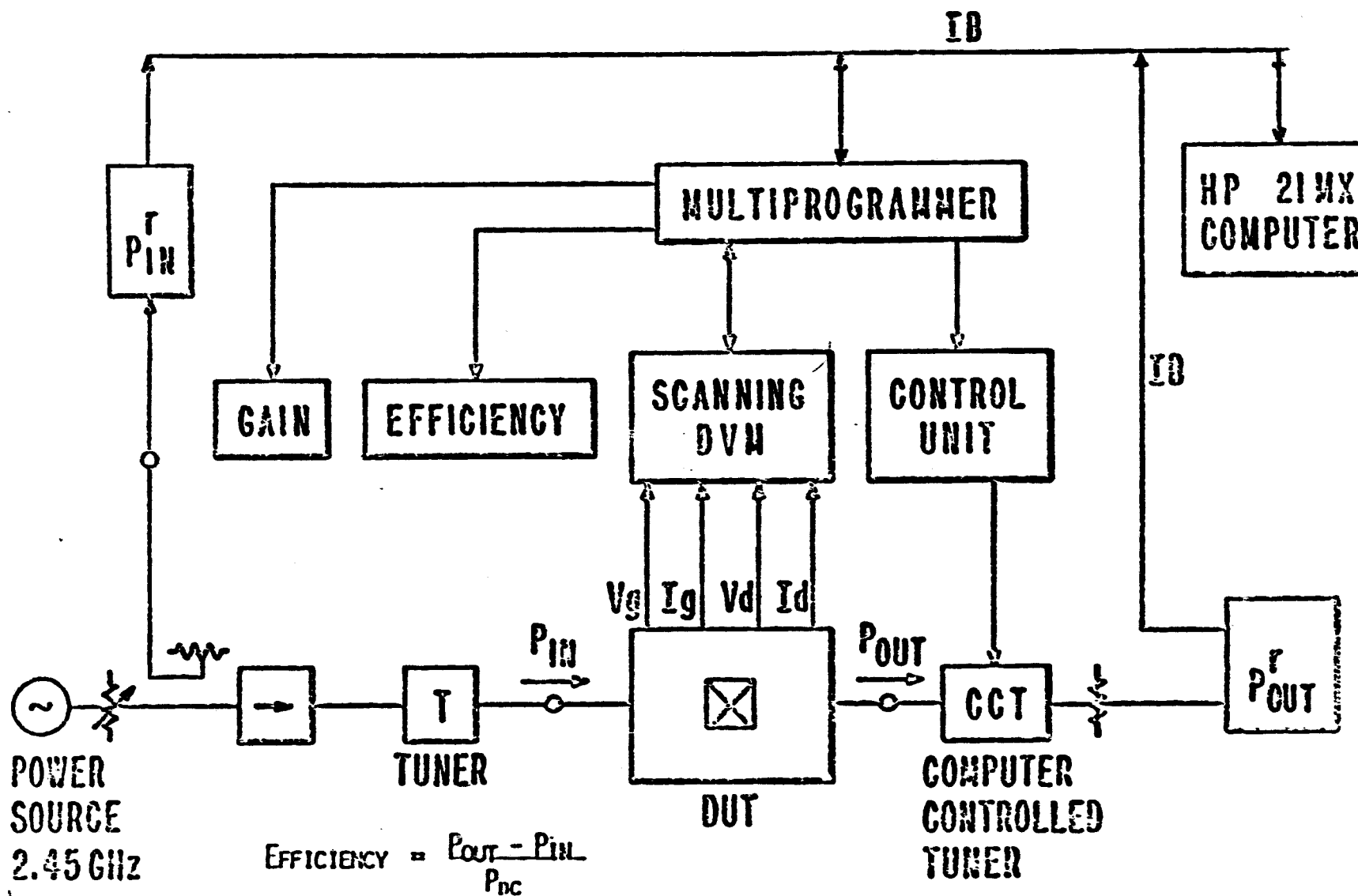
REAL

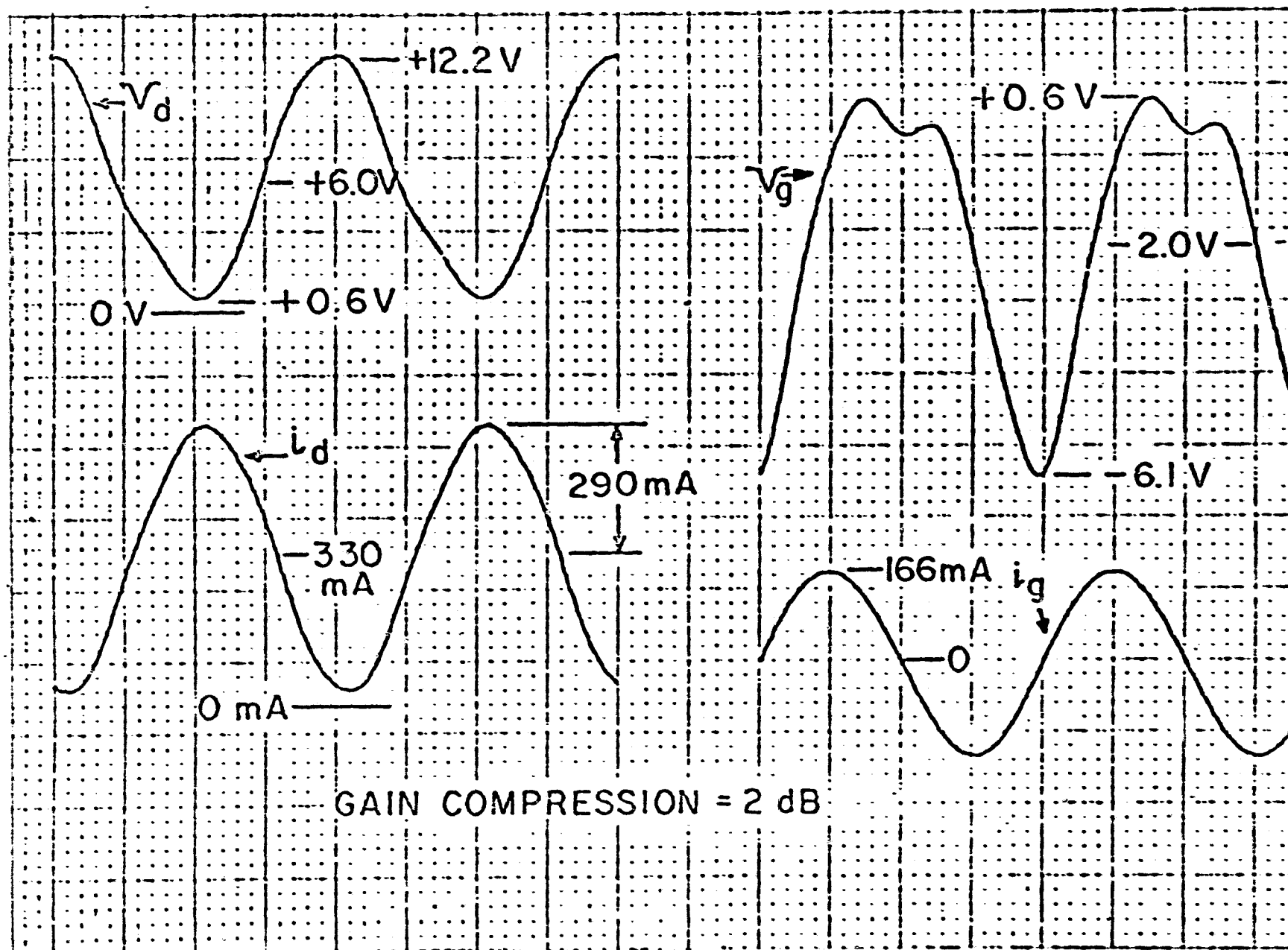
APPROACH

- o Sample best available GaAs FET devices.
- o Optimize performance using large signal computer-aided design routines.
- o Develop understanding of device and circuit operating modes and parameters using automated large-signal waveform sampling system.
- o Compare performance in different circuit configuration:
Single Pole Multi-Pole
- o Combine power amplifiers as required to achieve ^{goals} deliverable amplifiers.

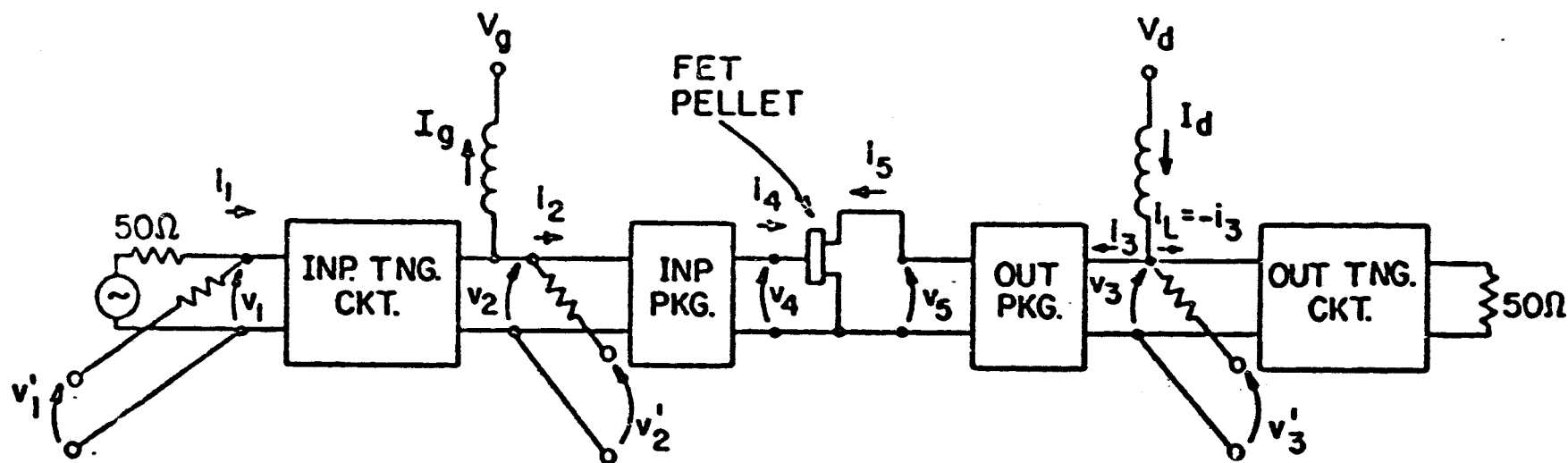
LOAD CONTOURS OF POWER TRANSISTOR AMPLIFIER



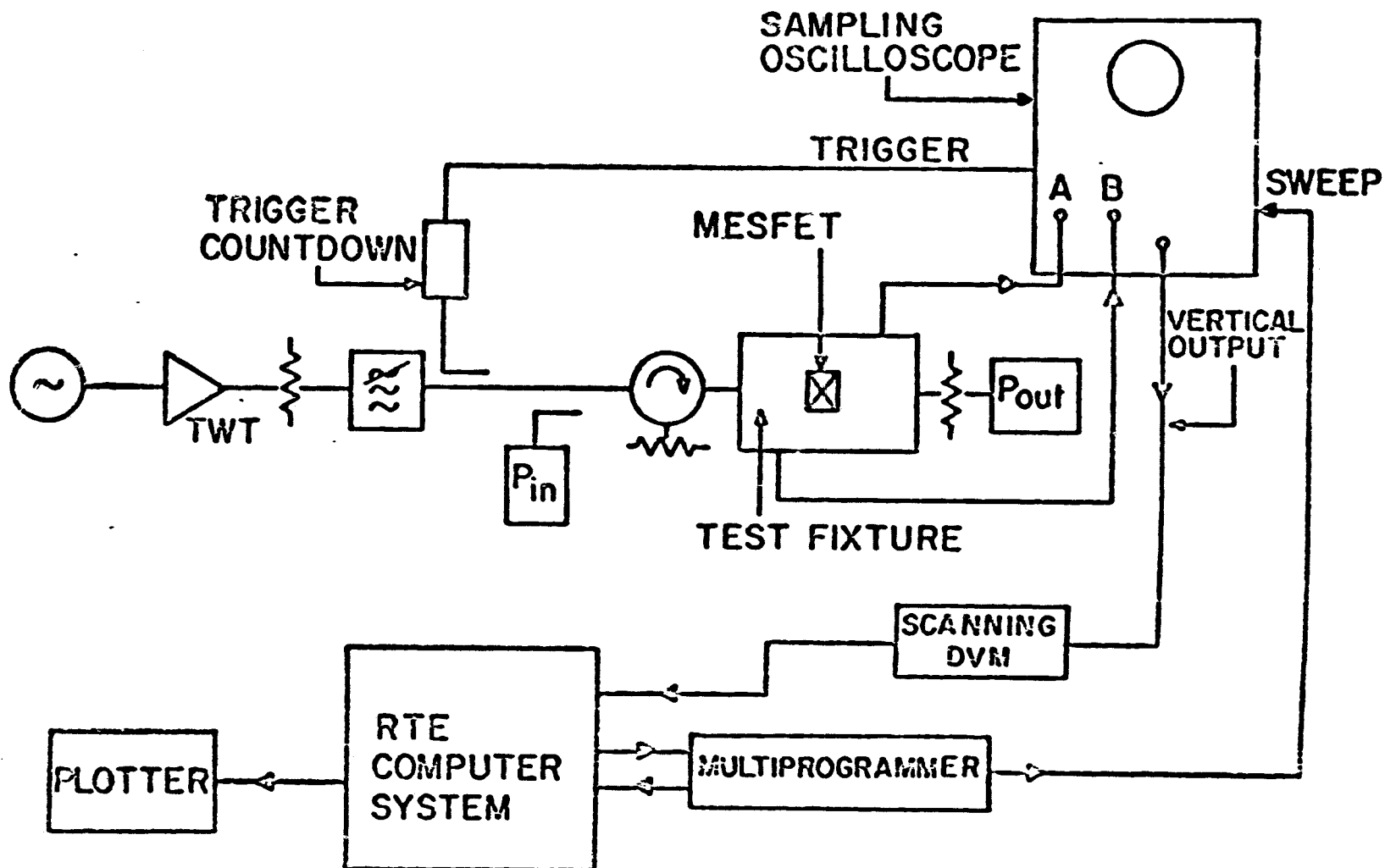




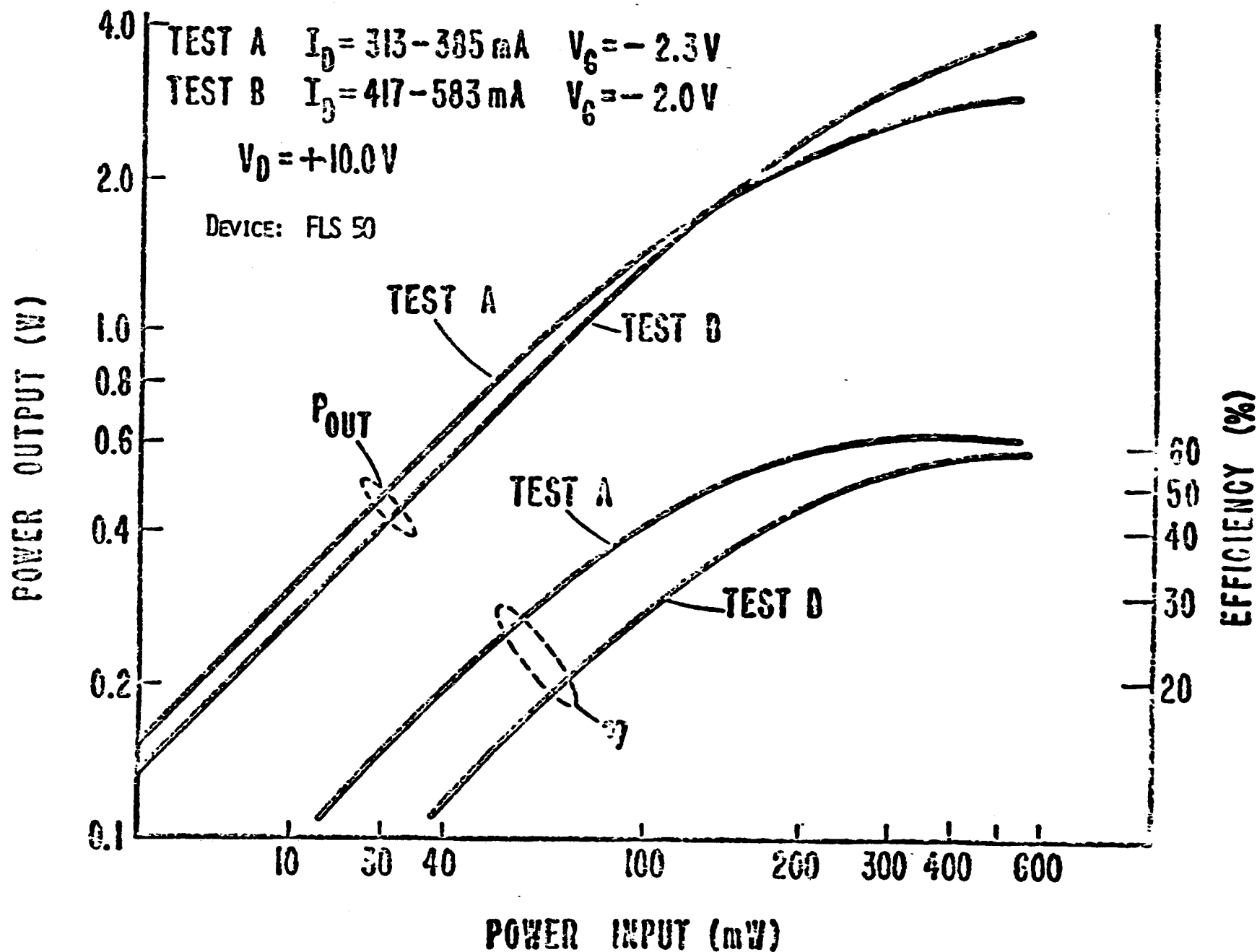
POWER FET DRAIN AND GATE WAVEFORMS



COMPUTATION OF VOLTAGE AND CURRENT WAVEFORMS



WAVEFORMS MEASUREMENT SET-UP



TEST RESULTS - MAX. POWER AND MAX. EFFICIENCY TUNING.

IRCAI

RESULTS TO DATE

- o Devices Sampled 6 Types Total 14
- o Devices tested in 3 Types Total 6
optimization circuit
- o Single stage (transistor) amplifier results. (Sample)

Device Type	Power per Chip	Efficiency
FLS 50	3.96 W	58%
MGF 2150	1 W	71%
NEC 86400	1.9 W	37%

- o Devices analyzed for η related parameter study 1

REM

Solid-State Technology Forecast

- Technology Direction is Favorable to SPS
- Efficiency Projections
- Cost Projections
- Technology Investigation Needed to Support SPS
- Totally Integrated Energy Conversion Chain

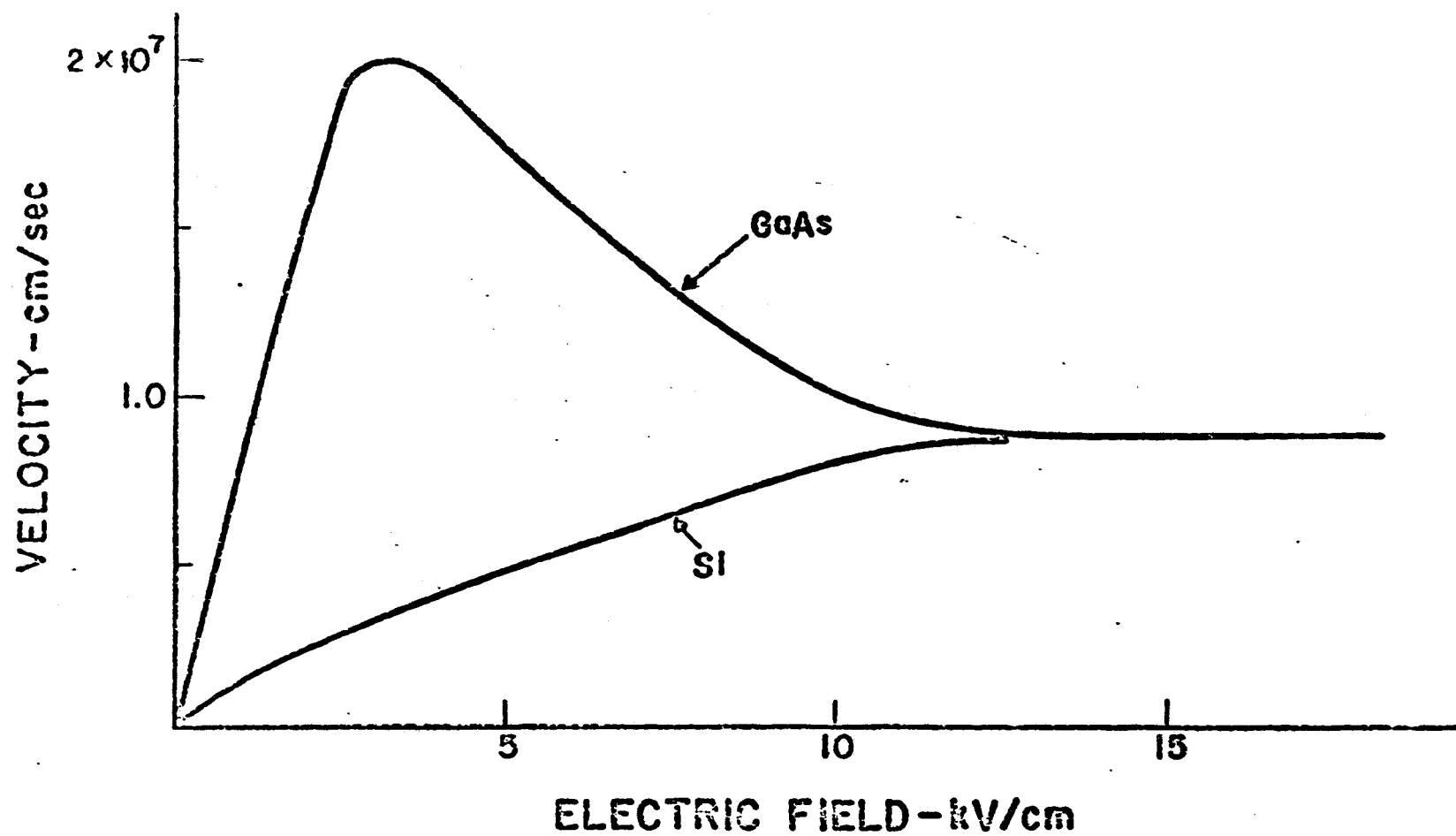
PROJECTIONS

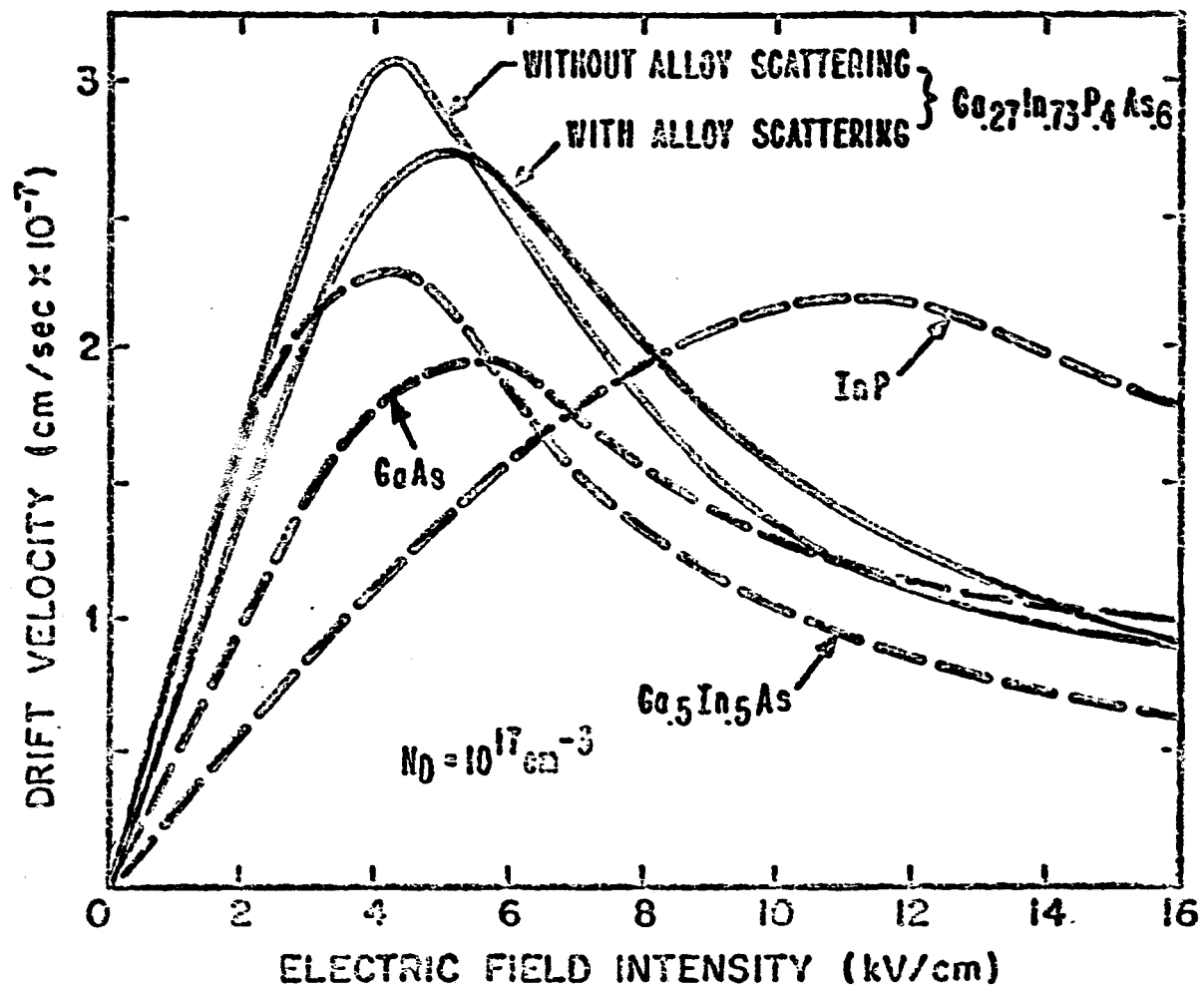
- AMPLIFIER PERFORMANCE
- DEVICE DESIGN INFORMATION

REAL

Technology Direction is Favorable to SPS

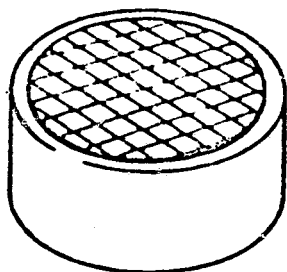
- o Rapid Growth, Heavy Funding in Micro-technology
- o Semiconductor Materials
- o New Device Concepts
- o Micro-circuitry
- o Processing and Manufacturing





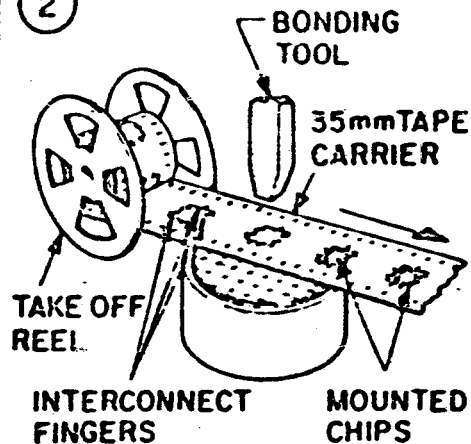
AMPLIFIER SUBMODULE FABRICATION

①



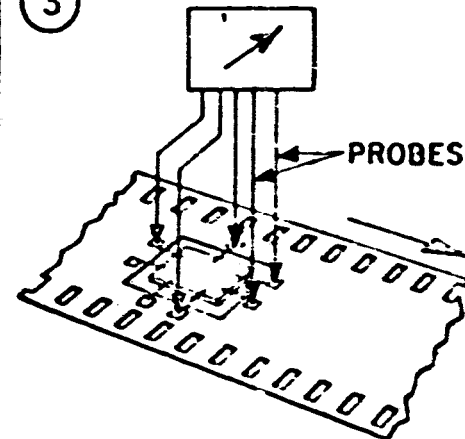
CIRCUIT WAFER WAXED DOWN
AND SAWED INTO CHIPS

②



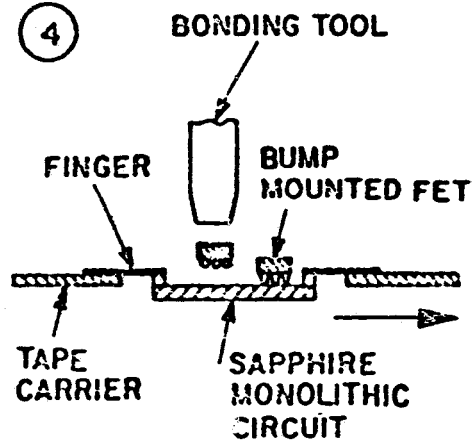
INTERCONNECT
FINGERS MOUNTED
CHIPS

③



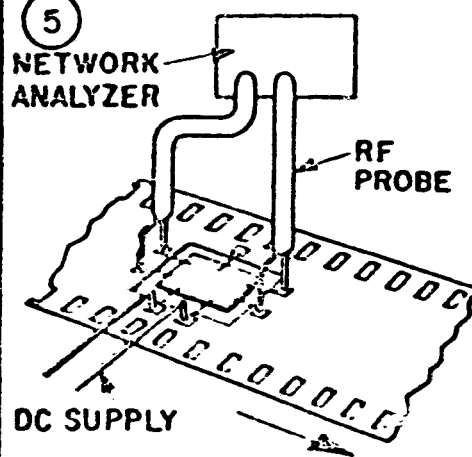
CIRCUIT DC TESTING

④



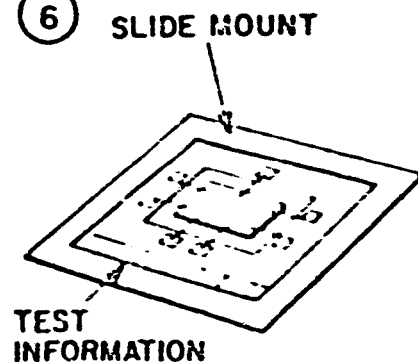
MOUNTING OF FET PELLETS

⑤



RF TESTING AND TRIMMING

⑥



SEPARATING, SLIDE MOUNTING,
BURN-IN, FINAL TESTING AND
STORAGE



Efficiency Projections

Single Device
Power Added Efficiency

80%

At 1-10 Watt

Module
DC/Radiated RF

70%

Including suf-
ficient gain and
phase control

Solar Energy to
Radiated RF

Solar Energy to
Power Grid

- o Status: 1 W, 71% Single Device - 10 dB Gain
- o Advantage: Just Started.

REAL

Technology Investigations Needed to Support SPS

- Total Integrated Energy Conversion Chain
- System Studies in Solid State
- Solar Cell Studies, Related to Above
- Alternate Device Studies
- Reliability & Space Environment Studies
- Production and Cost Reduction Studies

Cost Projections

Goals: \$/Watt-Years For Total SPS System

Microwave Transmitter Portion

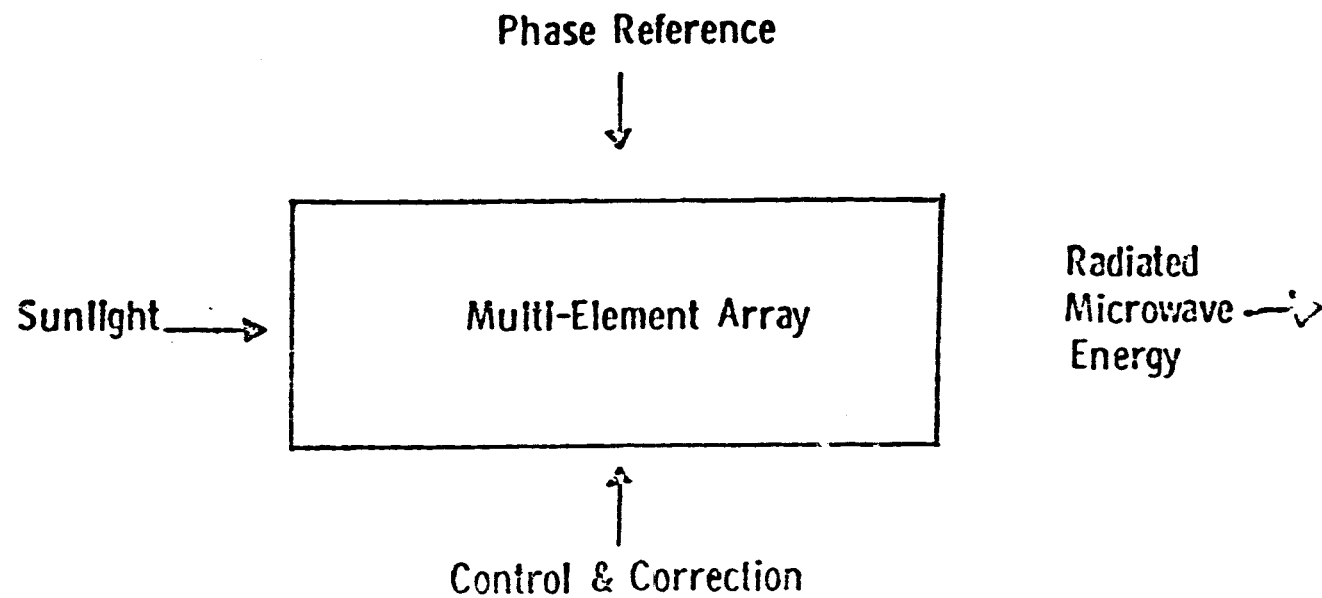
Material Costs - Today - Forecast

Processing Costs

REAL

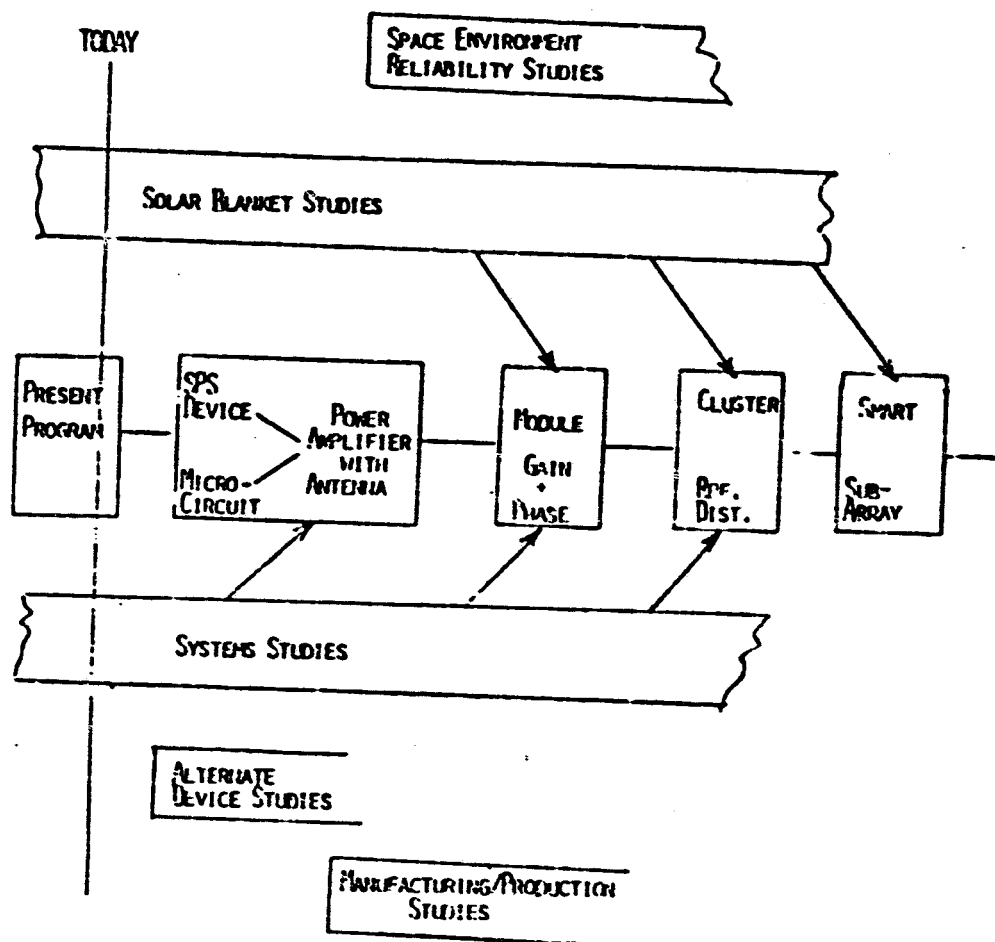
Totally Integrated Energy Conversion Chain

- Required to Optimize Performance
- Required to Minimize Cost



REAN

156



RCA

Advances in the Microwave Solid-State Technology and the continued steep rate of innovation within this technology (materials, devices, circuits) point increasingly toward its utilization as a principal ingredient in the Solar Power Satellite. Specific exploration studies of the solid-state antenna array and its functional elements should be vigorously pursued.

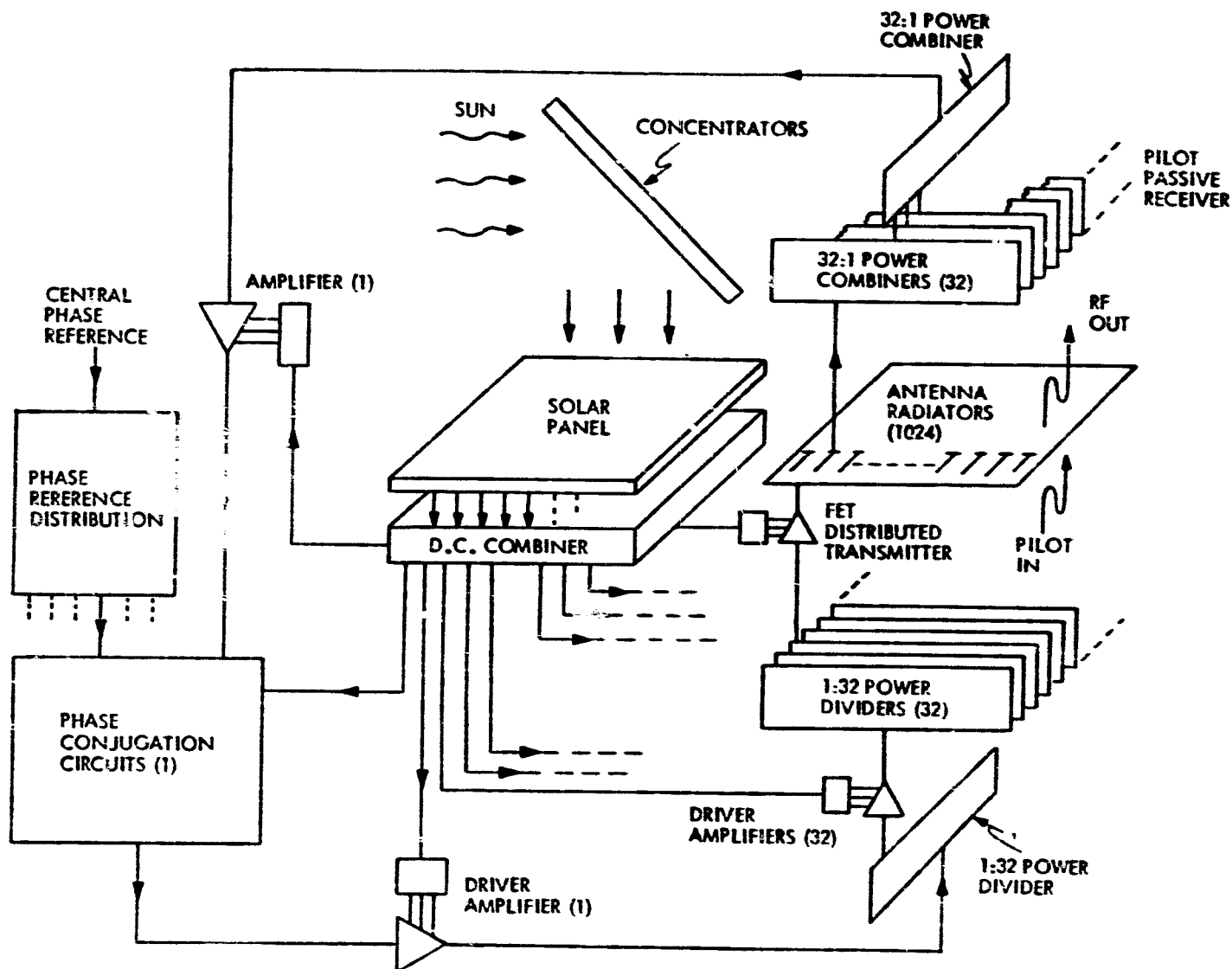
23
Solid State Sandwich Concept

*O. Maynard
Raytheon*

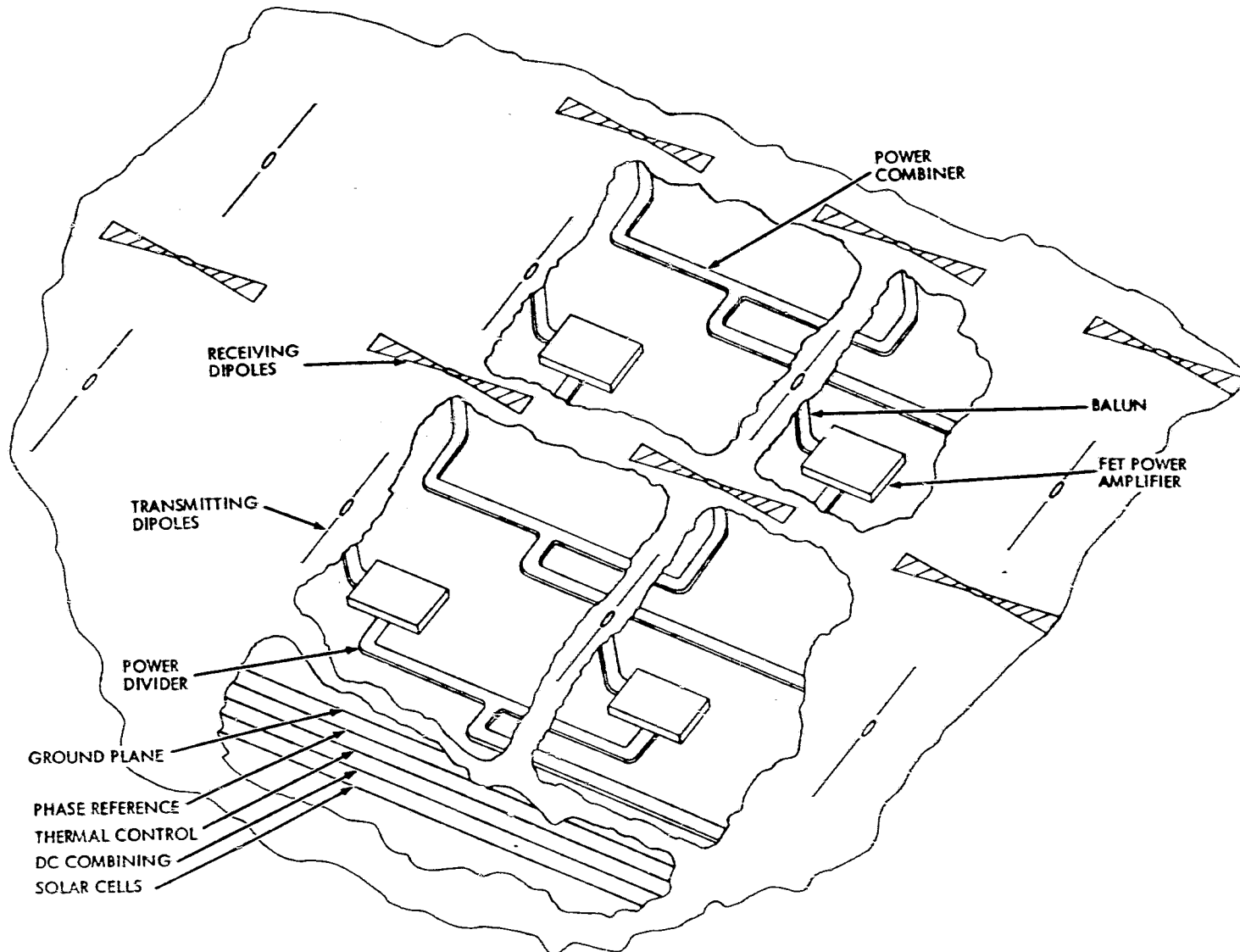
PRECEDING PAGE BLANK NOT FILMED

SOLID STATE MPTS SPACETENNA SUBARRAY CIRCUIT DIAGRAM

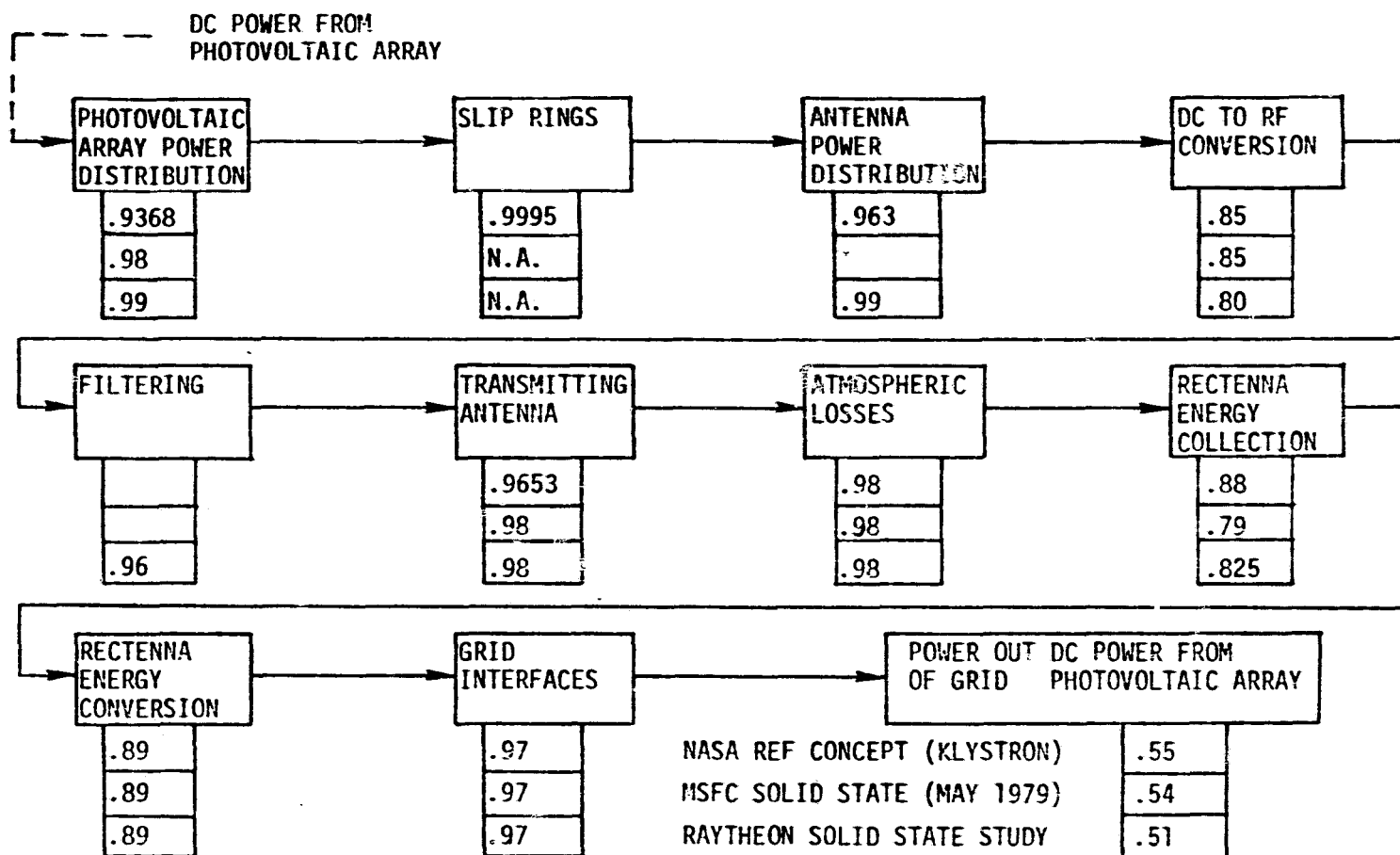
PRECEDING PAGE BLANK NOT FILMED



SPACETENNA - DIPOLE CONCEPT



PRELIMINARY ESTIMATES OF POWER TRANSMISSION AND CONVERSION EFFICIENCY CHAIN



ISSUES/CONSIDERATIONS

- LOW VOLTAGE DISTRIBUTION
- HARMONIC AND NOISE SUPPRESSION
- SUBARRAY SIZE
- MONOLITHIC TECHNOLOGY
- LIFETIME
- MUTUAL COUPLING
- INPUT TO OUTPUT ISOLATION
- CHARGED PARTICLE RADIATION EFFECTS
- TOPOLOGICAL CONSIDERATIONS
- SIDELobe SUPPRESSION

ISSUES/CONSIDERATIONS

RESOLUTION/STATUS

- LOW VOLTAGE DISTRIBUTION

FURTHER REFINEMENT REQUIRED TO MINIMIZE
WEIGHT AND CONTROL THERMAL LEAKAGE

- HARMONIC AND NOISE SUPPRESSION
- SUBARRAY SIZE
- MONOLITHIC TECHNOLOGY
- LIFETIME
- MUTUAL COUPLING
- INPUT TO OUTPUT ISOLATION
- CHARGED PARTICLE RADIATION EFFECTS
- TOPOLOGICAL CONSIDERATIONS
- SIDELobe SUPPRESSION

DC POWER CHARACTERISTICS OF SANDWICH

- DC POWER FROM PHOTOVOLTAIC BLANKET (PVB) TRANSMITTED TO POWER DISTRIBUTION LAYERS (+ GRID, - GROUND PLANE) (CONDUCTOR LENGTHS <20 CM).
- NEAR-UNIFORM VOLTAGE DIFFERENTIAL IS AVAILABLE CLOSE TO ALL USING EQUIPMENT ACROSS A SUBARRAY (15 V NOMINAL). LOCAL POWER CONDITIONING PROVIDED AT EACH AMPLIFIER MODULE.
- DC CONDUCTOR INCLUDING GROUND PLANE CROSS SECTIONS AND WEIGHT KEPT SMALL TO MINIMIZE "UNCONTROLLABLE" HEAT TRANSFER TO RF DEVICES HAVING LOWER CRITICAL JUNCTION TEMPERATURES THAN THOSE ASSOCIATED WITH PHOTOVOLTAIC PORTION OF SANDWICH.
 - TRANSFER OF POWER BETWEEN SUBARRAYS IS LIMITED BY GENERAL HEAT TRANSFER LIMITS AND BLOCKAGE FROM WASTE HEAT RADIATION POINT OF VIEW.
 - TRANSFER OF POWER FROM POWER GRID AND GROUND PLANE TO USING EQUIPMENT IS BY SHORT (DESIGN CONTROLLED) CONDUCTORS WITH BUILT-IN FUSES TO ISOLATE EQUIPMENT OVER-CURRENT FAILURES FROM THE POWER GRID AND GROUND PLANE.
- SPECIFIC WEIGHT OF GROUND PLANE IS .005 GM/WATT AND OF GRID IS .002 GM/WATT (WATTS ARE DC FROM PVB) FOR A SUBARRAY.

ISSUES/CONSIDERATIONS

RESOLUTION/STATUS

- LOW VOLTAGE DISTRIBUTION

- HARMONIC AND NOISE SUPPRESSION

FREQUENCY ALLOCATION NEEDS AT HARMONICS
SHOULD BE CONSIDERED OR CONSIDER SPREAD
SPECTRUM AND ACTIVE SUPPRESSION

- SUBARRAY SIZE
- MONOLITHIC TECHNOLOGY
- LIFETIME
- MUTUAL COUPLING
- INPUT TO OUTPUT ISOLATION
- CHARGED PARTICLE RADIATION EFFECTS
- TOPOLOGICAL CONSIDERATIONS
- SIDELobe SUPPRESSION

HARMONIC NOISE GENERATION, SUPPRESSION AND TRANSMISSION CHARACTERISTICS

- NOISE FILTERS ARE PROVIDED AT THE ELEMENT MODULE LEVEL ON TRANSMIT AND AT THE SUBARRAY CONJUGATING ELECTRONICS LEVEL ON RECEIVE.
- RESIDUAL NOISE IS NON-COHERENT BETWEEN SUBARRAYS.
- RESIDUAL HARMONICS MAY PERIODICALLY BE COHERENT OVER TOTAL TRANSMITTING ARRAY.
- NOISE AT EARTH IS ESTIMATED AS $-181 \text{ DBW/M}^2/4 \text{ KHZ}$.
- HARMONIC POWER DENSITY AT EARTH IS ESTIMATED AS -66 DBW/M^2 AT 3RD HARMONIC AND LESS AT HIGHER HARMONICS. GRATING LOBES FOR LOWER HARMONICS DO NOT INTERSECT THE EARTH.
- FREQUENCY ALLOCATION AT 3RD AND HIGHER HARMONICS SHOULD BE CONSIDERED. SPREAD SPECTRUM AND ACTIVE SUPPRESSION CONCEPTS SHOULD BE INVESTIGATED AS POSSIBLE MITIGATING APPROACHES.

ISSUES/CONSIDERATIONSRESOLUTION/STATUS

- LOW VOLTAGE DISTRIBUTION
- HARMONIC AND NOISE SUPPRESSION

- SUBARRAY SIZE

3M X 3M MAY BE CLOSE TO OPTIMUM, FURTHER
STUDY OF IMPLEMENTATION REQUIRED

- MONOLITHIC TECHNOLOGY
- LIFETIME
- MUTUAL COUPLING
- INPUT TO OUTPUT ISOLATION
- CHARGED PARTICLE RADIATION EFFECTS
- TOPOLOGICAL CONSIDERATIONS
- SIDELobe SUPPRESSION

SUBARRAY CHARACTERISTICS

THE FOLLOWING HAVE BEEN CONSIDERED IN SIZING OF THE SUBARRAY:

- TOPOLOGICAL CONSIDERATIONS TO MINIMIZE ELEMENT SPACING (MAXIMIZE TRANSMITTED POWER DENSITY), MINIMIZE DIVISIONS OF DRIVE POWER (MAXIMIZE EFFICIENCY) AND PROVIDE FOR OTHER FUNCTIONS WITH MINIMUM LAYERING (MINIMIZE INTER-LAYER CONNECTIONS) RESULTED IN A BASELINE SIZE OF 3.2M X 3.2M.
- SUBARRAY STEERING AND POINTING CONSIDERED SATISFACTORY.
- ARRAY FLATNESS CONSIDERED TO IMPOSE NO OVER-RIDING ISSUES.
- REMAINING COMPLEXITIES ARE PRIMARILY IN PACKAGING, THERMAL AND INTERFACING BETWEEN SUBARRAYS.
- KNOWN SPECIFIC WEIGHT ($\sim 3 \text{ KG/M}^2$) FOR 3.2M X 3.2M SUBARRAY MAY BE REDUCED BY 1% FOR 6.4M X 6.4M SUBARRAY WHILE POSSIBLE COMPLEXITY, HANDLING AND LOSSES NULLIFY THE KNOWN ADVANTAGE.
- LOSSES UNIQUE TO THE SUBARRAY ABOVE THE ELEMENT CELL LEVEL (ELEMENT SPACING 10 CM) HAVE BEEN ESTIMATED TO BE $< 0.5\%$.
- NEAR-IN SIDELobe INCREASES DUE TO THE SUBARRAY HAVE BEEN ESTIMATED TO BE $< 0.2 \text{ DB}$.

ISSUES/CONSIDERATIONS

RESOLUTION/STATUS

- LOW VOLTAGE DISTRIBUTION
- HARMONIC AND NOISE SUPPRESSION
- SUBARRAY SIZE

- MONOLITHIC TECHNOLOGY

MONOLITHIC APPROACHES APPLY AND REQUIRE
TECHNOLOGY DEVELOPMENT FOR
MINIMIZATION OF COST AND WEIGHT

- LIFETIME
- MUTUAL COUPLING
- INPUT TO OUTPUT ISOLATION
- CHARGED PARTICLE RADIATION EFFECTS
- TOPOLOGICAL CONSIDERATIONS
- SIDELobe SUPPRESSION

MONOLITHIC TECHNOLOGY FOR THE SANDWICH

- THE GENERAL CONCEPT OF MONOLITHIC TECHNOLOGY TO INCORPORATE MULTIPLE FUNCTIONS INTO ONE SERIES OF PROCESS AT BOTH THE AMPLIFIER LEVEL AND AT THE ANTENNA LAYER LEVEL IS THE SELECTED APPROACH FOR HIGH PRODUCTION RATE AND LOW COST PURPOSES.
- TOTAL SANDWICH CONCEPTS INCLUDE INTERCONNECTIONS BETWEEN LAYERS AND BETWEEN SUBARRAYS.

ISSUES/CONSIDERATIONSRESOLUTION/STATUS

- LOW VOLTAGE DISTRIBUTION
- HARMONIC AND NOISE SUPPRESSION
- SUBARRAY SIZE
- MONOLITHIC TECHNOLOGY

- LIFETIME

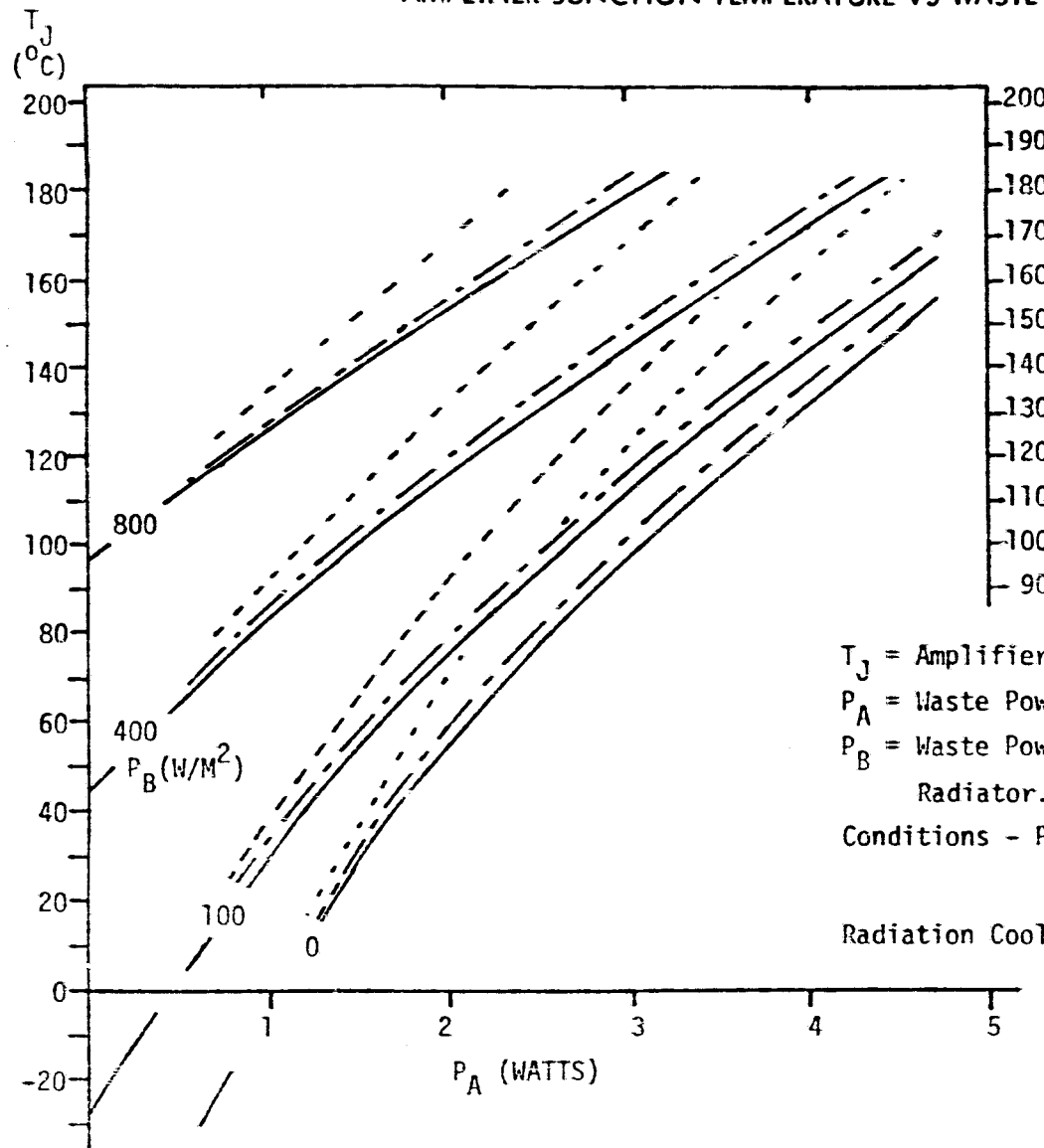
LIFETIME AFFECTED BY JUNCTION TEMPERATURE LIMITS AND CHARGED PARTICLES RADIATION REQUIRING TECHNOLOGY DEVELOPMENT IN BOTH AREAS.

- MUTUAL COUPLING
- INPUT TO OUTPUT ISOLATION
- CHARGED PARTICLE RADIATION EFFECTS
- TOPOLOGICAL CONSIDERATIONS
- SIDELobe SUPPRESSION

LIFETIME CONSIDERATIONS

- LIFETIME GOAL IS 30 YEARS WITH LOW PROBABILITY OF FAILURE.
- PRIMARY FAILURE MECHANISMS RELATE MOST DIRECTLY TO JUNCTION TEMPERATURE.
- RANGE OF INTEREST FOR JUNCTION TEMPERATURE IS 100°C TO 150°C REQUIRING ADVANCED TECHNOLOGY DEVELOPMENT FOR LONG LIFE.
- HEAT GENERATION AT AMPLIFIER DEVICES IS PRIMARY CONTRIBUTOR TO HIGH JUNCTION TEMPERATURE. ADVANCED TECHNOLOGY DEVELOPMENT REQUIRED FOR HIGH EFFICIENCY.
- HEAT TRANSPORT FROM DEVICE TO WASTE HEAT RADIATOR IS A MAJOR SANDWICH DESIGN CONSIDERATION INVOLVING:
 - HIGH CONDUCTIVITY MATERIALS
 - DEDICATED REGIONS FOR WASTE HEAT RADIATION TO COLD SPACE
 - HIGH EMISSIVITY AND LOW ABSORPTIVITY THERMAL CONTROL SURFACES-TO MAXIMIZE WASTE HEAT DISSIPATION WITHOUT EXCEEDING LONG-LIFE JUNCTION TEMPERATURES
- MATERIALS AND COATINGS MUTUAL TECHNOLOGY DEVELOPMENT GOALS HAVE BEEN ESTABLISHED
 - MATERIALS SUCH AS PYROLYTIC GRAPHITE, HAVING HIGH THERMAL CONDUCTIVITY, IN CONJUNCTION WITH HIGH PERFORMANCE THERMAL CONTROL COATINGS NEED TECHNOLOGY DEVELOPMENT TO ASSURE INTEGRITY AND PERFORMANCE OF HIGH EMISSIVITY AND LOW ABSORPTIVITY SURFACES.
 - WHERE WEIGHT IS NOT A SIGNIFICANT FACTOR COPPER MAY BE SATISFACTORY.
- OPTIMIZATION TOOLS HAVE BEEN CONCEIVED TO MAXIMIZE THE ABILITY OF THE TOTAL SANDWICH TO TRANSMIT HIGH POWER DENSITY.

AMPLIFIER JUNCTION TEMPERATURE VS WASTE HEAT

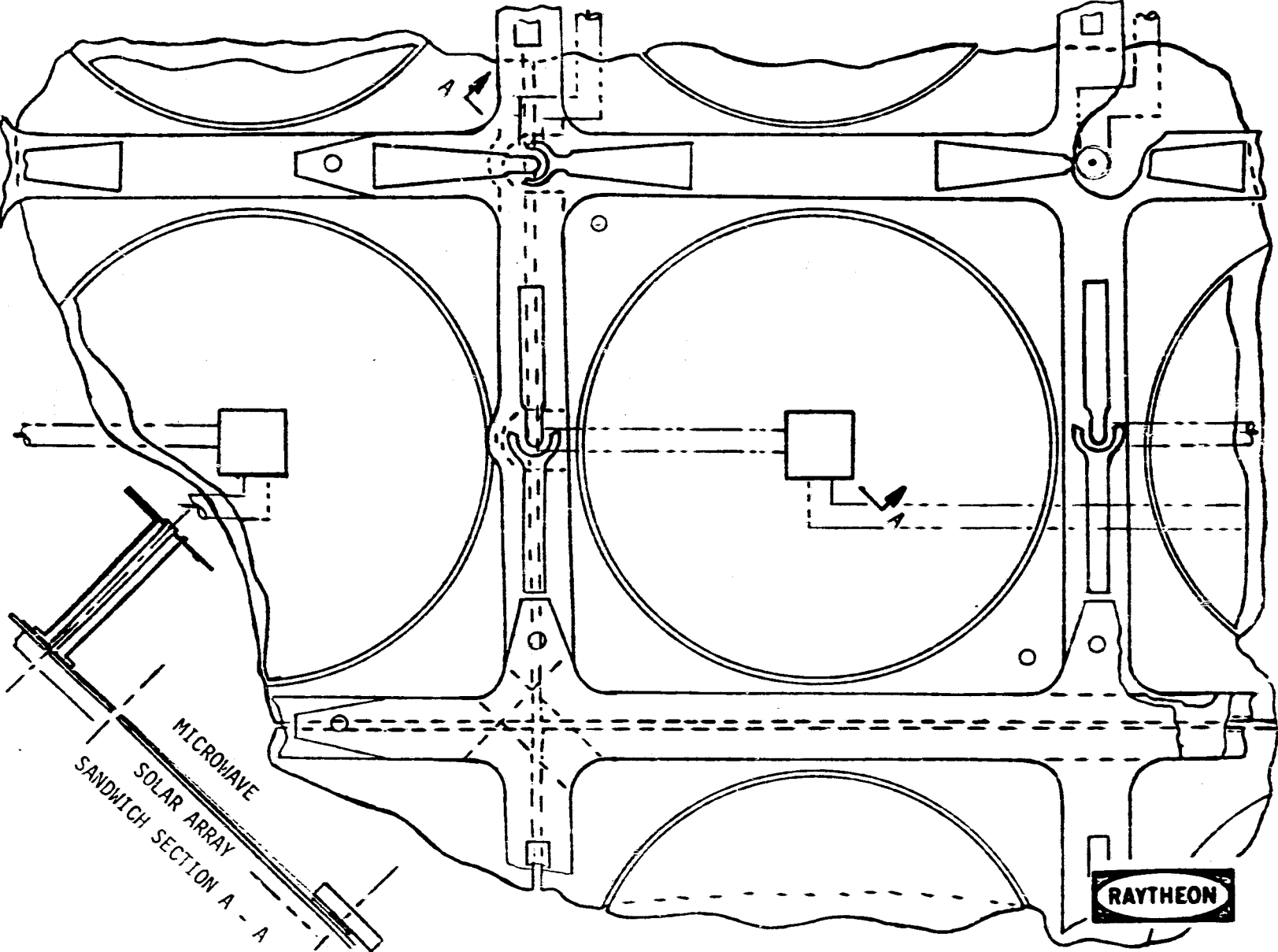


$\epsilon = 0.8$ Thermal Control
 $\alpha = 0.05$ Coating Wt = 1.59 gm
 Dia = 8.66 cm
 $t_{\text{root}} = 1.0$ mm
 $t_{\text{tip}} = 0.1$ mm

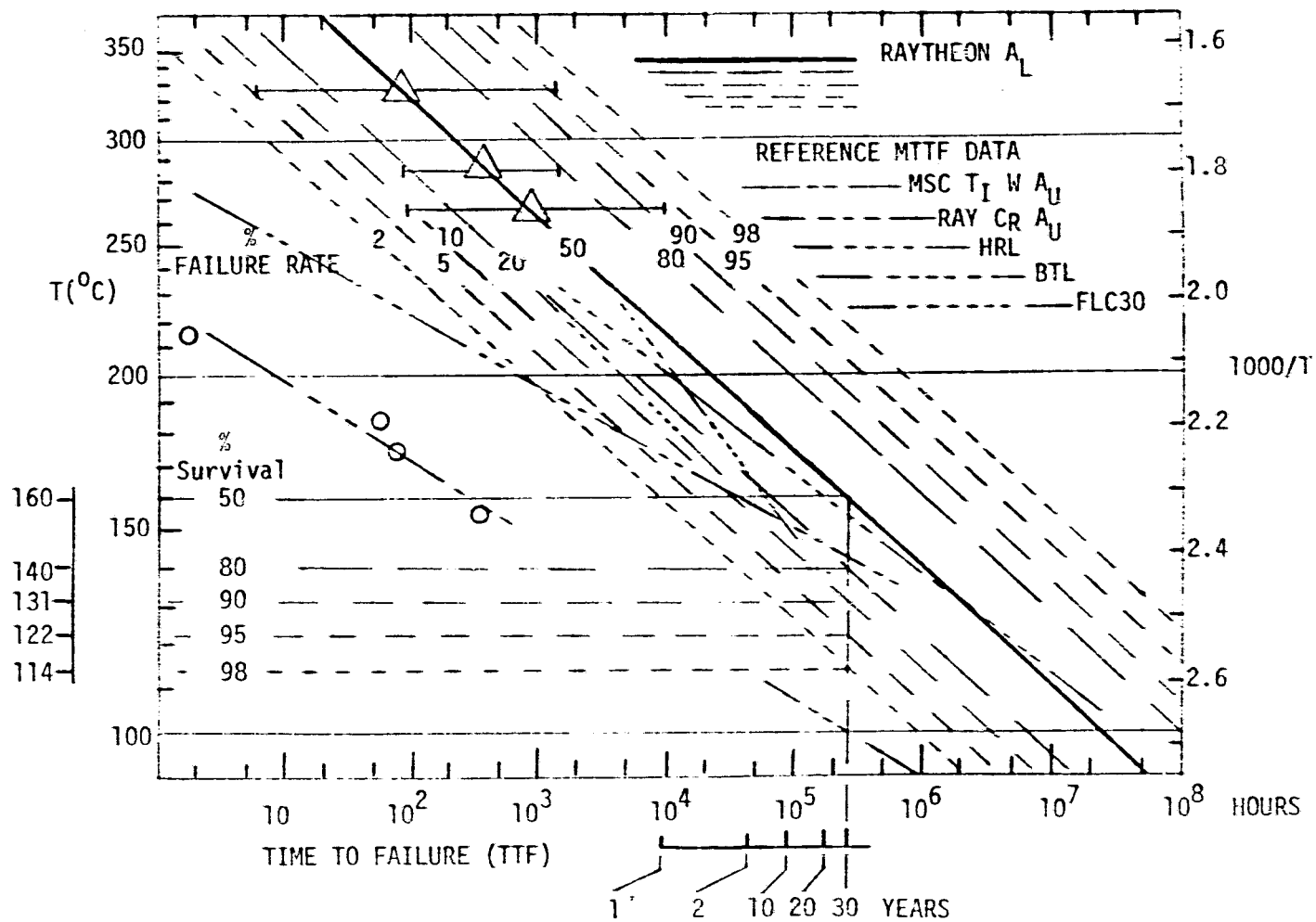
	Thermal Conductor Wt. (gm)
Aluminum	6.35
Copper	20.94
Pyrographite	5.29

T_J = Amplifier Junction Temperature
 P_A = Waste Power Generated at Amplifier Junction.
 P_B = Waste Power w/m² - Uniform Over Thermal Radiator.
 Conditions - P_S = Incident Solar Power (1300 W/m²)
 Radiation Cooling - To Absolute Zero

SUBARRAY LAYOUT - TYPICAL CORNER AND SECTION

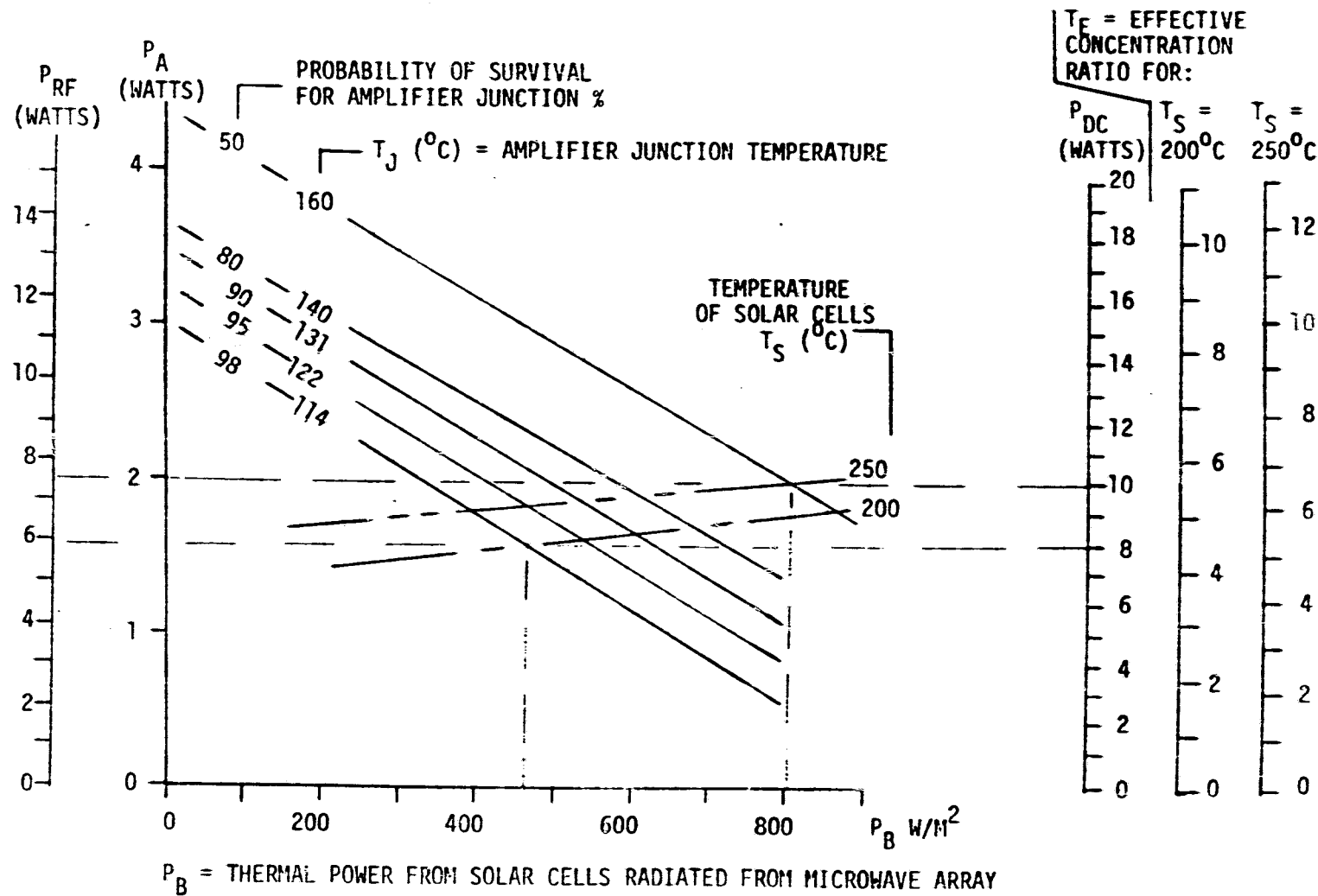


ACCELERATED LIFE DATA AND PROJECTIONS FOR SOLID STATE SPS MPTS STUDY



POWER PER ELEMENT CELL (10 CM X 10 CM) RELATIONSHIPS

- o PYROGRAPHITE RADIATORS (8.66 CM DIA)
- o AMPLIFIER EFFICIENCY = 0.8
- o DC TO RF EFFICIENCY = 0.7377



ISSUES/CONSIDERATIONS

RESOLUTION/STATUS

- LOW VOLTAGE DISTRIBUTION
- HARMONIC AND NOISE SUPPRESSION
- SUBARRAY SIZE
- MONOLITHIC TECHNOLOGY
- LIFETIME

- MUTUAL COUPLING

IMPLEMENTATION BY PRINTED DIPOLES SPACED FROM GROUND PLANE WITH BALUN IN CIRCUITRY AND CLOSE ELEMENT SPACING TO MINIMIZE DETRIMENTAL MUTUAL COUPLING EFFECTS

- INPUT TO OUTPUT ISOLATION
- CHARGED PARTICLE RADIATION EFFECTS
- TOPOLOGICAL CONSIDERATIONS
- SIDELobe SUPPRESSION

MUTUAL COUPLING CONSIDERATIONS

- ELEMENT SPACING (0.8λ) TO SUPPRESS GRATING LOBES.
- PHYSICAL IMPLEMENTATION OF DIPOLES SUPPORTED ABOVE (0.25λ) GROUND PLANE TO PREVENT SURFACE WAVE RESONANCES AND PROVIDE BALUN ACTION.
- DIPOLES AND TRANSFORMERS INCORPORATED IN CIRCUITRY USED FOR IMPEDANCE MATCHING IN PRESENCE OF MUTUAL COUPLING AMONG ELEMENTS.

ISSUES/CONSIDERATIONSRESOLUTION/STATUS

- LOW VOLTAGE DISTRIBUTION
- HARMONIC AND NOISE SUPPRESSION
- SUBARRAY SIZE
- MONOLITHIC TECHNOLOGY
- LIFETIME
- MUTUAL COUPLING

- INPUT TO OUTPUT ISOLATION

ORTHOGONAL DIPOLES, OFFSET FREQUENCIES
AND FILTERING PROVIDE SATISFACTORY
ISOLATION OF TRANSMIT FROM RECEIVE
SIGNALS

- CHARGED PARTICLE RADIATION EFFECTS
- TOPOLOGICAL CONSIDERATIONS
- SIDELobe SUPPRESSION

INPUT TO OUTPUT ISOLATION

- TRANSMIT AND RECEIVE DIPOLES ARE ORTHOGONAL TO MAXIMIZE INPUT/OUTPUT ISOLATION.
- SEPARATE PILOT FREQUENCIES FROM FUNDAMENTAL (OUTSIDE HIGH NOISE BAND).
- FILTERING PROVIDED ON PILOT RECEIVER WILL BE IMPLEMENTED AT THE PHASE CONJUGATION NETWORK AT THE SUBARRAY LEVEL.

ISSUES/CONSIDERATIONSRESOLUTION/STATUS

- LOW VOLTAGE DISTRIBUTION
- HARMONIC AND NOISE SUPPRESSION
- SUBARRAY SIZE
- MONOLITHIC TECHNOLOGY
- LIFETIME
- MUTUAL COUPLING
- INPUT TO OUTPUT ISOLATION
- CHARGED PARTICLE RADIATION EFFECTS
- TOPOLOGICAL CONSIDERATIONS
- SIDELOBE SUPPRESSION

GaAs IS CURRENTLY BEST TECHNOLOGY
(REQUIRES MORE ADVANCEMENT IN
"MECHANISMS" OF FAILURE)

CHARGED PARTICLE RADIATION EFFECTS/CONSIDERATIONS

- VAN ALLEN BELT DISTRIBUTION OF ELECTRONS GEOMAGNETICALLY GO OUT TO 40-50K NAUTICAL MILES. NO SINGLE PEAK BUT VARIES IN TIME.
- 11 YEAR SOLAR SUNSPOT CYCLE RESULTS IN CHARGED ELECTRONS AND PROTONS HAVING POSSIBLY SIGNIFICANT EFFECTS.
- SOLAR WINDS RESULT IN LOW ENERGY ELECTRONS HAVING MUCH SMALLER EFFECTS THAN CHARGED PARTICLES TRAPPED IN VAN ALLEN BELTS.
- GaAs MESFETS TEND TO BE HARDEST OF EXISTING TECHNOLOGIES.
- TEST RESULTS ARE NON-CONCLUSIVE RE FAILURE OR DEGRADATION MECHANISMS AND EFFECTS OF PROTECTIVE SCHEMES.
- SELECTION OF GaAs TECHNOLOGY AND SHIELDING APPEAR TO BE MOST EFFECTIVE APPROACH AT PRESENT.
- ADVANCED TECHNOLOGY DEVELOPMENT REQUIRED TO ADDRESS MATERIALS, FAILURE MECHANISMS AND PROTECTIVE SCHEMES.

ISSUES/CONSIDERATIONSRESOLUTION/STATUS

- LOW VOLTAGE DISTRIBUTION
- HARMONIC AND NOISE SUPPRESSION
- SUBARRAY SIZE
- MONOLITHIC TECHNOLOGY
- LIFETIME
- MUTUAL COUPLING
- INPUT TO OUTPUT ISOLATION
- CHARGED PARTICLE RADIATION EFFECTS
- TOPOLOGICAL CONSIDERATIONS
- SIDELOBE SUPPRESSION

REQUIRED FUNCTIONS CAN BE IMPLEMENTED
IN SANDWICH CONCEPT. FURTHER DETAILS
AT SUBARRAY BOUNDARIES REQUIRED.

TOPOLOGICAL CONSIDERATIONS

TOPOLOGICAL CONSIDERATIONS HAVE BEEN GIVEN AT THE TOTAL ARRAY, PHASE DISTRIBUTION SYSTEM, SUBARRAY AND ELEMENT MODULE LEVELS.

- STRUCTURAL SUPPORT FOR THE ARRAY IS CONSIDERED TO BE PROVIDED BY MAJOR STRUCTURAL RING AT PERIPHERY WITH TENSION GRID ASSURING RELATIVE FLATNESS. GRID MEMBERS ARE CONSIDERED TO BE SMALL WITH RESPECT TO SANDWICH THICKNESS AND DO NOT SHIELD RF OR WASTE HEAT RADIATION.
- MECHANICAL SUPPORT AT SUBARRAY BOUNDARIES ARE REQUIRED LARGELY FOR HANDLING, INSTALLATION AND REPLACEMENT PURPOSES. DETAILS OF HOW SUBARRAYS WILL BE MATED TO PRECLUDE ADVERSE DISCONTINUITIES ARE YET TO BE DEVELOPED.
- RF TRANSMIT ELEMENT LATTICE IS MAINTAINED IN REGION OF SUBARRAY EDGES TO MINIMIZE SYSTEMATIC ERROR SIDELOBES.
- FREE RADIATION OF WASTE HEAT FROM RADIATORS NEAR SUBARRAY EDGES IS COMPROMISED REQUIRING CUSTOMIZED EDGE TREATMENT TO MAXIMIZE THE EFFICIENCIES OF THE THERMAL RADIATORS AT THE EXPENSE OF WEIGHT AND COST. FURTHER INVESTIGATION IS REQUIRED.

ISSUES/CONSIDERATIONSRESOLUTION/STATUS

- LOW VOLTAGE DISTRIBUTION
- HARMONIC AND NOISE SUPPRESSION
- SUBARRAY SIZE
- MONOLITHIC TECHNOLOGY
- LIFETIME
- MUTUAL COUPLING
- INPUT TO OUTPUT ISOLATION
- CHARGED PARTICLE RADIATION EFFECTS
- TOPOLOGICAL CONSIDERATIONS

● SIDELobe SUPPRESSION

SINGLE STEP EDGE TAPER MAY BE REQUIRED

SIDELOBE SUPPRESSION CONSIDERATIONS

- UNIFORM VERSUS 10 DB GAUSSIAN ILLUMINATION AT SPACETENNA RESULTS IN THE FOLLOWING:

ADVANTAGES FOR UNIFORM

- SMALLEST TRANSMIT ANTENNA
- ALL AMPLIFIER MODULES OPERATE AT SAME POWER LEVEL
- EASY TRANSFER OF DC VOLTAGES FROM SOLAR ARRAY (IF DENSITY TAPERING IS EMPLOYED TO APPROXIMATE GAUSSIAN ILLUMINATION THEN DC DISTRIBUTION AND SOLAR ARRAY ARCHITECTURE BECOMES COMPLEX AND HEAVIER)

DISADVANTAGES FOR UNIFORM

- LOWER POWER BEAM EFFICIENCY
- HIGHER SIDELOBES (-17 DB, -24 DB, -28 DB BELOW $23 \text{ MW}/\text{CM}^2$ AND MORE LAND REQUIRED TO FENCE RECTENNA

- SINGLE STEP TAPER VERSUS UNIFORM (CONSTANT POWER DENSITY AT EACH LEVEL)

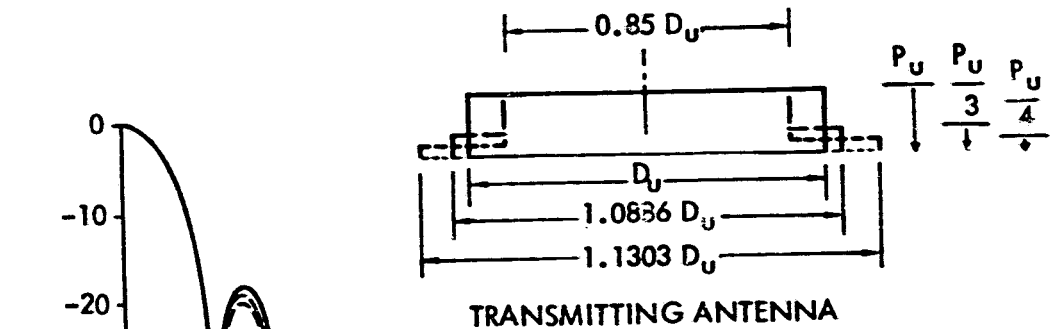
ADVANTAGES FOR STEP

- LOWER SIDELOBES (-28 DB BELOW $23 \text{ MW}/\text{CM}^2$)
- ALL AMPLIFIERS OPERATED AT SAME POWER LEVEL

DISADVANTAGES FOR STEP

- LESS POWER AVAILABLE
- LARGER SPACETENNA

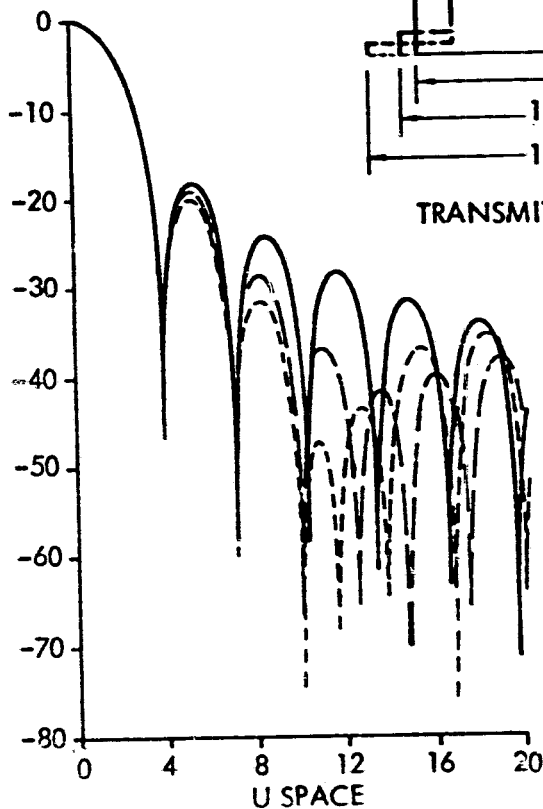
SIDELOBE COMPARISON OF UNIFORM POWER DISTRIBUTION WITH TWO EXAMPLES OF SINGLE STEP EDGE TAPER



KEY:

- UNIFORM POWER DISTRIBUTION
- - - 1/3 STEP AT EDGE
- - - - 1/4 STEP AT EDGE

POWER dB



RADIUS KM (FOR $D_u = 1.95$ KM
 $\lambda = 0.12$ M
 $R = 37,000$ KM)

P_u = POWER DENSITY AT TRANSMITTING ANTENNA

D_u = DIAMETER AT TRANSMITTING ANTENNA FOR UNIFORM POWER DISTRIBUTION

U SPACE

$$U = \frac{\pi D_u \sin \theta}{\lambda}$$

λ = WAVE LENGTH

θ = BEAM WIDTH (HALF ANGLE)

SUMMARY AND CONCLUSIONS
SOLID STATE SANDWICH CONCEPT ISSUES AND RESOLUTION SUMMARY

ISSUES/CONSIDERATIONS

LOW VOLTAGE DISTRIBUTION

HARMONIC AND NOISE SUPPRESSION

SUBARRAY SIZE

MONOLITHIC TECHNOLOGY

LIFETIME

MUTUAL COUPLING

INPUT TO OUTPUT ISOLATION

CHARGED PARTICLE RADIATION EFFECTS

TOPOLOGICAL CONSIDERATIONS

SIDELobe SUPPRESSION

RESOLUTION/STATUS

FURTHER REFINEMENT REQUIRED TO MINIMIZE
WEIGHT AND CONTROL THERMAL LEAKAGE

FREQUENCY ALLOCATION NEEDS AT HARMONICS SHOULD
BE CONSIDERED OR CONSIDER SPREAD SPECTRUM
AND ACTIVE SUPPRESSION

3M X 3M MAY BE CLOSE TO OPTIMUM, FURTHER
STUDY OF IMPLEMENTATION REQUIRED

MONOLITHIC APPROACHES APPLY AND REQUIRE
TECHNOLOGY DEVELOPMENT FOR MINIMIZATION
OF COST AND WEIGHT

LIFETIME AFFECTED BY JUNCTION TEMPERATURE
LIMITS AND CHARGED PARTICLE RADIATION
REQUIRING TECHNOLOGY DEVELOPMENT IN BOTH AREAS

IMPLEMENTATION BY PRINTED DIPOLES SPACED FROM
GROUND PLANE WITH BALUN IN CIRCUITRY AND CLOSE
ELEMENT SPACING TO MINIMIZE DETRIMENTAL MUTUAL
COUPLING EFFECTS

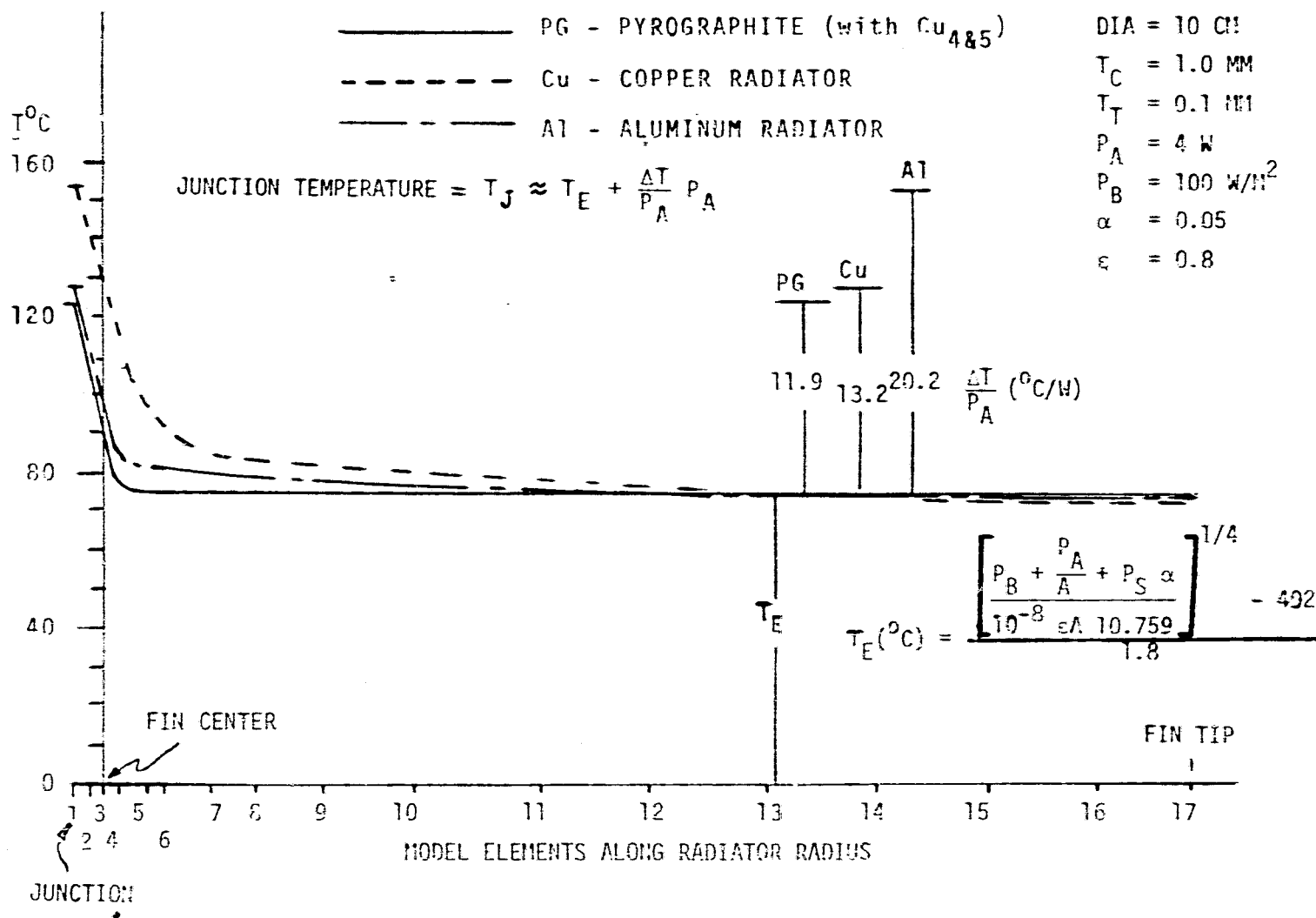
ORTHOGONAL DIPOLES, OFFSET FREQUENCIES AND
FILTERING PROVIDE SATISFACTORY ISOLATION OF
TRANSMIT FROM RECEIVE SIGNALS

GaAs IS CURRENTLY BEST TECHNOLOGY (REQUIRES
MORE ADVANCEMENT IN "MECHANISMS" OF FAILURE)

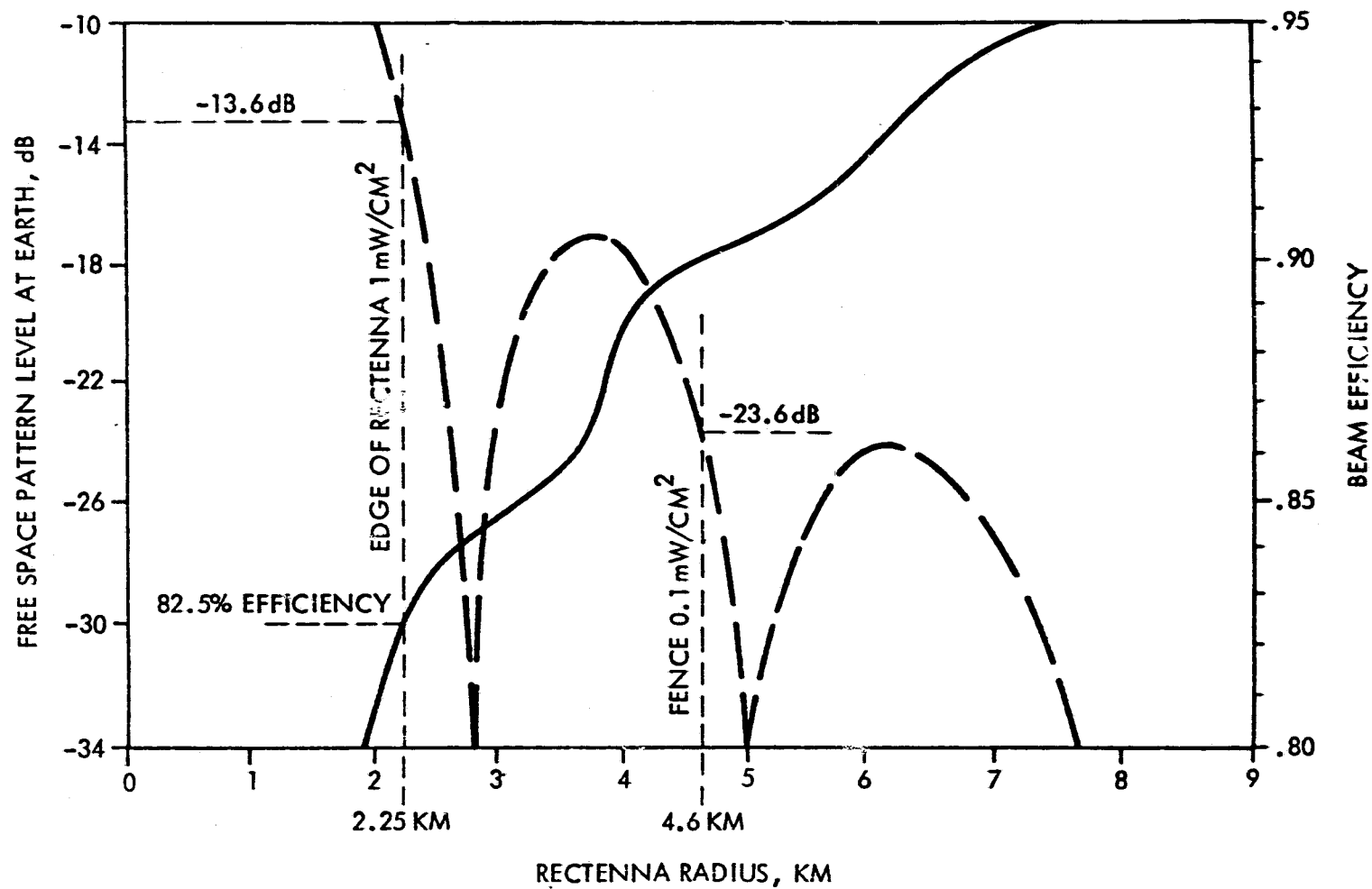
REQUIRED FUNCTIONS CAN BE IMPLEMENTED IN
SANDWICH CONCEPT. FURTHER DETAILS AT
SUBARRAY BOUNDARIES REQUIRED.

SINGLE STEP EDGE TAPER MAY BE REQUIRED.

AMPLIFIER THERMAL MODEL



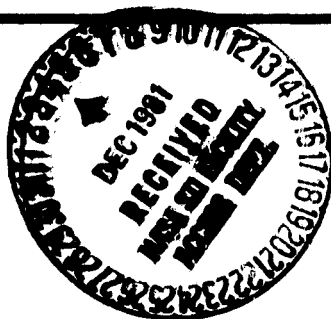
RECTENNA SIZE VS BEAM EFFICIENCY - UNIFORM ILLUMINATION





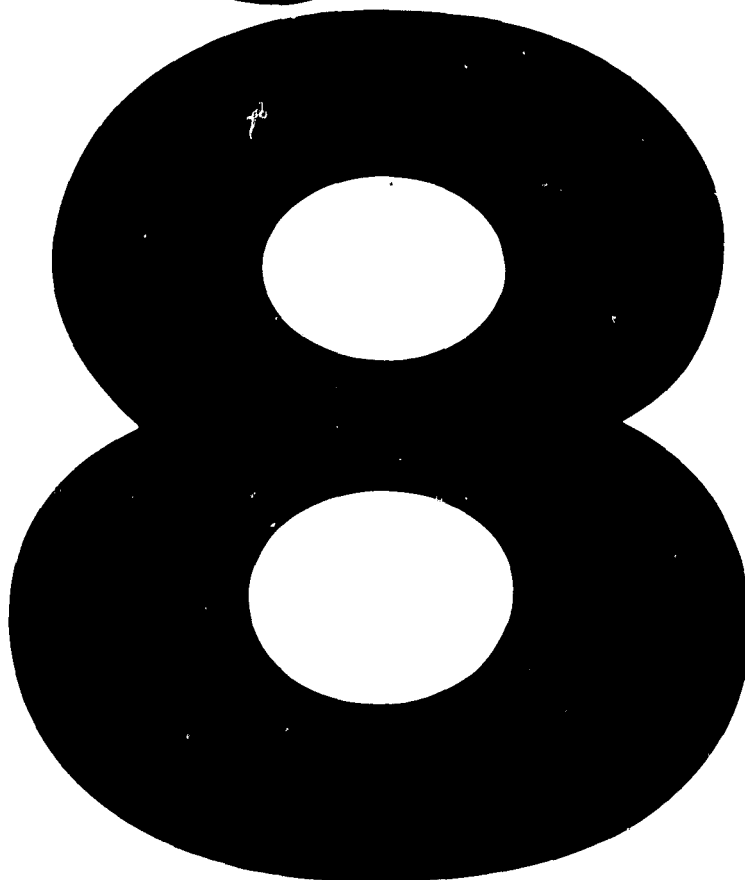
National Aeronautics and
Space Administration

Lyndon B. Johnson Space Center
Houston, Texas 77058



8

**Planned
Program
Activities**

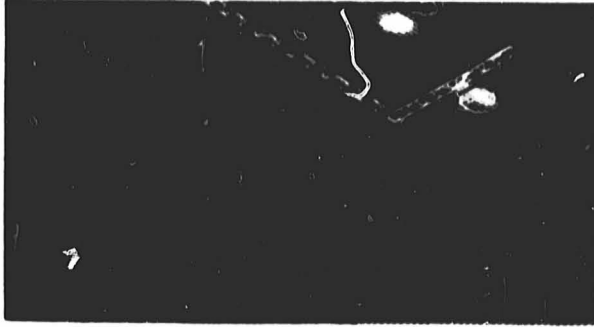


**NASA Solar Power
Satellite**

**Workshop on
Microwave Power
Transmission
and Reception**

**Session
Presentations**

**Jan
15-18
1980**



The presentation material herein was used in the Planned Program Activities Session of the Solar Power Satellite Workshop on Microwave Power Transmission and Reception held at the Lyndon B. Johnson Space Center, January 15-28, 1980. The workshop was conducted as part of the Technical assessment process of the DOE/NASA Solar Power Satellite Concept Evaluation program. All aspects of Solar Power Satellite microwave transmission and reception were addressed including studies, analyses, and laboratory investigations. Conclusions from these activities were presented as well as recommended follow-on work. The workshop was organized into eight sessions as follows:

- *General*
- *Microwave System Performance*
- *Phase Control*
- *Power Amplifiers*
- *Radiating Elements*
- *Rectenna*
- *Solid State Configurations*
- *Planned Program Activities*

The material contained herein supplements the workshop papers which were published and distributed at the time of the workshop. Together they are a comprehensive documentation of the numerous analytical and experimental activities in the field of microwave power transmission and reception.

- *Additional information regarding the workshop may be obtained by*

contacting: R.H. Dietz
EE4/SPS Microwave Systems
National Aeronautics &
Space Administration
Lyndon B. Johnson Space Center
Houston, Texas 77058
713 483 4507

Planned Program Activities Session

***R. H. Dietz
Lyndon B. Johnson Space Center***

NASA**Solar Power
Satellite****Planned Activities**

-
- **1980 funded efforts**
 - **Additional funded efforts**
 - **Ground Based Exploratory Development (GBED)**
 - Program overview (DOE/NASA)
 - Microwave systems
 - Reference system
 - System alternative (solid-state) (budgeted)
 - Sub-system alternatives
 - *Magnetron (not-budgeted)*
 - *Ground based phase control (budgeted)*
 - *Rectenna elements (budgeted)*
 - **Flight suitcase experiments**
 - Power module — power amplifier, phase control, waveguide, cooling, etc.
 - **Advanced technology candidates**
 - Photoklystron
 - Gyrocon
 - **Summary/Discussion**
-

NASA**Solar Power
Satellite****1980 Funded Efforts**

-
- **Phase control system definition phase IV
— JSC/LINCOM** **\$60K**
 - **Ground-based phase control system
breadboard — JSC** **\$50K**
 - **RF/harmonic measurement techniques
and systems — JSC/JPL** **\$50K**
 - **Solid state amplifier MSFC technology** **\$50K**
 - **Systems definition studies**
 - Complete solid state system studies
(Boeing/RI) **\$50K**
 - Magnetron powered SPS antenna study
(RI) **\$50K**

Note: Funding levels are approximate

- **Adapt sonic simulation techniques to evaluate effects of the disturbed ionosphere on the SPS phase control pilot signal's phase**
 - **Ionospheric scintillation characteristics associated with small aperture receivers**
 - **Model rectenna system and evaluate radio frequency interference levels and patterns resulting from scattering, harmonic generation, and fundamental reradiation**
 - **Investigate/evaluate multiple SPS system interference and environmental effects due to radio frequency beat signal generation**
- Estimated funding — \$50K**

Primary requirements for waveguide material

- **Good surface electrical conductivity**
- **High resistance to thermal distortion**
- **Preliminary tolerance requirements for waveguide**
 - **Length ± 30 mils**
 - **Width ± 3 mils**
 - **Slot offset ± 0.5 mils**

Thermal distortion can significantly decrease waveguide efficiency

- **Waveguide will alternately expand and contract during thermal cycling**
- **Waveguide will tend to bow due to thermal gradient between faces**

NASA**Solar Power
Satellite****Task Description**

- **Evaluation of waveguide requirements and fabrication processes to generate a graphite/metal matrix waveguide design**
- **Fabrication studies and development to verify ability to hold tolerances and establish tooling design**
- **Verification of composite properties on test specimens**
- **Fabricate waveguides to demonstrate reproducibility and provide test articles**
- **Perform physical and mechanical property testing (JSC, LMSC)**
 - RF performance (JSC)
 - Thermal distortion measurements (LMSC)
 - Thermal cycling effects (JSC)
- **Estimated cost of program**
 - FY1979/1980 \$175K

NASA**Solar Power
Satellite****DOE/NASA GBED
Program**

**Overall
Goal**

- **To provide information required to make a rational decision on whether to proceed to a technology verification phase of the SPS program**

Approach

- **Information generated through experiment, demonstration, and analysis, and would include:**
 - **Further development of system concept**
 - **Test/Demonstration of components necessary to construct and operate the system**
 - **Analysis of environmental effects and their mitigation**
 - **Assessment of economic factors including financing options**
 - **Programs to understand and solve problems in the international, institutional, and public concern areas**

NASA**Solar Power
Satellite****DOE/NASA GBED
Program**

**Program
Results**

- Data base that specifies/reduces uncertainty in all critical areas so that a decision can be made for or against a commitment to a technology verification program
 - Selection of preferred system(s)
 - Definition of a technology verification program, including required space projects

**Areas
to be
addressed**

- Systems analysis and technology
- Environmental research and assessment
- International affairs, institutional relations, and public concerns

NASA**Solar Power
Satellite****GBED - Systems Analysis
and Technology
*Technical Areas***

- System definition studies
 - Solar energy conversion
 - Electrical power processing and distribution
 - *Power transmission and reception*
 - Space structures, controls, and materials
 - Space operations
 - Space transportation
-

NASA

Solar Power
Satellite

**GBED - Power Transmission
and Reception**
Key Questions

- **Can the required performance be attained for SPS viability?**
 - *System efficiency*
 - *Focusing and pointing control*
 - *RFI*
 - **Can required long life and/or maintainability characteristics be achieved?**
 - **Can manufacturing techniques be devised to provide systems and components of required performance, production rates, and costs?**
-

NASA

Solar Power
Satellite

Microwave GBED
Summary

**General
objectives**

- **Investigate critical technology areas**
 - Phase control
 - Power amplifiers
 - *Power tubes*
 - *Solid-state*
 - Radiating module
 - Rectenna
 - System integration and performance
 - **Develop microwave system and subsystem hardware**
 - **Verify system performance through subsystem and system ground testing**
 - **Obtain required data for predicting performance of the full scale SPS microwave system**
 - **Establish SPS microwave system criteria and guidelines for continued development**
 - **Investigate potential microwave system/environmental impact areas**
-

NASA**Solar Power
Satellite**

**Microwave GBED
Summary**

- Approach**
- **Early test/facilities requirements definition phase**
 - Microwave system integration and test
 - Subsystem projects
 - **Establish system integration and testing project**
 - Coordinate all microwave activities
 - Progressive system integration tests
 - *Power amplifier/phase control*
 - *Power module using low power klystron*
 - *Power module environmental (high power klystron with heat-pipe radiator)*
 - *Transmit subarray (10.4 M x 10.4 m) using up to 36 power modules*
 - *Rectenna panel/subarray*
 - *Integrated microwave system*
-

NASA**Solar Power
Satellite**

**Microwave GBED
Summary**

- Approach**
- **Establish subsystem projects**
 - Klystron
 - Klystron thermal control
 - Solid-state power amplifier/SPS system
 - Phase control system
 - Radiating module
 - Rectenna
 - **Utilize existing specialized facilities**
 - **Obtain quantitative performance data at system/subsystem levels**
 - **Extrapolate performance to full scale SPS**
 - **System feasibility assessment and performance verification**
-

NASA

**Solar Power
Satellite**

GBED Plan Format

Issue Trees

**4.0 Power
Transmission
and
Reception**

**4.1 Microwave
Systems**

Milestone/Flow Chart

**4.0 Power
Transmission
and
Reception**

**4.1 Microwave
Systems**



Project Summary Sheets

**4.0 Power transmission and
reception**

4.1 Microwave systems

**4.1.1 Power amplifier
performance (tube/
solid-state)**

**4.1.2 Microwave system
performance (tube/
solid state)**

**4.1.3 Phase control system
performance (tube/
solid-state)**

**4.1.4 Transmit antenna
performance (tube/
solid-state)**

**4.1.5 Rectenna element
performance**

NASA

**Solar Power
Satellite**

Power Amplifier Project (Tube) Objectives

**Design, manufacture, test and analysis of
a high power, high efficiency power
amplifier tube to verify SPS performance
requirements (remaining issues)**

- Demonstrate thermal control capability
- Establish reliability data
- Establish cost data
- Verify detailed performance parameters
- Establish criteria and guidelines for continued development

NASA**Solar Power
Satellite****Power Amplifier
Thermal Control
*Objectives***

**Design, manufacture, test and analysis of
an efficient heat-pipe/radiator system to
dissipate waste heat from the SPS
configured power tubes**

- **Demonstrate heat-pipe operation at temperatures
of 200°C - 300°C**
 - **Assess restart capability**
 - **Establish heat-pipe operational lifetime data**
 - **Develop integrated heat-pipe radiator system**
 - **Establish operational efficiency**
 - **Establish efficiency/weight trade-offs**
 - **Establish heat-pipe/radiator criteria and guidelines
for continued development**
-

NASA**Solar Power
Satellite****Solid State
Power Amplifier Project
*Objectives***

**Design, manufacture, test and analysis of
a solid-state power amplifier(s) and power
module to verify SPS performance
requirements (remaining issues)**

- **Demonstrate thermal operating capability**
 - **Establish reliability/operating temperature
trade-offs**
 - **Determine noise characteristics**
 - **Establish cost data**
 - **Verify performance parameters**
 - **Integrated systems definition study**
-

- **Establish device concepts to meet requirements**
- **Develop the lumped element power module using highest efficiency amplifier**
- **Establish requirements for peripheral subsystems, e.g., phase control, power distribution, power processing, etc.**
- **Establish manufacturability requirements**
- **Perform as a parallel iterative process an SPS integration assessment**
- **Integrate power amplifier project/SPS system studies to provide data for programmatic decision**

- A Tube power amplifier performance**
 - **rf power > 50 kW**
 - **dc to rf conversion efficiency > 80%**
- B Solid state amplifier performance**
 - **rf power > 4 W**
 - **dc to rf conversion > 80%**
- C Tube power amplifier and electronics module performance**
 - **Noise suppression > 20dB (within 1 MHz of carrier)**
- D Power module performance**
 - **P/A efficiency > 80%**
 - **rfl < CCIR guidelines**
- E Subarray/rectenna performance**
 - **P/A efficiency > 80%**
 - **rfl < CCIR guidelines**

"Page missing from available version"

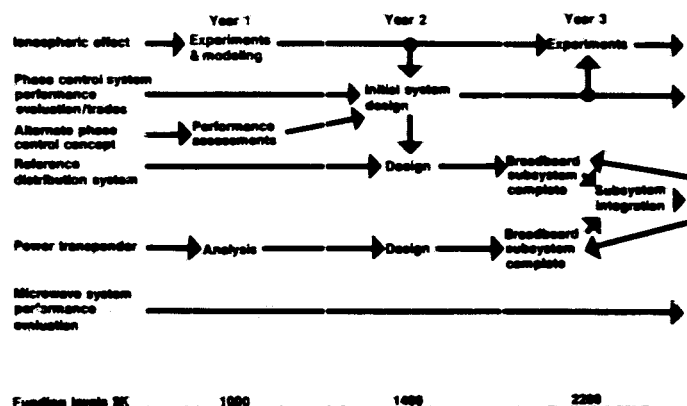
Design, manufacture, test and analysis of a phase control system to verify performance requirements (remaining issues)

- **Definition of ground-based/hybrid system**
- **Assessment of disturbed ionospheric effects**
- **Determine phase noise reduction by phase control loop around power amplifiers**
- **Establish rfi characteristics of power transponder for DOE environmental studies**
- **Obtain engineering data for future system performance analysis using full scale SPS computer simulation**
- **Identify hardware limitation and establish system performance criteria**

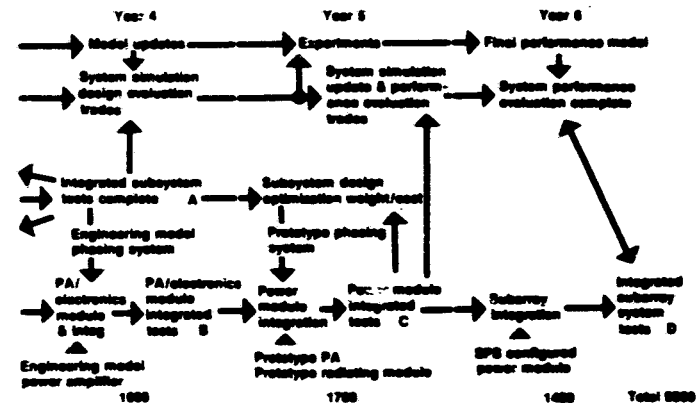
- **Early definition of ground based/hybrid system**
- **Early assessment of disturbed ionospheric effects on all phase control systems in conjunction with DOE**
- **Early solid state system configuration and phase error analysis**
- **Breadboard/prototype hardware testing and environmental tests**
- **End-to-end system model maintained/updated to predict full-scale SPS performance capabilities as hardware development matures**
- **Provide engineering support to integrated system tests**

NASA

Solar Power Satellite



Phase Control Project



A Phase control system performance

- Reference distribution phase error $< 5^\circ$ rms (referred to 2450 MHz)
- Power transponder phase error $< 5^\circ$ rms (referred to 2450 MHz)

B P/A - Phase control system performance

- Phase noise reduction < 20 dB [within ± 1 MHz of carrier]
- Phase error $< 5^\circ$ rms (referred to 2450 MHz)

C Power module system performance

- Phase error $< 10^\circ$ rms
- rfi $<$ CCIR guidelines

D Subarray system performance

- Phase error $< 12^\circ$ rms
 - rfi $<$ CCIR guidelines
-

Design, manufacture, test and analysis of the radiating module to verify performance requirements (remaining issues)

- Determine maximum radiating efficiency achievable - SPS goal is 96%
 - Develop measurement techniques for measuring rf radiated power levels to the accuracy required for SPS components
 - Evaluate low CTE composite materials for applications in the expected SPS environment
-

NASA

Solar Power
Satellite

**Radiating Module
Project**
Objectives

- **Define and characterize performance of potential pilot signal receiving techniques**
- **Define mechanical alignments and tolerances in terms of efficiency requirements and mass production**
- **Develop trade-offs between efficiency, tolerances, cost and mass manufacture**
- **Establish radiating module criteria and guidelines for continued development**

NASA

Solar Power
Satellite

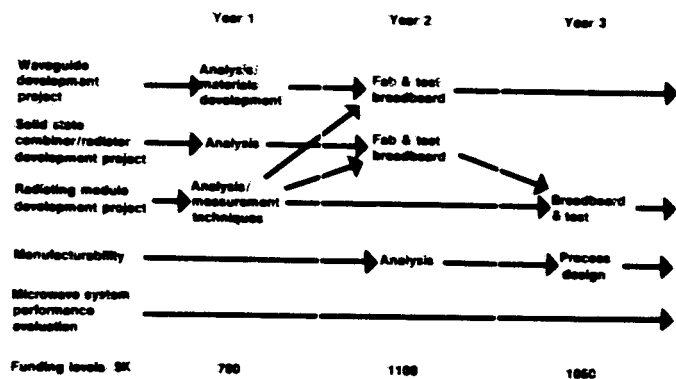
**Radiating Module
Project**
Approach

- **Analytical model development**
 - **Verification of efficiency as a function of tolerances and design details**
- **Radiating module development**
 - **Optimize detail design for maximum efficiency**
 - **Develop diplexing technique**
- **Test hardware fabrication**
 - **Supply test hardware for power module and subarray test**
- **Subarray efficiency test**
 - **Evaluate arraying effects: GAP spacing and positioning tolerance**

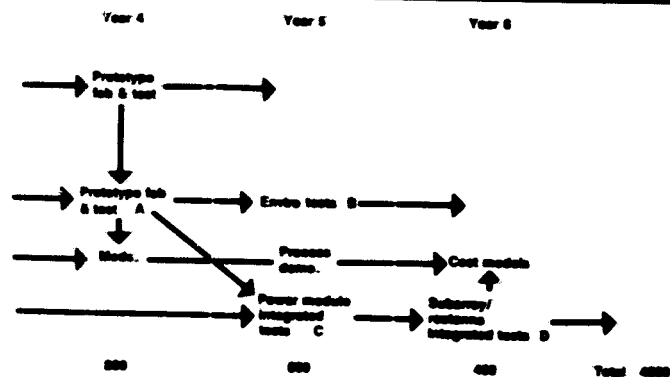
- **Materials evaluation**
 - **Viability of low CTE composites**
 - **Manufacturing techniques analysis**
 - **Analysis of fabrication techniques available vs. tolerance allowed**
 - **Design definition**
 - **Integration of total effort**
 - **Measurement techniques development**
 - **Test techniques**
 - **Data analysis techniques**
 - **Facilities**
 - **Test equipment**
-

NASA

Solar Power Satellite



Radiating Module Project



A Prototype antenna performance

- I²R losses < 5%
- Dimensional tolerances < 30 mils
- Combining losses < 2% (solid state configuration)

B Prototype antenna environmental performance

- Thermal effects < 2% loss efficiency

C Power module system tests

- Surface tolerance < 30 mils
- I²R losses < 5%
- Thermal effects less than 2% loss
- Solid state combining losses < 2%

D Subarray system tests

- Transmit efficiency > 93%
-

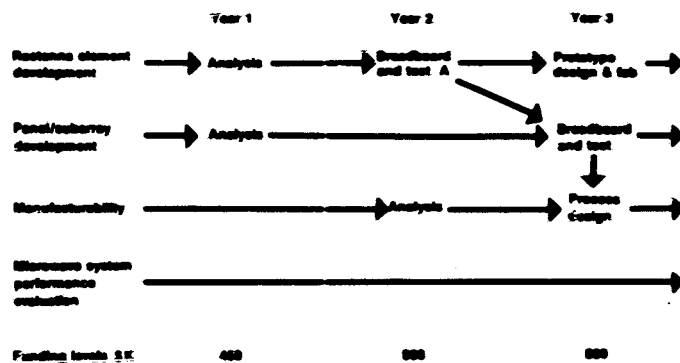
Design, manufacture, test and analysis of an SPS rectenna subarray of sufficient size to verify performance requirements (remaining issues)

- Demonstrate high efficiency antenna - rectifier designs which have potential for low cost mass production
 - Determine efficiency levels achievable - goal of approximately 89%
 - Develop detailed understanding of each component, element, and array for predicting performance and costs
 - Determine environmental and failure mode protection requirements and impacts
 - Develop techniques for predicting off-nominal performance including EMI effects of scattering
-

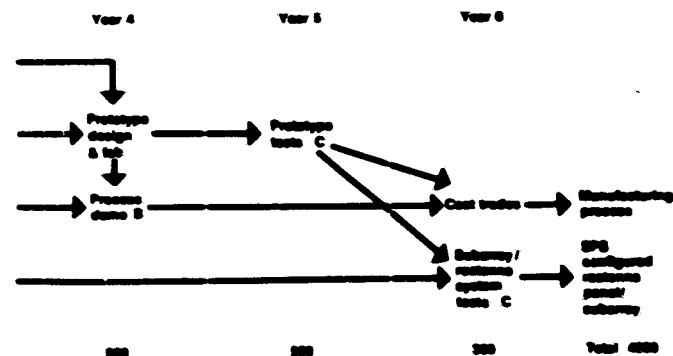
- **Indepth analytical evaluation of the available alternatives at the component, element, array and panel levels**
- **Development of analytical model to assist in evaluating design options, predict nominal efficiency, predict failure mode effects and evaluate manufacturing tolerances**
- **Optimize the rectenna design(s) including experimental effort**
- **Evaluate the effects of integrating rectenna elements into panels, units, and groups**
- **Provide hardware for panel/subarray test**
- **Determine nominal and off-nominal efficiency and reradiation characteristics for rectenna panel/subarray**

NASA

Solar Power Satellite



Rectenna Project



A Element performance

- Losses < 11%

B Manufacturing process

- Cost effective manufacturability demonstrated

C Subarray performance

- Conversion efficiency > 85%
- rfi < CCIR guidelines

- Effective management and technical integration of the various system elements
 - Experimental verification of critical microwave system parameters (remaining issues) at subarray level
 - Verify integrated system compatibility
 - Performance of microwave reference system configuration
 - Interaction of key subsystems/elements
 - Determine space environmental effects (remaining issues)
 - Determine rfi characteristics and effects for system performance evaluation and DOE environmental impact studies
 - Transmit antenna rfi characteristics
 - rfi effects on selected hardware
 - Rectenna reradiation characteristics
-

NASA**Solar Power
Satellite****Microwave Systems
Project
*Approach***

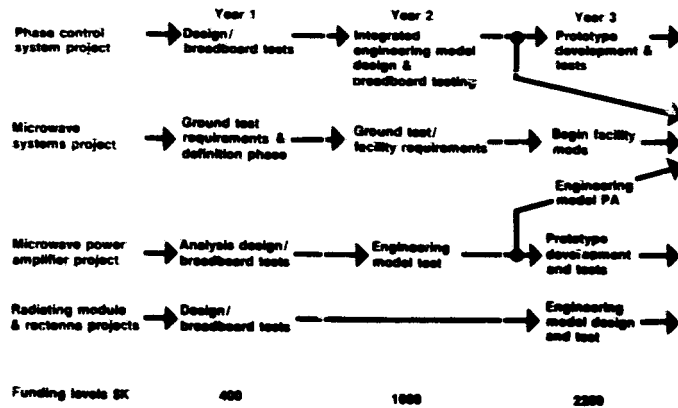
- **Early test/facilities requirements and test techniques definition phase**
- **Cost-effective utilization of existing facilities**
- **All ground tests (use thermal vacuum chamber for space environmental testing and antenna range/anechoic chamber for rf radiation testing)**
- **Obtain quantitative performance data at system/subsystem levels**
- **Supported by component contractors (hardware/engineering)**

NASA**Solar Power
Satellite****Remaining Issues
Microwave System/
*Environmentally Related***

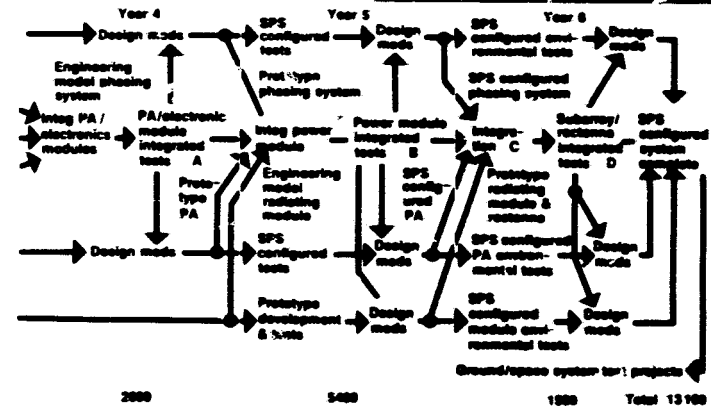
- 1 **Validity of the present ionospheric transmission limit of 23 mw/cm²**
 - **GBED evaluation - DOE prime**
 - 2 **Effects of heating/disturbing the ionosphere on communications**
 - **GBED evaluation - DOE prime**
 - 3 **Effects of heating/disturbing the ionosphere on performance of microwave system**
 - **GBED evaluation - NASA/DOE**
 - 4 **Electromagnetic compatibility**
 - **Radiated noise/harmonics at SPS**
 - **Reradiated noise/harmonics at rectenna**
 - **GBED evaluation - microwave systems project**
-

NASA

Solar Power Satellite



Microwave Systems Project



A Power amplifier/phase control systems performance

- Phase error < 5% rms (ref to 2450 MHz)
- Conversion efficiency 80%
- Noise suppression > 20dB
- rfi < CCIR guidelines

B Power module performance

- Phase error < 10% rms
- Transmission efficiency > [dc input to rf radiated]
- rfi < CCIR guidelines
- Cooling, corona, multipacting tests (after component environmental tests)

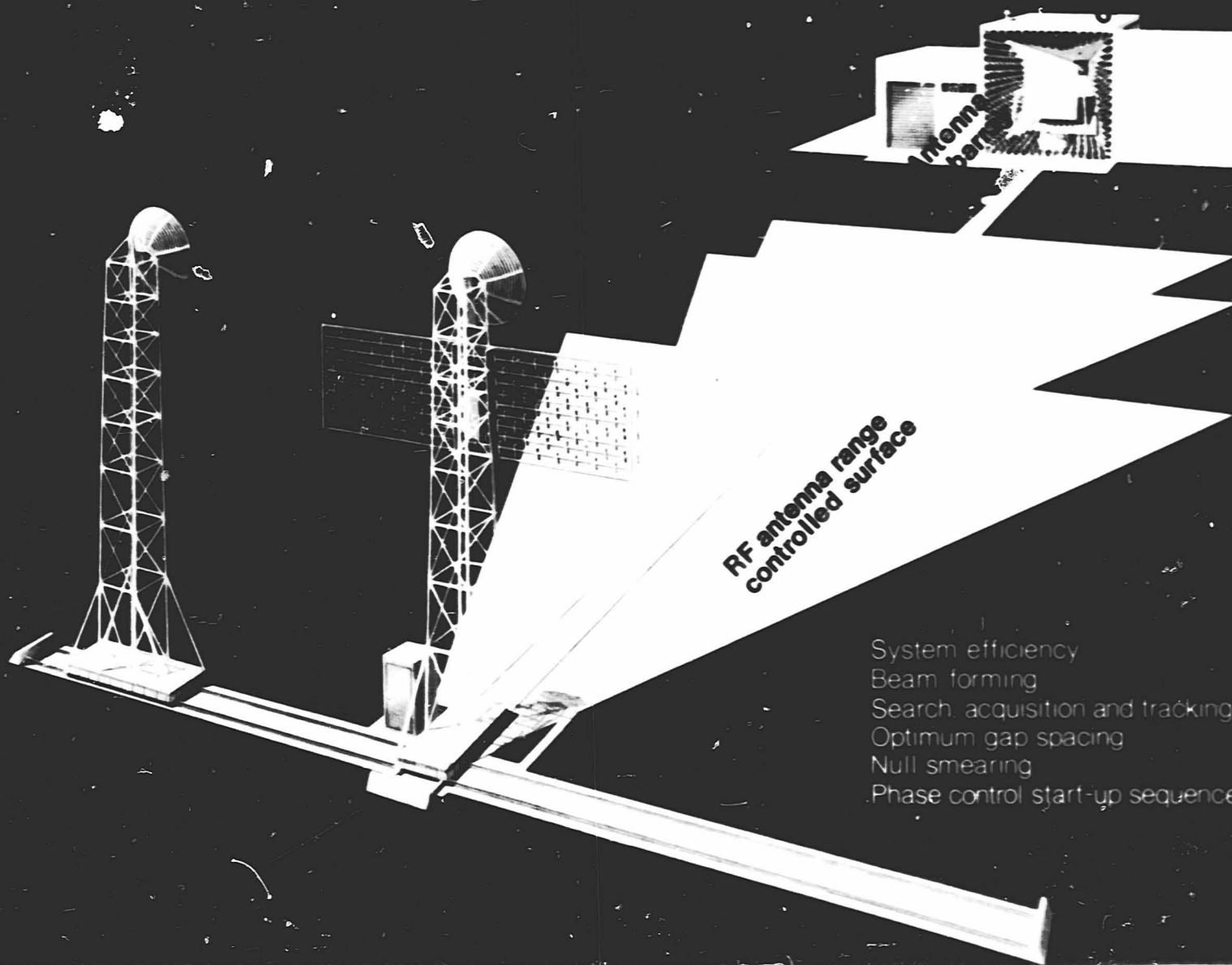
C Solid state vs tube power module configuration decision point**D Subarray/rectenna system performance**

- Phase error < 12% rms
- Overall efficiency > 55% [dc input to recovered dc output]
- rfi < CCIR guidelines
- Safe startup/shutdown

NASA

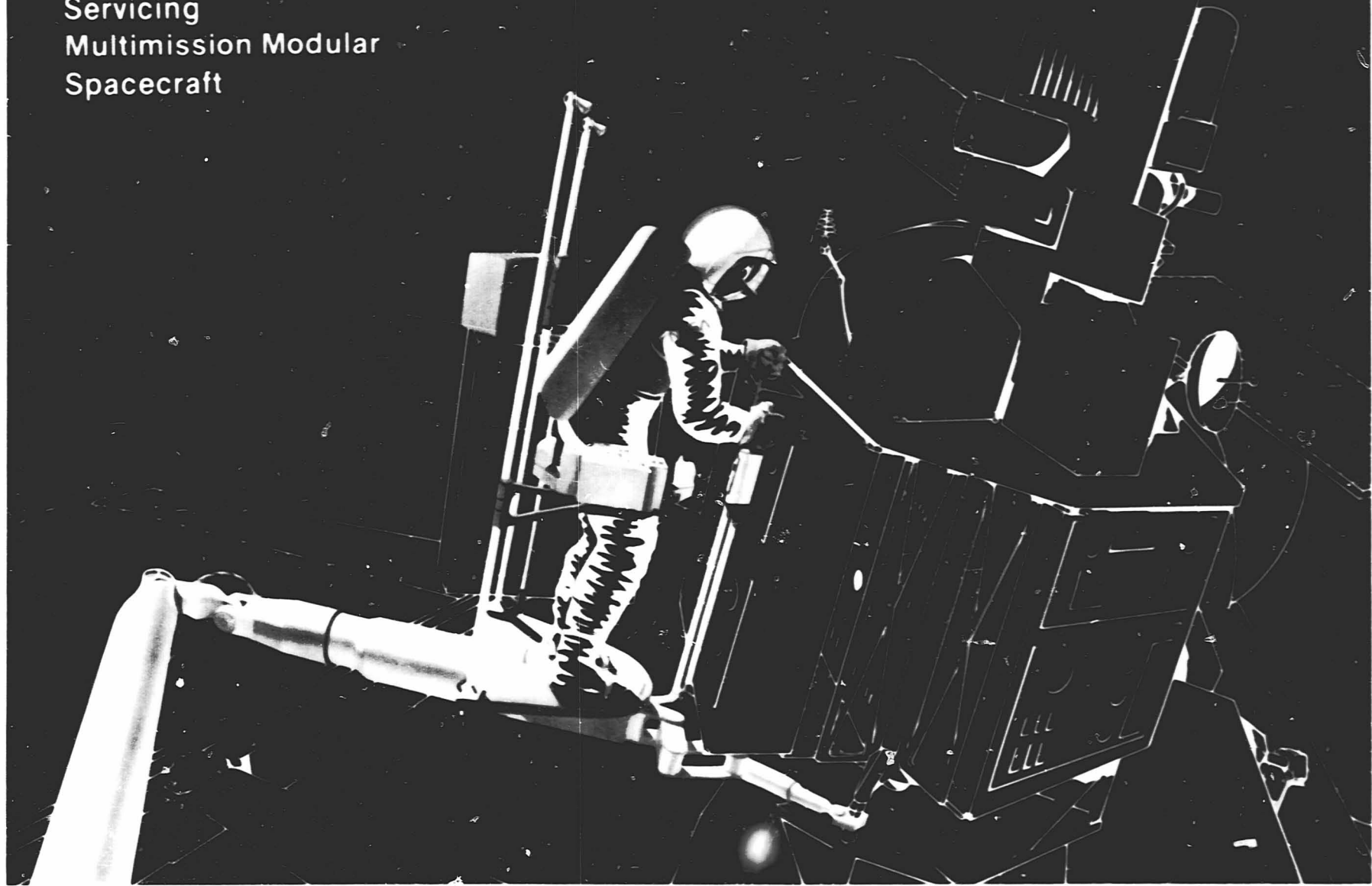
Solar Power
Satellite

MW System
Exploratory Research



System efficiency
Beam forming
Search, acquisition and tracking
Optimum gap spacing
Null smearing
Phase control start-up sequence

MRWS
Servicing
Multimission Modular
Spacecraft



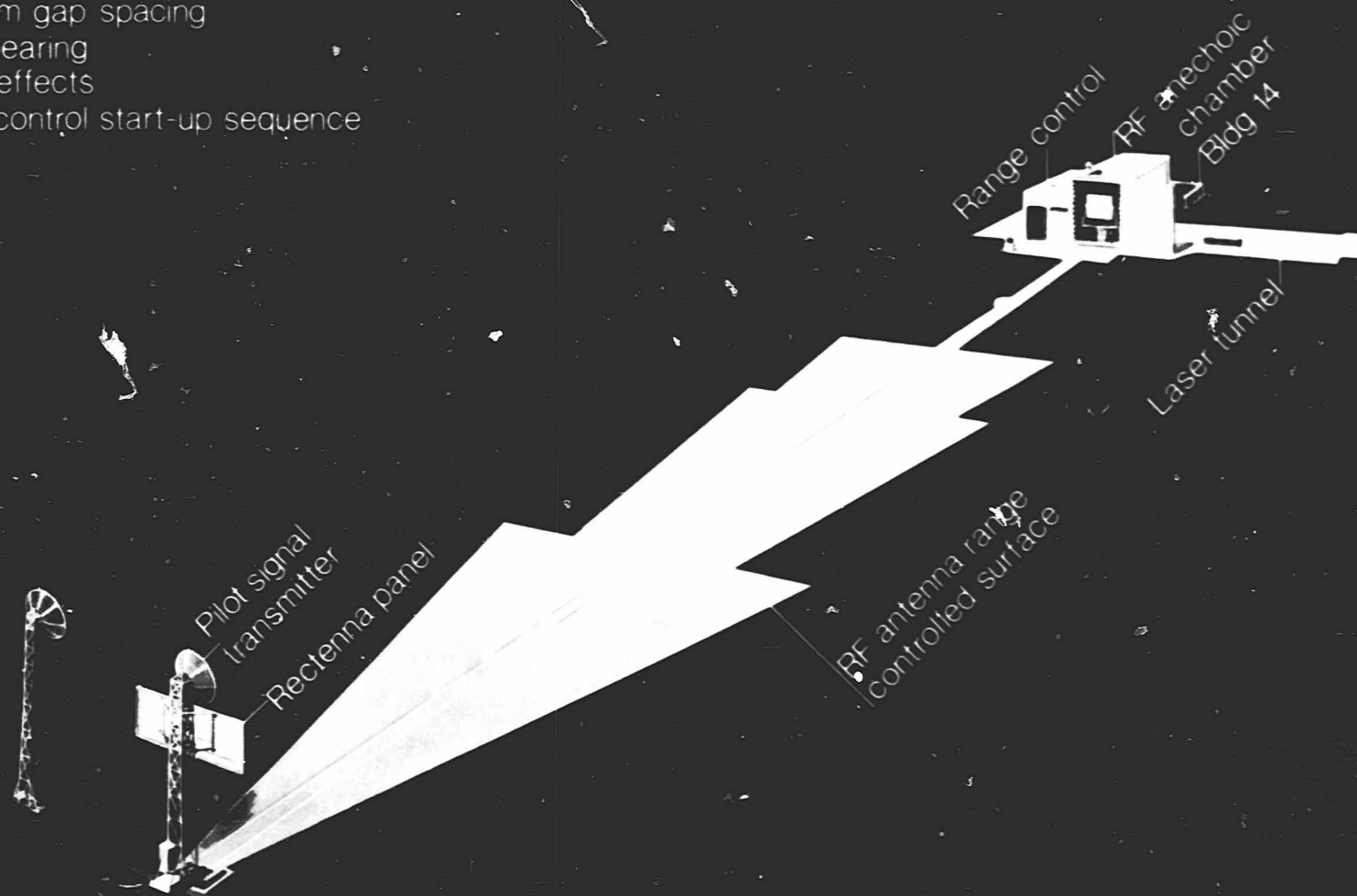
ORIGINAL PAGE IS
OF POOR QUALITY

SPS MW System Exploratory Research

measures:

- Beam mapping, gain-system efficiencies
- Search, acquisition and tracking
- Optimum gap spacing
- Null smearing
- Failure effects
- Phase control start-up sequence

Subarray, in chamber;
Mapper, Rectenna panel
down range



SPS MW System Exploratory Research

measures:

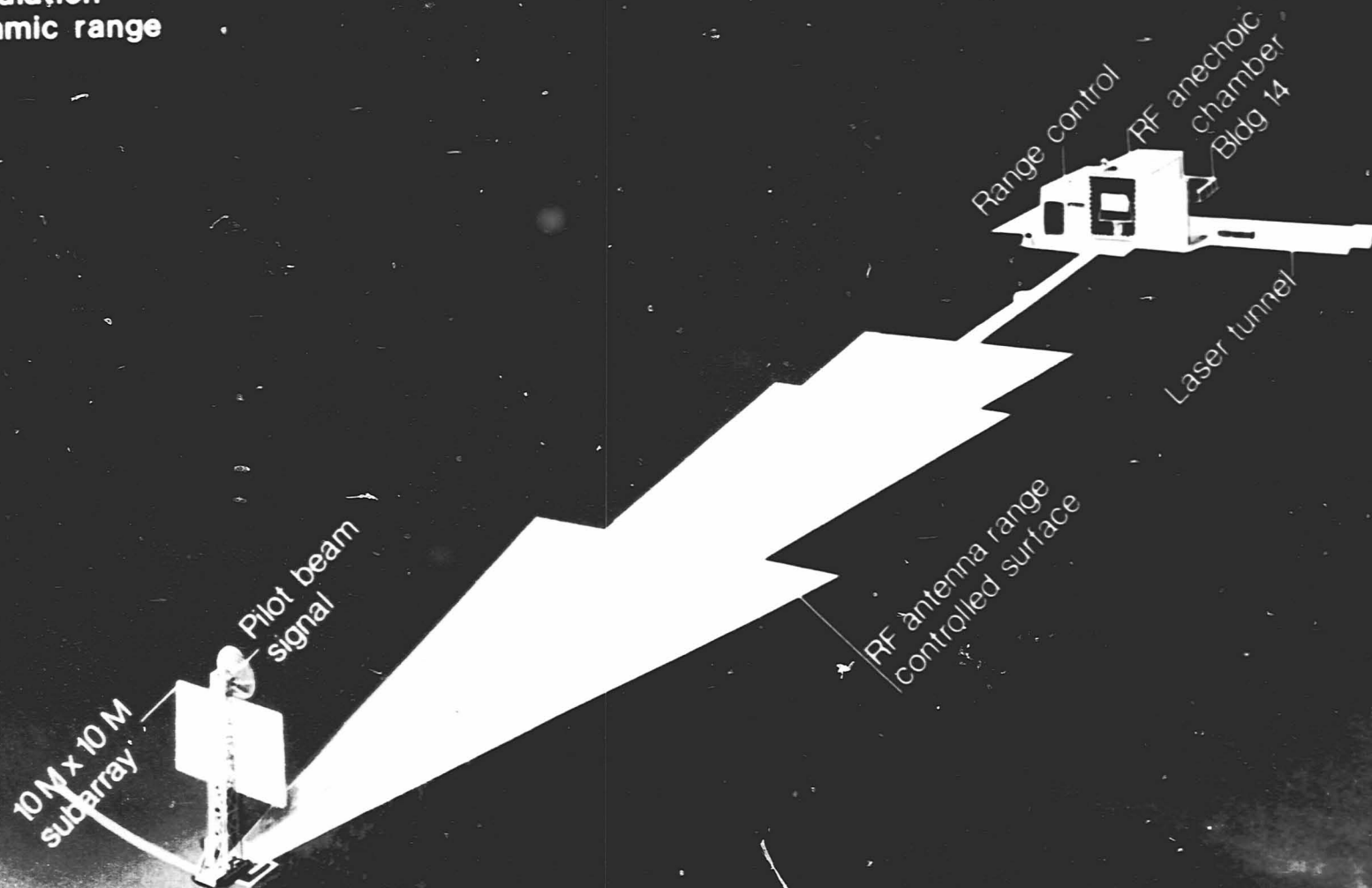
Rectenna efficiencies

Reradiation

Dynamic range

EMI

Rectenna in chamber,
Subarray down range



MW Power Module in Environmental Chamber

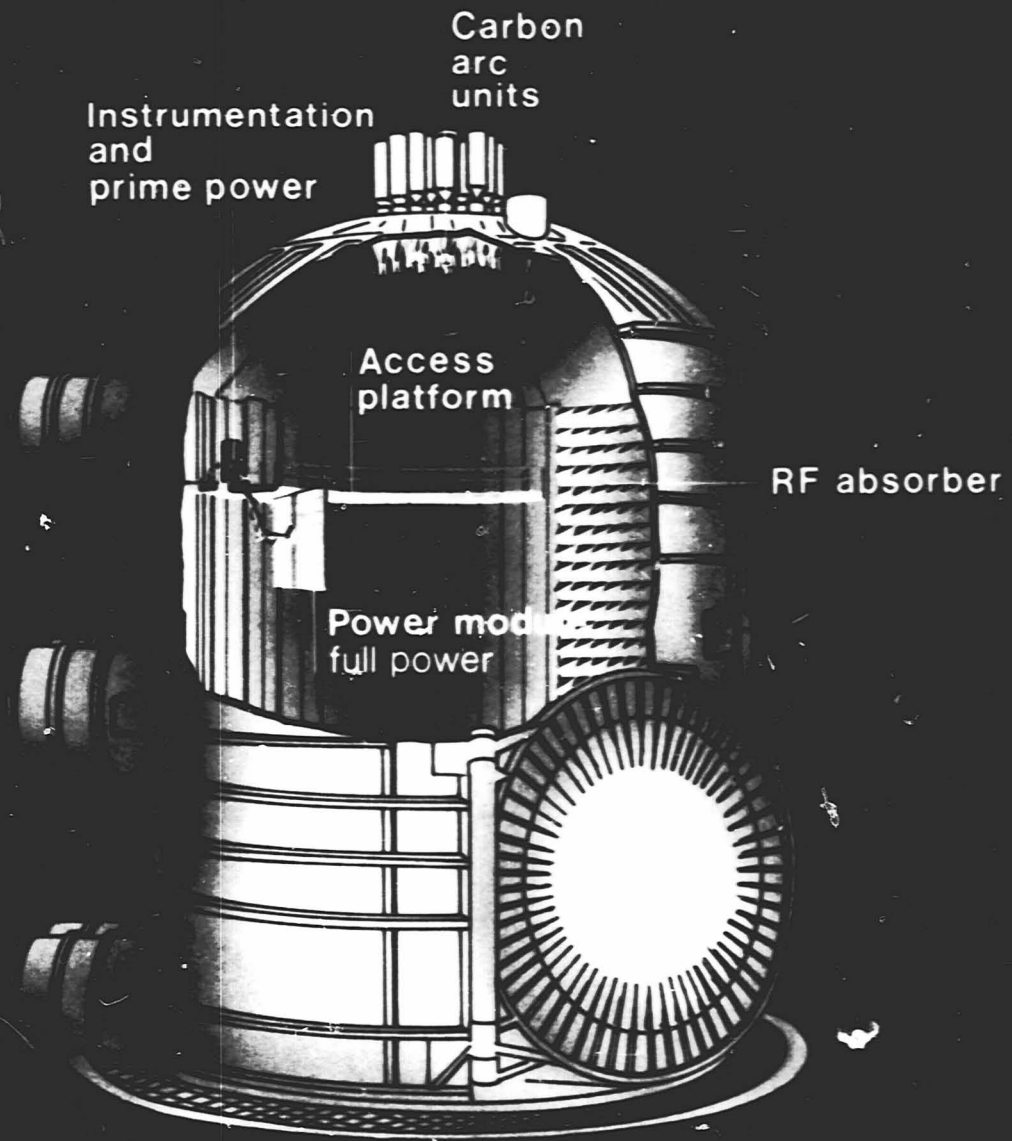
measures:

Thermal characteristics

Multipacting

Corona discharge

Plasma



ORIGINAL PAGE IS
OF POOR QUALITY

NASA**Solar Power
Satellite**

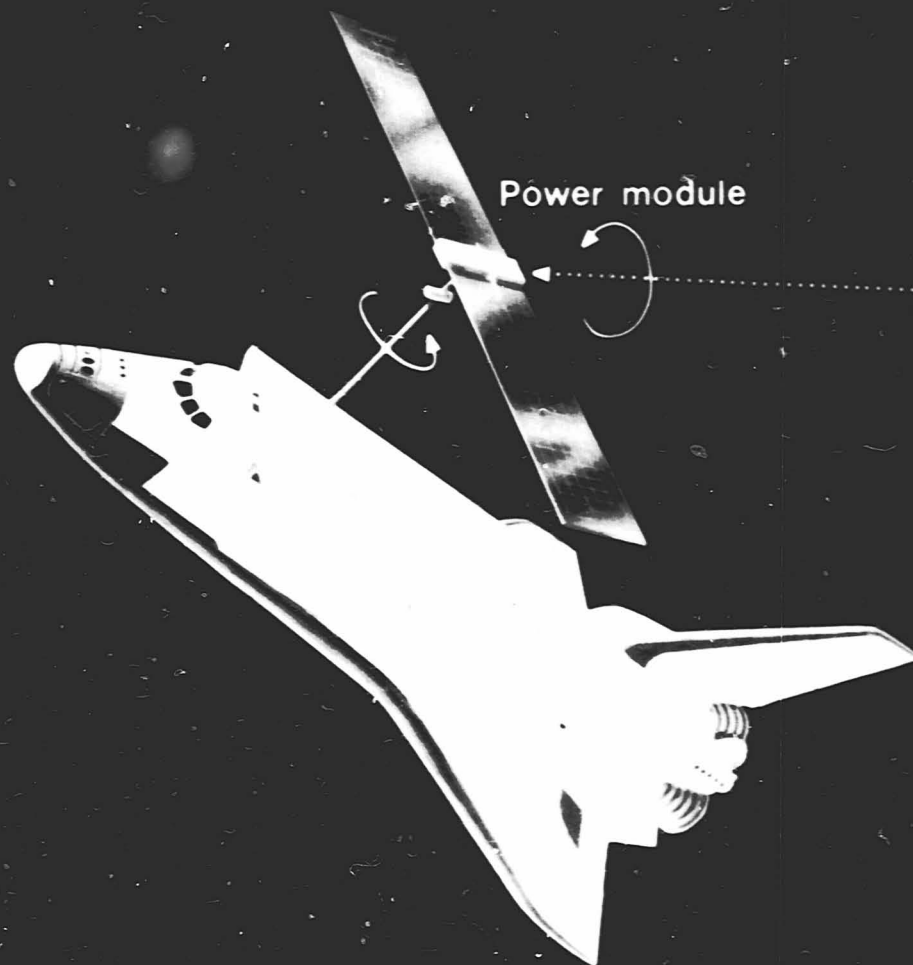
**Microwave System
GBED
Cost Summary**

By project	Microwave systems integration and test	\$13.1M
	Power amplifier tube/solid-state	15.7M
	Phase control system	9.3M
	Transmit antenna (radiating module)	4.7M
	Rectenna	4.0M
By operating category	Operating (includes contractor man-hours, simulations, management)	\$28.3M
	Equipment (includes test articles and test equipment)	11.9M
	Facilities (includes modifications and operating costs)	6.6M
By fiscal year	YR1 YR2 YR3 YR4 YR5 YR6 TOTAL	
	\$3.7M \$8M \$10.7M \$10.3M \$9.7M \$4.4M \$46.8M	

**Candidate flight experiments
(low Earth orbit)**

- **Single power module—radiating**
 - **Tube—requires space power supply > 50kW**
 - **Solid state—less power required**
 - **Pattern could be mapped if separate co-orbiting satellite available**
 - **Subarray performance**
 - **Phase control—mapping satellite required**
 - **Thermal control**
 - **Variable configuration if both phase and thermal control verified**
-

Shuttle Sortie Experiments

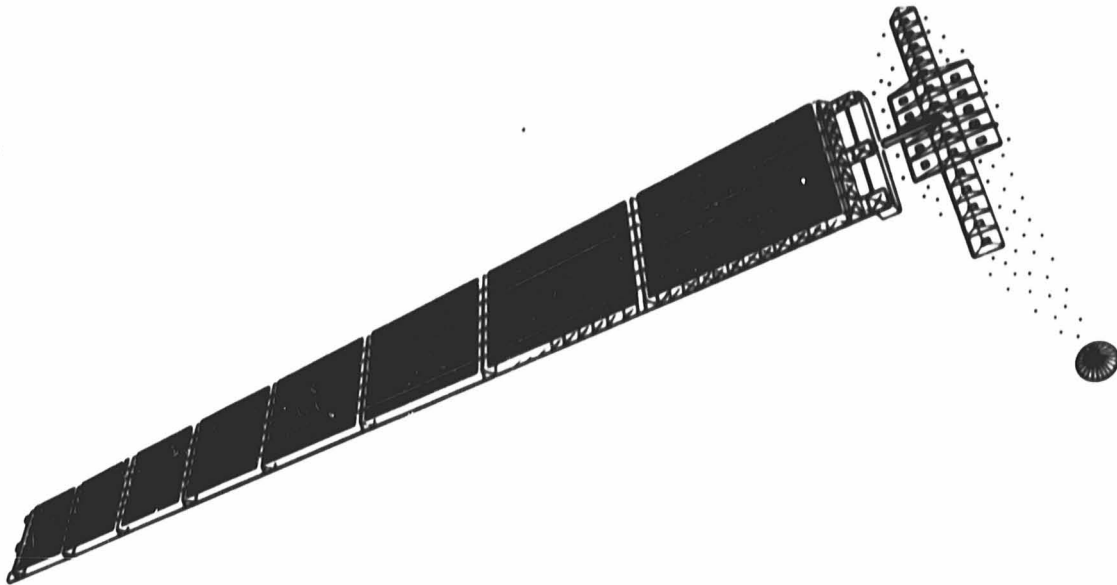


MW System Component Test

Detached
experiment
carrier

Beam
mapping
Pilot beam
transmitter

NASA**Solar Power
Satellite****System Development
Test Project**



NASA**Solar Power
Satellite****Gyrocon Power
Amplifier**

**Potential/
capabilities**

- **High power level - multi-megawatt**
- **High efficiency - theoretically approaching 100%**

History/status

- **Russian inventor - G. I. Budker - 1967**
- **Development/status**
 - **Russians demonstrated operating gyrocons - 1978**
 - *1 MW power, 75% efficiency, CW operation, 181 MHz frequency*
 - *50 MW power (peak), pulsed operation, 430 MHz frequency*
 - **Los Alamos scientific labs - 1979/1980 (P. J. Tellerico)**
 - *Design/develop/test - first American gyrocon*
 - *650 kW power, 450 MHz frequency*
 - *Calculated efficiency \approx 85%*

NASA**Solar Power
Satellite****Technology Research
Candidates**
Photoklystron

- **Oscillates at rf when illuminated by light**
- **rf is generated near solar incidence**
- **rf propagation vector at right angles to solar incidence**
- **SPS configuration would require rf or solar reflection**
- **High voltage solar arrays are eliminated**
- **dc bus bars reduced/sliprings are eliminated**
- **Proof-of-concept model developed**
- **1% efficiency demonstrated, 10% appears possible**
- **Efficiency, gain, operating voltages, phase stability parameters not well understood at SPS frequencies**
- **Appears to be a good technology research candidate**

NASA**Solar Power
Satellite****Planned Activities**

- **1980 funded efforts**
 - **Additional funded efforts**
 - **Ground Based Exploratory Development (GBED)**
 - **Program overview (DOE/NASA)**
 - **Microwave systems**
 - **Reference system**
 - **System alternative (solid-state) (budgeted)**
 - **Sub-system alternatives**
 - *Magnetron (not-budgeted)*
 - *Ground based phase control (budgeted)*
 - *Rectenna elements (budgeted)*
 - **Flight suitcase experiments**
 - **Power module — power amplifier, phase control, waveguide, cooling, etc.**
 - **Advanced technology candidates**
 - **Photoklystron**
 - **Gyrocon**
 - **Summary/Discussion**
-

NASA-JSC